www.segweb.org

REVIEWS IN ECONOMIC GEOLOGY
Volume 18

RARE EARTH AND CRITICAL ELEMENTS IN ORE DEPOSITS

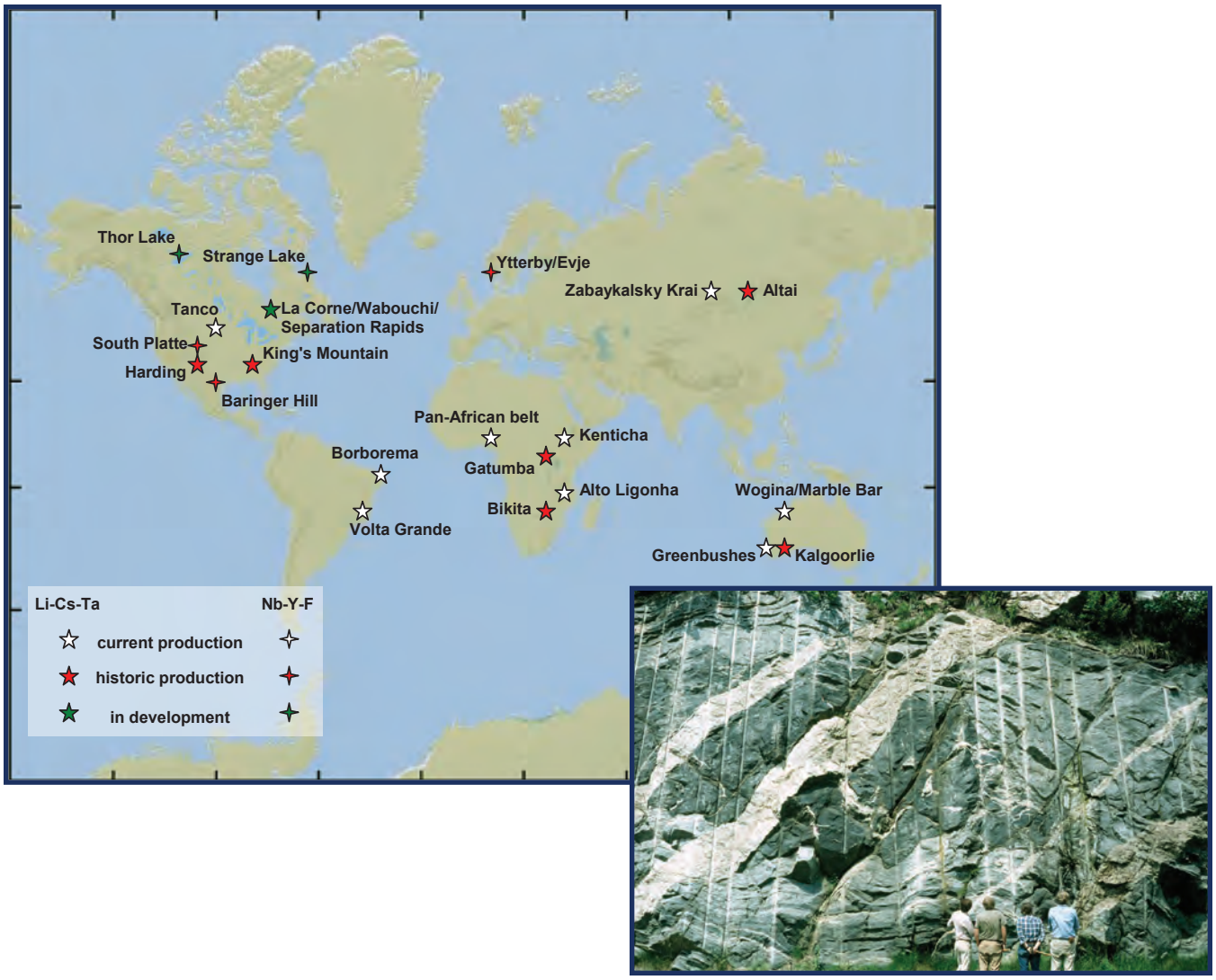

Editors
P.L. Verplanck and M.W. Hitzman

SOCIETY OF ECONOMIC GEOLOGISTS, INC.

www.segweb.org

REVIEWS IN
ECONOMIC GEOLOGY

Volume 18

RARE EARTH AND CRITICAL ELEMENTS IN ORE DEPOSITS

Volume Editors

Philip L. Verplanck
U.S. Geological Survey
Box 25046, MS 973
Denver Federal Center
Denver, CO 80225-0046

Murray W. Hitzman
Department of Geology & Geological Engineering
Colorado School of Mines
Golden, CO. 80401

SOCIETY OF ECONOMIC GEOLOGISTS, INC.

REVIEWS IN ECONOMIC GEOLOGY

Published by the Society of Economic Geologists, Inc.
7811 Shaffer Parkway
Littleton, CO 80127, USA

Website: segweb.org
E-mail: seg@segweb.org

Printed by
SpeedPro Imaging
10855 Dover St., Ste. 800
Broomfield, CO 80021

ISSN
0741-0123 (Print)
1933-1495 (Disc)
2374-443X (PDF)

ISBN
978-1-629492-18-6 (Print)
978-1-629492-19-3 (Disc)
978-1-629495-76-7 (PDF)

Reviews in Economic Geology is a series publication of the Society of Economic Geologists designed to accompany the Society's Short Course series. Like the Short Courses, each volume provides comprehensive updates on various applied and academic topics for practicing economic geologists and geochemists in exploration, development, research, and teaching. Volumes are produced in conjunction with each new Short Course, first serving as a textbook for that course, and subsequently made available to SEG members and others at a modest cost.

SEG Publications Board

Through 2016
Sarah A. Gleeson
Richard J. Goldfarb, *Chair*
Stuart F. Simmons

Through 2017
Zhaoshan Chang
Patrick Mercier-Langevin

Through 2018
Claire M. Chamberlain
Brian G. Hoal, *ex officio*
Lawrence D. Meinert

On the cover: The global distribution of some historically important, current, and potential future sources of rare elements from pegmatites. *Inset:* A set of common, unzoned pegmatite dikes that cut amphibolite and gneiss, Haddam, Connecticut, USA. Both images from the paper by D. London in this volume.

© Copyright 2016, Society of Economic Geologists, Inc.

CONTENTS

Sponsors v

Author Biographies vii

Introduction:
Rare Earth and Critical Elements in Ore Deposits 1
Philip L. Verplanck and Murray W. Hitzman

Chapter 1:
Rare Earth Element Ore Geology of Carbonatites 5
Philip L. Verplanck, Anthony N. Mariano, and Anthony Mariano, Jr.

Chapter 2:
Rare Metal Deposits Associated with Alkaline/Peralkaline Igneous Rocks 33
Jaroslav Dostal

Chapter 3:
Characteristics and Genesis of Ion Adsorption-Type Rare Earth Element Deposits 55
Kenzo Sanematsu and Yasushi Watanabe

Chapter 4:
Placer-Type Rare Earth Element Deposits 81
Debashish Sengupta and Bradley S. Van Gosen

Chapter 5:
Rare Earth Elements in Sedimentary Phosphorite Deposits: A Global Assessment 101
Poul Emsbo, Patrick I. McLaughlin, Edward A. du Bray, Eric D. Anderson, Thijs R.A. Vandenbroucke, and Robert A. Zielinski

Chapter 6:
Rare Earth Element Deposits in China 115
Yuling Xie, Zengqian Hou, Richard J. Goldfarb, Xiang Guo, and Lei Wang

Chapter 7:
By-Products of Porphyry Copper and Molybdenum Deposits 137
David A. John and Ryan D. Taylor

Chapter 8:
Rare-Element Granitic Pegmatites 165
David London

Chapter 9:
Critical Elements in Alkaline Igneous Rock-Related Epithermal Gold Deposits 195
Karen D. Kelley and Paul G. Spry

Chapter 10:
Critical Elements in Carlin, Epithermal, and Orogenic Gold Deposits 217
Richard J. Goldfarb, Albert H. Hofstra, and Stuart F. Simmons

Chapter 11:
The Minor Element Endowment of Modern Sea-Floor Massive Sulfides and Comparison with Deposits Hosted in Ancient Volcanic Successions 245
Thomas Monecke, Sven Petersen, Mark D. Hannington, Hannah Grant, and Iain M. Samson

Chapter 12:
Critical Elements in Sediment-Hosted Deposits (Clastic-Dominated Zn-Pb-Ag, Mississippi Valley-Type Zn-Pb, Sedimentary Rock-Hosted Stratiform Cu, and Carbonate-Hosted Polymetallic Deposits): A Review 307
Erin E. Marsh, Murray W. Hitzman, and David L. Leach

Chapter 13:
Resource Potential for Commodities in Addition to Uranium in Sandstone-Hosted Deposits 323
George N. Breit

Chapter 14: Lithium Brines: A Global Perspective 339
Lee Ann Munk, Scott A. Hynek, Dwight C. Bradley, David Boutt, Keith Labay, and Hillary Jochens

SEG
www.segweb.org

SPONSORS

The Society of Economic Geologists Publications Board thanks the U.S. Geological Survey and SGS for their generous financial support of this volume.

SGS

USGS
science for a changing world

This material is based upon work supported by the U.S. Geological Survey under Grant/Cooperative Agreement No. G16AP00122.

The views and conclusions contained in this document are those of the authors and should not be interpreted as representing the opinions or policies of the U.S. Geological Survey. Mention of trade names or commercial products does not constitute their endorsement by the U.S. Geological Survey.

AUTHOR BIOGRAPHIES

Eric D. Anderson received a B.A. degree in geology from Augustana College and an M.Sc. degree in geology and geochemistry from the University of Colorado, Boulder. His master's research focused on fluid evolution in the epithermal-porphyry environment. He went on to receive a Ph.D. from Colorado School of Mines. His dissertation integrated geophysical data and mineral deposit models, which resulted in a better understanding of the distribution of concealed mineral resources within an accreted island-arc setting. He currently works for the U.S. Geological Survey in Denver, specializing in geophysics and economic geology.

Dwight Bradley received his bachelor's degree in 1978 from the University of Vermont and a Ph.D. in 1984 from the State University of New York at Albany. He recently retired after a career as a research geologist with the U.S. Geological Survey in Alaska. He spent 26 summers in the field in Alaska, and has also worked in the Canadian Arctic, New England, Maritime Canada, and Mauritania. Bradley's field experience spans a range of tectonic settings, including collisional orogens, magmatic arcs, accretionary complexes, passive margins, foreland basins, and pull-apart basins. His research interests include earth history, plate tectonic interpretations of orogenic belts, geochronology, and tectonic aspects of ore-deposit genesis. He is currently studying the geochronology and tectonics of lithium-cesium-tantalum (LCT) pegmatites, both to elucidate the origins of these remarkable ore deposits, and, possibly, to develop LCT pegmatites as a tool in tectonic interpretations of orogenic belts.

George N. Breit earned a B.S. degree in geological sciences from Pennsylvania State University (1977) and M.S. (1980) and Ph.D. (1986) degrees in geochemistry from the Colorado School of Mines. He worked for the U.S. Geological Survey from 1978 to 2013, holding positions of increasing responsibility, from field assistant to project chief. George's initial work with the USGS focused on the geochemistry of formation of sandstone-hosted uranium deposits. He was also the vanadium resource specialist for 20 years. Later assignments included a range of investigations of low-temperature water-rock interaction, including rock alteration on active volcanoes, mobility of trace elements in the vadose zone in desert environments, natural trace element degradation of groundwater quality (south and southeast Asia and the United States), and controls on trace element distribution in sedimentary systems from deposition to weathering. He currently is conducting investigations of ore and environmental geochemical systems as a consultant.

David Boutt is an associate professor of hydrogeology in the Department of Geosciences at the University of Massachusetts-Amherst. Professor Boutt received his B.S. and M.S. degrees from the Department of Geological Sciences at Michigan State University in 1997 and 1999, respectively, followed by a Ph.D. degree in hydrology in 2004 from New Mexico Institute of Mining and Technology in Socorro, NM. Professor Boutt's research is focused primarily on advancing our scientific understanding of coupled processes and regional-scale groundwater flow in aquifer systems through the synthesis of physical, chemical, and thermal datasets with geologic and paleohydrologic information. Dr. Boutt has managed federal and private research grants and projects in the United States, Chile, the Caribbean, and Japan. He is an editor for the *Journal of Hydrological Processes*, the director of the UMass 1-year MS in geohydrology, and a codirector for the Environmental Sciences undergraduate program at UMass.

Jaroslav Dostal received a B.Sc. degree in geology from Charles University, Prague, where he subsequently worked as a lecturer at the Department of Mineral Deposits. After graduating from McMaster University, in Hamilton, Ontario, with a Ph.D. degree, he pursued postdoctoral studies at the Dalhousie University. He then became a professor of geology at Saint Mary's University, where he is currently professor emeritus. He is also an honorary professor at the Mongolian University of Science and Technology in Ulaanbaatar and an adjunct professor at the Department of Earth Sciences of Dalhousie University. At Saint Mary's, Dr. Dostal established a regional geochemical center and applied its analytical facilities to a variety of questions in earth sciences. His research has been recognized by scientific awards, including the Distinguished Scientist Award of the Atlantic Geoscience Society (Gesner Medal) and the Career Achievement Award of the Volcanology and Igneous Petrology Division of the Geological Association of Canada. Currently, he is a director of Ucore Rare Metals Ltd. His research interests are in geochemistry, mineral resources, igneous petrology, and geodynamics.

Edward A. Du Bray is a research geologist working as part of the U.S. Geological Survey Mineral Resources Program in Denver, Colorado, having obtained an M.S. degree in geology from Stanford University in 1977. He combines geologic mapping with petrologic and geochemical studies of igneous rocks throughout the western United States to understand the processes that govern the evolution of magmatic systems and their associated ore deposits. Recent studies of the 45–3 Ma ancestral Cascades arc along western North America characterize protracted continental arc magmatism and define the time-space-compositional variations that have controlled the evolution of subduction-related magmatism in this area. Currently, he is engaged in a study of voluminous ~1.4 Ga magmatism in the United States and evaluating relationships between the petrogenesis of these rocks and associated REE deposits.

Poul Emsbo is a research geologist with the U.S. Geological Survey in Denver, Colorado. He received his B.S. degree from Union College (1986) and earned his M.Sc. (1993) and Ph.D. (1999) degrees in economic geology-geochemistry from the Colorado School of Mines. Since arriving at the USGS in 1989, Poul has investigated the genesis of Carlin Au, MVT, sedex, sedimentary copper deposits, and high salinity brines. For the past several years he has explored the interplay between ocean chemistry, sea-floor hydrothermal deposits, marine sediment-hosted deposits, and metalliferous black shales.

Richard J. Goldfarb was a research geologist with the Minerals Program of the U.S. Geological Survey for 36 years. He has conducted studies on the distribution of gold deposits throughout the world, compiling comprehensive global descriptions of their spatial-temporal setting and evaluating their controlling factors. His research has been focused on global metallogeny, geology of ore deposits in the North American Cordillera with emphasis on orogenic gold, distribution and geology of lode gold deposits in China and elsewhere in Asia, and fluid inclusion and stable isotope applications to the understanding of ore genesis. Rich has senior-authored and co-authored more than 200 papers on mineral resources, with many recognized as the authoritative research on orogenic gold and on aspects of regional metallogeny. He has served as President of the Society of Economic Geologists, is a past Silver Medalist and lecturer of the Society, has served as chief editor of *Mineralium Deposita*, is currently on the editorial boards of *Economic Geology* and *Gondwana Research*, and was one of the co-editors of the *Economic Geology 100th Anniversary Volume*. He received his B.S. degree in geology from Bucknell University (1975), an M.S. degree in hydrology from MacKay School of Mines (1981), and Ph.D. degree in geology from the University of Colorado (1989). Currently, he is an adjunct professor at Colorado School of Mines and China University of Geosciences Beijing.

Xiang Guo is currently an exploration project manager in the Shaanxi Coal Geology Group Co. Ltd. He received his B.S. degree in geology (2010) and M.Sc. degree in mineral exploration (2014) from the University of Science & Technology Beijing (USTB). During undergraduate and graduate study at USTB, he examined mineral deposits in Inner Mongolia, Anhui, and Sichuan provinces. He has conducted field geology work, fluid inclusion research, and isotope geochemistry studies on REE, porphyry Mo, and epithermal Pb-Zn-Ag deposits.

Hannah Grant received an MGeol (International) degree in geological sciences from the University of Leeds in the United Kingdom, followed by an M.Sc. in geological sciences from Queen's University, Canada, where she investigated a silver-rich VMS deposit in the Canadian Arctic. After two years working as a geochemist for Newmont Mining Corporation in the United States, in 2014 she moved to GEOMAR, Helmholtz Centre for Ocean Research Kiel in Germany to pursue Ph.D. research into modern submarine hydrothermal systems. Her research is currently focused on the mineralogical and geochemical characterization of sea-floor massive sulfide deposits—specifically, the rare and critical metal content of these systems.

Mark Hannington is the Goldcorp Chair in Economic Geology at the University of Ottawa and Helmholtz Professor at GEOMAR-Helmholtz Center for Ocean Research Kiel, Germany. Prior to joining the University of Ottawa in 2005 and GEOMAR in 2014, he was a senior research scientist at the Geological Survey of Canada for 15 years. His research combines the study of ancient ore deposits and active hydrothermal systems on the modern sea floor. He and his students have worked extensively on Precambrian volcanogenic massive sulfide deposits and also have participated on more than 35 research cruises to active volcanic systems in the oceans. From 2001 to 2008, he served as editor of *Economic Geology*. He is the recipient of the Duncan Derry Medal of the Geological Association of Canada and the Silver Medal of the Society of Economic Geologists. He was made a Fellow of the Royal Society of Canada in 2012.

Murray W. Hitzman has B.A. degrees in geology and anthropology from Dartmouth College (1976), an M.S. degree in geology from University of Washington (1978), and a Ph.D. degree in geology from Stanford University (1983). He worked in the petroleum and minerals industries from 1976 to 1993, primarily doing mineral exploration worldwide, and he was largely responsible for Chevron Corporation's Lisheen Zn-Pb-Ag deposit discovery in Ireland (1990). Dr. Hitzman served in Washington, D.C., as a policy analyst in both the U.S. Senate for Senator Joseph Lieberman (1993–1994) and the White House Office of Science and Technology Policy (1994–1996). In 1996 he was named the Fogarty Professor in Economic Geology at the Colorado School of Mines and he served as head of the Department of Geology and Geological Engineering from 2002 to 2007. While his research in economic geology with graduate students has been conducted around the world, for the past 17 years he has focused his attention on the Central African Copperbelt. He served as the President of the Society of Economic Geologists in 2006. He is a member of the National Research Council (of the U.S. National Academy of Sciences) Committee on Geological and Geotechnical Engineering. He has previously served on the boards of a number of junior mineral exploration and mining companies.

Albert H. Hofstra is a research geologist at the U.S. Geological Survey, where he has worked to advance understanding of Carlin-type gold deposits in the Great Basin and Carlin-like gold deposits around the world (e.g., an upcoming *Reviews in Economic Geology* volume). His publications on these deposits address their age and relation to magmatism and tectonics, lithogeochemistry, alteration, mineral paragenesis and chemistry, P-T conditions, composition and source of ore fluids, processes of ore formation, and fluid flow modeling. His career path began with exploration for sediment-hosted gold deposits and a fluid inclusion study of the Jerritt Canyon district that developed into a comprehensive dissertation at the University of Colorado-Boulder. As leader of the Denver Inclusion Analysis Laboratory (http://minerals.cr.usgs.gov/dial/), he has recently begun to focus on melt and fluid inclusion studies of a myriad deposit types (IOA-REE, IOCG-Co, REE pegmatite, porphyry Mo, volcanogenic Be, Li brine, mesothermal Sb, epithermal Au-Ag, replacement and vein alunite).

Zengqian Hou has been a research geologist in the Chinese Academy of Geological Sciences (CAGS) for the past 25 years, since obtaining his M.Sc. (1985) and Ph.D. (1988)

degrees in economic geology from the China University of Geosciences (Beijing), China. He conducted postdoctoral research on modern sea-floor hydrothermal processes and mineralization while visiting the Geological Survey of Japan (1993–1994). Subsequently, he has become involved with a major government-funded mineral resources program in southwestern China (1995–2015). Hou's major interests include metallic metallogeny and mineral systems of orogenic belts, with emphasis on temporal-spatial distribution, geology, and geochemistry of porphyry, VMS, MVT, and carbonatite-associated REE deposits. He has supervised students studying a broad range of industry- and government-funded projects, including work in the Chinese Mainland and work on modern sea-floor hydrothermal environments. He is currently the Director of the Institute of Geology, CAGS (2005–2015) and was the Deputy-Director of the Institute of Mineral Resources, CAGS (2000–2005). He was in charge of a State Basic Research Plan of China (973 project) "Metallogensis of the Tibetan Collisional Orogen (2003–2008)." He is currently a chief scientist for a new 973 project, entitled "Continental Assembly and Related Metallogensis in Tibet (2011–2015)" and co-chair of an IGCP project on "Metallogenesis of Collisional Orogens in the East Tethyside Domain (2011–2015)."

Scott Hynek earned a B.A. degree in geology from Carleton College in 2001. He earned an M.S. (2003) and Ph.D. (2011) degrees in geology from the University of Utah. During this time he worked on both geochronology and paleo-environmental reconstruction from late Miocene–present in South America. As a postdoctoral scholar at the University of Utah, he applied mineralogy and geochemistry to characterize elemental fluxes associated with dust transport in the western United States. Later, as a postdoctoral scholar at Pennsylvania State University, he worked on chemical weathering and solute transport in the Luquillo Mountains of Puerto Rico. Currently, he is a research assistant at Penn State University where he manages the Metal Isotope Laboratory. The study of Li brine genesis is a primary research interest, and it draws upon his research experience in mineralogy, geochronology, chemical weathering, and elemental and isotopic geochemistry.

Hillary Jochens is a geologist practicing as an environmental consultant in Alaska, where she performs field investigations of contaminated sites. She received a B.S. degree in geological sciences from the University of Alaska Anchorage (2012). Recently her work is on modeling the nature and extent of contamination in both soil and groundwater.

David John is a research geologist with the U.S. Geological Survey in Menlo Park, California. He has a B.S. degree in earth sciences from the University of California, Santa Cruz (1976), and M.S. (1979) and Ph.D. (1987) degrees in geology with an economic geology emphasis from Stanford University. His Ph.D. thesis investigated variations in magmatic-hydrothermal systems and mineral deposits related to mid-Tertiary plutons emplaced over a 10-km-depth range in the central Wasatch Mountains, Utah. He has spent most of his career at the USGS studying volcanic and plutonic rocks and associated epithermal and porphyry deposits in the western United States. This work includes detailed studies of several Tertiary epithermal gold-silver deposits, hydrothermal systems associated with Quaternary volcanism in the Cascades and Yellowstone, and Cenozoic magmatism and associated hydrothermal systems in the Great Basin, including volcanic fields of the ancestral Cascade arc, the northern Nevada rift, and several large ignimbrite calderas.

Karen Kelley has been a research geologist with the U.S. Geological Survey in Denver for the past 33 years. She earned a B.S. degree at University of Colorado in Boulder, an M.S. degree in geology from the University of Reno (Mackay School of Mines), and a Ph.D. in economic geology from the Colorado School of Mines in 1996. Her dissertation focused on the geochronology and geochemistry of the Cripple Creek Au-Te deposit in Colorado. Other research interests include the genesis of sediment-hosted Pb-Zn massive sulfide deposits and exploration geochemistry, particularly techniques applied to buried deposits such as the giant Pebble porphyry Cu-Au-Mo deposit in Alaska. Karen has been a member of the editorial board for *Economic Geology* and served as guest editor of two special issues. She is currently on the editorial boards of *Mineralium Deposita* and *GEEA (Geochemistry: Exploration, Environment, Analysis)*. Karen was the 2015 SEG Thayer Lindsley Visiting Lecturer, and she has served as Councilor and chaired committees for the Society of Economic Geologists and Society for Geology Applied to Mineral Deposits.

Keith A. Labay is a physical scientist at the U.S. Geological Survey in Anchorage, where he performs geographic information system (GIS) work in the Alaska Science Center Geology Office. He received a B.S. degree in natural science from the University of Alaska Anchorage (1999). He has created spatial databases to accompany numerous new geologic maps and other publications within Alaska. Recently he has been applying spatial analysis techniques to a collaborative project, looking at mineral potential throughout Alaska.

David Leach received his B.S. degree at the Virginia Polytechnic Institute and his M.S. and Ph.D. (1973) degrees from the University of Missouri. He worked for the Lawrence Livermore National Laboratory for 5 years as a project scientist on uranium geochemistry, hydrothermal alteration experiments on porphyry ores, and exploration geochemistry. He joined the U.S. Geological Survey in 1978, where he worked for more than 34 years. He is currently an affiliated professor at the Colorado School of Mines and consultant to the minerals industry. He has authored or co-authored more than 200 papers on the geology and geochemistry of ore deposits and is a recognized expert on sediment-hosted base metal deposits. His career focused on hydrothermal mineral-rock interactions with special interest in Mississippi Valley-type and CD (SEDEX) Pb-Zn deposits, ore formation in metamorphic environments, global metallogeny, and deposit targeting using global geodynamics and secular distribution of ore deposits.

David London is a Stubbman-Drace Presidential Professor and Norman R. Gelphman Professor of Geology, and director of the University's electron microprobe laboratory at the University of Oklahoma. He obtained his B.A. degree in geology (1975) at Wesleyan University, Connecticut, and M.S. (1979) and Ph.D. (1981) degrees from Arizona State University. London joined the faculty at OU following a postdoctoral research fellowship (1981–1982, sponsored by Hatten S. Yoder, Jr.) at the Geophysical Laboratory of the Carnegie Institution of Washington. London's research pertains to the chemical evolution of silicic magmas, but with an emphasis on and application to the origins and internal evolution of granitic pegmatites. This work relies heavily on experimental studies and on the chemical attributes of common and rare minerals in granites and pegmatites. He is the author of the book *Pegmatites*, which was published in 2008 as Canadian Mineralogist Special Publication 10, and he is the chair and managing editor of the "Pegmatite Interest Group" of the Mineralogical Society of America. The mineral londonite, isometric $CsAl_4Be_4[B_{11}Be]O_{28}$ (Can. Mineral. 39: 747–755), is named after him.

Anthony N. Mariano and **Anthony Mariano Jr.** are mineral exploration geologists. They work as a team and specialize in the geology and mineralogy of rare elements on a world level. They have worked extensively in the field and in the laboratory for more than 50 years and in more than 50 countries. Their emphasis is on the economic evaluation and ranking of REE and other specialty metals deposits, which are often associated with carbonatites and alkaline complexes.

Erin Marsh is a research geologist with the Minerals Program at the U.S. Geological Survey in Denver, Colorado. She earned her B.S. (1998) and M.S. (2001) degrees from the University of Colorado, Boulder. She runs the fluid inclusion microthermometry and LA-ICP-MS labs at the Denver Federal Center. Generally, she is interested in the geochemistry of ore deposits. Her research emphasis is on the integrated application of multiple microanalytical techniques along with traditional field and laboratory work on understanding the formation of orogenic gold, placer gold, Te-rich Au deposits, Ni-Co laterite, and sedimentary rock-hosted base-metal deposits.

Patrick I. Mclaughlin is a research geologist with the Indiana Geological Survey (Indiana University). He obtained his B.Sc. degree from Illinois State University (1999) and completed his M.Sc. (2002) and Ph.D. (2006) work at the University of Cincinnati, where he studied sequence and event stratigraphy as a doctoral fellow. As an associate professor with the Wisconsin Geological Survey (2007–2015) he directed efforts in bedrock mapping. Pat's interest in high-resolution chronostratigraphy and sedimentary ore deposits has led him to develop new approaches to C-isotope and handheld XRF analysis of marine rocks and time-specific facies concepts. His field-based studies span the Proterozoic to Pliocene on three continents, with an emphasis on the lower Paleozoic of eastern North America.

Thomas Monecke obtained his Ph.D. degree at the TU Bergakademie Freiberg, Germany, in 2003. He subsequently spent five years as a postdoctoral fellow at the University of Ottawa and the Geological Survey of Canada. In 2006, he received the Waldemar Lindgren Award of the Society of Economic Geologists for his early career contributions to economic geology. He joined the Colorado School of Mines in 2008. His research focuses on the metallogeny of modern and ancient volcanic arcs and related extensional settings. He and his students have conducted extensive research on shallow marine hydrothermal systems and the volcanic setting, alteration mineralogy and geochemistry, and ore mineralogy of volcanogenic massive sulfide deposits.

Sven Petersen is currently a senior researcher at GEOMAR-Helmholtz Centre for Ocean Research Kiel, Germany. He received an M.Sc. degree in economic geology from the RWTH Aachen in Germany, investigating gold-rich sea-floor massive sulfide deposits in the Lau Basin. After almost 2 years at the Geological Survey of Canada, he moved to the TU Bergakademie Freiberg, Germany, where he obtained a Ph.D. degree for work on the TAG deposits in the central Atlantic. Since 2004 he has been working at GEOMAR, where his research focuses on understanding the processes that form and change sea-floor hydrothermal systems and associated mineral deposits. He participated in more than 30 research cruises to submarine hydrothermal systems in the Pacific, Atlantic, and Indian Ocean. The major aim of his research is to understand their chemical and mineralogical variability and the geological processes that affect them. He uses mobile drilling techniques and geophysical methods to investigate their resource potential and subseafloor processes as well as autonomous underwater vehicles for their exploration.

Lee Ann Munk is a professor of geochemistry in the Department of Geological Sciences at the University of Alaska Anchorage. Professor Munk received her B.S. degree in geology from St. Norbert College in 1995 and her M.S. degree from the Department of Geological Sciences at Michigan State University in 1997, followed by a Ph.D. degree in geochemistry in 2001 from The Ohio State University. Dr. Munk's research is focused primarily on investigating water-rock interactions across a spectrum of environments in order to understand sources, transport, and fate of trace elements. Major focus areas are acid-rock drainage, novel trace elements as tools for geochemical exploration, and origin of continental lithium brines. She has managed federal and private research grants and projects in Alaska, Chile, and the United States, and has worked on other collaborative research projects in Antarctica and the Caribbean. She is recognized as a global leader on the development of a lithium-brine resource model.

Iain Samson obtained B.Sc. and Ph.D. degrees from the University of Strathclyde in 1979 and 1983, respectively, and subsequently spent three years as a postdoctoral fellow at McGill University. His research interests are focused on the geochemistry of hydrothermal systems and the genesis of mineral deposits, and he has published on Irish-type Pb-Zn

deposits, intrusion-related W-Sn-Mo, Cu, PGE-Cu, and rare-element deposits, diagenetic systems, and fluid inclusions. He is currently a professor, and former Head, in the Department of Earth and Environmental Sciences at the University of Windsor, and was President of the Mineralogical Association of Canada from 2010 to 2012.

Kenzo Sanematsu received a B.Eng. degree in 2002 and a Ph.D. degree in earth resources engineering in 2007 from Kyushu University, Japan. He has been a research geologist since 2007 at the Geological Survey of Japan (GSJ), the National Institute of Advanced Industrial Science and Technology (AIST), and has investigated granite geochemistry, chemical weathering, and REE mineralization in Asia. For the past two years, he also was a visiting research fellow at the ARC Centre of Excellence in Ore Deposits, University of Tasmania. Currently, his research focuses on ore deposits of REE and other rare metals in Southeast Asia.

Debashish Sengupta is an applied geophysicist and professor at IIT Kharagpur. He has supervised 31 M.Sc. project dissertations, 12 M. Tech. project dissertations, and 11 doctoral dissertations. He has undertaken significant research work on rare earth and other economic deposits along the eastern coast of India for the past two decades. He has 90 papers published in journals of international repute and more than 50 publications in Conference Proceedings. He has collaborated with many national and international institutes, including Variable Energy Cyclotron Centre, Kolkata; Environmental Assessment Division, Bhabha Atomic Research Centre, Trombay, Mumbai; Research Reactor Institute, Kyoto University, Osaka, Japan; Department of Civil and Environmental Engineering, University of West Indies; Institute of Physics, University of São Paulo, Brazil; and Institute of Experimental Mineralogy, Moscow, Russia. He authored *Handbook on Radioactive Methods and Geochronology* and has edited a book titled *Recent Trends in Modelling of Environmental Contaminants*, published by Springer in 2014. In 2003, he was awarded the Society of Geoscientists and Applied Technologists (SGAT's) Award of Excellence in Earth Sciences.

Stuart Simmons is a consulting and research geoscientist. His work for clients is directed at finding mineral and energy resources, and his research is focused on geothermal energy and understanding precious metal transport and deposition and hydrothermal fluid flow in epithermal environments. He earned M.Sc. and Ph.D. degrees in economic geology (University of Minnesota), and he spent much of his professional career in New Zealand, at the Geothermal Institute, University of Auckland. He is currently a research professor at EGI, University of Utah.

Paul Spry is professor of geology at Iowa State University, where he has been since 1983. He earned B.S. (Honors) and M.S. degrees in geology at the University of Adelaide (Australia), and a Ph.D. degree in economic geology at the University of Toronto in 1984. Paul has focused his research efforts on the geology, mineralogy, and geochemistry of epizonal and mesozonal gold-silver telluride deposits, the effects of metamorphism on ore deposits, and the mineralogy of ore deposits, in general. He has also conducted research on Mississippi Valley-type, porphyry-style Cu and Mo, high-temperature carbonate replacement Pb-Zn-Ag, and intrusion-related gold deposits. Paul is currently on the editorial board of *Economic Geology* (on which he has served the last four editors), and he has also been a member of the editorial boards for *Ore Geology Reviews*, *Canadian Mineralogist*, and *Mineralogy and Petrology*. He was the SEG Thayer Lindsley Visiting Lecturer for 2012, and has served on or chaired several committees for the Society of Economic Geologists.

Ryan D. Taylor is a research geologist with the Minerals Program of the U.S. Geological Survey, a Ph.D. candidate at Colorado School of Mines, and the SEG student field trip guidebook editor. He obtained his B.S. (2006) and M.S. (2008) degrees in geology from Northern Arizona University. His general research interests include geochronology and geochemistry of ore deposits. Much of his work is focused on lode gold deposits and porphyry deposits of the western cordillera of North America, from California to Alaska. This includes correlating the timing of formation of these deposits with the tectonic evolution of the region and the processes that result in ore deposition in a regional framework. New research includes mineralogical studies of REE-bearing iron oxide-apatite deposits and mineral chemistry of alteration products of lode gold deposits.

Thijs R.A. Vandenbroucke received his Ph.D. degree in geology from Ghent University (Belgium) in 2005. His dissertation research focused on the chitinozoan biostratigraphy from the historical type area of the Upper Ordovician in the UK, compared to that of the series' new GSSPs. Following postdocs at the universities of Durham (UK), Leicester (UK), and Ghent, he held a research position at the French CNRS from 2009 to mid-2015. Vandenbroucke returned to Ghent University in 2015, where he is an assistant professor, lecturing on paleobiology, stratigraphy, and paleo-environments. His research has evolved into the application of integrated bio-chemo-stratigraphy to better understand the dynamic paleoclimate and paleo-oceanography of the early to middle Paleozoic.

Bradley Van Gosen received his B.A. degree in geology from the University of Colorado and his M.S. degree in geology from the Colorado School of Mines. He has been a research geologist for the U.S. Geological Survey in Denver for more than 30 years. His research career began with studies of uranium deposits hosted by solution-collapse breccia pipes in the Grand Canyon region. A recent withdrawal of about 1 million acres of public lands surrounding the Grand Canyon, enacted by the Secretary of the Interior, brought him back to these U deposits as the geologic consultant. Midcareer he studied a variety of deposit types for USGS assessments of mineral resources in public lands. In the last 15 years, he has focused more on industrial minerals—asbestos, talc, rare earth elements (REEs), and heavy-minerals sands. He has worked

extensively on the geology and distribution of natural occurrences of asbestos in the United States, providing insights that can be used to limit human exposures to asbestos. Currently, he serves as a project chief for a USGS project studying the mineral resources (Ti, Zr, REEs) of heavy mineral sands in the coastal plain of the southeastern United States. Brad serves as a U.S. delegate and Vice Chair for the United Nations Economic Commission for Europe (UNECE) Expert Group on Resource Classification. He also is the U.S. member of a collaborative uranium-thorium working group of the International Atomic Energy Agency (IAEA).

Philip L. Verplanck is a research geologist with the Mineral Resources Program of the U.S. Geological Survey. He received his B.S. degree in geology from Tufts University (1981), an M.S. degree in geology from Oregon State University (1986), and a Ph.D. degree in geology from the University of Colorado (1996). He has been with the U.S. Geological Survey since 1997. He has studied rare earth elements (REEs) since 1983, and his REE research includes lunar evolution, igneous petrology, aqueous geochemistry, and ore genesis. His current research focuses on carbonatite and alkaline intrusive-related REE deposits.

Yuling Xie is currently a professor at the University of Science and Technology Beijing (USTB), Beijing, China, and the team leader of the Economic Geology Group in USTB. Xie completed a B.Sc. degree at China University of Geosciences (Wuhan) in 1985 and a Ph.D. degree at China University of Geosciences (Beijing) in 1999. From December of 2008 to June 2009, Xie was a visiting professor in the ARC Centre of Excellence in Ore Deposits (CODES) of the University of Tasmania. As a research geologist, her interests include ore microscopy, fluid and melt inclusions, and metallic metallogeny. She has studied carbonatite-related REE, gold, porphyry Cu-Mo, and epithermal Pb-Zn-Ag deposits in Tibet, Sichuan, Anhui, Inner Mongolia, and Zhejiang.

Lei Wang earned her B.S. degree in mineral processing from Chang'an University (2011) and received her M.S. degree (2014) in mineralogy, petrology, and economic geology from the University of Science & Technology Beijing. Currently, she is working for the Northwest Bureau of the China Metallurgical Geology Bureau. During undergraduate and graduate studies, she examined mineral deposits in Inner Mongolia, Anhui, and Sichuan provinces. She has conducted research on the geology, fluid inclusion geochemistry, and mineralogy of REE, porphyry Mo, and epithermal Pb-Zn deposits. Currently, her work is focused on mineral deposit exploration design and assessment.

Yasushi Watanabe attended Hokkaido University, from which he received a B.Sc. degree in geology in 1982. He joined the Geological Survey of Japan (GSJ) in 1985 and has worked for the Survey for 29 years. He engaged in a metallogenic study of epithermal and porphyry Cu deposits in the circum-Pacific regions. He served as the leader of Mineral Resources Research Group from 2003 to 2008, and later, as Prime Senior Geologist of the GSJ. Since 2005, he has been involved in the "Rare Earth Exploration and Evaluation Project" of the GSJ, investigating rare earth deposits in the world. In April 2014, he began a new career at Akita University in Japan. He is currently a professor in the Faculty of International Resource Sciences of the university, and is teaching mineralogy and economic geology to undergraduate and graduate students.

Robert A. Zielinski received his B.A. degree in chemistry from Rutgers University and his Ph.D. degree in geochemistry from the Massachusetts Institute of Technology. He has enjoyed a full career as a research chemist with the U.S. Geological Survey in Denver. Areas of specialization include trace element geochemistry, isotope geology, and radiochemistry. Applications have included studies of igneous petrogenesis, trace element mobility during various alterations of volcanic rocks and formation of red beds, U-rich wetlands, and redistribution and environmental mobility of trace elements and radioisotopes during resource production (coal, oil and gas, phosphate, uranium). Most recently, his research has focused on the redistribution of uranium during ISR mining and on the occurrence and environmental mobility of radium in phosphogypsum and in scale deposits in oilfield equipment.

©2016 Society of Economic Geologists, Inc.
Reviews in Economic Geology, v. 18, pp. 1–3

Introduction:

Rare Earth and Critical Elements in Ore Deposits

Philip L. Verplanck,[1,†] and Murray W. Hitzman[2]

[1]*U.S. Geological Survey, Box 25046, Mail Stop 973, Denver, Colorado 80225*

[2]*Department of Geology and Geological Engineering, Colorado School of Mines, Golden, Colorado 80401*

This special volume provides a comprehensive review of the current state of knowledge for rare earth and critical elements in ore deposits. The first six chapters are devoted to rare earth elements (REEs) because of the unprecedented interest in these elements during the past several years. The following eight chapters describe critical elements in a number of important ore deposit types. These chapters include a description of the deposit type, major deposits, critical element mineralogy and geochemistry, processes controlling ore-grade enrichment, and exploration guides. This volume represents an important contribution to our understanding of where, how, and why individual critical elements occur and should be of use to both geoscientists and public policy analysts.

The term "critical minerals" was coined in a 2008 National Research Council report (National Research Council, 2008). Although the NRC report used the term "critical minerals," its focus was primarily on individual chemical elements. The two factors used in the NRC report to rank criticality were (1) the degree to which a commodity is essential, and (2) the risk of supply disruption for the commodity. Technological advancements and changes in lifestyles have changed the criticality of elements; many that had few historic uses are now essential for our current lifestyles, green technologies, and military applications. The concept of element criticality is useful for evaluation of the fragility of commodity markets. This fragility is commonly due to a potential risk of supply disruption, which may be difficult to quantify because it can be affected by political, economic, geologic, geographic, and environmental variables.

Following the NRC report, other groups, including the Japanese National Institute of Advanced Industrial Science and Technology (2008), the United States Department of Energy (2010), the European Commission (2010), and the American Physics Society and Materials Research Society (2010), evaluated the criticality of elements for their constituents. As these reports showed, element criticality is a conceptual framework. Rankings in these studies differed because supply risk can be different from one country to another, elements that are critical for one market may not be critical for another, and supply risks change with time.

Identifying potential sources for some of the elements deemed critical can be challenging. Because many of these elements have had minor historic usage, exploration for them has been limited. Thus, as this volume highlights, the understanding of the occurrence and genesis of critical elements in various ore deposit models is much less well defined than for base and precious metals. A better understanding of the geologic and geochemical processes that lead to ore-grade enrichment of critical elements will aid in determining supply risk and was a driving factor for preparation of this volume. Understanding the gaps in our knowledge of the geology and geochemistry of critical elements should help focus future research priorities.

Critical elements may be recovered either as primary commodities or as by-products from mining of other commodities. For example, nearly 90% of world production of niobium (Nb) is from the Araxá niobium mine (Brazil), whereas gallium (Ga) is recovered primarily as a by-product commodity of bauxite mining or as a by-product of zinc processing from a number of sources worldwide. Critical elements that are solely produced as by-product commodities pose a particular supply risk because their production is tied to other markets and thus fluctuations in their supply can be independent from their demand.

Whereas Nb and Ga are elements that are well documented as enriched in specific deposit types, the various geologic occurrences of many other critical elements is less well known. For these latter elements, a much better understanding of possible geologic sources is warranted to potentially alleviate supply disruptions. This volume provides some ideas for future exploration for such elements.

Rare earth elements are a focus of this volume because price spikes of these commodities over the past several years have created broad interest. As demonstrated in the papers in this volume, ore-grade enrichment of REEs can occur in a variety of deposit types. The REE enrichment in carbonatites, currently the world's primary source of light REEs, including La, Ce, Pr, Nd, Sm, and Eu, is described by Verplanck et al. (2016). This chapter also includes the ore geology of Nb because carbonatite-related deposits are the world's primary source of this element. Dostal (2016) reviewed REE enrichment in alkaline/peralkaline igneous rocks, which range from silica undersaturated (nepheline syenites) to silica oversaturated (granites). In addition to REEs, the processes controlling the enrichment of other rare elements, including beryllium (Be), hafnium (Hf), (Nb), tantalum (Ta), uranium (U), and thorium (Th), are considered. The ion-adsorption clay-type REE deposits, the primary source of the world's heavy REEs, are reviewed by Sanematsu and Watanabe (2016). These deposits, which are currently being exploited in southern China, are poorly described in the scientific literature; this chapter represents a significant step in our understanding of this deposit type. Placer-type REE deposits are described

† Corresponding author: e-mail, plv@usgs.gov

by Sengupta and Van Gosen (2016). Although these deposits are not currently a major source of REEs, they have been important historically. Prior to the discovery of the Mountain Pass REE deposit (California, United States) in the 1950s, placer deposits were the primary source of world's REEs. Emsbo et al. (2016) describe sedimentary phosphate deposits, the major source of phosphate for fertilizer. Enrichment of REEs is common in these deposits and this represents a potential source for meeting future global demands, although the REEs are presently not being recovered. The last chapter in the REE section, by Xie et al. (2016), is a comprehensive review of the REE deposits and deposit types in China, which currently dominates world REE production. The primary focus of this chapter is carbonatite and ion-adsorption clay deposits because they are the leading producers of light and heavy REEs, respectively, but the chapter also includes data on other deposit types, including placers, pegmatites, alkaline granites, and hydrothermal veins.

Porphyry copper (Cu) deposits, currently the world's major source of Cu and molybdenum (Mo), provide the majority of the world's rhenium (Re), selenium (Se), and tellurium (Te) as by-products (John and Taylor, 2016). The authors conclude that because of the immense size of known and potential porphyry Cu resources, these deposits will likely supply these elements to the global market for the foreseeable future. Although some porphyry deposits produce by-product platinum group elements (PGEs), the authors believe it is unlikely these deposits will become a major source for these elements.

Pegmatite deposits are currently the principal source of Ta and cesium (Cs) and a significant source of Li (London, 2016). In addition to these elements, individual pegmatites are also known to contain high concentrations of Be, Nb, rubidium (Rb), tin (Sn), U, yttrium (Y), and zirconium (Zr; London, 2016). London (2016) notes that although most pegmatite deposits are small in size, they are geographically widespread and may be important in the future as secondary, if not primary, sources of critical elements, particularly in times of disruption of global supplies from other types of deposits.

Precious metal deposits are not currently an important source of critical elements. However, antimony (Sb) is currently recovered from orogenic gold deposits and mercury (Hg) is recovered from some epithermal deposits to reduce environmental exposure (Goldfarb et al., 2016). Indium (In) and Te have been recovered in the past from epithermal deposits and some deposits may contain sufficient quantities to be future producers (Goldfarb et al., 2016). Thallium (Tl) has been produced from Carlin-type deposits outside the United States; such deposits in the United States could be a source of Tl as well as Sb, arsenic (As), Hg, Se, or vanadium (V; Goldfarb et al., 2016). Gold deposits in alkaline igneous rocks have historically contributed the by-products fluorine (F) and tungsten (W), although it is unclear if these elements are genetically related to Au mineralization. Some contain sufficient Te to be considered a future by-product commodity, and two deposits in China of uncertain classification contain Te as a primary producer. Although some deposits are enriched in PGEs, REEs, and V, it is unlikely they will be major sources of these commodities (Kelley and Spry, 2016).

Modern sea-floor massive sulfide deposits represent a new potential source of base and precious metal resources that may be exploited by future deep-sea mining operations. Chemical analyses of sulfide samples collected from sea-floor hydrothermal vent sites worldwide show that sea-floor massive sulfides can be enriched in critical elements such as Bi, Cd, Ga, Ge, Hg, In, Mo, Sb, Se, Te, and Tl, with concentrations ranging up to several tens or hundreds of parts per million. Based on a compilation of geochemical data from samples collected from hydrothermal vent sites worldwide, Monecke et al. (2016) make a first-order evaluation of the global minor element endowment of sea-floor sulfide deposits. Although some of the minor elements are potential commodities that could be recovered as primary or by-products from sulfide concentrates, they conclude that sea-floor massive sulfide deposits probably do not represent a significant future resource for these elements.

Sediment-hosted base metal deposits of copper, lead, and zinc have been, and are currently, sources of the critical elements cobalt (Co), Ga, Ge, and Re (Marsh et al., 2016). A significant portion of the world's Co is derived from sedimentary rock-hosted deposits in the Central African Copperbelt. In the past, much of the world's Ge was produced from carbonate-hosted polymetallic deposits, although most known deposits of this type have been mined out. Marsh et al. (2016) conclude that although data on the abundance of critical elements in the diverse ores of these deposit types are poor, there may be unrecognized and potentially important concentrations of these elements in a number of deposits.

Sandstone-hosted uranium deposits have been an important source of V in the past and, depending on market conditions, as well as political conditions in South Africa, could be an important source in the future (Breit, 2016). Processing of sandstone-hosted uranium ores has also recovered small amounts of Mo, Re, REEs, scandium (Sc), and Se (Breit, 2016). Future production of these critical elements from this type of deposit depends on development of new ore-processing technologies and market conditions (Breit, 2016).

Lithium has become a critical element due to its importance in some types of batteries and in a number of electronics products. Although pegmatites and Li-bearing clays are currently being mined for Li, three-quarters of the world's Li is recovered from continental brines. Munk et al. (2016) describe the characteristics of continental brine deposits and present exploration guidelines for their discovery. The authors also present two case studies of Li brines, one from Nevada and the other the world's largest producing Li brine at the Salar de Atacama in Chile.

Whereas the papers in this volume provide an overview of our state of knowledge concerning the economic geology of rare earth and critical elements, they also demonstrate that we lack adequate data on the occurrence of these elements in many deposit types. It is hoped that this volume will stimulate interest for additional research on the occurrence and concentration of the rare earth and critical elements in a wide range of deposit types. Additionally, these contributions may suggest possibilities for completely new types of critical element deposits.

REFERENCES

American Physics Society and Materials Research Society, 2011, Energy critical elements: Securing materials for emerging technologies: Washington, D.C., APS Panel on Public Affairs, 26 p.

Breit, G.N., 2016, Resource potential for commodities in addition to uranium in sandstone-hosted deposits: Reviews in Economic Geology, v. 18, p. 323–337.

Dostal, J., 2016, Rare metal deposits associated with alkaline/peralkaline igneous rocks: Reviews in Economic Geology, v. 18, p. 33–54.

Embso, P., McLaughlin, P.I., du Bray, E.A., Anderson, E.D., Vandenbroucke, T.R.A., and Zielinski, R.A., 2016, Rare earth elements in sedimentary phosphorite deposits: A global assessment: Reviews in Economic Geology, v. 18, p. 101–113.

European Commission, 2010, Critical raw materials for the EU: Report of the Ad-hoc Working Group on defining critical raw materials: 84 p. http://ec.europa.eu/enterprise/policies/raw-materials/critical/index_en.htm.

Goldfarb, R.J., Hofstra, A.H., and Simmons, S.F., 2016, Critical elements in Carlin, epithermal, and orogenic gold deposits: Reviews in Economic Geology, v. 18, p. 217–244.

John, D.A., and Taylor, R.D., 2016, By-products of porphyry copper and molybdenum deposits: Reviews in Economic Geology, v. 18, p. 137–164.

Kelley, K.D., and Spry, P.G., 2016, Critical elements in alkaline igneous rock-related epithermal gold deposits: Reviews in Economic Geology, v. 18, p. 195–216.

London, D., 2016, Rare-element granitic pegmatites: Reviews in Economic Geology, v. 18, p. 165–193.

Marsh, E.E., Hitzman, M.W., and Leach, D.L., 2016, Critical elements in sediment-hosted deposits (clastic-dominated Zn-Pb-Ag, Mississippi Valley-type Zn-Pb, sedimentary rock-hosted stratiform Cu, and carbonate-hosted polymetallic deposits): A review: Reviews in Economic Geology, v. 18, p. 307–321.

Monecke, T., Petersen, S., Hannington, M.D., Grant, H., and Samson, I.M., 2016, The minor element endowment of modern sea-floor massive sulfides and comparison with deposits hosted in ancient volcanic successions: Reviews in Economic Geology, v. 18, p. 245–306.

Munk, L.A., Hynek, S.A., Bradley, D.C., Boutt, D., Labay, K., and Jochens, H., 2016, Lithium brines: A global perspective: Reviews in Economic Geology, v. 18, p. 339–365.

National Institute of Advanced Industrial Science and Technology, 2008, Rare metals: Ibaraki, Japan, Publication Office AIST, 12 p.

National Research Council, 2008, Minerals, critical minerals, and the U.S. economy: Washington, D.C., National Academy Press, 264 p.

Sanematsu, K., and Watanabe, Y., 2016, Characteristics and genesis of ion-adsorption-type rare earth element deposits: Reviews in Economic Geology, v. 18, p. 55–79.

Sengupta, D., and Van Gosen, B.S., 2016, Placer-type rare earth element deposits: Reviews in Economic Geology, v. 18, p. 81–100.

Verplanck, P.L., Mariano, A.N., and Mariano, A., Jr., 2016, Rare earth element ore geology of carbonatites: Reviews in Economic Geology, v. 18, p. 5–32.

Xie, Y., Hou, Z., Goldfarb, R.J., Guo, X., and Wang, L., 2016, Rare earth element deposits in China: Reviews in Economic Geology, v. 18, p. 115–136.

U.S. Department of Energy, 2010, Critical materials strategy: Washington, D.C., Department of Energy, 165 p.

©2016 Society of Economic Geologists, Inc.
Reviews in Economic Geology, v. 18, pp. 5–32

Chapter 1

Rare Earth Element Ore Geology of Carbonatites

Philip L. Verplanck,[1,†] Anthony N. Mariano,[2] and Anthony Mariano, Jr.[3]

[1] *U.S. Geological Survey, MS 973, Denver Federal Center, Denver, Colorado 80225*

[2] *48 Page Brook Road, Carlisle, Massachusetts 01741*

[3] *1134 North Road, Carlisle, Massachusetts 01741*

Abstract

For nearly 50 years, carbonatites have been the primary source of niobium and rare earth elements (REEs), in particular the light REEs, including La, Ce, Pr, and Nd. Carbonatites are a relatively rare type of igneous rock composed of greater than 50 vol % primary carbonate minerals, primarily calcite and/or dolomite, and contain the highest concentrations of REEs of any igneous rocks. Although there are more than 500 known carbonatites in the world, currently only four are being mined for REEs: the Bayan Obo, Maoniuping, and Dalucao deposits in China, and the Mountain Pass deposit in California, United States. The carbonatite-derived laterite deposit at Mount Weld in Western Australia is also a REE producer. In addition to REEs, carbonatite-related deposits are the primary source of Nb, with the Araxá deposit, a carbonatite-derived laterite in Minas Gerais state, Brazil, being the dominant producer. Other commodities produced from carbonatite-related deposits include phosphates, iron, fluorite, copper, vanadium, titanium, uranium, and calcite.

Types of ores include those formed as primary magmatic minerals, from late magmatic hydrothermal fluids, and by supergene enrichment in weathered horizons. Although the principal REE-bearing mineral phases include fluorocarbonates (bastnäsite, parisite, and synchysite), hydrated carbonates (ancylite), and phosphates (monazite and apatite), the dominant mineral exploited at most mines is bastnäsite. Bastnäsite typically is coarse grained and contains approximately 75 wt % RE_2O_3 (rare earth oxides; REOs). Processes responsible for REE enrichment include fractional crystallization of the carbonatitic magma, enrichment of REEs in orthomagmatic or hydrothermal fluids and subsequent precipitation or subsolidus metasomatic redistribution of REEs, and breakdown of primary carbonatitic mineral phases by chemical weathering and sequestration of REEs in secondary minerals or in association with clays. Carbonatites are primarily associated with continental rifting, but some carbonatites are associated with orogenic activity. Although there is debate on how carbonatite magmas are generated, the parental magma and REEs are clearly derived from mantle sources.

Introduction

Carbonatites are volumetrically rare compared to silicate igneous rocks, but they have become important exploration targets because of their enrichments in critical elements. For nearly 50 years, carbonatites have been the primary source of rare earth elements (REEs), particularly the light REEs (LREEs) that include La, Ce, Pr, and Nd. Although most carbonatites contain elevated concentrations of REEs, only a few have sufficient quantities to warrant economic exploitation. In addition to LREE production, carbonatite-related deposits are the primary source of Nb (Araxá, Minas Gerais state, Brazil), an important source of phosphate, and a source of Cu (Palabora, South Africa). Furthermore, carbonatites are potential sources of Ta and heavy REEs (HREEs). The REE deposits include those formed as primary magmatic mineralization (Mountain Pass deposit, California, United States), by enrichment from late magmatic fluids (Bayan Obo, Inner Mongolia, China), and during supergene enrichment in weathered horizons (Mount Weld, Western Australia, Australia).

Carbonatites are defined by the International Union of Geological Sciences (IUGS) as igneous rocks composed of greater than 50 vol % primary carbonate minerals, primarily calcite and/or dolomite, and containing less than 20 wt % SiO_2 (Le Maitre, 2002). Varieties of carbonatites contain the highest concentrations of REEs of any igneous rocks (Cullers and Graf, 1984). The principal REE-bearing mineral phases include fluorocarbonates (bastnäsite, parisite, and synchysite), hydrated carbonates (ancylite), and phosphates (monazite and apatite; Table 1), with bastnäsite being the primary ore mineral. Because many REE-bearing mineral phases in these deposits form from hydrothermal fluids, the mineralogy consists of complex intergrowths of REE-rich phases and associated Sr- and Ba-rich phases.

Current mining operations associated with carbonatites include: (1) the REE deposits of Bayan Obo (Inner Mongolia, China), Maoniuping (Sichuan, China), Dalucao (or Daluxiang, Sichuan, China), and Mountain Pass (California, United States); (2) the Nb deposit at Araxá (Minas Gerais, Brazil)—the world's largest Nb producer, Catalão II (Minas Gerais, Brazil), and the Niobec niobium deposit (Saint-Honoré, Québec, Canada); and (3) Cu production at the Palabora deposit (South Africa; Fig. 1, Table 2). The Mount Weld REE deposit, Australia, recently began production of REEs from the weathered zone above a carbonatite. Carbonatites are extensively exploited for phosphate. Other carbonatite exploration targets include Adiounedj (Mali), Bear Lodge (Wyoming, United States), Eldor (Quebec, Canada), Elk Creek (Nebraska, United States), Glenover (South Africa), Kangankunde (Malawi), Lofdal (Namibia), Mushgai Khudag

† Corresponding author: e-mail, plv@usgs.gov

Table 1. Rare Earth Element (REE)-Bearing Minerals Found in Rare Earth Element Deposits[1]

Mineral	Formula
Allanite (Ce)	$(Ce,Ca,Y)_2(Al,Fe^{2+},Fe^{3+})_3(SiO_4)_3(OH)$
Ancylite (Ce)	$SrCe(CO_3)_2OH{\cdot}H_20$
Bastnäsite (Ce)	$(Ce,La)(CO_3)F$
Britholite (Ce)	$(Ce,Ca)_5(SiO_4,PO_4)_3(OH,F)$
Brockite	$(Ca,Th,Ce)(PO_4){\cdot}H_2O$
Burbankite	$(Na,Ca)_3(Sr,Ba,Ca,REE)_3(CO_3)_5$
Carbocernaite	$(Ca,Na)(Sr,REE)(CO_3)_2$
Cerianite (Ce)	$(Ce^{4+},Th)O_2$
Cerite (Ce)	$Ce_9Fe^{3+}(SiO_2)_6[(SiO_3)(OH)](OH)_3$
Cheralite	$(Ca,Ce,Th)(P,Si)O_4$
Chevkinite	$(Ca,Ce,Th)_4(Fe^{2+},Mg)_2(Ti,Fe^{3+})_3Si_4O_{22}$
Churchite (Y)	$YPO_4{\cdot}H_2O$
Florencite (Ce)	$CeAl_3(PO_4)_2(OH)_6$
Florencite (La)	$(La,Ce)Al_3(PO_4)_2(OH)_6$
Fluocerite (Ce)	$(Ce,La)F_3$
Fluorapatite	$(Ca,Ce)_5(PO_4)_3F$
Fluorite	$(Ca,REE)F$
Gorceixite	$(Ba,REE)Al_3[(PO_4)_2(OH)_5]{\cdot}H_2O$
Khanneshite	$(Na,Ca)_3(Ba,Sr,Ce,Ca)_3(CO_3)_5$
Monazite (Ce)	$(Ce,La,Nd,Th)PO_4$
Parisite (Ce)	$Ca(Ce,La)_2(CO_3)_3F_2$
Perovskite	$(Ca,REE)TiO_3$
Pyrochlore	$(Ca,Na,REE)_2Nb_2O_6(OH,F)$
Rhabdophane (Ce)	$(Ce,La)PO_4{\cdot}H_2O$
Rhabdophane (La)	$(La,Ce)PO_4{\cdot}H_2O$
Sahamalite	$(Mg,Fe)(Ce,La,Nd,Pr)_2(CO_3)_4$
Samarskite	$(REE,Fe^{2+},Fe^{3+},U,Th,Ca)(Nb,Ta,Ti)O_4$
Synchysite (Ce)	$Ca(Ce,La)(CO_3)_2F$
Xenotime (Y)	$(HREE,Y)PO_4$

[1] Minerals in bold have historically been processed to recover REEs; small quantities of other minerals may be found in deposits that are or have been mined, or in unmined deposits

(Mongolia), Sarfartôq (Greenland), Wigu Hill (Tanzania), Xiluvo (Mozambique), and Zandkopsdrft (South Africa). This chapter focuses on REE mineralization associated with carbonatites, but also contains information on other critical elements, primarily Nb, that are enriched in carbonatites. It includes an overview of the characteristics of these deposits, a description of important deposits, and a review of the processes responsible for ore-grade enrichment. Because this reviews volume is centered on critical elements, phosphates and copper mineralization will not be addressed.

Carbonatites

For the first half of the 20th century, petrologic controversy focused on whether or not carbonatitic rock occurrences were of sedimentary or igneous origin. Brøgger (1921) described the carbonatite and alkaline complex at Fen, Norway, and concluded that the carbonatite was probably of magmatic origin, sparking the debate on whether these rocks were sedimentary or magmatic. The controversy was ended by the experimental work of Wyllie and Tuttle (1960), which clearly demonstrated that calcite could crystallize from a carbonatitic magma, as well as numerous studies documenting intrusive relationships for carbonatite occurrences. In addition, Dawson (1962) reported the occurrence of carbonatite lavas at Oldoinyo Lengai, Tanzania. Although carbonatites are clearly formed by igneous processes, determining whether a rock unit is either a carbonatite (igneous) or a carbonate (sedimentary) can be controversial, as is the case with the world-class Bayan Obo deposit in China (see Wu, 2008).

Worldwide there are more than 500 known carbonatites, most of which do not display economic concentrations of REEs (Woolley and Kjarsgaard, 2008). Although much petrogenetic research has focused on the origin of nonmineralized carbonatites, the origin of carbonatitic magmas remains controversial. Radiogenic and stable isotope studies show that the parental magmas of carbonatites are derived from mantle melts (Bell and Blenkinsop, 1989), but questions that are still debated are what is the nature of the initial melts and how do the magmas evolve to form the observed rock types? As summarized by Winter (2001), petrogenetic discussion focuses on: (1) are carbonatite and alkali magmas developed separately by partial melting within the mantle, or do carbonatites evolve from parental alkali magmas?; (2) if carbonatites evolve from parental alkali magmas, then is it by fractional crystallization or liquid immiscibility, and at what depths does this occur?; and (3) if carbonatites are derived directly from a carbonatite magma, then what is the nature of the parental carbonatite magma? Field data, experimental petrology, stable and radiogenic isotope systematics, trace element geochemistry, and evaluation of mantle xenoliths provide insight into the nature of the initial melts and their possible evolutionary paths. Mitchell (2005) stressed that not all carbonatites are alike and suggested that the chemical variations of carbonatites could be the result of different mantle source characteristics. Current models for the generation of carbonatites are summarized in reviews by Le Bas (1987), Gittins (1989), Bailey (1993), Winter (2001), Mitchell (2005), and Millonig and Groat (2013). These models may be divided into those in which carbonatites are postulated to be produced directly as primary melts from carbonated mantle peridotite, and those in which carbonatite magmas are produced as a derivative magma from a silicate parent through direct differentiation or liquid immiscibility.

Important to the understanding of critical element enrichment in deposits associated with carbonatites is that the generation of primary carbonatite melts or alkali-rich silicate melts in the mantle requires a mantle source enriched in lithophile elements, as well as H_2O and CO_2 (Bailey, 1987; Winter, 2001). These components are not only necessary to generate carbonatite melts, but also play an important role in the concentration of REEs to form an ore deposit. Bailey (1987) provided an excellent review of insight gained from studying mantle xenoliths and experimental petrology to constrain the nature of metasomatized mantle as the source of alkaline magmas. He called upon the introduction of H, C, F, Na, Al, P, S, Cl, K, Ca, Ti, Fe, Rb, Y, Zr, Nb, Ba, and REEs to preexisting garnet or spinel lherzolite. This influx of constituents can lead to changes in mantle mineralogy, including the formation of minerals such as biotite, amphibole, clinopyroxene, and carbonates. Experimental studies (Wyllie and Huang, 1975; Wyllie, 1977, 1989; Wyllie and Lee, 1999) demonstrated that carbonatite melts can be generated directly from a metasomatized mantle source by small degrees of partial melting. Furthermore, the formation of different types of carbonatites may reflect melting of different types of mantle

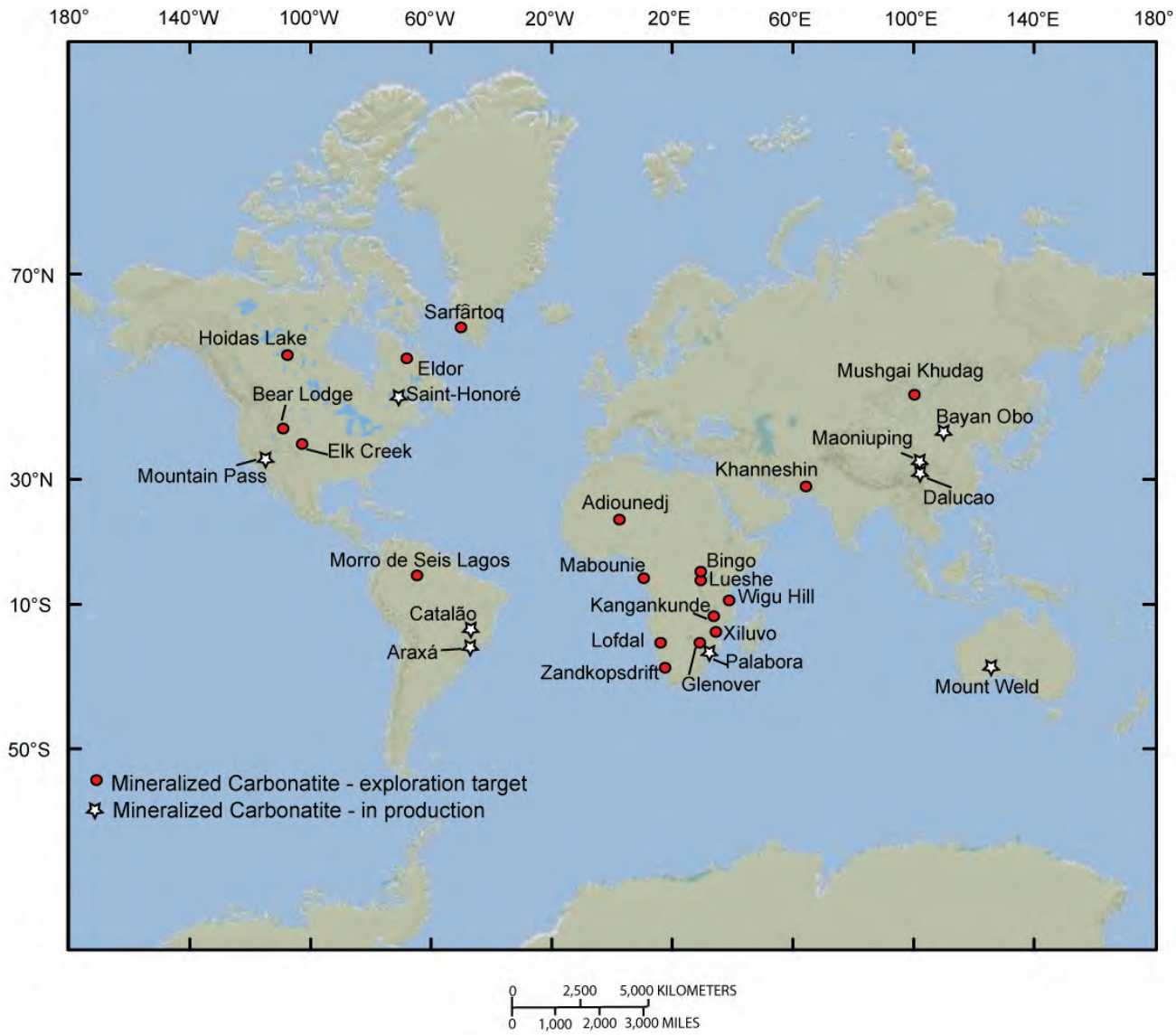

Fig. 1. Distribution of rare earth element and niobium mineralized carbonatites, including deposits in production and exploration targets discussed in this paper.

source material or variations in melt conditions (Mitchell, 2005).

Although the process or processes responsible for the generation of carbonatitic magmas are debated, the evolution of these magmas leads to REE enrichments. In general, carbonatite magmas evolve by fractional crystallization and the gravitational separation of early-formed crystals (Twyman and Gittins, 1987). Crystallization of the magma occurs as pressure and temperature decrease. Early major mineral phases can include calcite, dolomite, olivine, diopside, and apatite (Gittens, 1989; Kjarsgaard and Hamilton, 1989). Unlike most rock-forming minerals in silicate magmas, calcite, dolomite, and apatite can include REEs in their crystal structure. Although apatite is a common REE-bearing phase that can form early in the crystallization sequence, its crystallization history depends on the phosphate content of the magma. Magnetite can also be an early-forming phase, but its crystallization behavior is driven by the oxygen fugacity and magma composition. Carbonatite magmas have low viscosities (Jones et al., 2012), such that gravitational settling and/or flotation of crystals are efficient mechanisms for solid phase separation and concentration. Although major carbonate phases incorporate REEs, only a small fraction of the total REEs partition into these phases because the distribution coefficient between the magma and these phases is generally less than one, and the remaining magma can become enriched in REEs. The distribution of Nb in the system is driven by the crystallization of Nb-bearing phases, such as pyrochlore, perovskite, and lueshite (Mitchell and Kjarsgaard, 2004; Mitchell, 2015).

Carbonatite magmas may contain a variety of volatile components that include CO_2, H_2O, Cl, F, and S. As crystallization progresses, these components become enriched in the residual magma along with various incompatible elements, and they can exsolve into a separate fluid phase. Fluid inclusions and fenitization (alkali metasomatism) provide clear evidence for the separation of a volatile-rich fluid phase. Alkali

Table 2. Carbonatite-Related Ore Deposits (REE, rare earth element)

	Deposit	Reported resource (metric tons)	Reported ore grade	Comment	Reference
Rare earth element deposits			Total REE oxide %		
Active mines	Bayan Obo, Inner Mongolia, China	118,000,000	6	Tonnage represents estimated mineral resource of the deposit; see Xie et al. (2015) for more detail	Berger et al. (2009), Fan et al. (2014)
	Maoniuping, Sichuan, China	3,170,000	2.95	Reserve of REE oxide is estimated to be 3.17 million metric tons (Mt)	Geological Brigade (109) of Sichuan Bureau of Geology and Mineral Resource (2010)
	Dalucao (Daluxiang), Sichuan, China	81,556	5.2	Reserve of REE oxide is estimated to be 0.082 Mt	Geological Brigade (109) of Sichuan Bureau of Geology and Mineral Resource (2010)
	Mountain Pass, California, United States	16,700,000	7.98	Tonnage represents proven and probable reserves using a cutoff grade of 5%	Molycorp, Inc. (2012)
	Mount Weld, Western Australia	23,900,000	7.9	Tonnage represents total mineral resource estimate, as of January 2012, for two deposits at Mount Weld: (1) the Central Lanthanide deposit and (2) the Duncan deposit	Lynas Corporation (2012)
Advanced exploration projects	Bear Lodge Mountains, Wyoming, United States	6,800,000	3.79	Tonnage and grade data represent measured and indicated resources using a cutoff grade of 1.5% REE oxide; inferred resource estimated at 23,300,000 t at a grade of 2.86% REE oxide	Rare Element Resources Ltd. (2012)
Niobium deposits			Nb_2O_5 %		
Active mines	Araxá, Brazil	462,000,000	2.48		Cordeiro et al,. 2011
	Catalão II, Brazil	24,000,000	0.95	Proven and probable reserves for Boa Vista fresh carbonatite	Anglo American, 2013
	Saint-Honoré, Canada	419,000,000	0.42	Niobec mine	IAMGOLD, 2011
Exploration projects	Elk Creek, Nebraska, United States	81,200,000	0.71	Tonnage and grade represent indicated Nb oxide resource estimate; inferred resources of 99,800,000 t at 0.56% niobium oxide	NioCorp Developments Ltd. (2015)

metasomatism associated with carbonatite intrusions is characterized by Na and K enrichment and Si depletion.

The IUGS definition of carbonatites is broad and nongenetic, which permits for the inclusion of rocks that have varying petrogenetic evolutions. Carbonatites are classified by the dominant carbonate mineralogy and include calcite carbonatite (sövite), dolomite carbonatite (beforsite), and ferrocarbonatite (ankerite carbonatite; Streckeisen, 1980). A similar compositional classification is also used that includes calciocarbonatite, magnesiocarbonatite, and ferrocarbonatite (Woolley and Kempe, 1989). Variations in composition and mineralogy of carbonatites can reflect changes due to magmatic evolution, be the result of mineral segregation in a magma chamber, or reflect overprinting by later stage fluids exsolving from magma. Many carbonatite bodies contain a variety of lithologic units that are subdivided based on mineralogical and textural variations as well as crosscutting relationships. The term "transgressive carbonatite" is applied to some carbonatite lithologies that occur relatively late in the evolutionary sequence. Another approach to classify carbonatites is based on the composition of the associated silicate lithologies. Woolley (2003) compiled carbonatite data, including data for spatially associated alkaline igneous rocks, and recognized that a variety of alkaline rock series can be associated with carbonatites. Mitchell (2005) created a mineralogical-genetic classification for carbonatites and redefined carbonatites as containing greater than 30 vol % primary igneous carbonate, regardless of silica content. Mitchell (2005) came up with nine genetically distinct types of carbonatite, each related to a specific magma type and tried to link various types of elemental enrichment with individual classes of carbonatites. Essential to the application of this mineralogical-genetic approach in understanding carbonatites is the accurate and thorough characterization of the associated alkaline rock, which can be hampered by poor exposure and overprinting of hydrothermal fluids.

Carbonatites tend to be enriched, to varying degrees, in a variety of elements that include REEs, Sr, Ba, U, Th, Nb, Ta, P, and F. Although the overall REE content of carbonatites can be variable, the shape of the chondrite-normalized REE pattern of carbonatites almost invariably displays LREE enrichment and no Eu depletion (Fig. 2). Rare earth mineral phases have the highest REE contents, but major carbonate minerals, including calcite and dolomite, can contain substantial quantities of REEs (Mariano, 1989b). Barium and strontium abundances are generally high, whereas those of uranium, thorium, niobium, and phosphate are variable. Titanium and zirconium are commonly enriched in accessory minerals.

Mineral Deposits Related to Carbonatite Rocks

All carbonatites are enriched in REEs compared to most silicate igneous rocks, but only a small fraction of these reach economic concentrations. Deposit types include those formed from primary hypogene mineralization, those enriched by late-stage fluids, and those developed during supergene enrichment in weathered horizons. Processes potentially responsible for REE enrichment include fractional crystallization of the carbonatitic magma, enrichment of REEs in orthomagmatic fluids and subsequent precipitation or subsolidus metasomatic

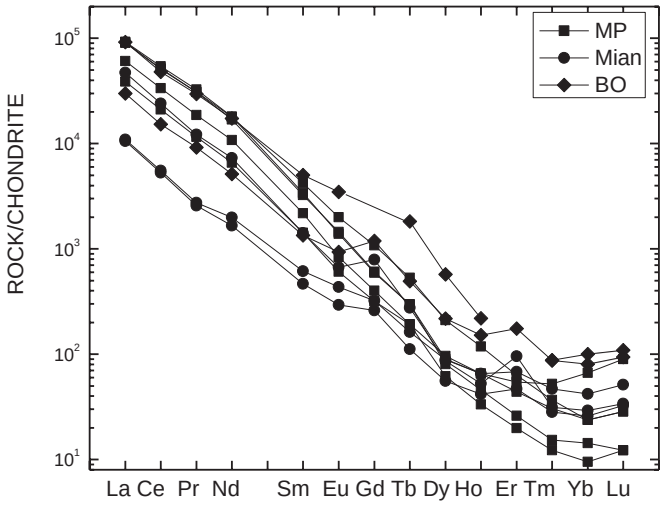

Fig. 2. Chondrite-normalized rare earth element diagram for select carbonatite deposits. The deposits include Mountain Pass (MP), with data from Table 3; Bayan Obo (BO), with data from Lai et al. (2012); and the Mianning deposits (Mian), using Lizhuang carbonatite samples from Huo et al. (2006). Concentrations normalized to C1 chondrite values from Anders and Ebihara (1982).

redistribution of REEs, and breakdown of primary carbonatitic minerals by chemical weathering and sequestration of REEs in secondary minerals. Currently, carbonatite-related deposits are being mined for REEs, Nb, phosphates, and Cu. Actively mined REE deposits include Bayan Obo (Inner Mongolia, China), Maoniuping (Sichuan, China), Dalucao (Sichuan, China), Mountain Pass (California, United States), and Mount Weld (Western Australia, Australia). Active Nb mining occurs at Araxá and Catalão II, Brazil, and St. Honoré, Canada. This section will review these major deposits; further discussion of the major Chinese deposits can be found in Xie et al. (2016).

Mountain Pass, California, United States

The Mountain Pass REE deposit is located on the eastern edge of the Mojave Desert in San Bernardino County, southeastern California, and is hosted by the Sulphide Queen carbonatite. Between 1965 and 1995, the deposit was the world's leading source of REEs (Castor, 2008a). Detailed descriptions of the carbonatite and surrounding rock units can be found in Olson et al. (1954), Mariano (1976, 1989a, b), Castor (2008a, b), and Mariano and Mariano (2012). The Sulphide Queen carbonatite is a composite, tabular body made up of REE-bearing sövites and beforsites. The body has a strike length of approximately 700 m, an average width of 75 m, and dips to the southwest at approximately 45°. The carbonatite is the youngest intrusive unit and follows a series of ultrapotassic alkaline intrusions that include shonkinite, syenite, and granite. The radiometric age of the carbonatite is 1375 ± 5 Ma, and the shonkinite and syenite are 1410 ± 5 and 1403 ± 5 Ma, respectively, of Dewitt et al. (1987). The complex represents a classic example of the spatial association between carbonatite and alkaline silicate rocks.

The Sulphide Queen carbonatite body is not uniform and has been divided into various lithologies based on mineralogical and textural features. Descriptions of the various

carbonatite lithologies have changed through time because of the level of detail of study and extent of exposure. Overall, calcite and dolomite in varying proportions are the primary mineral phases, with subordinate and variable amounts of barite, celestine, strontianite, cerussite, phlogopite, and fluorite (Castor, 2008b; Mariano and Mariano, 2012). Bastnäsite is the primary REE mineral, with parisite, synchysite, and monazite, and less abundant allanite, ancylite, apatite, cerite, florencite, hydroxyl bastnäsite, and sahamalite (Castor and Nason, 2004; Castor, 2008b; Mariano and Mariano, 2012). Initially, Olson et al. (1954) described three main types of carbonatite within the Sulphide Queen orebody that include a ferruginous dolomite, a gray calcite-pink barite unit, and a silicified carbonatite. This work primarily utilized samples from surface exposures, and the authors noted that the three units were quite variable in mineralogy and texture. Castor (2008b) also noted that the carbonatite was chemically and mineralogically variable and described a bastnäsite-barite sövite (calcite-dominant carbonatite) unit, a bastnäsite-barite-dolomite carbonatite (beforsite) unit, and a compositionally intermediate unit of bastnäsite-barite dolomite-sövite. Castor (2008b) provided further descriptions of the two primary units with the bastnäsite-barite sövite typically containing about 65 vol % calcite, 25 vol % strontian barite, and 10 vol % bastnäsite (Fig. 3), and the bastnäsite-barite-dolomite carbonatite (beforsite) typically comprising 55 vol % dolomite, 25 vol % barite, 15 vol % bastnäsite, and 5 vol % calcite. Castor (2008b) also described three subunits based on mineralogical variations of the three main types of carbonatite that include a white bastnäsite-barite sövite, a parisite-barite sövite, and a monazite-bearing carbonatite.

Work by the above authors, as well as detailed mapping and drill core analysis by R.L. Sherer and A.N. Mariano, show that the mineralogy of the carbonatite at Mountain Pass is quite heterogeneous with the dominant carbonate mineral being either calcite or dolomite. Barite and bastnäsite are generally the second, third, or fourth most abundant mineral phases. Other REE-rich phases are present generally in trace amounts, but locally can make up a few percent of the rock. Because the mineralogy variations in the carbonatite can affect milling and processing procedures, during the early days of mining at Mountain Pass in the 1960s, six major rock types were defined to describe the orebody. The ore types include hard brown ore, black ore, pink ore, white ore, breccia, and blue fibrous ore. Although these "miner terms" may still be in use today, these descriptive terms represent alteration and fenitization rather than individual carbonatite units. They are caused by silicification, introduction of iron, and crocidolite. This overprint is caused by hydrothermal and fenitization processes that may or may not be spatially controlled by structure.

Bastnäsite at Mountain Pass can be coarse grained (as shown in Fig. 4 from the Birthday vein) and displays primary igneous textures. Textural evidence shows that bastnäsite and parisite crystallized with euhedral morphology in association with calcite, barite, and dolomite, and thus probably formed as primary magmatic phases (Figs. 5, 6; Mariano, 1989a, b). Celestine ($SrSO_4$) occurs as a primary exsolution phase from barite at Mountain Pass, whereas strontianite ($SrCO_3$) occurs mostly as late veins and clusters cutting earlier primary minerals, including bastnäsite, barite, calcite, and dolomite.

Monazite is subordinate to bastnäsite, but it occurs in all of the major carbonatite units at Mountain Pass; in some areas, it is the major REE-bearing mineral. Euhedral, primary magmatic monazite is illustrated by the image in Figure 7. Based on detailed mineral processing observations, monazite may represent up to10 to 15 wt % of the REE mineral concentrates (E. McNew, oral commun., 2010). Although pyrochlore is only infrequently encountered in the carbonatite rocks, it is most commonly found associated with monazite.

The reported proven and probable ore reserves at Mountain Pass, as of April 2012, are 16.7 million tonnes at a grade of 7.89 wt % REOs, with a cutoff grade of 5 wt % (Molycorp, Inc., 2012). This high grade of the ore is primarily the result of the high modal bastnäsite abundance, as much as 15 to 20 vol %, and the fact that bastnäsite consists of approximately 75 wt % REOs.

Bayan Obo, north-central China

As of 2014, the Bayan Obo deposit, Inner Mongolia, China, is the world's primary source of LREEs (Long et al., 2010; U.S.

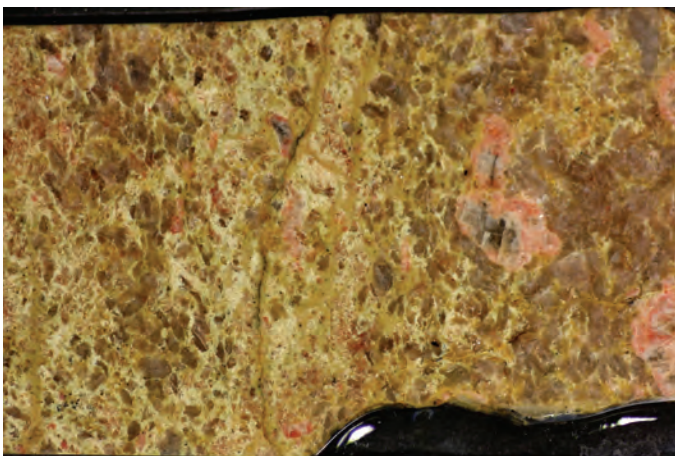

Fig. 3. Bastnäsite-rich barite sövite (calcite carbonatite), normal-light photograph, horizontal distance = 3.6 cm, Mountain Pass, California. Bastnäsite is brownish green in color and barite is pink.

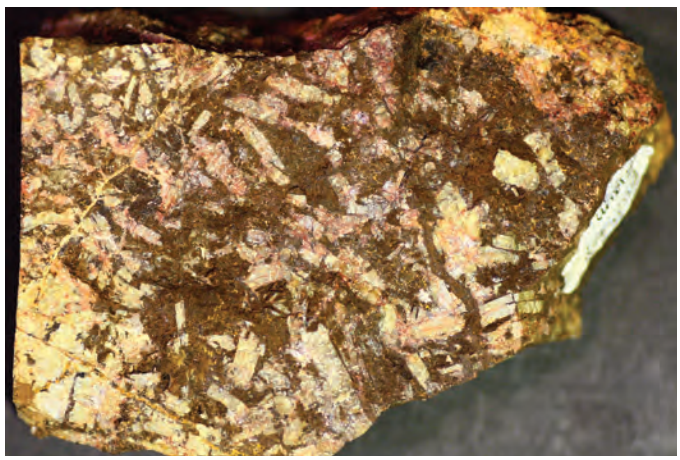

Fig. 4. Coarse-grained, tabular bastnäsite in a ferruginous dolomite matrix, normal-light photograph, from the "Birthday Claim," Mountain Pass, California. Horizontal distance = 8 cm.

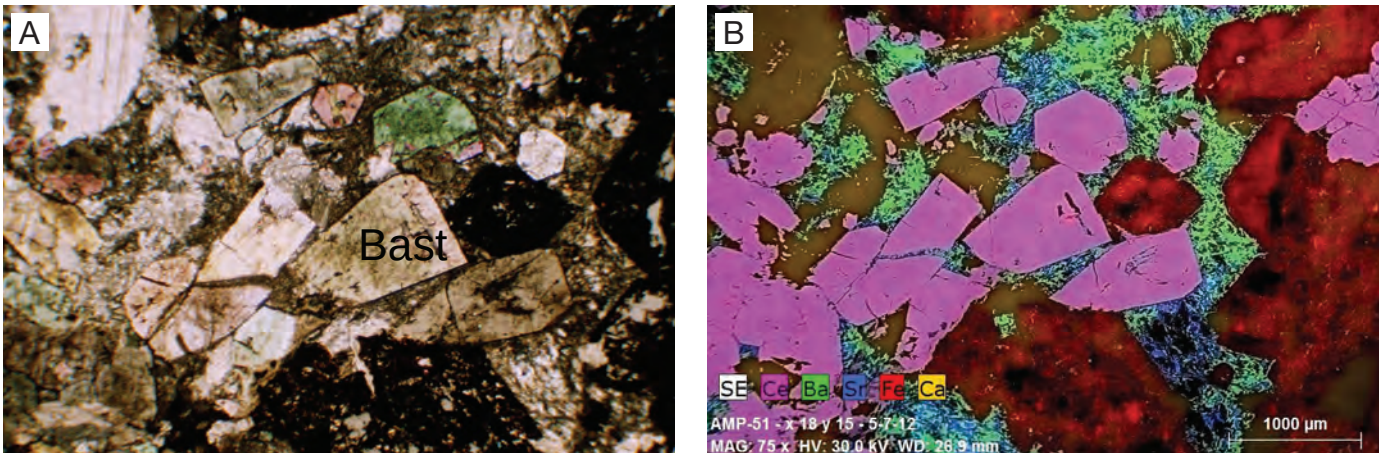

Fig. 5. Images of Mountain Pass ore sample. A. Plane-polarized light photomicrograph of "black ore" bastnäsite (Bast) in ferruginous calcite carbonatite, displaying primary igneous texture with a horizontal distance of 5 mm. B. X-ray element map of the section with pink = bastnäsite, green = barite, blue = strontianite, red = dispersed Fe oxide in calcite, and mustard brown = calcite.

Department of Energy, 2010). It is described in more detail by Xie et al. (2016) elsewhere in this volume. Historically, the primary commodity at Bayan Obo was iron from hematite-magnetite iron ore, and the REEs were by-products. Currently, REE orebodies are being mined separate from the iron-ore mining. The origin of the world-class Bayan Obo deposit remains controversial, primarily because the origin of the host lithology, the H8 dolomite, as either a sedimentary or igneous rock, has been debated for more than 30 years (Yuan et al., 1992). Yang et al. (2011) identified contact relationships that show the H8 dolomite intruded its host rock and this confirms a magmatic origin. These relationships, and the geochemical and mineralogical character of the deposit, allow us to include the Bayan Obo deposit in our classification of carbonatite-related REE deposits. In contrast, Kynicky et al. (2012) interpreted the host dolomite marble as part of a Proterozoic metasedimentary sequence, with the REE mineralization formed by hydrothermal replacement. The age of mineralization is also debated with ages ranging from approximately 1400 to 350 Ma. Xie et al. (2016) provide a summary of the geochronology and are in favor of a circa 1400 Ma age of mineralization with the younger dates reflecting with post ore-forming events. General discussions of the Bayan Obo deposit include Mariano (1989a), Drew et al. (1990), Chao et al. (1992), Yuan et al. (1992), Smith et al. (2000), Le Bas et al. (2007), Wu (2008), Xu et al. (2008), and Yang et al. (2009), Yang et al. (2011).

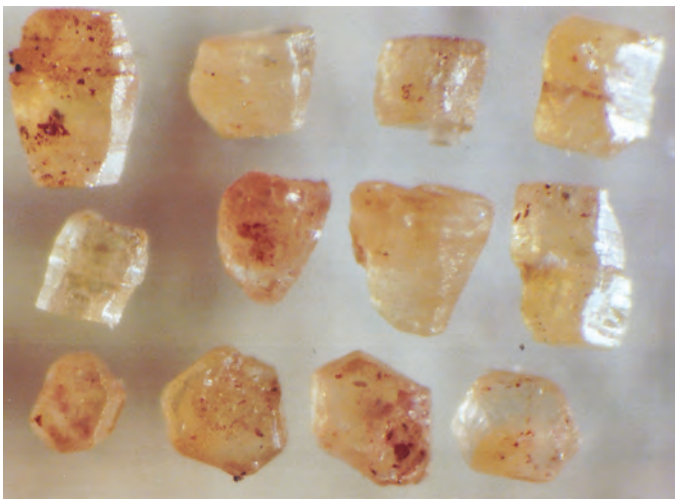

Fig. 6. Parisite mineral separates from Mountain Pass. The individual grains of parisite are euhedral, stubby crystals of primary magmatic origin. Average grain size = 3.5 mm. Note that clear crystals of parisite are quite rare.

The Bayan Obo deposit is operated by Baotou Steel. It consists of three orebodies (main, east, and west) that are lenticular in shape within the H8 dolomite marble (Yang et al., 2011). The H8 dolomite marble outcrop is 18 km in strike length, 1 km in maximum width, and consists dominantly of dolomite and calcite, with subordinate feldspar, quartz, Na-tremolite, magnesio-arfvedsonite, phlogopite, apatite, fluorite, barite, and ore minerals (Xu et al., 2008). Ore minerals at Bayan Obo are mainly bastnäsite, with lesser amounts of monazite. Making general statements about the nature of the mineralization at Bayan Obo is difficult because the nomenclature used in the literature to describe the primary lithologies is not consistent owing to the different hypotheses for the host and ore genesis. Recent work by Yang et al. (2011) delineates four types of Bayan Obo ore that include riebeckite type, aegirine type, banded, and massive. However, they do not describe the mineralogy of these ores. The summary of the Bayan Obo deposits by Xu et al. (2010) separated the ore types, on the basis of textural evidence, into disseminated, massive, and banded. They describe fluorite, apatite, and aegirine as the primary gangue minerals. Hydrothermal alteration is intense and widespread at Bayan Obo, encompassing an area of approximately 50 km^2 (Drew et al., 1990). The intensity and complexity of the hydrothermal alteration is one reason that the origin of the deposit is controversial, particularly because primary mineralogy and textures are overprinted by multiple hydrothermal alteration events. Yang et al. (2011) noted that the fenitization at Bayan Obo between the host dolomite (H8) and wall-rock slates consisted of the addition of K resulting in the occurrence

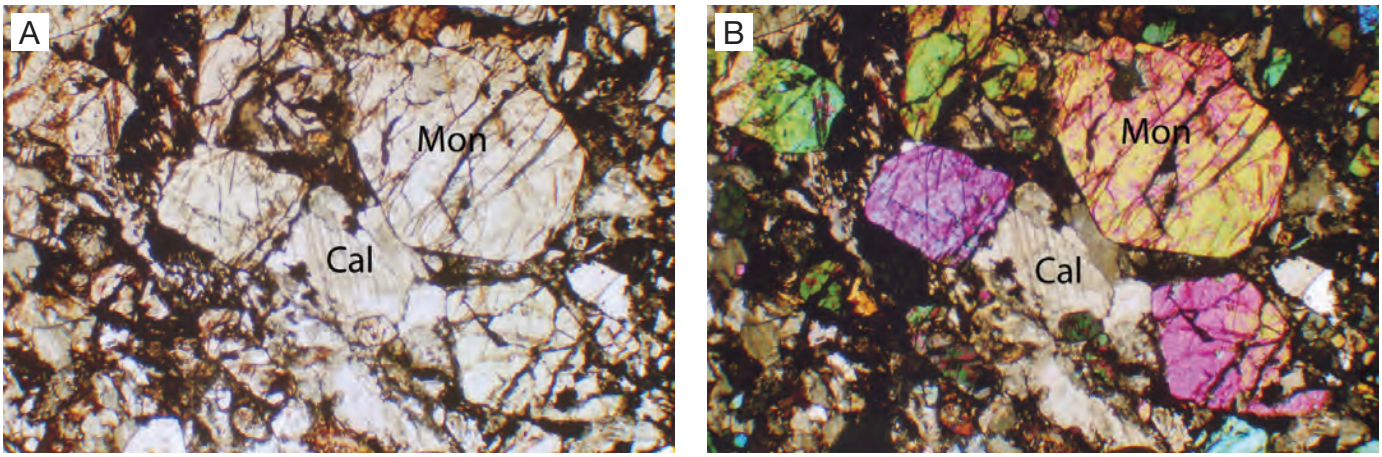

Fig. 7. Photomicrographs displaying euhedral monazite from the Mountain Pass carbonatite, California. A. Plane-polarized light photomicrograph with monazite (Mon) having higher relief than calcite (Cal). B. Cross-polarized light of the same section. Horizontal distance = 1.76 mm.

of riebeckite and phlogopite. The extensive fenitization is indicative of a strong influence of alkali activity, further supporting a carbonatite-mantle origin.

Mianning-Dechang REE belt, Sichuan, China

Two active carbonatite-related REE deposits are located within the Mianning-Dechang REE belt, Sichuan Province, China. These are the Maoniuping and the Dalucao deposits; the Maoniuping deposit is the second largest REE deposit in China (Yuan et al., 1992, 1995; Mariano, 1994; Wang et al., 2008; Kynicky et al., 2012). In addition, two smaller deposits in the same belt, Muluo and Lizhuang, are major REE exploration targets. The tectonic setting for these deposits is a bit anomalous because the deposits are located along the western margin of the Yangtze craton that was reactivated during the Indo-Asian Himalayan collisional orogen (Xie et al., 2016) and thus not in an extensional setting. Recent descriptions of these deposits include Xu et al. (2008, 2012), Hou et al. (2009), Xie et al. (2009), and Kynicky et al. (2012). The REE deposits occur as carbonatite-related sills and dikes within an alkaline complex of syenite (nordmarkite) and diorite stocks (Hou et al., 2009).

Ages for the Maoniuping deposit and host nordmarkite range from ca. 40 to 24 Ma (Shi, 1993; Xie et al., 2009). The deposit consists of a series of veins, stringers, and stockworks that are 1 to 30 m in width and 10 to 1,170 m in length. Mineralization styles include pegmatitic, carbonatitic, breccia, and stockwork (Yuan et al., 1995; Hou et al., 2009). The most abundant mineralization occurs as calcite-barite pegmatitic veins that contain coarse-grained bastnäsite, as well as fluorite, with local aegirine and augite, and minor amounts of microcline, arfvedsonite, biotite, apatite, quartz, and sulfides (Fig. 8; Xu et al., 2008, 2012). The REE mineralization is accompanied by intense late-stage fenitization. This alteration is dominated by an aegirine-augite assemblage, with also calcite, barite, and fluorite (Xu et al., 2012). Bastnäsite is also the primary ore mineral at Dalucao, and gangue minerals include calcite with subordinate microcline, quartz, arfvedsonite, Ba-rich celestine, strontiobarite, fluorite, aegirine, apatite, and sulfides (Xu et al., 2008).

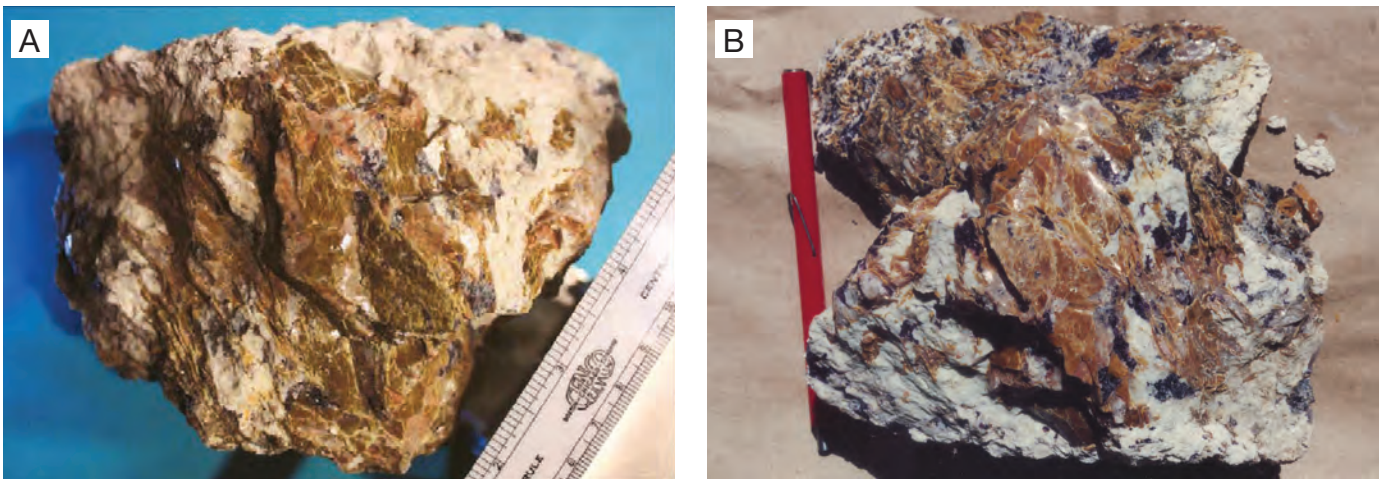

Fig. 8A and B. Photographs of hand samples from the Mianning area, China, with coarse-grained bastnäsite (mottled brown to pinkish-orange), calcite (white), and fluorite (purple).

Mount Weld, Australia

The Mount Weld REE deposit in Western Australia (Fig. 1) is hosted in a lateritic sequence that reflects supergene enrichment of the underlying carbonatite complex. The significant lateritic REE mineralization was first recognized by Mariano in 1980, and the supergene REE mineralization was first reported by Mariano (1981) and was described in a more detailed report by Mariano (1984). Other descriptions of the deposit include those by Lottermoser (1990) and Hoatson et al. (2011). The laterite sequence consists of a supergene enrichment zone as thick as 90 m, which is located above a 3- to 30-m-thick residual zone that overlays the unweathered carbonatite. The laterite is covered by 20 to 80 m of lacustrine and alluvial sedimentary rocks. A representative sample of unweathered carbonatite has a moderate REE content (Table 3, Fig. 9). The composition reported in Table 3 is for a calcite carbonatite (sövite) from a drill core (sample GRC-29 from drill core MWED-6 at 798 ft.). It is composed of calcite with minor magnetite, apatite, olivine, biotite, and pyrochlore. Rare earth element-rich minerals include calcite, apatite, and possibly pyrochlore (Mariano, 1981). The carbonatite is part of an alkaline complex within the Eastern Goldfields province of the Yilgarn craton. Graham et al. (2004) dated magnetite from the carbonatite to obtain an age of 2025 ± 10 Ma by the Re-Os method.

Secondary monazite is the dominant REE-bearing phase in the laterite ore. Other REE-bearing phases include cerianite, churchite, florencite, and other crandallite subgroup minerals (Mariano, 1984, 1989b). Lottermoser (1990) also noted the presence of secondary rhabdophane. Monazite is typically fine grained and can occur as pseudomorphs after apatite and rhabdophane (Fig. 10). Monazite is the most abundant REE mineral in the sample analyzed for this study (GRC-24 from drill hole MWRC-18 at 57–60 m). In addition, a cerium phase is pseudomorphous after apatite. Gangue minerals in the Mount Weld laterite include goethite and hematite, with minor calcite, cryptomelane, dolomite, hollandite, kaolinite, maghemite, montmorillinite, magnetite, pyrochlore, ilmentite, and rutile, and traces of quartz, barite, anatase, and vermiculite (Lottermoser, 1990). The calcite in the laterite is of supergene origin and is not a remnant of the primary carbonatite (Mariano, 1984).

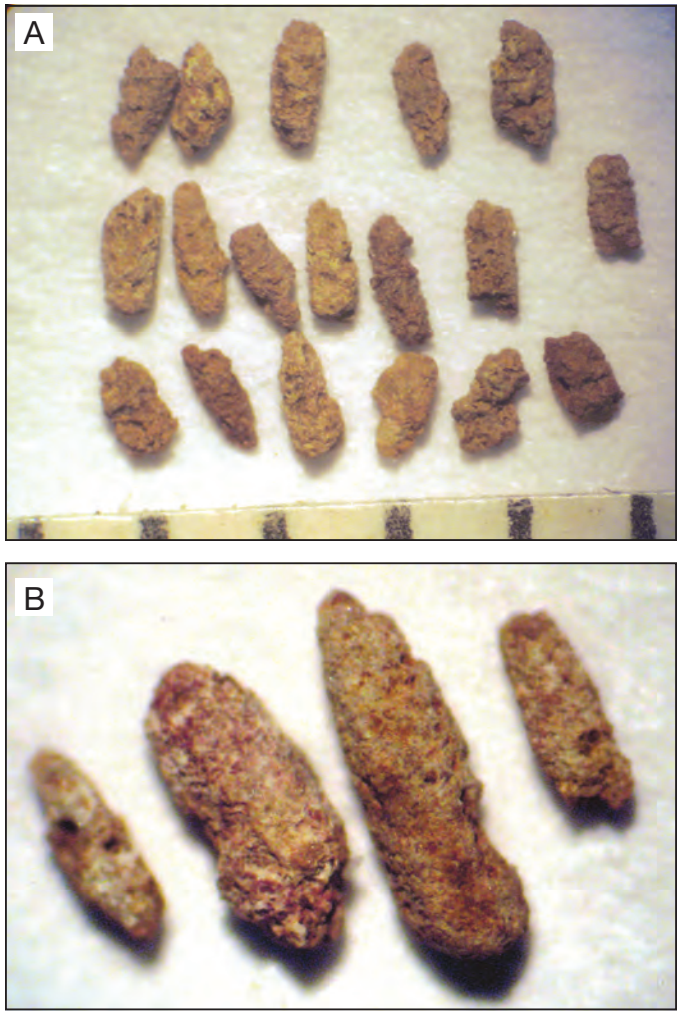

Fig. 10. Normal-light photographs of monazite pseudomorphs after apatite. Minerals separated from the Mount Weld laterite. Scale in (A) in mm increments. Long dimension of minerals in (B) is ~0.7–1.2 mm.

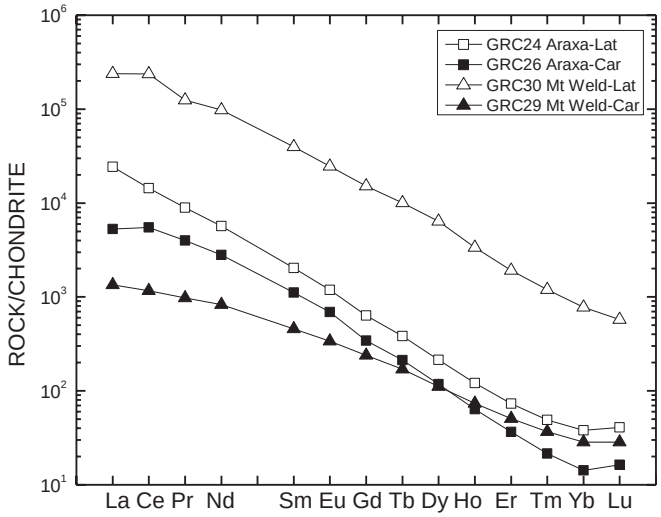

Fig. 9. Chondrite-normalized rare earth element diagram for laterite (Lat) and carbonatite (Car) samples from the Mount Weld and Araxá deposits. Data from Table 3. Concentrations normalized to C1 chondrite values from Anders and Ebihara (1982).

Araxá, Brazil

The Araxá carbonatite in Minas Gerais, Brazil, contains the world's largest known and highest grade resource of Nb contained in pyrochlore. The deposit occurs in a central plug of transgressive carbonatite and is mined by Companhia Brasileira de Metalurgia e Mineração. Outcrop and drill core at the Araxá deposit, and the similar Catalão deposits, provide clear evidence that the parent rock is carbonatite, which is termed the Barreiro carbonatite complex at Araxá (Mariano, 1989a; Morteani and Preinfalk, 1996). Although these deposits are enriched in REEs, they are currently only being mined by open-pit methods for Nb (Fig. 11).

The Araxá carbonatite occurs as a circular plug with an approximate diameter of 5 km (Fig. 12). Apatite fission-track ages for two samples from the carbonatite were 81.9 ± 3.4 and

Table 3. Chemical Composition of Carbonatite, Laterite, and "Apatitite" Samples

Sample no.	GRC-1	GRC-2	11PV01	11PV02	11PV04	GRC-6	GRC-24	GRC-26	GRC-30	GRC-29	GRC-32	GRC-34	T-724G
Lithology	Calcite carbonatite	Dolo carbonatite	Carbonatite ore	Carbonatite ore	Carbonatite ore	Carbonatite	Laterite	Carbonatite	Laterite	Carbonatite	Carbonatite	Carbonatite	Apatitite
Location	Mtn. Pass	Mtn. Pass	Mtn. Pass	Mtn. Pass	Mtn. Pass	Kangan-kunde	Araxa, Brazil	Araxa, Brazil	Mt. Weld	Mt. Weld	Bear Lodge, WY	Adiouned, Mali	Mushgai Khudag
Constituent[1] (wt %)													
SiO_2	8.64	22.2	12.0	3.93	2.81	0.71	5.38	1.14	4.41	0.98	0.54	2.96	3.83
TiO_2	<0.01	<0.01	<0.01	<0.01	<0.01	<0.01	2.97	1.39	0.92	0.02	0.03	0.22	<0.01
Al_2O_3	0.03	0.03	0.03	0.03	0.03	0.04	10.5	0.02	4.04	<0.01	0.10	1.00	1.86
Fe_2O_3	4.09	4.21	0.98	1.56	2.12	2.42	45.7	39.1	16.6	4.33	12.1	9.07	17.5
MgO	1.10	7.88	0.43	10.6	5.44	7.07	0.31	7.12	0.23	1.39	0.12	0.64	0.23
CaO	33.9	17.5	2.39	16.6	17.7	12.7	0.33	17.8	3.05	50.9	22.9	49.8	32.5
MnO	1.18	0.44	0.25	0.44	0.64	0.93	0.26	0.29	0.66	0.14	0.36	2.00	0.06
Na_2O	0.03	0.05	0.05	0.06	0.06	0.08	0.07	0.29	0.09	0.16	0.11	0.09	0.49
K_2O	0.01	<0.01	<0.01	<0.01	<0.01	<0.01	0.04	0.17	0.08	0.10	0.05	0.06	0.12
P_2O_5	0.24	0.52	0.19	0.10	0.13	7.49	5.95	6.91	17.2	5.52	0.02	1.72	23.5
Loss on ignition	30.6	17.8	10.4	28.3	24.5	27.2	10.4	15.0	8.66	NA	17.9	20.7	7.54
Constituent[2] (ppm)													
F	2,190	4,060	4,940	6,440	3,120	200	1,030	6,400	1,160	1,830	24,400	155,000	20,200
La	12,100	18,900	28,800	28,700	28,200	46,300	7,590	1,650	74,400	420	23,800	6,100	19,000
Ce	17,100	27,300	44,100	41,400	42,000	70,400	11,700	4,480	192,900	950	32,100	10,900	30,300
Pr	1,420	2,300	4,010	3,810	3,790	6,250	1,100	490	15,300	120	2,690	1,070	2,820
Nd	3,970	6,500	10,900	10,800	10,200	18,000	3,420	1,690	59,000	500	7,140	3,720	8,860
Sm	280	430	670	830	640	1,190	400	220	7,830	90	490	530	990
Eu	45	62	103	148	107	192	88	51	1,820	25	73	127	230
Gd	83	104	154	281	158	283	165	89	3,950	62	127	284	454
Tb	9	9	14	25	14	25	18	10	473	8	11	32	52
Dy	31	20	29	68	26	49	69	38	2,060	36	29	137	229
Ho	4.7	2.4	4.7	8.5	3.3	5	8.7	4.6	242	5.3	4.1	18.6	37.2
Er	9.3	4.2	11.5	13.3	5.5	6.5	15.4	7.7	405	10.7	7.5	36.1	87.8
Tm	1	0.4	1.7	1.2	0.5	0.4	1.6	0.7	39.1	1.2	0.7	4.2	11.3
Yb	5	2	14	5	3	2	8	3	163	6	3	24	66
Lu	0.7	0.3	2.2	0.7	0.3	<0.2	1	0.4	14.1	0.7	0.4	3.3	8.7
Y	125	58	111	181	65	79	167	92	4,710	122	121	421	1,230
Ba	80,200	117,000	113,100	128,700	169,200	24,400	67,800	23,100	1,940	1,140	12,200	12,100	290
Sr	7,130	15,700	83,100	13,600	26,100	159,500	9,160	10,600	3,100	7,220	167,900	2,290	11,100
Th	98	150	179	146	219	227	2,180	2,630	911	44	230	899	212
U	12	4	103	17	7	1	40	13	91	104	18	4	311
Nb	2	6	21	5	2	202	24,100	39,200	757	492	23	234	7
Sc	11	7	13	6	6	9	51	8	238	<5	<5	<5	14
Ta	<0.5	<0.5	<0.5	<0.5	<0.5	<0.5	33.2	51.2	7.1	102	<0.5	0.8	<0.5
Zr	4.2	3.2	NA	NA	NA	47.3	1,860	438	293	100	56.5	310	95.3
Rb	0.6	0.5	0.6	0.4	0.3	<0.2	2.9	6.7	1.5	5.4	2.3	1.6	1.9
Cu	40	26	17	25	<5	23	481	690	183	75	602	15	328
Pb	14,200	3,110	1,930	2,510	217	73	528	40	136	53	429	275	1,210
Zn	91	193	15	39	29	1,470	1,030	254	911	48	588	656	596
Mo	24	29	7	35	8	13	11	<2	200	2	26	15	80
Cd	0.8	<0.2	<0.2	<0.2	0.3	29.2	0.4	0.4	12.4	<0.2	0.7	0.8	10.6
Co	8.5	8.6	3.5	3	4.9	1.5	60.1	52.4	30.9	10.8	6.6	2	72.9
Cr	10	10	<10	<10	<10	<10	100	110	70	<10	<10	40	10
Ni	<5	<5	<5	<5	<5	<5	47	58	16	<5	<5	<5	38
V	63	19	<0.1	<0.1	<0.1	30	566	453	180	16	40	20	272

[1] Major oxides determined by wavelength dispersive X-ray fluorescence spectrometry
[2] Fluoride determined by ion selective electrode; other elements determined by inductively coupled plasma-mass spectrometry

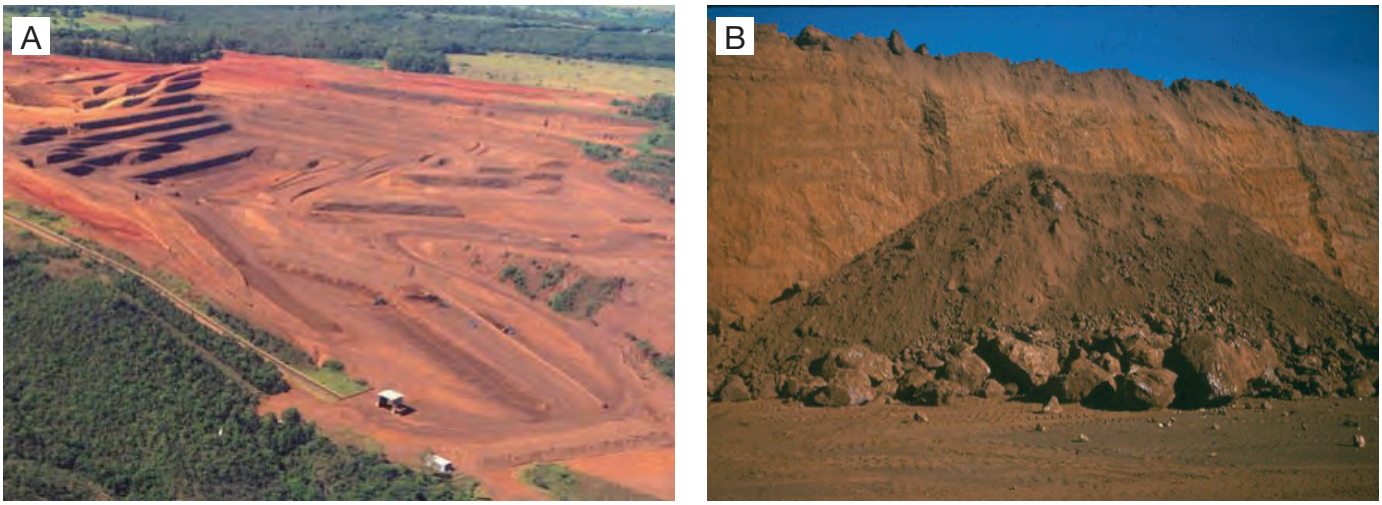

Fig. 11. Photographs of the Araxá niobium mine (Brazil). A. Overview of the open-pit mine in Araxá laterite above the carbonatite. Photograph courtesy of Companhia Brasileira de Metalurgia e Mineração (CBMM). B. Photograph from within the open pit showing bench and ore pile. Approximate height of the bench = 15 m.

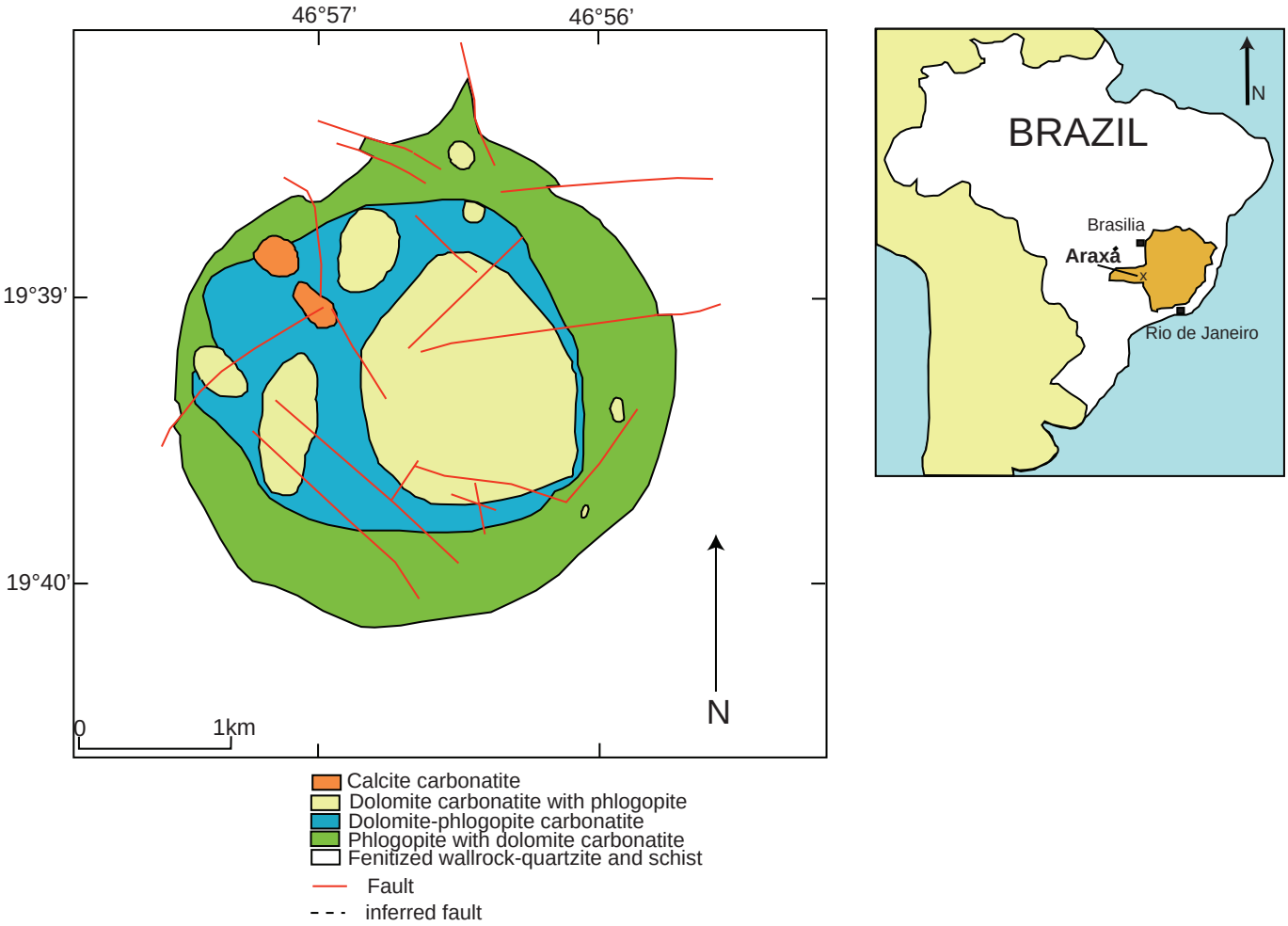

Fig. 12. Geology of the Araxá carbonatite complex (after Silva et al., 1979) with location map.

84.4 ± 1.9 Ma (Eby and Mariano, 1992). The carbonatite plug intrudes Precambrian schists and gniesses of the Barreiro Group. The carbonatite is dominantly a magnesiocarbonatite that contains variable amounts of phlogopite; lesser volumes of calciocarbonatite are also present. Fenitization overprints sections of the carbonatite, as well as the surrounding country rock. Peripheral doming of the metamorphic country rocks provides evidence that the carbonatite did not breach the contemporary land surface during emplacement. Extensional fractures produced within the domed metamorphic rocks during igneous intrusion enhanced subsequent erosion and exposure of the buried carbonatite. The strongly domed peripheral metasedimentary rocks were subjected to intense silicification during the intrusive episode. Consequently, they crop out as resistant ridges surrounding a topographically depressed, lateritically weathered carbonatite plug with deep internal drainage. The entire plug is weathered to laterite in the near surface, with an average depth of laterization of 150 m. A major fault has allowed laterization to locally form to a depth of 350 m in the southeastern part of the intrusion.

Mineralogy of the weathered zone consists primarily of ferric oxides (goethite and hematite), magnetite, bariopyrochlore, secondary monazite, and barite, with subordinate gorceixite, kaolinite, apatite, quartz, vermiculite, plumbopyrochlore, and cerian pyrochlore (Mariano, 1978, 1989b; Woolley, 1987; Morteani and Preinfalk, 1996). Electron microprobe analyses of pyrochlore, the most abundant ore mineral in the laterite orebody at Araxá, determined 63.51 and 56.35 wt % Nb_2O_5 for a bariopyrochlore and a plumbopyrochlore, respectively (Mariano, 1989b). The dominant REE phase is supergene monazite.

Bariopyrochlore from the Araxá laterite is not a product of weathering of the primary pyrochlore. Sodium and Ca are replaced at the "A" site by Ba and Sr during hydrothermal alteration. In a fresh carbonatite sampled from core drilled near the center of the Araxá complex, the pyrochlores are normal Na-Ca type, but microveinlets within the pyrochlore show incipient alteration to bariopyrochlore (Mariano, 1989b). Although no outcrops of Nb-mineralized carbonatite are present at Araxá, they were present at Catalão, and included ore-grade bariopyrochlore, with magnetite present in the carbonatite and in the mineralized laterite (Fig. 13).

Bariopyrochlore in the Araxá laterite ore has not undergone any chemical Nb enrichment during weathering. The B site cations were not affected during early hydrothermal alteration of the fresh carbonatite, or during the subsequent lateritic weathering stage. Niobium enrichment in the laterite is primarily due to the physical accumulation of pyrochlore and the removal of the soluble minerals calcite, dolomite, apatite, and some magnetite during laterization. We conclude that enrichment of Nb in the carbonatite laterites of Araxá, Catalão I, Catalão II, Morro de Seis Lagos (Brazil), Lueshe and Bingo (Democratic Republic of the Congo), Mabounie (Gabon), and Mount Weld is almost exclusively physical and does not constitute a chemical enrichment of Nb in pyrochlore.

The grade, tonnage, and ease of mining and processing of the Araxá laterite deposit suggests that it may dominant the Nb world marketplace for the foreseeable future. However, in 1975 the company drilled holes beneath the laterite to test the mineralogy of the fresh, unweathered carbonatite. The drilling into unweathered carbonatite revealed the presence of pyrochlore mineralization in quantities far exceeding pyrochlore grades from most Nb-mineralized carbonatites. The mineralization consists of euhedral pyrochlore cocrystallized with magnetite, apatite, phlogopite, and dolomite with minor barite and monazite and accessory zircon and baddeleyite. Other trace minerals include ilmenite, calcite, and isokite (Mariano, 1978). An example of the impressive pyrochlore mineralization and associated minerals is shown in Figure 14. A representative sample included for this study (GRC-26, Table 3) from the carbonatite underlying the weathered zone, located from a depth of 180.18 to 180.26 m, is magnetite-apatite dolomite carbonatite with pyrochlore and minor phlogopite.

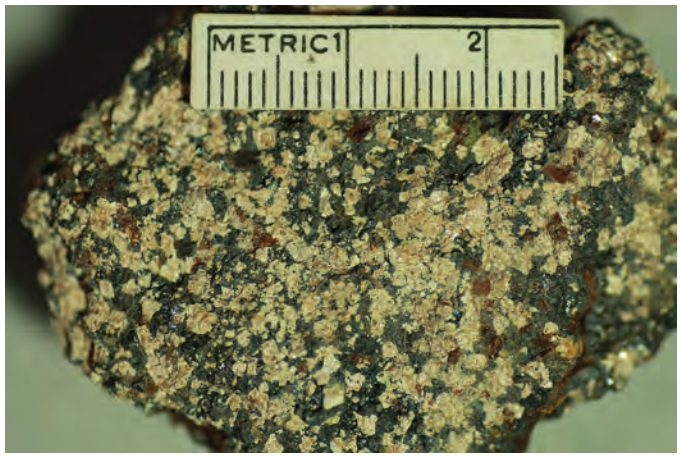

Fig. 13. Hand sample of bariopyrochlore with magnetite from a carbonatite outcrop at Catalão, Brazil. Note that this is not from Araxá but is an excellent example of a bariopyrochlore occurrence. The bariopyrochlore is formed by hydrothermal alteration of primary pyrochlore by substitution of Ba for Na and Ca at the A site. Occurrence of bariopyrochlore in the carbonatite documents that bariopyrochlore within the laterite may not simply be formed by weathering processes.

The petrology of this type of pyrochlore ore-bearing carbonatite at Araxá and Catalão has been described as being "phoscorite" or "nelsonite" (Biondi, 2005; Cordeiro et al., 2010). However, this terminology may be misleading because the high-grade Nb mineralization at both deposits is hosted in transgressive carbonatite magma pulses that intruded earlier carbonatite. Furthermore, olivine is critical to the definition of phoscorite (Le Maitre, 2002), but it does not cocrystallize with pyrochlore at Araxá and Catalão. This suggests that the pyrochlore orebodies at Araxá and Catalão may warrant a different petrologic name, and Mitchell (2015) made a similar suggestion.

Other Mineralized Carbonatites

We have analyzed a suite of samples from other mineralized carbonatites that include Bear Lodge, Wyoming (United States), Kangankunde (Malawi), Adiounedj (Mali), and Mushgai Khudag (Mongolia; Tables 3, 4). This suite represents a range in deposit mineralogy and composition, and highlights the REE variability in carbonatites. We recognize that individual carbonatites are quite heterogeneous in their mineralogy, such that one or a few samples may not truly represent the intrusive body. Samples were, however, chosen that are representative of major units, particularly mineralized zones.

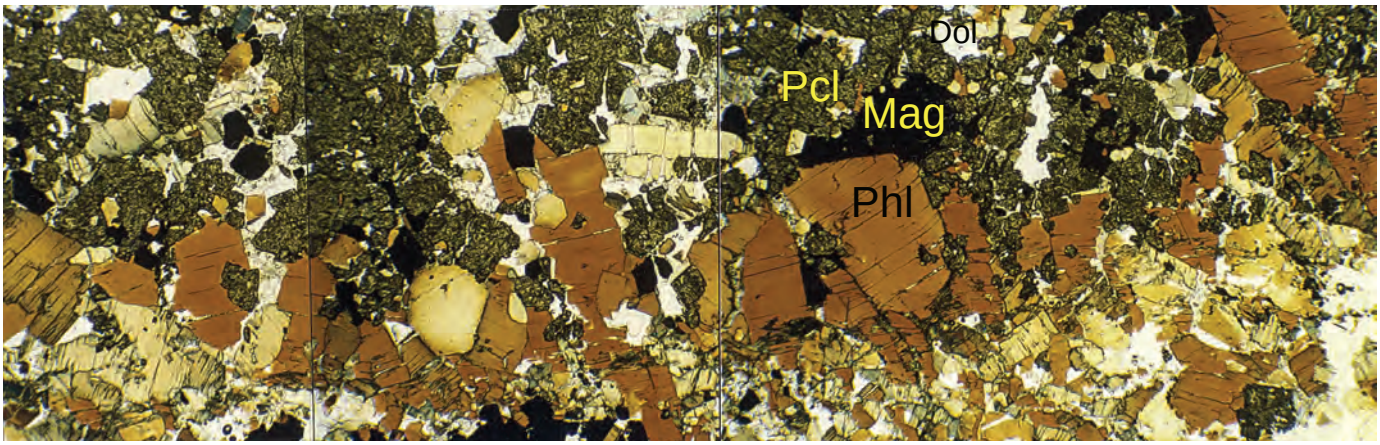

Fig. 14. Composite, normal-light photomicrograph of Araxá carbonatite, drill core from the central plug at a depth of 126 m below the surface. The photomicrograph displays pyrochlore-rich zone and primary igneous textures within fresh carbonatite below the laterite. Pyrochlore = Pcl) = high relief, dark grains; dolomite (Dol) = white grains; phlogopite (Phl)-brown, platey grains; and magnetite (Mag) = black grains. Horizontal dimension ~7 cm.

Bear Lodge deposit, Wyoming

The mineralization in the central part of the Bear Lodge deposit, hosted by the Bull Hill carbonatite in northeastern Wyoming, is characterized by REE-mineralized dikes, veins, and stockworks cutting a diatreme breccia and adjacent carbonatite. Identified zones include an unoxidized zone, a transitional zone, an oxide-carbonate zone, and an oxidized zone. The deeper zone is characterized by unoxidized carbonatite with mineralized veins carrying a REE mineral assemblage of predominantly ancylite with bastnäsite group minerals, carbocernaite, burbankite, and minor monazite (Mariano and Mariano, 2012). The sample analyzed for this study (GRC-32) is from a hydrothermal vein containing ancylite-strontianite pseudomorphs and minor fluorite from the unoxidized zone (Fig. 15). The precursor mineral is hexagonal in shape and is thought to be burbankite. The upper part of the deposit primarily consists of intensely oxidized dikes and veins termed FMR dikes (FeOx-MnOx-REE). Sulfides are completely oxidized, and groundmass carbonate is completely leached. The REE phase assemblage consists of bastnäsite group minerals, with variable, but subordinate, monazite and cerianite. The oxidized zone is as much as 150 m thick and may result from hydrothermal and/or supergene processes. The thin transition zone, generally 6 m thick, occurs at the top of the unoxidized zone and represents the initiation of sulfide oxidation and breakdown of ancylite to bastnäsite group minerals (Larochelle et al., 2012). The oxide-carbonate zone (OxCa) extends from the top of the transition zone to the base of the oxidized zone. It is characterized by nearly total oxidation of sulfides, variable partial leaching of groundmass calcite, and significant breakdown of ancylite to form bastnäsite group minerals. The $^{40}Ar/^{39}Ar$ age determinations of biotite and orthoclase phenocrysts constrain the age of carbonatite magmatism to between 51.6 ± 0.2 and 51.15 ± 0.04 Ma (Andersen et al., 2013). Recent work in the Bear Lodge deposit area has identified locations enriched in HREEs adjacent to the better known areas of LREEs in the Bull Hill zone. Preliminary

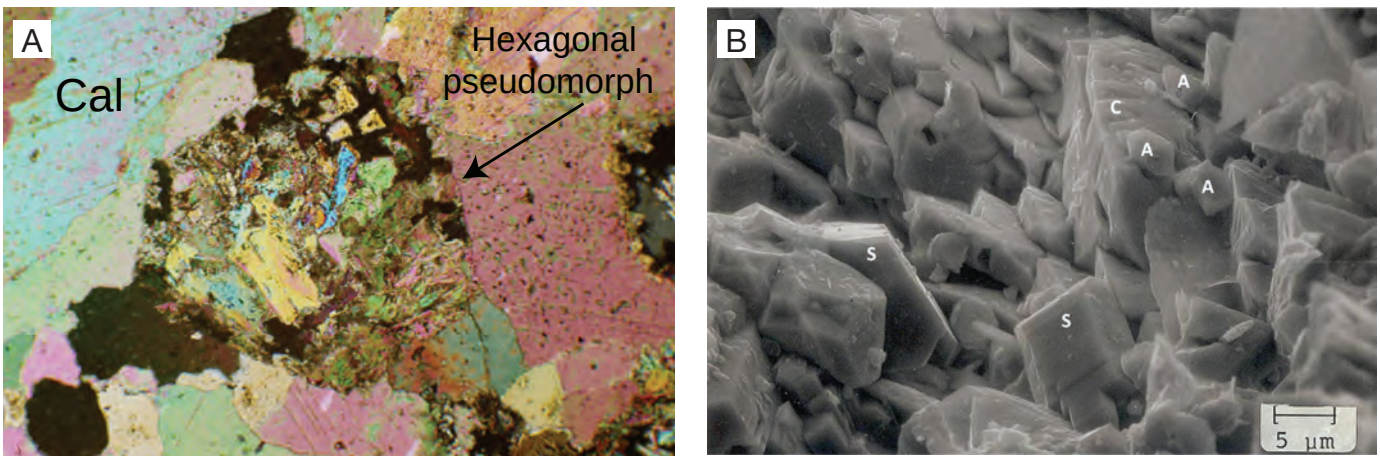

Fig. 15. Hexagonal pseudomorph with contained ancylite, carbocernaite, and strontianite in sövite, Bear Lodge, Wyoming. Horizontal distance = 1.8 mm. A. Cross-polarized photomicrograph. B. Secondary electron image of secondary crystals in hexagonal pseudomorph; carbocernaite (C), strontianite (S), and ancylite (A).

Table 4. Nd and Sr Isotope Compositions of Selected Carbonatites

Sample	Label	Rb (ppm)	Sr (ppm)	Sm (ppm)	Nd (ppm)	AGE (Ma)[1]	$^{143}Nd/^{144}Nd_m$[2]	2σ uncertainty	ε_{Nd}[3]	$^{87}Sr/^{86}Sr_m$[2]	2σ uncertainty	$^{87}Sr/^{86}Sr$[3]
GRC-1	Mtn. Pass, United States-carbonatite	0.6	7130	280	3970	1385	0.511052	0.000011	–3.2	0.705233	0.000010	0.70523
GRC-2	Mtn. Pass, United States-carbonatite	0.5	15,700	430	6500	1385	0.511027	0.000010	–3.6	0.705325	0.000009	0.70532
11PV01	Mtn. Pass, United States-carbonatite	0.6	83,100	670	10,900	1385	0.510996	0.000006	–3.7	0.705556	0.000012	0.70556
11PV02	Mtn. Pass, United States-carbonatite	0.4	13,600	830	10,800	1385	0.511093	0.000015	–3.5	0.705945	0.000011	0.70594
11PV04	Mtn. Pass, United States-carbonatite	0.3	26,100	640	10,200	1385	0.511004	0.000011	–3.7	0.705117	0.000008	0.70512
GRC-6	Kangankunde, Malawi-carbonatite	<0.2	159,500	1190	18,000	123	0.512679	0.000010	3.3	0.703097	0.000011	0.70310
GRC-26	Araxá, Brazil-central core, drill core, carbonatite	6.7	10,600	220	1690	87.2	0.512344	0.000008	–4.4	0.704951	0.000011	0.70495
GRC-24	Araxá, Brazil-laterite	2.9	9160	400	3420	87.2	0.512246	0.000007	–6.1	0.705450	0.000013	0.70545
GRC-29	Mt. Weld, Australia-drill core, carbonatite	5.4	7220	90	500	2025	0.511501	0.000010	0.7	0.702056	0.000011	0.70197
GRC-30	Mt. Weld, Australia-laterite	1.5	3100	7830	59,000	2025	0.510996	0.000011	–2.4	0.705809	0.000012	0.70575
GRC-32	Bear Lodge, United States-ancylite vein in carbonatite	2.3	167,900	490	7140	51.5	0.512591	0.000014	0.1	0.704406	0.000012	0.70441
GRC-34	Adiounedj, Mali-carbonatite	1.6	2290	530	3720	275	0.512418	0.000007	–0.1	0.705593	0.000011	0.70558
T-724G	Mushgai Khudag, Mongolia-"apatitite"	1.9	11,100	990	8860	139.9	0.512452	0.000011	–1.3	0.706365	0.000008	0.70636

Notes: Elemental abundances from Table 3; Nd and Sr isotope compositions were obtained at the University of Colorado, Boulder, using a Finnigan-MAT 261 six-collector solid-source mass spectrometer

[1] Age citations in text

[2] Measured values

[3] Initial isotopic composition

mineralogical assessment identifies HREE-enriched fluorocarbonates, monazite, and xenotime, in addition to bastnäsite group minerals (Larochelle et al., 2012).

Adiounedj, Mali

This occurrence is described by Sauvage and Savard (1985). Woolley (2001) summarized the carbonatites as small plugs and dikes within a syenitic host. No age determinations for this locality have been published. The carbonatite complex includes sövites, calcite carbonatites rich in iron and manganese oxide minerals, and ferrocarbonatites. Other minerals present include barite, apatite, and fluorite, with subordinate synchysite and pyrochlore. The sample analyzed for this study (GRC-34) is a ferrocarbonatite consisting of calcite, fluorite, apatite, Fe oxide minerals, and synchysite.

Kangankunde, Malawi

Wall and Mariano (1996) provided a detailed description of this occurrence. The Kangankunde carbonatite complex, which lies within the Chilwa alkaline province of southern Malawi, is an example of a carbonatite complex without associated silicate rocks. The K-Ar age of phlogopite from the carbonatite is 123 ± 6 Ma (Cahen and Snelling, 1966). The carbonatite is composed of dolomite and ankerite carbonatites surrounded by a fenitized aureole (Wall and Mariano, 1996). Rare earth element mineral phases include monazite, bastnäsite, and minor florencite-goyazite. Rare earth element mineralization can occur as hexagonal pseudomorphs of monazite, strontianite, and barite, or as clusters of euhedral monazite (Fig. 16). The sample included in this study (GRC-6) is a ferrocarbonatite with strontianite, monazite, apatite, and barite. The strontianite content is approximately 27 wt %, and the monazite content is approximately 10 wt %.

Mushgai Khudag, Mongolia

The Mushgai Khudag REE deposit is another occurrence with few descriptions in the literature (Baskina et al., 1978; Andreeva et al., 2001). Sanematsu et al. (2010) described the deposit as a sheet-like magnetite-apatite body adjacent to a syenite porphyry that is "locally accompanied by carbonatite dikes and veins of high-grade ores." The magnetite-apatite body is composed of apatite, celestine, magnetite, hematite, goethite, fluorite, gypsum, phlogopite, calcite, pyrite, and monazite, and the carbonatite dike ores consist of monazite, apatite, carbonates, pyrite, and magnetite (Sanematsu et al., 2010). Sanematsu et al. (2010) concluded that the REE mineralization in the magnetite-apatite ores and high-grade carbonatite ores at the Mushgai Khudag deposit result from exsolution from the syenite magmas during crystallization. The sample utilized in this study (T724G) was collected from the apatite-magnetite body and can be termed "apatitite" because it consists of >50 vol % apatite, with celestine, gypsum, and lesser monazite. The fine-grained monazite and celestine appear to be supergene products that crystallized during the weathering process. An Rb-Sr isochron age of syenite yields an age of 139.9 ± 5.9 Ma (Munkhtsengel and Ilzumi, 1999).

Lofdal, Namibia

Although we do not include new data from Lofdal, we provide a brief description of the deposit because of its anomalous

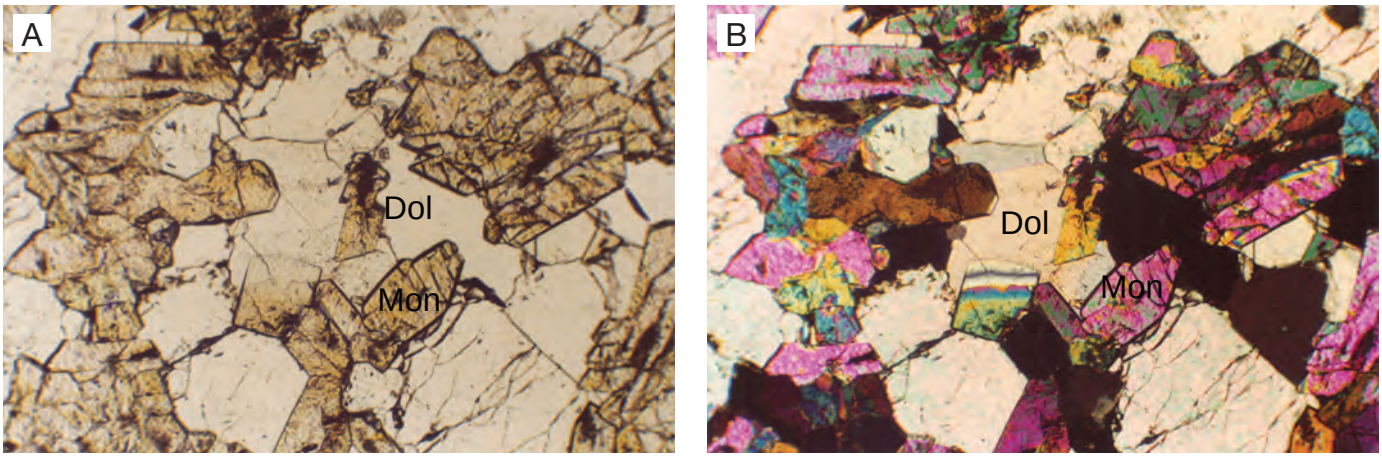

Fig. 16. Primary, euhedral monazite in carbonatite, Kangankunde, Malawi. A. Plane-polarized light photomicrograph with monazite (Mon) having higher relief than dolomite (Dol). B. Cross-polarized light photomicrograph. Horizontal distance = 1.76 mm.

mineralogical and geochemical character relative to other carbonatite-hosted REE deposits. Rare earth element deposits associated with carbonatites are generally characterized by extreme LREE enrichment, with steep chondrite-normalized REE patterns and relatively low concentrations of HREEs. The REE mineralization associated with the Lofdal deposit is an exception because it has a relatively high proportion of HREEs. At Lofdal, the carbonatites occur as a series of subparallel dikes, generally 0.5 to 5 m in width and as long as 5 km (Mariano, 2001a, b; Mariano and Siegfried, 2001; Wall et al., 2008). Xenotime-bearing carbonatite veins at Lofdal are the major source of the HREEs (Mariano, 2001a, b). The enhanced recognition of HREEs by the utilization of cathodoluminescence was an effective analytical tool during exploration at Lofdal.

Geologic Setting of Carbonatites

Carbonatites typically occur within stable continental tectonic settings, in areas defined as shields, cratons, and crystalline blocks. They are generally associated with intracontinental rift and fault systems (Berger et al., 2009). Crustal thinning in rift environments enables magmas derived from the asthenospheric or lithospheric mantle to ascend high in the upper crust, because there is a minimal distance to travel and it is a region of high heat flow. For example, the East African rift hosts the Oldoinyo Lengai volcano and its recent natrocarbonatite lavas. However, less commonly carbonatites can also be associated with orogenic activity along continental margins (Woolley, 1989). Carbonatite bodies have been described as tabular and moderately dipping (Mountain Pass; Castor, 2008b), lenses (Bayan Obo; Yang et al., 2011), veins (Maoniuping; Xie et al., 2009), and large stocks (Iron Hill, Colorado; Olson and Hedlund, 1981).

Many carbonatites occur with alkaline intrusive rocks, but not all carbonatite districts contain documented alkaline intrusive rocks (Woolley, 2003; Mitchell, 2005; Woolley and Kjarsgaard, 2008). When they do occur together, carbonatites tend to be surrounded by alkaline intrusive rocks, and the carbonatites are generally younger. Carbonatites can be associated with different suites of alkaline rocks, as summarized by Bell (1998), Woolley (2003), and Mitchell (2005). Although some authors propose a genetic link between carbonatite and associated alkaline silicate rocks, other evaluations question the relationship, based on the observation that these rock types are quite different chemically and mineralogically, and some carbonatites lack associated alkaline rocks (Gittens and Harmer, 2003). For example, the mineralized carbonatite at Mountain Pass lies within an ultrapotassic alkaline complex that includes shonkinites, melasyenites, syenites, quartz syenites, and granites. Castor (2008b) suggested that the genesis of the carbonatite is linked to the ultrapotassic alkaline units because of the spatial association and chemical similarities. Dating by DeWitt et al. (1987) documents the carbonatite to be approximately 20 m.y. younger than the alkaline suite, which may bring into question the genetic link. However, hiatus periods between multiple injections of carbonatites have been measured that exceed 20 m.y. (Eby and Mariano, 1992).

Mineralized carbonatites can occur as tabular bodies of sills and dikes (Mountain Pass) or as veins (Maoniuping and Lofdal). Veins can vary from clusters of veinlets, which are centimeters in width, to large veins which are tens of meters wide. Most mineralized carbonatites have associated breccias that can contain mineralized clasts or have a mineralized matrix. Deposits with breccia zones include Mountain Pass, Bayan Obo, Maoniuping, and Dalucao. A common feature of most carbonatite deposits is that the surrounding rocks are hydrothermally altered by alkali metasomatism. This style of alteration is known as fenitization because it was first described at the Fen alkaline complex in southern Norway. Alkali-rich fluids from the crystallizing magma react with the country rocks and convert the adjacent wall-rock minerals to an assemblage of alkali-bearing minerals. Summary papers that describe the nature of fenitization include Le Bas (1981, 2008), Woolley (1982), and Morogan (1994). Whereas fenitization is characteristic of most carbonatites, the extent of alteration is variable from zones a few meters to hundreds of meters in extent. In some complexes, fenitized zones are discontinuous adjacent to carbonatites or their genetically associated igneous rocks.

Fenites can be classified as Na or K rich. Sodium-rich fenites are characterized by the presence of alkali feldspar, as well as sodic-potassic amphibole or sodic pyroxene, and potassium-rich fenites contain potassium feldspar (Le Bas, 2008). Intermediate fenites, which are rich in both Na and K, are common. Mineralogy, mineral compositions, and textures can be complex in fenites because of heterogeneity in the original lithologies, variable proximity to the intrusion, variations in the fluid chemistry, and overprinting by multiple hydrothermal events. Common minerals resulting from fenitization include aegirine, alkali-amphibole, nepheline, phlogopite, alkali-feldspar, and carbonates.

Ore and Gangue Character: Mineralogy, Texture, Zonations

General reviews of carbonatite-hosted REE mineralization include those by Neary and Highly (1984), Mariano (1989a, b), Richardson and Birkett (1996), Castor and Hedrick (2006), Castor (2008b), Long et al. (2010), Millonig and Groat (2013), and Verplanck et al. (2014). Overall, the ore mineralogy of carbonatite REE deposits is complex. The principal REE-bearing minerals associated with carbonatites are fluorocarbonates (bastnäsite, parisite, and synchysite), hydrated carbonates (ancylite), and phosphates (monazite; Zaitsev et al., 1998), with other REE-bearing phases, such as apatite, britholite, and burbankite, being less common (Table 1). Because most carbonatites experience a complex petrogenetic evolution, including hydrothermal overprinting of primary magmatic phases, their mineralogical and textural characteristics can be quite varied and intricate. For this reason, limited data are available with regards to paragenesis and zoning patterns. As described in the deposit section, bastnäsite is the primary REE ore mineral for the all the magmatic deposits currently being mined, including Mountain Pass, Bayan Obo, Maoniuping, and Dalucao. Bastnäsite consists of 75 wt % RE_2O_3, with La, Ce, and Nd as the primary REEs in this mineral.

The Mountain Pass deposit is the largest REE deposit in the United States and appears to be a rare example of primary magmatic REE mineralization, as we discuss in the section describing the Mountain Pass deposit. That conclusion is based on textural evidence that suggests bastnäsite and parisite cocrystallized with primary calcite and barite.

A second example of REE carbonatite mineralization of primary magmatic origin occurs in the Khanneshin carbonatite complex in southern Afghanistan. Tucker et al. (2012) described two types of LREE mineralization, with their "type 2 mineralization" being present as mineralized dikes containing primary magmatic LREE mineralization. Euhedral to subhedral khanneshite, monazite, and fluorite in these dikes are interpreted as evidence for primary magmatic mineralization.

More typically, carbonatite-hosted deposits are characterized by REE mineralization derived from magmatic-hydrothermal processes, in which common, hypogene REE-bearing ore minerals include bastnäsite, parisite, ancylite, synchysite, and monazite. According to Mariano (1989a), bastnäsite of hydrothermal origin typically occurs as fine-grained, fibrous or platy masses (Fig. 17) in vugs, microfractures, and veinlets, commonly associated with quartz, fluorite, strontianite, barite, and hematite.

Ancylite is described as a minor or trace phase in unweathered carbonatites in the Kola region (Russia) and at Araxá and Catalão I (Brazil; Mariano, 1989a). Ancylite has never been described as a primary magmatic mineral; thus, ancylite may be a useful indicator of hydrothermal ore formation (Wall and Zaitsev, 2004). At Bear Lodge, ancylite is a predominant REE-bearing phase in the unoxidized zone, where it is commonly intergrown with strontianite and barite in hexagonal pseudomorphs. These pseudomorphs are likely replacements of an earlier hexagonal mineral (Mariano, 1989a). Similarly, Zaitsev et al. (1998) described ancylite in the Khibina carbonatites of the Kola Peninsula, where ancylite occurs in an alteration assemblage with strontianite replacing the hexagonal crystal form of burbankite. The chondrite-normalized REE patterns of ancylite from both Khibina and Bear Lodge display strong LREE enrichment (Zaitsev et al., 1998; Moore et al., 2015).

As is the case for ancylite, synchysite in the Khibina carbonatite is present as a pseudomorph of burbankite, or as fine-grained syntaxial intergowths with parisite (Zaitsev et al., 1998). The authors described synchysite as forming

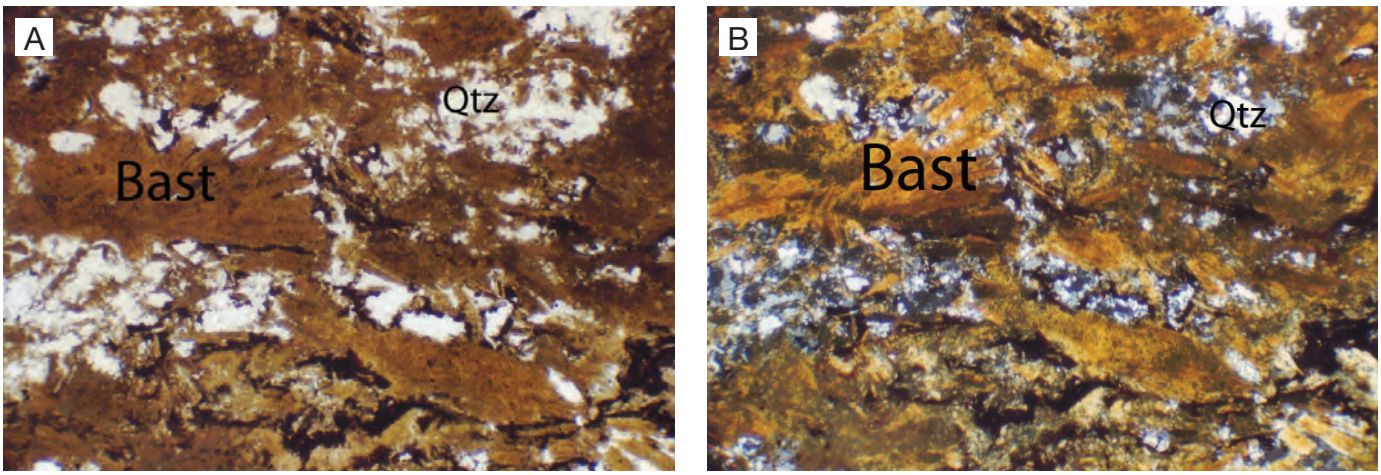

Fig. 17A and B. Cross-polarized light photomicrographs of hydrothermal bastnäsite (Bast, yellow-brown, radiating fan-shaped clusters) with quartz (Qtz, white), Dong Pao carbonatite, North Vietnam. Horizontal dimension ≈1.76 mm.

porous aggregates, which are enriched in LREEs. Monazite is observed in many REE mineral deposits and can form as a primary magmatic (Mountain Pass), hydrothermal (Bear Lodge, Kola carbonatites, and Dalucao), or supergene (Araxá, Catalão, and Mount Weld) phase.

Apatite can be an important REE-bearing mineral phase, such as at Mushgai Khudag where the modal abundance of apatite can be as high as 85 vol %. Another example is the coarse-grained fluorapatite at Nolans Bore (Australia), where it occurs within veins with allanite, kaolinite, and other clays. Nolans Bore was not described in this review paper because carbonatites have not been identified at this deposit, although the geochemistry is consistent with carbonatite-related REE mineralization.

The primary REE ore mineral in lateritic deposits associated with carbonatites is supergene monazite, and the primary Nb ore minerals are bariopyrochlore and pyrochlore. At Mount Weld and Araxá, supergene monazite is fine grained and can occur as polycrystalline aggregates or as pseudomorphs after apatite. At Araxá, the bariopyrochlore is a residual mineral from hydrothermal alteration of primary pyrochlore in fresh carbonatite and not a supergene phase.

Gangue Mineralogy

The most common hypogene gangue minerals in carbonatites include calcite, dolomite, barite, ankerite, fluorite, fluorapatite, aegirine-augite, phlogopite, strontianite, quartz, magnetite, and hematite. The most common U- and Th-rich phases in carbonatites are accessory minerals, such as perovskite, pyrochlore, monazite, and thorite. As discussed above, the Sulphide Queen orebody at Mountain Pass is interpreted as a rare example of a carbonatitic REE deposit of magmatic origin. Calcite, dolomite, barite, celestine, strontianite, and secondary quartz are the dominant gangue minerals in this deposit.

Mineralization at the Bayan Obo deposit is hosted in a massive dolomitic marble. Xu et al. (2010) summarized the ore mineralogy and stated that fluorite, apatite, and aegirine are the primary gangue minerals. The primary gangue mineral associated with REE mineralization at the Maoniuping deposit is coarse-grained calcite, which is accompanied by subordinate fluorite biotite, barite, microcline, aegirine, arfvedsonite, and apatite (Xu et al., 2008). Gangue minerals within the Dalucao deposit include calcite and subordinate microcline, quartz, arfvedsonite, barium-rich celestine, strontiobarite, fluorite, aegirine, apatite, and sulfide minerals (Xu et al., 2008). Accessory minerals in the Mianning carbonatites include maoniupingite, thorite, and rare xenotime (Mariano, 1994).

Many carbonatites contain variable, but minor amounts of sulfide gangue minerals. Little attention is paid to the nature of the sulfide minerals because they are generally not considered an economic resource. The one exception to this is the Palabora deposit in South Africa, where Cu mineralization is hosted in a carbonatite pipe. Olson et al. (1954) reported pyrite and galena from the Sulfide Queen carbonatite at Mountain Pass; Moore et al. (2015) reported pyrite and pyrrhotite in the unoxidized zone at Bear Lodge; and Heinrich (1966) reported pyrite, sphalerite, galena, and molybdenite associated with late-stage carbonatization at Kangankunde.

Geochemistry

Elemental variations

By definition, carbonatite mineralogy is dominated by carbonate mineral phases, such that the major element chemistry is characterized by high Ca and abundant carbonate, and by low SiO_2 concentrations compared to most igneous rocks. In addition, carbonatites can be enriched to varying degrees in Fe, Mg, and high field strength elements (HFSEs; Zr, Nb, Hf, REEs, Th, U, and Ta), Ba, Sr, P, and F. Interpretation of the chemistry of carbonatite rock samples is problematic compared to many silicate igneous rocks, because of uncertainty as to whether the samples directly represent magmatic compositions. In silicate systems, numerous examples of preserved glasses can be used to identify quenched magmas and many lavas represent near-magmatic compositions. Few carbonatite lavas have been discovered, and those that have contain no glasses. Furthermore, the low viscosity of carbonatite magmas promotes the separation of crystals from magma, such that many carbonatite samples are likely to be cumulates; thus, the bulk composition would not be representative of the parental magma composition. Finally, most carbonatites display evidence of hydrothermal overprinting and subsolidus recrystallization. Although these features make the interpretation of carbonatite chemistry problematic, it is still possible to use the chemistry to describe general characteristics of different carbonatites.

Woolley and Kempe (1989) compiled published mineralogical, compositional, and occurrence data on carbonatite, and calculated the median chemical compositions of calciocarbonatite, magnesiocarbonatite, and ferrocarbonatite (Table 3). This is a good summary of the nonmineralized carbonatites because most of these published carbonatite studies were for nonmineralized carbonatites. For this review, however, we compiled data from other workers in the Bayan Obo and Mianning districts, as well as our own samples from a suite of deposits including Mountain Pass, United States; Bear Lodge, United States; Kangankunde, Malawi; Mount Weld, Australia; Araxá, Brazil; Adiounedj, Mali; and Mushgai Khudag, Mongolia (Table 3).

Woolley and Kempe (1989) devised a ternary plot with CaO, MgO, and FeO + Fe_2O_3 + MnO to display major element data for carbonatites, such that calciocarbonatites have >80% CaO, magnesiocarbonatites have MgO > FeO + Fe_2O_3 + Mn, and ferrocarbonatites have FeO + Fe_2O_3 + MnO > MgO (Fig. 18). We display data (Fig. 18) from mineralized REE and Nb deposits (Bayan Obo, Mianning district, Mountain Pass, Mount Weld, and Araxá), as well as those data for average calciocarbonatite, magnesiocarbonatite, and ferrocarbonatite from Woolley and Kempe (1989). The REE mineralized carbonatites plot in all three fields, with Mianning samples plotting near the CaO end member, Mountain Pass within all three fields, and Bayan Obo samples within the ferrocarbonatite field. These results are consistent with deposit descriptions. The primary commodity at Bayan Obo is Fe and the REEs are by-products. The deposits near Mianning (Maonioping and Dalucao) are associated with calcite carbonatites (Yang and Woolley, 2006; Xu et al., 2010). Carbonatite samples from Mountain Pass plot in all three fields, similar to results presented in Castor and Nason (2004), with the

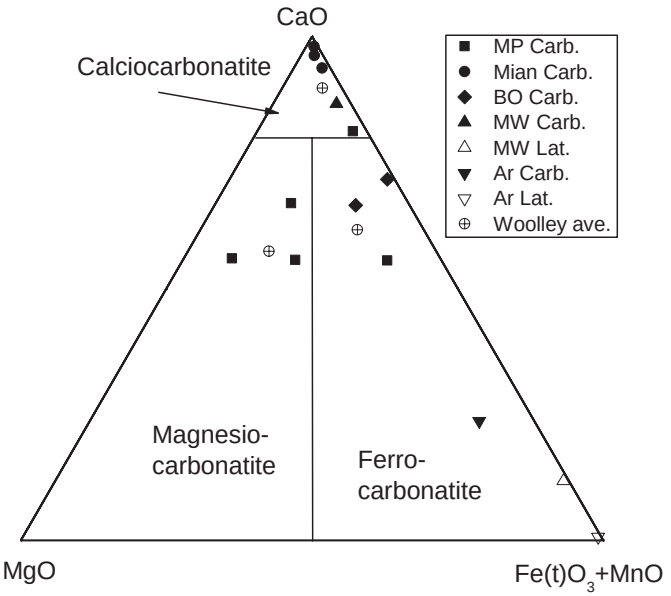

Fig. 18. Ternary diagram of major element concentration data for actively mined carbonatites including Mountain Pass, Bayan Obo, Mianning, Mount Weld, and Araxá. Bayan Obo (BO) data from Lai et al. (2012), Mianning deposits (Mian) data from Lizhuang carbonatite samples from Huo et al. (2006), and other data this study with carb = carbonatite, lat. = laterite, MW = Mount Weld, Ar = Araxá. Field boundaries and average values of ferro-, calcio-, and magnesio-carbonatite (⊕) from Woolley and Kempe (1989).

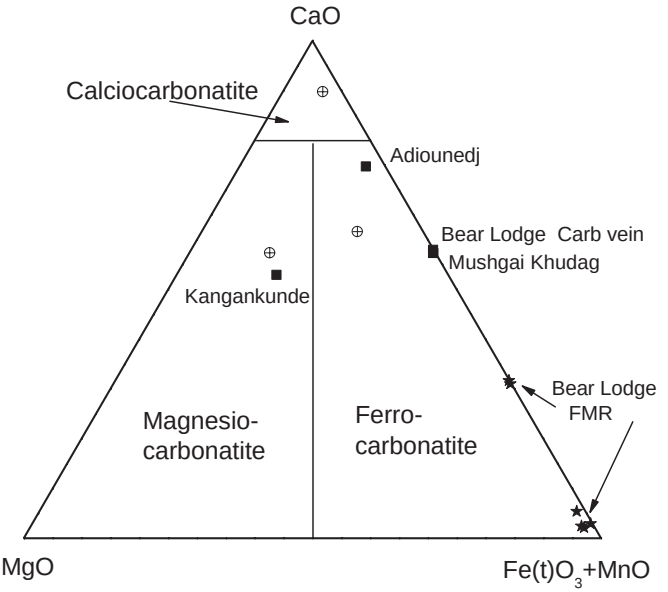

Fig. 19. Ternary diagram of major element concentration data for other carbonatites from this study. Field boundaries and average values of ferro-, calcio-, and magnesio-carbonatite (⊕) from Woolley and Kempe (1989).

calcite-rich carbonatite plotting in the calicocarbonatite field and the dolomite-rich samples in the magnesiocarbonatite field. Carbonatite samples underlying the Mount Weld and Araxá laterite-related deposits plot within the calciocarbonatite and ferrocarbonatite fields, respectively, and their corresponding laterites plot near the FeO + Fe_2O_3 + MnO end member, consistent with the breakdown of primary calcium-bearing minerals and the retention of Fe in the weathering products.

Figure 19 displays major element variations from other REE mineralized carbonatites. Samples plot within the magnesiocarbonatite and ferrocarbonatite fields. The Kangankunde sample plots within the magnesiocarbonatite field, and Adiounedj, Mushgai Khudag, and Bear Lodge samples plot within the ferrocarbonatite field. The unoxidized Bear Lodge ancylite-fluorite vein plots between the CaO and FeO + Fe_2O_3 + MnO end members, and the FMR vein samples plot toward the FeO + Fe_2O_3 + MnO end member. The matrix carbonate in the FMR zone has been leached, and thus these samples plot toward the FeO + Fe_2O_3 + MnO end member.

Chondrite-normalized REE diagrams for economic REE carbonatites display extreme LREE abundances (Fig. 2), with La approaching 10^5 times chondrite or approximately 30,000 ppm. Features that are typical of carbonatite chondrite-normalized REE patterns include LREE enrichments, steep negative slopes, and no negative Ce or Eu anomalies. Samples from various deposits have a range in REE abundances that likely reflects the relative proportions of ore and gauge minerals in the sample. One way to evaluate the slope of the chondrite-normalized REE pattern is to plot La_{cn} versus La_{cn}/Yb_{cn} (with cn = chondrite-normalized; Fig. 20). The samples from deposits being actively mined generally display steeper slopes compared to other mineralized carbonatites, in part because the LREE abundances are slightly to substantially greater (Fig. 20). Rare earth element patterns for carbonatites that are mineralized, but not currently economic, also display high REE abundances, particularly for the LREEs, compared to other rocks including many carbonatites (Fig. 21). Some of the presently uneconomic deposits (Mushgai Khudag and Adiounedj) have HREE abundances significantly higher than the mined carbonatites (Fig. 20).

Based on the samples analyzed in this study, the REE abundances for the underlying carbonatites at Mount Weld and Araxá are more similar to average carbonatites compared to other mineralized carbonatites (Table 3). Nevertheless, the laterite ore at Mount Weld displays extreme REE enrichment comparable to the highest abundances from the mined carbonatites (Figs. 2, 9). Rare earth element enrichment in the laterite sample from Araxá does not reach these extreme concentrations, but the primary commodity at Araxá is Nb, not REEs.

Carbonatites can be enriched in other elements, which include Sr, Ba, U, Th, Nb, Ta, P, and F. Figure 22 displays variations in Sr and Ba for mined and other mineralized carbonatites from this study. All samples from mined carbonatites (Bayan Obo, Mountain Pass, and the Mianning deposits) have Ba abundances greater than 10,000 ppm, with some greater than 100,000 ppm. The Mountain Pass carbonatite samples have the highest Ba abundances. Furthermore, the Sr abundances of these mine-related samples (Bayan Obo, Mountain Pass, and the Mianning deposits) show covariance with the Ba abundances. The Sr abundances of the mineralized samples from unmined deposits are similar to those of the mined samples. The Bear Lodge vein sample and the Kangankunde sample contain >100,000 ppm Sr. Strontium has a similar ionic radius and charge to Ca, such that these two elements tend to behave similarly. For this suite of samples, Sr abundances

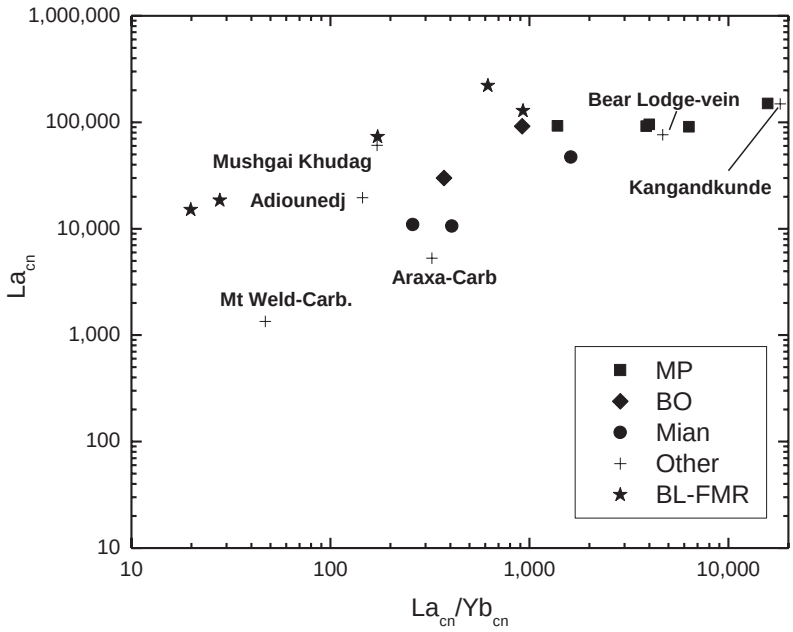

Fig. 20. Diagram displaying variation in chondrite-normalized La concentration (La_{cn}) in relationship to chondrite-normalized ratio of La over Yb (La_{cn}/Yb_{cn}) for mineralized carbonatites. Bayan Obo (BO) data from Lai et al. (2012), Mianning deposits (Mian) data from Lizhuang carbonatite samples from Huo et al. (2006), and other data this study. Concentrations normalized to C1 chondrite values from Anders and Ebihara (1982).

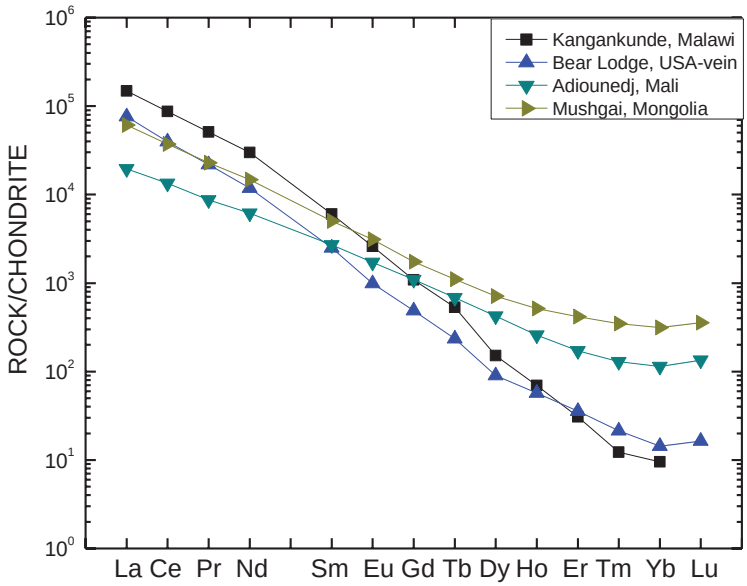

Fig. 21. Chondrite-normalized rare earth element diagram for selected carbonatite deposits (this study). Concentrations normalized to C1 chondrite values from Anders and Ebihara (1982).

do not covary with those of Ca (Fig. 23), consistent with the observed presence of primary Sr mineral phases. That is to say, Sr is a primary element and not simply a minor element substituting into Ca minerals.

Two other elements of interest are F and P, because these elements are major constituents in apatite, monazite, and fluorocarbonates (bastnäsite, parisite, and synchysite), all potentially important REE mineral phases, and fluorite (CaF_2) is present in the REE ore zones of some deposits, including Bayan Obo and the Mianning district. In addition, low-temperature geochemistry studies demonstrate that P and F are important ligands controlling the disposition and transport of REEs (Wood, 2003). Regrettably, published data from Bayan Obo and Mianning do not contain F analyses. Abundances of F and P can be quite variable in carbonatites (Fig. 24). Note that Mountain Pass samples are relatively low in P. The two samples with the highest F abundances (Mushgai Khudag and Adiounedj) have the highest HREE abundances, and Mushgai Khudag also has the highest P concentrations.

The unweathered carbonatite core sample from beneath the Araxá laterite deposit is strongly enriched in Nb (24,100 ppm), and the lateritic ore sample contains 39,200 ppm Nb (5.61 wt % Nb_2O_5). These samples have substantially greater Nb abundances than our other analyzed samples (Table 3), with all other samples containing <1,000 ppm Nb and most <100 ppm Nb. The average grade of ore mined at the Araxá deposit is 2.5 to 3.0 wt % Nb_2O_5, with grades locally as high as 8 wt % Nb_2O_5.

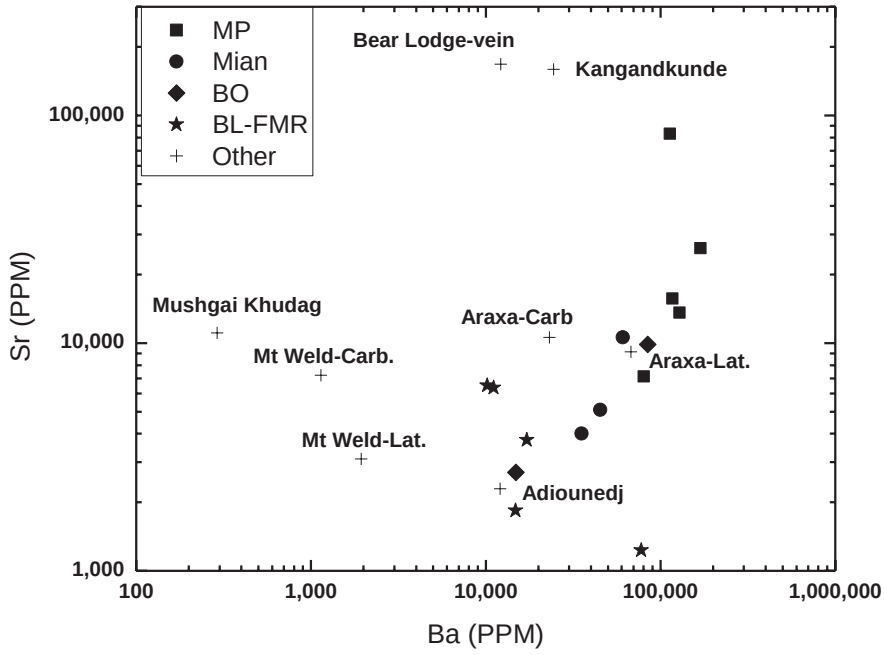

Fig. 22. Diagram displaying variation in strontium (Sr) and barium (Ba) in mineralized carbonatites. Bayan Obo (BO) data from Lai et al. (2012), Mianning deposits (Mian) data from Lizhuang carbonatite samples from Huo et al. (2006), and other data this study.

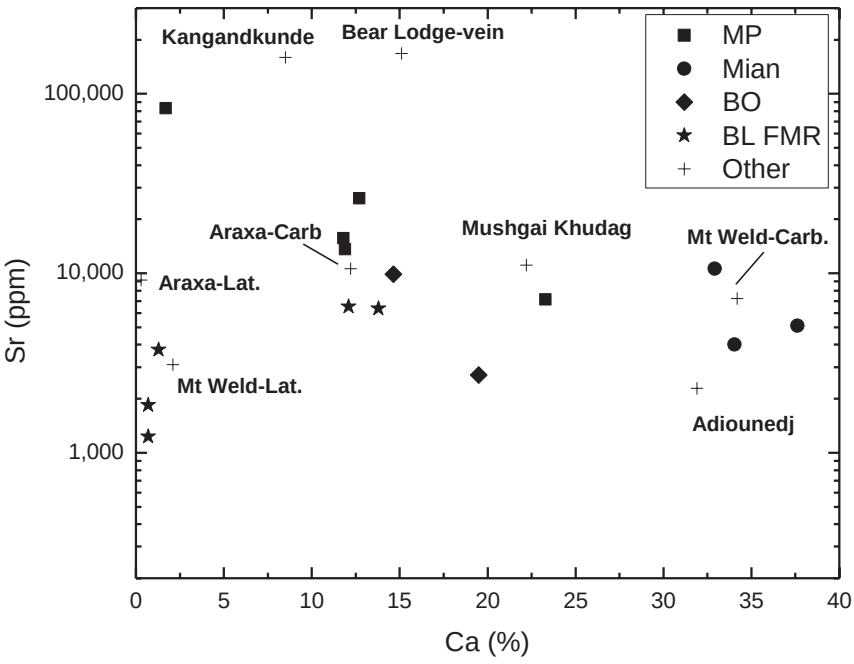

Fig. 23. Diagram displaying variation in strontium (Sr) and calcium (Ca) in mineralized carbonatites. Bayan Obo (BO) data from Lai et al. (2012), Mianning deposits (Mian) data from Lizhuang carbonatite samples from Huo et al. (2006), and other data this study.

Isotopic constraints

Most isotopic studies of carbonatites have focused on constraining the origin of carbonatitic magmas, with only a few recent studies dedicated to the nature of mineralization. A summary of stable isotope studies (O, H, C, and S) of carbonatites is presented in Deines (1989). Carbon isotopes can be used to differentiate between sedimentary carbonates and carbonatites because carbonate sedimentary rocks have a carbon isotope composition similar to sea water ($\delta^{13}C$ –2 to +2‰) and carbonatites generally have lower values ($\delta^{13}C$ –8 to –2‰; Deines, 1989). Most carbonatites have a C isotope composition that is consistent with mantle derivation and magmatic origin. Andersen (1987), Pearce et al. (1997), Demény et al. (2004), and Drüppel et al. (2005) determined the carbon and oxygen isotope composition of samples from the Fen complex (Norway), the Grønnedal-Ika complex (Greenland), the Kola Alkaline Provence (Russia), and Swartbooisdrif (Namibia), respectively, and all concluded that the parental magmas were derived from the mantle.

Recent studies at Bayan Obo were undertaken to gain insight into the origin of the dolomite and carbonatite units. Yang et al. (2009) report $\delta^{13}C$ and $\delta^{18}O$ of carbonatite dikes and H8 dolomite samples from Bayan Obo and determined that isotopic composition of the dolomite samples generally

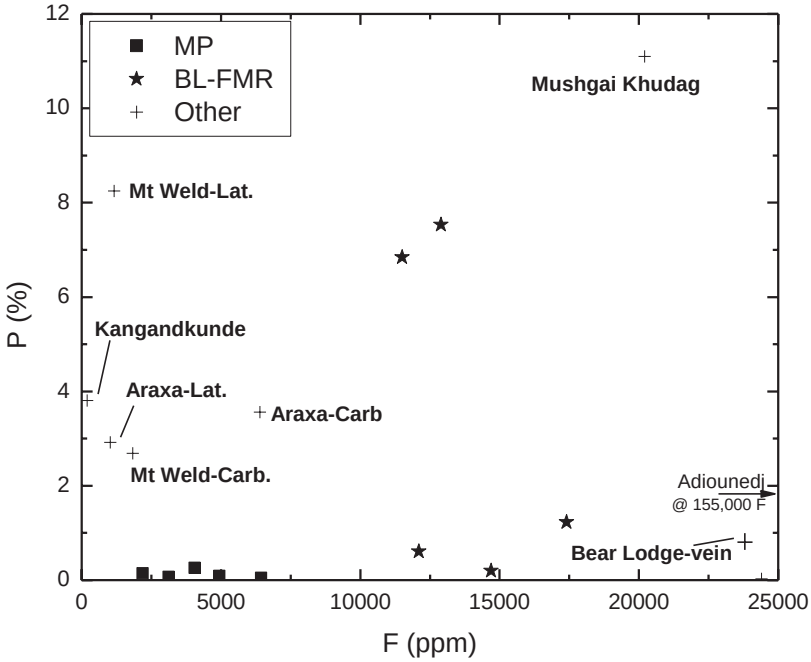

Fig. 24. Diagram displaying the variation of phosphorous (P) and fluorine (F) in mineralized carbonatites. Bayan Obo (BO) data from Lai et al. (2012), Mianning deposits (Mian) data from Lizhuang carbonatite samples from Huo et al. (2006), and other data this study.

fall between the mantle and marine end members. Based on these isotopic data, they concluded that the dolomite is probably of marine origin, and the mineralization is produced by metasomatism by mantle-derived fluids. These mantle-derived fluids were likely associated with the nearby carbonatite dikes and were thus responsible for the REE mineralization in the H8 dolomite (Yang et al., 2009).

Oxygen isotope compositions of minerals in REE mineralized carbonatites may be useful to evaluate the role of meteoric water in the origin of mineralization in carbonatites that display metasomatic overprinting. Isotopic studies at the Fen complex by Andersen (1986, 1987) concluded that the parental magmas at the Fen were derived from mantle sources, but postmagmatic oxygen and carbon isotope reequilibration resulted from groundwater-derived hydrothermal solutions.

As is the case for the stable isotope studies, the vast majority of radiogenic isotope studies (Nd, Sr, and Pb) of carbonatites are focused on the origin of carbonatites and not ore genesis. Bell and Blenkinsop (1989) and Bell (1998) summarized much of the radiogenic isotope work conducted to determine the origin of carbonatites and associated alkaline rocks. The radiogenic isotope data document that the carbonatites are of mantle origin, but the range in isotopic data suggests that the subcontinental upper mantle is inhomogeneous (Bell and Blenkinsop, 1989).

We determined the Nd and Sr isotope compositions of a suite of mineralized carbonatites (Table 4). Our data are similar to previously published data from the same localities. For example, Nelsen et al. (1988) reported ε_{Ndi} and $^{87}Sr/^{86}Sr_i$ values of 3.1 and 0.7031, respectively, for a carbonatite sample from Kangankunde, Malawi, whereas we measured ε_{Ndi} and $^{87}Sr/^{86}Sr_i$ values of 3.26 and 0.703097 for a carbonatite sample from the same locality. Nelsen et al. (1988) also reporte ε_{Ndi} (0.3 and 0.4) and $^{87}Sr/^{86}Sr_i$ (0.7020 and 0.7020) values for two carbonatite samples from Mount Weld, and we report similar ε_{Ndi} (0.66) and $^{87}Sr/^{86}Sr_i$ (0.702056) values for a carbonatite sample from Mount Weld.

Our results, together with the data set compiled by Bell (1998) for primarily nonmineralized carbonatites, are shown in Figure 25. Our new data display a large range in $^{87}Sr/^{86}Sr_i$ from 0.702056 to 0.706365, and ε_{Ndi}, from +3.26 to –3.73, with the exclusion of the two laterite samples. The carbonatite samples have a large range in age as well, from approximately 51.5 Ma (Bear Lodge) to 2025 Ma (Mount Weld), and are located in five continents.

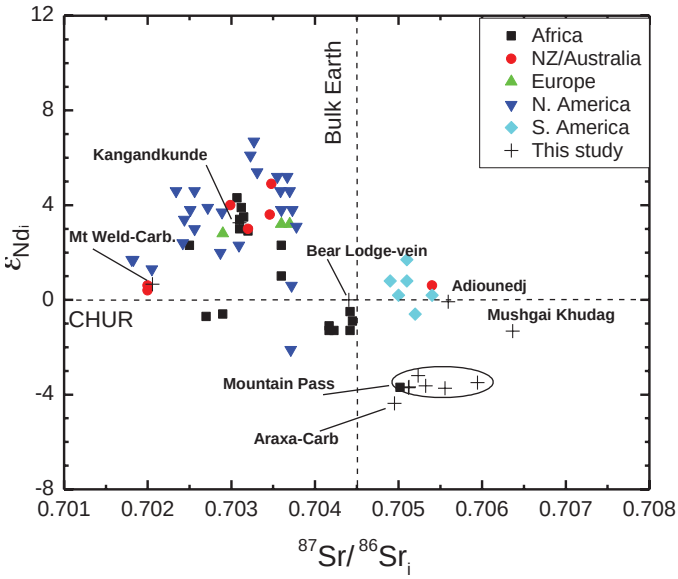

Fig. 25. Variation in Nd isotope composition in relationship to Sr isotope composition of carbonatites. All data calculated as initial values. Data from various continents from Bell and Blenkinsop (1989), other data from this study (Table 4).

These samples clearly demonstrate that mineralized carbonatites have a mantle signature, and that the REEs are derived from a mantle reservoir. As discussed previously, petrologists are not in agreement on the processes responsible for carbonatite genesis. Radiogenic isotopic data from carbonatites may help constrain the source of the REEs, because of the Nd isotope systematics, but these data do not provide adequate constraints on the evolution of the magma from the mantle source, except to preclude assimilation of substantial crustal material.

Fluid inclusion studies

Fluid inclusion studies document that a volatile alkali-rich fluid phase can become saturated and separate from the magma at some point during magmatic evolution. Gittens et al. (1990), Rankin (2005), and Veksler and Lentz (2006) summarized the state of the knowledge, describing detailed fluid inclusion studies from carbonatites in North America, Asia, and Africa. Fluids released from carbonatite magmas tend to be Na-K-Cl carbonate/bicarbonate brines, with K to Na weight ratios of 0.1 to 0.6 (Rankin, 2005). Furthermore, experimental work by Keppler (2003) showed that alkali elements are preferentially partitioned into water within the carbonatite melts, providing the appropriate constituents to fenitize wall rock. Xie et al. (2009) undertook a fluid inclusion study of the Maoniuping deposit and documented a complex melt-fluid history. Using melt and fluid inclusions in quartz and fluorite, they concluded that the initial ore-forming fluid was high temperature (600°–850°C), high pressure (>350 MPa), sulfate rich, and contained K, Na, Ca, Ba, Sr, and REEs. The initial fluid evolved to a moderate temperature (227°–453°C), CO_2-rich fluid, and then to a lower temperature (<200°C), aqueous fluid. The REE mineralization was determined to precipitate from the moderate temperature, CO_2-rich fluid (Xie et al., 2009).

Bühn and Rankin (1999) looked in detail at fluid inclusions trapped in the quartzite country rock of the Kalkfield carbonatite complex, Namibia. Fluid types included a low-density CO_2 fluid and a Na-, K-, Ca-, Cl-, and bicarbonate-bearing aqueous brine (Bühn and Rankin, 1999). The chondrite-normalized REE patterns of the trapped fluids display LREE enrichment. Bühn and Rankin (1999) concluded that virtually all the alkali metals and chloride, as well as significant F, Th, Ti, and U, preferentially partitioned into a mixed alkali-carbonic fluid.

Ore Genesis

Magmatic and metasomatic processes

Summarizing the genesis of critical element deposits associated with carbonatites is a difficult task, because many aspects are poorly understood. To start with, petrologists are not in agreement with the origin of carbonatitic magmas. Neodymium isotope studies demonstrate the Nd has a mantle signature such that the source of the REEs found in carbonatite deposits is the mantle. Experimental work shows that carbonatites can be produced as low-percentage partial melts in the mantle (Wallace and Green, 1988; Dalton and Wood, 1993; Sweeney, 1994), and that the concentration of REEs to form mineral deposits is a function of sufficient REE abundance in the source magma and a mechanism that leads to ore-grade enrichments of the REEs. Other studies demonstrate that carbonatitic magma can form from alkaline magmas. As the isotopic data point to a mantle source, the initial alkaline magma must be derived from the mantle, and the REEs must be present in sufficient quantities to eventually reach ore-grade enrichment. Fractional crystallization and liquid immiscibility are two processes put forth to generate carbonatite magmas from alkaline magmas. In either scenario, a substantial fraction of the REEs and Nb must partition into the carbonatitic magma. In the case of liquid immiscibility, these elements need to become preferentially enriched in the carbonatite magma relative to the silicate magma. Experimental work by Veksler et al. (2012) evaluated the partitioning of REEs and HFSEs between silicate magma and immiscible carbonatite melts. They demonstrate that these elements do not significantly partition into the immiscible carbonatite melts when moderate quantities of P, F, and Cl are present. These results point to extensive fractional crystallization of a carbonatite-silicate magma as probably being the process for forming ore-grade, rare-metal carbonatite deposits (Veksler et al., 2012).

Irrespective of which process or processes are responsible for the generation of carbonatitic magma, a carbonatite magma is generated at some point, and high concentrations of the elements of interest are needed in this magma to form an ore deposit. Furthermore, carbonatitic magmas can be enriched in volatiles (CO_2, H_2O, Cl, F, S, and P), alkalis, large ion lithophile elements (LILE), and HFSE. The evolution of the magma is dependent, not only on variations in pressure and temperature, but also on the magma composition, crystal chemistry and structure, and kinetics of crystal growth. In general, early crystallizing phases include olivine, calcite, and magnetite, as well as apatite if sufficient P is present. As is the case with Mountain Pass, primary REE-bearing mineral phases can crystallize from the magma in sufficient modal abundances to reach ore-grade REE concentrations. Other deposits might have had primary REE phases that were subsequently overprinted and upgraded by later magmatic hydrothermal fluids. Examples of this include burbankite at Bear Lodge (United States) and Khibina (Russia; Fig. 15). Monazite is another REE-rich phase that can also be primary magmatic in origin, as is the case at Mountain Pass and Kangankunde (Figs. 7, 16).

Although primary REE mineral phases can crystallize directly from the carbonatitic magma, it appears more common for the residual magma to become enriched in REEs, volatiles, and alkalis. Wall and Mariano (1996) noted that REE mineralization tends to be best developed in units emplaced late in the magmatic sequence, typically ferrocarbonates. As crystallization progresses, the residual magma becomes enriched in H_2O until it becomes saturated and a fluid phase exsolves. Keppler (2003) undertook a series of experiments to evaluate water solubility in carbonatite magmas at 900°C and 0.25 to 2.25 kbars. At 1 kbar and an approximate depth of 3 km, the water solubility of the carbonatite magma is approximately 10%, solubility that is two to three times greater than that of silicate magmas at similar pressures. The point where saturation is reached depends on pressure, temperature, H_2O content, and magma composition (Gittens, 1989). The extent

to which the fluid removes alkali elements and REEs from the magma is due to the partitioning of ligands, such as Cl and F, from the magma to the fluid phase. Fluid inclusion studies are consistent with this scenario (e.g., Morogan and Lindblom, 1995). The common presence of fenitized wall rock supports the concept of the separation of alkali-rich fluids from the evolving carbonatite magma. In addition, many carbonatite REE deposits contain breccias, which may result from the build-up and explosive release of volatile-rich fluids from the magmatic system.

Although clear evidence for late-stage metasomatic fluids exists for many carbonatites, the role of these fluids in ore deposit genesis is poorly understood. Many factors influence the fluid composition, and hence the role late-stage fluids play in REE transport and deposition. The initial magma composition and petrogenetic evolutionary path control the composition of the crystallizing phases, and thus the composition of the residual melt. The exsolution of the fluid phase from the melt is dependent not only on the melt composition, but also on pressure and temperature variations. Fluid inclusion studies provide general characteristics of fluid phases exsolved from carbonatite melts, and document the presence of H_2O, CO_2, alkalis, and ligands, including F^-, OH^-, Cl^-, SO_4^{2-}, CO_3^{2-}, and PO_4^{2-}. These ligands play a key role in the disposition of REEs in magmatic and aqueous systems. Rare earth elements are primarily trivalent with relatively small ionic radii, and thus behave as "hard ions" in the Pearson classification (Pearson, 1963). These "hard ions" preferentially bond with "hard ligands" including monovalent ligands (F^-, OH, and Cl^-) and divalent ligands SO_4^{2-}, CO_3^{2-}, and PO_4^{2-}. Complexation of REEs with various ligands influences both the disposition and transport of REEs as a group. It can also lead to fractionation of the REEs, because the strength of the bonds can vary across the REEs owing to the minor, but systematic, decrease in ionic radii with increasing mass (Wood, 2003).

The disposition of the REEs associated with an exsolved fluid is not well understood and is likely variable. These fluids have the potential to transport REEs, precipitate REE phases, and remobilize REEs from earlier formed phases. The occurrence of metasomatically recrystallized primary REE phases, for example burbankite at Bear Lodge and Khibina, documents that late-stage fluids can alter primary REE distributions. The stability of REE complexes within aqueous fluids influences the transport and disposition of the REEs, and it can vary with temperature, pressures, pH, and solution chemistry. For example, if the REEs are transported as F complexes and an F-rich mineral precipitates, then the REEs are likely to be much less stable in solution. Similarly, if the REEs are transported as complexes with PO_4^{2-}, then a P-rich mineral precipitates. Another potential mechanism to dramatically alter the composition of the exsolved fluid is interaction with a second fluid, such as groundwater.

Coupled comprehensive petrologic studies and experimental work are needed to better understand the role late-stage, predominantly magmatic hydrothermal fluids play in the formation of carbonatite-related REE deposits. With the increased interest in these deposits, many studies are currently underway and are likely to provide a strong framework for unraveling these complex processes.

Enrichment by weathering processes

Near-surface enrichment of REEs above a plutonic rock substrate can be an important step in the development of economic REE deposits. At present, the mining of laterites in southeastern China produces much of the world's supply of HREEs. These deposits are associated with weathered granites, not carbonatites (Sanematsu and Watanabe, 2016). Examples of significant lateritic deposits of LREEs associated with carbonatites include Mount Weld (Australia), Araxá (Brazil), Mrima Hill (Kenya), and Zandkopsdrift (South Africa). Laterite is a term used to describe highly weathered subsoils that form in tropical or subtropical settings. In the weathering environment, some primary REE-bearing phases can be stable and lead to the formation of REE placer deposits (Sengupta and Van Gosen, 2016). Other minerals containing REEs can more easily breakdown as a consequence of chemical weathering. As lateritic weathering progresses, the REEs can be released even from the more stable phases (Bao and Zhoa, 2008). In the lateritic zone, REEs can be present within: (1) primary igneous minerals, such as apatite, monazite, xenotime, and zircon; (2) secondary minerals that include apatite, monazite, cerianite, churchite, florencite, gorceixite, plumbogummite group (part of the crandallite subgroup), xenotime, and rhabdophane; and (3) clays and iron and aluminum oxyhydroxides (Mariano, 1984, 1989a, Lottermoser, 1990; Wu et al., 1990; Morteani and Preinfalk, 1996; Chi and Tian, 2008; Bao and Zhoa, 2008). Secondary REE minerals formed in this environment are commonly fine grained and occur as polycrystalline aggregates (Mariano, 1989a).

Laterites form from the intense weathering of the underlying bedrock. Factors controlling the degree of laterization include climate, topography, length of time exposed in a stable environment, and bedrock composition (e.g., Marsh et al., 2013). Optimal conditions for the formation of substantial lateritic zones include a topography that allows the entrapment of newly formed residual minerals and a tectonically stable region so that denudation rates are low and weathering profiles preserved. Laterization is driven by the interaction between infiltrating groundwater and the bedrock it contacts. Physical properties, such as cleavage and porosity, are important because they control the amount of mineral surfaces available for interaction. The properties of aqueous solutions, such as temperature, acidity, redox potential, and dissolved constituents, affect the type and rate of chemical reactions that will occur. The primary mineralogy of the rock being weathered plays a role both in the rate of weathering and influences the composition of the aqueous phase, which in turn can control the formation of secondary phases. In general, Ca, Mg, K, and Na partition into the aqueous phase and are leached from the system. In contrast, Fe and often Al are quite reactive, and these elements are sequestered by secondary phases, such as goethite, hematite, gibbsite, and various clay minerals. Bao and Zhao (2008) showed that the concentrations of Ca, Mg, K, and Na in the solid phase decrease as the degree of weathering increases, whereas Al is enriched during the process. Supergene elemental enrichment in laterites can occur via the physical and chemical breakdown of mineral phases where (1) some constituents are transported out of the weathering zone, thus leading to an increase in concentration of the remaining

constituents, and (2) where some constituents are further concentrated within the weathering zone and sequestered by secondary phases.

In most carbonatites, the REEs are hosted in calcite, dolomite, and apatite, and these minerals are quite susceptible to dissolution in the lateritic weathering environment. Oxygenated groundwater in the near-surface environment can be slightly acidic and, if it interacts with sulfide minerals, then the waters can become more acidic. Acidic water interacts with primary minerals, such as calcite, dolomite, and apatite, to mobilize Ca and Mg and liberate REEs. Other elements, such as Al, Fe, P, K, and Na, are also released from these and other phases. Mobility of the REEs in this environment is quite complex owing to variations in solution chemistries and properties. Whether the REEs sorb to clays or form secondary phases depends on the pH and Eh of the solution, the availability of ligands for complexation, and the mineral saturation state. In this environment, dissolved ligands likely available to complex REEs include phosphate, carbonate, fluoride, and chloride. Because of these complexities, it is difficult to make general statements concerning the mineralogy of lateritic REE deposits.

At Mount Weld, the underlying carbonatite is only moderately enriched in REEs, and the REEs are hosted within calcite, dolomite, and apatite. Primary REE minerals are absent in fresh unweathered carbonatite drill core. Detailed mineralogical analyses of the Mount Weld laterite show that the LREEs are primarily sequestered by secondary monazite, rhabdophane, and the plumbogummite group (Mariano, 1984; Lottermoser, 1990). The HREEs were mobilized deeper in the weathering profile and became adsorbed into noncrystalline phases and incorporated into churchite (Lottermoser, 1990). Work by Mariano (1989a) also highlighted the importance of secondary monazite, as well as cerianite and crandallite subgroup minerals, as host phases for REEs at Mount Weld. Similarly, fresh unweathered drill core from the central plug carbonatite at Araxá is only moderately enriched in REEs, and primary REE minerals are absent. In the Araxá carbonatite, the REEs are hosted by calcite, dolomite, and apatite. Within the laterites at Araxá and Catalão, secondary phases host the REEs and include apatite, monazite, rhabdophane, florencite, and gorceixite (Mariano, 1989a; Morteani and Preinfalk, 1996). Leaching experiments by Morteani and Preinfalk (1996) documented that only 2 to 30 wt % of the REEs are bound to iron hydroxides in the laterite at Araxá.

In summary, the development of extensive supergene REE mineralization on a carbonatite substrate does not require the presence of early crystallized, discreet REE-rich minerals. Primary REE minerals are absent in unweathered drill core from the central plug of both Araxá and Mount Weld. The extensive supergene REE mineralization that developed subsequently to carbonatite emplacement is derived from REEs that occurred initially as substitutional impurities in primary calcite, dolomite, and apatite. In addition, the supergene mineralization consists almost exclusively of monazite, crandallite group phosphates, and rhapdophane. Cerianite is also present under conditions of strong oxidation, and the spatially associated REE phosphate minerals exhibit Ce depletion. Bastnäsite and other REE carbonates are only observed where all of the phosphate has been consumed.

The laterite deposit at Araxá is the world's primary source of Nb, with bariopyrochlore as the primary Nb host mineral. As discussed in the section describing the Araxá deposit, the Nb enrichment in the laterite is a consequence of the physical enrichment of pyrochlore, resulting from the chemical destruction and removal of the major and minor minerals, including calcite, dolomite, and apatite, in the weathered carbonatite during laterization. Care must be taken when describing pyrochlore in carbonatite-related lateritic deposits as a product of supergene enrichment because the Nb in the pyrochlore was not enhanced but the relative abundance of pyrochlore increased due to the removal of other phases. Thus, to avoid this confusion, Nb enrichment by residual pyrochlore in the laterites of Araxá, Catalão I and II, Mrima, Leushe, and Mount Weld should not be referred to as "supergene" enrichment. Of note, pyrochlore crystals in many carbonatite laterites, including Araxá, retain their octahedral morphology, but they become friable and are easily broken during the physical processing operation. This has an adverse effect on recovery. In the case of the Araxá carbonatite, the grade of Nb_2O_5 in the laterite is so unusually high such that consequent losses of Nb to the tailings can be tolerated.

The laterite deposits at Araxá occur in a subtropical Brazil at approximate latitude 19° S. The climate is warm and humid, and the region receives 1,700 mm of annual precipitation. Similarly, the lateritic clay REE deposits in China, which are not associated with carbonatites, occur mainly in areas south of latitude 28° N, again in a subtropical climate that is warm, humid, and is characterized by more than 1,500 mm of annual precipitation (Bao and Zhoa, 2008).

The chemical breakdown of pyrochlore only occurs under conditions of extreme lateritic weathering (Mariano, 1984; Mitchell, 2015). This occurs only in environments of Amazon-type climatic conditions and where lateritic weathering has occurred in the Precambrian. In some carbonatites that are Precambrian in age and exposed to extreme lateritic weathering over a long period, both pyrochlore and magnetite are destroyed. This includes the upper layers of laterite at Mount Weld (Australia), Morro dos Seis Lagos (Brazil), Cerro Impacto (Venezuela), and Twarietau (Guyana). Under these conditions the more strongly bonded "B" sites of pyrochlore are also destroyed releasing Nb into the laterite, where it is chemically dispersed, but not enriched. The Nb is mainly present in some ferric iron oxides. As such, this is not a potential economic source of Nb.

Exploration

Although features of carbonatite-related ore deposits can aid in exploration, finding a deposit that can compete with the grade, tonnage, and extraction practices of currently mined deposits is a significant task. The search for REE deposits associated with carbonatites begins with a thorough study of existing deposits, because a working understanding of general deposit features is crucial for exploration study design and data evaluation. Identifying, exploring, and evaluating provinces comprising alkaline igneous rocks and known carbonatites is a starting point. Carbonatites are primarily found in rift settings because crustal thinning and high heat flow can facilitate ascent of mantle-derived magmas high in the crust. Carbonatites can, however, occur within orogenic belts, such

as those of the carbonatites within the Qinling orogenic belt of central China, suggesting that carbonatites within orogenic belts maybe important and underappreciated targets.

Potential geochemical indicators include fenitized wall rock, enrichment in LILE and particularly Ba (see Fig. 22), and radioactivity. Many known carbonatites have a halo of fenitized wall rock that surrounds mineralized bodies and that can be an indicator of late-stage alkaline fluids. Fenitization is a relatively rare style of hydrothermal alteration that is characterized by alkali-ferric iron metasomatism. Some elements anomalously enriched in the carbonatite (P, Nb, REEs, Ti, U, and Th) may reside in relatively resistant minerals, such that regional heavy mineral stream-sediment surveys could help locate targets.

Geophysical surveys can be useful for the identification of buried or concealed targets, and a variety of survey methods (radiometric, magnetic, and gravimetric) can be used successfully in carbonatite systems. Slight to moderate enrichments in U and Th relative to host rocks are general characteristics of many carbonatite systems and can be evaluated by ground or airborne radiometric surveys. As described above, carbonatites may contain radioactive minerals including monazite and pyrochlore, and thus have a positive radiometric signal. Mineralized carbonatites tend to have zones of magnetite enrichment, such that parts of the deposits may display positive magnetic anomalies relative to their host rocks. If the carbonatite is enveloped by a fenitized aureole, then an associated negative magnetic anomaly would be expected, owing to the destruction of mineral magnetism by the hydrothermal fluids. The Mount Weld deposit was initially identified during the interpretation of a regional aeromagnetic survey (Gunn and Dentith, 1997). Another example is the Elk Creek deposit in Nebraska, which is buried by approximately 200 m of sedimentary rocks. It was initially identified during a regional aeromagnetic survey and ground-based gravity survey (Burfeind et al., 1971). Subsequently, the anomaly was drilled and Nb mineralized carbonatite discovered (Brookins et al., 1975).

Carbonatite REE deposits are the primary source of LREEs (La, Ce, Pr, and Sm), and the deposits currently being mined have exceptional grade and tonnage. Bastnäsite is the primary ore mineral, and the ore processing of bastnäsite is well established. Furthermore, bastnäsite does not generally contain elevated U or Th abundances. These characteristics make REE deposits where bastnäsite is the main ore mineral favorable for exploration targets. Conversely, carbonatite LREE exploration targets dominated by other REE mineral phases need to establish that they can compete with these producing deposits, particularly on the ore-processing side. The increased REE exploration activity at carbonatites has identified localities, for example Bear Lodge and Lofdal, which are enriched in other REEs (Eu, Tb, and Dy). Identifying carbonatite-related exploration targets with enrichments in the more valued middle and HREEs is economically beneficial and could provide new sources of these critical elements.

Acknowledgments

We would like to thank Roger Mitchell, James Clark, Lee Groat, Richard Grauch, John Landreth, Adrian Van Rythoven, and Richard Goldfarb for thoughtful reviews. Any use of trade, product, or firm names is for descriptive purposes only and does not imply endorsement by the U.S. Government.

REFERENCES

Anders, E., and Ebihara, M., 1982, Solar-system abundances of the elements: Geochimica et Cosmochimica Acta, v. 46, p. 2362–2380.

Andersen, A.K., Cosca, M.A., and Larson, P.B., 2013, Timing of carbonatite magmatism in the Bear Lodge alkaline complex, WY [abs.]: Geological Society of America Abstracts with Programs, v. 45, p. 499.

Andersen, T., 1986, Magmatic fluids in the Fen carbonatite complex, S.E. Norway—evidence of mid-crustal fractionation from solid and fluid inclusions in apatite: Contributions to Mineralogy and Petrology, v. 93, p. 491–503.

——1987, Mantle and crustal components in a carbonatite complex, and the evolution of carbonatite magma: REE and isotopic evidence from the Fen complex, southeast Norway: Chemical Geology (Isotope Geosciences), v. 65, p. 147–166.

Andreeva, I.A., Kovalenko, V.I., and Naumov, V.B., 2001, Origin, magma content, and genesis of silicate magma of alkaline carbonatite-bearing complex of Mushgai Khudag, south Mongolia: Petrology, v. 9, p. 563–582 (in Russian).

Anglo American, 2013, Ore reserves and mineral resources report 2013, 49 p.

Bailey, D.K., 1987, Mantle metasomatism-perspective and prospect: Geological Society Special Publication 30, p. 1–13.

——1993, Carbonatite magmas: Journal of the Geological Society London, v. 150, p. 637–651.

Bao, Z., and Zhao, Z., 2008, Geochemistry of mineralization with exchangeable REY in the weathering crusts of granitic rocks in South China: Ore Geology Reviews, v. 33, p. 519–535.

Baskina, B.A., Volchanskaya, I.K., and Kovalenko, V. I., 1978, Potassic alkaline volcanic-plutonic complex of Mushgai Khudag in south Mongolia and related mineralization: Sovetskaya Geologiya, v. 4, 1978, p. 86–99 (in Russian).

Bell, K., 1998, Radiogenic isotope constraints on relationships between carbonatites and associated silicate rocks—a brief review: Journal of Petrology, v. 39, p. 1987–1996.

Bell, K., and Blenkinsop, J., 1989, Neodymium and strontium isotope geochemistry of carbonatites, *in* Bell, K. ed., Carbonatites: Genesis and evolution: London, Unwin Hyman, p. 278–300.

Berger, V.I., Singer, D.A., and Orris, G.J., 2009, Carbonatites of the world, explored deposits of Nb and REE—database and grade and tonnage models: U.S. Geological Survey Open-File Report 2009-1139, 17 p., text plus database.

Biondi, J.C., 2005, Brazilian mineral deposits associated with alkaline and alkaline-carbonatite complexes, *in* Comin-Chiaramonti, P. and Gomes, C.B., eds., Mesozoic to Cenozoic alkaline magmatism in the Brazilian Platform, Editora da Universidade de Sao Paulo: Fapesp, São Paulo, p. 707–750.

Brøgger, W.C., 1921, Die Eruptivgesteine des Kristianiagebietes. IV. Das Fengebiet in Telemark, Norwegen.Videns.Skrift. I. Mat-Naturv. Klasse 91.

Brookins, D.G., Treves, S.B., and Bolivar, S.L., 1975, Elk Creek, Nebraska carbonatite: Strontium geochemistry: Earth and Planetary Science Letters, v. 28, p. 79–82.

Bühn, B., and Rankin, A.H., 1999, Composition of natural, volatile-rich Na-Ca-REE-Sr carbonatitic fluids trapped in fluid inclusions: Geochimica et Cosmochimica Acta, v. 63, p. 3781–3797.

Burfeind, W.J., Carlson, M.P., and Smith, R., 1971, The Elk Creek geophysical anomaly, Johnson and Pawnee Counties, Nebraska [abs.]: Geological Society of America Abstracts with Programs, v. 3, no. 4, p. 254.

Cahen, L., and Snelling, N.J., 1966, The geochronology of equatorial Africa: Amsterdam, North-Holland Publishing, 195 p.

Castor, S.B., 2008a, Rare earth deposits of North America: Resource Geology, v. 58, p. 337–347.

——2008b, The Mountain Pass rare-earth carbonatite and associated ultrapotassic rocks, California: Canadian Mineralogist, v. 46, p. 779–806.

Castor, S.B., and Hedrick, J.B., 2006, Rare earth elements, *in* Kogel, J.E., Trivedi, N.C., Barker, J.M., and Krukowski, S.T., eds., Industrial minerals & rocks—Commodities, markets, and uses, 7th ed.: Littleton, CO, Society for Mining, Metallurgy, and Exploration, Inc. (SME), p. 769–792.

Castor, S.B., and Nason, G.W., 2004, Mountain Pass rare earth deposit, California: Nevada Bureau of Mines and Geology Special Publication 33, p. 68–81.

Chao, E.C.T., Back, J.M., Minkin, J.A., and Yingchen, R., 1992, Host-rock controlled epigenetic, hydrothermal metasomatic origin of the Bayan Obo REE Fe-Nb ore deposit, Inner Mongolia, P.R.C: Applied Geochemistry, v. 7, p. 443–458.

Chi, R., and Tian, J., 2008, Weathered crust elution-deposited rare earth ores: New York, N.Y., Nova Science Publishers, 286 p.

Cordeiro, P.F.O., Brod, J.A., Dantas, E.L., and Barbosa, E.S.R., 2010, Mineral chemistry, isotope geochemistry and petrogenesis of niobium-rich rocks from the Catalão I carbonatite-phoscorite complex, Central Brazil: Lithos, v. 118, p. 223–237.

Cordeiro, P.F.O., Brod, J.A., Palmieri, M., de Oliveira, C.G., Barbosa, E.S.R., Santos, R.V., Gaspar, J.C., and Assis, L.C., 2011, The Catalão I niobium deposit, central Brazil: Resources, geology and pyrochlore chemistry: Ore Geology Reviews, v. 41, p. 112–121.

Cullers, R.L., and Graf, J.L., 1984, Rare earth elements in igneous rocks of the continental crust: Intermediate and silicic rocks-ore petrogenesis, *in* Henderson, P., ed., Rare earth element geochemistry: Amsterdam, Elsevier, p. 275–316.

Dalton, J.A., and Wood, B.J., 1993, The compositions of primary carbonate melts and their evolution through wall rock reaction in the mantle: Earth and Planetary Science Letters, v. 119, p. 511–525.

Dawson, J.B., 1962, Sodium carbonate lavas from Oldoinyo Lengai, Tanganyika: Nature, v. 195, p. 1075–1076.

Deines, P., 1989, Stable isotope variations in carbonatites, *in* Bell, K. ed., Carbonatites: Genesis and evolution: London, Unwin Hyman, p. 301–359.

Demény, A., Sitnikova, M.A., and Karchevsky, P.I., 2004, Stable C and O isotope compositions of carbonatite complexes of the Kola alkaline province: Phoscorite-carbonatite relationships and source compositions: London, Mineralogical Society of Great Britain and Ireland Series 10, p. 407–431.

DeWitt, E., Kwak, L.M., and Zartman, R.E., 1987, U-Th-Pb and $^{40}Ar/^{39}Ar$ dating of the Mountain Pass carbonatite and alkalic igneous rocks, S.E. Cal. [abs.]: Geological Society of America Abstracts with Programs, v. 19, p. 642.

Drew, L.J., Qingrun, M., and Weijun, S., 1990, The Bayan Obo iron-rare-earth-niobium deposits, Inner Mongolia, China: Lithos, v. 26, p. 43–65.

Drüppel, K., Hoefs, J., and Okrusch, M., 2005, Fenitizing processes induced by ferrocarbonatite at Swartbooisdrif, NW Namibia: Journal of Petrology, v. 46, p. 377–406.

Eby, G.N., and Mariano, A.N., 1992, Geology and geochronology of carbonatites and associated alkaline rocks peripheral to the Paranfi basin, Brazil-Paraguay: Journal of South American Earth Sciences, v. 6, p. 207–216.

Fan, H.R., Hu, F.F., Yang, K.F., Pirajno, F., Liu, X., and Wang, K-Y., 2014, Integrated U-Pb and Sm-Nd geochronology for a REE-rich carbonatite dyke at the giant Bayan Obo REE deposit, northern China: Ore Geology Reviews, v. 63, p. 510–519.

Geological Brigade (109) of Sichuan Bureau of Geology and Mineral Resource, 2010, Exploration report of Maoniuping REE deposit in Mianning, Sichuan province (in Chinese).

Gittins, J., 1989, The origin and evolution of carbonatite magmas, *in* Bell, K. ed., Carbonatites: Genesis and evolution: London, Unwin Hyman, p. 580–600.

Gittins, J., and Harmer, R.E., 2003, Myth and reality in the carbonatite-silicate rock "association:" Periodico di Mineralogia, v. 72, p. 19–26.

Gittins, J., Beckett, M.F., and Jago, M.F., 1990, Composition of the fluid accompanying carbonatite magma: A critical examination: American Mineralogist, v. 75, p. 1106–1109.

Graham, S., Lambert, D.D., and Shee, S.R., 2004, The petrogenesis of carbonatite, melnoite and kimberlite from the Eastern Goldfields province, Yilgarn craton: Lithos, v. 76, p. 519–533.

Gunn, P.J., and Dentith, M.C., 1997, Magnetic responses associated with mineral deposits: AGSO Journal of Australian Geology and Geophysics, v. 17, p. 145–158.

Heinrich, E.W., 1966, The geology of carbonatites: Chicago, Rand McNally, 585 p.

Hoatson, D.M., Jaireth, S., and Miezitis, Y., 2011, The major rare-earth-element deposits of Australia: Geologic setting, exploration, and resources: Geoscience Australia, 204 p.

Hou, Z.Q., Tian, S.H., Yuan, Z.X., Xie, Y.L., Yin, S.P., Yi, L.S., Fei, H.C., and Yang, Z.M., 2006, The Himalayan collision zone carbonatites in western Sichuan, SW China: Petrogenesis, mantle source and tectonic implication: Earth and Planetary Science Letters, v. 244, p. 234–250.

Hou, Z.Q., Tian, S.H., Xie, Y.L., Yang, Z., Yuan, Z., Yin, S., Yi, L., Fei, H., Zou, T., Bai, G., and Li, X., 2009, The Himalayan Mianning-Dechang REE belt associated with carbonatite-alkaline complexes, eastern Indo-Asian collision zone, SW China: Ore Geology Reviews, v. 36, p. 65–89.

Jones, A.P., Genge, M., and Carmody, L., 2012, Carbonate melts and carbonatites: Reviews in Mineralogy and Geochemistry, v. 75, p. 289–322.

Keppler, H., 2003, Water solubility in carbonatite melts: American Mineralogist, v. 88, p. 1822–1824.

Kjarsgaard, B.A., and Hamilton, D.L., 1989, The genesis of carbonatites by immiscibility, *in* Bell, K. ed., Carbonatites: Genesis and evolution: London, Unwin Hyman, p. 388–404.

Kynicky, J., Smith, M.P., and Xu, C., 2012, Diversity of rare earth deposits—the key example of China: Elements, v. 8, p. 361–367.

Lai, X., Yang, X., and Sun, W., 2012, Geochemical constraints on genesis of dolomite marble in the Bayan Obo REE-Nb-Fe deposit, Inner Mongolia: Implications for REE mineralization: Journal of Asian Earth Sciences, v. 64, p. 90–102.

Larochelle, E.F., Noble, A.C., and Richardson, M.P., 2012, Technical report on the mineral reserves and development of the Bull Hill mine, Bear Lodge, Wyoming: NI 43-101 Report, 456 p.; accessed May 17, 2012, http://www.bearlodgeproject.com/BearLodgeHome.aspx

Le Bas, M.J., 1981, Carbonatite magmas: Mineralogical Magazine, v. 44, p. 133–140.

——1987, Nephelinites and carbonatites: Geological Society Special Publication 30, p. 53–83.

——2008, Fenites associated with carbonatites: Canadian Mineralogist, v. 46, p. 915–932.

Le Bas, M.J., Xueming, Y, Taylor, R.N., Spiro, B., Milton, J.A., and Peishan, Z., 2007, New evidence from a calcite-dolomite carbonatite dyke for the magmatic origin of the massive Bayan Obo ore-bearing dolomite marble, Inner Mongolia, China: Mineralogy and Petrology, v. 90, p. 223–248.

Le Maitre, R.W., 2002, Igneous rocks: A classification and glossary of terms, 2nd ed.: Cambridge, UK, Cambridge University Press, 236 p.

Long, K.R., Van Gosen, B.S., Foley, N.K., and Cordier, D., 2010, The principal rare earth elements deposits of the United States—a summary of domestic deposits and a global perspective: U.S. Geological Survey Scientific Investigations Report 2010-5220, 96 p.

Lottermoser, B.G., 1990, Rare-earth element mineralization within the Mt. Weld carbonatite laterite, Western Australia: Lithos, v. 24, p. 151–167.

Lynas Corporation, 2012, Resource estimates: Lynas Corporation website; accessed May 16, 2012, at http://www.lynascorp.com/page.asp?category_id=2&page_id=4

Mariano, A.N., 1976, A study of the Mountain Pass carbonatite: Confidential report to Molycorp Inc., 208 p.

——1978, The application of cathodoluminescence for carbonatite exploration and characterization: International Symposium on Carbonatites, 1st Poços de Caldas, Minas Gerais, Brazil, p. 39–57.

——1981, Characterization of selected drill core from the Mount Weld carbonatite complex, Laverton, Western Australia: Confidential report to Molycorp Inc., 79 p.

——1984, Report on the mineralogy of Nb, Ta, and REE in the Mount Weld laterite: Confidential report to Molycorp Inc. January, 1984, 79 p.

——1989a, Economic geology of rare earth minerals: Reviews in Mineralogy, v. 21, p. 309–338.

——1989b, Nature of economic mineralization in carbonatites and related rocks, *in* Bell, K., ed., Carbonatites—genesis and evolution: London, Unwin Hyman, p. 149–176.

——1994, Preliminary evaluation of the bastnäsite-bearing carbonatite occurrences south of Mianning, Sichuan, China: Confidential report to AMR Technologies, Inc., 91 p.

——1998, Report on field trip to the Mushgai Khudag carbonatite complex Gobi Desert, Mongolia: Confidential report to Norsk Hydro ASA, 29 p.

——2001a, Xenotime-bearing carbonatite veins from Lofdal, Damaraland, Namibia: Confidential Report to AMR Technologies, Inc., 6 p.

——2001b, Geologic field evaluation, sampling and mapping of carbonatite dikes in the Lofdal area of Damaraland, Namibia: Confidential report to AMR Technologies, Inc., 11 p.

Mariano, A.N., and Mariano, A.N., Jr., 2012, Rare earth mining and exploration in North America: Elements, v. 8, p. 369–376.

Mariano, A.N., and Siegfried, P., 2001, Summary of reconnaissance mapping of the carbonatite occurrences at Lofdal, Khorixas district, Namibia: Confidential report to AMR Technologies, Inc., 10 p.

Marsh, E.E., Anderson, E.D., and Gray, F., 2013, Nickel-cobalt laterites—a deposit model: U.S. Geological Survey Scientific Investigations Report 2010-5070-H, chapter H, 38 p.

Millonig, L.J., and Groat, L.A., 2013, Carbonatites in Western North America—occurrences and metallogeny: Society of Economic Geologists, Special Publication 17, p. 245–264.
Mitchell, R.H., 2005, Carbonatites and carbonatites and carbonatites: Canadian Mineralogist, v. 43, p. 2049–2068.
——2015, Primary and secondary niobium mineral deposits associated with carbonatites: Ore Geology Reviews, v. 64, p. 626–641.
Mitchell, R.H., and Kjarsgaard, B.A., 2004. Solubility of niobium in the system $CaCO_3$-CaF_2-$NaNbO_3$ at 0.1 GPa pressure: Implications for the crystallization of pyrochlore from carbonatite magma: Contributions to Mineralogy and Petrology, v. 148, p. 281–287.
Molycorp, Inc., 2012, Molycorp's rare earth reserves at Mountain Pass increase by 36%: Molycorp Press Release, April 9, 2012.
Moore, M., Chakhmouradian, A.R., Mariano, A.N., and Sidhu, R., 2015, Evolution of rare-earth mineralization in the Bear Lodge carbonatite, Wyoming: Mineralogical and isotopic evidence: Ore Geology Reviews, v. 64, p. 499–521.
Morogan, V., 1994, Ijolite versus carbonatite as sources of fenitization: Terra Nova, v. 6, p. 166–176.
Morogan, V., and Lindblom, S., 1995, Volatiles associated with the alkaline-carbonatite magmatism at Alnö, Sweden: A study of fluid and solid inclusions in minerals from the Langarsholmen ring complex: Contributions to Mineralogy and Petrology, v. 122, p. 262–274.
Morteani, G., and Preinfalk, C., 1996, REE distribution and REE carriers in laterites formed on the alkaline complexes of Araxá and Catalão (Brazil): London, Chapman and Hall, Mineralogical Society Series 7, p. 227–256.
Munkhtsengel, B., and Ilzumi, S., 1999, Rb-Sr geochronology and Sr-Nd isotope systematics of the Mushgai Khudag syenite and Bayan Khoshuu monzonite in south Mongolia: International Geological Symposium on East Asia, Mongolian Geoscientist Special Issue, v. 14, p. 14–16.
Neary, C.R., and Highley, D.E., 1984, The economic importance of the rare earth elements, *in* Henderson, P., ed., Rare earth element geochemistry: Amsterdam, Elsevier, p. 423–466.
Nelson, D.R., Chivas, A.R., Chappell, B.W., and McCulloch, M.T., 1988, Geochemical and isotopic systematics in carbonatites and implications for the evolution of ocean-island sources: Geochimica et Cosmochimica Acta, v. 58, p. 1–17.
NioCorp Developments Ltd., 2015, Elk Creek, Nebraska Niobium Project: NioCorp Developments Ltd. website, accessed February 17, 2015, at http://www.niocorp.com/index.php/projects/elkcreekniobium
Olson, J.C., and Hedlund, D.C., 1981, Alkalic rocks and resources of thorium and associated elements in the Powderhorn district, Gunnison County, Colorado: U.S. Geological Survey Professional Paper 1049-C, 34 p.
Olson, J.C., Shawe, D.R., Pray, L.C., and Sharp, W.N., 1954, Rare-earth mineral deposits of the Mountain Pass district, San Bernardino County, California: U.S. Geological Survey Professional Paper 261, 75 p.
Palabora Mining Company Limited Mine Geological and Mineralogical Staff, 1976, The geology and the economic deposits of copper, iron, and vermiculite in the Palabora Igneous Complex—a brief review: Economic Geology, v. 71, p. 177–192.
Pearce, N.J.G., Leng, M.J., Emeleus, C.H., and Bedford, C.M., 1997, The origins of carbonatites and related rocks from the Grønnedal-Íka nepheline syenite complex south Greenland: C-O-Sr isotope evidence: Mineralogical Magazine, v. 61, p. 515–529.
Pearson, R.G., 1963, Hard and soft acids and bases: Journal of the American Chemical Society, v. 85, p. 3533–3539.
Rankin, A.H., 2005, Carbonatite-associated rare metal deposits: Composition and evolution of ore-forming fluids—the fluid inclusion evidence: Geological Association of Canada, Short Course Notes 17, p. 299–314.
Rare Element Resources Ltd., 2012, Rare element reports 10 percent increase of M & I rare-earth mineral resources and 61 percent increase of oxide and oxide-carbonate inferred resources: Rare Element Resources News Release, May 7, 2012.
Richardson, D.G., and Birkett, T.C., 1996, Carbonatite associated deposits: Geological Survey of Canada, Geology of Canada Number 8, p. 541–558.
Samoilov, V.S., and Kovalenko, V.I., 1983, Complexes of alkaline rocks and carbonatites in south Mongolia: Nauka, v. 35, 196 p. (in Russian).
Sanematsu, K., and Watanabe, Y., 2016, Characteristics and genesis of ion-adsorption-type rare earth element deposits: Reviews in Economic Geology, v. 18, p. 55–79.
Sanematsu, K., Kon, Y., Hirano, H., and Watanabe, Y., 2010, Mineralogy and geochemistry of the Mushgai Khudag REE deposit, Mongolia [abs.]: Geological Society of America Abstracts with Programs, v. 42, p. 335.
Sauvage, J.-F. and Savard, R., 1985, Les complexes alcalins sous-saturés à carbonatites de la région d'In Imanal (Sahara malien): Journal of African Earth Sciences, v. 3, p. 143–149.
Sengupta, D., and Van Gosen, B.S., 2016, Placer-type rare earth element deposits: Reviews in Economic Geology, v. 18, p. 81–100.
Shi, Z.M., 1993, Age conjecture and meaning of Himalayan REE deposit in Maoniuping: Sichuan Geology Acta, v. 13, p. 247–254 (in Chinese with English abs.).
Silva, A.B.da., Marchetto, M., and Souza, O.M.de., 1979, Geologia do complex carbonititico de Araxá (Barreiro), Minas Gerais: Mineracao Metalurgia, v. 43, p. 8–14.
Smith, M.P., Henderson, P., and Campbell, L.S., 2000, Fractionation of the REE during hydrothermal processes: Constraints from the Bayan Obo Fe-REE-Nb deposit, Inner Mongolia, China: Geochimica et Cosmochimica Acta, v. 64, p. 3141–3160.
Streckeisen, A., 1980, Classification and nomenclature of volcanic rocks, lamprophyres, carbonatites and melilitic rocks IUGS Subcommission on the Systematics of Igneous Rocks Recommendations and Suggestions: Geologische Rundschau, v. 69, p. 194–207.
Sweeney, R.J., 1994, Carbonatite melt compositions in the Earth's mantle: Earth and Planetary Science Letters, v. 128, p. 259–270.
Tucker, R.D., Belkin, H.E., Schulz, K.J., Peters, S.G., Horton, F., Buttleman, K., and Scott, E.R., 2012, A major light rare-earth element (LREE) resource in the Khanneshin carbonatite complex, southern Afghanistan: Economic Geology, v. 107, p. 197–208.
Twyman, J.D., and Gittins, J., 1987, Alkalic carbonatite magmas: Parental or derivatives: Geological Society Special Publication 30, p. 85–94.
U.S. Department of Energy, 2010, Critical materials strategy: U.S. Department of Energy Report, 170 p., accessed January 26, 2011, at http://www.energy.gov/news/documents/criticalmaterialsstrategy.pdf.
Veksler, I.V., and Lentz, D., 2006, Parental magmas of plutonic carbonatites, carbonate-silicate immiscibility and decarbonation reactions: Evidence from melt and fluid inclusions: Mineralogical Association of Canada Short Course, v. 36, p. 123–150.
Veksler, I.V., Dorfman, A.M., Dulski, P., Kamenetsky, V.S., Danyushevsky, L.V., Jeffries, T., and Dingwell, D.B., 2012, Partitioning of elements between silicate melt and immiscible fluoride, chloride, carbonate, phosphate and sulfate melts, with implications to the origin of natrocarbonatite: Geochimica et Cosmochimica Acta, v. 79, p. 20–40.
Verplanck, P.L., Van Gosen, B.S., Seal, R.R, and McCafferty, A.E., 2014, A deposit model for carbonatite and peralkaline intrusion-related rare earth element deposits: U.S. Geological Survey Scientific Investigations Report 2010-5070J, 58 p.
Wall, F., and Mariano, A.N., 1996, Rare earth minerals in carbonatites: A discussion centered on the Kangankunde carbonatite, Malawi, *in* Jones, A.P., Wall, F., and Williams, C.T., eds., Rare earth minerals: Chemistry, origin and ore deposits: Mineralogical Society, Ser. 7, p. 193–225.
Wall, F., and Zaitsev, A.N., 2004, Rare earth minerals in Kola carbonatites: London, Mineral Society of Great Britain and Ireland Series 10, p. 341–373.
Wall, F., Vistorina, N., Niku-Paavola, V.N., Storey, C., Müller, A., and Jeffries, T., 2008, Xenotime-(Y) from carbonatite dykes at Lofdal, Namibia: Unusually low LREE:HREE ratio in carbonatite, and the first dating of xenotime overgrowths on zircon: Canadian Mineralogist, v. 46, p. 861–877.
Wallace, M.E., and Green, D.H., 1988, An experimental determination of primary carbonatite magma composition: Nature, v. 335, p. 343–346.
Wang, D., Yang, J., Yan, S., Xu, J., Chen, Y., Pu, G., and Luo, Y., 2008, A special orogenic-type rare earth element deposit in Maoniuping, Sichuan, China: Geology and Geochemistry: Resource Geology, v. 51, p. 177–188.
Winter, J.D., 2001, An introduction to igneous and metamorphic petrology: New Jersey, Prentice Hall, 697 p.
Wood, S.A., 2003, The geochemistry of rare earth elements and yttrium in geothermal waters: Society of Economic Geologists Special Publication 10, p. 133–158.
Woolley, A.R., 1982, A discussion of carbonatite evolution and nomenclature, and the generation of sodic and potassic fenites: Mineralogical Magazine, v. 46, p. 13–17.
——1987, Alkaline rocks and carbonatites of the world, Part 1: North and South America: Austin, University of Texas Press, and British Museum of Natural History, 216 p.
——1989, The spatial and temporal distribution of carbonatites, *in* Bell, K., ed., Carbonatites: Genesis and evolution: London, Unwin Hyman, p. 15–37.
——2001, The alkaline rocks and carbonatites of the world. 3. Africa: London, U.K., Geological Society of London, 372 p.

——2003, Igneous silicate rocks associated with carbonatites: Their diversity, relative abundances and implications for carbonatite genesis: Periodico di Mineralogia, v. 72, p. 9–17.
Woolley, A.R., and Kempe, D.R.C., 1989, Carbonatites—nomenclature, average chemical compositions, and element distribution, *in* Bell, K., ed., Carbonatites—genesis and evolution: London, Unwin Hyman, p. 1–14.
Woolley, A.R., and Kjarsgaard, B.A., 2008, Global carbonatite database: Geological Survey of Canada Open-File 5796.
Wu, C., 2008, Bayan Obo controversy: Carbonatite versus iron oxide-Cu-Au-(REE-U): Resource Geology, v. 58, p. 348–354.
Wu, C., Huang, D., and Guo, Z., 1990, REE geochemistry in the weathered crust of granites, Longnan area, Jiangxi province: Acta Geologica Sinica, v. 3, p. 193–210.
Wu, C., Yuan, Z., and Bai, G., 1996, Rare element deposits in China: London, Chapman and Hall, Mineralogical Society Series 7, p. 281–310.
Wyllie, P.J., 1977, Mantle fluid compositions buffered by carbonates in peridiote-CO_2-H_2O: Journal of Geology, v. 85, p. 187–207.
——1989, Origin of carbonatites: Evidence from phase equilibrium studies, *in* Bell, K., ed., Carbonatites, genesis and evolution: London, Unwin Hyman, p. 500–545.
Wyllie, P.J., and Huang, W.-L., 1975, Influence of mantle CO_2 in the generation of carbonatites and kimberlites: Nature, v. 257, p. 297–299.
Wyllie, P.J., and Lee, W.-J., 1999, Model system controls on conditions for formation of magnesiocarbonatite and calciocarbonatite magmas from the mantle: Journal of Petrology, v. 39, p. 1885–1893.
Wyllie, P.J., and Tuttle, O.F., 1960, The system CaO-CO_2-H_2O and the origin of carbonatites: Journal of Petrology, v. 1, p. 1–46.
Xie, Y., Hou, Z., Yin, S., Dominy, S.C., Xu, J., Tian, S., and Xu, W., 2009, Continuous carbonatitic melt-fluid evolution of a REE mineralization system: Evidence from inclusions in the Maoniuping REE deposit, Western Sichuan, China: Ore Geology Reviews, v. 36, p. 90–105.
Xie, Y., Hou, Z., Goldfarb, R.J., Guo, X., and Wang, L., 2016, Rare earth element deposits in China: Reviews in Economic Geology, v. 18, p. 115–136.
Xu, C., Campbell, I.H., Kynicky, J., Allen, C.M., Chen, Y.J., Huang, Z.L., and Qi, L., 2008, Comparison of the Daluxiang and Maoniuping carbonatitic REE deposits with Bayan Obo REE deposit, China: Lithos, v. 106, p. 12–24.
Xu, C., Wang, L., Song, W., and Wu, M., 2010, Carbonatites in China: A review for genesis and mineralization: Geoscience Frontiers, v. 1, p. 105–114.
Xu, C., Taylor, R.E., Li, W., Kynicky, J., Chakhmouradian, A.R., and Song, W., 2012, Comparison of fluorite geochemistry from REE deposits in the Panxi region and Bayan Obo, China: Journal of Asian Earth Sciences, v. 57, p. 76–89.
Yang, K-F, Fan, H-R., Santosh, M., Hu, F-F., and Wang, K-Y., 2011, Mesoproterozoic carbonatitic magmatism in the Bayan Obo deposit, Inner Mongolia, North China: Constraints for the mechanism of super accumulation of rare earth elements: Ore Geology Reviews, v. 40, p. 122–131.
Yang, X-Y, Sun, W-D, Zhang, Y.X., and Zheng, Y.-F., 2009, Geochemical constraints on the genesis of the Bayan Obo Fe-Nb-REE deposit in Inner Mongolia, China: Geochimica et Cosmochimica Acta, v. 73, p. 1417–1435.
Yang, Z., and Woolley, A., 2006, Carbonatites in China—a review: Journal of Asian Earth Sciences, v. 27, p. 559–575.
Yuan, Z., Bai, G., Wu, C., Zhang, Z., and Ye, X., 1992, Geological features and genesis of the Bayan Obo REE ore deposit, Inner Mongolia, China: Applied Geochemistry, v. 7, p. 429–442.
Yuan, Z.X., Shi, Z., Bai, G., Wu, C., Chi, R. and Li, X., 1995, Rare earth element deposit in Maoniuping Mianning, Sichuan province: Beijing, Geological Publishing House, 150 p. (in Chinese).
Zaitsev, A.N., Wall, F., and Le Bas, M.J., 1998, REE-Sr-Ba minerals from the Khibina carbonatites, Kola Peninsula, Russia: Their mineralogy, paragenesis and evolution: Mineralogical Magazine, v. 62, p. 225–250.

©2016 Society of Economic Geologists, Inc.
Reviews in Economic Geology, v. 18, pp. 33–54

Chapter 2

Rare Metal Deposits Associated with Alkaline/Peralkaline Igneous Rocks

Jaroslav Dostal†

Department of Geology, Saint Mary's University, Halifax, Nova Scotia B3H 3C3, Canada

Abstract

Highly evolved alkaline/peralkaline igneous rocks host deposits of rare earth elements (REE), including Y as well as Zr, Hf, Nb, Ta, U, and Th. The host rocks spanning from silica-undersaturated (nepheline syenites) to silica-oversaturated (granites) occur in intraplate tectonic environments, mainly in continental settings and are typically associated with rifting, faulting, and/or crustal extension. They range in age from Neoarchean/Paleoproterozoic to Mesozoic, but several significant deposits are of Mesoproterozoic age. The deposits/prospects can be subdivided into three types. The first is hosted by nepheline syenitic rocks of large, layered alkaline intrusions where the mineralization commonly occurs in layers rich in REE-bearing minerals, which mostly show cumulate textures (e.g., Thor Lake/Nechalacho, Canada; Ilimaussaq, Greenland; Lovozero, Russia; Kipawa, Canada; Norra Kärr, Sweden; Pilanesberg, South Africa). The second type includes mineralization in peralkaline granitic rocks where REE-bearing minerals are usually disseminated. The mineralization is typically hosted by pegmatites (including the Nb-Y-F type), felsic dikes, and minor granitic intrusions (e.g., Strange Lake, Canada; Khaldzan-Buregtey, Mongolia; Ghurayyah, Saudi Arabia; Bokan, Alaska, United States). The third type is disseminated, very fine grained, and hosted by peralkaline felsic volcanic/volcaniclastic rocks, mostly of trachytic composition (e.g., Dubbo Zirconia and Brockman/Hastings, Australia).

The bulk of the REE is present in ore/accessory minerals which in some mineralized zones, particularly in cumulate rocks from alkaline complexes, can reach >10 vol %. Mineralization is composed of a variety of REE-bearing minerals, which frequently show complex replacement textures. They include fluorocarbonates, phosphates, silicates, and oxides. Economically most important are bastnäsite, monazite, xenotime, loparite, eudialyte, synchysite, and parasite. Many other minerals are either sparse or it is difficult with present technology to profitably extract REE from them on a commercial scale. Compared to carbonatite-hosted REE deposits, the REE mineralization in alkaline/peralkaline complexes has lower light REE concentrations but has commonly higher contents of heavy REE and Y and shows a relative depletion of Eu. Elevated concentrations of U and Th in the ore assemblages make gamma-ray (radiometric) surveys an important exploration tool.

The host peralkaline (granitic, trachytic, and nepheline syenitic) magmas undergo extensive fractional crystallization, which is protracted in part due to high contents of halogens and alkalis. The REE mineralization in these rocks is related to late stages of magma evolution and typically records two mineralization periods. The first mineralization period produces the primary magmatic ore assemblages, which are associated with the crystallization of fractionated peralkaline magma rich in rare metals. This assemblage is commonly overprinted during the second mineralization period by the late magmatic to hydrothermal fluids, which remobilize and enrich the original ore. The parent magmas are derived from a metasomatically enriched mantle-related lithospheric source by very low degrees of partial melting triggered probably by uplift (adiabatic) or mantle plume activity. The rare metal deposits/mineralization related to peralkaline igneous rocks represent one of the most economically important resources of heavy REE including Y. In addition to REE, some of these deposits contain economically valuable concentrations of other rare metals including Zr, Nb, Ta, Hf, Be, U, and Th, as well as phosphates.

Introduction

Evolved alkaline/peralkaline igneous rocks are associated with economically important mineralization of rare metals, particularly of rare earth elements (REE) including yttrium (Y), zirconium (Zr), niobium (Nb), tantalum (Ta), uranium (U), thorium (Th), and beryllium (Be). Typically several of these elements are concentrated together in a deposit. In the past 20 years or so, the demand for REE has dramatically increased together with the prices of individual REE leading to an exploration boom. Thus the evolved alkaline/peralkaline rocks, some of which host economically important deposits of REE, have attracted a great deal of interest in the exploration industry, as well as in geologic literature (e.g., Richardson and Birkett, 1996; Orris and Grauch, 2002; Castor, 2008a; Kynicky et al., 2012; Mariano and Mariano, 2012; Verplanck et al., 2014), particularly as highly evolved, rare metal-rich, alkaline/peralkaline igneous rocks occur only rarely in the geologic record. These deposits represent one of the most economically important resources of heavy REE (HREE), including yttrium (Y). Compared to light REE (LREE), HREE (europium through to lutetium) are relatively rare in nature and so, in general, more valuable than the LREE (lanthanum to samarium). The prices of individual REE vary by one or two order of magnitude.

Rare earth elements, which include lanthanides and yttrium, as well as some other rare metals hosted in peralkaline rocks such as Zr, Nb, Ta, U, and Th, do not readily enter into the crystal structure of common rock-forming minerals and become progressively enriched in magma during crystallization. Thus, these elements can be concentrated in

† E-mail: jdostal@smu.ca

highly fractionated rocks, such as evolved granites and nepheline syenites (e.g., Richardson and Birkett, 1996; Cerny et al., 2005). A characteristic feature of the mineralization is that rare metal-bearing minerals are intimately related to the crystallization history of magma, particularly to the late stages of its evolution, although the mineralization is frequently associated with hydrothermal alteration, which itself is typically linked to late-stage magmatic fluids (e.g., Salvi and Williams-Jones, 2005; Chakhmouradian and Zaitsev, 2012; Sheard et al., 2012; Walters et al., 2013).

Alkaline intrusive rocks hosting significant REE mineralization include two distinct rock types—peralkaline granites and silica undersaturated (feldspathoid-bearing) syenites (e.g., Richardson and Birkett, 1996; Salvi and Williams-Jones, 2005). Ore-bearing volcanic equivalents are less common (e.g., Taylor et al., 1995a; Mungall and Martin, 1996). The mineralized granites occur as isolated bodies, pegmatites, or in the most fractionated parts of the differentiated plutons. The REE-rich silica-undersaturated syenites typically belong to the nepheline syenite clan and are present in strongly evolved parts of the large layered alkaline complexes. Both the granites and syenites and their volcanic equivalents usually occur in intraplate tectonic environments where they are typically associated with intracontinental rift and fault systems (Berger et al., 2009). This chapter focusses on rare earth mineralization associated with peralkaline granites and syenites and their volcanic equivalents. It summarizes the characteristics of the deposits, reviews the processes involved in their origin, and describes some important examples of these deposits.

Rare Earth Element Minerals of Peralkaline Rocks and Their Deposits

In alkaline/peralkaline rocks, REE are present in a wide range of mineral species (Table 1). There are about 270 minerals which contain REE as an essential component in their crystal structure and chemical formula and many of them occur in alkaline/peralkaline rocks. Most common are silicates, followed by fluorocarbonates, oxides, and phosphates. Although these minerals generally contain most of the REE, they tend to be biased toward either LREE or HREE (Fig. 1). The most abundant rare earth element in a mineral is frequently indicated as the parenthesized element symbol in the name of some minerals (Table 1; Levinson, 1966). For example in xenotime-(Y), yttrium is the predominant REE although it can also contain other rare earths. Yttrium (at. no. 39) is considered a REE as it has similar chemical and physical properties. It is usually included with HREE because of their shared occurrences and its ionic radius which is nearly identical to that of Ho (Fig. 1).

The accessory (or ore) minerals typically contain >90% of the total REE in the peralkaline rocks (Bea, 1996; Chakhmouradian and Zaitsev, 2012) although Abdel-Rahman (1994) showed that alkali amphiboles can have significant concentrations of REE. The modal abundances of accessory (ore) minerals in some mineralized zones, particularly of cumulate rocks, can reach 10 vol % or even more. Peralkaline rock-associated REE mineralization contains a variety of REE-bearing minerals (Table 1; e.g., Mariano, 1989; Chakhmouradian and Wall, 2012; Mariano and Mariano, 2012) and can show replacement textures in part due to late magmatic to hydrothermal overprinting of the primary mineralogy. REE mineralogy of deposits is variable both within individual deposits and particularly among the various deposits. Hydrothermal overprinting of primary magmatic phases produced complex and varied assemblages where many REE ore phases occur as pseudomorphs of preexisting minerals. Mineral phases including zircon can occur in at least two generations. In some deposits, the mineral assemblages were modified by more than one hydrothermal stage. The relative proportions of primary and postmagmatic phases are variable even within the individual deposits. The grain size of the ore minerals varies from coarse, particularly of primary cumulate phases, to fine grained in volcanic rocks and replacement textures. Hydrothermal fluids also altered the host rocks. Gangue minerals of the deposits are also rather varied in part due to the hydrothermal overprint. In nepheline syenite-hosted deposits the dominant gangue minerals are nepheline, alkali feldspar, sodalite,

Table 1. Names and Formulae of REE-Bearing and Related Minerals Associated with REE Mineralization

Mineral	Formula	Approx. REE oxides (wt %)
Aeschynite	$(Ln,Ca,Fe,Th)(Ti,Nb)_2O_6$	32
Allanite (Ce)	$(Ln,Ca,Y)_2(Al,Fe^{3+})_3(SiO_4)_3(OH)$	38
Allanite (Y)	$(Y,Ln,Ca)_2(Al,Fe^{3+})_3(SiO_4)_3(OH)$	39
Apatite	$(Ca,Ln)_5(PO_4)_3(F,Cl,OH)$	19
Armstrongite	$CaZrSi_6O_{15}\cdot 3H_2O$	
Barylate	$BaBe_2Si_2O_7$	
Bastnäsite (Ce)	$(Ln,Y)(CO_3)F$	75
Britholite (Ce)	$(Ln,Th,Ca)_5(SiO_4,PO_4)_3(OH,F)$	32
Cerite (Ce)	$Ce_9Fe^{3+}(SiO_4)_6[(SiO_3)(OH)](OH)_3$	73
Columbite	$Fe^{2+}Nb_2O_6$	
Elpidite	$Na_2ZrSi_6O_{15}\cdot 3H_2O$	
Eudialyte	$Na_4(Ca,Ln)_2(Fe^{2+},Mn^{2+},Y)ZrSi_8O_{22}(OH,Cl)_2$	9
Euxenite (Y)	$(Y,Ca,Ln,U,Th)(Nb,Ta,Ti)_2O_6$	24
Fergusonite (Ce)	$(Ln,Y)NbO_4$	53
Fergusonite (Y)	$YNbO_4$	46
Fluorite	CaF_2	
Gadolinite (Ce)	$(Ln,Y)_2Fe^{2+}Be_2Si_2O_{10}$	60
Gadolinite (Y)	$Y_2Fe^{2+}Be_2Si_2O_{10}$	48
Gittinsite	$CaZrSi_2O_7$	
Iimoriite (Y)	$Y_2(SiO_4)(CO_3)$	68
Kainosite (Y)	$Ca_2(Y,Ln)_2Si_4O_{12}(CO_3)\cdot H_2O$	38
Loparite (Ce)	$(Ln,Na,Ca)(Ti,Nb)O_3$	30
Monazite	$(Ln,Th)PO_4$	65
Parisite (Ce)	$Ca(Ln)_2(CO_3)_3F_2$	61
Pyrochlore	$(Ca,Na,Ln)_2Nb_2O_6(OH,F)$	
Rinkite (rinkolite)	$(Ca,Ln)_4Na(Na,Ca)_2Ti(Si_2O_7)_2(O,F)_2$	20
Samarskite	$(Ln,Y,Fe^{3+},U,Th,Ca)(Nb,Ta)_5O_4$	24
Steenstrupine (Ce)	$Na_{14}Ln_6Mn_2Fe_2(Zr,Th)(Si_6O_{18})_2(PO_4)_7\cdot 3H_2O$	31
Synchysite (Ce)	$Ca(Ln)(CO_3)_2F$	51
Synchysite (Y)	$Ca(Y,Ln)(CO_3)_2F$	42
Thalenite (Y)	$Y_3Si_3O_{10}(F,OH)$	64
Thorite	$(Th,U)SiO_4$	
Titanite	$(Ca,Ln)TiSiO_5$	4
Uraninite	$(U,Th)O_2$	
Xenotime (Y)	YPO_4	61
Zircon	$(Zr,Ln)SiO_4$	4

Notes: Ln = lanthanides; estimates of REE oxide content (lanthanides + Y as trivalent oxides) are based on Webmineral composition (www.webmineral.com); the mineral name followed by brackets refers to the formula of specific chemical variant of the mineral

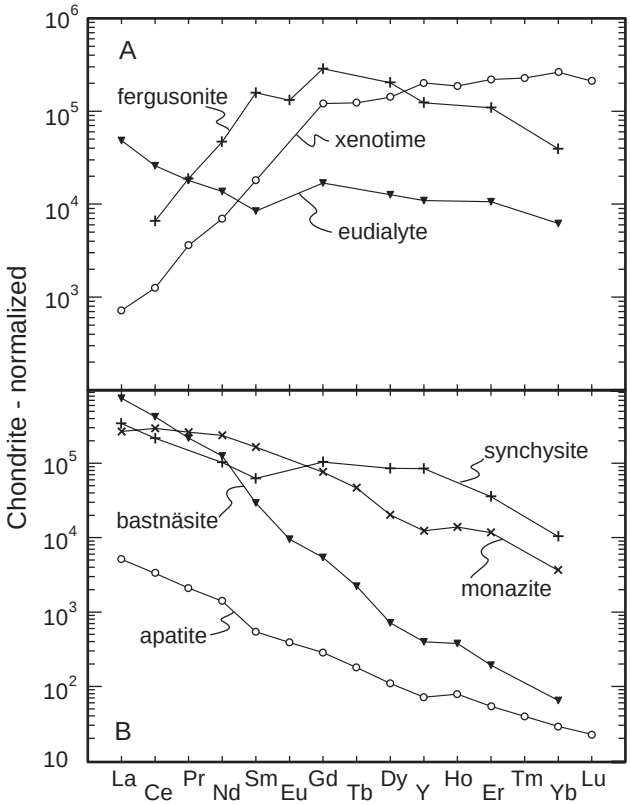

Fig. 1. Chondrite-normalized REE (lanthanides and Y) patterns of selected minerals which are major constituents of REE ores hosted by peralkaline rocks: apatite (Arzamastsev et al., 2002), monazite, xenotime (Förster et al., 1999), eudialyte, fergusonite (Sheard et al., 2012), synchysite (Dostal et al., 2011), and bastnäsite (Castor, 2008b). Note that yttrium is plotted as a pseudo-lanthanide between Dy and Ho. Normalizing values are after Sun and McDonough (1989).

aegerine, and arfvedsonite and their alteration products. The main gangue minerals of peralkaline granite-hosted deposits are quartz and alkali feldspar.

At present, there are only a limited number of REE minerals which are/or can be commercially exploited. According to Chakhmouradian and Wall (2012) it is less than 20 minerals. They include bastnäsite, monazite, xenotime, synchysite (Fig. 1), loparite, and parasite. Many others are either sparse or it is difficult at present to profitably extract REE from them on a commercial scale. In addition to these minerals, REE are hosted in subordinate to minor amounts in many other minerals, including rock-forming phases, where they substitute for other cations of comparable radius and charge.

Peralkaline Igneous Rocks

There is no precise and generally accepted definition of the term "alkaline," which implies an enrichment of Na_2O and K_2O in a rock (Winter, 2001). In particular, there is no agreement as to the amounts of the alkali elements that need to be in a rock to be termed alkaline (Mitchell, 1996) although several alkali-silica classification diagrams have been proposed (e.g., Cox et al., 1979; Le Bas et al., 1986; LeMaitre et al., 2002). Rather than adopt some arbitrary alkali element content, petrologists frequently use a classification based upon mineralogy. Thus, the alkaline igneous rocks are rocks containing sodium-or potassium-rich major rock-forming minerals, namely feldspathoids, alkali amphiboles, or alkali pyroxenes (e.g., Cox et al., 1979; Winter, 2001). This definition applies to both silica-oversaturated and undersaturated alkaline rocks. Peralkaline rocks are a subset in which the molecular amount of alkalis ($Na_2O + K_2O$) exceeds aluminum (Al_2O_3). If the ($Na_2O + K_2O$)/Al_2O_3 (molecular) ratio is greater than unity the rocks are termed peralkaline, i.e., they have more alkalis than Al (Fig. 2; e.g., Shand, 1943; Frost et al., 2001; Frost and Frost, 2011). Originally, the term peralkaline was used to be synonymous with agpaitic (Ussing, 1912). Subsequently, the term agpaitic referred to peralkaline nepheline syenites containing Zr- and Ti-rich minerals (Sørensen, 1992). Recently, Frost and Frost (2008) proposed the original usage with a subdivision of peralkaline/agpaitic rocks into feldspathoid- and quartz-bearing. Unlike granitoid rocks (Fig. 2), the feldspathoid-bearing rocks with a ($Na_2O + K_2O$)/Al_2O_3 (molecular) ratio less than 1 are called miaskitic (Hall, 1996; Mitchell, 1996).

The peralkaline rocks include types with a wide range of silica, spanning from silica-oversaturated granites through syenites to feldspathoid-bearing silica-undersaturated rocks (Richardson and Birkett, 1996). Their mineralogy is characterized by the common occurrence of alkali pyroxenes (aegirine) and alkali amphiboles (arfvedsonite and/or riebeckite). The peralkalinity reflects not only the mineralogy and major element chemistry of the rocks but has a bearing on the behavior of rare elements during fractionation. The peralkaline intrusive rocks, as well as their volcanic equivalents, show many similar chemical characteristics and types of rare metal enrichment (e.g., Sørensen, 1992; Marks et al., 2003, 2011; Salvi and Williams-Jones, 2005; Verplanck and Van Gosen, 2011; Dostal et al., 2014; Verplanck et al., 2014).

Evolved peralkaline rocks usually have high Fe (incorporated into alkali pyroxene and alkali amphibole) and Fe/Mg ratios. Their characteristic feature is a distinct enrichment in REE, Th, U, and high-field strength elements (HFSE), such

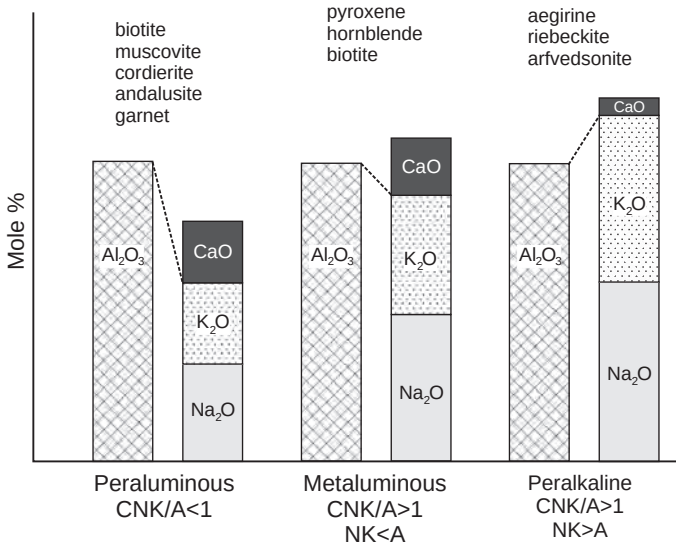

Fig. 2. Classification of granitoid rocks based upon molar proportions of Al_2O_3, CaO, Na_2O, and K_2O after Shand (1943). Common nonquartz-feldspathic minerals for each type are shown. Vertical axis is schematic. Modified after Clarke (1992). A = Al_2O_3, CNK = CaO + Na_2O + K_2O, NK= Na_2O+K_2O.

as Zr, Hf, Nb, and Ta and halogens (F and Cl). These highly fractionated rocks are low in Ca, Eu, and Sr and are relatively anhydrous with a high F/H_2O ratio (e.g., Cerny et al., 2005; Salvi and Williams-Jones, 2005; Cuney and Kyser, 2008). The deposits of rare metals are hosted mainly in rocks of granitic and nepheline syenitic composition. Pegmatites hosting rare metal mineralization are commonly subdivided into the Li-Cs-Ta and Nb-Y-F types (Cerny and Ercit, 2005). The latter type, which is enriched in Be, REE, Th, U, Zr, and Sc, has been correlated with peralkaline granite (Linnen and Cuney, 2005).

Alkaline/peralkaline rocks are most commonly found in intraplate environments, typically continental rift zones, although they may also be formed in postcollisional to post-orogenic settings. In terms of genetic classifications of granitic rocks based upon both tectonic and chemical characteristics, the peralkaline rocks represent the A-type (the A denoting anorogenic and/or anhydrous) granitoids, which occur along rift zones and within stable continental blocks (Loiselle and Wones, 1979; Clemens et al., 1986; Whalen et al., 1987; Bonin, 2007). Eby (1990, 1992) further subdivided these granitoids, mainly according to their chemical composition, into two subgroups A1 and A2. The A1 type (referred to as anorogenic) was inferred to be derived by differentiation of an ocean-island basalt (OIB)-like magma unlike the A2 type (postcollisional or post-tectonic). The peralkaline rocks typically correspond to the A1 type.

Rare Earth Element Deposits of Alkaline/Peralkaline Rocks

Evolved alkaline/peralkaline igneous rocks host economic or subeconomic resources of rare metals, some of which are deposits or advanced exploration targets (Fig. 3). Peralkaline rock-associated rare metal deposits are particularly valued for their heavy REE. In addition to REE, some of these deposits contain economically valuable concentrations of other rare metals, including Zr, Nb, Ta, Hf, Be, U, and Th. The calculated ore reserves in these deposits range in size from about 5 million metric tons (Mt) to >600 Mt (Table 2). The grades of REE (including Y) range from about 0.2 to 1.5 wt % and are generally <1 wt % for Nb, Ta, Hf , Be, U, and Th, while Zr ranges from about 0.25 to 5 wt % (Table 2; Richardson and Birkett, 1996, Verplanck et al., 2014). However, there are some exceptions, for example, the former Ross-Adams mine at the Bokan Mountain (Alaska) produced ore with 1 wt % U_3O_8 and 3 wt % ThO_2. In the Khibiny complex of the Kola Peninsula (Russia), REE-bearing apatite is mined for phosphate.

Compared to the carbonatite deposits, the REE mineralization in peralkaline complexes has lower LREE concentrations but has higher contents of HREE, including Y (Figs. 4, 5). The chondrite-normalized plots of the peralkaline rocks typically show a negative Eu anomaly, which is commonly lacking in those of carbonatites (Figs. 4, 5). Unlike peralkaline rock-associated mineralization, the carbonatite REE deposits are mainly valued for their contents of LREE.

The peralkaline complexes with rare metal deposits occur in continental intraplate settings where their locations are frequently controlled by rift/fault zones. The emplacement of shallow-seated intrusions can be also controlled by ring fractures. Some of the high-level intrusions are known to be associated with contemporaneous volcanic rocks (e.g., Nigeria; Bowden, 1985; Bowden et al., 1987). The age of mineralized peralkaline igneous complexes spans from Neoarchean/Paleoproterozoic

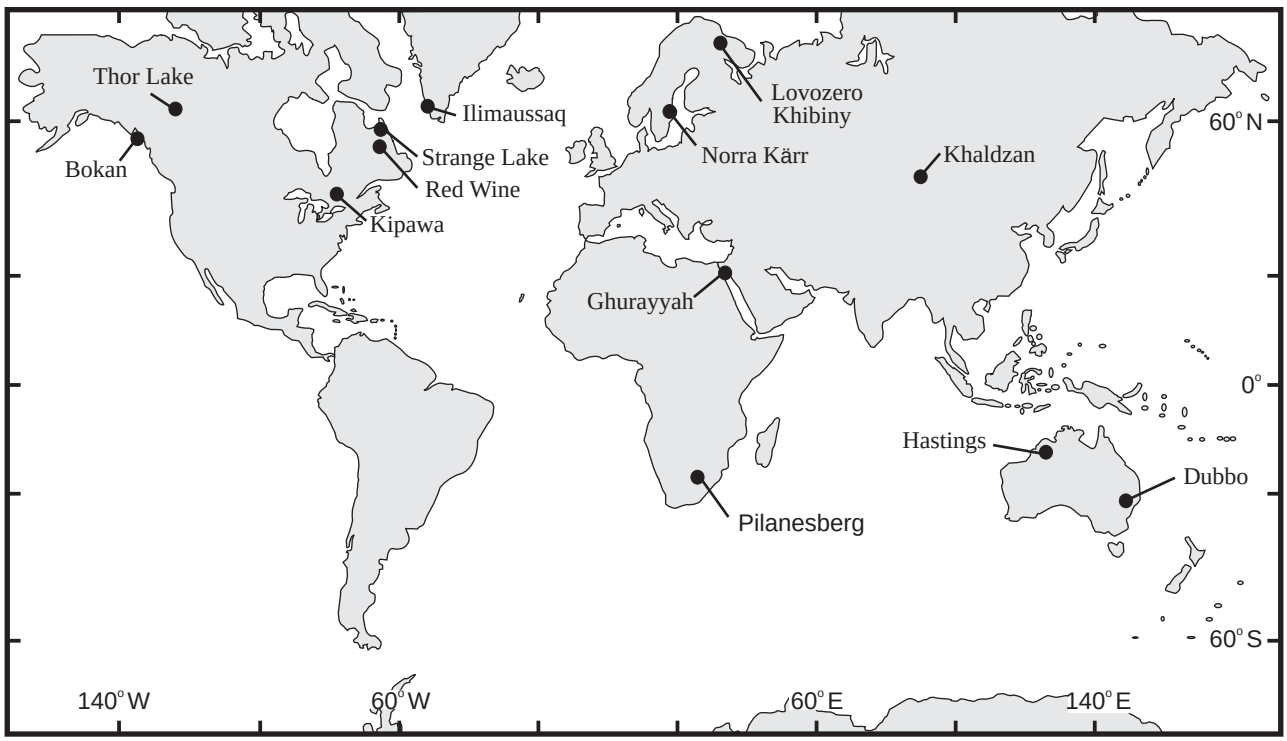

Fig. 3. World map showing the locations of major REE deposits and advanced exploration projects hosted in alkaline/peralkaline igneous rocks.

Table 2. Tonnage and Ore Grade of Selected Advanced REE Exploration Projects Related to Peralkaline Igneous Rocks

Deposit	TREO reserves (Mt)	Ore reserve (Mt)	HREO/TREO (%)	Ore grade (wt %)						
				TREO	ZrO_2	HfO_2	Nb_2O_5	Ta_2O_5	U_3O_8	ThO_2
Thor Lake (Nechalacho), Northwest Territories, Canada										
Basal	1.799	125.7	20.9	1.43	2.89		0.38	0.04		
Upper	2.353	177.7	10.0	1.32	2.13		0.31	0.02		
Ilimaussaq Complex, Greenland										
Kvanefjeld	6.547	619.0	11.8	1.06					0.03	
Sørensen	2.667	242.0	11.7	1.10					0.03	
Zone 3	1.106	95.3	12.1	1.16					0.03	
Kipawa (Zeus), Quebec, Canada	0.107	27.1	36.2	0.40	0.93					0.03
Norra Kärr, Sweden	0.343	58.1	50.3	0.59	1.72	0.03				
Strange Lake, Quebec/Labrador, Canada										
Enriched	0.288	20.0	49.7	1.44	2.59	0.06	0.34		0.01	0.06
Granite	4.118	472.5	36.5	0.87	1.79	0.05	0.15		0.01	0.03
Bokan, Alaska, United States	0.030	4.9	40.1	0.61	0.25		0.06		0.01	0.01
Two Tom, Labrador, Canada	0.480	40.6	6.3	1.18			0.26			0.06
Dubbo, Australia	0.651	73.2	23.3	0.89	1.96	0.04	0.46	0.03	0.01	
Hastings/Brockman, Australia	0.076	36.2	85.8	0.21	0.89	0.03	0.35	0.02		

Notes: Recent data are not available for some deposits discussed in the text, including Lovozero, Khibiny, Khaldzan-Buregtey, Ghurayyah, and Pilansberg; data from Hatch (2014) for REE, for other elements: Ciuculescu et al. (2013) for Thor Lake; Gowans et al. (2013) for Strange Lake; Tasman Metals (2012) for Norra Kärr; Greenland Metals and Energy (2014) for Illimaussaq Complex; Saucier et al. (2013) for Kipawa; Robinson et al. (2011) for Bokan; Hastings Rare Metals (2014) for Hastings/Brockman; and Alkane Resources (2014) for Dubbo; abbreviations:Mt = million metric tons, TREO = oxides of lanthanides and Y; HREO = oxides of heavy REE (Eu to Lu) and Y

to Mesozoic, although a disproportionally large number of the intrusions are Mesoproterozoic (1,000–1,460 Ma).

The evolved peralkaline felsic igneous rocks which host rare metal deposits predominantly include nepheline syenites, peralkaline granites, and trachytes. Typically, the rare metal mineralization is closely related to the crystallization of magma, particularly to its late stages.

The REE deposits associated with peralkaline complexes can be subdivided into three groups: (1) deposits in layered nepheline syenitic complexes, (2) deposits in peralkaline granitic intrusions and related rocks, and (3) deposits in peralkaline felsic volcanic rocks. The first group includes the REE-rich peralkaline silica-undersaturated host rocks that are associated with layered intrusions composed mainly of nepheline syenites, which in turn are generally a part of a larger alkaline layered complex (Verplanck et al., 2014). They show textures suggestive of crystal accumulation where the REE mineralization occurs in layers or bands containing mineral cumulates that are rich in REE-bearing minerals such as eudialyte (Salvi and Williams-Jones, 2005). Cumulate textures indicate that the initial REE enrichment was due to magmatic processes and the ore-bearing layers represent cumulate layers within a magma chamber. The thickness of the ore horizons is variable. For example, REE mineralization at the Nechalacho deposit is concentrated into two zones—an upper that is 15 to 30 m thick and a lower that is 15 to 60 m thick (Sheard et al., 2012). Examples of this group of deposits (Fig. 3) include the Nechalacho deposit at Thor Lake (NWT, Canada), Kvanefjeld, Sørensen, Zone 3, and Kringlerne at Ilímaussaq (southern Greenland), Lovozero and Khibiny at Kola Peninsula (Russia), Kipawa (Quebec, Canada), Red Wine (Labrador, Canada), Norra Kärr (Sweden), and Pilanesberg (South Africa).

The second group is related to peralkaline granites. The REE mineralization occurs in pegmatites (including the Nb-Y-F type) hosted by peralkaline granites (e.g., Strange Lake, Quebec-Labrador, Canada) or in small, highly evolved peralkaline granitic stocks as hydrothermal disseminations (e.g., Khaldzan-Buregtey, western Mongolia; Ghurayyah, Saudi Arabia). Unlike the first type, the mineralization and its host rocks do not show any features of crystal accumulation. The second group also includes the mineralization hosted by structurally controlled late-magmatic to hydrothermal quartz-feldspathic dikes related to peralkaline granites (e.g., Bokan Mountain, southeastern Alaska). At Bokan, the Dotson vein system has a strike length of more than 2,000 m and an average width of 50 m while individual dikes have a maximum width of 3 m (Robinson et al., 2011). The third group includes rare metal mineralization in peralkaline felsic volcanic rocks, typically trachytes where ore minerals are disseminated and are very fine grained (e.g., Dubbo Zirconia and Brockman/Hastings, Australia). The deposits hosted by nepheline syenites are more frequent, whereas the deposits of volcanic rocks are relatively rare.

All these deposits have several common characteristics: (1) they are enriched in U and Th and thus radioactivity makes a gamma-ray (radiometric) survey an effective exploration tool; (2) the host intrusions frequently have alteration halos (including fenitization) due to the escape of alkali-rich fluids from the magma into the country rocks; (3) the deposits are relatively enriched in HREE but depleted in LREE compared to carbonatites; and (4) they contain a wide variety of ore minerals that frequently show complex replacement textures and display late hydrothermal overprints, which appear to represent late stages of the evolution of the magmatic systems.

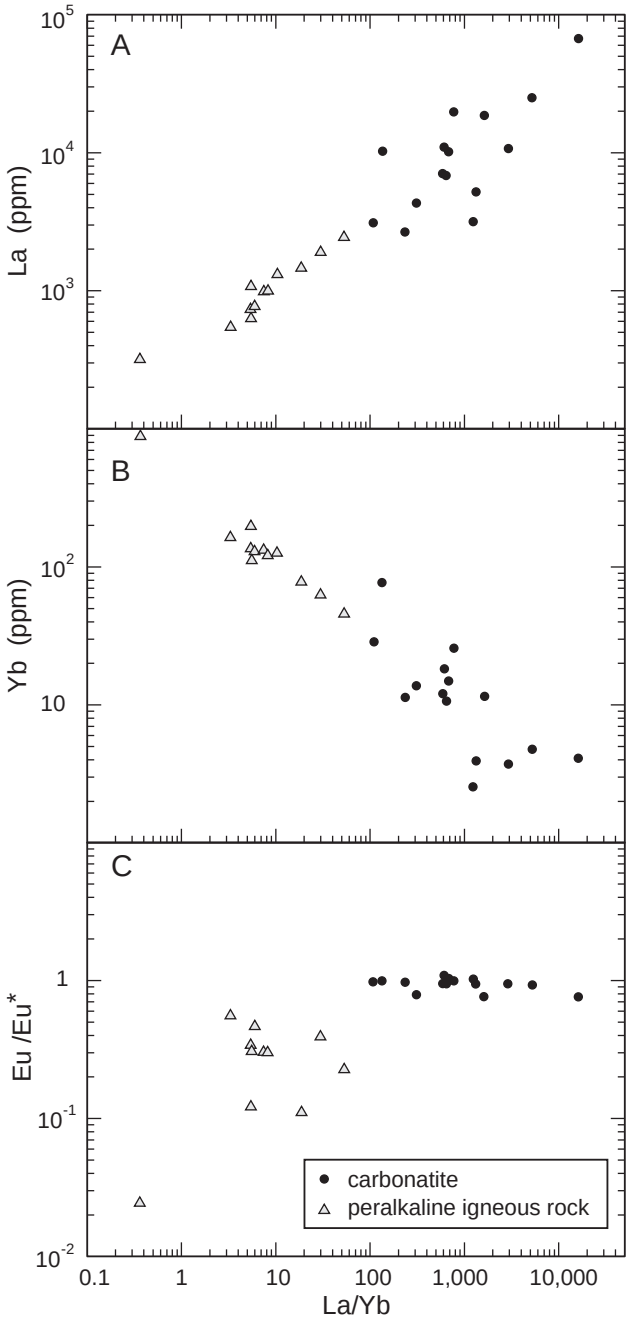

Fig. 4. The variations of La (ppm), Yb (ppm), and Eu/Eu* relative to La/Yb ratios in mineralized carbonatites and peralkaline granitic and nepheline syenitic rocks. Eu anomalies are calculated as $(Eu/Eu^*) = Eu_n/((Sm_n) x(Gd_n))^{1/2}$, where subscript n denotes the chondrite-normalized value and Eu* represents the Eu value expected for a smooth chondrite-normalized REE pattern (McLennan, 1989). Most data are the average grades of the REE reserves in the deposits and exploration projects reported by Hatch (2012).

The only REE deposits of peralkaline igneous rocks that are being actively mined are those in Kola Pensinsula in Russia. However, at present, a number of deposits are in advanced stages of exploration. The description of several prominent deposits are given below while the reserve estimates of some of the advanced exploration projects are given in Table 2 and their locations are shown in Figure 3.

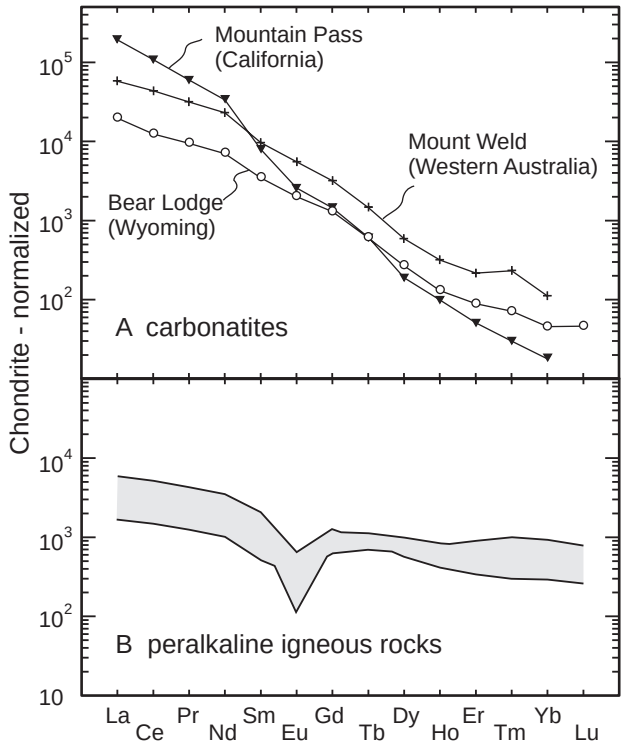

Fig. 5. Chondrite-normalized REE patterns of (A) the average ore of the major carbonatite-hosted REE deposits (Mountain Pass [California), Mount Weld [Western Australia], and Bear Lodge Mountains [Wyoming]), and (B) the range of the average ore of the REE deposits associated with peralkaline igneous rocks (Thor Lake, Strange Lake, Kipawa, Norra Kärr, and Bokan). The data from Hatch (2012), Saucier et al. (2012), Tasman Metal Ltd. (2012), Bakker et al. (2011), and Robinson et al. (2011). Normalizing values are after Sun and McDonough (1989).

Quality assurance/quality control (QA/QC) programs during exploration, as well as chemical analyses of the mineralized samples from these deposits, face additional analytical problems since the bulk of REE and HFSE is present in ore/accessory minerals. Some of these minerals are refractory in nature and thus analytical quality is an issue. Furthermore, QA/QC is typically based upon the use of reference samples to determine precision (repeatability) and accuracy (closeness to the "true" value) of the data. However, there are only a few proper Certified Reference Material standards high in REE and HFSE for undertaking QA/QC on analytical data.

The abbreviations TREE (total rare earth elements) or TREO (total rare earth element oxides), which are commonly used in exploration reports, include Y or oxide of Y in totals (Table 2). In the exploration industry, rare earths are typically reported as oxides in wt %, whereas in the research sector, they are reported as elemental values in ppm (g/t).

Deposits Associated with Nepheline Syenites

Thor Lake (Nechalacho), Northwest Territories, Canada

The Thor Lake deposit (also known as the Nechalacho deposit) is located about 100 km south of Yellowknife, Northwest Territories, Canada (Fig. 6), along the southern margin of the Slave Province of the Canadian Shield (e.g., Taylor and Pollard, 1996; Sheard et al., 2012). It is hosted by the

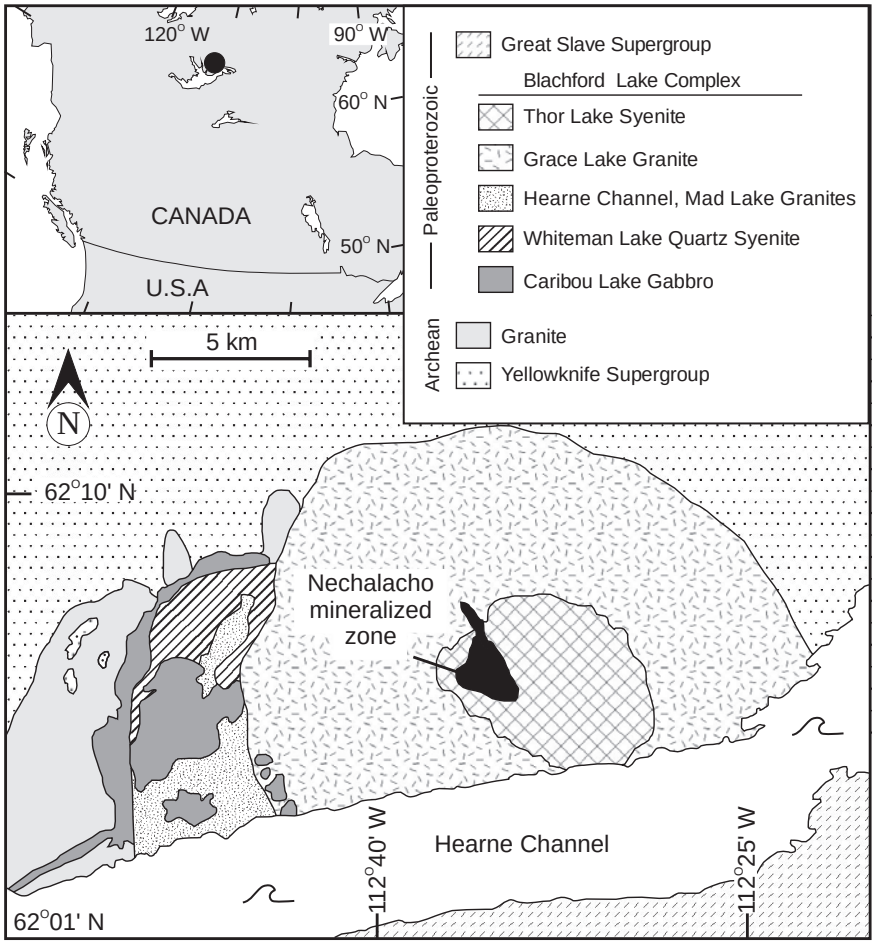

Fig. 6. Geologic sketch map of the Blachford Lake intrusive complex (Northwest Territories, Canada), showing the location of the Nechalacho mineralized zone. Modified after Sheard et al. (2012). The insert map shows the location of the deposit.

Precambrian Blatchford Lake Complex (2.1 Ga old), an elliptical-shaped intrusion about 16 × 33 km in size, which was emplaced in a failed rift zone. The complex (Taylor and Pollard, 1996; Sheard et al., 2012) consists of an earlier suite of gabbro (Caribou Lake gabbro), quartz syenite (Whiteman Lake quartz syenite), and granite (Hearne Channel and Mad Lake granites) and a later granitic intrusion (Grace Lake granite) intruded by the Thor Lake syenite. The two units (Grace Lake and Thor Lake) of the late suite are peralkaline and show a distinct enrichment in Nb, Zr, REE, U, and Th. However, the bulk of REE mineralization is hosted by an even younger unit in the core of the Thor Lake syenite (Sheard et al., 2012), the Nechalacho layered alkaline complex dated at 2094 ± 10 Ma (Bowring et al., 1984). The unit, which is only locally exposed at the surface, has been drilled over an area of ~5 km². This layered alkaline suite consists primarily of aegirine nepheline syenite (Sheard et al., 2012), which includes from top down: sodalite-bearing syenite roof cumulates, pegmatitic aegerine nepheline syenite, and a basal zone of foyaitic syenite, all of which show cumulate textures. The mineralization occurs primarily within two subhorizontal tabular zones: the 15- to 30-m-thick upper zone and the 15- to 60-m-thick lower zone (Sheard et al., 2012). The sodalite cumulate zone hosts the "upper mineralized zone" and the foyaitic syenite hosts the "basal zone mineralization" (Table 2).

The dominant primary accessory/ore phase in the upper zone is magmatic cumulate zircon while in the lower zone it is eudialyte. The presence of cumulate textures indicates that the initial REE mineralization was due to magmatic processes. Fluorine-rich orthomagmatic hydrothermal fluids altered the primary phases to form a complex assemblage of secondary REE-bearing phases and further concentrated the REE (Taylor and Pollard, 1996; Williams-Jones, 2010; Sheard et al., 2012). The primary ore minerals are largely pseudomorphed. At present, the major ore minerals in the upper and lower ore zones include zircon, fergusonite, allanite, synchysite, and bastnäsite (Sheard et al., 2012).

The REE pattern of the Thor Lake average ore (Fig. 7) is highly fractionated with $(La/Yb)_n$ ~18, $(Gd/Yb)_n$ ~4.4 (n-chondrite-normalized), and shows a distinct negative Eu anomaly. The La_n values reach ~6,000 (~1,400 ppm). The shape of the pattern differs from those of some other syenite-hosted REE deposits, such as Kipawa and Norra Kärr (Fig. 7), insofar as the Thor Lake pattern has higher LREE but lower HREE. Tonnage and grade of reported ore resources are given in Table 2.

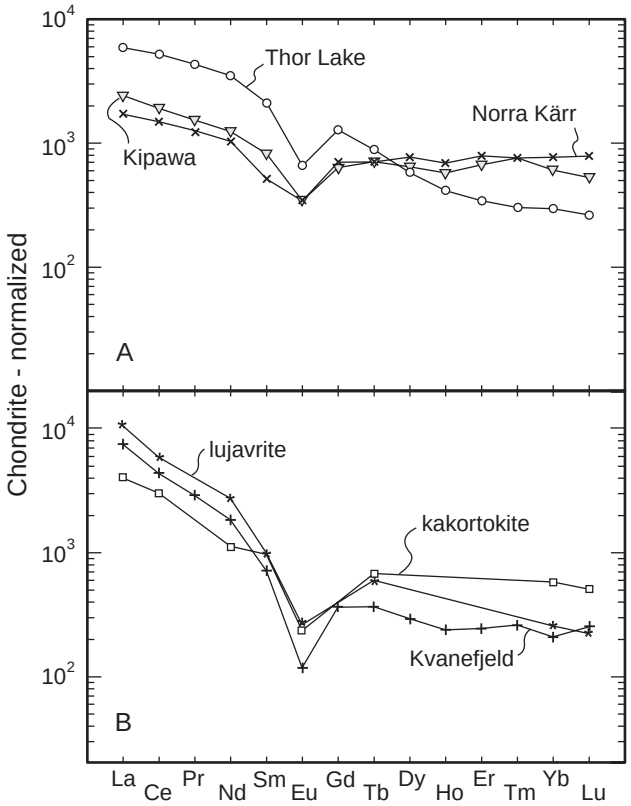

Fig. 7. Chondrite-normalized REE abundances of deposits hosted by nepheline syenites. (A). Average of the ore reserves of the Thor Lake, Kipawa, and Norra Kärr deposits. The data are from Saucier et al. (2012) for Kipawa, Tasman Metal Ltd. (2012) for Norra Kärr, and Bakker et al. (2011) for the Thor Lake (Nechalacho). (B). The eudialyte-rich kakortokite (layered eudialyte-bearing nepheline syenite) and the average of mineralized arfvedsonite lujavrites (meso- to melanocratic nepheline syenite) are from the Ilimaussaq Complex (after Bailey et al., 2001, and Sørensen et al., 2006). Also shown are the average REE concentrations of the ore reserves of the Kvanefjeld deposit (Hatch, 2012). Normalizing values are after Sun and McDonough (1989).

Ilimaussaq, Greenland

The 1.13 Ga-old Ilimaussaq intrusion (Paslick et al., 1993) is a part of the 1.1 to 1.3 Ga Gardar igneous province, an intracratonic rift zone in southern Greenland (Sørensen, 2001). It is one of the best known alkaline intrusions in the world with the famous occurrence of >200 mineral species, some of which are unique to the intrusion (Sørensen, 2001, 2006). The complex (Fig. 8) is the type locality for eudialyte, sodalite, arfvedsonite, and many other minerals (33 in total), as well as a type locality of agpaitic rocks (peralkaline nepheline syenite, Ussing, 1912).

The complex has the shape of an ellipsoid ~17 km in length and 8 km in width and an exposed vertical thickness of about 1,700 m (Sørensen, 2001, 2006). It is composed of a variety of syenitic/nepheline syenitic and peralkaline granitic rocks which were emplaced in three successive magma pulses at a shallow depth of ~3 to 4 km (Larsen and Sørensen, 1987). Successive "leaking" of the deep-seated magma chamber filled by mantle-derived alkali basaltic/nephelinitic parent magma was responsible for the three magma pulses rising to the high-level reservoir, where the melt underwent low-pressure closed-system fractionation (Markl et al., 2001, 2010; Sørensen, 2001, 2006). The earliest of these three stages (Stage I) is the weakly silica-undersaturated augite syenite (Larsen and Sørensen, 1987); it forms a few hundred meters-thick zone along the margin of the intrusion as well as a 150-m-thick lid on top of the intrusion (Marks and Markl, 2001). The lid was later intruded by a minor pulse of quartz syenite and peralkaline granite of Stage II. The high silica content of these rocks is attributed to crustal contamination (e.g., Larsen and Sørensen, 1987; Marks and Markl, 2001).

Stage III corresponds to the intrusion of a nepheline- and sodalite-bearing syenite magma which produced a series of roof and floor cumulates. The roof cumulate rocks crystallized in situ from the top downward, forming the succession: pulaskite (nepheline-bearing alkali feldspar syenite), foyaite (K-feldspar-rich nepheline syenite), sodalite foyaite, and naujaite (sodalite-rich nepheline syenite; Ussing, 1912; Bailey et al., 2001). The earliest exposed floor cumulates are kakortokites (layered eudialyte-bearing nepheline syenite) that are overlain by lujavrites (meso- to melanocratic nepheline syenite; Larsen and Sørensen, 1987), which show pronounced magmatic layering. Lujavrite also occurs as dikes and irregular masses cutting through all other rock types. The floor cumulates are younger than the roof cumulates and represent a separate pulse of magma which is volatile rich and distinctly enriched in incompatible elements such as REE, Be, U, and Nb (Friis and Mair, 2010). The magmatic evolution of the complex ends with the emplacement of pegmatites, hydrothermal veins rich in Zr, U, and REE minerals (e.g., steenstrupine, pyrochlore; Sørensen, 2001) and fenitization of the country rocks.

The Ilimaussaq Complex was explored by Danish geologists in the 1950s to 1970's. This work focused on finding uranium, particularly in an area known as Kvanefjeld, situated at the northwestern edge of the intrusion (Fig. 8; type locality for seven minerals). The uranium deposit, which was discovered there in 1956, is related to lujavrite. The ore is rich in both U and Th as well as in REE, Nb, and Zr (Sørensen et al., 2006, 2011).

Cuney and Kyser (2008) recognized two types of mineralization. One is related to magmatic processes, whereas the other is associated with late- to postmagmatic processes related to the exsolution of an orthomagmatic fluid phase. The chondrite-normalized REE pattern of the mineralized lujavrite is highly fractionated with $(La/Yb)_n$ ~40–100; Fig. 7); it is similar to that of the REE composition of the ore reserves of the Kvanefjeld deposit (Hatch, 2012).

In the Kangerluarsul area of the Ilimaussaq intrusion, a layered kakortokite sequence at least 285 m thick consists of 29 repetitive (rhythmically layered) units containing distinct eudialyte-bearing layers which are interpreted to be formed by the crystal settling and the repeated injection of magma (Sørensen, 1992). The chondrite-normalized REE pattern of eudialyte kakortokite ore (Fig. 7) is enriched in LREE with $(La/Yb)_n$ ~6 but with a flat HREE segment $(Gd/Yb)_n$ ~1 and with La_n ~4,000 (~1,000 ppm).

The main REE-bearing minerals in the complex are eudialyte, rinkite, and steenstrupine (Table 1). The latter is a major ore mineral in lujavrites and in the REE-U deposit at Kvanefjeld. The major host of Nb is pyrochlore while uraninite is the main U mineral. Tonnage and grades of the REE resources of

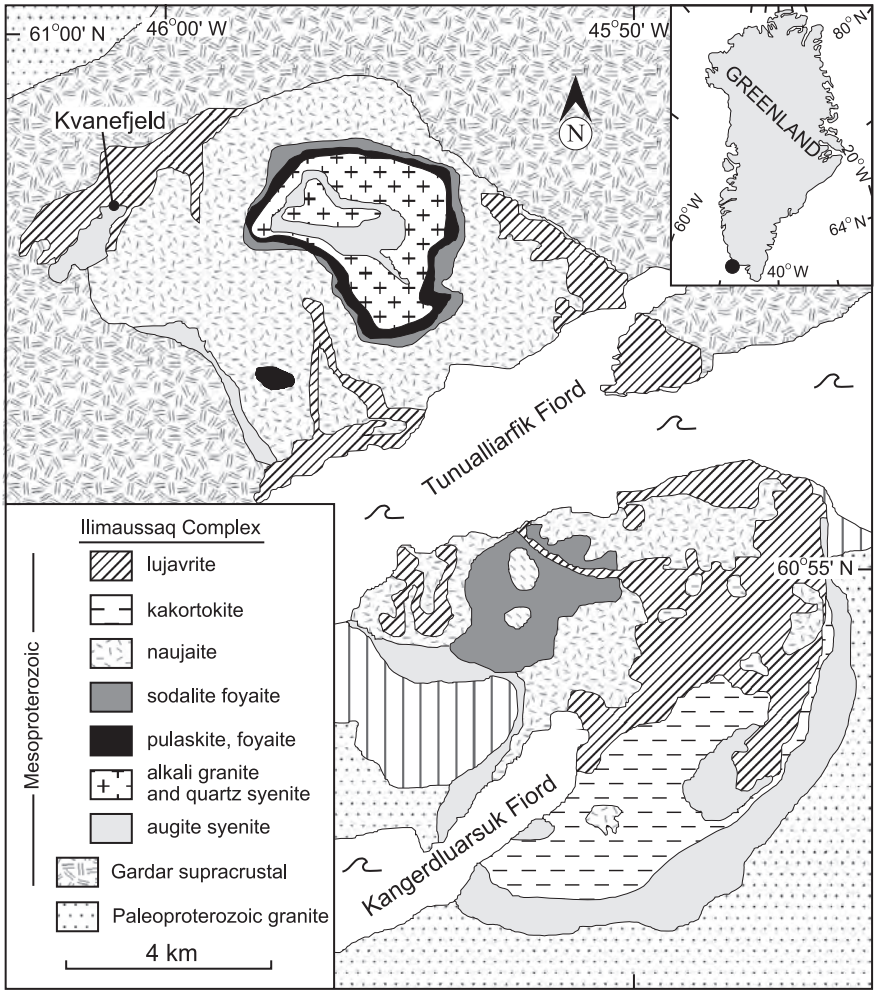

Fig. 8. Geologic sketch map of the Ilimaussaq peralkaline complex (southern Greenland). Modified after Bailey et al., (2001), Sørensen (2001), and Salvi and Williams-Jones (2005). The insert map shows the location of the complex. The roof cumulate rocks: pulaskite (nepheline-bearing alkali feldspar syenite), foyaite (K-feldspar-rich nepheline syenite), sodalite foyaite and naujaite (sodalite-rich nepheline syenite); the floor cumulates: kakortokite (layered eudialyte-bearing nepheline syenite) and lujavrite (meso- to melanocratic nepheline syenite).

the Kvanefjeld deposit are reported in Table 2. In the vicinity of Kvanefjeld, there are two other advanced projects with estimated ore reserves—Sørensen and Zone 3 (Table 2), which are geologically closely comparable to the Kvanefjeld deposit. In the Kangerluarsul area, which features multiple eudialyte-rich layers, the total rare metal resource was estimated to be ~2 Mt of ore containing 3 wt % ZrO_2, 1.6 wt % total rare earth element oxides, and 0.1 wt % Nb_2O_5 (Secher, 2002, Salvi and Williams-Jones, 2005).

Lovozero and Khibiny, Russia

The Devonian (~370 Ma) Lovozero Complex of the Kola Peninsula alkaline province of Russia (Fig. 9) is one of the world's largest peralkaline layered intrusions (Kramm and Kogarko, 1994; Kogarko et al., 1995). It forms a layered sheet-like lopolith the emplacement of which was tectonically controlled by a major NE-SW–trending fault. Geophysical data suggest that the intrusion continues to a depth of several kilometers (Kogarko et al., 2002, 2010). The oval-shaped ring intrusion (Fig. 9), which is hosted by the Precambrian rocks, underlies an area of about 650 km² and is composed of peralkaline nepheline syenitic rocks. It mainly consists of two intrusive phases. The older one, which forms the margin of the massif (Fig. 9), is made up of a strongly differentiated and layered sequence of urtites (80–90% nepheline, 10% aegirine, and also containing loparite), foyaites (leucocratic nepheline syenites with massive or trachytic texture), and lujavrites (meso- to melanocratic peralkaline nepheline syenite). The sequence ("differentiated complex") is rhythmically layered with layers ranging in thickness from a few centimeters to hundreds of meters (Kogarko et al., 2010). The total thickness of this sequence is about 2.5 km (Mitchell and Chakhmouradian, 1996).

The second magmatic phase, which represents a distinct magma pulse, overlies the differentiated sequence and forms the core of the complex. The second sequence is composed predominantly of eudialyte lujavrite and constitutes a sheet-like layered body about 450 m thick (Kogarko et al., 2010), which locally could reach a thickness of about 800 m (Chakhmouradian and Zaitsev, 2012; Linnen et al.,

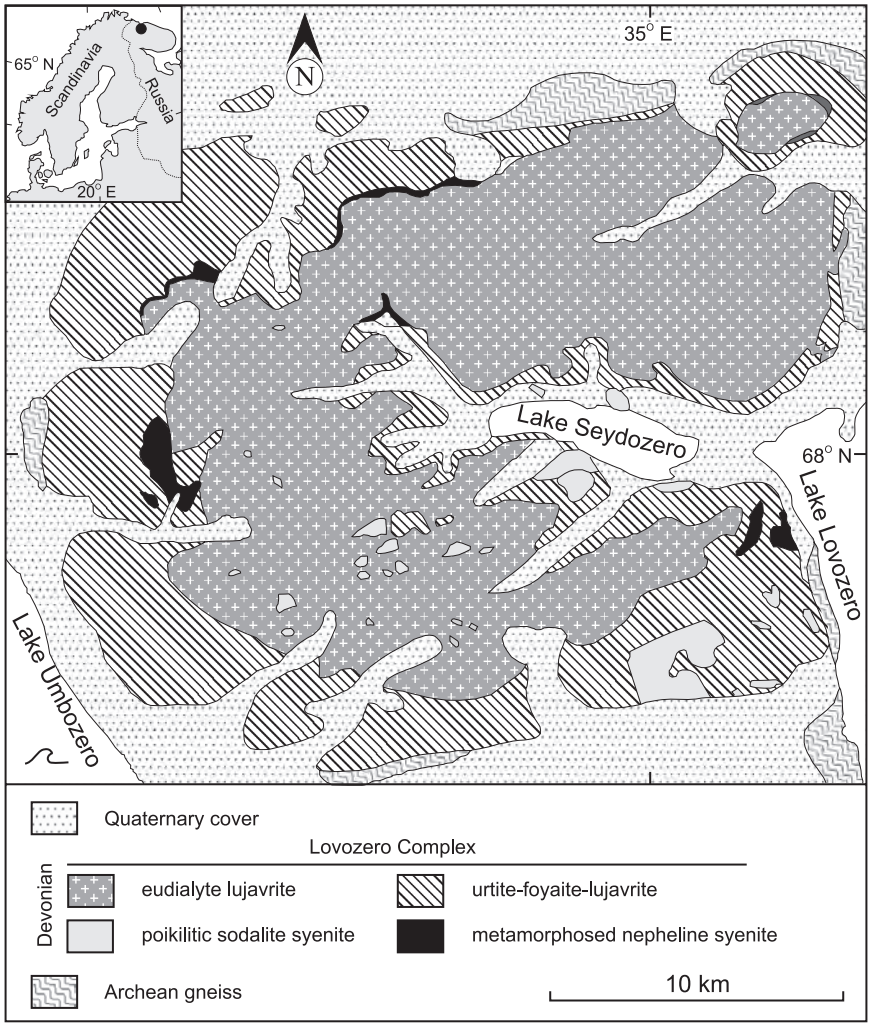

Fig. 9. Geologic sketch map of the Lovozero Complex of the Kola Peninsula of northwestern Russia. Modified after Kogarko et al. (2002) and Salvi and Williams-Jones (2005). The insert map shows the location of the complex. The older phase (differentiated sequence): urtite (80–90% nepheline, 10% aegirine, and also containing loparite), foyaite (leucocratic nepheline syenite with massive or trachytic texture), and lujavrite (meso- to melanocratic peralkaline nepheline syenite), the second phase: eudialyte lujavrite.

2014). The main rock-forming mineral phases of both these pulses are nepheline, K-Na feldspar, aegirine, arfvedsonite, and eudialyte (Kogarko et al., 2010). Eudialyte of the second phase is euhedral unlike in the lujavrites of the differentiated complex where it forms interstitial anhedral crystals. The Sr-Nd-Hf isotope signatures suggest that the rocks of the Lovozero massif are mantle derived and are not affected by crustal contamination (Kramm and Kogarko, 1994; Kogarko et al., 2010).

The two most important ore minerals of the Lovozero massif are loparite and eudialyte. Loparite occurs as a cumulus phase with grains mostly 0.2 to 0.6 mm in size (Castor and Hedrick, 2006), particularly in the urtites of the differentiated series. The loparite-rich ore bands are several centimeters to several meters thick and contain 2 to 3 vol % loparite (Castor and Hedrick, 2006), although in some layers loparite reaches up to 25 vol % (Kogarko et al., 2002). Loparite has been mined for more than a half-century. Current annual production in the Lovozero massif is about 6,000 t of loparite containing 30 to 35 wt % total rare earth element oxides, 8 to 12 wt % Nb_2O_5, and 0.6 to 0.8 wt % Ta_2O_5 (Zaitsev and Kogarko, 2012).The reserves of the loparite deposits are estimated at >1,000 Mt with 0.8 to 1.5 wt % total rare earth element oxides (Linnen et al., 2014).

Eudialyte of eudialyte lujavrite of the overlying unit occurs in layers or lenses (with >10 vol %, locally up to 50–85 vol % eudialyte) with 8 to 10 wt % ZrO_2 (Kogarko et al., 2010). Eudialyte is also an important source of REE (~2–2.5 wt % total rare earth element oxides; Chakhmouradian and Zaitsev, 2012), Hf, Y, Nb, and Ta (Kogarko et al., 2010). However, this mineral has not been commercially exploited because of difficulties with the REE extraction.

Kogarko et al. (2010) documented a cryptic compositional variation in the cumulate loparite implying that crystal accumulation played an important role during the evolution of the massif and that loparite deposits are of magmatic origin. Volatiles became concentrated in the residual melts, triggering a replacement of loparite during the postcumulus stage by

a variety of interstitial REE-bearing minerals, such as steenstrupine, monazite, and cerite.

In the proximity of the Lovozero massif there is another peralkaline intrusion of similar age (~368 Ma, Kramm and Kogarko, 1994; Kramm and Sindern, 2004)—the Khibiny massif, which is also the source of a wide range of exotic minerals and hosts the world's largest apatite deposit (Zaitsev et al., 1998). The intrusion is considered to be closely related to the Lovozero massif but both bodies have separate roots. The Khibiny massif is an elliptical-shaped ring complex about 40 km long and cropping out over an area of 1,327 km^2. The multiphase ring complex is composed of several concentric zones the age of which decreases inward. Each ring represents a separate intrusion mostly of nepheline syenitic magma and most of them show well-developed primary magmatic layering. The massif hosts several large apatite-nepheline deposits containing in total ~8,000 Mt of ore with 15 wt % P_2O_5 and 0.4 wt % total rare earth element oxides (Linnen et al., 2014). The ore is typically made up of ~60 to 90% apatite and has been mined for phosphate over 80 years. The apatite, which contains about 0.9 wt % total rare earth element oxides (Chakhmouradian and Zaitsev, 2012), is believed to be a result of the accumulation of apatite during the fractional crystallization of the magma (Kogarko et al., 1984). The REE are not extracted from apatite because of technical problems.

Red Wine Mountains, Labrador, Canada

The peralkaline Red Wine intrusive suite and related volcanic and subvolcanic rocks of the Letitia Lake Group (Curtis and Currie, 1981; Hill and Miller, 1991) of central Labrador (as well as the Strange Lake deposit) were emplaced during a major Mesoproterozoic anorogenic magmatic event in Labrador and northeastern Quebec, which took place between ~1460 and ~1240 Ma (Kerr, 2011); they are considered to represent an extension of the Gardar igneous province of Greenland, which has a comparable age (Currie, 1985). In central Labrador, the rare metal mineralization is hosted in intrusive and less commonly in volcanic rocks. The Red Wine intrusive suite (dated at 1330 Ma; Kerr, 2011) intrudes the coeval Letitia Lake Group, which consists of dominantly peralkaline felsic volcanic and pyroclastic rocks and small syenitic intrusions. All these rocks are strongly affected by the ~1 Ga Grenvillian orogeny; they are highly deformed and metamorphosed and have gneissic textures (Kerr, 2011).

The Red Wine suite forms two high-level intrusions (North and South Red Wine plutons, Curtis and Currie, 1981; Hill and Miller, 1991), each about 15 km long and 5 km wide occurring about 2 km apart. They consist of metamorphosed peralkaline felsic rocks, ranging from nepheline- to quartz-bearing varieties. The silica-oversaturated rocks typically form thick envelops around a smaller core composed of the silica-undersaturated rocks. The rocks occur mainly as banded gneisses with only relicts of the original igneous textures (Kerr, 2011). Both rock types contain two feldspars, arfvedsonite and aegirine. The undersaturated rocks have nepheline and eudialyte, whereas the oversaturated type contains quartz. The main rare metal-bearing mineral is eudialyte, which is disseminated or occurs in discrete layers locally composed of up to 50% eudialyte. The mineralized zones contain on average about 1 wt % total rare earth element oxides (Kerr, 2011). Kerr (2011) noted similarities of the Red Wine intrusive suite to the mineralized sequences of Kipawa (Quebec, Canada) and Illimaussaq (Greenland). On this basis, the Red Wine mineralization is considered to belong to the first deposit type (associated with nepheline syenites), although the relationship is less clear due to strong metamorphism and deformation.

The Letitia Lake Group (dated at 1327 ± 4 Ma, U-Pb zircon; Hill and Thomas, 1991; Kerr, 2011) occurs just east of the Red Wine plutons. It also contains several REE-Nb-Be prospects hosted by strongly deformed peralkaline quartz syenites and related volcanic rocks (Miller, 1987). One of the advanced exploration prospects is the Two Tom Lake project which occurs in a small (~2 km diam) peralkaline, alkali amphibole-bearing syenite stock that intrudes volcanic rocks of the Letitia Lake Group. Exposure of the mineralization is poor. The deposit, which is composed of multiple mineralized zones, is steeply dipping, at least 1.1 km long and 80 to >200 m wide (Daigle, 2012). LREE are mostly present in monazite and undetermined Ce-Ca-bearing silicate, whereas the latter hosts the bulk of HREE. The majority of Nb is contained in pyrochlore and niobophyllite while Be is in barylite. Other ore minerals are allanite, britholite, thorite, and gadolinite (Kerr, 2011; Daigle, 2012). The reported mineral resources of the Two Tom Lake project are given in Table 2. The ore has a relatively low HREE oxide/total rare earth element oxide ratio (6.26%; Table 2). The Two Tom Lake prospect probably belongs to the second type of the REE deposits (associated with peralkaline granites). However, due to tectono-thermal overprinting and a limited amount of published data, its classification is uncertain.

Pilanesberg, South Africa

The Pilanesberg Complex is a circular differentiated alkaline intrusion about 25 km in diameter and underlying an area of approximately 530 km^2. It crops out at the junction of the granitic and noritic phases of the Bushveld Complex, north of Rustenburg in the western Transvaal, South Africa (Ferguson, 1973; Lurie and Cawthorn, 1984; Lurie, 1986). The complex was emplaced about 1,250 ± 50 m.y. ago (Lurie and Cawthorn, 1984) at the intersection of two tectonic lineaments, and consists of partly eroded alkaline volcanics (pyroclastics and lava-flow units) intruded by ring dikes and cone sheets concentrically arranged around the core (Laurie, 1986). The core and rings/cones are composed mainly of nepheline syenites; some nepheline syenites display trachytoid textures (foyaites; Lurie and Cawthorn, 1984; Lurie, 1986). In addition, there are also tinguaites (phonolites), which form sheets and dikes, and syenites that constitute the oldest intrusive phase of the complex. The dominant minerals of the silica-undersaturated rocks are K-feldspar, albite, nepheline, and aegirine-augite although their proportions are variable. These rocks were affected by extensive autometasomatic processes (Olivo and Williams-Jones, 1999; Mitchell and Liferovich, 2006), which led to a significant enrichment of rare metals including REE and HFSE in some highly fractionated nepheline syenites. One of the major rock-types,"green foyaite," which occurs in the outer zone of the body contains up to 19,900 ppm Zr and 6,500 ppm REE (Olivo and Williams-Jones, 1999). These elements are present mainly in eudialyte which constitutes up to 20 vol % of the rock (Olivo and Williams-Jones, 1999). In

addition, this mineralized rock type contains zircon, britholite, and fergusonite. The rocks are also high in fluorite (typically 0.45 vol %). Lurie (1986) and Lurie and Cawthorn (1984) described rare metal mineralization from Thabayadiotsa, one of the sites within the "green foyaite" zone at the eastern sector of the complex. There the mineralized bands, which are 0.5 to 2 m thick, contain 1.3 to 10% of combined total rare earth element oxides and ThO_2. Estimated reserves at this site are 13.5 Mt ore containing 0.7 wt % total rare earth element oxides + ThO_2. The complex is located within a national park and there has not been recent exploration.

Deposits Associated with Peralkaline Granites

Strange Lake, Quebec-Labrador, Canada

The Strange Lake deposit is hosted by a circular ring complex about 8 km in diameter that is composed of peralkaline granite (Fig. 10). The complex straddles the boundary between the Canadian provinces of Quebec and Newfoundland and Labrador. The complex dated at 1240 ± 2 Ma (U-Pb zircon, Miller et al., 1997) intrudes Archean metamorphic rocks of the Rae Province of the Canadian Shield and Mesoproterozoic (~1.5–1.4 Ga) granitic rocks.

The complex which is bounded by an outwardly dipping ring fracture, filled by a fluorite-rich breccia, contains three main phases. The core of the intrusion, which is the oldest phase (Kerr, 2011), is composed of hypersolvus granite (contains one alkali feldspar: perthitic K-feldspar, in addition to quartz, and interstitial arfvedsonite). This granite is termed "exotic poor" by Miller (1986) as it has relatively low contents of rare metal (exotic) minerals, although the rock is still strongly enriched in incompatible elements, including REE, compared to most granites. The outer zone of the pluton is younger and is formed by subsolvus granite (i.e., containing two alkali feldspars: discrete crystals of microcline and albite in addition to quartz and arfvedsonite, which can be present both as phenocrysts and in the groundmass). It is termed the "exotic" granite by Miller (1986) as it has significantly higher contents of HFSE and REE than the hypersolvus granite. The third phase of the intrusion is a minor unit in the center of the complex composed of subsolvus granite strongly enriched in HFSE and REE. It is termed the "exotic-rich" granite by Miller (1986) and represents the youngest phase of the intrusion. There are also numerous mineralized pegmatite dikes (10–50 cm thick), which are subvertical and located mainly in subsolvus granites. Kerr (2011) considered them to be a part of the third phase. At the center of the complex, a 6- to 20-m-thick pegmatite dike hosted by subsolvus granite represents the bulk of the potential ore zone (Miller, 1990; Boily and Williams-Jones, 1994).

According to Kerr and Rafuse (2012) there are two types of mineralization, i.e., low-grade orthomagmatic, disseminated mineralization hosted primarily by the exotic-rich granite and high-grade mineralization hosted by pegmatites and pegmatite-aplite zones. A well-developed textural and chemical zonation in pegmatites suggests in situ crystallization from volatile-rich silicate magma (Kerr and Rafuse, 2012). The mineralization consists of a number of unusual minerals, including gittinsite, pyrochlore, bastnäsite, monazite, kainosite-(Y), elpidite, and gadolinite. Many of these minerals are secondary. Hydrothermal overprinting of primary mineral assemblages played an important role during the formation of the ore (Salvi and Williams-Jones, 1990, 1996). Many ore minerals occur in multiphase mineral assemblages typically as pseudomorphs of preexisting phases. Fluid inclusions suggest that the complex was emplaced at a shallow depth (<3 km; Salvi and Williams-Jones, 1990, 2005).

The chondrite-normalized REE pattern of the mineralization (Fig. 11) shows an enrichment in LREE but flat HREE segment with $(La/Yb)_n$ ~3.3, $(Gd/Yb)_n$ ~0.8, and a pronounced

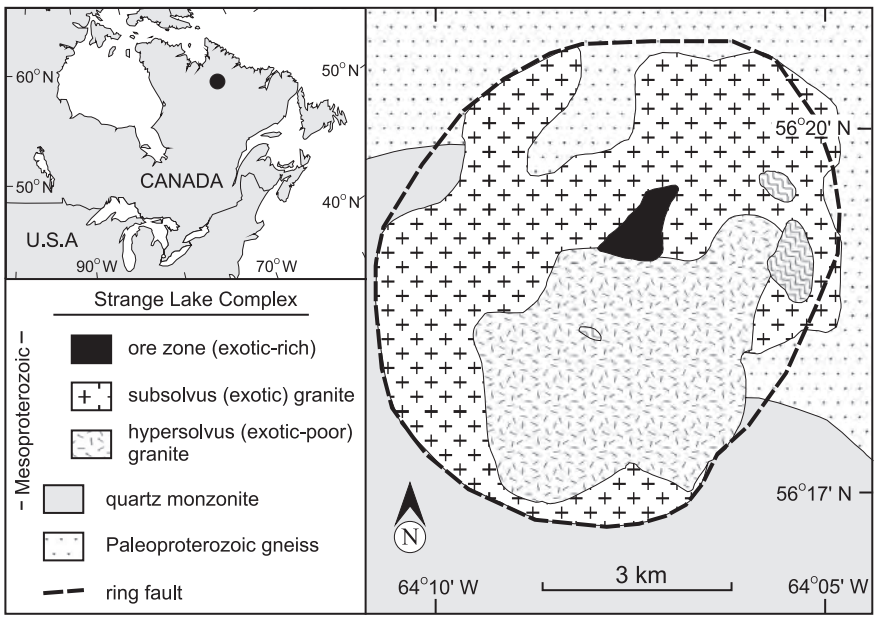

Fig. 10. Geologic sketch map of the Strange Lake Complex (Quebec/Labrador, Canada). Modified after Miller (1986), Salvi and Williams-Jones (1996, 2005), and Kerr and Rafuse (2012). The insert map shows the location of the complex.

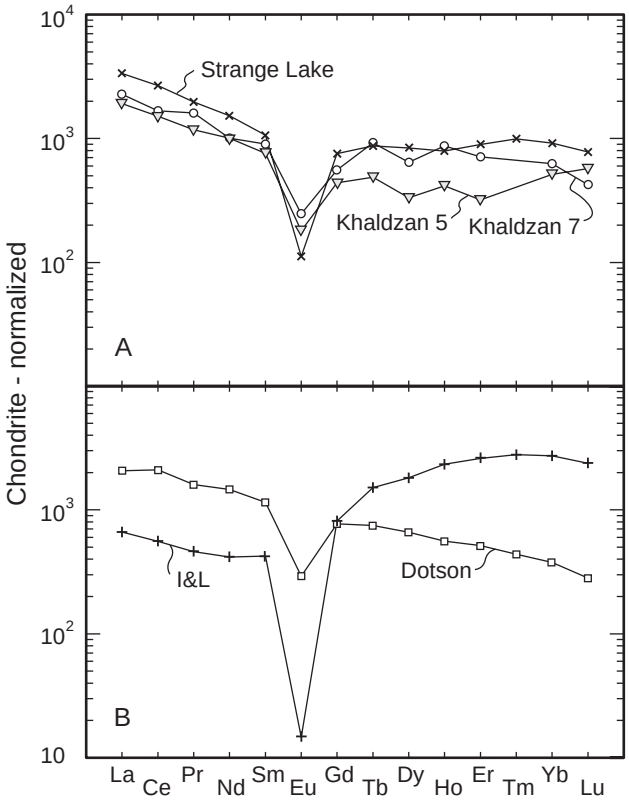

Fig. 11. Chondrite-normalized REE abundances of deposits hosted by peralkaline granites. (A). The average of the ore reserves of the Strange Lake deposit as well as the averages of two mineralized phases (phase 5 and 7 of Kovalenko et al., 1995) of the Khaldzan-Buregtey intrusion of Mongolia (after Kovalenko et al., 1995). The average of the REE concentrations of the Strange Lake deposit is from Daigle et al. (2011). (B). The average ore reserves of the Dotson and I and L mineralized zones of the Bokan Mountain deposit (Robinson et al., 2011). Normalizing values are after Sun and McDonough (1989).

negative Eu anomaly. Tonnage and grade of the estimated REE reserves of the Strange Lake deposit are given in Table 2.

Khaldzan-Buregtey, Mongolia

The Khaldzan-Buregtey massif is a composite intrusion of peralkaline granitoids located in Mongolian Altay, western Mongolia (Kovalenko et al., 1995, 2007; Kempe et al., 1999; Salvi and Williams-Jones, 2005) and is a part of a Paleozoic belt of alkaline intrusions within the prominent Tsagan-Shibetin fault zone. This Devonian (392–395 Ma, Kovalenko et al., 2007), oval-shaped complex is about 30 km long and up to 8 km wide. It is composed predominantly of nordmarkite (peralkaline quartz syenite), which forms the outer rim of the complex, and younger peralkaline granite. These rocks were intruded by dikes of peralkaline granites as well as by two small mineralized stocks. The larger of the two mineralized granites crops out over an area of about 0.85 km^2 and is composed of medium-grained arfvedsonite- and aegirine-bearing peralkaline granite. The stock is in turn intruded by a small body of fine- to medium-grained miarolitic peralkaline granite. The geochemical characteristics, including the high positive ε_{Nd} values (~4.4–6.5; Kovalenko et al., 2007), suggest that the rocks of this multiphase intrusion were derived from the same mantle-related source (Kovalenko et al., 2007).

The rare metal minerals are disseminated through the mineralized zones within both mineralized stocks and include bastnäsite, monazite, elpidite, gittinsite, zircon, and pyrochlore and are accompanied by fluorite. However, some of these minerals are secondary. Although the rare metal-rich peralkaline granites were modified by alteration processes, a melt inclusion study (Kovalenko et al., 1995) indicates that the original magma was enriched in rare metals.

The massif hosts one large Zr-Nb-REE deposit (Khaldzan-Buregtey, Kovalenko et al., 1995; Kempe et al., 1999) and several smaller ones. The reserves of the deposit have not yet been calculated. Kempe et al. (1999) provided an estimate of resources for the main deposit: 0.6 Mt Nb_2O_5, 0.035 Mt Ta_2O_5, 4 Mt ZrO_2, 1 Mt REE oxides, 0.1 Mt Y_2O_3, while Salvi and Williams-Jones (2005) reported an estimate of the average ore grade (2 wt % Zr, 0.4 wt % Nb, and 0.3 wt % REE). Kovalenko et al. (1995, 2007) and Salvi and Williams-Jones (2005) noted that the mineralization of Khaldzan-Buregtey is similar to that of Strange Lake. In fact, the chondrite-normalized REE patterns of the two mineralized zones are similar to the pattern of the Strange Lake deposit (Fig. 11), although they have a smaller negative Eu anomaly.

Ghurayyah, Saudi Arabia

The Ghurayyah deposit (Küster, 2009) is hosted by a Neoproterozoic granitic complex in the northwestern Arabian Shield (northwestern Saudi Arabia). The shallow-seated intrusion is a circular stock about 900 m in diameter with steeply dipping contacts, located at the intersection of two prominent tectonic lineaments (Drysdall and Douch, 1986; Küster, 2009). The emplacement occurred between 610 and 570 Ma (Küster, 2009) during postorogenic extension (Stoeser, 1986) in an intraplate setting (Küster, 2009). The stock is composed of porphyritic peralkaline microgranites containing euhedral phenocrysts of quartz, K-feldspar, and subordinate sodic amphibole (arfvedsonite) which encloses aegirine cores. The groundmass is made up of quartz, albite, K-feldspar, and minor mica and fluorite, which also occurs as veinlets. Accessory/ore minerals are fine grained (<1 mm in size) and disseminated in the groundmass throughout the stock; they reach up to 5 vol % (Jackson and Ramsay, 1986). They are mainly zircon, columbite-tantalite, pyrochlore, samarskite, aeschynite, xenotime, monazite, uraninite, and thorite as well as monazite, bastnäsite, and synchysite Y, which are the main REE carriers (Harris and Marriner, 1980, Drysdall et al., 1984). The deposit contains an estimate of 385 Mt of ore with 245 g/t (ppm) Ta_2O_5, 2,840 ppm Nb_2O_5, 8,915 ppm ZrO_2, 1,270 ppm Y_2O_3, and 140 ppm U_3O_8 (Küster, 2009). The REE concentrations are also elevated (Küster, 2009; Fig. 12) but the reserves have not yet been calculated. The chondrite-normalized REE patterns of the mineralized samples (Fig. 12) are distinctly enriched in HREE with $(La/Yb)_n$ ~0.07 to 0.25 and $(Gd/Yb)_n$ ~0.1 to 0.24 and with a pronounced negative Eu anomaly.

Bokan Mountain, Alaska

The Bokan Mountain Complex is a small circular stock of about 3 km in diameter located near the southern tip of

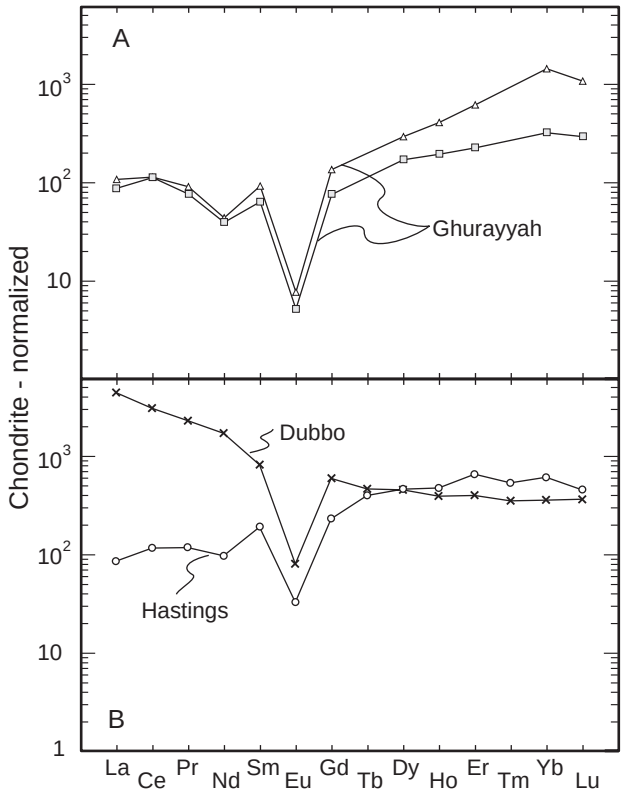

Fig. 12. Chondrite-normalized REE abundances of (A) two mineralized peralkaline granites from the Ghurayyah intrusion (Drysdall et al., 1984), and (B) ore reserves of the Dubbo Zirconia and Hastings/Brockman deposits (Hatch, 2014). Normalizing values are after Sun and McDonough (1989).

Prince of Wales Island (southeastern Alaska) where it (Fig. 13) intrudes Lower Paleozoic rocks of the Alexander terrane of the North American Cordillera (Dostal et al., 2011, 2013, 2014). The Jurassic (177 Ma) Bokan Mountain Complex is concentrically zoned and consists of (1) a core made up of arfvedsonite granite, and (2) an outer ring composed predominantly of aegirine granite (Fig. 13). The high positive ε_{Nd} values of the peralkaline granitic rocks suggest that the rocks were derived from a mantle-related source (Philpotts et al., 1998; Dostal et al., 2011, 2014).

The major REE prospects predominantly occur as clusters of subparallel mineralized dikes or veins and metasomatically enriched alteration halos associated with shear fault zones. These mineralized bodies occur both within the complex (e.g., I and L zone), as well as in the Paleozoic granitic host rocks (e.g., Dotson zone). The largest cluster is the ca. 50-m-wide Dotson zone that extends for >2 km (Fig. 13). REE are present in various accessory/ore minerals, including xenotime, monazite, fergusonite, pyrochlore, bastnäsite, synchysite, allanite, zircon, iimoriite, kainosite, and cerite (Staatz, 1978; Philpotts et al., 1998; Dostal et al., 2011, 2014; Robinson et al., 2011). Many of these minerals are secondary occurring as the partial to complete replacement of preexisting minerals or mineral assemblages and frequently form complex intergrowths due to postmagmatic and hydrothermal processes.

The REE concentrations of the two most significant prospects, Dotson and I and L zones differ (Fig. 11). The average concentrations of the mineralized parts of the I and L zone are distinctly enriched in HREE with $(La/Yb)_n$ ~0.22, and $(Gd/Yb)_n$ ~0.3 whereas the similar average for the Dotson zone yields $(La/Yb)_n$ ~5, $(La/Sm)_n$ ~1.6, and $(Gd/Yb)_n$ ~2.0. Tonnage and grade of ore resources in the dominant Dotson zone are reported in Table 2.

The complex also hosts a U-Th deposit (Ross-Adams mine; Fig. 13), which was mined intermittently between 1957 and 1971. The mine produced about 85,000 t of ore with a grade

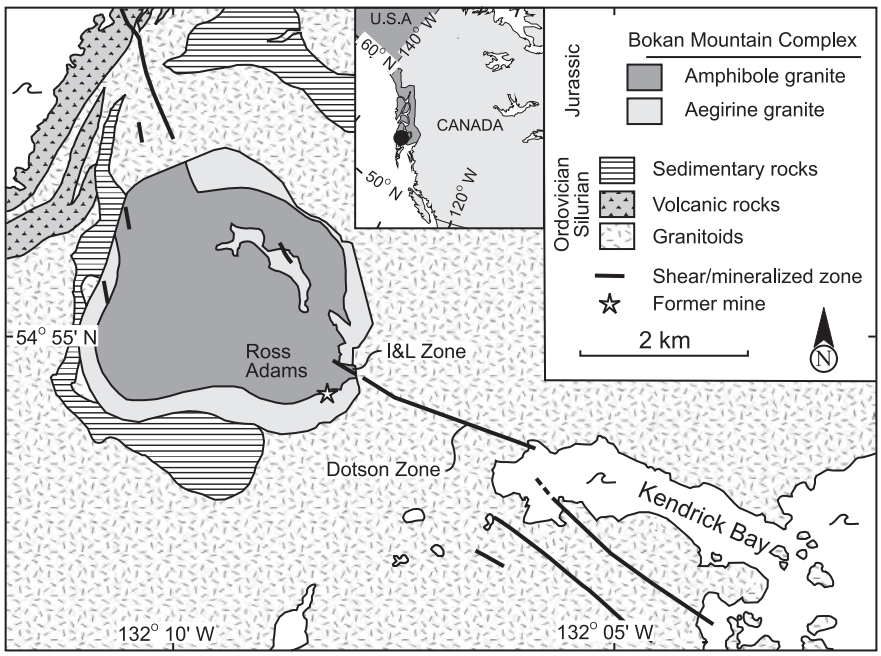

Fig. 13. Geologic sketch map of Bokan Mountain Complex (southernmost Alaska, United States). Modified after MacKevett (1963) and Thompson (1988). The insert map shows the location of the complex.

of ~1 wt % U_3O_8 and 3 wt % ThO_2 (Long et al., 2010). The main ore minerals are thorite and uraninite. The deposit is a mineralized alteration zone along a sheared fault. It has the shape of an irregular pipe which was about 24 m wide and mined along the strike for more than 300 m (Thompson, 1988; Long et al., 2010).

The thorium-uranium, REE, and HFSE mineralization is genetically related to the Bokan Complex and is thought to be of magmato-hydrothermal origin (Thompson, 1988; Philpotts et al., 1998; Barker and Van Gosen, 2012; Dostal et al., 2014). Most of the REE and HFSE mineralization reflects both an initial magmatic event and, more importantly, a pervasive orthomagmatic hydrothermal metasomatism which upgraded the mineralized zones (Dostal et al., 2011, 2014; Barker and Van Gosen, 2012; Verplanck et al., 2014).

Deposits Associated with Peralkaline Volcanic Rocks

Dubbo Zirconia, Australia

The Dubbo Zirconia (or Toongi) deposit located about 400 km northwest of Sydney in New South Wales (Australia) is hosted by the Toongi intrusive which is a nearly vertical Jurassic trachyte plug about 900 m long and 600 m wide (Chalmers, 2012). This body belongs to an aerial to subaerial Mesozoic alkaline volcanic intraplate complex, which is about 15 to 20 km in diameter. The complex which was emplaced on top of Triassic clastic sediments consists of two parts. The lower part is composed of alkali basalt flows dated at 200 Ma and the upper part is made up of trachyte-trachyandesite lava flows, tuff sheets, plugs, and domes associated with minor nepheline syenite intrusions. The 184-m.y.-old Toongi peralkaline trachyte, which belongs to the upper part of the complex, is composed of microphenocrysts of K-feldspar (~30–40%), plagioclase (30–40%), and aegirine (~15–20%) set in a fine-grained (cryptocrystalline) matrix also containing accessory ore minerals. Ore minerals are very fine grained and less than 100 μm in size (typically <20 μm). They include eudialyte and armstrongite, the main carriers of Zr, Y, and HREE, niobite which hosts the bulk of Nb and Ta, and bastnäsite containing most of REE, particularly LREE. The REE and HFSE mineralization is dispersed relatively uniformly throughout the plug. It is assumed that the parent alkali basalt-trachyandesite magma underwent extensive in situ fractionation with an enrichment of volatiles and incompatible elements (HFSE and REE) at the top of magma chamber (Chalmers, 2012). Ore minerals appear to be primary interstitial phases that crystallized at the last stages of magma evolution. Late magmatic to hydrothermal fluids led to the enrichment of primary magmatic mineralization (Chalmers, 2012). The chondrite-normalized REE pattern of the average mineralization (Fig. 12) is characterized by a distinct enrichment of LREE with $(La/Yb)_n$ ~11.2, $(Gd/Yb)_n$ ~4.8, and a distinct negative Eu anomaly. The rare metal reserves are given in Table 2.

Hastings/Brockman, Australia

The Hastings (or Brockman) deposit located ~18 km southeast of Halls Creek, Western Australia, occurs within the Proterozoic Halls Creek mobile zone. The mineralization is hosted by a fluorite-bearing, felsic volcaniclastic unit informally known as the "Niobium tuff." It is the lowermost unit of the Brockman volcanics, a sequence composed of trachytic and rhyolitic lavas, volcaniclastic units, and subvolcanic intrusions (Taylor et al., 1995b), which are part of the Halls Creek Group, a thick early Proterozoic volcano-sedimentary sequence. The Niobium tuff varies in thickness from 5 to 35 m and can be traced for over 3.5 km. This trachytic volcaniclastic rock contains variable proportions of pumice, quartz, albite, and lithic fragments enclosed in a devitrified microcrystalline groundmass (Ramsden et al., 1993). The volcanic detritus of the tuffs is ~1,870 m.y. old (Taylor et al., 1995b). The Niobium tuff contains distinct enrichment in HFSE and HREE (Taylor et al., 1995a). The ore minerals are very fine grained (<20 μm) and disseminated. They include zircon, gel zircon (unusual hydrous Y-Th-Nb-bearing secondary zircon; Ramsden et al., 1993), Y-REE niobates as well as bastnäsite, parasite, and synchysite. The main carrier of HREE is gel zircon, which contains ~5,000 ppm Dy, 5,000 ppm Er, 6,000 ppm Yb, 1,400 ppm Gd, and 600 pm Sm (Ramsden et al.,1993). LREE are mainly in bastnäsite, parasite, and synchysite. Fluorite is intimately associated with the ore minerals. Trachytic flows overlying the Niobium tuff contain the same ore minerals but in minor amounts. The Niobium tuff is probably a result of the pyroclastic eruption of highly fractionated intraplate trachytic magma in a rift-related basin in a shallow-marine setting (Ramsden et al., 1993; Taylor et al., 1995a, b). Its mineralization is considered to be the product of extreme fractionation of magma concentrated in the upper parts of the magma chamber, which was subsequently overprinted by late-stage fluorine-rich fluids that enhanced rare metal grades in the rocks. Late-stage hydrothermal fluids associated with the magma reacted with precursor magmatic minerals, particularly columbite and zircon, and produced the observed mineralization (Ramsden et al., 1993; Taylor et al., 1995a). The mineralization shows a pronounced relative depletion of LREE relative to HREE (Fig. 12) with $(La/Yb)_n$ ~0.13 and $(Gd/Yb)_n$ ~0.38, and a negative Eu anomaly. The ore reserves are given in Table 2.

Discussion

In intracontinental rift and fault zones, alkaline rocks are not uncommonly spatially associated with carbonatites (e.g., Bell, 1998; Berger et al., 2009; Verplanck and Van Gosen, 2011; Jones et al., 2013; Verplanck et al., 2014), which also host economically important REE deposits. The relationship of mantle-derived alkaline silicate and carbonatite magmas is still under discussion. Carbonatite and primitive alkaline magmas could have been derived separately from a metasomatically enriched upper mantle source by a small degree of partial melting. For example, Martin and De Vito (2005) suggested that in an extensional environment the difference between two magmas can be related to the type of metasomatism, whereby an enrichment by mantle-derived CO_2-rich fluids would lead to carbonatitic melts, whereas the metasomatism by H_2O-rich fluids would generate A-type granites (Linnen et al., 2014). Alternatively, carbonatites have also been considered to be derived from parent alkaline magmas either by fractional crystallization or by liquid immiscibility (e.g., Bell, 1998; Jones et al., 2013). Carbonate-silicate liquid immiscibility has frequently been invoked and is supported by experimental works (e.g., Veksler, 2004; Veksler and Lentz, 2006; Jones et al., 2013; Martin et al., 2013).

There is still some controversy regarding the origin of the peralkaline magmas and their high concentrations of rare metals, as well as a debate about whether the HFSE, REE, Th, and U mineralization associated with these rocks is due to purely magmatic processes (i.e., extensive fractional crystallization/crystal accumulation) or is associated with late magmatic-hydrothermal activities. If fluids played a role during the formation, a question arises regarding whether the fluids are orthomagmatic or derived from country rocks. These topics will be discussed in turn.

Evolution of the host peralkaline granitic and syenitic rocks

It is generally well documented that peralkaline nepheline syenites, syenites, and granites can be generated by extensive low-pressure fractionation from a nephelinitic, basanitic, or basaltic parent (Platt, 1996; Winter, 2001; Frost and Frost, 2008). This process will drive parent liquid compositions toward low-temperature residual liquids rich in alkalis, silica, and alumina and generate melts with phonolitic (nepheline syenitic), trachytic (syenitic), and pantelleritic (peralkaline granitic) characteristics.

High contents of rare metals in peralkaline felsic rocks are usually attributed in part to protracted fractional crystallization. In peralkaline granitic and syenitic rocks, these elements are highly incompatible. Their solid-liquid partition coefficients (K_D = concentration in mineral/concentration in liquid) for common rock-forming minerals, including feldspars and feldspathoids in alkaline melts, are very low (<<1), and thus these elements do not easily enter into their crystal structure (e.g., Shaw, 2006). Rather, they are progressively enriched in the residual magmas during fractional crystallization and show extreme enrichment at the last stage of crystallization. The compositional characteristics of these rocks are consistent with the model of protracted evolution of the alkaline magmas leading to an extremely fractionated melt composition at low temperatures (e.g., Markl et al., 2001: <450°C). This is in part due to the role of volatiles, particularly fluorine (Linnen, 1998), which depress the solidus temperature in the rock systems, thus extending the range of crystallization to anomalously low temperatures (Dostal and Chatterjee, 1995, 2000; Markl et al., 2001). Alkalis and fluorine also increase the solubility of Zr, Nb, Ta, REE, Th, and U in volatile-bearing peralkaline felsic magmas (Linnen and Keppler, 1997, 2002). Thus, fractionation is further enhanced by high concentrations of alkalis and fluorine in the peralkaline magmas which suppresses crystallization of HFSE- and REE-bearing accessory/ore minerals until the last stages of crystallization (Linnen, 1998; Halter and Webster, 2004).

Negative Eu anomalies in the chondrite-normalized patterns of peralkaline felsic rocks (Fig. 5), as well as the Sr and Ba depletion on the primitive mantle normalized plots (Fig. 14), reflect the fractionation of feldspars (the phases enriched in Eu, Sr, and Ba with K_D >>1), suggesting that these rocks (both nepheline syenite and granite) solidified from highly evolved melts which underwent extensive, low-pressure, feldspar-dominated crystal fractionation. This is consistent with the observation that the rare metal mineralization of both nepheline syenites and peralkaline granites is typically associated with the most fractionated parts of the intrusions.

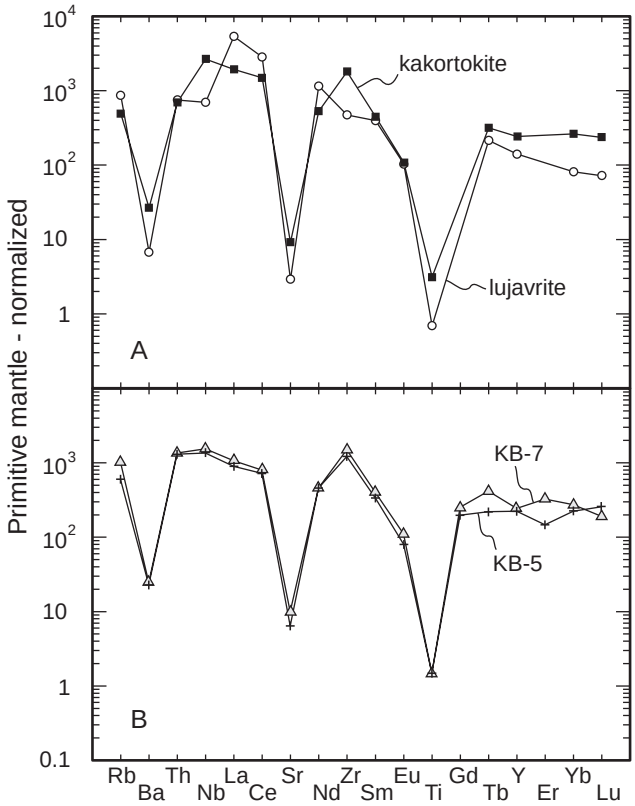

Fig. 14. Primitive mantle-normalized trace element abundances in (A) mineralized nepheline syenites (eudialyte kakortokite and mineralized arfvedsonite lujavrite) from the Ilimaussaq intrusion (after Bailey et al., 2001, and Sørensen et al., 2006; kakortokite - layered eudialyte-bearing nepheline syenite and lujavrite-meso- to melanocratic nepheline syenite), and (B) mineralized peralkaline granites from Khaldzan-Buregtey intrusion of Mongolia (after Kovalenko et al., 1995). KB-5 = average composition of mineralized intrusive phase 5, KB-7 = average composition of the mineralized intrusive phase 7. Normalizing values are after Sun and McDonough (1989).

Source rock composition

Alkaline/peralkaline magmas, including parents to nepheline syenitic melts, are typically assumed to be derived by a low degree of melting of a mantle source (e.g., Platt, 1996; Pilet et al., 2008). The high contents of incompatible rare metals observed in these rocks require a metasomatically enriched lithospheric mantle rather than primitive mantle source (e.g., Shaw et al., 2007; Pilet et al., 2008). Moreover, the high concentrations of halogens suggest the presence of amphibole or phlogopite in the mantle source. The bulk of the REE in the mantle source was either in amphibole or in accessory minerals such as Ti oxides (Chakhmouradin and Zaitsev, 2012). The large size of some silica-undersaturated layered intrusions such as those in the Kola Peninsula implies the involvement of a large volume of metasomatized mantle source.

There is still some debate about the origin of the peralkaline silica-oversaturated felsic rocks. Peralkaline granitic magma cannot be readily derived by partial melting of common crustal source rocks, which are typically peraluminous. In order to account for the chemical composition of peralkaline granitic rocks, several source-related models/processes have been invoked: (1) crustal contamination of

silica-undersaturated alkaline magmas (e.g., Goodenough et al., 2000; Marks and Markl, 2001); (2) melting of lower crustal material, possibly metasomatized by mantle-derived fluids (e.g., Lentz, 1996; Martin and De Vito, 2005); (3) melting of an underplated alkali-rich mafic source (e.g., Bonin, 2007; Jahn et al., 2009); and (4) melting of metasomatically enriched lithospheric mantle (e.g., Upton et al., 2003; Shaw et al., 2007; Pilet et al., 2008).

Crustal contamination of silica-undersaturated alkaline magma was suggested for quartz syenites associated with nepheline syenites of the Ilimaussaq Complex (Marks and Markl, 2001). Although this process can account for the Ilimaussaq quartz syenites, it does not apply to all peralkaline granitic rocks. In the Bokan Mountain Complex, for example, the consistently high positive ε_{Nd} values in peralkaline granites and oxygen isotopice ratios argue against extensive crustal contamination (Philpotts et al., 1998, Dostal et al., 2011). Furthermore, contamination by typical crustal material would not lead to the observed distinct enrichment of incompatible trace elements and to the unusual composition of peralkaline rocks.

Although all these models for the origin of the peralkaline granite are plausible, these rocks are compositionally similar to their volcanic equivalents. Thus, it can be speculated that the origin of the peralkaline granitic rocks probably resembled that of recent peralkaline volcanic rocks, such as pantellerites, for which mantle melting followed by fractional crystallization has been invoked (Mungall and Martin, 1996; Civetta et al., 1998; Ronga et al., 2010). Regardless of the model, the parent magmas of peralkaline granitic rocks not associated with alkaline silica-undersaturated rocks have probably been derived by a low degree of melting of enriched lithospheric source (mantle or mantle derived). Such a mantle source is enriched in incompatible trace elements and possesses positive ε_{Nd}.

Origin of mineralization

The genesis of the HFSE and REE mineralization associated with the peralkaline rocks is not well understood and there is still considerable debate as to whether the mineralization is magmatic, hydrothermal, or a combination of the two (e.g., Salvi and Williams-Jones, 1990, 1996, 2005; Dostal et al., 2004; Halter and Webster, 2004; Veksler, 2004; Cerny et al., 2005; Linnen and Cuney, 2005). The magmatic model assumes that the rare metal enrichment is mainly due to extensive fractional crystallization. However, the mineralization is typically associated with altered parts of alkaline intrusions, suggesting that the enrichment is related to hydrothermal activities unless the association is only coincidental.

Volatiles undoubtedly play an important role in the evolution of the highly evolved peralkaline rocks (e.g., Marks et al., 2003; Salvi and Williams-Jones, 2005; Markl et al., 2010). The parent melts of the peralkaline felsic rocks are generated under relatively dry and reducing conditions (Salvi and Williams-Jones, 2005; Frost and Frost, 2008). When these magmas undergo extensive fractionation, they become saturated with aqueous fluids only very late in the crystallization history. At these advanced stages of fractionation, the aqueous fluids escape from the magma highly enriched in incompatible elements (such as REE, HFSE, Th, and U) and containing significant amounts of halogens, particularly fluorine. Thus the hydrothermal fluids, which are enriched in all these elements, can play an important role in concentrating HFSE, REE, Th, and U as well as during autometasomatism (e.g., Halter and Webster, 2004, Veksler, 2004; Salvi and Williams-Jones, 2005). It appears that both magmatic and hydrothermal processes are likely to have contributed to the formation of the rare metal deposits of peralkaline rocks. The initial magmatic mineralization of rare metals was subsequently remobilized and enriched by volatile-rich magmatic fluids, which were released during the late stage of the evolution of the magma.

The deposits related to layered silica-undersaturated syenite complexes display various indicators of crystal accumulation such as cumulate textures. As most rare metal-bearing minerals have high specific gravity, they tend to accumulate at the bottom of the evolved magma chamber. In these intrusions, REE mineralization is frequently associated with layers rich in REE-bearing minerals (Salvi and Williams-Jones, 2005) including, for example, many distinct eudialyte-rich layers in the Ilimaussaq Complex (Sørensen, 2001). On the other hand, in pegmatites like those at in Strange Lake, minor intrusions at Khaldzan-Buregtey and felsic dikes at Bokan Mountain, there are no obvious indications of crystal accumulation. The primary magmatic mineralization is probably related to crystallization of highly fractionated, late-stage, fluorine-rich peralkaline magma in pegmatites, minor intrusions, and dikes. In deposits such as Bokan Mountain, where the mineralization is frequently associated with altered zones and largely composed of secondary minerals, most of which pseudomorphically replaced primary minerals, the secondary hydrothermal processes played a rather important role.

All these deposits typically show imprints of hydrothermal processes that led to the remobilization of REE, HFSE, U, and Th and their redeposition in the nearby mineralized sites as secondary phases. The secondary processes not only redistributed but also enriched REE in the mineralized zones (e.g., Salvi and Williams-Jones, 2005; Verplanck et al., 2014). During remobilization, LREE moved greater distances than HREE (Williams-Jones et al., 2012). Salvi and Williams-Jones (1996) inferred that the remobilization took place at low temperatures ($\leq$350°C).

Evidence for hydrothermal alteration of large layered intrusions, such as Lovozero, that lack signs of crustal input suggest that hydrothermal fluids are orthomagmatic, although a minor contribution of crust-derived fluids in some smaller intrusions is possible. The orthomagmatic origin of the bulk of the fluids is also in accordance with available oxygen isotope data (e.g., Taylor and Pollard, 1996; Kovalenko et al., 2007).

Exploration

REE mineralization is closely associated with alkaline/peralkaline igneous rocks. Thus exploration for REE deposits typically encompasses a search for these host rocks. Exploration guides for peralkaline rock-associated REE deposits include:

1. Tectonic environment: The deposits and their host peralkaline complexes typically occur in continental anorogenic tectonic settings and are associated with zones of rifting and/or faulting. If hosted by a layered alkaline/peralkaline complex, the mineralization is typically associated with evolved, differentiated parts of the complex.

2. Mineralogy: Peralkaline complexes, particularly those which are mineralized, can contain relatively rare but colorful indicator minerals. According to Richardson and Birkett (1996), these potentially useful minerals include eudialyte (pink/red), sodalite (dark blue), aegirine (dark green), riebeckite/arfvedsonite (dark bluish-green), and fluorite (purple). Other mineralogical reconnaissance indicators of REE mineralization are heavy minerals. A significant part of the mineralization is hosted in ore/accessory minerals which are resistant to weathering. Thus, the presence of abundant resistate rare metal-rich minerals in heavy mineral concentrates of stream sediments or soils is a useful exploration tool. These indicator minerals include monazite, xenotime, zircon, pyrochlore, allanite, and thorite (Barker and Van Gosen, 2012; Verplanck et al., 2014).
3. Geochemistry: Peralkaline rocks associated with REE mineralization have anomalously high concentrations of REE, Zr, Hf, Nb, Ta, Th, U, and F compared to most granitic rocks (Bowden, 1985; Linnen and Cuney, 2005). The elevated abundances of these elements typically contrast with regional background concentrations (Richardson and Birkett, 1996) and are useful reconnaissance indicators of the mineralization during geochemical surveys of stream sediments, residual soils, and rocks (Richardson and Birkett, 1996; Verplanck et al., 2014). Regional lake water surveys revealed that F, U, and Pb can be useful pathfinders for REE mineralization (Richardson and Birkett, 1996).
4. Wall-rock alteration: The country rocks in contact with peralkaline intrusive bodies frequently have alteration halos due to the escape of alkali-rich magmatic fluids into the surrounding country rocks, causing alkali metasomatism including fenitization (Le Bas, 2008). The alkali-rich fluids hydrothermally altered the rocks and converted at least some minerals to alkali-rich phases such as alkali feldspars. However, compared to the carbonatite complexes, the alteration halos surrounding the peralkaline intrusions are less extensive, ranging from tens to a few hundred meters in width (Richardson and Birkett, 1996; Verplanck et al., 2014).
5. Geophysics: Ground and airborne geophysical exploration methods are excellent exploration tools for these deposits. Radiometric (gamma-ray), magnetic, and gravity surveys have been recently used in the exploration for these deposits to identify and delineate peralkaline/alkaline igneous complexes and their mineral deposits (Thomas et al., 2010). The REE deposits are enriched in U and Th and thus radioactivity inherent to them makes gamma-ray (radiometric) survey an effective exploration tool. In fact, many known REE deposits/advanced exploration projects (e.g., Kipawa, Bokan, Greenland) were discovered during the search for uranium deposits (Verplanck et al., 2014). Magnetic and gravity surveys can be used to locate peralkaline intrusions; their anomalies do not reflect REE mineralization but are typically produced by the magnetic and density characteristics of intrusions. Distinct magnetic and gravity anomalies can delineate igneous bodies or tectonic lineaments. Richardson and Birkett (1996) and Verplanck et al. (2014) noted that several REE deposits, including Strange Lake, Kipawa, and Bokan, displayed distinct positive radiometric but negative magnetic anomalies during an airborne geophysical survey.

Conclusions

Peralkaline igneous rocks host mineralization and deposits of REE, HFSE, U, and Th. The host rocks are typically peralkaline granites and nepheline syenites and less commonly volcanic rocks, particularly trachytes. These rocks occur in intraplate tectonic environments, mostly in continental settings where they are related to rifting faulting and/or crustal extension. They range in age from Neoarchean/Paleoproterozoic to Mesozoic although several important deposits are Mesoproterozoic (1000–1460 Ma) in age. Likewise, large REE deposits hosted by carbonatites are of Mesoproterozoic age including the Mountain Pass (~1400 Ma) and Bayan Obo (~1300 Ma).

The mineralization is intimately related to the crystallization history of magma, particularly to the late stages of the evolution. The bulk of rare metals is present in ore minerals and includes a variety of REE-bearing phases, which commonly show complex replacement textures. REE-bearing minerals include fluorocarbonates, phosphates, silicates, and oxides. Economically most important are bastnäsite, monazite, xenotime, loparite, eudialyte, synchysite, and parasite. Compared to the carbonatite deposits, the mineralization typically has lower LREE concentrations but has higher contents of HREE.

The deposits include three distinct types. The first is hosted by nepheline syenitic rocks of layered peralkaline/alkaline intrusions. The mineralization mostly occurs in layers rich in rare metal-bearing minerals, which show cumulate textures. The minerals accumulated at highly fractionated parts of the intrusions because of the high specific gravity and low viscosity of the melts. These deposits include Thor Lake/Nechalacho (Canada), Ilimaussaq (Greenland), Lovozero (Russia), Kipawa (Canada), Norra Kärr (Sweden), and Pilanesberg (South Africa). The second type corresponds to mineralization in the Nb-Y-F-type pegmatites, felsic dikes, and veins and in minor highly fractionated peralkaline granitic intrusions where REE-bearing minerals are commonly disseminated. Examples of the deposits of this type are at Strange Lake (Canada), Khaldzan-Buregtey (Mongolia), Ghurayyah (Saudi Arabia), and Bokan (Alaska, United States). The third type is associated with peralkaline felsic volcanic rocks, commonly trachytes, where fine-grained ore minerals are disseminated through the body. The examples of this mineralization are the Dubbo Zirconia and Brockman/Hastings deposits in Australia.

Elevated concentrations of U and Th of the ore assemblages make gamma-ray (radiometric) survey an important exploration tool. Other useful geophysical techniques when exploring for the alkaline/peralkaline intrusions are magnetic and gravity surveys. Geologic exploration indicators of REE-bearing alkaline hosts include intraplate continental environments rifting and/faulting, alteration halos, and indicator minerals.

The parent alkali or transitional basaltic magmas of peralkaline nepheline syenites and granites were derived from a lithospheric source metasomatically enriched in HFSE, REE, Th, U, and halogens by low degrees of partial melting. The melting was triggered probably by adiabatic uplift or mantle plume activities. The melts underwent fractional crystallization

during their ascent achieving syenitic or granitic composition. The host peralkaline (nepheline syenitic and granitic) magmas were derived by extensive fractional crystallization, which was protracted in part due to high contents of halogens and alkalis. At the late stages of differentiation when magma becomes fluid saturated and rich in rare metals, rare metal-bearing minerals started to crystalize.

The deposits typically record two periods of mineralization. The primary magmatic mineralization is associated with crystallization of highly fractionated peralkaline magma rich in HFSE, REE, Th, and U. The primary mineralization was overprinted during the second period, by late magmatic to hydrothermal fluids rich in REE, HFSE, Th, and U that remobilized and enriched the original ore probably during multiple metasomatic events. These fluids were dominantly orthomagmatic, released during the last stages of the magma evolution. These deposits and prospects represent one of the most economically important resources of heavy REE including Y.

Acknowledgments

I would like to thank Phil Verplanck and Rich Goldfarb for soliciting this contribution to the volume. The research was supported by U.S. Geological Survey Mineral Resources External Research Program, the Natural Sciences and Engineering Research Council of Canada, and Ucore Rare Metals. Thanks are also due to Phil Verplanck, Rich Goldfarb, David Lentz, and Victor Owen for careful reviews and Randy Corney for technical assistance.

REFERENCES

Abdel-Rahman, A.M., 1994, Alkali amphibole: A potential source of rare earth elements in felsic alkaline rocks: Exploration and Mining, v. 3, p. 81–94.

Alkane Resources Ltd., 2014, Research reports—projects: Dubbo Zirconia project: http://www.alkane.com.au/index.php/projects/current-projects/dubbo.

Arzamastsev, A.A., Bea, F., Arzamastseva, L.V., and Montero, P., 2002, Rare earth elements in rocks and minerals from alkaline plutons of the Kola Peninsula, NW Russia, as indicators of alkaline magma evolution: Russian Journal of Earth Sciences, v. 4, p. 187–209.

Bailey, J.C., Gwozdz, R., Rose-Hansen, J., and Sørensen, H., 2001, Geochemical overview of the Ilímaussaq alkaline complex, South Greenland: Geology of Greenland Survey Bulletin, v. 190, p. 35–54.

Bakker, F., Delaney, B., Mercer, B., and Qi, D., 2011, Technical report on the Nechalacho deposit, Thor Lake project, Northwest Territories, Canada: Report NI43-101, 289 p., http://www.avalonraremetals.com/.

Barker, J.C., and Van Gosen, B.S., 2012, Alaska's rare earth deposits and resource potential: Mining Engineering, v. 64, p. 20–32.

Bea, F., 1996, Residence of REE, Y, Th and U in granites and crustal protoliths: Implications for the chemistry of crustal melts: Journal of Petrology, v. 37, p. 521–552.

Bell, K., 1998, Radiogenic isotope constraints on relationships between carbonatites and associated silicate rocks—a brief review: Journal of Petrology, v. 39, p. 1987–1996.

Berger, V.I., Singer, D.A., and Orris, G.J., 2009, Carbonatites of the world, explored deposits of Nb and REE-database and grade and tonnage models: U.S. Geological Survey Open-File Report 2009-1139, 17 p., http://pubs.usgs.gov/of/2009/1139/.

Boily, M., and Williams-Jones, A.E., 1994, The role of magmatic and hydrothermal processes in the chemical evolution of the Strange Lake plutonic complex, Québec-Labrador: Contributions to Mineralogy and Petrology, v. 118, p. 33–47.

Bonin, B., 2007, A-type granites and related rocks: Evolution of a concept, problems and prospects: Lithos, v. 97, p. 1–29.

Bowden, P., 1985, The geochemistry and mineralization of alkaline ring complexes in Africa (a review): Journal of African Earth Sciences, v. 3, p. 17–39.

Bowden, P., Black, R., Martin, R.F., Ike, E.C., Kinnaird, J.A., and Batchelor, R.A., 1987, Niger-Nigerian alkaline ring complexes: A classic example of African Phanerozoic anorogenic mid-plate magmatism: Geological Society Special Publication 30, p. 357–379.

Bowring, S.A., Van Schmus, W.R., and Hoffman, P.F., 1984, U-Pb zircon ages from Athapuscow Aulacogen, East Arm of Great Slave Lake, N.W.T., Canada: Canadian Journal of Earth Sciences, v. 21, p. 1315–1324.

Castor, S.B., 2008a, Rare earth deposits of North America: Resource Geology, v. 58, p. 337–347.

——2008b, The Mountain Pass rare-earth carbonatite and associated ultrapotassic rocks, California: Canadian Mineralogist, v. 46, p. 779–806.

Castor, S.B., and Hedrick, J.B., 2006, Rare earth elements, *in* Kogel, J.E., Trivedi, N.C., Barker, J.M., and Krukowski, S.T., eds., Industrial minerals and rocks—commodities, markets, and uses, 7th ed.: Littleton, CO, Society for Mining, Metallurgy, and Exploration, p. 769–792.

Cerny, P., and Ercit, T.S., 2005, Classification of granitic pegmatites revisited: Canadian Mineralogist, v. 43, p. 2005–2026.

Cerny, P., Blevin, P.L., Cuney M., and London, D., 2005, Granite-related ore deposits: Economic Geology, v. 100, p. 337–370.

Chakhmouradian, A.R., and Wall, F., 2012, Rare earth elements: Minerals, mines, magnets (and more): Elements, v. 8, p. 333–340.

Chakhmouradian, A.R., and Zaitsev, A.N., 2012, Rare earth mineralization in igneous rocks: Sources and processes: Elements, v. 8, p. 347–353.

Chalmers, I., 2012, The Toongi rare metal and rare earth deposit-Dubbo zirconia project: International Geological Congress, 34th, Brisbane, Australia, www.alkane.com.au/pdf/presentations/20120808.pdf

Ciuculescu, T., Foo, B., Gowans, R., Hawton, K., Jacobs, C., and Spooner, J., 2013, Technical report disclosing the results of the feasibility study on the Nechalacho rare earth elements project: Mincon International Ltd., http://www.avalonraremetals.com/_resources/projects/may_2013_ni43_report.pdf.

Civetta, L., D'Antonio, M., Orsi, G., and Tilton, G.R., 1998, The geochemistry of volcanic rocks from Pantelleria Island, Sicily Channel: Petrogenesis and characteristics of the mantle source region: Journal of Petrology, v. 39, p. 1453–1491.

Clarke, D.B., 1992, Granitoid rocks: London, UK, Chapman and Hall, 283 p.

Clemens, J.D., Holloway, J.R., and White, A.J.R., 1986, Origin of an A-type granite: Experimental constraints: American Mineralogist, v. 71, p. 317–324.

Cox, K.G., Bell, J.D., and Pankhurst, R.J., 1979, The interpretation of igneous rocks: London, UK, George Allen and Unwin, 450 p.

Cuney, M., and Kyser, T.K., 2008, Deposits related to magmatic differentiation: Mineralogical Association of Canada Short Course, v. 39, p. 55–77.

Currie, K.L., 1985, An unusual peralkaline granite near Lac Brisson, Quebec-Labrador: Geological Survey of Canada Paper 85-1A, p. 73–80.

Curtis, L.W. and Currie, K.L., 1981, Geology and petrology of the Red Wine Alkaline Complex, central Labrador: Geological Survey of Canada Bulletin 294, 61 p.

Daigle, P., 2012, Resource estimate and technical report for the Two Tom REE deposit of the Red Wine Complex, Labrador, Canada: Report to Rare Earth Metals Inc., 163 p., http://www.canadarareearth.com/upload/documents/twotom-43-101.pdf

Daigle, P., Robinson, J., and Baughman, D., 2011, Strange Lake, resource model update: Report to Quest Rare Minerals, 116 p., http://www.questrareminerals.com/.

Dostal, J., and Chatterjee, A.K., 1995, Origin of topaz-bearing and related peraluminous granites of Late Devonian Davis Lake pluton, Nova Scotia, Canada: Crystal versus fluid fractionation: Chemical Geology, v. 123, p. 67–88.

——2000, Contrasting behaviour of Nb/Ta and Zr/Hf ratios in a peraluminous granitic pluton (Nova Scotia, Canada): Chemical Geology, v. 163, p. 207–218.

Dostal, J., Chatterjee, A.K., and Kontak, D.J., 2004, Chemical and isotopic (Pb, Sr) zonation in a peraluminous granite pluton: Role of fluid fractionation: Contributions to Mineralogy and Petrology, v. 147, p. 74–90.

Dostal, J., Kontak. D.J., Hanley, J., and Owen, V., 2011, Geological investigation of rare earth element and uranium deposits of the Bokan Mountain Complex, Prince of Wales Island, southeastern Alaska: U.S. Geological Survey Mineral Resources External Research Program Report GO9PA00039, 122 p.

Dostal, J., Karl, S.M., Keppie, J.D., Kontak, D.J., and Shellnutt, J.G., 2013, Bokan Mountain peralkaline granitic complex, Alexander terrane (southeastern Alaska): Evidence for Early Jurassic rifting prior to accretion with North America: Canadian Journal of Earth Sciences, v. 50, p. 678–691.

Dostal, J., Kontak, D.J., and Karl, S.M., 2014, The Early Jurassic Bokan Mountain peralkaline granitic complex (southeastern Alaska): Geochemistry, petrogenesis and rare-metal mineralization: Lithos, v. 202–203, p. 395–412.

Drysdall, A.R., and Douch, C.J., 1986, Nb-Th-Zr mineralization in microgranite-microsyenite at Jabal Tawish, Midyan region, Kingdom of Saudi Arabia: Journal of African Earth Sciences, v. 4, p. 275–288.

Drysdall, A.R., Jackson, N.J., Ramsay, C.R., Douch, C.J., and Hackett, D., 1984, Rare element mineralization related to Precambrian alkali granites in the Arabian Shield: Economic Geology, v. 79, p. 1366–1377.

Eby, G.N., 1990, The A-type granitoids: A review of their occurrence and chemical characteristics and speculations on their petrogenesis: Lithos, v. 26, p. 115–134.

——1992, Chemical subdivision of the A-type granitoids: Petrogenetic and tectonic implications: Geology, v. 20, p. 641–644.

Ferguson, J., 1973, The Pilansberg alkaline province: Transactions Geological Society of South Africa, v. 76, p. 207–214.

Förster, H.J., Tischendorf, G., Trumbull, R.B., and Gottesmann, B., 1999, Late-collisional granites in the Variscan Erzgebirge, Germany: Journal of Petrology, v. 40, p. 1613–1645.

Friis, H., and Mair, J.L., 2010, Ilímaussaq alkaline complex, a unique rare element deposit: British Columbia Geological Survey Open File 2010-10, p. 37–40.

Frost, B.R., and Frost, C.D., 2008, A geochemical classification for feldspathic igneous rocks: Journal of Petrology, v. 49, p. 1955–1969.

Frost, C.D., and Frost, B.R., 2011, On ferroan (A-type) granitoids: Their compositional variability and modes of origin: Journal of Petrology, v. 52, p. 39–53.

Frost, B.R., Barnes, C.G., Collins, W.J., Arculus, R.J., Ellis, D.J., and Frost, C.D., 2001, A geochemical classification for granitic rocks: Journal of Petrology, v. 42, p. 2033–2048.

Goodenough, K.M., Upton, B.G.J., and Ellam, R.M., 2000, Geochemical evolution of the Ivigtut granite, South Greenland: A fluorine-rich "A-type" intrusion: Lithos, v. 51, p. 205–221.

Gowans, R.M., Hutchinson, I., Lewis,W.J., Shoemaker, S., Spooner, J., and Zalnieriunas, R.V., 2013, NI 43-101: Technical report on the pre-feasibility study for the Strange Lake property, Quebec, Canada. Report to Quest Rare Minerals, 232 p., http://www.questrareminerals.com/

Greenland Minerals and Energy Ltd., 2014, Projects—Kvanefjeld: http://www.ggg.gl/projects/specialty-metals-kvanefjeld/.

Hall, A., 1996, Igneous Petrology, 2nd ed.: London, UK, Longman Scientific, 573 p.

Halter, W., and Webster, J.D., 2004, The magmatic to hydrothermal transition and its bearing on ore-forming systems: Chemical Geology, v. 210, p. 1–6.

Harris, N.B.W., and Marriner, C.F., 1980, Geochemistry and petrogenesis of a peralkaline granite complex from the Midian Mountains, Saudi Arabia: Lithos, v. 13, p. 325–337.

Hastings Rare Metals Ltd., 2014, Projects: Hastings: http://www.hastingsraremetals.com/projects/hastings-project/jorc-resource/.

Hatch, G.P., 2012, TMR Advanced Rare-Earth Projects Index. Technology Metal Research, October 2012: http://www.techmetalsresearch.com/metrics-indices/tmr-advanced-rare-earth-projects-index/.

——2014, TMR Advanced Rare-Earth Projects Index. Technology Metal Research, March 2014: http://www.techmetalsresearch.com/metrics-indices/tmr-advanced-rare-earth-projects-index/.

Hill, J.D., and Miller, R.R., 1991, A review of Middle Proterozoic epigenetic felsic magmatism in Labrador: Geological Association of Canada Special Paper 38, p. 417–431.

Hill, J.D., and Thomas, A., 1991, Correlation of two Helikian peralkaline granite-volcanic centres in central Labrador: Canadian Journal of Earth Sciences, v. 20, p. 753–763.

Jackson, N.J., and Ramsay, C.R., 1986, Post-orogenic felsic plutonism, mineralization and chemical specialization in the Arabian Shield: Transactions of the Institution of Mining and Metallurgy, v. B95, p. 83–93.

Jahn, B.M., Litvinovsky, B.A., Zanvilevich, A.N., and Reichow, M., 2009, Peralkaline granitoid magmatism in the Mongolian-Transbaikalian belt: Evolution, petrogenesis and tectonic significance: Lithos, v. 113, p. 521–539.

Jones, A.P., Genge, M., and Carmody, L., 2013, Carbonate melts and carbonatites: Reviews in Mineralogy and Geochemistry, v. 75, p. 289–322.

Kempe, U., Goetze, J., Dandar, S., and Habermann, D., 1999, Magmatic and metasomatic processes during formation of the Nb-Zr-REE deposits-Khaldzan Buregte and Tsakhir (Mongolian Altai): Indications from a combined CL-SEM study: Mineralogical Magazine, v. 63, p. 165–177.

Kerr, A., 2011, Rare earth element mineralization in Labrador: A review of known environments and the geological context of current exploration activity: Newfoundland and Labrador Department of Natural Resources, Geological Survey Branch, Report 2011-1, p. 109–145.

Kerr, A., and Rafuse, H., 2012, Rare-earth element geochemistry of the Strange Lake deposits: Implications for resource estimation and metallogenic models: Newfoundland and Labrador Department of Natural Resources, Geological Survey Branch, Report 2012-1, p. 39–60.

Kogarko, L.N., Krigma, L.D., and Belyakova, Y.N., 1984, The nepheline-diopside-apatite system and liquid evolution during the crystallization of an apatite-bearing ijolite-urtite magma: Geochemistry International, v. 21, p. 38–58.

Kogarko, L.N., Kononova, V.A., Orlova, M.P., and Woolley, A.R., 1995, Alkaline rocks and carbonatites of the world. Part two, Former USSR: London, UK, Chapman and Hall, 226 p.

Kogarko, L.N., Williams, C.T., and Woolley, A.R., 2002, Chemical evolution and petrogenetic implications of loparite in layered, agpaitic Lovozero complex, Kola Peninsula, Russia: Mineralogy and Petrology, v. 74, p. 1–24.

Kogarko, L.N., Lahaye, Y., and Brey, G.P., 2010, Plume-related mantle source of super-large rare metal deposits from the Lovozero and Khibina massifs on the Kola Peninsula, Eastern part of Baltic Shield: Sr, Nd and Hf isotopic systematics: Mineralogy and Petrology, v. 98, p. 197–208.

Kovalenko, V.I., Tsaryeva, G.M., Goreglyad, A.V., Yarmolyuk, V.V., Troitsky, V.A., Hervig, R.L., and Farmer, G.L., 1995, The peralkaline granite-related Khaldzan-Buregtey rare metal (Zr, Nb, REE) deposit, western Mongolia: Economic Geology, v. 90, p. 530–547.

Kovalenko, V.I., Yarmolyuk, V.V., Kozlovsky, A.M., Kovach, V.P., Salnikova, F.B., Kotov, A.B., and Vladykin, N.V., 2007, Two types of magma sources of rare-metal alkali granites: Geology of Ore Deposits, v. 49, p. 442–466.

Kramm, U., and Kogarko, L.N., 1994, Nd and Sr isotope signatures of the Khibina and Lovozero agpaitic centres, Kola alkaline province, Russia: Lithos, v. 32, p. 225–242.

Kramm, U., and Sindern, S., 2004, Timing of Kola ultrabasic, alkaline and phoscorite-carbonatite magmatism, *in* Wall, F., and Zaitsev, A.N., eds., Phoscorites and carbonatites from mantle to mine: The key example of the Kola alkaline province: London, Mineralogical Society, p. 75–97.

Küster, D., 2009, Granitoid-hosted Ta mineralization in the Arabian-Nubian Shield: Ore deposit types, tectono-metallogenic setting and petrogenetic framework: Ore Geology Reviews, v. 35, p. 68–86.

Kynicky, J., Smith, M.P., and Xu, C., 2012, Diversity of rare earth deposits: the key example of China: Elements, v. 8, p. 361–367.

Larsen, L.M., and Sørensen, H., 1987, The Ilímaussaq intrusion-progressive crystallization and formation of layering in an agpaitic magma: Geological Society Special Publication 30, p. 473–488.

Le Bas, M.J., 2008, Fenites associated with carbonatites: Canadian Mineralogist, v. 46, p. 915–932.

Le Bas, M.J., Le Maitre, R.W., Streckeisen, A., and Zanettin, B., 1986, A chemical classification of volcanic rocks based on the total alkali-silica diagram: Journal of Petrology, v. 27, p. 745–750.

Le Maitre, R.W., and others, 2002, Igneous rocks. A classification and glossary of terms, 2nd ed.: Cambridge, Cambridge University Press, 236 p.

Lentz, D.R., 1996, U, Mo and REE mineralization in late tectonic granitic pegmatites, southwestern Grenville province, Canada: Ore Geology Reviews, v. 11, p. 197–227.

Levinson, A.A., 1966, A system of nomenclature for rare-earth minerals: American Mineralogist, v. 51, p. 152–158.

Linnen, R.L., 1998, The solubility of Nb-Ta-Zr-Hf-W in granitic melts with Li and Li-F: Constraints for mineralization in rare-metal granites and pegmatites: Economic Geology, v. 93, p. 1013–1025.

Linnen, R.L., and Cuney, M., 2005, Granite-related rare-element deposits and experimental constraints on Ta-Nb-W-Sn-Zr-Hf mineralization: Geological Association of Canada Short Course Notes, v. 17, p. 45–68.

Linnen, R.L., and Keppler, H., 1997, Columbite solubility in granitic melts: Consequences for the enrichment and fractionation of Nb and Ta in the Earth's crust: Contributions to Mineralogy and Petrology, v. 128, p. 213–227.

——2002, Melt composition control on Zr/Hf fractionation in magmatic processes: Geochimica et Cosmochimica Acta, v. 66, p. 3293–3301.

Linnen, R.L., Samson, I.M., Williams-Jones, A.E., and Chakhmouradian, A.R., 2014, Geochemistry of the rare-earth element, Nb, Ta, Hf and Zr deposits: Treatise on Geochemistry, 2nd ed. v. 13, p. 543–568.

Loiselle, M.C., and Wones, D.R., 1979, Characteristics and origin of anorogenic granites [abs.]: Geological Society of America Abstracts with Programs, v. 11, p. 468.

Long, K.R., Van Gosen, B.S., Foley, N.K., and Cordier, D., 2010, The principal rare earth element deposits of the United States—a summary of domestic deposits and a global perspective: U.S. Geological Survey Scientific Investigations Report 2010-5220, 96 p.

Lurie, J., 1986, Mineralization of the Pilanesberg alkaline complex, *in* Mineral deposits of South Africa: Geological Society of South Africa, v. 2, p. 2215–2228.

Lurie, J., and Cawthorn, G., 1984, An excursion through the Pilanesberg Complex: Geological Congress of the Geological Society of South Africa, 20th, Field Guide, 24 p.

MacKevett, E.M., Jr., 1963, Geology and ore deposits of the Bokan Mountain uranium-thorium area, southeastern Alaska: U. S. Geological Survey Bulletin 1154, 125 p.

Mariano, A.N., 1989, Economic geology of rare earth minerals: Reviews in Mineralogy, v. 21, p. 309–338.

Mariano, A.N., and Mariano, A., Jr., 2012, Rare earth elements: Rare earth mining and exploration in North America: Elements, v. 8, p. 369–376.

Markl, G., Marks, M., Schwinn, G., and Sommer, H., 2001, Phase equilibrium constraints on intensive crystallization parameters of the Ilimaussaq Complex, South Greenland: Journal of Petrology, v. 42, p. 2231–2258.

Markl, G., Marks, M.A., and Frost B.R., 2010, On the controls of oxygen fugacity in the generation and crystallization of peralkaline melts: Journal of Petrology, v. 51, p. 1831–1847.

Marks, M., and Markl, G., 2001, Fractionation and assimilation processes in the alkaline augite syenite unit of the Ilímaussaq intrusion, South Greenland, as deduced from phase equilibria: Journal of Petrology, v. 42, p. 1947–1969.

Marks, M., Vennemann, T., Siebel, W., and Markl, G., 2003, Quantification of magmatic and hydrothermal processes in a peralkaline syenite-alkali granite complex based upon textures, phase equilibria, and stable and radiogenic isotopes: Journal of Petrology, v. 44, p. 1247–1280.

Marks, M.A., Hettmann, K., Schilling, J., Frost, B.R., and Markl, G., 2011, The mineralogical diversity of alkaline igneous rocks: Critical factors for the transition from miaskitic to agpaitic phase assemblages: Journal of Petrology, v. 52, p. 439–455.

Martin, L.H.J., Schmidt, M.W., Mattsson, H.B., and Guenther, D., 2013, Element partitioning between immiscible carbonatite and silicate melts for dry and H_2O-bearing systems at 1-3 GPa: Journal of Petrology, v. 54, p. 2301–2338.

Martin, R.F., and De Vito, C., 2005, The patterns of enrichment in felsic pegmatites ultimately depend on tectonic setting: Canadian Mineralogist, v. 43, p. 2027–2048.

McLennan, S.M., 1989, Rare earth elements in sedimentary rocks: Influence of provenance and sedimentary processes: Reviews in Mineralogy, v. 21, p. 169–200.

Miller, R.R., 1986, Geology of the Strange Lake alkalic complex and associated Zr-Y-Nb-Be-REE mineralization: Newfoundland Department of Mines and Energy, Mineral Development Division, Report 86-1, p. 11–19.

——1987, The relationship between Mann-type Nb-Be mineralization and felsic peralkaline intrusives, Letitia Lake project, Labrador: Newfoundland Department of Mines and Energy, Mineral Development Division, Report 87-1, p. 83–91.

——1990, The Strange Lake pegmatite-aplite hosted rare metal deposit, Labrador: Newfoundland Department of Mines and Energy, Geological Survey Branch, Report 90-1, p. 171–182.

Miller, R.R., Heaman, L.M., and Birkett, T.C., 1997, U-Pb zircon age of the Strange Lake peralkaline complex: Implications for Mesoproterozoic peralkaline magmatism in north-central Labrador: Precambrian Research, v. 81, p. 67–82.

Mitchell, R.H., 1996, Classification of undersaturated and related alkaline rocks: Mineralogical Association of Canada Short Course Notes, v. 24, p. 2–22.

Mitchell, R.H., and Chakhmouradian, A. R., 1996, Compositional variation of loparite from the Lovozero alkaline complex, Russia: Canadian Mineralogist, v. 34, p. 977–990.

Mitchell, R.H., and Liferovich, R.P., 2006, Subsolidus deuteric/hydrothermal alteration of eudialyte in lujavrite from the Pilanesberg alkaline complex, South Africa: Lithos, v. 91, p. 352–372.

Mungall, J.E., and Martin, R.F., 1996, Extreme differentiation of peralkaline rhyolite, Terceira, Azores: A modern analogue of Strange Lake, Labrador?: Canadian Mineralogist, v. 34, p. 769–777.

Olivo, G.R., and Williams-Jones, A.E., 1999, Hydrothermal REE-rich eudialyte from the Pilanesberg Complex, South Africa: Canadian Mineralogist, v. 37, p. 653–663.

Orris, G.J., and Grauch, R.I., 2002, Rare earth element mines, deposits, and occurrences: U.S. Geological Survey Open-File Report 02-189.

Paslick, C.R., Halliday, A.N., Davies, G.R., Mezger, K., and Upton, B.G.J., 1993, Timing of Proterozoic magmatism in the Gardar province, southern Greenland: Bulletin of Geological Society of America, v. 105, p. 272–278.

Philpotts, J.A., Taylor, C.D., Tatsumoto, M., and Belkin, H.E., 1998, Petrogenesis of late-stage granites and Y-REE-Zr-Nb-enriched vein dikes of the Bokan Mountain stock, Prince of Wales Island, southeastern Alaska: U.S. Geological Survey Open-File Report 98-459, 71 p.

Pilet, S., Baker, M.B., and Stolper, E.M., 2008, Metasomatized lithosphere and the origin of alkaline lavas: Science, v. 320, p. 916–919.

Platt, R.G., 1996, Nepheline syenite complexes-an overview: Mineralogical Association of Canada Short Course Notes, v. 24, p. 63–99.

Richardson, D.G., and Birkett, T.C., 1996, Peralkaline rock-associated rare metals: Geological Society of America, Geology of North America, v. P-1, p. 523–540.

Robinson, R.J., Power, M.A., and Barker, J.C., 2011, Technical report on the exploration program and mineral resource estimate for the Bokan Mountain property, Prince of Wales Island, Alaska: NI 43-101 Report, 190 p., http://ucore.com/projects/bokan-mountain-alaska/43-101

Ramsden, A.R., French, D.H., and Chalmers, D.I., 1993, Volcanic-hosted rare-metals deposit at Brockman, Western Australia: Mineralogy and geochemistry of the Niobium tuff: Mineralium Deposita, v. 28, p. 1–12.

Ronga, F., Lustrino, M., Marzoli, A., and Melluso, L., 2010, Petrogenesis of a basalt-comendite-pantellerite rock suite: the Boseti Volcanic Complex (Main Ethiopian rift): Mineralogy and Petrology, v. 98, p. 227–243.

Salvi, S., and Williams-Jones, A.E., 1990, The role of hydrothermal processes in the granite-hosted Zr, Y, REE deposit at Strange Lake, Quebec/Labrador: Evidence from fluid inclusions: Geochimica et Cosmochimica Acta, v. 54, p. 2403–2418.

——1996, The role of hydrothermal processes in concentrating HFSE in the Strange Lake peralkaline complex, northeastern Canada: Geochimica et Cosmochimica Acta, v. 60, p. 1917–1932.

——2005, Alkaline granite-syenite deposits: Geological Association of Canada Short Course Notes, v. 17, p. 315–341.

Saucier, G., Roy, A., Casgrain, P., Côté, P., Thomassin, Y., Bilodeau, M., Cannus, Y., and Hayden, A., 2012, NI 43-101 Report—preliminary economic assessment study for Kipawa project: Roche's Ref.: 061623.001-200, submitted to Matamec Explorations, Inc., 229 p., http://www.matamec.com/vns-site/page-technical_reports-en.html

Saucier, G. and 14 others, 2013, NI 43-101 Report—feasibility study for the Kipawa project, Temiscaminque area, Quebec, Canada. Roche Consulting: http://matamec.com/vns-site/uploads/documents/061623-003-finrep_matamec-n143-101-20131017-001-appen.pdf.

Secher, K., 2002, Deposits of speciality metals in South Greenland, *in* Secher, K., ed., Greenland mineral resources fact sheet: Copenhagen, GEUS, no. 3, 2 p.

Shand, S.J., 1943, The Eruptive Rocks, 2nd edition: New York, John Wiley, 444 p.

Shaw, D.M., 2006, Trace elements in magmas: A theoretical treatment: Cambridge, UK, Cambridge University Press, 243 p.

Shaw, J.E., Baker, J.A., Kent, A.J.R., Ibrahim, K.M., and Menzies, M.A., 2007, The geochemistry of the Arabian lithospheric mantle—a source for intraplate volcanism?: Journal of Petrology, v. 48, p. 1495–1512.

Sheard, E.R., Williams-Jones, A.E., Heiligmann, M., Pederson, C., and Trueman, D.L., 2012, Controls on the concentration of zirconium, niobium, and the rare earth elements in the Thor Lake rare metal deposit, Northwest Territories, Canada: Economic Geology, v. 107, p. 81–104.

Sørensen, H., 1992, Agpaitic nepheline syenites: A potential source of rare elements: Applied Geochemistry, v. 7, p. 417–427.

——2001, Brief introduction to the geology of the Ilímaussaq alkaline complex, South Greenland, and its exploration history: Geology of Greenland Survey Bulletin 190, p. 7–23.

——2006, The Ilimaussaq alkaline complex, South Greenland—an overview of 200 years of research and an outlook: Meddelelser om Gronland Geoscience, v. 45, 71 p.

Sørensen, H., Bohse, H., and Bailey, J.C., 2006, The origin and mode of emplacement of lujavrites in the Ilímaussaq alkaline complex, South Greenland: Lithos, v. 91, p. 286–300.

Sørensen, H., Bailey, J.C., and Rose-Hansen, J., 2011, The emplacement and crystallization of the U-Th-REE-rich agpaitic and hyperagpaitic lujavrites at Kvanefjeld, Ilimaussaq alkaline complex, South Greenland: Bulletin of the Geological Society of Denmark, v. 59, p. 69–92.

Staatz, M.H., 1978, I and L uranium and thorium vein system, Bokan Mountain, and southeastern Alaska: Economic Geology, v. 73, p. 512–523.

Stoeser, D.B., 1986, Distribution and tectonic setting of plutonic rocks of the Arabian Shield: Journal of African Earth Sciences, v. 4, p. 21–46.

Sun, S.S., and McDonough, W.F., 1989, Chemical and isotopic systematics of oceanic basalts: Implications for mantle composition and processes: Geological Society London Special Publication 42, p. 313–345.

Tasman Metals Ltd., 2012, Sweden-Norra Kärr rare element project: http://www.tasmanmetals.com/s/Norra-Karr.asp

Taylor, R.P., and Pollard, P.J., 1996, Rare earth element mineralization in peralkaline systems: the T-zone-REE-Y-Be deposit, Thor Lake, Northwest Territories, Canada: Mineralogical Society Series 7, p. 167–192.

Taylor, W.R., Esslemont, G., and Sun, S.S., 1995a, Geology of the volcanic-hosted Brockman rare-metals deposit, Halls Cree mobile zone, northwest Australia. II. Geochemistry and petrogenesis of the Brockman volcanics: Mineralogy and Petrology, v. 52, p. 231–255.

Taylor, W.R., Page, R.W., Esslemont, G., Rock, N.M. S., and Chalmers, D.I., 1995b, Geology of the volcanic-hosted Brockman rare-metals deposit, Halls Cree mobile zone, northwest Australia. I. Volcanic environment, geochronology and petrography the Brockman volcanics: Mineralogy and Petrology, v. 52, p. 209–230.

Thomas, M.D., Ford, K.L., and Keating, P., 2010, Exploration geophysics for intrusion-hosted rare earth metals [ab.]: British Columbia Geological Survey Open File 2010-10, p. 59–61.

Thompson, T.B., 1988, Geology and uranium-thorium mineral deposits of the Bokan Mountain granite complex, southeastern Alaska: Ore Geology Reviews, v. 3, p. 193–210.

Upton, B.G.J., Emeleus, C.H., Heaman, L.M., Goodenough, K.M., and Finch, A.A., 2003, Magmatism of the mid-Proterozoic Garder province, South Greenland: Chronology, petrogenesis and geological setting: Lithos, v. 68, p. 43–65.

Ussing, N.V., 1912, Geology of the country around Julianehaab, Greenland: Meddelelser om Grønland, v. 38, 426 p.

Veksler, I.V., 2004, Liquid immiscibility and its role at the magmatic-hydrothermal transition: A summary of experimental studies: Chemical Geology, v. 210, p. 7–31.

Veksler, I.V., and Lentz, D., 2006, Parental magmas of plutonic carbonatites, carbonate-silicate immiscibility and decarbonation reactions: Evidence from melt and fluid inclusions: Mineralogical Association of Canada, Short Course, v. 36, p. 123–150.

Verplanck, P.L., and Van Gosen, B.S., 2011, Carbonatite and alkaline intrusion-related rare earth element deposits—a deposit model: U.S. Geological Survey Open-File Report 2011-1256.

Verplanck, P.L., Van Gosen, B.S., Seal, R.R., and McCafferty, A.E., 2014, A deposit model for carbonatite and alkaline intrusion-related rare earth element deposits: U.S. Geological Survey Scientific Investigations Report 2010-5070-J, 58 p.

Walters, A.S., Goodenough, K.M., Hughes, H.S.R., Roberts, N.M.W., Gunn, A.G., Rushton, J., and Lacinska, A., 2013, Enrichment of rare earth elements during magmatic and post-magmatic processes: A case study from the Loch Loyal syenite complex, northern Scotland: Contributions to Mineralogy and Petrology, v. 166, p. 1177–1202.

Whalen, J.B., Currie, K.L., and Chappell, B.W., 1987, A-type granites: Geochemical characteristics, discrimination and petrogenesis: Contributions to Mineralogy and Petrology, v. 95, p. 407–419.

Williams-Jones, A.E., 2010, The Nechalacho rare earth deposit, Thor Lake, Northwest Territories [abs.]: British Columbia Geological Survey Open File 2010-10, p. 41.

Williams-Jones, A.E., Migdisov, A.A., and Samson, I.M., 2012, Hydrothermal mobilization of the rare earth elements: A tale of "ceria" and "yttria": Elements, v. 8, p. 355–360.

Winter, J.D., 2001, An introduction to igneous and metamorphic petrology: New Jersey, Prentice Hall, 697 p.

Zaitsev, A.N., Wall, F., and Le Bas, M.J., 1998, REE-Sr-Ba minerals from the Khibina carbonatites, Kola Peninsula, Russia: Their mineralogy, paragenesis and evolution: Mineralogical Magazine, v. 62, p. 225–250.

Zaitsev, V., and Kogarko, L. N., 2012, Sources and perspective of REE in the Lovozero massif (Kola Peninsula, Russia): European Mineralogical Conference 2012, Frankfurt, Germany, v. 1, p. 290.

©2016 Society of Economic Geologists, Inc.
Reviews in Economic Geology, v. 18, pp. 55–79

Chapter 3

Characteristics and Genesis of Ion Adsorption-Type Rare Earth Element Deposits

Kenzo Sanematsu[1,2,†] and Yasushi Watanabe[1,*]

[1] *Geological Survey of Japan, AIST, Central 7, 1-1-1 Higashi, Tsukuba, Ibaraki 305-8567, Japan*

[2] *CODES ARC Centre of Excellence in Ore Deposits, University of Tasmania, Private Bag 126, Hobart, Tasmania 7001, Australia*

Abstract

Ion adsorption-type rare earth element (REE) deposits are the predominant source of heavy REE (HREEs) and yttrium in the world. Economic examples of the deposits are confined almost exclusively to areas underlain by granitic rocks in southern China. These deposits are termed "ion adsorption-type" because the weathered granites contain more than ~50% ion-exchangeable REY (REE + Y), relative to whole-rock REY. The ore grades range from 140 to 6,500 ppm (typically ~800 ppm) REY, and some of the deposits are remarkably enriched in HREEs. The Yanshanian (Jurassic-Cretaceous) granites that weather to form the deposits are products of subduction-related or extensional intraplate magmatism. These parent granites for the REE deposits are biotite- and/or muscovite-bearing granites and are characterized by >70% SiO_2, <0.08% P_2O_5, and metaluminous to weakly peraluminous (ASI < 1.1) compositions. The highly differentiated (SiO_2 >~75%) muscovite granites are HREE enriched relative to the biotite granites and are notably characterized by occurrences of fluorite and hydrothermal REE-bearing minerals, particularly REE fluorocarbonates that formed in a deuteric alteration event. Magmatic allanite and titanite are either altered to form hydrothermal REE-bearing minerals or almost completely broken down during weathering.

The weatherable REE-bearing minerals, including fluorocarbonates, allanite, and titanite, are the source minerals for the ion adsorption ores. The HREE grades of the ion adsorption ores are strongly influenced by the relative abundances and weathering susceptibilities of these REE-bearing minerals in the parent granites. The presence of easily weathered HREE minerals in the underlying granites appears to be the primary control of the HREE-rich deposits, although solution and solid phase chemistry during development of the weathering profile may influence REE fractionation. Monazite, zircon, and xenotime are also present in the granites, but because they are more resistant to chemical weathering, they are typically not a source of REEs in the weathered materials.

The REE-bearing minerals are decomposed by acidic soil water at shallow levels in the weathering profile, and the REE^{3+} ions move downward in the profile. The REEs are complexed with humic substances, with carbonate and bicarbonate ions, or carried as REE^{3+} ions in soil and ground water at a near-neutral pH of 5 to 9. The REE^{3+} ions are removed from solution by adsorption onto or incorporated into secondary minerals. The removal from the aqueous phase is due to a pH increase, which results from either water-rock interaction or mixing with a higher pH ground water. The REEs commonly adsorb on the surfaces of kaolinite and halloysite, to form the ion adsorption ores, due to their abundances and points of zero charge. In addition, some REEs are immobilized in secondary minerals consisting mainly of REE-bearing phosphates (e.g., rhabdophane and florencite). In contrast to the other REEs that move downward in the weathering profile, Ce is less mobile and is incorporated into the Mn oxides and cerianite (CeO_2) as Ce^{4+} under near-surface, oxidizing conditions. As a result, the weathering profile of the deposits can be divided into a REE-leached zone in the upper part of the profile, with a positive Ce anomaly, and a REE accumulation zone with the ion adsorption ores in the lower part of the profile that is characterized by a negative Ce anomaly. The thickness of the weathering profiles generally ranges from 6 to 10 m but can be as much as 30 m and rarely up to 60 m. The negative Ce anomaly in weathered granite terrane is thus a good exploration indicator for ion adsorption ores. A temperate or tropical climate, with moderate to high temperatures and precipitation rates, is essential for chemical weathering and ion adsorption REE ore formation. Low to moderate denudation, characteristic of such a climate in areas of low relief, are favorable for the preservation of thick weathering profiles with the REE orebodies.

Introduction

Rare earth elements (REEs: La-Lu) are divided into light REEs (LREEs: La-Eu) and heavy REEs (HREEs: Gd-Lu). Crustal abundances of HREEs are lower than those of LREEs (Rudnick and Gao, 2003), suggesting that resources of HREEs are scarcer than those of LREEs. Demand for HREEs has increased in the past decade (Kanazawa and Kamitani, 2006; Wall, 2014); for example, dysprosium (Dy) is an indispensable additive for production of Nd magnets (Minowa, 2008). The HREEs generally occur with Y because of their geochemical affinity, and they have been mined predominantly from ion adsorption-type REE deposits in southern China (Roskill, 2015; U.S. Geological Survey, 2015). The total production of REEs from the ion adsorption-type deposits in China accounted for 20% of the world production in 2010 (Roskill, 2015), ranking fourth behind the Bayan Obo, Weishan, and Maoniuping deposits also in China, which both consist of LREE-rich carbonatitic ores (Wu et al., 1996; Wall, 2014).

† Corresponding author: e-mail, k-sanematsu@aist.go.jp

*Present address: Mining Museum of Akita University 28-2 Osawa, Tegata, Akita, 010-8502, Japan.

After the discovery of the Longnan deposits in Jiangxi province in 1969, more than 200 HREE- and LREE-rich ion adsorption-type deposits were discovered and mined in southern China (Chen, 1996; Ding, 2012; Wall, 2014). Additional ion adsorption-type REE deposits and occurrences have been discovered outside of China, in Madagascar, Malawi (Le Couteur, 2011), Brazil (Rocha et al., 2013), and Southeast Asia (e.g., Mentani, 2012; Sanematsu et al., 2013). The ion adsorption-type occurrences are located in the temperate (C) and tropical (A) areas of the Köppen-Geiger climate classification (Köppen, 1936; Peel et al., 2007; Fig. 1) because chemical weathering and breakdown of REE-bearing minerals are promoted by moderate to high temperatures and precipitation rates.

Rare earth element deposits produced by weathering processes include ion adsorption-type and residual REE deposits, with the difference in these deposit types being whether the REEs are adsorbed on weathering products or are incorporated in minerals, either primary or secondary. Placer deposits are a subset of residual deposits that undergo mechanical erosion in addition to chemical weathering. The ion adsorption ores do not require crushing, grinding, or mineral processing, and REEs are easily extracted by ion-exchange using a dilute electrolyte solution, such as ammonium sulfate solution at room temperature (e.g., Wu et al., 1990a; Chi and Tian, 2008; Chi et al., 2012; Moldoveanu and Papangelakis, 2012, 2013a; Tian et al., 2013). This metallurgical process enables mining of low-grade ores. The REE grades of ion adsorption deposits are lower than those of placer deposits, and placer REE ores are generally rich in LREEs because of abundant monazite and lesser xenotime (Orris and Grauch, 2002; Sengupta and Van Gosen, 2016). Ion adsorption ores generally contain lower amounts of radioactive elements (Th and U) than residual REE ores, and the Th and U concentrations in the leachate are low (Chi and Tian, 2009; Sanematsu and Kon, 2013). Economic issues with developing ion adsorption-type deposits include a large stripping ratio, large leach residue, overexploitation, and environmental restoration costs (Ding, 2012; Wang et al., 2013). Ion adsorption ore grades and tonnages have been decreasing, thus extraction costs are increasing because more extraction reagent is required (Tian et al., 2013). Contamination of local water resources near the mining sites with NH^{4+}-N (ammonium nitrogen) is an issue with decreasing ore grades (Tian et al., 2013).

In this paper, we review the geologic settings and lithogeochemistry of parent granites for the ion adsorption deposits, and the geochemical and mineralogical characteristics of the ores in southern China and some prospective areas outside of China. We also review previous work on the mineralogy of REE-bearing minerals in granites, and mobility, fractionation, and adsorption of REEs during granite weathering in order to elucidate the genesis of ion adsorption-type deposits and to provide implications for exploration.

Characteristics of Ion Adsorption-Type REE Deposits

Exploration for weathering-type REE deposits in southern China started in the 1960s, when it was recognized that they developed in thick weathering profiles on igneous rocks as a result of the temperate climate conditions (Fig. 1). In 1969, the HREE-rich Zudong intrusion and its weathering profile (Orebody 701) were recognized in Longnan County, Jiangxi province (Chen, 1996; Ding, 2012). Following the public disclosure of the preliminary REE extraction method for this ion-exchangeable ore in 1971, exploration for ion adsorption-type deposits became widespread and the LREE-rich Heling deposits were discovered in Xunwu County, Jiangxi province in 1972. Other deposits in Xinfeng County, Guangdong province were discovered in 1986 to 1987. These deposits were considered to be a state secret (Ding, 2012).

The ion adsorption-type deposits that have been mined in southern China (Table 1) include deposits of Jiangxi, Guangdong, Fujiang, Guangxi (Zhuang Autonomous Region), Hunan, and Yunnan provinces, which are listed in decreasing order of resource size (Zhou et al., 2012). Jiangxi province has thelargest ore reserves and greatest production of ion adsorption ores, with the majority of deposits located near Ganzhou

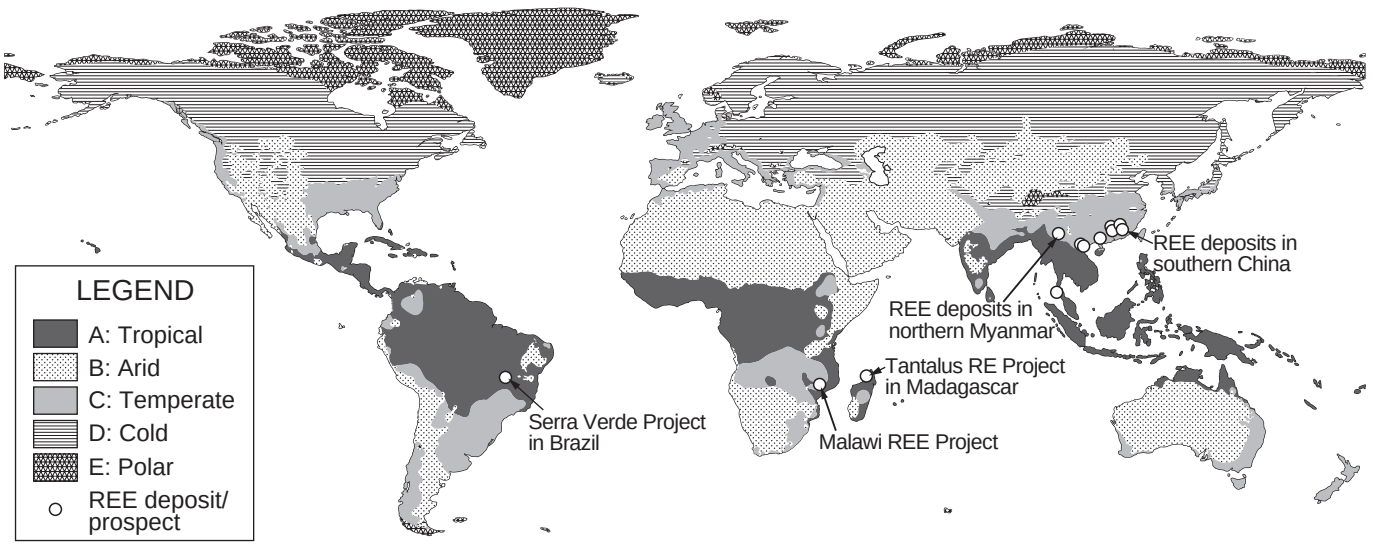

Fig. 1. World map of the Köppen-Geiger climate classification (modified after Peel et al., 2007). Ion adsorption-type REE deposits and prospects are shown in the map.

City in southern Jiangxi (Fig. 2). The economic ores contain approximately greater than 500 ppm of ion-exchangeable REY (Bao and Zhao, 2008).

Limited data are available on mineral resources and ore reserves of ion adsorption-type deposits (Table 1). They are smaller than REE deposits associated with carbonatites and peralkaline rocks (Castor and Hedrick, 2006; Castor 2008; Linnen et al., 2014; Wall, 2014) because the orebodies are confined to the near-surface weathering profiles. Ore reserves of the ion adsorption-type deposits are classified into large (>0.5 million metric tons (Mt)), medium (0.05–0.5 Mt), and small (<0.01 Mt) categories (Zhu, 1999). Only several large REE deposits have been identified, but more than 100 (probably ~200) medium and small REE deposits are known in southern China (Zhang, 1990; British Geological Survey, 2011; Ding, 2012; Wang et al., 2013; Wall, 2014). The thickness of the weathering profiles generally ranges from 6 to 10 m, but locally can reach 30 m and rarely may be 60 m (Yang et al., 1981; Wu et al., 1990a, 1996; Zhang, 1990; Huo, 1992; Chen, 1996; Zhu, 1999; Bao and Zhao, 2008; Li and Li, 2010; Pan, 2011; Yang and Xiao, 2011; Chen, 2013; Tong, 2013; Wang et al., 2013). Parent rocks of ion adsorption-type deposits consist mostly of calc-alkaline granite and minor alkali granite, felsic volcanic rocks, and metamorphic rocks including phyllites (Zhang, 1990; Huo, 1992; Chi and Tian, 2008).

Ion adsorption ores generally have over 50% ion-exchangeable REY, which are dominantly present on the surface of clays, including kaolinite and halloysite (Yang et al., 1981; Song and Shen, 1986; Yang, 1987; Wu et al., 1990a, 1993a, 1996; Zhang, 1990; Chi et al., 2005, 2012; Bao and Zhao, 2008; Chi and Tian, 2008; Pan, 2011; Chen, 2013; Tong, 2013). Typically, the REY contents in calc-alkaline parent rocks range

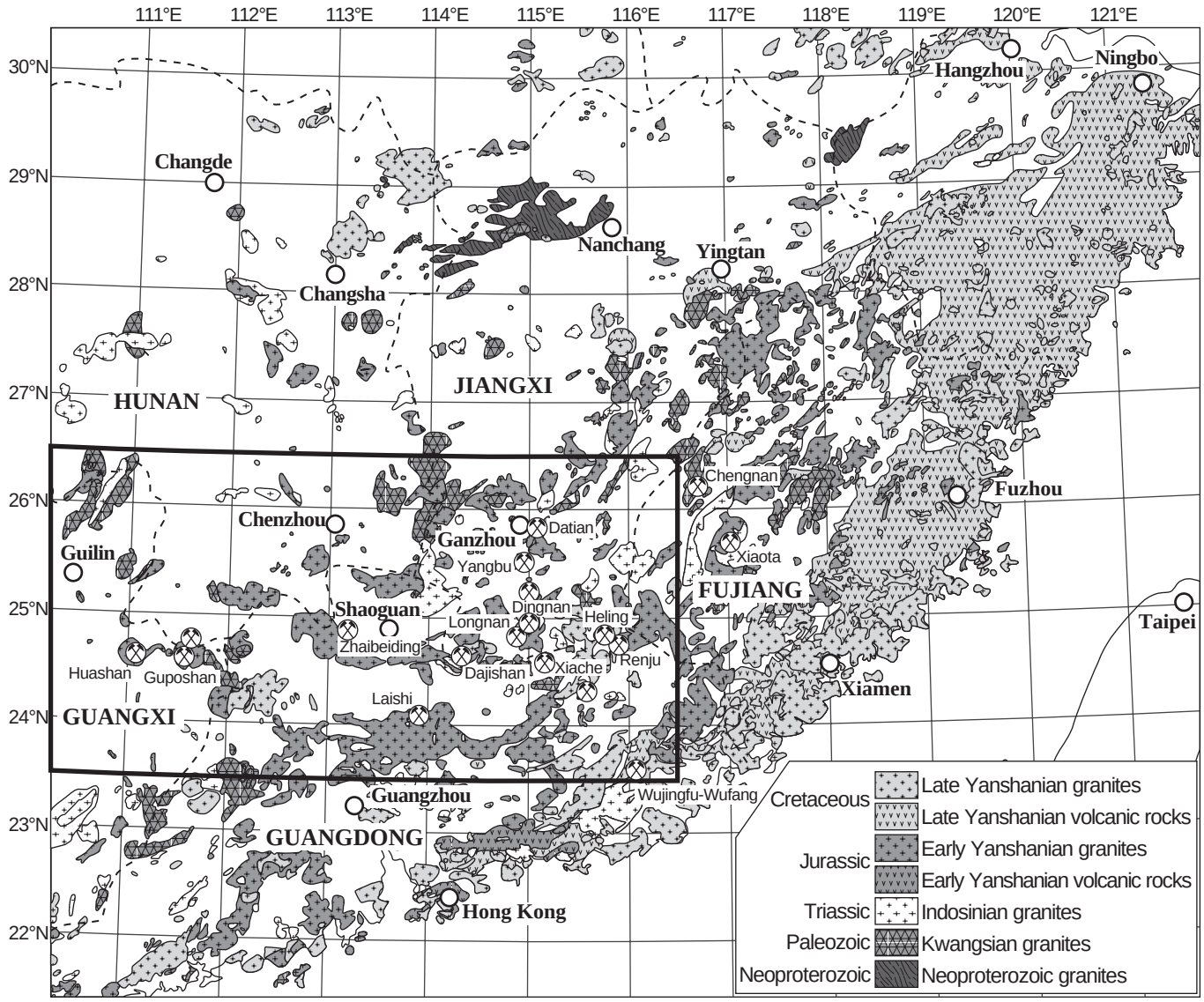

Fig. 2. Geologic map showing distribution of granitic rocks and volcanic rocks in southern China (Sun, 2006; Zhou et al., 2006; Wang, Y.J. et al., 2011; Zhang et al., 2012). Localities of typical REE deposits are from Huo (1992), JOGMEC (2011), Wang et al. (2012), Wang et al. (2013), and this study. Refer to Wang et al. (2013) for detailed localities. A bold rectangle area shows the Nanling Range.

Table 1. Major Ion-Adsorption-Type

Province or region	Reserves[1]	Resources[1]	Deposits (County/City)	Elevation	REY grade	Recovery of ion-exchangeable REY	Thickness of weathering crusts[2]
Jiangxi province	9.4 Mt	Unknown	Longnan (Longnan County)	300–400 m	143–1,228 ppm in Zudong 336–886 ppm in Guanxi	47–~100%	~10 m (Up to 30m)
			Heling (Xunwu County)	250–300 m	1,020–1,530 ppm (avg 1,350 ppm; up to 6,460 ppm) in porphyry 510–1,530 ppm (avg 910 ppm; up to 4,900 ppm) in rhyolite	>60%	6–9 m (Up to 28 m)
			Dingnan (Dingnan County)	300–800 m	287–651 ppm	>42%	~10 m
			Dajishan (Quannan County)	350–400 m	311–990 ppm	Unknown	Up to 30 m
			Datian (Gan County)	<400 m	Unknown	>60%	Unknown
			Yangbu (Gan County)	200–300 m	Unknown	Unknown	Average ~7 m
Guangdong Province	Unknown	0.52 Mt (?)	Wujingfu and Wufang (Jiexi and Jiedong Counties)	100 m	680–1,800 ppm	>60%	Unknown
			Laishi (Xinfeng County)	100–200 m	680–1,800 ppm (avg ~800 ppm)	80–90%	Up to 30 m
			Zhaibeiding (Ruyuan County)	<300 m	680–1,800 ppm (avg ~800 ppm)	>70%	Unknown
			Renju (Pingyuan County)	250–400 m	680–1,800 ppm (up to ~4,100 ppm)	>65%	Unknown
			Xiache (Heping County)	200–300 m	850–1,250 ppm (up to ~2,800 ppm)	72.6–85.5%	Unknown
Guangxi Zhuang Autonomous Region	1.1 Mt	Unknown	Huashan (Zhongshan County)	Unknown	429–679 ppm	Unknown	Unknown
			Guposhan[3] (Hezhou City)	Unknown	699–1,324 ppm	Unknown	Unknown
			Qinghu (Liuchuan County)	20–144 m	640–1,700 ppm	57.7%	8.3–22.6 m (avg 15.1 m)
			Majigang (Bobai County)	150–200 m	590–2,260 ppm (avg ~1,130 ppm)	74.0%	20–30 m (avg 22 m)
Fujian province	4 Mt	Unknown	Chengnan (Ninghua County)	330–410 m	420–1,700 ppm (avg ~840 ppm)	41–72%	0.72–7.45 m (Up to 17.3 m)
			Xiaota (Yong'an City)	< 500m	510–1,700 ppm	Unknown	8–20 m (Up to 30 m)
Hunan province	Unknown	0.02 Mt	Guposhan (Jianghua County)	300–700 m	Up to 1,327 ppm	Unknown	Unknown
Yunnan province	Unknown	Unknown	Long'an (Longchuan County)	1,000–1,100 m (?)	Up to ~2,900 ppm (avg ~1,100 ppm)	30–40%	4–13 m (avg 6.6 m)

[1] Reserves and resources of REY oxides are from Roskill (2011) and JOGMEC (2011), respectively; note that these values may be smaller than the current acctual reserves and resources
[2] Includes thickness of barren overburden
[3] Guposhan deposits belong partly to Hunan province

REE Deposits in Southern China

Parent rocks (geologic age)	Constituent minerals of parent rocks	References	Characteristics
Zudong Ms granite and Bt granite (148 and 124 Ma), and Guanxi Bt granite (176 and 170 Ma; Yanshanian age)	Qtz, Kfs, Pl, Ab, Ms, and Bt in Zudong See Table 3 for accessary minerals Qtz, Kfs, Pl, Ab, Bt, Hlb, and accessary minerals in Guanxi	Yang et al. (1981), Huang et al. (1989), Zhang (1990), Wu et al. (1990a, 1993b), and Bao and Zhao (2008)	Large deposits rich in HREE and Y
Bt granite porphyry, and rhyolitic lava and tuff (Yanshanian age)	Qtz, Kfs, Pl, Bt, Apt, RFC, Zrn, Mnz, Frg, Tur, and Fl in granite porphyry	Yang et al. (1981), Song and Shen (1982), Zhang (1990), Yu et al. (2004), and Bao and Zhao (2008)	Large deposits rich in LREE
(Ms-bearing) Bt granite (Yanshanian age)	Qtz, Kfs, Pl, Bt, Ms, Apt, RFC, Mnz, Xen, Thr, and Fl	Zhang (1990), Ishihara et al. (2008), Murakami and Ishihara (2008), and Wang et al. (2013a)	Large deposits
Wuliting Bt granodiorite (238 Ma; Indoshinian age)	Qtz, Kfs, Pl, Bt, Mag, Ttn, Apt, Py, Zrn, Aln, and Chl	Yang et al. (1999), Qiu et al. (2004), Hua et al. (2007), and Ishihara et al. (2008)	
Datian Ms granite and Bt granite (124 Ma; Yanshanian age)	Qtz, Kfs, Pl, Bt, Ms, Apt, Gar, Zrn, Mnz, Xen, Frg, Exn, Fl, Ilm, and Mag(?)	Deng (1988), Zhang (1990), Wu et al. (1992, 1993b)	Rich in HREE and Y
Yangbu Hlb-bearing Bt granite and porphyry (461 Ma)	Qtz, Kfs, Pl, Bt, Hlb, Apt, Epi, Mag, Zrn, and Ttn.	Zhao et al. (2012)	
Bt granite (Yanshanian)	Unknown	Zhang (1990), Lu (2008), and Yang and Xiao (2011)	Large deposits
Fogang (Hlb-bearing) Bt granite (165–159 Ma; Yanshanian age)	Qtz, Kfs, Pl, Bt, Hlb, Aln, Ttn, Apt, Zrn, Mnz, Xen, Ilm, Rtl, Mag, and Smk	Huang (1989), Li et al. (2007), Xu et al. (2007), Yang and Xiao (2011), and Xinfeng County (2014)	Large and medium deposits
Ms granite and Bt granite (145 Ma; Yanshanian age)	Qtz, Kfs, Pl, Ab, Bt, Ms, Gar, Frg, Gdn, RFC, Tur, Fl, Mnz, Smk, Xen, and Py	Ma et al. (1991), Wu et al. (1990b, 1992, 1993b), Yang and Xiao (2011), and Ruyuan Yao Autonomous County (2014)	Medium deposits rich in HREE and Y
Bt granite, Bt granite porphyry, and intermediate volcanic rock (Yanshanian age)	Qtz, Kfs, Pl, Bt, Ttn, Apt, Zrn, Mnz, Fl, Mag, and Ilm in granite and granite porphyry	Zhang (1990), Chen and Yu (1994), and Yang and Xiao (2011)	Medium deposits
Hlb-Bt granite porphyry and partly intermediate volanic rock (Yanshanian age)	Qtz, Kfs, Pl, Bt, Hlb, Aln, Mnz, Xen, and other accessary minerals	Yang and Xiao (2011), Deng (2013)	Medium deposits
(Hlb-bearing) Bt granite (163–160 Ma; Yanshanian age)	Qtz, Kfs, Pl, Bt, Apt, Zrn Aln, Mnz, Xen, and Frg	Zhu et al. (2006), Hua et al. (2007), Bao and Zhao (2008), and Feng et al. (2012)	
(Hlb-bearing) Bt granite (165–151 Ma; Yanshanian age)	Qtz, Kfs, Pl, Bt, Apt, Zrn Aln, Mnz, Xen, Frg, and Gdn	Zhu et al. (2006), Gu et al. (2007), Hua et al. (2007), Bao and Zhao (2008), and Feng et al. (2012)	
Hlb-Bt monzonite and partly syenite (158 Ma: Yanshanian age)	Qtz, Kfs, Pl, Bt, Hlb, Apt, Ttn, Zrn, Aln, Ilm, and Mag	Xu and Yuan (1992), Yuan et al. (1993), and Pan (2011)	
Qtz monzonite porphyry and Px monzonite (Yanshanian age)	Unknown	Pan (2011)	
Bt granite (422–400 Ma)	Unknown	Zhang (1990), and Chen (2013)	
Hlb-bearing Bt granite (Yanshanian age)	Qtz, Kfs, Pl, Bt, Hlb, Apt, Ttn, Aln, Mnz, Xen, and Frg	Tong (2013)	
Bt granite (Yanshanian age)	Probably same as Guposhan in Guangxi	Luo (2011), and Li and Shen (2013)	
Granite (Indosinian age)	Unknown	Li and Li (2010)	

Abbreviations: Ab = albite, Aln = allanite, Apt = apatite, Bt = biotite, Chl = chlorite, Epi = epidote, Exn = euxenite, Fl = fluorite, Frg = fergusonite, Gar = garnet, Gdn = gadolinite, Hlb = hornblende, Ilm = ilmenite, Kfs = K-feldspar, Mag = magnetite, Mnz = monazite, Ms = muscovite, Pl = plagioclase, Px = pyroxene, Py = pyrite, Qtz = quartz, RFC = REE fluorocarbonates, Rtl = rutile, Smk = samarskite, Thr = thorite, Ttn = titanite, Tur = tourmaline, Xen = xenotime, Zrn = zircon

from 110 to 590 ppm (Huang, 1989; Huang et al., 1989; Ma et al., 1991; Wu et al., 1993b; Yang et al., 1999; Hua et al., 2007; Bao and Zhao, 2008; Ishihara et al., 2008; Luo, 2011; Pan, 2011; Chen, 2013; Li and Shen, 2013), and the higher REY contents are found in LREE-rich alkali granite and granite porphyry (Chen and Yu, 1994; Bao and Zhao, 2008). The REY grades of ion adsorption ores range from 140 up to 6,500 ppm (Yang et al., 1981; Wu et al., 1990a; Zhang, 1990; Yang et al., 1999; Hua et al., 2007; Bao and Zhao, 2008; Murakami and Ishihara, 2008; Li and Li, 2010; Pan, 2011; Yang and Xiao, 2011; Chen, 2013; Li and Shen, 2013; Tong, 2013), and they can be nearly six times greater than the REY abundances of parent granites (Huang et al., 1989; Wu et al., 1990a; Bao and Zhao, 2008; Yang and Xiao, 2011). Although ore grades are lower than those of REE ores of carbonatites or peralkaline rocks (Castor and Hedrick, 2006; Castor, 2008; Chakhmouradian and Zaitsev, 2012; Mariano and Mariano, 2012; Linnen et al., 2014; Wall, 2014), some ion adsorption ores are moderately to strongly enriched in HREEs and generally easy to process. The LREE/HREE ratios of the ion adsorption deposits are variable from HREE-rich deposits (e.g., Longnan in Jiangxi) to LREE-rich deposits (e.g., Heling in Jiangxi; Zhu, 1999). The LREE/HREE ratios of ion adsorption ores reflect those of parent granites, such that HREE-rich ores are derived from HREE-enriched (low LREE/HREE ratio) parent granites.

Longnan deposits

The HREE-rich Longnan deposits, located in Longnan County, Jiangxi province, are underlain by the Zudong and Guangxi intrusions (Fig. 3). Characteristics of the granite intrusions were summarized by Huang et al. (1989). The Zudong intrusion crops out in an area of 4 by 9 km along a NNE-SSW-trending structure and consists of a main body of muscovite granite, which is the parent rock for the most HREE-rich ion adsorption orebodies and smaller biotite granite bodies. The Guanxi intrusion consists mainly of biotite granite. Zircon U-Pb and whole-rock Rb-Sr ages of the Zudong intrusion are 124 and 148 Ma, respectively, and those of the Guanxi intrusion are 170 and 176 Ma (Huang et al., 1989). As shown in Figure 4, these biotite and muscovite granites primarily have high SiO_2 contents of 72 to 76%, low P_2O_5 contents of <0.06% and ASI (alumina saturation index = molar Al_2O_3/($CaO + Na_2O + K_2O$) ratio) below ~1.1 (Yang et al., 1981; Wu et al., 1990a; Zhang, 1990; Bao and Zhao, 2008). Huang et al. (1989) reported REY contents of the Zudong muscovite granite ranging from 193 to 307 ppm (avg 262 ppm) and those of the biotite granite from 262 to 275 ppm. Although the REY contents of these granites are not significantly different (Fig. 4D), the muscovite granite is remarkably enriched in HREE(+Y), with very low La_N/Yb_N (N: chondrite normalized by Sun and McDonough, 1989) ratios of 0.31 to 0.95 (Fig. 4E), whereas La_N/Yb_N ratios of the biotite granite are 2.0 and 1.9 (Huang et al., 1989). The LREE/HREE ratios of the ion adsorption ores reflect those of the parent granite, except for Ce, as shown in chondrite-normalized REE patterns in Figure 5A. The Guanxi biotite granite has higher REY contents of 319 to 405 ppm and higher La_N/Yb_N ratios of 4.4 to 7.5, indicating that this intrusion is relatively depleted in HREEs compared to the Zudong intrusion (Fig. 4D, E).

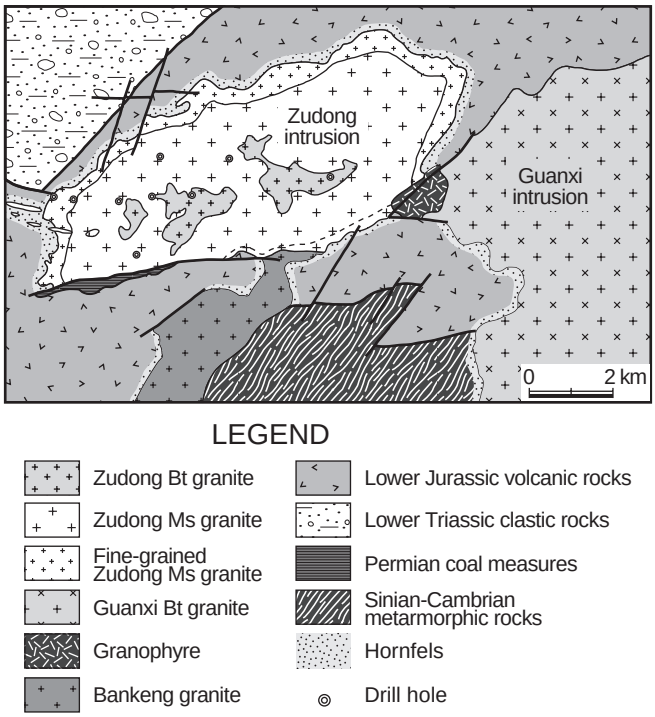

Fig. 3. Geologic map of the HREE-rich Longnan deposits in southern China (partly modified from Huang et al., 1989). Bt = biotite, Ms = muscovite.

Huang et al. (1989) documented a different suite of accessory minerals for muscovite granite compared to the biotite granite of the Zudong intrusion in Longnan. In their work, the muscovite granite, parent rock of the most HREE-rich ion adsorption-type ores in Longnan, contains abundant fluorite and synchysite-(Y), with subordinate zircon, xenotime, monazite, gadolinite, aeschynite-(Y), pyrochlore, topaz, and columbite, and lesser amounts of fergusonite, grossular, apatite, ilmenite, and magnetite (Table 2). In contrast, the biotite granite contains zircon, xenotime, monazite, apatite, and trace amounts of other REE-bearing minerals, including synchysite-(Y) (Table 2). The different HREE enrichment between the weathered muscovite granite and biotite granite results from different mineral assemblages in the parent rocks (Tables 2, 3). Since synchysite-(Y) is rarely found in the weathered muscovite granite, it is considered to be the predominant source of HREE-rich ores. Huang et al. (1989) concluded that the synchysite-(Y) formed during deuteric alteration by the breakdown of primary REE phases. The deuteric alteration consisted of the formation of secondary albite, muscovite, and fluorite. During subsequent weathering, the synchysite-(Y) and probably other minerals broke down. Weathering products are dominated by kaolinite and halloysite, with subdominant montmorillonite, vermiculite, and gibbsite, and, in some cases, mixed layer clays (Yang, 1987; Wu et al., 1990a).

Heling deposits

The LREE-rich Heling deposits, located in Xunwu County, Jiangxi province, were studied by Song and Shen (1982, 1986) and summarized by Bao and Zhao (2008). The weathering profile is primarily developed on the Heling granite porphyry, which is surrounded by rhyolitic lava and tuff. The granite

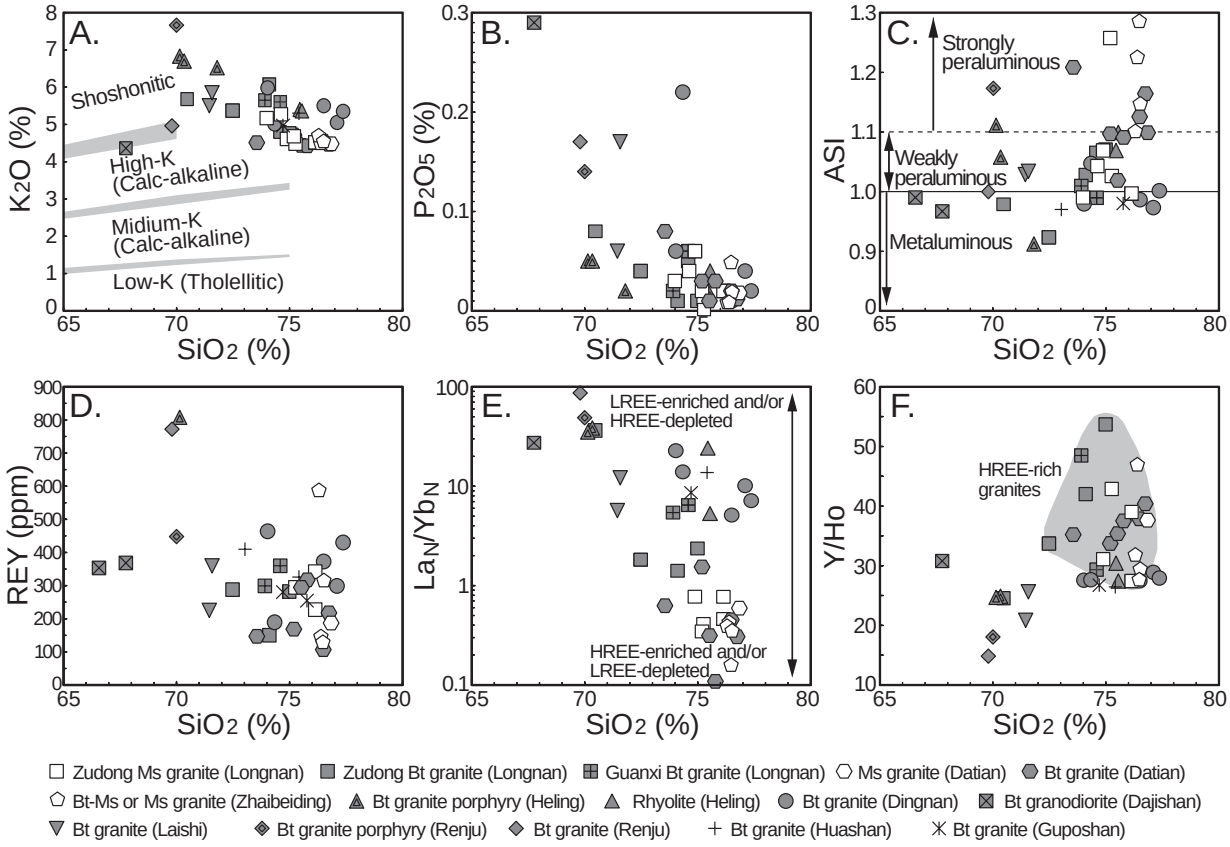

Fig. 4. Diagrams of (A) K_2O contents, (B) P_2O_5 contents, (C) ASI (alumina saturation index = molar $Al_2O_3/(CaO + Na_2O + K_2O)$ ratio), (D) REY contents, (E) La_N/Yb_N ratios and (F) Y/Ho ratios of the parent granites of ion adsorption-type REE deposits in southern China (Yang et al., 1981; Deng, 1988; Huang, 1989; Huang et al., 1989; Zhang, 1990; Wu et al., 1990a, 1993b; Yuan et al., 1993; Chen and Yu, 1994; Hua et al., 2007; Bao and Zhao, 2008; Ishihara et al., 2008). Boundary lines for K contents are from Rickwood (1989). The subscript N indicates normalization by chondrite components (Sun and McDonough, 1989). Note that differentiated biotite and/or muscovite granites occur in the HREE-rich Longnan, Datian, and Zhaibeiding deposits, whereas alkali granite porphyry occurs in the LREE-rich Heling deposits. Bt = biotite, Ms = muscovite.

porphyry has high alkali contents (Yang et al., 1981; Zhang, 1990; Bao and Zhao, 2008) compared to calc-alkaline granites in other deposits (Fig. 4A), suggesting a low degree of partial melting. The REY content of the granite porphyry is 808 ppm, which is significantly higher than those of calc-alkaline granites associated with other deposits (Fig. 4D). The Heling granite porphyry is enriched in LREEs and depleted in HREEs and the REEs are predominantly hosted by bastnäsite-(Ce), apatite, and lesser zircon, monazite, fergusonite, and synchysite-(Y). The REY grades in the weathered zone are relatively high (1,212–3,797 ppm), and they have high La_N/Yb_N ratios of 42 to 121, when compared to the Longnan ores (Fig. 5), again reflective of the underlying lithology. Clay minerals of these ion adsorption ores consist mainly of kaolinite and halloysite (Song and Shen, 1982).

Guangdong province deposits

Guangdong province contains the second largest resources of ion adsorption ores, which are represented by the Wujingfu-Wufang, Laishi, Zhaibeiding, Renju, and Xiache deposits (Table 1), but published data on the deposits and parent granites are limited. Yang and Xiao (2011) reported that the thickness of weathering profiles with REE ores generally range from 5 to 15 m, and that REY grades range from approximately 690 to 1,700 ppm with as high as 4,100 ppm at the Renju deposits in Pingyuan County. The HREE-rich Zhaibeiding deposits in Ruyuan County overlie muscovite granite and biotite granite, similar to the Longnan deposits, with REY contents ranging from 131 to 589 ppm and La_N/Yb_N ratios from 0.23 to 1.5 (Ma et al., 1991; Wu et al., 1993b). The muscovite granite consists of quartz, albite, K-feldspar, muscovite, fluorite, tourmaline, zircon synchysite-(Y), gadolinite, xenotime, cassiterite, and pyrite (Wu et al., 1993b). A U-Pb zircon age of 144.8 Ma was obtained from the muscovite granite (Wu et al., 1990b). The thickness of weathering crusts on the granites is variable and may locally reach up to 60 m (Yang and Xiao, 2011). The Fogang batholith, considered to the parent rocks of the Laishi and other REE deposits in Guangdong (Wang et al., 2012), has an exposed area of nearly 6,000 km^2 (Xu et al., 2007; Fig. 2). It consists mainly of calc-alkaline biotite granite, with small intrusions of hornblende-bearing biotite granodiorite and syenite, which are metaluminous to weakly peraluminous (ASI <1.1), and an A-type alkali granite pluton (Li et al., 2007; Xu et al., 2007). The Fogang batholith has U-Pb zircon ages of 159 to 165 Ma, and the age of the alkali granite is 158 Ma (Li et al., 2007).

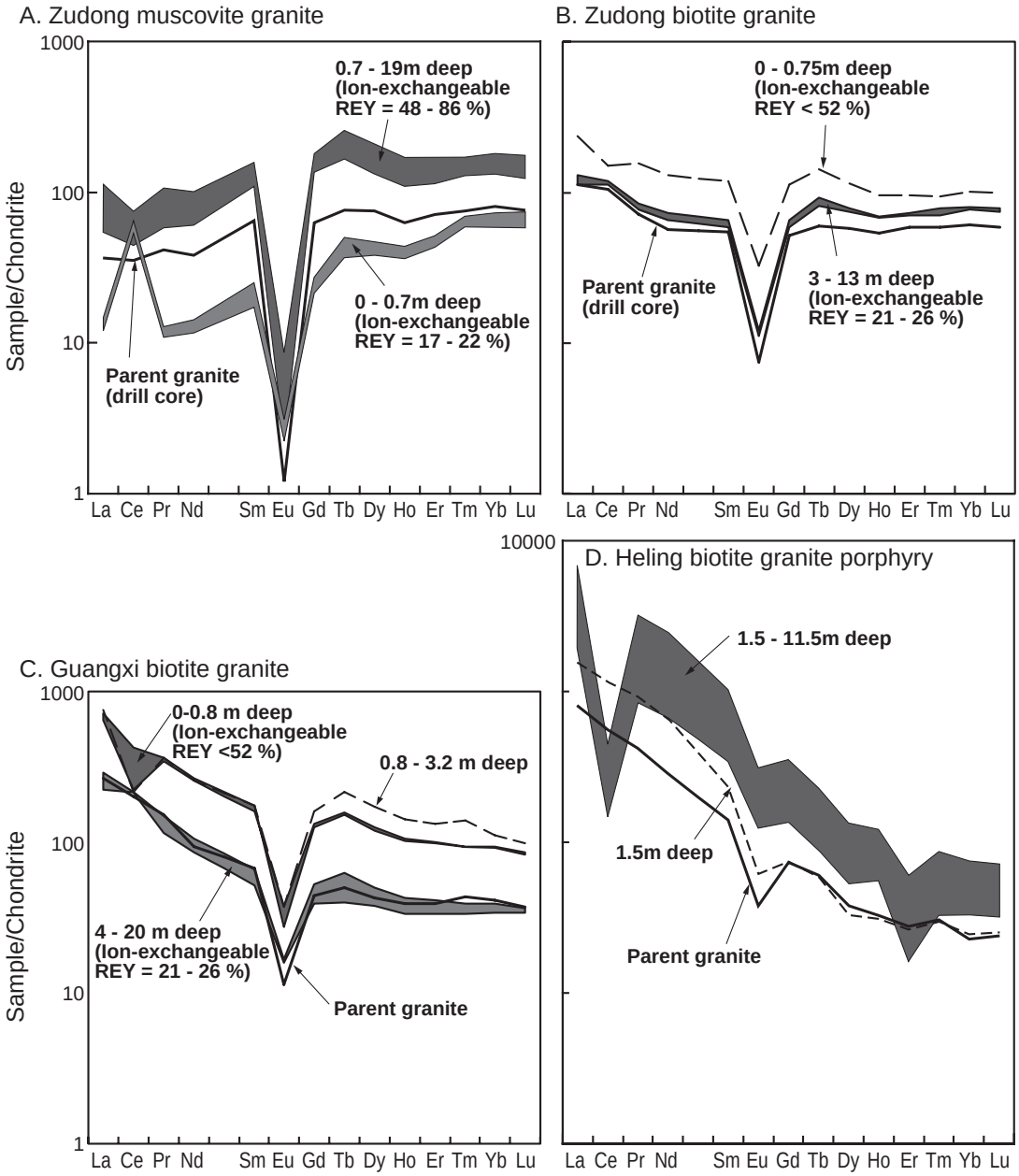

Fig. 5. Chondrite-normalized REE pattern (Sun and McDonough, 1989) of ion adsorption ores developed on (A) the HREE-rich Zudong muscovite granite, (B) HREE-rich Zudong biotite granite, (C) Guangxi biotite granite in Longnan (Wu et al., 1990a), and (D) LREE-rich Heling biotite granite porphyry (Bao and Zhao, 2008) in Jiangxi province, southern China. Note that ion adsorption ores show significant negative Ce anomalies.

The REY contents range from 125 to 411 ppm and La_N/Yb_N ratios are 6.1 to 11 in the Fogang batholith (Xu et al., 2007; Hsieh et al., 2008), and thus it is not strongly enriched in HREEs compared to the HREE-rich Zudong intrusion in Longnan and Zhaibeiding granite in Ruyuan. Identified REE-bearing minerals are allanite, titanite, apatite, zircon, monazite, xenotime, samarskite, and fergusonite (Zhu and Ruan, 1984; Huang, 1989; Hsieh et al., 2008).

Huashan-Guposhan deposits

The ion adsorption type of REE deposits in Guangxi and Hunan are less productive than the deposits in Jiangxi and Guangdong and are underlain by the Huashan-Guposhan granite plutons. The granites have REY contents of 171 to 618 ppm and La_N/Yb_N ratios of 1.8 to 21 (Gu et al., 2006; Zhu et al., 2006; Hua et al., 2007; Bao and Zhao, 2008; Feng et al., 2012). The U-Pb zircon ages of the different granite plutons range typically from 165 to 151 Ma (Gu et al., 2006; Zhu et al., 2006). Identified REE-bearing minerals consist of apatite, zircon, allanite, monazite, xenotime, fergusonite, and gadolinite (Bao and Zhao, 2008). The REY contents of the ores range from 429 to 1,327 ppm with La_N/Yb_N ratios of 7.1 to 24 (Bao and Zhao, 2008; Li and Shen, 2013). No information on the thickness of weathering crusts is available.

Table 2. Comparison of Main Accessory Minerals of the HREE-Rich Zudong Intrusion in the Longnan Deposits (partly modified from Huang et al., 1989)

Rock	Zudon muscovite granite		Zudon biotite granite	
	Parent rock	Weathered rock	Parent rock	Weathered rock
Mineral	Content (g/t)		Content (g/t)	
Zircon	40–71	80–100	115.8	100–200
Xenotime	Trace–20.7	20–30	31.4	Minor >200
Monazite	2–16.4	10	99.2	100
Columbite	3.6	1–5	-	Trace
Fergusonite	0.7	Trace	Trace	7
Pyrochlore	0.7–13.8	5–7	Trace	Trace
Aeschynite-(Y)	>10	20–30	Trace	Trace
Gadolinite	0.9–17.0	Up to 32	Trace	Trace
Chernovite	6	Up to 151	-	Trace
Synchysite-(Y)	233	-	Minor	-
Apatite	Minor	Uncertain	4.8	Uncertain
Topaz	6.1	Uncertain	-	-
Fluorite	421–2308	Uncertain		
Grossular	Trace–4.7		Minor	Uncertain
Magnetite	Minor		Minor	
Ilmenite	0.7		Minor	

See Table 3 for empirical chemical formula of minerals

Soil-water data for ion adsorption-type deposits in southern China

At ambient temperatures, the solubility of REEs is strongly controlled by pH (Brookins, 1988), thus the pH of soil and soil water has been measured at many different deposits. The pH values of water associated with weathered granites of the Zudong and Guanxi intrusions vary from a moderately low pH of 4.4 to 5.2 in the surface soil, to a pH of 5.5 to 6.0 in the strongly weathered zone that includes the ion adsorption ores, and to a pH of 6.3 in the weakly weathered zone on parent granites (Wu et al., 1990a). Similar pH values were reported in other mining sites of Xunwu, Dingnan, and Gan Counties in Jiangxi province, consisting of 4.13 to 4.80 in the surface soil, 4.36 to 4.84 in the strongly weathered zone, and 5.01 to 5.77 in the weakly weathered zone (Wei et al., 2001). At other mining sites of Guangdong province, Yang and Xiao (2011) reported similar pH values consisting of 4.8 to 5.96 in the surface soil, 5.22 to 6.80 in the strongly weathered zone including ion adsorption ores, and 6.23 to 6.48 in the weakly weathered zone on parent rocks. The moderately lower pH values in the surface soils are attributed to humic substances (Wu et al., 1990a; Wei et al., 2001) and to CO_2 in the atmosphere. Song and Shen (1982) concluded that REE adsorption onto clays occurred when the pH values were between 4.7 and 5.6 at the Heling deposits. On the other hand, Pang (2011) reported that REE adsorption was most likely to occur at a higher pH range, between 5.5 and 6.5, in the Qinghu and Majigang deposits in Guangxi.

Other prospective areas for ion adsorption deposits

The Malawi REE deposit was recently discovered in the Chambe basin located northwest of the Mulanje Massif, southern Malawi (Le Couteur, 2011). The basement rocks of the deposit consist of Precambrian to Paleozoic hornblende-biotite gneissic complex, which is intruded by Late Jurassic to Early Cretaceous syenitic plutons accompanied by carbonatite

Table 3. REE-Bearing Minerals Associated with Ion-Adsorption Ore Formation

Mineral name	Empirical chemical formula	Dominant REE(+Y)
Aeschynite-(Ce)	$(Y,Ca,Fe^{2+})(Ti,Nb)_2(O,OH)_6$	LREE
Aeschynite-(Y)	$(Y,Ca,Fe^{2+})(Ti,Nb)_2(O,OH)_6$	HREE + Y
Allanite-(Ce)	$(Ce,Ca,Y)_2(Al,Fe^{3+})_3(SiO_4)_3(OH)$	LREE
Almandine	$Fe_3Al_2(SiO_4)_3$	HREE + Y
Anatase	TiO_2	
Apatite	$Ca_5(PO_4)_3F$	LREE
Bastnasite-(Ce)	$Ce(CO_3)F$	LREE
Britholite-(Ce)	$(Ce,Ca)_5(SiO_4,PO_4)_3(OH,F)$	LREE
Columbite-(Fe)	$Fe^{2+}Nb_2O_6$	
Columbite-(Mn)	$MnNb_2O_6$	
Cerianite	$(Ce^{4+},Th)O_2$	Ce
Chernovite-(Y)	$YAsO_4$	HREE + Y
Coffinite	$U(SiO_4) \cdot nH_2O$	
Crandallite	$CaAl_3(PO_4)_2(OH)_5 \cdot H_2O$	LREE
Euxenite-(Y)	$(Y,Ca,Ce)(Nb,Ta,Ti)_2O_6$	HREE + Y
Fergusonite-(Y)	$YNbO_4$	HREE + Y
Florencite-(Ce)	$CeAl_3(PO_4)_2(OH)_6$	LREE
Fluorite	CaF_2	
Gadolinite-(Y)	$Y_2Fe^{2+}Be_2Si_2O_{10}$	HREE + Y
Gorceixite	$BaAl_3(PO_4)_2(OH)_5 \cdot H_2O$	LREE
Goyazite	$SrAl_3(PO_4)_2(OH)_5 \cdot H_2O$	LREE
Grossular	$Ca_3Al_2(SiO_4)_3$	HREE + Y
Hornblende	$Ca[(Fe^{2+},Mg^{2+})_4(Al,Fe^{3+})]Si_7AlO_{22}(OH)_2$	HREE + Y
Ilmenite	$FeTiO_3$	
Monazite-(Ce)	$(Ce,Th)PO_4$	LREE
Parisite-(Ce)	$CaCe_2(CO_3)_3F_2$	LREE
Pyrochlore	$(Na,Ca)_2Nb_2O_6(OH,F)$	HREE + Y
Rhabdophane-(Ce)	$(Ce,La)PO_4 \cdot H_2O$	LREE
Rutile	TiO_2	
Samarskite-(Y)	$(Y,Fe^{3+},U)(Nb,Ta)_5O_4$	HREE + Y
Spessartine	$Mn_3Al_2(SiO_4)_3$	HREE + Y
Tantalite-(Fe)	$Fe^{2+}Ta_2O_6$	
Tantalite-(Mn)	$MnTa_2O_6$	
Titanite	$CaTiSiO_5$	HREE + Y
Synchysite-(Ce)	$CaCe(CO_3)_2F$	LREE
Synchysite-(Y)	$CaY(CO_3)_2F$	HREE + Y
Thorite	$ThSiO_4$	
Uraninite	UO_2	
Xenotime-(Y)	YPO_4	HREE + Y
Yttrofluorite	$(Ca_{1-x},Y_x)F_{2+x}$	HREE + Y
Zircon	$ZrSiO_4$	HREE + Y

References: Yang et al., 1981; Huang, 1989; Huang et al., 1989; Zhang et al., 1990; Wu et al., 1992, 1993a; Chen and Yu, 1994; Yang et al., 1999; Bao and Zhao, 2008; Yang and Xiao, 2011; Tong, 2013; Sanematsu et al., 2013; Sanematsu and Kon, 2013; this study

Note: REE and Y are present as minor components in minerals that do not include Ce or Y in the formula

belonging to the Chilwa alkaline province in southern Malawi and Mozambique (Garson and Walshaw, 1969). Syenitic plutons consist mainly of syenite and quartz syenite in the Chambe basin, whereas elsewhere they are more variable in compositions (e.g., syenite, quartz syenite, and granite). Chevkinite, yttrofluorite, and other REE minerals are found in the main part of the massif, but the dominant REE minerals have not been identified (Platt and Woolley, 1986). The thickness of the weathering profile on syenite is up to 15 m. The center of the basin is covered by kaolinitic soil with bauxite (Garson and Walshaw, 1969). Geochemical data from three kaolinitic soil samples show REY contents ranging from 475 to 739 ppm with La_N/Yb_N ratios of 10 to 12, and the percent of ion-exchangeable REY concentrations relative to whole-rock REY contents

(hereinafter PER) ranges from 31 to 74% (Le Couteur, 2011). Saprolitic weathered syenite samples have lower REY contents of 198 to 642 ppm and the PERs are less than 30% (Le Couteur, 2011). Most of these samples have low contents of Th (<10 ppm) and U (<30 ppm). Chondrite-normalized REE patterns of weathered rock samples display negative Ce anomalies similar to ion adsorption ores in southern China.

The Tantalus REE deposit in northern Madagascar is being explored by Tantalus Rare Earths Ag. In northern Madagascar, Jurassic sedimentary basement rocks are intruded by a NW-trending Tertiary alkaline complex, which consists of syenite and smaller intrusions of alkali granite and quartz syenite that host REE-Ta-Nb-Zr mineralization (Ganzeev and Grechishchev, 2003). These igneous rocks are overlain by weathering profiles consisting of a saprolitic layer and an overlying Fe-rich lateritic layer. These clay-rich weathering profiles have PERs of 60 to 76%, and Th and U are not in ion-exchangeable states (Moldoveanu and Papangelakis, 2013b).

The Serra Verde REE deposit located in Goiás province of Brazil is currently being explored by Mineração Serra Verde. This deposit has the total resources (measured + indicated + inferred) of 909 Mt at a cut-off grade of 0.16 REY oxides (data from website of Mineração Serra Verde). The REEs occur in weathered granites of 6 m thickness and more than 50% of them are ion-exchangeable except for Ce (Rocha et al., 2013). In the processed oxide product from the ores, the fraction of oxides of HREEs and Y (note that Eu is included in HREEs in this project) is 38% (Rocha et al., 2013), suggesting the ores are significantly rich in HREEs. The high REY grades and HREE enrichment of the Serra Verde deposit probably reflects the underlying Serra Dourada granitic pluton, which is characterized by high REY and HREE contents (Marini et al., 1992; Santana, 2013).

In recent years, relatively small ion adsorption-type deposits and prospects have been recognized in Southeast Asia (Fig. 1). Ion adsorption ores are locally mined in Myanmar (e.g., eastern Kachin state, northern Shan state), however the geologic information is very limited. In the vicinity of a polymetallic W deposit in northern Vietnam, the Nui Phao Granite with zircon U-Pb ages of ~250 Ma (Ishihara and Orihashi, 2014), has 10-m-thick weathering profiles (Mentani, 2012). The weathered granite is moderately rich in HREEs, and the average REE content and PERs are 549 ppm and 67%, respectively, in the northern part of the exposed granite area (Mentani, 2012). In the Ben Den area of Lao Cai province in northern Vietnam, ion-absorption-type ores are identified in weathering profiles with thicknesses ranging from 7 to more than 20 m (CCOP, 2012). On Phuket Island in Thailand, the Late Cretaceous Kata Beach granite (Pollard et al., 1995) has a weathering profile of 12 m in thickness in which REY contents range from 181 to 1,158 ppm and PERs range from 34 to 88% (Sanematsu et al., 2013). The economic potential of these areas is still unknown.

Geologic Settings of Ion Adsorption-Type Deposits of Southern China

Numerous lithogeochemical and geochronological studies have been conducted in the granite terranes of southern China. Mesozoic granitic rocks are widely distributed in southern China (Fig. 2), and the majority of the productive ion adsorption-type REE deposits occur in areas underlain by granite in the Nanling Range in southern China (Zhang, 1990; Huo, 1992; Wu et al., 1992; Wang et al., 2013). The Phanerozoic igneous rocks of the southern China were formed during three major tectonic events: the middle Paleozoic Kwangsian, Triassic Indosinian, and Jurassic-Cretaceous Yanshanian events (e.g., Zhou et al., 2006; Wang, F.Y. et al., 2011; Zhang et al., 2012). Zircon U-Pb ages of the Kwangsian granites and gneissic granites range from 454 to 400 Ma (Zhang et al., 2012) and from 457 to 415 Ma (Wang, Y.J. et al., 2011), respectively. The Kwangsian granites were formed by crustal anatexis of mainly Proterozoic metapelitic rocks and/or igneous rocks with minor input of mantle-derived magma (Wang, Y.J. et al., 2011; Zhang et al., 2012). These granites are primarily peraluminous (ASI >1.0), with the gneissic granites being more peraluminous, and they are enriched in LREEs relative to HREEs with moderate REY contents (Wang, Y.J. et al., 2011; Zhang et al., 2012).

Some relatively minor ion adsorption-type deposits, such as Dajishan, Qingxi, Huangfang, Huangsha, and Long'an, are associated with the Indosinian granites (Wang et al., 2013; Table 1; Fig. 2), which have a total outcrop area of 14,300 km^2 (Zhou et al., 2006). The Indosinian granites are primarily (90.9%) peraluminous compositions and are related to the Triassic syncollisional event (Zhou et al., 2006). The granites have REY contents of 75 to 195 ppm and La_N/Yb_N of 8.0 to 59 (Wang et al., 2007). Zircon U-Pb ages of the granites range from 251 to 205 Ma (Zhou et al., 2006; Wang et al., 2007).

The Yanshanian magmatism is closely related to widespread base and precious metal deposit formation in southern China and is a result of the southwestward subduction of the Pacific Plate and intraplate tectonics within the Yangtze block (Wang, F.Y. et al., 2011). The Early Yanshanian granites (ca. 180–142 Ma; e.g., Zhou et al., 2006) are of the calc-alkaline series and are distributed over a total area of 64,100 km^2 in southern China (Sun, 2006; Fig. 2). The HREE-rich granites of the Early Yanshanian are aligned in E-W directions in the middle (southern Jiangxi and northern Guangdong) and southern (Fogang in Guangdong) parts of the Nanling Range (Wu et al., 1992; Fig. 2). These calc-alkaline granites, A-type granites, alkali granites, and syenites were formed by intraplate rifting (Zhou et al., 2006; Guo et al., 2012) in an extensional tectonic setting in the Yangtze block (Hua et al., 2007; Guo et al., 2012), and from the Pacific flat-slab subduction and subsequent break-off (Li and Li, 2007; Li et al., 2007). The Xihuashan granite, which was derived from the Proterozoic lower crust with a small fraction of mantle-derived magma, is enriched in HREEs as well (Guo et al., 2012). The regional distribution of the HREE-rich granites is not consistently related to the distribution of the HREE-rich ion adsorption deposits. This is in part because to form HREE-rich ion adsorption deposits, the series of events does not only include differentiation of a specific magma but also required postmagmatic processes, including deuteric alteration and chemical weathering.

Discussion

Geochemistry and REE-bearing minerals of granite

The REE contents of igneous rocks are generally dependent on both the degree of partial melting of the source and magmatic differentiation (e.g., Chakhmouradian and Zaitsev,

2012; Linnen et al., 2014). Igneous rocks are widely distributed in southern China; however, ion adsorption-type REE deposits are primarily developed on granites in the Nanling Range (Fig. 2). Wang et al. (2013) summarized ages of the parent granites and the data indicate that the majority of the major deposits were associated with the Yanshanian intrusions. The parent granites of the deposits are biotite granite or muscovite granite with medium to high $Na_2O + K_2O$ (approx 8–10%) contents and low P_2O_5 contents of <~0.08% (Yang et al., 1981; Deng, 1988; Huang et al., 1989; Zhang, 1990; Ma et al., 1991; Yu et al., 2004; Gu et al., 2006; Hua et al., 2007; Li et al., 2007; Bao and Zhao, 2008; Ishihara et al., 2008; Yang and Xiao, 2011; Feng et al., 2012; Fig. 4B), although some granites show higher P_2O_5 contents (Huang, 1989; Chen and Yu, 1994). They primarily are metaluminous to weakly peraluminous (ASI <1.1) in composition, and have I-type affinities (Chappell and White, 1974), although the granites become increasingly peraluminous with magmatic differentiation. Based on the classification of granitoid series (Ishihara, 1977), the parent granites are primarily classified into ilmenite series with some exceptions, such as granites in Dajishan and Qinghu (Table1), which are likely magnetite series.

Parent granites of the HREE-rich deposits are highly differentiated muscovite granites with abundant alkali feldspars, SiO_2 contents greater than ~75%, and very low P_2O_5 contents of <~0.02% (Yang et al, 1981; Deng, 1988; Huang et al., 1989; Zhang, 1990; Ma et al., 1991; Wu et al., 1992, 1993b; Yuan et al., 2007; Bao and Zhao, 2008; Yang and Xiao, 2011). Significant enrichment of HREEs by magmatic differentiation was recognized in some high SiO_2 I-type granites of the Lachlan fold belt of southeastern Australia (Chappell, 1999) and in southwestern Japan (Ishihara and Murakami, 2006). The highly differentiated granites associated with the REE deposits that contain a variety of fine-grained hydrothermal minerals, including REE fluorocarbonates, fluorite, monazite, xenotime, fergusonite, gadolinite, and samarskite (Table 1). The occurrence of hydrothermal minerals is suggested by elevated Y/Ho ratios of whole-rock compositions (Fig. 4F), because a fractionation of Y/Ho is controlled by fluids generated from differentiated melts (Bau and Dulski, 1995; Bau, 1996). For example, the Zudong muscovite granite is characterized by enrichment of HREEs (La_N/Yb_N = 0.31–0.95), Y/Ho ratios ranging from 27 to 50 (Fig. 4), and the occurrence of hydrothermal minerals (Table 2; Huang et al., 1989; Wu et al., 1990a, Bao and Zhao, 2008). In contrast, less differentiated biotite granites associated with Longnan and other deposits tend to have lower Y/Ho ratios of 15 to 34 (Fig. 4F), and they are more enriched in LREEs (La_N/Yb_N = 1.8–35; Fig. 4E). These biotite granites contain less hydrothermal minerals than the more differentiated granites with high Y/Ho ratios (Table 1).

The occurrence of REE fluorocarbonates in granites is important for the formation of ion adsorption ores because the fluorocarbonates are more easily dissolved in moderately low pH soil water than silicates, oxides, and phosphates during weathering. The REE fluorocarbonates occur along grain boundaries, such as veinlets and in cavities (Fig. 6A), and it is

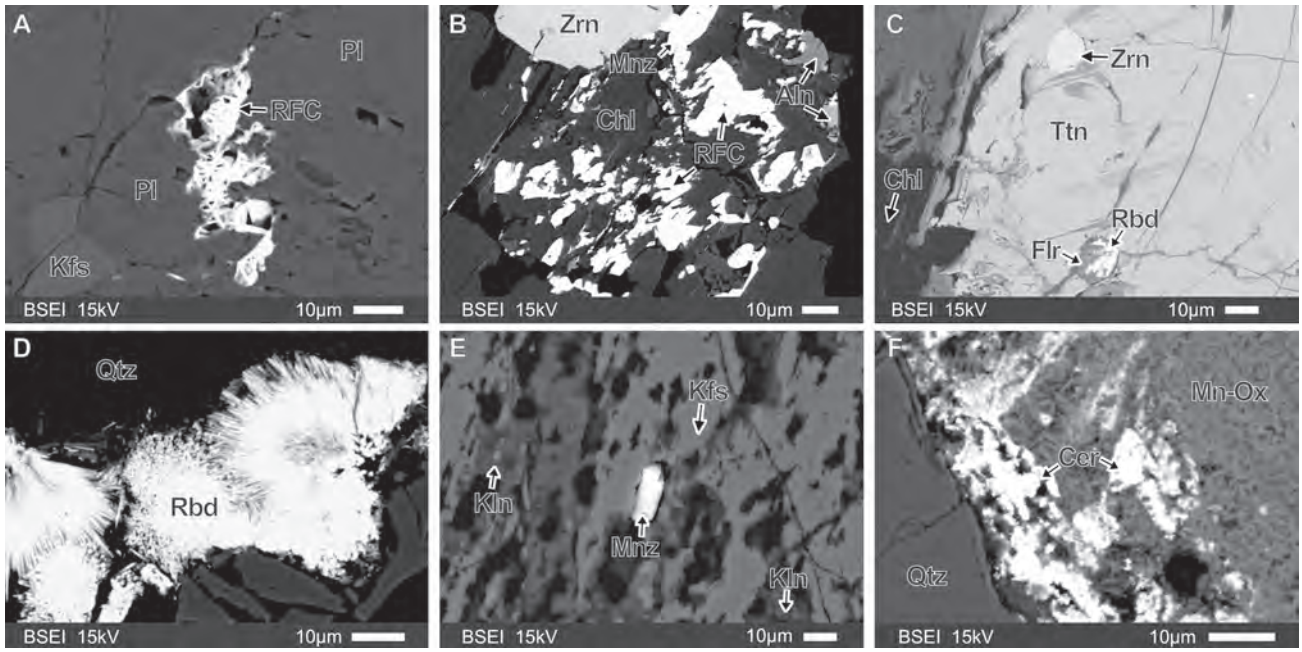

Fig. 6. SEM-backscattered electron images of REE-bearing minerals in granites and ion adsorption ores. A. Occurrence of REE fluorocarbonate along a crack in K-feldspar in biotite granite in Phuket, Thailand (Sanematsu et al., 2013). B. Replacement of precursor allanite by REE fluorocarbonate and lesser amount of monazite during deuteric alteration of muscovite-biotite granite (SiO_2 = 75.3%) in southern Myanmar. C. Replacement of precursor apatite by florencite and rhabdophane in the incipient weathering stage of biotite granite in southern Myanmar. D. Rhabdophane-(Ce) in weathered biotite granite (Sanematsu et al., 2013). E. Residual monazite-(Ce) in the ion adsorption ore from Dingnan, southern China (sample 1130S3; Murakami and Ishihara, 2008). F. Aggregate of fine-grained cerianite (CeO_2) and Mn oxyhydroxide in the ion adsorption ore with positive Ce anomaly ($Ce/Ce^* = 2.3$) from Dingnan, southern China (sample 1130S3). Ab = albite, Aln = allanite, Cer = cerianite, Chl = chlorite, Flr = florencite-(Ce), Kfs = K-feldspar, Kln = kaolinite, Mn-Ox = Mn oxyhydroxide, Mnz = monazite-(Ce), Qtz = quartz, Rbd = rhabdophane-(Ce), RFC = REE fluorocarbonate, Zrn = zircon.

believed that they formed by F- and CO_2-rich fluids during deuteric alteration at the last stage of magmatic differentiation (e.g., Huang et al., 1989; Maruéjol et al., 1990; Bea, 1996; Förster, 2001; Berger et al., 2008; Ishihara et al., 2008; Sanematsu et al., 2013). The muscovite granite, which underlies the main orebody of the HREE-rich Zudong deposit, contains abundant F-bearing minerals, such as fluorite, synchysite-(Y), and topaz, whereas the Zudong biotite granite contains only F-bearing biotite and apatite (Huang et al., 1989). Wu et al. (1992) studied a variety of HREE-rich granites throughout the Nanling Range and documented relatively high F contents of 340 to 6,700 ppm, with a median value of 1,400 ppm.

Fluorine plays an important role in the alteration of magmatic REE-bearing silicates and the formation of REE source minerals for ion adsorption ores. Pan et al. (1993) reported that titanite may destabilize to form fine-grained REE minerals (e.g., allanite and monazite), rutile, quartz, calcite, apatite, and chlorite in CO_2-PO_4^{3-}-F_2 fluids at low temperatures. These results suggest that allanite and titanite are important REE sources for ion adsorption ores. An experimental study by Price et al. (1999) showed that titanite is unstable in F-rich melts because it reacts with F to form fluorite. Middleton et al. (2013) documented that titanite in metaluminous granite degrades into anatase + calcite + quartz + synchysite-(Ce) ± bastnäsite-(Ce) in CO_2-F_2-dominant fluids, or into anatase + calcite + quartz + monazite-(Ce) + xenotime ± thorite in CO_2-HPO_4^{2-}-dominant fluids. Allanite in granitic rocks commonly alters to secondary minerals, including fluorite and REE fluorocarbonates, such as bastnäsite and synchysite (Caruso and Simmons, 1985; Lira and Ripley, 1990; Bea 1996; Gieré, 1996; Gieré and Sorensen, 2004; Berger et al., 2008). Allanite can be replaced by a monazite-fluorite mineral assemblage upon interaction with fluorine- and phosphate-rich fluids (Wood and Ricketts, 2000), although this mineral assemblage is not common (Gieré and Sorensen, 2004). Figure 6B shows the replacement of allanite by REE-rich fluorocarbonate and lesser monazite during deuteric alteration of granite. These studies of allanite and titanite alteration are consistent with the occurrence of REE fluorocarbonates, with lesser amounts of allanite and titanite, in the highly differentiated granites that form the REE deposits (Yang et al., 1981; Huang et al., 1989; Bao and Zhao, 2008; Ishihara et al., 2008), suggesting that the alteration of allanite and titanite to REE fluorocarbonates by fluorine-dominant and phosphate-poor hydrothermal fluids is important for formation of the ion adsorption ores.

Occurrences of REE fluorocarbonates suggest that REE^{3+} ions are transported by carbonate (CO_3^{2-}), bicarbonate (HCO_3^-), and fluoride ligands, as predicted by Wood (1990a). However, (bi)carbonate species are dominant over fluoride species, and the stability constants are likely to increase with increasing temperatures. Stability constants of REE fluorides and chloride complexes in acidic fluid at 300° to 500°C were theoretically predicted (Wood, 1990a; Haas et al., 1995), however experimental data from Migdisov et al. (2009) indicate that the previous studies overestimated the stabilities of REE fluoride complexes, particularly HREE fluoride complexes, at temperatures above 150°C. Migdisov et al. (2009) also pointed out that the previous theoretical studies underestimated the stabilities of LREE chloride complexes. The recent studies indicate that REEs are predominantly transported as REE chloride complexes even in fluorine-bearing hydrothermal solutions (Migdisov and Williams-Jones, 2014).

Allanite and titanite, which are common REE-bearing minerals in monazite-free granites, contribute significantly to whole-rock REE contents (Gromet and Silver, 1983; Bea, 1996), and they can be precursor minerals of REE fluorocarbonates formed by hydrothermal alteration as discussed above. Partition coefficients for REEs between allanite and melt indicate that allanite incorporates LREEs rather than HREEs and Y (e.g., Gieré and Sorensen, 2004), and that titanite is moderately rich in HREEs and Y in contrast to allanite (e.g., Green and Pearson, 1986; Prowatke and Klemme, 2005). Modal and electron probe microanalysis (EPMA) analyses of Gromet and Silver (1983) indicated that allanite and titanite together contribute 80 to 95% of REEs in a monazite-free granodiorite. Bea (1996) analyzed accessory minerals of different granitoids and crustal protoliths using LA-ICPMS and EPMA and noted that strongly peraluminous granites contain monazite, xenotime, apatite, zircon, Th silicates (thorite and/or huttonite), and pyrochlore, and that metaluminous and weakly peraluminous granites contain allanite, titanite, apatite, zircon, monazite, and Th silicates. In the study by Bea (1996), a proportion of LREEs (except for Eu) of each mineral relative to whole-rock LREEs is primarily dominated by monazite in the allanite-free granites, and by allanite in the other monazite-free granites. Predominant HREE-bearing minerals are zircon, apatite, and xenotime in the allanite-free granites and zircon and titanite in the other monazite-free granites. As the quantitative data of Bea (1996) showed, magmatic allanite and monazite rarely coexist in granitoids.

Phosphates, including monazite and xenotime, in contrast to REE fluorocarbonates, allanite, and titanite, are not favorable as REE source minerals for ion adsorption deposits because of their resistance to chemical weathering, as discussed by Sengupta and Van Gosen (2016). Apatite, the most common phosphate in granites, incorporates less REY, with contents ranging from 61 to 45,300 ppm (Sha and Chappell, 1999; Belousova et al., 2002), compared to monazite and xenotime. Experimental studies indicate that the solubility of apatite and monazite in magma is dependent on SiO_2 content, temperature, and ASI of magma (e.g., Harrison and Watson, 1984; Pichavant et al., 1992; Piccoli and Candela, 2002). Solubilities of apatite (Watson, 1979, 1980; Watson and Capobianco, 1981; Harrison and Watson, 1984) and monazite (Montel, 1986, 1993; Rapp and Watson, 1986; Rapp et al., 1987) decrease with increasing SiO_2 or decreasing temperature of melt. This leads to saturation and fractional crystallization of apatite and/or monazite in melt of intermediate to felsic compositions, resulting in depletion of LREEs and relative enrichment of HREE + Y (Miller and Mittlefehldt, 1982). Solubility of apatite is influenced by the ASI of melt (Pichavant et al., 1992) and, in a peraluminous melt, it increases linearly with increasing ASI up to P_2O_5 = ~0.63% at ASI = 1.3 (Wolf and London, 1994). Solubilities of monazite and xenotime in a peraluminous melt are much lower than apatite (Wolf and London, 1995). These experimental results are consistent with granite geochemistry from different localities, which indicated that P_2O_5 contents of I- and S-type granites decrease with increasing SiO_2 by fractional crystallization of phosphates (mostly apatite); however, those of differentiated S-type granites with

higher ASI tend to increase (Bea et al., 1992; Chappell, 1999; Broska et al., 2004).

In hydrothermally altered granite, apatite is associated with hydrothermal REE minerals, such as REE fluorocarbonates, as well as fluorite (Gieré, 1996), whereas monazite is less reactive with hydrothermal fluids. Poitrasson et al. (1996) compared the effect of hydrothermal alteration on monazite in two contrasting granites, one chloritized at ~284°C and the other greisenized at ~200°C. In their study, alteration and substitution of REEs are recognized in monazite in both granites, and the phosphate framework was partly destroyed in monazite of the greisenized granite. Cuney and Mathieu (2000) reported that REEs were significantly leached from monazite in sandstone by diagenetic fluids of high salinity (from 28 wt % NaCl to 30 wt % $CaCl_2$ equiv; Mathieu et al., 2000) at ~140°C and 1 kbar. These studies indicate that the solubility products of REE phosphates is influenced by the presence of fluoride, chloride, carbonate, or hydroxide in acidic fluids (pH <2) up to 300°C and it decreases with increasing temperature (Poitrasson et al., 2004; Cetiner et al., 2005). These studies also suggest that monazite can be partly altered by acidic fluids in the presence of specific ligands.

Zircon is a ubiquitous HREE-bearing mineral in granitoids (Hoskin and Schaltegger, 2003) and is the first or second most significant host mineral for HREEs in xenotime-free granite (Gromet and Silver, 1983; Bea, 1996). However, the abundance of zircon in granite decreases in the late stages of fractional crystallization, as typically recorded by a decrease in Zr content. Wu et al. (1992) showed that Zr contents are less than 100 ppm for all HREE-rich granites in the Nanling Range and average 60 ppm for 11 muscovite granite samples of the Zudong intrusion. The REE-bearing oxide minerals, dominated by Y, REE, U, Th, Nb, Ta, and Ti, may form by magmatic or magmatic-hydrothermal processes and consist of fergusonite, samarskite, euxenite, aeschynite, and pyrochlore groups. These oxide minerals are quantitatively less significant than REE-bearing silicates and phosphate, except in many peralkaline rocks (Gromet and Silver, 1983; Bea, 1996; Mariano and Mariano, 2012; Linnen et al., 2014).

Numerous studies have indicated that REY contents and associated magmatic and hydrothermal REE-bearing mineral occurrences in granites are influenced by magmatic differentiation. High REY contents of some alkali granites (e.g., Heling granite porphyry, Fig. 4A) are most likely caused by a lower degree of partial melting than for other calc-alkaline granites. However, these alkali granites do not necessarily contain high HREE contents. The LREE/HREE ratios of granites are constrained by fractional crystallization of LREE-bearing minerals and the occurrence of HREE-bearing hydrothermal minerals as shown by the differences between the adjacent muscovite granite and biotite granite at the Zudong deposit, and the Guanxi biotite granite at the Longnan deposits (Table 2; Figs. 3, 4). The significant enrichment of HREEs is found in highly differentiated muscovite granites (SiO_2 >~75%), with associated deuteric alteration including albitization and fluoritization. It is also notable that the parent granites of the ion adsorption-type deposits in southern China primarily have metaluminous to weakly peraluminous (ASI <1.1) compositions in the Yanshanian age (Table 1) and contain low P_2O_5 contents of <0.08%. Major ion adsorption-type deposits are relatively uncommon in areas underlain by Kwangsian and Indosinian granites. The Kwangsian granites are metaluminous to strongly peraluminous (ASI = 0.93–1.44), and their P_2O_5 contents range from 0.01 to 0.27% (Zhang et al., 2012). The Kwangsian gneissic granites are weakly to strongly peraluminous (ASI = 1.04–1.42), and the P_2O_5 contents range from 0.05 to 0.22% (Wang et al., Y.J., 2011). The Indosinian granites are weakly to strongly peraluminous (ASI = 1.00–1.20) in compositions, and their P_2O_5 contents range from 0.08 to 0.20% (Wang et al., 2007).

Weathering of granite and REE-bearing minerals

During granite weathering, elements, including REEs and Y, can be released from primary magmatic, hydrothermal, and secondary minerals. The secondary REE-bearing minerals are formed by alteration of and dissolution of the precursor minerals during weathering of granite at ambient temperatures. During weathering, REE fluorocarbonates dissolve in acidic soil water, and REE-bearing phosphates, oxides, and silicates are likely to dissolve more slowly. Dissolution rates of some REE-bearing minerals at ambient temperatures were reported and discussed by previous studies (Ewing et al., 1981; Tole, 1985; Valsami-Jones et al., 1998; Ewing, 1999; Balan et al., 2001; Oelkers and Poitrasson, 2002; Guidry and MacKenzie, 2003; Tromans, 2006; Chaïrat et al., 2007; Harouiya et al., 2007; Oelkers et al., 2008), suggesting potential source minerals for ion adsorption ores. Another factor that can significantly affect the susceptibility of a mineral to chemical weathering is the decrease in crystallinity caused by metamictization. Because REE-bearing minerals generally contain radioactive Th and U as trace to major components, the crystal lattice can become disrupted due to radiation damage (Ewing and Haaker, 1980; Ewing, 1994). Metamict minerals can be partly to completely amorphous, and the metamict state influences the extent of alteration of REE-bearing minerals and the ease of dissolution in soil water. The metamict state is variable among REE-bearing minerals because it depends on irradiation time and metamictization rate, which is constrained by crystal structure, adsorbed water content, mineral composition, alpha-particle dose rate, and annealing rates of minerals (Ewing and Haaker, 1980; Ewing, 1994).

In addition to secondary REE fluorocarbonates, primary magmatic allanite and titanite are important REE sources, particularly LREE and HREE sources, respectively, for ion adsorption ores. The REE fluorocarbonates generally dissolve during weathering of parent granites (Huang et al., 1989), although the tiny grains can be present in the ores (Sanematsu and Kon, 2013). Allanite undergoes various degrees of metamictization (Ewing and Haaker, 1980; Ewing, 1994; Gieré and Sorensen, 2004), and this probably enhances alteration and dissolution of the mineral during weathering. Allanite likely breaks down releasing REE^{3+} into soil water because it is rarely found in weathering crusts on allanite-bearing igneous rocks (Banfield and Eggleton, 1989; Braun and Pagel, 1994; Condie et al., 1995; Schroeder et al., 2000; Harlavan and Erel, 2002; Gieré and Sorensen, 2004; Price et al., 2005; Sanematsu et al., 2013; Berger et al., 2014). Titanite is rarely found in clastic sediments derived from igneous rocks (Deer et al., 1982) or is quantitatively reduced in a weathering crust on titanite-bearing granodiorite (Condie et al., 1995).

It is more resistant to weathering than allanite and apatite because of the estimated weathering rates of accessary minerals: allanite > apatite > titanite by dissolution experiments of granite and soil samples (Harlavan and Erel, 2002). These study results suggest that allanite and titanite are important REE sources for ion adsorption ores.

Secondary REE-bearing phosphate minerals, such as the rhabdophane and crandallite group (e.g., florencite), commonly occur after dissolution of apatite in weathered granitic rocks and soils. Apatite is altered and replaced by secondary phosphates, such as rhabdophane and florencite, in weathered granites and syenites (Banfield and Eggleton, 1989; Braun et al., 1990, 1993, 1998; Braun and Pagel, 1994; Taunton et al., 2000; Aubert et al., 2001; Laveuf and Cornu, 2009; Stille et al., 2009; Aide and Aide, 2012; Du et al., 2012; Sanematsu et al., 2013; Berger et al., 2014; Janots et al., 2015), and these minerals have an important role in controlling REE concentrations and fractionation in soil water and ground water (Aubert et al., 2001; Köhler et al., 2005; Oelkers et al., 2008; Stille et al., 2009). The secondary REE-bearing phosphates occur even in the incipient weathering stage of granite (Fig. 6C), and apatite is commonly dissolved or replaced in weathered granite (Fig. 6D). Experimental studies indicate that apatite dissolution rates increase with decreasing pH of solution (Valsami-Jones et al., 1998; Guidry and MacKenzie, 2003; Chaïrat et al., 2007; Harouiya et al., 2007) and that temperature differences are not significant below 50°C (Harouiya et al., 2007). In acidic solutions at ambient temperatures, REE mobility related to apatite dissolution is strongly influenced by rhabdophane precipitation and dissolution because this secondary phase can immobilize the REEs (Köhler et al., 2005).

In contrast, the dissolution rate of monazite at room temperature is much lower than that of apatite, even in acidic ($2 < pH < 6$) solutions (Valsami-Jones et al., 1998; Oelkers and Poitrasson, 2002; Guidry and MacKenzie, 2003; Chaïrat et al., 2007; Harouiya et al., 2007; Oelkers et al., 2008). Monazite occurs in nature in a crystalline state, rather than in a metamict state, even after large radiation doses, because it is relatively easy to anneal the radiation damage at low temperatures over geologic time (Boatner and Sales, 1988; Meldrum et al., 1998, 2000). Relatively few modern studies have been conducted on radiation damage and annealing of xenotime. However, some old studies indicate that monazite and xenotime are mostly crystalline and are not in a metamict state (Hutton, 1950; Hurley and Fairbairn, 1953; Ueda, 1957). In weathered granites, fine-grained residual monazite and xenotime are common (Fig. 6E), whereas apatite is relatively scarce. Huang et al. (1989) demonstrated that masses of monazite and xenotime were not significantly reduced during weathering of the HREE-rich Zudong intrusion. The low dissolution rate of monazite in soil water and its resistance to weathering accounts for the typical occurrences of monazite in placer heavy minerals and REE deposits (Hutton, 1950; Jackson and Christiansen1993; Roy, 1999; Orris and Grauch, 2002; Kanazawa and Kamitani, 2006; Ravindra Kumar and Sreejith, 2010; Sengupta and Van Gosen, 2016).

Whole-rock P_2O_5 contents of fresh and weathered granite most likely play a significant role in the potential mobility of REEs during weathering. If whole-rock P_2O_5 contents are elevated, the phosphate released during weathering will likely lead to the formation of secondary phosphate minerals (e.g., rhabdophane and florencite), sequestering the REEs. These results suggest that phosphate-rich rocks, which are generally found in less differentiated granitoids (e.g., granodiorite) or strongly peraluminous granites, are not preferable for a parent rock of ion adsorption ores, but there are a few exceptions, for example the Dajishan deposits and Renju deposits are underlain by granodiorite and granite with high P_2O_5 content up to 0.29% as shown in Figure 4B (Ishihara et al., 2008). From these study results, the REE incorporation into the secondary phosphates is more likely to occur in phosphate-dominant circumstances than REE adsorption on clays during weathering.

Zircon is resistant to chemical weathering, and residual zircon crystals are commonly found in ion adsorption ores (Huang et al., 1989; Sanematsu and Kon, 2013). The common occurrence of zircon in placer sands and sediment reflects the resistance to chemical weathering (e.g., Hutton, 1950; Orris and Grauch, 2002). Lång (2000) indicated that zircon is more stable than other heavy minerals in soils, such as apatite, titanite, garnet, and epidote, in pH 4 to 5 conditions. Zircon is commonly found in a moderately to highly metamict state in granites, but its crystallinity can be preserved by annealing of the radiation damage even at relatively low temperatures (Ewing, 1994; Ewing et al., 2003). Nevertheless, the common occurrence of damaged zircon is attributed to an annealing process that is slower in zircon than in monazite at low temperatures (Ewing et al., 2003). Experimental studies suggest that a dissolution rate of zircon is generally low and that the dissolution rate of metamict zircon is higher than that of crystalline zircon at low temperatures (<150°C; Tole, 1985; Ewing et al., 1981, Ewing, 1999; Balan et al., 2001; Tromans, 2006). Balan et al. (2001) studied influences of radiation damage on the chemical durability of detrital zircon. Their results indicated that moderately damaged zircons retain U, Th, and Pb, but highly-damaged zircons can release U, Th, and Pb during weathering, although REE contents were not reported. These results suggest that REE dissolution from zircon and contribution to ion adsorption ores is minor to insignificant.

Granite contains REE-bearing mineral groups expressed as (Y, REE, U, Th)-(Nb,Ta,Ti) oxides which are commonly metamict and altered (Ewing, 1975; Lumpkin and Ewing, 1995; Ercit, 2005). These REE oxides occur in small quantities in the parent granites of REE deposits (Yang et al., 1981; Huang et al., 1989), but they could be rich in HREE and Y. Huang et al. (1989) reported that abundances of fergusonite, pyrochlore, aeschynite, and gadolinite were not significantly reduced after weathering of the HREE-rich Zudong intrusion (Table 2). Also, placer deposits of fergusonite and cassiterite were mined in areas surrounding the Huashan and Guposhan granites (Institute of Geology, Chinese Academy of Sciences, 1965). Fergusonite and pyrochlore are relatively uncommon minerals in placers (Hutton, 1950; Orris and Grauch, 2002; Patyk-Kara, 2002). These results suggest that REEs may have been leached under certain conditions. For example, Ruschel et al. (2010) found that Y was leached from highly metamict fergusonite-(Y), whereas U and Th were immobile. Resistance to weathering of, or the mobility of REEs and other elements from, REE-rich oxide minerals may depend on the degree of metamictization and solution chemistry.

Mobility of REEs during weathering

Mobility and fractionation of REEs during weathering of igneous rocks are strongly dependent on which REE-bearing minerals are present and the degree of weathering (e.g., Nesbitt, 1979; Braun et al., 1990, 1993, 1998; Middleburg et al., 1988; Nesbitt and Markovics, 1997; Taunton et al., 2000; Aubert et al., 2001; Stille et al., 2009; Yusoff et al., 2013). In southern China, REY contents of ion adsorption ores can be as much as 5.4 times greater than those of the parent granites (e.g., Bao and Zhao, 2008; Yang and Xiao, 2011), with the REY enrichments in the middle to lower part of the weathering profile (Fig. 7; Huang et al., 1989; Wu et al., 1990a; Bao and Zhao, 2008). Where the surface is covered by vegetation, soil water is acidic because of the presence of dissolved atmospheric CO_2 and humic and fulvic acids that are produced by decay of organic matter. Minerals in the soil released from the weathered granites, including REE-bearing minerals, are altered and may dissolve by reactions with acidic soil water.

A schematic diagram (Fig. 7) displays REE mobility in a weathering profile and the formation of ion adsorption ore. Mobile elements in soil water, including REEs, migrate downward in the weathered granite soil profile. In this process, REEs are transported in soil water by forming aqueous complexes or as REE^{3+} ions, and they are either immobilized by adsorption or incorporation into secondary minerals or mobilized away from the weathering profile. This REE reprecipitation is caused by a pH increase resulting from the soil water-mineral interaction or mixing with a high pH ground water. Ground-water levels typically have larger fluctuations in tropical areas than in the temperate areas due to alternating dry and rainy seasons. This can cause variability in location of the REEs that are being concentrated in the weathering profile. The weathering profile can be divided into an REE-leached zone in the upper part of the profile and an REE accumulation zone with more ion-exchangeable REEs in the lower part of the profile (Wu et al., 1990a; Zhang, 1990; Bao and Zhao, 2008; Yang and Xiao, 2011; Chi et al., 2012; Sanematsu et al., 2013). During weathering, because Ce is rarely scavenged from the leached zone, fractionation occurs between Ce and other REEs. In addition, the LREEs and HREEs(+Y) can fractionate during weathering and precipitation of secondary minerals.

The fractionation between Ce and other REEs is commonly recognized in weathering profiles and some studies have reported positive Ce anomalies in weathered granitic rocks (e.g., Banfield and Eggleton, 1989; Huang et al., 1989; Mongelli, 1993) and laterite formed on syenite (e.g., Braun et al., 1990, 1993, 1998; Braun and Pagel, 1994; Marker and de Oliveira, 1994; Berger et al., 2014). The positive Ce anomaly results from oxidization of Ce^{3+} to Ce^{4+} to form CeO_2, with

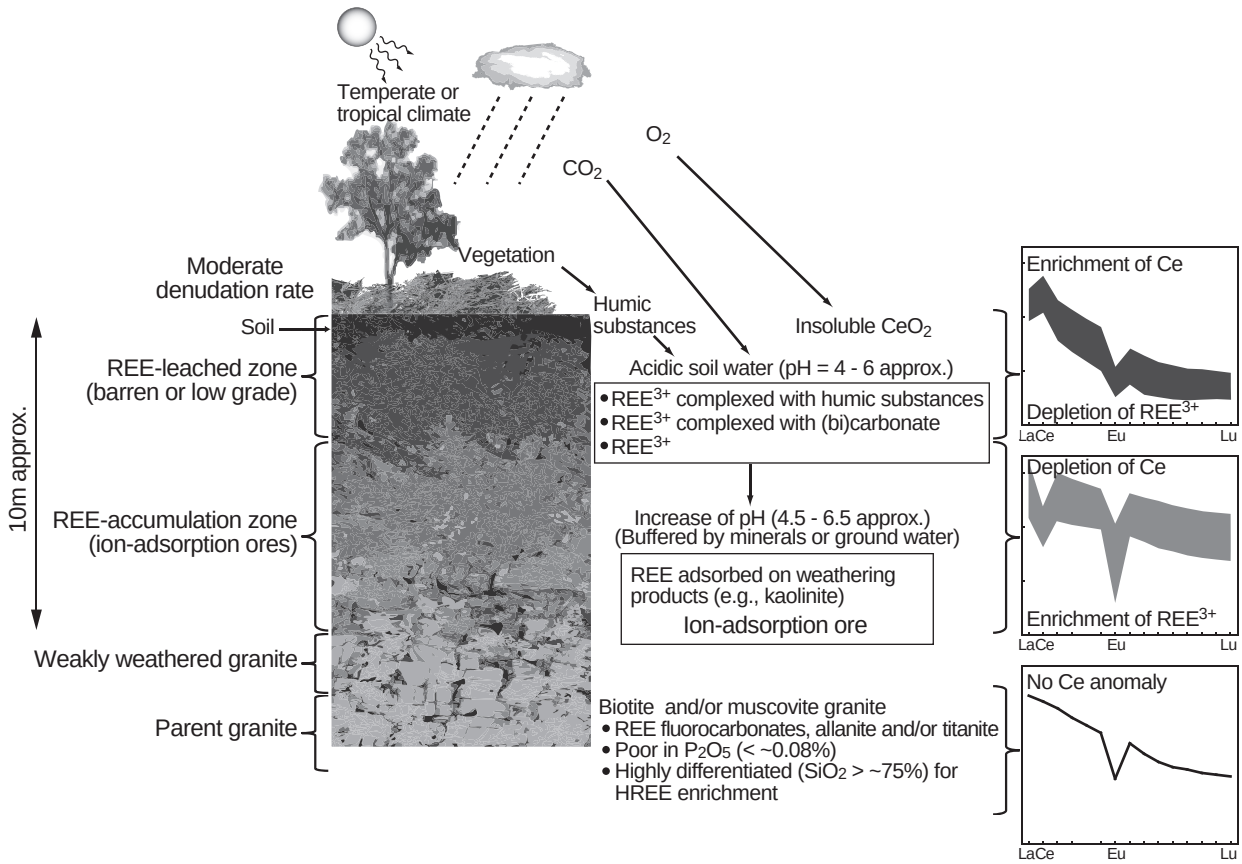

Fig. 7. Schematic model of the genesis of ion adsorption-type REE ores developed on granites. Columnar diagram represents a typical weathering profile hosting the REE ores. Graphs show the typical examples of chondrite-normalized REE patterns of the REE leached zone, REE accumulation zone (ion adsorption ores), and parent granite. See the body text for details.

Ce^{4+} being less soluble than the other REE^{3+} ions at 25°C under atmospheric pressure (Brookins, 1988). As a result, the accumulation zone lower in the weathering profile is enriched in REEs but is depleted in Ce. This migration and fractionation of REEs leads to the relative negative Ce anomaly in the accumulation zone and the corresponding ion adsorption ores (e.g., Wu et al., 1990a; Chi et al., 2005; Bao and Zhao, 2008; Sanematsu et al., 2013). Aggregates of fine-grained CeO_2 commonly occur with feldspars, clays, and Mn oxides in weathered granite, particularly in the REE-leached zone (Fig. 6F). In some ion adsorption ores in southern China, Fe-Mn oxides occur within the clay zones and are enriched in REEs. Wu et al. (1993a) described two examples, with REY = 2,645 and 13,707 ppm and positive Ce anomalies, but their PERs are only 27 and 4.4%, respectively. Significant Ce enrichment in Mn oxides is caused by oxidization of Ce^{3+} to Ce^{4+} during adsorption by δ-MnO_2 (De Carlo et al., 1998; Ohta and Kawabe, 2001). With increasing solution pH from 4.8 to 6.8, Mn oxides preferentially adsorb LREEs relative to HREEs (Ohta and Kawabe, 2001). Figure 6F illustrates cerianite and Ce-bearing Mn oxyhydroxide in the ion adsorption ore, and these minerals are consistent with a positive Ce anomaly ($Ce/Ce^* = 2.2$) of the parent granite (Murakami and Ishihara, 2008).

Thermodynamic studies and analyses of natural waters suggest that REEs are primarily complexed with carbonate and bicarbonate ions in soil water or ground water at circum-neutral pH (5–9), and that the predominant ligand is dependent on pH and the concentration of the species. Experimental and theoretical studies suggest that REEs dissolve in solution at room temperature by forming the carbonate and bicarbonate complexes $REECO_3^+$ and $REEHCO_3^{2+}$, respectively, at pH values above 5; REE^{3+} ions are present at pH values below 5 to 6 (Cantrell and Byrne, 1987; Wood, 1990b; Liu and Byrne, 1998). Rare earth element fluoride complexes, such as $REEF^{2+}$ and $REEF_2^+$, may also be present, because F^- is released during weathering of REE fluorocarbonate, fluorite, and biotite. However, the (bi)carbonate complexes or REE^{3+} are more abundant than fluoride and other inorganic complexes in solutions with pH values above 6.5 at low temperature (Cantrell and Byrne, 1987; Wood, 1990b). Phosphate complexes of REE^{3+} may be significant where there are high dissolved phosphate concentrations at a pH range of 7 to 9 (Byrne et al., 1991; Lee and Byrne, 1992), although the REE carbonate complexes are predominant at the same pH range (Johannesson et al., 1996). Experimental studies suggest that the HREEs are more easily complexed by carbonate and bicarbonate than the LREEs (Cantrell and Byrne, 1987; Lee and Byrne, 1993; Pourret et al., 2007a). The stability constant of bicarbonate increases from La to Lu (Cantrell and Byrne, 1987; Lee and Byrne, 1993), suggesting HREEs should be enriched in CO_2-rich solutions.

In addition to (bi)carbonate ions, humic substances are critical for leaching and complexing REEs during granite weathering. Experimental studies by Chen et al. (2001) showed REEs were leached by 0.01 mol/L organic acids from weathered granites in Guangdong province and HREEs were selectively leached relative to LREEs by citric and acetic acids. Thermodynamic studies indicated that the amount of REEs complexed with humic acid is strongly dependent on pH (Takahashi et al., 1997, 1999; Glaus et al., 2000; Sonke and Salters, 2006; Pourret et al., 2007b), and the carboxyl site of humic acid is the main binding site of REEs (Takahashi et al., 1997; Pourret et al., 2007b). Similar to humic acid, fulvic acid is also important for complexing of REEs (Pourret et al., 2007b). Binding between REEs and humic substances becomes more stable with decreasing ionic radii from La to Lu (Takahashi et al., 1997; Sonke and Salter, 2006), and this suggests that HREEs are more strongly bound to humic substances than LREEs. Using the model calculations of World Average River Water, Tang and Johannesson (2003) and Pourret et al. (2007a, b) predicted that REEs are more likely complexed with humic substances than carbonate ions at a pH range of 5 to 8. The model calculation by Tang and Johannesson (2003) suggested that complexation of REEs with humic substances occurs when there are significantly high concentrations of dissolved organic carbon in natural water at pH values of 4.8 to 7.9. It is considered that soil water in ion adsorption-type deposits has higher concentrations of dissolving organic carbon than natural river water because river waters tend to be more dilute.

Although fractionation of LREEs from HREEs is influenced by complexing with humic substances and (bi)carbonate ions during ion adsorption ore formation, this appears to be of secondary importance when compared to the primary fractionation caused by weathering susceptibilities of initial magmatic and hydrothermal minerals (REE fluorocarbonates, allanite, titanite, etc.) as explained above. Ion adsorption ores became enriched in HREEs relative to the parent granite in Longnan because of the dissolution of HREE-rich fluorocarbonate of synchysite-(Y) (Huang et al., 1989; Wu et al., 1990a; Bao and Zhao, 2008). In contrast, ion adsorption ores became enriched in LREEs relative to the parent granite because the dominant REE minerals being leached were LREE-rich fluorocarbonates, such as at Heling (Bao and Zhao, 2008) and Phuket (Sanematsu et al., 2013).

Adsorption of REEs

As reviewed by Laveuf and Cornu (2009), REE adsorption in soils and weathered rocks is dependent on the nature of adsorption materials, and the pH and ionic strength of the soil waters. Granites decay to fine-grained weathering products which are capable of cation-exchange. Kaolinite and halloysite (kaolin group) are the main clays most likely to adsorb REEs in southern China (Yang, 1987; Wu et al., 1990a, 1993a; Bao and Zhao, 2008; Murakami and Ishihara, 2008; Chi and Tian, 2008; Chi et al., 2012) and in Thailand (Imai et al., 2013; Sanematsu et al., 2013). Kaolinite (or halloysite) has two types of cation exchange resulting from isomorphous substitution of Al^{3+} for Si^{4+} (permanent charge) and basal surface (variable charge). Ferris and Jepson (1975), and Ma and Eggleton (1999) documented that exchangeable cations of kaolinite occur mostly on the edges and on the basal surface of the mineral. In addition, the permanent negative charge from the isomorphous substitution is not very significant in exchangeable cations. Cation exchange capacity is similar for kaolinite and halloysite, but tube halloysite may have a higher capacity (Ma and Eggleton, 1999; Joussein et al., 2005). The cation exchange capacities of kaolinite and halloysite increase with decreasing particle size because of the edge and surface

effects. This is strongly dependent on the pH of the solution (Ma and Eggleton, 1999; Joussein et al., 2005).

Not only kaolin group minerals, but also other clay minerals (e.g., illite), as well as amorphous materials, are capable of exchanging REEs because they have permanent charge and/or pH-dependent surface charge (variable charge), which can be expressed as the pH of the point of zero charge. The surfaces of minerals and amorphous materials are more positively charged below their own points of zero charge, and they are more negatively charged above the points of zero charge. In general, silicate minerals have higher points of zero charge, and metal oxides have lower point of zero charges (Kosmulski, 2009, 2011). The REEs are adsorbed onto the surface of negatively charged materials because they dissolved in soil water predominantly as species with positive charge (e.g., $REECO_3^+$, $REEHCO_3^{2+}$, and REE^{3+}; Cantrell and Byrne, 1987; Wood 1990b; Liu and Byrne, 1998), and as complexes of REE humic substances which are likely to be positively charged because of the carboxyl. The point of zero charge of kaolinite is less than 3.6 (Schroth and Sposito, 1997; Kosmulski, 2009, 2011), suggesting that kaolinite is negatively charged in ion adsorption ores with low pH of 4.1 to 6.5 (Wu et al., 1990a; Wei et al., 2001; Pan, 2011; Yang and Xiao, 2011) and thus is capable of adsorbing REEs. Although halloysite lacks data for point of zero charges, it is likely to have a point of zero charge similar to kaolinite because it possesses almost the same composition and crystal structure. Experimental studies and surface complexation modeling suggest that REE^{3+} ions are likely adsorbed on the surface of silica and alumina in clays as $REE(OH)_2^+$ in acidic solutions (Kosmulski, 1997; Marmier et al., 1997, 1999; Piasecki and Sverjensky, 2008). Cation exchange capacities of 2/1 layer clays, such as illite and montmorillonite, are generally higher than those of kaolinite and halloysite (e.g., Carroll, 1959; Laveuf and Cornu, 2009) because they have both permanent and variable charges. Illite, which is also found in ion adsorption ores, may adsorb REEs because its point of zero charge is ~2.5 (Kosmulski, 2009, 2011). On the other hand, the higher point of zero charge of montmorillonite (7–9; Kosmulski, 2009, 2011) indicates that it is unlikely to adsorb REEs at its basal surface because of its positive variable charge. In summary, these point of zero charge values suggest that kaolin group minerals and/or illite are capable of adsorbing REEs in natural soil and ground water, although occurrences of illite-rich ion adsorption ores have not been reported.

Experimental studies suggest that fractionation between LREEs and HREEs is influenced by pH, ionic radii, ionic strength, and presence of humic substances, but the extent of REE fractionation during the adsorption process is difficult to constrain. Coppin et al. (2002) indicated that REEs are increasingly adsorbed on kaolinite with increasing solution pH. In their experiments, HREEs are more selectively adsorbed than LREEs at high ionic strength (I = 0.5 *M*), but this ionic strength is much greater than found in most soil and ground waters. No significant REE fractionation is recognized at lower ionic strength of I = 0.025 *M* (Coppin et al., 2002), suggesting that REE fractionation within kaolinite is minor during soil and ground-water interaction. Wan and Liu (2005) conducted experimental studies of REE adsorption onto kaolinite at low REE concentrations typical of natural solutions, and their results indicated that REEs have a greater tendency to be adsorbed at higher pH and that HREEs have a greater tendency to be adsorbed than LREEs at near-neutral pH. Wan and Liu (2006) studied the effect of humic acid on the adsorption of REEs onto the kaolin over a wide range of pH (3–10), and the results indicate that REE adsorption increases with decreasing pH, with decreasing concentration of humic acid, and with increasing ionic strength. The results also showed that LREEs have a greater tendency to be adsorbed onto kaolin than HREEs in the presence of a significant amount of humic acid, and this is attributed to stronger binding between humic acid and HREEs with smaller ionic radii by lanthanide contraction (Takahashi et al., 1997; Sonke and Salter, 2006).

Preservation of orebodies

Chemical weathering is preferentially promoted by temperate and tropical climatic conditions because the chemical weathering rate increases with the increase in annual precipitation and temperature (White and Blum, 1995; Oliva et al., 2004; Gislason et al., 2009; Viers et al., 2014). A comparison between southern China (temperate) and Southeast Asia (mostly tropical) suggests that a temperate climate appears to be more favorable for preservation of ion adsorption-type REE deposits than a tropical climate. Kaolin-bearing weathering profiles are commonly developed on Late Permian-Early Jurassic and Cretaceous ilmenite-series granites in Southeast Asia (Cobbing et al., 1992; Khin Zaw et al., 2014). However, weathered granites with high PERs were found only in limited localities (Sanematsu et al., 2009, 2013, 2015; Imai et al., 2013). The lower PERs may be attributed to desorption of ion-exchangeable REY and this may be the result of seasonal fluctuations in ground-water level. Further research is required to quantitatively evaluate ion-exchangeable REY concentrations of weathered granite in different climatic settings.

Not only chemical weathering, but also low amounts of mechanical erosion are required to preserve ion adsorption orebodies. The weathering profile of the Zudong muscovite granite, which hosts the Longnan deposits, has a thin REE-leached zone with a positive Ce anomaly to depths of only 0.7 m and a thick REE accumulation zone, which represents the ion adsorption orebody, with a negative Ce anomaly from 0.7 to 19 m (Wu et al., 1990a; Fig. 5A). Above the Heiling, Guposhan, and Huashan deposits, the REE-leached zone with a positive Ce anomaly is equally thin (Bao and Zhao, 2008). Such a thin REE-leached zone suggests that most of the zone was eroded after providing REEs to the lower part of the weathering profiles in the Nanling Range and is consistent with a low to moderate erosion rate where part of the section is removed but the lower ore zone remains. In the eastern part of the range, including southern Jiangxi province, graben basins were formed by crustal thinning (Wang and Shu, 2012), and this may have kept the erosion rate low, thus preserving the ion adsorption orebodies at deposits such as Longnan and Heling.

Limited data are available on the topographic relief of the REE deposit areas and thickness of weathering profiles. However, climate and elevation of granite terranes appear to have important roles for preservation of the orebodies because they are closely related to denudation (erosion) of weathered

rocks (Einsele, 2000). The low to moderate denudation rate in southern China is favorable for the formation and preservation of weathering profiles and their included ion adsorption orebodies. The ion adsorption-type deposits in southern China are located in areas of low hills (Bao and Zhao, 2008), mainly below an elevation of 550 m (Zhang, 1990). Wang et al. (2013) summarized the elevation ranges for the ores as being mostly from 160 to 400 m, with some exceptions in the higher hills at the Dingnan (Wang et al., 2013), Guposhan (Li and Shen, 2013), and Long'an deposits (Table 1). Denudation rates for low hills are lower than those of high mountains (Milliman and Syvitski, 1992; Einsele, 2000), and this likely helps to preserve thick weathering profiles of ion adsorption ores in southern China. Because the denudation rate is controlled by both weathering and transport rates of weathered materials, thick weathering profiles can be preserved where more weathered material can be produced than can be removed by transport processes (Einsele, 2000). The largest amount of material removal will correlate with the highest rainfall, surface runoff, and river flow (Einsele, 2000), and thus thick weathering profiles are likely to be developed in areas with moderate rainfall where transport is limited and chemical weathering is promoted. Southern China is characterized by a temperate climate (Fig. 1), with an annual temperature of 18° to 21°C and annual precipitation averaging 1,500 to 2,000 mm (Wang et al., 2013). Denudation rates may basically be defined by annual suspended sediment load discharge volumes (Milliman and Meade, 1983; Einsele, 2000). Milliman and Meade (1983) reported an annual sediment discharge of 100 to 500 t/km^2/yr in southern China and northern Vietnam with temperate climates, but substantially greater values of 500 to 1,000 t/km^2/yr in the mainland of Southeast Asia, with a tropical climate and in Madagascar with a temperate climate. The tropical climate and high erosion rate in Southeast Asia is consistent with the weathering profiles only ranging from typically <1 to 10 m in thickness, which is much thinner than the weathering profiles containing ion adsorption-type deposits in southern China.

Implications for Exploration

Ion adsorption-type REE deposits are formed by the following processes: (1) the emplacement of a biotite or muscovite granite with REE source minerals such as REE fluorocarbonates, allanite, and titanite; (2) development of thick weathering profiles and adsorption of REEs to form the orebodies; and (3) preservation of the orebodies as illustrated in Figure 7. Ilmenite-series granite terranes exposed as low hills in areas of temperate or tropical climate with low to moderate erosion rates are likely to meet these conditions. Alkali granites could be good source rocks for REE-rich deposits, as for example, the Heling granite porphyry, but they are generally rich in LREEs. Low P_2O_5 content is preferable for high recovery of REEs in the ion-exchange process because REEs are incorporated in secondary phosphate minerals during weathering (Sanematsu et al., 2015). Immobilization of REEs into secondary phosphates limits the amount of REEs available to be adsorbed onto clays. For economic deposits of HREEs, highly differentiated muscovite granite is essential and high SiO_2 content (>~75%) of such an intrusion is a good indicator for exploration, although these granites are not necessarily all rich in HREEs. Because the fine-grained REE source minerals are difficult to identify in highly differentiated granites, the occurrence of fine-grained fluorite may be a useful indicator of the alteration of magmatic REE-bearing minerals and the occurrence of hydrothermal minerals including REE fluorocarbonates.

Laterite, which is strongly weathered, Fe_2O_3-Al_2O_3 enriched, SiO_2 depleted, and formed under tropical and subtropical climates, can be enriched in REEs from the weathering of parent rocks. Lateritic REE deposits are typically underlain by carbonatites not granites, and the REEs are mainly contained in secondary phosphates, not adsorbed onto clays. One of the most significant lateritic REE deposits is Mount Weld in Australia, where laterite is developed from weathering of a Proterozoic carbonatite. This deposit consists of high-grade lateritic ores, with the majority of the REEs present in secondary phosphates and aluminophosphates (Lottermoser, 1990; Verplanck et al., 2016). For another example, Sanematsu et al. (2011) studied ion-exchangeable REEs and REE-bearing minerals in laterite derived from alkali basalt in Laos. They reported that REEs migrated significantly during weathering, but PERs are very low (1–2%), because REEs are incorporated in crandallite group minerals, including florencite-(Ce).

Negative Ce anomalies in a weathering profile underlain by granite is a helpful indicator to target favorable areas for ion adsorption ores during geochemical exploration surveys (Wu et al., 1990a; Sanematsu et al., 2013). Previous studies have indicated that typical ion adsorption ores have negative Ce anomalies, whereas low-grade ion adsorption occurrences that are commonly uneconomic and overburden have positive Ce anomalies (e.g., Yang et al., 1981; Wu et al., 1990a; Bao and Zhao, 2008; Sanematsu et al., 2009, 2013, 2015). Sanematsu et al. (2013) conducted a sequential leaching test on ion adsorption ores from Phuket, Thailand, and documented the positive correlation between negative Ce anomalies and PERs. They found strongly negative Ce anomalies in an ion-exchangeable fraction, strongly positive Ce anomalies in a leachate fraction of Mn and Fe oxides, and little or small positive Ce anomalies in a leachate fraction of organic matter. The REE concentrations are greatest in the ion-exchangeable fraction because the majority of the REEs (>~50%) are ion-exchangeable in the ion adsorption ores such that the whole-rock REE patterns of the ion adsorption ores commonly show negative Ce anomalies.

Negative Ce anomalies have a positive correlation with PERs or with concentrations of ion-exchangeable REEs in weathering profiles underlain by granites, such as occurrences in the northern and western parts of Thailand and in Dingnan County in southern China (Fig. 8; Sanematsu et al., 2013, 2015; Sanematsu and Kon, 2013; Sanematsu, unpub. data). The positive correlation between negative Ce anomalies and PERs (Fig. 8A) results from weathering processes described previously: the dissolution of REE-bearing mineral phases in the parent granite, the downward movement of ground and soil waters, and the removal of a substantial fraction of the REEs (except Ce) by adsorption onto clays. Because of redox processes, Ce behaves differently and is removed from solution into a nonexchangeable fraction (mineral phase) in oxidizing conditions. The cause of the positive correlation between negative Ce anomalies and concentrations of

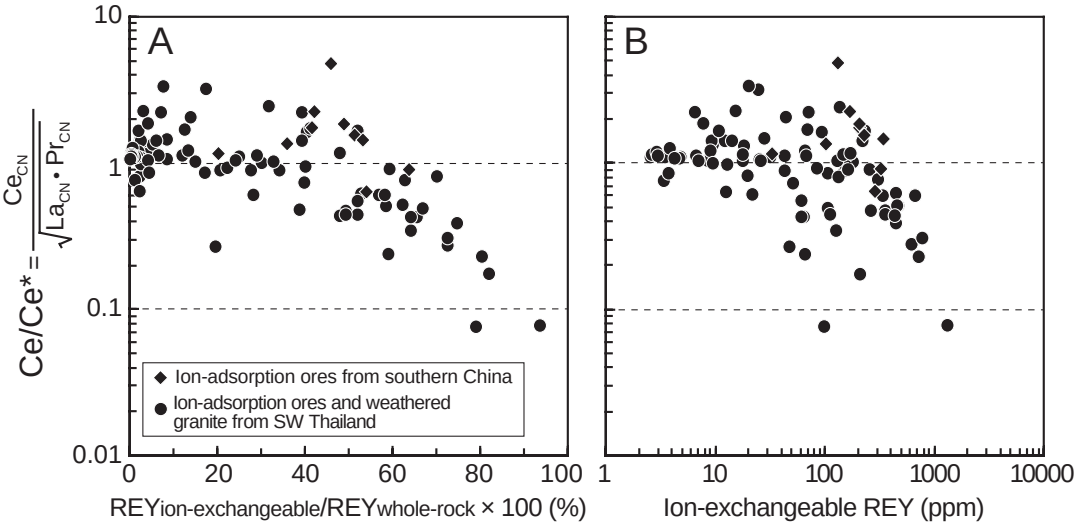

Fig. 8. A. Plots of Ce anomalies vs. PERs (percentages of ion-exchangeable REY relative to whole-rock REY). B. Plots of Ce anomalies vs. concentrations of ion-exchangeable REY. Samples consist of ion adsorption ores from Dingnan County of southern China (Murakami and Ishihara, 2008; Sanematsu and Kon, 2013) and from Thailand (Imai et al., 2013; Sanematsu et al., 2013, 2015; Sanematsu, unpub. data). Ion-exchangeable REY were extracted by reacting with 0.5 mol/L ammonium sulfate solution for 24 hr (Sanematsu and Kon, 2013).

ion-exchangeable REY is relatively unclear (Fig. 8B) but likely due to the variability in REE concentrations and host minerals in the parent granites.

Conclusions

Ion adsorption-type REE deposits are located primarily in the area underlain by the Jurassic-Cretaceous Yanshanian granites in the Nanling Range, southern China. The granite magmatism resulted from subduction of the Pacific Plate and extensional intraplate tectonics. The parent granites for the REE deposits are generally composed of biotite and muscovite granite characterized by metaluminous to weakly peraluminous (ASI <~1.1) compositions and low P_2O_5 contents (<~0.08%). The HREE-rich granites are confined to highly differentiated (SiO_2 >~75%) muscovite granite, which contain fluorite and hydrothermal REE minerals formed during deuteric alteration. These characteristics of the favorable source granites probably characterize other granites outside of southern China that could weather to form ion adsorption ores.

The most favorable REE source minerals for formation of ion adsorption ores are REE fluorocarbonates, such as synchysite and bastnäsite, because they release REE^{3+} during weathering and dissolve in low-pH soil water. Allanite and titanite, which occur in magmatic monazite-free granite (typically ASI <~1.1), are the dominant sources of LREEs and HREEs, respectively. These silicates are replaced by alteration minerals, such as REE fluorocarbonates if fluorine-dominant hydrothermal fluids are present, or interact with downward-moving soil water. In contrast, monazite and xenotime are strongly resistant to chemical weathering because of their less metamict state and low solubility in the soil water. Because apatite is altered and replaced by secondary phosphates, including rhabdophane and florencite, an abundance of phosphates is not a favorable scenario for formation of ion adsorption-type deposits.

During weathering, REE-bearing minerals in parent granites are decomposed by acidic soil water and the REEs migrate downward in the weathering profile. The REEs are immobilized by adsorption or incorporation into secondary minerals due to pH increase, which results from the interaction of the soil water with various minerals or higher pH ground water. The weathering profile of the deposits can be divided into a REE-leached zone in the upper part of the profile and a REE accumulation zone in the lower part of the profile. The REE-leached zone displays a positive Ce anomaly due to the immobile nature of CeO_2, which formed from oxidation of Ce^{3+} to Ce^{4+}. In contrast, the accumulation zone, corresponding to the ion adsorption ores, exhibits a negative Ce anomaly because the other REE^{3+} are preferentially adsorbed onto clays and weathering products. As a result, the negative Ce anomaly of ion adsorption ores has a positive correlation with the ion-exchangeable REY, and this anomaly is a useful indicator in geochemical exploration.

Many studies suggest that REEs are transported in complexes with humic substances and (bi)carbonate ions or as REE^{3+} ions in soil and ground water at circum-neutral pH ($5 \leq pH \leq 9$). The predominant ligand is dependent on pH and concentration of the species. The REEs are most likely to adsorb onto the surface of kaolinite and halloysite in ion adsorption ores because of their points of zero charge and the abundances of these clays in weathered granites.

The fractionation between LREEs and HREEs in ion adsorption ores is constrained by the weathering susceptibilities and relative abundances of REE-bearing minerals in parent granites, that is, HREE-rich ion adsorption ores are derived from HREE-rich granites. Additionally, fractionation may occur during weathering by the formation of secondary minerals, including REE-bearing phosphates, Fe-Mn oxides, and cerianite, which preferentially scavenge LREEs from soil water.

A temperate or tropical climate, a moderate denudation rate, and a setting of low relief hills are preferable conditions for both

chemical weathering of granite and preservation of thick weathering profiles that may host ion adsorption orebodies. However, the tropical climate may lead to accelerated denudation rates of the weathering profiles or desorption of ion-exchangeable REEs due to seasonal fluctuations of ground-water level.

Acknowledgments

We thank Shunso Ishihara, Akira Imai, and Khin Zaw for helpful advice and for supporting sample collection. Thanks also to an anonymous reviewer, Chengyu Wu, Philip L. Verplanck, and Richard Goldfarb for constructive comments on our earlier manuscript. A part of SEM-EDS work was helped by Karsten Goemann and Sandrin Feig at the Central Science Laboratory in University of Tasmania. This study was financially supported by the JSPS Grant-in-Aid for Scientific Research (A) of 19253005, JSPS Grant-in-Aid for Young Scientists (B) of 23760796, JSPS Postdoctoral Fellowships for Research Abroad, Japan Mining Promotive Foundation and CODES ARC Centre of Excellence in Ore Deposits (CODES), University of Tasmania.

REFERENCES

Aide, M.T., and Aide, C., 2012, Rare earth elements: Their importance in understanding soil genesis: International Scholarly Research Network, ISRN Soil Science 2012, Article ID 783876, 11 p.

Aubert, D., Stille, P., and Probst, A., 2001, REE fractionation during granite weathering and removal by waters and suspended loads: Sr and Nd isotopic evidence: Geochimica et Cosmochimica Acta, v. 65, p. 387–406.

Balan, E., Neuville, D.R., Trocellier, P., Fritsch, E., Muller, J.P., and Calas, G., 2001, Metamictization and chemical durability of detrital zircon: American Mineralogist, v. 86, p. 1025–1033.

Banfield, J.F., and Eggleton, R.A., 1989, Apatite replacement and rare earth mobolization, fractionation, and fixation during weathering: Clays and Clay Minerals, v. 37, p. 113–127.

Bao, Z., and Zhao, Z., 2008, Geochemistry of mineralization with exchangeable REY in the weathering crusts of granitic rocks in South China: Ore Geology Review, v. 33, p. 519–535.

Bau, M., 1996, Controls on the fractionation of isovalent trace elements in magmatic and aqueous systems: evidence from Y/Ho, Zr/Hf and lanthanide tetrad effect: Contributions of Mineralogy and Petrology, v. 123, p. 323–333.

Bau, M., and Dulski, P., 1995, Comparative study of yttrium and rare-earth element behaviours in fluorine-rich hydrothermal fluids: Contributions of Mineralogy and Petrology, v. 119, p. 213–223.

Bea, F., 1996, Residence of REE, Y, Th and U in granites and crustal protoliths: Implication for the chemistry of crustal melts: Journal of Petrology, v. 37, p. 521–552.

Bea, F., Fershtater, G., and Corretgé, L.G., 1992, The geochemistry of phosphorus in granite rocks and the effect of aluminium: Lithos, v. 29, p. 43–56.

Belousova, E.A., Griffin, W.L., O'Reilly, S.Y., and Fisher, N.I., 2002, Apatite as an indicator mineral for mineral exploration: trace-element compositions and their relationship to host rock type: Journal of Geochemical Exploration, v. 76, p. 45–69.

Berger, A., Gnos, E., Janots, E., Fernandez, A., and Giese, J., 2008, Formation and composition of rhabdophane, bastnäsite and hydrated thorium minerals during alteration: Implications for geochronology and low-temperature processes: Chemical Geology, v. 254, p. 238–248.

Berger, A., Janots, E., Gnos, E., Frei, R., and Bernier, F., 2014, Rare earth element mineralogy and geochemistry in a laterite profile from Madagascar: Applied Geochemistry, v. 41, p. 218–228.

Boatner, L.A., and Sales, B.C., 1988, Monazite, *in* Lutze, W. and Ewing, R.C., eds., Radioactive waste forms for the future, North Holland, New York, p. 495–564.

Braun, J.J., and Pagel, M., 1994, Geochemical and mineralogical behavior of REE, Th and U in the Akongo lateritic profile (SW Cameroon): Catena, v. 21, p. 173–177.

Braun, J.J., Pagel, M., Muller, J.P., Bilong, P., Michard, A., and Guillet, B., 1990, Cerium anoamalies in lateritic profiles: Geochimica et Cosmochimica Acta, v. 54, p. 781–795.

Braun, J.J., Pagel, M., Herbillon, A., and Rosin, C., 1993, Mobilization and redistribution of REEs and thorium in a syenitic lateritic profile: a mass balance study: Geochimica et Cosmochimica Acta, v. 57, p. 4419–4434.

Braun, J.J., Viers, J., Dupré, B., Polve, M., Ndam, J., and Muller, J.P., 1998, Solid/liquid REE fractionation in the lateritic system of Goyoum, East Cameroon: The implication for the present dynamics of the soil covers of the humid tropical regions: Geochimica et Cosmochimica Acta, v. 62, p. 273–299.

British Geological Survey, 2011, Rare Earth Elements Mineral Profile, British Geological Survey, Nottingham, United Kingdom: http://www.bgs.ac.uk/mineralsuk/search/home.html

Brookins, D.G., 1988, Eh-pH Diagrams for Geochemistry, Springer-Verlag, New York, 176 p.

Broska, I., Williams, C.T., Uher, P., Konečný, P., and Leichmann, J., 2004, The geochemistry of phosphorus in different granite suites of the Western Carpathians, Slovakia: the role of apatite and P-bearing feldspar: Chemical Geology, v. 205, p. 1–15.

Byrne, R.H., Lee, J.H., and Bingler, L.S., 1991, Rare earth element complexation by PO_4^{3-} ions in aqueous solution: Geochimica et Cosmochimica Acta, v. 55, p. 2729–2735.

Cantrell, K.J., and Byrne, R.H., 1987, Rare earth element complexation by carbonate and oxalate ions: Geochimica et Cosmochimica Acta, v. 51, p. 597–605.

Carroll, D., 1959, Ion exchange in clays and other minerals: Geological Society of America Bulletin, v. 70, p. 749–780.

Caruso, L., and Simmons, G., 1985, Uranium and microcracks in a 1,000-meter core, Redstone, New Hampshire: Contributions to Mineralogy and Petrology, v. 90, p. 1–17.

Castor, S.B., 2008, Rare earth deposits of North America: Resource Geology, v. 58, p. 337–347.

Castor, S.B., and Hedrick, J.B., 2006, Rare earth elements. Industrial Minerals Volume, 7th edition: Society for Mining, Metallurgy, and Exploration, Littleton, Colorado, p. 769–792.

CCOP (Coordinating Committee for Geoscience Programmes in East and Southeast Asia), 2012, Member Country Report of Vietnam: 48th CCOP Annual Session 4–8 November 2012, Langkawi, Malaysia, CCOP-48AS/3-16, p. 1–18.

Cetiner, Z.S., Wood, S.A., and Gammons, C.H., 2005, The aqueous geochemistry of the rare earth elements. Part XIV. The solubility of rare earth element phosphates from 23 to 150°C: Chemical Geology, v. 217, p. 147–169.

Chaïrat C., Schott J., Oelkers E.H., Lartigue J.-E., and Harouiya N., 2007, Kinetics and mechanism of natural fluorapatite dissolution at 25°C and pH from 3 to 12: Geochimica et Cosmochimica Acta., v. 71, p. 5901–5912.

Chakhmouradian, A.R., and Zaitsev, A.N., 2012, Rare earth mineralization in igneous rocks: Sources and processes: Elements, v. 8, p. 347–353.

Chappell, B.W., 1999, Aluminium saturation in I- and S-type granites and the characterization of fractionated haplogranites: Lithos, v. 46, p. 535–551.

Chappell, B.W., and White, A.J.R., 1974, Two contrasting granite types: Pacific Geology, v. 8, p. 173–174.

Chen, B.H., Wu, F.H., and Liu, F.F., 2001, Experimental study on the effects of organic acids on the dissolution of REE in the weathering crust of granite: Chinese Journal of Geochemistry, v. 20, p. 144–151.

Chen, B.H., and Yu S.J., 1994, The geological and geochemical characteristics of Late Yanshanian granites in Renju-Huangshe area, Pingyuan Guangdong: Journal of Zhongshan University, v. 33, p. 130–133 (in Chinese with English abstract).

Chen, D., 1996, The discovery history of mineral deposits of Jiangxi Province, China: Geological Publishing House, Beijing, 245 p. (in Chinese with English summary).

Chen, R.G., 2013, Characteristics and regularity analysis of the Chengnan rare earth ores in Ninghua County, Fujian Province: Journal of Yangtze University (Natural Science Edition), v. 10, p. 65–67 (in Chinese).

Chi, R.A., and Tian, J., 2008, Weathered crust elution-deposited rare earth ores: New York, Nova Science Publishers, 288 p.

Chi, R.A., Tian, J., Li, Z.J., Peng, C., Wu, Y.X., Li, S.R., Wang, C.W., and Zhou, Z.A., 2005, Existing state and partitioning of rare earth on weathered ores: Journal of Rare Earths, v. 23, p. 756–759.

Chi, R.A., Tian, J., Luo, X.P., Xu, Z.G., and He, Z.Y., 2012, The basic research on the weathered crust elution-deposited rare earths ores: Nonferrous Metals Science and Engineering, v. 3, p. 1–14 (in Chinese with English abstract).

Cobbing, E.J., Pitfield, P.E.J., Darbyshire, D.P.E., and Mallick, D.J.J., 1992, The Granites of the South-East Asian tin belt: Overseas Memoir 10. British Geological Survey, London, 369 p.

Condie, K.C., Dengate, J., and Cullers, R., 1995, Behavior of rare earth elements in a paleoweathering profile on granodiorite in the Front Range, Colorado, USA: Geochimica et Cosmochimica Acta, v. 59, p. 279–294.

Coppin, F., Berger, G., Bauer, A., Castet, S., and Loubet, M., 2002, Sorption of lanthanides on smectite and kaolinite: Chemical Geology, v. 182, p. 57–68.

Cuney, M., and Mathieu, R., 2000, Extreme light rare earth element mobilization by diagenetic fluids in the geological environment of the Oklo natural reactor zones, Franceville basin, Gabon: Geology, v. 28, p. 743–746.

De Carlo, E.H., Wen, X.Y., and Irving, M., 1998, The influence of redox reactions on the uptake of dissolved Ce by suspended Fe and Mn oxide particles: Aquatic Geochemistry, v. 3, p. 357–389.

Deer, W.A., Howie, R.A., and Zussman, J., 1982, Rock-Forming Minerals. Volume 1A Orthosilicates, Longman, London and New York, p. 444–465.

Deng, J., 2013, Geological characteristics and metallogenic conditions of the Xiache REE deposits in Heping County, Guangdong Province, Earth, v. 5, p. 5 (in Chinese).

Deng, Z.C., 1988, Characteristics and genesis of the Datian HREE granite, southern Jiangxi: Journal of Guilin College of Geology, v. 8, p. 39–48 (in Chinese with English abstract).

Ding, J.Y., 2012, Historical review of the ionic rare earth mining: In honor of the 60 anniversary of GNMRI: Nonferrous Metals Science and Engineering, v. 3, p. 14–19 (in Chinese with English abstract).

Du, X., Rate, A.W., and Gee, M.A.M., 2012, Redistribution and mobilization of titanium, zirconium and thorium in an intensely weathered lateritic profile in Western Australia: Chemical Geology, v. 330–331, p. 101–115.

Einsele, G., 2000, Sedimentary Basins: Evolution, Facies, and Sediment Budget. Second, completely revised and enlarged edition. Springer, Berlin, Heidelberg, New York, London, Paris, Tokyo, Hong Kong, 792 p.

Ercit, T.S., 2005, Identification and alteration trends of granitic-pegmatite-hosted (Y,REE,U,Th)-(Nb,Ta,Ti) oxide minerals: A statistical approach: The Canadian Mineralogist, v. 43, p. 1291–1303.

Ewing, R.C., 1975, Alteration of metamict, rare-earth, AB_2O_6-type Nb–Ta–Ti oxides: Geochimica Cosmochimica et Acta, v. 39, p. 521–530.

——1994, The metamict state: 1993–the centennial: Nuclear Instruments and Methods in Physics Research, B91, p. 22–29.

——1999, Nuclear waste forms for actinides: Proceedings of the National Academy of Sciences, v. 96, p. 3432–3439.

Ewing, R.C., and Haaker, R.F., 1980, The metamict state: Implications for radiation damage in crystalline waste forms: Nuclear and Chemical Waste Management, v. 1, p. 51–57.

Ewing, R.C., Haaker, R.F., and Lutze, W., 1981, Leachability of zircon as a function of alpha dose: MRS Proceedings, v. 11, p. 389.

Ewing, R.C., Meldrum, A., Wang, L., Weber, W.J., and Corrales, L.R., 2003, Radiation effects in zircon, *in* Hanchar, J.M., and Hoskin, P.W.O., eds., Zircon: Reviews in Mineralogy and Geochemistry, Mineralogical Society of America, v. 53, p. 387–425.

Feng, Z.H., Wang, C.Z., Zhang, M.H., and Liang, J.C., 2012, Unusually dumbbell-shaped Guposhan-Huashan twin granite plutons in Nanling Range of south China: Discussion on their incremental emplacement and growth mechanism: Journal of Asian Earth Sciences, v. 48, p. 9–23.

Ferris, A.P., and Jepson, W.B., 1975, The exchange capacities of kaolinite and the preparation of homoionic clays: Journal of Colloid Interface Science, v. 51, p. 245–259.

Förster, H.J., 2001, Synchysite-(Y)–synchysite-(Ce) solid solutions from Markersbach, Erzgebirge, Germany: REE and Th mobility during high-T alteration of highly fractionated aluminous A-type granites: Mineralogy and Petrology, v. 72, p. 259–280.

Ganzeev, A.A., and Grechishchev, O.K., 2003, A new genetic type of rare-metal alkali granites of Madagascar: Geologiya i Geofizika, v. 44, p. 539–553.

Garson, M.S., and Walshaw, R.D., 1969, The geology of the Mlanje area: Bulletin of the Geological Survey of Malawi, v. 21, p. 1–157.

Gieré, R., 1996, Formation of Rare Earth Minerals in Hydrothermal Systems. *in* Rare Earth Minerals: Chemistry, Origin and Ore Deposits. Jones, A.P., Williams, C.T., Wall, F., eds.: Mineralogical Society Series, Chapman & Hall, 7, p 105–150.

Gieré, R., and Sorensen, S.S., 2004, Allanite and other REE-rich epidote-group minerals: Reviews in Mineralogy and Geochemistry, v. 56, p. 431–493.

Gislason, S. R., Oelkers, E. H., Eiriksdottir, E. S., Kardjilov, M. I., Gisladottir, G., Sigfusson, B., Snorrason, A., Elefsen, S., Hardardottir, J., Torssander, P., and Oskarsson, N., 2009, Direct evidence of the feedback between climate and weathering: Earth and Planetary Science Letters, v. 277, p. 213–222.

Glaus, M.A., Hummel, W., and Van Loon, L.R., 2000, Trace metal-humate interactions. I. Experimental determination of conditional stability constants: Applied Geochemistry, v. 15, p. 953–973.

Green, T.H., and Pearson, N.J., 1986, Rare earth element partitioning between sphene and coexisting silicate liquid at high pressure and temperature: Chemical Geology, v. 55, p. 105–119.

Gromet, L.P., and Silver, L.T., 1983, Rare earth element distributions among minerals in a granodiorite and their petrogenetic implications: Geochimica et Cosmochimica Acta, v. 47, p. 925–939.

Gu, S.Y., Hua, R.M., and Qi, H.W., 2006, Geochemistry and petrogenesis of the Yanshanian Huashan-Guposhan granites in Guanxi: Acta Petrogica et Mineralogica, v. 25, p. 97–109 (in Chinese with English abstract).

Guidry, M.W., and MacKenzie, F.T., 2003, Experimental study of igneous and sedimentary apatite dissolution: Control of pH, distance from equilibrium, and temperature on dissolution rates: Geochimica et Cosmochimica Acta, v. 67, p. 2949–2963.

Guo, C.L., Chen, Y.C., Zeng, Z.L., and Lou, F.S., 2012, Petrogenesis of the Xihuashan granites in southeastern China: Constraints from geochemistry and in-situ analyses of zircon U-Pb-Hf-O isotopes: Lithos, v. 148, p. 209–227.

Haas, J.R., Shock, E.L., and Sassani, D.C., 1995, Rare earth elements in hydrothermal systems: estimates of standard partial molal thermodynamic properties of aqueous complexes of the rare earth elements at high pressure and temperatures: Geochimica et Cosmochimca Acta, v. 59, p. 4329–4350.

Harouiya, N., Chaïrat, C., Köhler, S.J., Gout, R., and Oelkers, E.H., 2007, The dissolution kinetics and apparent solubility of natural apatite in closed reactors at temperatures from 5 to 50 °C and pH from 1 to 6: Chemical Geology, v. 244, p. 554–568.

Harlavan, Y., and Erel, Y., 2002, The release of Pb and REE from granitoids by the dissolution of accessory phases: Geochimica et Cosmochimica Acta, v. 66, p. 837–848.

Harrison, T.M., and Watson, E.B., 1984, The behaviour of apatite during crustal anatexis: equilibrium and kinetic considerations: Geochimica et Cosmochimica Acta, v. 48, p. 1468–1477.

Hoskin, P.W., and Schaltegger, U., 2003, The composition of zircon and igneous and metamorphic petrogenesis: Reviews in mineralogy and geochemistry, v. 53, p. 27–62.

Hsieh, P.S., Chen, C.-H., Yang, H.J., and Lee C.Y., 2008, Petrogenesis of the Naling Muntains granites from South China: Constraints from systematic apatite geochemistry and whole-rock geochemical and Sr-Nd isotope compositions: Journal of Asian Earth Science, v. 33, p. 428–451.

Hua, R.M., Zhang, W.L., Gu, S.Y., and Chen, P.R., 2007, Comparison between REE granite and W–Sn granite in the Nanling region, South China, and their mineralizations: Acta Petrologica Sinica, v. 23, p. 2321–2328 (in Chinese with English abstract).

Huang, D.H., Wu, C.G., and Han, J.Z., 1989, REE geochemistry and mineralization characteristics of the Zudong and Guanxi Granites, Jiangxi Province: Acta Geologica Sinica, v. 2, p. 139–157.

Huang, W.H., 1989, Geochemical characteristics of the Laishi REE deposits in Xinfeng County, Guangdong Province: Geology of Nonferrous Metals of Guangdong Province, v. 2, p. 26–37 (in Chinese).

Huo, M.Y., 1992, Distribution characteristics of the weathering-crust-type rare-earth resources in Nanling, China: Journal of Natural Resources, v. 7, p. 64–70 (in Chinese with English abstract).

Hurley, P.M., and Fairbairn, H.W., 1953, Radiation damage in zircon, a possible age method: Bulletin of Geological Society of America, v. 64, p. 659–674.

Hutton, C.O., 1950, Studies of heavy detrital minerals: Bulletin of Geological Society of America, v. 61, p. 635–716.

Imai, A., Yonezu, K., Sanematsu, K., Ikuno, T., Ishida, S, Watanabe, K., Pisutha-Arnond, V., Nakapadungrat, S., and Boosayasak, J., 2013, Rare earth elements in hydrothermally altered granitic rocks in the Ranong and Takua Pa tin-field, southern Thailand: Resource Geology, v. 63, p. 84–98.

Institute of Geology, Chinese Academy of Sciences, 1965, Study on Minerals From Fuchuan-Hexian-Zhongshan Area. Science Press, Beijing. 101 p. (in Chinese).

Ishihara, S., 1977, The magnetite-series and ilmenite-series granitoids: Mining Geology, v. 27, p. 293–305.

Ishihara, S., and Murakami, H., 2006, Fractionated ilmenite-series granites in Southwest Japan: Source magma for REE-Sn-W mineralizations: Resource Geology, v. 56, p. 245–256.

Ishihara, S., Renmin, H., Hoshino, M., and Murakami, H., 2008, REE abundance and REE minerals in granitic rocks in the Nanling Range, Jiangxi

Province, Southern China, and generation of the REE-rich weathered crust deposits: Resource Geology, v. 58, p. 355–372.
Ishihara, S. and Orihashi, Y., 2014, Zircon U-Pb age of the Triassic granitoids at Nui Phao, northern Viet Nam: Bulletin of Geological Survey of Japan, v. 65, p. 17–22.
Jackson, W.D., and Christiansen, G., 1993, International strategic minerals inventory summary report—Rare-earth oxides: U.S. Geological Survey Circular 930-N, 68 p.
Janots, E., Bernier, F., Brunet, F., Muñoz, M., Trcera, N., Berger, A., and Lanson, M., 2015, Ce (III) and Ce (IV) (re)distribution and fractionation in a laterite profile from Madagascar: insights from in situ XANES spectroscopy at the Ce L_{III}-edge: Geochimica Cosmochimica et Acta, 153, 134–148.
JOGMEC (Japan Oil, Gas and Metals National Corporation), 2011, Restructuring trend and resources of REE industry in China: JOGMEC Metal Resources Report, March 2011, p. 57–70 (in Japanese).
Johannesson, K.H., Stetzenbach, K.J., Hodge, V.F., and Lyons, W.B., 1996, Rare earth element complexation behavior in circumneutral pH groundwaters: assessing the role of carbonate and phosphate ions: Earth and Planetary Sciences Letters, v. 139, p. 305–319.
Joussein, E., Petit, S., Churchman, J., Theng, B., Righi, D., and Delvaux, B., 2005, Halloysite clay minerals — A review: Clay Minerals, v. 40, p. 383–426.
Kanazawa, Y., and Kamitani, M., 2006, Rare earth minerals and resources in the world: Journal of alloys and compounds, v. 408, p. 1339–1343.
Khin Zaw, Meffre, S., Lai, C.K., Burrett, C., Santosh, M., Graham, I., Manaka, T., Salam, A., Kamvong, T., and Cromie, P., 2014, Tectonics and metallogeny of mainland Southeast Asia — A review and contribution: Gondwana Research, v. 26, p. 5–30.
Kosmulski, M., 1997, Standard enthalpies of adsorption of di- and trivalent cations on alumina: Journal of Colloid Interface Science, v. 192, p. 215–227.
——2009, pH-dependant surface charging and points of zero charge. IV. Update and new approach: Journal of Colloid Interface Science, v. 337, p. 439–448.
——2011, The pH-dependent surface charging and points of zero charge V. Update: Journal of Colloid and Interface Science, v. 353, p. 1–15.
Köhler, S.J., Harouiya, N., Chaïrat, C., and Oelkers, E.H., 2005, Experimental studies of REE fractionation during water–mineral interactions: REE release rates during apatite dissolution from pH 2.8 to 9.2: Chemical Geology, v. 222, p. 168–182.
Köppen, W., 1936, Das geographische System der Klimate, *in* Handbuch der Klimatologie, Köppen, W. and Geiger, R.M., eds., C. Gebr, Borntraeger, p. 1–44 (in German).
Lång, L.O., 2000, Heavy mineral weathering under acidic soil conditions: Applied Geochemistry, v. 15, p. 415–423.
Laveuf, C., and Cornu, S., 2009, A review on the potentiality of rare earth elements to trace pedogenetic processes: Geoderma, v. 154, p. 1–12.
Le Couteur, P.C., 2011, Geological report on the Chambe Basin area of exclusive prospecting license EPL0325/11 Mulanje Massif, Southern Malawi, East Africa. Vancoucer, Micron Geological Ltd., 101 p.
Lee, H.G., and Byrne, R.H., 1992, Examination of comparative rare earth element complexation behavior using linear free-energy relationships: Geochimica et Cosmochimica Acta, v. 56, p. 1127–1137.
Lee, J.H., and Byrne, R.H., 1993, Complexation of trivalent rare earth elements (Ce, Eu, Gd, Tb, Yb) by carbonate ions: Geochimica et Cosmochimica Acta, v. 57, p. 295–302.
Li, C.C., and Shen, X.K., 2013, Investigation of geological conditions of weathering crust type rare earth deposits in Hunan Province: Geological Review, v. 59, p. 497–498 (in Chinese).
Li, J.Y., and Li, Z.P., 2010, Predictive study of REE deposits in the Long'an area, Yunnan Province: Yunnan Geology, no. 4, p. 429–430 (in Chinese).
Li, X.H., Li, Z.X., Li, W.X., Liu, Y., Yuan, C., Wei, G.J., and Qi, C.S., 2007, U-Pb zircon, geochemical and Sr-Nd-Hf isotopic constraints on age and origin of Jurassic I- and A-type granites from central Guangdong, SE China: A major igneous event in response to foundering of a subducted flat-slab?: Lithos, v. 96, p. 186–204.
Li, Z.X., and Li, X.H., 2007, Formation of the 1300-km-wide intracontinental orogen and postorogenic magmatic province in Mesozoic South China: A flat-slab subduction model: Geology, v. 35, p. 179–182.
Linnen, R.L., Samson, I.M., Williams-Jones, A.E., Chakhmouradian, A.R., 2014, Geochemistry of the Rare-Earth Element, Nb, Ta, Hf, and Zr Deposits: *in* Holland, H.D. and Turekian, K.K., eds., Geochemistry of Mineral Deposits, Scott, S.D. ed., Vol. 13, Treatise on Geochemistry (2nd Edition), Elsevier-Pergamon, Oxford, p. 543–568.
Lira, R., and Ripley, E.M., 1990, Fluid inclusion studies of the Rodeo de Los Molles REE and Th deposit, Las Chacras Batholith, Central Argentina: Geochimica et Cosmochimica Acta, v. 54, p. 663–671.
Liu, X.W., and Byrne, R.H., 1998, Comprehensive investigation of yttrium and rare earth element complexation by carbonate ions using ICP-Mass Spectrometry: Journal of Solution Chemistry, v. 27, p. 803–815.
Lottermoser, B.G., 1990, Rare-earth element mineralization within the Mt. Weld carbonatite laterite, Western Australia: Lithos, v. 24, 151–167.
Lu, C.B., 2008, Geological characteristics of the Wujingfu REE metallogenic province in Jiexi County, Guangdong Province: West-China Exploration Engineering, v. 20, p. 86–87 (in Chinese).
Luo, X.Y., 2011, Mechanism of REE mineralization and ion adsorption type ore formation in Hunan Province: Acta Mineralogica Sinica, no. 1, p. 332–333 (in Chinese).
Lumpkin, G.R., and Ewing, R.C., 1995, Geochemical alteration of pyrochlore group minerals: Pyrochlore subgroup: American Mineralogists, v. 80, p. 732–743.
Ma, C., and Eggleton, R.A., 1999, Cation exchange capacity of kaolinite: Clays and Clay Minerals, v. 47, p. 174–180.
Ma, P.X., Liu, Z.X., and Bai, G., 1991, On geochemical features and origin of Zhaibeiding HREE-rich granite in Guangdong: Journal of Hebei College of Geology, v. 14, p. 351–360 (in Chinese with English abstract).
Mariano, A.N., and Mariano A.N.Jr., 2012, Rare earth mining and exploration in North America: Elements, v. 8, p. 369–376.
Marini, O.J., Botelho, N.F., and Rossi, P., 1992, Elementos Terra Raras em granitóides da Província Estanífera de Goiás: Brazilian Journal of Geology, v. 22, p. 61–72 (in Portuguese with English abstract).
Marker, A., and de Oliveira, J.J., 1994, Climatic and morphological control of rare earth distribution in weathering mantles on alkaline rocks: Catena, v. 21, p. 179–193.
Marmier, N., Dumonceau, A. J., and Fromage, F., (1997) Surface complexation modeling of Yb(III) sorption and desorption on hematite and alumina: Journal of Contaminant Hydrology, v. 26, p. 159–167.
Marmier, N., Deliseé, A., and Fromage, F., 1999, Surface complexation modeling of Yb(III) and Cs(I) sorption on silica: Journal of Colloid Interface Science, v. 212, p. 228–233.
Maruéjol, P., Cuney, M., and Turpin, L., 1990, Magmatic and hydrothermal REE fractionation in the Xihuashan granites (SE China): Contributions to Mineralogy and Petrology, v. 104, p. 668–680.
Mathieu, R., Cuney, M., and Cathelineau, M, 2000, Geochemistry of palaeofluids circulation in the Franceville basin and around Oklo natural nuclear reaction zones (Gabon): Journal of Geochemical Exploration, v. 69–70, p. 245–249.
Meldrum, A., Boatner, L.A., Weber, W.J., and Ewing, R.C., 1998, Radiation damage in zircon and monazite: Geochimica et Cosmochimica Acta, v. 62, p. 2509–2520.
Meldrum, A., Boatner, L.A., and Ewing, R.C., 2000, A comparison of radiation effects in crystalline ABO_4-type phosphates and silicates: Mineralogical Magazine, v. 64, p. 185–194.
Mentani, T., 2012, So-called "ion-adsorption type" REE deposits found in weathered crust of ilmenite-series granite in northern Vietnam: Master's thesis, University of Tokyo, 107 p.
Middleburg, J.J., van der Weijden, C.H., and Woittiez, J.R.W., 1988, Chemical processes affecting the mobility of major, minor and trace elements during weathering of granitic rocks: Chemical Geology, v. 68, p. 253–273.
Middleton, A.W., Föster, H.-J., Uysal, I.T., Golding, S.D., and Rhede, D., 2013, Accessory phases from the Soultz monzogranite, Soultz-sous-Forêts, France: Implications for titanite destabilisation and differential REE, Y and Th mobility in hydrothermal systems: Chemical Geology, v. 335, p. 105–117.
Migdisov, A.A., and Williams-Jones, A.E., 2014, Hydrothermal transport and deposition of the rare earth elements by fluorine-bearing aqueous liquids: Mineralium Deposita, v 49, p. 987–997.
Migdisov, A.A., Williams-Jones, A.E., and Wagner, T., 2009, An experimental study of the solubility and speciation of the Rare Earth Elements (III) in fluoride-and chloride-bearing aqueous solutions at temperatures up to 300°C: Geochimica et Cosmochimica Acta, v. 73, p. 7087–7109.
Miller, C.F., and Mittlefehldt, D.W., 1982, Depletion of light rare-earth elements in felsic magmas: Geology, v. 10, p. 129–133.
Milliman, J.D., and Meade, R.H., 1983, World-wide delivery of river sediment to the oceans: The Journal of Geology, v. 91, p. 1–21.
Milliman, J.D., and Syvitski, P.M., 1992, Geomorphic/tectonic control of sediment discharge to the ocean: The importance of small mountainous rivers: The Journal of Geology, v. 100, p. 525–544.

Minowa, T., 2008, Rare earth magnets: Conservation of energy and the environment: Resource Geology, v. 58, p. 414–422.
Moldoveanu, G.A., and Papangelakis, V.G., 2012, Recovery of rare earth elements adsorbed on clay minerals: I. Desorption mechanism: Hydrometallurgy, v. 117–118, p. 71–78.
——2013a, Recovery of rare earth elements adsorbed on clay minerals: II. Leaching with ammonium sulfate: Hydrometallurgy, v. 131–132, p. 158–166.
——2013b, Leaching of rare earths elements from clay materials — Summary report to Tantalus Rare Earths AG January 9, 2013: Department of Chemical Engineering and Applied Chemistry, University of Toronto. p. 1–9.
Mongelli, G., 1993, REE and other trace elements in a granitic weathering profile from Serre, southern Italy: Chemical Geology, v. 103, p. 17–25.
Montel, J.M., 1986, Experimental determination of the solubility of Ce-monazite in SiO_2-Al_2O_3-K_2O-Na_2O melts at 800°C, 2 kbar, under H_2O-saturated conditions: Geology, v. 14, p. 659–662.
——1993, A model for monazite/melt equilibrium and application to the generation of granitic magmas: Chemical Geology, v. 110, p. 127–146.
Murakami, H., and Ishihara, S., 2008, REE mineralization of weathered crust and clay sediment on granitic rocks in the Sanyo Belt, SW Japan and the southern Jiangxi Province, China: Resource Geology, v. 58, p. 373–401.
Nesbitt, H.W., 1979, Mobility and fractionation of rare earth elements during weathering of a granodiorite: Nature, v. 279, p. 206–210.
Nesbitt, H.W., and Markovics, G., 1997, Weathering of granodioritic crust, long-term storage of elements in weathering profiles, and petrogenesis of siliciclastic sediments: Geochimica et Cosmochimica Acta, v. 61, p. 1653–1670.
Oelkers, E.H., and Poitrasson, F., 2002, An experimental study of the dissolution stoichiometry and rates of a natural monazite as a function of temperature from 50 to 230°C and pH from 1.5 to 10: Chemical Geology, v. 191, p. 73–87.
Oelkers, E.H., Valsami-Jones, E., and Roncal-Herrero, T., 2008, Phosphate mineral reactivity: from global cycles to sustainable development: Mineralogical Magazine, v. 72, p. 337–340.
Ohta, A., and Kawabe, I., 2001, REE(III) adsorption onto Mn dioxide (δ-MnO_2) and Fe oxyhydroxide: Ce(III) oxidation by δ-MnO_2: Geochimica et Cosmochimica Acta, v. 65, p. 695–703.
Oliva, P., Dupré, B., Martin, F., and Viers, J., 2004, The role of trace minerals in chemical weathering in a high-elevation granitic watershed (Estibere, France): Chemical and mineralogical evidence: Geochimica et Cosmochimica Acta, v. 68, p. 2223–2243.
Orris, G.J., and Grauch, R.I, 2002, Rare earth element mines, deposits, and occurrences: U.S. Geological Survey Open-File Report 02–189, 174 p.
Pan, H., 2011, Characteristics and ore genesis of weathering-crust ion adsorption type REE deposits in the Yunkai Area, Guangxi Region: Land and Resources of Southern China, v. 9, p. 37–40 (in Chinese).
Pan, Y., Fleet, M.E., and MacRae, N., 1993, Late alteration in titanite ($CaTiSiO_5$): Redistribution and remobilisation of rare earth elements and implications for U/Pb and Th/Pb geochronology and nuclear waste disposal: Geochimica et Cosmochimica Acta, v. 57, p. 355–367.
Patyk-Kara, N.G., 2002, Placers in the system of sedimentogenesis: Lithology and Mineral Resources, v. 37, p. 429–441.
Peel, M.C., Finlayson, B.L., and McMahon, T.A., 2007, Updated world map of the Köppen-Geiger climate classification: Hydrology and Earth System Sciences, v. 11, p. 1633–1644.
Piasecki, W., and Sverjensky, D.A., 2008, Speciation of adsorbed yttrium and rare earth elements on oxide surfaces: Geochimica et Cosmochimica Acta, v. 72, p. 3964–3979.
Piccoli, P.M., and Candela, P.A., 2002, Apatite in igneous systems: Reviews in Mineralogy and Geochemistry, v. 48, p. 255–292.
Pichavant, M., Montel, J.M., and Richard, L.R., 1992, Apatite solubility in peraluminous liquids: Experimental data and an extension of the Harrison-Watson model: Geochimica et Cosmochimica Acta, v. 56, p. 3855–3861.
Platt, R.G., and Woolley, A.R., 1986, The mafic mineralogy of the peralkaline syenites and granites of the Mulanje complex Malawi: Mineralogical Magazine, v. 50, p. 85–99.
Poitrasson, F., Chenery, S., and Bland, D.J., 1996, Contrasted monazite hydrothermal alteration mechanisms and their geochemical implications: Earth and Planetary Science Letters, v. 145, p. 79–96.
Poitrasson, F., Oelkers, E., Schott, J., and Montel, J.M., 2004, Experimental determination of synthetic $NdPO_4$ monazite end-member solubility in water from 21° C to 300° C: implications for rare earth element mobility in crustal fluids: Geochimica et Cosmochimica Acta, v. 68, p. 2207–2221.
Pollard, P.J., Nakapadungrat, S., Taylor, R.G., 1995, The Phuket Supersuite, southwest Thailand: fractionated I-type granites associated with tin-tantalum mineralization: Economic Geology, v. 90, p. 586–602.
Pourret, O., Davranche, M., Gruau, G., and Dia, A., 2007a, Competition between humic acid and carbonates for rare earth elements complexation: Journal of Colloid and Interface Science, v. 305, p. 25–31.
——2007b, Rare earth elements complexation with humic acid: Chemical Geology, v. 243, p. 128–141.
Price, J.D., Hogan, J.P., Gilbert, M.C., London, D., and Morgan, G.B.VI, 1999, Experimental study of titanite–fluorite equilibria in the A-type Mount Scott Granite; implications for assessing F contents of felsic magma: Geology, 27, p. 951–954.
Price, J.R., Velbel, M.A., and Patino, L.C., 2005, Allanite and epidote weathering at the Coweeta Hydrologic Laboratory, western North Carolina, USA: American Mineralogist, v. 90, p. 101–114.
Prowatke, S., and Klemme, S., 2005, Effect of melt composition on the partitioning of trace elements between titanite and silicate melt: Geochimica et Cosmochimica Acta, v. 69, p. 695–709.
Rapp, R.P., and E.B. Watson, 1986, Monazite solubility and dissolution kinetics: Implications for the thorium and light rare earth chemistry of felsic magmas: Contribution of Mineralogy and Petrology, v. 94, p. 304–316.
Rapp, R.P., Ryerson, F.J., and Miller, C.F., 1987, Experimental evidence bearing on the stability of monazite during crustal anatexis: Geophysical Research Letters, v. 14, p. 307–310.
Ravindra Kumar, G.R., and Sreejith, C., 2010, Relationship between heavy mineral placer deposits and hinterland rocks of southern Kerala: A new approach for source-to-sink link from the chemistry of garnets: Indian Journal of Geo-Marine Sciences, v. 39, p. 562–571.
Rickwood, P.C., 1989, Boundary lines within petrologic diagrams which use oxides of major and minor elements: Lithos, v. 22, p. 247–263.
Rocha, A., Schissel, D., Sprecher,, A., de Tarso, P., and Goode, J., 2013, Process Development for the Serra Verde Weathered Crust Elution-deposited Rare Earth Deposit in Brazil, *in* Rare Earth Elements — Proceedings of the 52nd Conference of Metallurgists (COM 2013), London, I., Goode, J., Moldoveanu, G., and Rayat, M. eds., Metallurgical Society of the Canadian Institute of Mining, Metallurgy and Petroleum (MetSoc-CIM), Montreal, Canada.
Roskill, 2011, Rare Earths & Yttrium: Market Outlook to 2015, 14th edition, 2011: Roskill Information Services, Ltd., London, 492 p.
——2014, Rare earths: Market outlook for 2020, 15th edition: London, Roskill Information Services, Ltd., 337 p.
Roy, P.S., 1999, Heavy mineral beach placers in southeastern Australia: their nature and genesis: Economic Geology, v. 94, p. 567–588.
Rudnick, R.L., and Gao, S., 2003, The Composition of the Continental Crust, *in* Rudnick, R.L. ed., The Crust, Vol. 3, Treatise on Geochemistry, Holland, H.D., and Turekian, K.K., eds., Elsevier-Pergamon, Oxford, p. 1–64.
Ruschel, K., Nasdala, L., Rhede, D., Wirth, R., Lengauer, C.L., and Libowitzky, E., 2010, Chemical alteration patterns in metamict fergusonite: European Journal of Mineralogy, v. 22, p. 425–433.
Ruyuan Yao Autonomous County, 2014, General Plan of Mineral Resources in Ruyuan Yao Autonomous County, 75 p. (in Chinese)
Sanematsu, K., and Kon, Y., 2013, Geochemical characteristics determined by multiple extraction from ion-adsorption type REE ores in Dingnan County of Jiangxi Province, South China: Bulletin of the Geological Survey of Japan, v. 64, p. 313–330.
Sanematsu, K., Murakami, H., Watanabe, Y., Duangsurigna, S., and Vilayhack, S., 2009, Enrichment of rare earth elements (REE) in granitic rocks and their weathered crusts in central and southern Laos: Bulletin of Geological Survey of Japan, v. 60, p. 527–558.
Sanematsu, K., Moriyama, T., Sotouky, L., and Watanabe, Y., 2011, Mobility of rare earth elements in basalt-derived laterite at the Bolaven Plateau, southern Laos: Resource Geology, v. 61, p. 140–158.
Sanematsu, K., Kon, Y., Imai, A., Watanabe, K., and Watanabe Y., 2013, Geochemical and mineralogical characteristics of ion-adsorption type REE mineralization in Phuket, Thailand: Mineralium Deposita, v. 48, p. 437–451.
Sanematsu, K., Kon, Y., and Imai, A., 2015, Influence of phosphate on mobility and adsorption of REEs during weathering of granites in Thailand: Journal of Asian Earth Sciences, in press.
Santana, I.V., 2013, Caracterização mineralógica e geoquímica de ocorrências de terras raras no maciço granítico Serra Dourada, Goiás/Tocantins, Brasil: Master's thesis (MSc) of Institute of Geosciences, University of Brasília, Brasília, 82 p. (in Portuguese with English abstract).

Schroeder, P.A., Melear, N.D., West, L.T., and Hamilton, D.A., 2000, Metagabbro weathering in the Georgia Piedmont, USA: implications for global silicate weathering rates: Chemical Geology, v. 163, p. 235–245.
Schroth, B.K., and Sposito, G., 1997, Surface charge properties of kaolinite: Clays and Clay Minerals, v. 45, p. 85–91.
Sengupta, D., and Van Gosen, B.S., 2016, Placer-type rare earth element deposits: Reviews in Economic Geology, v. 18, p. 81–100.
Sha, L.K., and Chappell, B.W., 1999, Apatite chemical composition, determined by electron microprobe and laser-ablation inductively coupled plasma mass spectrometry, as a probe into granite petrogenesis: Geochimica et Cosmochimica Acta, v. 63, p. 3861–3881.
Song, Y.H., and Shen, L.P., 1982, Discussion on clay minerals occurring in the weathered crust of a certain acid volcanic rock in Jiangxi Province and their formation conditions: Acta Mineralogica Sinica, v. 3, p. 207–212 (in Chinese with English abstract).
Song, Y.H., and Shen, L.P., 1986, REE geochemistry of the weathered crust of acid volcanic rocks — An experimental study: Geochimica, v. 3, p. 225–234 (in Chinese with English abstract).
Sonke, J.E., and Salters, V.J.M., 2006, Lanthanide-humic substances complexation. I. Experimental evidence for a lanthanide contraction effect: Geochimica et Cosmochimica Acta, v. 70, p. 1495–1506.
Stille, P., Pierret, M. C., Steinmann, M., Chabaux, F., Boutin, R., Aubert, D., Pourcelot, L., Morvan, G., 2009, Impact of atmospheric deposition, biogeochemical cycling and water-mineral interaction on REE fractionation in acidic surface soils and soil water (the Strengbach case): Chemical Geology, v. 264, p. 173–186.
Sun, S.S., and McDonough, W.F., 1989, Chemical and isotopic systematics of oceanic basalts: implications for mantle composition and processes, *in* Saunders, A.D., and Norry, M.J., eds., Magmatism in the ocean basins: Geological Society Special Publication, no. 42, p. 313–345.
Sun, T., 2006, A new map showing the distribution of granites in South China and its explanatory notes: Geological Bulletin of China, v. 25, p. 332–335 (in Chinese with English abstract).
Takahashi, Y., Minai, Y., Ambe, S., Makide, Y., Ambe, F., and Tominaga, T., 1997, Simultaneous determination of stability constants of humate complexes with various metal ions using multitracer technique: Science of the Total Environment, v. 198, p. 61–71.
Takahashi, Y., Minai, Y., Ambe, S., Makide, Y., and Ambe, F., 1999, Comparison of adsorption behavior of multiple inorganic ions on kaolinite and silica in the presence of humic acid using the multitracer technique: Geochimica et Cosmochimica Acta, v. 63, p. 815–836.
Tang, J., and Johannesson, K.H., 2003, Speciation of rare earth elements in natural terrestrial waters: assessing the role of dissolved organic matter from the modeling approach: Geochimica et Cosmochimica Acta, v. 67, p. 2321–2339.
Taunton, A.E., Welch, S.A., and Banfield, J.F., 2000, Microbial controls on phosphate and lanthanide distributions during granite weathering and soil formation: Chemical Geology, v. 169, p. 371–382.
Tian, J., Tang, X.K., Yin, J.Q., Luo, X.P., Rao, G.H., and Jiang, M.T., 2013, Process optimization on leaching of a lean weathered crust elution-deposited rare earth ores: International Journal of Mineral Processing, v. 119, p. 83–88.
Tole, M.P., 1985, The kinetics of dissolution of zircon ($ZrSiO_4$): Geochimica et Cosmochimica Acta, v. 49, p. 453–458.
Tong, Q.H., 2013, Study on the metallogenic regularity of the Xiaotao ion-adsorption type REE deposits in Fujian Province: Earth, v. 6, p. 26–27 (in Chinese).
Tromans, D., 2006, Solubility of crystalline and metamict zircon: A thermodynamic analysis: Journal of Nuclear Materials, v. 357, p. 221–233.
Ueda, T., 1957, Studies on the metamictization of radioactive minerals: Memoirs of the College of Science, University of Kyoto, Series B, v. 24, No. 2, p. 81–120.
U.S. Geological Survey, 2015, Mineral Commodity Summaries 2015: U.S. Geological Survey, 196 p.
Valsami-Jones, E., Ragnarsdottir, K.V., Putnis, A., Bosbach, D., Kemp, A.J., and Cressey, G., 1998, The dissolution of apatite in the presence of aqueous metal cations at pH 2–7: Chemical Geology, v. 151, p. 215–233.
Viers, J., Oliva, P., Dandurand, J.-L., and Dupré, B., 2014, Chemical weathering rates, CO_2 consumption, and control parameters deduced from the chemical composition of rivers, *in* Drever, J.I. ed., Surface and Groundwater, Weathering and Soils, Vol. 7, Treatise on Geochemistry (2nd Edition), Holland, H.D. and Turekian, K.K., eds., Elsevier-Pergamon, Oxford, p. 175–194.
Wall, F., 2014, Rare earth elements, *in* Critical Metals Handbook, Gunn, G. ed., John Wiley and Sons, p. 312–339.
Wan, Y.X., and Liu, C.Q., 2005, Study on adsorption of rare earth elements by kaolinite: Journal of Rare Earth: v. 23, p. 377–381.
——2006, The effect of humic acid on the adsorption of REEs on kaolin: Colloids and Surfaces, v. 290, p. 112–117.
Wang, D.H., Zhao, Z., Yu, Y., Zhao, T., Li, J.K., Dai, J.J., Liu, X.X., and He, H.H., 2013, Progress, problems and research orientation of ion-adsorption type rare earth resources: Rock and Mineral Analysis, v. 32, p. 796–802 (in Chinese with English abstract).
Wang, D.Z., and Shu, L.S., 2012, Late Mesozoic basin and range tectonics and related magmatism in Southeast China: Geoscience Frontiers, v. 3, p. 109–124.
Wang, F.Y., Ling, M.X., Ding, X., Hu, Y.H., Zhou, J.B., Yang, X.Y., Liang, H.Y., Fan, W.M., and Sun, W.D., 2011, Mesozoic large magmatism events and mineralization in SE China: oblique subduction of the Pacific plate: International Geology Review, v. 53, p. 704–726.
Wang, G.M., Huang, T.L., Zhu, J.F., and Xu, Y.J., 2012, Remote sensing quantitative forecast of the potential of ion adsorption type rare earth resources: Land form research based on SPOT 5 data: Remote Sensing for Land & Resources, v. 24, p. 127–131 (in Chinese with English abstract).
Wang, Y.J., Fan, W.M., Sun, M., Liang, X.Q., Zhang, Y.H., and Peng, T.P., 2007, Geochronological, geochemical and geothermal constraints on petrogenesis of the Indosinian peraluminous granites in the South China Block: A case study in the Hunan Province: Lithos, v. 96, p. 475–502.
Wang, Y.J., Zhang, A.M., Fan, W.M., Zhao, G.C., Zhang, G.W., Zhang, Y.Z., Zhang, F.F., and Li, S.Z., 2011, Kwangsian crustal anatexis within the eastern South China Block: geochemical, zircon U-Pb geochronological and Hf isotopic fingerprints from the gneissoid granites of Wugong and Wuyi–Yunkai Domains: Lithos, v. 127, p. 239–260.
Watson, E.B., 1979, Apatite saturation in basic to intermediate magmas: Geophysical Research Letters, v. 6, p. 937–940.
——1980, Apatite and phosphorus in mantle source regions: An experimental study of apatite/melt equilibria at pressures to 25 kbar: Earth and Planetary Science Letters, v. 51, p. 322–335.
Watson, E.B., and Capobianco, C.J., 1981, Phosphorus and the rare earth elements in felsic magmas: An assessment of the role of apatite: Geochimica et Cosmochimica Acta, v. 45, p. 2349–2358.
Wei, Z., Yin, M., Zhang, X., Hong, F., Li, B., Tao, Y., Zhao, G. and Yan C., 2001, Rare earth elements in naturally grown fern Dicranopteris linearis in relation to their variation in soils in South-Jiangxi region: Environmental Pollution, v. 114, p. 345–355.
White, A.F., and Blum, A.E., 1995, Effects of climate on chemical weathering in watersheds: Geochimica et Cosmochimica Acta, v. 59, p. 1729–1747.
Wolf, M.B., and London, D., 1994, Apatite dissolution into peraluminous haplogranitic melts: An experimental study of solubilities and mechanisms: Geochimica et Cosmochimica Acta, v. 58, p. 4127–4145.
——1995, Incongruent dissolution of REE- and Sr-rich apatite in peraluminous granitic liquids: Differential apatite, monazite, and xenotime solubilities during anatexis: American Mineralogist, v. 80, p. 765–775.
Wood, S.A., 1990a, The aqueous geochemistry of the rare–earth elements and yttrium. Part 2. Theoretical predictions of speciation in hydrothermal solutions to 350°C at saturated water vapor pressure: Chemical Geology, v. 88, p. 99–125.
——1990b, The aqueous geochemistry of the rare-earth elements and yttrium. 1. Review of available low-temperature data for inorganic complexes and the inorganic REE speciation of natural waters: Chemical Geology, v. 82, p. 159–186.
Wood, S.A., and Ricketts, A., 2000, Allanite-(Ce) from the Eocene Casto granite, Idaho: response to hydrothermal alteration: The Canadian Mineralogist, v. 38, p. 81–100.
Wu, C.Y., Huang, D.H., and Guo, Z.G., 1990a, REE geochemistry in the weathered crust of granites, Longnan area, Jiangxi Province: Acta Geologica Sinica, v. 3, p. 193–210.
Wu, C.Y., Huang, D.H., Bai, G., and Ding, X.S., 1990b, Differentiation of rare earth elements and origin of granitic rocks, Nanling Mountain area. Acta Petrologica Mineralogica, 9, 106–116 (in Chinese).
Wu, C.Y., Bai, G., and Huang, D.H., 1992, Characteristics and significance of HREE-rich granitoids of the Nanling Mountain area: Bulletin of the Chinese Academy of Geological Sciences, v. 25, p. 43–58 (in Chinese with English abstract).
Wu, C.Y., Lu, H.L., Xu, L.M., and Hou, L., 1993a, A preliminary study on modes of occurrence of rare earth elements in the tropical-subtropical

weathering crust of Nanling region: Mineral Deposits, v. 12, p. 297–307 (in Chinese with English abstract).

Wu, C.Y., Huang, D.H., Yuan, Z.X., Bai, G., Nakajima, T., and Ishihara, S., 1993b, Trace elements geochemistry and genetic implications for highly evolved granitic rocks from south China: Resource Geology Special Issue, No. 16, p. 9–24.

Wu, C.Y, Yuan, Z.X., and Bai, G. 1996, Rare earth deposits in China, *in* Jones, A.P., Williams, C.T., Wall, F., eds., Rare Earth Minerals: Chemistry, Origin and Ore Deposits: Mineralogical Society Series, 7, Chapman & Hall, p. 105–150.

Xinfeng County, 2014, General Plan of Mineral Resources in Xinfeng County, 85 p. (in Chinese).

Xu, L.M., and Yuan, Z.X., 1992, Zircon U-Pb isotopic age of the Qinghu monzonite in Guangxi and its geological significance: Geology of Guangxi, v. 5, p. 33–36 (in Chinese).

Xu, X.S., Lu, W.M., and He, Z.H., 2007, Age and generation of Fogang granite batholith and Wushi diorite-hornblende gabbro body: Science in China (Series D), v. 50, p. 209–220.

Yang, D.H., and Xiao, G.M., 2011, Regional metallogenic regularities of the ion adsorption type of rare-earth deposits in Guangdong Province: Geology and Resources, v. 20, p. 462–468 (in Chinese with English abstract).

Yang, X.M., Yang, X.Y., Zhang, P.S., Zhan, W.L., and Tao, K.J., 1999, Geochemical study of REE from granite weathering crusts in Dajishan of Jiangxi Province: Chinese Rare Earths, v. 20, p. 1–5 (in Chinese with English abstract).

Yang, Y.Q., Hu, Z.S., and Luo, Z.M., 1981, Geological characteristics of mineralization of rare earth deposits of the ion-adsorption type and their prospecting direction: Bulletin of Institute of Mineral Deposit, Chinese Academy of Geological Sciences, v. 2, p. 102–118 (in Chinese with English abstract).

Yang, Z.M., 1987, A study on clay minerals from the REE-rich weathered crust developed on the Longnan Granite in Jiangxi: Acta Geologica Sinica, v. 1, p. 70–80 (in Chinese with English abstract).

Yu, B., Xie, J.T., Ji, Z.N., and Liu, J., 2004, Study on insitu-leaching methods of the Yanfutang ion-adsorption type REE deposits: Metallic Ore Dressing Abroad, v. 41, p. 37–40 (in Chinese).

Yuan, Z.X., Wu, C.Y., Xu, L.M., and Ni, Y.X., 1993, The distribution of trace elements in granitoids in the Nanling Region of China: Chinese Journal of Geochemistry, v. 12, p. 193–205.

Yusoff, Z.M., Ngwenya, B.T., and Parsons, I., 2013, Mobility and fractionation of REEs during deep weathering of geochemically contrasting granites in a tropical setting, Malaysia. Chemical Geology v. 349, p. 71–86.

Zhang, F.F., Wang, Y.J., Zhang, A.M., Fan, W.M., Zhang, Y.Z., and Zi, J., 2012, Geochronological and geochemical constrants on the petrogenesis of Middle Paleozoic (Kwangsian) massive granites in the eastern South China Block: Lithos, v. 150, p. 188–208.

Zhang, Z.H., 1990, A study on weathering crust ion adsorption type REE deposit, South China: Contributions to Geology and Mineral Resources Research, v. 5, p. 57–71 (in Chinese with English abstract).

Zhao, Z. Chen, Z.Y., Chen, Z.H., Hou K.J., Zhao, Z., Xu, J.X., Zhang, J.J., Zeng, Z.L., 2012, Zircon U-Pb dating, tectonic setting and ore-bearing properties evaluation of the Caledonian Yangbu pluton in South Jiangxi: Rock and Mineral Analysis, v. 31 p. 530–535 (in Chinese with English abstract).

Zhou, X.M., Sun, T., Shen, W.Z., Shu, L.S., and Niu, Y.L., 2006, Petrogenesis of Mesozoic granitoids and volcanic rocks in South China: a response to tectonic evolution: Episodes, v. 29, p. 26–33.

Zhou, X.W., Wen, D.X., and Luo, X.P., 2012, The status quo and development trend of the extraction of ion-adsorbed rare earth in southern China: Nonferrous Metals Science and Engineering, v. 3, p. 81–85 (in Chinese with English abstract).

Zhu, J.C., Zhang, P.H., Xie, C.F., Zhang, H., and Yang, C., 2006, The Huashan–Guposhan A-type granitoid belt in the Western part of the Nanling mountains: Petrology, geochemistry and genetic interpretations: Acta Geologica Sinica, v. 80, p. 529–542 (in Chinese with English abstract).

Zhu, X., 1999, Mineral Facts of China, Beijing, Science Press, 665 p. (in Chinese).

Zhu, Y.D., and Ruan, D.Y., 1984, A preliminary study on REE distribution pattern in Xinfeng granite: Journal of Central–South Institute of Mining and Metallurgy, v. 4, p. 101–107 (in Chinese with English abstract).

©2016 Society of Economic Geologists, Inc.
Reviews in Economic Geology, v. 18, pp. 81–100

Chapter 4

Placer-Type Rare Earth Element Deposits

Debashish Sengupta[1] and Bradley S. Van Gosen[2,†]

[1] *Department of Geology and Geophysics, Indian Institute of Technology, Kharagpur West Bengal, India*

[2] *U.S. Geological Survey, Box 25046, MS 973, Denver, Colorado 80225*

Abstract

Ancient and modern types of sedimentary placer deposits formed in both alluvial and coastal environments have been signficant sources of the rare earth elements (REEs). The REE-bearing minerals in placer-type deposits are primarily monazite [(Ce,La,Nd,Th)PO_4] and sometimes xenotime (YPO_4), which are high-density (heavy) minerals that accumulate with the suite of heavy minerals. Monazite has been extracted from many heavy mineral placers as a coproduct of the economic recovery of associated industrial minerals, such as titanium oxide minerals (ilmenite, rutile), zircon, sillimanite, garnet, staurolite, and others. Xenotime has been produced from some alluvial deposits as a coproduct of tin (cassiterite) placer mining.

Placers are mineral deposits formed by the mechanical concentration of minerals from weathered debris. Placers can be classified as eluvial, alluvial, eolian, beach, and fossil (paleo) deposit types. Monazite-bearing placer-type deposits can occur in residual weathering zones, beaches, rivers and streams, dunes, and offshore areas. The detrital mixture of sand, silt, clays, and heavy (dense) minerals deposited in placers are derived primarily from the erosion of crystalline rocks, mainly igneous rocks and moderate- to high-grade metamorphic rocks (amphibolite facies and higher). In fluvial settings, slope is an important factor for the concentration of heavy minerals from detritus. In coastal settings, the actions of waves, currents, tides, and wind are forces that concentrate and sort mineral particles based on size and density.

Placer deposits containing monazite are known on all continents. In the past, by-product monazite has been recovered from placers in Australia, Brazil, India, Malaysia, Thailand, China, New Zealand, Sri Lanka, Indonesia, Zaire, Korea, and the United States. More recently, monazite has been recovered from coastal and alluvial placers in India, Malaysia, Sri Lanka, Thailand, and Brazil. In particular, along the southwestern and southeastern coasts of India, beach deposits rich in heavy minerals have experienced renewed exploration and development, partly to recover monazite for its REEs as well as its Th, to be used as a nuclear fuel source.

Exploration designed to locate heavy mineral placers in coastal environments should identify bedrock terranes containing abundant high-grade metamorphic rocks or igneous rocks and identify ancient or modern coastal plains sourced by streams and rivers that drain these terranes. Trace elements associated with heavy mineral placers, useful as pathfinder elements, primarily include Ti, Hf, the REEs, Th, and U. Radiometric methods of geophysical exploration are useful in discovering and delineating deposits of heavy mineral sands. Several minerals in these deposits can produce a radiometric anomaly, but especially monazite, due to its high thorium content. Some beach districts in India and Brazil have been demonstrated as areas of high background radiation with potential dose exposure to humans and others, primarily due to the Th and U in detrital grains of monazite and zircon.

Monazite- or xenotime-bearing placers offer several advantages as sources of REEs. Ancient and modern deposits of heavy mineral sands that formed in coastal settings can be voluminous with individual deposits as much as about 1 km wide and more than 5 km long. Grains of monazite or xenotime in placer deposits are mingled with other heavy minerals of industrial value. Monazite and xenotime are durable and often the heaviest minerals within the sand-silt deposit, which makes them relatively easy to mechanically separate. Thus, the REE ore minerals, monazite or xenotime, can be recovered from heavy mineral placers as a low-cost coproduct along with the economic production of the associated industrial minerals.

Introduction

Alluvial and coastal placer deposits have been, and continue to be, important sources of many mineral commodities, such as gold, tin (in cassiterite), titanium oxide (in ilmenite, rutile, leucoxene), and zirconium (in zircons), as well as additional industrial minerals (sand and gravel, sillimanite, garnet, staurolite, as examples). Placers are also sources of the rare earth elements (REEs), chiefly via the minerals monazite [(Ce,La,Nd,Th)PO_4] and sometimes xenotime (YPO_4). In fact, until the mid-1960s, when full-scale production of rare earths began at the Mountain Pass carbonatite deposit in southeastern California, placer mines recovering monazite as a coproduct were the world's principal source of the REEs (Tse, 2011; Fig. 1).

With the increasing demand for REEs in modern technologies, combined with potential supply restrictions for specific REEs, placer deposits have reemerged as viable sources of rare earths, specifically through the recovery of monazite and/or xenotime from placers composed of heavy mineral-rich sands. Presently, the purposeful recovery of monazite occurs from heavy mineral beach deposits mined and processed at several coastal sites along the southwestern and southeastern shores of India. These operations recover ilmenite, rutile, leucoxene, rutile, sillimanite, garnet, and sometimes other

† Corresponding author: e-mail, bvangose@usgs.gov

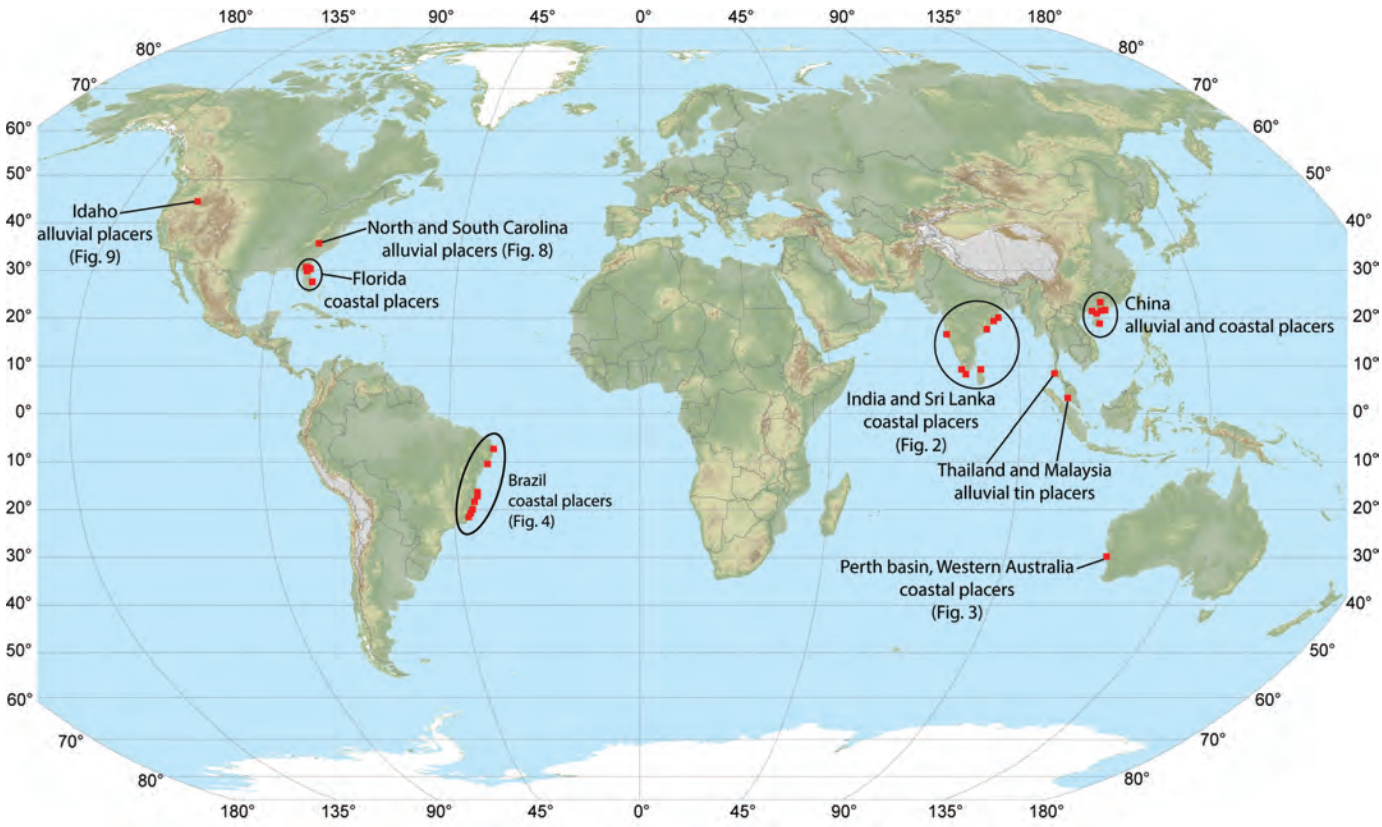

Fig. 1. Global map showing significant placer districts (red squares) that produced monazite and/or xenotime in the past or presently; these minerals were recovered as by- or coproduct commodities with other economic heavy minerals. Current monazite production occurs at modern beach placers in India and coastal placers at the Buena district, Brazil.

industrial minerals as primary commodities, and also separate monazite as a coproduct. The REEs within the monazite are extracted for sale, and the thorium (Th) in the mineral is sought as a fuel source for a nationally coordinated program in India to develop thorium-based nuclear power.

Ancient and modern coastal deposits of heavy mineral sands offer several advantages as ore deposits. As examples, these deposits are relatively easy to mine because they are weakly to poorly consolidated, and likewise are relatively easy to process. Examples of heavy mineral sands deposits are known on every continent and most likely also exist in Antartica. Ancient and modern deposits of heavy mineral sands that formed in coastal environments can be voluminous. Individual bodies of heavy mineral-rich sands are typically about 1 km wide and more than 5 km long. Many heavy mineral sands districts extend for more than 10 km, encompassing several individual deposits that are spread along an ancient or modern strandline. Reported thicknesses of economic deposits range from 3 to 45 m. Individual ore deposits typically comprise at least 10 million metric tons (Mt) of ore (the total size of the individual sand-silt body), with an overall heavy mineral content of 2 to >10%.

This paper describes examples of alluvial and coastal placer deposits known to host economic concentrations of monazite or xenotime (economic in the past or present). Descriptions of these deposits and their geologic setting provide insights into source rocks, transport mechanisms, and the depositional environments that form potentially economic REE placer deposits. Separately discussed is a classification scheme for placer deposits in general, followed by explanations of ore-gangue mineralogy and geochemistry characteristic of REE-bearing placers. These insights contribute to discussions on genetic models and exploration criteria relevant to monazite- or xenotime-bearing placers, particulary coastal placer deposits. Next, the aspect of radiation exposures from these deposits is discussed; relatively high levels of natural radioactivity, produced by monazite and zircon in some coastal sands, have been studied, particular in India. Finally, the significance of monazite-bearing placers is reemphasized—monazite in placers can contribute much-needed REEs to the global supply as well as thorium, obtaining the monazite (and/or xenotime) as a coproduct of the economic production of titanium oxide minerals, zircons, and other industrial minerals.

Terminology

Much of the terminology used to describe placer deposits is not commonly used in geologic discussions. To aid the reader and avoid confusion, some terms often used in discussions of this general deposit type are as follows.

"Heavy minerals" are generally defined as dense minerals that have a specific gravity greater than 2.85. For comparison, quartz has a specific gravity of approximately 2.65.

"Heavy mineral suite" is a term that refers to the entire group of heavy minerals identified within a particular deposit.

"Grade," in reference to a heavy mineral sands deposit, most often refers to the average heavy mineral content of the deposit (usually reported in wt %).

As noted earlier, placers are sedimentary deposits formed by the physical-mechanical concentration of minerals orginally derived from weathered debris. Some of these deposits can contain economic (or potentially economic) concentrations of heavy minerals; in addition to "placer," this deposit type is also commonly referred to as "heavy mineral sands." In the context of this discussion, placer and heavy mineral sands are interchangeable.

General geology

Placers are mineral deposits formed by the mechanical concentration of minerals from weathered debris. Examples of placer deposits occur in beaches, rivers and streams, dunes and offshore areas. The economic minerals hosted by placer deposits are very resistant to chemical and physical breakdown (durable), and typically have high density. The detrital mixture of sand, silt, clays, and "heavy" (dense) minerals deposited in placers are primarily derived from the erosion of crystalline rocks. The source rocks include a wide variety of igneous rocks and moderate- to high-grade metamorphic rocks (amphibolite facies and higher), and some sandstones and conglomerates. This detritus is transported by mechanisms such as moving water and aeolian activity, carrying the dense minerals in a mixture of sand, silt, and clay to downgradient areas where they are deposited and further concentrated. It is important to note that the processes of major concentration of heavy minerals are due to flowing waters in rivers or streams and wind. In fluvial settings, slope provides an important factor for the concentration heavy mineral placers. In coastal settings, the actions of waves, currents, tides, and wind are forces that concentrate the heavy dense minerals, including the minerals of economic value.

The major thorium deposits in various parts of coastal Asia and South America are classified as sedimentary thorium deposits (Dill, 2010), which could also be described as thorium placers (Table 1). Both modern placer and paleoplacer deposits could cater to the world demand of thorium. Thorium-bearing minerals are widely known to accumulate in modern coastal placer deposits, with examples in India, Brazil, Sri Lanka, and Malaysia, to name a few (Fig. 1, Table 1). In India, shoreline-parallel concentrations of monazite in coastal sands in the States of Kerala, Tamil Nadu, and the recently discovered deposits in Orissa (Fig. 2; Mohanty et al., 2003a, b) have pushed India to the top level in production of thorium. These placer deposits resulted from fluvial drainage systems during the Quaternary. These monazite sands are of interest as a resource for economic recovery of the REEs, primarily cerium (Ce), obtained as a coproduct of titanium (Ti) oxide production in the form of ilmenite and rutile and zirconium (Zr) recovery from zircon.

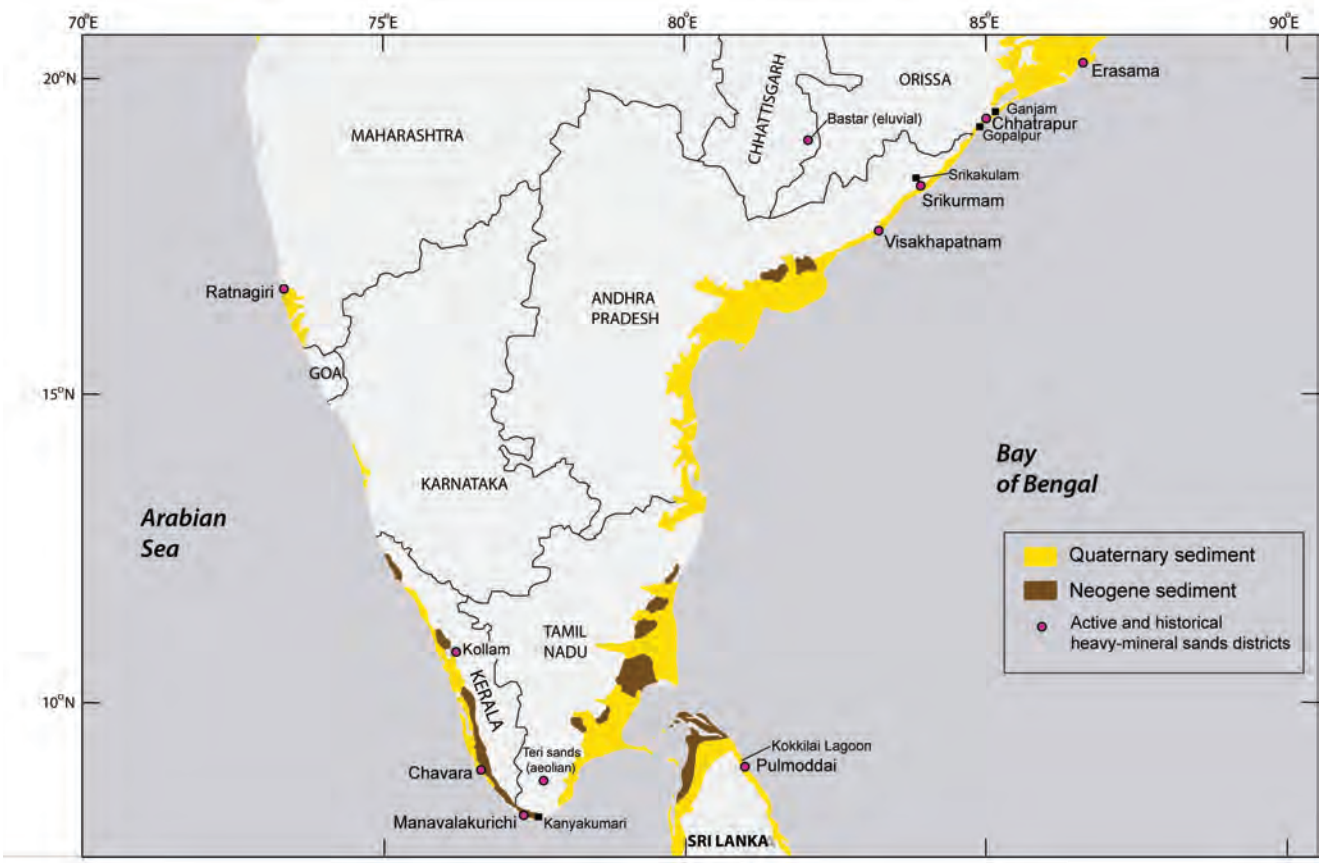

Fig. 2. Index map of southern India and northern Sri Lanka, showing locations of (1) historic and active heavy mineral sands operations discussed in this report, and (2) areas of Quaternary and Neogene sediments.

Table 1. Major Coastal and Fluvial Thorium (Monazite) Placer Deposits

Country	State	Placer district	Latitude	Longitude	Comments	References
Australia	Western Australia	Eneabba, Perth basin	–29.79	115.30	About 2,500 t of monazite produced annually as a coproduct prior to 1995	Sheppard (1990); Castor and Hedrick (2006)
Brazil	Bahia	Alcobaça	–17.26	–39.22	Coastal placer; past producer of monazite	Overstreet (1967); Orris and Grauch (2002)
Brazil	Espírito Santo	Anchieta (Parati, Imbiri, Pipa de Viho, Mãebá)	–20.77	–40.57	Coastal placer; past producer of monazite	Overstreet (1967); Orris and Grauch (2002)
Brazil	Espírito Santo	Aracruz	–19.95	–40.15	Coastal placer; past producer of monazite	Overstreet (1967); Orris and Grauch (2002)
Brazil	Sergipe	Brejo Grande - Pacatuba	–10.43	–36.47	Coastal placer; past producer of monazite	Overstreet (1967); Orris and Grauch (2002)
Brazil	Rio de Janeiro	Buena (Buena Norte, Buena Sol)	–21.52	–41.07	Active producer of monazite from beach placers	Indústrias Nucleares do Brasil SA (2013)
Brazil	Rio Grande do Norte	Camaratuba	–6.89	–34.89	Coastal placer; past producer of monazite	Overstreet (1967); Orris and Grauch (2002)
Brazil	Bahia	Cumuruxatiba (Curumuxatiba, Comoxatiba)	–18.31	–39.66	Coastal placer; past producer of monazite	Overstreet (1967); Orris and Grauch (2002)
Brazil	Espírito Santo	Guarapari (Praia do Vaz, Vila Velha, Rastinga, Canto do Riacho, Praia de Diogo)	–20.70	–40.51	Coastal placer; past producer of monazite	Overstreet (1967); Orris and Grauch (2002)
Brazil	Espírito Santo	Itapemirim (Boa Vista, Siri)	–21.17	–40.91	Coastal placer; past producer of monazite	Overstreet (1967); Orris and Grauch (2002)
Brazil	Paraiba	Mataraca	–6.48	–34.97	Coastal placer; past producer of monazite	Overstreet (1967); Orris and Grauch (2002)
Brazil	Bahia	Porto Seguro district	–16.43	–39.08	Coastal placer; past producer of monazite	Overstreet (1967); Orris and Grauch (2002)
Brazil	Bahia	Prado area	–17.39	–39.21	Coastal placer; past producer of monazite	Overstreet (1967); Orris and Grauch (2002)
Brazil	Rio de Janeiro	Sao Joao de Barra (Barra Sao Joao)	–21.40	–41.00	Coastal placer; past producer of monazite	Overstreet (1967); Orris and Grauch (2002)
Brazil	Espírito Santo	Serra (Jacareipe)	–20.17	–40.19	Coastal placer; past producer of monazite	Overstreet (1967); Orris and Grauch (2002)
Brazil	Bahia, Espirito Santo	Vitoria	–18.33	–39.66	Coastal placer; past producer of monazite	Overstreet (1967); Orris and Grauch (2002)
China	Guangxi	Beihei	21.48	109.10	River and coastal placers; byproduct monazite	Jackson and Christiansen (1993); Orris and Grauch (2002)
China	Guangdong	Dianbai	21.50	111.02	Coastal placers; by-product monazite	Jackson and Christiansen (1993); Orris and Grauch (2002)
China	Guangdong	Haikang	20.98	110.07	River and coastal placers; by-product monazite	Jackson and Christiansen (1993); Orris and Grauch (2002)
China	Guangdong	Nanshanhai	21.55	111.67	Coastal placers; by-product monazite	Jackson and Christiansen (1993); Orris and Grauch (2002)
China	Hainan Island	Sai-Lao, Wuzhaung, and Xinglong districts	18.68	110.38	Coastal placers; by-product monazite	Jackson and Christiansen (1993); Orris and Grauch (2002)
China	Guangxi	Xun Jiang	23.50	110.83	River placers; by-product monazite	Jackson and Christiansen (1993); Orris and Grauch (2002)
India	Orissa	Erasama	20.15	86.51	Coastal placers containing monazite	Mohanty et al. (2003a, b, 2004)
India	Orissa	Chhatrapur	19.34	85.01	Coastal placers containing monazite	Mohanty et al. (2003a, b, 2004)
India	Andhra Pradesh	Visakhapatnam	17.66	83.27	Coastal placers containing monazite	Raju et al. (2001)
India	Kerala	Manavalakurichi	8.14	77.30	Coastal placers containing monazite	Tipper (1914); Raju et al. (2001)
India	Kerala	Chavara	8.99	76.52	Coastal placers containing monazite	Prakash et al. (1991)
India	Maharashtra	Ratnagiri	17.02	73.28	Coastal placers containing monazite	Raju et al. (2001)
Malaysia	Selangor	Batang Berjuntai	3.39	101.42	Fluvial tin placers; by-product monazite and xenotime	Orris and Grauch (2002)
Sri Lanka	Eastern Province	Pulmoddai	8.95	80.99	Coastal placers containing monazite	Lanka Mineral Sands Limited (2013)
Thailand	Phang-nga	Takua-Pa	8.87	98.35	Fluvial tin placers; by-product monazite and xenotime	Economic and Social Commission for Asia and the Pacific (2001)
United States	Idaho	Central Idaho fluvial placers	44.42	–116.02	Fluvial placers; by-product monazite	Staatz et al. (1980)
United States	North Carolina and South Carolina	Piedmont region fluvial placers	35.31	–81.54	5,000 t of monazite produced from 1887 to 1917	Overstreet et. al. (1968); Staatz et al. (1979)
United States	Florida	Mineral City	30.24	–81.39	About 1 t of monazite produced in 1925	Staatz et al. (1980)
United States	Florida	Rutile Mining Co. mine	30.34	–81.60	Small amounts of monazite recovered from beach sands	Staatz et al. (1980)
United States	Florida	Riz Mining Co. mine	27.64	–80.35	Dune sands; monazite as by-product from 1940s to 1955	Staatz et al. (1980)
United States	Florida	Green Cove Springs	29.87	–81.71	Beach deposits; monazite recovered as coproduct	Staatz et al. (1980); Castor and Hedrick (2006)
United States	Florida	Boulogne	30.77	–81.98	Beach deposits; monazite recovered as coproduct	Staatz et al. (1980)

Classification of Placer Deposits

Based on their mode of transportation and the site of deposition, placers are classified as (1) eluvial, (2) alluvial or fluvial, (3) eolian, (4) beach, and (5) fossil placers.

1. Eluvial placers are formed upon the release of minerals from the rock matrix, caused by the decomposition of rock in place from weathered deposits primarily due to precipitation and aeolian activity. This is the embryonic stage in the development of placers (Gupta, 2003). Notable Indian examples are the cassiterite, columbite, and tantalite placer deposits in the Bastar district in the state of Madhya Pradesh in central India (Fig. 2; Suryanarayan et al., 1979).
2. Alluvial placers represent the next stage in the placer formation. The heavy minerals are introduced into the fluvial system by the action of runoff, gravity, and/or by the erosive action of the stream itself. Renowned examples are the gold-bearing alluvial placer deposits that fed the famous California (United States) gold rush in the 19th century. Economic examples of xenotime-bearing fluvial placer deposits occur in India (Rai et al., 1991), Malaysia (Castor and Hedrick, 2006), and Thailand (Economic and Social Commission for Asia and the Pacific, 2001, p. 72–74).
3. Eolian deposits, formed by the actions of winds, can hold concentrations of heavy minerals. These types of deposits occur in arid/semiarid regions, where the influence of wind is strong and sufficient vegetation does not exist to cover the soil. Wind action progressively concentrates the heavy minerals by blowing away the associated light minerals over time (Nikiforova et al., 2005, 2007). Prominent examples are eolian gold deposits of Australia. The Teri deposits of Tamil Nadu (Fig. 2) are aeolian in origin. The Trail Ridge deposit of north-central Florida is a Pliocene-age complex of aeolian sands, from which DuPont produces titanium minerals, zircon, and staurolite (Dupont, 2014). The sand dunes of the Richards Bay area (Richards Bay Minerals, 2013) on the east coast of South Africa have been a highly productive source of zircon, rutile, and ilmenite.
4. Beach placers are formed by the interaction of terrestrial processess with coastal hydrodynamics. The heavy minerals are carried in sediments, transported to the coastal area by various processes of detrital transport, then selectively panned, sorted and deposited at suitable locations by the action of waves and currents. The factors controlling the formation of beach placers are complex and include geomorphology of the area, climate, drainage pattern, coastal processes, and neotectonics. The heavy minerals are concentrated by a combination of these processes in the upper part of the beach, where the actions of the wind may erode them and form heavy mineral-rich coastal dune deposits (deposit type 3 above; Kudrass, 2000). Most of the important deposits of ilmenite, rutile, zircon, monazite, and garnet occur in the form of beach placers. India has some of the world's largest placer deposits along its long southeast and southwest coastlines.
5. Fossil (paleo) placers formed in the geologic past due to processes similar to modern deposits. Fossil placers become exposed by factors such as climate change and/orepirogenic movements and eustasy. Along the coasts of India and adjoining areas of Sri Lanka (Singhvi et al., 1986) there are considerable reserves of fossil placers known to exist (Ali et al., 2001); these deposits formed during previous low stands of sea level. Other examples of fossil placers are discussed in this article. Fossil placers can be reworked by erosion and act as sources of recent deposits.

Examples of Monazite-Bearing Placer Districts

By-product monazite has been recovered in the past from placer deposits in Australia, Brazil, India, Malaysia, Thailand, China, New Zealand, Sri Lanka, Indonesia, Zaire, Korea, and the United States. Until the mid-1960s, with the advent of full rare earth production from the Mountain Pass carbonatite deposit in southeastern California, monazite placers were the world's principal source of REE production (Tse, 2011, Fig. 1). Monazite has recently been recovered from beach and alluvial placers in India, Malaysia, Sri Lanka, Thailand, and Brazil (Table 1). Indian beach placers are the principal source for ongoing production of monazite and for this reason the Indian deposits are described in more detail as examples of this deposit type.

Heavy mineral sands deposits (placers) occur on every continent, likely including Antarctica. The REE deposit dataset of Orris and Grauch (2002) lists 369 REE-bearing placer deposits and occurrences, including 264 shoreline placers, 78 alluvial placers, 13 paleoplacers, and 14 unclassified placers. The examples of monazite-bearing placers that follow should not be regarded as a complete listing of all known occurrences of this deposit type throughout the world. Rather, the deposits described here are examples of significant deposits of monazite-rich, heavy mineral sands that have been worked in the past or are being mined at this time.

Australia

The vast majority of the heavy mineral and associated monazite resources of Australia are hosted by ancient beach and sand dune deposits that formed along middle Eocene to Pleistocene strandlines (Hoatson et al., 2011). Significant fossil beach deposits of heavy minerals occur in three inland Cenozoic-age sedimentary basins of western and southern Australia, which are the Canning, Perth, Murray, and Eucla basins (Fig. 3). In the northeastern part of the Canning basin in the northeastern part of Western Australia, heavy mineral sands are currently (2014) mined inland of the coast near Derby. The Perth basin, in the southwestern part of Western Australia, hosts substantial deposits of heavy minerals within Cenozoic strandline strata that parallel the coast north and south of Perth. The heavy mineral beach deposits of the Murray basin occur in Cenozoic paleostrandlines in New South Wales, Victoria, and South Australia. The Eucla basin bounds the coast of the southwestern part of South Australia and southeastern part of Western Australia.

Heavy mineral-rich beach and dune sand deposits in the Perth basin of Western Australia have been extensively mined since the 1970s. The sands were deposited along strandlines from the Pliocene to early Pleistocene. The Eneabba mining district in the northern part of the Perth basin (north of Perth, Fig. 3) has been a substantial producer of heavy minerals, principally rutile, zircon, and ilmenite, as well as a former producer of monazite as a coproduct. Reportedly, prior to 1995 about 2,500 t of monazite were recovered annually as a coproduct of titanium minerals and zircon processing

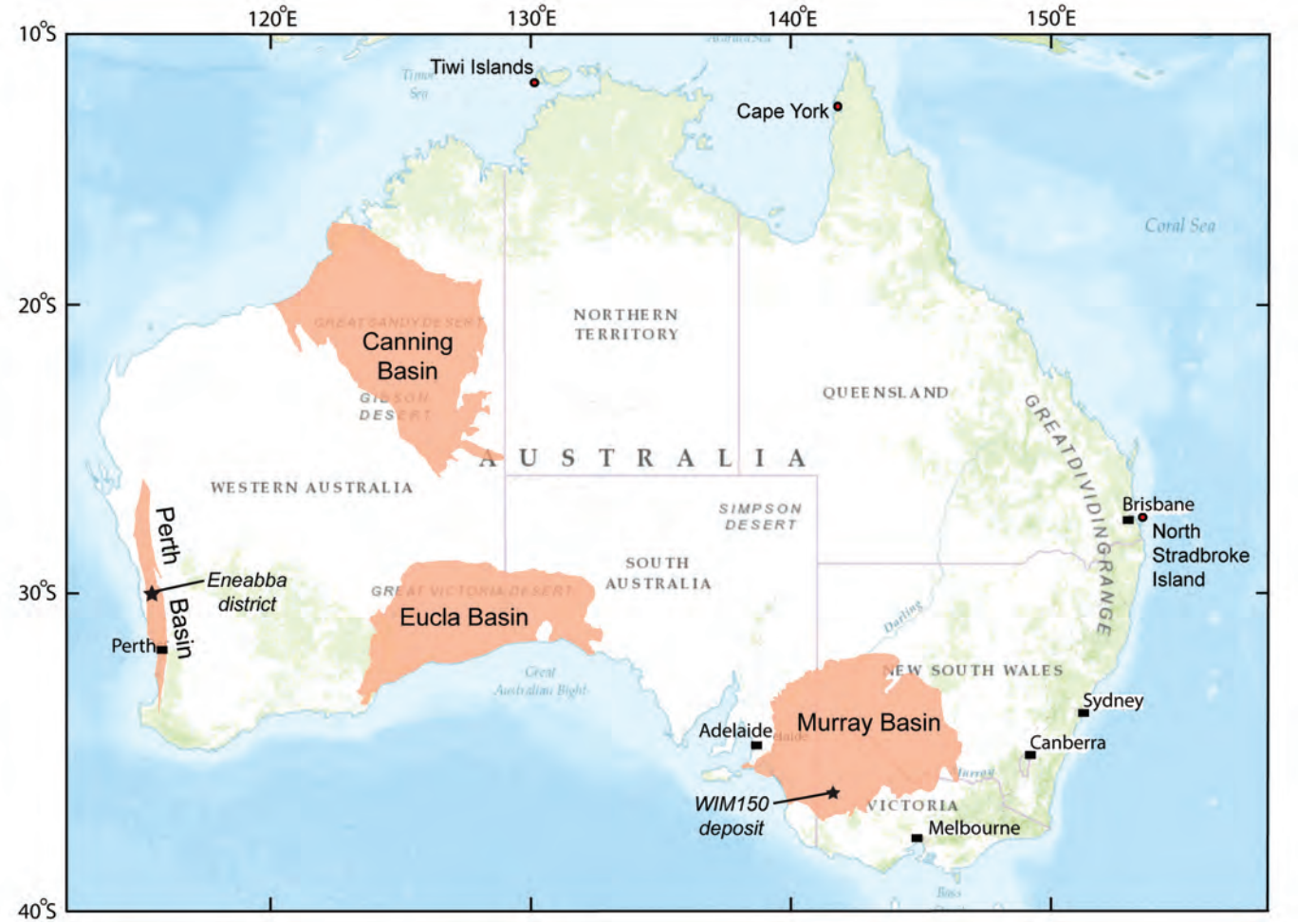

Fig. 3. Index map of Australia showing the Cenozoic sedimentary basins and other districts (red dots; Tiwi Islands, Cape York, North Stradbroke Island) that host deposits of heavy mineral sands that are currently being mined.

in the Eneabba district (Castor and Hedrick, 2006; Hoatson et al., 2011). Production of monazite in the district peaked between 1975 and 1985 (Shepherd, 1990). The source of the monazite in the ancient dune and beach sands of the Eneabba district are thought to be underlying Mesozoic sedimentary rocks, with Archean crystalline rocks of the basement being the original source (Shepherd, 1990). In the Eneabba deposits, monazite concentrations can be as much as 7% near the southern end of the barrier complex, deposited in the direction of the longshore drift near a relic headland (Shepherd, 1990). On average, heavy minerals compose about 6% of the paleoshore sands mined in this district, with monazite composing 0.5 to 7.0% of this heavy mineral suite (Shepherd, 1990). Heavy mineral production remains active today in the district, but monazite is not currently recovered as a product and is returned to the mined site. As an example of recent heavy mineral production capacity, in 2010 Iluka Resources reported a mining and processing output from their Perth basin operations of 41,500 t of rutile, 347,500 t of synthetic rutile, 255,800 t of ilmenite, and 46,200 t of zircon (Geoscience Australia, 2012).

Within the Murray basin, near Horsham in the Wimmera region of western Victoria, the WIM150 mineral sands deposit (Fig. 3) reportedly contains substantial resources of monazite and xenotime, associated with titanium minerals and zircon in the heavy mineral suite. The deposit is about 14 m thick, comprises titanium-zircon-rich sand bodies formed along a late Tertiary strandline. The mineral sands project here is in an advanced stage of premining development and permitting, with plans to recover the titanium minerals and zircon. It appears that the associated monazite and xenotime will not be exploited in the foreseeable future of this project; however, the deposit reportedly contains more than 580,000 t of monazite and 170,000 t of xenotime (O'Driscoll, 1988).

Roy and Whitehouse (2003) attributed the high concentrations of heavy minerals in strandline sands in the Murray basin to barrier sand complexes, totaling 400 km in length, which formed during Pliocene seashore progradation driven by sea-level oscillations. They suggest that the heavy minerals in the sand deposits were derived from storm and wave reworking of underlying heavy mineral-bearing Miocene sands, and that erosion and deposition were aided by growth faults.

Brazil

The monazite placers of the Brazilian coast include elevated paleobeaches, modern beaches, sand dunes, and the banks,

channels, and bars of streams that deposit sediments near the shore. Cretaceous and Tertiary sandstones that formed along paleostrandlines crop out near the modern beach; some sandstone intervals are rich in monazite, ilmenite, and zircon. These sandstones are eroded and disaggregated by high-tide waves and storm surges. These processes redeposit sand and heavy minerals into the surf zone, where the heavy minerals are again reworked and sorted by waves, longshore drift, and tides. Thus, the Cretaceous-Tertiary strandline deposits, which occur in slightly higher outcrops near the modern beach, are another source (often richer source) of monazite. According to the study of Leonardos (1974), the principal inland sources of detrital monazite along the central Brazilian coast are Archean amphibolite-granulite rocks and Cretaceous and Tertiary sedimentary rocks derived from erosion of these Archean rocks.

More than a dozen mined monazite-bearing placer districts occur intermittently along the central coast of Brazil (Overstreet, 1967; Orris and Grauch, 2002). Coastal placers that were past producers of monazite occur scattered along the coast between the city of Campos in the state of Rio de Janeiro on the southern end to the southernmost area of the coast in the state of Rio Grande do Norte on the north end (Fig. 4). Monazite was recovered as a coproduct of the more profitable titanium minerals (ilmenite, rutile) and zircon. In contrast to most heavy mineral sands operations, many of the Brazilian deposits were mined primarily for their monazite, sought foremost as a source of thorium. According to Overstreet (1967), from 1900 to 1947 Brazil exported 62,115 short tons (56,350 t) of monazite concentrate, with the monazite recovered from beach placers. Since the early 1990s, the Buena placer district (Fig. 4), which includes the Buena Norte and Buena Sol deposits, has been the only active Brazilian producer of monazite through a state-administered program (Indústrias Nucleares do Brasil SA (INB), 2013).

The coastal sand deposits of Brazil have some of the highest monazite concentrations known in the world, with as much as 8% average monazite content in some sand bodies (Overstreet, 1967). The Guarapari coastline of Espiroto Santo, near Campos (Fig. 4), is a popular tourist destination known for its white sand beaches, but this shoreline is also known for its very high level of background radioactivity due to abundant monazite. In this area, the recently and historically mined Buena Norte deposit has a reported monazite content of 0.83% (Jackson and Christiansen, 1993). Analyses of Brazilian monazites suggest that their average REE oxide content is typically around 57 to 60%, with preferential enrichment in the light REEs (Overstreet, 1967; Orris and Grauch, 2002).

Summarizing the monazite endowment in Brazil's coastal deposits state-by-state, Hedrick (1997, p. 61.4) reported the following "measured reserves" of monazite (more properly stated, "measured resources"): "Measured reserves were 16,622 tons [metric tons] grading 53.88% REOs in Bahia, 29,210 tons grading 57% REOs in Ceara, 697,382 tons grading 60% REOs in Espirito Santo, 326,766 tons grading 59.72% REOs in Minas Gerais, and 17,166 tons grading 60% REOs in the state of Rio De Janeiro." Most of these monazite resources remain. The proximity of many of these mineral-rich beach deposits to resorts and other population centers has been a major factor in restricting their development.

China

China has considerable resources of monazite within placer deposits; however, scant information on the characteristics and production of these resources has been published. Jackson and Christiansen (1993) reported that China produced 10,200 t REOs from placer deposits in 1989. Since that time, rare earth production from placer deposits in China is unavailable.

Some of the productive monazite-bearing placer districts in China (Jackson and Christiansen, 1993; Orris and Grauch, 2002) are as follows:

1. Beihei district, located near 21° 29' N, 109° 06' E in the Guangxi province. A mixture of river and marine placers along the coast, containing about 1.5% heavy minerals comprised of ilmenite, rutile, zircon, and monazite. A producer of by-product monazite.
2. Dianbai district, located near 21° 30' N, 111° 01' E in the Guangdong province. Placers on the coast, containing about 2.3% heavy minerals comprise ilmenite, rutile, zircon, and monazite. A producer of by-product monazite.
3. Haikang district, located near 20° 56' N, 110° 04' E in the Guangdong province. A mixture of river and marine placers that contain ilmenite, zircon, rutile, monazite, and xenotime. A producer of by-product monazite.
4. Nanshanhai district, located near 21° 32' 45" N, 111° 40' 00" E in the Guangdong province. Coastal placers that contain ilmenite, zircon, rutile, monazite, and xenotime. A producer of by-product monazite.
5. Sai-Lao, Wuzhaung, and Xinglong placer districts, all located on Hainan Island (see Orris and Grauch, 2002). These placers contain ilmenite, zircon, anatase, cassiterite, monazite, magnetite, and chromite. Producers of by-product monazite.
6. Xun Jiang district, located near 23° 30' N, 110° 50' E in the Guangxi province. River deposits containing 6.0% heavy minerals comprise ilmenite, rutile, zircon, and monazite.

India

The history of placer deposits as a source of economic minerals began with the discovery of monazite in the beach sands of Manavalakurichi (Tipper, 1914) in southernmost India (Fig. 2). The beach sands were first worked in 1911 and subsequently were rapidly developed with the establishment of the TiO_2 (titania) pigment industry in Europe and America. However, by the 1950s ilmenite production saw a sudden decrease in India. This was in part due to the discoveries of new deposits in Australia and Canada, compounded by the presence of undesirable impurities, such as chromium and ferric iron, in Indian ilmenite. However, after nationalization of all the major deposits in India, the national production of ilmenite and rutile has increased over the years. The current production rate is about 140,000 t of ilmenite and 6,000 t of rutile. Governmental concerns, such as the Indian Rare Earths Ltd. and Kerala Minerals and Metals Ltd., are involved in the production and marketing of the placer minerals.

Over the last few decades new deposits have been discovered in coastal placers of India, such as Chhatrapur in Orissa and Visakhapatnam in Andhra Pradesh along the east coast, and Ratnagiri in Maharashtra on the west coast of the country (Fig. 2). Along the coastal stretches of Tamil Nadu, deposits

Fig. 4. Index map showing monazite-producing placer deposits (red squares) along the central coastline of Brazil. The active monazite producer is the Buena district (Indústrias Nucleares do Brasil SA (INB), 2013), the southernmost placer district shown in the map.

of heavy minerals occur in the inland areas in the form of teri sands, also known as red sands in Tamil Nadu (Babu et al., 2009). The current reserves of the placer minerals in India are as follows: 278 Mt ilmenite, 13.49 Mt rutile, 18 Mt zircon, 7 Mt monazite, 84 Mt sillimanite, and 86 Mt garnet (Raju et al., 2001).

The major placer concentrations of India are located along the east and west coasts (Fig. 2). For example, detrital monazite occurs in ilmenite-bearing heavy mineral sands of Chavara and Manavalakurichi, as well as less extensive detrital monazite deposits in parts of coastal Orissa, Andhra Pradesh, and Tamil Nadu. Thus, the Eastern Ghats group of rocks have been more widely spread, though as localized deposits, in comparison to sediments derived from the Western Ghats group, which is mostly concentrated in Kerala. Apart from these coastal placers, there are numerous inland placers in Maharashtra. These deposits generally occur in stream segments with low current velocity, such as point bar deposits, within ripple marks, around submerged bars, or in narrow zones at the bottom of a stream.

The heavy mineral content of beach placers along the southern coast of Orissa primarily depends on the nature of the hinterland rocks present in the region. The source rocks are dominated by granulite facies of khondalites, charnockites, and leptynolites (Mohanty et al., 2003b), plus the presence of granite intrusions, pegmatites, quartz veins, and metasediments. Based on the thorium oxide concentration in the monazite sands, it was inferred that the monazite grains were derived primarily from the granulite-facies metamorphic rocks belonging to the Eastern Ghats group of rocks (Mohanty et al., 2003b). Radioactive elements thorium (Th) and uranium (U) and rare earth elements (lanthanum (La), cerium (Ce), praseodymium (Pr), neodymium (Nd), and samarium (Sm)) are highly enriched in the monazite sands of coastal Orissa. Ilmenites are the major heavy minerals and constituite about 65 to 80% of the total heavy mineral assemblage (Mohanty et al., 2003b). Earlier studies (Mohanty et al., 2003a) suggest that the ilmenite grains are derived from higher grade (granulite-facies) metamorphic rocks. The important feature observed commonly in the monazites is the abundance of total REE as compared to the actinides; additionally, the monazites are enriched in La, Ce and Nd. The greater content of yttrium oxide (Y_2O_3) has been attributed to the garnet-free paragenesis (Mohanty et al., 2003a).

In extensive studies undertaken along peninsular India, especially along the eastern and western coasts, in addition to the marine regressions and transgressions during the Quartenary the rivers also play a significant role in beach placer development (Prakash et al., 1991; Mohanty et al., 2004; Sengupta et al., 2005). Three factors responsible for placer mineralization, especially the radioactive minerals, are (1) their distribution in the hinterland rocks, (2) geologic controls due to presence of rivers attributed to its morphology, and (3) structures that control the drainage patterns (Sinha-Roy, 1982). This implies the significant role of weathering and transport in the formation of heavy mineral placers. This relationship is true for not only the placer mineralization along the Western Ghats group of rocks, especially the southern coast of Kerala, such as the Chavara placer deposit, but also in the Eastern Ghats (Prakash et al., 1991). The latter comprises rich placer deposits along the southern Orissa coast, such as the Erasama (Fig. 5) and Chhatrapur deposits (Fig. 6). The southern rivers in Kerala, India, for example, the Neyyar, Karamana, and Vamanapuram Rivers, carry enhanced concentrations of heavy minerals (that include radioactive minerals) into the pensisular region, aided by the southwestern monsoon (Prakash et al., 1991). In Tamil Nadu, extensive studies of zircons in placer deposits located along the southern coast show the zircons are enriched in REEs, especially europium (Eu) and (Ce); this indicates that the bedrock source for the zircons was primarily charnockites (Angusamy et al., 2004). In a similar manner, the role of Rushikulya River, in the Ganjam district, southern coast of Orissa (Fig. 7), aided in the formation of the rich placer deposits sourced from the Eastern Ghats group of rocks for Chhatrapur placers. Additionally, high-grade metasedimentary rocks along the hinterland, transported by the Mahanadi River drainage basin, formed the Erasama placer deposit (Mohanty et al., 2004; Sengupta et al., 2005). For the Eastern Ghats group of rocks, it has been observed that charckonites and the khondalites are primarly responsible for the enhanced concentration of thorium as compared to uranium. Along the Eastern Ghats there are major and notable heavy mineral placers, located in the States of Tamil Nadu, Andhra Pradesh, and Orissa, respectively (Ali et al., 2001; Mohanty

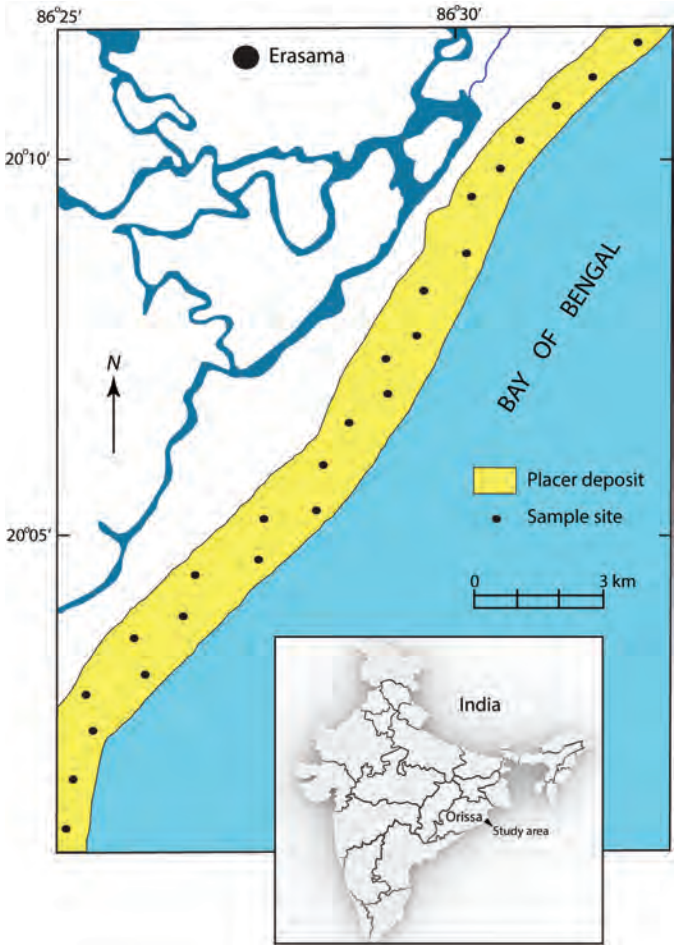

Fig. 5. Map showing the sample locations in the Erasama beach placer deposit, Orissa, India (after Mohanty et al., 2004).

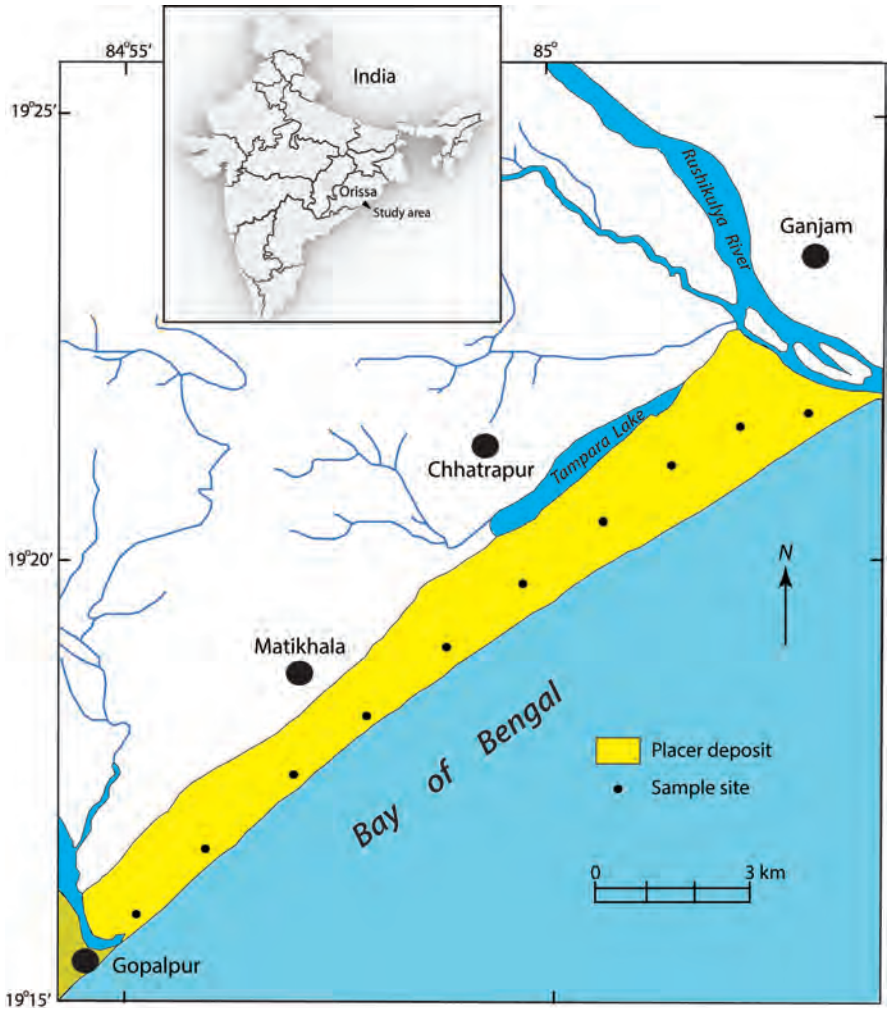

Fig. 6. Map showing sample locations in the Chhatrapur beach placer deposit, Orissa, India (after Mohanty et al., 2004).

et al., 2003b). Recent studies indicate that the Eastern Ghats group is the major source for the heavy mineral assemblage observed in the placer deposits (Raju et al., 2001). The heavy mineral placers both in the eastern and western part of India are highly enriched in thorium (Mohanty et al., 2003a, b, 2004; Sengupta et al., 2005).

Malaysia

Prior to the domination of global yttrium production by China in the late 1980s, xenotime-bearing alluvial placer deposits in Malaysia were the largest sources of yttrium in the world (Castor and Hedrick, 2006). The sources within Malaysia are alluvial tin placer deposits, which carry considerable cassiterite accompanied by ilmenite, monazite, and xenotime. Recently, tailings produced from past tin placer mining have been reprocessed to recover monazite and xenotime. In this manner, 350 t REOs were produced from Malaysia in 2012 (Gambogi, 2013).

Sri Lanka

Modern beach deposits on the northeastern coast of Sri Lanka have some of the highest concentrations of heavy minerals in the world. Beach sands of this region are mined and processed by Lanka Minerals Sands Ltd. (2013), a company owned by the Government of Sri Lanka, and the successor to Ceylon Mineral Sands Corp. The company's primary mining operations and processing plants are located just east of Pulmoddai on the northeast coast of Sri Lanka (Fig. 2). Products from the beach sands are ilmenite, rutile, and zircon; sillimanite, monazite and garnet also exist, with monazite reportedly composing 0.3% of the heavy mineral fraction (Herath, 1990). According to the company, in some stretches of beach the heavy minerals can compose as much as 90% of the sand deposits; ilmenite forms 65% of the heavies, rutile forms 10%, and zircon forms 10% (Lanka Minerals Sands Ltd., 2013). Heavy mineral-rich beach sands extend along the shore about 8 km south from Kokkilai Lagoon (Fig. 2) and they extend inland from the ocean for about 370 m. The stretch of beach that extends about 40 km north and south of Pulmoddai in northeastern Sri Lanka represents one of the richest deposits of heavy mineral sands in the world (Lanka Minerals Sands Ltd., 2013).

Monazite-bearing alluvium in southwestern Sri Lanka, specifically stream sediments of the Bentota River, have been described as "one of the world's most thorium rich sediments" (Rupasinghe et al., 1983, p. 1). Monazite is carried by this river system into seasonal beach sand deposits at Kaikawala

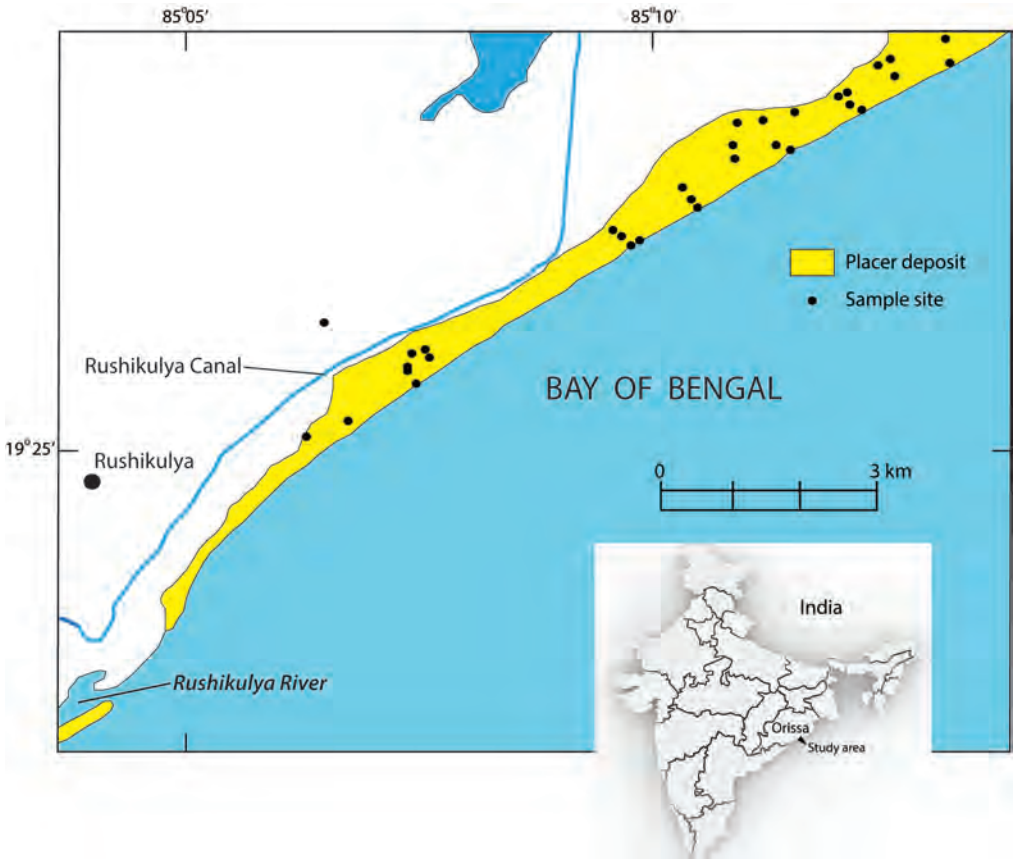

Fig. 7. Index map of the Rushikulya beach placer deposit along the Orissa coast, southeast India, showing sample locations (after Sulekha Roa et al., 2009).

and Beruwala. Monazite was once mined on a small scale at Kaikawala beach. Analyses of these monazites by Rupasinghe et al. (1983) found them to be highly enriched in the light REEs relative to the heavy REEs, with a negative Eu anomaly when normalized to chondrite values (Rupasinghe and Dissanayake, 1984).

Thailand

Tin (in cassiterite) has been mined from alluvial placers in Thailand for over 1,000 years, but much more recently they initiated by-product recovery of monazite (starting in 1969), ilmenite (in 1976), and xenotime (in 1977; Economic and Social Commission for Asia and the Pacific, 2001, p. 72–74). Production of REOs from Thailand decreased steadily from the 1980s to 1995, which was their last year of significant monazite and xenotime production. Similar to the Malaysian rare-earth resources, in Thailand the monazite and xenotime are recovered as by-products from the retreatment of earlier processing plant tailings derived from tin placers. The host tin placers, those enriched in monazite and xenotime, are alluvial deposits that were mined by gravel pump; these deposits occur mainly in southern Thailand (shown in Economic and Social Commission for Asia and the Pacific, 2001, p. 72–74).

United States

Monazite-bearing, heavy mineral placers of both alluvial and coastal origins are well known in the United States. Some of these placers produced modest tonnages of monazite in the past. A century ago, monazite was produced from alluvial placers in mountain valleys of North Carolina and South Carolina, and during the 1950s monazite was recovered from stream alluvium in mountain valleys of central Idaho. As recently as 1994, heavy mineral sands deposits in Florida, which formed along Pliocene and Pleistocene strandlines, were worked for titanium minerals and zircon but also produced monazite as a coproduct. As of 2014, monazite is not recovered at an active placer operation in the United States.

Monazite-brearing alluvial placers in North and South Carolina: In 1887, a few short tons of monazite were produced from stream deposits in the Piedmont region of North and South Carolina, giving this region the distinction of being the world's first supplier of thorium (Olson and Overstreet, 1964). Monazite-bearing placers of this region were worked by small-scale sluice operations from 1887 to 1911 and 1915 to 1917, producing a total of about 5,000 t of monazite (Overstreet et al., 1968). Monazite mining ended here in 1917, not because reserves had been exhausted, but rather because the beach deposits of India and Brazil were producing thorium at lower cost.

The high-grade monazite placers of the Piedmont of North and South Carolina occur between the Catawba River in the northeast and the Savannah River in the southwest (Fig. 8). The stream-sediment deposits across this region are generally consistent in character; the heavy mineral concentrations

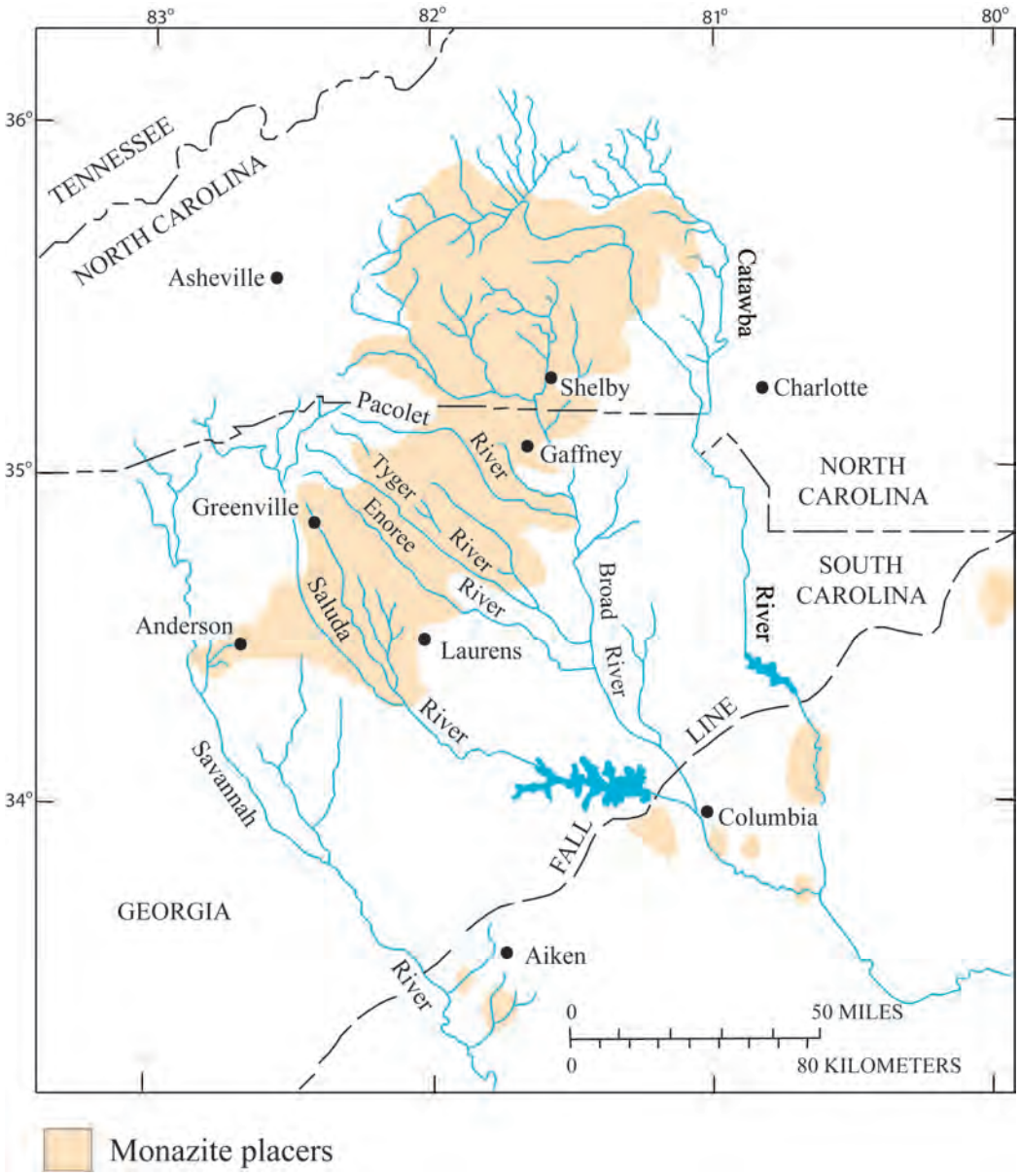

Fig. 8. Map of monazite-bearing alluvial placers in North and South Carolina, United States. Modified from Staatz et al. (1979).

are greatest in the headwaters areas. Stacked layers of unconsolidated sediments of gravel, sand, clay, and clayey silt form an average total thickness of about 4.5 m (15 ft; Staatz et al., 1979). Monazite typically occurs in all units, but is generally most abundant in the basal gravel layers and least abundant in the clay layers. Dredging in this region between the summers of 1955 and 1958 (Williams, 1967) found heavy mineral contents of about 1 to 1.5%, with monazite forming about 8% of this fraction (Mertie, 1975). Overall, these dredging operations recovered monazite, ilmenite, rutile, zircon, and staurolite (Williams, 1967).

According to Staatz et al. (1979), the heavy mineral content of the placer deposits of the Piedmont region ranges from 0.15 to 2.0%, with monazite forming about 3.5 to 13% of the heavy minerals. Other parts of the heavy mineral fraction include ilmenite, 20 to 70%; garnet, 2 to 50%; rutile, 0.3 to 7%; zircon, trace to 14%; and sillimanite and kyanite together, trace to 20%. In some Piedmont placer deposits, additional heavy minerals include epidote, magnetite, xenotime, tourmaline, sphene, staurolite, andalusite, and an unidentified black radioactive mineral (Staatz et al., 1979). Analysis of 52 samples of alluvial monazite from this region (Mertie, 1975) found that the monazite contains 60 to 63% total REE oxides and 2.5 to 7.8% Th oxide content, with a mean value of 5.67% Th.

The Piedmont region of the southeastern United States is underlain by crystalline, high-grade metamorphic rocks intruded by quartz monzonite and pegmatite. The monzonite and pegmatite intrusions vary from monazite-bearing to monazite-free. Overstreet (1967) suggested that the primary

source of the alluvial monazite was the high-grade metamorphic rocks, particularly sillimanite schist.

Monazite alluvial placers in Idaho: At least 11 monazite-bearing placer districts exist in the valleys of a region extending north of Boise, Idaho, and along the western flank of the Idaho batholith (Fig. 9). Monazite was first recognized here in 1896, as the heavy, yellow to brownish-yellow mineral that collected with other heavy minerals and gold within the sluice boxes of gold placer operations in the Boise basin near Idaho City, Centerville, and Placerville (Lindgren, 1897). In 1909, a mill designed to capture the monazite was built by the Centerville Mining and Milling Co. Only a small amount of monazite concentrate was produced for its Th content before the mill burned down in a forest fire in 1910.

In the 1950s, two areas of west-central Idaho were mined by dredges for monazite recovery—Long Valley and Bear Valley (Fig. 9). Beginning in September 1950, Long Valley was worked by three dredges that were earlier used to recover gold but later converted to recover monazite. The dredges were redesigned for monazite recovery with assistance from the U.S. Bureau of Mines under the sponsorship of the U.S. Atomic Energy Commission. The history of these dredging operations is described by Argall (1954) and Staatz et al. (1980, p. 9–16, and references cited therein). The heavy minerals recovered in the Long Valley district were dominated by ilmenite (84% of heavies), followed by monazite (8%), garnet (5%), and zircon (3%). During this five-year period, Staatz et al. (1980) estimated that the three dredges recovered 6,430 t

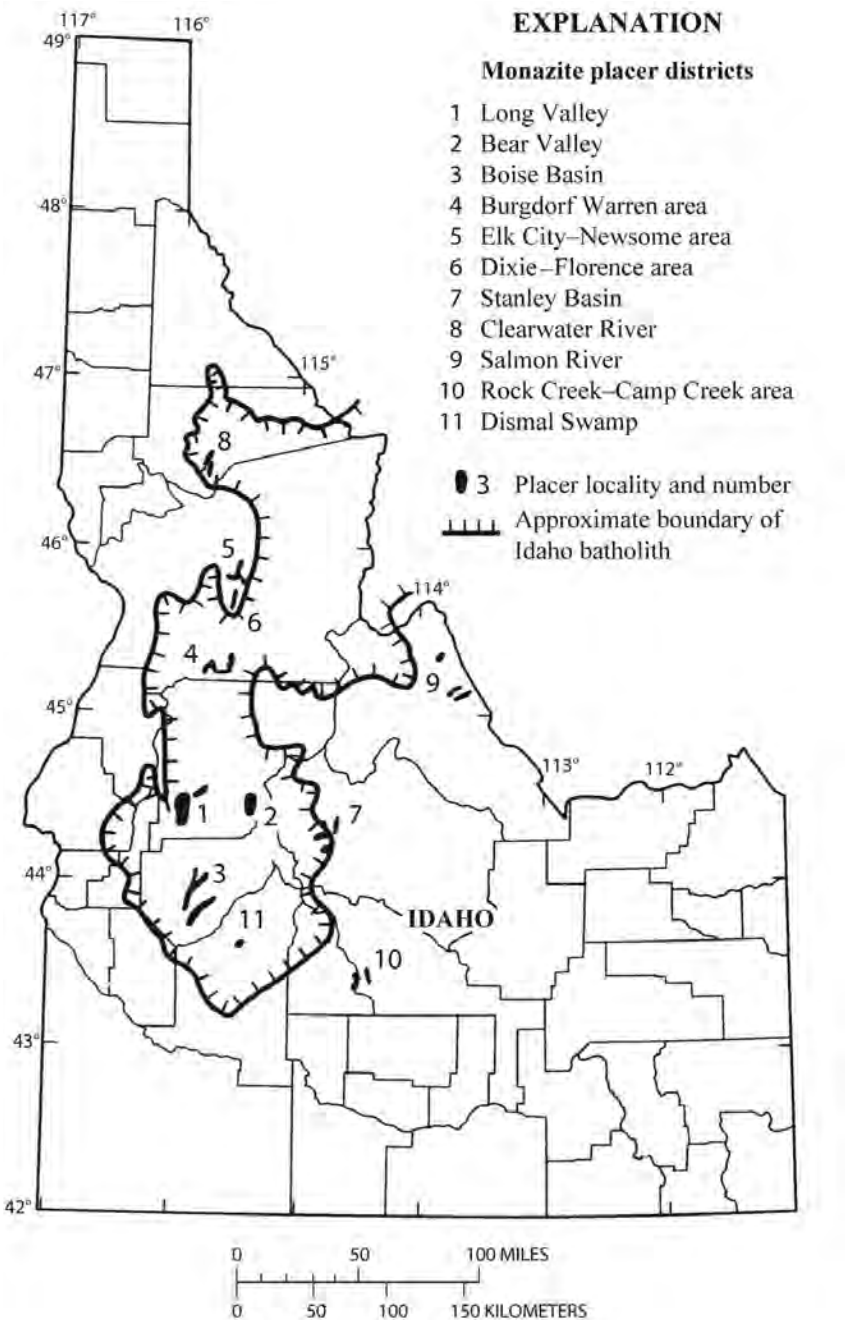

Fig. 9. Generalized map of known monazite-bearing alluvial placer districts in Idaho. Modified from Staatz et al. (1980).

of monazite. The dredging ended here in mid-1955, when the government stockpile order was fulfilled.

Rare earth elements and thorium were also unintentionally recovered within the minerals euxenite and monazite from the Bear Valley placers. The Bear Valley placers were worked by first one dredge in 1955, then a second in 1956, with the intent to recover niobium (Nb) and tantalum (Ta) for another federal government contract. According to Staatz et al. (1980, p. 10), "from alluvium of Bear Valley, 2,049 short tons [1,858 metric tons] of euxenite, 83.5 tons [75.7 metric tons] of columbite, and 54,862 tons [49,760 metric tons] of ilmenite were recovered." No records of the monazite recovery were kept.

The U.S. Geological Survey (Staatz et al., 1980) determined that the five most important monazite districts in Idaho are Long Valley, Bear Valley, the Boise basin, the Burgdorf Warren area, and the Elk City-Newsome area (Fig. 9). The reported thorium oxide contents of monazite in the Idaho placer deposits range from 2.2 to 6.24%. Only a few analyses for REE were conducted on monazites from Idaho placers, which indicated these monazites contain 63% total REE oxides. Staatz et al. (1980) calculated thorium reserves for each of the five major placer districts individually, indicating the five districts have total reserves of about 9,130 t of Th oxide. The REE resources of the five placer districts would presumably be at least 10 times the Th resource, because the typical monazite contains about 63% total REE oxides and 2.2 to 6.24% Th oxide.

The primary source of the resistant REE-thorium-bearing minerals in the Idaho placers is thought to be the Idaho batholith, in particular the quartz monzonite and pegmatite phases of the batholith (Mackin and Schmidt, 1957). The most common heavy minerals in the alluvial deposits (in generally decreasing amounts) are ilmenite, magnetite, sphene, garnet, monazite, euxenite, zircon, and uranothorite (uranium-rich thorite).

Monazite-bearing coastal sands in northeastern Florida: Modern beach sands near Mineral City (now known as Ponte Vedra) were mined chiefly for ilmenite from 1916 to 1929 (Staatz et al., 1980), about 1 km west of the ocean and just east of Jacksonville. Reportedly one short ton (0.9 t) of monazite was produced in 1925 (Staatz et al., 1980).

From 1943 to 1968, the Rutile Mining Co. recovered ilmenite, rutile, zircon, and small amounts of monazite from Pleistocene and Pliocene beach sands just east of Jacksonville.

The Riz Mineral Co. mined dune sands near Vero Beach from the early 1940s until 1955, recovering ilmenite, rutile, zircon, and monazite (Staatz et al., 1980).

A variety of companies mined and processed Pleistocene beach deposits at Green Cove Springs to recover their heavy minerals, particularly titanium minerals and zircons (the Duval Upland ridge deposit); these deposits are located south of Jacksonville and west of St. Johns River. Reportedly, about 500 t of monazite per year were recovered as a coproduct from the Green Cove Springs deposits (Castor and Hedrick, 2006). Recently, Iluka Resources resumed mining from this deposit to recover titanium minerals and zircon; they ended their mining activities there in 2005 and the site is now being reclaimed by the company. The deposits at Green Cove Springs contained an average of 3% heavy minerals, which included ilmenite, leucoxene, rutile, zircon, and monazite (Staatz et al., 1980).

From 1974 to 1978, Humphrey Minerals mined a Pleistocene beach deposit near Boulogne in northeastern Florida. This ore body averaged about 4% heavy minerals; titanium minerals, zircon, and monazite were recovered. Reportedly, monazite composes 0.3 to 0.4% of the heavy mineral assemblage in this deposit (Staatz et al., 1980). This Pleistocene shoreline facies extends to the north into Georgia, where this unit was earlier mined by the same company at nearby Folkston, Georgia.

Industrial Mineral Commodities in Heavy Mineral Placers

Placer deposits are the main source of titanium feedstock for the titanium dioxide (TiO_2) pigments industry (Murphy and Frick, 2006), through recovery of the minerals ilmenite ($Fe^{2+}TiO_3$), rutile (TiO_2), and leucoxene (an alteration product of ilmenite). Heavy mineral sands (placers) are also the principal source of zircon ($ZrSiO_4$), which is often recovered as a coproduct. Other heavy minerals produced as coproducts from some deposits are sillimanite/kyanite, staurolite, monazite, and garnet.

Prior to full-scale mining and production from the Mountain Pass carbonatite deposit, California, in the mid-1960s, alluvial placers were the primary source of rare-earth elements for the world. Today, deposits of monazite [$(Ce,La,Nd,Th)PO_4$], mainly in beach placers, are again sought as a source of rare earth elements as well as thorium, most particularly at several coastal sand deposits in southern India. The processed Th is to be used in Th-based nuclear power under development in India and elsewhere.

Ore and Gangue Mineralogy

Heavy mineral-rich placer deposits encompass a wide range of minerals with varying values of specific gravity. They have been generally classified (Emery and Noakes, 1968) as placers that contain: (1) "very heavy" minerals with specific gravity between 6.8 and 21, such as cassiterite and native gold; (2) "light" heavy minerals with specific gravity between 4.2 and 5.3, such as ilmenite, rutile, monazite, xenotime, and zircon; and (3) minerals with densities between 2.9 and 4.1, such as garnet, sillimanite, and hypersthene. Folk (1980) divided the heavy minerals into four groups, based on their physical and chemical nature—opaques, micas, ultrastables, and metastables.

The economic heavy minerals in placer deposits are especially durable and resistant to chemical breakdown, and thus survive the torturous journey from the bedrock source area to the site of deposition, as distant as the coast or the sea (offshore deposition). The suite of heavy minerals most commonly includes Ti-bearing minerals (ilmenite, rutile, and leucoxene) and zircon, and can also contain sillimanite/kyanite, staurolite, monazite, garnets, xenotime, and others. In the vast majority of economic heavy mineral coastal deposits ("heavy mineral sands"), ilmenite is the most abundant heavy mineral and the principal ore mineral, followed by rutile, leucoxene ("altered ilmenite"), and zircon. Together, ilmenite, rutile, and zircon often compose more than 80% of the heavy mineral suite. Other heavy minerals that are sometimes recovered as economic coproducts include garnets, sillimanite, staurolite, cassiterite ("tin placers"), monazite, and xenotime. Economic

deposits can contain less than 1% heavy mineral content, but composite grades are usually more than 2% and locally can exceed 10%. The economic viability of a heavy mineral sand deposit is dependent on the interplay of many factors, such as its location, depth, size, heavy mineral grade and mineralogy, and market prices.

Resources of REEs in placer deposits occur principally in monazite [$(Ce,La,Nd,Th)PO_4$], as a source of light REEs, and/or xenotime (YPO_4), as a potential source of Y and heavy REEs. The light minerals (gangue) in heavy minerals sands are dominated by quartz sand, clay minerals, and silt-size quartz and iron-oxide minerals. Feldspars are typically minor or absent constituents. Carbonate minerals are rare.

Mineralogical characteristics in beach placer deposits vary from region to region depending on the host rocks, their provenance, ambient climate, mechanism of transport, and the hydraulic conditions during the depositional stage (Borreswara Rao, 1957; Force, 1976, 1991). The roles of aeolian and marine processes along with the local hydrodynamic conditions and coastal geomorphology have a dominant role in the distribution of the placer minerals, as demonstrated along coastal Orissa, India (Komar and Wang, 1984).

Geochemistry

Trace elements associated with heavy mineral placers primarily include Ti, Hf, the REEs (such as La, Ce, Pr, Nd, Sm, Eu, Gd, Tb, Dy, Ho, Er, Tm, Yb, and Lu) and Y, Th, and U. These elements have been used from the analyses of stream sediments to evaluate the presence of heavy mineral sands on a regional scale (e.g., Grosz, 1993). These pathfinder (exploration) elements reflect the composition of the potentially economic heavy minerals of this deposit type, including ilmenite ($FeTiO_3$), rutile (TiO_2), zircon ($(Zr,Hf,U)SiO_4$), monazite ($(La,Ce,Th,U)PO_4$), and xenotime (YPO_4). Monazite is preferentially enriched in the light REEs relative to the heavy REEs (Fig. 10).

Variation in chemistry at a deposit scale most likely indicates the variations in heavy mineral content rather than geochemical gradients due to hypogene, hydrothermal, or supergene processes. Hydrothermal alteration and other forms of geochemical diffusion that are typical of most ore deposits are not associated with heavy mineral sands.

The thorium to uranium ratio is useful in the recognition of "geochemical facies" (Macfarlane et al., 1990) and a possible indicator of oxidizing and reducing conditions (Adams and Weaver, 1958; Anjos et al, 2006). Average equivalent Th/equivalent U (eTh/eU) ratios for Gopalpur and Rushikulya beach samples, India (Figs. 6, 7), are observed to be in the range of 22 to 49 (Fig. 11). Both sets of beach samples lie in heavy mineral and clay mineral fields, indicating a generally higher presence of thorium in Gopalpur and higher potassium in Rushikulya. This could be attributed to adsorption and the chemical composition in this region (Doveton and Presnky, 1992). The detailed mechanism has been discussed by Sulekha Rao et al. (2009).

Higher concentrations of radioactive elements (Th, U) and REEs (La, Ce and Nd) have been observed in the monazite sands of Chhatrapur, India (Mohanty et al., 2003a). The chondrite-normalized REE distribution pattern of the monazite grains indicated uniformly enriched light REEs, which has been attributed to the preferential incorporation of lighter lanthanides formed during partial melting. The majority of the beach samples studied fall in both heavy minerals and clay mineral fields (Fig. 11). However, samples of beach sands from Gopalpur fall primarily in the heavy minerals field while Rushikulya beach samples plot mainly in the clay minerals field, indicating that both Th and K are associated with clay minerals due to adsorption and chemical composition (Doveton and Presnsky, 1992).

Most of the earlier studies on monazite REE chemistry are either related to igneous or metamorphic rocks, with few studies reported on placers. Geochemical studies of the REE

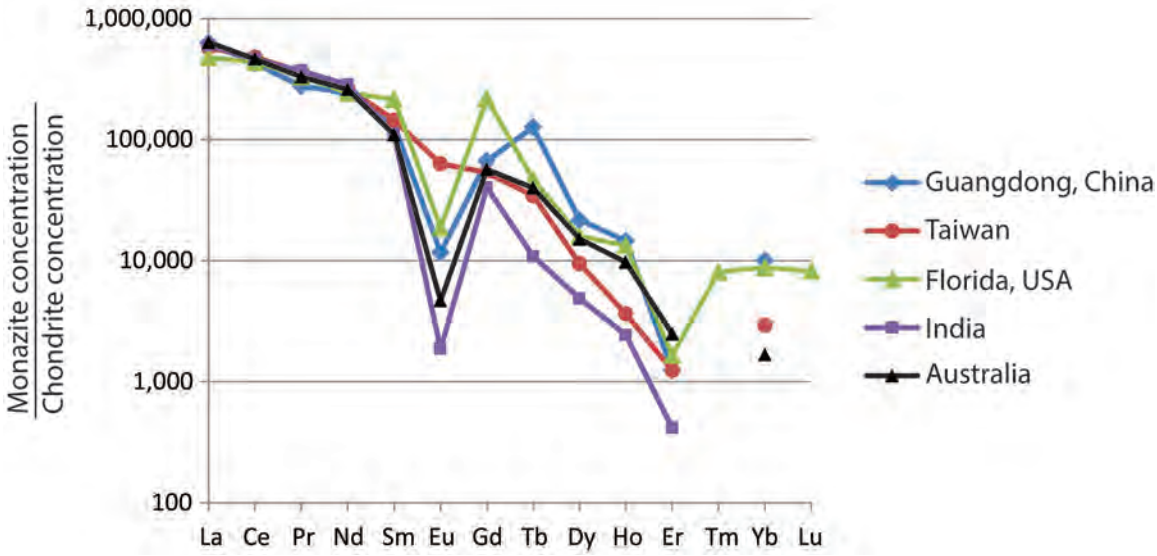

Fig. 10. Chondrite-normalized plot showing the REE distribution in selected monazites separated from heavy mineral sands deposits from a few continents. Chondrite-normalized europium values that lie below the trend of the other REEs are typical of monazite, but are not universal, as displayed by the monazite sample from a heavy mineral sand deposit in Taiwan. Data from Mukherjee (2007). Chondrite REE concentrations from Boynton (1984).

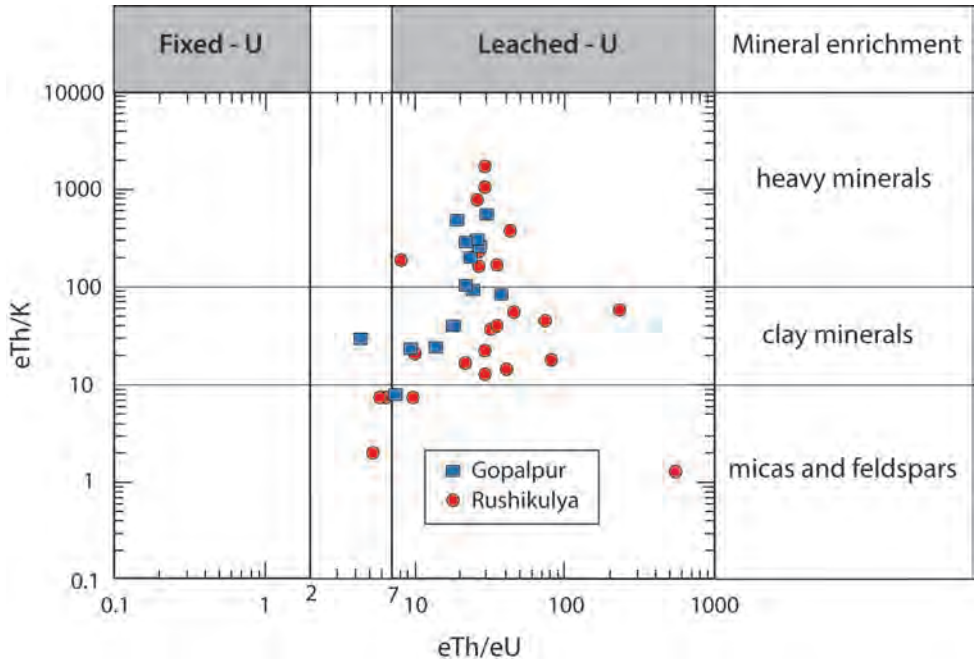

Fig. 11. Discrimination diagram plot of eTh/eU vs. eTh/eK in bulk sand samples collected from the Gopalpur and Rushikulya beach placer deposits, Orissa, India. The vertical bars represent values of eTh/eU = 2 or 7. Diagram modified from Sulekha Rao et al. (2009).

chemistry in placers are important because sustained mining of placer deposits depletes their reserves. An important additional aspect is to utilize better techniques for enhanced recovery of the REEs from beach washings.

Typically, monazite extracted from beach placers is preferentially enriched in the light REEs. Dawood and El-Naby (2007) reported light REE enrichment from Sinai beach, Egypt. This monazite is sourced primarily by pegmatites and granites. The chondrite-normalized REE pattern from zircons (Fig. 12) of the Kanayakumari beach areas, located on the southernmost tip of India, exhibits light REE enrichment compared to heavy REE as well as Ce and Eu anomalies (Angusamy et al., 2004); these monazites are thought to be sourced by charnockites. Chhatrapur monazite placers in Orissa, on the east coast of India (Fig. 6), also show similar trends of light REE enrichment in zircons (Fig. 13) relative to heavy REEs as well as an Eu anomaly (Mohanty et al., 2003b). Chondrite-normalized REE fractionation patterns for the lunar and terrestrial monazite indicate that the light REEs (ie., La to Sm) are highly enriched relative to heavy REEs (i.e., Gd to Lu; Lovering et al., 1974).

Genesis of Heavy Mineral Placers

Whether the ultimate deposition of the heavy mineral-rich sediments occurs in an alluvial or coastal setting, the processes that form these deposits begin inland. High-grade metamorphic rocks (of amphibolite facies and higher) and a variety of plutonic igneous rocks are the principal sources of heavy minerals, including monazite. These bedrocks weather and erode, contributing detritus composed of sand, silt, clay, and heavy minerals to fluvial systems. Streams and rivers carry the detritus to the coast, where they are deposited in a variety of coastal environments, including deltas, the beach face (foreshore), nearshore, barrier islands, dunes, or tidal lagoons, as well as the channels and floodplains of streams and rivers in the coastal plain. The sediments are worked by the actions of waves, tides, longshore currents, and wind, which are effective mechanisms for sorting the mineral grains based on differences in their size and density. The finest-grained, most dense heavy minerals are the most effectively sorted. The result is that heavy minerals accumulate together, forming laminated or lens-shaped packages of sediments several meters and as much as tens of meters thick that are rich in heavy minerals. Generally, economic deposits of heavy mineral sands contain at least 1% total heavy mineral content. Most economic deposits of coastal heavy mineral sands (coastal placers) are Paleogene, Neogene, and Quaternary deposits, as well as some modern coastal deposits.

Factors influencing the formation of placer deposits

Climate: Climate influences the weathering processes, and ultimately decomposes the rock matrix and liberates the minerals. Tropical to subtropical climates promote chemical weathering, which has given rise to a decomposed stage of crystalline rocks called laterites. This could be considered as the preconcentration process of the placer minerals. Most of the rich, modern placer deposits of the world are in tropical regions.

Drainage pattern: Fluvial processes act as a conductor of sediment transport from the source rock to the zone of concentration. The erosive power of rivers is strong, releasing heavy minerals from the parent rock and transporting them downstream. For example, in the Kerala State of southwestern India, west-flowing rivers with steep gradients were the major agent of erosion and transportation of sediments to the Arabian Sea.

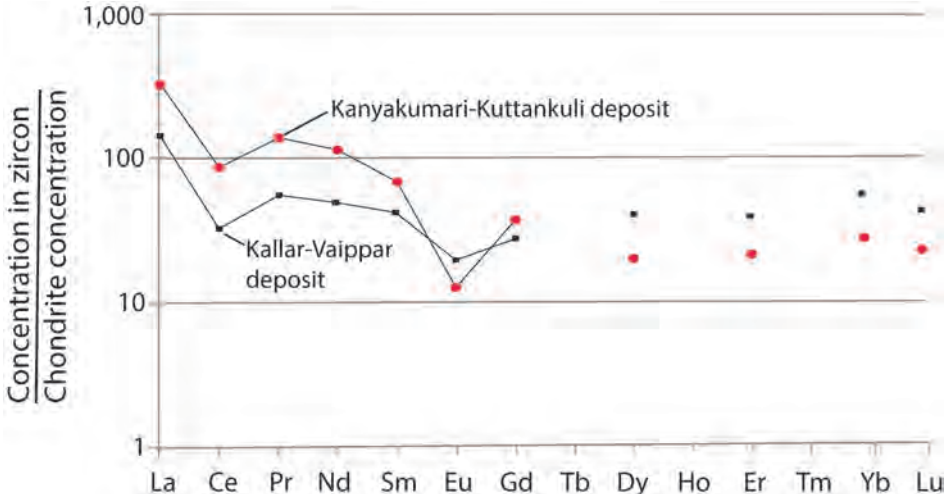

Fig. 12. Chondrite-normalized pattern of REEs in zircons from Kanyakumari beach placers, showing Ce and Eu anomalies (Angusamy et al., 2004).

Coastal processes: Beach deposits result from the interplay of coastal hydrodynamics of rivers, waves, and currents. The direction and strength of the coastal currents along with the geomorphology of the coast, sometimes influenced by localized faulting, determine the location of the deposit. Strong, sustained wave action moves sand from offshore to the shore. Waves sort out the heavy minerals based on their size and specific gravity, respectively. Studies suggest that mineral sorting occurs mainly on the upper part of the high-tide swash (wave) zone. Fine-grained sands and heavy minerals on the foreshore (beach face) can be remobilized by winds, forming heavy mineral-rich sand dunes behind the beach. Sea-level changes are a function of climatic changes, such as ice ages. Rises in regional sea level (transgression) and fall of sea level (regression) strongly influence the deposition and preservation of heavy mineral sands, both along the strandline and inland fluvial deposits. Major episodes of heavy mineral sands accumulation have been linked to seaward progradation of the shore during regression events as well as prolonged transgressive events.

Exploration Considerations

Beach placer deposits—also referred to as "heavy mineral sands"—are well known from different parts of the world (Mero, 1965). Discoveries of beach placer deposits occurred along the Brazilian coast (Da Silva, 1979), China (Highley et al., 1988), Egypt, France, Bangladesh, and Iran (UNSCEAR, 1993). The beach placer deposits have primarily been investigated for their economic resources of heavy minerals, in particular ilmenite, rutile, zircon, sillimanite and garnet, apart from monazite and zircon and their actinide and rare-earth elements. Two basic criteria provide the foundation for locating significant deposits of heavy mineral sands (placers) in coastal environments: (1) identify bedrock terranes that contain abundant high-grade metamorphic rocks or igneous rocks; and (2) identify ancient or modern coastal plains sourced by streams and rivers that drain these terranes.

For several decades, the mineable (economic) deposits of heavy mineral sands are those formed during the Paleogene,

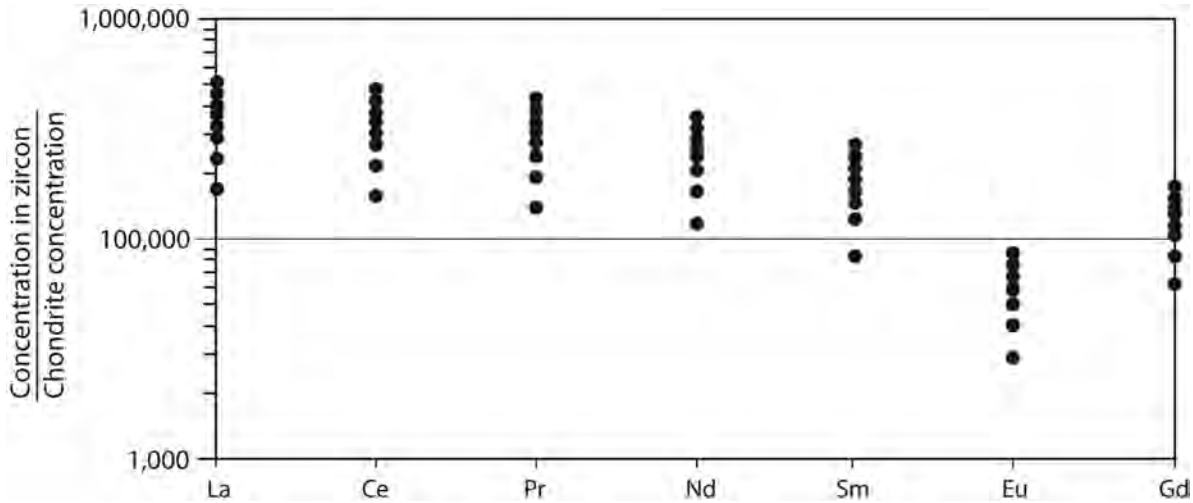

Fig. 13. Chondrite-normalized pattern of the light REEs in zircons from Chhatrapur beach, India, showing LREE enrichment and Eu anomaly (after Mohanty et al., 2003a).

Neogene, or Quaternary. Heavy mineral deposits of Cretaceous age or older are likely to be hosted by lithified, well-cemented sandstones. Thus, restricting the assessment areas to unconsolidated Paleogene, Neogene, and Quaternary sediments deposited in coastal environments is a first-level exploration and assessment guideline.

Detailed geologic mapping that divides sedimentary units by time period (such as epoch) can benefit the search for deposits. For example, during the Pliocene many economic deposits of heavy mineral sands formed along the cratonic margins of widely separated continents. Also, within a single coastal basin, time-equivalent sedimentary units can indicate the extent of ancient strandlines, and thus the possible locations of related deposits.

Grosz (1993) described the application of stream sediments to locate deposits of heavy mineral sands in the mid-Atlantic coastal plain of the United States. His study analyzed concentrations of Ti, Hf, the REEs, Th, and U in stream sediments. These pathfinder (exploration) elements were selected to detect the presence of the heavy minerals typical of this deposit type, including ilmenite ($FeTiO_3$), rutile (TiO_2), zircon ($(Zr,Hf,U)SiO_4$), monazite ($(Ce,La,Y,Th,U)PO_4$), and xenotime (YPO_4). Grosz (1993) concluded that geochemical data may be used to locate deposits of heavy minerals, especially by indicating areas in the mid-Atlantic region of the eastern United States that merit more detailed sampling and analyses.

Monazite-Bearing Beach Placer Deposits and Natural Radioactivity

Radiometric methods of geophysical exploration are useful in discovering and delineating deposits of heavy mineral-rich beach placers (heavy mineral sands). Several minerals in these deposits can produce a radiometric anomaly, in particular monazite, due to its thorium content (Force et al., 1982; Grosz et al., 1989, 1992; Grosz and Schruben, 1994). Zircon grains may also generate thorium and uranium anomalies. Potassium-bearing minerals, such as K-feldspar and micas, can also contribute to total count surveys, appearing as K highs in the gamma spectra.

A factor that is equally important is the potential radiation dose to humans and others from some high-grade placers, specifically, the exposure to natural radioactivity caused by the radioactive minerals in these deposits, principally monazite and zircon. The Erasama and Chhtarapur placer districts in the Orissa State along the east coast of India (Figs. 5–7) have been shown to be "high background radiation areas," primarily due to the presence of thorium and uranium (Mohanty et al., 2004; Sengupta et al., 2005). Similarly, in Brazil the Guarapari coastline of Espírito Santo is a popular tourist destination known for its white sand beaches, but this shoreline is also known for its very high level of background radioactivity due to abundant detrital monazite.

The Significance of Monazite Placers

Monazite hosted by placer deposits offers several advantages. First, it has a two-fold value as an ore mineral—it contains several rare earth elements as well as thorium. Second, grains of monazite in placer deposits are mingled with other minerals of industrial value, such as ilmenite, rutile, zircon, garnet, sillimanite, and other heavy minerals; thus, monazite is recovered as a low-cost coproduct. Third, monazite is resistant to mechanical and chemical degradation and is typically the heaviest (highest density) mineral in the sand-silt deposit; these qualities make monazite relatively easy to mechanically separate and recover from heavy mineral sands.

Thorium has wide applications apart from its potential use as source of nuclear energy (International Atomic Energy Agency, 2005; Hongjie, 2012), such as its use in glasses of high refractive indices and as a source of neutrons. The major applications of thorium presently are in refractory usage, aerospace alloys, ceramics, and lighting. Thorium's host minerals—monazite, thorite, thorianite, bedafite and zircon—are normally associated with other minerals that have a better control on the ore grade rather than thorium itself (Dill, 2010).

Because of the effect of the natural radiation environment and its enhancement due to the presence of monazite and the zircon in these placers, there is dire need to quantify the radiation background and its possible effects on the population. These studies are more so because quite a large number of beach placer areas, such as Gopalpur and other adjacent beaches, are also famous beach resorts of the southern part of coastal Orissa (east coast of India). Recently, these beach areas have become important centers of tourism with a large influx of people throughout the year (Mohanty et al., 2003a).

China, Japan, and the United States constitute about 90% of global product manufacturing that involves the REEs. The product distribution differences among the countries are substantial. Automobile catalytic converters accounted for 32% of rare earth use in the United States in 2007; the second biggest use was in metallurgical additives and alloys (around 21%). Japan used 28 and 27% of total rare earths in permanent magnets and polishing powders, and 15% in automobile catalytic converters. China has experienced the most dramatic changes in recent REE use. China has traditionally employed rare earths in applications such as metallurgical additives and alloys, petroleum refining, and glass and ceramics, but new applications in China have grown significantly since 2002. The end-use history demonstrates the dramatic increase in these new applications, which are primarily permanent magnets, polishing powders, nickel hydride batteries, phosphors, and automobile catalytic converters.

PIXE and EDXRF analyses on monazite sands from Chhatrapur and Erasama (Figs. 5–7) indicate the higher abundance of the oxides of cerium followed by lanthanum and neodymium. Cerium has wide applications, mainly in the fields of specialty glasses and ceramics. In addition, cerium lasers are used to locate atmospheric pollutants such as ozone and sulfur dioxide. Cerium compounds are also used to make phosphors. The primary uses of lanthanum are in hybrid car batteries, hydrogen sponge alloys, "mischmetal" (an alloy with approximate composition of 50% Ce, 25% La, and the remainder mostly Nd and Pr), and in cerium-doped lanthanum-based scintillators. Lanthanum is also used to enhance the alkali resistance of glasses, such as infrared absorbing glasses. Neodymium is useful in crycoolers and frequently used in countries such as China as a fertilizer. In addition, neodymium compounds are used in manufacturing neodymium magnets, which are the strongest permanent magnets at this time.

The sector with the largest consumption use of REEs is metallurgical applications—mainly in the form of mischmetal.

With the growing demand for Nd and Pr in magnets, current processing methods sometimes recover those elements individually, leaving a mischmetal composition consisting almost entirely of Ce and La. The sector with the next highest use of REEs is computer components, which contain Nd, Pr, Dy, Gd, and Tb. Automobile catalytic converters rank third among rare earth consumption, mostly using Ce. Six other product sectors are also significant users of REEs: audio systems (mostly Ce), glass additives (Ce and La), nickel metal hydride batteries for computers (Nd, Pr, Dy, and Tb), catalysts (predominantly La), automobiles (Nd and Pr), and wind turbines (Nd and Pr). Together, the consumption of REEs in these nine product sectors constitutes nearly 88% of the total REE use (Du and Graedel, 2011).

Heavy mineral placers offer several advantages as sources of mineral feedstock:

1. The deposits are usually unconsolidated or weakly consolidated sediments, and thus relatively easy to excavate;
2. These deposits are sizeable, with orebodies of at least 10 Mt;
3. Well-established techniques are used to separate the heavy minerals from the ore body (mixture of sand-silt-clay);
4. A single deposit and operation can produce multiple salable products, such a Ti oxide minerals (ilmenite, rutile), zircons, garnet, staurolite, tourmaline, kyanite, and/or sillimanite, as well as monazite, a potential source of the light REEs and thorium.

An aspect of utmost significance is the depletion of heavy mineral content and the associated rare earth minerals due to continuous mining of the beach placers. Thus, additional deposits of heavy minerals (including inland paleodeposits) will be needed to fill increasing world demand for many industrial minerals, REEs, and perhaps thorium.

Disclaimer

Any use of trade, product, or firm names is for descriptive purposes only and does not imply endorsement by the U.S. Government.

REFERENCES

Adams, J.A.S., and Weaver, C.E., 1958, Thorium-to-uranium ratios as indications of sedimentary processes—example of concept of geochemical facies: American Association of Petroleum Geologists Bulletin, v. 42, p. 387–430.

Ali, M.A., Krishnan, S., and Banerjee, D.C., 2001, Beach and inland heavy mineral sand investigation and deposits in India—an overview: Exploration and Research for Atomic Minerals, v. 13, p. 1–21.

Angusamy, N., Loveson, V.J., and Rajamanickam, G.V., 2004, Zircon and ilmenite from the beach placers of southern coast of Tamil Nadu, east coast of India: Indian Journal of Marine Sciences, v. 33, p. 138–149.

Anjos, R.M., Veiga, R., Macario, K., Carvalho, C., Sanches, N., Bastos, J., and Gomes, P.R.S., 2006, Radiometric analysis of Quaternary deposits from the southeastern Brazilian coast: Marine Geology, v. 229, p. 29–43.

Argall, G.O., Jr., 1954, New dredging techniques recover Idaho monazite: Mining World, v. 16, p. 26–30.

Babu, N., Vasumathi, N., and Rao, B.R., 2009, Recovery of ilmenite and other heavy minerals from Teri Sands (Red Sands) of Tamil Nadu, India: Journal of Minerals and Materials Characterization and Engineering, v. 8, p. 149–159.

Borreswara Rao, C., 1957, Beach erosion and concentration of heavy mineral sands: Journal of Sedimentary Petrology, v. 27, p. 143–147.

Boynton, W.V., 1984, Cosmochemistry of the rare earth elements—meteorite studies, *in* Henderson, P., ed., Rare earth geochemistry, Developments in geochemistry 2: Amsterdam, Elsevier Science Publishers B.V., p. 63–114.

Castor, S.B., and Hedrick, J.B., 2006, Rare earth elements, *in* Kogel, J.E., Trivedi, N.C., Barker, J.M., and Krukowski, S.T., eds., Industrial minerals and rocks—commodities, markets, and uses, 7th ed.: Littleton, CO, Society for Mining, Metallurgy, and Exploration, Inc. (SME), p. 769–792.

Da Silva, M.A.M., 1979, Provenance of heavy minerals in beach sands, southeastern Brazil—from Rio Grande to Chui (Rio Grande do Sul State): Sedimentary Geology, v. 24, p. 133–148.

Dawood, Y.H., and El-Naby, H.H.A., 2007, Mineral chemistry of monazite from the black sand deposits, northern Sinai, Egypt—a provenance perspective: Mineralogical Magazine, v. 71, p. 389–406.

Dill, H.G., 2010, The "chessboard" classification scheme of mineral deposits—mineralogy and geology from aluminum to zirconium: Earth-Science Reviews, v. 100, p. 1–420.

Doveton, J. H., and Prensky, S. E., 1992, Geological applications of wireline logs—a synopsis of developments and trends: Log Analyst, v. 33, p. 286–303.

Du, X., and Graedel, T.E., 2011, Global in-use stocks of rare earth elements—a first estimate: Environmental Science and Technology, v. 45, p. 4096–4101.

DuPont, 2014, Dupont company website, accessed December 14, 2014, at http://www2.dupont.com/Florida_Mine/en_US/about.html

Economic and Social Commission for Asia and the Pacific (ESCAP), 2001, Mineral resources of Thailand: United Nations publication, Atlas of Mineral Resources of the ESCAP Region, v. 16, 239 p.

Emery, K.O., and Noakes, L.C., 1968, Economic placer deposits of the continental shelf: Technical Bulletin—United Nations, Economic and Social Commission for Asia and the Pacific (ESCAP), Committee for Coordination of Joint Prospecting for Mineral Resources in Asian Offshore Areas (CCOP), v. 1, p. 95–111.

Folk, R.L., 1980, Petrology of sedimentary rocks: Austin, Texas, Hemphill Publishing, 184 p.

Force, E.R., 1976, Metamorphic source rocks of titanium placer deposits—a geochemical cycle: U.S. Geological Survey Professional Paper 959-B, 16 p.

——1991, Geology of titanium-mineral deposits: Geological Society of America Special Paper 259, 112 p.

Force, E.R., Grosz, A.E., Loferski, P.J., and Maybin, A.H., 1982, Aeroradioactivity maps in heavy mineral exploration—Charleston, South Carolina, area: U.S. Geological Survey Professional Paper 1218, 19 p.

Gambogi, J., 2013, Rare earths: U.S. Geological Survey Mineral Commodity Summaries, 2013. Available at http://minerals.usgs.gov/minerals/pubs/commodity/rare_earths/.

Geoscience Australia, 2012, Australia's identified mineral resources 2011: Canberra, Geoscience Australia, 123 p.

Grosz, A.E., 1993, Use of geochemical surveys in Ti-Hf-REE-Th-U placer exploration—a Mid-Atlantic-States example: U.S. Geological Survey Bulletin 2039, p. 181–188.

Grosz, A.E., and Schruben, P.G., 1994, NURE geochemical and geophysical surveys—defining prospective terranes for United States placer exploration: U.S. Geological Survey Bulletin 2097, 9 p.

Grosz, A.E., Cathcart, J.B., Macke, D.L., Knapp, M.S., Schmidt, Walter, and Scott, T.M., 1989, Geologic interpretation of the gamma-ray aeroradiometric maps of central and northern Florida: U.S. Geological Survey Professional Paper 1461, 48 p.

Grosz, A.E., San Juan, F.C., Jr., and Reid, J.C., 1992, Heavy-mineral concentrations associated with some gamma-ray aeroradiometric anomalies over Cretaceous sediments in North Carolina—implications for locating placer mineral deposits near the Fall zone: U.S. Geological Survey Open-File Report 92-396, 27 p.

Gupta, C.K., 2003, Chemical metallurgy—principles and practice: Wiley-VCH Verlag GmbH and Co. KGaA, Weinheim, 824 p.

Hedrick, J.B., 1997, Rare-earth metals: U.S. Geological Survey Minerals Yearbook, p. 61.1–61.6.

Herath, J.W., 1990, Sri Lanka's minerals and national development: Industrial Minerals, no. 270, p. 133–135.

Highley, D.E., Slater, D., and Chapman, G.R., 1988, Geological occurrence of elements consumed in the electronics industry: Transactions of the Institution of Mining and Metallurgy, v. 97, sec. C, p. 34–49.

Hoatson, D.M., Jaireth, S., and Miezitis, Y., 2011, The major rare-earth-element deposits of Australia—geological setting, exploration, and resources: Geoscience Australia, 204 p.

Hongjie, Xu, 2012, Chinese Academy of Sciences Thorium Molten Salt Reactor program: Presentation at the Thorium Energy Conference, 2102. Available at https://www.youtube.com/watch?v=5Chj2iJsGSU&feature=player_embedded.

International Atomic Energy Agency, 2005, Thorium fuel cycle—potential benefits and challenges: International Atomic Energy Agency TECDOC Series 1450 (IAEA-TECDOC-1450), 113 p.

Indústrias Nucleares do Brasil SA (INB), 2013, INB Buena—mineral treatment unit: Indústrias Nucleares do Brasil SA website, accessed November 13, 2013, at http://www.inb.gov.br/eng/WebForms/interna.aspx?secao_id=62.

Jackson, W.D., and Christiansen, G., 1993, International strategic minerals inventory summary report—rare-earth oxides: U.S. Geological Survey Circular 930-N, 68 p.

Komar, P. D., and Wang, C., 1984, Processes of selective grain transport and the formation of placers on beaches: Journal of Geology, v. 92, p. 637–655.

Kudrass, H.R., 2000, Marine placer deposits and sea-level changes, *in* Cronan, D.S., ed., Handbook of marine mineral deposits: Boca Raton, Florida, CRC Press, p. 3–12.

Lanka Minerals Sands Limited, 2013, Welcome to Lanka Mineral Sands: Lanka Mineral Sands Limited company website, accessed November 14, 2013, at http://www.lankamineralsands.com/.

Leonardos, O.H., Jr., 1974, Origin and provenance of fossil and recent monazite deposits in Brazil: Economic Geology, v. 69, p. 1126–1128.

Lindgren, W., 1897, Monazite from Idaho: American Journal of Science, 4th series, v. 4, p. 63–64.

Lovering, J.F., Wark, D.A., Gleadow, A.J.W., and Britten, R., 1974, Lunar monazite—a late-stage (mesostatis) phase in mare basalt: Earth and Planetary Science Letters, v. 21, p. 164–168.

Macfarlane, P.A., Whittemore, D.O., Townsend, M.A., Doveton, J.H., Hamilton, V.J., Coyle, W.G., III, Wade, A., Macpherson, G.L., and Black, R.D., 1990, The Dakota aquifer program annual report, FY89, Appendix B: Kansas Geological Survey Open-File Report 90-27, 301 p. Available at http://www.kgs.ku.edu/Dakota/vol3/fy89/index.htm.

Mackin, J.H., and Schmidt, D.L., 1957, Uranium and thorium-bearing minerals in placer deposits in Idaho: Idaho Bureau of Mines and Geology Mineral Resources Report 7, 9 p.

Mero, J.L., 1965, The mineral resources of the sea: Amsterdam, Elsevier, 312 p.

Mertie, J.B., Jr., 1975, Monazite placers in the southeastern Atlantic States: U.S. Geological Survey Bulletin 1390, 41 p.

Mohanty, A.K., Das, S.K., Vijayan, V., Sengupta, D., and Saha, S.K., 2003a, Geochemical studies of monazite sands of Chhatrapur beach placer deposit of Orissa, India by PIXE and EDXRF method: Nuclear Instruments and Methods in Physics Research, v. 211, sec. B, no. 1, p. 145–154.

Mohanty, A.K., Vijayan, V., Sengupta, D., Das, S.K., and Saha, S.K., 2003b, Geochemical characteristics of ilmenite sands of Chhatrapur beach placer deposit of Orissa, India—a PIXE study: International Journal of PIXE, v. 13, p. 121–131.

Mohanty, A.K., Sengupta, D., Das, S.K., Saha, S.K., and Van, K.V., 2004, Natural radioactivity and radiation exposure in the high background area at Chhatrapur beach placer deposit of Orissa, India: Journal of Environmental Radioactivity, v. 75, p. 15–33.

Mukherjee, T.K., 2007, Thorium resources in India, its mining, separation and chemical processing: International Atomic Energy Agency (IAEA) Technical Meeting, "Thorium Based Fuels and Fuel Cycle Options for Pressurized Heavy Water Cooled Reactors, Light Water Reactors and High Temperature Gas-Cooled Reactors," October 22–25, 2007, Istanbul, Turkey.

Murphy, P., and Frick, L., 2006, Titanium, *in* Kogel, J.E., Trivedi, N.C., Barker, J.M., and Krukowski, S.T., eds., Industrial minerals and rocks—commodities, markets, and uses, 7th ed.: Littleton, CO, Society for Mining, Metallurgy, and Exploration, Inc. (SME), p. 987–1003.

Nikiforova, Z.S., Filippov, V.E., and Gerasimov, B.B., 2005, Influence of eolian processes on placer formation during various epochs of the Earth's evolution: Russian Geology and Geophysics, v. 46, p. 517–528.

Nikiforova, Z.S., Prudnikov, S.G., Lebedev, V.I., Oidup, C.K., and Tulaeva, E.G., 2007, Possibility of the discovery of eolian gold placers in Tuva: Lithology and Mineral Resources, v. 42, p. 21–27.

O'Driscoll, M., 1988, Rare earths—enter the dragon: Industrial Minerals, v. 254, p. 21–55.

Olson, J.C., and Overstreet, W.C., 1964, Geologic distribution and resources of thorium: U.S. Geological Survey Bulletin 1204, 61 p.

Orris, G.J., and Grauch, R.I., 2002, Rare earth element mines, deposits, and occurrences: U.S. Geological Survey Open-File Report 02-189, version 1.0. Available at http://pubs.usgs.gov/of/2002/of02-189/.

Overstreet, W.C., 1967, The geologic occurrence of monazite: U.S. Geological Survey Professional Paper 530, 327 p.

Overstreet, W.C., White, A.M., Whitlow, J.W., Theobald, P.K., Jr., Caldwell, D.W., and Cuppels, N.P., 1968, Fluvial monazite deposits in the southeastern United States: U.S. Geological Survey Professional Paper 568, 85 p.

Prakash, T.N., Raju, G.K., and Prithviraj, M., 1991, Radioelement distribution in river, beach, and offshore areas and their significance to Chavara placer deposit, southern Kerala coast of India: Geo-Marine Letters, v. 11, p. 32–38.

Rai, S.D., Shivananda, S.R., Tiwary, K.N., Banerjee, D.C., and Kaul, Ravi, 1991, Xenotime-bearing inland placers in India and their beneficiation: Exploration and Research for Atomic Minerals, v. 4, p. 77–92.

Raju, R.D., Ali, M.A., and Krishnan, S., eds., 2001, Special issue, "Beach and inland heavy sand deposits of India": Exploration and Research for Atomic Minerals, v. 13, 159 p.

Richards Bay Minerals, 2013, History: Richards Bay Minerals company website, accessed December 23, 2014, at http://www.riotinto.com/aboutus/history-4705.aspx.

Roy, P.S., and Whitehouse, J., 2003, Changing Pliocene sea levels and formation of heavy mineral beach placers in the Murray basin, southeastern Australia: Economic Geology, v. 98, p. 975–983.

Rupasinghe, M.S., and Dissanayake, C.B., 1984, The rare-earth element abundance in the sedimentary gem deposits of Sri Lanka: Lithos, v. 17, p. 329–342.

Rupasinghe, M.S., Gocht, W., and Dissanayake, C.B., 1983, The genesis of thorium-rich monazite placer deposits in Sri Lanka: Journal of the National Science Council of Sri Lanka, v. 11, no. 1, p. 99–110.

Sengupta, D., Mohanty, A.K., Das, S.K., and Saha, S.K., 2005, Natural radioactivity and radiation exposure in the high background area of the Chhatrapur beach placer deposits of Orissa, India, *in* McLaughlin, J.P., Simopoulos, E.S., and Steinhäusler, F., eds., The Natural Radiation Environment VII—International Symposium on the Natural Radiation Environment (NRE-VII), 7th, Rhodes, Greece, May 20–24, 2002: Amsterdam, Elsevier, v. 7, p. 1148–1151.

Shepherd, M.S., 1990, Eneabba heavy mineral sand placers, *in* Hughes, F.E., ed., Geology and mineral deposits of Australia and Papua New Guinea: Parkville, Victoria, Australasian Institute of Mining and Metallurgy, p. 1591–1594.

Singhvi, A.K., Deraniyagala, S.U., and Sengupta, D., 1986, Thermoluminescence dating of Quaternary red-sand beds—a case study of coastal dunes in Sri Lanka: Earth and Planetary Sciences, v. 80, p. 139–144.

Sinha-Roy, S., 1982, Grain characteristics of zircons on beach sands from southwest coast of India: Journal of the Geological Society of India, v. 23, p. 431–440.

Staatz, M.H., Armbrustmacher, T.J., Olson, J.C., Brownfield, I.K., Brock, M.R., Lemons, J.F., Jr., Coppa, L.V., and Clingan, B.V., 1979, Principal thorium resources in the United States: U.S. Geological Survey Circular 805, 42 p.

Staatz, M.H., Hall, R.B., Macke, D.L., Armbrustmacher, T.J., and Brownfield, I.K., 1980, Thorium resources of selected regions in the United States: U.S. Geological Survey Circular 824, 32 p.

Sulekha Rao, N., Sengupta, D., Guin, R., and Saha, S.K., 2009, Natural radioactivity measurements in beach sand along southern coast of Orissa, eastern India: Environmental Earth Sciences, v. 59, p. 593–601.

Suryanarayan, M., Babu, T.M., Mahapatra, T.B., Upadhyay, S.N., Babu, P.V.R., Dougall, N. K., and Ramachar, T.M., 1979, On the occurrence of cassiterite, tantalian-cassiterite, columbite-tantalite and other uranium minerals in Bastar district, Madhya Pradesh: Indian Minerals, v. 33, no. 2, p. 36–38.

Tipper, G.H., 1914, The monazite sands of Travancore: Records of the Geological Survey of India, v. 44, pt. 3, p. 186–196.

Tse, P.K., 2011, China's rare-earth industry: U.S. Geological Survey Open-File Report 2011-1042, 11 p. Available only on-line at http://pubs.usgs.gov/of/2011/1042/.

UNSCEAR, 1993, UNSCEAR 1993 report—sources and effects of ionizing radiation: United Nations Scientific Committee on the Effects of Atomic Radiation (UNSCEAR). Available at http://www.unscear.org/unscear/en/publications/1993.html.

Williams, L., 1967, Heavy minerals in South Carolina: Columbia, S.C., South Carolina State Development Board, Division of Geology, Bulletin 35, 35 p.

©2016 Society of Economic Geologists, Inc.
Reviews in Economic Geology, v. 18, pp. 101–113

Chapter 5

Rare Earth Elements in Sedimentary Phosphorite Deposits: A Global Assessment

Poul Emsbo,[1,†] Patrick I. McLaughlin,[2] Edward A. du Bray,[1] Eric D. Anderson,[1] Thijs R.A. Vandenbroucke,[3] and Robert A. Zielinski[4]

[1] *U.S. Geological Survey, Box 25046, MS 973, Denver Federal Center, Denver, Colorado 80225*

[2] *Indiana Geological Survey, Indiana University, Bloomington, Indiana 47405*

[3] *Department of Geology, Ghent University, Krijgslaan 281/S8, 9000 Ghent, Belgium*

[4] *U.S. Geological Survey, Box 25046, MS 939, Denver Federal Center, Denver, Colorado 80225*

Abstract

Each year an estimated 56,000 metric tons (t) of rare earth elements (REEs), including 23,000 t of heavy REEs (HREEs), are mined, beneficiated, and put into solution, but not recovered, by operations associated with the global phosphate fertilizer industry. Importantly, the REEs in sedimentary phosphorites are nearly 100% extractable, using technologies currently employed to meet global phosphate fertilizer needs. Our evaluation suggests that by-product REE production from these phosphate mines could meet global REE requirements. For example, the calculated REE flux accompanying phosphate production in the United States is approximately 40% of the world's total and, alone, could supply 65% of global HREEs needs. Moreover, recognition that the tonnages and HREE concentrations of some unmined phosphorite deposits dwarf the world's richest REE deposits suggests that these deposits might constitute stand-alone REE deposits. The hypothesized genesis of these REE-rich occurrences strongly supports the long-debated suggestion that oceanic REE contents vary in a secular fashion and that associated high-grade REE abundances reflect oceanic redox state transitions during specific time periods. Here, we use this new process-based model, based on observed variations in global-secular REE abundances, to identify phosphorite horizons deposited during periods favorable for high-grade REE accumulation.

Introduction

Rare earth element-based technologies underpin an increasingly broad range of industrial sectors (Service, 2010). These elements, grouped because of their chemical and physical similarities, include the 14 naturally occurring lanthanides, and Y (Long et al., 2010). Rare earth elements (REEs) are informally classified into light REEs (LREEs) and heavy REEs (HREEs). While the division between categories varies among different academic and industry groups, we have chosen to designate LREEs as La through Sm, and HREEs as Eu through Lu and Y in conformance with several recent papers on HREEs (cf. Kato et al., 2011). The HREE group is particularly important to emerging technologic requirements of the green energy, defense, and electronic industries (Humphries, 2010; Long et al., 2010; British Geological Survey, 2011; Kato et al., 2011).

Currently, nearly 97% of the world's REEs are produced by China from two ore deposit types (Humphries, 2010; U.S. Geological Survey, 2011). The Bayan Obo deposit, the largest REE deposit in the world, is a high-grade, igneous-related carbonatite deposit that supplies 80% of the world's LREEs (U.S. Geological Survey, 2011; Kynicky et al., 2012; Verplanck et al., 2016; Xie et al., 2016). As is common among carbonatite deposits, the deposit is preferentially LREE enriched relative to the HREEs. Ion-adsorption clay-type deposits of South China constitute the second important REE deposit type. While small and low grade, these deposits have allowed China to dominate the HREE market because these deposits are HREE enriched and the associated ore is easily mined and processed (Long et al., 2010; Kynicky et al., 2012; Sanematsu and Watanabe, 2016). Recent renewed production from the giant, high-grade carbonatite-type Mountain Pass deposit in California, along with the development of similar carbonatite-type deposits, has eased the current LREE shortage (Humphries, 2010; Long et al., 2010; British Geological Survey, 2011). More daunting, however, is the challenge to meet growing HREE requirements because most recent efforts to identify HREE-enriched clay-type deposits have been unsuccessful (Long et al., 2010; British Geological Survey, 2011) .

The need to identify viable new HREE sources has prompted consideration of unconventional sources. Recognition that deep-sea muds contain appreciable REEs, for example, has led to exploration of areas as remote as the sea floor, more than 4 km below the surface. While these REE-enriched sediments have been proposed as REE resources (Kato et al., 2011), their profitable exploitation depends on overcoming the technical and environmental obstacles associated with deep seafloor mining. Emsbo et al. (2015) identified sedimentary phosphate deposits (phosphorites) in the United States as a potential REE source and demonstrated that some of these deposits are highly REE enriched and may constitute potential HREE sources. They determined that by-product REE production from phosphate rock currently mined in the United States could meet a large proportion of world's REE demand. Moreover, the size of some unmined phosphorite deposits and their HREE concentrations dwarf those of the world's richest REE deposits, which suggest that these sedimentary rocks might constitute stand-alone REE

† Corresponding author: e-mail, pemsbo@usgs.gov

deposits. They discovered, for example, phosphorites that are more than an order of magnitude higher grade than the China HREE clays; importantly, REEs contained in these phosphorites are nearly 100% extractable using technologies currently employed to meet global phosphate fertilizer needs. Phosphorite REE concentrations are generally consistent within temporally equivalent occurrences, but vary by as much as three orders of magnitude among geologic periods (Fig. 1). Systematic REE concentration variations of this sort strongly support the much debated suggestion that oceanic REE contents vary in a secular fashion in accord with varying oceanic redox conditions. Consequently, a small amount of horizon-specific data can be used to reasonably extrapolate contained REE abundances from reserve and production data because phosphate beds in age-equivalent horizons have strikingly similar REE contents over strike lengths of 100s of km.

The primary objective of this paper is to use published values for known horizons and/or published values for equivalent-age horizons (Emsbo et al., 2015, and references therein), combined with the supposition that REE concentrations in francolite from specific phosphate horizons are relatively consistent, to approximate REE grades and tonnages of currently mined phosphorites. These estimates are speculative and not intended as formal reserve estimates but rather provide approximations of REE flux through mining, beneficiation, and dissolution operations associated with ongoing phosphate fertilizer production. In addition, we use documented global-secular REE abundance variations to identify phosphorite occurrences deposited during periods that were favorable for deposition of high REEs containing strata.

Sedimentary Phosphorites

Sedimentary marine phosphorites are the world's principal source of phosphorus for the fertilizer industry, and thus an essential ingredient of modern agriculture. The availability of low-cost phosphorus has been fundamental to the "Green Revolution," which has allowed modern agricultural systems to meet increasing food demands resulting from global population growth. Phosphate, a nonrenewable commodity, resides in "francolite" (an informal name for a carbonate-rich fluorapatite mineral) that has been periodically deposited as a constituent of seafloor sediment on >1,000s km^2 areas at continental and sedimentary basin margins, forming enormous deposits in the process. The REE assessment described herein pertains to marine phosphorite deposits formed along passive and convergent continental ocean-basin margins and marginal to cratonic epeiric ocean basins; it does not include marine insular and seamount deposits.

Phosphorite is a marine sedimentary rock in which phosphate minerals are the major constituents (more than ~18% P_2O_5; Cathcart, 1980b). The principal gangue or diluent minerals in all marine phosphorite deposits are quartz, carbonate minerals (calcite and dolomite), clay minerals (i.e., montmorillonite, illite, chlorite, and kaolinite), and Fe oxide minerals (goethite, hematite, limonite). In addition, organic material is a constituent of many deposits. These diluents affect processing and chemical uses of the phosphorite (Cathcart, 1980a).

"Francolite" is essentially the only phosphate-bearing mineral present in phosphorites unaltered by metamorphism or weathering. This structurally and chemically complex mineral is a carbonate-fluorapatite with >1% F and believed to contain appreciable amounts of CO_2 (Jarvis et al., 1994). Francolite is not a Commission on New Minerals, Nomenclature and Classification–approved mineral, and it is has yet to be demonstrated that (CO_3) groups substitute for (PO_4) groups in the structure of apatite (Pasero et al., 2010). Nonetheless, we use the informal mineral name to agree with a vast phosphorite literature. The major element geochemistry of unaltered francolite is relatively uniform and includes approximately 32 to 40% P_20_5, ~50% CaO, ~5% CO_2, ~4% F, ~3% SO_4, and ~1% Na (Jarvis et al., 1994; Piper, 2001). The apatite structure allows numerous trace element substitutions, including REEs. Rare earth element enrichment in francolite, whereby a REE substitutes for Ca in the mineral lattice (Jarvis et al., 1994; Piper, 1999), was documented more than a century ago (Jarvis et al., 1994). Emsbo et al. (2015) confirmed that the REEs contained in phosphate-rich rocks are almost entirely bound in francolite. Historically, the prime impetus for studies of REEs in phosphate pertained to phosphate genesis and paleo-ocean chemistry (Jarvis et al., 1994; Piper, 1999; Lécuyer et al., 2004). Early investigations recognized the potential for by-product REE extraction during production of phosphoric acid from the Hawthorn Group and the Phosphoria Formation phosphorites (McKelvey et al., 1951; Altschuler et al., 1967). However, sedimentary phosphorites have generally been viewed as having low-grade and therefore uneconomic REE contents. In contrast, an assessment of U.S. phosphorites by Emsbo et al. (2015) shows that phosphorite rock currently mined in the United States potentially could meet a substantial proportion of world's REE needs as a by-product; that work also demonstrates that these rocks have HREE contents that are considerably greater than those characteristic of ore mined in presently active REE deposits (Fig. 1).

Fig. 1. Shale-normalized REE (North American Shale Composite, McLennan, 1989) plots for francolite from sedimentary phosphorites, grouped by geologic age. REE patterns for francolite are consistent for any particular time, which indicates that geologic age is a predictive tool for the assessment and exploration of phosphorite-hosted REE deposits (modified from Emsbo et al., 2015). Plotted data: for comparison purposes (see text for details) whole-rock samples with P_2O_5 >10% and phosphate grain separates, normalized to pure francolite (see Emsbo et al., 2015, for data and references). First panel shows mean REEs of major deposits: deep-sea muds (site 76: Kato et al. (2011), Bokan Mountain (Bentzen et al., 2013), Mountain Pass (Haxel, 2005; Long et al., 2010), and China clay-type deposits (Bao and Zhao, 2008)) plotted relative to francolite from three United States phosphorites. Direct comparison between ores whole-rock REE values and francolite values requires lowering francolite values between 5 and 30% to adjust for dilution by gangue minerals in the phosphorites. Subsequent panels depict 1st (blue), 2nd (red), 3rd (green) quantiles of REE abundances in francolite from global phosphorites. Dotted patterns: median values of coeval biogenic phosphate from Lécuyer et al. (2004) that document similar patterns as those in the phosphorites.

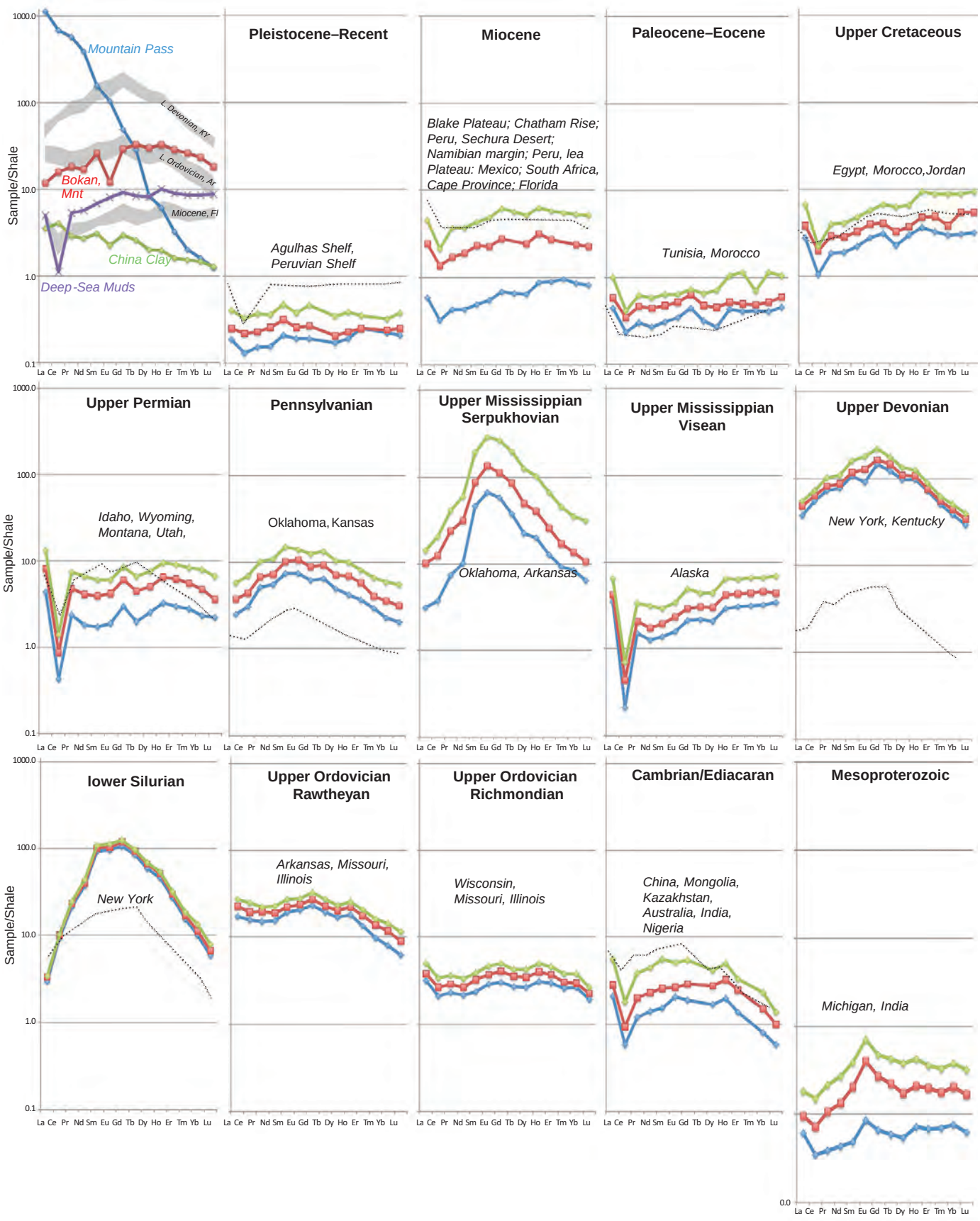
Sample/Shale
1000.0
100.0
10.0
1.0
0.1
La Ce Pr Nd Sm Eu Gd Tb Dy Ho Er Tm Yb Lu
Mountain Pass
L. Devonian, KY
L. Ordovician, Ar
Bokan, Mnt
Miocene, Fl
China Clay
Deep-Sea Muds
Pleistocene–Recent
Agulhas Shelf, Peruvian Shelf
Miocene
Blake Plateau; Chatham Rise; Peru, Sechura Desert; Namibian margin; Peru, lea Plateau: Mexico; South Africa, Cape Province; Florida
Paleocene–Eocene
Tunisia, Morocco
Upper Cretaceous
Egypt, Morocco,Jordan
Upper Permian
Idaho, Wyoming, Montana, Utah,
Pennsylvanian
Oklahoma, Kansas
Upper Mississippian Serpukhovian
Oklahoma, Arkansas
Upper Mississippian Visean
Alaska
Upper Devonian
New York, Kentucky
lower Silurian
New York
Upper Ordovician Rawtheyan
Arkansas, Missouri, Illinois
Upper Ordovician Richmondian
Wisconsin, Missouri, Illinois
Cambrian/Ediacaran
China, Mongolia, Kazakhstan, Australia, India, Nigeria
Mesoproterozoic
Michigan, India
0.0

Genesis of Phosphorites and Processes of REE Enrichment

The processes and geochemical cycles of phosphogenesis have been debated for more than 100 years and are still poorly understood (Glenn et al., 1994). The "upwelling hypothesis" first introduced by Kazakov (1939) and subsequently refined (e.g., McKelvey et al., 1959; Cook et al., 1990) has been the overarching hypothesis for the formation of phosphate deposits. This hypothesis suggests that phosphorites form where deep, cold, phosphate-rich marine water upwells along continental margins. In fact, modern phosphorites are known to form beneath upwelled waters along modern continental margins (Glenn et al., 1994). The chemical mechanisms that foster phosphate accumulation (i.e., microbial concentration, redox pumping of phosphorus via Fe-FeOOH redox pairs) and subsequent hydraulic reworking/winnowing processes (cf. Glenn et al., 1994) promote high-grade phosphorite formation but are beyond the scope of this paper. Despite its prominence, the upwelling model is inconsistent with the intermittent distribution of giant phosphate deposits in the secular stratigraphic record and, importantly, not all modern phosphorites seem to have formed beneath upwelling zones. Glenn and Arthur (1990) observed that the effects of upwelled waters are limited to the locus of upwelling, and that some of Tethyan deposits formed in shallow basins, tens to hundreds of kilometers removed from the open Tethyan margin. Together, these observations suggest that simple upwelling may be insufficient to cause formation of super giant phosphate deposits in the geologic record (Glenn et al., 1994). Similarly, the genesis of the giant districts formed in shallow intracratonic basins (i.e., Cambrian Georgina, Neoproterozoic/Cambrian Nanhua rift, and even the Permian phosphoria basins), located markedly inboard from the open-marine margin, is potentially inconsistent with upwelling. Alternatively, intriguing relationships between secular carbon isotope excursions (Follmi et al., 1994; Emsbo et al., 2010; McLaughlin et al., 2012) suggest that other processes might be critical to phosphate deposit genesis. Emsbo et al. (2010, 2015) suggested that correspondence between carbon isotope excursions and phosphorites reflects fundamental changes in ocean chemistry that dramatically influenced chemical redox cycling of elements, including phosphate. Specifically, linked redox cycling might promote temporally systematic REE enrichment and abundance pattern variations (Fig. 1).

Geologic processes controlling phosphorite REE contents are intensely debated. Many interpret normalized REE patterns that resemble modern seawater as primary (Elderfield and Pagett, 1986; Wright et al., 1987; Piper et al., 1988; Picard et al., 2002; Martin and Scher, 2004). In contrast, deviations from modern REE patterns and concentrations are also considered by some as primary and the result of ocean chemistry secular variation (Wright et al., 1987; Picard et al., 2002; Lécuyer et al., 2004). However, some consider these variations as reflecting postdepositional alteration and diagenetic equilibration (McArthur and Walsh, 1984; Ilyin, 1998; Shields and Stille, 2001; Shields and Webb, 2004; Bright et al., 2009); facies, grain size, and duration and depth of burial variations are suggested as responsible for these purported secondary effects (McArthur and Walsh, 1984; Ilyin, 1998; Shields and Stille, 2001; Shields and Webb, 2004). However, Emsbo et al. (2015) showed that systematically increasing REE contents are uncorrelated with increasing deposit age and demonstrate that the oldest phosphorites (Cambrian and Proterozoic) have considerably lower REE contents than younger analogues (Fig. 1). Moreover, Emsbo et al. (2015) documented individual phosphate beds, extensive over 1,000s km^2, that have similar REE contents, despite (1) deposition in a wide range of depositional environments; (2) different sedimentary host-rock compositions, grain morphologies, and sizes; and (3) diverse burial depth. These systematics contradict the hypothesis that phosphorite REE contents are determined by the depth and duration of burial, depositional setting, phosphate grain morphology, or host-rock composition. Emsbo et al. (2015) further observed that coeval biogenic and phosphorite materials have similar REE abundance characteristics. Accordingly, temporal correspondences of REE concentrations among coeval, though lithologically diverse deposits, and among coeval strata from widely separated, across-continent sites most likely reflect systematic oceanic REE compositional variations through time (Fig. 1).

The processes primarily responsible for REE seawater compositional variations through time are unknown, and the concept that REE contents of oceanic sedimentary deposits are related to secular oceanic compositional REE variation has been criticized for lack of a theoretical basis for seawater REE composition shifts (cf. Shields and Webb, 2004). However, Emsbo et al. (2015) marshalled extensive published findings, documenting the mass balance, cycling, and fractionations of REEs that accompany marine geochemical cycles in the modern ocean (cf. Elderfield and Greaves, 1982; Sholkovitz, 1994) in support of the hypothesis that oceanic secular REE abundance variations are not only possible, but expected. The dominant control on REE content of the modern ocean is adsorptive scavenging of REEs by particles (dominantly Fe-Mn oxyhydroxides) that settle through the water column, thereby sequestering REEs in marine sediments. Similarly, preferential removal of Ce and LREEs by oxyhydroxide particles is responsible for distinctive REE patterns characteristic of modern seawater (cf. Emsbo et al., 2015). Adsorptive scavenging limits oceanic REE aqueous concentrations and, thus, oceanic REE residence times; correspondingly, dissolution of REE adsorbing oxyhydroxides in modern dysoxic and anoxic water columns can locally increase seawater REE concentrations as much as tenfold (German et al., 1991). Furthermore, reductive dissolution of oxyhydroxides in anoxic sediments generates large benthic fluxes of Mn, Fe, and REEs (Elderfield and Greaves, 1982; Elderfield et al., 1990; Sholkovitz et al., 1992), which, in anoxic/dysoxic environments, can be transferred back into the overlying water column, thereby contributing to relative increases in dissolved LREEs and pronounced middle REEs (MREEs) and Ce enrichments.

Large Mesozoic and Paleozoic positive carbon isotope excursions correspond to periods of global anoxia that profoundly affected ocean and marine biologic systems (Jenkyns, 2010; Gill et al., 2011; McLaughlin et al., 2012; Liu et al., 2013; Harper et al., 2014; Kaiho et al., 2014). Emsbo et al. (2015) suggested that transitions from oxic to anoxic oceanic conditions during these events triggered massive shifts in Fe-Mn oxyhydroxide cycling, which in turn caused a net decrease in

the REE burial and sequestration. Modern analogs suggest that reductive dissolution of already formed oxyhydroxides in shallowly buried sediments can cause a benthic flux of REEs, with relative abundances similar to those observed in modern anoxic pore waters, to seawater, thereby greatly increasing oceanic MREE and Ce abundances.

Coincidence among anomalous REE patterns/abundances, phosphorites, and changes in ocean redox conditions define potentially important relationships (Emsbo et al., 2010, 2015; McLaughlin et al., 2012). Whereas formation of phosphate deposits has generally been ascribed to deep, cold, phosphate-rich marine water upwelling along continental margins, inconsistencies involving the intermittent distribution of giant phosphate deposits in the secular stratigraphic record, inconsistent paleogeographic phosphorite distributions, and the association between ferruginous sediments and phosphorites more plausibly reflect oceanic redox variations. The potential link between REE patterns and phosphogenesis reflects adsorptive scavenging of phosphorous by oxyhydroxides, thereby controlling oceanic phosphorous abundances (Van Cappellen and Ingall, 1994; Ingall and Jahnke, 1997; Palastanga et al., 2011). Thus, the coincidence of REE patterns distinct from modern seawater, intermittent distributions of sedimentary phosphate deposits in the geologic record, and emerging associations with C isotope excursions suggest that processes responsible for these variations are linked and reflect fundamental transitions from oxic to anoxic marine conditions.

Nonetheless, the documentation that phosphorite REE contents vary in a secular fashion and that age-equivalent horizons have similar REE contents over 1,000s km^2, independent of depositional environments, sedimentary host-rock compositions, grain morphologies and sizes, and postdepositional processes, has important implications for the assessment of phosphorite REEs. For example, these observations suggest that a small amount of horizon-specific data can be used to reasonably extrapolate contained REE abundances from reserve and production data for phosphorites hosted in the same horizon. Moreover, secular variations in phosphate REE concentrations should allow identification of phosphorite horizons deposited during periods favorable for high-grade REE accumulation.

Potential Extraction of REEs from Phosphorites

The viability of REE resources is heavily dependent on the cost of beneficiation and chemical REE extraction. For example, using a simple acid leach to liberate REEs adsorbed on clay surfaces has allowed low-grade South China clay-type deposits to dominate global HREE production (Long et al., 2010). Driven by the ever-increasing demand for new HREE resources, recent exploration has identified a number of HREE-enriched deposits, primarily igneous rock associated, of various types. However, exploitation of igneous rock-associated HREE-enriched deposits can be inhibited by REE residences within a diverse array of fine-grained, refractory minerals that are difficult to physically concentrate (beneficiate) and dissolve (Long et al., 2010).

The ease of mining, beneficiating, and chemically dissolving sedimentary francolite allows production of 215 million metric tons per year (Mt/yr) of cost-effective phosphate fertilizer by the world's fertilizer industry. Many of the world's phosphorite deposits occur as flat-lying horizons that can be efficiently mined using opencast dragline or open-pit mining methods (Zhang et al., 2006). Ore beneficiation processes, utilizing a combination of physical processes, including washing, screening, and flotation, are highly efficient in concentrating ores. For example, rocks of the Hawthorn Group remain a premier phosphate source because low-cost beneficiation allows upgrading ore containing as little as 3% P_2O_5 to nearly pure francolite (>30% P_2O_5; Zhang et al., 2006). Carbonaceous and calcareous (calcite/dolomite) ores are commonly treated by calcination, roasting ores at temperatures above 700°C, which removes diluents. After beneficiation, the vast majority of phosphate rock is dissolved in sulfuric acid to produce phosphoric acid, mainly consumed to produce fertilizer, animal feed, and various phosphorus chemicals (Zhang et al., 2006). During phosphate rock dissolution, phosphogypsum ($CaSO_4$) precipitates as a waste-product, yielding 4 to 5 t of phosphogypsum for every ton of phosphoric acid produced (Zielinski et al., 2011).

Rare earth elements in phosphorites are almost entirely hosted in lattice substitutions in francolite, a characteristic unique to these rocks (cf. Emsbo et al., 2015). The REE residence distinction is critical because easily dissolved francolite allows near-quantitative extraction of the REEs from phosphorites. For example, simple dissolutions of francolite contained in phosphate ores from the Hawthorn, Phosphoria, and Love Hollow strata, using dilute H_2SO_4 (0.4 *N*) and HCl (0.5 *N*), extracted nearly 100% (within analytical error) of their total REE content (Emsbo et al., 2015). The crucial issue of scalability, specifically the chemical behavior of REEs within actual phosphoric acid-producing plants, regrettably remains untested. However, Zielinski et al. (2011) conducted a geochemical and mass-balance environmental study of radium (Ra) in phosphogypsum produced by a large phosphoric acid plant in Jordan. Their results document the trace and REE chemistry of phosphogypsum and suggest that >70% of the REEs contained in primary phosphate ore becomes sequestered in phosphogypsum. In addition, they used REE head-grades concentrations between 85 and 40 ppm (not including Y content), based on literature-reported abundances measured in low-grade phosphate samples. Given that REEs are almost entirely hosted in francolite and values reported from the Duwi Formation (the ore horizon in Jordan and Egypt), REE contents of pure beneficiated ore are likely between 450 and 1,000 ppm (median 710 ppm ΣREE) (Emsbo et al., 2015 and references therein), which suggests that <20% of the total REEs become sequestered in phosphogypsum. Regardless, Zielinski et al. (2011) demonstrated that 70 to 85% of the REEs contained in the phosphogypsum is water soluble. Crucially, phosphogypsum-hosted REEs were, in fact, dissolved and reprecipitated with the phosphogypsum; these REEs were neither sequestered in, nor governed by, the physical transport of high REE refractory minerals, which would otherwise result in consignment to waste piles. Accordingly, results of this geochemical study confirm laboratory-scale studies by Emsbo et al. (2015), which indicate near-quantitative dissolution (>90%) of REEs during phosphoric acid production. Of course, as with all REE deposit types, the winning and refining of REEs from solution is a complex and costly process that is beyond the scope of this study.

Quantity of REEs in Global Phosphorites

In 2012, approximately 215 Mt of phosphate rock, averaging about 30% P_2O_5 (predominantly beneficiated), were produced globally (Jasinski, 2011). About 71% of phosphate rock was produced by China (95.3 Mt), the United States (30.1 Mt), and Morocco (27.1 Mt) from phosphorite deposits. Phosphate from marine phosphorites supplies more than 85% of global phosphate and the top 10 phosphate producing nations generate >95% of all phosphate rock mined from phosphorite (Jasinski, 2011). Over the last decade, production has steadily increased by approximately 7%, mainly as a consequence of increased production in China; production by other producers has varied little. As demonstrated in Figures 2 through 7, phosphorite occurrences span the entire geologic column. The goal of the following discussion, however, is to identify the chronostratigraphy and regional correlations in order to constrain the age of the world's major phosphorite horizons so that their REE contents can be evaluated using the data compiled in Emsbo et al. (2015).

Emsbo et al. (2015) used the documented uniformity of REEs in phosphate districts, the fact that nearly all REEs in phosphate deposits reside in the francolite lattice, and yearly U.S. phosphate production figures, to estimate the amount of REEs being mined and processed, but not recovered by the U.S phosphate industry. Similarly, assuming that REE abundances in individual time horizons are relatively uniform, we approximate the REE inventory hosted in global phosphorites and the amount of REEs resident in the world's phosphate mines using data compiled by Emsbo et al. (2015). To foster calculation of the REE endowment of phosphate mines, and to facilitate comparisons of REE contents between phosphorites, all REE abundances discussed below pertain to pure francolite. In cases for which only whole-rock data are available, francolite concentrations are calculated from measured whole-rock REE and P_2O_5 concentrations. In many instances, the phosphate industry reports P_2O_5 grades for beneficiated ore because of the ease of concentrating francolite from phosphate ore during beneficiation. Similarly, REE grades reported in Table 1 are not whole-rock values but instead are the values expected of beneficiated ore. Yttrium for samples with unreported values was calculated using the Dy concentration and the database mean Y/Dy ratio of 11. In instances for which abundances are not directly measured from particular ore horizons, we use the demonstrated abundances derived from documented secular variation of francolite REE contents to establish approximate concentrations. Again, the intent here is not to provide rigorous ore reserve estimates, but rather to provide order of magnitude REE contents of global phosphorites.

North America

Yearly, the United States produces nearly 30 Mt of phosphate rock, nearly all of which is dissolved in sulfuric acid to produce fertilizer (Jasinski, 2011). Approximately 80% of the United States phosphate is sourced from Miocene/Pliocene strata (Miocene Hawthorn Group and age-equivalent formations) present in the southeast coastal United States region; the remainder is produced from the Permian Phosphoria Formation in Idaho, Wyoming, Utah, and Montana (Fig. 2; Jasinski, 2011). Phosphate beds in the Hawthorn Group, deposited in marginal marine to deeper water environments, have uniform REE concentrations with median ΣREE francolite values of 900 ppm, of which 400 ppm are ΣHREE (Emsbo et al., 2015). Similarly, the REE concentrations of the Phosphoria Formation are strikingly uniform across Utah, Idaho, and Wyoming with mean values of 1,200 ppm ΣREE and 600 ppm ΣHREE,

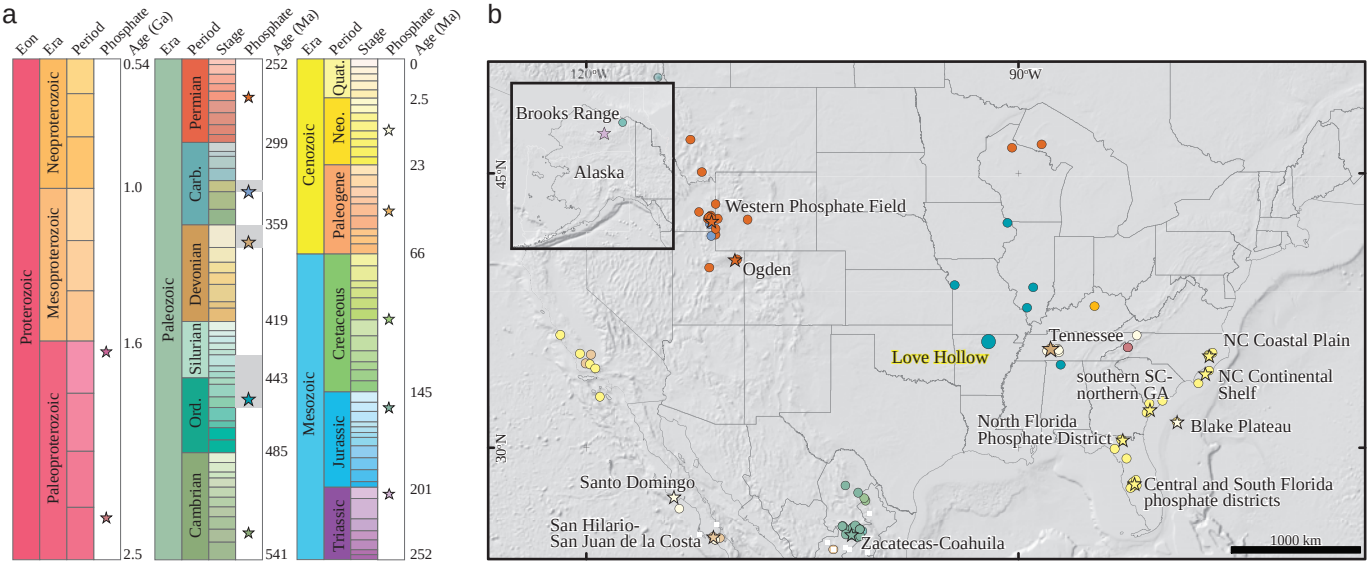

Fig. 2. Localities and stratigraphic age of world phosphate deposits. a. Ages and color-coding in the stratigraphic chart are adapted from the International Commission on Stratigraphy. Stars indicate time periods of major deposits. Gray shaded areas represent favorable REE enrichment time periods. (www.stratigraphy.org/ICSChart/ChronostratChart2013-01.pdf). b. Temporal and spatial distribution of major (i.e., mined, Notholt et al., 1989f) and minor phosphorite occurrences (Chernoff and Orris, 2002) in North America. Colored circles in the maps are keyed to time periods with larger circles and localities outlined in yellow indicating phosphorites hosted in favorable time periods.

Table 1. REE Potential of Sedimentary Phosphate Deposits

Age/country	Resource (Mt)	Average P_2O_5 (%)	Annual production Francolite (t)	Total resource		Annual production (t)	
				Total REE	Heavy REE	Total REE	Heavy REE
Africa, Middle East							
Neogene-Quaternary (53, 17)							
South Africa	1,500	9		335,667	110,500		
Paleocene-Eocene (107, 37)							
Algeria	500	24	986,842	84,708	30,063	106	37
Guinea Bissau	112	30					
Malie	12	25					
Mauritania	100	20					
Morocco	56,250	28	23,684,211	8,168,304	2,824,554	2,534	876
Senegal	65	31	955,263	8,525	2,948	102	35
Togo	100	36	1,052,632	11,294	3,906	113	39
Tunisia	3,000	16	2,105,263	762,375	263,625	225	78
Iran	165	20	28,947	34,427	11,905	3	1
Iraq	4050	22	197,368	768,211	265,643	21	7
Saudi Arabia	3600	20	2,526,316	751,140	259,740	270	93
Syria	414	4		431,906	149,351		
Upper Cretaceous (710, 310)							
Egypt	3,000	22	4,431,579	3,679,091	1,606,364	3,146	1,374
Israel	1000	26	2,526,316	1,065,000	465,000	1,794	783
Jordan	1574	28	5,000,000	1,556,574	679,631	3,550	1,550
Saudi Arabia	4280	20		5,925,660	2,587,260		
Syria	643	25	1,210,526	712,187	310,955	859	375
Precambrian (250, 100)							
Burkina Faso	60	25		22,800	9,120		
Asia, E Europe, Australia							
Cambrian (250, 100)							
China	4000	22	37,500,000	1,772,727	709,091	9,375	3,750
India	45	17	861,842	25,809	10,324	215	86
Pakistan	22	17	15,000	12,618	5,047	4	2
Vietnam	1400	23	710,000	593,478	237,391	178	71
Precambrian (250, 100)							
China	8000	25	37,500,000	3,120,000	1,248,000	9,375	3,750
India	132	23	861,842	55,957	22,383	215	86
Korea (D.R.)	88	13	789,474	66,000	26,400	197	79
Australia	3352	17	1,578,947	1,922,471	768,988	395	158
Kazakhstan	3000	23	921,053	1,271,739	508,696	230	92
Paleocene-Eocene (107, 37)							
Uzbekistan	2600	24	492,105	440,483	156,325	53	18
Lower Ordovician (NA)							
Basltic Basin	65000	10					
North America							
Miocene (900,400)							
United States	14,600	30	18,000,000	17,082,000	7,592,000	16,200	7,200
Paleogene (107, 37)							
Mexico	900	14	1,360,526	261,386	92,764	146	50
Jurassic (NA)							
Mexico	154	16					
Triassic (NA)							
United States - Alaska	5700	12					
Permian (1200, 600)							
United States	7600	24	4,600,000	14,820,000	7,410,000	5,520	2,760
South America							
Miocene (900,400)							
Peru	1453	31	768,000	1,645,171	731,187	691	307
Chile	374	9		1,458,600	648,267		
Venezuela	45	23		68,674	30,522		
Cretaceous (710, 310)							
Colombia	744	21	9000	955,863	417,349	6	3
Venezuela	208	20	115,000	280,592	122,512	82	36
Precambrian (250, 100)							
Brazil	227	13					
Total	200,069		150,788,053	70,171,436	30,317,807	55,606	23,697

Notes: Total contained REE and potential annual REE production from operating phosphate mines is calculated using estimated phosphate resources and age (Notholt et al., 1989a-g), mean phosphate REE concentration (ΣREE, ΣHREE; ppm) from the specific age horizon (Emsbo et al., 2015), and the annual phosphate production (Jasinski, 2011); these estimates are not intended as formal REE ore reserve estimations, but rather as rough approximations to illustrate the relative potential of phosphorite-hosted REEs

respectively (Fig 1). Based on these figures, approximately 23,000 t ΣREE (of which 10,000 t are ΣHREE) are mined, beneficiated, and dissolved in acid by the United States phosphate industry, annually, from Miocene phosphorite deposits in Florida and North and South Carolina and from the Permian Phosphoria Formation in the western United States (Table 1; Emsbo et al., 2015). The monetary value of phosphate fertilizer-contained REEs, even at today's lower values, rivals that of the fertilizer itself and this quantity of REEs represents approximately 15% of ΣREE and more than 65% of ΣHREE global demand.

Triassic phosphorites in the Shublik Formation of Alaska and Upper Jurassic phosphorites of central Mexico are substantial but remain unexploited. The REE content of these phosphorites is unknown and the REE composition of these Mesozoic intervals remains undocumented, and thus we are unable to estimate the REE content of these deposits. The majority of phosphate production in Mexico, however, is from middle Miocene deposits in Baja California that may have REE values similar to those in the Miocene Hawthorn Group in the southeast coastal United States region.

Africa and the Middle East

The world's largest phosphate province includes several Upper Cretaceous and Paleocene-Eocene horizons that can be traced for approximately 7,000 km across the paleo-Tethyan margin of the Arabian platform, from northern Africa to southeastern Turkey and western Iran (Figs. 3, 4; Notholt et al., 1989b). Although the entire Upper Cretaceous to Paleocene-Eocene sequence across the strike length of this province contains phosphorite, nearly all of the ore in North Africa is contained in Paleocene-Eocene horizons, whereas most of the ore in the Middle East countries is contained in the older, Upper Cretaceous (Campanian/Maastrichtian) strata. Most of the production in Syria is presumably from the Upper Cretaceous because the Paleocene-Eocene phosphorites are usually thin (1 m thick), lower grade (4%), and are only locally developed (Notholt et al., 1989b). The Sirhan-Turayf region of Saudi Arabia constitutes a large phosphate-producing region in which Maastrichtian (Upper Cretaceous) to Lutetian (middle Eocene) strata contain minable horizons. Both Upper Cretaceous and Paleocene-Eocene strata contain phosphate, but production is reportedly from the younger horizon (International Business Publications, 2013). Paleocene-Eocene francolite from Tunisia and Morocco has a median REE concentration of 107 ppm ΣREE (37 ppm ΣHREE; Fig. 1, Table 1), whereas concentrations in Upper Cretaceous phosphorites in Egypt, Morocco, and Jordan are markedly higher; the median value is 710 ppm ΣREE (310 ppm ΣHREE). Thus, despite immense size and production, because most of Morocco's production is from Paleocene-Eocene strata, the REE by-product potential for Morocco is less than for smaller producers like Jordan, Egypt, and Israel, which produce ore from the Upper Cretaceous strata with higher REE concentrations (Table 1).

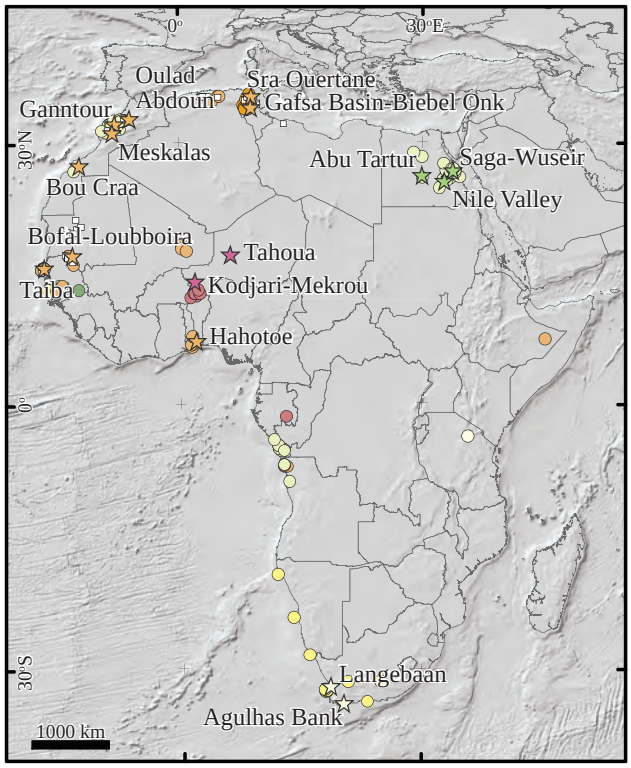

Fig. 3. Temporal and spatial distribution of major (i.e., mined, Notholt et al., 1989g) and minor phosphorite occurrences (Chernoff and Orris, 2002) in Africa. See Figure 2 for symbol key.

Asia, Europe, Russia, and Australia

The Precambrian/Cambrian boundary marks an extraordinary phosphogenesis period in Earth's history (Cook and Shergold, 1986). During this time, nearly 200 upper Neoproterozoic (Ediacaran) to lower Cambrian phosphate deposits formed in a belt that extends from Kazakhstan through central Asia into southern China, Vietnam, and Australia (Fig. 5; Cook and Shergold, 1986). Ilyin (1998) measured the REE concentrations of deposits in the Khubsugul basin in Mongolia, Karatau basin in Kazakhstan, Lesser Himalaya in India, Volta basin in Burkina Faso, Nanhua basin in China, and the Georgina basin in Australia. Phosphorite horizons in each of these basins have strikingly uniform REE concentrations with median ΣREE values of 250 ppm, of which 100 ppm are ΣHREE (Fig. 1, Table 1). China is the world's largest phosphate producer; nearly all of its ore is contained in deposits hosted within the Ediacaran Doushantuo and lower Cambrian Meishucun Formations in the Nanhua rift basin along the southern margin of the Yangtze craton. REE values of the Doushantuo and Meishucun horizons are relatively uniform; mean values correspond to those characteristic of other Precambrian/Cambrian boundary deposits (Ilyin, 1998; Shields and Stille, 2001; Chen et al., 2003). In central Asia, the Kisil Kum area of Uzbekistan includes a large middle Eocene phosphate-producing district (Ilyin and Boiko, 1989).

Russia is also a noteworthy phosphate producer; however, nearly all production is from igneous deposits. The Kingisepp mine, hosted by Lower Ordovician strata, stopped production in 2006. In Europe, the Baltic basin contains Lower Ordovician phosphorites that can be traced from the Finnish Bay (Gulf of Finland) along the north coast of Estonia from Paldiski eastward through Tallin to Maardu to Kingisepp, about 125 km southwest of Leningrad, and as far east as Volkhov, a total distance of at least 400 km (Notholt et al., 1989d).

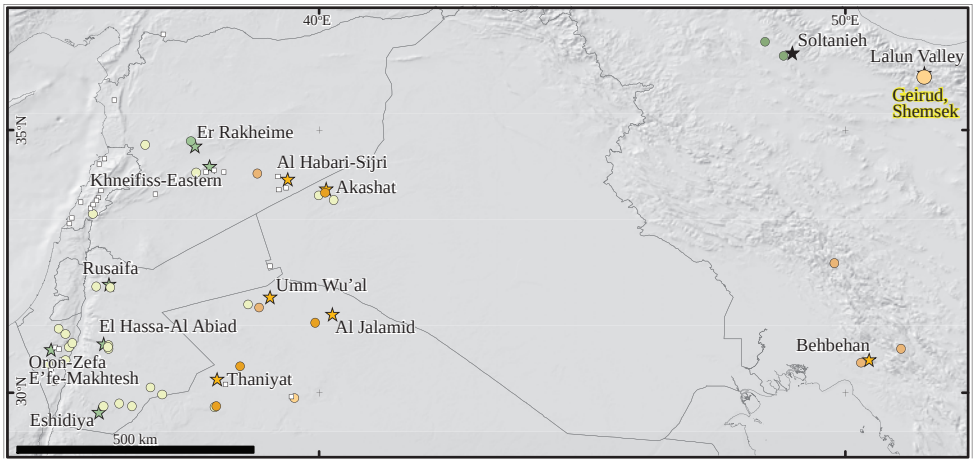

Fig. 4. Temporal and spatial distribution of major (i.e., mined, Notholt et al., 1989a-d) and minor phosphorite occurrences (Chernoff and Orris, 2002) in the Middle East. See Figure 2 for symbol key.

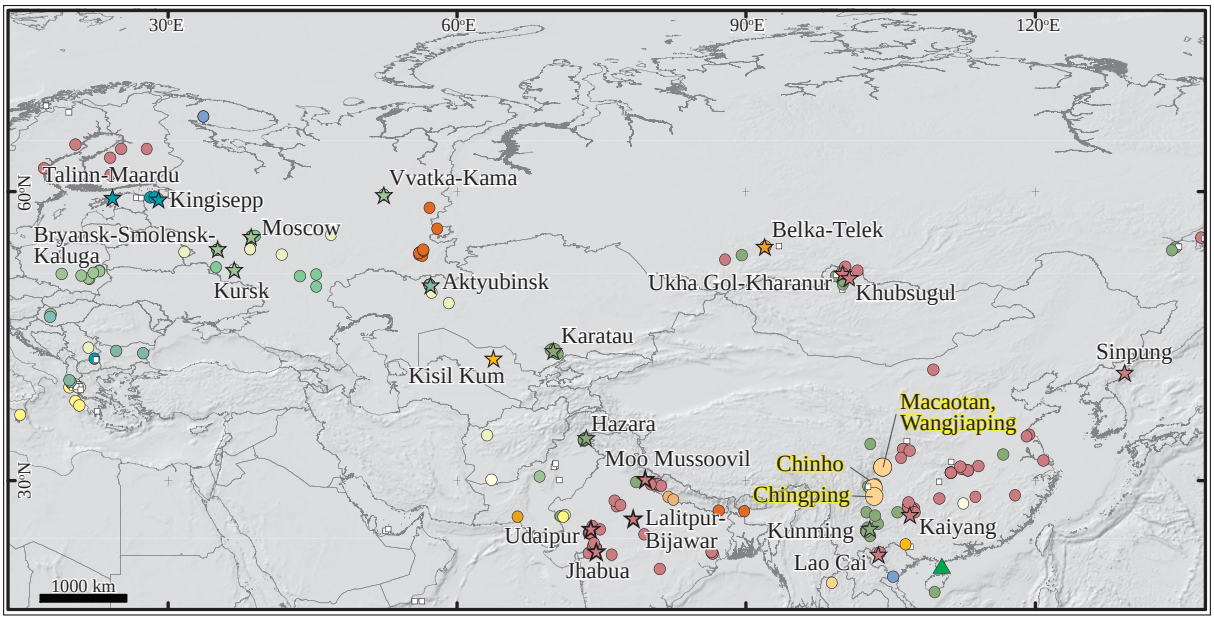

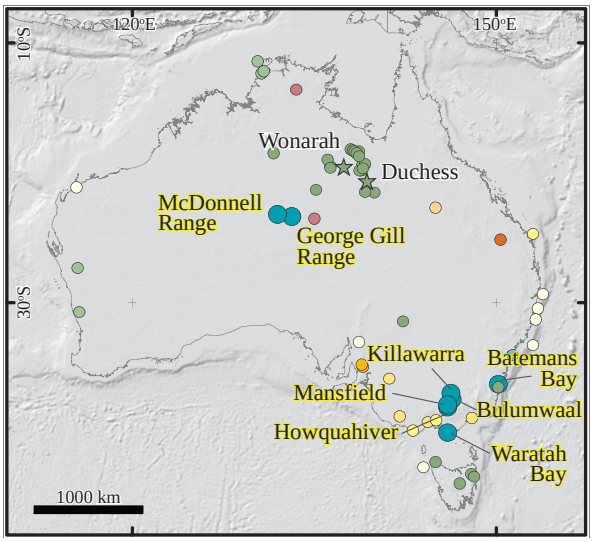

Fig. 5. Temporal and spatial distribution of major (i.e., mined, Notholt et al., 1989e) and minor phosphorite occurrences (Chernoff and Orris, 2002) in Asia, Eastern Europe and Russia, and Australia. See Figure 2 for symbol key.

Finland is the only current Western European phosphate producer from igneous phosphate (Notholt et al., 1989a; Zhang et al., 2006). Although small phosphorite deposits of Paleozoic, Mesozoic, and Cenozoic age occur throughout Western Europe (Fig. 6), none have produced phosphate since World War II (Notholt et al., 1989a).

South America

Phosphate production in South America is dominated by production from igneous deposits in Brazil (Notholt et al., 1989c; Zhang et al., 2006). Phosphate deposits of sedimentary origin are of relatively limited distribution in South America. Noteworthy phosphorites are found mainly in Cretaceous and Neogene sediments. In addition, the Neoproterozoic Bambui Group in the State of Minas Gerais (Brazil) hosts small phosphate occurrences, and other potentially economic deposits are in northwest Patas de Minas. In Columbia and Venezuela, Upper Cretaceous rocks host several large phosphate deposits (Fig. 7). During the last 10 years, a large middle Miocene phosphate resource was developed in the coastal Sechura Desert, northwestern Peru; associated phosphate production is substantial. Generally equivalent, potentially significant deposits occur in Chile. Even though the REE contents of these South American Neoproterozoic, Upper Cretaceous, and middle Miocene phosphorites have not been measured directly, the REE composition of these stratigraphic intervals have been well characterized elsewhere (Fig. 1), and these values were used to estimate the REE inventory of South America in Table 1.

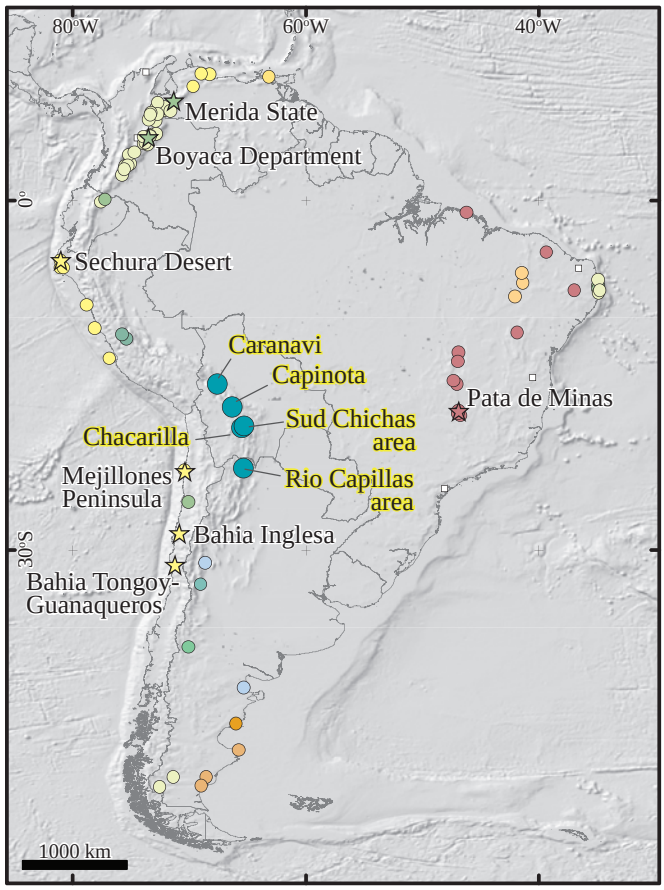

Fig. 7. Temporal and spatial distribution of major (i.e., mined, Notholt et al., 1989c) and minor phosphorite occurrences (Chernoff and Orris, 2002) in South America. See Figure 2 for symbol key.

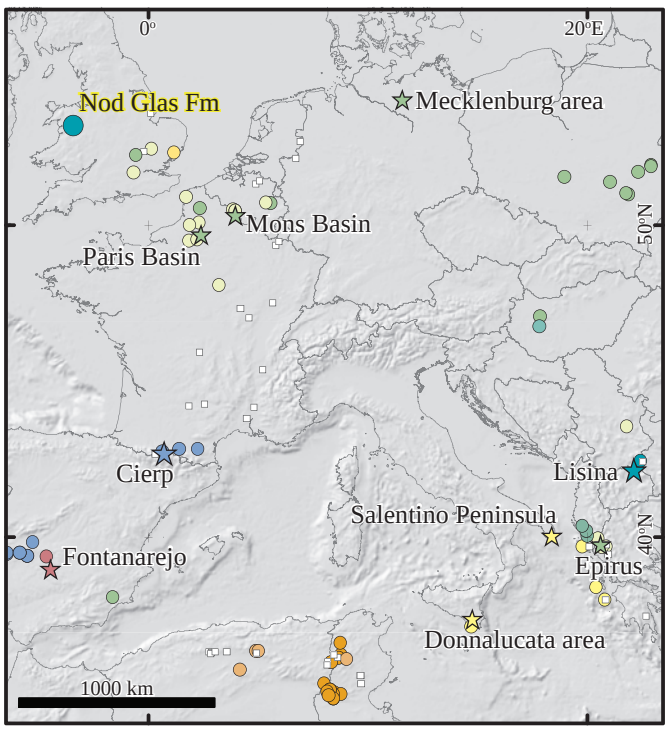

Fig. 6. Temporal and spatial distribution of major (i.e., mined, Notholt et al. 1989a) and minor phosphorite occurrences (Chernoff and Orris, 2002) in Europe. See Figure 2 for symbol key.

Exploration for Phosphorites Enriched in REEs

The discovery that unmined phosphorites appear to have higher grades and tonnage than the world's richest HREE deposits suggests that these rocks could be a primary source of REEs. Systematic secular variations of phosphorite REE content indicate that deposits formed during certain geologic time periods are likely uniformly REE enriched. Upper Mississippian, Devonian, Ordovician, and lower Silurian phosphorite deposits are particularly prospective (Emsbo et al., 2015). As such, deposits that formed during these time periods are emphasized in Figures 2 to 7 and briefly discussed below as important REE exploration targets. What follows is not a comprehensive assessment. Instead, we demonstrate a process-based assessment strategy for REE resources, based on the supposition that phosphorite REE contents are predictable and noteworthy. While the ages of identified phosphorites considered in this review are plausible, in most cases, temporal resolution is too imprecise to allow exact authoritative correlation. Also, while only Upper Devonian and Upper Ordovician examples of the prospective horizons are recognized in this review, many of the world's phosphorite occurrences are not considered because their ages are insufficiently well documented. Age determinations and correlations can be refined through evaluation of pertinent biostratigraphic and stratigraphic data.

Upper Devonian phosphorites in New York and Kentucky contain francolite with startlingly high REE concentrations (18,000 ppm ΣREE, 7,000 ppm ΣHREE), but these samples were collected from strata of great but incompletely known extent (Emsbo et al., 2015). The similarly aged Upper Devonian phosphorites in lower Famennian strata of the Geirud Formation (Iran) are small historic producers with modest reserves (46 Mt at 15% P_2O_5). However, this horizon, as much as 7 m thick, can be traced throughout the Elburz Mountains and to the north where it has been locally recognized in northern Azerbaijan and, possibly, into the Yenisei basin in the northwestern part of the Siberian platform (Notholt et al., 1989b; Salehi, 1989). The age of the Geirud Formation deposits suggests that these deposits may, in fact, have very high REE contents. Similarly, several deposits in the Sichuan province (China) occur in a 5-m-thick horizon that contains up to 18% P_2O_5 that has been constrained to a Middle to Late Devonian age (Notholt et al., 1989e). Though the age of this horizon is not well known, these rocks are emphasized because Upper Devonian phosphorite deposits have demonstrably high REE potential.

Emsbo et al. (2015) used francolite REE concentrations from the better delineated (though lower grade, 5,400 ΣREE and 1,600 ppm ΣHREE) informal Upper Ordovician Love Hollow phosphorite within the Fernvale Limestone, to demonstrate the potential of phosphorite-hosted REE deposits. Francolite from the Love Hollow phosphorite, exposed throughout an area of over 100 km² in Arkansas and in isolated localities in Missouri and Illinois, have uniform REE contents that are more than 10 times higher than those characteristic of clay-type deposits and similar to ore grades projected for the Bokan Mountain prospect, the peralkaline-type deposit in southeast Alaska that is one of the largest, most high grade HREE resources known in the United States. (Fig 1). Using the known phosphorite distribution and the average measured phosphate content (23% P_2O_5), Emsbo et al. (2015) estimated that the 100 km² of exposed Love Hollow strata contain approximately 235 Mt of phosphate rock that in turn contains 1.3 Mt of extractable ΣREE, of which 0.37 Mt are ΣHREE. These abundances are nearly twice the ΣHREE likely contained in the South China clays and 60 times that contained in the Bokan Mountain deposit. Moreover, mining 1 km² of this horizon (about 5% of the area mined annually for phosphate in Florida), where beds are as much as 9 m thick, would yield an amount of ΣREE approximately equivalent to five times that contained in the entire Bokan Mountain deposit, or 50% of the ΣREE and more than 150% of the ΣHREE projected global annual demand. Although the REE content of the Love Hollow phosphorite suggests that it may constitute a world-class REE deposit, similar-sized deposits in the Upper Devonian or Mississippian plausibly contain 4 to 5 times more REEs.

Importantly, phosphorite deposits also formed during several other Late Ordovician events. However, Emsbo et al. (2015) demonstrated that nearly coeval phosphorites can be compositionally distinct. Phosphorite within the Maquoketa Shale, for example, is just slightly older than that in the Love Hollow and can be traced throughout the United States midcontinent. In places these phosphorites are separated by just a few meters of intervening strata and yet, the REE content of these two horizons are quite distinct; the REE content of the Maquoketa rocks is only about 15% that of the Love Hollow phosphorites (Emsbo et al., 2015, Fig. 4). Upper Ordovician rocks in Bolivia, Australia, and the U.K. contain a series of phosphorite deposits that appear to be slightly older than both the Love Hollow strata and Maquoketa Shale (i.e., upper Caradoc). However, given the uncertainty of their age and the complexity of Upper Ordovician stratigraphy (Ghienne et al., 2014), these rocks must be considered to have substantial phosphorite-hosted REE potential because in general Upper Ordovician phosphorites have high REE potential.

Discussion and Conclusions

As demonstrated above, nearly all of the world's phosphate fertilizer is derived from phosphorites contained in Lower Cambrian/Ediacaran, Permian, Upper Cretaceous, Paleocene-Eocene, or Miocene strata. The REE content of most of these units has been well characterized. Current global phosphate resource estimates combined with the documented uniformity of REEs in phosphate districts, the near-total residence of REEs in francolite, and the supposition that REE abundances in individual time horizons are relatively uniform, was used to construct the rough assessment of the REE inventory hosted in global phosphorites in Table 1. Moreover, phosphate REE compositions combined with world phosphate production data permit an estimate of the quantity of REEs that are mined, beneficiated, and put into solution, but not recovered, by the global phosphate fertilizer industry.

The integration of all these data with phosphate ore resource estimates in Table 1, suggests that approximately 70 Mt ΣREE, including 30 Mt ΣHREE, are hosted in the world's major phosphate-producing districts (Table 1). Global phosphate production figures, estimated REE contents, and evidence for near-quantitative dissolution of REEs during phosphoric acid production indicates that 56,000 t ΣREE (23,000 t ΣHREE) pass, in solution, through phosphate mills each year. Recovery of a fraction of the REE flux through these mills as by-product production could meet global REE needs. The United States produces phosphate from rocks of two of the more REE enriched ages (Miocene and Permian); though producing only about 14% of the world's phosphate, about 40% of the global phosphorite REE budget is presently passing through United States phosphate mills. The United States, alone, could produce as much as 65% of the world's ΣHREE demand. Rare earth elements as a group can seemingly be extracted economically as a by-product of current mining activity because the value of the REEs contained in processed phosphate ore rivals the value of the phosphate itself.

The volume and HREE content of some currently unmined phosphorite deposits dwarf those of the world's richest REE deposits. For example, some phosphorites have grades more than an order of magnitude greater than that of the Chinese HREE clays that currently produce most of the world's HREEs. These sedimentary rocks might themselves constitute stand-alone REE deposits because beneficiation, dissolution, and production of sedimentary phosphate ore is sufficiently economical and efficient to produce the phosphate required to fertilize the fields that feed the world's population. This is economically feasible because the value of

the REEs contained in these deposits exceeds the monetary value of the phosphate itself. Their extraordinary endowment, combined with the ease of REE extraction, suggests that the REE-enriched phosphorites might constitute a primary source of REEs, one with potential to resolve the global REE (particularly HREE) supply shortage.

We have used documented global-secular REE abundance variations as an assessment tool to identify phosphorite deposited during periods, including the Late Mississippian, Devonian, and Ordovician, favorable for deposition of high REE-containing strata that are enriched in REE. The hypothesis that the REE content of phosphorites has varied systematically through time and that this variation reflects ocean chemistry variations agrees with available data. However, the hypothesis that phosphorite REE contents are directly related to host-rock age and the nascent exploration strategy based on this premise warrant further testing. Rigorous examination of this hypothesis via determinations of REE contents of temporally well-constrained phosphorite deposits combined with systematic analysis of marine biogenic (skeletal) francolite REE contents through geologic time would test the utility of this assessment strategy (Emsbo et al., 2010, 2015). Importantly, the REE content of rocks associated with several prominent phosphogenic periods of Earth history (i.e., upper Cambrian, Lower Ordovician, Lower Jurassic, and Upper Triassic deposits) remain undocumented and thus their REE endowment is unknown.

Acknowledgments

The authors would like to thank the staff from the Florida, Michigan, Wisconsin, and Illinois State Geological Surveys for access to samples and logistical support. Reviews by Philip Verplanck, Jeff Mauk, and Richard Goldfarb improved the manuscript.

REFERENCES

Altschuler, Z.S., Berman, S., and Cuttitta, F., 1967, Rare earths in phosphorites—geochemistry and potential recovery: U.S. Geological Survey Professional Paper, p. 1–9.

Bao, Z., and Zhao, Z., 2008, Geochemistry of mineralization with exchangeable REY in the weathering crusts of granitic rocks in South China: Ore Geology Reviews, v. 33, p. 519–535.

Bentzen, E.H., Hassan, G., Galbraith, L., Hammen, R.F., Robinson, R.J., Hafez, S.A., and Annavarapu, S., 2013, Preliminary economic assessment on the Bokan Mountain rare earth element project, near Ketchikan, Alaska: Vancover, BC, Tetra Tech, 227 p.

Bright, C.A., Cruse, A.M., Lyons, T.W., MacLeod, K.G., Glascock, M.D., and Ethington, R.L., 2009, Seawater rare-earth element patterns preserved in apatite of Pennsylvanian conodonts?: Geochimica et Cosmochimica Acta, v. 73, p. 1609–1624.

British Geological Survey, 2011, Rare earth elements mineral profile: Centre for Sustainable Mineral Development, 54 p.

Cathcart, J.B., 1980a, The phosphate industry of the United States, *in* Khasawneh, F.E., ed., The role of phosphorus in agriculture: Madison, Wisconsin, American Society of Agronomy, p. 19–42.

——1980b, World phosphate reserves and resources: The role of phosphorus in agriculture: Madison, Wisconsin, American Society of Agronomy, p. 1–18.

Chen, D.F., Dong, W.Q., Qi, L., Chen, G.Q., and Chen, X.P., 2003, Possible REE constraints on the depositional and diagenetic environment of Doushantuo Formation phosphorites containing the earliest metazoan fauna: Chemical Geology, v. 201, p. 103–118.

Chernoff, C.B., and Orris, G.J., 2002, Data set of world phosphate mines, deposits, and occurrences: Part A. geologic data; Part B. Location and mineral economic data: U.S. Geological Survey Open-File Report 2002-156, p. 680.

Cook, P.J., and Shergold, J.H., 1986, Proterozoic and Cambrian phosphorites—nature and origin, *in* Cook, P. J., and Shergold, J.H., eds., Phosphate deposits of the world—Proterozoic and Cambrian phosphorites, 1: New York, Cambridge University Press, p. 369–386.

Cook, P.J., Shergold, J.H., Burnett, W.C., and Riggs, S.R., 1990, Phosphorite research—a historical overview, *in* Notholt, A.J.G., and Jarvis, I., eds., Phosphorite research and development: Geological Society, London, Special Publication, p. 1–22.

Elderfield, H., and Greaves, M., 1982, The rare earth elements in seawater: Nature, v. 296, p. 214–219.

Elderfield, H., and Pagett, R., 1986, Rare earth elements in ichthyoliths: Variations with redox conditions and depositional environment: Science of the Total Environment, v. 49, p. 175–197.

Elderfield, H., Upstill-Goddard, R., and Sholkovitz, E.R., 1990, The rare earth elements in rivers, estuaries, and coastal seas and their significance to the composition of ocean waters: Geochimica et Cosmochimica Acta, v. 54, p. 971–991.

Emsbo, P., McLaughlin, P.I., Munnecke, A., Breit, G.N., Koenig, A.E., Jeppsson, L., and Verplanck, P.L., 2010, The Ireviken Event: a Silurian OAE: Geological Society of America 2010, 561 p.

Emsbo, P., McLaughlin, P. I., Breit, G.N., du Bray, E.A., and Koenig, A.E., 2015, Rare earth elements in sedimentary phosphate deposits: Solution to the global REE crisis?: Gondwana Research, v. 27, p. 776–785.

Follmi, K.B., Weissert, H., Bisping, M., and Funk, H., 1994, Phosphogenesis, carbon-isotope stratigraphy, and carbonate-platform evolution along the Lower Cretaceous northern Tethyan margin: Geological Society of America Bulletin, v. 106, p. 729–746.

German, C.R., Holliday, B.P., and Elderfield, H., 1991, Redox cycling of rare earth elements in the suboxic zone of the Black Sea: Geochimica et Cosmochimica Acta, v. 55, p. 3553–3558.

Ghienne, J.F., Desrochers, A., Vandenbroucke, T.R., Achab, A., Asselin, E., Dabard, M.P., Farley, C., Loi, A., Paris, F., Wickson, S., and Veizer, J., 2014, A Cenozoic-style scenario for the end-Ordovician glaciation: Nature Communications, v. 5, p. 4485.

Gill, B.C., Lyons, T.W., Young, S.A., Kump, L.R., Knoll, A.H., and Saltzman, M.R., 2011, Geochemical evidence for widespread euxinia in the later Cambrian ocean: Nature, v. 469, p. 80–83.

Glenn, C.R., and Arthur, M.A., 1990, Anatomy and origin of a Cretaceous phosphorite-greensand giant, Egypt: Sedimentology, v. 37, p. 123–154.

Glenn, C.R., Föllmi, K.B., Riggs, S.R., Baturin, G.N., Grimm, K.A., Trappe, J., Abed, A.M., Galli-Olivier, C., Garrison, R.E., Ilyin, A.V., Jehl, C., Rohrlich, V., Sadaqah, R.M.Y., Schidlowski, M., Sheldon, R.E., and Siegmund, H., 1994, Phosphorus and phosphorites—sedimentology and environments of formation: Eclogae Geologicae Helvetiae (Journal of the Swiss Geological Society), v. 87, p. 747–788.

Harper, D.A.T., Hammarlund, E.U., and Rasmussen, C.M.Ø., 2014, End Ordovician extinctions: A coincidence of causes: Gondwana Research, v. 25, p. 1294–1307.

Haxel, G.B., 2005, Ultrapotassic mafic dikes and rare earth element- and barium-rich carbonatite at Mountain Pass, Mojave Desert, Southern California: Summary and field trip localities: U.S.Geological Survey Open-File Report 2005-1219, p. 56–56.

Humphries, M., 2010, Rare earth elements: The global supply chain: Congressional Research Service, CRS Report no. R41347, 27 p.

Ilyin, A.V., 1998, Rare-earth geochemistry of "old" phosphorites and probability of syngenetic precipitation and accumulation of phosphate: Chemical Geology, v. 144, p. 243–256.

Ilyin, A.V., and Boiko, V. S., 1989, The Kisil Kum phosphorite deposits, Middle Asia, USSR, *in* Notholt, A.J.G., Sheldon, R.P., and Davidson, D.F., eds., Phosphate deposits of the world—phosphate rock resources, 2: New York, Cambridge University Press, p. 507–509.

Ingall, E., and Jahnke, R., 1997, Influence of water-column anoxia on the elemental fractionation of carbon and phosphorus during sediment diagenesis: Marine Geology, v. 139, p. 219–229.

International Business Publications, U.S.A., 2013, Saudi Arabia Mineral & Mining Sector Investment and Business Guide: Washington, DC, International Business Publication, 73 p.

Jarvis, I., Burnett, W.C., Nathan, Y., Almbaydin, F.S.M., Attia, A.K.M., Castro, L.N., Flicoteaux, R., Hilmy, M.E., Husain, V., Qutawnah, A.A., Serjani, A., and Zanin, Y.N., 1994, Phosphorite geochemistry—state-of-the-art and environmental concerns: Eclogae Geologicae Helvetiae (Journal of the Swiss Geological Society), v. 87, p. 643–700.

Jasinski, S.M., 2011, Phosphate rock: U.S.Geological Survey Mineral Commodity Summaries, p. 118–119.
Jenkyns, H.C., 2010, Geochemistry of oceanic anoxic events: Geochemistry, Geophysics, Geosystems, v. 11, p. 1–30.
Kaiho, K., Katabuchi, M., Oba, M., and Lamolda, M., 2014, Repeated anoxia-extinction episodes progressing from slope to shelf during the latest Cenomanian: Gondwana Research, v. 25, p. 1357–1368.
Kato, Y., Fujinaga, K., Nakamura, K., Takaya, Y., Kitamura, K., Ohta, J., Toda, R., Nakashima, T., and Iwamori, H., 2011, Deep-sea mud in the Pacific Ocean as a potential resource for rare-earth elements: Nature Geoscience, v. 4, p. 535–539.
Kazakov, A.V., 1939, The phosphate facies: Origin of the phosphorites and the geologic factors of formation of the deposits: Transactions Scientific Institute for Fertilizers and Insect-Fungicides, v. 145, p. 1–106.
Kynicky, J., Smith, M.P., and Xu, C., 2012, Diversity of rare earth deposits: The key example of China: Elements, v. 8, p. 361–367.
Lécuyer, C., Reynard, B., and Grandjean, P., 2004, Rare earth element evolution of Phanerozoic seawater recorded in biogenic apatites: Chemical Geology, v. 204, p. 63–102.
Liu, X.-c., Wang, W., Shen, S.-z., Gorgij, M.N., Ye, F.-c., Zhang, Y.-c., Furuyama, S., Kano, A., and Chen, X.-z., 2013, Late Guadalupian to Lopingian (Permian) carbon and strontium isotopic chemostratigraphy in the Abadeh section, central Iran: Gondwana Research, v. 24, p. 222–232.
Long, K.R., Van Gosen, B.S., Foley, N.K., and Cordier, D., 2010, The principal rare earth elements deposits of the United States—a summary of domestic deposits and a global perspective: U.S.Geological Survey Scientific Investigations Report 2010-5220, 96 p.
Martin, E.E., and Scher, H.D., 2004, Preservation of seawater Sr and Nd isotopes in fossil fish teeth: Bad news and good news: Earth and Planetary Science Letters, v. 220, p. 25–39.
McArthur, J.M., and Walsh, J.N., 1984, Rare-earth geochemistry of phosphorites: Chemical Geology, v. 47, p. 191—220.
McKelvey, V.E., Cathcart, J.B., and Worthing, H.W., 1951, Preliminary note on the minor-metal content of Florida phosphate rock: Trace Elements Investigations, Memorandum 236, 6 p.
McKelvey, V.E., Williams, J.S., Sheldon, R.P., Cressman, E.R., Cheney, T.M., and Swanson, R.W., 1959, The Phosphoria, Park City and Shedhorn Formations in the western phosphate field, U.S. Geological Survey Professional Paper 313-A, 47 p.
McLaughlin, P.I., Emsbo, P., and Brett, C.E., 2012, Beyond black shales: The sedimentary and stable isotope records of oceanic anoxic events in a dominantly oxic basin (Silurian; Appalachian basin, USA): Palaeogeography, Palaeoclimatology, Palaeoecology, v. 367–368, p. 153–177.
McLennan, S.M., 1989, Rare earth elements in sedimentary rocks: Influence of provenance and sedimentary processes: Reviews in Mineralogy, v. 21, p. 169–200.
Notholt, A.J.G., Sheldon, R.P., and Davidson, D.F., 1989a, Europe—introduction, *in* Notholt, A.J.G., Sheldon, R.P., and Davidson, D.F., eds., Phosphate deposits of the world—phosphate rock resources, 2: New York, Cambridge University Press, p. 363–369.
——1989b, Middle East—introduction, *in* Notholt, A.J.G., Sheldon, R.P., and Davidson, D.F., eds., Phosphate deposits of the world—phosphate rock resources, 2: New York, Cambridge University Press, p. 312–315.
——1989c, South America—introduction, *in* Notholt, A.J.G., Sheldon, R.P., and Davidson, D.F., eds., Phosphate deposits of the world—phosphate rock resources, 2: New York, Cambridge University Press, p. 90–94.
——1989d, USSR and Mongolian People's Republic—introduction, *in* Notholt, A.J.G., Sheldon, R.P., and Davidson, D.F., eds., Phosphate deposits of the world—phosphate rock resources, 2: New York, Cambridge University Press, p. 478–481.
——1989e, Asia—introduction, *in* Notholt, A.J.G., Sheldon, R.P., and Davidson, D.F., eds., Phosphate deposits of the world—phosphate rock resources, 2: New York, Cambridge University Press, p. 437–442.
——1989f, North America and Greenland—Introduction, *in* Notholt, A.J.G., Sheldon, R.P., and Davidson, D.F., eds., Phosphate deposits of the world—Phosphate rock resources, 2: New York, Cambridge University Press, p. 1–5.
——1989g, Africa—introduction, *in* Notholt, A.J.G., Sheldon, R.P., and Davidson, D.F., eds., Phosphate deposits of the world—Phosphate rock resources, 2: New York, Cambridge University Press, p. 164–170.
Palastanga, V., Slomp, C.P., and Heinze, C., 2011, Long-term controls on ocean phosphorus and oxygen in a global biogeochemical model: Global Biogeochemical Cycles, v. 25, p. 1–19.
Pasero, M., Kampf, A.R., Ferraris, C., Pekov, I.V., Rakovan, J., and White, T.J., 2010, Nomenclature of the apatite supergroup minerals: European Journal of Mineralogy, v. 22, p. 163–179.
Picard, S., Le'cuyer, C., Barrat, J.-A., Garcia, J.-P., Dromart, G., and Sheppard, S.M.F., 2002, Rare earth element contents of Jurassic fish and reptile teeth and their potential relation to seawater composition (Anglo-Paris basin, France and England): Chemical Geology, v. 186, p. 1–16.
Piper, D.Z., 1999, Trace elements and major element oxides in the Phosphoria Formation at Enoch Valley, Idaho-Permian sources and current reactivities: U.S.Geological Survey Open-File Report 99-163, 66 p.
——2001, Marine chemistry of the Permian Phosphoria Formation and basin, southeast Idaho: Economic Geology, v. 96, p. 599–620.
Piper, D.Z., Baedecker, P.A., Crock, J.G., Burnett, W.C., and Loebner, B.J., 1988, Rare earth elements in the phosphatic-enriched sediment of the Peru shelf: Marine Geology, v. 80, p. 269–285.
Salehi, H., 1989, The sedimentary phosphate resources of Iran, *in* Notholt, A.J.G., Sheldon, R.P., and Davidson, D.F., eds., Phosphate deposits of the world—phosphate rock resources, 2: New York, Cambridge University Press, p. 323–328.
Sanematsu, K., and Watanabe, Y., 2016, Characteristics and genesis of ion-adsorption-type rare earth element deposits: Reviews in Economic Geology, v. 18, p. 55–79.
Service, R.F., 2010, Nations move to head off shortages of rare earths: Science, v. 327, p. 1596–1597.
Shields, G.A., and Stille, P., 2001, Diagenetic constraints on the use of cerium anomalies as palaeoseawater redox proxies: An isotopic and REE study of Cambrian phosphorites: Chemical Geology, v. 175, p. 29–48.
Shields, G.A., and Webb, G.E., 2004, Has the REE composition of seawater changed over geological time?: Chemical Geology, v. 204, p. 103–107.
Sholkovitz, E.R., 1994, Ocean particle chemistry: The fractionation of rare earth elements between suspended particles and seawater: Geochimica et Cosmochimica Acta, v. 58, p. 1567–1579.
Sholkovitz, E.R., Shaw, T.J., and Schneider, D.L., 1992, The geochemistry of rare earth elements in the seasonally anoxic water column and porewaters of Chesapeake Bay: Geochimica et Cosmochimica Acta, v. 56, p. 3389–3402.
U.S. Geological Survey, 2011, Phosphate rock, minerals yearbook,v. I: Metals and minerals: Mineral commodity summaries: U.S.Government Printing Office, p. 118–119.
Van Cappellen, P., and Ingall, E.D., 1994, Benthic phosphorus regeneration, net primary production, and ocean anoxia: A model of the coupled marine biogeochemical cycles of carbon and phosphorus: Paleoceanography, v. 9, p. 677–692.
Verplanck, P.L., Mariano, A.N., and Mariano, A., Jr., 2016, Rare earth element ore geology of carbonatites: Reviews in Economic Geology, v. 18, p. 5–32.
Wright, J., Schrader, H., and Holser, W.T., 1987, Paleoredox variations in ancient oceans recorded by rare earth elements in fossil apatite: Geochimica et Cosmochimica Acta, v. 51, p. 631–644.
Xie, Y., Hou, Z., Goldfarb, R.J., Guo, X., and Wang, L., 2016, Rare earth element deposits in China: Reviews in Economic Geology, v. 18, p. 115–136.
Zhang, P., Wiegel, R., and El-Shall, H., 2006, Phosphate rock, *in* Kogel, J.E., Trivedi, N.C., Barker, J.M., and Krukowski, S.T., eds., Industrial minerals and rocks—commodities, markets, and uses: Littleton, Colorado, Society for Mining, Metallurgy, and Exploration, Inc. (SME), p. 703–722.
Zielinski, R.A., Al-Hwaiti, M.S., Budahn, J.A., and Ranville, J.F, 2011, Radionuclides, trace elements, and radium residence in phosphogypsum of Jordan: Environmental Geochemistry and Health, v. 33, p. 149–165.

©2016 Society of Economic Geologists, Inc.
Reviews in Economic Geology, v. 18, pp. 115–136

Chapter 6

Rare Earth Element Deposits in China

Yuling Xie,[1,†] Zengqian Hou,[2] Richard J. Goldfarb,[3,4] Xiang Guo,[1] and Lei Wang[1]

[1]*University of Science and Technology Beijing, Beijing 100083, P.R. China*

[2]*Institute of Geology, Chinese Academy of Geological Science, Beijing 100037, P.R. China*

[3]*U.S. Geological Survey, Denver Federal Center, Denver, Colorado 80225*

[4]*State Key Laboratory of Geological Processes and Mineral Resources, China University of Geosciences, Beijing 100083, P.R. China*

Abstract

China is the world's leading rare earth element (REE) producer and hosts a variety of deposit types. Carbonatite-related REE deposits, the most significant deposit type, include two giant deposits presently being mined in China, Bayan Obo and Maoniuping, the first and third largest deposits of this type in the world, respectively. The carbonatite-related deposits host the majority of China's REE resource and are the primary supplier of the world's light REE. The REE-bearing clay deposits, or ion adsorption-type deposits, are second in importance and are the main source in China for heavy REE resources. Other REE resources include those within monazite or xenotime placers, beach placers, alkaline granites, pegmatites, and hydrothermal veins, as well as some additional deposit types in which REE are recovered as by-products.

Carbonatite-related REE deposits in China occur along craton margins, both in rifts (e.g., Bayan Obo) and in reactivated transpressional margins (e.g., Maoniuping). They comprise those along the northern, eastern, and southern margins of the North China block, and along the western margin of the Yangtze block. Major structural features along the craton margins provide first-order controls for REE-related Proterozoic to Cenozoic carbonatite alkaline complexes; these are emplaced in continental margin rifts or strike-slip faults.

The ion adsorption-type REE deposits, mainly situated in the South China block, are genetically linked to the weathering of granite and, less commonly, volcanic rocks and lamprophyres. Indosinian (early Mesozoic) and Yanshanian (late Mesozoic) granites are the most important parent rocks for these REE deposits, although Caledonian (early Paleozoic) granites are also of local importance. The primary REE enrichment is hosted in various mineral phases in the igneous rocks and, during the weathering process, the REE are released and adsorbed by clay minerals in the weathering profile. Currently, these REE-rich clays are primarily mined from open-pit operations in southern China.

The complex geologic evolution of China's Precambrian blocks, particularly the long-term subduction of ocean crust below the North and South China blocks, enabled recycling of REE-rich pelagic sediments into mantle lithosphere. This resulted in the REE-enriched nature of the mantle below the Precambrian cratons, which were reactivated and thus essentially decratonized during various tectonic episodes throughout the Proterozoic and Phanerozoic. Deep fault zones within and along the edges of the blocks, including continental rifts and strike-slip faults, provided pathways for upwelling of mantle material.

Introduction

China is responsible for more than 95% of the world's rare earth element (REE) production (Tse, 2011) and contains a number of giant deposits. As of the end of 2011, the REE resource in China was about 136 million metric tons (Mt). The Bayan Obo and Maoniuping REE deposits are the first and third largest REE deposits in the world, respectively. In addition, yttrium (Y) reserves in China are 0.22 Mt, which represents more than one-third of the world's Y reserve of 0.54 Mt (U.S. Geological Survey, 2012).

World REE resources are contained dominantly in bastnaesite and monazite. Bastnaesite-rich ($REE[CO_3]F$) deposits in China contain most of the economic REE resources, whereas monazite-rich ($REE[PO_4]$) deposits are less significant. Large numbers of REE deposits have been mined in China, which include the economically important carbonatite-related and ion adsorption (IAR) deposit types, as well as less significant residual placer, monazite or xenotime placer, beach placer, pegmatite-hosted, alkaline granite-related, and hydrothermal vein deposits. Other REE production is as a by-product from the development of other deposit types. Carbonatite-related REE deposits are the most important for the light REE (LREE), whereas the IAR deposits are second in significance and are the most important heavy REE (HREE) source in China. A large amount of literature, both in English and Chinese, has been published about the REE deposits in China, but details regarding geologic settings, geochronology, and structural controls are still controversial.

Focusing on the available information regarding the tectonic, geologic, and geochemical features of known REE provinces and deposits, this paper provides an up-to-date review of REE deposits in China. The various types of REE resources are summarized in Tables 1 to 5, and the relative importance of each type is displayed in Figure 1.

Deposit Types and Recognized Resources

The carbonatite-related REE deposits (Table 1) comprise the main source of LREE resources in China. The two largest

† Corresponding author: e-mail, yulingxie63@hotmail.com

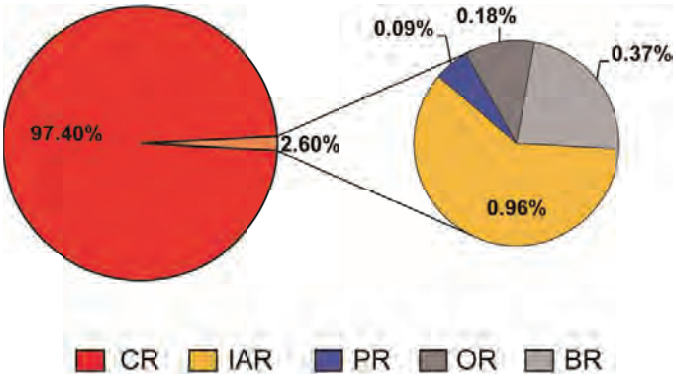

Fig. 1. Relative resource percentages of various REE deposit types in China. Abbreviations: BR = deposits with REE as by-products, CR = carbonatite-related REE deposits, IAR = ion adsorption REE deposits, PR = placer and beach placer REE deposits, OR = other and unknown types of REE deposits.

of these are the Bayan Obo deposit in Inner Mongolia and the Maoniuping deposit in Sichuan province, and they are described in detail below. As of the end of 2011, about 20 carbonatite-related REE deposits were stated to contain total REE resources of more than 134 million metric tons (Mt) as rare earth oxides (REO), representing 98.40% of the total REE resource in China (Fig. 1). In addition to the two giant deposits, other carbonatite-related REE deposits are associated with the Tan-Lu fault system in eastern China, the eastern Qinling-Dabie orogenic belt, and carbonatite complexes in the northern part of Xinjiang in northwestern China (Fig. 2).

The IAR deposits (Table 2) are generally of low grade, but the HREE and LREE, as well as Y, can be easily extracted from the clays and, therefore, these have been referred to as the easily worked deposits of REE (Neary and Highley, 1984). In the past few decades, more than 169 IAR deposits have been exploited. Because of the confidential nature of the mining activity, most tonnage data for IAR deposits are not available. Based on limited published material, the estimated total REE resource in IAR deposits, including some resources in associated residual placers, is more than 1.3 Mt or about 0.97% of the total REE resource of China (Fig. 1). These deposits are spatially restricted to southeastern China (Fig. 3).

Placer and beach placer REE deposits (Table 3) contribute very minor amounts of REE to China's overall total resource. The REE placers are distributed mostly in the South China block, where they have a close spatial association with the IAR deposits (Fig. 4). Additional minor placers are in the North China block and Alpine-Himalayan orogen. The REE are concentrated in resistant minerals, such as monazite and xenotime. As of the end of 2011, 26 placer and beach placer REE deposits were recognized and they had a combined resource of 0.12 Mt, accounting for 0.09% of the total REE resource of China.

Other REE resources in China include those in pegmatites, alkaline granites, and hydrothermal veins (Table 4, Fig. 4). A total of 27 REE deposits of these types or types of unclear affinity have been reported in China, with an additional

Table 1. Carbonatite-Related REE Deposits in China

No	Deposit	Location	Main commodity	Average grade (REO wt %)	Total resource (REO)	Reporting year	Reference
C1	Baynan Obo (Main and East orebody)	Baotou, Inner Mongolia	LREE, Nb, Th, Fe	6	57.4 Mt	2014	Fan et al. (2014)
	Baynan Obo (West orebody)	Baotou, Inner Mongolia	LREE, Nb, Th, Fe	1.158–3.026	60.67 Mt	2005	*
	Bayan Obo surrounding area (including Boluotou, East Jielegele, etc.)	Baotou, Inner Mongolia	LREE, Nb, Th, Fe	3.14	10.47 Mt	2009	*
C2	Baerzhe (801)	Zhalute, Inner Mongolia	Nb	/	245,757 t (Nb_2O_5)	2009	*
C3	Taohualashan	Alashanyouqi, Inner Mongolia	Nb	/	7,760 t (Nb_2O_5)	1975	*
C4	Dulahala	Baotou, Inner Mongolia	Nb, Fe, REE	0.3–3	21.76 Mt	1967	*
C5	Ganluodi	Xichang, Sichuan province	Nb, Zr	/	/	1966	*
C6	Lizhuang	Mianning, Sichuan province	LRE, Nb, Th, Ba	1.47–1.63	5,764 t	2006	*
C7	Muluo	Mianning, Sichuan province	LREE, fluorite	/	0.1 Mt	2011	*
C8	Maoniuping	Mianning, Sichuan province	LREE	2.95	3.17 Mt	2010	**
C9	Nanhe	Mianning, Sichuan province	LREE, Y	5.25–6.4	14,725 t	2005	*
C10	Haha	Mianning, Sichuan province	LREE	3.15–4.05	966 t	2005	*
C11	Baozishan	Mianning, Sichuan province	LREE	/	/	1966	*
C12	Sanchahe	Mianning, Sichuan province	LREE	1.86	6,177 t	2009	*
C13	Dalucao	Dechang, Sichuan province	LREE, Pb	5.21	81,556 t	2007	*
C14	Chishan	Weishan, Shandong province	LREE	3.25	119,962 t	1975	*
C15	Longbaoshan	Cangshan, Shandong province	LREE	2.1–3.54	12,431 t	1997	*
C16	Badoushan	Zibo, Shandong province	LREE	0.13–0.21	1,952 t	2001	*
C17	Hujiazhuang	Laiwu, Shandong province	Nb, REE, P	1	9,994 t	1973	*
C18	Miaoya	Zhushan, Hubei province	REE, Nb	1.5	392,974 t	1981	*
C19	Jiertage	Kashi area, Xinjing	REE	3.46	5,678 t	2002	Zou et al. (2002)
C20	Sitaduwei	Baicheng, Xinjing	REE	0.037–0.111	REE occurence	2002	Zou et al. (2002)

Notes: * = Online material from National Geology Archives of China (http://www.ngac.cn/) and the references herein; ** = 109 Geological Brigade of Sichuan Bureau of Geology and Mineral Resource (2010); "/" = grade or tonnage data not acquired

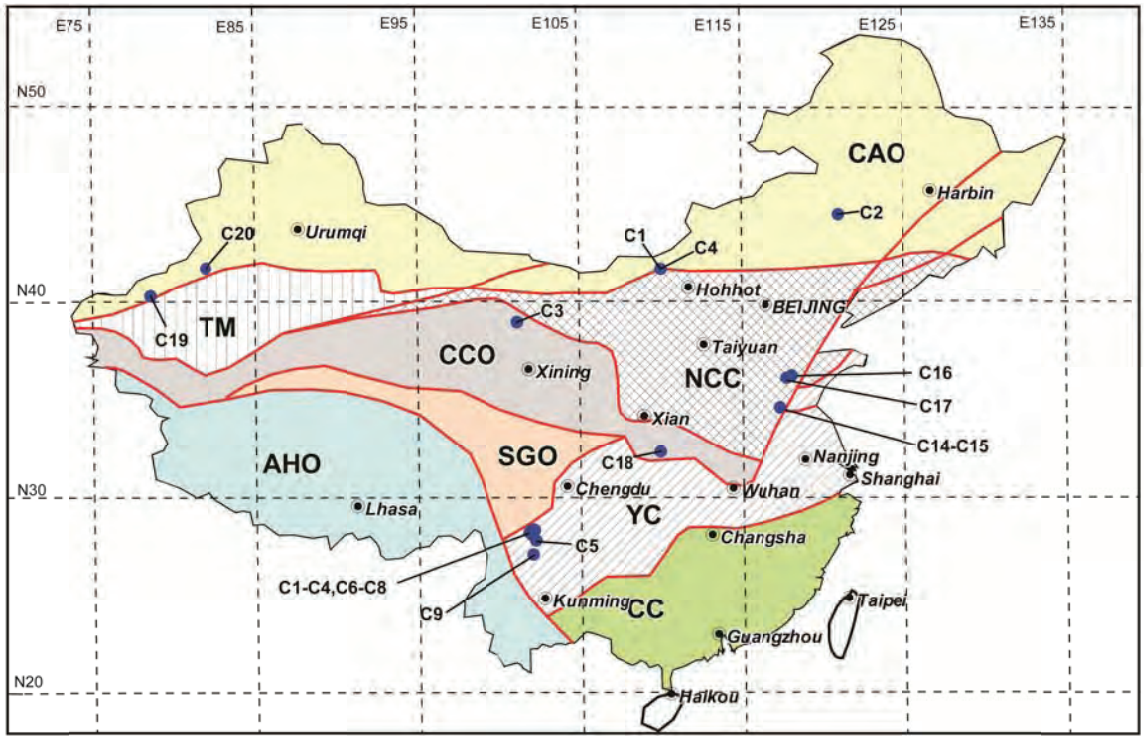

Fig. 2. The distribution of carbonatite-related REE deposits in China with tectonic setting (for deposit numbers, see Table 1; tectonic setting based on Kusky et al., 2007). Abbreviations: AHO = Alpine-Himalayan orogen, CAO = Central Asia orogen, CC = Cathaysia craton, CCO = central China orogen, NCC = North China craton, SGO = Songpan-Ganzi orogen, TM = Tarim block, YC = Yangtze craton.

Table 2. Ion Adsorption-Type (including associated residue placer) REE Deposits in China[1]

No.	Deposit	Location	Type	Main commodities	Average grade (REO wt%)	Reporting year	Total REO resource (t)
Jiangxi province							
R1	Zudong (701)	Longnan	IAR	Y dominated HREE	0.0979–0.1072	1979	17,622
	Lintang, Fukeng, Dongjiang, Wenlong, Liren, Huangsha, Guanxi, Dongjiang	Longnan (8 deposits)	IAR	/	/	2003	/
	Zhulanfu	Huichang	IAR	LREE	0.117	1988	2,836
	Chongxianaobei	Xingguo	IAR	Y	0.03–0.081	1972	22,878
	Nanyuan	Zixi	IAR	LREE	0.1084–0.106	1987	519
	Heling	Xunwu	IAR	LREE	/	1977	239,456
	Xiangmukeng	Xunwu	IAR	LREE	0.082	1990	2,520
	Nanqiao	Xunwu	IAR+RP	LREE	0.189	1986	102,386
	Dinglong	Xingguo	IAR	Y, Eu, LREE	0.083	1988	310
	Zhonghe, Youkeng, Yaoxia-Hantangao, Waxia, Tuziao, Tongmu, Lannikeng, Hejicha, Dongkengao, Datangkeng, Chigang, Anxi	Xinfeng (13 deposits)	IAR	/	/	2003	/
	Longshe	Xinfeng	IAR	REE	0.102–0.160	1988	1,884
	Beipu	Shanjiang	IAR	HREE	0.0824–0.1240	1974	/
	Aoshan	Shanjiang	IAR	REE	\	1990	206
	Xiazao	Wanan	IAR	REE	0.091–0.098	1989	202
	Xinwuzai	Shangyou	IAR	LREE	0.055–0.077	1988	521
	Wantianchating	Ruijin	IAR	REE	0.06	1988	259
	Boying	Ruijin	IAR	LREE	0.088	1989	474
	Yukeng	Quannan	IAR	REE	0.134–0.214	1981	83,800
	Changcheng	Quannan	IAR	/	/	2003	/
	Dongshang	Ninggang	IAR	HREE	0.1%	1989	176.59
	Datang	Ninggang	IAR	REE	0.08	1990	414.88
	Getian	Ninggang	IAR	REE	0.074	1990	3,609
	Xiaobu	Ningdu	IAR	REE	/	2003	/
	Huangpi, Dagu	Ningdu	IAR	REE	/	2003	/
	Dongshanba	Ningdu	IAR	REE	0.113	1989	859.2

Table 2. *(Cont.)*

No.	Deposit	Location	Type	Main commodities	Average grade (REO wt%)	Reporting year	Total REO resource (t)
Jiangxi province *(cont.)*							
	Yangfu, Tiancun, Jifu, Huxin, Hanfang, Datian, Dafu	Ganxian	IAR	/	/	2003	/
	Shatou	Dingnan, Ganzhou,	IAR+PR	LREE, Moz	0.0995	1976	79,700
	Zhushanbei, Yingjia, Mazhukeng, Changkengwei, Zhangtiantang, Xiaoman, Xikeng, Tianluokeng, Tianlaolikeng, Kaizidong, Tianchenao, Sanqiutian, Qingjingtang, Nongji No. 6, Shengcaoping, Neitoukeng, Muzishan, Longchuankeng, Laopengshan, Laolikeng, Laohukeng, Laishuikeng, Jingbei, Jingtoukeng, Jiazibei, Dashuishan, Dakeng, Bengguang, Baishuizhai, Aonao, Aobeitang, Anshan	Dingnan, Ganzhou (32 deposits)	IAR	REE	/	2003	/
	Bijiashan	Dingnan, Ganzhou	IAR+PR	Xt	0.0425	1977	769.2
	Shitoukeng	Dingnan, Ganzhou	IAR	REE	0.091	1988	3,997
	Zhangkeng	Anyuan	IAR	REE	0.104	1989	1,341
	Lidong	Anyuan	IAR	REE	0.132	1988	965
	Changli, Xikeng, Tuwu, Tongluo, Niupiqi, Lengkeng, Gutian, Gangxia, Dashiao, Chetou	Anyuan(10 deposits)	IAR	REE	/	2003	/
	Donghu	Lean, Fuzhou	RP+AP	Xt, Moz	Xt: 41.6–134.0g/t; Moz: 149.3–197.8g/t	1974	Xt: 118; Moz: 287
	Hukeng	Anfu	RP	Xt, Moz, Eux, Tn, Nbt	/	1973	REO: 5,122; Xt: 1,442; Tn+Nbt+ Eux: 1,615
	Luokeng	Dayu	RP	Xt, Moz, Eux, Th	Xt: 136.2g/m^3; Moz: 86.9g/m^3; Zr: 140.8 g/m^3; a	1970	Xt: 10,944; Moz: 819; Zr: 1,061
	Changling	Shangyou	IAR+RP	REO, Xt, Moz, Zr	Xt: 98.5g/t; Moz: 99.32g/t; Zr: 121.28g/t; REO: 0.0355	1971	Xt: 5,230; Moz: 5,514; Zr: 6,837
	Zhangjiapai	Shicheng	IAR+RP	HREE	0.0379–0.0455	1976	REO: 762
	Tangfang	Guangchang	IAR+RP	Moz, Xt	0.0502	1981	REO: 257
Guangdong province							
	Gonghe	Jiangmen	IAR	REE	/	2011	REO: 62,200
	Datang-7369	Xingning	IAR	LREE	0.118–0.623	1986	REO: 4,459
	Zhongheling	Xingning	IAR	LREE	0.143	1986	REO: 1,322
	Laishi (Luilong)	Xinfeng	IAR	REE	0.056	1979	REO: 56,449
	Xinyi	Wuhua, Meizhou	IAR	HREE dominated	0.07	1987	REO: 372
	Huacheng	Wuhua, Meizhou	IAR	Y, HREE	0.067–0.090	1987	REO: 257
	Zhaibeiding	Ruyuan	IAR+RP	HREE, Kao	0.00095	1988	REO: 7,957
	Shantang	Qingyuan	IAR	HREE	0.092	1988	REO: 216
	Renju	Pingyuan, Meizhou	IAR	REE	0.173	2004	REO: 11,914
	Bachi	Pingyuan, Meizhou	IAR	LREE	0.167	1987	REO: 28,369
	Renhedian	Luhe	IAR	REE	0.104	1989	REO: 692
	Hongxingcun	Longchuan	IAR	REE	0.116	1989	REO: 1,332
	Baimiao	Liannan	IAR	REE	0.064–0.084	1989	REO: 22
	Wufang	Jieyang-Jiexi	IAR	HREE	0.099	1992	REO: 115,241
	Mantoushan	Jiexi-Jieyang	IAR	HREE dominated	0.074–0.119	1992	REO: 73,384
	Sishui	Jiaoling-Pingyuan	IAR	LREE dominated	0.1–0.115	1992	REO: 28,015
	Kengtou	Jiaoling	IAR	HREE	0.07	1987	REO: 142
	Zuokeng	Huidong	IAR	Y+LREE	0.122	1990	REO: 21,505
	Gonghe	Heshan	IAR	LREE+HREE	0.151	1989-	REO: 12,376
	Longpi	Heping	IAR	LREE dominated	0.14–0.197	1986	REO: 1,156
	Yousheng	Heping	IAR	REE	0.171	1987	REO: 10,853
	Shihan	Heping	IAR	LREE	0.163	1987	REO: 14,412
	Shiziao	Heping	IAR	LREE	0.188–0.168	1986	REO: 443
	Guyun	Dongyuan	IAR	LREE+HREE	0.14	2006	REO: 930
	Wufeng	Dabu	IAR	REE	0.093	2010	REO: 5,481
	Fenlangzhen	Meizhou	IAR	LREE	0.126	1988	REO: 200
	Fengtian	Shaoguan	IAR	HREE dominated	0.037–0.088	1987	REO: 215
	512 xenotime mine	Guangning	RP	Moz	Xt: 71g/t	1972	Xt: 3,763; Moz: 6,958; Zr: 10,311

Table 2. *(Cont.)*

No.	Deposit	Location	Type	Main commodities	Average grade (REO wt%)	Reporting year	Total REO resource (t)
Hunan province							
	Mangshan (Cibaling)	Yizhang	IAR+RP	REE	0.112	1986	REO: 1,469
	Yijiang	Rucheng	IAR	REE, Sc	10.102	1990	REO: 4,221.8
	Dadi	Guidong	IAR	LREE+HREE	0.065–0.099	1989	REO: 245
	Gupeshan	Jianghua	IAR+RP	REE	0.1	1986	REO: 113,318
Fujiang province							
	Guanpi (Shangtu segment)	Zhaoan	IAR	LREE dominated	0.0607	1987	REO: 123
	Zhongjiape	Changting	IAR	REE	/	1986	REO: 277
	Zhongfang	Changting	IAR	REE	0.093	2009	REO: 1,776
	Yangmeikeng	Changting	IAR	REE	0.0508–0.0608	1987	REO: 152
	Nantang	Changting	IAR	REE	0.082	1988	REO: 11,211
	Luodi	Changting	IAR	REE	0.05309–0.05603	1987	REO: 308
	Yangguling	Changting	IAR	HREE dominated	0.0364–0.0504	1986	REO: 304
	Jiuxi	Yunxiao	IAR	Y, Sm, Eu, Dy	0.03843–0.0419	1986	REO: 46
	Liangshan	Wuping	IAR	Y, Eu	0.0455%	1987	REO: 19
	Dayangquan	Wuping	IAR	Y, Eu	0.0405–0.036542	1986	REO: 63
	Fuxian	Shanghang	IAR	REE	0.0150–0.0200	1987	REO: 18
	Shaxiaba	Shanghang	IAR	Y, Eu	0.0484	1986	REO: 98
	Lingbeikeng	Shanghang	IAR	Y, Eu	0.05195–0.04354	1986	REO: 346
	Jiazhuang	Shanghang	IAR	REE	0.059	2007	REO: 315.89
	Qiankeng	Qingliu	IAR	REE	0.0624	1987	REO: 117.32
	Wei	Qingliu	IAR	REE	0.061343	1986	REO: 156
	Qingzhou	Qingliu	IAR	Ce	0.058245–0.064355	1986	REO: 303
	Niuyun	Pinghe	IAR	LREE	0.071–0.087	1986	REO: 250
	Zhangjiatang	Ninghua	IAR+RP	Eu, Y, LREE	0.07–0.09	1989	REO: 1,192
	Fengdouchao	Ninghua	IAR	LREE	0.074–0.077	2006	REO: 334
	Sipu	Liancheng	IAR	Ce, La	0.0350–0.0600	1987	REO: 95
	Pengkou	Liancheng	IAR	Y, Eu	0.03–0.06	1986-1987	REO: 1,381
	Wenfang	Liancheng	IAR	REE	0.047	2006	REO: 780
	Huangfang	Liancheng	IAR	REE	0.079	2005	REO: 714
	Lutian-Shangli	Jianning	IAR	Er, Eu, Y	Er_2O_3:0.083%	1988	REO: 504
	Houyang	Mingxi	RP	Xt, Moz, Zr	/	1972	REO: 76,773; Xt: 8,278; Moz: 1231; 6
	Aiyang xenotime mine	Jianning	RP	Xt, Moz, Zr	Xt: 147.34 g/m^3; Moz: 138.82 g/m^3; Zr: 99.39 g/m^3	1972	Xt: 25; Moz: 22; Zr: 17
	Houyang xenotime mine	Mingxi	RP	Xt, Moz, Zr	Xt: 60.76–96.5; 9 g/m^3	1974	Xt: 177; Moz: 285; Zr: 1,093
Zhejiang province							
	Daping	Suichang	IAR	LREE	0.05	1991	REO: 2434
	Banqiao	Songyang	IAR	REE	0.109	1996	REO: 1143
	Hedi	Qingyuan	IAR	La, Nd, Eu	/	1997	REO: 3583
Guangxi province							
	Huashan	Zhongshan-Fuchuan,	IAR	REE	0.1–0.181	1992	REO: 136400
	Liutang	Chongzuo	IAR	REE	/	1999	/
Yunnan province							
	Adebo monazite mine	Jinping, Yunnan province	RP	Moz, Zr	250–300	1963	Moz: 2878
Heilongjiang province							
	Lianzhuzhen	Mishan city, Heilongjiang province	IAR	REE	0.138–1.05	1991	/

Notes: Abbreviations: Cas = cassiterite, Eux = euxenite, Fet = fergusonite, Gar = garnet, Ilm = ilmenite, Kao = kaolinite, Moz = monazite, Nb = niobite; Ru = rutile, Wf = wolframite, Xt = xenotime, Zr = zircon; AP = placer REE deposit, IAR = ion adsorption-type REE deposit, RP = residue placer REE deposit; "/" = grade or tonnage data not acquired

[1] Online material from National Geology Archives of China (http://www.ngac.cn/) and the references herein

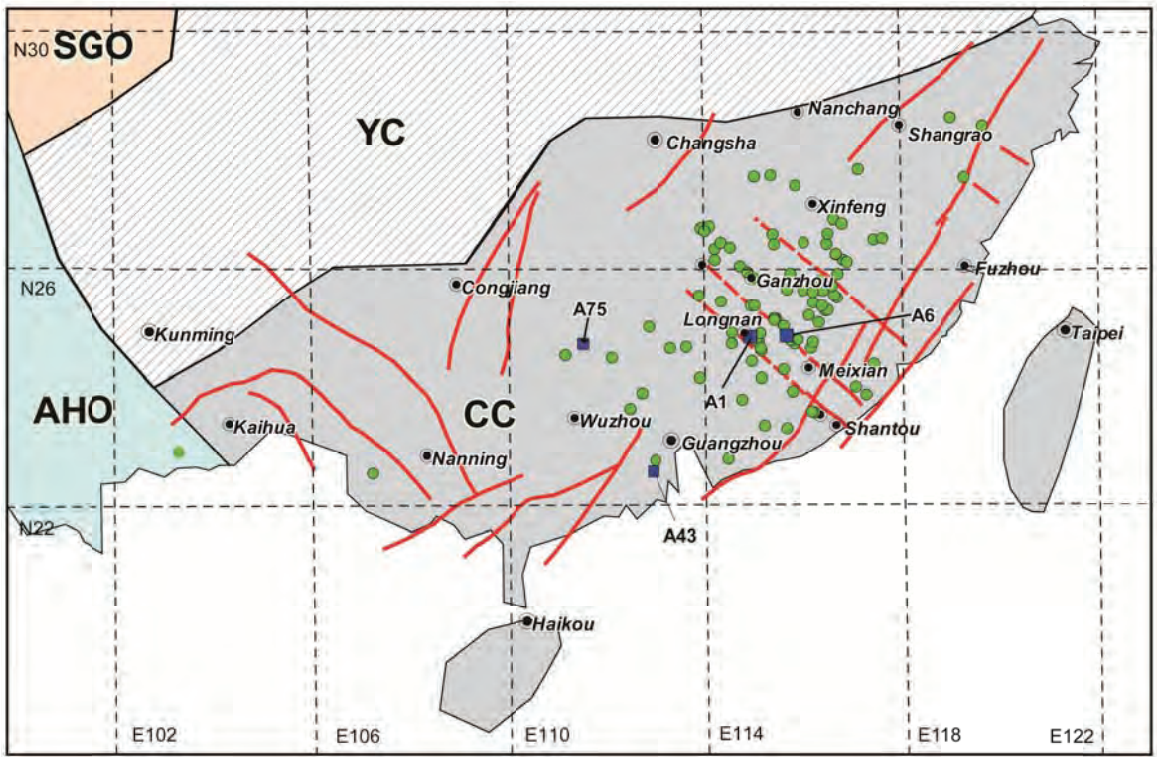

Fig. 3. The distribution of ion adsorption REE deposits in China with tectonic settings (for deposit numbers, see Table 2; tectonic setting same as Fig. 2). Green filled circle = deposit, blue filled square = key deposits, red line = regional fault (based on Ren et al., 1999); red dashed line = estimated regional fault based on RS image.

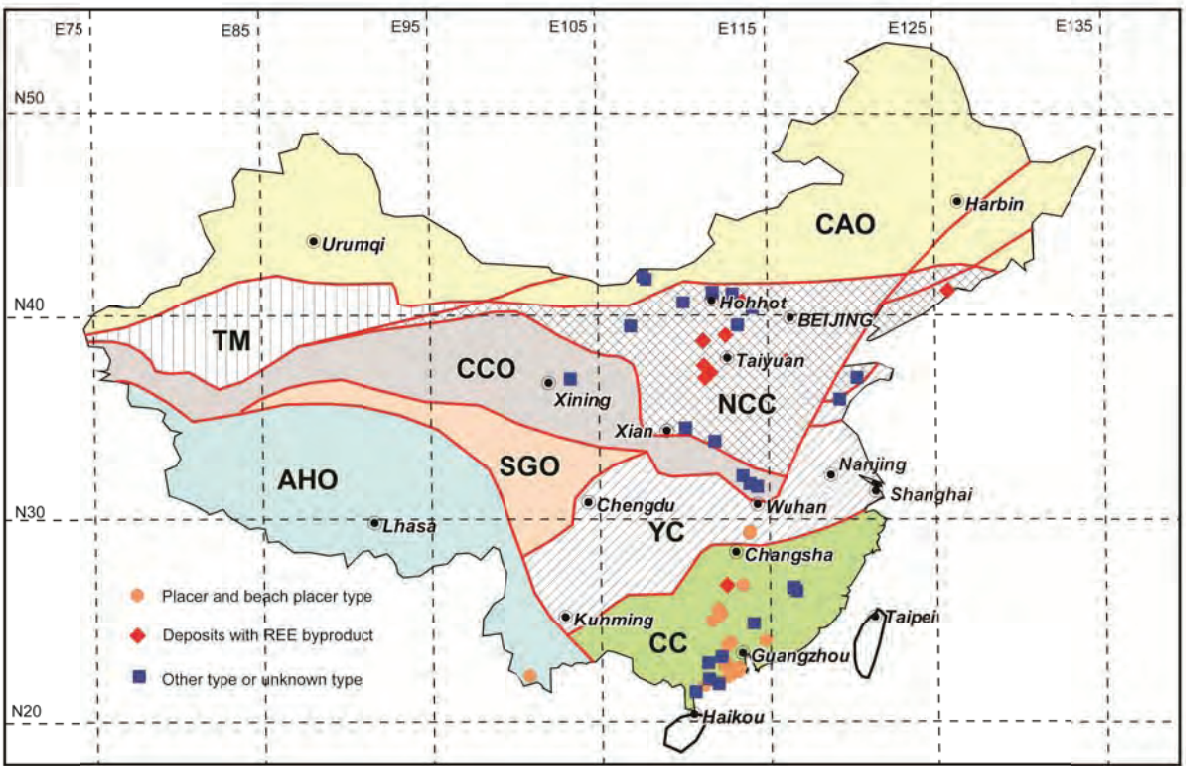

Fig. 4. The distribution of placer, beach placer, and other types of REE deposits in China with tectonic settings (tectonic setting same as Fig. 2).

Table 3. Placer and Beach Placer-Type REE Deposits in China[1]

No	Deposit	Location	Main commodities	Average grade (g/m^3)	Total resource (t)	Reporting year
S1	Mengwang monazite deposit	Menghai, Yunnan province	Moz, Zr, Ilm, Ru	Moz: 620; Zr: 690; Ilm: 5,052	Moz: 12,645; Zr: 13,863; Ilm: 101,522	1963
S2	Niulanyong monazite deposit	Yangjiang, Guangdong province	Moz	/	Moz: 5,725	1959
S3	Helukou fergusonite deposit	Jianghua, Hunan province	Fet	Fet: 50–150	Fet: 172,039	1961
S4	Qiancaochong-Yangjiaping fergusonite deposit	Lanjia, Hunan province	Fet, Xt, Moz, Zr, Nt, Ilm, Cas, Wof	Fet: 50–70	Fet: 6	1960
S5	Shilichong fergusonite deposit	Lanjia, Hunan province	Fet, Moz	Fet: 50; Moz: 40	Fet: 2; Moz: 4	1960
S6	Dazipengwa fergusonite deposit	Lanjia, Hunan province	Fet	Fe: 50; Moz: 1,120	Fet: 16; Moz: 48	1960
S7	Yiyang river deposit	Anren, Hunan province	Zr, Moz	/	Zr: 470; Moz: 80; Ilm:13,660	1960
S8	Liuli'ao monazite deposit	Tongcheng, Hubei province	Moz, Zr, Ru	/	Moz: 1,375	1960
S9	Juanshui monazite deposit	Chongyang, Hubei province	Moz, Zr, Gar, Ru	Moz: 334–611	Moz: 13,937	1960
S10	Wudong monazite deposit	Xinxing, Guangdong province	Moz	/	747	1955
S11	Sheyu monazite and zircon deposit	Xinxing, Guangdong province	Moz, Zr, Ilm	Moz: 312; Zr: 441	Moz: 8,975; Zr: 11,777; Ilm: 7,541	1960
S12	Jiaokeng deposit	Taishan, Guangdong province	Fet	Fet: 88.44	Fet: 18	1960
S13	Gudoutianchang REE deposit	Xinhui, Guangdong province	Fet, Moz, Zr, Cas	Fet: 56–251; Moz: 3.8–20.6; Zr: 2.2; Cas: 42.5–248.4	Fet: 4; Cas: 5	1959
S14	Taling fergusonite deposit	Xinhui, Guangdong province	Fet, Moz	Fet: 93; Moz: 190; Zr: 165	Fet: 85; Moz: 174; Zr: 151	1960
S15	Sancun REE deposit	Xinhui, Guangdong province	Fet, Moz, Zr	Fet: 58.4; Moz: 207; Zr: 67	Moz: 939; Fet: 183; Zr: 533	1960
S16	West bank of Tan river (Tanjiangxi'an) monazite and zircon deposit	Xinhui, Guangdong province	Moz, Zr	Moz: 350–228; Zr: 291–168	Moz: 952; Zr: 924; Fet: 6	1960
S17	Hengshui REE deposit	Xinhui, Guangdong province	Fet, Moz, Zr	Fet: 5.4–95.9; Moz: 11.15–260.48; Zr: 24.08–255	Fet 34; Moz 75	1959
S18	Shikengkou deposit	Taishan, Guangdong province	Fet, Moz, Zr	Moz: 52.6; Fet: 39	Fet: 9	1960
S19	Goupili monazite deposit	Heyuan, Guangdong province	Moz	/	/	1958
S20	Jingqu Ta-niobite deposit	Zhaoqing, Guangdong province	Tn, Moz, Ilm	Tn: 119	Nb_2O_5: 5; Ilm: 3; Moz: 2	1972
S21	Madianhe xenotime deposit	Dianbai, Guangdong province	Xt, Moz, Zr	Xt: 111–133; Moz: 90–350; Zr: 744–860; Ilm: 450–463	Xt: 1,069; Ilm: 4,437	1973
S22	Wuhe deposit	Guangning, Guangdong province	Moz, Xt, Zr, Ilm	Moz: 423; Xt: 132; Zr: 100–200; Ilm: 150–300	Moz: 495; Xt: 155	1970
S23	Nansandao deposit	Zhanjiang, Guangdong province	Xt, Moz	Zr: 1,021–1,882; Moz: 118–354	Zr: 19,836	1959
S24	Zhapozhen deposit	Yangjiang, Guangdong province	Moz	Moz: 550	Moz: 236	1959
S25	Wangcungang deposit	Dianbai, Guangdong province	Zr, Moz, Ilm	Zr: 1,640; Moz: 222	Zr: 2,304	1959

Notes: Abbreviations: Cas = cassiterite, Fet = fergusonite, Gar = garnet, Ilm = ilmenite, Moz = monazite, Nb = niobite, Nt = niotanite, Ru = rutile, Tn = tanniobite, Wf = wolframite, Xt = xenotime, Zr = zircon; "/" = grade or tonnage data not acquired

[1] Online material from National Geology Archives of China (http://www.ngac.cn/) and the references herein

combined REE resource of 0.24 Mt or 0.18% of the total REE resource of China. Some resources are also defined as by-products in the mining of phosphate, bauxite, uranium, and kaolinite deposits. Twelve deposits with REE as a by-product commodity (Table 5) have a reported combined REO resource of 0.5 Mt, accounting for 0.37% of the total REE resource of China.

Carbonatite-Related LREE deposits

Carbonatite-related LREE deposits in China occur in continental rifts and in collisional orogens and were formed throughout the past 1.5 billion years during the Mesoproterozoic Jinningian (e.g., Bayan Obo), late Paleozoic Hercynian (e.g., Miaoya), late Mesozoic Yanshanian (e.g., Chishan), and Cenozoic Himalayan (e.g., Maoniuping) orogenies. These different aged deposits are typically associated with belts of REE deposits, such as the Bayan Obo-Langshan,Weishan-Laiwu-Zibo (e.g., Chisan), and Mianning-Dechang (e.g., Maoniuping) REE belts. Miaoya, however, is, at least presently, an isolated occurrence in the Qinling-Dabie orogen.

The Bayan Obo-Langshan REE belt is located along the northern margin of the North China block and is about 400 km long from east to west. The belt is dominated by the giant Bayan Obo deposit (57.4 Mt REO), which was discovered as

Table 4. Other REE Deposit Types in China

No	Deposit	Location	Main commodities	Average grade (REO wt % [3])	Deposite type	Reporting year	Total resource (REO, t)	Reference
O1	Zhoujiagou	Fangshan; Shanxi province	Eux, Xt	/	Granite-related	1972	3,069[1]	*
O2	Yuantou	Huayin; Shanxi province	Moz, Alt	/	Vein style	1972	2,490	*
O3	Zhuangzishang	Suozhou, Shanxi province	Apt, REE	/	Vein style	1962	7,085	*
O4	Wanghuizhuang	Datong; Shanxi province	P_2O_5, REE	1.95-3.75	Vein style	1974	2,200	*
O5	Dazhuzhi	Rizhao; Shandong province	Moz, U, Th	/	Unknown	1980	51,000	*
O6	Butou	Laixi; Shandong province	Moz, U, Th	0.016	Pegmatite	1974	398	*
O7	Ninghua	Ninghua; Fujian province	REE, Sc	/	Unknown	1988	8,000	*
O8	Yihenchahan	Wulate; Inner Mongolia	Alt, REE	/	Unknown	2009	6,714	*
O9	Zhaojinggou	Wuchuan, Inner Mongolia	Nb, Tb, REE	/	Unknown	1972	864	*
O10	Hayehutong	Baotou; Inner Mongolia	Alt, REE	0.0054	Pegmatite	1957	906	*
O11	Chahangou	Chayou; Inner Mongolia	LREE, Te	0.0204	Pegmatite	1972	229	*
O12	Chaganmiao	Wulate; Inner Mongolia	REE, Nb, Th, U, Be0.0020	Granite	1959	4,324	*	
O13	Laohuchong	Yingshan; Hubei province	Y0.074-0.082	Metamorphosed volcanic	1979	3,454	*	
O14	Guangshui	Yingshan; Hubei province	Y 0.0009	Unknown	1980	8,334	*	
O15	Dengjiawan	Dawu; Hubei province	Y0.054-0.064	Unknown	1979	246	*	
O16	Dazhaiyu	Luanchuan; Henan province	Y	Hydrothermal	1971	684	*	
O17	514	Yunfu; Guangdong province	Xt 0.0005	Granite	1973	/	*	
O18	Aizizhen	Shixing; Guangdong province	Fe, Xt, Moz	/	Pegmatite	1970	21	*
O19	Xiangumiao and Shanglai	Luoding; Guangdong province	Xt, Moz	/	Granite	1972	/	*
O20	Xijiangpai	Shicheng; Jiangxi province	Xt, Eux, Moz	0.0002	Pegmatite	1972	532	*
O21	Liantang	Shicheng; Jiangxi province	Nb, Ta, REE	0.0002	Pegmatite	1977	1,487	*
O22	Ganshahenao	Tianzhu; Gansu province	Zr, Ilm0.0089	Pegmatite	1999	136,136	*	
O23	301	Wuhai; N Inner Mongolia	Li, Th, REE	0.08-0.19	Alkaline rock	1961	4,738	*
O24	Ketagexi	Weili county, Xinjing	REE, Nb, Ta, Zr	0.045-0.099	Alkaline syenite	2002	Not confirmed	Zou et al. (2002)
O25	Boziguoer	Baicheng, Xinjiang	REE, Y, Nb, Ta	0.07-0.19	Alkaline granite	2002	Not confirmed	Zou et al. (2002)
O26	Yilankeli	Baicheng, Xinjiang	REE, Y	1.559	Alkaline pegmatite	2002	Not confirmed	Zou et al. (2002)
O27	Kuoshibulake	Atushi city, Xinjiang	REE, Y	2.433	Hydrothermal	2002	Not confirmed	Zou et al. (2002)

Notes: * = Online material from National Geology Archives of China (http://www.ngac.cn/) and the references herein; abbreviations: Alt = allanite, Eux = euxenite, Ilm = ilmenite, Moz = monazite, Xt = xenotime, Zr = zircon; "/" = grade or tonnage data not acquired

[1] For Xt, not REO

an iron deposit in 1927 and began producing REE as a by-product 30 years later (Tse, 2011). In recent years, the REE resources in Bayan Obo have taken more of an important role. Although iron is important, the REE have become a major commodity in this area and some solely REE orebodies are being exploited. Although there are still different opinions regarding the mineralization age and the genesis of the Bayan Obo deposit, the majority of researchers now suggest that the REE mineralization is related to Mesoproterozoic carbonatites and alkaline rocks that formed in a continental margin rift environment (Zhang et al., 1994; Fan et al., 2006; Le Bas, 2006; Yang et al., 2011). There are some features at the deposit that resemble those of the iron oxide-copper-gold (IOCG) deposits (e.g., Wu, 2008), a class of deposits that shows some overlap with the carbonatite-related REE deposits (e.g., Groves et al., 2010). The northern margin of the North China block and the Bayan Obo deposit itself both were subjected to early and late Paleozoic magmatism (Zhang et al., 1994; Liu et al., 2004) and deformation (Zhang et al., 2003), which have led to much of the complexity and controversy associated with geochronological studies of the deposit.

The Himalayan Mianning-Dechang REE belt in western Sichuan province, southwestern China, is approximately 270 km long and 15 km wide along a general north-south trend. It includes one giant (Maoniuping: 3.17 Mt REO), two intermediate (Dalucao: 0.082 Mt REO; Muluo: 0.1 Mt REO), and a number of small REE deposits (e.g., Lizhuang) and occurrences (Fig. 2, Table 2). The REE belt is located within the western margin of Yangtze craton of the South China block (Fig. 2) and follows a Permian paleorift zone. The host carbonatite rocks and associated alkaline rocks were emplaced between ca. 36 and 13 Ma (Tian, 2006, 2008a, b; Hu et al., 2012), which was a period when the western margin of the block was reactivated as the eastern part of the Indo-Asian Himalayan collisional orogen. The REE mineralization that is associated with the carbonatite-alkalic complexes is

Table 5. Deposits with REE As By-products In China

No.	Deposit	Location	Economic commodity	Average grade (REO, wt %)	Discovery date	Total REE resource (REO, t)
B1	Xiangwang	Xiaoyi; Shanxi province	Bauxite	/	2003	373,407
B2	Xihonghe	Xinzhou; Shanxi province	Bauxite	/	2007	6,717
B3	Tuanshuitou	Lvliang; Shanxi province	Bauxite	/	2006	19,248
B4	Houtashang	Lvliang; Shanxi province	Bauxite	/	2006	7,193
B5	Tiejincun	Lvliang; Shanxi province	Bauxite	/	2004	36,281
B6	Puyi	Lvliang; Shanxi province	Bauxite	/	2006	35,500
B7	Qinghe	Ji'an; Jilin province	U	0.014–0.043	/	/
B8	Shiqiehe	Baode; Shanxi province	Bauxite	/	2005	9,959
B9	Aoshan	Maanshan; Anhui province	Fe	/	1959	/
B10	Qiganliang	Fengzhen; Neimeng province	P	/	1973	13,425
B11	Kenwei	Qingyuan; Guangdong province	Kao	/	1987	175
B12.	Shawei	Huiyang	Kao, Ta, Y, Moz, Xt	/	1977	Nb_2O_5: 497; Ta_2O_5: 514; Xt: 1,674; Moz: 487

Notes: * = Online material from National Geology Archives of China (http://www.ngac.cn/) and the references herein; abbreviations: Kao = kaolinite, Moz = monazite, Xt = xenotime; "/" = grade or tonnage data not acquired

spatially associated with a series of Cenozoic strike-slip faults constrained by the ancient Panxi rift. The complexes consist of carbonatitic sills or dikes, and associated alkaline syenite stocks, which intruded Yanshanian granites, Proterozoic basement, and Devonian-Cretaceous sedimentary rock sequences. The REE mineralization is dated by molybdenite Re-Os and by Rb-Sr techniques, with results indicating ore formation at 28.5 Ma (Y-L. Xie, unpub. data, 2014) at the Lizhuang deposit and 29.9 Ma at the Maoniuping deposit (Hu et al., 2012), respectively. These dates overlap those of the widespread postcollisional magmatism throughout the Qinghai-Tibet plateau area (Hou et al., 2006).

The Weishan-Laiwu-Zibo REE belt in Shandong province is situated in the eastern margin of the North China block. The belt is about 250 km long and 50 km wide and trends north-south along the western side of the continental-scale Tan-Lu fault zone. Some of the REE mineralization is genetically related to emplacement of a syenite-related, carbonatite-alkaline complex that is imprecisely dated on unspecified minerals by K-Ar methods at 174 to 119 Ma (Yu et al., 2010). The mineralization, as dated by both K-Ar (unspecified minerals) and Rb-Sr (muscovite), is more narrowly constrained to the period of 119.5 to 107 Ma (Lan et al., 2011; Yu et al., 2010). Four REE deposits and a number of carbonatite-hosted occurrences are known in this belt, including the Chishan deposit in Weishan County (C14, Fig. 2), Longbaoshan deposit in Cangshan County (C15, Fig. 2), Badoushan deposit in the Zibo area (C16, Fig. 2), and Hujiazhuang deposit in the Laiwu area (C17, Fig. 2; Table 1).

The Miaoya REE deposit, which is located in Hubei province, is the only identified carbonatite-related REE deposit in the 2,400-km-long Qinling-Dabie orogenic belt. The NW-trending orogen and the Miaoya REE deposit are situated in the reactivated southern margin of the North China block. The REE mineralization is genetically related to a Hercynian carbonatite that has a K-Ar biotite age of 278 Ma (Li, 1980, 1991). In addition to the Miaoya deposit, two REE deposits of uncertain type have also been reported in the eastern edge of the orogen (e.g., Denjawan and Zhuangzishang in Hubei provinces). Furthermore, a number of carbonatite-related Mo deposits have been dated by Re-Os methods in the western part of the orogen, which include the ca. 209.5 Ma Huangshui'an and ca. 220–221 Ma Huanglongpu deposits in Shannxi province (Huang et al., 2009; Xu et al., 2009). Therefore, the orogen has a high favorability for the discovery of future carbonatite-related REE deposits.

Bayan Obo REE deposit

Geology: The giant Bayan Obo deposit in Inner Mongolia is the largest REE deposit in the world and also contains important resources of Nb and Fe. Reported reserves for the main and east orebodies are 57.4 Mt at an average grade of 6% REO, 2.2 Mt averaging 0.13% Nb_2O_5, and at least 1,500 Mt averaging 35% Fe (Fan et al., 2004a, b, 2014). It was primarily explored and mined as an Fe deposit with REE recovered as a by-product. Bayan Obo is located in the Langshan-Bayan Obo continental margin rift at the northern margin of North China block (Drew et al., 1990; Chao et al., 1997). Geologic features, mineral assemblages, geochemistry, and geochronology of the deposit have been extensively studied during the past 25 years (e.g., Institute of Geochemistry, 1988; Drew et al., 1990; Yuan et al., 1991, 1995; Chao et al., 1992, 1997; Smith et al., 2000; Smith, 2007; Zhang, P.S. et al., 2002; Zhang, Z.Q. et al., 2003; Fan et al., 2006; Wang et al., 2010; Qiu et al., 2011; Yang et al., 2011; Lai and Yang, 2013).

The strata in the deposit region are mainly those of the Mesoproterozoic Lower Bayan Obo Group and, to a lesser extent, the Archean Wutai Group. The Bayan Obo Group has been divided into nine lithologic units from H1 to H9, with the H8 dolomite being the dominant host rock for the REE orebodies (Fig. 5). Gentle regional east-west folds are distributed throughout the deposit area. The major fault in the Bayan Obo area is the Kuangou fault, which also strikes east-west.

Igneous rocks in the Bayan Obo district include a Hercynian dioritic-granitic pluton, which is composed of granite, K-feldspar granite, granitic diorite, gabbro diorite, gabbro, monzonitic granite, and biotite granite (Fan et al., 2009), and numerous Proterozoic anorogenic igneous rocks, which are composed of trachyte, magnesioarfvedesonite-feldspatite, potash-rhyolite, dacite, rhyolite, quartz porphyry, trachy basalt (Wang et al., 2003), and carbonatite (Drew et al., 1990;

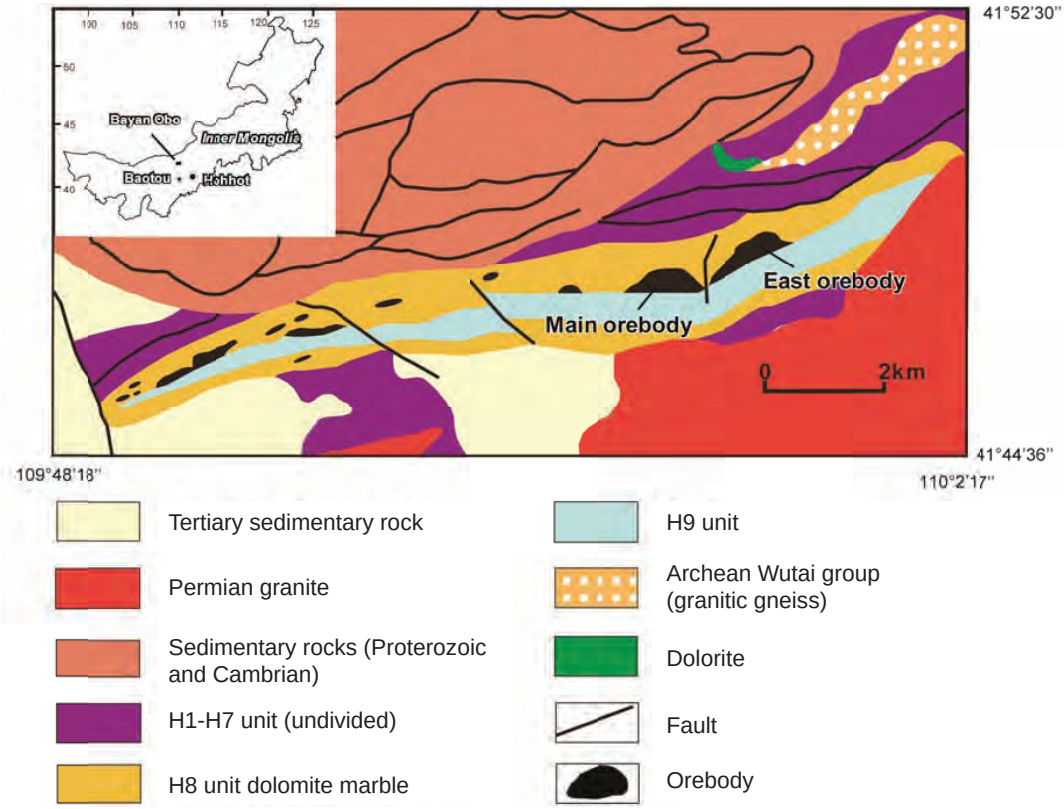

Fig. 5. Simplified geologic map of the Bayan Obo REE deposit, Inner Mongolia (modified after Chao et al., 1997).

Yuan et al., 1991; Fan et al., 2006; Le Bas et al., 2007). The carbonatite occurs as dikes and as a unit of massive dolomite marble, assuming that the H8 unit is indeed carbonatite, an assumption that is well supported by recent geochemical data (e.g., Yang et al., 2011). Based on the mineral assemblages and geochemical data, the carbonatite can be divided into a calcite carbonatite, dolomite carbonatite (or the so-called dolomite marble), and calcite-dolomite carbonatite (Wang et al., 2002).

The deposit consists of a main orebody, an east orebody, and a series of small west orebodies, as well as a skarn that is related to the Hercynian granite (Fan et al., 2004a; Liu et al., 2004) in the eastern part of the deposit. In 2009, exploration identified an additional REO resource of >10 Mt, mainly located in deposits to the east (Boluotou) and south (East Jielegele) of the main deposit (Table 1). The orebodies of the main deposit are aligned along an E-W-striking belt. The main and east orebodies occur as large lenses trending east-west and northeast, respectively. The dominant alteration in this deposit is fenitization, reflecting widespread Na metasomatism, with a resulting mineral assemblage of fluorite, aegirine, riebeckite, albite, and quartz. Fenitization along the contact between the dolomite marble and K-rich country-rock slates is common. The main orebodies occur in dolomite marble of the H8 unit, which has been interpreted as a carbonatite comprising both volcanic rock (Xiao et al., 2003; Wang et al., 2010) and intrusive rock (Liu, 1985; Wang et al., 2002; Le Bas et al., 2007; Yang et al., 2011; Liu et al., 2012), as well as a sedimentary rock that has undergone a hydrothermal overprint (Hou, 1989; Meng and Drew, 1992; Yang, X.Y. et al., 2000; Qin et al., 2007), a sedimentary rock (Yang and Drew, 1994; Zhang et al., 2012), and a hydrothermal-replacement body of a sedimentary rock (Lai et al., 2012). The various interpretations of the H8 unit have been at the center of the long-term argument about the genesis of the deposit, but detailed geochemical data (e.g., Yang et al., 2011) indicate that H8 is likely a Mesoproterozoic carbonatite intrusion.

The mineral assemblage of the Bayan Obo deposit is extremely complex. The dominant ore minerals include magnetite, niobite ($[Fe, Mn]Nb_2O_6$), bastnaesite, bunsite ($REE_2Ca[CO3]_3F_2$), aechynite, monazite, and xenotime. New REE-bearing minerals discovered in the deposit include baotite ($Ba(Nb, Ti)_2SiO_7$) and baiyuneboite ($NaBaCe_2[F(CO_3)_4]$). Details of the mineral assemblages are described by Zhang et al. (2001, 2002). From the periphery of the carbonatite bodies inward, the mineralization varies from disseminated ores in dolomite, to banded ore, aegirine-rich assemblages, riebeckite-rich assemblages, and finally to a massive ore (Fig. 6).

Geochronology/geochemistry: Many papers discuss the geochemistry of the Bayan Obo deposit, including the major and trace element compositions, stable and radiogenic isotopes, geochronology of the dolomite marble (H8), carbonatite dikes, and REE ores. Although the genesis of the H8 dolomite is still a controversial topic, the genetic link between the carbonatite and the ores has been widely accepted. Carbonatite-related hydrothermal fluids are most commonly called upon to explain the formation of the REE ores (e.g., Smith et al., 2000; Fan et al., 2006; Qin et al., 2007).

Results from many geochronology studies of Bayan Obo have most consistently been interpreted to indicate that the main REE-related magmatism and the mineralization events

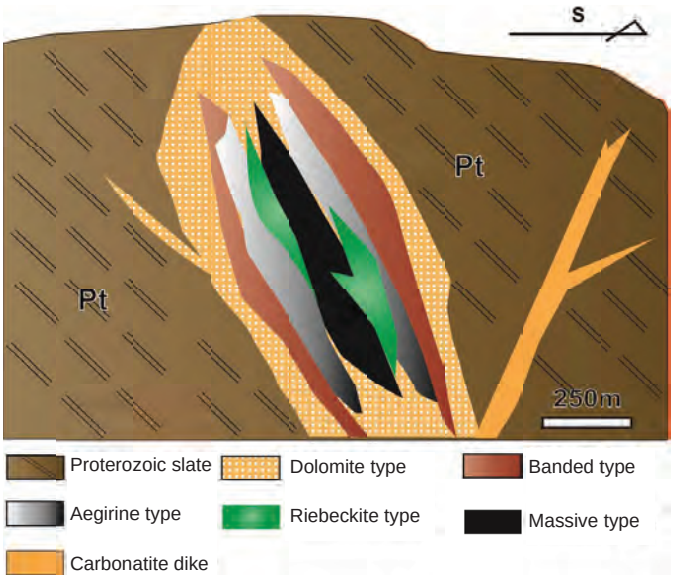

Fig. 6. Ore deposit model for the Bayan Obo REE deposit, showing the ore-style variations in the deposit.

are Mesoproterozoic (e.g., Liu et al., 2001; Zhang et al., 2003). Mineral Sm-Nd isochrons yielded ages of 1313 Ma (Ren et al., 1994) and 1250 Ma (Zhang et al., 2003), whereas whole-rock Sm-Nd isochrons yielded ages of 1580 Ma (Yuan et al., 1991) and 1286 Ma (Zhang et al., 1994, 2003). Fan et al. (2014) obtained a U-Pb age for zircons from an REE-rich carbonatite dike of ca. 1400 Ma. We agree with the Mesoproterozoic interpretation and argue that many of the younger Neoproterozoic and early Paleozoic dates referenced below are best interpreted as part of the complicated postore geologic history of the deposit.

Conflicting younger age estimates include SHRIMP analyses of monazite grains that gave U-Pb apparent ages ranging from 1000 to 400 Ma (Qiu, 1997), monazite internal Th-Pb isochrones that ranged from 555 to 398 Ma (Wang et al., 1994; Chao et al., 1997), and ^{40}Ar-^{39}Ar plateau ages of riebeckite from 395 to 343 Ma (Chao et al., 1997). Liu et al. (1996) obtained an Re-Os apparent age of 439 Ma for molybdenite in the REE ore. Qiu (1997) suggested that the Bayan Obo deposit underwent multistage ore-forming events and the early mineralization event occurred before 1000 to 800 Ma, whereas the major ore-forming event happened at 340 Ma (based on the U-Pb age of monazite) or 408 Ma (based on the Pb-Th age of monazite). Zhang et al. (2003) preferred that the main ore-forming event occurred in the Mesoproterozoic or Neoproterozoic and was overprinted in the early Paleozoic. Based on Sr-Nd isotope results, Yang et al. (2011) proposed a 1.35 Ga mineralization event and Paleozoic modification of the ores, a geochronological model that now is widely accepted. Smith et al. (2014) also suggested two ore-forming stages, one initial stage at ca. 1300 Ma and the second defined by remobilization of Fe and REE, as well as the introduction of Nb at ca. 450 Ma; later Permian magmatism was the preferred cause of the overprinting skarn assemblage. Campbell et al. (2014), based upon zircon SHRIMP ages, argued that the initial ore elements were deposited at 1325 ± 60 Ma and were remobilized during a 456 ± 28 Ma alteration event.

Yang et al. (2011) presented the most recent petrochemical data for calcite carbonatite, calcite-dolomite carbonatite, and dolomite carbonatite dikes, as well as for the dolomite marble unit. Their results show that the carbonatite dikes and dolomite marble have similar Sr-Nd isotope compositions and Sr-Nd isochron ages, thus implying a magmatic origin for the dolomite marble. The initial $^{87}Sr/^{86}Sr$ values range from 0.7064 to 0.7089 for the calcite carbonatite, 0.7032 to 0.7082 for the calcite-dolomite carbonatite, and 0.7048 to 0.7055 for the dolomite carbonatite. The $\varepsilon_{Nd(t)}$ values range from –0.47 to +0.65 (Yang et al., 2011). The calcite carbonatite is characterized by a LREE enrichment pattern, whereas the dolomite carbonatite has a flat REE pattern. Yang et al. (2011) interpreted the geochemical data as indicative of a crystal fractionation of an evolving Mesoproterozoic carbonatite magma.

Melt and fluid inclusions have been studied in calcite and barite from the carbonatite dikes and in fluorite from the REE ore (Fan et al., 2004b, 2006; Qin et al., 2007). Melt, melt-fluid, aqueous-vapor, gas, and solid inclusions have all been reported by Qin et al. (2007) as indicating a magmatic origin for the carbonatite dikes. Two- or three-phase CO_2-rich, three-phase hypersaline liquid-vapor-solid, and two-phase liquid-rich inclusions have been recognized in fluorite and quartz from the REE ores (Fan et al., 2006). Microthermometric results show a wide range of homogenization temperatures for different types of inclusions, from less than 100° to 450°C. The carbonic phase in the CO_2-rich inclusions is nearly pure CO_2. Fluids involved in formation of the REE-Nb-Fe mineralization at Bayan Obo have been suggested to be mainly in the H_2O-CO_2-NaCl-(F-REE) system (Fan et al., 2006). The sylvite, barite, and calcite daughter phases in the inclusions (Fan et al., 2006) also indicate high K, Ca, Ba, and SO_4 in the fluid. Coexistence of brine inclusions and CO_2-rich inclusions with similar homogenization temperatures has been taken as evidence that immiscibility of a carbonatite-derived fluid accompanied REE mineralization. The abundant REE-bearing carbonate daughter phases in fluid inclusions provide support that the original ore-forming fluids were very rich in REE. The relatively high homogenization temperatures and salinities of some fluid inclusions indicate an initial dense brine, probably of magmatic/carbonatitic origin, as described by Smith et al. (2000). Carbonatite-related fluids have been shown to include alkali-chloride brines, alkali-carbonate brines (Samson et al., 1995), aqueous carbonic fluids (Ting et al., 1994), and a distinctively dense REE-rich H_2O-CO_2-SO_4 supercritical fluid with elevated Sr, Ba, Ca, Pb, and Zn (Xie et al., 2011). All of these are somewhat consistent with the numerous fluid compositions suggested for the ore-forming solutions at Bayan Obo. The reported inclusions containing different numbers and types of solid phases, including REE-bearing minerals, at Bayan Obo, imply a high solubility of REE and other components.

Genesis and deposit model: The Bayan Obo deposit formed during multiple episodes of hydrothermal activity (Drew et al., 1990; Yuan et al., 1991; Chao et al., 1992, 1997). Workers have suggested that it may be an IOCG deposit (Mao et al., 2008), a SEDEX deposit (Yang and Drew, 1994), a deposit formed from meteorite impact (Yao et al., 1998), a magmatic hydrothermal replacement deposit (Chao et al., 1997; Wang

et al., 2003), and a carbonatite-derived replacement deposit of a sedimentary carbonate unit (Lai et al., 2012). Ling et al. (2013) further developed the sedimentary carbonate replacement model, arguing that the release of Si-rich fluids from a subducting Neoproterozoic through late Paleozoic slab was critical for formation of the giant REE resource. Nevertheless, most geochronological and geochemical data have led the majority of workers to accept a Mesoproterozoic carbonatite-related hypothesis for ore genesis (Le Bas et al., 1992; Yuan et al., 2000; Yang, X.M. et al., 2000, 2003, Fan et al., 2006).

Geochemical data indicate that the carbonatite and ore material have a mantle source, whereas the high Re/Os ratios, highly radiogenic $^{187}Os/^{188}Os$ ratios, and very low Os concentrations in a late-stage pyrite grain suggest a crustal origin for the reduced sulfur (Liu et al., 2004). The REE-, Nb-, Fe-, and Ta-bearing minerals in the Bayan Obo deposit are related to magmatic-hydrothermal events associated with the Mesoproterozoic evolution of a carbonatite magma. Dolomite carbonatite represents the earlier phase of carbonatite, and the calcite carbonatite represents the later phase of the carbonatite (Yang et al., 2011). The mineralization style shows a variation from disseminated ore in altered wall rock, to deformed ore in dolomite, and to massive ore in the center of the dolomite marble (Fig. 6).

The REE mineralization formed in a continental rift environment during the Mesoproterozoic and thus within the ancient Columbia or Nuna supercontinent. This rift may have been originally active as far back as ca. 1900 Ma (e.g., Fan et al., 2014). Reconstructions of the Mesoproterozoic supercontinent suggested that the North China block was amalgamated with the Australian cratons in East Nuna by 1650 to 1580 Ma, and breakup of East Nuna took place between 1450 and 1380 Ma (Pisarevsky et al., 2014). It is very possible that the initial REE mineralization at Bayan Obo correlates with this period of breakup. However, the late pyrite and Nb enrichment at Bayan Obo most likely was formed by hydrothermal events during Paleozoic deformation along the North China block margin (Liu et al., 2004), when the Paleo-Asia Ocean was being subducted below the block after it was rifted from Gondwana (e.g., Goldfarb et al., 2014). Therefore, the present-day ultimate configuration of the orebodies and the final mineral assemblages at Bayan Obo reflect more than 1 b.y. of tectonism and magmatism.

Maoniuping REE deposit

Geology: The Maoniuping giant REE deposit is the most important deposit in the Mianning-Dechang REE belt of southwestern China, and thus the one deposit in the region that has been studied in detail. The reported resources of the deposit include 3.17 Mt REO at an average grade of 2.95 wt %, 0.6 Mt Pb, 0.08 Mt Mo, 13.24 Mt CaF_2, 19.76 Mt $BaSO_4$, and 0.83 Mt $SrSO_4$ (109 Geological Brigade of Sichuan Bureau of Geology and Mineral Resource, 2010). The REE mineralization is associated with Himalayan age carbonatite-alkalic complexes. The geology of the Maoniuping district is described in detail by Hou et al. (2006, 2009). A 146 Ma granite pluton (Zhang et al., 1988) underlies much of the district, which also includes Devonian metamorphosed clastic country rocks, a rhyolite unit of unknown age, and the carbonatite-alkalic complex (Fig. 7).

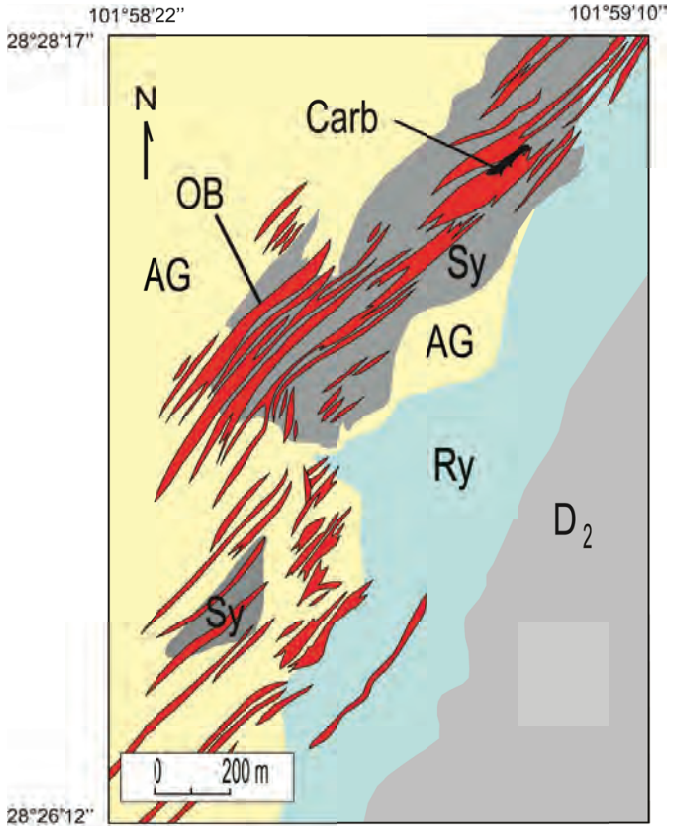

Fig. 7. Simplified geologic map of the Maoniuping REE deposit (after Yuan et al, 1995). Abbreviations: AG = alkaline granite, Carb = carbonatite, D_2 = Middle Devonian, OB = orebody, Ry = rhyolite, Sy = syenite.

The carbonatite-alkalic complex, which was emplaced into the granite and rhyolite, comprises mainly syenite and minor carbonatite sills, stocks, and dikes that have a 29.9 Ma Sm-Nd isochron age (Hu et al., 2012). The mineral assemblages of the carbonatites are dominated by calcite, fluorite, biotite, aegirine, aegirine-augite, arfvedsonite, barite, microcline, apatite, quartz, and REE-bearing minerals, with minor magnetite and sulfides. The 27 to 26 Ma REE mineralization (Hu et al., 2012) occurs as vein systems hosted in carbonatite, nordmarkite, and, to a lesser extent, altered granite and rhyolite. The alteration at Maoniuping is characterized by a fenite halo surrounding the carbonatite and enveloping the REE orebodies. The REE-bearing veinlets, stringers, and stockwork zones surround the carbonatites; some of the ores are also pegmatitic, disseminated, or breccias. The REE orebodies vary in shapes from layerlike, to lenticular, and to pipelike in different ore zones. Bastnaesite is the main REE-bearing mineral, although minor bunsite and chevkinite also contribute to the resource. The pegmatitic ore occurs mainly as large dikes in the upper parts of the carbonatite complex, surrounded by veinlets and stockworks, and zoning downward to disseminated ore in the carbonatite. The minor breccia ore at Maoniuping has carbonatite and pegmatite as cement. No crosscutting relationships have been confirmed among the stockworks, veins, pegmatites, and carbonatite; they all appear to be relatively coeval and interrelated (Xie et al., 2015).

Geochemistry: Mineralogical and geochemical studies indicate that the carbonatites at Maoniuping are dominated by calcite carbonatite and have low concentrations of SiO_2, FeO, and MgO (Xu et al., 2002). The carbonatites are extremely enriched in large ion lithophile elements (LILE; Sr, Ba) and LREE, but relatively depleted in high-field strength elements (HFSE; Nb, Ta, P, Zr, Hf, Ti; Xu et al., 2002), suggesting a metasomatized mantle source. Their O, C, and S isotope compositions are similar to those of primary, mantle-derived carbonatites, also suggesting a mantle source (Xu et al., 2002; Li et al., 2007). Low $\xi_{Nd(t)}$ (–3.2 to –4.2) and relative high $^{87}Sr/^{86}Sr$ (0.706074–0.706149) values, as well as a wide range of $^{207}Pb/^{204}Pb$ (15.526–15.567) and $^{208}Pb/^{204}Pb$ ratios (38.283–39.390; Hou et al., 2006), distinguish them from the Bayan Obo carbonatites. Their Sr, Nd, and Pb isotope signatures indicate notable contamination by crustal materials. Overlapping emplacement ages, isotopic compositions, and mantle-normalized trace element patterns for the spatially associated syenites suggest a liquid immiscibility origin for the carbonatites (Xu et al., 2002; Hou et al., 2006).

Complex melt, melt-fluid, and fluid inclusion assemblages exist in fluorite, quartz, barite, and bastnaesite from carbonatite and REE ores. Net-like sulfate-bearing melt-fluid inclusions are most common in carbonatite-hosted fluoritegrains, which show an early crystallization character and are characterized by consistent solid/aqueous/vapor ratios, indicating that these are the most representative samples of the primary carbonatitic fluid (Xie et al., 2011, 2015). Quartz, barite, and bastnaesite contain a CO_2-rich fluid inclusion assemblage and crystallized later than the fluorite (Xie et al., 2009). Paragenetically heterogeneous trapping of unmixed phases during the carbonatite fluid evolution lead to preservation of varied inclusion assemblages, such as a melt and a melt-fluid inclusion assemblage, a solid-rich and solid-poor CO_2-rich fluid inclusion assemblage, and a CO_2-rich and pure CO_2 fluid inclusion assemblage (Xie et al., 2011, 2015). Microthermometric results demonstrate that the primary carbonatite fluid was a high temperature (650°–850°C), high pressure (>350 MPa) supercritical fluid (Xie et al., 2009) and followed an evolutionary path that included phase separation of a critical fluid at 650° to 850°C, sulfate-melt exsolution from aqueous fluid at 335° to 455°C, and sulfate crystallization over a wide range of temperature (Xie et al., 2011, 2015). The LA-ICP-MS analyses of primary melt-fluid inclusions in fluorite show high LREE concentrations in the primary carbonatite fluid, as well as elevated Pb, Zn, Sr, and Ba. Exsolution of sulfate melt and crystal fractionation of sulfate minerals may have caused the further enrichment of REE and base metals in the residual CO_2-rich fluid that deposited the bastnaesite and quartz (Xie et al., 2009).

Scanning electron microscopy/energy dispersive spectrometer (SEM/EDS) and laser raman microprobe (LRM) analyses of solid phases in melt-fluid and solid-rich fluid inclusions show that almost all solid phases are sulfate minerals, including syngenite ($K_2Ca(SO_4)_2 \cdot H_2O$), glauberite ($Na_2Ca(SO_4)_2$), aphthitalite ($K_3Na(SO_4)_2$, mirabilite ($Na_2SO_4 \cdot 10H_2O$), anhydrite ($CaSO_4$), and celestite ($SrSO_4$; Xie et al., 2011, 2015). The dominance of SO_4 and H_2O in the aqueous phase and CO_2 in the vapor phase is confirmed by LRM results (Xie et al., 2009). The LRM and SEM/EDS data imply a distinctive sulfate-rich ore-forming fluid at Maoniuping.

The microthermometric results for the CO_2-rich inclusions in bastnaesite and quartz indicate that the REE deposition occurred at approximately 275° to 325°C and the unmixing between CO_2 and H_2O was an important mechanism for REE ore formation. Oxygen and carbon isotope data for calcite gangue, combined with $\delta^{13}C_{V\text{-}PDB}$ and δD of fluid inclusions in fluorite and quartz, were interpreted to indicate that the ore-forming fluids were dominantly of orthomagmatic origin, but mixed with an external fluid during the late stages of fluid evolution (Hou et al., 2009).

Ore genesis and deposit model: On the basis of tectonic setting, ore geology, and geochemical data, an ore-forming model can be developed for the Maoniuping REE deposit. Geochemical studies indicate an enriched mantle source for the alkaline carbonatite complexes and an unmixing between the syenite and carbonatite magmas as described by Hou et al. (2006). During the Tertiary India-Asia collision, the Panxi paleorift was reactivated as a series of strike-slip faults along the ancient zone of structural weakness and the carbonatite-alkaline complex was emplaced along the faults. The rapid ascent of the carbonatite magma, and the associated pressure decrease, caused exsolution of a sulfate melt and a CO_2-dominant, REE-rich fluid from the magma. This may have been associated with minor REE precipitation. Further evolution of the fluid, particularly the unmixing between CO_2 and H_2O, caused the bulk of the REE precipitation.

A giant carbonatite body, large fluid volume, and a deep magma chamber are not necessary for the formation of a giant REE deposit because of the high water solubility in a carbonatite magma (Keppler, 2003), effective fluid exsolution, and high REE contents in such a primary carbonatite fluid. A dense primary carbonatite fluid and rapid fluid evolution prevent long distance migration of the REE. Thus, the fenite alteration and REE mineralization occur in or immediately surrounding the causative carbonatite. Maoniuping, and many other carbonatite-related REE deposits of the Mianning-Dechang REE belt are characterized by a zonation from an outer (upper) REE vein system, to a middle REE-bearing pegmatite ore style, and then to an inner (lower) disseminated style (Fig. 8). Breccia-style mineralization may also be present with the pegmatitic and disseminated ores in the carbonatite body.

Ion-Adsorbed Clay REE (IAR) Deposits in Southern China

Almost all IAR deposits are located in southern China, in the Jiangxi, Hunan, Guangdong, Guangxi, and Fujian provinces, although a few are also in the Guizhou and Yunnan provinces. Minor IAR deposits have been also reported in Inner Mongolia, Shandong, and the Shanxi provinces of northern China (Table 2, Fig. 3). The Longnan-Xunwu area is the most important IAR district in China, with widespread Mesozoic granite, and lesser Paleozoic granite and Mesozoic volcanic rock (Fig. 9), determined to be the parent rocks for the deposits. The IAR deposits in southern China occur in the lateritic weathering profiles of mainly felsic intrusive to acidic volcanic rocks, particularly in highly evolved Mesozoic granitoids that are REE rich (Bao and Zhao, 2008). A few small IAR deposits are also reported in the weathering profiles of tuff, diabase, lamprophyre, and basalt (Wu, 1988; Wang et al., 2006; Bao and Zhao, 2008; Yang et al., 2008). The REE in the

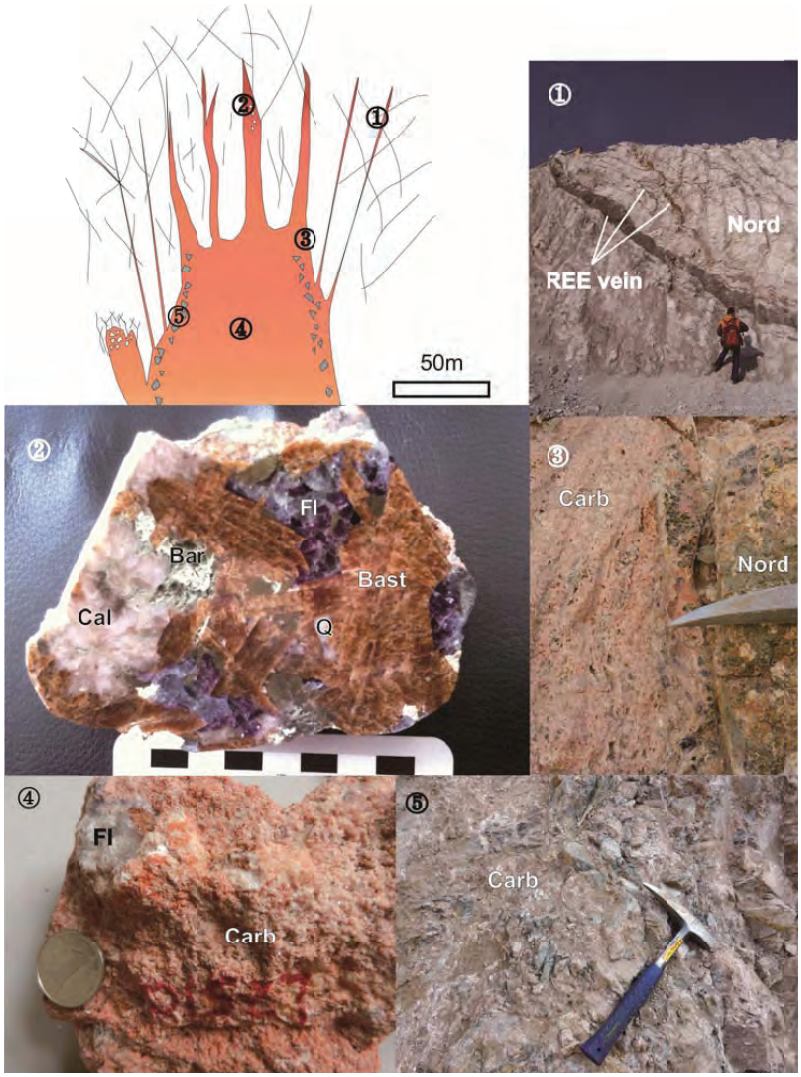

Fig. 8. Deposit model showing the zonation of mineralizing style for deposits of the Mianning-Dechang REE belt. 1 = REE vein and stockwork in nordmarkite, 2 = ore in pegmatite dike, 3 = ore along the contact between carbonatite and nordmarkite, 4 = disseminated ore in the center of carbonatite dike, 5 = breccia ore with carbonatite cement in the outer zone of carbonatite dike; Carb = carbonatite; Bar = barite, Bast = bastnaesite, Cal = calcite, Fl = fluorite, Nord = nordmarkite, Q = quartz.

IAR deposits have been suggested to adsorb to clay minerals, such as kaolinite, during lateritic weathering (Bao and Zhao, 2008). Mentani et al. (2010), however, noted that much of the REE resource could be associated with secondary amorphous phosphates that are mixed with the kaolin group minerals. In Japan, Murakami and Ishihara (2008) noted that much of the HREE resource in IAR deposits might, at least in some cases, be present in residual REE-bearing minerals, such as zircon, that were weathered from parent granitoids. Sanematsu and Watanabe (2016) suggest that the HREE are restricted to the weathering of highly evolved muscovite granites and are concentrated in fluorocarbonates precipitated during late hydrothermal alteration events.

Whitish zones in well-preserved soil profiles are mined for their REE by small pits on many of the hillsides in southern China. The REE had traditionally been leached in pits by sulfuric acid, the solutions were then moved to a second pit, and eventually mixed with oxalic acid to precipitate REE $(COOH)_2$, which is typically rich in the HREE and Y. More recently, however, due to environmental concerns, leaching operations have been moved from the pits to local processing plants.

The IAR deposits in China have been divided into LREE (with Y_2O_3 <50% of the total REE resources) and HREE (with Y_2O_3 >50% of the total REE resources) types, and seven subtypes that include Y-rich HREE; medium Y HREE; Eu-rich, medium Y LREE; La-Nd-Eu-rich, low Y LREE; medium Y, low Eu LREE; Ce-rich LREE; and those of uncertain affinity (He and Wang, 1989). The Longnan-Xunwu-Xinfeng district in Jiangxi province is the largest IAR district and is the most significant HREE producer in the world. The Zudong and Heling REE deposits in the district are typical of the HREE- and LREE-type IAR deposits in China, respectively, and are described in detail below.

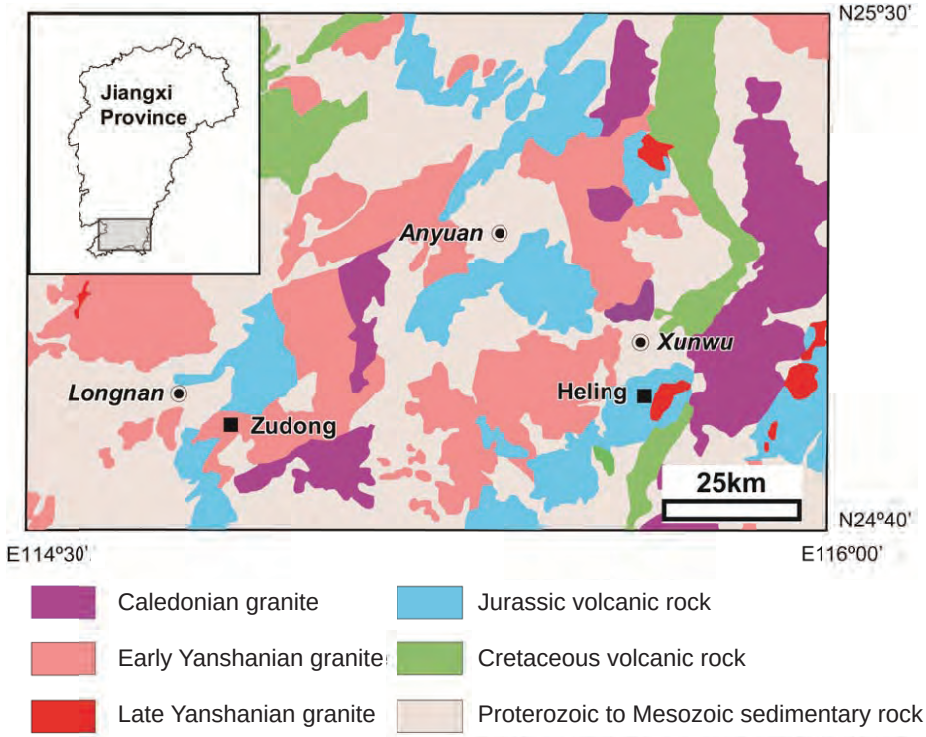

Fig. 9. The distribution of intrusive and volcanic rocks in the Longnan-Xunwu area with deposit location (after Guo, 2010).

Zudong HREE deposit

The Zudong HREE deposit is located in Longnan county, South Jiangxi province (Fig. 9), and was the first discovered IAR deposit in China in the late 1960s. It had a pre-mining total REE resource of 131,000 t at an average grade of 0.048 wt % of yttrium oxide, with the Y estimated to define 35.8 to 62.5% of the total REE resource. There are more than seven other similar REE deposits in the area of Zudong, including Lintang, Fukeng, Dongjiang, Wenlong, Liren, Huangsha, and Guanxi.

The REE mineralization occurs in the weathering profile of the Zudong granite, which was emplaced into an Early Jurassic sequence of tuffs, rhyolite, and rhyolite porphyry (Fig. 10). The Zudong intrusive body is composed of medium-grained, muscovite-, K-feldspar-, and alkali feldspar-bearing granite and medium-grained, biotite- and K-feldspar-bearing granite (Wu, 1988; Huang et al., 1989a, 1993; Wu et al., 1990). Both of the intrusive phases crop out at an elevation of 300 to 400 m, in an area of low-relief hills. Weathered lateritic crusts have a considerable thickness, generally from several meters to 30 m on the tops and ridges of the hills, and they become gradually thinner in downslope areas (Wu, 1988; Wu et al., 1990).

The accessory minerals in the muscovite-bearing granite consist mainly of doverite, fluorite, and zircon, with minor monazite, gadolinite, xenotime, and chernovite. Doverite hosts about 60% of the REE in the intrusion and is the major contributor to REE accumulation in the weathering profile owing to its weak resistance to weathering processes. In contrast, the accessory mineral assemblage of the biotite-bearing granite is simple and dominated by monazite, xenotime, and zircon, with minor apatite and fluorite. Bao and Zhao (2008) indicated that the Zudong granite was altered to an albite-muscovite-fluorite-carbonate assemblage and the muscovite-bearing rocks are more altered than the biotote-bearing phases. The degree of alteration is the possible cause of the difference in accessory mineral assemblages. It is possible, in other words, that some of the REE-bearing accessory minerals in the granite may be hydrothermal alteration products formed prior to the extensive weathering.

The Zudong granite has an Rb-Sr isochron age of 147.7 ± 3.0 Ma and an initial $^{87}Sr/^{86}Sr$ value of 0.7188 (Huang et al., 1989b). The chemical composition is within the range of most S-type granites (Bao and Zhao, 2008). A well-developed weathering profile has formed above the granite. From the top downward, the profile includes a surface soil zone (A horizon), a completely weathered zone (B horizon), a semi-weathered zone (C horizon), a weathering front (D), and an unweathered granite (E). Zones B and C compose the REE orebody (Fig. 11). A changing sequence of mineral assemblages can be correlated with the progressive development of the weathered crust. The uppermost Zone A has a mineral assemblage of kaolinite + halloysite ± gibbsite + goethite, Zone B is dominated by halloysite + kaolinite + vermiculite, and Zone C includes halloysite + kaolinite + montmorillonite + mica.

Huang et al. (1989a) proposed a model for the enrichment of REE in the Zudong deposit that included a parent granite with a high HREE concentration. During hydrothermal alteration of the granite, the REE-bearing minerals were converted to more easily liberated, F-bearing, HREE-rich carbonate. During the long-term weathering and leaching process, the REE were adsorbed by clay minerals, and perhaps phosphates, to form the economic IAR deposit.

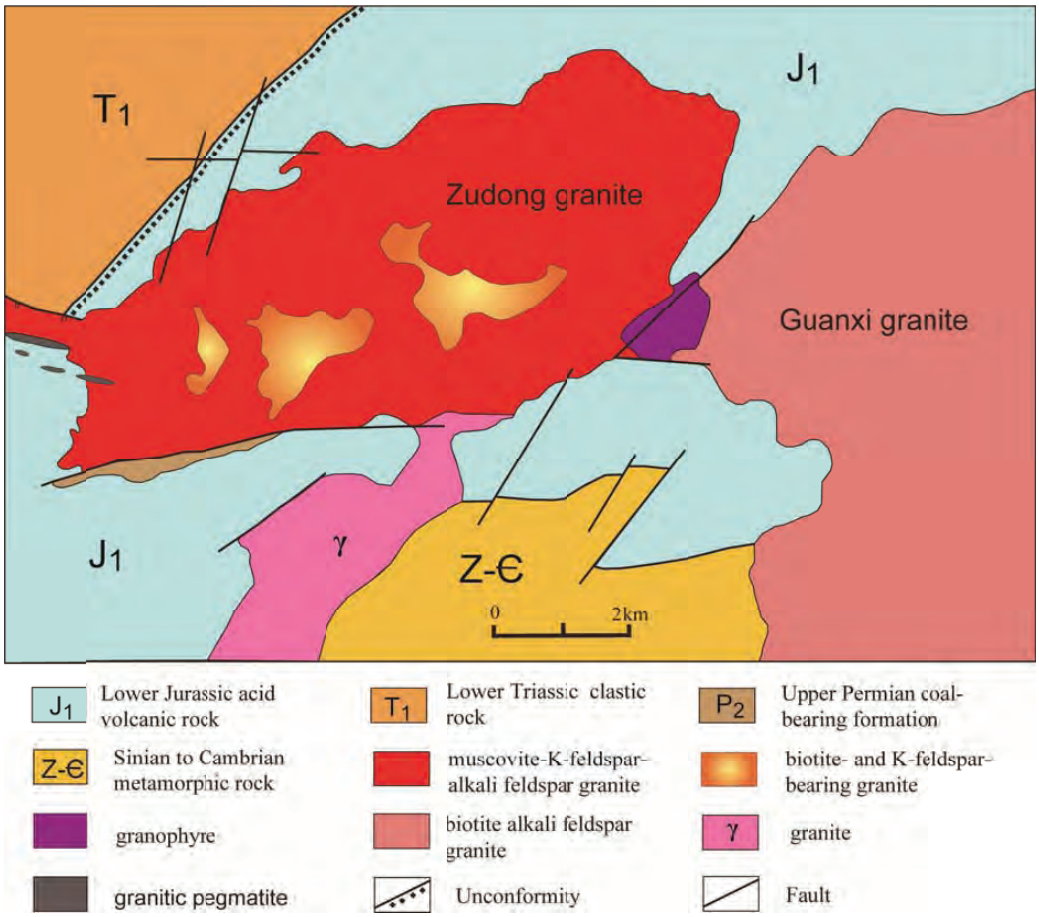

Fig. 10. Geologic map of Zudong HREE deposit (after Huang et al., 1988).

Heling LREE deposit

The Heling LREE deposit, discovered in 1972, is located in Xunwu county, South Jiangxi province (Figs. 9, 12), and has a total REO resource of 239,000 t (Table 2). The REE mineralization mainly occurs in the weathering profile of an acid volcanic rock and granite porphyry body (Wang and Ruan, 1989). The thickness of the orebody averages 8 to 9 m, but locally can be 28 m (Bao and Zhao, 2008). The granite porphyry, with an outcrop area of about 32 km², was emplaced into the Late Jurassic volcanic rock sequence of the Jilongzhang Formation (Fig. 12) in the Heling basin (Lai and Wang, 1996; Zuo et al., 2000). The volcanic rocks include agglomerate-bearing tuff, rhyolitic ignimbrite, and rhyolitic porphyroclastic lava (Zhang and Ye, 1995). Whole-rock Rb-Sr isochron dating of the volcanic rocks yields dates from 154 to 138 Ma (Lai and Wang, 1996) and the biotite K-Ar age of the granite porphyry is 114 Ma (Wang and Ruan, 1989).

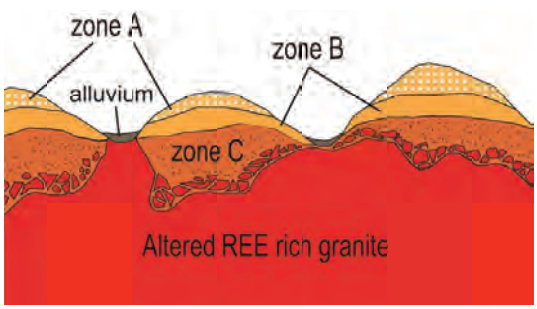

Fig. 11. Deposit model for the Zudong IAR deposit, Jiangxi province (based on Wu et al., 1988). Zone A = soil cap, Zone B = wholly weathered zone, Zone C = semi-weathered zone.

Phenocrysts in the granite porphyry are plagioclase feldspar (>40%), K-feldspar (15–40%), quartz (15–30%), and biotite (>2%), and the matrix is mainly quartz and feldspar. The accessory minerals in the granite porphyry are magnetite, apatite, bastnaesite, and Ce apatite, whereas in the acid volcanic rocks the accessory minerals are Ti magnetite, monazite, bastnaesite, chevkinite, and minor apatite (Wang and Ruan, 1989). The granite porphyry has a higher accessory mineral volume percentage than volcanic rock. The geochemical results show that the granite porphyry has a high K and low Ca content, with high Ba (279 ppm), Sr (36 ppm), and REE (376–2,460 ppm), a high LREE/HREE (4.07) ratio, and a negative Eu anomaly. The REE data indicate a LREE enrichment pattern (Wang and Ruan, 1989).

Petrochemical data show that the volcanic rocks have high SiO_2 (60–75.8 wt %), high K_2O (2.12–7.03 wt %), low CaO (0.03–4.09 wt %), and low Na_2O (0.14–4.0 wt %), as well as an $Al_2O_3 > K_2O + Na_2O + CaO$ character implying an Al-oversaturated volcanic rock (Zuo et al., 2000). The volcanic rocks have higher Si and lower amounts of alkaline elements

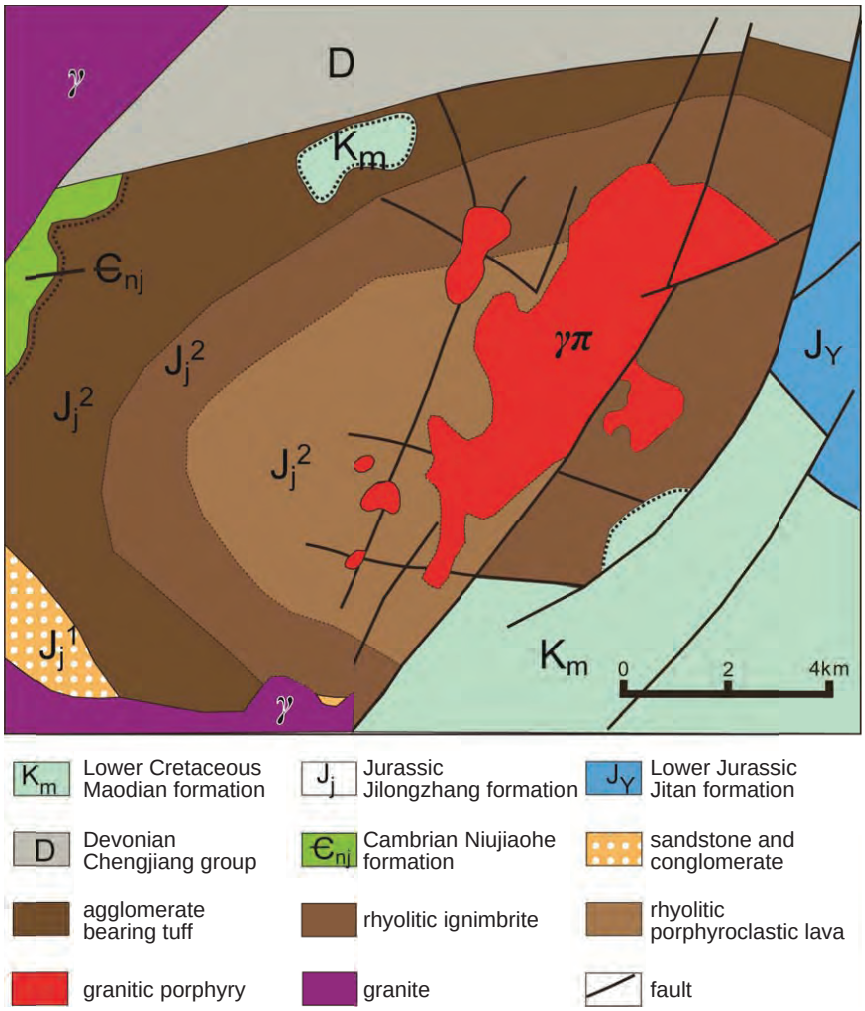

Fig. 12. Geologic map of the Heling LREE deposit (after Zhang and Ye, 1995).

than the granite porphyry. The total REE concentration (391–482 ppm) and LREE/HREE (2.91) ratios of the volcanic rock are lower than granite porphyry. The Eu negative anomaly is similar to the granite porphyry (Wang and Ruan, 1989). The volcanic rocks are considered to be an evolutionary product of the same source magma as that responsible for the granite porphyry, despite the significant reported age discrepancies that probably reflect imprecise geochronological data.

Discussion

Regional controls on LREE deposits in China

The regional tectonic and associated structural settings provide important controls on the LREE resources in China. Tectonically, China is composed of a number of Precambrian blocks, such as North China, Yangtze, Tarim, and Cathaysia, and their interstitial fold belts (Zhang et al., 1984; Wang and Mo, 1995; Zheng et al., 2013) that mainly reflect Paleozoic-Mesozoic ocean closures between the blocks. Almost all of the large LREE deposits in China are associated with carbonatites formed in craton margin environments. These include the northern margin of the North China block (e.g., Bayan Obo), western margin of the Yangtze block (e.g., Maoniuping), and southern and eastern margins of the North China block (e.g., Miaoya and Chishan, respectively; Fig. 2).

The North China and Yangtze blocks have undergone complex geologic histories. The subduction of the Proterozoic oceanic crust (Zheng and Zhang, 2007) and late Mesozoic Paleotethys Ocean below the western margin of Yangtze block (Wang et al., 2013), the Mianlue Ocean below the southern margin of the North China block during late Paleozoic (Lai et al., 2004), and the Pacific Ocean below the eastern margin of both blocks during early Mesozoic (Ren and Huang, 2002) obviously affected the evolution of the margins of these cratonic fragments. Long-term subduction enhanced the contribution of REE-rich pelagic sediment into the asthenosphere and also back to the mantle lithosphere by underplating. These cycled pelagic sediments led to the REE enrichment in the mantle under the margins of the North China and Yangtze Precambrian blocks.

Bayan Obo is the only Precambrian giant carbonatite-related REE deposit in China and situated along the northern margin of the North China block. Subduction of Precambrian oceanic crust may have contributed to an exceptional REE enrichment of the mantle under this area. It has been recognized that the North China block comprises distinct Eastern and Western

blocks (Zhao et al., 2001) and underwent a complex Precambrian evolution of subduction and continent-continent collision (Zhao et al., 2001; Kusky, 2011). Zhao et al. (2001) suggested that the Eastern and Western blocks were separate entities in the Archean until an active margin and E-dipping Andean-type subduction zone developed on the west edge of Eastern block sometime between 2.5 and 1.85 Ga, as the two blocks collided. Recent seismic results show that there was also a second, E-dipping paleosubduction zone located to the east of the suture and dipping beneath the Western block (Kusky, 2011). This westward subduction may have brought REE-rich pelagic sediments into the asthenosphere and led to REE-enriched mantle below the area of Bayan Obo.

The activated margins of the Precambrian blocks comprise the first-order controls on LREE resources in China. Reactivation of the ancient craton margins produced a series of rifts and deep faults, such as the continental margin rift along the northern margin of the North China block (e.g., Langshan-Bayan Obo rift) and the major strike-slip fault system along the western margin of the Yangtze block. These deep and near vertical conduits, transecting much of the lithosphere, channeled ascending mantle magmas that contained components of REE-rich pelagic sediment. The recently reported, but very poorly documented, carbonatite-related Jongju deposit in North Korea, claimed in press releases to be larger than Bayan Obo (August 13, 2014 website: http://www.ctoccapital.com/largest-known-rare-earth-deposit-discovered-in-north-korea/), also is located along the northern margin of the North China block.

The difference in tectonic setting between China's two main LREE deposits, Bayan Obo and Maoniuping, is reflected by the differences in magma sources and magma evolution paths. These differences in tectonomagmatic history may ultimately be responsible for the variation in the mineralization styles and mineral assemblages. The Bayan Obo deposit is enriched in Fe, Nb, and Ta, whereas the Maoniuping lacks economic Nb and Ta mineralization. The REE mineralization in Bayan Obo occurs mainly as massive ore in carbonatite (dolomite marble) and as disseminations in the wall rock. Vein systems are not well developed. Maoniuping is solely mined for its REE and is dominated by veinlet- and stockwork-style ores surrounding the carbonatite.

Bayan Obo is located in a Mesoproterozoic continental margin rift, whereas the Maoniuping deposit occurs within a Himalayan strike-slip fault system, although the system is localized along a Permian rift. The carbonatite at Bayan Obo includes calcite carbonatite, calcite-dolomite carbonatite, and dolomite carbonatite (Wang et al., 2003; Yang et al., 2011) and is more Mg rich than that at Maoniuping. The carbonatite in Maoniuping is dominated by calcite carbonatite, with minor Sr-rich carbonatite, but lacks dolomite carbonatite (Hou et al., 2006; Xie et al., 2011). The Sr-Nd isotope data show lower $\xi_{Nd(t)}$ for Maoniuping relative to Bayan Obo, implying an enriched mantle source with crustal material involvement at Maoniuping. The carbonatite originated from the unmixing between carbonatite melt and an alkaline silicate melt. The isotope results for Bayan Obo, however, show much higher $\xi_{Nd(t)}$ and a wide range of initial $^{87}Sr/^{86}Sr$ values (Yang et al., 2011), which indicate a slightly depleted mantle origin. From the early dolomite carbonatite phase to the later calcite carbonatite phase, the Sr-Nd isotope values show a flat trend with a narrow range of $\xi_{Nd(t)}$ and a wide range of $^{87}Sr/^{86}Sr$. The absence of any associated alkaline silicate rocks, such as syenite, but the presence of associated basic rocks at Bayan Obo, implies a different evolution path compared to Maoniuping. The unmixing between alkaline silicate magma and carbonatite melt might not have happened at Bayan Obo.

Parent granitoids for HREE-rich IAR deposits in southern China

Almost all of the major IAR deposits in southern China occur in the weathering profile of granitoids. The parent granitic rocks, some of which are Sn-rich granites, include quartz syenite, quartz monzonite, granite porphyry, granzerite granite, dacite-rhyolite, migmatitic granite, biotite granite, biotite granodiorite, biotite monzonitic granite, biotite syenogranite, two-mica granite, muscovite granite, and muscovite alkaline granite. They range widely in age from Mesoproterozoic to Cenozoic (e.g., Wu, 1988, and references therein; Gu et al., 2007; Li et al., 2012). Yanshanian granites (e.g., Zudong and Heling in Jiangxi province: Bao and Zhao, 2008, and references therein) and Indosinian granites (e.g., Gonghe in Guangdong province and Dajishan in Jiangxi province: Zhuang et al., 2000) have been recognized as the most common parent rocks for IAR mineralization. Recent geochronological results, however, for two IAR-related granites in Jiangxi province give ages of 445.2 Ma (Hanfang granite) and 457.5 Ma (Longshe granite; Li et al., 2012; Sun et al., 2012), thus indicating that Caledonian granitoids also are associated with the IAR ores.

The S-type granites have been emphasized as the most important source for IAR deposits (Bao and Zhao, 2008), but increasing amounts of evidence show that A- and I-type granites also play an important role in REE mineralization in southern China (Hua et al., 2007). Although there are still arguments about classification of some of the suggested A-type granites (Hua et al., 2007), petrochemical data demonstrate that the A-type granites in southern China have much higher REE concentrations than S- and I-type bodies in the region (Wu et al., 2007). The Zudong granite has been referred to as an S-type granite, but its high ξ_{Nd} and young model age imply a source from evolved mantle. Hua et al. (2007) believe that the major IAR deposits in South Jiangxi province are all related to A-type granites. Indosinian peraluminous to metaluminous granite, Yanshanian A-type granite, and middle to late Yanshanian biotite monzonitic granite or alkaline-feldspar granite all are recognized parent intrusions for the southern China IAR deposits (Hua et al., 2007). The middle to late Yanshanian intrusions show a low degree of differentiation, high total REE, LREE enrichment patterns, a strong negative Eu anomaly, and accessory biotite and REE-bearing minerals, together implying they are most likely an I- or syntectonic-type granite (Hua et al., 2007).

The IAR deposits are the main HREE resource in China. The IAR deposits are clustered in the center of the South China block, but show both NE- and NW-striking trends controlled by Mesozoic granitoids and regional fault systems (e.g., Shantou-Jieyang-Longnan and Meixian-Ganzhou), respectively (Fig. 8). The South China block was underplated by Paleotethys oceanic crust during early Paleozoic, adding the

REE-rich pelagic sediments to the mantle lithosphere below the block. Similar to controls for the carbonatite-related REE deposits, deep faults and lithospheric discontinuities provide the paths for REE-rich mantle material to return to shallow levels of the crust in evolved granite magmas.

HREE mobilization and enrichment during weathering and genesis of IAR deposits

The REE element enrichment may be added to the parent granite rock during hydrothermal processes, such as documented at the Zudong deposit (Huang et al., 1989b). This, therefore, indicates that at least some of the anomalous REE in the granite need not be the product of primary magmatic evolution. The Middle Jurassic Guanxi biotite granite located to the east of the Zudong granite (Fig. 6) is associated with the Guangxi REE deposit. The Guangxi granite has an initial $^{87}Sr/^{86}Sr$ value of 0.7056, indicating a different source from the Late Jurassic Zudong granite (Huang et al., 1989b), although both are associated with important REE deposits, and the Guanxi deposit is more LREE enriched. Different chondrite-normalized REE patterns also characterize the two granites (Huang et al., 1989b). Consequently, Zhang (1993) proposed that hypogene hydrothermal alteration played an important role in enriching some, but not all, granites that weathered to form the IAR mineralization. Furthermore, large variations in REE patterns in the weathered crust are not consistent with fractionation during the weathering process (Wang and Liu, 2012).

The enrichment of REE in the weathering profile, nevertheless, is not only controlled by parent rock type, mineral assemblage, and the occurrence and content of REE in the parent rock, but also by the local climate, groundwater patterns, and deposit area geomorphology. The REE mobilization and accumulation in the weathering profiles appears to be controlled specifically by the abundance and distribution of REE-bearing minerals in the parent granites, as well as the stability of these minerals during weathering, (e.g., Humphris, 1984). The enrichment of REE in the weathering profile is also partly controlled by the adsorption ability of organic matter, clay minerals, phosphates, and Fe oxides/hydroxides (Song et al., 2006). The REE-bearing minerals in the parent rock include fluorine-bearing carbonate (e.g., bastnaesite, synchysite, and yttroparisite), silicates (e.g., zircon, allanite, and spinthere), or phosphates (e.g., monazite and xenotime), as well as isomorphic phases in hornblende, feldspar, biotite, and zircon. Fluorine-bearing carbonate is much easier to break down during the weathering process than the silicates and phosphates because the carbonate dissolves easily in acidic groundwater.

The local elevation provides critical controls on IAR deposit formation. Where the altitude is less than 500 m, and the local relief is less than 150 m, a large and deep lateritic weathering cap forms with a strong layered structure (He and Wang, 1989). Subtropical climatic conditions, such as the warm and humid environment of southern China with locally more than 1,500 mm of precipitation annually, enhance development of IAR mineralization (Bao and Zhao, 2008). The abundance of organic matter in the soil profile plays an important role in the REE mobilization (Chen et al., 1993). Based on experimental results, Lin and Zheng (1994) indicated that the REE concentrations of the leaching solutions, their pH and ionic strength, water-to-rock ratios, and temperature are the dominant factors affecting REE adsorption to clay minerals. Continued leaching, coupled with a low rate of denudation, preferentially results in the accumulation of REE in the subsurface B and C soil horizons of mature weathering profiles (Bao and Zhao, 2008). Additional discussion of IAR deposits can be found in Sanematsu and Watanabe (2016).

Conclusions

1. China has the largest REE resources in the world, with confirmed 208 Mt of REE oxide resources. Deposit types include carbonatite-related, ion-adsorbed clays, placers and beach placers, and pegmatite-hosted, as well as by-product production from clay, bauxite, and U deposits. The carbonatite-related deposits define the largest LREE resources, accounting for 98.15% of the total resource in China, and the IAR deposits provide the most important HREE resources in China.
2. The major LREE deposits in China occurs within four metallogenic areas, including the Langshan-Bayan Obo belt along the northern margin of North China craton, the Weishan-Laiwu-Zibo belt along the eastern margin of North China block, the Mianning-Dechang belt in the western margin of Yangtze block, and the Miaoya deposit in the southern margin of the North China block. The margins to the Precambrian cratonic blocks define the first-order structural control for the major LREE deposits in China.
3. Almost all the hypogene REE deposits in China occur along margins of Precambrian blocks that are reactivated cratonic fragments. The ores are associated with continental rift zones and strike-slip faults, which comprise major lithosphere discontinuities. Long-term subduction from Neoarchean to Phanerozoic contributed REE-rich pelagic sediment to the underlying mantle and developed REE-rich mantle lithosphere reservoirs below much of the North China and South China blocks. Reactivation of the margins to the blocks allowed the deep fault zones to tap and aid the ascent of REE-rich mantle magma.
4. The IAR deposits in China occur mainly in the weathering profile of granitoids that vary in age from Mesoproterozoic to Cenozoic in the South China block. Minor IAR deposits also occur in the weathering profile of lamprophyre, basalt, and tuff.
5. In addition to the REE enrichment associated with the supergene weathering process, earlier hypogene REE concentration during hydrothermal alteration caused an enrichment in granitic parent rock for the IAR. The wide range of parent-rock compositions, magma sources, ages associated with the IAR deposits, and the spatial distribution of these deposits implies that REE-enriched mantle and major structures were important for the significant HREE resources.

Acknowledgments

This paper was financially supported by the National Nature Science Foundation of China (41072066) and the IGCP/SIDA-600 project. Many thanks to Philip Verplanck for his kind invitation to submit this review paper. Many thanks to

Baoshun Liu and Quanli Wang for their help in data processing and drafting. The use of trade, product, industry, or firm names in this report is for descriptive purpose only and does not constitute endorsement by the U.S. Geological Survey and the U.S. Government.

REFERENCES

109 Geological Brigade of Sichuan Bureau of Geology and Mineral Resource, 2010, Exploration report of Maoniuping REE deposit in Mianning, Sichuan province: Whole report not acquired (in Chinese).

Bao, Z.W., and Zhao, Z.H., 2008, Geochemistry of mineralization with exchangeable REY in the weathering crusts of granitic rocks in South China: Ore Geology Reviews, v. 33, p. 519–535.

Campbell, L.S., Compston, W., Sircombe, K.N., and Wilkinson, C.C., 2014, Zircon from the East orebody of the Bayan Obo Fe-Nb-REE deposit, China, and SHRIMP ages for carbonatite-related magmatism and REE mineralization events: Contributions to Mineralogy and Petrology, v. 168, doi:10.1007/s00410-014-1041-3.

Chao, E.C.T., Back, J.M., Minkin, J.A., and Ren, Y., 1992, Host-rock controlled epigenetic, hydrothermal metasomatic origin of the Bayan Obo REE-Fe-Nb ore deposit, Inner Mongolia, PRC: Applied Geochemistry, v. 7, p. 443–458.

Chao, E.C.T., Back, J.M., Minkin, J.A., Tatsumoto, M., Wang, J., Conrad, J.E., Makee, E.H., Hou, Z., Meng, Q., and Huang, S., 1997, The sedimentary carbonate-hosted giant Bayan Obo REE-Fe-Nb ore deposit of Inner Mongolia, China: A cornerstone example for giant polymetallic ore deposits of hydrothermal original: U.S. Geological Survey Bulletin, v. 2143, 65 p.

Chen, Z.C., Zhuang, W.M., and Yu, S.J., 1993, A new study of transforming and accumulating behaviors of REE in the weathering crust of granites in South China: Advances in Earth Science, v. 8, p. 47–48 (in Chinese).

Drew, L.J., Meng, Q., and Sun, W., 1990, The Bayan Obo iron-rare earth-niobium deposit, Inner Mongolia, China: Lithos, v. 26, p. 46–65.

Fan, H.R., Xie, Y.H., Wang, K.Y., and Wilde, S.A., 2004a, Methane-rich fluid inclusions in skarn near the giant REE-Nb-Fe deposit at Bayan Obo, northern China: Ore Geology Reviews, v. 25, p. 301–309.

Fan, H.R., Xie, Y.H., Wang, K.Y., Tao, K.J., and Wilde, S.A., 2004b, REE daughter minerals trapped in fluid inclusions in the giant Bayan Obo REE-Nb-Fe deposit, Inner Mongolia, China: International Geology Review, v. 46, p. 638–645.

Fan, H.R., Hu, F.F., Yang, K.F., and Wang, K.Y., 2006, Fluid unmixing/immiscibility as an ore-forming process in the giant REE-Nb-Fe deposit, Inner Mongolian, China: Evidence from fluid inclusions: Journal of Geochemical Exploration, v. 89, p. 104–107.

Fan, H.R., Hu, F.F., Yang, K.F., Wang, K.Y., and Liu Y.S., 2009, Geochronology framework of late Paleozoic diorite-granitic plutons in the Bayan Obo area, Inner Mongolia, and tectonic significance: Acta Petrologica Sinica, v. 25, p. 2933–2938 (in Chinese with English abs.).

Fan, H.R., Hu, F.F., Yang, K.F., Pirajno, F., Liu, X., and Wang, K-Y., 2014, Integrated U-Pb and Sm-Nd geochronology for a REE-rich carbonatite dyke at the giant Bayan Obo REE deposit, northern China: Ore Geology Reviews, v. 63, p. 510–519.

Goldfarb, R.J., Taylor, R.D., Collins, G.S., Goryachev, N.A., and Orlandini, O.F., 2014, Phanerozoic continental growth and gold metallogeny of Asia: Gondwana Research, v. 25, p. 48–102.

Groves, D., Bierlein, F.P., Meinert, L.D., and Hitzman, M.W., 2010, Iron oxide copper-gold (IOCG) deposits through Earth history: Implications for origin, lithospheric setting, and distinction from other epigenetic iron oxide deposits: Economic Geology, v. 105, p. 641–654.

Gu, S.Y., Hua, R.M., and Qi, H.W., 2007, Zircon LA-ICP-MS U-Pb dating and Sr-Nd isotope study of the Guposhan granite complex, Guangxi, China: Chinese Journal of Geochemistry, v. 26, p. 290–296.

Guo, C.L., 2010, Study on mineralization-related Mesozoic granitoids in Chongyi-Shangyou counties, South Jiangxi, and comparison to corresponding granitoids in the Nanling region, South China: PhD dissertation, China Academy of Geological Science, 239 p. (in Chinese with English abs.).

He, L.Y., and Wang, S.N., 1989, The ion adsorption type rare earth deposits in South China: Rare Earth, v. 1, p. 39–44 (in Chinese).

Hou, Z.L., 1989, The Bayan Obo FE-Nb-REE-deposit: Its basic geological features, metallogensis and genetic model: Geology and Prospecting, v. 25, p. 1–5 (in Chinese with English abs.).

Hou, Z.Q., Tian, S.H., Yuan, Z.X., Xie, Y.L., Yin, S.P., Yi, L.S., Fei, H.C., and Yang, Z.M., 2006, The Himalayan collision zone carbonatites in western Sichuan, SW China: Petrogenesis, mantle source and tectonic implication: Earth and Planetary Science Letters, v. 244, p. 234–250.

Hou, Z.Q., Tian, S.H., Xie, Y.L., Yuan, Z.X., Yin, S.P., Yi, L.S., Fei, H.C., Zou, T.R., Bai, G., and Li, X., 2009, The Himalayan Mianning-Dechang REE belt associated with carbonatite-alkalic complex in the eastern Indo-Asian collision zone, SW China: Ore Geology Reviews, v. 36, p. 65–89.

Hu, W.J., Tian, S.H., Wang, S.P., Chen, L.J., Su, Y.N., Yue, L., and Wang, Y.X., 2012, Sm-Nd isochron age of carbonatite from the Maoniuping REE deposit, Sichuan province and their geological implications: Mineral Resources and Geology, v. 26, p. 237–241 (in Chinese with English abs.).

Hua, R.M., Zhang, W.L., Gu, S.Y., and Chen, P.R., 2007, The rock characteristics and evolution of granite related to the weathering crust type REE deposit in South China: Acta Mineralogica Sinica, (sup.), v. 27, p. 17–19 (in Chinese).

Huang, D.H., Wu, C.Y., and Han, J.Z., 1989a, REE geochemistry and mineralization characteristics of the Zudong and Guanxi granites, Jiangxi province: Acta Geologica Sinica, v. 2, p. 139–157.

Huang, D.H., Wu, C.Y., Han, J.Z., and Zhang, Q.D., 1989b, Characteristics of isotopic systematics of U-Pb and Rb-Sr and their geological implications for Zudong and Guanxi granitic intrusives, Longnan county, Jiangxi province: Acta Petrologica Sinica, v. 1, p. 37–48 (in Chinese with English abs.).

Huang, D.H., Wu, C.Y., and Han, J.Z., 1993, Petrology, REE geochemistry and rock-forming mechanism of the Zudong and Guanxi granites, Jiangxi: Bulletin of the Chinese Academy of Geological Sciences, nos. 27–28, p. 69–94 (in Chinese with English abs.).

Huang, D.H., Hou, Z.Q., Yang, Z.M., Li, Z.Q., and Xu, D.X., 2009, Geological and geochemical characteristics: Metallogentic mechanism and tectonic setting of carbonatite vein-type Mo (Pb) deposits in the East Qinling molybdenum ore belt: Acta Geologica Sinica, v. 83, p. 1968–1984 (in Chinese with English abs.).

Huang, Z.L., Xu, C., Liu, C.Q., Xu, D.R., Li, W.B., and Guan, T., 2003, Sr and Nd isotope geochemistry of fluorites from the Maoniuping REE deposit, Sichuan province, China: Implications for the source of ore-forming fluids: Journal of Geochemical Exploration, nos. 78–79, p. 643–648.

Humphris, S.E., 1984, The mobility of the rare earth elements in the crust, *in* Henderson, P., ed., Rare earth element geochemistry: Amsterdam, Elsevier, p. 317–342.

Institute of Geochemistry, Chinese Academy of Sciences, 1988, Geochemistry of the Bayan Obo ore deposit: Beijing, Science Press, 546 p. (in Chinese).

Keppler, H., 2003, Water solubility in carbonatite melts: American Mineralogist, v. 88, p. 1822–1824.

Kusky, T., 2011, Geophysical and geological tests of tectonic models of the North China craton: Gondwana Research, v. 20, p. 26–35.

Kusky, T., Li, J., and Santosh, M., 2007, The Paleoproterozoic North Hebei orogen: North China craton's collisional suture with the Columbia supercontinent: Gondwana Research, v. 12, p. 4–28.

Lai, S.C., Zhang, G.W., Dong, Y.P., Pei, X.Z., and Chen, L., 2004, Geochemistry and regional distribution of ophiolites and associated volcanics in Mianlüe suture, Qinling-Dabie Mountains: Science in China (series D), v. 33, p. 289–299.

Lai, X.D., and Yang, X.Y., 2013, Geochemical characteristics of the Bayan Obo giant REE-Nb-Fe deposit: Constraints on its genesis: Journal of South American Earth Sciences, v. 41, p. 99–112.

Lai, X.D., Yang, X.Y., and Sun, W.D., 2012, Geochemical constraints on genesis of dolomite marble in the Bayan Obo REE-Nb-Fe deposit, Inner Mongolia: Implications for REE mineralization: Journal of Asian Earth Sciences, v. 57, p. 90–102.

Lai, Z.Z., and Wang, A.C., 1996, The Mesozoic volcanic age and the source of magma in south Jiangxi: Geology of Jiangxi, v. 10, p. 111–117 (in Chinese with English abs.).

Lan, T.G., Fan, H.R., Hu, F.F., Yang, K.F., and Wang, Y., 2011, Genesis of the Weishan REE deposit, Shandong province: Evidence from Rb-Sr isochron age, LA-MC-ICPMS Nd isotopic compositions and fluid inclusions: Geochemica, v. 40, p. 428–442 (in Chinese with English abs.).

Le Bas, M.J., 2006, Re-interpretation of zircon date in a carbonatite dyke at the Bayan Obo giant REE-Fe-Nb deposit, China: Acta Petrologica Sinica, v. 22, p. 517–518.

Le Bas, M.J., Keller, J., Tao, K.J., Wall, F., Williams, C.T., and Zhang, P.S., 1992, Carbonatite dykes at Bayan Obo, Inner Mongolia, China: Mineralogy and Petrology, v. 46, p. 195–228.

Le Bas, M.J., Yang, X.M., Taylor, R.N., Spiro, B., Milton, J.A., and Zhang, P.S., 2007, New evidence from a calcite-dolomite carbonatite dyke for the magmatic origin of the massive Bayan Obo ore-bearing dolomite marble, Inner Mongolia, China: Mineralogy and Petrology, v. 90, p. 223–248.

Li, B., Huang, Z.L., Xu, C., and Qi, L., 2007, A preliminary study on geochemistry of platinum group elements(PGE) of carbonatites in the Mianning REE deposit, Sichuan province, China: Acta Mineralogica Sinica, v. 27, p. 423–429 (in Chinese with English abs.).

Li, J.K., Chen, Z.Y., Chen, Z.H., Hou, K.J., and Zhao, Z., 2012, The dating and analysis of ore-forming conditions for Hanfang granite intrusions in Ganxian, Jiangxi province: Rock and Mineral Analysis, v. 31, p. 717–723 (in Chinese with English abs.).

Li S., 1980, Geochemical features and petrogenesis of Miaoya carbonatites, Hubei: Chinese Journal of Geochemistry, no. 4, p. 345–355 (in Chinese with English abs.).

——1991, Geochemistry and petrogenesis of the Shaxiongdong carbonatite complex, Hubei province: Geochemica, v. 3, p. 245–254 (in Chinese with English abs.).

Lin, C.S., and Zheng, Z.P., 1994, Experimental studies on metallogenetic mechanism of weathering crust-leaching REE deposit in southern China: Geochimica, v. 23, p. 189–198 (in Chinese with English abs.).

Ling, M.X., Liu Y.L., Williams, I.S., Teng, F.Z., Yang, X.Y., Ding, X., Wei G.J., Xie L.H., Deng, W.F., and Sun, W.D., 2013, Formation of the world's largest REE deposit through protracted fluxing of carbonatite by subduction-derived fluids: Nature, Scientific Reports 3: 1776, p. 1–8.

Liu, L.S., Gao, L., Du, A.D., and Sun, Y.L., 1996, The Re-Os isotopic age of molybdenite from Bayan Obo REE ore deposits: Mineral Deposits, v. 15, p. 188–191 (in Chinese with English abs.).

Liu, T.G., 1985, Geological and geochemical character of Baiyou Eborauhuagite: Acta Petrologica Sinica, v. 1, p. 15–28 (in Chinese with English abs.).

Liu, T.G., Zhang, Z.W., Ye, L., Shen, N.P., Yang, Z.F., Li, C.X., and Feng, J.R., 2012, Geological and geochemical characteristics and genesis of "dolomite" at Bayan Obo, China: Acta Geologica Sinica, v. 86, p. 723–734 (in Chinese with English abs.).

Liu, Y.L., Peng, G.Y., Zhang, X., Li, H.M., and Chen, J.F., 2001, U-Pb and Pb-Pb dating of the host rock-H8 dolomite in Bayan Obo ore deposit: Bulletin of Mineralogy, Petrology and Geochemistry, v. 20, p. 274–277 (in Chinese with English abs.).

Liu, Y.L., Yang, G., Chen, J.F., Du, A.D. and Xie, Z., 2004, Re-Os dating of pyrite from Giant Bayan Obo REE-Nb-Fe deposit: Chinese Science Bulletin, v. 49, p. 2627–2631.

Mao, J.W., Yu, J.J., Yuan, S.D., Cheng, Y.B., Xie, G.Q., Hou, K.J., and Yang, Z.X., 2008, Iron oxide-copper-gold deposits: Characteristics, present research situation and ore prospecting: Mineral Deposits, v. 27, p. 267–278 (in Chinese with English abs.).

Meng, Q.R., and Drew, L.J., 1992, Study on oxygen and carbon isotope and the implication for genesis of Baiyan Obo ore-bearing H8 dolomite: Contributions to Geology and Mineral Resources Research, v. 7, p. 46–54 (in Chinese with English abs.).

Mentani, T., Ohmura, T., Watanabe, Y., and Urabe, T., 2010, So-called "ion-adsorption type" REE deposits found in northern Vietnam [abs.]: Geological Society of America Abstracts with Programs, v. 4, p. 336.

Murakami, H., and Ishihara, S., 2008, REE mineralization of weathered crust and clay sediment on granitic rocks in the Sanyo belt, SW Japan and the southern Jiangxi province, China: Resource Geology, v. 58, p. 373–401.

Neary, C.R., and Highley, D.E., 1984, The economic importance of the rare earth elements, *in* Henderson P., ed., Rare earth element geochemistry: Amsterdam, Elseviere, p. 423–466.

Pisarevsky, S.A., Elming, S-A.,Pesonen, L.J., and Li, Z.X., 2014, Mesoproterozoic paleogeography: Supercontinent and beyond: Precambrian Research, v. 244, p. 207–225.

Qin, C.J., Qiu, Y.Z., Zhou, G.F., Guo, F., Wang, Z.G., Zhang, T.R., and Xiao, G.W., 2007, Fluid inclusion study of carbonatite dykes/veins and ore-hosted dolostone at the Bayan Obo ore deposit: Acta Petrologica Sinica, v. 23, p. 161–168 (in Chinese with English abs.).

Qiu, Y.Z., 1997, Thought on SHRIMP dating of Bayan Obo monazite: Acta Geoscientia Sinica, v. 18 (sup.), p. 211–213 (in Chinese with English title).

Qiu, Y.Z., Wen, H.J., and Qin, C.J., 2011, The chronology of Hercynian granite and the discovery of Yanshanian granite: Acta Mineralogica Sinica, v. 31 (S1), p. 631–632 (in Chinese).

Ren, J.S., Wang Z.X., Chen B.W., Jiang C.F., and Niu B.G., 1999, Tectonic map of China and neighbouring area: Beijing, Geological Publishing House (in Chinese).

Ren, S.M., and Huang, B.C., 2002, Preliminary study on post-late Paleozoic kinematics of the main clocks of the Paleo-Asia ocean: Progress in Geophysics, v. 17, p. 1–8 (in Chinese with English abs.).

Ren, Y.C., Zhang, Y.C., and Zhang, Z.Q., 1994, Study on heat events of ore-forming Bayan Obo deposit: Acta Geoscientia Sinica, v. 1–2, p. 95–101 (in Chinese with English abs.).

Samson, I.M., Liu, W.N., and Williams-Jones, A.E., 1995, The nature of orthomagmatic hydrothermal fluids in the Oka carbonatite, Quebec, Canada: Evidence from fluid inclusion: Geochimica et Cosmochimica Acta, v. 59, p. 1963–1977.

Sanematsu, K., and Watanabe, Y., 2016, Characteristics and genesis of ion-adsorption-type rare earth element deposits: Reviews in Economic Geology, v. 18, p. 55–79.

Smith, M.P., 2007, Metasomatic silicate chemistry at the Bayan Obo Fe-REE-Nb deposit, Inner Mongolia, China: Contrasting chemistry and evolution of fenitising and mineralising fluids: Lithos, v. 93, p. 126–148.

Smith, M.P., Henderson, P., and Campbell, L.S., 2000, Fractionation of the REE during hydrothermal processes: Constraints from the Bayan Obo Fe-REE-Nb deposit, Inner Mongolia, China: Geochimica et Cosmochimica Acta, v. 64, p. 3141–3160.

Smith, M.P., Campbell, L.S., and Kynicky, J., 2014, A review of the genesis of the world-class Bayan Obo Fe-REE-Nb deposits, Inner Mongolia, China: Multistage processes and outstanding questions: Ore Geology Reviews, http://dx.doi.org/10.1016/j.oregeorev.2014.03.007.

Song, Z.L., Liu, C.Q., Han, G.L., Wang, Z.L., Zhu, Z.Z., and Yang, C., 2006, Enrichment and release of rare earth elements during weathering of sedimentary rocks in Wujiang catchment, southeast China: Journal of Rare Earths, v. 24, p. 491–496.

Sun, Y., Li, J.K., Chen, Z.Y., Chen, Z.H., Hou, K.J., and Zhao, Z., 2012, LA-MC-ICP-MS zircon U-Pb dating and rare earth potential of the Longshe granite in Ganzhou, Jiangxi province: Geotectonica et Metallogenia, v. 36, p. 422–426 (in Chinese with English abs.).

Tian, S.H., Hou, Z.Q., Yuan, Z.X., Chen, W., Xie, Y.L., Fei, H.C., Yin, S.P., Yi, L.S., and Zhou, S., 2006, ^{40}Ar-^{39}Ar geochronology of rocks and ores from the Muluozhai REE deposit in Mianning County, Sichuan province: Acta Petrologica Sinica, v. 22, p. 2431–2436 (in Chinese with English abs.).

Tian, S.H., Hou, Z.Q., Yang, Z.S., Chen, W., Yang, Z.M., Yuan, Z.X., Xie, Y.L., Fei, H.C., Yin, S.P., Liu, Y.C., Li, Z., and Li, X.Y., 2008a, Geochronology of REE deposits in Mianning-Dechang REE metallogenetic belt: Constraints on duration of hydrothermal activities and tectonic model for carbonatite-alkalic complexes in south western Sichuan: Mineral Deposits, v. 27, p. 177–187 (in Chinese with English abs.).

Tian, S.H., Hou, Z.Q., Yang, Z.S., Yang, Z.M., Yuan, Z.X., Wang, Y.B., Xie, Y.L., Liu, Y.C., and Li, Z., 2008b, Zircon U-Pb ages, Hf isotopic compositions and geological significance: A case study of carbonatite and nordmarkite from the Dalucao REE deposit, Sichuan province: Acta Petrologica Sinica, v. 24, p. 544–554 (in Chinese with English abs.).

Ting, W., Burke, E.A.J., Rankin, A.H., and Woolley, A.R., 1994, Characteristics and petrogenetic significance of CO_2, H_2O and CH_4 fluid inclusions in apatite from the Sukulu carbonatite, Uganda: European Journal of Mineralogy, v. 6, p. 787–803.

Tse, P.K., 2011, China's rare-earth industry: U.S. Geological Survey Open-File Report 2011-1042, 11 p.

U.S. Geological Survey and U.S. Department of Interior, 2012, Mineral commodity summaries 2012, 198 p.

Wang, H.Z., and Mo, X.X., 1995, An outline of the tectonic evolution of China: Episodes, v. 18, p. 6–16.

Wang, J.B., and Ruan, D.Y., 1989, Evolution and RE concentration of Heling-type RE acidic volcanic rock series: Journal of the Chinese Rare Earth Society, v. 7, p. 68–72 (in Chinese with English abs.).

Wang, J., Tatsumoto, M., Li, X., Premo, W.R., and Chao, E.C.T., 1994, A precise ^{232}Th-^{208}Pb chronology of fine-grained monazite: Age of the Bayan Obo REE-Fe-Nb ore deposit, China: Geochimica et Cosmochimica Acta, v. 58, p. 3155–3169.

Wang, K.Y., Fan, H.R., Xie, Y.H., and Li, H.M., 2002, Zircon U-Pb dating of basement gneisses in the super-large Bayan Obo REE-Fe-Nb deposit, Inner Mongolia: Chinese Science Bulletin, v. 47, p. 243–246.

Wang, K.Y., Fan, H.R., Yang, K.F., Hu, F.F., and Ma, Y.G., 2010, Bayan Obo carbonatites: Texture evidence from polyphase intrusive and extrusive carbonatite: Acta Geologica Sinica, v. 84, p. 1365–1376 (English ed.).

Wang, W., Yang, R.D., Bao, M., Wei, H., and Wang, Q., 2006, Discussion on the mineralization associated with the weathering crust on Emeishan basalt in Guizhou province, China: Journal of Guizhou University (Nature Science), v. 23, p. 366–370 (in Chinese with English abs.).

Wang, X.N., and Liu, R.Q., 2012, The geochemical characteristics and ore genesis of a granite weathering crust ion adsorption type of rare earth ore

deposit in North Guangdong: Science and Technology Information, v. 15, 233 p. (in Chinese).
Wang, Y.J., Fan, W.M., Zhang, G.W., and Zhang, Y.H., 2013, Phanerozoic tectonics of South China Block: Key observations and controversies: Gondwana Research, v. 23, p. 1273–1305.
Wang, Y.X., Qiu, Y.Z., Gao, J.Y., and Zhang, Q., 2003, Proterozoic anorogenic magmatic rocks and their constraints on mineralizations in the Bayan Obo deposit region, Inner Mongolia: Science in China (series D), v. 46, p. 26–40.
Wu, C.Y., 1988, The study of ion-adsorbed type of rare earth deposits in weathering crust from south Jiangxi and north Guangdong provinces: Ph.D. dissertation of China Academy of Geological Science, 1988, 158 p. (in Chinese with English abs.).
——2008, Bayan Obo controversy: Carbonatite versus iron oxide-Cu-Au-(REE-U): Resource Geology, v. 58, p. 348–354.
Wu, C.Y., Huang, D.H., and Guo, Z.X., 1989, REE geochemistry in the weathering process of granites in Longnan county, Jiangxi province: Acta Geologica Sinica, v. 4, p. 349–362 (in Chinese with English abs.).
Wu, C.Y., Huang, D.H., Bai, G., and Ding, X.S., 1990, Differentiation of rare earth elements and origin of granitic rocks, Nanling mountain area: Acta PetrologicaMineralogica, v. 9, p. 106–116 (in Chinese with English abs.).
Wu, S.P., Wang, M.Y., and Qi, K.J., 2007, Present situation of researches on A-type granites: A review: Acta Petrologica Mineralogica, v. 26, p. 57–66 (in Chinese with English abs.).
Xiao, R.G., Fei, H.C., An, G.Y., Zhang, H.C., and Hou, W.R., 2003, Lithology and genesis of dolomite in Baiyun'Ebo mine, Inner Mongolia: Geoscience, v. 17, p. 287–293 (in Chinese with English abs.).
Xie, Y.L., Hou, Z.Q., Yin, S.P., Dominy, S.C., Xu, J.H., Tian, S.H., and Xu, W.Y., 2009, Continuous carbonatitic melt-fluid evolution for REE mineralization system: Evidence from inclusions in the Maoniuping REE deposit in western Sichuan, China: Ore Geology Reviews, v. 36, p. 90–105.
Xie, Y.L., Li, Y.X., Cooke, D.R., Kamenetsky, V., Chang, Z., Danyushevsky, L., Dominy, S.C., Ryan, C., and Laird, J., 2011, Geochemical characteristics of carbonatite fluids at the Maoniuping REE deposit, western Sichuan, China: SGA Biennial Meeting, 11th, Antofagasta, Chile, September 26–29, 2011, Proceedings, p. 196–198.
Xie, Y.L., Li, Y.X., Hou Z.Q., Cooke, D.R., Danyushevsky, L., Dominy, S.C., and Yin, S.P., 2015, A model for carbonatite hosted REE mineralization—the Mianning-Dechang REE belt, Western Sichuan Province, China: Ore Geology Reviews, v. 70, p. 595–612.
Xu, C., Huang, Z.L., Qi, L., Xiao, H.Y, Li, W.B., and Liu, C.Q., 2002, REE and isotopic geochemistry of fluorites in the Maoniuping rare-earth deposit, Sichuan province: Geochimica, v. 31, p. 180–190 (in Chinese with English abs.).
Xu, C., Zhang, H., Huang, Z.L., Liu, C.Q., Qi, L., Li, W.B., and Guan, T., 2004, Genesis of the carbonatite-syenite complex and REE deposit at Maoniuping, Sichuan province, China: Evidence from Pb isotope geochemistry: Geochemical Journal, v. 38, p. 67–76.
Xu, C., Song, W.L., Qi, L., and Wang, L.J., 2009, Geochemical characteristics and tectonic setting of ore-bearing carbonatites in Huanglongpu Mo ore field: Acta Petrologica Sinica, v. 25, 422–430 (in Chinese with English abs.).
Yang, K.F., Fan, H.R., Santosh, M., Hu, F.F., and Wang, K.Y., 2011, Mesoproterozoic carbonatitic magmatism in the Bayan Obo deposit, Inner Mongolia, North China: Constraints for the mechanism of super accumulation of rare earth elements: Ore Geology Reviews, v. 40, p. 122–131.
Yang, R.D., Wang, W., Zhang, X.D., Liu, L., Wei, H.R., Bao, M., and Wang, J.X., 2008, A new type of rare earth elements deposit in weathering crust of Permian basalt in western Guizhou, NW China: Journal of Rare Earths, v. 26, p. 753–759.
Yang, X.M., Yang, X.Y., Chen, T.H., Zhang, P.S., Tao, K.J., Le Bas, M.J., and Henderson, P., 2000, Geochemical characteristics of a carbonatite dyke rich in rare earths from Bayan Obo, China: Journal of Rare Earths, v. 18, p. 1–8.
Yang, X.M., Yang, X.Y., Zheng, Y.F., and Le Bas, M.J., 2003, A rare earth element-rich carbonatite dyke at Bayan Obo, Inner Mongolia, North China: Mineralogy and Petrology, v. 78, p. 93–110.
Yang, X.Y., Zhang, Y.X., Zheng, Y.F., Yang, X.M., Xu, B.L., Zhao, Y.B., Peng, Y., and Hao, Z.G., 2000, Carbon and oxygen isotope compositions of ore-bearing dolostone in the Bayan Obo deposit as well as two typical micrite mounds and a carbonatite dyke: Acta Geologica Sinica, v. 74, p. 169–180 (in Chinese with English abs.).
Yang, Z.Y., and Drew, L.J., 1994, On the hot-water sedimentary origin of dolomite-host rock of Bayan Obo deposit, Inner Mongolia, China: Contributions to Geology and Mineral Resources Research, v. 9, p. 39–48 (in Chinese with English abs.).
Yao, D., Zhang, L.J., Wiltshire, J., Malahoff, A., and Ye, Y.G., 1998, Geology and meteorite impact origin of Bayan Obo Fe-Nb-REE deposit, Inner Mongolia, China: Marine Geology and Quaternary Geology, v. 18, p. 87–96 (in Chinese with English abs.).
Yu, X.F., Tang, H.S., Han, Z.Z., and Li, C.Y., 2010, Geological characteristics and origin of rare earth elements deposits related with alkaline rock in the Chishan-Longbaoshan area, Shandong province: Acta Geologica Sinica, v. 84, p. 407–417 (in Chinese with English abs.).
Yuan, Z.X., Bai, G., and Wu, C.Y., 1991, Genesis and metallogenic age of Bayan Obo Ni, REE and Fe ore deposit, Inner Mongolia: Mineral Deposit Geology, v. 10, p. 59–70 (in Chinese with English abs.).
Yuan, Z.X., Shi, Z., Bai, G., Wu, C., Chi, R., and Li, X., 1995, Rare earth element deposit in Maoniuping Mianning, Sichuan province: Beijing, Geological Publishing House, 150 p. (in Chinese).
Yuan, Z.X., Bai, G., and Zhang, Z.Q., 2000, Trachytic rock and associated fenitization in the Bayan Obo ore deposit, Inner Mongolia, China: Evidence for magmatic-hydrothermal mineralization related to a carbonatitic complex: Acta Geologica Sinica, v. 74, p. 148–153 (in Chinese with English abs.).
Zhang, F.R., and Ye, B.Z., 1995, The lithofacies features of Hululian volcanic dome, Xunwu county, Jiangxi: Geology of Jiangxi, v. 9, p. 45–51 (in Chinese with English abs.).
Zhang, P.S., Tao, K.J., Yang, Z.M., and Song, R.K., 2001, Genesis of rare earths, niobium and tantalum minerals in Bayan Obo ore deposit of China: Journal of the Chinese Rare Earth Society, v. 19, p. 97–102 (in Chinese with English abs.).
Zhang, P.S., Tao, K.J., Yang, Z.M., Yang, X.M. and Song, R.K., 2002, Rare earths, niobium and tantalum minerals in Bayan Obo ore deposit and discussion on their genesis: Journal of Rare Earths, v. 20, p. 81–86 (in Chinese with English abs.).
Zhang, Y.X., Luo, Y.N., and Yang, C.X., 1988, The Panxi rift: Beijing, Geological Publishing House, 325 p. (in Chinese).
Zhang, Y.X., Lu, H.B., Wang, J., Liu, J.Y., Meng, Q.W., and Huang, M., 2012, Analysis of ore-forming tectonic setting of the Bayan Obo REE deposit: Acta Geologica Sinica, v. 86, p. 768–774 (in Chinese with English abs.).
Zhang, Z.H., 1993, The ore-forming geological characteristics and ore-controlling factors of the ion adsorption type of rare earth deposit: Guangdong Non-ferrous Metal Geology, v. 1, p. 22–31 (in Chinese).
Zhang, Z.M., Liou, J.G., and Coleman, R.G., 1984, An outline of the plate tectonics of China: Geological Society of America Bulletin, v. 95, p. 295–312.
Zhang, Z.Q., Tang, S.H., Wang, J.H., Yuan, Z.X., and Bai, G., 1994, New data for ore-forming age of the Bayan Obo REE ore deposit, Inner Mongolia: Chinese Rare Earths, v. 1–2, p. 85–94 (in Chinese with English abs.).
Zhang, Z.Q., Tang, S.H., Wang, J.H., Yuan, Z.X., and Bai, G., 2003, Information about ore deposit formation in different epochs: Age of the orebodies of the Bayan Obo deposit with a discussion: Geology in China, v. 30, p. 130–137 (in Chinese with English abs.).
Zhao G.C., 2001, Palaeoproterozoic assembly of the North China craton: Geologic Magazine, v. 138, p. 89–91.
Zheng, Y.F., and Zhang, S.B., 2007, Formation and evolution of Precambrian continental crust in South China: Chinese Science Bulletin, v. 52, p. 1–12.
Zheng, Y.F., Xiao, W.J., and Zhao, G.C., 2013, Introduction to tectonics of China: Gondwana Research, v. 23, p. 1189–1206.
Zhuang, W.M., Huang, Y.Y., and Chen, S.Q., 2000, Basic features and tectonic setting of Indosinian granitiods in central Guangdong: Guangdong Geology, v. 15, p. 33–39 (in Chinese with English abs.).
Zou, T.R., Xu, J., Chen, W.S., and Xia, F.R., 2002, Study on alkaline rock type rare and rare earth deposit on the northern margin of the Tarim basin: Mineral Deposits, v. 21 (sup), p. 845–848 (in Chinese with English abs.).
Zuo, Y.M., Zhang, S.M., Wu, J.H., and Zhou, W.X., 2000, A discussion on the petrological and petrochemical features of volcanic rocks of the Jilongzhang Formation in south Jiangxi-north Guangdong: Jiangxi Geology, v. 14, p. 93–99 (in Chinese with English abs.).

©2016 Society of Economic Geologists, Inc.
Reviews in Economic Geology, v. 18, pp. 137–164

Chapter 7

By-Products of Porphyry Copper and Molybdenum Deposits

David A. John[1,†] and Ryan D. Taylor[2]

[1] *U.S. Geological Survey, MS 901, 345 Middlefield Rd., Menlo Park, California 94025-3591*

[2] *U.S. Geological Survey, Denver Federal Center, MS 973, Box 25046, Denver, Colorado 80225*

Abstract

Porphyry Cu and porphyry Mo deposits are large to giant deposits ranging up to >20 and 1.6 Gt of ore, respectively, that supply about 60 and 95% of the world's copper and molybdenum, as well as significant amounts of gold and silver. These deposits form from hydrothermal systems that affect 10s to >100 km^3 of the upper crust and result in enormous mass redistribution and potential concentration of many elements.

Several critical elements, including Re, Se, and Te, which lack primary ores, are concentrated locally in some porphyry Cu deposits, and despite their low average concentrations in Cu-Mo-Au ores (100s of ppb to a few ppm), about 80% of the Re and nearly all of the Se and Te produced by mining is from porphyry Cu deposits.

Rhenium is concentrated in molybdenite, whose Re content varies from about 100 to 3,000 ppm in porphyry Cu deposits, ≤150 ppm in arc-related porphyry Mo deposits, and ≤35 ppm in alkali-feldspar rhyolite-granite (Climax-type) porphyry Mo deposits. Because of the relatively small size of porphyry Mo deposits compared to porphyry Cu deposits and the generally low Re contents of molybdenites in them, rhenium is not recovered from porphyry Mo deposits. The potential causes of the variation in Re content of molybdenites in porphyry deposits are numerous and complex, and this variation is likely the result of a combination of processes that may change between and within deposits. These processes range from variations in source and composition of parental magmas to physiochemical changes in the shallow hydrothermal environment. Because of the immense size of known and potential porphyry Cu resources, especially continental margin arc deposits, these deposits likely will provide most of the global supply of Re, Te, and Se for the foreseeable future.

Although Pd and lesser Pt are recovered from some deposits, platinum group metals are not strongly enriched in porphyry Cu deposits and PGM resources contained in known porphyry deposits are small. Because there are much larger known PGM resources in deposits in which PGMs are the primary commodities, it is unlikely that porphyry deposits will become a major source of PGMs.

Other critical commodities, such as In and Nb, may eventually be recovered from porphyry Cu and Mo deposits, but available data do not clearly define significant resources of these commodities in porphyry deposits. Although alkali-feldspar rhyolite-granite porphyry Mo deposits and their cogenetic intrusions are locally enriched in many rare metals (such as Li, Nb, Rb, Sn, Ta, and REEs) and minor amounts of REEs and Sn have been recovered from the Climax mine, these elements are generally found in uneconomic concentrations.

As global demand increases for critical elements that are essential for the modern world, porphyry deposits will play an increasingly important role as suppliers of some of these metals. The affinity of these metals and the larger size and greater number of porphyry Cu deposits suggest that they will remain more significant than porphyry Mo deposits in supplying many of these critical metals.

Introduction

Porphyry copper and porphyry molybdenum deposits are the world's largest sources of copper (~60%) and molybdenum (~95%) and commonly contain 100s of million metric tons (Mt) to >20 billion metric tons (Gt) of ore (Seedorff et al., 2005; Sinclair, 2007; Singer et al., 2008; John et al., 2010; Sillitoe, 2010; Taylor et al., 2012). These deposits formed from large magmatic-hydrothermal systems that affected 10s to >100 km^3 of upper crustal rocks, thereby resulting in enormous mass redistribution and local concentration of many elements (Barton, 2010). There is a broad spectrum of types of porphyry Cu deposits ranging from those in which Cu is the only metal recovered to Au- and/or Mo-rich deposits in which Au and Mo are co- or important by-products to porphyry Au deposits in which Au is the major product and only minor Cu is recovered (Sillitoe, 2000; Singer et al., 2008). Similarly, there is a spectrum of characteristics of porphyry Mo deposits, and these deposits are generally subdivided into two end-member types, arc-related (also called quartz monzonite or low fluorine) and alkali-feldspar rhyolite-granite (AFRG; also called Climax) types (Sillitoe, 1980; White et al., 1981; Westra and Keith, 1981; Ludington et al., 2009; Taylor et al., 2012).

In addition to Cu, Mo, and Au, significant amounts of other elements, including Ag, As, Re, platinum group metals (PGMs, especially Pd), Se, and Te, are recovered from some porphyry Cu deposits (Table 1). Small amounts of W, Sn, Th and light rare earth elements (REEs) have been recovered from alkali-feldspar rhyolite-granite porphyry Mo deposits. Due to the large volume of rocks affected by the ore-forming hydrothermal systems and the large tonnages of ore processed from these deposits, other elements concentrated in trace quantities may become economic in future years. In this chapter, we review the characteristics of porphyry Cu and Mo deposits and discuss by-products and potential by-products from them. We also briefly mention other types of porphyry

† Corresponding author, e-mail, djohn@usgs.gov

Table 1. By-Products of Porphyry Copper and Porphyry Molybdenum Deposits

Commodity	Deposit type	Location/paragenesis	Mineralogy	Grade	Examples	Notes	References
Silver	Porphyry Cu	Mostly in central Cu-(Mo-Au) ores in potassic alteration	Mostly in solid solution in Cu-Fe sulfides; less commonly in electrum, argentite, tetrahedrite-tennantite, sphalerite, galena, and Ag tellurides	<0.1 to 21 g/t	Batu Haiju, Bingham, Butte, Chuquicamata, Escondida		Ballantyne et al. (1998); Arif and Baker (2004); Singer et al. (2008)
Rhenium	Porphyry Cu, especially continental arc deposits	In molybdenite; higher Re contents of molybdenite at shallower depths in some deposits	Solid solution in molybdenite	0.01 to 0.6 g/t	Bingham, Chuquicamata, El Teniente, Pebble	Recovered from flue dust produced by roasting molybdenite concentrates	Giles and Schilling (1972); Berzina et al. (2005); Sinclair et al. (2009); John et al. (in press); Millensifer et al. (2013)
Selenium	Porphyry Cu	Cu-(Mo-Au) sulfide ores	Solid solution in Cu and Fe sulfides; uncommon selenides	1 to 600 ppm (typically <10 ppm)	Bingham, Elatsite, Pebble, Skouriés	Recovered from anode slimes that typically contain about 7% Se	Tomakchieva (2002); Gregory et al. (2013)
Tellurium	Porphyry Cu	Cu-(Mo-Au) sulfide ores	Au, Ag, and Pd tellurides (petzite, hessite, merenskyite)	<0.1 to >100 ppm (typically 1-10 ppm)	Bingham, Elatsite, Pebble, Skouriés	Recovered from anode slimes that typically contain 1-4 % Te	Economou-Eliopoulos and Eliopoulos (2000); Tomakchieva (2002); Gregory et al. (2013)
Platinum Group Metals (Pd and Pt)	Porphyry Cu, especially island arc deposits in alkaline rocks	Mostly in central Cu-Au zone in potassic alteration; in late stage pyrophyllite alteration at Pebble	Tellurides (merenskyite); solid solution in pyrite (Pebble)	<0.1 to 60 ppb Pt + Pd	Allard, Elatsite, Mt. Polley, Mount Milligan, Pebble, Santo Tomas II, Skouriés	Pd/Pt ranges from 0.6 to >20; commonly only Pd reported	Tarkian and Stribrny (1999;) Economou-Eliopoulos (2005;) Gregory et al. (2013)
Arsenic	Porphyry Cu	Commonly in advanced argillic alteration in upper and outer parts of deposits and in late stage veins	Enargite-luzonite, tennantite-tetrahedrite, arsenopyrite; solid solution in pyrite, chalcopyrite, bornite	Highly variable; Schwartz (1995) reports 300 to 2000 ppm in Cu ore	Bingham, Butte, Chuquicamata	Recovered from smelter flue dust; considered an environmental hazard	Meyer et al. (1968); Schwartz (1995); Ossandón et al. (2001); Singer et al. (2008)
Zinc	Porphyry Cu	Advanced argillic alteration in upper and outer parts of deposits and in late stage veins	Sphalerite; solid solution in tennantite	>8,000 ppm as sphalerite overgrowths on Cu sulfides at Chuquicamata	Butte, Chuquicamata	Mostly with enargite in "Main stage" veins at Butte and late veins at Chuquicamata	Meyer et al. (1968); Ossandón et al. (2001)
Tungsten	Alk. granite and arc-related porphyry Mo, porphyry Cu	Late-stage veins (porphyry Mo deposits); breccia pipes inferred related to porphyry Cu deposits	Scheelite, wolframite, huebnerite	0.1 to 0.3% W in porphyry W-Mo; 0.02 to 0.06% WO_3 (porphyry Cu breccias)	Climax, Endako, Pine Nut, Sunrise	Porphyry W deposits	Sinclair (2007); Singer et al. (2008)
Bismuth	Arc-related porphyry Mo	Late-stage, upper ore zones associated with W	Bismuthinite, aikinite, native bismuth	<150 ppm	Davidson, Endako, Koktenkol, Pidgeon	Treated as an impurity in some ores such as at Endako	Noble et al. (1995); Mazurov (1996)
Uranium	Porphyry Cu	Cu-(Mo-Au) ores and in exotic Cu ore	Unknown	Unknown	Bingham, Chuquicamata (Mina Sur exotic Cu), Twin Buttes	At Bingham recovered from Cu-leach liquor that averaged 8 to 12 ppm U	Dahlkamp (2009)
Tin	Alk. Granite porphyry Mo; porphyry Sn	Sericitic alteration, paragenetically related to W at Climax	Cassiterite	0.2 to 0.5% Sn in porphyry Sn deposits	Climax, porphyry Sn deposits of Bolivia and Japan	Primary commodity in porphyry Sn deposits	Ohta (1995)

Table 1. *(Cont.)*

Commodity	Deposit type	Location/paragenesis	Mineralogy	Grade	Examples	Notes	References
Cerium, LREE	Alk. Granite porphyry Mo and porphyry Sn	Unknown, possibly derived from the alkaline host intrusion	Monazite	0.005% monazite in ore at Climax	Climax	Monazite is a relatively abundant accessory mineral in alkaline plutons	Overstreet (1967); Wallace et al. (1968)
Indium	Porphyry Mo-W	Late-stage in veins and breccia	Solid solution in sphalerite, chalcopyrite	Trace to 280 ppm; up to ~7 wt % in sphalerite	Mount Pleasant, Bingham	Mostly in sphalerite; lesser amounts in chalcopyrite	Briskey (2005); Sinclair et al. (2006)
Niobium	Alk. Granite porphyry Mo	Breccia pipes, veins, intrusive host	Columbite	Ppm to 0.1% Nb_2O_5	Cave Peak, Shapinggou	Nb is concentrated in alkaline igneous rocks and carbonatites with tantalum	Audetat (2010); Xu et al. (2011)
Silica	Porphyry Cu	Oxidized advanced argillic alteration and silica lithocap	Quartz	>95 to 99% SiO_2	White River		John et al. (2003)
Sulfuric acid	Porphyry Cu	Cu-(Mo-Au) sulfide ores	Cu-Fe sulfide minerals		Bingham	Produced during smelting of Cu-Fe sulfide ores	Kennecott Utah Copper (2013)

deposits that may contain critical commodity by-products. In this report, critical commodities are defined as elements, such as Re, PGMs, Te, Se, REEs, In, Li, Nb, and Ta, which are important in use in modern society and technology and may have potential for supply restriction (e.g., National Research Council, 2008; American Physical Society, 2011; British Geological Survey, 2012).

Porphyry Copper and Molybdenum Deposits

General description

Porphyry Cu deposits and encompassing porphyry Cu systems are the subject of extensive ongoing research, and many aspects of these systems are discussed in recent summary papers that include Sillitoe (2000, 2005, 2010), Tosdal and Richards (2001), Richards (2003, 2009, 2011), Cooke et al. (2005), Seedorff et al. (2005), Sinclair (2007), Singer et al. (2008), and John et al. (2010). Similarly, characteristics of porphyry Mo deposits are summarized in recent papers by Ludington and Plumlee (2009), Ludington et al. (2009), and Taylor et al. (2012). The following section highlights some pertinent aspects of porphyry Cu and Mo deposits and systems. For more detailed description and discussion, the reader is referred to the aforementioned papers and the references contained therein.

Porphyry Cu deposits are parts of porphyry Cu systems, which are large volumes of hydrothermally altered rock centered on porphyry Cu stocks and other intrusions. The deposits may include associated skarn, carbonate-replacement, sediment-hosted, and high- and intermediate-sulfidation epithermal base and precious metal mineralization (Sillitoe, 2010). Porphyry Cu systems most commonly form above active subduction zones at convergent plate margins and are associated with calc-alkaline batholiths and volcanic arcs (Fig. 1; Sillitoe, 1972; Richards, 2003, 2011). They commonly occur in linear, typically orogen-parallel belts, which range from a few tens to thousands of kilometers long, as epitomized by the Andes of western South America (Sillitoe and Perelló, 2005). Isolated porphyry Cu systems can form in postcollisional and other tectonic settings after subduction ends (Richards, 2009; Hou et al., 2011).

Porphyry Cu deposits are among the world's largest metallic mineral deposits, generally containing large tonnages (>100 Mt and ranging up to 20 Bt) with typical hypogene grades of 0.5 to 1.5% Cu, <0.01 to 0.04% Mo, and 0 to 1.5 g/t Au (Singer et al., 2008; Sillitoe, 2010). Porphyry Cu deposits are the world's most important source of Cu, accounting for more than 60% of the annual world Cu production and about 65% of known Cu resources. Together with related skarn, replacement, and epithermal deposits, porphyry copper systems presently supply nearly three-quarters of the world's Cu, half the Mo, as much as one-fifth of the Au, about 80% of the Re, most of the Se and Te, and minor amounts of Ag, Pd, Pt, Bi, Zn, and Pb (Sillitoe, 2010). Hydrothermal activity related to porphyry Cu systems results in concentration, redistribution, or depletion of dozens of other major and trace elements within the much larger volume of rock (~10–100 times) affected by hydrothermal fluids (Seedorff et al., 2005; Barton, 2010), potentially forming economic concentration of numerous other elements.

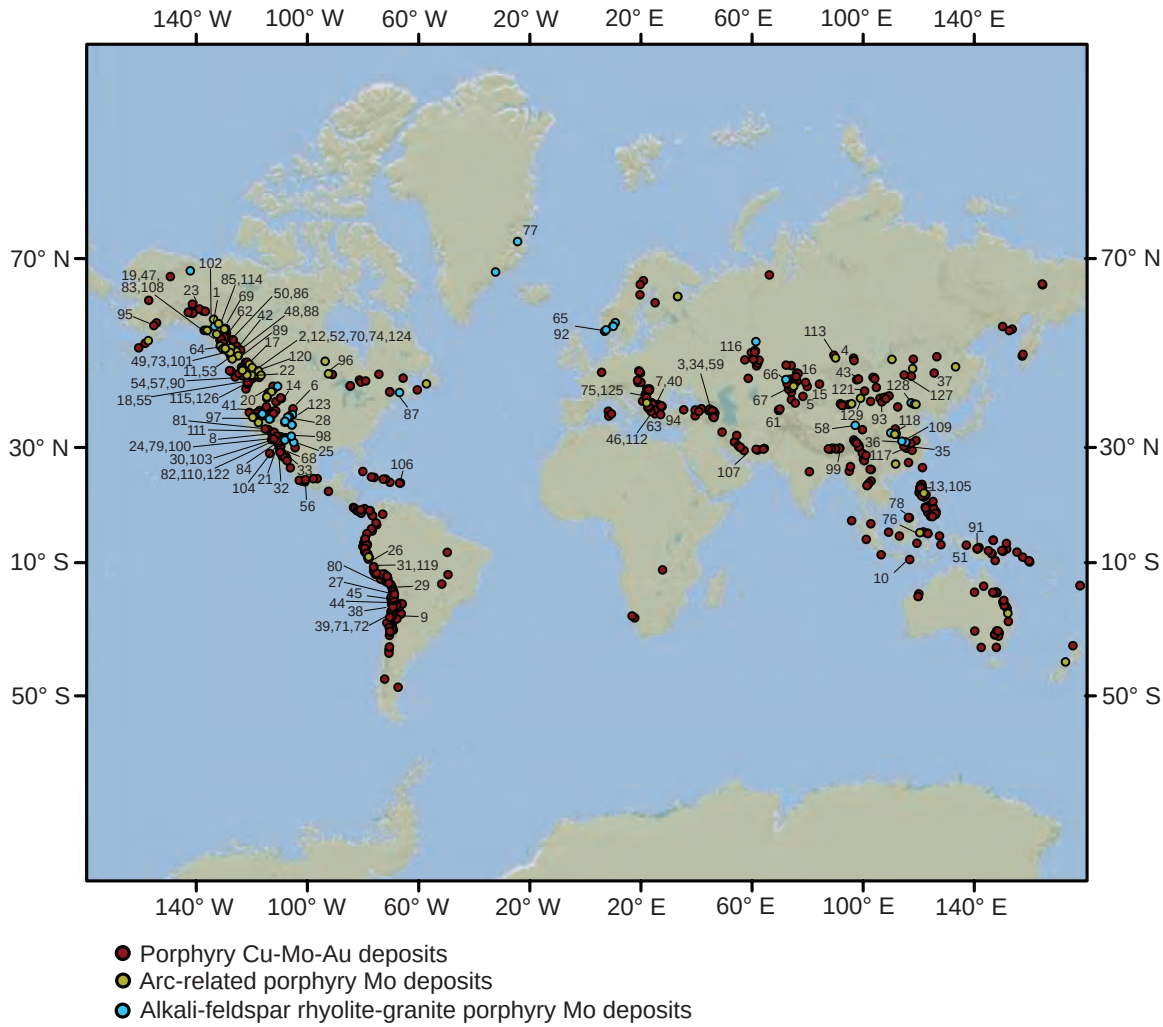

Fig. 1. Global distribution of porphyry Cu and porphyry Mo deposits from Singer et al. (2008) and Taylor et al. (2012). Numbered deposits mentioned in the text and tables:1 = Adanac (Ruby Creek), 2 = Afton-Ajax, 3 = Agarak, 4 = Aksug, 5 = Aktogai, 6 = Allard, 7 = Assarel-Medet, 8 = Bagdad, 9 = Bajo de la Alumbrera, 10 = Batu Hijau, 11 = Berg, 12 = Bethlehem, 13 = Biga, 14 = Bingham, 15 = Borly, 16 = Boshcekul, 17 = Boss Mountain, 18 = Brenda, 19 = Bronson Slope, 20 = Butte, 21 = Cananea, 22 = Carmi, 23 = Casino, 24 = Castle Dome (Pinto Valley), 25 = Cave Peak, 26 = Cerro Verde, 27 = Chuquicamata, 28 = Climax, 29 = Collahuasi, 30 = Copper Creek, 31 = Cuajone, 32 = Cuatro Hermanos, 33 = Cumobabi, 34 = Dastakert, 35 = Dexing, 36 = Donggou, 37 = Duobaoshan, 38 = El Salvador, 39 = El Teniente, 40 = Elatsite, 41 = Ely, 42 = Endako, 43 = Erdenet (Erdenetuin-Obo), 44 = Escondida, 45 = Esperanza, 46 = Fissoka, 47 = Galore Creek, 48 = Gibraltor, 49 = Glacier Gulch (Davidson), 50 = Granisle, 51 = Grasberg, 52 = Highmont, 53 = Huckleberry, 54 = Hushamu, 55 = Ingerbelle, 56 = Inguaran, 57 = Island Copper, 58 = Jinduicheng, 59 = Kadjaran (Kadzharan), 61 = Kalmakyr (Almalyk), 62 = Kemess South, 63 = Kirki, 64 = Kitsault (Lime Creek), 65 = Knaben, 66 = Koktenkol, 67 = Kounrad, 68 = La Caridad, 69 = Logtung, 70 = Lornex, 71 = Los Bronces/Rio Blanco (Andina) 72 = Los Pelambres, 73 = Lucky Ship, 74 = Maggie, 75 = Majdanpek, 76 = Malala, 77 = Malmbjerg, 78 = Mamut, 79 = Miami, 80 = Mina Sura, 81 = Mineral Park (Ithica Peak), 82 = Mission-Pima, 83 = Mitchell (Sulphurets), 84 = Morenci, 85 = Mount Haskin, 86 = Mount Milligan, 87 = Mount Pleasant, 88 = Mount Polley, 89 = Nithi Mountain, 90 = Ok, 91 = Ok Tedi, 92 = Orsdalen, 93 = Oyu Tolgoi, 94 = Pagoni Rachi, 95 = Pebble, 96 = Pidgeon, 97 = Pine Nut, 98 = Questa, 99 = Qulong, 100 = Ray, 101 = Red Bird, 102 = Red Mountain, 103 = San Manuel-Kalamazoo, 104 = Santa Rita, 105 = Santo Tomas II (Philex), 106 = Sapo Alegre, 107 = Sar Cheshmeh, 108 = Schaft Creek, 109 = Shaping-gou, 110 = Sierrita-Esperanza, 111 = Silver Bell, 112 = Skouriés, 113 = Sora (Sorsk), 114 = Storie Moly, 115 = Sunrise, 116 = Tominskoe, 117 = Tongchankou, 118 = Tonkuangyu, 119 = Toquepala, 120 = Trout Lake (Max), 121 = Tsagaan Suvarga, 122 = Twin Buttes, 123 = Urad-Henderson, 124 = Valley Copper, 125 = Veliki Krivelj, 126 = White River, 127 = Wunugetushan, 128 = Xiaodonggou, 129 = Zuun Mod Molybdenum.

The primary and by-product commodities for both types of porphyry Mo deposits are similar, but they are found in varying concentrations. Alkali-feldspar rhyolite-granite deposits are commonly higher grade (commonly ≤0.1–0.3% Mo; Ludington and Plumlee, 2009) than arc-related deposits (commonly 0.03–0.2% Mo; Taylor et al., 2012), and both have moderate to large sizes (a few to >1,500 Mt). Arc-related porphyry Mo deposits are considered to be an end member of the porphyry Cu deposit spectrum that formed at slightly greater crustal depths due to differences in the behavior of Mo and Cu during magmatic evolution (Candela and Holland, 1986; Misra, 2000).

Geologic setting

Porphyry Cu systems are widespread with nearly 700 deposits and prospects known as of 2008 (Fig. 1; Singer et al., 2008). They formed throughout most of Earth's history beginning in the Archean, but because they generally form in the upper crust (less than 5- to10-km depth) in tectonically unstable convergent plate margins and are prone to erosion, more than 90% of known deposits are Cenozoic or Mesozoic in age (Singer et al., 2008). Porphyry Cu systems mostly form in subduction-related magmatic arc environments along convergent plate margins under regional stress regimes ranging from moderately extensional through oblique slip to contractional (Sillitoe, 1972, 2010; Tosdal and Richards, 2001; Richards, 2003, 2011). Some porphyry Cu systems form in back-arc or post-subduction (post-collisional) magmatic settings, in both extensional and compressional environments (Richards, 2009; Hou et al., 2011). In convergent plate margins, arc-type magmatism generates hydrous, oxidized upper crustal granitoids genetically related to ores. In most cases, arc crust is relatively thick, and there is evidence for broadly coeval compressional or transpressional tectonism (e.g., Tosdal and Richards, 2001; Sillitoe and Perelló, 2005). Many porphyry Cu deposits formed during unusual periods of subduction, including flat subduction induced by subduction of buoyant oceanic structures, such as ridges, ocean plateaus, and seamount chains, or during episodes of plate reorganization (e.g., Sillitoe and Perelló, 2005). Within this broadly compressional environment, transpression is expressed as strike-slip faults with significant reverse movement, and it has been suggested that stress relaxation to transtensional or mildly extensional conditions is associated with emplacement of mineralized porphyry intrusions (e.g., Tosdal and Richards, 2001; Richards, 2003).

Porphyry Cu deposits formed in postcollisional settings tend to be small volume, spatially isolated, and mildly alkaline (high K ± Na calc-alkaline) to strongly alkaline in composition, although some of the world's largest porphyry Cu-(Mo-Au) deposits are interpreted to have formed in this tectonic setting (e.g., Grasberg, Indonesia: Richards, 2009; Pebble, Alaska: Goldfarb et al., 2013).

The overwhelming majority of porphyry Mo deposits formed within continental crust, and deposits developed within oceanic crust, are exceedingly rare (e.g., Malala in Indonesia: van Leeuwen et al., 1994). Alkali-feldspar rhyolite-granite deposits formed within back-arc extensional to transtensional zones and rift zones. The most famous of these deposits, Climax and Urad-Henderson, occur within the Colorado Mineral Belt and are associated with a reduction in tectonic stress accompanied by extension following the Laramide orogeny.

Intrusive rocks associated with porphyry copper and molybdenum deposits

Porphyry intrusions in porphyry Cu deposits are I-type and magnetite-series, mostly metaluminous, and range from medium K calc-alkaline to high K calc-alkaline (shoshonitic) or alkaline (Seedorff et al., 2005; Sillitoe, 2010). These intrusions span a range of compositions from calc-alkaline diorite and quartz diorite through granodiorite to quartz monzonite (monzogranite), and alkaline diorite through monzonite to uncommon syenite. Molybdenum-rich porphyry Cu deposits are usually associated with more felsic intrusions, whereas Au-rich porphyry Cu deposits tend to be related to the more mafic end members (Sillitoe, 2010). Lamprophyres are present in some deposits, and commingling of lamprophyric (minette) with silicic magmas at Bingham may have contributed sulfur and chalcophile elements to the Bingham system (Keith et al., 1997; Hattori and Keith, 2001). Contributions from ultramafic magmas might account for platinum-group metal (PGM) concentrations in deposits such as Bingham and Skouriés, Greece (Tarkian and Stribrny, 1999; Economou-Eliopoulos, 2005). Radiogenic isotope compositions (Pb-Nd-Sr-Hf-Os) of rocks comprising porphyry copper systems have wide variations, which imply that a wide range of contributions from normal and enriched mantle, oceanic crust, and continental crust are involved with porphyry copper metallogenesis (Ayuso, 2010).

Intrusions associated with arc-related porphyry Mo deposits are peraluminous I-type calc-alkaline magmas. Most are quartz monzonite to granodiorite in composition, although they vary from diorite to granite, and have both oxidized and reduced compositions (Westra and Keith, 1981; Sinclair, 2007; Taylor et al., 2012).

Alkali-feldspar rhyolite-granite porphyry Mo deposits are related to highly evolved, fluorine-rich rare metal granites. Alkaline igneous rocks, like those associated with many alkali-feldspar rhyolite-granite porphyry molybdenum deposits, are unusually enriched in elements, such as Zr, Ba, Li, REEs, Nb, Rb, and Ta. These are commonly A-type granites that contain magnetite and have a significant crustal input (Ludington and Plumlee, 2009).

Subtypes of porphyry copper and molybdenum deposits and related metals

Porphyry Cu deposits commonly are divided on the basis of their Cu, Mo, and Au contents and/or on the composition of associated igneous rocks. Kesler (1973), Sillitoe (1979, 1993, 2000), Kirkham and Sinclair (1995), and Kesler et al. (2002) defined Au-rich porphyry deposits on the basis of their Au content or Cu/Au with differing classification cut-offs. Although early studies suggested that most Au-rich porphyry systems formed in island-arc settings (Kesler, 1973), more recent studies (e.g., Cox and Singer, 1992; Sillitoe, 2000; Kesler et al., 2002) note that Au-rich porphyry deposits are not limited to any specific tectonic setting or type of crust.

Cox and Singer (1992) used Au/Mo to divide porphyry copper deposits into three subtypes, Cu-Au (Au/Mo ≥30), Cu-Au-Mo (Au/Mo = 3–30), and Cu-Mo (Au/Mo ≤3), in which gold is in parts per million and molybdenum is in weight percent. They noted that this classification is not based on tectonic setting and that it is common for multiple subtypes to exist in the same broad arcs that formed at about the same time. The Cox and Singer (1992) classification is adopted in this paper (Table 2).

Types of porphyry Mo deposits are best distinguished on the basis of the composition of associated intrusive rocks and tectonic environment of formation. Sillitoe (1980) distinguished these deposits based upon whether they were related to subduction or continental rifting. Westra and Keith (1981) more quantitatively distinguished the types based on the K, F, Nb, Rb, and Sr concentrations within source plutons. There is

Table 2. Rhenium Data for Porphyry Copper

Deposit	Country	Deposit subtype[1]	Tectonic setting	Cu (wt %)	Mo (wt %)	Au (g/t)	Mininmum Re in MoS_2 (ppm)	Maximum Re in MoS_2 (ppm)	Preferred mean Re in MoS_2 (ppm)
Porphyry copper deposits									
Agarak	Armenia	Cu	Continental arc	0.56	0.025	0.6	57	6,310	820
Ajax West	Canada	Cu	Island arc	0.31	0.005	0.2			3,161
Aksug	Russia	Cu	Postcollisional	0.67	0.015	0.12			460
Aktogai	Kazakhstan	Cu-Mo	Continental arc	0.39	0.01	0.026	50	2,700	850
Bagdad	United States	Cu-Mo	Continental arc	0.4	0.01	0.0011	330	642	460
Berg	Canada	Cu-Mo	Continental arc	0.39	0.031	0.06	67	215	152
Bethlehem--Huestis	Canada	Cu-Mo	Island arc	0.4	0.005	0.012			417
Bethlehem--Iona	Canada	Cu-Mo	Island arc	0.52	0.006	0.012			1,015
Bethlehem--JA	Canada	Cu-Mo	Island arc	0.43	0.017	0.01	200	246	222
Bingham	United States	Cu	Postcollisional	0.882	0.053	0.38	130	2,000	250
Borly	Kazakhstan	Cu	Continental arc	0.34	0.011	0.3	250	5,500	3,160
Boschekul	Kazakhstan	Cu-Mo	Island arc	0.67	0.0023	0.049	230	1,500	825
Brenda	Canada	Cu-Mo	Island arc	0.152	0.037	0.013	80	145	115
Bronson Slope	Canada	Cu-Au	Island arc	0.17	0.006	0.44			180
Butte	United States	Cu-Mo	Continental arc	0.673	0.028	0.042			240
Cananea	Mexico	Cu	Continental arc	0.45	0.002	0.035			700
Casino	Canada	Cu	Continental arc	0.25	0.025		65	289	197
Castle Dome (Pinto Valley)	United States	Cu-Au	Continental arc	0.33	0.0055	0.34	1,200	1,750	1,750
Cerro Verde	Peru	Cu	Continental arc	0.495	0.01		3,060	3,497	3,280
Chuquicamata	Chile	Cu-Mo	Continental arc	0.86	0.04	0.013	93	262	265
Collahuasi	Chile	Cu-Mo	Continental arc	0.592	0.04	0.01	368	448	395
Copper Creek	United States	Cu	Continental arc	0.75	0.0046		534	2,107	1,165
Cuajone	Peru	Cu	Continental arc	0.69	0.0214				580
Cuatro Hermanos	Mexico	Cu	Continental arc	0.431	0.035				469
Cumobabi	Mexico	Cu-Mo	Continental arc	0.266	0.099		189	368	279
Dastakert	Armenia	Cu	Continental arc	0.62	0.048		130	300	220
Duobaoshan	China	Cu	Island arc	0.46	0.016	0.128	122	885	560
El Salvador	Chile	Cu	Continental arc	0.86	0.022	0.1			585
El Teniente	Chile	Cu-Mo	Continental arc	0.62	0.019	0.005	25	1,154	420
Elatsite	Bulgaria	Cu	Continental arc	0.39	0.01	0.26	273	2,740	1,250
Ely	United States	Cu	Continental arc	0.613	0.01	0.27	1,250	2,840	1,600
Erdenet (Erdenetuin-Obo)	Mongolia	Cu	Postcollisional	0.62	0.025		104	534	199
Escondida	Chile	Cu-Au	Continental arc	0.769	0.0062	0.25	95	1,805	886
Gibraltar	Canada	Cu	Island arc	0.29	0.006	0.07	238	750	443
Granisle	Canada	Cu	Continental arc	0.43	0.005	0.13	522	528	526
Highmont West Pit	Canada	Cu-Mo	Island arc	0.15	0.05	0.04			157
Huckleberry	Canada	Cu	Continental arc	0.49	0.014	0.04	247	258	253
Hushamu	Canada	Cu-Au	Island arc	0.198	0.0092	0.278			3,140
Ingerbelle	Canada	Cu-Au	Island arc	0.329	0.002	0.17			1,620
Island Copper	Canada	Cu	Island arc	0.338	0.0088	0.19	1,654	1,863	1,730
Kadjaran (Kadzharan)	Armenia	Cu	Continental arc	0.27	0.055	0.65	33	2,620	280
Kalmakyr (Almalyk)	Uzbekistan	Cu-Au	Continental arc	0.38	0.006	0.6	700	2,000	1,500
Kemess South	Canada	Cu-Au	Island arc	0.22	0.008	0.65	3,106	4,609	3,858
Kounrad	Kazakhstan	Cu	Continental arc	0.589	0.011	0.19	620	4,050	1,540
La Caridad	Mexico	Cu	Continental arc	0.452	0.0247				570
Lomex	Canada	Cu-Mo	Island arc	0.404	0.014	0.006	286	427	351
Los Bronces/Rio Blanco (Andina)	Chile	Cu-Mo	Continental arc	0.601	0.02		104	898	265
Los Pelambres	Chile	Cu-Mo	Continental arc	0.617	0.015	0.028	450	820	600
Machangqing	China	Cu-Au	Collision belt(?)	0.64	0.08	0.35	31	125	80
Maggie	Canada	Cu-Mo	Continental arc	0.28	0.029				643
Majdanpek	Serbia	Cu-Au	Continental arc	0.6	0.005	0.35	2,320	3,550	2,770
Medet	Bulgaria	Cu	Continental arc	0.37	0.01	0.1			905
Miami	United States	Cu-Mo	Continental arc	0.63	0.01	0.009			600
Mineral Park (Ithica Peak)	United States	Cu	Continental arc	0.489	0.011		250	290	270

and Porphyry Molybdenum Deposits

Number of Re analyses[2]	Preferred sample type[3]	Re grade (g/t)[4]	Ore tonnage (Mt)	Mo (t)[5]	Re (t)[6]	Mo/Re	References
106,0,0	1	0.342	125	31,250	43	732	Berzina et al. (2005); Singer et al. (2008)
1,0,0	1	0.263	365	18,250	96	190	Sinclair et al. (2009)
0,0,1	3	0.115	337	50,550	39	1,304	Berzina et al. (2005); Singer et al. (2008)
30,0,0	1	0.142	2,636	263,600	374	704	Berzina et al. (2005); Singer et al. (2008)
0,7,2	2	0.077	1,600	160,000	123	1,299	Sutulov (1974); Nadler (1997); Barra et al. (2003); Singer et al. (2008)
4,0,0	1	0.079	238	73,780	19	3,947	Sinclair et al. (2009)
1,0,0	1	0.035	1.4	70	0.05	1,439	Sinclair et al. (2009)
0,0,1	1	0.102	30	1,770	3	591	Sinclair et al. (2009)
4,0,0	1	0.063	260	44,200	16	2,703	Sinclair et al (2009)
36,6,1	3	0.221	3,230	1,711,900	714	2,398	Giles and Schilling (1972); McCandless and Ruiz (1993); Chesley and Ruiz (1998; Singer et al. (2008); Austen and Ballantyne (2010); J. Chesley, writ. commun. (2013)
19,0,0	1	0.579	94	10,384	55	190	Berzina et al. (2005); Singer et al. (2008)
23,0,0	1	0.032	1,000	23,000	32	727	Singer et al. (2008); Sinclair et al. (2009)
11,0,2	1	0.071	182	67,229	13	5,211	Sutulov (1974); Sinclair et al. (2009); W.D. Sinclair, writ. commun. (2013)
1,0,1	1	0.018	79	4,740	1.4	3,333	Sinclair et al. (2009)
1,0,0	1	0.112	5,220	1,461,600	585	2,500	Giles and Schilling (1972); Singer et al. (2008)
0,0,1	3	0.023	5,141	102,820	118	870	Giles and Schilling (1972); Sutulov (1974); Singer et al. (2008)
4,0,0	1	0.082	559	139,750	46	3,049	Sinclair et al. (2009)
3,0,2	1	0.160	1,438	79,090	230	344	Giles and Schilling (1972); Singer et al. (2008)
0,2,0	2	0.116	2,528	252,800	293	862	Mathur et al. (2001); Singer et al. (2008)
1,6,2	3	0.177	21,277	8,510,800	3766	2,260	Giles and Schilling (1974); Sutulov (1974); Nadler (1997); Singer et al. (2008); Barra et al. (2013)
0,3,0	2	0.263	3,100	1,240,000	815	1,521	Mathur et al. (2001); Masterman et al. (2004); Singer et al. (2008)
0,3,0	2	0.089	75	3,464	7	517	McCandless and Ruiz (1993); Barra et al. (2005); Singer et al. (2008)
1,0,1	3	0.207	1,630	348,820	337	1,034	Nadler (1997); Mathur et al. (2001); Singer et al. (2008)
0,1,0	2	0.274	233	81,550	64	1,277	Barra et al. (2005); Singer et al. (2008)
0,2,0	2	0.460	67	66,330	31	2,152	Barra et al. (2005); Singer et al. (2008)
8,0,1	1	0.176	36	17,040	6	2,727	Sutulov (1974); Berzina et al. (2005); http://www.globalmetals.am/en/projects/molibdeny_ashkharh/
0,8,0	2	0.149	951	152,160	142	1,074	Zhao et al. (1997); Singer et al. (2008); Zeng et al. (2013)
1,0,2	3	0.215	3,836	843,986	825	1,023	Giles and Schilling (1972); Sutulov (1974); Nadler (1997); Singer et al. (2008)
1,14,2	3	0.133	20,731	3,938,890	2757	1,429	Giles and Schilling (1974); Sutulov (1974); Nadler (1997); Maksaev et al. (2004); Cannell (2004); Klemm et al. (2007); Singer et al. (2008)
19,0,0	1	0.208	350	35,000	73	481	Singer et al. (2008); Sinclair et al. (2009)
4,0,0	3	0.267	754	75,400	201	375	Giles and Schilling (1972); Sutulov (1974); Singer et al. (2008)
2,1,1	3	0.043	1,780	445,000	77	5,814	Watanabe and Stein (2000); Berzina et al. (2005); Singer et al. (2008)
0,7,0	2	0.092	11,158	691,796	1027	674	Mathur et al. (2001); Singer et al. (2008); Romero et al. (2010)
3,0,1	1	0.044	935	56,100	41	1,364	Sinclair et al. (2009); W.D. Sinclair, writ. commun. (2013)
0,0,5	3	0.044	171	8,560	8	1,136	Sinclair et al. (2009); W.D. Sinclair, writ. commun. (2013)
2,0,0	1	0.131	0.8	400	0.1	3,817	Sinclair et al. (2009)
2,0,0	1	0.059	73	10,276	4	2,373	Sinclair et al. (2009)
1,0,0	4	0.481	510	46,883	245	191	NorthIsle Copper and Gold, Inc. (2012)
1,0,0	1	0.054	78	1,564	4	370	Sinclair et al. (2009)
0,0,11	3	0.262	600	52,800	157	336	Sinclair et al. (2009); W.D. Sinclair, writ. commun. (2013)
237,0,1	1	0.257	1,700	935,000	437	2,140	Nadler (1997); Berzina et al. (2005); Singer et al. (2008)
20,0,1	1	0.150	2,000	120,000	300	400	Sutulov (1974); Singer et al. (2008); Pasava et al. (2010)
2,0,0	1	0.514	213	17,040	109	156	Sinclair et al. (2009)
20,0,1	1	0.282	637	70,070	180	390	Sutulov (1974); Berzina et al. (2005); Singer et al. (2008)
0,2,1	3	0.235	1,800	444,600	423	1,051	Nadler (1997); Valencia et al. (2005); Singer et al. (2008)
2,0,20	3	0.081	460	64,400	37	1,728	Sinclair et al. (2009); W.D. Sinclair, writ. commun. (2013)
0,13,2	2	0.088	16,816	3,363,200	1480	2,273	Mathur et al. (2001); Singer et al. (2008); Deckert et al. (2013)
0,3,0	2	0.150	7,458	1,118,700	1119	1,000	Mathur et al. (2001); Singer et al. (2008)
0,0,5	3	0.107	39	31,200	4	7,477	Hou et al. (2006)
1,0,0	1	0.311	181	52,606	56	932	Sinclair et al. (2009)
3,0,0	1	0.231	1,000	50,000	231	216	Todorov and Staikov (1985); Singer et al. (2008)
22,0,1	1	0.151	244	24,400	37	662	Sutulov (1974); Berzina et al. (2005); Singer et al. (2008)
1,0,0	1	0.100	1,591	159,100	159	1,000	Berzina et al. (2005); Singer et al. (2008)
2,0,1	1	0.050	876	96,360	44	2,200	Giles and Schilling (1972); Sutulov (1974); Singer et al. (2008)

Table 2.

Deposit	Country	Deposit subtype[1]	Tectonic setting	Cu (wt %)	Mo (wt %)	Au (g/t)	Mininmum Re in MoS_2 (ppm)	Maximum Re in MoS_2 (ppm)	Preferred mean Re in MoS_2 (ppm)
Mission-Pima	United States	Cu	Continental arc	0.52	0.015				600
Mitchell (Sulphurets)	Canada	Cu-Au	Island arc	0.18	0.005	0.69	7,012	8,170	7,590
Morenci	United States	Cu-Mo	Continental arc	0.524	0.0095	0.028	270	640	455
Mt. Tolman	United States	Cu-Mo	Continental arc	0.09	0.054				182
Ok	Canada	Cu	Continental arc	0.34	0.016				746
Pebble	United States	Cu	Postcollisional	0.592	0.0243	0.342	329	2,070	1,100
Qulong	China	Cu-Mo	Postcollisional	0.52	0.032		16	303	125
Ray	United States	Cu	Continental arc	0.68	0.001		440	1,500	820
San Manuel-Kalamazoo	United States	Cu-Mo	Continental arc	0.6	0.011	0.017	700	1,200	900
Santa Rita	United States	Cu	Continental arc	0.468	0.008	0.056	700	1,200	800
Sar Cheshmeh	Iran	Cu	Continental arc	1.2	0.03	0.27	11	517	597
Schaft Creek	Canada	Cu	Island arc	0.25	0.019	0.18			590
Sierrita-Esperanza	United States	Cu-Mo	Continental arc	0.294	0.0292	0.003	90	1,800	238
Silver Bell	United States	Cu-Mo	Continental arc	0.66	0.013	0.026	340	620	531
Skouriés	Greece	Cu-Au	Postcollisional	0.35	0.002	0.47	800	1,000	900
Snowfields	Canada	Cu-Au	Island arc	0.08	0.008	0.50			3,600
Sora (Sorsk)	Russia	Cu	Postcollisional?	0.17	0.058		6	18	14
Tominskoe	Russia	Cu	Island arc	0.58	0.004	0.12			1,080
Tongchankou	China	Cu	Uncertain	0.94	0.04		176	235	208
Toquepala	Peru	Cu-Mo	Continental arc	0.55	0.04		387	1,496	600
Tsagaan Suvarga	Mongolia	Cu	Continental arc	0.53	0.018	0.084	80	156	118
Twin Buttes	United States	Cu-Mo	Continental arc	0.502	0.023	0.019			600
Valley Copper	Canada	Cu-Au	Island arc	0.44	0.0067	0.006			294
Veliki Krivelj	Serbia	Cu	Continental arc	0.44	0.004	0.068			302
Wunugetushan	China	Cu-Mo	Postcollisional?	0.46	0.053		142	369	199
Yulong	China	Cu-Au	Postcollisional?	0.99	0.028	0.35	291	665	444
Zuun Mod Molybdenum	Mongolia	Cu-Mo	Continental arc?	0.069	0.059		250	300	275
Porphyry Molybdenum Deposits									
Boss Mountain	Canada	Arc-related	Continental arc		0.074		49	157	80
Carmi	Canada	Arc-related	Continental arc		0.064		10	139	58
Endako	Canada	Arc-related	Continental arc	0.002	0.07		15	67	35
Glacier Gulch (Davidson)	Canada	Arc-related	Continental arc	0.04	0.177		34	41	38
Kitsault (Lime Creek)	Canada	Arc-related	Continental arc	0.004	0.115		36	129	71
Lucky Ship	Canada	Arc-related	Continental arc		0.067				41
Mount Haskin	Canada	Arc-related	Continental arc		0.09				108
Nithi Mountain	Canada	Arc-related	Continental arc		0.02				76.9
Quartz Hill	United States	Arc-related	Continental arc	0.003	0.0762				149
Red Bird	Canada	Arc-related	Continental arc	0.07	0.065		6	43	25
Red Mountain	Canada	Arc-related	Continental arc		0.1				32
Storie Moly	Canada	Arc-related	Continental arc		0.078		15	22	20
Thompson Creek	United States	Arc-related	Continental arc		0.071				120
Trout Lake (Max)	Canada	Arc-related	Continental arc		0.12		56	73	56
Adanac (Ruby Creek)	Canada	Alk-granite/ hybrid?	Extensional continental arc	0.001	0.059		8	22	12
Climax	United States	Alk-granite	Continental rift		0.2		10	80	13
Donggou	China	Alk-granite	Collision belt		0.116		4.1	4.3	4.2
Jinduicheng	China	Alk-granite	Collision belt		0.099		15.5	16.2	15.9
Questa	United States	Alk-granite	Continental rift		0.15		6	145	36
Shapinggou	China	Alk-granite	Collision belt		0.126		0.4	14.7	4.7
Urad Henderson	United States	Alk-granite	Continental rift		0.228		7	20	20
Xiaodonggou	China	Alk-granite	Collision belt(?)		0.109		4.5	8.4	7.1

[1] Cox and Singer (1992) porphyry Cu models; Taylor et al. (2012) and Ludington and Plumlee (2009) porphyry Mo models

[2] Number of analyses of MoS_2 separates, MoS_2 analyzed for Re-Os dating, MoS_2 mill concentrates

[3] Sample type used in calculating Re grade: 1 = molybdenite separate; 2 = molybdenite separate used in Re-Os dating; 3 = molybdenite mill concentrate; 4 = average grade of total resources calculated from drilling

(Cont.)

Number of Re analyses[2]	Preferred sample type[3]	Re grade (g/t)[4]	Ore tonnage (Mt)	Mo (t)[5]	Re (t)[6]	Mo/Re	References
0,1,1	3	0.150	900	135,000	135	1,000	Sutulov (1974); McCandless and Ruiz (1993); Singer et al. (2008)
2,0,0	1	0.633	734	36,700	465	79	Sinclair et al. (2009)
3,1,0	1	0.072	6,470	614,650	466	1,319	Giles and Schilling (1972); McCandless and Ruiz (1993); Singer et al. (2008)
0,0,1	3	0.163	2,177	1,175,580	355	3,313	Carten et al. (1993); W.D. Sinclair, writ. commun. (2013)
1,0,0	1	0.199	64	10,240	13	804	Sinclair et al. (2009)
0,6,2	3	0.446	5,940	1,443,420	2649	545	Northern Dynasty Minerals, Ltd. (2011); Lang et al. (2013)
0,4,0	2	0.067	1,517	485,440	102	4,776	Singer et al. (2008); Hou et al. (2009)
9,0,0	1	0.014	1,583	15,830	22	714	Giles and Schilling (1972); Singer et al. (2008)
2,0,2	3	0.165	1,390	152,900	229	667	Giles and Schilling (1972); Sutulov (1974); Nadler (1997); Singer et al. (2008)
8,0,1	3	0.107	3,030	242,400	324	748	Giles and Schilling (1972); Sutulov (1974); Singer et al. (2008)
15,0,5	3	0.299	1,200	360,000	359	1,003	Singer et al. (2008); Aminzadeh et al. (2011)
1,0,0	1	0.187	1,393	264,670	260	1,016	Sinclair et al. (2009)
6,1,2	2	0.116	2,262	660,504	262	2,517	Giles and Schilling (1972); Sutulov (1974); McCandless and Ruiz (1993); Nadler (1997); Singer et al. (2008)
18,1,0	2	0.115	268	34,840	31	1,130	Giles and Schilling (1972); Barra et al. (2005); Singer et al. (2008)
4,0,0	1	0.030	568	11,360	17	667	Singer et al. (2008); Sinclair et al. (2009)
1,0,0	4	0.480	2,203	176,240	1057	167	Pretium Resources Inc. (2011
9,0,0	1	0.014	300	174,000	4.2	41,429	Sotnikov et al. (2001); Berzina et al. (2005); Berzina and Korobeinikov (2007)
1,0,0	1	0.072	241	9,640	17	556	Singer et al. (2008); Sinclair et al. (2009)
0,6,0	2	0.139	45	17,840	6.2	2,878	Xie et al. (2007); Singer et al. (2008)
1,2,2	3	0.400	2,320	928,000	928	1,000	Giles and Schilling (1972); Sutulov (1974); Nadler (1997); Mathur et al. (2001); Singer et al. (2008)
0,2,0	2	0.035	240	43,200	8.4	5,143	Wantanbe and Stein (1999; Singer et al. (2008)
0,0,1	3	0.230	940	216,200	216	1,000	Sutulov (1974); Singer et al. (2008)
0,0,1	3	0.033	791	52,997	26	2,030	Sinclair et al. (2009); W.D. Sinclair, writ. commun. (2013)
1,0,0	1	0.020	750	30,000	15	2,000	Singer et al. (2008); Sinclair et al. (2009)
0,7,0	2	0.176	850	450,341	150	3,011	Chen et al. (2011)
0,0,2	3	0.207	628	175,840	130	1,353	Hou et al. (2006)
2,0,0	4	0.270	218	128,620	59	2,185	Erdene Resource Development Corp. (2011)
7,0,0	1	0.099	63	46,620	6.2	7,500	Sinclair et al. (2009)
3,0,0	1	0.062	21	13,248	1.3	10,345	Sinclair et al. (2009)
14,12,1	1	0.041	600	420,000	25	17,143	Giles and Schilling (1972); Selby and Creaser (2001); Sinclair et al. (2009); W.D. Sinclair, writ. commun. (2013)
2,0,0	1	0.112	75	133,281	8.4	15,789	Sinclair et al. (2009)
9,0,0	1	0.136	104	119,600	14	8,451	Sinclair et al. (2009)
1,0,0	1	0.046	62	41,205	2.8	14,634	Sinclair et al. (2009)
1,0,0	1	0.162	12	11,025	2.0	5,556	Sinclair et al. (2009)
0,1,0	2	0.026	240	47,920	6.2	7,692	Selby and Creaser (2001); Mosher (2001)
0,0,1	3	0.189	1,600	1,219,200	302	4,032	Hudson et al. (1979; Wolfe (1995); W.D. Sinclair, writ. commun. (2013)
2,0,0	1	0.027	75	48,945	2.0	24,000	Sinclair et al. (2009)
1,0,0	1	0.053	187	187,000	10	18,750	Sinclair et al. (2009)
3,0,0	1	0.026	101	78,390	2.6	30,000	Sinclair et al. (2009)
0,0,1	3	0.142	212	150,520	30	5,000	Carten et al. (1993); W.D. Sinclair, writ. commun. (2013)
1,0,1	3	0.112	43	51,480	4.8	10,714	Sinclair et al. (2009)
4,0,0	1	0.012	144	84,783	1.7	50,000	Sinclair et al. (2009)
13,0,4	3	0.043	800	1,600,000	35	45,714	Giles and Schilling (1972); Nadler (1997); Singer et al. (1993); Sinclair et al. (2009); W.D. Sinclair, writ. commun. (2013)
0,2,0	2	0.008	594	689,000	4.8	145,000	Mao et al. (2011); Deng et al. (2013)
0,7,0	2	0.026	1,089	1,078,000	28	38,077	Mao et al. (2011); Deng et al. (2013)
14,8,1	2	0.090	424	636,000	38	16,667	Giles and Schilling (1972); Singer et al. (1993); Rosera et al. (2013); W.D. Sinclair, writ. commun. (2013)
0,9,0	2	0.010	1,270	1,600,000	13	126,000	Mao et al. (2011); Deng et al. (2013)
2,0,2	3	0.076	437	996,360	33	30,000	Giles and Schilling (1972); Nadler (1997); Seedorff and Einaudi (2004); Markey et al. (2007); W.D. Sinclair, writ. commun. (2013)
0,6,0	2	0.013	42	45,235	0.5	83,846	Zeng et al. (2010)

[4] Re grade calculated from mean Re content of MoS_2 and Mo grade of deposit
[5] Contained Mo (t)
[6] Contained Re (t)

a nearly complete range in Mo-Cu contents between Mo-rich, Cu-poor porphyry Cu deposits and arc-related porphyry Mo deposits with the latter restricted to deposits that generally contain <100 ppm Cu (Ludington et al., 2009; Taylor et al., 2012).

In addition to variations in principal commodities produced from each of these subtypes, by-products tend to vary between subtypes. For example, some alkaline porphyry Cu systems are enriched in Au, Te, and PGMs, and Au-rich porphyry Cu deposits formed in island-arc settings are more likely to be enriched in PGMs than porphyry Cu deposits formed in continental margin arcs (Tarkian et al., 2003).

Hydrothermal alteration, mineralization, and metal zoning in porphyry copper and molybdenum systems

Hydrothermal alteration minerals and assemblages in porphyry Cu and Mo deposits are zoned spatially and temporally (Fig. 2; cf. Meyer and Hemley, 1967; Seedorff et al., 2005; Sinclair, 2007; Dilles, 2010; Sillitoe, 2010). Hydrothermal alteration zones have kilometer-scale vertical and lateral dimensions that show significant variation in geometry, largely as a function of rock composition, depth, and orientation of more permeable zones, such as hydrofractured rock and porphyry dikes. Alteration in porphyry Cu deposits shows a consistent zoning pattern that comprises, centrally from the bottom upward, several of sodic/sodic-calcic, potassic, chlorite-sericite (intermediate argillic), sericitic, and advanced argillic types (Fig. 2). Chloritic and propylitic alteration develop distally at shallow and deeper levels, respectively (Fig. 2). Potassic alteration tends to be more centrally located, deeper, and formed at higher temperatures and earlier relative to sericitic alteration. Advanced argillic and sericitic alteration are commonly zonally arranged around fluid-flow conduits, but advanced argillic and sericite-clay-chlorite

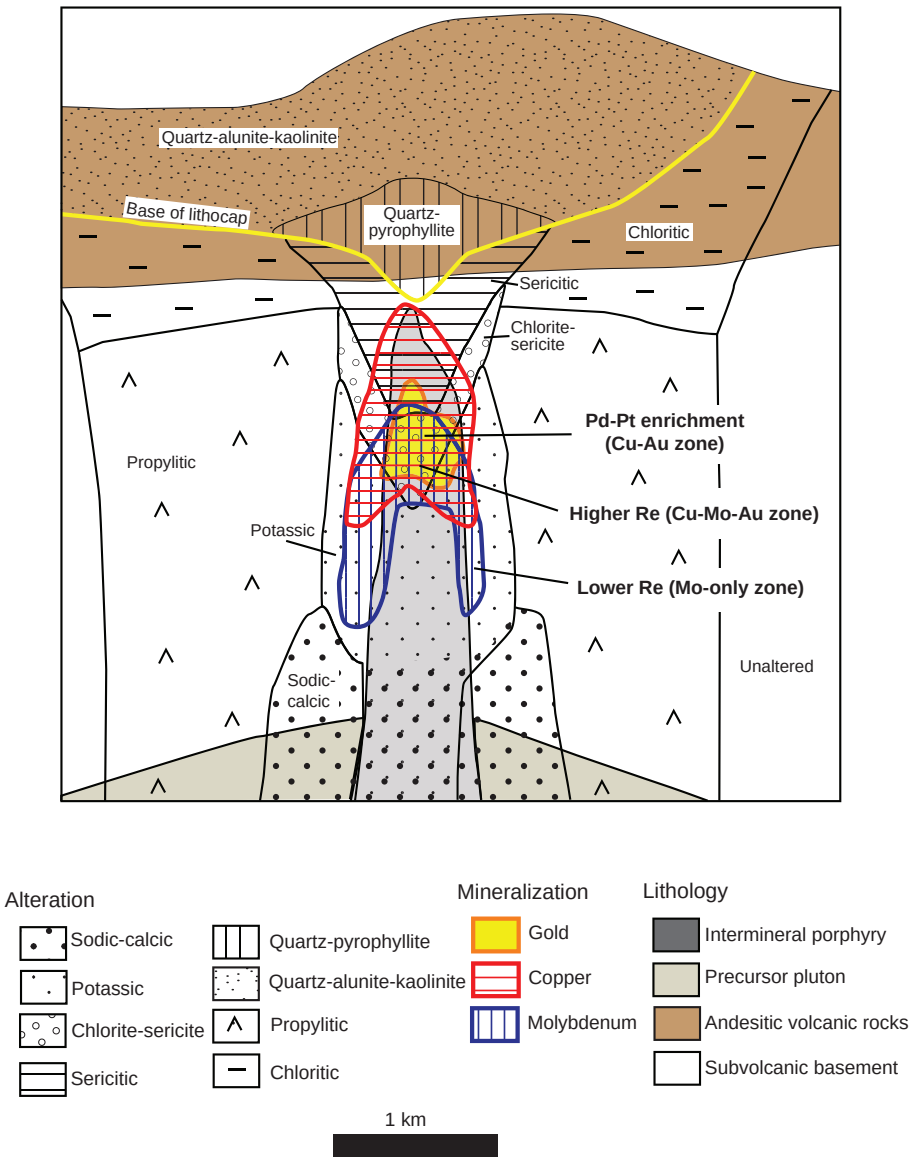

Fig. 2. Cross section showing generalized model of hydrothermal alteration and metal zoning in porphyry copper deposits. Modified from Sillitoe (2010, Figs. 6, 10).

(SCC; also called intermediate argillic) alteration assemblages may be adjacent to one another in the low-temperature and near-surface epithermal quartz-alunite environment overlying some porphyry systems. Advanced argillic alteration generally overlies potassic and sericitic alteration zones. Greisen forms sets of sheeted quartz-muscovite veins in the deep root zones of some porphyry Cu systems that are formed from silicic, hornblende-poor granites. Sodic-calcic and sodic alteration formed at deep levels and along the sides of some porphyry Cu deposits. Chloritic and propylitic alteration generally form at shallow to moderate depths, respectively, peripheral to central zones of advanced argillic, sericitic, and potassic alteration in porphyry Cu systems; propylitic zones may grade downward into deeper zones of sodic-calcic or sodic alteration. Fluorine-rich alteration minerals, such as topaz, zunyite, and/or fluorite, are common in a few porphyry Cu systems (e.g., Oyu Tolgoi, Khashgerel et al., 2008).

The mineralizing plutons in alkali-feldspar rhyolite-granite porphyry Mo systems are enriched in fluorine (commonly in excess of 1%), and a unique feature of these systems is the ubiquitous occurrence of fluorite. These high F systems produce mica with 1 to 3% F in the sericitic alteration zone and ore-bearing veins with abundant gangue fluorite (Ludington and Plumlee, 2009). These alkaline melts also produce a more intense K-feldspar-rich alteration than is found in the calc-alkaline porphyry systems. The hydrothermal fluids also can produce variable abundances of topaz and garnet. Topaz and other hydroxyl minerals are invariably fluorine enriched. Alteration is best characterized at the Urad-Henderson deposit (e.g., White and Mackenzie, 1973; White et al., 1981; Seedorff and Einaudi, 2004), although alteration described at Climax is similar (Hall et al., 1974). Major alteration zones include silicic, potassic, quartz-sericite-pyrite (QSP), argillic, and propylitic. Additional minor alteration zones denoted at Urad-Henderson include magnetite, topaz, greisen, and garnet. The silicic zone is found in the core of the system and is surrounded and overlain by the potassic zone that is associated with Mo mineralization. The QSP zone is generally found above the potassic zone. Peripheral to this is the argillic zone and a broad area of propylitic alteration extends beyond this. As with porphyry Cu deposits, the greisen zone at Urad-Henderson is located in the deep root zone. Mineral associations suggest that the garnet zone is genetically related to a late-tage Pb-Zn-Mn event of the Henderson orebody (White et al., 1981).

Metal zoning in porphyry Cu systems is systematic and characteristically mimics alteration zoning (Fig. 2; Sillitoe, 2010). Copper ± molybdenum ± gold ore is invariably associated with the potassic, sericitic, and sericite-chlorite cores of porphyry copper systems. Cu-Fe sulfides commonly are zoned outward from inner bornite-chalcopyrite to chalcopyrite-pyrite, and with increasing sulfide contents, this grades into pyrite halos, typically in the surrounding propylitic zones. Sericitic alteration is commonly pyrite dominant, implying removal of the copper precipitated in earlier potassic alteration. However, sericitic alteration may also constitute ore where appreciable copper remains with the pyrite, either in chalcopyrite or in high sulfidation-state assemblages (i.e., pyrite-bornite, pyrite-chalcocite, pyrite-covellite, pyrite-tennantite, and pyrite-enargite).

Molybdenite is the primary ore mineral in porphyry Mo deposits, and there is no metal zoning of various Mo-bearing minerals. Molybdenum mineralization is spatially associated with the potassic and sericitic alteration zones and ore may be highest grade near the contact and overlap between these two alteration zones. The Mo ore zone is generally surrounded by pyrite as the dominant sulfide in sericitic (QSP) zones. Peripheral Ag-Pb-Zn veins may form at some deposits. Tungsten and tin mineralization may also form distal to the molybdenum ore zone.

In Au-rich porphyry Cu deposits, gold is in centrally located potassic zones and generally correlates with copper content (Fig. 2). Gold is present in solid solution in bornite and chalcopyrite and as fine-grained, high-fineness elemental gold particles that probably are exsolved from bornite and chalcopyrite (Kesler at al., 2002). Gold solubility is greater in high-temperature precursors to bornite than in intermediate solid solution (the high-temperature precursor to chalcopyrite), and bornite-rich ore typically has higher gold grades than chalcopyrite-rich ore. The gold grains in some deposits contain minor amounts of PGM minerals, especially Pd tellurides (e.g., Tarkian and Stribrny, 1999).

In contrast to gold, copper and molybdenum are less strongly correlated, with spatial separation of the two metals commonly resulting from the different timing of their introduction (e.g., Bingham: Chesley and Ruiz, 1998; Redmond and Einaudi, 2010; Seo et al., 2012). In many Au-rich porphyry Cu deposits, Mo tends to be concentrated as external annuli partly overlapping the Cu-Au cores (e.g., Batu Hijau, Bajo de la Alumbrera, and Esperanza: Garwin, 2002; Ulrich and Heinrich, 2002; Proffett, 2003; Perelló et al., 2004). Other porphyry Cu-Au-Mo deposits have deep, centrally located molybdenite zones (e.g., Bingham: John, 1978; Redmond and Einaudi, 2010; Seo et al., 2012). Molybdenum-rich deposits tend to form at greater depths and are commonly associated with more felsic composition igneous rocks than Au-rich deposits (Cox and Singer, 1992; Sillitoe, 2010).

Primary commodities of porphyry copper and molybdenum deposits

Copper is the primary commodity of all porphyry Cu deposits, although molybdenum and/or gold commonly are coproducts or important by-products and silver is commonly a by-product. Copper grade reported for 422 deposits and prospects in 2008 ranged from several hundred ppm to about 1.8% and averaged 0.48% (Singer et al., 2008). The predominant copper minerals in hypogene ore are chalcopyrite, which occurs in nearly all deposits, and bornite, found in about 75% of deposits (Singer et al., 2008). Lesser amounts of hypogene copper are recovered from digenite, covellite, enargite, and tetrahedrite/tennantite. Common copper minerals in oxide ores include malachite, azurite, cuprite, tenorite, chrysocolla, native copper, copper wad, and atacamite.

Molybdenum grades are reported for about half of the porphyry copper deposits in Singer et al. (2008), range from less than 0.001 to 0.1% Mo, and average about 0.018% Mo. Molybdenite is the only molybdenum mineral of significance and is reported in about 70% of the deposits in Singer et al. (2008).

Gold grades, ranging from 0.0011 to 1.3 g/t Au and averaging 0.276 g/t Au, are reported for about 60% of the porphyry

copper deposits in the Singer et al. (2008) database. Gold is present both in solid solution in chalcopyrite and bornite and as native gold/electrum grains; native gold may be exsolved from Cu-Fe sulfides at low temperature (Kesler et al., 2002).

Molybdenum is the primary, and often only, commodity in porphyry Mo deposits. Molybdenum mineralization occurs chiefly as molybdenite, and supergene enrichment is negligible, because molybdenite is relatively stable in the supergene environment (Plumlee, 1999). Arc-related porphyry Mo deposits have grades ranging from 0.027 to 0.2% Mo with an average grade of 0.076% Mo (Taylor et al., 2012). Alkali-feldspar rhyolite-granite deposits typically have Mo grades of ≤0.1 to 0.3%, but range from 0.024 to possibly as high as 0.5% with an average of about 0.13% Mo (R. Kamilli, writ. commun., 2013).

By-products of porphyry copper and molybdenum deposits

By-products recovered from porphyry Cu deposits include Ag, As, PGMs, Re, Se, Te, W, U, and Zn, and industrial materials, including silica and sulfuric acid (Table 1; Sillitoe, 1983). By-products of alkali-feldspar rhyolite-granite Mo deposits include Sn, W, and monazite, a light rare earth element-bearing phosphate mineral.

Silver grades reported for 172 deposits in Singer et al. (2008) range from 0.095 to 21 g/t Ag and average about 2.90 g/t Ag. Silver is thought to occur mostly in solid solution in Cu-Fe sulfides, but it also is present in electrum, argentite, tetrahedrite-tennantite, sphalerite, galena, and telluride minerals (e.g., Ballantyne et al., 1998; Arif and Baker, 2004; Singer et al., 2008). Silver is primarily in Cu-Au ± Mo ore zones in the central parts of porphyry copper deposits.

Arsenic is commonly enriched in advanced argillic lithocaps of porphyry Cu deposits and in late-stage enargite-gold veins (e.g., "Main stage" veins at Butte; Meyer et al., 1968). Tennantite and enargite are the primary As minerals (Schwartz, 1995). Arsenic is primarily recovered from smelter dust and is currently viewed mostly as an environmental hazard (e.g., Schwartz, 1995).

Tungsten has many of the same properties as molybdenum. Porphyry W deposits are rare and are usually accompanied by significant concentrations of Mo. More commonly, tungsten is a minor to trace commodity within porphyry Mo deposits. Tungsten has been recovered in trace amounts from the Climax deposit, both from wolframite and huebnerite ($MnWO_4$; Wallace et al., 1968). Crosscutting relationships of molybdenite- and huebnerite-bearing veins show that tungsten mineralization is paragenetically later at Climax. Wolframite and/or scheelite also occur at porphyry Mo deposits, such as Endako, British Columbia (e.g., Selby et al., 2000), Davidson, British Columbia (e.g. Atkinson, 1995), Pine Nut, Nevada, and elsewhere.

Singer et al. (2008) reported scheelite in 51 of 691 porphyry Cu deposits, although in some of these deposits it is probably present in adjacent skarns. Scheelite was recovered from mine tailings at a reported grade of 0.02 to 0.04% tungsten from the Inguaran copper breccia pipe deposit, Mexico (Osoria et al., 1991), and the Sunrise copper breccia pipe, Washington, has a reported grade of 0.062% WO_3 (Lasmanis, 1995). Both deposits are inferred to be part of porphyry copper systems.

Small amounts of uranium were recovered from several porphyry Cu deposits in the 1970s and 1980s. From 1978 to 1989 at Bingham, uranium was extracted at a maximum rate of about 50 t U/yr from Cu leach liquor containing 8 to 12 ppm U (Dahlkamp, 2009). No uranium mineral was identified, but Dahlkamp suggested that uranium may be present as uraninite or uranothorianite. Uranium averages about 5 to 7 ppm in Cu–Mo-Au ore at Bingham (Austen and Ballantyne, 2010). At Twin Buttes, Arizona, uranium was recovered from 1980 to 1985 at a rate of up to 100 t U/yr from Cu ore (Dahlkamp, 2009). At the Mina Sur exotic Cu deposit, south of the giant Chuquicamata deposit, uranium was recovered as a by-product of Cu production in 1982 (Nanjari, 2009). The potential for recovering uranium from the Climax porphyry Mo deposit has been investigated (D'Arcy, 1950; Desborough and Sharp, 1978).

Additional minor constituents that have been recovered from the Climax mine include cassiterite (SnO_2) and monazite (LREE-bearing phosphate). Cassiterite is associated with quartz-sericite-pyrite veinlets that are more abundant within tungsten zones, suggesting that tin and tungsten may be paragenetically related (Wallace et al., 1968). The monazite that has been recovered may not be directly related to the Climax hydrothermal system, however, and instead may be derived from the Precambrian metamorphic and igneous country rocks and/or the alkaline porphyries.

Beryllium in the form of beryl [$Be_3Al_2(Si_6O_{18}$] and helvite [$Mn(Be_3Si_3O_{12})S$] is present as a trace constituent in some porphyry Mo deposits, including deposits in New Mexico (McLemore, 2010). At the Logtung porphyry W-Mo deposit in British Columbia, beryl crystals can reach to lengths greater than 1 cm and are abundant enough to be considered a source of beryllium (Mihalynuk and Heaman, 2002). Minor amounts of beryl also are present at Endako. At Questa, New Mexico, quartz-beryl veins crosscut the stockwork molybdenite veins and lack molybdenum mineralization; accessory minerals within these veins include chalcopyrite, fluorite, carbonates, and scheelite and the veins do not have associated wall-rock alteration (Klemm et al., 2008).

Bismuth is enriched in some porphyry Mo and Cu deposits. In addition to trace Cu and W minerals, the Endako deposit also contains bismuthinite (Bi_2S_3). However, bismuth is treated as an impurity and is not recovered (Marek, 2011). Other arc-related porphyry Mo deposits in British Columbia, such as Boss Mountain and Davidson, and other deposits around the world, also have reported bismuthinite. Bismuth is considered a secondary commodity at the Koktenkol W-Mo porphyry deposit in Kazakhstan. The most important bismuth minerals at Koktenkol are in the aikinite-bismuthinite series and native bismuth, and a decision to build a factory to produce rare metals was made in 1986 but was later abandoned due to the collapse of the Soviet Union (Mazurov, 1996). Bismuthinite is an accessory mineral associated with W and Mo mineralization at the Logtung, Yukon porphyry W-Mo deposit (Noble et al., 1995).

Critical element by-products of porphyry copper and molybdenum deposits

Rhenium, platinum group metals, selenium, and tellurium are the other critical elements most commonly enriched in or recovered from porphyry Cu deposits (Table 1). Although

these elements generally are present in only trace abundances in Cu-Mo-Au ore zones in porphyry Cu deposits, the large volume of ore processed makes their recovery economically feasible in some instances. Other critical elements, notably rare earth elements and gallium, are locally enriched in parts of porphyry Cu deposits (e.g., advanced argillic alteration in the Oyu Tolgoi deposit, Mongolia; Khashgerel et al., 2008), but they have not been found in sufficient concentrations to make their recovery economically feasible. Additionally, porphyry Mo deposits have produced or may potentially produce Nb and In. Although not necessarily deemed as "critical elements," Cs, F, Li, Rb, Sn, and Ta also may have elevated concentrations within some alkali-feldspar rhyolite-granite porphyry Mo deposits.

Rhenium

Rhenium is the most important critical element by-product of porphyry deposits. Porphyry Cu deposits are the world's largest source of rhenium, accounting for about 80% of the annual mine production (Polyak, 2013). Global mine production of Re in 2011 was an estimated 54,000 kg of which about 26,000 kg was produced from porphyry Cu mines in Chile (Polyak, 2013). Large porphyry Cu deposits formed in continental arcs dominate Re resources contained in porphyry deposits (Table 2, Fig. 3).

Rhenium is consumed mostly in high-temperature super alloys (an estimated 83% of 2011 worldwide consumption), which are used primarily in construction of single-crystal turbine blades in jet aircraft engines, and in Pt-Re catalysts (10%) that are used to produce high-octane, lead-free gasoline (Polyak, 2013). Rhenium is one of the most widely dispersed elements in the crust, with an estimated average abundance of 0.4 ppb in the continental crust (Taylor and McLennan, 1995; estimates range from 0.18–2 ppb; Rudnick and Gao, 2003; Sun et al., 2003). Magmatic-hydrothermal processes can concentrate rhenium by a factor of 100 to >1,000 in Cu ± Mo ± Au ores of porphyry Cu deposits (Table 2). Rhenium is recovered from molybdenite concentrates that are separated from copper-(iron) sulfides by flotation methods. During roasting of the molybdenite concentrates to produce molybdenum oxide, rhenium is oxidized to Re_2O_7 and passes up the flue stack with sulfur gases. When the flue dusts and gases are scrubbed, rhenium is dissolved in the resulting sulfuric acid and is eventually precipitated out as ammonium perrhenate (NH_4ReO_4; Sutulov, 1974; Nadler, 1997).

Publically available data about rhenium resources are limited. Of more than 225 porphyry Cu deposits with published Mo grades and tonnages as of 2008 (Singer et al., 2008), Re concentration data are available for only about 80 deposits, several of which are represented by a single rhenium analysis

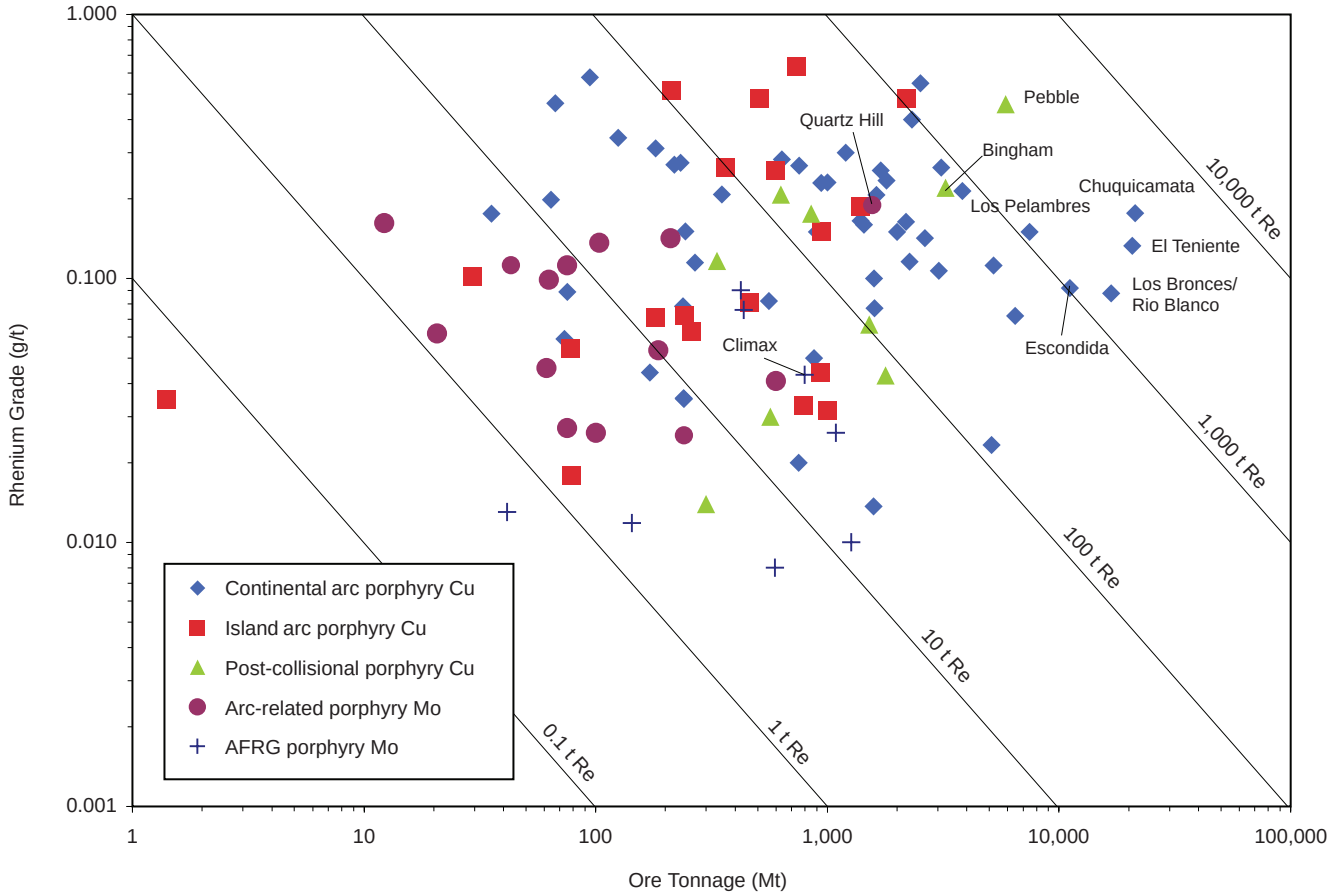

Fig. 3. Rhenium grade vs. deposit tonnage for porphyry Cu and porphyry Mo deposits. Porphyry Cu deposits divided by tectonic setting and porphyry Mo deposits divided into alkali-feldspar rhyolite-granite- and arc-related types. Data listed in Table 2.

(Table 2; John et al., in press). There are similarly few rhenium data for porphyry Mo deposits. The available rhenium analytical data are a mixture of analyses of (1) small molybdenite separates (e.g., Giles and Schilling, 1972; Sinclair et al., 2009; Millensifer et al., 2013), (2) smaller molybdenite separates used in Re-Os dating studies (e.g., McCandless and Ruiz, 1993; Barra et al., 2013), and less commonly, (3) bulk molybdenite mill concentrates (mostly from Sutulov, 1974, and Nadler, 1997), and (4) analyses of drill core (e.g., Northisle Copper and Gold Inc., 2012). The molybdenite separates and mill concentrates are subject to impurities, and some of the variation in rhenium content within deposits may be the result of variable purity of these molybdenite separates. Electron microprobe analyses of the rhenium contents of molybdenites are available for some deposits (e.g., Newberry, 1979a; McCandless et al., 1993), but these analyses have relatively high detection limits and low precision and were not included in our data compilation.

Calculated rhenium resources in porphyry Cu and porphyry Mo deposits are based on the average concentration of Re in molybdenite, the average Mo grade for the entire deposit, and the total tonnage of the deposit. For some deposits, there are multiple types of Re analyses, which in many cases have significantly different values. For these deposits, a "preferred" Re content of molybdenite was selected based on the types of analyses and when the analyses were made, and these preferred values were used in the resource calculation (see Table 2). Molybdenum grades and tonnages for porphyry Cu deposits are mostly from Singer et al. (2008) and subject to the rules specified in their data compilation. For example, average Mo grades and the associated tonnages are based on the total production, reserves, and resources at the lowest possible cutoff grade, and all mineralized rock and alteration within 2 km are combined into one deposit. Tonnages therefore are premining resources. Because many porphyry Cu deposits have been mined for decades or longer (for example, the Bingham Canyon deposit has been mined since 1906), remaining tonnages and rhenium resources for these deposits are smaller than indicated in Table 2.

Rhenium in porphyry deposits is contained primarily as ReS_2 in solid solution in molybdenite (Fleischer, 1959) at concentrations ranging from <10 ppm to several wt %. In such a paragenesis, rhenium is the quintessential "byproduct of a byproduct" of porphyry deposits (Lifton, 2007). Maximum reported Re concentrations in molybdenite from porphyry systems range up to 4.2% in the Kirki prospect and 4.7% in the Pagoni Rachi prospect, both in northern Greece (Melfos et al., 2001; Voudouris et al., 2009), although they are seldom >1 wt % in porphyry deposits (Table 2). Rhenium contents of other sulfide minerals common in porphyry copper deposits, including chalcopyrite, bornite, pyrite, and sphalerite, are <1 to 100 ppb, indicating that the vast majority of rhenium is contained in molybdenite (Freydier et al., 1997; Ruiz and Mathur, 1999; Mathur et al., 2000; Barra et al., 2003).

Calculated rhenium grades of Cu-Mo-(Au) ores in porphyry copper deposits range from about 0.01 to 0.6 g/t Re, although most are between 0.03 and 0.4 g/t Re (Table 2; Sinclair et al., 2009; Millensifer et al., 2013; John et al., in press). Despite the low average Re grades of porphyry Cu deposits, the total Re contents of these deposits can be considerable due to their large size (Table 2, Figs. 3, 4). For example, the giant Chuquicamata deposit contained an estimated 3,750 t Re at an average grade of about 0.18 g/t Re and measured and indicated resources of the giant unmined Pebble deposit are about 2,650 t Re at an average grade of about 0.45 g/t Re. The rhenium resources of these deposits are about 70 and 45 times, respectively, the world's current annual production. Most porphyry deposits with estimated resources of >500 t Re are porphyry Cu deposits that formed in continental margin arcs, mostly in the Andes in South America (Fig. 3); two notable exceptions are Pebble and Bingham, which formed in postcontractional tectonic settings on continental crust (Richards, 2009; Goldfarb et al., 2013). In contrast, the Re contents of molybdenites in porphyry Mo deposits generally are much lower (mostly ≤100 ppm, Fig. 5, Table 2), and despite their generally higher Mo grades, Re resources in these deposits are small relative to large porphyry Cu deposits (Figs. 3, 4), and rhenium is not currently recovered from porphyry Mo deposits.

Reported Re contents of molybdenites vary by more than an order of magnitude within some porphyry Cu deposits (Table 2). For example, Giles and Schilling (1972) reported that Re contents of molybdenites in the Bingham deposit range from 130 to 2,000 ppm with a mean of 360 ppm. They suggested that the Re content of molybdenite decreases inward and downward in the mineralized intrusive complex, and that there is a steady decrease in Re content with increasing depth into the Mo-rich core of the system, which underlies the Cu-rich zone. Giles and Schilling (1972) also suggested that there is an inverse relationship between the Re content of molybdenite and the bulk Mo grade with high Re molybdenites in Cu-rich zones. More recent studies of Bingham confirm these general relationships but also show that Mo mineralization postdates most Cu-Au mineralization (e.g., Redmond and Einaudi, 2010; Landtwing et al., 2010; Austen and Ballantyne, 2010; Redmond and Einaudi, 2010; Seo et al., 2012). Austen and Ballantyne (2010) showed that higher Re grades (avg 0.55 g/t) and calculated Re contents of molybdenite (avg about 310 ppm Re) are in Cu-Mo-Au ores (>0.35% Cu, >0.05 % Mo) in the center of the deposit, whereas the Re grade (avg 0.19 g/t Re) and calculated Re in molybdenite (about 120 ppm Re) are significantly lower in deeper, Mo-only ores (>0.05% Mo, <0.35% Cu) and in the "barren" core (<0.05% Mo, <0.35% Cu).

Similar to Bingham, Aminzadeh et al. (2011) reported that Re contents of molybdenite samples range from 11 to 517 ppm and appear to be a function of depth and molybdenite paragenesis in the Sar Cheshmeh deposit, Iran. More deeply formed molybdenite in quartz-rich veins has lower Re contents than molybdenite in quartz-poor veins associated with intense sericitic alteration in shallower parts of the deposit. Aminzadeh et al. (2011) suggested that the higher Re contents of molybdenites in the shallow, sericitic alteration formed at lower temperatures and from more acidic (lower pH) fluids than the molybdenites in the deeper, higher temperature quartz-molybdenite veins. However, the Re contents of five molybdenite mill concentrates also reported by Aminzadeh et al. (2011) are relatively homogeneous (550–631 ppm) and average 597 ppm, substantially more than the

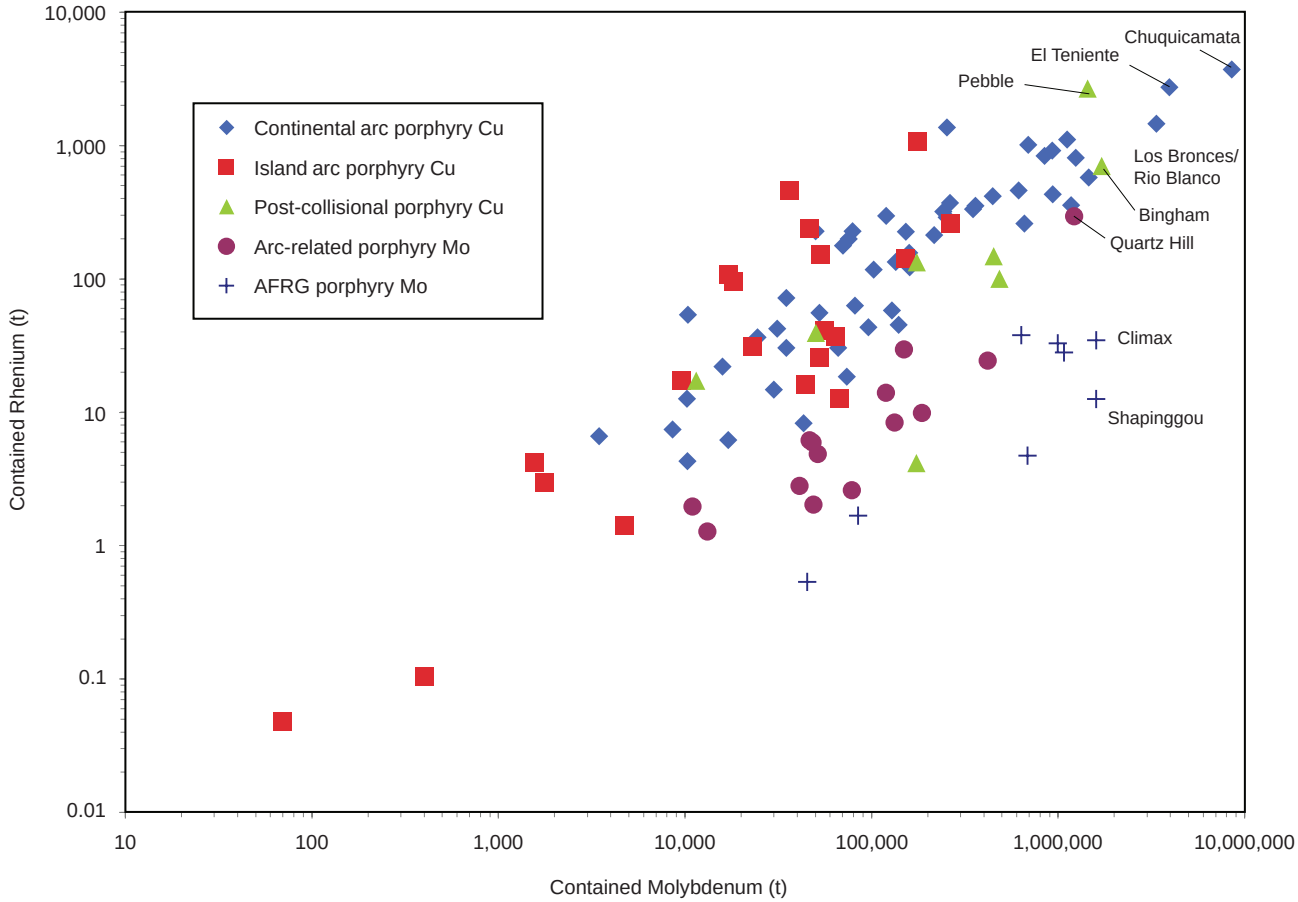

Fig. 4. Contained Re vs. contained Mo for porphyry Cu and porphyry Mo deposits. Porphyry Cu deposits divided by tectonic setting and porphyry Mo deposits divided into alkali-feldspar rhyolite-granite- and arc-related types. Data listed in Table 2.

highest reported value for an individual molybdenite sample (517 ppm), thereby raising questions about their reported Re zoning patterns.

Molybdenite occurs as two polytypes with rhombohedral (3R) and hexagonal (2H) structures. The 2H polytype is the stable form and is much more common in naturally occurring samples (Newberry, 1979a, b). Newberry (1979a) found that most 3R-rich molybdenites in porphyry and skarn deposits are associated with high levels of Re and concluded that the natural formation of 3R molybdenite results from nonequilibrium growth processes, which in general are impurity related. He suggested that early-formed 3R molybdenite may recrystallize to the 2H polytype with the concomitant loss of Re, which, for example, may happen during late-stage sericitic alteration in porphyry systems. Newberry (1979b) also suggested that Re contents and polytypes of molybdenites change through time during the evolution of porphyry systems: early Re-poor, 2H molybdenite in "A" veins gives way to 3R- and Re-rich molybdenite in "B" veins, and finally to "D" veins containing 2H molybdenites with variable Re contents. However, recent analyses of molybdenites from the Pagoni Rachi porphyry prospect in northern Greece that have some of the highest Re contents ever reported in nature show that they crystallized as the 2H polytype, therefore suggesting that Re concentration does not correlate with a specific polytype (Voudouris et al., 2009).

In summary, available data for the Re contents of molybdenites in porphyry systems suggest that there are significant variations in the Re contents of molybdenites (1) between different types and subtypes of porphyry deposits (i.e., between porphyry Cu and porphyry Mo deposits), and (2) within individual deposits (Table 2). In particular, Re contents of molybdenites in all types of porphyry Cu-(Mo-Au) deposits generally are much greater than Re contents of molybdenites in alkali-feldspar rhyolite-granite porphyry Mo deposits, molybdenites associated with sericitic alteration tend to have greater Re contents than those associated with potassic alteration, and molybdenites precipitated at lower temperatures or at higher oxygen fugacities tend to have greater Re contents. There are a myriad of possible causes of these variations, including simple mass-balance relationships; variable magma sources (e.g., crustal versus mantle); variations in magma crystallization histories, including fractionation and wall-rock assimilation; variations in the physical (pressure, temperature) and chemical (e.g., f_{S_2}, f_{O_2}, pH, Cl, and F activities) properties during Re and Mo transport and deposition; and fluid phase separation and possible decoupling of Mo and Re during hydrothermal processes (e.g., Giles and Schilling, 1972; Newberry, 1979b; Stein et al., 2001; Xiong and Wood, 2001, 2002; Berzina et al., 2005; Klemm et al., 2008; Voudouris et al., 2009; Seo et al., 2012; Barra et al., 2013). In

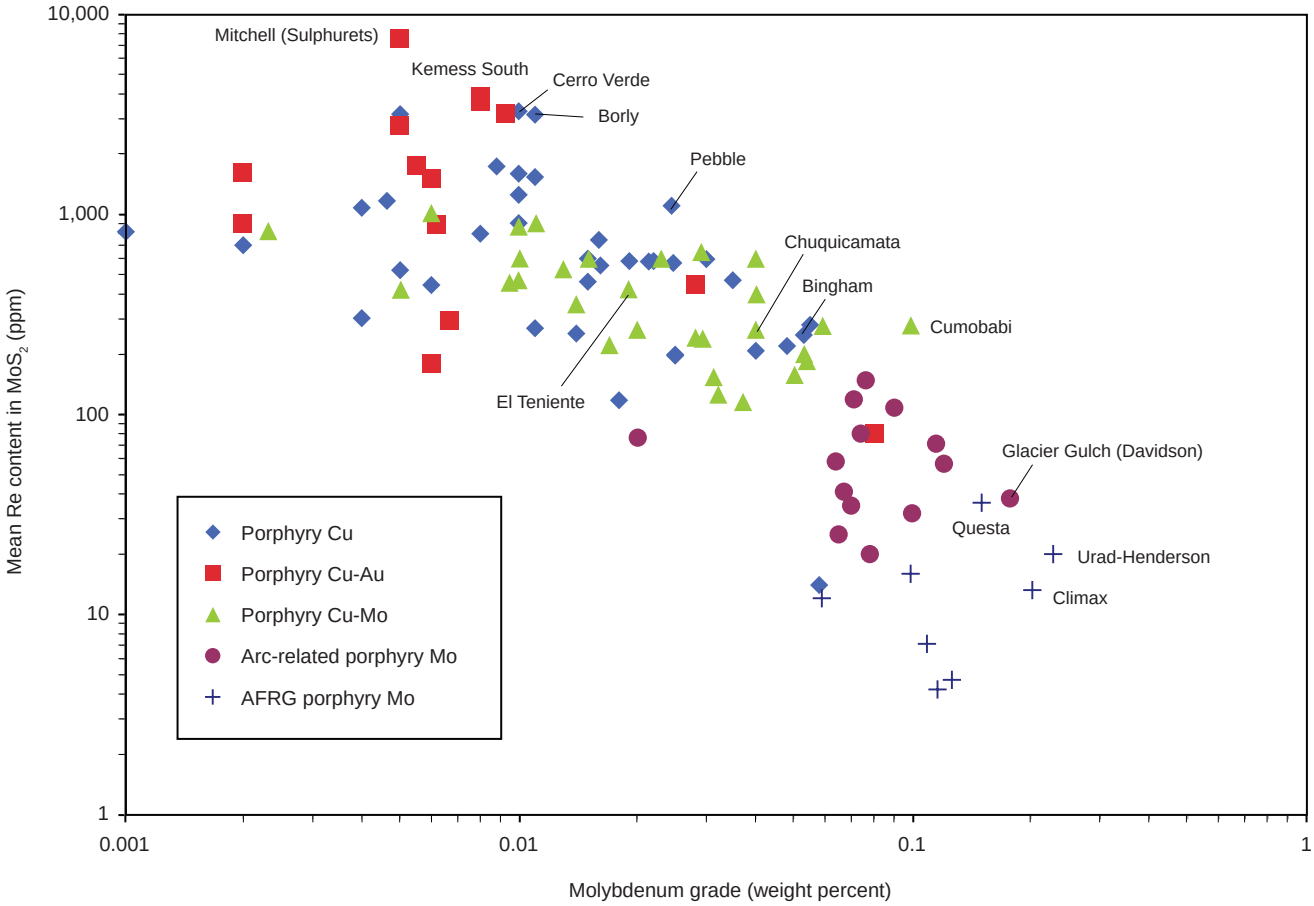

Fig. 5. Mean Re content of molybdenite in porphyry Cu and Mo deposits. Porphyry Cu deposits separated in subtypes using criteria of Cox and Singer (1992). Data listed in Table 2.

the following paragraphs, we briefly discuss several of these potential causes for the observed variations in Re contents of molybdenites in porphyry systems.

Several authors suggest that variation of Re contents of molybdenites in different deposit types and subtypes is a simple "mass-balance phenomenon" (e.g., Stein et al., 2001). In this model, because essentially all Re is contained in molybdenite, less abundant molybdenite in porphyry Cu deposits has higher Re concentrations than the more abundant but Re-poor molybdenite in porphyry Mo deposits (Giles and Schilling, 1972; Newberry, 1979b; Stein et al., 2001; Sinclair et al., 2009). This model seemingly predicts that Re grades of porphyry deposits should be relatively constant, and Giles and Schilling (1972) noted that average Re grades of the Ely, Bingham, and Climax deposits are approximately equal (0.14–0.16 g/t) despite large differences in average Mo grade of these deposits (0.008, 0.04, and 0.4%, respectively). However, more recent grade-tonnage data for these deposits suggest that Re grades are significantly higher for Bingham and Ely than Climax (Table 2), and the overall greater than 60-fold range of Re grades in porphyry Cu and Mo deposits (Figs. 3, 4) suggests that this model is too simple.

Rhenium contents of magmas derived from mantle sources may be greater than those derived from crustal sources. Rhenium is highly siderophilic and is a moderately incompatible element during mantle melting events. Therefore, it is considered to be relatively depleted within the upper mantle (Hauri and Hart, 1997). However, the Re content of molybdenite in porphyry deposits has been suggested to be higher within mantle-derived magma sources than in deposits with crustal-derived melt sources (Mao et al., 1999; Stein et al., 2001; Stein, 2006). Due to the high volatility of inorganic rhenium compounds, many subaerial volcanic rocks are depleted in rhenium by post- and syn-eruptive degassing (e.g., Lassiter, 2003). The behavior of rhenium during subduction and mantle metasomatism remains controversial (e.g., Chesley et al., 2002); however, there is evidence that the mantle wedge in arc environments is actually enriched in rhenium by addition of rhenium from the subducted slab (Sun et al., 2003, 2004). Sun et al. (2004) confirmed that Re is mobile in subduction zone fluids and that arc magmas are enriched in Re from fluids released by dehydration of subducted slabs. Fumarolic gases in the Kurile-Kamchatka volcanic arc are significantly enriched in rhenium, which has been attributed to addition of rhenium transported by fluids derived from subducted sediments into the mantle wedge (Tessalina et al., 2008). These studies suggest that undegassed arc-related, mantle-derived magmas will be enriched in rhenium compared to the depleted asthenosphere and average continental crust, and supports proposals of the importance of melt source on rhenium content.

Similar subduction zone processes lead to metasomatism of the subcontinental lithospheric mantle. Comparison of ultramafic xenoliths in Tanzania showed that metasomatized samples have elevated Re (ppb vs. ppt level), K_2O, Ba, and Rb contents relative to samples that were not metasomatized (Burton et al., 2000). Therefore, porphyry deposits in which metals and/or magma have metasomatized lithospheric mantle sources would be expected to contain elevated Re contents. Pilet et al. (2008) and Richards (2009) suggested that partial melting of metasomatized subcontinental lithospheric mantle could generate alkaline magmas in postsubduction continental settings. Pettke et al. (2010) suggested that giant porphyry deposits in the western United States, including both porphyry Cu (Bingham and Butte) and alkali-feldspar rhyolite granite porphyry Mo (Climax and Urad-Henderson) deposits, are derived from metasomatized subcontinental mantle lithosphere. This model could explain elevated Re contents in some postsubduction porphyry Cu deposits (e.g., Bingham), but it is in contrast to the low Re contents characteristic of alkali-feldspar rhyolite granite porphyry Mo deposits. This observation, along with complications due to possible contamination of magmas by Re-rich crustal reservoirs of reduced sediments (e.g. Crusius et al., 1996), render this model for Re enrichment too simple.

Variations in composition and/or oxidation state of magmas that are inferred to be genetically related to porphyry deposits might cause the variable behavior of rhenium. Ishihara (1988) noted that molybdenites in oxidized, magnetite-series granitic rocks and related copper deposits had higher Re contents than molybdenites related to more reduced ilmenite-series granitic rocks in Japan. This observation is consistent with the generally higher oxidation state of magmatic-hydrothermal systems related to porphyry Cu systems relative to those forming porphyry Mo systems (e.g., Einaudi et al., 2003; Seedorff et al., 2005). However, because igneous rocks related to porphyry Mo systems span a large range of compositions (although mostly felsic) that overlap compositions of porphyry Cu-related intrusive rocks (e.g., Seedorff et al., 2005; Sinclair, 2007; Taylor et al., 2012), it is unlikely that magma composition or source alone plays the controlling role in Re behavior.

Alternatively, the chemical and physical properties of fluids transporting Re, Mo, and other metals may be more important factors in determining the variable Re contents of molybdenites. Because Re and Mo are highly volatile elements, there can be significant transport of these elements by magmatic vapors, and studies of high-temperature fumaroles suggest that Mo and Re may be transported as different types of complexes. Bernard et al. (1990) showed that Mo is predominantly transported as molybdic acid (H_2MoO_4) in high-temperature (>500°C) magmatic gases, and that oxychlorides are present only at lower temperatures (<400°C) or at high HCl fugacities (>10 mol %). They speculated that Re also was likely transported as rhenic acid (H_2ReO_4). However, more recent studies of fumaroles in the Kurile-Kamchatka volcanic arc indicate that Re is transported as oxide and oxychloride complexes and is precipitated at high temperatures (400°–850°C) as sulfide (rheniite and Re-rich molybdenite) and oxide phases (Tessalina et al., 2008; Yudovskaya et al., 2008). This suggests that Mo and Re could be differentially partitioned into, and transported by, magmatic vapor depending on the oxidation state and HCl activity.

Coexisting low-density vapor and high-density brine phases have long been known in porphyry systems (e.g., Roedder, 1971). As first proposed by Henley and McNabb (1978) and supported by recent studies of fluid inclusions by LA-ICP-MS techniques, low-density vapors likely transport and deposit much of Cu and Au in many porphyry Cu deposits (e.g., Heinrich et al., 1999; Ulrich and Heinrich, 2002; Williams-Jones and Heinrich, 2005; Landtwing et al., 2010). Recent experimental studies indicate that there also is significant Mo solubility in high-temperature water vapor (Rempel et al., 2006, 2008, 2009), and LA-ICP-MS fluid inclusion studies of Mo mineralization in the Bingham porphyry Cu deposit suggest that more than 70% of the Mo was transported and deposited by a low-density, aqueous vapor phase (Seo et al., 2012).

In porphyry Cu deposits, Cu-(Au) mineralization commonly predates most Mo mineralization (e.g., Gustafson and Hunt, 1975; Soregaroli, 1975; Ulrich and Heinrich, 2002; Rusk et al., 2008). For example, at Bingham, early Cu-Au mineralization is cut by younger porphyry dikes, which are in turn cut by quartz-molybdenite veins, and high-grade Mo mineralization is generally deeper and spatially distinct from high-grade Cu-Au mineralization (Babcock et al., 1995; Chesley and Ruiz, 1998; Landtwing et al., 2010; Redmond and Einaudi, 2010; Seo et al., 2012). Similarly, at Bajo de la Alumbrera, Mo mineralization is late, peripheral to, and not correlated with, Cu-Au mineralization (Ulrich and Heinrich, 2002), and at El Teniente, most Mo mineralization is relatively late and associated with sericitic alteration, whereas Cu mineralization is associated with potassic alteration (Klemm et al., 2007).

At Bingham, although Cu-Au and Mo mineralization are separate events, both formed from intermediate density and salinity fluids that initially had similar Cu, Mo, and S contents and underwent decompressional phase separation into low-density vapor and brine phases (Landtwing et al., 2010; Seo et al., 2012). Seo et al. (2012) suggested that early Cu-stage fluids had a relatively neutral pH and were oxidized, thereby resulting in precipitation of Cu-Fe sulfides, while Mo remained in solution and was lost from the system. During subsequent Mo mineralization, fluids were slightly more acidic and reduced, which resulted in molybdenite as the first sulfide phase to precipitate. Both Cu-Au and Mo stages were dominated by vapor phases with vapor/brine mass values of about 9. Seo et al. (2012) suggested that slight variations in pH and/or redox state may be the ultimate cause for the temporal separation of Cu-(Au) and Mo. Because Mo was predominantly precipitated from a vapor phase, this suggests that significant Re was also present in the vapor phase. The apparently more Re rich compositions of molybdenites in the more shallowly formed Cu-Mo-Au ores (Giles and Schilling, 1972; Austen and Ballantyne, 2010) may be consistent with the high volatility of Re and Mo and progressive degassing of Mo and Re from the magma that formed the later Mo mineralization.

In contrast to Bingham, molybdenite in the Questa porphyry Mo deposit has low Re contents (Table 2), and there are very low overall Cu and Au contents in the deposit. Klemm et al. (2008) showed that Mo ore at Questa was deposited from high-salinity brines formed by extensive boiling. At Questa, initial ore fluids were moderate density and salinity with high Cu contents (>>Mo) similar to parental ore fluids at Bingham. Decompression from near-lithostatic to near-hydrostatic

pressures led to fluid phase separation and boiling off of most of the Cu-enriched vapor, thereby forming Mo-enriched but Cu-, and probably S-, poor brines (Klemm et al., 2008). Klemm et al. (2008) suggested that similar Mo-rich, Cu-Au-poor porphyry Mo deposits in the western United States (e.g., Climax and Urad-Henderson) may result in part from selective removal of Cu (and probably Au and S) into an escaping vapor phase. Rhenium also may have been partitioned into the vapor and lost from these systems, thereby resulting in the Re-poor molybdenite and overall low rhenium content characteristic of these deposits.

In contrast to multiple fluid phases at high temperatures, Xiong and Wood (2002) suggested that the observed greater Re contents of molybdenites in relatively low temperature, oxidized, low pH, sericitic alteration in some porphyry Cu deposits may be partly explained by Re solubility and mobility in aqueous fluids. Based on their experiments under supercritical conditions at 400° to 500°C applicable to porphyry deposits, they suggest that (1) Re is much more soluble as chloride complexes ($ReCl_4^o$ and $ReCl_3^-$) than as sulfide (ReS_2) or oxide (ReO_2) complexes, (2) oxidizing environments have greater capacity for transporting Re than reducing environments, and (3) ReS_2 has slight prograde solubility in the 400° to 500°C temperature range. These factors favor transport and deposition of rhenium in lower temperature, oxidized environments, and they suggest that mixing of an oxidized fluid containing Re with a reduced, sulfur-bearing fluid is an effective mechanism for depositing ReS_2. Berzina et al. (2005) similarly suggested that the Re content of molybdenites formed by reduced, acidic fluids related to sericitic alteration are greater than those derived from more oxidized, alkaline fluids related to potassic alteration in several deposits in Siberia and Mongolia.

In summary, the potential causes of the variation in Re content of molybdenites in porphyry deposits are numerous and complex, and this variation is likely the result of a combination of processes that may change from deposit to deposit. These processes range from variations in source and composition of parental magmas to physiochemical changes in the shallow hydrothermal environment. Although molybdenites in porphyry Cu deposits from which rhenium is recovered typically have Re contents ranging from about 200 to 3,000 ppm that are significantly enriched relative to other major deposit types, typical Re grades of these deposits are lower than some other major deposit types (e.g., strata-bound Cu deposits in Poland and Kazakhstan: Sinclair et al., 2009; Millensifer et al., 2013; John et al., in press). Most importantly to the economics and global supply of rhenium, these porphyry deposits are large to giant deposits with 10s of millions of tons of ore mined per year that contain sufficient molybdenite to allow economic recovery of Mo, as well as the Re incorporated into molybdenite.

Platinum-group metals (palladium and platinum)

Platinum-group metals (PGMs) are another critical commodity by-product of porphyry Cu deposits that have generated significant exploration interest in recent years, because of their high value and enrichment in some porphyry deposits. Small amounts of PGMs, mostly palladium, are recovered from refinery anode slimes in some deposits (e.g., Bingham: Phillips and Krahulec, 2006). Economou-Eliopoulos (2005) provided an extensive overview of PGMs in porphyry systems.

Platinum-group metals are a group of six elements, platinum (Pt), palladium (Pd), rhodium (Rh), iridium (Ir), osmium (Os), and ruthenium (Ru), which are among the rarest elements in the continental crust. Average continental crust abundances are estimated as Pt, 1.5 ppb; Pd, 1.5 ppb; Rh, no estimate; Os, 0.041 ppb; Ir, 0.037 ppb; and Ru, 0.56 ppb (Rudnick and Gao, 2003). Only platinum and palladium are concentrated in sufficient abundances in porphyry deposits to allow their recovery. Platinum and palladium are used primarily as catalysts to decrease harmful emissions from both light-duty (Pd) and heavy-duty (Pt) vehicles (71 and 39% of the world consumption of Pd and Pt, respectively, in 2011), in the jewelry industry (31% Pt and 6% Pd), in the electronics (16% Pd) and glass (7% Pt) industries, in dentistry (7% Pd), in a variety of other industries, including chemical, electrical, medical and biomedical, and as an investment (Loferski, 2013).

Concentrations of Pd and Pt in 37 porphyry Cu and in three porphyry Mo deposits are summarized in Table 3. The concentrations of PGMs in porphyry Cu ores are relatively low (generally ≤50 ppb Pd + Pt), and most published analyses are reported as the Pd and Pt contents of sulfide or flotation concentrate samples (e.g., Tarkian and Stribrny, 1999) or of exceptionally Cu rich ore samples (e.g., Thompson et al., 2001). Therefore, most estimates of Pt and Pd contents of ores and total Pd + Pt resources listed in Table 3 and plotted in Figure 6 are calculated from their concentrations in concentrate samples that are normalized to the average Cu grade of the deposit (Table 3; Economou-Eliopoulos, 2005). As indicated in Table 3, a few estimates of Pt and Pd resources are calculated from analyses of high-grade ore samples normalized to the average Cu grade of the deposit or from the Pd + Pt contents in molybdenite concentrates normalized to the average Mo grade of the deposit.

Calculated average Pd + Pt concentrations of ores range from <0.1 to about 92 ppb in porphyry Cu deposits and ≤1 ppb in three porphyry Mo deposits (Table 3). Skouriés has the highest reported average Pd + Pt content (Economou-Eliopoulos, 2005). Pd/Pt varies widely from <1 to about 40, although most deposits have values between 2 and 10 and about a quarter of the deposits report Pd but not Pt concentrations (Table 3).

Notable examples of PGM-enriched porphyry Cu systems include the Mount Milligan, Mount Polley, Galore Creek, and Afton-Ajax systems in British Columbia (Mutschler et al., 1985; Thompson et al., 2001; Sinclair et al., 2009; LeFort et al., 2011); Skouriés, Greece (Eliopoulos and Economou-Eliopoulos, 1991; Economou-Eliopoulos and Eliopoulos, 2000); Elatsite, Bulgaria (Tarkian et al., 2003); Boschekul, Kazakhstan (Tarkian and Stribrny, 1999); Kalmakyr, Uzbekistan (Pasava et al., 2010); Mamut, Malaysia (Tarkian and Stribrny, 1999); Ok Tedi, Papua New Guinea (Tarkian and Stribrny, 1999); Santo Tomas II, Philippines (Tarkian and Koopmann, 1995); Allard, Colorado (Mutschler et al., 1985); and Pebble, Alaska (Northern Dynasty Minerals, 2011; Gregory et al., 2013). Intrusive rocks related to PGE-enriched porphyry systems have compositions ranging from alkaline (British Columbia deposits and Allard prospect), to subalkaline (Pebble, Skouriés), and

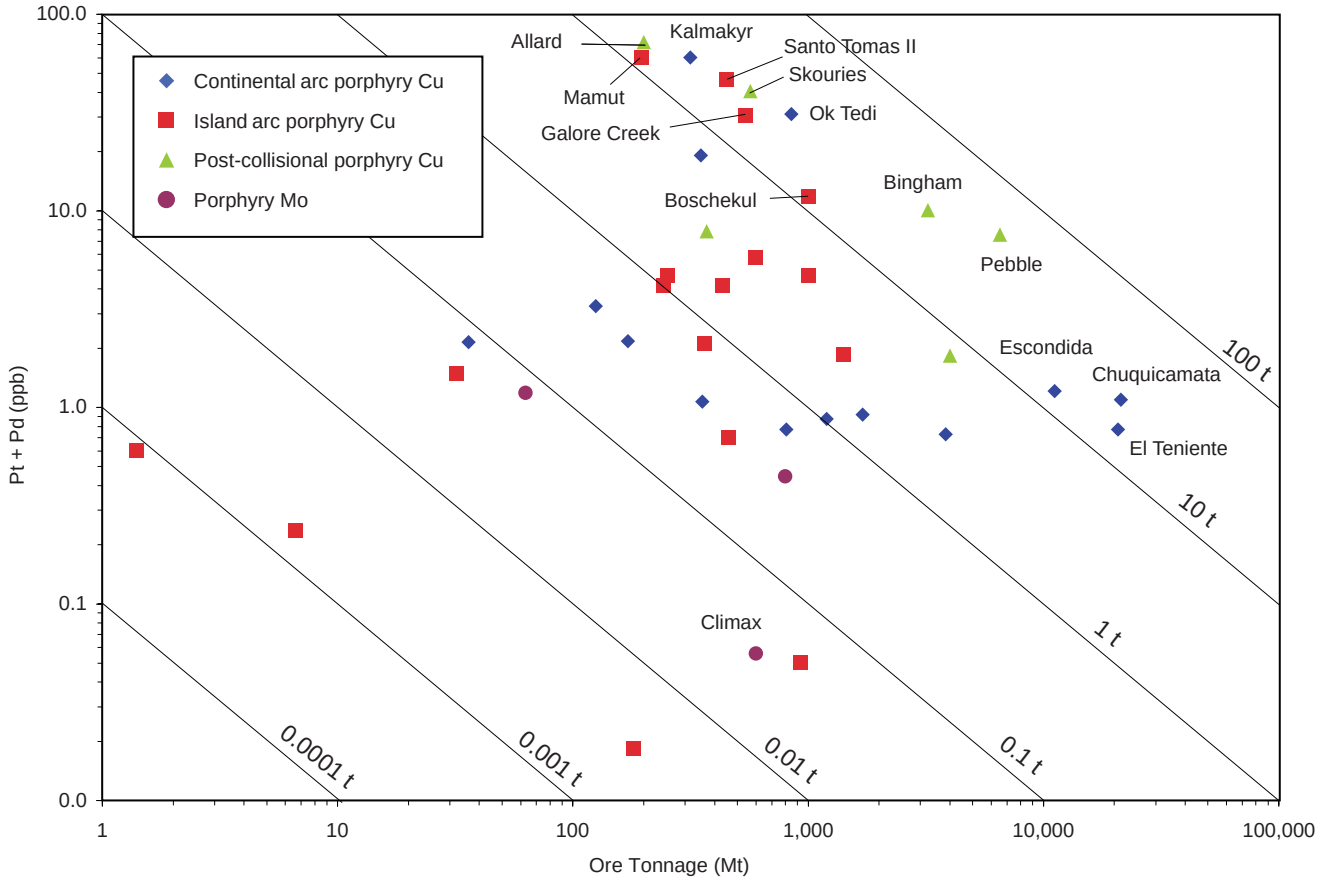

Fig. 6. Grade-tonnage plot of platinum group metals (Pd + Pt) in porphyry Cu and Mo deposits. Porphyry Cu deposits divided by tectonic setting. Data listed in Table 3.

calc-alkaline (Boschekul, Mamut, Ok Tedi), although PGMs are most commonly enriched in Au-rich alkaline porphyry Cu systems, especially in K-rich shoshonitic intrusions (Economou-Eliopoulos, 2005). Although some PGM-enriched porphyry deposits formed in continental arcs (Kalmakyr, Elatsite) or postcollisional (Skouriés, Allard, Pebble) tectonic settings, deposits formed in island arcs are most common and include the British Columbia deposits, Santo Tomas II, Mamut, and Boschekul. As noted by Tarkian and Stribrny (1999), Tarkian et al. (2003), and Economou-Eliopoulos (2005), although no unique characteristic features of PGM-bearing porphyry Cu deposits have been defined, Au-rich porphyry Cu deposits are the most promising exploration targets for Pd and Pt.

Platinum-group metals commonly are grouped together with Au and Re as highly siderophilic elements, as defined by their tendency to partition into metallic phases. However, in porphyry Cu deposits, PGMs tend to exhibit chalcophile behavior and form sulfide minerals that are commonly associated with native gold or electrum. PGMs are generally enriched in Cu- and Au-rich ore zones associated with magnetite-rich potassic alteration (Economou-Eliopoulos, 2005). There is textural evidence that some platinum group minerals may be exsolved from chalcopyrite. In the Kalmakyr deposit, laser ablation ICP-MS analysis of Cu sulfide minerals showed that Pd is homogeneously distributed in chalcopyrite (up to 110 ppm Pd) and tetrahedrite (up to 20 ppm Pd) and is likely bound to the crystal lattice of these minerals (Pasava et al., 2010).

In the Santo Tomas II and Elatsite porphyry Cu deposits, PGMs are enriched in magnetite-bearing bornite-chalcopyrite ore associated with potassic alteration and have much lower concentrations in chalcopyrite-pyrite ore in sericitic alteration (Tarkian and Koopmann, 1995). In the Elatsite deposit, Tokmakchieva (2002) showed that Pd and Pt are enriched in magnetite-bearing bornite-chalcopyrite ores relative to chalcopyrite-pyrite-molybdenite ore and that Pt and Pd are concentrated in chalcopyrite as inclusions of platinum, merenskyite, palladium-arsenite, palladium, and rammelsbergite($NiAs_2$).

Merenskyite ($PdTe_2$) is the main platinum group mineral described in porphyry Cu-Au deposits, such as at Skouriés, Santo Tomas II, Biga (Atlas), Elatsite, Majdanpek, and Mamut (Tarkian and Koopmann, 1995; Tarkian et al., 2003; Economou-Eliopoulos, 2005). Merenskyite occurs mostly as inclusions in chalcopyrite and bornite, at grain boundaries of chalcopyrite and bornite crystals, or enclosed by electrum and hessite (Ag_2Te) inclusions in chalcopyrite. Merenskyite varies from nearly pure $PdTe_2$ to a member of the merenskyite-moncheite $(Pt,Pd)Te_2$ solid-solution series with small amounts of Ni, Bi, and Ag.

In contrast to other porphyry deposits, Pd in the Pebble deposit is concentrated in pyrite in quartz-pyrophyllite

Table 3. Platinum Group Metals in Porphyry

Deposit	Country	Deposit subtype[1]	Tectonic setting	Cu (wt %)	Mo (wt %)	Au (g/t)	Ore tonnage (Mt)	Pd + Pt in concentrate (ppb)
Porphyry Cu deposits								
Agarak	Armenia	Cu	Continental arc	0.56	0.025	0.6	125	105
Ajax West	Canada	Cu	Island arc	0.31	0.005	0.2	365	205
Aksug	Russia	Cu	Postcollisional	0.67	0.015	0.12	371	
Allard	United States	Cu	Postcollisional	0.4	0		200	
Assarel	Bulgaria	Cu	Continental arc	0.44		0.2	354	
Bajo de la Alumbrera	Argentina	Cu-Au	Continental arc	0.53		0.64	806	
Bethlehem-Huestis	Canada	Cu-Mo	Island arc	0.4	0.005	0.012	1.4	37.6
Bingham	United States	Cu	Postcollisional	0.882	0.053	0.38	3,230	
Boschekul	Kazakhstan	Cu-Mo	Island arc	0.67	0.0023	0.049	1,000	
Brenda	Canada	Cu-Mo	Island arc	0.152	0.037	0.013	182	3
Chuquicamata	Chile	Cu-Mo	Continental arc	0.86	0.04	0.013	21,277	
Dastakert	Armenia	Cu-Mo	Continental arc	0.77	0.064		36	67
El Salvador	Chile	Cu	Continental arc	0.86	0.022	0.1	3,836	
El Teniente	Chile	Cu-Mo	Continental arc	0.62	0.019	0.005	20,731	
Elatsite1	Bulgaria	Cu	Continental arc	0.39	0.01	0.26	350	
Elatsite2	Bulgaria	Cu	Continental arc	0.39	0.01	0.26	350	
Elatsite3	Bulgaria	Cu	Continental arc	0.39	0.01	0.26	350	
Elatsite4	**Bulgaria**	**Cu**	**Continental arc**	**0.39**	**0.01**	**0.26**	**350**	
Elatsite5	Bulgaria	Cu	Continental arc	0.39	0.01	0.26	350	
Galore Creek	Canada	Cu	Island arc	0.554	0.0007	0.31	541	
Gibraltar	Canada	Cu	Island arc	0.29	0.006	0.07	935	4
Granisle	Canada	Cu	Continental arc	0.43	0.005	0.13	171	126
Grasberg	Indonesia	Cu-Au	Postcollisional	0.6		0.64	4,000	
Island Copper	Canada	Cu	Island arc	0.338	0.0088	0.19	600	
Island Copper	**Canada**	**Cu**	**Island arc**	**0.338**	**0.0088**	**0.19**	**600**	**51**
Kadjaran (Kadzharan)	Armenia	Cu	Continental arc	0.27	0.055	0.65	1,700	
Kalmakyr1	**Uzbekistan**	**Cu-Au**	**Continental arc**	**2.4**	**0.18**	**4.1**	**316**	
Kalmakyr2	Uzbekistan	Cu-Au	Continental arc	0.38	0.006	0.6	2,000	60
Kalmakyr (Almalyk2)	Uzbekistan	Cu-Au	Continental arc	0.38	0.006	0.6	2,000	
La Escondida	Chile	Cu-Au	Continental arc	0.769	0.0062	0.25	11,158	
Lomex	Canada	Cu-Mo	Island arc	0.404	0.014	0.006	460	45
Lorraine	Canada		Island arc	0.66		0.26	32	
Majdanpek	Serbia	Cu-Au	Island arc?	0.6	0.005	0.35	1,000	
Mamut1	Malaysia	Cu-Au	Island arc	0.48	0.001	0.5	196	
Medet	Bulgaria	Cu	Island arc?	0.37	0.01	0.1	244	
Mount Polley	Canada		Island arc	0.23	0.001	0.3	253	
Ok Tedi	Papua New Guinea	Cu-Au	Island arc	0.64	0.011	0.78	854	
Panguna1	Papua New Guinea	Cu-Au	Island arc	0.465	0.005	0.57	1420	
Panguna2	**Papua New Guinea**	**Cu-Au**	**Island arc**	**0.465**	**0.005**	**0.57**	**1420**	
Pebble	United States	Cu	Postcollisional	0.592	0.0243	0.342	6,528	
Santo Tomas II	Phillipines	Cu-Au	Island arc	0.375	0.0005	0.7	449	
Sar Cheshmeh1	Iran	Cu	Continental arc	1.2	0.03	0.27	1,200	
Sar Cheshmeh2	**Iran**	**Cu**	**Continental arc**	**1.2**	**0.03**	**0.27**	**1,200**	
Skouriés1	Greece	Cu-Au	Postcollisional	0.35	0.002	0.47	568	
Skouriés2	**Greece**	**Cu-Au**	**Postcollisional**	**0.35**	**0.002**	**0.47**	**568**	**2,440**
Skouriés3	Greece	Cu-Au	Postcollisional	0.35	0.002	0.47	568	
Sora (Sorsk)	Russia	Cu	Island arc	0.17	0.058		435	
Tzar Assen	Bulgaria	Cu	Island arc	0.47			6.6	
Porphyry Mo deposits								
Boss Mountain	Canada	Arc-related Mo	Continental arc		0.074		63	849
Endako	Canada	Arc-related Mo	Continental arc	0.002	0.07		600	24
Climax	United States	Alk-granite	Continental rift		0.2		800	120

[1] Cox and Singer (1992) porphyry Cu models; Taylor et al. (2012) and Ludington and Plumlee (2009)) porphyry Mo models
[2] Calculated from Pt + Pd contents of Cu or Mo concentrates
[3] Contained Pt + Pd (t) calculated from Pt + Pd grade and deposit tonnage
[4] For deposits with multiple analyses, analysis in bold plotted in Figure 6

Copper and Molybdenum Deposits

Pd in concentrate (ppb)	Pt in concentrate (ppb)	Pd/Pt	Cu or Mo in concentrate (wt %)	Pd + Pt grade (ppb)[2]	Pd + Pt (t)[3,4]	Comments	References
			18.0	3.3	0.4		Faramazyan et al. (1970); Singer et al. (2008); Sinclair et al. (2009)
			30.0	2.1	0.8		Sinclair et al. (2009)
54	67	0.8	10.3	7.9	2.9		Sotnikov et al. (2001); Singer et al. (2008)
1750	2770	0.6	25.0	72.3	14.5	Avg of three ore samples	Mutschler et al. (1985); Tarkian et al. (2003); Singer et al. (2008)
54	14	3.9	27.9	1.1	0.4		Tarkian and Stribrny (1999); Singer et al. (2008)
35	8	4.4	29.5	0.8	0.6		Tarkian and Stribrny (1999); Singer et al. (2008)
			25.0	0.6	0.001		Sinclair et al. (2009)
8			0.7	10.1	32.6		Tarkian and Stribrny (1999); Singer et al. (2008)
245			13.9	11.8	11.8		Tarkian and Stribrny (1999); Singer et al. (2008)
			25.0	0.02	0.003		Sinclair et al. (2009)
36			28.3	1.1	23.3		Tarkian and Stribrny (1999); Singer et al. (2008)
			24.0	2.1	0.08		Faramazyan et al. (1970)
16	8	2.0	28.3	0.7	2.8		Tarkian and Stribrny (1999); Singer et al. (2008)
32	8	4.0	32.1	0.8	16.0		Tarkian and Stribrny (1999); Singer et al. (2008)
760	170	4.5	19.0	19.1	6.7		Tarkian and Stribrny (1999); Singer et al. (2008)
1900	72	26.4	25.9	29.7	10.4		Tarkian and Stribrny (1999); Singer et al. (2008)
550	160	3.4	25.0	11.1	3.9	Avg of 35 ore samples	Tarkian et al. (2003)
1000	**230**	**4.3**	**25.0**	**19.2**	**6.7**	**Sulfide concentrate**	**Tarkian et al. (2003)**
740	155	4.8	25.6	13.6	4.8	Flotation concentrate	Tarkian et al. (2003)
783	48	16.3	15.1	30.5	16.5	Avg of four ore samples	Thompson et al. (2001); Singer et al. (2008)
			23.0	0.1	0.05		Sinclair et al. (2009)
			25.0	2.2	0.4		Sinclair et al. (2009)
58	15	3.9	23.8	1.8	7.4		Tarkian and Stribrny (1999); Singer et al. (2008)
30	6	5.0	3.2	3.9	2.3	Avg of two ore samples	Thompson et al. (2001); Sinclair et al. (2009)
			3.0	**5.7**	**3.4**		**Sinclair et al. (2009)**
24	84	0.3	31.7	0.9	1.6		Tarkian and Stribrny (1999); Singer et al. (2008)
55	**5**	**10.0**		**60.4**	**19.1**	**Pd + Pt estimate from average of high-grade ore only**	**Pasava et al. (2010)**
			2.4	9.6	19.1		Pasava et al. (2010)
20			31.3	0.2	0.5		Tarkian and Stribrny (1999)
44	8	5.5	33.0	1.2	13.5		Tarkian and Stribrny (1999); Singer et al. (2008)
			26.0	0.7	0.3		Sinclair et al. (2009)
19	11	1.7	13.3	1.5	0.05	One ore sample	Thompson et al. (2001); Singer et al. (2008)
185	20	9.3	26.2	4.7	4.7	Avg of two ore samples	Tarkian and Stribrny (1999); Singer et al. (2008)
1390	470	3.0	20.4	54.8	10.7	Avg of two flotation concentrates	Tarkian and Stribrny (1999); Singer et al. (2008)
160	8	20.0	14.9	4.2	1.0		Tarkian and Stribrny (1999); Singer et al. (2008)
142	19	7.5	7.9	4.7	1.2	Avg of three ore samples	Thompson et al. (2001); Singer et al. (2008)
775			18	30	25.2	Avg of two flotation concentrates	Tarkian and Stribrny (1999); Singer et al. (2008)
40	8	5.0	35.2	0.6	0.9		Tarkian and Stribrny (1999); Singer et al. (2008)
52			**7.7**	**3.1**	**4.5**		**Tarkian and Stribrny (1999); Singer et al. (2008)**
8				7.6	49.4		Northern Dynasty Minerals, Ltd. (2011)
48	14	3.4	0.5	46.5	20.9	Pd and Pt are average of five mineralized samples	Tarkian and Koopmann (1995); Singer et al. (2008)
8			21.8	0.4	0.5		Tarkian and Stribrny (1999); Singer et al. (2008)
24			**32.9**	**0.9**	**1.1**		**Tarkian and Stribrny (1999); Singer et al. (2008)**
160	8	20.0	2.4	24.5	13.9		Tarkian and Stribrny (1999); Singer et al. (2008)
			21.0	**40.7**	**23.1**		**Economou-Eliopoulos (2005); Singer et al. (2008)**
2670	200	13.4	25.0	40.2	22.8	Avg of nine rocks from Eliopoulos and Economou-Eliopoulos (1991)	Tarkian et al. (2003)
39	66	0.6	4.3	4.2	1.8	Tonnage calculated using contained Mo and average Mo grade	Sotnikov et al. (2001); Berzina et al. (2005)
8			15.9	0.2	0.002		Tarkian and Stribrny (1999); Singer et al. (2008)
			53.0	1.19	0.07		Sinclair et al. (2009)
			30.0	0.06	0.02		Sinclair et al. (2009)
			54.0	0.44	0.4		Singer et al. (1993); Sinclair et al.. (2009)

alteration, which overprints early potassic and sodic-potassic alteration and Cu-Au mineralization (Gregory et al., 2013; Lang et al., 2013). Elevated concentrations of Pd (>3 ppm) are in pyrite in samples with massive pyrophyllite replacement and are associated with high-fineness gold inclusions in pyrite and chalcopyrite and gold in solid solution in bornite. The highest 3-m drill core assay is 1.17 ppm Pd, and numerous drill intersections tens of meters long exceed 0.1 ppm Pd (Lang et al., 2013). Total Pd resources at Pebble are estimated as 49,454 kg at an average grade of 0.0076 g/t (Northern Dynasty Minerals, 2011), which is the largest estimated PGM resource in a porphyry Cu deposit (Table 3, Fig. 6).

Global mine production in 2012 is estimated to have been 179,000 kg of platinum and 200,000 kg of palladium (Loferski, 2013). Global resources of PGMs in mineral concentrations that can be mined economically are estimated to total more than 100 Mkg (Loferski, 2013). The total annual global production of Pd and Pt from porphyry Cu deposits is unknown but likely no greater than a few thousand kg. Total potential Pd + Pt resources from known PGM-enriched porphyry Cu deposits listed in Table 3 is about 300,000 kg, less than the current annual global mine production and only about 0.3% of the estimated global PGM resources. Consequently, porphyry Cu deposits are unlikely to become an important source of PGMs. Their potential value lies as a minor by-product of Cu-Au-Mo ores (e.g., Pebble, Bingham) or in selective mining of high-grade zones where deep epithermal Au-PGM mineralization may be superimposed on porphyry Cu mineralization (e.g., Mount Milligan: LeFort et al., 2011).

Selenium

Most of the global mine production of selenium is a by-product of porphyry Cu deposits where most Se is as a substitute for sulfur in Cu-Fe sulfide minerals. Selenium is recovered from the anode slimes produced during the electrolytic refining of Cu ore (Butterman and Brown, 2004; George, 2012). These slimes average about 7 wt % Se, with a few containing as much as 25% Se (Moats et al., 2007). Selenium is consumed in a variety of industries; in 2011 the estimated global consumption of selenium by application was metallurgy, 40%; glass manufacturing, 25%; agriculture, 10%; chemicals and pigments, 10%; electronics, 10%; and other uses, 5% (George, 2012).

Selenide minerals are uncommon in porphyry deposits. Instead, Se mostly occurs as a stoichiometric substitution for S in hypogene sulfides, likely because the elevated reduced sulfur activity and low f_{Se_2}/f_{S_2} of the hydrothermal fluids and the buffering of the f_{Se_2} and f_{S_2} by the sulfide assemblages do not allow the stabilization of selenide minerals (Simon and Essene, 1996; Simon et al., 1997). Substitution of Se for S in sulfides is a result of their similar ionic radii and oxidation state (–2; Simon et al., 1997; Ciobanu et al., 2006). Selenium substitution may occur in any sulfide mineral, but data compiled by Berrow and Ure (1989) suggested that the higher concentrations of Se occur in cinnabar, stibnite, and chalcopyrite than in other sulfide minerals.

Selenium mineralogy and concentrations of Se in porphyry ores are seldom reported. Treatment of 400 t of porphyry Cu ore typically yields about 1 kg of Se (suggesting about 2.5 ppm recoverable Se; Selenium Tellurium Development Association, 2012). Broadhurst et al. (2007) estimated that a typical run of mine porphyry Cu sulfide ore contains 10 to 100 ppm Se. Chalcopyrite-pyrite-molybdenite and magnetite-bornite-chalcopyrite assemblages at Elatsite contain 20 to 410 and 250 to 600 ppm Se, respectively, and Se averages 6 ppm overall in the ores (Tokmakchieva, 2002). The Se-rich magnetite-bornite-chalcopyrite assemblage is mainly found in the central potassic alteration zone, where bornite and/or chalcopyrite contain exsolved grains of the selenide minerals, clausthalite and bohdanowiczite (Bogdanov et al., 2005). Individual chalcopyrite crystals contain 100 to 2,400 ppm Se (Tokmakchieva, 1999). The Assarel deposit contains 3 to 40 ppm of Se in chalcopyrite, pyrite, chalcocite, and covellite ores (Tokmakchieva, 2002). The Se content of chalcopyrite averages 200 ppm in the Skouriés deposit (Nicolaidou, 1998). Ion microprobe analyses of pyrite from the Dexing porphyry Cu deposit typically have Se contents <70 ppm (Reich et al., 2013). Selenium is found as inclusions within bornite and chalcopyrite in breccias at the Mount Polley deposit, where Se mineralization is associated with higher Cu and Ag grades, higher bornite contents, and higher Cu/Au than in other breccias in the deposit (Logan and Mihalynuk, 2005). Selenium is in solid solution in molybdenite, chalcopyrite, pyrite, and bornite in the Erdenet deposit (Malyutin et al., 2007). Gregory et al. (2013) described four types of pyrite at Pebble and noted that late-stage pyrite-4 has a mean Se content of 142 ppm, which is significantly higher than the other types of pyrite (mean Se contents from 63–81 ppm), and also has high Au, As, and Ni contents. Selenium contents of high-grade Cu-Au ore in potassic alteration at Batu Hijau average 8.8 ppm (Idrus et al., 2009). High-grade Cu-Au-Mo ore at Bingham averages 12 ppm Se (Austin and Ballantyne, 2010).

Huston et al. (1995) calculated that Se levels in pyrite negatively correlate with hydrothermal fluid temperature as long as native Se is not stable and after removing variations that may result from changing H_2Se/H_2S. Data from the Assarel and Medet porphyry deposits support this model with higher Se concentrations associated with lower homogenization temperatures and lower salinities in fluid inclusions in late-stage pyrite-chalcopyrite ± molybdenite veins (Economou-Eliopoulos and Eliopoulos, 2000). Similarly, Gregory et al. (2013) suggested that Se- and As-rich pyrite-4 at Pebble may have formed at relatively low temperatures based on the findings of Huston et al. (1995).

Global Se production in 2011 was estimated to be about 3,000 to 3,500 t (George, 2012). Estimated global reserves of Se are 98,000 t based on identified Cu deposits (George, 2013a). Although coal generally contains between 0.5 and 12 ppm Se, recovery of Se from coal is not currently economical (George, 2013a). Therefore, most Se likely will continue to be recovered from porphyry Cu deposits.

Tellurium

Porphyry Cu deposits are the world's principal source of tellurium, although Te production from these deposits is more a reflection of the large tonnages of ore processed rather than the Te grade (George, 2013b; Goldfarb et al., in press). All Te produced in the United States is from the ASARCO refinery in Texas, which processes anode slimes derived from several

porphyry Cu deposits. Tellurium and selenium are extracted from copper that is refined by the electrolytic process, a technique cost effective only for high-grade Cu ores (Moss et al., 2011). Typically, the slimes contain 1 to 4% Te, although as much as 8 to 9% Te in the slimes has been reported at some refineries (Moats et al., 2007). Lower grade Cu ores are refined by the more economical solvent-leach process, which is currently not capable of recovering Te.

Tellurium is used mainly as a Cd-Te film in photovoltaic solar cells and as an additive to steel, copper, and lead alloys to improve machine efficiency, particularly in thermoelectric cooling applications. Together, the photovoltaic solar and thermoelectric applications account for more than two-thirds of the world's Te usage (George, 2013). Tellurium also is used in copying machines and as a coloring agent in ceramic and glass. Other uses include its application as a vulcanizing agent in the chemical industry, as an accelerator in the rubber industry, and in integrated circuits, laser diodes, and medical instrumentation.

Tellurium is enriched in porphyry Cu deposits, although Te contents of porphyry deposits are seldom reported. Broadhurst et al. (2007) estimated that typical run of mine porphyry copper sulfide ore contains 0.1 to 1 ppm Te. Economou-Eliopoulos and Eliopoulos (2000) reported whole-rock concentrations of Te from 0.33 to 2.7 ppm in ore samples from the Skouriés deposit and Fissoka prospect, and Tokmakchieva (2002) and Tarkian et al. (2003) reported as much as 106 ppm Te in ore samples from the Elatsite deposit. Economou-Eliopoulos and Eliopoulos (2000) also reported 4 and 18.5 ppm Te in two chalcopyrite concentrate samples from Skouriés. Tellurium averages 4.8 ppm in high-grade Cu-Mo-Au ore at Bingham (Austen and Ballantyne, 2010). High Te contents may reflect both solid solution of Te in sulfide minerals and discrete Te-bearing minerals (Goldfarb et al., in press).

Gold, Ag, and Pd tellurides are the most commonly reported Te minerals in porphyry Cu deposits. At the Pebble deposit, Gregory et al. (2013) estimated that 2.5 to 3% of the gold contained in chalcopyrite, the main Cu ore mineral, is hosted by inclusions of petzite (Ag_3AuTe_2) and calaverite ($AuTe_2$). In other porphyry Cu deposits, anomalous Pd contents reflect the presence of Pd-bearing telluride minerals as distinct grains or as inclusions in bornite and chalcopyrite (see previous section on PGMs). For example, merenskyite ($PdTe_2$), locally associated with lesser kotulskite (Pd(Te,Bi)) and hessite (Ag_2Te), are commonly reported in porphyry Cu deposits (Economou-Eliopoulos, 2005).

Wall rocks surrounding some porphyry Cu deposits are enriched in Te. For example, the main Cu ± Au porphyry ores at Ely, Nevada, which are not enriched in Te, have an Ag-rich halo that averages about 100 ppm Te (Gott and McCarthy, 1966). Watterson et al. (1977) also found high concentrations of Te in silicified rocks in a halo surrounding the Ely porphyry Cu ores. Chaffee (1982) identified two zones with anomalous whole-rock Te contents at the Kalamazoo deposit, Arizona. The highest concentrations of Te were present in the outer pyritic halo to the porphyry deposit, whereas lower but anomalous Te values corresponded with the Cu-Au ore zone. Cox et al. (1975) identified a similar dual zonation at the Sapo Alegre deposit, Puerto Rico. Therefore, future Te resources may be evaluated in the alteration halos to Cu-(Mo-Au) ores in some porphyry Cu deposits if Te demand increases.

Many porphyry systems with abundant telluride minerals are associated with subduction-related alkalic intrusions. These include deposits of the Late Triassic-Early Jurassic continental arc in British Columbia. The Mount Milligan Cu-Au deposit, one of the larger deposits of this group, is characterized by a late-stage "subepithermal" or intermediate-sulfidation overprinting event that deposited an Au-PGM-As-Sb-Bi-Te-Hg assemblage (LeFort et al., 2011). Many Au-rich epithermal deposits with significant Te concentrations may be postporphyry ores, thus reflecting late-stage events in an evolving porphyry-epithermal magmatic-hydrothermal system most consistently of an alkalic nature. La Plata, Colorado, may be such an example, where gold-telluride vein and replacement deposits surround an alkaline intrusion that is rich in Au and Cu (Jones, 1992).

Annual global production of tellurium is estimated to be 450 to 470 t, of which more than 75% is a by-product of Cu mining (George, 2013b). Estimated global reserves for Te are 24,000 t, which include only Te contained in Cu reserves and assume that only about one-half of the Te contained in unrefined copper anodes is actually recovered (George, 2013b).

Other critical or rare metal commodities

Indium is becoming increasingly important for high-tech applications. The highest In concentrations in porphyry deposits are found in sphalerite and chalcopyrite (Briskey, 2005). In porphyry Cu deposits, indium occurs mostly as a trace constituent in chalcopyrite. Chalcopyrite from the Bingham porphyry Cu deposit contains up to 150 ppm In, but averaged only 11 ppm in 42 analyzed samples (Briskey, 2005). Porphyry tin deposits that contain sphalerite may produce In as a by-product if Zn is recovered, but this possibility remains remote.

Other rare metals, such as Cs, F, Li, Nb, Rb, Sn, and Ta, are concentrated in parts of alkali-feldspar rhyolite-granite porphyry Mo deposits (Ludington and Plumlee, 2009). The undeveloped (as of 2013) Cave Peak prospect, Texas, has been correlated with other alkali-feldspar rhyolite-granite porphyry Mo deposits (Sharp, 1979; Audétat, 2010). Its accessory mineralogy includes columbite [$(Fe, Mn)Nb_2O_6$], huebnerite, and cassiterite. Quaterra Resources Inc. (2008) is currently assessing the property and has indicated that W, Be, and Nb might be produced as by-products. Mineralization is found in the largest of three breccia pipes associated with porphyritic granitoid plugs. A significant concentration of niobium exists at a grade of 0.1% Nb_2O_5 (Long, 1992). The Climax-style Mo mineralization at Shapinggou, China, includes resources that make it the world's second largest Mo mine, and it is reported to contain niobium ore (Xu et al., 2011).

Summary and Conclusions

Porphyry Cu and Mo deposits are large to giant deposits, which formed from hydrothermal systems that affected large volumes of the upper crust, thereby resulting in enormous mass redistribution. Several critical elements, which lack primary ores, including Re, Se, and Te, are concentrated locally within porphyry Cu deposits at relatively low concentrations

(a few 100 ppb to a few ppm). Because porphyry Cu mines commonly process 100s of Mt of Cu-Au-Mo ore annually, Re, Se, and Te can be recovered from these deposits if proper ore-processing circuits are available. For example, 80% of global Re mine production is a by-product of Mo recovery, which is itself a by-product of Cu mining in some porphyry Cu deposits. However, Re recovery requires both the production of molybdenite concentrates and special facilities for the processing of Re-enriched flue dust produced during roasting of molybdenite concentrates. Because of the immense size of known and potential resources in some continental margin and postcollisional porphyry Cu deposits, these deposits likely will provide most of the global supply of Re, Te, and Se for the foreseeable future.

In contrast, platinum group metals are not strongly enriched in porphyry Cu deposits, and although Pd and lesser Pt are recovered from some deposits, estimated PGM resources contained in known porphyry deposits are small. Because there are much larger known PGM resources in deposits in which PGMs are the primary commodities, it is unlikely that porphyry deposits will become a major source of PGMs.

Other critical commodities, such as In, may eventually be recovered from porphyry Cu and Mo deposits, but available data do not clearly define significant resources of these commodities in porphyry deposits and their recovery remains unlikely.

Acknowledgments

We thank Dave Sinclair, Don Singer, Steve Ludington, and John Chesley for discussions and unpublished data, and Dick Sillitoe and Dave Sinclair for helpful reviews.

REFERENCES

American Physical Society and the Material Research Society, 2011, Energy critical minerals: Powering our high-tech world, 24 p., http://www.aps.org/policy/reports/popa-reports/loader.cfm?csModule=security/getfile&PageID=236337 (accessed 7/3/13).

Aminzadeh, B., Shahbpour, J., and Maghami, M., 2011, Variation of rhenium contents in molybdenites from the Sar Cheshmeh porphyry Cu-Mo deposit in Iran: Resource Geology, v. 61, p. 290–295.

Arif, J., and Baker, T., 2004, Gold paragenesis and chemistry at Batu Hijau, Indonesia: Implications for gold-rich porphyry copper deposits: Mineralium Deposita, v. 39, p. 523–535.

Atkinson, D., 1995, The Glacier Gulch (Hudson Bay Mountain or Yorke-Hardy) porphyry molybdenum-tungsten deposit, west-central British Columbia: Canadian Institute of Mining, Metallurgy, and Petroleum Special Volume 46, p. 704–707.

Audétat, A., 2010, Source and evolution of molybdenum in the porphyry Mo (-Nb) deposit at Cave Peak, Texas: Journal of Petrology, v. 51, p. 1739–1760.

Austen, G., and Ballantyne, G., 2010, Geology and geochemistry of deep molybdenum mineralization at the Bingham Canyon mine, Utah, USA: Society of Economic Geologists Guidebook Series, v. 41, p. 35–49.

Ayuso, R.A., 2010, Isotope geochemistry: U.S. Geological Survey Scientific Investigations Report 2010-5070-B, p. 100–106.

Babcock, R.C., Ballantyne, G.H., and Phillips, C.H., 1995, Summary of the geology of the Bingham district, Utah: Arizona Geological Society Digest, v. 20, p. 316–335.

Ballantyne, G.H., Smith, T.W., and Redmond, P.B., 1998, Distribution and mineralogy of gold and silver in the Bingham Canyon porphyry copper deposit, Utah: Society of Economic Geologists Guidebook Series, v. 29, p. 147–153.

Barra, F., Ruiz, J., Mathur, R., and Titley, S., 2003, A Re-Os study of sulfide minerals from the Bagdad porphyry Cu-Mo deposit, northern Arizona, USA: Mineralium Deposita, v. 38, p. 585–596.

Barra, F., Ruiz, J., Valencia, V.A., Ochoa-Landin, L., Chesley, J.T., and Zurcher, L., 2005, Laramide porphyry Cu-Mo mineralization in northern Mexico: Age constraints from Re-Os geochronology in molybdenite: Economic Geology, v. 100, p. 1605–1616.

Barra, F. Alcota, H., Rivera, S., Valenica, V., Munizaga, F., and Maksaev, V., 2013, Timing and formation of porphyry Cu-Mo mineralization in the Chuquicamata district, northern Chile: New constraints from the Toki cluster: Mineralium Deposita, DOI 10.1007/s00126-012-0452-1.

Barton, M.D., 2010, Broader implications and societal relevance of porphyry copper systems: U.S. Geological Survey Scientific Investigations Report 2010-5070-B, p. 126–130.

BC Minfile 092L 158: Ministry of Energy, Mines and Petroleum Resources, 5 p.

Bernard, A., Symonds, R.B., and Rose, W.I., Jr., 1990, Volatile transport and deposition of Mo, W, and Re in high temperature magmatic fluids: Applied Geochemistry, v. 5, p. 317–326.

Berrow, M.L., and Ure, A.M., 1989, Geological meterials and soils, *in* Ihnat, M., ed., Occurrence and distribution of selenium: Florida, CRC Press, p. 213–242.

Berzina, A.N., and Korobeinikov, A.F., 2007, Rhenium and precious metal (Pt, Pd, and Au) abundances in porphyry Cu-Mo deposits of central-Asian mobile belt: Acta Petrologica Sinica, v. 23, p. 1957–1972.

Berzina, A.N., Sotnikov, V.I., Economou-Eliopoulos, M., and Eliopoulos, D.G., 2005, Distribution of rhenium in molybdenite from porphyry Cu-Mo and Mo-Cu deposits of Russia (Siberia) and Mongolia: Ore Geology Reviews, v. 26, p. 91–113.

Bogdanov, K., Filipov, A., and Kehayov, R., 2005, Au-Ag-Te-Se minerals in the Elatsite porphyry-copper deposit, Bulgaria: Geochemistry, Mineralogy and Petrology, v. 43, p. 13–19.

Briskey, J.A., 2005, Indium in zinc-lead and other mineral deposits—a reconnaissance survey of 1118 indium analyses published before 1985: U.S. Geological Survey Open-File Report 2005-1209, 8 p.

British Geological Survey, 2012, Risk list 2012, http://www.bgs.ac.uk/mineralsuk/statistics/risklist.html, accessed 7/3/13

Broadhurst, J.L., Petrie, J.G., and von Blottnitz, H., 2007, Understanding element distribution during mineral metal production: Mineral Processing and Extractive Metallurgy, v. 116, p. 1–16.

Burton, K.W., Schiano, P., Birck, J.-L., Allègre, C.J., Rehkämper, M., Halliday, A.N., and Dawson, J.B., 2000, The distribution and behavior of rhenium and osmium amongst mantle minerals and the age of the lithospheric mantle beneath Tanzania: Earth and Planetary Science Letters, v. 183, p. 93–106.

Butterman, W.C., and Brown, R.D., Jr., 2004, Mineral commodity profiles—selenium: U.S. Geological Survey Open-File Report 03-018, 20 p.

Candela, P.A., and Holland, H.D., 1986, A mass transfer model for copper and molybdenum in magmatic hydrothermal systems: the origin of porphyry-type ore deposits: Economic Geology, v. 81, p. 1–19.

Cannell, J.B., 2004, El Teniente porphyry copper molybdenum deposit, central Chile: Ph.D. thesis, Hobart, University of Tasmania, 317 p.

Carten, R.B., White, W.H. and Stein, H.J., 1993, High-grade granite-related molybdenum systems: Classification and origin: Geological Association of Canada Special Paper 40, p. 521–554.

Chaffee, M.A., 1982, A geochemical study of the Kalamazoo porphyry copper deposit, *in* Titley, S.R., ed., Advances in the geology of the porphyry copper deposits, southwestern North America: Tucson, Arizona, University of Arizona Press, p. 211–225.

Chen, Z., Zhang, L., Wan, B., Wu, H., and Cleven, N., 2011, Geochronology and geochemistry of the Wunugetushan porphyry Cu-Mo deposit in NE China, and their geological significance: Ore Geology Reviews, v. 43, p. 92–105.

Chesley, J.T., and Ruiz, J., 1998, Preliminary Re-Os dating on molybdenite mineralization from the Bingham Canyon porphyry copper deposit, Utah: Society of Economic Geologists Guidebook Series, v. 29, p. 165–169.

Chesley, J., Righter, K., and Ruiz, J., 2002, Large-scale metasomatism—a Re-Os perspective: Earth and Planetary Science Letters, v. 219, p. 49–60.

Ciobanu, C.L., Cook, N.J., and Spry, P.G., 2006, Preface—Special Issue: Telluride and selenide minerals in gold deposits—how and why?: Mineralogy and Petrology, v. 87, p. 163–169.

Cooke, D.R., Hollings, P., and Walshe, J.L., 2005, Giant porphyry deposits: Characteristics, distribution, and tectonic controls: Economic Geology, v. 100, p. 801–818.

Cox, D.P., and Singer, D.A., 1992, Distribution of gold in porphyry copper deposits: U.S. Geological Survey Bulletin 1877, p. C1–C14.

Cox, D.P., Perez, G., and Nash, J.T., 1975, Geology, geochemistry, and fluid inclusion petrography of the Sapo Alegre porphyry copper prospect and its

metavolcanic wall rocks, west-central Puerto Rico: U.S. Geological Survey Journal of Research, v. 3, p. 313–327.
Crusius, J., Calvert, S.E., Peersen, T.F., and Sage, D., 1996, Rhenium and molybdenum enrichments in sediments as indicators of oxic, suboxic and anoxic conditions of deposition: Earth and Planetary Science Letters, v. 145, p. 65–79.
Dahlkamp, F.J., 2009. Uranium deposits of the world, USA and Latin America: Berlin, Springer-Verlag, 4 volumes, 516 p.
D'Arcy, R.G., 1950, Recovery of uranium from Climax brannerite concentrate C-7: Topical Report MITG-231, MIT Mineral Engineering Laboratory, Contract AT-30-3-Gen-211, 10 p.
Deckert, K., Clark, A.H., Cuadra, P., and Fanning, M., 2013, Refinement of the time-space evolution of the giant Mio-Pliocene Río Blanco-Los Bronces porphyry Cu-Mo cluster, central Chile: New U-Pb (SHRIMP II) and Re-Os geochronology and $^{40}Ar/^{39}Ar$ thermochronology data: Mineralium Deposita, v. 48, p. 57–79.
Deng, X.H., Chen, Y.J., Santosh, M., Zhao, G.C., and Yao, J.M., 2013, Metallogeny during continental outgrowth in the Columbia supercontinent: Isotopic characterization of the Zhaiwa Mo-Cu system in the North China craton: Ore Geology Reviews, v. 51, p. 43–56.
Desborough, G.A., and Sharp, W.N., 1978, Tantalum, uranium, and scandium in heavy accessory oxides, Climax molybdenum mine, Climax, Colorado: Economic Geology, v. 73, p. 1749–1751.
Dilles, J.H., 2010, Hydrothermal alteration: U.S. Geological Survey Scientific Investigations Report 2010-5070-B, p. 57–62.
Eliopoulos, D.G., and Economou-Eliopoulos, M., 1991, Platinum-group element and gold contents in the Skouriés porphyry copper deposit, Chalkidiki Pennisula, northern Greece: Economic Geology, v. 86, p. 740–749.
Economou-Eliopoulos, M., 2005, Platinum-group element potential of porphyry deposits: Mineralogical Association of Canada Short Course Series, v. 35, p. 203–246.
Economou-Eliopoulos, M., and Eliopoulos, D.G., 2000, Palladium, platinum and gold concentration in porphyry copper systems of Greece and their genetic significance: Ore Geology Reviews, v. 16, p. 59–70.
Einaudi, M.T., Hedenquist, J.W., and Inan, E.E., 2003, Sulfidation state of fluids in active and extinct hydrothermal systems: Transitions from porphyry to epithermal environments: Society of Economic Geologists Special Publication 10, p. 285–313.
Erdene Resource Development Corp., 2011, Zuun Mod porphyry molybdenum-copper project, south-western Mongolia: Minarco-Mine Consultant, NI 43-101 report, 64 p., accessed March 18, 2013 at: http://www.erdene.com/assets/pdf/ZuunMod43-101TechnicalReport_MinarcoJune2011.pdf.
Faramazyan, A.S., Kalinin, S.K., and Terekhovich, S.L., 1970, Geochemistry of Pt group elements in the ores of Cu-Mo deposits of Armenia: Doklady Earth Science Sections, v. 190, p. 220–221.
Fleischer, M., 1959, The geochemistry of rhenium, with special reference to its occurrence in molybdenite: Economic Geology, v. 54, p. 1406–1413.
Freydier, C., Ruiz, J., Chesley, J., McCandless, T., and Muizaga, F., 1997, Re-Os isotope systematics of sulfides from felsic igneous rocks: Application to base metal porphyry mineralization in Chile: Geology, v. 25, p. 775–778.
Garwin, S. L., 2002, The geologic setting of intrusion-related hydrothermal systems near the Batu Hijau porphyry copper- gold deposit, Sumbawa, Indonesia: Society of Economic Geologists Special Publication 9, p. 333–366.
George, M.W., 2012, Selenium and tellurium: U.S. Geological Survey 2011 Minerals Yearbook, p. 65-1–65-9.
——2013a, Selenium: U.S. Geological Survey Minerals Commodity Summaries 2013, p. 143–144. http://minerals.usgs.gov/minerals/pubs/commodity/selenium/mcs-2013-selen.pdf (accessed 4/25/2013)
——2013b, Tellurium: U.S. Geological Survey Minerals Commodity Summaries 2013, p. 164–165. http://minerals.usgs.gov/minerals/pubs/commodity/tellurium/mcs-2013-tellu.pdf (accessed 4/25/2013)
Giles, D.L., and Schilling, J.H., 1972, Variation in the rhenium content of molybdenite: International Geological Congress, 24th, Proceedings of Section 10, p. 145–153.
Goldfarb, R.J., Anderson, E.D., and Hart, C.J.R., 2013, Tectonic setting of the Pebble and other copper-gold-molybdenum porphyry deposits within the evolving middle Cretaceous continental margin of northwestern North America: Economic Geology, v. 108, p. 405–419.
Goldfarb, R.J., Berger, B.R., George, M., and Seal, R., in press, Tellurium—economic and environmental geology, and prospects: U.S. Geological Survey Professional Paper.
Gott, G.B., and McCarthy, J.H., Jr., 1966, Distribution of gold, silver, tellurium, and mercury in the Ely mining district, White Pine County, Nevada: U.S. Geological Survey Circular 535, 5 p.
Gregory, M.J., Lang, J.R., Gilbert, S., and Hoal, K.O., 2013, Geometallurgy of the Pebble porphyry copper-gold-molybdenum deposit, Alaska: Implications for gold distribution and paragenesis: Economic Geology, v. 108, p. 463–482.
Gustafson, L.B., and Hunt, J.P., 1975, The porphyry copper deposit at El Salvador, Chile: Economic Geology, v. 70, p. 857–912.
Hall, W.E., Friedman, I., and Nash, J.T., 1974, Fluid inclusion and light stable isotope study of the Climax molybdenum deposits, Colorado: Economic Geology, v. 69, p. 884–901,
Hattori, K.H., and Keith, J.D., 2001, Contribution of mafic melt to porphyry copper mineralization: Evidence from Mount Pinatubo, Philippines, and Bingham Canyon, Utah, USA: Mineralium Deposita, v. 36, p. 799–806.
Hauri, E.H., and Hart, S.R., 1997, Rhenium abundances and systematics in oceanic basalts: Chemical Geology, v. 139, p. 185–205.
Heinrich, C.A., Günter, D., Audétat, A., Ulrich, T., and Frischknecht, R., 1999, Metal fractionation between magmatic brine and vapor determined by microanalysis of fluid inclusions: Geology, v. 27, p. 755–758.
Henley, R.W., and McNabb, A., 1978, Magmatic vapor plumes and groundwater interaction in porphyry copper emplacement: Economic Geology, v. 73, p. 1–20.
Hou, Z., Zeng, P., Gao, Y., Du, A., and Deming, F., 2006, Himalayan Cu-Mo-Au mineralization in the eastern Indo-Asian collision zone: Constraints from Re-Os dating of molybdenite: Mineralium Deposita, v. 41, p. 33–45.
Hou, Z., Yang, Z, Qu, X, Meng, X., Li, Z., Beaudoin, G., Rui, Z., Gao, Y., and Zaw, K., 2009, The Miocene Gangdese porphyry copper belt generated during post-collisional extension in the Tibetan orogen: Ore Geology Reviews, v. 36, p. 25–51.
Hou, Z., Zhang, H, Pan, X., and Yang, Z., 2011, Porphyry Cu (-Mo-Au) deposits related to melting of thickened mafic lower crust: Examples from the eastern Tethyan metallogenic domain: Ore Geology Reviews, v. 39, p. 21–45.
Huston, D.L., Sie, S.H., Suter, G.F., Cooke, D.R., and Both, R.A., 1995, Trace elements in sulfide minerals from eastern Australian volcanic-hosted massive sulfide deposits—Part I. Proton microprobe analyses of pyrite, chalcopyrite, and sphalerite, and Part II. Selenium levels in pyrite—comparison with $\delta^{34}S$ values and implications for the source of sulfur in volcanogenic hydrothermal systems: Economic Geology, v. 90, p. 1167–1196.
Idrus, A., Kolb, J., and Meyer, F.M., 2009 Mineralogy, lithogeochemistry and elemental mass balance of the hydrothermal alteration associated with the gold-rich Batu Hijau porphyry copper deposit, Sumbawa Island, Indonesia: Resource Geology, v. 59, p. 215–230.
Ishihara, S., 1988, Rhenium contents of molybdenites in granitoid-series rocks in Japan: Economic Geology, v. 83, p. 1047–1051.
John, D.A., Rytuba, J.J., Ashley, R.P., Blakely, R.J., Vallance, J.W., Newport, G.R., and Heinemeyer, G.R., 2003, Field guide to hydrothermal alteration in the White River altered area and in the Osceola mudflow, Washington: U.S. Geological Survey Bulletin 2217, 58 p.
John, D.A., Ayuso, R.A., Barton, M.D., Blakely, R.J., Bodnar, R.J., Dilles, J.H., Gray, Floyd, Graybeal, F.T., Mars, J.C., McPhee, D.K., Seal, R.R., Taylor, R.D., and Vikre, P.G., 2010, Porphyry copper deposit model: U.S. Geological Survey Scientific Investigations Report 2010–5070-B, 169 p.
John, D.A., Seal, R.R., II, and Polyak, D.E., in press, Rhenium: Economic and environmental geology, and prospects for future supply: U.S. Geological Survey Professional Paper.
John, E.C., 1978, Mineral zones in the Utah copper orebody: Economic Geology, v. 73, p. 1250–1259.
Jones, B.K., 1992, Application of metal zoning to gold exploration in porphyry copper systems: Journal of Geochemical Exploration, v. 43, p. 127–155.
Keith, J.D., Whitney, J.A., Hattori, K., Ballantyne, G.H., Christiansen, E.H., Barr, D.L., Cannan, T.M., and Hooks, C.J., 1997, The role of magmatic sulphides and mafic alkaline magmas in the Bingham and Tintic mining districts, Utah: Journal of Petrology. v. 38, p. 1679–1690.
Kennecott Utah Copper, 2013, http://www.kennecott.com/products (accessed 4/29/13).
Kesler, S.E., 1973, Copper, molybdenum, and gold abundances in porphyry copper deposits: Economic Geology, v. 68, p. 106–112.
Kesler, S.E., Chryssoulis, S.L., and Simon, G., 2002, Gold in porphyry copper deposits: Its distribution and fate: Ore Geology Reviews, v. 21, p. 103–124.
Khashgerel, B.-E., Kavalieris, I., and Hayashi, K.-I., 2008, Mineralogy, textures, and whole-rock geochemistry of advanced argillic alteration: Hugo

Dummett porphyry Cu-Au deposit, Oyu Tolgoi mineral district, Mongolia: Mineralium Deposita, v. 43, p. 913–932.
Kirkham, R.V., and Sinclair, W.D., 1995, Porphyry copper, gold, molybdenum, tungsten, tin, silver: Geological Society of America, The Geology of North America, v. P-1, p. 421–446.
Klemm, L.M., Pettke, T., Heinrich, C.A., and Campos, E., 2007, Hydrothermal evolution of the El Teniente deposit, Chile: Porphyry Cu-Mo ore deposition from low-salinity magmatic fluids: Economic Geology, v. 102, p. 1021–1045.
Klemm, L.M., Pettke, T., and Heinrich, C.A., 2008, Fluid and source magma evolution of the Questa porphyry Mo deposit, New Mexico, USA: Mineralium Deposita, v. 43, p. 533–553.
Lang, J.R., Gregory, M.J., Rebagliati, C.M., Payne, J.G., Oliver, J.L., and Roberts, K., 2013, Geology and magmatic-hydrothermal evolution of the giant Pebble porphyry copper-gold-molybdenum deposit, southwest Alaska: Economic Geology, v. 108, p. 437–462.
Landtwing, M.R., Furrer, C., Redmond, P.B., Pettke, T., Guillong, M., and Heinrich, C.A., 2010, The Bingham Canyon porphyry Cu-Mo-Au deposit. III. Zoned copper-gold ore deposition by magmatic vapor expansion: Economic Geology, v. 105, p. 91–118.
Lasmanis, R., 1995, Regional geological and tectonic setting of porphyry deposits in Washington State: Canadian Institute of Mining, Metallurgy and Petroleum Special Volume 46, p. 77–102.
Lassiter, J.C., 2003, Rhenium volatility in subaerial lavas: Constraints from subaerial and submarine portions of the HSDP-2 Mauna Kea drillcore: Earth and Planetary Science Letters, v. 214, p. 311–325.
LeFort, D., Hanley, J., and Guillong, M., 2011, Subepithermal Au-Pd mineralization associated with an alkali porphyry Cu-Au deposit, Mount Milligan, Quesnel terrane, British Columbia, Canada: Economic Geology, v. 106, p. 781–808.
Leybourne, M.I., and Cameron, E.M., 2008, Source, transport, and fate of rhenium, selenium, molybdenum, arsenic, and copper in groundwater associated with porphyry-Cu deposits, Atacama Desert, Chile: Chemical Geology, v. 247, p. 208–228.
Lifton, Jack, 2007, Byproducts IV: Rhenium, a byproduct of a byproduct, http://www.resourceinvestor.com/2007/10/04/byproducts-iv-rhenium-a-byproduct-of-a-byproduct (accessed 12/11/12).
Loferski, P.J., 2013, Platinum-group metals: U.S. Geological Survey Mineral Commodity Summary, p. 120–121.
Logan, J.M., and Mihalynuk, M.G., 2005, Regional geology and setting of the Cariboo, Bell, Springer and Northeast porphyry Cu-Au zones at Mount Polley, south-central British Columbia: British Columbia Geological Survey, Geological Fieldwork 2004, Paper 2005-1, p. 249–270.
Long, K.R., 1992, Reserves and production data for selected ore deposits in the United States found in the files of the Anaconda Copper Company: U.S. Geological Survey Open-File Report 92-002, 21 p.
Ludington, S., and Plumlee, G.S., 2009, Climax-type porphyry molybdenum deposits: U.S. Geological Survey Open-File Report 2009-1215, 16 p.
Ludington, S., Hammarstrom, J., and Piatak, N., 2009, Low-fluorine stockwork molybdenite deposits: U.S. Geological Survey Open-File Report 2009-1211, 9 p.
Maksaev, V., Munizaga, F., McWilliams, M., Fanning, M., Mathur, R., Ruiz, J., and Zentilli, M., 2004, New chronology for El Teniente, Chilean Andes, from U-Pb, $^{40}Ar/^{39}Ar$, Re-Os, and fission track dating: Implications for the evolution of a supergiant porphyry Cu-Mo deposit Society of Economic Geologists Special Publication 11, p. 15–54.
Malyutin, Y.A., Maksimyuk, I.E., Gavrilova, S.P., Zhigachev, A.L., and Erdenetsogt, P., 2007, Geological and geochemical features of the Erdenetiin-Ovoo deposit: Moscow University Geology Bulletin, v. 62, p. 325–333.
Mao, J.W., Zhang, Z.C., Zhang, Z.H., and Du, A.D., 1999, Re-Os dating of molybdenites in the Xiaoliugou W-(Mo) deposit in the northern Qilian Mountains and its geological significances: Geochimica et Cosmochimica Acta, v. 63, p. 1815–1818.
Mao, J.W., Pirajno, F., Xiang, J.F., Gao, J.J., Ye, H.S., Li, Y.F., and Guo, B.J., 2011, Mesozoic molybdenum deposits in the east Qinling-Dabie orogenic belt: Characteristics and tectonic settings: Ore Geology Reviews, v. 43, p. 264–293.
Marek, J.M., 2011, Technical report Endako molybdenum mine: Prepared for Thompson Creek Metals Company Inc., 103 p.
Markey, R., Stein, H.J., Hannah, J.L., Zimmeerman, A., Selby, D., and Creaser, R.A., 2007, Standardizing Re-Os geochronology: A new molybdenite reference material (Henderson, USA) and the stoichiometry of Os salts: Chemical Geology, v. 244, p. 74–87.
Masterman, G.J., Cooke, D.R., Berry, R.F., Clark, A.H., Archibald, D.A., Mathur, R., Walshe, J.L., and Durán, M., 2004, $^{40}Ar/^{39}Ar$ and Re-Os geochronology of porphyry copper-molybdenum deposits and related copper-silver veins in the Collahuasi district, northern Chile: Economic Geology, v. 99, p. 673–690.
Mathur, R., Ruiz, J., and Munizaga, F., 2000, Relationship between copper tonnage of Chilean base-metal porphyry deposits and Os isotope ratios: Geology, v. 28, p. 555–558.
——2001, Insights into Andean metallogenesis from the perspective of Re-Os analyses of sulfides: (http://www.cec.uchile.cl/~vmaksaev/S5_Mathur.pdf)
Mazurov, A.K., 1996, The Koktenkol stockwork W-Mo deposit, central Kazakhstan, *in* Shatov, V., Seltmann, R., Kremenetsky, A., Lehmann, B., Popov, V., and Ermolov, P., eds., Granite-related ore deposits of central Kazakhstan and adjacent areas: St. Petersburg, Russia, Glagol Publishing House, p. 155–165.
McCandless, T.E., and Ruiz, J., 1993, Rhenium-osmium evidence for regional mineralization in southwestern North America: Science, v. 261, p. 1282–1286.
McCandless, T.E., Ruiz, J., and Campbell, A.R., 1993, Rhenium behavior in molybdenite in hypogene and near-surface environments: Implications for Re-Os geochronometry: Geochimica et Cosmochimica Acta, v. 57, p. 889–905.
McLemore, V.T., 2010, Beryllium resources in New Mexico and adjacent areas: New Mexico Bureau of Geology and Mineral Resources Open-file Report OF-533, 105 p.
Melfos, V., Voudouris, P., Arikas, K. and Vavelidis, M., 2001, Rhenium-rich molybdenites in Thracian porphyry Cu-Mo occurrences, NE Greece: Bulletin of the Geological Society of Greece, v. 34, p. 1015–1022.
Meyer, C., and Hemley, J.J., 1967, Wall rock alteration, *in* Barnes, H.L., ed., Geochemistry of hydrothermal ore deposits: New York, Holt, Rinehart, and Winston, Inc., p. 166–235.
Meyer, C., Shea, E.P., Goddard, C.C., Jr., and staff, 1968, Ore deposits at Butte, Montana, *in* Ridge, J.D., ed., Ore Deposits of the United States, 1933–1967 (Graton-Sales volume): New York, American Institute of Mining, Metallurgical, and Petroleum Engineers, v. 2, p. 1373–1416.
Mihalynuk, M.G., and Heaman, L.M., 2002, Age of mineralized porphyry at the Logtung deposit W-Mo-Bi-Be (beryl, aquamarine), northwest BC: British Columbia Geological Survey, Geological Fieldwork 2001, Paper 2002-1, p. 35–40.
Millensifer, T.A., Sinclair, W.D., Jonasson, I.R., and Lipmann, A., 2013. Rhenium, *in* Gunn, A.G., ed., Critical metals handbook: American Geophysical Union, p. 340–360.
Misra, K.C., 2000, Understanding mineral deposits: Netherlands, Kluwer Academic Publishers, 845 p.
Moats, M., Davenport, W., Demetrio, S., Robinson, T., and Karcas, G., 2007, Electrolytic copper refining—2007 world tankhouse operating data: Copper Electrorefining and Electrowinning, International Copper-Cobre Conference, 6th, Toronto, Ontario, Canada, Proceedings, v. 5, p. 195–241.
Mosher, G.Z., 2001, Technical report on the Nithi Mountain molybdenum property, British Columbia, Canada: Report to Leeward Capital Corp., 50 p. http://leewardcapital.com/NewsFiles/1192110100-REP-L0001-00%20FINAL.pdf; accessed 4-2013.
Moss, R.L., Tzimas, E., Kara, H., Willis, P., and Kooroshy, J., 2011, Critical metals in strategic energy technologies: European Commission, Joint Research Centre Institute for Energy and Transport Technical Report EUR 24884 EN, 162 p.
Mutschler, F.E., Griffen, M.E., Stevens, S.D., and Shannon, S.S., 1985, Precious metal deposits related to alkaline rocks in the north American Cordillera—an interpretive review: Geological Society of South Africa Transactions, v. 88, p. 355–377.
Nadler, H.-G., 1997, Rhenium, *in* Habashi, Fathi, ed., Handbook of extractive metallurgy: Weinheim, Wiley-VCH, v. III, p. 1491–1501.
Nanjari, M.A., 2009, Historical review of unconventional sources of uranium in northern Chile: Vienna, International Atomic Energy Agency, Technical Meeting on Uranium Form Unconventional Resources, Nov. 4-6, 2009, Powerpoint presentation slides, http://www.iaea.org/OurWork/ST/NE/NEFW/documents/RawMaterials/TM_Vienna2009/presentations/20_Arancibia_Chile.pdf (accessed 12/14/12).
National Research Council, 2008, Minerals, critical minerals, and the U.S. economy: Washington, D.C., National Academy Press, 264 p.
Newberry, R.J.J., 1979a, Polytypism in molybdenite (I): A non-equilibrium, impurity-induced phenomenon: American Mineralogist, v. 64, p. 758–767.

——1979b, Polytypism in molybdenite (II): Relationships between polytypism, ore deposition/alteration stages and rhenium contents: American Mineralogist, v. 64, p. 768–775.
Nicolaidou, A.E., 1998, Selenium content in sulfide ores from the Chalkidiki peninsula, Greece: Journal of Environmental Pathology, Toxicology and Oncology, v. 17, p. 189.
Noble, S.R., Spooner, E.T.C., and Harris, F.R., 1995, Logtung—a porphyry W-Mo deposit in the southern Yukon: Canadian Institute of Mining, Metallurgy, and Petroleum Special Volume 46, p. 732–746.
Northern Dynasty Minerals Ltd., 2011, Preliminary assessment of the Pebble project, southwest Alaska: Document 1056140100-REP-R0001-00, 579 p.
Northisle Copper and Gold Inc., 2012, Updated resource report for the Hushamu deposit, northern Vancouver Island, British Columbia, Canada: NI-43-101 report, 86 p. http://www.northisle.ca/i/pdf/techreports/NI43-101-Updated_Resource_Report_Hushamu_Deposit_2012.pdf (accessed 4/25/13)
Ohta, E., 1995, Common features and genesis of tin-polymetallic veins: Resource Geology Special Issue 18, p. 187–195.
Osoria, A.H., Leija, N.V., and Esquivel, R., 1991, Economic geology of the Inguaran mining district, Michoacan: Geological Society of America, The Geology of North America, v. P-3, p. 365–368.
Ossandón C, G., Fréraut C, R., Gustafson, L.B., Lindsay, D.D., and Zentilli, M., 2001, Geology of the Chuquicamata mine: A progress report: Economic Geology, v. 96, p. 249–270.
Overstreet, W.C., 1967, The geologic occurrence of monazite: U.S. Geological Survey Professional Paper 530, 327 p.
Pašava, J., Vymazalova, A., Košler, J., Koneev, R.I., Jukov, A.V., and Khalmatov, R.A., 2010, Platinum-group elements in ores from the Kalmakyr porphyry Cu-Au-Mo deposit, Uzbekistan: Bulk geochemical and laser abalation ICP-MS data: Mineralium Deposita, v. 45, p. 411–418.
Perelló, J., Brockway, H., and Martini, R., 2004, Discovery and geology of the Esperanza porphyry copper-gold deposit, Antofagasta region, northern Chile: Society of Economic Geologists Special Publication 11, p. 167–186.
Pettke, T., Oberli, F., and Heinrich, C.A., 2010, The magma and metal source of giant porphyry-type ore deposits, based on lead isotope microanalysis of individual fluid inclusions: Earth and Planetary Science Letters, v. 296, p. 267–277.
Pilet, S., Baker, M.B., and Stolper, E.M., 2008, Metasomatized lithosphere and the origin of alkaline lavas: Science, v. 320, p. 916–919.
Phillips, C.H., and Krahulec, K., 2006, Geology and history of the Bingham mining sistrict, Salt Lake County, Utah: Utah Geological Association Publication 32, p. 6–41.
Polyak, D.E., 2013, Rhenium: U.S. Geological Survey, 2011 Minerals Yearbook, 6 p. http://minerals.usgs.gov/minerals/pubs/commodity/rhenium/myb1-2011-rheni.pdfaccessed 4/25/2013.
Plumlee, G.S., 1999, The environmental geology of mineral deposits: Reviews in Economic Geology, v. 6A, p. 71–116.
Proffett, J.M., Jr., 2003, Geology of the Bajo de la Alumbrera porphyry copper-gold deposit, Argentina: Economic Geology, v. 98, p. 1535–1574.
Quaterra Resources Inc., 2008, Quaterra acquires Cave Peak molybdenum prospect in Texas, http://quaterra.com/news/new_releases_2008/index.php?&content_id=142 (accessed 4/30/13)
Redmond, P.B., and Einaudi, M.T., 2010, The Bingham Canyon porphyry Cu-Mo-Au deposit. I. Sequence of intrusions, vein formation, and sulfide deposition: Economic Geology, v. 105, p. 43–68.
Reich, M., Deditius, A., Chryssoulis, S., Li, J.W., Ma, C.Q., Parada, M.A., Barra, F., and Mittermayr, F., 2013, Pyrite as a record of hydrothermal fluid evolution in a porphyry copper system—a SIMS/EMPA trace element study: Geochimica et Cosmochimica Acta, v. 104, p. 42–62.
Rempel, K.U., Migdisov, A.A., and Williams-Jones, A.E., 2006, The solubility and speciation of molybdenum in water vapour at elevated temperatures and pressures: Implications for ore genesis: Geochimica et Cosmochimica Acta, v. 70, p. 687–696.
Rempel, K.U., Williams-Jones, A.E., and Migdisov, A.A., 2008, The solubility of molybdenum dioxide and trioxide in HCl-bearing water vapour at 350 degrees C and pressures up to 160 bars: Geochimica et Cosmochimica Acta, v. 72, p. 3074–3083.
——2009, The partitioning of molybdenum(VI) between aqueous liquid and vapour at temperatures up to 370 degrees C: Geochimica et Cosmochimica Acta, v. 73, p. 3381–3392.
Richards, J.P., 2003, Tectono-magmatic precursors for porphyry Cu-(Mo-Au) deposit formation: Economic Geology, v. 98, p. 1515–1533.
——2009, Post-subduction porphyry Cu-Au and epithermal Au deposits—products of remelting of subduction modified lithosphere: Geology, v. 37, p. 247–250.
——2011, Magmatic to hydrothermal metal fluxes in convergent and collided margins: Ore Geology Reviews, v. 40, p. 1–26.
Roedder, E., 1971, Fluid inclusion studies on the porphyry-type ore deposits at Bingham, Utah, Butte, Montana, and Climax, Colorado: Economic Geology, v. 66, p. 98–118.
Romero, K.S., Wong, C., Barra, F., Véliz, W., and Ruiz, J., 2010, Molybdenite mineralization and Re-Os geochronology of the Escondida and Escondida Norte porphyry deposits, northern Chile: Resource Geology, v. 61, p. 91–100.
Rosera, J.M., Coleman, D.S., and Stein, H.J., 2013, Re-evaluating genetic models for porphyry Mo mineralization at Questa, New Mexico: Implications for ore deposition following silicic ignimbrite eruption: Geochemistry, Geophysics, and Geosystems, v. 14, doi:10.1002/ggge.20048.
Rudnick, R.L. and Gao, S., 2003, The composition of the continental: Treatise on Geochemistry, v. 3, p. 1–64.
Ruiz, J., and Mathur, R., 1999, Metallogenesis in continental margins: Re-Os evidence from porphyry copper deposits in Chile: Reviews in Economic Geology, v. 12, p. 59–72.
Rusk, B.G., Reed, M.H., and Dilles, J.H., 2008, Fluid inclusion evidence for magmatic-hydrothermal fluid evolution in the porphyry copper-molybdenum deposit at Butte, Montana: Economic Geology, v. 103, p. 307–334.
Schwartz, M.O., 1995, Arsenic in porphyry copper deposits: Economic geology of a polluting element: International Geology Review, v. 37, p. 9–25.
Seedorff, E., and Einaudi, M.T., 2004, Henderson porphyry molybdenum system, Colorado: I. Sequence and abundance of hydrothermal mineral assemblages, flow paths of evolving fluids, and evolutionary style: Economic Geology, v. 99, p. 3–37.
Seedorff, E., Dilles, J.H., Proffett, J.M., Jr., Einaudi, M.T., Zurcher, L., Stavast, W.J.A., Johnson, D.A., and Barton, M.D., 2005, Porphyry deposits—characteristics and origin of hypogene features: Economic Geology 100th Anniversary Volume, p. 251–298.
Selby, D., and Creaser, R.A., 2001, Re-Os geochronology and systematics in molybdenite from the Endako porphyry molybdenum deposit, British Columbia, Canada: Economic Geology, v. 96, p. 197–204.
Selby, D., Nesbitt, B.E., Muehlenbachs, K., and Prochaska, W., 2000, Hydrothermal alteration and fluid chemistry of the Endako porphyry molybdenum deposit, British Columbia: Economic Geology, v. 95, p. 183–202.
Selenium and Tellurium Development Association, 2013, http://www.stda.org/se-te.htm (accessed April 23, 2013).
Seo, J.H., Guillong, M., and Heinrich, C.A., 2012, Separation of molybdenum and copper in porphyry deposits: the roles of sulfur, redox, and pH in ore mineral deposition at Bingham Canyon: Economic Geology, v. 107, p. 333–356.
Sharp, J.E., 1979, Cave Peak, a molybdenum-mineralized breccia pipe complex in Culberson County, Texas: Economic Geology, v. 74, p. 517–534.
Sillitoe, R.H., 1972, A plate tectonic model for the origin of porphyry copper deposits: Economic Geology, v. 67, p. 184–197.
——1979, Some thoughts on gold-rich porphyry copper deposits: Mineralium Deposita, v. 14, p. 161–174.
——1980, Types of porphyry molybdenum deposits: Mining Magazine, v. 142, p. 550–553.
——1983, Unconventional metals in porphyry deposits, *in* Shanks, W. C., III, ed., Cameron volume on unconventional mineral deposits: New York, Society of Mining Engineers of AIME, p. 207–221.
——1993, Gold-rich porphyry copper deposits: Geological model and exploration implications: Geological Association of Canada Special Paper 40, p. 465–478.
——2000, Gold-rich porphyry deposits: Descriptive and genetic models and their role in exploration and discovery: Reviews in Economic Geology, v. 13, p. 315–344.
——2005, Supergene oxidized and enriched porphyry copper and related deposits: Economic Geology 100th Anniversary Volume, p. 723–768.
——2010, Porphyry copper systems: Economic Geology, v. 105, p. 3–41.
Sillitoe, R.H., and Perelló, J., 2005, Andean copper province: Tectonomagmatic settings, deposit types, metallogeny, exploration, and discovery: Economic Geology 100th Anniversary Volume, p. 845–890.
Simon, G., and Essene, E.J., 1996, Phase relations among selenides, sulfides, tellurides and oxides: I. Thermodynamic properties and calculated equilibria: Economic Geology, v. 91, p. 1183–1208.

Simon, G., Kesler, S.E., and Essene, E.J., 1997, Phase relations among selenides, sulfides, tellurides, and oxides: II. Applications to selenide-bearing ore deposits: Economic Geology, v. 92, p. 468–484.
Sinclair, W.D., 2007, Porphyry deposits: Geological Association of Canada Special Publication 5, p. 223–243.
Sinclair, W.D., Kooiman, G.J.A., Martin, D.A., and Kjarsgaard, I.M., 2006, Geology, geochemistry and mineralogy of indium resources at Mount Pleasant, New Brunswick, Canada: Ore Geology Reviews, v. 28, p. 123–145.
Sinclair, W.D., Jonasson, L.R., Kirkham, R.V., and Soregaroli, A.E., 2009, Rhenium and other platinum-group metals in porphyry deposits: Geological Survey of Canada, Open File 6181, 1 sheet.
Singer, D.A., Mosier, D.L., and Menzie, W.D., 1993, Digital grade and tonnage data for 50 types of mineral deposits: U.S. Geological Survey Open-File Report 93-280, 1 computer disk.
Singer, D.A., Berger, V.I., and Moring, B.C., 2008, Porphyry copper deposits of the world—database and grade and tonnage models, 2008: U.S. Geological Survey Open- File Report 2008-1155, 45 p., http://pubs.usgs.gov/of/2008/1155/.
Soregaroli, A.E., 1975, Important characteristics of some Canadian Cordillera porphyry deposits: Current Research, Geological Survey of Canada, Paper 75-1, Pt. B, p. 59–62.
Sotnikov, V.I., Berzina, A.N., Economou-Eliopoulos, M., and Eliopoulos, D.G., 2001, Palladium, platinum and gold distribution in porphyry Cu ± Mo deposits of Russia and Mongolia: Ore Geology Reviews, v. 18, p. 95–111.
Stein, H.J., 2006, Low-rhenium molybdenite by metamorphism in northern Sweden—recognition, genesis, and global implications: Lithos, v. 87, p. 300–327.
Stein, H.J., Markey, R.J., Morgan, J.W., Hannah, J.L., and Schersten, A., 2001, The remarkable Re-Os chronometer in molybdenite: How and why it works: Terra Nova, v. 13, p. 479–486.
Sun W., Bennett V.C., Eggins S.M., Kamenetsky V.S., and Arculus R.J., 2003, Evidence for enhanced mantle to crust rhenium transfer from undegassed arc magmas: Nature, v. 422, p. 294–297.
Sun, W., Bennet, V.C., and Kamenetsky, V.S., 2004, The mechanism of Re enrichment in arc magmas—evidence from Lau basin basaltic glasses and primitive melt inclusions: Earth and Planetary Science Letters, v. 222, p. 101–114.
Sutulov, A., 1974, Copper porphyries: Salt Lake City, University of Utah Printing Services, 200 p.
Tarkian, M., and Koopmann, G., 1995, Platinum-group minerals in the Santo Tomas II (Philex) porphyry copper-gold deposit, Luzon Island, Philippines: Mineralium Deposita, v. 30, p. 39–47.
Tarkian, M., and Stribrny, B., 1999, Platinum-group elements in porphyry copper deposits: A reconnaissance study: Mineralogy and Petrology, v. 65, 161–183.
Tarkian, M., Hunken, U., Tokakchieva, M., and Bogdanow, B., 2003, Precious-metal distribution and fluid inclusion petrography of the Elatsite porphyry copper deposit, Bulgaria: Mineralium Deposita, v. 38, p. 261–281.
Taylor, R.D., Hammarstrom, J.M., Piatak, N.M., and Seal, R.R., 2012, Arc-related porphyry molybdenum deposit model: U.S. Geological Survey Scientific Investigations Report 2010-5070-D, 64 p.
Taylor, S.R., and McLennan, S.M., 1995, The geochemical evolution of the continental crust: Reviews of Geophysics, v. 33, p. 241–265.
Thompson, J.F.H., Lang, J.R., and Stanley, C.R., 2001, Platinum group elements in alkaline porphyry deposits, British Columbia: Exploration and Mining in British Columbia, Mines Branch, Pt. B, p. 57–64.
Todorov, T., and Staikov, M., 1985, Rhenium content in molybdenite from ore mineralizations in Bulgaria: Geologica Balcanica, v. 15, p. 45–58.
Tokmakchieva, M., 1999, Bornite mineralization in the content of copper deposits in our country: Geology and Mineral Resources, No. 8-9, p. 40–44.
——2002, Valuable minor components in the composition of porphyry copper deposits: Annual of the University of Mining and Geology "St. Ivan Rilski," Sofia, Bulgaria, v. 45, pt. 1, p. 71–75.
Tosdal, R.M., and Richards, J.P., 2001, Magmatic and structural controls on the development of porphyry copper ±Mo ±Au deposits: Reviews in Economic Geology, v. 14, p. 157–181.
Ulrich, T., and Heinrich, C.A., 2002, Geology and alteration geochemistry of the porphyry Cu-Au deposit at Bajo de la Alumbrera, Argentina: Economic Geology, v. 97, p. 1865–1888.
Valenica, V.A., Ruiz, J., Barra, F., Geherls, G., Ducea, M., Titley, S.R., and Ochoa-Landin, L., 2005, U-Pb zircon and Re-Os molybdenite geochronology from La Caridad porphyry copper deposit: Insights for the duration of magmatism and mineralization in the Nacozari district, Sonora, Mexico: Mineralium Deposita, v. 40, p. 175–191.
van Leeuwen, T.M., Taylor, R., Coote, A., and Longstaffe, F.J., 1994, Porphyry molybdenum mineralization in a continental collision setting at Malala, northwest Sulawesi, Indonesia: Journal of Geochemical Exploration, v. 50, p. 279–315.
Voudouris, P.C., Melfos, V., Spry, P.G., Kartal, T., Arikas, K., Moritz, R., and Ortelli, M., 2009, Rhenium-rich molybdenite and rheniite in the Pagonia Rachi Mo-Cu-Te-Ag-Au prospect, northern Greece: Implications for the Re geochemistry of porphyry-style Cu-Mo and Mo mineralization: Canadian Mineralogist, v. 47, p. 1013–1036.
Wallace, S.R., Muncaster, N.K., Jonson, D.C., MacKenzie, W.B., Bookstrom, A.A., and Surface, V.E., 1968, Multiple intrusion and mineralization at Climax, Colorado, *in* Ridge, J.D., ed., Ore deposits of the United States, 1933–1967 (Graton-Sales volume): New York, American Institute of Mining, Metallurgical, and Petroleum Engineers, p. 605–640.
Watanabe, Y., and Stein, H.J., 2000, Re-Os ages for the Erdenet and Tsagaan Suvarga porphyry Cu-Mo deposits, Mongolia, and tectonic implications: Economic Geology, v. 95, p. 1537–1542.
Watterson, J.R., Gott, G.B., Neuerburg G.J., Lakin, H.W., and Cathrall, J.B., 1977, Tellurium, a guide to mineral deposits: Journal of Geochemical Exploration, v. 8, p. 31–48.
Westra, G., and Keith, S.B., 1981, Classification and genesis of stockwork molybdenum deposits: Economic Geology, v. 76, p. 844–873.
White, W.H., and MacKenzie, W. B., 1974, Hydrothermal alteration associated with the Henderson molybdenite deposit, Colorado [abs.]: Economic Geology, v. 68, p. 142.
White, W.H., Bookstrom, A.A., Kamilli, R.J., Ganster, M.W., Smith, R.P., Ranta, D.E., and Steininger, R.C., 1981, Character and origin of Climax-type molybdenum deposits: Economic Geology 75th Anniversary Volume, p. 270–316.
Williams-Jones, A.E., and Heinrich, C.A., 2005, Vapor transport of metals and the formation of magmatic-hydrothermal ore deposits: Economic Geology, v. 100, p. 1287–1312.
Wolfe, W.J., 1995, Exploration and geology of the Quartz Hill molybdenum deposit, southeast Alaska: Geological Society of the Canadian Institute of Mining, Metallurgy and Petroleum (CIM) Special Volume 46, p. 764–770.
Xie, G.-Q., Mao, J.-W., Li, R.-L., Qu, W.-J., Pirajno, F., and Du, A.-D., 2007, Re-Os molybdenite and Ar-Ar phlogopite dating of Cu-Fe-Au-Mo (W) deposits in southeastern Hubei, China: Mineralogy and Petrology, v. 90, p. 249–270.
Xiong, Y., and Wood, S., 2001, Hydrothermal transport and deposition of rhenium under subcritical conditions (up to 200°C) in light of experimental studies: Economic Geology v. 96, p. 1429–1444.
——2002, Experimental determination of the hydrothermal solubility of ReS_2 and the Re-ReO_2 buffer assemblage and transport of rhenium under supercritical conditions: Geochemical Transactions, v. 3, p. 1–10.
Xu, X.C., Lou, J.W., Xie, Q.Q., Xiao, Q., Liang, J., and Lu, S.M., 2011, Geochronology and tectonic setting of Pb-Zn-Mo deposits and related igneous rocks in the Yinshan region, Jinzhai, Anhui province, China: Ore Geology Reviews, v. 43, p. 132–141.
Yudovskaya, M.A., Tessalina, S., Distler, V.V., Chaplygin, I.V., Chugaev, A.V., and Dikov, Y.P., 2008, Behavior of highly-siderophile elements during magma degassing: A case study at the Kudryavy volcano: Chemical Geology, v. 248, p. 318–341.
Zeng, Q.D., Liu, J.-M., Chu, S.-X., Want, Y.-B., Sun, Yan, Duan, X.-X., Zhou, L.L., and Qu, W.-J., 2013, Re-Os and U-Pb geochronology of the Duobaoshan porphyry Cu-Mo-(Au) deposit, northeast China, and its geological significance: Journal of Asian Earth Sciences, v. 79, p. 895–909.
Zhao, Y.M, Bi, C.S., and Zhang, D.Q., 1997, The Re-Os isotopic age of molybdenite from Duobaoshan and Tongshan porphyry copper (molybdenum deposits: Acta Geoscientica Sinica, v. 18, p. 61–67.
Zheng, Q., Liu, J., Qin, F., and Zhang, Z., 2010, Geochronology of the Xiaodonggou porphyry Mo deposit in northern margin of North China craton: Resource Geology, v. 60, p. 192–202.

©2016 Society of Economic Geologists, Inc.
Reviews in Economic Geology, v. 18, pp. 165–193

Chapter 8

Rare-Element Granitic Pegmatites

David London†

School of Geology & Geophysics, University of Oklahoma, 100 East Boyd Street, Room 710, Sarkeys Energy Center, Norman, Oklahoma 73019

Abstract

Rare-element granitic pegmatites represent highly concentrated sources of rare metals, including Li, Rb, Cs, Be, Sn, Nb, Ta, Zr, Y, REE, and U. In today's markets, pegmatites are the principal sources of Ta, and one pegmatite (Tanco, Canada) is the sole commercial producer of Cs for use as deep drilling fluid in the form of Cs formate solution. Growth in the demand for Li-based batteries has prompted exploration for spodumene- and petalite-bearing pegmatites, and several new Canadian prospects are slated for mining. Pegmatite bodies that contain minerals in which these elements are essential structural constituents constitute less than ~1 to 2% of all pegmatites in a given pegmatite-bearing terrane, and the economic production from many such bodies is limited by their small size (i.e., they may be economic in grade, but not for mechanized mining). Because pegmatites are found in cratons and orogenic belts, however, pegmatite-hosted resources are widespread and likely to be significant secondary, if not primary sources of rare metals for local economies or in times of disruption of global supplies from other types of deposits.

Pegmatites are primarily igneous in origin, and the most likely processes that enrich them in rare elements include crystal-melt fractionation together with the creation of locally flux- and rare-element-enriched domains of melt in otherwise rather ordinary granitic melt. The mechanism of constitutional zone refining, in which fluxes and incompatible components are enriched in a boundary layer of melt adjacent to crystal growth fronts, represents the most effective means of concentrating rare elements. Whereas Rayleigh fractionation produces an exponential increase in the abundances of incompatible rare elements, constitutional zone refining leads to a sharp, "L"-shaped inflection in the concentration of incompatible elements with the progress of crystallization. The absolute concentrations of trace elements at the end of constitutional zone refining can be orders of magnitude greater that those that are attainable by Rayleigh fractionation (between mineral and bulk melt). In rare-element pegmatites, some trace-element enrichment patterns show the gradual increase in abundance that is expected of Rayleigh fractionation, whereas pegmatites in which the transition from ordinary mineral assemblages to those enriched in rare elements is sharply defined, more closely match the elemental fractionation that is derived from constitutional zone refining.

Although pegmatites are igneous, pegmatite-forming melts crystallize well below their liquidus, and perhaps even below solidus temperatures. The textures and zonation that are hallmarks of pegmatites arise in response to the inception of crystallization from highly undercooled, viscous melt. Graphic granite, the one texture that is unique to pegmatites, constitutes prima facie evidence of such conditions. The crystallization of rare-element minerals, such as beryl, spodumene, tantalite, and pollucite can also be reconciled to the low-temperature crystallization of melts.

Pegmatite-hosted ores are entirely endogenic, and many pegmatites exhibit little or no exogenic wall-rock alteration. Narrow and sporadic zones of alteration envelopes, unpredictable size in relationship to degree of fractionation, and sharply defined zonation of rare-element ores to inner units combine to make granitic pegmatites difficult targets for exploration.

Introduction

Pegmatites constitute small (by industry standards) but highly concentrated resources of industrial minerals, rare metals, and gem materials. As sources of feldspar, quartz, and mica for applications in glasses, ceramics, electronics, and fillers, large granitic pegmatites constitute nearly 100% minable rock (Glover et al., 2012). Minerals of rare metals occur in less than ~2% of pegmatites, and minable resources are found in a much smaller fraction of those (e.g., Černý, 1991a). The elements that are enriched in pegmatites to minable (ore) grades include Li, Cs, Be, Sn, Nb, Ta, U, Y, Zr, and REE. This large and diverse list of elements, together with significant enrichments in B, P, F, Rb, Bi, Hf, etc., make the most fractionated pegmatites also among the most mineralogically complex deposits on earth. In addition to the industrial minerals and critical metals described above, a very small proportion of the rare-element pegmatites culminate with miarolitic cavities that yield many of the world's finest and most valuable mineral specimens and colored gemstones (Simmons et al., 2012).

This manuscript reviews some of the past and current concepts of pegmatite formation, toward an understanding of those processes that foster the accumulation of rare elements to ore grades. The emphasis here is on deposits associated with pegmatites of granitic composition. Most pegmatites possess compositions close to the composition of granite at its thermal minimum or eutectic in the system $NaAlSi_3O_8$-$KAlSi_3O_8$-SiO_2, with deviations to peraluminous and to slightly alkaline compositions. Deposits associated with alkaline granites, syenites, and carbonatites normally contain some pegmatitic facies, but

† E-mail, dlondon@ou.edu

these are detailed elsewhere in this volume (Dostal, 2016; Verplanck et al., 2016).

Definitions

Pegmatites are essentially igneous rocks. This statement can be construed to mean that pegmatites are necessarily igneous in origin, or that they are mostly of igneous origin, but that hydrothermal processes may play a part in their formation. Both meanings are implied. Strictly speaking, pegmatites are defined by texture, not composition. Pegmatitic textures occur in most of the common (gabbroic and granitic) and uncommon (syenitic and carbonatitic) igneous rocks. Pegmatites are far more prevalent in granitic compositions than any others, for reasons that will be explained below. As used here, the term "pegmatite" will refer to those of granitic composition unless noted otherwise.

Whereas the common plutonic rocks form large bodies that are texturally and mineralogically homogeneous, pegmatites are precisely the opposite. They constitute small areas of segregation within their igneous sources, or dikes and small isolated bodies that intrude other igneous and metamorphic hosts (Fig. 1). Exceedingly coarse crystal size is the hallmark of pegmatites, but heterogeneity of textures, including variations in grain size and the anisotropy of rock fabrics, is more definitive. Pegmatitic textures are marked by sharp changes in crystal size (coarsening inward), abrupt zonation of mineral assemblages, prominently oriented crystal growth directions (inward-directed or radial), layered structures, and skeletal intergrowths of minerals (Fig. 2). A skeletal intergrowth of quartz and feldspars, termed "graphic granite" (Fig. 3), is the defining texture of pegmatites, and it is the only texture that is unique to pegmatites and that is not shared in common with hydrothermal veins. The graphic intergrowths arise through rapid crystallization of one phase (quartz or feldspar) from viscous silicate melt, with simultaneous saturation in the other along the growth front (Fenn, 1986). Graphic granite is solely igneous in origin and cannot be generated by precipitation from hydrothermal fluids (London, 2009). Graphic intergrowths between quartz-tourmaline, quartz-garnet, and phosphates (apatite, amblygonite, triphylite, etc.) with sodic plagioclase also are common.

Tectonic Environments

Pegmatites are associated with all of the known cratons and orogenic belts throughout geologic time (Tkachev, 2011). Important historic, current, and potential pegmatite resources have been found in every continent except Antarctica (Fig. 4), and this deficiency likely results from limited exposure and exploration. In association with orogenic belts, pegmatites arise from continental collision and partial melting of the crust (though this environment is less well defined for Precambrian rocks). However, crustal thickening in the absence of tectonism may bring low-melting metasedimentary rocks to anatectic conditions, which in turn generates granites that are capable of spawning pegmatites (Bea, 2012); pegmatites enriched in Sn, Li, and Ta in the Iberian peninsula appear to have formed by this mechanism.

Pegmatites and their source granites, where exposed, do not normally possess a pervasive foliation that might be indicative of syntectonic deformation. Therefore, orogenic pegmatites are mostly associated with a post-tectonic phase following crustal thickening after continental collisions (Tchakev, 2011; cf. Martin and De Vito, 2005). Sufficient heat to bring source rocks to their solidus temperatures follows from burial, and from a large amount of radiogenic heat that is produced from schists of sedimentary origin (Bea, 2012). Pegmatite belts of the Hindu Kush (Afghanistan and Pakistan) and along the entirety of the Appalachian orogen (United States) are

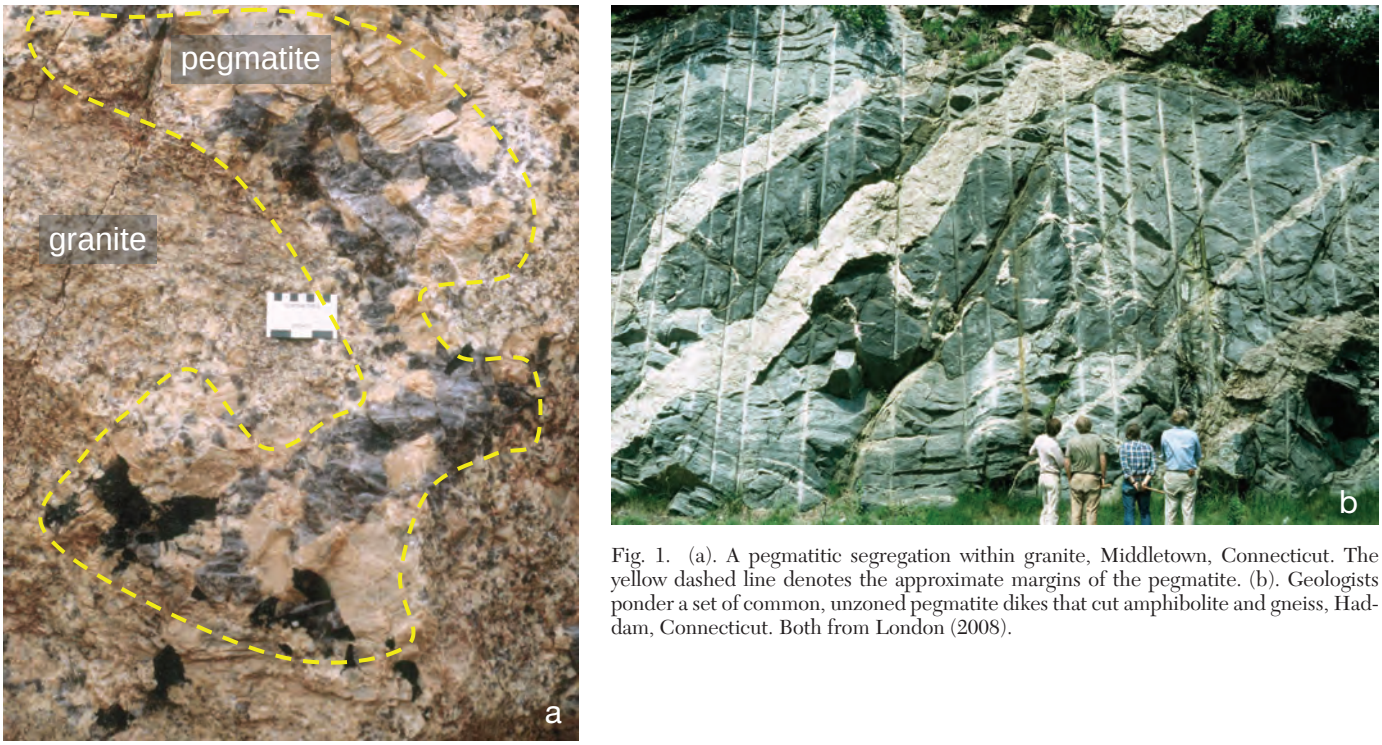

Fig. 1. (a). A pegmatitic segregation within granite, Middletown, Connecticut. The yellow dashed line denotes the approximate margins of the pegmatite. (b). Geologists ponder a set of common, unzoned pegmatite dikes that cut amphibolite and gneiss, Haddam, Connecticut. Both from London (2008).

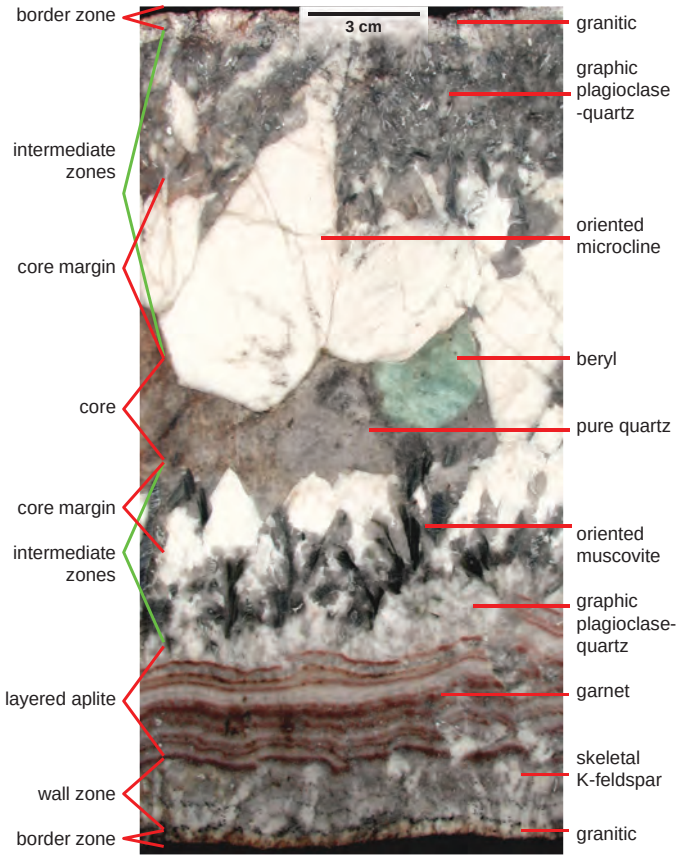

Fig. 2. Textural and zonal attributes of pegmatites. The image shows a complete section of a pegmatite dike, 28 cm thick, located near Palomar Mountain, San Diego County, California. Zonal portions of the dike are described on the left. Mineralogical features are listed on the right. From London and Kontak (2012).

representatives of pegmatites in a largely postcollisional tectonic setting.

Pegmatites (and their granites) are also associated with rifts within continents, or with extension in the back-arc regions of subduction zones along continental margins. Where this tectonic setting is known beyond a reasonable doubt, the associated pegmatites typically form very small but abundant segregations within their source plutons, but only rarely emanate from those plutons as dikes of any size. These pegmatites are commonly miarolitic (containing clay-filled or empty cavities), and many contain gem deposits of topaz, aquamarine beryl, optical-grade fluorite, and "morion," which refers to large, clear quartz crystals for use in optical or electronic applications. Pegmatites of this type include deposits at Gross Spitkoppe, Namibia (Frindt et al., 2004), and at Volodarsk, Ukraine (Lyckberg et al., 2009).

Fig. 3. Graphic granite, the defining texture of pegmatites, from the Little Three mine, Ramona, California, consists of a skeletal intergrowth of quartz and alkali feldspar. Graphic intergrowths between quartz-sodic plagioclase, quartz-tourmaline, quartz-garnet, and phosphates (apatite, amblygonite, triphylite, etc.) with plagioclase also are common in pegmatites.

Affiliations based on composition

Many pegmatite fields possess no known granitic sources. Going back into the Precambrian, tectonic environment becomes more equivocal. However, an affiliation has been established that associates pegmatites, by their chemistry, to certain granite types. In turn, those granite types can be linked to postcollisional or extensional tectonic environments, even where these may not be evident from regional geologic constructions.

Černý (1991a) introduced the notion of pegmatite "families," which recognizes distinctive trace-element enrichments in pegmatite groups (a group is a population of pegmatites that possess a common history or source). He proposed two families of pegmatites—"LCT" (for Li-Cs-Ta) and "NYF" (for Nb-Y-F)—that correspond to the two prevalent types of rare-element enrichments found in pegmatites.

Marine shales, which are the predominant component of clastic sediments, are the principal protoliths for the S-type granites (Chappell and White, 1992) and their associated LCT family of pegmatites. Compositional hallmarks of the S-type granites and their pegmatites include moderate to strongly peraluminous compositions (ASI or A/CNK values >1.1), a marked enrichment in (biogenic) phosphorus, and among the elements of the LCT family, a distinct enrichment in Cs (London, 2008), whose preconcentration in sediments comes by adsorption onto clay minerals that constitute a large fraction of marine shales (e.g., Wahlberg and Fishman, 1962). A high Li and Cs content relative to Rb is imparted during subsequent anatexis, and is controlled by the partitioning of Li, Rb, and Cs between alkali feldspar (and biotite) and granitic melt, in which Rb is more compatible in the crystalline phases than is either Li or Cs (London, 1995). The trend toward enrichment in Ta over Nb may be controlled partly by the solubilities of Nb and Ta oxides as functions of temperature (e.g., Linnen and Cuney, 2005), but the crystal/melt partition coefficients for Nb and Ta between common accessory minerals (titanite, ilmenite, etc.) and melts do not show a consistent trend of enrichment of one element over another. Pegmatites of the LCT family are also notably enriched in B, which may be adsorbed from seawater onto pelagic clays or may be hosted by tourmaline that forms strata-bound layers adjacent to deep marine hydrothermal vents (e.g., Jiang et al., 2000). This abundance contrasts with the low B content of mantle and most volcanogenic sources.

The NYF family of pegmatites is associated with A-type granites that are emplaced into rift zones within continents or in association with hot spots within continents (e.g., Eby,

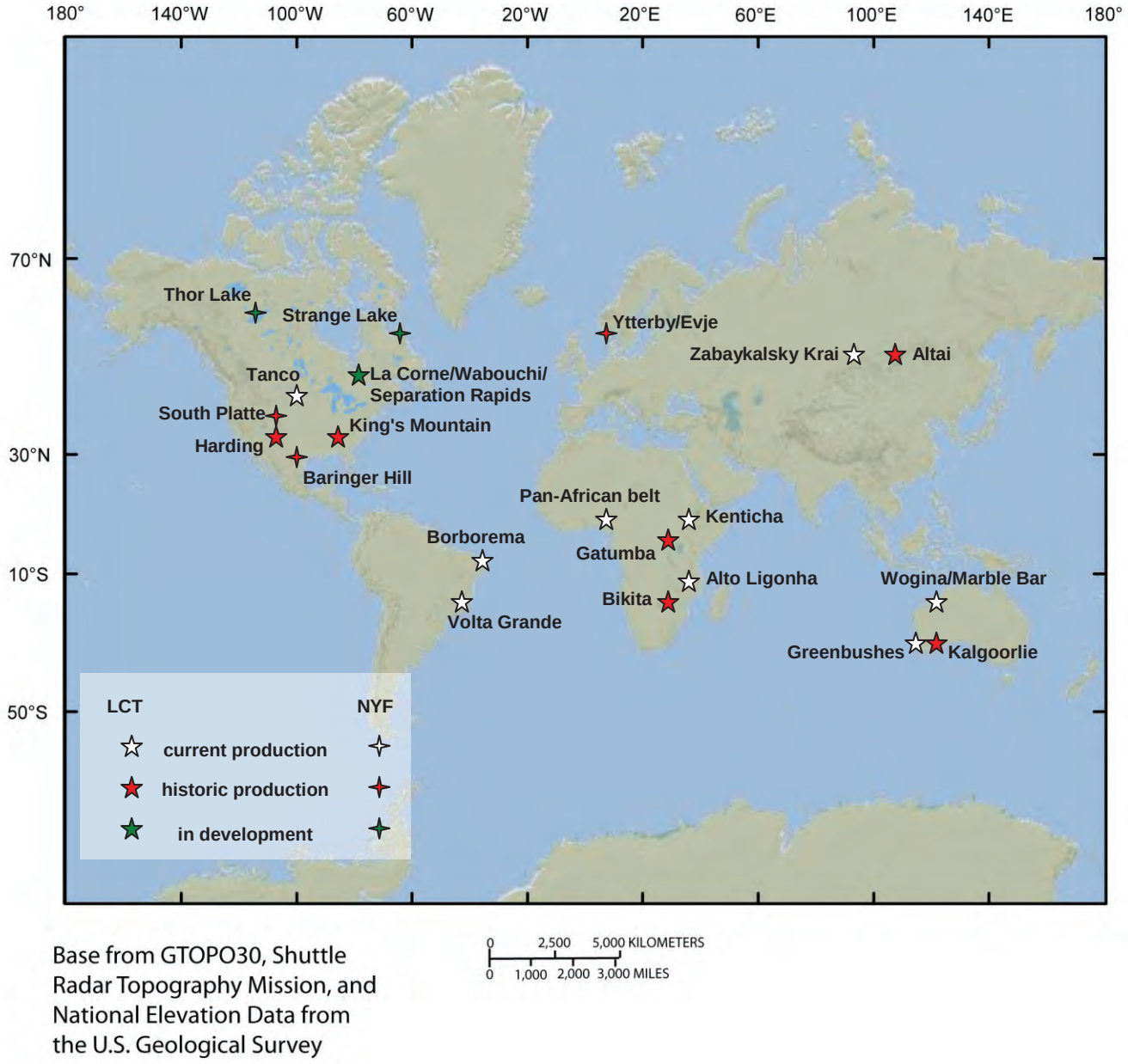

Fig. 4. The global distribution of some historically important, current, and potential future sources of rare elements from pegmatites. LCT stands for a lithium-cesium-tantalum signature of rare-element enrichment. Most current production from LCT pegmatites is for Ta, but Li, Cs, gem materials, and (historically) Be are important ores. Three new prospects in Canada are being developed for production of Li. NYF is short for niobium-yttrium-fluorine enrichment. These pegmatites have historically been mined for REE, but Zr, Nb, and U are potential ores. The NYF deposits include pegmatites that are associated with alkaline igneous rock suites.

1990). The "A" refers to "anorogenic," though crustal deformation associated with rifting is present. In this setting, A-type granites and layered gabbroic intrusions (or their volcanic equivalents) comprise a bimodal igneous suite, with contributions to the granites from mantle and crustal sources (e.g. Christiansen et al., 2007). The A-type granites and NYF pegmatites tend toward alkaline bulk compositions (they contain modal or normative aegirine), are notably low in phosphorus, and are enriched in heavy rare earth elements (HREE) and in F. Melting of amphiboles and biotite to pyroxene-quartz assemblages in the lower crust provides the likely source of F. In turn, the solubility of the HREE may be selectively enhanced in F-rich melts and fluids (e.g., Timm et al., 2011; Dalou et al., 2012), which may explain the enrichment in Y and HREE. It is not known, however, if the high Nb/Ta ratio arises from a characteristic enrichment at the source, or from mineral-melt fractionation within derivative magmas.

The vast majority of pegmatites, referred to as "simple" or "common" pegmatites (London, 2008) consist of nearly equal modal or normative proportions of sodic plagioclase, alkali feldspar, and quartz. Micas, both white (mostly muscovite) and dark (biotite) are major to minor constituents, and garnet,

tourmaline, mafic oxides or spinel, and apatite are common accessories. The common pegmatites lack the exotic minerals that are the basis for the classification of granitic pegmatites (Černý and Ercit, 2005). However, Černý's pegmatite families were never meant to apply to a single pegmatite body, but rather to a comagmatic pegmatite group in which only a few individual deposits evolve to show the chemical affinity of the group. In the absence of exotic minerals, geochemical trends in the abundances of trace elements contained by major and common accessory minerals usually point unambiguously to the chemical affinity or pegmatite family to which the entire group belongs (Černý et al., 1985).

Geologic Setting

Where pegmatites can be associated with their source granites, the pegmatites form segregations near the tops or margins of plutons. They do not arise from the centers of their source granites, and where such pegmatites occur as dikes well within the confines of granites, they are intrusive from another source. Segregations with pegmatitic textures accumulate upward, and coalesce into a pegmatitic carapace. The pegmatite groups that develop the LCT chemical signature and that originate from peraluminous granites tend to comprise a large fraction of the entire igneous complex, forming a thick pegmatitic carapace that emanates outward as a dense swarm of dikes into host rocks. Among the NYF pegmatites of Paleozoic age, whose tectonic setting and sources are comparatively well defined, the fraction of the entire magma body that develops pegmatitic texture is small, and the pegmatites mostly lie within their source pluton, rather than forming an extensive dike swarm around it (see Chapter 5 of London, 2008, for specific examples of each).

Pegmatite dike swarms close to their granitic source commonly occur as concentric ring systems rather than radial dikes (Fig. 5). Further from source, however, pegmatites have a tendency to follow large-scale deformation structures, including axial planes of folds or regional-scale faults (see examples in Černý, 1991b). There are exceptions to every point, and some pegmatite fields follow clearly delineated trends that bear no known relation to regional structures. The pegmatite field known as the Middletown district, Connecticut, is such a case. All of the regional ductile structure (derived from Acadian and Appalachian orogenies) strikes north-northeast. From a pegmatitic granite source northeast of Middletown, however, the pegmatite swarm strikes east-southeast, across the grain of all known ductile and brittle deformation structures (London, 1985).

Migration from source

The distance that pegmatite dikes can travel from source is poorly known. A kinematic model developed by Rubin (1995) led him to conclude that granite (pegmatite)-forming dikes leave their granite source only after a significant fraction of the heat contained by the main plutonic magma has dissipated into the surrounding rocks, and that small dikes cannot migrate past the thermal aureole of their granite source. Preheating is necessary to prevent a rapid increase in the viscosity of melt due to heat loss from dikes as they propagate outward. Therefore, the distance from source, and the consequent zonation of pegmatite bodies within a pegmatite group,

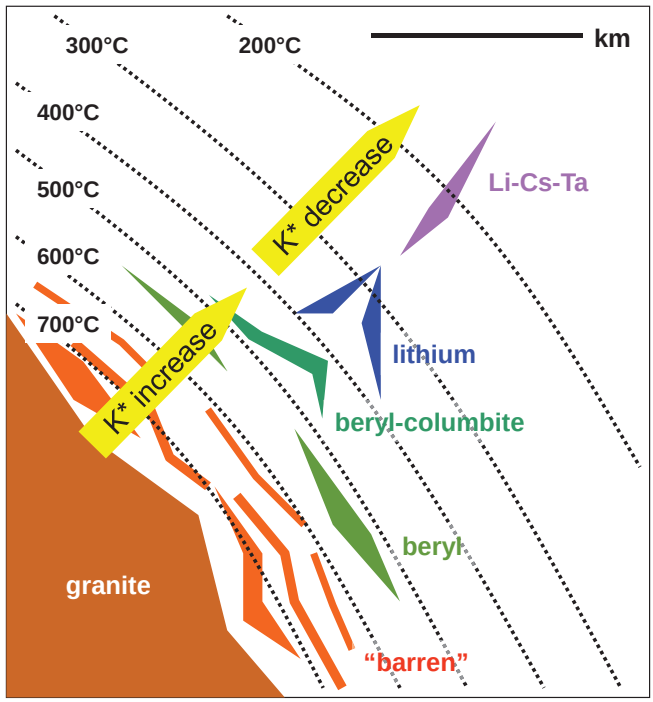

Fig. 5. Chemical evolution through an LCT pegmatite group with distance from the granitic source. A schematic plan (map) view of a granite source and surrounding pegmatite field. Common ("barren") pegmatites by the hundreds occur close to the pluton as a ring dike system. At distance, pegmatite bodies follow preexisting regional structures. Isotherms correspond to the approximate temperatures of host at the time of pegmatite emplacement. Values of K* (molar K/[K + Na] of whole rocks) initially increase from the granite to the less evolved but K-feldspar-rich rare-element pegmatites, then decrease outward to the sodic Li-Cs-Ta and albite-lepidolite/spodumene subtypes of rare-element pegmatites.

is correlated with the size and depth of their source intrusion. Deeper and larger intrusions foster emplacement farther from source than do smaller or shallow bodies. As a generality, the A-type granites that generate the NYF family of pegmatites are emplaced at shallow levels of ~2 to 4 km. Their pegmatites are mostly small, and mostly within or immediately adjacent to the granites themselves. The S-type granites that spawn LCT pegmatites are deeper (~8–12 km); consequently, a large proportion of their pegmatites are external to the granites, and those pegmatites may extend kilometers from source (e.g., Baker, 1998).

Zonation within pegmatite fields

Based mostly on exposures of pegmatite fields in the Canadian Shield province, Trueman and Černý (1982) proposed that the zonation of pegmatites followed a regular progression of fractionation from source (Fig. 5). Vlasov (1961) portrayed a similar evolution, in which distal pegmatites contained all of the major zonal assemblages as more proximal bodies, but with increasing development of chemically and texturally complex internal zones and hydrothermal overprint with distance from source (Fig. 6). The regional zonation of rare-element minerals in LCT pegmatite fields became the foundation of the classification scheme presented by Černý (1991a) and Černý and Ercit (2005), which is the classification that is in widespread use today.

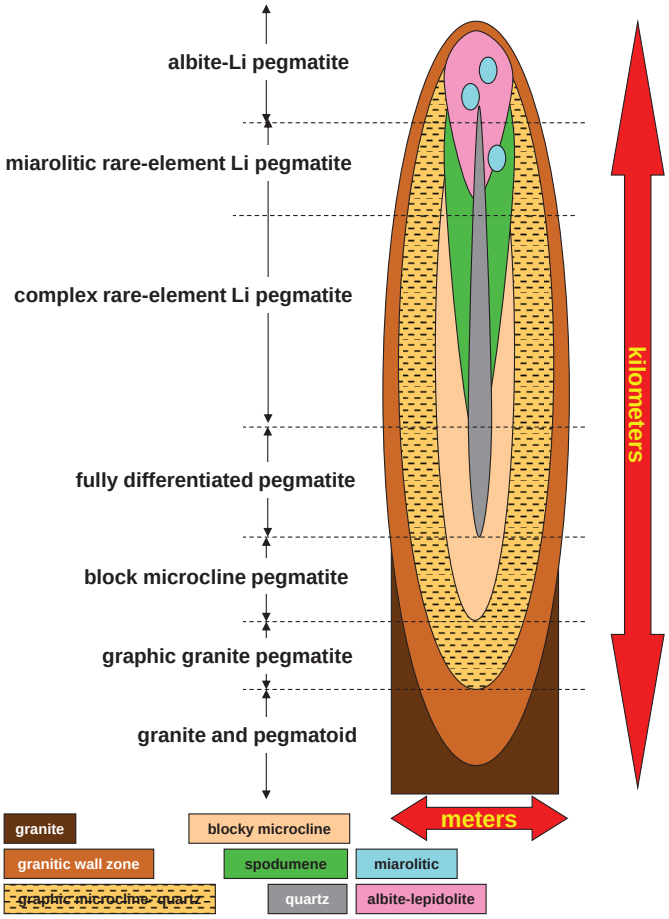

Fig. 6. Regional and internal zoning sequence of Vlasov (1961). From the granitic source, Vlasov (1961) recognized five textural-paragenetic types of pegmatites: type I: graphic (graphic microcline-quartz intergrowths), type II: block (coarse perthitic microcline cores), type III: fully differentiated (granitic borders, block microcline intermediate zones, quartz core), type IV: complex rare-element (Li-rich), and type V: albite-spodumene or albite-lepidolite. Modified from London (2008).

Taken together, the metamorphic aureoles associated with granitic plutons, and the regular zonation of pegmatites within that gradient, constitute a first-order basis for exploration. Ceramic pegmatites ("barren" in the classification of Černý, 1991a, as shown in Fig. 5), those mined for industrial materials, lie closest to source. Beryl-rich pegmatites appear rather abruptly outward from those (London, 2008, fig. 12-3). Then come lithium-rich pegmatites (sources of spodumene and petalite for ceramic, pharmaceutical, and solid-state battery applications: Kesler et al., 2012). The most distal pegmatites are those that carry mineralization in Sn, Ta, and Cs, in addition to Li and Be. These may be massive bodies, or rarely miarolitic (cavity-bearing), in which case they are more valuable as sources of gem and mineral specimens than as metal ores.

This zonation model applies to the LCT pegmatites, which appear to far outnumber those that are typed as NYF (Fig. 4). No comparable zonation model has been presented for the NYF family of pegmatites, as there are too few exposures of these, or else they are not so well studied.

Ore-Forming Processes

Pegmatites are sources of many different types of ores. The ceramic pegmatites ("barren" in the classification of Černý, 1991a, "common" in the nomenclature used by London, 2008) derive their ores by simple crystal fractionation from large masses of granitic magma. As those magmas fractionate, the feldspars evolve to low contents of Fe (imparting less color) and Ca (imparting a lower melting temperature), which makes them suitable for glasses and ceramics. Muscovite becomes coarse grained, lower in Fe (and hence lower in color) for use as sheet and scrap mica, joint tape compound, and cosmetics (e.g., see Glover et al., 2012). Quartz from pegmatites is suitable for glass-making, but with very few exceptions (e.g., the Spruce Pine district of North Carolina), pegmatitic quartz lacks the purity that is needed for electronic applications (see Chapter 4 of London, 2008, for a lengthier explanation).

Rare-element enrichment

Figure 7 is constructed to illustrate the spatial relationships of magma sources (region of partial melting), coalescence upward into a large granite pluton, with pegmatite dikes emanating from that. The abundances of various rare elements (Table 1) are also shown at each stage in the evolutionary process, ending with rare-element pegmatites.

The enrichment factors in rare-element pegmatites are large in magnitude (Table 2), but they are not atypical of

Table 1. Abundances of Selected Major, Minor, and Trace Elements in Continental Crust, Rhyolite Obsidians, and Pegmatites (ppm wt)

	(1)	(2)	(3)	(4)	(5)
Li		57	344	3440	3427
Na	28,000	32,000	34,100	30,400	28,236
K	26,000	34,500	36,900	29,300	24,572
Rb	90	156	1,370	1,160	5,212
Cs	3	6	40	580	2,641
Be	3	4	68	39	169
Mg	21,000	1,400	100	200	60
Ca	36,000	6,300	3,000	1,600	1,071
Sr	375	72	8	1	---
Ba	400	447	92	2	---
Fe*	50,000	12,444	5,056	4,044	124
Mn	950	542	<77	<464	1,394
Ti	4,400	2,997	<59	<12	45
Nb	20	32	81	51	56
Ta	2	3	37	24	300
Sn	2	4	21	200	128
B	10	---	143	1,924	217
P	1,050	131	357	2,528	3,748
F	625	1,200	8,000	13,000	1,220

(1): Average crustal abundance, ppm (Mason and Moore, 1982)
(2): Average abundance in subcalcic obsidians from continental margins and continental interiors, ppm (subset of 151 analyses in Macdonald et al., 1992, that include Be)
(3): A-type rhyolite: vitrophyre from Honeycomb Hills, Utah, ppm (Congdon and Nash, 1991)
(4): S-type rhyolite: green obsidian pebbles from) Macusani, Peru, ppm (London et al., 1988) except Sn (unpublished ion probe analysis)
(5): Tanco pegmatite, Manitoba (Stilling et al., 2006)
* = total Fe as Fe^{2+}

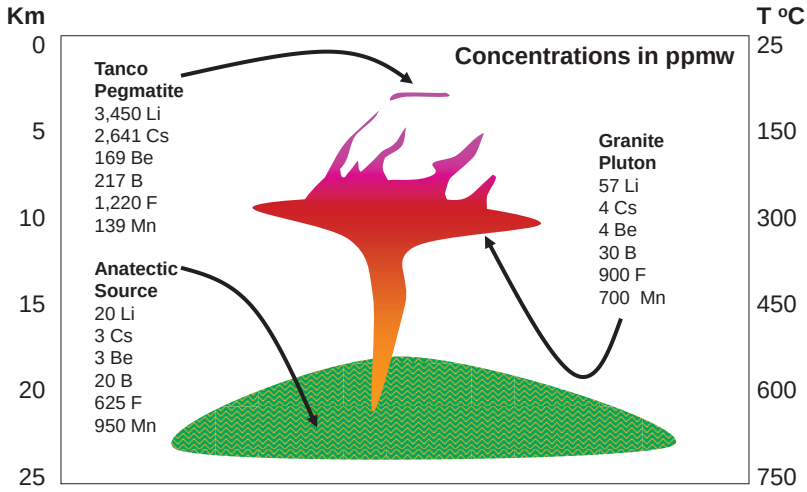

Fig. 7. Chemical fractionation from source to pegmatite. The abundances of several important trace elements found in rare-element pegmatites are traced from their crustal sources (Mason and Moore, 1982), through to large granitic plutons (data from Macdonald et al., 1992), through to a rare-element pegmatite, represented by the bulk composition of the Tanco deposit (Stilling et al., 2006).

other metal deposits. What is different in the formation of rare-element pegmatites (in comparison to hydrothermal base-metal deposits, which typically are large, open systems) is that pegmatites are produced essentially within a closed system, by chemical refinement of an ever-dwindling fraction of melt. Throughout this process, that residual melt is continuously extracted and coalesced. To appreciate how much earth material is involved, London (2008) used the Cs content of the Tanco pegmatite to estimate that the pegmatite deposit (<2 km^3) might have involved as much as 18,000 km^3 of rock in the initial partial melting event.

Chemical coherency of incompatible and volatile components

Tables 1 and 2 list most of the rare elements that are enriched through the pegmatite-forming process, excluding Ba, Sr, Fe, and Ti, which are depleted in pegmatites relative to granites (as represented by rhyolite obsidians). The rare elements in Tables 1 and 2 are, under most circumstances, incompatible in quartz and feldspars, which are the principal rock-forming minerals of pegmatites. Rare alkalis can be compatible in micas (Icenhower and London, 1995), and the high field-strength elements (HFSE, e.g., Sn, Nb, Ta) are normally compatible in oxides and in titanite (e.g. Linnen and Cuney, 2005). In order to be concentrated to form pegmatitic ores, either the abundances of micas and oxides are not sufficient to deplete (i.e., disperse) the rare alkalis and HFSE, or else the mineral-melt partition coefficients must decrease as crystallization proceeds. The mineral/melt partition coefficients depend both on the mineral structure (i.e., rules of diadochy) and on the structure of the melt as a function of its composition. Of the two, changes in melt composition are more likely to affect, and possibly lower, the mineral/melt partition coefficients.

Table 3 compiles a summary of element volatility in systems comprised of granitic melts (sensu lato) and aqueous fluid.

Table 2. Enrichment (incompatibility) Factors for Rhyolite Obsidians and Tanco Pegmatite (values are $C_i^{\text{rhyolite or pegmatite}}/C_i^{\text{crustal average}}$ from Table 1)

All obsidians		Spor Mtn vitrophyre		Macusani obsidian		Tanco	
Li	2.85	Be	22.67	Cs	193.33	Cs	880.34
Cs	2.00	Ta	18.50	Li	172.00	Li	171.34
Sn	1.80	Li	17.20	Sn	100.00	Ta	149.86
Rb	1.73	Rb	15.22	Be	13.00	Sn	63.80
Nb	1.60	Cs	13.20	Rb	12.89	Rb	57.91
Ta	1.40	Sn	10.50	Ta	12.05	Be	56.40
Be	1.33	Nb	4.04	Nb	2.57	Nb	2.80
K	1.33	K	1.42	K	1.13	Na	1.01
Na	1.14	Na	1.22	Na	1.09	---	---
Ba	1.12	---	---	---	---	K	0.95
---	---	Ba	0.23	Ca	0.04	Ca	0.03
Sr	0.19	Ca	0.08	Mg	0.01	Ba	---
Ca	0.18	Sr	0.02	Ba	0.00	Sr	---
Mg	0.07	Mg	0.00	Sr	0.00	Mg	0.00

Notes: All obsidians from Macdonald et al. (1992); Spor Mountain vitrophyre from Congdon and Nash (1991); Macusani obsidian from London et al. (1988); Tanco pegmatite from Stilling et al. (2006); columns are arranged by enrichment (incompatibility) increasing upward; horizontal line across columns separates compatible (below) from incompatible elements (above)

Table 3. Vapor/Melt Partition Coefficients at 200 MPa for Macusani Obsidian (London et al., 1988) and for Spor Mountain Vitrophyre (Webster et al., 1989).

	Macusani		Spor Mountain
T, °C:	775	650	850
Li	0.4	0.3	3.7
Rb	0.2	0.1	2.5
Cs	0.1	0.0	2.3
Be	0.2	0.2	0.9
Sr	0.4	0.5	0.0
Ba	0.8	1.1	0.0
Nb	0.0	0.1	0.0
Zr	0.0	0.2	0.0
Y	0.0	0.2	2.0
B	2.3	1.0	0.0
P	0.9	0.2	---
F	0.4	0.3	---

Notes: Macusani glass containing 0.045 wt % Cl was equilibrated with an equal volume of H_2O; Spor Mountain vitrophyre was equilibrated with 0.2 *m* NaCl solution (1.2 wt% NaCl)

Volatility is measured by the partition coefficient of an element between vapor/melt. The summary shows a few elements (B, Cs) that are significantly to moderately volatile ($D_i^{v/m}$ >1), whereas the HFSE are highly nonvolatile ($D_i^{v/m}$ «1). The data sources derive from experiments with the Macusani obsidian, Peru (London et al., 1988), which is an archetypal representative of the S-type/LCT association, and the Spor Mountain vitrophyre (Utah), which possesses a distinctly A-type signature (Webster et al., 1989). Both starting materials, Macusani obsidian and Spor Mountain vitrophyre, are peraluminous, F rich, and Cl poor. However, Cl was added to the experiments with Spor Mountain vitrophyre, which accounts for the higher volatility of some of its rare elements. Note that some components that are commonly referred to as volatiles are not (e.g., F, P). Jahns (1953) described the components of H, B, P, and F as "hyperfusible," rather than volatile, in reference to their fluxing effects on silicate-H_2O systems. These components will be described collectively as "fluxes" hereafter.

All of these elements exhibit chemical coherency in pegmatite-forming systems, meaning that they are all enriched together in the final products of pegmatites. These include volatile components like Cs and B, and nonvolatile components like Ta and Sn (Table 2). Saturation of melt in aqueous fluid fractionates volatile from nonvolatile elements. In order to maintain chemical coherency among volatile and nonvolatile components, an aqueous fluid phase cannot be liberated and removed from the magma system, at least up to the point of the formation of pegmatites.

Models based on the measured fractionation of Be and Cs between minerals and melt indicate that the average crustal granite must undergo >95% of crystal fractionation to achieve ore-grade concentrations of these elements (London, 2008). Based on the Rb and Cs contents of muscovite in the border zones of pegmatites, Jolliff et al. (1992) also concluded that ≥75% fractional crystallization of the Harney Peak granite was necessary to produce the trace-element signatures of the common pegmatites of the Black Hills district, South Dakota, and at least 90% of fractional crystallization of the source granite would be needed to generate the rare-element pegmatites. It is difficult to imagine that an aqueous fluid is not evolved from those same granitic magmas at a lesser extent of crystal fractionation, which would deplete subsequent melt fractions in B, Cs, and some significant proportion of Li, Rb, and Be. London (2008) described this disparity as one of the fundamental unknowns in igneous petrology.

Rare-element pegmatites by direct anatexis

Stewart (1978) appears to be the first petrologist to make a substantive case that the Li-rich rare-element pegmatites originate at the inception of anatexis, by a very small fraction of partial melting, rather than at the end of the granite-forming process. His argument was that the average Li content of granites is too low to yield the weight-percent levels of Li found in major spodumene or petalite-bearing pegmatites. Though lacking a Rayleigh fractionation model as his basis, Stewart (1978) also understood that only a very small fraction of granitic melt could achieve the concentrations needed to precipitate lithium aluminosilicates, and he doubted that this small fraction could be extracted from a granitic pluton.

The absence of a plutonic source and the trace-element signatures of some pegmatite groups have led others to propose that the most evolved pegmatites of some districts arose more or less directly from metasedimentary sources, without coalescence and extended crystal fractionation in a large, plutonic magma chamber. Shearer et al. (1992) proposed that the Li-rich pegmatites of the Black Hills district, South Dakota, might have formed by the anatexis of metasedimentary rocks similar to those that host the associated Harney Peak granite. They based this proposal on the lack of convergence between the trace-element contents of the Harney Peak granite and those of the pegmatites based on Rayleigh fractionation models (i.e., the same argument as that of Stewart, 1978). Roda-Robles et al. (1999) use the compositions of micas and feldspars to describe a model by which rare-element pegmatites are derived by limited fractionation of partial melts from quartzofeldspathic metamorphic sources.

Occurrences of rare-element pegmatites formed directly from a low melt fraction during anatexis of metamorphic rocks are not impossible, but they would be exceptional. It is now clear that under normal conditions, the rare-element pegmatites cannot arise by very low degrees of partial melting; that is, more or less directly by partial melting of a metamorphic protolith. Stewart (1978) assumed that partial melting and fractional crystallization are true equilibrium processes, and hence are perfectly reversible. Thus, if a small fraction of evolved melt could persist to uncommonly low temperatures, then the reverse should be true—that a rare-element-enriched melt could be produced by a small amount of partial melting at the same low-temperature condition. That presumption is incorrect. Bea (1996) demonstrated convincingly that the diffusion of trace elements within crystals is orders of magnitude slower than are the likely rates of melting and melt extraction from source. Therefore in the first-formed melts, the partition coefficients for trace elements ($D_i^{mineral/melt}$) are close to unity. Thus, it is not by chance that the trace-element contents of relatively unfractionated granites, represented by

rhyolite obsidians in Table 1, are only slightly more chemically evolved than is the average continental crust, and about the same as their abundances in metasediments and gneisses at anatectic conditions (e.g., Bebout et al., 2007). The fraction of melt produced at the onset of anatexis in juvenile crustal rocks is large, because the bulk compositions of such rocks (e.g., aluminous schists and felsic gneisses) do not lie far from the composition of the minimum melt (e.g., London, 2008, fig. 10-2; London et al., 2012a,). Consequently, at the lowest temperatures of anatexis, a rather large fraction of melt (~10 vol % or more) is produced in which the abundances of the trace elements (e.g., the rare alkalis, rare HFSE, etc.) are at or below their abundances in the starting protoliths. The first-formed melts are close to the hydrous minimum in a quartzofeldspathic system in composition, and hence in temperature of formation. Therefore, the incipient melting temperatures are ≥700°C. As discussed below, the solubilities of rare-element minerals (e.g., beryl, tourmaline, spodumene, etc.) are far too high to achieve saturation in the partial melts at such temperatures.

Solubilities of ore-forming minerals

The solubilities of minerals in which rare alkalis, ore-forming HFSE, and fluxing components are essential structural constituents have been determined rather extensively through petrologic experiments involving hydrous granitic melts (e.g., Wolf and London, 1997, Evensen et al., 1999, London et al., 1998, 1999, 2001a, b; Linnen and Cuney, 2005). By fixing the activities of common components through saturation in other minerals with which they occur, the solubilities of lithium aluminosilicates, beryl, pollucite, cassiterite, columbite, and tantalite can be reduced to the abundances of their rare-element constituents in melt. Table 4 presents published mineral solubility data for melt-saturating rare-element minerals at 700°C, near the minimum temperature of the hydrous granite liquidus at 200 MPa. The liquidus saturation values for each of these minerals at 700°C can be compared to their elemental abundances in the Tanco pegmatite, for which the mineralogy and composition are well constrained. In all cases, the concentrations of rare elements in the Tanco pegmatite are far below the values required to saturate the melt in tourmaline, pollucite, and tantalite at liquidus temperatures, even though these minerals appear as primary phases at Tanco. This apparent conundrum is reconciled by considering the temperature-dependence of the rare-element ore minerals in relationship to the actual temperatures at which pegmatites crystallize.

Table 4. Rare-Element Concentrations (ppm) in Pegmatite and in Melt at Saturation of Mineral at 700°C, 200 MPa H_2O

Element	Tanco	700°C	% of saturation
Be	169	430	39 beryl
Li	3,453	7,000	49 petalite
Cs	2,641	51,880	5 pollucite
B	216	4,085	5 tourmaline
F	1,220	30,000	4 topaz
Mn	1,394	8,520	16 spessartine
Ta	300	7,500	4 Mn-tantalite

Notes: Values at saturation in ppm as derived from experiments: beryl (Evensen et al., 1999), petalite (Stewart, 1978), pollucite (London et al., 1998), tourmaline (Wolf and London, 1997), topaz (London et al., 2001b), spessartine (London et al., 2001a), Mn tantalite (Linnen and Cuney, 2005)

Cooling Histories of Pegmatites

Pegmatites are widely recognized for the gigantic size of their crystals. Students of geology are taught a basic proportionality between crystal size and rate of cooling: crystal size increases as rate of cooling decreases. Most professional geoscientists learn little or nothing more about this relationship. Thus, in the case of pegmatites, some definitions state that pegmatites are the products of exceedingly slow cooling, thereby explaining the enormity of their crystals.

Conductive cooling models

Chakoumakos and Lumpkin (1990) were the first to apply a model for conductive heat loss to derive the cooling history of a pegmatite, the Harding pegmatite, near Dixon, New Mexico. The Harding deposit is a large (20 m thick in their thermal model), strategic reserve of Ta, Be, and Li. Using the conductive cooling model published by Jaeger (1968), Chakoumakos and Lumpkin (1990) estimated that the body would have cooled to 550°C at its center, ~150°C below its liquidus temperature, in less than three years. Following this lead, Morgan and London (1999) and Webber et al. (1999) calculated cooling profiles through much thinner, miarolitic, gem-bearing pegmatite dikes in San Diego County, California. Those bodies, varying from ~18 cm to 2 m thick, would have cooled to 450°C, close to their glass transition temperatures, in a few days to a few months. Employing the concepts of Rubin (1995), London (2008) modeled the cooling history of thin (1 m thick) dikes within and beyond the thermal aureole of a large granitic sill. In all of these cases, even within the thermal aureole of a 0.5-km-thick granite sill, the pegmatite bodies would have cooled to temperatures 200° to 250°C below their liquidus temperatures in a matter of days to weeks.

Other monitors of temperature

A limited number of studies that utilize stable isotope partitioning between coexisting minerals (e.g., Karin Siegel et al., pers. commun., 2012), fluid inclusion analysis (e.g., Sirbescu and Nabelek, 2003), or feldspar solvus thermometry (e.g. London et al., 2012b) cite temperatures mostly in the range of 350° to 450°C for pegmatite systems. Where present, wall-rock alteration assemblages are indicative of conditions of the zeolite to lower greenschist facies of metamorphism (i.e., 350°–450°C). Alteration minerals in the contact metamorphic aureoles of pegmatites include typical greenschist assemblages (Ep-Chl-Qtz-Cc), argillic alteration, and near end-member spessartine (Shearer et al., 1984; London, 1986b; Morgan and London, 1987).

In relationship to a liquidus temperature of 650° to 700°C for a near-minimum or eutectic hydrous granitic liquid, the actual temperature of pegmatite crystallization appears to lie ~200°C below the minimum. That is, pegmatite-forming liquids are undercooled and supersaturated to this extent prior to the onset of crystallization. Liquidus undercooling prior to the onset of crystallization is the single most important cause of pegmatitic textures (London, 2008, 2009, 2014b).

Crystal nucleation delay

All liquids require some measure of supersaturation in order to nucleate stable crystals. Thermodynamic and kinetic factors both play a part. In granitic liquids, the kinetic factor becomes especially important, because the reorganization of melt to form stable crystal nuclei entails chemical diffusion, and the rate of chemical diffusion is inversely proportional to the viscosity of the fluid medium (e.g., Mungall, 2002). At 450°C, H_2O-saturated granitic melt possesses a viscosity of ~10^8 Pa·s (calculated from Baker, 1996), about the same as semisolid asphaltic pitch at 25°C. This high viscosity impedes the reorganization of the melt structure, and consequently, crystal nucleation is delayed, metastably, as cooling continues. The time between cooling below the liquidus and the first appearance of discernible crystals is called the nucleation delay or nucleation lag time. The magnitude of undercooling and the time interval of the nucleation delay define a parabolic shape for the first appearance of crystals upon undercooling of granitic liquid (Fig. 8). The value of 450°C, which is 240°C below the liquidus-solidus temperature of the minimum melt composition, coincides with the minimum in crystal nucleation delay (2 weeks) in the hydrous granite system (Evensen, 2001), and with the maximum rate of growth for alkali feldspars and quartz (Fenn, 1977; Swanson, 1977).

Temperatures of crystallization in pegmatites

The foregoing discussion presents theoretical and empirical evidence that pegmatite bodies cool quickly to temperatures that are 150° to 250°C below their likely liquidus temperatures. Crystal nucleation, which starts along the margins of bodies, cannot commence much before the magmas have reached this range of temperature. Feldspar solvus thermometry (London et al., 2012b) and stable isotope temperatures (Karin Siegel et al., pers. commun., 2012) indicate that crystallization within pegmatites is nearly isothermal, following the ingress of the 450° ± 25°C isotherm. This assessment of cooling history can reconcile the high solubilities of rare-element minerals with their much lower actual concentrations of rare essential structural constituents at saturation in pegmatites.

Temperature-dependence of rare-element saturation

The solubilities of tourmaline, beryl, tantalite, and pollucite all decrease sharply with decreasing temperature (see citations in Table 4). Pegmatites such as the Tanco deposit would have become saturated in most of these minerals below 450°C at the concentrations of their rare essential structural constituents in the bulk composition. London (2008) examined the specific case of pollucite. Using experimentally determined temperature-composition relationships, pollucite at Tanco should have crystallized at ~385°C based on its leucite component (London et al., 1998). At that temperature, a supercooled melt with ~0.48 wt % Cs_2O could precipitate pollucite. This is twice the amount of Cs in the Tanco bulk composition, which implies that the pegmatite should have been saturated with respect to pollucite at that temperature after about 50% of the bulk melt had crystallized. However, it is only 5% of the Cs that would be necessary to saturate a granitic melt in pollucite at 700°C and 200 MPa H_2O.

Beryl-rich pegmatites contain approximately 40 to 65% of the Be they should require to be saturated in beryl at liquidus temperatures (Table 5). However, beryl is a common constituent of the border zones of pegmatites (Cameron et al., 1949), which means that pegmatite-forming melts must be saturated from the start with respect to beryl. The disparity can be resolved by considering the temperature-dependence of beryl solubility (Evensen et al., 1999). Granitic melts containing as little as 30 ppm Be can become abruptly saturated in beryl as

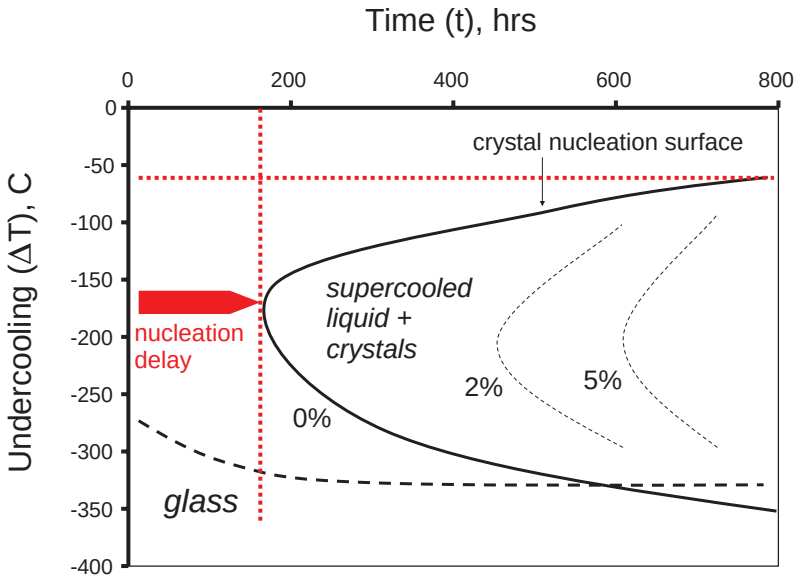

Fig. 8. Graph illustrating the crystal-nucleation delay, the time interval between the onset of undercooling and the first appearance of macroscopic crystals, in the granite system. The solid curve delineates the first appearance of crystals to form (K-feldspar) upon undercooling (ΔT) of H_2O-saturated granitic melt ($Ab_{38.23}Or_{28.72}Qtz_{33.04}Crn_{0.01}$) at 200 MPa. Contours delineate the volume % of crystals as functions of time (in hours) and undercooling (in °C). The gray dashed line represents the approximate location of the liquid ⇔ glass transition. From Evensen (2001), modified by London (2008).

Table 5. Beryllium Content of Beryl-Bearing Granitic Pegmatites

Location	Pegmatite type (where known)	Average Be ppm	Source
Tanco	Complex Li	163	Stilling et al. (2006)
Manitoba, Canada	Petalite		
Sparrow Pluton	Beryl	260	Kretz et al. (1989)
Yellowknife, NWT, Canada			
Helen Beryl	Beryl	91	Staatz et al. (1963)
Black Hills, SD USA			
Tin Mountain	Complex Li	223	Staatz et al. (1963)
Black Hills, SD USA	Spodumene		
Souchon	Complex Li	202	Gallagher (1975)
Kamativi mine, Zimbabwe	Lepidolite		Rijks and van der Veen (1972)
Augustus	Complex Li	202	Gallagher (1975)
near Salisbury, Zimbabwe	Lepidolite		Ackermann et al. (1968)
Mistress	Complex Li	432	Gallagher (1975)
near Salisbury, Zimbabwe	Lepidolite		Ackermann et al. (1968)
Benson 1	Complex Li	576	Gallagher (1975)
Mtoko district, Zimbabwe	Lepidolite		Ackermann et al. (1968)
Benson 4	Complex Li	76	Gallagher (1975)
Mtoko district, Zimbabwe	Lepidolite		Ackermann et al. (1968)
Benson 2	Complex Li	36	Gallagher (1975)
Mtoko district, Zimbabwe	Lepidolite		Ackermann et al. (1968)
Al Hayat	Complex Li	126	Gallagher (1975)
Bikita district, Zimbabwe	Spodumene		Ackermann et al. (1968)
Bikita Main	Complex Li	180	Gallagher (1975)
Bikita district, Zimbabwe	Petalite		Ackermann et al. (1968)
Beryl Rose		152	Gallagher (1975)
Darwin district, Zimbabwe			
Unnamed pegmatite	Complex Li	155	Rossovskiy and Matrosov (1974)
Gobi Field, E. Gobi, Mongolia	Lepidolite		
Average:		205	

a result of liquidus undercooling below 600°C (London, 2008, fig. 12-3; 2015a).

Similar temperature-composition relationships hold for columbite (Nb) and tantalite (Ta). At 700°C and 200 MPa, the Nb content of peraluminous granitic melt at saturation in columbite is ~700 ppm, and the Ta content at saturation in tantalite is ~2,000 ppm (Linnen and Cuney, 2005). These are minimum solubility values, which increase with increasing alkalinity, F, or Li content of melt, individually (Linnen and Cuney, 2005). Hence, the problem of Nb-Ta oxide mineralization is not one of limited solubility in the melt, but rather one of high solubility in the melt.

The Tanco pegmatite, for example, contains just 300 ppm Ta in its bulk composition (Stilling et al., 2006), yet it is a world-class Ta deposit. Using the temperature-solubility data from Linnen and Cuney (2005), London (2008) observed that 300 ppm Ta is sufficient to saturate a peraluminous granitic melt in tantalite at 450°C. Though some Ta oxides are associated with fine-grained massive mica or with albite only, van Lichtervelde et al. (2007) concluded that most mineralization of Nb and Ta oxides at Tanco was magmatic in origin.

Undercooling also accounts for the common appearance of columbite in the border zones of pegmatites (Cameron et al., 1949). Using the same data and logic as cited above, a pegmatite containing 50 ppm Nb (e.g., Tanco, with 56 ppm Nb: Stilling et al., 2006) could become saturated in columbite below ~525°C. The estimated temperatures of crystallization along the margins of pegmatites are below 525°C, which explains why columbite is a common accessory mineral of the border zones.

Pegmatite Fabrics and Mineral Zonation

The majority of pegmatites occur as dikes, and as dikes they commonly manifest axially bilateral or layered zonation in texture and mineral assemblages. The outer zones (border and wall), aplites (if present, layered or massive), and feldspathic intermediate zones possess some combination of fine-grain size, graphic intergrowths, and a marked asymmetry in the orientation of layering or the directional growth of crystals (London, 2014a). All of these fabrics are attributable to the effects of liquidus undercooling, nucleation delay, and the consequent growth of crystals from a highly viscous melt in the absence of an intervening aqueous fluid (Fenn, 1986; London, 2009, 2014a). Fine-grain size of border zones and aplites, and graphic intergrowths of quartz and feldspar arise from essentially one-dimensional inward growth, in which the high viscosity of melt precludes the dispersion of excluded components back into the melt, or their redistribution laterally along the crystallization front. Alternations of mineral layering (e.g., garnet or tourmaline in layered aplites) could arise from local saturation in these minerals due to the episodic pile-up of their constituents along the crystallization front (London, 1999, 2008, 2009).

Why are pegmatites granitic?

High viscosity impedes the diffusion needed to promote nucleation. Consequently, during continuous cooling to the temperatures of their host rocks, polymerized (silica-rich) melts of high viscosity experience several tens to hundreds of degrees of undercooling before the driving force of

crystallization overcomes the kinetic barriers to nucleation that result from that high viscosity. In Figure 8, notice that the crystal nucleation surface, which marks the first appearance of crystals, becomes asymptotic to the liquidus within ~50°C of undercooling. It appears, therefore, that at least 50°C of undercooling is necessary to start the nucleation of crystals from granitic melt of the composition of the thermal minimum or eutectic, irrespective of the cooling rate. When crystallization commences from crystal-free or even crystal-bearing melts, that nucleation always begins along the margins of the melt volume. The resultant textures are those associated with the outer zones of pegmatites: fine-grained aplitic, layered aplitic, skeletal, and graphic intergrowths, and oriented, inwardly flaring crystals (e.g., London et al., 1989; London, 1999).

Low-viscosity melts, which correspond to less polymerized, low-silica liquids represented by basalts, phonolites, and carbonatites, do not inhibit the diffusion of essential structural constituents to the same extent, and consequently crystals can nucleate more readily and closer to the liquidus than in granitic melts (e.g., Lofgren, 1980; Lofgren and Russell, 1986). The lower viscosities of nongranitic melts foster the nucleation of crystals with negligible undercooling (i.e., they track the liquidus closely), which makes their ordinary phaneritic textures the norm.

Transition to coarse-grained texture

The interior intermediate zones and the cores (if not pure quartz) of pegmatites possess coarse crystal size and more isotropic fabrics. Graphic intergrowths of quartz and feldspar in the outer zones give way to segregated monocrystals in the interior units. The growth of large monocrystals requires a change from one-dimensional inward growth to two-dimensional crystallization along a surface. That surface must expand laterally and must be able to grow by the diffusion of its essential structural constituents to its surface while excluded components diffuse away at a rate that does not lead them to saturate in a new mineral phase that may terminate (starve or poison) the growth of the substrate crystal (London, 2009).

The roles of fluxing components

In order for aluminosilicate crystals to grow to giant size in a closed system, either the rate of cooling must be very slow, such that slow-diffusing components, including Si and Al, can migrate to and away from growing crystal surfaces, or else the viscosity of the melt must drop in order to facilitate more rapid diffusion of these components. Based on the current understanding of the thermal history of pegmatites, crystallization at low temperatures (~450°C) from highly viscous granite liquid would preclude the former hypothesis. Alternatively, diffusion could proceed quickly if the viscosity of the growth medium were dramatically reduced. Components that could reduce the viscosity of silicate melt include the components of H, B, P, F, and alkalis in excess of Al , i.e., peralkaline composition (e.g., Dingwell et al., 1996). These fluxing components have been implicated in the formation of pegmatite textures since the inception of petrologic study. In addition to their effects on viscosity, the components of B, P, and F are now known to lower the solidus temperatures of silicate melts, and to enhance the solubility of H_2O (as H^+: London, 2009), thereby further reducing the viscosity of the melt and forestalling the exsolution of an aqueous fluid.

Though the fluxing components appear to be necessary to effect the changes in melt structure that facilitate the growth of large crystals and the concentration of ore-forming elements, the abundances of H, B, P, and F in pegmatites are manifestly low. Minerals that contain a few weight percent of these components (micas, tourmaline, apatite) are normally present at accessory levels in pegmatites. The whole-rock contents of the fluxes rarely exceed a few tenths of a weight percent. A dearth of wall-rock alteration around all but the few largest and most evolved pegmatites confirms that large quantities of the fluxes, including H_2O, are not normally lost from pegmatite bodies. Even the exceptionally fractionated Tanco body contains <1 wt % of B, P, and F (Table 1). When the mass of these components introduced into the host rocks is added back to the mass of pegmatite (Morgan and London, 1989), the total flux content exclusive of H_2O remains <2 wt %.

Current and Recurrent Concepts of Pegmatite Formation

In the first comprehensive summary of pegmatite studies, Jahns (1955) presented the models for the internal evolution and development of pegmatites, all of which dated from the late 19th century. Although much science has been done since then, and the study of pegmatites has become more factual and less intuitive with time, it could be said that nothing fundamentally new has been discovered or put forward since these earliest studies.

Pegmatites in the context of ore deposits

Lindgren (1933) placed pegmatites at a transition between granite-hosted ores on the one hand and hydrothermal vein deposits on the other. He observed that pegmatites have affinities both to igneous and to hydrothermal rocks, but he regarded them as essentially igneous in origin. An interesting point is that Lindgren (1933) believed that there was no change of phase in the evolution of granitic melt to hydrothermal fluid through the transition in which pegmatites resided. An important role for fluxing components had already been proposed, and to this extent, even the earliest petrologists and economic geologists believed, or hypothesized, that fluxing components were essential to the pegmatite-forming process (Crosby and Fuller, 1896); these are the same components that are known to promote increased miscibility between magmatic and aqueous phases.

The critical role of aqueous fluid

From the 19th century to modern times, a few petrologists have ascribed pegmatites to a purely hydrothermal origin. Gresens (1969) developed a model based on volume changes associated with the reaction among muscovite, quartz, and K-feldspar, and related that to local variations in pressure (volume) during ductile deformation and regional metamorphism in mountain belts. Roedder (1981) proposed that "simple" granitic pegmatites are igneous, but that "complex" pegmatites might be hydrothermal. Though not explained in detail, Roedder thought that the exotic compositions of

rare-element pegmatites would make their silicate constituents more soluble in aqueous fluid, and hence transportable through that medium. Once the igneous origins of granites were established, and the compositions of pegmatites were determined to be those of granites, the purely hydrothermal models mostly vanished from the scientific literature.

Though proposed more than half a century earlier (Brögger, 1890), Jahns and Burnham (1969) are widely credited with the concept that pegmatites arise from the action of an aqueous fluid that has exsolved from silicate melt. In that model, the buoyant ascent of an aqueous fluid through granitic melt was thought to fractionate Na (downward) from K (upward) and the corresponding changes in the composition of melt result in the precipitation of fine-grained sodic aplite along the footwall, and giant-textured K-feldspar along the hanging wall. Later, Jahns (1982) stated that "discoidal lenses" of pure quartz crystallize simultaneously within melt in the central portions of a body. The Jahns-Burnham model, which has been championed recently by Nabelek et al. (2010), has been reviewed and assessed extensively by London (2008), and readers are referred to that source for a full discussion. However, some of the weakness of that model are the following:

1. An experimental basis on which the model was founded does not exist, except for some "failed" experiments (London, 2005a), which Jahns evidently did not perform (Robert F. Martin, pers. commun., 2008). In those failed experiments, material transport and fractionation of Na from K occurred along and because of a thermal gradient in the reaction vessels.
2. The fractionation of K and Na that was the foundation of the Jahns-Burnham model for zonation in pegmatites has been invalidated by at least three separate and methodologically different experimental programs.
3. In the Jahns-Burnham model, the concept of "compositional quench" was employed to explain two completely different textures—those of the layered aplites (fine-grained) and of giant K-feldspar megacrysts.
4. Graphic granite, the defining texture of pegmatites and prima facie evidence of high-viscosity melt, was not considered in the Jahns-Burnham model.
5. Jahns hypothesized that quartz cores were primary, but Burnham and Nevkasil (1986) claimed that the pure quartz bodies in pegmatites must be hydrothermal. To accomplish that, Burnham and Nekvasil (1986) stated that "vigorous convection" must occur in pegmatites, but Jahns (1982) argued convincingly against any role for convection in pegmatite bodies.

One of the key problems with the Jahns-Burnham model, as with the purely hydrothermal models, is that the solubility of silicate components in a typical aqueous fluid (that is, moderately saline, and sometimes containing CO_2) at pegmatite-forming conditions is approximately 2 wt % dissolve solids (Hermann et al., 2013), in which aluminum is almost completely insoluble (Anderson and Burnham, 1983). To make the point, base-metal Cu porphyry systems that are purely I-type, and lacking the B and F that are sometimes present and reflect a sedimentary component in the source, are felsic melts that achieve early saturation in a saline aqueous fluid (e.g., Bodnar, 1998). In the model of Jahns and Burnham (1969), those bodies should develop abundant pegmatitic textures. Instead, they are devoid of pegmatites, and their hydrothermal deposits consist of vein quartz.

Immiscible and flux-rich liquids

Based on the current knowledge of the bulk compositions of pegmatites, and the various mineralogical monitors of melt composition (e.g., Table 4 and references therein), the compositions of pegmatites appear to be very close to the bulk compositions of the melts from which they form. In contrast, Thomas et al. (1998, 2012) and Thomas and Davidson (2012) advocated that pegmatite-forming melts routinely contain tens of weight percent of these constituents, including Be, and that such high concentrations of fluxing components lead to saturation in three or more fluid phases during the consolidation of pegmatites (silicate melt, dense salt melt, and aqueous fluid). Much of the evidence that Thomas et al. (2012) cited comes from studies of crystalline inclusions that are construed to be trapped melts. They reported solidus temperatures of ~550° to 650°C and liquidus temperatures from 750° to 950°C for exceedingly hydrous and flux-rich "melt" inclusions (Thomas, 1994; Thomas et al., 1996; Thomas and Klemm, 1997; Thomas and Webster, 2000). As derivative melts, and in particular as hydrous, flux-rich granitic melts, their solidus and liquidus must be lower (e.g., near the solidus of the hydrous Macusani obsidian, 450°C at 200 MPa: London et al., 1989), not higher, than that of hydrous haplogranitic liquids. One possibility is that these inclusions constitute mixtures of fluids that were immiscible at the conditions of entrapment, and this is one of the hypotheses put forward by Thomas and Webster (2000) and by Veksler et al. (2003). However, entrapment of immiscible fluids might account for the high liquidus temperatures of these inclusions, but not their high solidi, which should be close to the solidus of hydrous macusanite (i.e., if one of the phases trapped was a low-melting flux-rich melt). Alternatively, inclusions with final-melting temperatures as high as 750° to 950°C could easily be explained as cases of trapped melt plus accidentally trapped crystalline phases (Roedder, 1984), leading to widely variable compositions (e.g., 100–7,000 ppmw Sn in a single quartz sample: Thomas and Webster, 2000) or immiscible liquids resulting from complete laboratory melting (Thomas et al., 1996). Thomas and Davidson (2012) reported what they interpret as melt inclusions containing up to 38,000 ppm Be, which is more than 10^2 greater than the Be contents of the most beryl-rich pegmatites. However, Thomas and Davidson (2012) also noted that the Be content of laboratory-melted inclusions increases with their homogenization temperatures. This behavior is characteristic of inclusions containing variable fluid-crystal proportions upon entrapment. This topic has now been thoroughly debated through a public comment and reply (London, 2015b; Thomas and Davidson, 2015)

Constitutional zone refining

Based on experiments with the flux- and Li-rich obsidian from Macusani, Peru (London et al., 1989), London (1992) proposed that constitutional zone refining might be a viable mechanism to produce local enrichment in fluxes adjacent to crystal surfaces, even if the concentrations of fluxes in the bulk melt are low. By this mechanism, fluxes and other

incompatible (i.e., ore-forming) components could be concentrated by exclusion from quartz and feldspar into a boundary layer of melt adjacent to the surfaces of crystal growth. The model gained traction from experimental simulations, in which a flux-rich boundary layer liquid was quenched to glass in advance of a crystallization front (London, 1999). Since that initial discovery, the nature of boundary layer enrichment has been studied in other bulk compositions (Morgan and London, 2005), including the green obsidian from Macusani, Peru, whose composition closely resembles that of a highly fractionated Li pegmatite such as the Tanco deposit. An experiment with the Macusani glass (Fig. 9) illustrates the efficacy of consititutional zone refining in the concentration of fluxes and incompatible components in a boundary layer liquid. Importantly, the liquid represented by that boundary layer quenches to a durable, insoluble, and single-phase glass. Though the hydrous melt generated from the Macusani obsidian possesses low viscosity at high temperature (cf. Bartels et al., 2011), the viscosity increase upon cooling to pegmatite-forming temperatures is sufficient to keep fluxes including B and F from diffusing rapidly away from the crystallization front, thereby preserving the flux-rich character of the boundary layer liquid. The same is true for melt compositions containing >18 wt % of B_2O_3 and >13 wt % of H_2O, which quenched to a durable, single-phase glass (London, 1999).

With the increase in B, P, or F in residual melt upon the fractional crystallization of quartz and feldspars, the melt composition and the composition of the cognate mineral assemblage

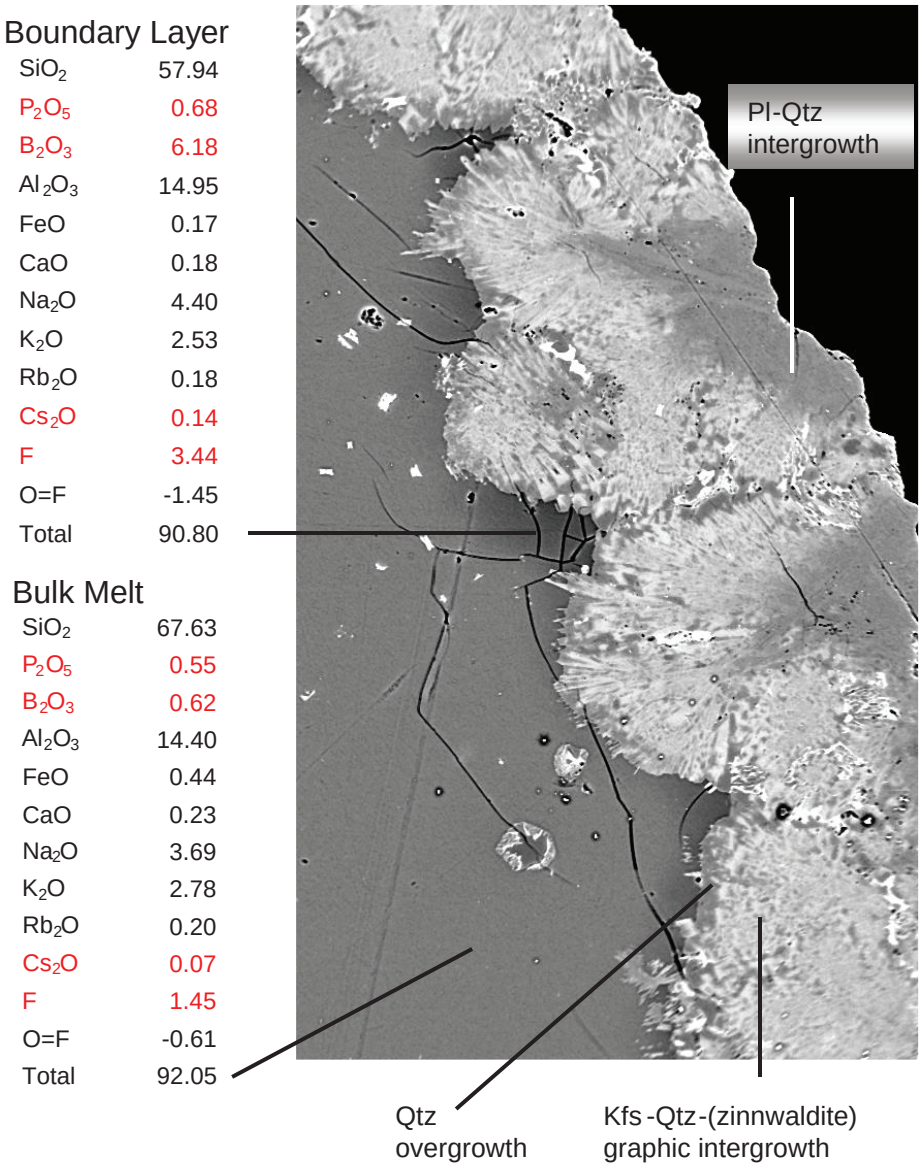

Fig. 9. Backscattered electron image from experiment MAC-92 (London et al., 1989). The experimental charge consisted of macusanite obsidian (USNM 2143) with 3.5 wt % H_2O; the experiment was conducted at 500°C (ΔT = 300°C) and 200 MPa. The crystal assemblage and compositions of the bulk melt (medium gray) and boundary layer liquid (dark gray) are shown. Concentrations of fluxing and other incompatible components are highlighted in red font. Kfs = K-feldspar, Pl = plagioclase, Qtz = quartz. From London and Morgan (2012).

begin to diverge away from the minimum in the hydrous granite system (London, 1986a, 1989, 2008, fig. 14-10). With reference to the analyses in Figure 9, the melt composition becomes increasingly sodic and alkaline in character (measured by ASI or A/CNK <1), and silica poor, though the melt remains saturated in quartz. The corresponding mineral assemblage becomes potassic (initially in K-feldspar), peraluminous (K-feldspar is succeeded by white mica, muscovite, or lepidolite solid solutions), and quartz rich. The liquid line of descent toward sodic, alkaline residual melt occurs even in initially peraluminous bulk compositions (London et al., 1989). Increasing alkalinity in this manner leads to further reductions in viscosity and solidus temperatures and promotes an increase in the solubility of H_2O in the melt (e.g., Dingwell et al., 1996).

Additional details of how constitutional zone refining might operate to promote the formation of giant crystals are presented elsewhere (London, 2008, 2009). In that model, the outer zones of pegmatites, which are marked by fine-grain size, layered structures, unidirectional solidification textures, and graphic quartz-feldspar intergrowths are the hallmarks of crystallization from a viscous melt. Boundary layer exclusion of incompatible elements should begin from the inception of crystallization, and the width and chemical complexity of the boundary layer liquid will increase with the amount of bulk melt that undergoes zone refining. However, the dissolution of constituents from the bulk melt into and through the boundary layer to the surfaces of growing (quartz-feldspar) crystals serves to dilute the content of incompatible elements in the boundary layer liquid until the bulk melt is consumed or has fractionated toward the boundary layer composition.

In the model presented by London (2009), the transition from the fine-grained and anisotropic fabrics to the coarse-grained internal zones marks the development of a flux-rich boundary layer liquid. The boundary layer liquid is likely the only liquid present, as the miscibility of H_2O and silicate components increase with increasing flux content and increasing alkalinity of the residual melt. Eventually, crystallization evolves from the diffusion of bulk melt components through the boundary layer liquid, to crystallization of the boundary layer liquid itself. The products are quartz-poor albite-lepidolite units that contain most of the HFSE mineralization (Nb, Ta, Sn, REE, U) and fluxes (tourmaline, phosphates, topaz, rarely fluorite) that are found in mineralized pegmatites. These late-stage liquids can escape to form their own intrusive bodies, which are represented by the albite-lepidolite and albite-spodumene subtypes of the rare-element pegmatites (Černý, 1991a). As internal units or discrete bodies, this is the culmination of magmatic fractionation of granitic pegmatites from either metallogenic family. Massive bodies of essentially pure albite or of pure muscovite are common in most types of pegmatites, and they may host mineralization in Sn, Nb, and Ta. The interpretive origins of these monominerallic masses are rarely unambiguous or unequivocal. Because of their essentially monominerallic compositions, they have mostly been thought of as replacement bodies, though not necessarily at subsolidus conditions. Cameron et al. (1949) astutely pointed out that peritectic reactions between early-formed minerals and more fractionated late-stage melt were likely to occur in pegmatites because pegmatite-forming melts fractionate so considerably from start to finish.

The mechanism of constitutional zone refining, in which fluxes and incompatible components are enriched in a boundary layer of melt adjacent to crystal growth fronts, represents the most effective means of concentrating rare elements. During Rayleigh fractionation, the concentrations of incompatible trace elements rise exponentially in crystals and in melt because the crystal-melt partition coefficients are taken as constants, and the surfaces of crystals are in chemical equilibrium with the bulk melt as crystal fractionation proceeds. In contrast, consititutional zone refining leads to a sharp, "L"-shaped inflection in the concentration of incompatible elements with the progress of crystallization. The incompatible trace element concentrations of crystals remain constant and near zero, such that the absolute concentrations of trace elements at the end of consititutional zone refining can be orders of magnitude greater that those that are attainable by Rayleigh fractionation (between mineral and bulk melt). In rare-element pegmatites, some trace-element enrichment patterns show the gradual increase in abundance that is expected of Rayleigh fractionation (e.g., plagioclase and alkali feldspar: London et al., 2012b), whereas pegmatites in which the transition from ordinary mineral assemblages to those enriched in rare elements is sharply defined more closely match the elemental fractionation that is derived from constitutional zone refining (e.g., tourmaline and garnet: Morgan and London, 1999). This behavior is to be expected, because the partitioning of incompatible trace elements between crystals and melt are likely to differ based on the precise composition of the evolving boundary layer liquid and the solubility of crystal-incompatible elements within it (e.g., between Cs and Be: London, 2005b).

Geology of Rare-Metal Ores

The nature of occurrences and ore-forming processes in pegmatites vary with the chemical diversity of the rare elements and their host minerals. Zonation of ore-forming minerals is systematic in most pegmatites, but different among different ore-forming minerals. In addition, silicate and phosphate minerals tend to possess the giant crystal size that is distinctive of pegmatites (cm to m), whereas the ores of HFSE oxides (of Nb, Ta, Sn, REE, and U) are comparatively fine grained (mm to a few cm).

Lithium

Spodumene (α-$LiAlSi_2O_6$) and petalite ($LiAlSi_4O_{10}$) are the only significant ores of Li in pegmatites. In the quartz-saturated environment of granitic pegmatites, the stability relationships of spodumene, petalite, and eucryptite (α-$LiAlSiO_4$) are functions only of pressure and temperature (Fig. 10). Solid solutions of Mn, Fe, or Cr in the place of Al extend the stability field of spodumene to lower pressure and higher temperature (London, 1984). However, the composition of spodumene in most pegmatites is near enough to the ideal end-member composition that minor quantities of these additional components do not have any important bearing on the stability field of the phase.

At the giant Tanco mine, Canada, and at the equally large Bikita pegmatite, Zimbabwe (Cooper, 1964; Fig. 4), petalite was the initial lithium aluminosilicate to crystallize, followed by spodumene (+ quartz) as a primary assemblage and also as

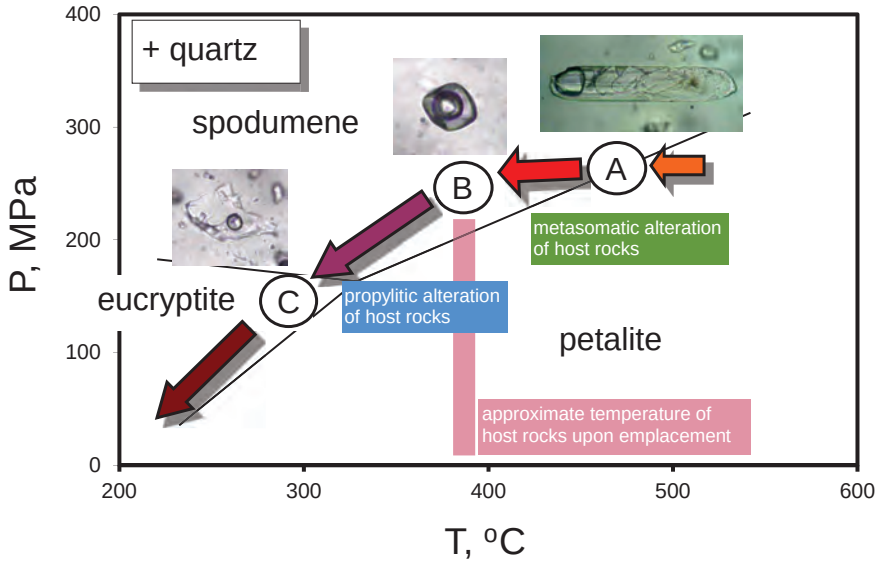

Fig. 10. Lithium aluminosilicate stability relations in quartz-saturated systems, together with (a) the cooling history of the Tanco pegmatite based on estimated conditions of fluid-inclusion entrapment in the lithium aluminosilicates and quartz as host minerals, and (b) wall-rock alteration. Point A marks the P-T point at which the Tanco pegmatite crossed the reaction boundary petalite ⇒ spodumene + 2 quartz; crystal-rich inclusions in spodumene homogenize at this temperature. Point B denotes transition from melt- to vapor-dominated crystallization; the fluid phase was a single homogeneous aqueous-carbonic fluid containing ~4 mole % CO_2 and low salt content. Point C marks the conditions of fluid entrapment (based on the intersection of isochors for aqueous and carbonic fluids in eucryptite and associated quartz) in the stability field of eucryptite + quartz. Photomicrographs show typical fluid inclusions: crystal-fluid inclusion (~100 μm) trapped at condition A, mixed aqueous-carbonic inclusion (~20 μm) hosted by quartz at the magmatic-hydrothermal transition B, and aqueous brine inclusion (~40 μm) hosted by eucryptite + quartz at condition C; nearly pure carbonic fluid inclusions occur together with aqueous brine. Metasomatic alteration of host rocks converted amphibolite to tourmaline, holmquistite, and Li-Rb-Cs dark mica near the solidus condition for the pegmatite. Later and lower temperature propylitic alteration converted amphibolite to epidote-albite-titanite-calcite-quartz-chlorite. The inflection in the cooling curved (denoted by the vertical magenta bar) denotes the transition from isobaric cooling to uplift, and hence corresponds to the temperature of the host rocks upon the emplacement of the pegmatite. Modified from London (2008).

pseudomorphs after petalite (referred to as SQI, spodumene-quartz intergrowth), and finally eucryptite + quartz. These assemblages constrain the cooling history of these pegmatites to an initial period of what might be isobaric cooling of the primary assemblages, followed by subsolidus cooling along a geotherm into the field of eucryptite + quartz (Fig. 10).

Hydrous silicate liquids in the system $NaAlSi_3O_8$-$LiAlSiO_4$-SiO_2-H_2O contain ~1.8 wt % Li_2O on the liquidus surface (200 MPa) at saturation in eucryptite, spodumene, or petalite (Stewart, 1978). That is approximately twice the Li content in the Tanco, Bikita, and Harding pegmatite whole-rock compositions (Table 4). This disparity has two possible explanations: (1) the lithium aluminosilicates did not appear in these pegmatites until ~50% of the melt had already crystallized, or (2) crystallization of undercooled melt brought these pegmatites to saturation in lithium aluminosilicates at lower concentrations of Li in melt. At each of these pegmatites, lithium aluminosilicates first appear in interior zones; hence, both explanations may be applicable.

Spodumene-rich pegmatites at King's Mountain, North Carolina, constitute a rarer but economically significant type of rare-metal pegmatite deposit (Fig. 4). The thick pegmatite bodies at King's Mountain are weakly zoned, in contrast to the sharp mineralogical zonation that is prevalent in other rare-element pegmatites. Spodumene forms phenocrysts (cm-scale) in a groundmass of only slightly finer grained quartz-albite-K feldspar pegmatite (Kunasz, 1982). The deposits were hosts to a variety of rare secondary phosphates, but primary phosphates other than apatite, and tourmaline, topaz, or fluorite are rare to absent (i.e., the pegmatite is notably depleted in fluxing components). Host amphibolites to the pegmatites, however, exhibit tourmalinization along their contacts with the pegmatite bodies, and holmquistite, a lithium amphibole, is also present (London, 1986b).

As a source of Li metal or carbonate, spodumene possesses higher concentrations of Li. However, for ceramic applications, spodumene typically contains enough of Fe, Mn, Cr that act as chromophores to give unwanted color to ceramics. The Foote mine at King's Mountain employed a chlorine leach process that rendered their product suitable for ceramic materials (Kunasz, 1982). Petalite does not accommodate these chromophores because petalite does not contain an octahedral (6-coordinate) site in which the transition metals normally fit. Because natural petalite compositions closely approach the ideal formula, the spodumene + quartz intergrowths (SQI) that replace petalite are essentially iron free. Tanco and the giant Greenbushes pegmatite, Western Australia (Fig. 4), currently meet much of the world's demand for ceramic-grade Li minerals (Linnen et al., 2012). Recently discovered pegmatite deposits in eastern Canada (Fig. 4) are potentially as large and high in grade as Greenbushes (Linnen et al., 2012).

The compositions of lithium aluminosilicate glass ceramics (e.g., Corningware™ and Visionsware™) are close to that of petalite, which makes petalite or spodumene + quartz pseudomorphs after petalite ideal raw materials for this application. Otherwise, salars and brines of the Atacama desert (Chile), similar deposits in Argentina and Bolivia, and zeolitized tuffs in Nevada represent the most attractive sources of Li metal for large-scale mining operations (Kesler et al., 2012). However, Kesler et al. (2012) noted that pegmatites are highly concentrated sources of Li by comparison, suitable for small-scale and artisanal mining, and may be regarded as strategic reserves because of the potential for political or economic instability in the principal known sources of brines. A few pegmatites are mined for their Li metal content: the giant Greenbushes pegmatite, Western Australia, produces $LiCO_3$ from spodumene for electronic markets in Asia. Production in 2011 exceeded 11,000 metric tons (t; Jaskula, 2012).

Beryllium

As is the case for Li, large tonnage, low-grade deposits of bertrandite in zeolitized tuffs near Spor Mountain, Utah (Lindsey, 2001) have replaced pegmatitic beryl as the principal economic source of beryllium. Because beryl occurs as coarse crystals in pegmatites, however, it is amenable to hand cobbing where labor is abundant and inexpensive. Thirty-eight species or groups of beryllium minerals are reported from pegmatites (Černý, 2002), but beryl is the only one that carries any potential as an ore in pegmatites.

The average beryllium content of 14 of the most beryl rich pegmatites known (Table 5) is 205 ppm Be by weight (London and Evensen, 2002). In contrast, the Be content of hydrous granitic melts saturated in beryl lies between 200 to 1,200 ppm at a liquidus temperature of 700°C (Evensen et al., 1999), with 430 ppm Be at beryl saturation of a metaluminous granitic liquid (Table 4).

Evensen et al. (1999) treated the solubility of beryl as an activity product of its constituent oxides in melt, i.e., $a_{Be_3Al_2Si_6O_{12}} = a_{BeO}^3 \cdot a_{Al_2O_3} \cdot a_{SiO_2}^6$. Granitic pegmatites are quartz saturated, which fixes the activity of silica in the melt, and that makes the solubility of beryl a function of the activity-concentration relationships between beryllia and alumina. Consequently, the solubility of beryl is lowest in peraluminous but otherwise chemically simple pegmatites, such as those represented by the muscovite-rare element class of Černý (1991a). Beryl exhibited the highest solubility in the chemically complex Macusani glass, which is a suitable analogue to the highly fractionated LCT pegmatites. Evensen et al. (1999) hypothesized that speciation reactions involving Be, Al, and components such as F, lowered the activities of the constituent oxides in the activity product, thereby requiring higher total concentrations of both elements to saturation melts in beryl.

The absence of beryl in the common pegmatites arises from the higher concentrations required to saturate the melt in beryl at the liquidus temperature of granite (~700°C), and from the relative compatibility of Be in muscovite and in plagioclase, which is typically in the range of oligoclase in composition (Evensen and London, 2002; London and Evensen, 2002). The compatibility of Be in these two phases effectively suppresses Be accumulation and beryl saturation in the melt. With a drop of only 100° to 600°C, however, a peraluminous melt containing 140 ppmw Be and depleted in Ca (i.e., in which the plagioclase composition is albite $<An_{10}$) would crystallize beryl in profusion (London, 2008, fig. 12-3). Thus, it is not surprising that the pegmatite type normally recognized just beyond the "barren zone" of muscovite pegmatites is of the beryl class (e.g., Trueman and Černý, 1982). If partition coefficients do not change with temperature or composition, then the abundance and distribution of beryl in the distal pegmatites will resemble those of the beryl class. The most distal pegmatites are chemically more evolved, and from the work of Evensen et al. (1999), one might expect that higher concentrations of Be would be needed to saturate these melts in beryl. However, the most distal pegmatites of a group, the rare-element pegmatites, may crystallize at lower temperatures, and hence come to beryl saturation earlier in their consolidation.

A recurrent question in the geology of pegmatites is whether the compositions of the rocks are representative of the melts from which they crystallize. Strong differences of opinion have existed, and persist today, and the Be content of beryl-bearing pegmatites is a case in point that is important enough that it is reiterated again. Several lines of evidence indicate that beryl-rich pegmatites do not contain more than a few hundred ppm Be in the bulk compositions of their magmas. The richest pegmatitic deposits of beryl contain only 205 ppm Be on average (Table 5). Experimental melt compositions from simple haplogranites to flux- and rare-element-enriched melts contain only a few hundred ppm Be at beryl saturation on the liquidus at temperatures of 650° to 700°C and 200 MPa (Evensen et al., 1999).

A field geochemical survey by Smeds (1992) found ~125 ppm Be in muscovite from "barren" pegmatites, but muscovite from beryl-rich pegmatites contains ~25 ppm Be (Smeds, 1992). This is precisely the trend described by the model above, in which muscovite is a principal host for Be at near-liquidus temperatures, but beryl becomes abundant when melts are substantially undercooled prior to crystallization (London, 2008). Using muscovite-melt partition coefficients established by Evensen and London (2002), muscovite containing 25 ppm Be would coexist with a melt that contained only ~30 ppm Be.

These low values for beryl-rich pegmatites, beryl-saturated experimental melts, and field studies of mineral-melt partitioning contrast sharply with the interpretations stemming from remelted crystalline inclusions. Thomas et al. (2011, p. 492) stated that inclusions containing 1,234 to 11,025 ppm Be provide "the evidence [that] supports the view that MI compositions in pegmatite minerals reflect the pegmatite forming magma." Those magmas in question, the granites of Ehrenfriedersdorf, Germany, contain 8.3 ± 2.5 ppm Be in their whole rocks (Thomas et al., 2011). Actual occurrences of beryl in these granites are restricted to rare hydrothermal miaroles and veins.

Beryl is common in the border zones, where its precipitation can be explained by crystallization from a highly undercooled melt along the margins of a pegmatite body. Beryl is a prevalent component of the late-stage albite-lepidolite units described above, where its accumulation can be ascribed to the process of constitutional zone refinement. A beryl-rich "fringe" commonly lies at the boundary between internal

feldspathic zones (K-feldspar or albite) and the pure quartz cores that are present in many moderately to highly fractionated pegmatites (Fig. 11). In this case, a pure beryl layer, like other monominerallic layers of garnet, tourmaline, mica, and phosphates, might be the result of localized (boundary-layer) saturation along a rapidly advancing crystallization front. (Note, however, that Thomas et al. (2012) rejected the notion of flux-enriched boundary layers as a possible explanation for their anomalously high rare-element crystalline inclusions.) The regularity of this occurrence, however, whether adjacent to giant-textured microcline or fine-grained albitic aplite, and always adjacent to massive quartz, is one of the consistent spatial associations in the zonation of pegmatite minerals.

Niobium, tin, and tantalum

The progressive enrichment of Nb, Ta, and Sn upon the fractional crystallization of granites culminates in ores of columbite or pyrochlore (Nb) and other niobates in the NYF pegmatites, and cassiterite (Sn), columbite-tantalite or microlite (Ta) in the LCT family of pegmatites (Černý, 1986; Linnen and Cuney, 2005). Kovalenko et al. (1977) and Raimbault and Burnol (1998) published phenocryst-groundmass partition coefficients that showed Nb to be compatible in "white mica," nominally muscovite, while Ta exhibited incompatible behavior. They suggested that the crystallization of white mica would lead to a decreasing Nb/Ta ratio in residual melts and their derivative rocks, which trend is seen in the evolution from granite to rare-element pegmatite (Černý et al., 1985). In a study that included trace-element partition coefficients between minerals and coexisting peraluminous (S-type) glasses, Acosta-Vigil et al. (2010) cited values of $D_{Nb}^{Bt/glass}$ = 8.55, but $D_{Ta}^{Bt/glass}$ = 3.92; for coexisting ilmenite, $D_{Nb}^{Ilm/glass}$ = 66.5, and $D_{Ta}^{Ilm/glass}$ = 41.2. In high-pressure melting experiments at 800°C and 2.5 GPa, Stepanov and Hermann (2013) reported $D_{Nb}^{Bt/glass}$ = 1.96 and $D_{Ta}^{Bt/glass}$ = 0.91. Thus the trend for both micas, biotite and muscovite, is to fractionate Nb over Ta. Stepanov and Hermann (2013) pointed out, however, that the melting intervals of muscovite and biotite are quite different. Muscovite melts almost congruently at the onset of anatexis. Near-minimum peraluminous granitic melts, representative of the S-type granites, contain 20 wt % normative muscovite component (Icenhower and London, 1995). Magnetite and hercynite are typical peritectic phases. Partial melts derived from the anatexis of aluminous gneisses and schists, however, are conspicuously low in mafic components (e.g., Stevens et al., 2007; London et al., 2012b), and consequently Fe-Ti oxides exert a negligible effect on the concentration or dispersion of HFSE during the subsequent fractional crystallization of granitic magmas. Biotite persists well beyond the initial anatectic condition (e.g., Acosta-Vigil et al., 2012), biotite recrystallizes readily with changes in the intensive conditions of its environment (London et al., 2012a), and thus biotite is likely to be in continuous chemical equilibrium with melt. Irrespective of the oxides, biotite alone in restite would lower the Nb/Ta ratio of the melt, and hence impart a Ta-enriched signature to the melts that eventually spawn the LCT family of pegmatites. Because the mass fraction of biotite in aluminous gneisses and schists tends to be large, and biotite is comparatively reactive with melt, biotite, rather than oxides, may exert the primary control on the Nb/Ta ratio at source. The subsequent crystallization of biotite and muscovite in two-mica granites should drop the Nb/Ta ratio further. The fact that the LCT family of rare-element pegmatites winds up with sufficient Nb to precipitate columbite from the start, and possesses especially high Ta concentrations, indicates that neither micas nor oxides remove sufficient HFSE to

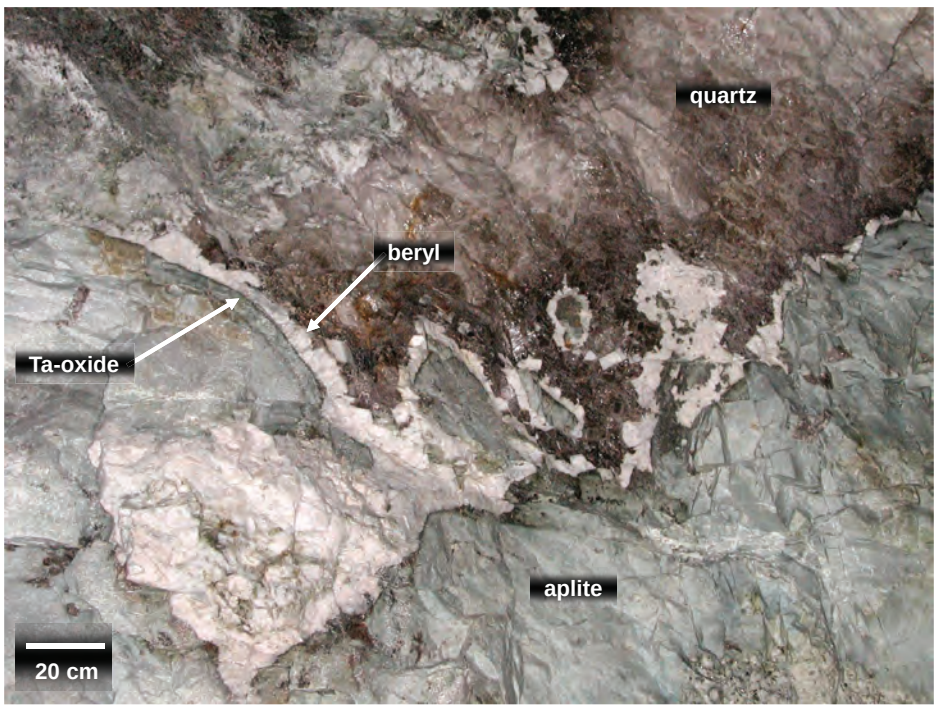

Fig. 11. A beryl "fringe" at aplite-quartz contact in the Tanco pegmatite, Manitoba (photo dated 04 November 2012). A layer of uranium-rich Ta oxides at the surface of the aplite has induced smokiness (radiation damage) in adjacent quartz.

give these components compatible behavior ($D_{HFSE}^{bulk\ mineral/melt} > 1$) as crystallization proceeds from granites to their pegmatitic stages.

Mineralization in these HFSE is normally associated with the late-stage albite-lepidolite bodies (with spodumene, beryl, apatite, etc.) or with fine-grained monominerallic albite or mica (muscovite or lepidolite). Geoscientists debate the extent to which these units are magmatic or postmagmatic in origin (e.g., van Lichtervelde et al., 2007), but that distinction may be more semantic than real. A case has been made that the miscibility between magmatic and otherwise hydrothermal fluids increases with increasing alkalinity and increasing flux content of the chemical system, such that a continuous, supercritical transition from one condition or state to the other might be feasible in some of the most evolved pegmatites (e.g., London, 1986a, Thomas et al., 2000; Sowerby and Keppler, 2002). What is evident from the geology of these HFSE is that their solubilities are high enough that they do not normally precipitate early in the evolutionary history of a pegmatite body, yet they are almost entirely endogenic in their occurrence, and at least in pegmatites, they do not form vein stockworks nor are they transported to host wall rocks by pegmatite-derived hydrothermal fluids to any appreciable extent.

Occurrences of columbite in the border zones of relatively primitive pegmatites, and sometimes tantalite in the near-margin zones of more fractionated bodies, attest to other factors that may bring a pegmatite-forming melt to saturation in HFSE at an early stage. The case for columbite in the border zones of pegmatites has been made (above) on the basis of undercooling along the pegmatite contact that brings the melt to saturation in columbite at Nb concentrations far below those of the liquidus temperature. At the Tanco mine, some of the highest grade tantalite mineralization is spatially associated with rafts or xenoliths of amphibolite in the pegmatite. This close association led Linnen (2004) to hypothesize that the diffusion of Fe from amphibolite into pegmatite-forming melt raised the solubility product of the oxides, expressed generally as $a_{A^{2+}O} \cdot a_{B^{5+}{}_2O_5}$, to the point of local saturation in the oxides. From a subsequent and detailed analysis of the Tanco pegmatite, van Lichtervelde et al. (2006) concluded that there is no statistically significant positive association of Ta mineralization with the proximity of mafic enclaves.

Zirconium, uranium, yttrium, and the rare earth elements

Ores of these HFSE are more commonly associated with alkaline igneous rocks, especially the mantle-derived family of shonkinite-ijolite-syenite-carbonatite, than with granitic compositions. However, the NYF pegmatites, which are clearly linked to the A-type granites, are quartz saturated but weakly alkaline, as they contain minor aegirine and riebeckite. Their source granites (A-type by major- and trace-element composition) are mostly characterized as metaluminous, alkalic-calcic, and ferroan (Ercit, 2005).

In the principal publication on the subject of REE-enriched pegmatites that populate the NYF family, Ercit (2005) noted that so little research has been done on these deposits that generalities or guides to exploration are difficult to draw. Ercit (2005) did observe that in the few instances where pegmatites have been mined for REE, those bodies were actually poor in lanthanides, but what they did contain was highly enriched in small portions of the pegmatite bodies. This observation is true also of the LCT pegmatites, which are REE depleted overall, but which sometimes contain high concentrations of zircon, monazite, along with the other HFSE (Nb, Ta, P, etc.) in albite-rich bodies. As noted above, the albite-rich bodies appear to fractionate from B-, P-, or F-rich residual melts, which become highly sodic and silica depleted (though quartz saturated) through this process. To this extent, the liquid line of descent in any B-, P-, or F-bearing granitic melt whose minerals do not buffer the concentrations of the fluxes will evolve toward the alkaline, sodic compositions that syenites possess.

Pegmatitic facies are commonly associated with syenite-alkaline granite complexes that constitute important deposits of REE, U, Nb, and Zr, and less commonly, Be and P. These deposits are addressed in detail by Dostal (2016). There are few fundamental differences between these deposits and those associated with the NYF family of pegmatites, except that the NYF pegmatites and their sources are always silica saturated, whereas those of the syenite-granite suites are foid bearing and normative, and they are commonly associated with carbonatites. In the syenite-carbonatite-(granite) suite, apatite tends to be abundant, whereas the NYF family of pegmatites and their A-type source granites are exceedingly depleted in P. Fluid inclusions from NYF pegmatites and from minerals associated with the alkaline granite suites are Cl rich (e.g., Roedder, 1981, 1984), whereas those from pegmatites of the LCT family tend to be exceedingly Cl poor (e.g., London et al., 2012). Whereas hydrothermal alteration and hydrothermal redistribution of ore-forming minerals is negligible within pegmatites of the LCT family, hydrothermal overprints and remobilization of HFSE is endemic to the alkaline types (e.g., Salvi and Williams-Jones, 2005).

Zonal distribution of primary ore

Following conventional usage, primary ores are those that can be ascribed to precipitation from the silicate melt, whether as bulk melt, immiscible melts, or exotic boundary layer liquids. Hydrothermal deposits are also construed as primary if they can be shown to have been deposited in the fluid-filled space without replacement of preexisting minerals. Crystals that line and fill miarolitic cavities would meet this criterion if the cavity itself did not result from a secondary process involving dissolution. Replacement bodies are those that can be ascribed to the deposition of minerals in the place of preexisting minerals. Though replacement processes in pegmatites are normally thought of as hydrothermal, or subsolidus, that is not a necessary constraint (Cameron et al., 1949).

In the summary views of Cameron et al. (1949), replacement bodies in pegmatites are uncommon to rare and relatively insignificant. Part of the reason for this point of view is that the wartime study examined all granitic pegmatites. Only the very small proportion of them that qualified as complex rare-element types might have contained some demonstrably secondary mineralogy. Because of the mineralogical and economic interest in the rare-element pegmatites, however, the large, published body of otherwise descriptive geology contains many references to replacement bodies or units in

connection with rare-element ores. In most cases, textural evidence of replacement is absent. Assemblages (including monominerallic masses) were construed as replacements simply because their compositions lie so far from that of granite.

Hydrothermal alteration and redistribution of ores

The notable distinction between rare-element pegmatites and most other types of metal deposits is the paucity of hydrothermal recrystallization within pegmatites, and the general lack of a hydrothermal redistribution of ore-forming minerals in pegmatites (except for the large, alkaline syenite-granite plutons of NYF affinity). The most prevalent characteristic of subsolidus hydrothermal alteration in Li-rich pegmatites entails exchange of K and Na for Li, which converts the lithium aluminosilicates to assemblages of eucryptite + albite, albite + muscovite, or muscovite only (London and Burt, 1982). Montebrasite first shows a loss of F, followed by metasomatic replacement by apatite and other Ca-Na phosphates, and mica. Alteration of lithiophilite-triphylite is market first by hydration and leaching of Li, then oxidation of Mn and Fe from 2+ to 3+, and the metasomatic exchange of Ca for Mn and Fe (e.g., London and Burt, 1982). Each of these hydrothermal replacements is pseudomorphic, and hence is readily discernible as secondary in origin.

Much of the lithium that is removed from the primary lithium aluminosilicates and phosphates is incorporated into Li muscovite or lepidolite that replaces large primary crystals of microcline. The secondary Li muscovite or lepidolite bodies contain appreciable quantities of Sn or Ta oxides, and hence internal redistribution of primary HFSE ores occurs to some extent (Černý, 1986).

Highly instructive exposures of the relationships between primary and secondary ore zones are accessible for viewing at the Harding pegmatite, near Dixon, New Mexico, with permission (http://epswww.unm.edu/harding/release/relform.htm). The old working face of the main cut exposes the core unit, which is comprised of small (cm-scale) spodumene laths in a random "jackstraw" arrangement, with an interstitial assemblage of albite (clevelandite habit), lepidolite, quartz, beryl (cesian), glassy fresh K-feldspar (some with the blue-green color of amazonite), manganoan apatite, and microlite (calcium tantalite; Fig. 12). That primary central ore zone grades abruptly (northward along the cut) into a replacement body in which an earlier generation of giant microcline and some spodumene crystals were replaced by lepidolite, minor quartz, uranian microlite, and the same, second generation of glassy microcline crystals. Jahns and Ewing (1977) aptly named the replacement body as the "spotted rock" zone. Though they construed the spotted rock zone as an "alternative" core unit, it is clearly secondary (replacive) in origin, and it is contiguous with the primary assemblage of the core as described above. A characteristic of complex lithium pegmatites, such as the Harding, is they may contain multiple generations of the same mineral, a later generation that remained stable and an earlier generation that did not, whose compositions are negligibly different. Dissolution and replacement within pegmatites can be highly selective, even on the scale of individual crystals (e.g., London, 2008, figs. 3-14, 4-12h, 4-19, and 8-10b).

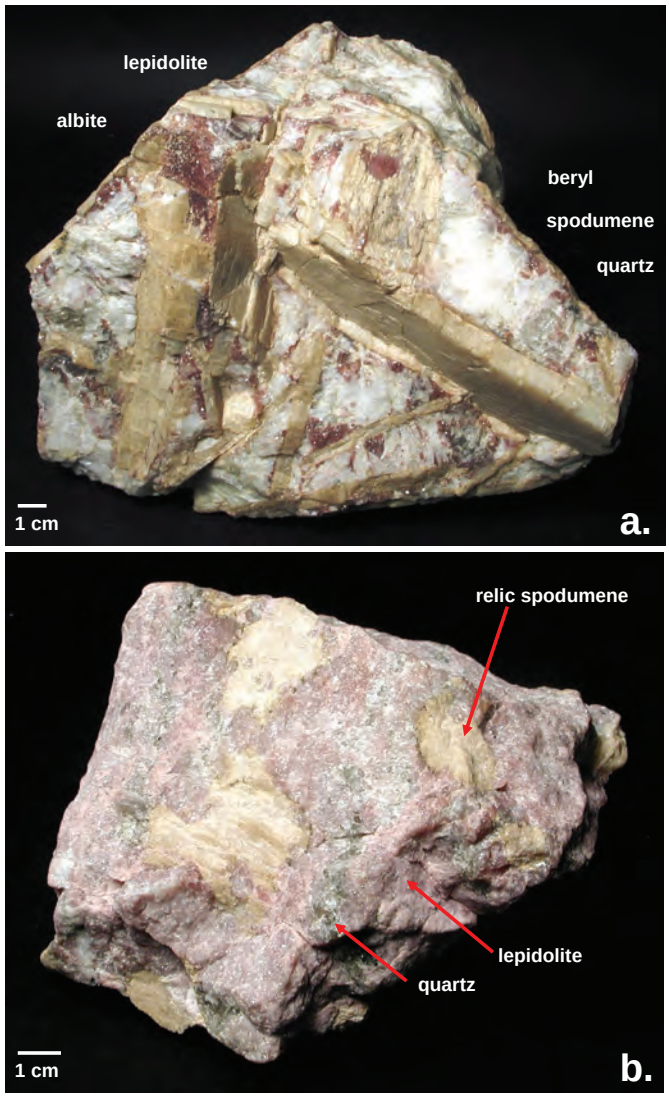

Fig. 12. (a). The primary core assemblage at the Harding pegmatite, New Mexico, consists of lath-shaped spodumene with an interstitial assemblage of platy albite, Li mica, beryl, quartz, K-feldspar (glassy white and rarely light blue), apatite, and accessory microlite. (b). Metasomatic replacement of primary pegmatite adjacent to the core left ovoid relics of spodumene and K-feldspar in a fine-grained assemblage of Li mica with sporadic patches of crystallized (glassy-white) K-feldspar, and accessory uranian microlite.

Alteration of Host Rocks

Wall-rock alteration is absent around the vast majority of the common pegmatites. It is sporadic and localized around the highly fractionated rare-element types, and only the largest few of those are surrounded by a semicontinuous aureole of altered rock. The alteration mostly entails metasomatic reactions between the host lithologies and fluids emanating from the adjacent pegmatite. Characteristic products include tourmaline, rare alkali-enriched dark mica (chemically similar to zinnwaldite), and holmquistite. Propylitic alteration indicative of the greenschist facies involves mostly hydration reactions that produce chlorite-epidote-calcite-quartz (-albite) in mafic hosts and muscovite-spessartine-"zinnwaldite"(-albite) in aluminous schists.

Tourmalinization is the most common type of replacement. With the introduction of boron (and aluminum) from pegmatite-derived fluids, almost any host rock is a candidate to produce tourmaline (Shearer et al., 1984; Morgan and London, 1989; London, 2011). In miarolitic pegmatites, tourmalinization is restricted to the host rocks that are in close proximity to miarolitic cavities, and to this extent tourmalinized wall rock is a guide to gem exploration.

Holmquistite is found around the largest Li-rich pegmatites, including Tanco, King's Mountain, and Harding (Fig. 4). In thin section, its intense blue pleochroism resembles glaucophane (Fig. 13). London (1986b) used this characteristic to locate holmquistite that had been misidentified as glaucophane in Western Australia; that is, published reports of glaucophane around pegmatites that are not associated with blueschist-facies metamorphism were construed to be holmquistite. One such location was at Ubini Station, north of the Kalgoorlie pegmatite district (Fig. 4). That pegmatite is described as having a strike length of ~1.5 km, and overlying eluvial prospects have produced manganotantalite.

Extent of wall-rock alteration

Morgan and London (1987) mapped out the metasomatic aureole around the Tanco pegmatite as evidenced by replacements of amphibolite (hornblende + plagioclase) by assemblages containing holmquistite, rare-alkali dark mica, or tourmaline. Shearer et al. (1984) similarly studied the nature and extent of metasomatic alteration around the Tip Top pegmatite, South Dakota. Both studies documented that the recognizable aureole extends only a few meters at most away from the pegmatite contacts. However, replacement reactions went nearly to completion (i.e., complete elimination of the host assemblage) in many locations. Based on the limits and extent of alteration, Shearer et al. (1984) characterized the metasomatic event as involving a small quantity of solute-rich aqueous fluid.

Not all of the alteration entails an addition of solutes from the pegmatite. In places around the Tanco body, alteration of the amphibolite produced retrograde recrystallization of the amphibolite (the propylitic assemblage) that entailed mostly hydration. Although the alteration envelope surrounds Tanco rather completely, samples of unaltered amphibolite are encountered up to the pegmatite contact.

Morgan and London (1987) noted that the spatial distribution of alteration around Tanco correlated with the mineralogy of the interior pegmatite zones that were in closest proximity to the host amphibolite. Holmquistite was developed mostly above the spodumene- and petalite-rich upper intermediate zone. Dark mica is conspicuously Cs rich above giant masses of pollucite within the upper portions of the pegmatite. Tourmaline is more prevalent in hosts along the footwall contact, where albitic rocks in the lower units of the pegmatite are tourmaline rich. Morgan and London (1987) also noted that calcite is more abundant in the propylitic assemblage along the hanging-wall contact than along the footwall. They correlated this distribution, and the preservation of petalite in the upper zones of the pegmatite, with the buoyant ascent of CO_2 fluid following solvus unmixing of an aqueous-carbonic saline solution (London, 1986).

The record of host-rock metasomatism around large lithium pegmatites corresponds to the latest and most fractionated of the internal zones. This correlation requires that the latest zones within the pegmatite have been crystallized, and the fluid egress from the pegmatite to the surrounding hosts follows from that as a subsolidus event. There is no documented evidence around any pegmatite for an early stage of fluid release to hosts. Following emplacement, chemical interaction between pegmatites and their hosts appears to entail only an influx of externally derived components from the host into the pegmatite (e.g., London, 1990; Thomas and Spooner, 1992), but no diffusive or advective counterflow until the end of consolidation. Thus, there is no evidence from pegmatite-hosted interactions that an aqueous-carbonic fluid is present in the pegmatite until the end of consolidation. From an exploration standpoint, that exogenic alteration carries the predominant chemical signature of the inner and latest pegmatite units.

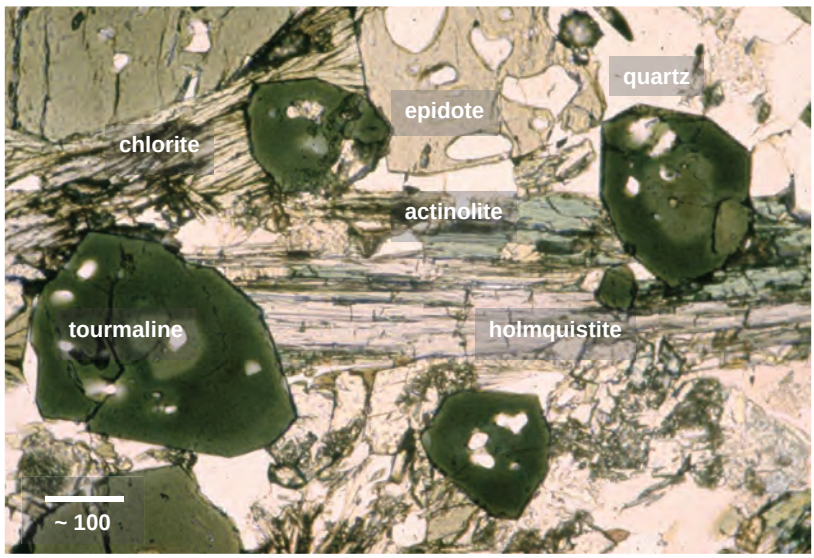

Fig. 13. Photomicrograph in plane-polarized light of the metasomatic assemblage holmquistite-tourmaline-epidote-quartz-chlorite-actinolite after amphibolite at the contact with Harding pegmatite, New Mexico. From London (2008).

Criteria for Exploration

Exploration for rare-element pegmatites has been conducted successfully based on current models for pegmatite zonation and from the signatures of chemical alteration around pegmatite bodies. The summary below lists some factors that may augment or obviate an effective exploration program for rare-element pegmatites.

Regional zonation

Vlasov (1961) attempted to use a graphic depiction to convey the regional zonation of pegmatite compositions (of the LCT family) with distance from source (Fig. 6). Trueman and Černý (1982) also illustrated this zonation schematically as a progression in the appearance of key rare-element minerals, from beryl to the lithium aluminosilicates to tantalite and pollucite (Fig. 5). What was not so evident from either zoning model is the decreasing frequency of individual bodies with increasing chemical complexity. For example, Page et al. (1953) cited only 32 out of ~24,000 pegmatite bodies in the Black Hills, South Dakota, as beryl rich, and only seven are notably lithium rich (Fig. 14). Although regional zoning within a pegmatite group points the way toward the more fractionated bodies (e.g., London, 1986), finding those very few, most evolved pegmatites becomes a matter of extensive field coverage and a serendipitous level of exposure (e.g., Tanco: Hutchinson, 1959).

Though Shearer et al. (1992) proposed that the evolved Li-rich pegmatites of the Black Hills district, South Dakota, are not genetically related to the Harney Peak granite, which is the apparent source of the many thousands of common pegmatites in the district, most of the major Li pegmatites of the Black Hills district lie near its margins, as they would if they were the distal members of a large pegmatite group. Figure 14 plots the locations of the Li-rich pegmatites on a pegmatite density contour map (from Redden et al., 1982). Most of the Li pegmatites lie close to the limits of the pegmatite field (the zero-density contour), and mostly in host rocks whose metamorphic peak did not exceed the first sillimanite isograd (i.e., on the staurolite side of that metamorphic zone). The

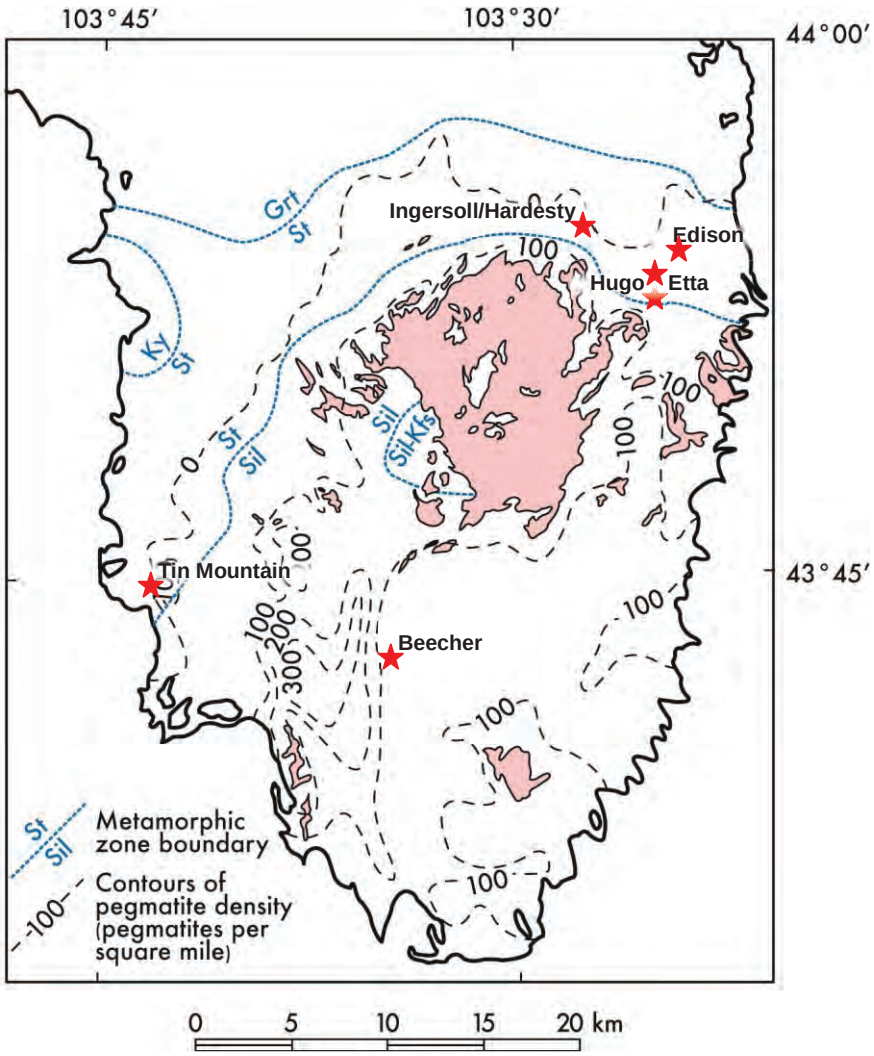

Fig. 14. Pegmatite density contour map (pegmatite bodies per square mile) in the Black Hills district, South Dakota, redrafted from Redden et al. (1982). Metamorphic zones and isograd reactions are shown in blue. Granite bodies are presented in pink. Six of the largest Li-rich pegmatites in the district are plotted as red stars.

Beecher lode lies within the mapped zone of the sillimanite-in isograd, but beyond the limits of the lowest contour of pegmatite density (100 bodies/mi^2). In short, the regional distribution of rare-element pegmatites in the Black Hills mostly conforms to the model of zonation from source within a single pegmatite group.

Chemistry of border zones

Vlasov (1961) was the first petrologist to explicitly state that each of the more fractionated, distal pegmatites in a group inherits most of the same textural-mineralogical zones of the less fractionated bodies closer to the source. This statement is certainly true of the border zones of pegmatites, which are the medium-grained granitic marginal facies, and which are similar in mineralogy and texture among all pegmatites of a group regardless of the extent of their internal differentiation. Although these are properly construed as chilled margins, they do not capture the bulk compositions of their magmas, as do chilled margins around basaltic to intermediate magma bodies. One way to explain this disparity is that the crystallization of pegmatites begins with significant fractionation of incompatible elements into the melt adjacent to the crystallization front (London, 2008). However, the textures in the outer portions of pegmatites are not indicative of growth from a flux-rich melt. Beryl and columbite also are common accessory minerals in the border zone assemblages of pegmatites. Their precipitation indicates that the melt formed upon initial crystallization of the border zones is not sufficiently flux rich to enhance their solubility and thereby preclude local saturation. For the purposes of exploration, the question is whether the border (and wall) zones of pegmatites contain chemical information that may distinguish common from rare-element pegmatites when the interior portions of individual bodies are not exposed.

An explanation for the compositions of the border zones, which are far from the bulk composition of the pegmatite-forming melt yet commonly saturated in beryl, apatite, tourmaline, garnet, and columbite, was presented as the concept "subsolidus isothermal fractional crystallization" (London, 2014a, p. 91, 2014b). In that concept, when crystallization of a multicomponent melt begins from a state of high supersaturation as caused by undercooling, the first phases to crystallize are those whose compositions are farthest from the equilibrium of the undercooled state. Hence, the first-formed feldspar is plagioclase as calcic as ~$An_{12–15}$, even though the bulk composition is far less calcic and K rich, and the composition of plagioclase within the pegmatite quickly drops to ~$An_{0–3}$.

Jolliff et al. (1992) tested the hypothesis that the border zones of pegmatites are quenched melts, and as such should reflect the bulk compositions of their pegmatites. They focused on the rare-alkali content of muscovite of the border zones around pegmatites in the Black Hill district (South Dakota) as their indicator of fractionation. Jolliff et al. (1992) observed appreciable heterogeneity in the modal compositions of border zone samples around individual pegmatites, and a statistically poor correlation of Rb and Cs contents of muscovite with the known internal zonation of the bodies. However, they did recognize a trend in K/Rb versus Cs values that correlated in a general sense with the overall chemical fractionation of the body (Jolliff et al., 1992, fig. 3b). In some instances, they recognized regions where more fractionated fluid from the inner zones had modified the composition of the border zone mica as that fluid exited the pegmatite. Thus, although the variable modal and chemical compositions of the border zones negated their efforts to apply a numerical fractionation model for the derivation of the pegmatites from the Harney Peak granite, they did ascertain that the chemistry of micas in the border zones was a useful indicator of internal composition, and that the pegmatites studied could be derived from the Harney Peak granite by 75 to 90% of fractionation crystallization from the least evolved, common pegmatites to the Li-rich rare element bodies.

The compositions of pegmatitic micas and K-feldspar have been similarly used to assess the extent of chemical fractionation in a pegmatitic body. For K-feldspars, Černý et al. (1985) demonstrated the utility of the ratio of K/Rb to Cs. These measures vary inversely with increasing chemical fractionation from parental granites to evolved pegmatites. Smeds (1992) augmented the existing data bases on trace-element contents of pegmatitic muscovite by studying unmineralized (common) pegmatites as well as those that had proven to be rich in Li, Be, and Sn. Thought the Li content of muscovite increased with the chemical fractionation of the dike, the same was not always true for Sn, and Be contents were substantially higher in beryl-absent, common pegmatites (120 ppm Be) than in beryl-mineralized rare-element dikes (25 ppm).

Exogenic chemical halos

The limit of observable metasomatic reactions in host rocks is not necessarily the limit of migration of pegmatite-derived elements. Galeschuk and Vanstone (2005) make this point through their geochemical survey in soil horizons above and around the Tanco pegmatite and a buried pegmatite, the Dibs deposit, to the east. Strontium, Mn, and Mo showed the strongest positive anomalies directly over the buried Dibs deposit. In reference to the Dibs deposit, Galeschuk and Vanstone (2005) denote "combination anomalies," which are positive concentration anomalies directly above the body and on its flanks. Two of the most geochemically mobile elements, Rb and Cs, form combination anomalies, along with two of the most immobile elements, Re and Ti. A plan contour map of Li concentrations in soils (Galeschuk and Vanstone, 2005, fig. 18) showed positive anomalies that extended a kilometer or more laterally away from the source pegmatites (Tanco and Dibs). The case study of the Dibs deposit (Galeschuk and Vanstone, 2005, table 1) may be an important guide to geochemical exploration; however, the general applicability of this technique and the elemental signatures identified with it await similar published geochemical studies from other locations.

Pegmatite textures as functions of size

London (2008, 2009) described how pegmatitic textures might evolve from the interplay between liquidus undercooling and the accumulation of fluxes in melts. Undercooling promotes the formation of fine-grained, layered, graphic, and oriented crystal fabrics. The greater the rate of heat loss in relationship to the inception and growth of crystals, the more the fabrics of pegmatites are dominated by fine-grain size,

graphic intergrowths, and unidirectional crystal growth habits that are markedly aligned inward from the margins toward the residual body of melt. The inward transition from these to more isotropic and coarse-grained textures can result from a decrease in the rate of cooling, or a decrease in the viscosity of the melt through the accumulation of fluxing components. A third factor, size, may play a part in the evolution of texture. The temperatures at the margins of thin and thick dikes may be equivalent (all else being the same except dike thickness). However, the greater heat content of thick dikes allows their interiors to cool more slowly. In large bodies, graphic quartz-feldspar intergrowths may be completely absent, and the orientational anisotropy tends to be less pronounced.

Because thinner dikes possess less heat, and hence cool more quickly than do thick magma bodies, thin dikes tend to be marked throughout by a high degree of textural anisotropy. Oriented crystals and graphic microcline-quartz intergrowths persist from margins to the well-defined centers of most dikes (e.g., London, 2008, figs. 8-6, 8-7, and 8-8). Despite the accumulation of fluxes that produce cavities filled with tourmaline, spodumene, topaz, etc., the melts from which these dikes crystallized evidently remained high in viscosity because of their low temperature of crystallization. In pegmatite dikes of Ramona, California, thin portions of dikes possess graphic textures to their centers, but graphic intergrowths evolve to monophase individual crystals of quartz and K-feldspar where the dikes thicken (London et al., 2012a).

Uebel (1977) divided pegmatites into two zones: a shell and a core. Uebel (1977) characterized the pegmatite shell by its variable grain size among different minerals and by the pronounced UST fabric of K-feldspar, tourmaline, etc. In contrast, pegmatite cores were marked by a more uniformly coarse-grained assemblage, in which crystal shapes were more equant and growth directions more isotropic. Uebel's (1977) divisions were identical to those cited in London (2009), in which London (2009) attributed the prevalence of fine-grain size and UST fabrics in the outer pegmatite zones (border, wall, and aplite) to the effects of liquidus undercooling, and the more uniform and coarse-grained interior units (intermediate and core zones) to the accumulation of fluxing components via constitutional zone refining of the bulk melt. Thin and thick portions of the same dike commonly possess different degrees of chemical fractionation, as indicated by their interior mineral assemblages. The thin portion of a dike might consist only of "common" pegmatite, with the UST fabrics that are common to the "shell" zone. As those dikes thicken, they develop not only coarser and more isotropic fabrics, but also more chemically evolved assemblages. Uebel (1977) made a similar observation, but London (2008; London et al., 2012b) explained it by the consititutional zone refining model. When consititutional zone refining operates, the more melt that is processed, the greater is the chemical fractionation of the last zone. Thus, thicker bodies achieve a greater degree of chemical fractionation at their centers than do thin bodies of the same melt composition. That contrasts with the more traditional process of Rayleigh fractionation between minerals and the bulk melt. When Rayleigh fractionation operates, the concentration profiles and final abundances of trace elements from start to finish are the same, irregardless of the thickness of the melt body.

The most common pegmatites are chemically simple (granitic) and unzoned dikes with coarse grain size. Using texture and composition as a guide, such dikes would most likely be the result of slow cooling, and crystallization closer to their liquidus temperature. That is, the temperature difference between the liquidus of the pegmatite-forming melts and their hosts would be small, and hence these pegmatites would be emplaced at depths (and temperatures) not far from their magmatic points of origin.

How different, though, are the textures of thicker dikes? The lower wall zone of the Tanco pegmatite is marked by enormous, upward-branching skeletal crystals of quartz (meters in width and length) in fine-grained albite, with interspersed giant crystals of graphic microcline-quartz that are highly oriented toward the dike center. This zone is overlain by several meters of faintly banded aplite, followed by nongraphic but still highly oriented assemblages of petalite, microcline, and montebrasite, and then quartz, with abundant beryl at the margins of the quartz bodies. This inward transition in texture at the scale of tens of meters is identical in the textural sequence and in the proportionate thickness of units as seen in dikes that are only 30 cm thick (London, 2008, figs. 8-6–8-8). At the Tanco footwall contact, the texture of the border zone is aphanitic—a porcelaneous rock of plagioclase + muscovite + quartz with skeletal Fe-Mn phosphates, tourmaline, columbite, etc. (London, 2015b, fig. 3). Despite its huge dimensions, the first melt in contact with host rocks quenched the magma, perhaps initially to glass.

The most significant consequence of body size might lie in the internal distribution of zones containing rare-element minerals. In thin miarolitic pegmatites of San Diego County, the Hindu Kush regions of Afghanistan and Pakistan, and the famous gem-bearing pegmatites of Elba (Italy), rare-element minerals including beryl, spodumene, tantalates, and pollucite are concentrated abruptly at the dike centers in a well-defined centerline array of pods or miarolitic cavities (London, 2008, fig. 3-5). In larger bodies, the final distribution of melt pools, like the fabric of the minerals themselves, is more isotropic, meaning random. Consequently, the internal zonation of rare-element ore-bearing units is more erratic, and rather than being concentrated exclusively at the center-line of the body, these residual melt pockets are distributed throughout the interior units. There is no better example of this relationship between pegmatite size and complexity of ore-bearing units than the Tanco mine (Fig. 15). As complex as that zonation is at the scale of mapping, the upper and lower intermediate zones are themselves heterogeneous, each containing isolated domains of rare-element-enriched mineral assemblages. The pattern is that of a honeycomb of more ordinary pegmatite that contains cells of highly fractionated pegmatite. For this reason, mine geologists lumped the upper and lower intermediate zones in to one "mixed zone" in earlier maps (e.g., Morgan and London, 1987, fig. 3).

Age and Distribution

Rare-element pegmatites that achieve the same high degree of chemical fractionation (e.g., to yield pollucite) are known to occur in all of the major continental terranes except Antarctica (Černý, 1991b). They span most of the known history of the earth, from the Archean to the Cenozoic (Tkachev, 2011).

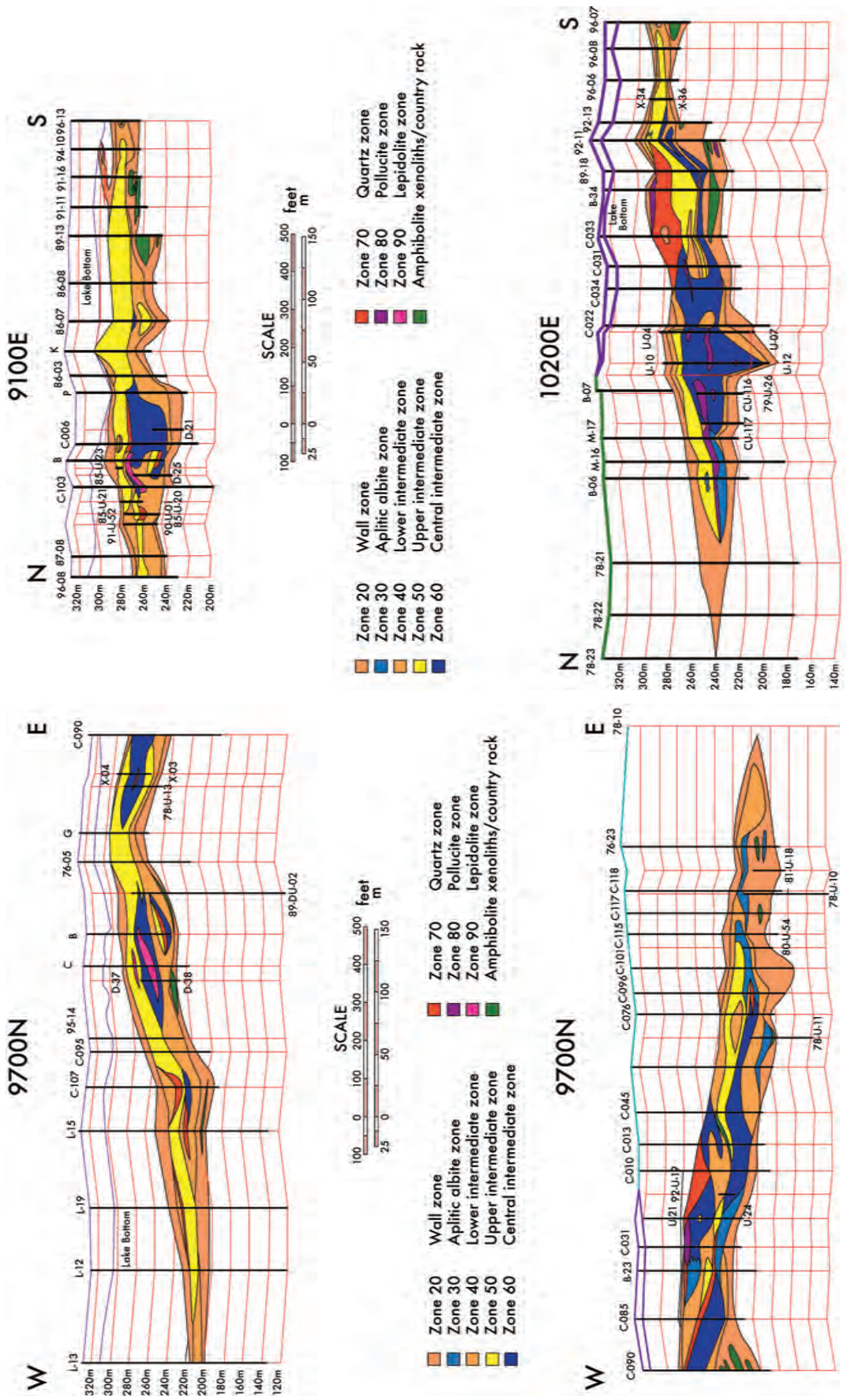

Fig. 15. Geologic cross sections NE-W (a) and N-S (b) through the Tanco pegmatite, Bernic Lake, Manitoba (Canada). The border zone (not shown) consists of albite-quartz-(tourmaline-apatite-beryl-biotite-triphylite); wall zone: albite-quartz-(beryl-muscovite-perthite-tourmaline); aplitic albite: albite-quartz-(muscovite-Ta oxides-beryl-apatite-tourmaline-sulfides-ilmenite-zircon); lower intermediate zone: microcline-albite-quartz-spodumene-montebrasite-(Li micas-lithiophilite-petalite-Ta oxides); upper intermediate zone: spodumene-quartz-montebrasite-(perthite-pollucite-lithiophilite-albite-Li micas-petalite-encryptite-Ta oxides); central intermediate zone: perthite-quartz-albite-muscovite-(beryl-Ta oxides-zircon-ilmenite-spodumene-sulfides-lithiophilite-apatite-cassiterite); quartz zone: quartz-(spodumene-montebrasite); pollucite zone: pollucite-(quartz-spodumene-petalite-Li micas-albite-microcline-apatite-elbaite); lepidolite zone: Li micas, perthite-(albite-quartz-beryl-Ta oxides-cassiterite-zircon). Redrafted from Stilling et al. (2006).

The largest pegmatitic rare-element deposits, the supergiants large enough to be minable on a mechanized scale, are all Precambrian in age. The Tanco deposit, Canada, is dated at 2641 ± 3 Ma (Camacho et al., 2012). The main pegmatite at Bikita, Zimbabwe, is 2640 ± 40 Ma (Holmes, 1954). The Greenbushes pegmatite, Western Australia, has an initial crystallization age of 2527 ± 2 Ma (Partington et al., 1995). The Harding pegmatite, New Mexico, is dated at ~1350 ± 50 Ma (Brookins, 1986) based on Rb-Sr (all others are U-Pb ages). Most are hosted by greenstones or amphibolites, even if they belong to the LCT family and are likely to have been sourced from metasediments.

Is there a fundamental difference in the volume of granite magmatism between the Precambrian and the Phanerozoic? Production of larger volumes of granite in the Archean would lead to larger volumes of melts at the pegmatite-forming stage. Larger magma bodies produce not only larger bodies but also larger rare-element orebodies. This is because of the way in which constitutional zone refining operates. The more magma that undergoes zone refining, the larger and more concentrated are the final flux- and rare-element-rich zones.

Other than size, there is no other important distinction between rare-element granites of the Precambrian and those of the Phanerozoic, except perhaps that miarolitic, gem-bearing pegmatites are more abundant in younger rocks than similarly evolved pegmatites in Precambrian terranes. Tkachev (2011) questioned this long-held conjecture, citing the older miarolitic pegmatite fields of Brazil and Africa. It might be correct to state that the very large rare-element pegmatites are all Precambrian, whereas the important districts of miarolitic pegmatites are mostly Phanerozoic.

Concluding Remarks

A few giant rare-element pegmatites are past and present major suppliers of Li and Ta. However, the worldwide distribution and locally high concentrations of minable rare-element ores in pegmatites makes them important secondary reserves of many strategic commodities, and primary sources of industrial minerals and colored gem materials. The large, "common" pegmatites represent industrial-scale sources of quartz, feldspar, and mica. The smaller rare-element and gem-bearing pegmatites remain suitable for artisanal mining, especially where labor is abundant and costs are low. Insofar as the rare metals remain strategic to modern society, their global (bulk crustal) rarity dictates that pegmatitic sources will remain as potentially important orebodies, especially in times of crisis or political instability.

Acknowledgments

Colleagues and students at the University of Oklahoma have contributed much of the data that underpins this summary. The National Science Foundation has provided numerous grants in support of this research. The electron microprobe lab, which is the source of much of the data used here, was created with a grant from the U.S. Department of Energy and is supported annually by the Vice President of Research at the University of Oklahoma. I thank Dan Kontak and Encar Roda-Robles for their detailed and constructive reviews of the manuscript.

REFERENCES

Ackermann, K.J., Branscombe, K.C., Hawkes, J.R., and Tidy, A.J.L., 1968, The geology of some beryl pegmatites in southern Rhodesia: Transactions of the Geological Society of South Africa, v. 69, p. 1–38.

Acosta-Vigil, A., Buick, I., Cesare, B., London, D., and Morgan, G.B. VI, 2012, The extent of equilibration between melt and residuum during regional anatexis and its implications for differentiation of the continental crust: A study of partially melted metapelitic enclaves: Journal of Petrology, v. 53, p. 1319–1356.

Anderson, G.M., and Burnham, C.W., 1983, Feldspar solubility and the transport of aluminum under metamorphic conditions: American Journal of Science, v. 283-A, p. 283–297.

Baker, D.R., 1996, Granitic melt viscosities: Empirical and configurational entropy models for their calculation: American Mineralogist, v. 81, p. 126–134.

——1998, The escape of pegmatite dikes from granitic plutons: Constraints from new models of viscosity and dike propagation: Canadian Mineralogist, v. 36, p. 255–263.

Bartels, A., Vetere, F., Holtz, F., Behrens, H., and Linnen, R.L., 2011, Viscosity of flux-rich pegmatitic melts: Contributions to Mineralogy and Petrology, v. 162, p. 51–60.

Bea, F., 1996, Controls on the trace element composition of crustal melts: Geological Society of America Special Paper 315, p. 33–41

——2012, The sources of energy for crustal melting and the geochemistry of heat-producing elements: Lithos, v. 153, p. 278–291.

Bebout, G.E., Bebout, A.E., and Graham, C.M., 2007, Cycling of B, Li, and LILE (K, Cs, Rb, Ba, Sr) into subduction zones: SIMS evidence from micas in high-P/T metasedimentary rocks: Chemical Geology, v. 239, p. 284–304.

Bodnar, R.J., 1998, Fluid evolution in porphyry copper deposits [abs.]: Mineralogical Magazine, v. 62A, p. 180–181.

Brögger, W.C., 1890, Die mineralien der syenitpegmatitgänge der Südnorwegischen augit und nephelinsyenite: Zeitschrift für Kristallographie und Mineralogie, v. 16, p. 1–63 and 213.

Brookins, D.G., 1986, Rubidium-strontium geochronologic studies of large granitic pegmatites: Neues Jahrbuch für Mineralogie, Abhandlungen, v. 156, p. 81–97.

Burnham, C.W., and Nekvasil, H., 1986, Equilibrium properties of granite pegmatite magmas: American Mineralogist, v. 71, p. 239–263.

Camacho, A., Baadsgaard H., Davis, D.W., and Černý, P., 2012, Radiogenic isotope systematics of the Tanco and Silverleaf granitic pegmatites, Winnipeg River pegmatite district, Manitoba: Canadian Mineralogist, v. 50, p. 1775–1792.

Cameron, E.N., Jahns, R.H., McNair, A.H., and Page, L.R., 1949, Internal structure of granitic pegmatites: Economic Geology Monograph 2, 115 p.

Černý, P., 1986, Characteristics of pegmatite deposits of tantalum, *in* Moeller, P., Cerny, P, and Saupe, F., eds., Lanthanides, tantalum and niobium: mineralogy, geochemistry, characteristics of primary ore deposits, prospecting, processing and application: Berlin, Springer, p. 195–239.

——1991a, Rare-element granite pegmatites. Part I: Anatomy and internal evolution of pegmatite deposits: Geoscience Canada, v. 18, p. 49–67.

——1991b, Rare-element granite pegmatites. Part II: Regional to global environments and petrogenesis: Geoscience Canada, v. 18, p. 68–81.

——2002, Mineralogy of beryllium in granitic pegmatites: Reviews in Mineralogy and Geochemistry, v. 50, p. 405–444.

Černý, P., and Ercit, T.S., 2005, The classification of granitic pegmatites revisited: Canadian Mineralogist, v. 43, p. 2005–2026.

Černý, P., Meintzer, R.E., and Anderson, A.J., 1985, Extreme fractionation in rare-element granitic pegmatites: Selected examples of data and mechanisms: Canadian Mineralogist, v. 23, p. 381–421.

Chakoumakos, B.C., and Lumpkin, G.R., 1990, Pressure-temperature constraints on the crystallization of the Harding pegmatite, Taos County, New Mexico: Canadian Mineralogist, v. 28, p. 287–298.

Chappell, B.W., and White, A.J.R., 1992, I- and S-type granites in the Lachlan fold belt: Transactions of the Royal Society of Edinburgh, Earth Sciences, v. 83, p. 1–26.

Christiansen, E.H., Haapala, I., and Hart, G.L., 2007, Are Cenozoic topaz rhyolites the erupted equivalents of Proterozoic rapakivi granites? Examples from the Western United States and Finland: Lithos, v. 97, p. 219–246.

Congdon, R.D., and Nash, W.P., 1991, Eruptive pegmatite magma: Rhyolite of the Honeycomb Hills, Utah: American Mineralogist, v. 76, p. 1261–1278.

Cooper, D.G., 1964, The geology of the Bikita pegmatite, *in* Haughton, S.H., ed., The geology of some ore deposits of southern Africa: Johannesburg, Geological Survey of South Africa, v. 2, p. 441–461.

Crosby, W.O., and Fuller, M.L., 1896, Origin of pegmatite: Massachusetts Institute of Geology Quarterly, v. 9, p. 326–356.
Dalou, C., Koga, K.T., Shimizu, N, Boulon, J., and Devidal, J.-L., 2012, Experimental determination of F and Cl partitioning between lherzolite and basaltic melt: Contributions to Mineralogy and Petrology, v. 163, p. 591–609.
Dingwell, D.B., Hess, K.-U., and Knoche, R., 1996, Granite and granitic pegmatite melts: Volumes and viscosities: Transactions of the Royal Society of Edinburgh, Earth Sciences, v. 87, p. 65–72.
Dostal, J., 2016, Rare metal deposits associated with alkaline/peralkaline igneous rocks: Reviews in Economic Geology, v. 18, p. 33–54.
Eby, G.N., 1990, The A-type granitoids: A review of their occurrence and chemical characteristics and speculations on their petrogenesis: Lithos, v. 26, p. 115–134.
Ercit, T.S., 2005, REE-enriched granitic pegmatites: Geological Association of Canada Short Course Notes, v. 17, p. 175–199.
Evensen, J.M., 2001, The geochemical budget of beryllium in silicic melts and superliquidus, subliquidus, and starting state effects on the kinetics of crystallization in hydrous haplogranite melts: Ph.D. dissertation, Norman, Oklahoma, University of Oklahoma, 293 p.
Evensen, J.M., and London, D., 2002, Experimental silicate mineral/melt partition coefficients for beryllium, and the beryllium cycle from migmatite to pegmatite: Geochimica et Cosmochimica Acta, v. 66, p. 2239–2265.
Evensen, J.M., London, D., and Wendlandt, R.F., 1999, Solubility and stability of beryl in granitic melts: American Mineralogist, v. 84, p. 733–745.
Fenn, P.M., 1977, The nucleation and growth of alkali feldspars from hydrous melts: Canadian Mineralogist, v. 15, p. 135–161.
——1986, On the origin of graphic granite: American Mineralogist, v. 71, p. 325–330.
Frindt, S., Haapala, I., and Pakken, L., 2004, Anorogenic Gross Spitzkoppe granite stock in central western Namibia. Part I. Petrology and geochemistry: American Mineralogist, v. 89, p. 841–856.
Galeschuk, C.R, and Vanstone, P.J., 2005, Exploration for buried rare-element pegmatites in the Bernic Lake area of southeastern Manitoba: Geological Association of Canada Short Course Notes, v. 17, p. 159–173.
Gallagher, M.J., 1975, Composition of some Rhodesian lithium-beryllium pegmatites: Transactions of the Geological Society of South Africa, v. 78, p. 35–41.
Glover, A.S., Rogers, W.Z., and Barton, J.E., 2012, Granitic pegmatites: Storehouses of industrial minerals: Elements, v. 8, p. 269–273.
Gresens, R.H., 1969, Tectonic-hydrothermal pegmatites. I. The model: Contributions to Mineralogy and Petrology, v. 15, p. 345–355.
Hermann, J., Zheng, Y.-F., and Rubatto, D., 2013, Deep fluids in subducted continental crust: Elements, v. 9, p. 281–287.
Holmes, A., 1954, The oldest dated minerals of the Rhodesian shield: Nature, v. 173, p. 612–614.
Hutchinson, R.W., 1959, Geology of the Montgary pegmatite (Manitoba) Economic Geology, v. 54, p. 1525–1542.
Icenhower, J.P., and London. D., 1995, An experimental study of element partitioning between biotite, muscovite and coexisting peraluminous granitic melt at 200 MPa (H_2O): American Mineralogist, v. 80, p. 1229–1251.
Jaeger, J.C., 1968, Cooling and solidification of igneous rocks, *in* Hess, H.H., and Poldervart, A., eds., Basalts: The Poldervaart treatise on rocks of basaltic composition: New York, John Wiley and Sons, p. 503–536.
Jahns, R.H., 1953, The genesis of pegmatites. I. Occurrence and origin of giant crystals: American Mineralogist, v. 38, p. 563–598.
——1955, The study of pegmatites: Economic Geology 50th Anniversary Volume, p. 1025–1130.
——1982, Internal evolution of pegmatite bodies: Mineralogical Association of Canada Short Course Handbook, v. 8, p. 293–327.
Jahns, R.H., and Burnham, C.W., 1969, Experimental studies of pegmatite genesis: I. A model for the derivation and crystallization of granitic pegmatites: Economic Geology, v. 64, p. 843–864.
Jahns, R.H., and Ewing, R.C., 1977, The Harding mine, Taos County, New Mexico: Mineralogical Record, v. 8, p. 115–126.
Jaskula, B.W., 2012, Lithium: U.S. Geological Survey, 2012, Mineral commodity summaries 2012, p. 94–95.
Jiang, S.-Y., Palmer, M.R., Slack, J.F., Yang, J.-H., and Shaw, D.R., 2000, Trace element and rare earth element geochemistry of tourmalinites and related rocks and ores from the Sullivan deposit and vicinity, southeastern British Columbia: Geological Association of Canada, Mineral Deposits Division Special Publication, v. 1, p. 482–495.
Jolliff, B.L., Papike, J.J., and Shearer, C.K., 1992, Petrogenetic relationships between pegmatite and granite based on geochemistry of muscovite in pegmatite wall zones, Black Hills, South Dakota, United States: Geochimica et Cosmochimica Acta, v. 56, p. 1915–1939.
Kesler, S.E., Gruber, P.W., Medina, P.A., Keoliean, G.A., Everson, M.P., and Wallington, M.P., 2012, Global lithium resources: Relative importance of pegmatite, brine and other deposits. Ore Geology Reviews (http://dx.doi.org/10.1016/j.oregeorev.2012.05.006).
Kovalenko, V.I., Antipin, V.S., Konusova, V.V., Kostyukova, Ye.S., and Pisarskaya, V.A., 1977, Partition coefficients of fluorine, niobium, tantalum, lanthanum, ytterbium, ytrium, tin, and tungsten in ongonite: Doklady Earth Science, v. 233, p. 203–205.
Kretz, R., Loop, J., and Hartree, R., 1989, Petrology and Li-Be-B geochemistry of muscovite-biotite granite and associated pegmatite near Yellowknife, Canada: Contributions to Mineralogy and Petrology, v. 102, p. 174–190.
Kunasz, I.A., 1982. Foote Mineral Company, Kings Mountain operation: Mineralogical Association of Canada Short Course Handbook, v. 8, p. 505–511.
Lindgren, W., 1933 Mineral deposits, 4th ed.: New York, NY, McGraw-Hill, 930 p.
Lindsey, D.A., 2001, Beryllium deposits at Spor Mountain, Utah: Utah Geological Survey Miscellaneous Publications, p. 73–78.
Linnen, R.L., 2004, The importance of mafic wallrocks to the generation of large pegmatite-hosted tantalum deposits [abs.]: Geological and Mineralogical Associations of Canada Abstracts Volume 29 (CD-ROM).
Linnen, R.L., and Cuney, M., 2005, Granite-related rare-element deposits and experimental constraints on Ta-Nb-W-Sn-Zr-Hf mineralization: Geological Association of Canada Short Course Notes, v. 17, p. 45–68.
Linnen, R.L., van Lichtervelde, M., and Cerny, P., 2012, Granitic pegmatites as sources of strategic metals: Elements, v. 8, p. 275–280.
Lofgren, G.E., 1980, Experimental studies on the dynamic crystallization of silicate melts, *in* Hargraves, R.B., ed., Physics of magmatic processes: Princeton, NJ, Princeton University Press, p. 487–551.
Lofgren, G.E., and Russell, W.J., 1986, Dynamic crystallization of chondrule melts of porphyritic and radial pyroxene composition: Geochimica et Cosmochimica Acta, v. 50, p. 1715–1726.
London, D., 1984, Experimental phase equilibria in the system $LiAlSiO_4$-SiO_2-H_2O: A petrogenetic grid for lithium-rich pegmatites: American Mineralogist, v. 69, p. 995–1004.
——1985, Pegmatites of the Middletown district, Connecticut: Connecticut Geological and Natural History Survey Guidebook 6, p. 509–533.
——1986a, The magmatic-hydrothermal transition in the Tanco rare-element pegmatite: Evidence from fluid inclusions and phase equilibrium experiments: American Mineralogist, v. 71, p. 376–395.
——1986b, Holmquistite as a guide to pegmatitic rare metal deposits: Economic Geology, v. 81, p. 704–712.
——1989, Lithophile rare element concentration in silicic rocks: the alkaline trend in granitic systems [abs.]: Geological and Mineralogical Associations of Canada, Program with Abstracts, v. 14, p. A21.
——1990, Internal differentiation of rare-element pegmatites: A synthesis of recent research: Geological Society of America Special Paper 246, p. 35–50.
——1992, The application of experimental petrology to the genesis and crystallization of granitic pegmatites: Canadian Mineralogist, v. 30, p. 499–540.
——1995, Geochemical features of peraluminous granites, pegmatites, and rhyolites as sources of lithophile metal deposits: Mineralogical Association of Canada Short Course Handbook, v. 23, p. 175–202.
——1999, Melt boundary layers and the growth of pegmatitic textures [abs.]: Canadian Mineralogist, v. 37, p. 826–827.
——2005a, Granitic pegmatites: an assessment of current concepts and directions for the future: Lithos, v. 80, p. 281–303.
——2005b, Geochemistry of alkalis and alkaline earths in ore-forming granites, pegmatites, and rhyolites: Geological Association of Canada Short Course Handbook, v. 17, p. 17–43.
——2008, Pegmatites: Canadian Mineralogist Special Publication 10, 368 p.
——2009, The origin of primary textures in granitic pegmatites: Canadian Mineralogist, v. 47, p. 697–724.
——2011, Experimental synthesis and stability of tourmaline: a historical overview: Canadian Mineralogist, v. 49, p. 117–136.
——2014a, A petrologic assessment of internal zonation in granitic pegmatites: Lithos, v. 184–187, p. 74–104.
——2014b, Subsolidus isothermal fractional crystallization: American Mineralogist, v. 99, p. 543–546.
——2015a, Reading pegmatites: What beryl says: Rocks and Minerals, in press.

——2015b, Reply to Thomas and Davidson on "A petrologic assessment of internal aonation in granitic pegmatites" (London 2014a): Lithos, v. 212–215, p. 469–484.
London, D., and Burt, D.M., 1982, Alteration of spodumene, montebrasite, and lithiophilite in pegmatites of the White Picacho district, Arizona: American Mineralogist, v. 67, p. 97–113.
London, D., and Evensen, J.M., 2002, Beryllium in silicic magmas and the origin of beryl-bearing pegmatites: Reviews in Mineralogy and Geochemistry, v. 50, p. 445–486.
London, D., and Kontak, D.J., 2012, Granitic pegmatites: Scientific wonders and economic bonanzas: Elements, v. 8, p. 257–261.
London, D., and Morgan, G.B. VI, 2012, The pegmatite puzzle: Elements, v. 8, p. 263–268.
London, D., Hervig, R.L., and Morgan, G.B., VI, 1988, Melt-vapor solubilities and element partitioning in peraluminous granite-pegmatite systems: Experimental results with Macusani glass at 200 MPa: Contributions to Mineralogy and Petrology, v. 99, p. 360–373.
London, D., Morgan, G.B., VI, and Hervig, R.L., 1989, Vapor-undersaturated experiments in the system macusanite-H_2O at 200 MPa, and the internal differentiation of granitic pegmatites: Contributions to Mineralogy and Petrology, v. 102, p. 1–17.
London, D., Morgan, G.B. VI, and Icenhower, J., 1998, Stability and solubility of pollucite in granitic systems at 200 MPa H_2O: Canadian Mineralogist, v. 36, p. 497–510.
London, D., Wolf, M.B., Morgan, G.B. VI, and Gallego Garrido, M., 1999, Experimental silicate-phosphate equilibria in peraluminous granitic magmas, with a case study of the Alburquerque batholith at Tres Arroyos, Badajoz, Spain: Journal of Petrology, v. 40, p. 215–240.
London, D., Evensen, J.M., Fritz, E., Icenhower, J.P., Morgan, G.B. VI, and Wolf, M.B., 2001a, Enrichment and accommodation of manganese in granite-pegmatite systems [abs.]: Annual Goldschmidt Conference, 11th, Lunar Planetary Institute Contribution 1088, Houston, Lunar Planetary Institute, Abstract 3369 (CD-ROM).
London, D., Morgan, G.B. VI, and Wolf, M.B., 2001b, Amblygonite-montebrasite solid solutions as monitors of fluorine in evolved granitic and pegmatitic melts: American Mineralogist, v. 86, p. 225–233.
London, D., Morgan, G.B. VI, and Acosta-Vigil, A., 2012a, Experimental simulations of anatexis and assimilation involving metapelite and granitic melt: Lithos, v. 153, p. 292–307.
London, D., Morgan, G.B. VI, Paul, K.A., and Guttery, B.M., 2012b, Internal evolution of a miarolitic granitic pegmatite: the Little Three mine, Ramona, California (United States): Canadian Mineralogist, in press.
Lyckberg, P., Chornousenko, V., and Wilson, W.E., 2009, Volodarsk-Volynski Zhitomir Oblast, Ukraine: Mineralogical Record, v. 40, p. 473–506.
MacDonald, R., Smith, R.L., and Thomas, J.E., 1992, Chemistry of the subalkalic silicic obsidians: U.S. Geological Survey Professional Paper 1523, 214 p.
Martin, R.F., and De Vito, C., 2005, The patterns of enrichment in felsic pegmatites ultimately depend on tectonic setting: Canadian Mineralogist, v. 43, p. 2027–2048.
Mason, B.H., and Moore, C.B., 1982, Principles of geochemistry, 4th ed.: New York, John Wiley and Sons, 344 p.
Morgan, G.B., VI, and London, D., 1987, Alteration of amphibolitic wallrocks around the Tanco rare-element pegmatite, Bernic Lake, Manitoba: American Mineralogist, v. 72, p. 1097–1121.
——1989, Experimental reactions of amphibolite with boron-bearing aqueous fluids at 200 MPa: Implications for tourmaline stability and partial melting in mafic rocks: Contributions to Mineralogy and Petrology, v. 102, p. 281–297.
——1999, Crystallization of the Little Three layered pegmatite-aplite dike, Ramona district, California: Contributions to Mineralogy and Petrology, v. 136, p. 310–330.
——2005, Phosphorus distribution between potassic alkali feldspar and metaluminous haplogranite liquid at 200 MPa (H_2O): the effect of undercooling on crystal-liquid systematics: Contributions to Mineralogy and Petrology, v. 150, p. 456–471.
Mungall, J.E., 2002, Empirical models relating viscosity and tracer diffusion in magmatic silicate melts: Geochimica et Cosmochimica Acta, v. 66, p. 125–143.
Nabelek, P.I., Whittington, A.G., and Sirbescu, M.-L.C., 2010, The role of H_2O in rapid emplacement and crystallization of granite pegmatites: Resolving the paradox of large crystals in highly undercooled melts: Contributions to Mineralogy and Petrology, v. 160, p. 313–325.
Page, L.R., Norton, J.J., Stoll, W.C., Hanley, J.B., Adams, J.W., Pray, L.C., Steven, T.A., Erickson, M.P., Joralemon, P., Stopper, R.F., and Hall, W.E., 1953, Pegmatite investigations, 1942–1945, Black Hills, South Dakota: U.S. Geological Survey Professional Paper 247, 228 p.
Partington, G.A., McNaughton, N.J., and Williams, I.S., 1995, A review of the geology, mineralization, and geochronology of the Greenbushes Pegmatite, Western Australia: Economic Geology, v. 90, p. 616–635.
Raimbault, L., and Burnol, L., 1998, The Richemont rhyolite dyke, Massif Central, France: A subvolcanic equivalent of rare-element granites: Canadian Mineralogist, v. 36, p. 265–282.
Redden, J.A., Norton, J.J., and MacLaughlin, R.J., 1982, Geology of the Harney Peak Granite, Black Hills, South Dakota: U.S. Geological Survey Open File Report 82-481, 18 p.
Rijks, H.R.P., and van-der-Veen, A.H., 1972, The geology of the tin-bearing pegmatites in the eastern part of the Kamativi district, Rhodesia: Mineralium Deposita, v. 7, p. 383–395.
Roda-Robles, E., Pesquera Perez, A., Velasco Roldan, F., and Fontan, F., 1999, The granitic pegmatites of the Fregeneda area (Salamanca, Spain): Characteristics and petrogenesis: Mineralogical Magazine, v. 63, p. 535–558.
Roedder, E., 1981, Natural occurrence and significance of fluids indicating high pressure and temperature: Physics and Chemistry of the Earth, v. 13, p. 9–39.
——1984, Fluid inclusions: Reviews in Mineralogy, v.12, 644 p.
Rossovskiy, L.N., and Matrosov, I.I., 1974, Geochemical features of topaz-lepidolite-albite pegmatites of the East Gobi, Mongolia: Geochemistry International, v. 11, p. 1323–1327.
Rubin, A.M., 1995, Getting granite dikes out of the source region: Journal of Geophysical Research, v. 100B, p. 5911–5929.
Salvi, S., and Williams-Jones, A.E., 2005, Alkaline granite-syenite deposits: Geological Association of Canada Short Course Handbook, v. 17, p. 315–341.
Shearer, C.K., Papike, J.J., Simon, S.B., Laul, J.C., and Christian, R.P., 1984, Pegmatite/wallrock interactions, Black Hills, South Dakota: Progressive boron metasomatism adjacent to the Tip Top pegmatite: Geochimica et Cosmochimica Acta, v. 48, p. 2563–2579.
Shearer, C.K., Papike, J.J., and Laul, J.C., 1987, Mineralogical and chemical evolution of a rare-element granite-pegmatite system, Harney Peak Granite, Black Hills, South Dakota: Geochimica et Cosmochimica Acta, v. 51, p. 473–486.
Shearer, C.K., Papike, J.J., and Jolliff, B.L., 1992, Petrogenetic links among granites and pegmatites in the Harney Peak rare-element granite-pegmatite system, Black Hills, South Dakota: Canadian Mineralogist, v. 30, p. 785–809.
Simmons, W.B., Pezzotta, F., Shigley, J.E., and Beurlen, H., 2012, Granitic pegmatites: Storehouses of colored gemstones: Elements, v. 8, p. 281–287.
Sirbescu, M.L., and Nabelek, P.I., 2003, Crystallization conditions and evolution of magmatic fluids in the Harney Peak Granite and associated pegmatites, Black Hills, South Dakota: Evidence from fluid inclusions: Geochimica et Cosmochimica Acta, v. 67, p. 2443–2465.
Smeds, S.A., 1992, Trace elements in potassium-feldspar and muscovite as a guide in the prospecting for lithium- and tin-bearing pegmatites in Sweden: Journal of Geochemical Exploration, v. 42, p. 351–469.
Sowerby, J.R. and Keppler, H., 2002, The effect of fluorine, boron, and excess sodium on the critical curve in the albite-H_2O system: Contributions to Mineralogy and Petrology, v. 143, p. 32–37.
Staatz, M.B., Page, L.R., Norton, J.J., and Wilmarth, V.R., 1963, Exploration for beryllium at the Helen Beryl, Elkhorn and Tin Mountain pegmatites, Custer County, South Dakota: U. S. Geological Survey Professional Paper 297C, p. 129–197.
Stepanov, A.S. and Hermann, J., 2013, Fractionation of Nb and Ta by biotite and phengite: Implications for the "missing Nb paradox:" Geology, v. 41, p. 303–306.
Stevens, G., Villaros, A., and Moyen, J., 2007, Selective peritectic garnet entrainment as the origin of geochemical diversity in S-type granites: Geology, v. 35, p. 9–12.
Stewart, D.B., 1978, Petrogenesis of lithium-rich pegmatites: American Mineralogist, v. 63, p. 970–980.
Stilling, A., Cerny, P., and Vanstone, P.J., 2006, The Tanco pegmatite at Bernic Lake, Manitoba. XVI. Zonal and bulk compositions and their petrogenetic significance: Canadian Mineralogist, v. 44, p. 599–623.
Swanson, S.E., 1977, Relation of nucleation and crystal-growth to the development of granitic textures: American Mineralogist, v, 62, p. 966–978.

Thomas, A.V., and Spooner, E.T.C., 1992, The volatile geochemistry of magmatic H_2O-CO_2 fluid inclusions from the Tanco zoned granitic pegmatite, southeastern Manitoba, Canada: Geochimica et Cosmochimica Acta, v. 56, p. 49–65.

Thomas, R., 1994, Fluid evolution in relation to the emplacement of the Variscan granites in the Erzgebirge region: A review of the melt and fluid inclusion evidence, *in* Seltmann, R., Kämpf, H., and Möller, P., eds., Metallogeny of collisional orogens: Czech Geological Survey, p. 70–81.

Thomas, R., and Davidson, P., 2012, Water in granite and pegmatite-forming melts: Ore Geology Reviews, v. 46, p. 32–46.

——2015, Comment on "A petrologic assessment of internal zonation in granitic pegmatites" by David London (2014): Lithos, v. 212–215, p. 462–468.

Thomas, R., and Klemm, W., 1997, Microthermometric study of silicate melt inclusions in Variscan granites from SE Germany: Volatile contents and entrapment conditions: Journal of Petrology, v. 38, p. 1753–1765.

Thomas, R., and Webster, J.D., 2000, Strong tin enrichment in a pegmatite-forming melt: Mineralium Deposita, v. 35, p. 570–582.

Thomas, R., Reide, D., and Turnbull, R.B., 1996, Microthermometry of volatile-rich silicate melt inclusions in granitic rocks: Zeitschrift für Geologische Wissenschaften, v. 24, p. 505–526.

Thomas, R., Webster, J.D., and Rhede, D., 1998, Strong phosphorus enrichment in a pegmatite-forming melt: Acta Universitatis Carolinae Geologica, v. 42, p. 150–164.

Thomas, R., Webster, J.D., and Heinrich, W., 2000, Melt inclusions in pegmatitic quartz: complete miscibility between silicate melts and hydrous fluids at low pressure: Contributions to Mineralogy and Petrology, v. 139, p. 394–401.

Thomas, R., Webster, J.D., and Davidson, P., 2011, Be-daughter minerals in fluid and melt inclusions: implications for the enrichment of Be in granite–pegmatite systems. Contributions to Mineralogy and Petrology, v. 161, p. 483–495.

Thomas, R., Davidson, P., and Beurlen, H., 2012, The competing models for the origin and internal evolution of granitic pegmatites in the light of melt and fluid inclusion research: Mineralogy and Petrology, v. 106, p. 55–73.

Timm, J., Klem, R., Klemme, S., Pfänder, J., Hoffman, J.E., and Gao, J., 2011, Nb-Ta fractionation by partial melting at the titanite-rutile transition: Contributions to Mineralogy and Petrology, v. 161, p. 35–45.

Tkachev, A.V., 2011. Evolution of metallogeny of granitic pegmatites associated with orogens throughout geologic time: Geological Society of London Special Publication 350, p. 7–23.

Trueman, D.L., and Cerny, P., 1982, Exploration for rare-element granitic pegmatites: Mineralogical Association of Canada Short Course Handbook, v. 8, p. 463–493.

Uebel, P.-J., 1977, Internal structure of pegmatites, its origin and nomenclature: Neues Jahrbuch für Mineralogie Abhandlungen, v. 131, p. 83–113.

van Lichtervelde, M., Linnen, R.L., Salvi S., and Beziat, D., 2006, The role of metagabbro rafts on tantalum mineralization in the Tanco granitic pegmatite, Manitoba: Canadian Mineralogist, v. 44, p. 625–644.

van Lichtervelde, M., Salvi, S., Didiear, B., and Linnen, R.L., 2007, Textural teatures and chemical evolution in tantalum oxides: Magmatic versus hydrothermal origins for Ta mineralization in the Tanco Lower Pegmatite, Manitoba, Canada: Economic Geology, v. 102, p. 257–276.

Veksler, I.V., Thomas, R., and Wirth, R., 2003, Crystallization of $AlPO_4$-SiO_2 solid solutions from granitic melt and implications for P-rich melt inclusions in pegmatitic quartz: American Mineralogist, v. 88, p. 1724–1730.

Verplanck, P.L., Mariano, A.N., and Mariano, A., Jr., 2016, Rare earth element ore geology of carbonatites: Reviews in Economic Geology, v. 18, p. 5–32.

Vlasov, K.A., 1961, Principles of classifying granite pegmatites and their textural-paragenetic types: Transactions of the Academy of Sciences U.S.S.R., Geologic Series, v. 1, p. 5–20.

Wahlberg, J.S., and Fishman, M.J., 1962, Adsorption of cesium on clay minerals: U. S. Geological Survey Bulletin, v. 1962, p. 30.

Webber, K.L., Simmons, W.B., Falster, A.U., and Foord, E.E., 1999, Cooling rates and crystallization dynamics of shallow level pegmatite-aplite dikes, San Diego County, California: American Mineralogist, v. 84, p. 708–717.

Webster, J.D., Holloway, J.R., and Hervig, R.L., 1989, Partitioning of lithophile trace elements between H_2O and H_2O + CO_2 fluids and topaz rhyolite melt: Economic Geology, v. 84, p. 116–134.

Wolf, M.B., and London, D., 1997, Boron in granitic magmas: Stability of tourmaline in equilibrium with biotite and cordierite: Contributions to Mineralogy and Petrology, v. 130, p. 12–30.

©2016 Society of Economic Geologists, Inc.
Reviews in Economic Geology, v. 18, pp. 195–216

Chapter 9

Critical Elements in Alkaline Igneous Rock-Related Epithermal Gold Deposits

Karen D. Kelley[1] and Paul G. Spry[2,†]

[1] *U.S. Geological Survey, Box 25046, Mail Stop 973, Denver, Colorado 80225*

[2] *Department of Geological and Atmospheric Sciences, 253 Science I, Iowa State University, Ames, Iowa 50011-3212*

Abstract

Alkaline igneous rock-related gold deposits, primarily of Mesozoic to Neogene age, are among the largest epithermal gold deposits in the world. These deposits are a subset of low-sulfidation epithermal deposits and are spatially and genetically linked to small stocks or clusters of intrusions possessing high alkali-element contents. Critical-, near-critical, or energy-critical elements associated with these deposits are F, platinum-group elements (PGEs), rare earth elements (REEs), Te, V, and W. Fluorine and tungsten have been locally recovered in the past, and some other elements could be considered as future by-products depending on trends in demand and supply.

The Jamestown district in Boulder County, Colorado, historically produced F from large lenticular fluorite-bearing breccia bodies and Au-Te veins in and adjacent to the Jamestown monzonite stock. Several hundred thousand metric tons (t) of fluorspar were produced. Some alkalic epithermal gold deposits contain tungsten-bearing minerals, such as scheelite, ferberite, or wolframite. Small tungsten orebodies adjacent to and/or overlapping the belt of Au telluride epithermal deposits in Boulder County were mined historically, but it is unclear in all cases how the tungsten mineralization is related genetically to the Au-Te stage. Micron-sized gold within deposits in the Ortiz Mountains in New Mexico contain scheelite but no record of tungsten production from these deposits exists.

The most common critical element in alkaline igneous-rock related gold deposits is tellurium, which is enriched (>0.5%) in many deposits and could be considered a future commodity as global demand increases and if developments are made in the processing of Au-Te ores. It occurs as precious metal telluride minerals, although native Te and tetradymite (Bi_2Te_2S) have been reported in a few localities. Assuming that the Dashigou and adjacent Majiagou deposits in Sichuan province, China, are correctly classified as alkalic-related epithermal gold deposits (exact origin remains unclear), they represent the only primary producers of Te (as tetradymite) from this deposit type.

It is worth noting that some epithermal veins (and spatially or genetically related porphyry deposits) contain high contents of Pt or Pd, or both. The Mount Milligan deposit typically contains >100 ppb Pd, and some values exceed 1,000 ppb. However, owing to the presence of other large known PGE resources in deposits in which PGEs are the primary commodities, it is unlikely that alkaline-related epithermal gold deposits will become a major source of PGEs. Similarly, many epithermal gold deposits related to alkaline rocks have high vanadium contents, but are unlikely to be considered vanadium resources in the future. Roscoelite (V-rich mica) is a characteristic mineral of alkalic-related epithermal deposits and is particularly abundant in deposits in Fiji where it occurs with other V-rich minerals, such as karelianite, Ti-free nolanite, vanadium rutile, schreyerite, and an unnamed vanadium silicate. A few alkaline intrusive complexes that contain anomalous concentrations of gold or were prospected for gold in the past are also host to REE occurrences.The best examples are the Bear Lodge Mountains in Wyoming and Cu-REE-F (±Ag, Au) vein deposits in the Gallinas Mountains in New Mexico, which have REE contents ranging up to 5.6% in addition to anomalous Au.

Introduction

On the basis of geologic environment, fluid chemistry, and alteration mineralogy, epithermal gold deposits have been divided into low-sulfidation deposits, in which the most common alteration assemblage is quartz-adularia-sericite-carbonate, and high-sulfidation deposits, which are characterized by the assemblage quartz-alunite-kaolinite-pyrophyllite (e.g., Hedenquist, 1987; White and Hedenquist, 1990, 1995; Cooke and Simmons, 2000; Hedenquist et al., 2000; Simmons et al., 2005). A subset of low-sulfidation epithermal gold deposits is specifically associated with igneous rocks possessing high alkali-element contents (e.g., Lindgren, 1933; Bonham and Giles, 1983; Bonham, 1984, 1986; Mutschler et al., 1984, 1985; Kelley et al., 1995; Richards, 1995; Jensen and Barton, 2000; Spry and Scherbarth, 2006). Comprehensive summaries of these deposits, most commonly referred to as alkalic-type epithermal gold deposits or alkaline igneous rock-related epithermal gold deposits, have been published by Mutschler et al. (1985), Richards (1995), and Jenson and Barton (2000).

Although not common, epithermal gold deposits associated with alkaline magmatism are distributed globally (Fig. 1).These deposits range widely in size and grade (Table 1). Several deposits or districts contain greater than 100 metric tons (t) of Au, including Cripple Creek, Golden Sunlight, and combined deposits in the Northern Black Hills district (Gilt Edge, Annie Creek, Foley Ridge, and Golden Reward) in the United States; the Mount Milligan porphyry and epithermal deposits in British Columbia; the Porgera-Mount Kare and Ladolam deposits in Papua New Guinea, and the Emperor deposit in Fiji (Fig. 1; Table 1). Resource estimates are poorly

† Corresponding author: e-mail, pgspry@iastate.edu

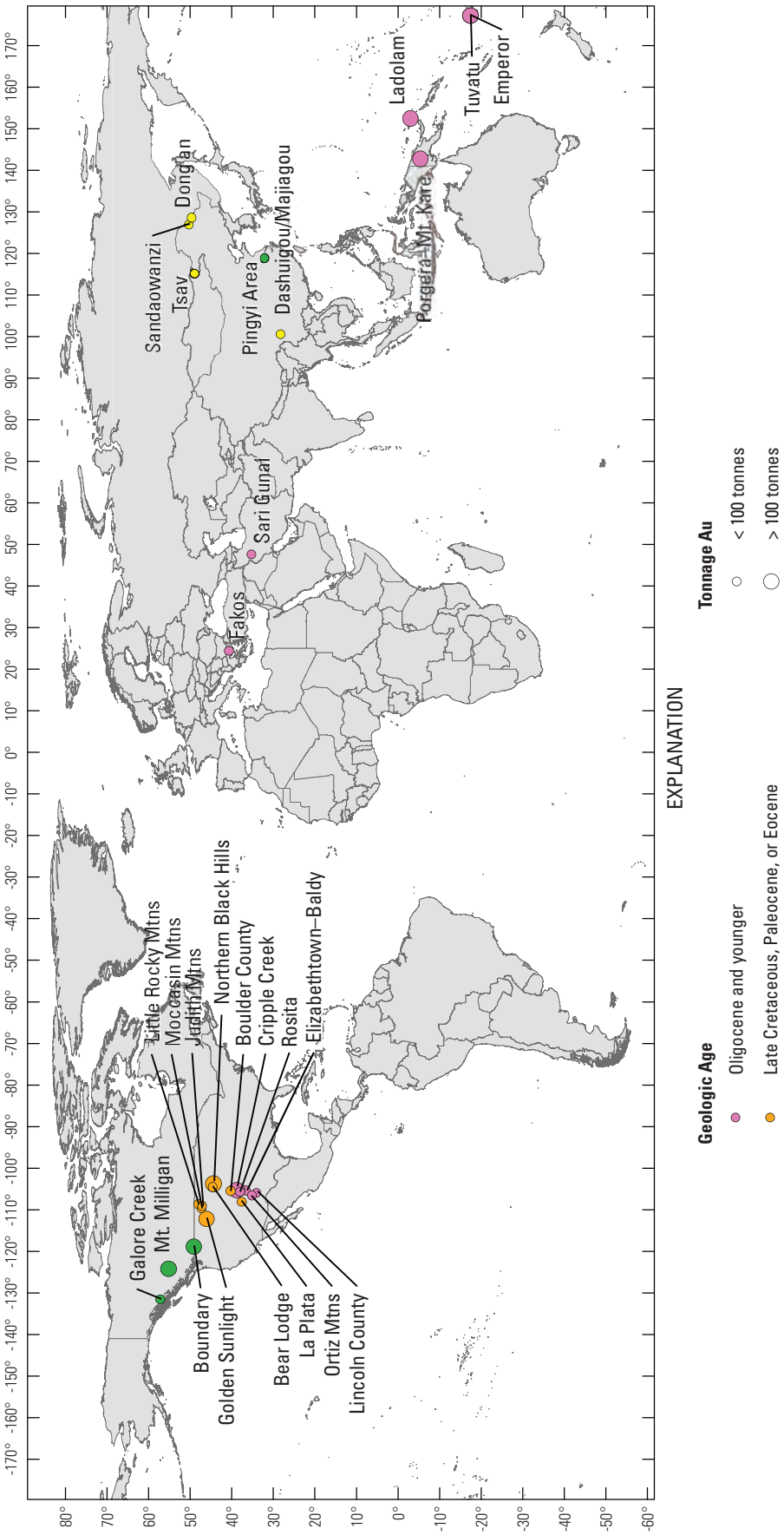

Fig. 1. Locations of epithermal gold deposits associated with alkaline rocks. Some porphyry deposits (Galore Creek, Mount Milligan) that are transitional to epithermal deposits are also shown. Deposits or districts (made up of several deposits) containing >100 t Au are shown as large solid circles. Color of circle corresponds to age of deposit or associated alkaline rocks. See Table 1 for details.

constrained for many deposits in regions of Europe and Asia. The ages of major deposits are Mesozoic to Neogene (Table 1; Fig. 1).

In addition to Au, the most common geochemical signatures displayed by these deposits include Ag, Ba, F, Te, and V, with less common Mo and W (Table 1). High concentrations of As and Sb, and enrichments in base metals characterize some deposits and a few have anomalous PGE (Mutschler et al., 1985) and elevated REE contents (Table 1). Many commodities that are commonly enriched in epithermal Au deposits associated with alkaline magmatism are defined as critical, energy critical, or near-critical in recent reports (National Institute of Advanced Industrial Science and Technology, 2008; National Research Council, 2008; U.S. Department of Energy, 2010) because they are necessary to maintain a modern standard of living. The elements that are considered to be critical depend upon location, shortage, and need. For example, the European Union considers the following 14 elements/minerals to be critical: Sb, Be, Co, F, Ga, Ge, graphite, In, Mg, Nb, PGEs, REEs, Ta, and W (e.g., Melfos and Voudouris, 2012), whereas energy critical elements (required for alternative energy technology) for sustainable development in the United States include Ag, Co, Ga, Ge, Li, PGEs, REEs, Pt, Re, Sc, Se, Te, V, and Y (Jaffe et al., 2011).

For the purpose of this paper, elements that are considered "critical elements" as defined above, and which are significantly enriched in alkaline rock-related epithermal gold deposits, are F, PGE, REE, Te, V, and W. The aim of the paper is to discuss (1) the geological and geochemical characteristics of alkaline rock-related epithermal gold deposits, and (2) the enrichments of critical elements that either have been or could be by-products if such commodities increase in criticality. A discussion of the critical elements in low- and high-sulfidation epithermal deposits is included in Goldfarb et al. (2016). Owing to the fact that many of the alkalic-related epithermal deposits are high-level expressions of deeper porphyry systems, some important aspects of the associated porphyry deposits are mentioned. However, a description of the critical elements in porphyry Cu and Mo deposits is included in a separate chapter (John and Taylor, 2016).

Deposit Characteristics

The genetic model for epithermal gold deposits must take into account the numerous shared characteristics among deposits (Table 1), which suggest similar controls on ore formation, as well as differences among deposits. Common features include the spatial association with alkaline igneous rocks, the presence of Au telluride, F, V-, or W-rich minerals, the role of early magmatic-hydrothermal fluids and involvement of externally derived groundwaters during later phases as indicated by fluid inclusion and stable isotope studies, clear relationships with alkalic porphyry-type activity, and large-scale structural control on emplacement and mineralization (Richards, 1995; Mutschler et al., 1998; Jensen and Barton, 2000; Table 1). Differences among deposits are the style and superficial characteristics of the deposit and minor differences in alteration and ore minerals. Such differences could be due to variations in host-rock composition and/or the magmatic source rocks, or to depth of erosion of the deposits.

Petrology and geochemistry of alkaline igneous rocks

There is general consensus that alkaline magmas are derived from the partial melting of metasomatic rocks in the mantle (e.g., Gast, 1968). However, debate centers on whether such melting should generate silicic or alkaline melts (e.g., Niu, 2008). Pilet et al. (2008) proposed that small partial melts of metasomatized mantle may generate amphibole-, volatile- and alkali-rich veins. Niu (2008) suggested that various degrees of mixing of melted vein material with "plume" melts may produce an alkalic magma with a broad compositional range, including syenite, monzonite, alkali basalt, diorite, latite, phonolite, vogesite, banakite, hawaiite, monchiquite, andesite, trachyte, bostonite, absarokite, and shoshonite. Alkaline magmas generally form small, isolated intrusions or clusters of intrusions that are manifested as stocks, laccoliths, dikes, and sills. The genetic relationship to lamprophyres and tinguaites remains unclear, but they may have crystallized contemporaneously with ore deposition (e.g., Gies deposit, Judith Mountains, Montana: Zhang and Spry, 1994) perhaps providing volatiles, but they also may have been emplaced postore (e.g., Golden Sunlight, Montana: Spry et al., 1996, 1997; Spry and Thieben, 2000; Cripple Creek, Colorado: Kelley et al., 1998; Jensen and Barton, 2000).

Silica contents of alkali rocks span a range from <40 to >80 wt % SiO_2, and K_2O + Na_2O contents from <2 to almost 16 wt %. When plotted in terms of alkalis versus silica (Le Bas et al., 1986), the rocks have alkali compositions close to or overlapping the alkalic-subalkalic boundary (Fig. 2). The Na/K ratio of these rocks can be highly variable within a district (see Jensen and Barton, 2000, fig. 3c, p. 286), and overlap the ultrapotassic, shoshonitic, and calc-alkaline fields of Peccerillo and Taylor (1976). Such variability characterizes rocks spatially associated with the Fakos porphyry-epithermal and Ladolam, Papua New Guinea epithermal deposits, where ultrapotassic, shoshonitic, and calc-alkaline rock compositions are indicated (Müller et al., 2001; Fornadel et al., 2012).

There are many chemical characteristics of alkaline magmas that are likely prerequisites to forming deposits rich in critical metals such as F, PGEs, REEs, Te, V, and W, as discussed in later sections. Alkaline igneous rocks associated with epithermal gold deposits typically contain an abundance of hydrous phases (e.g., hornblende and biotite), have high oxygen fugacities (as evidenced by Fe^{3+}-bearing phases such as magnetite and aegerine; Jenson and Barton, 2000), are enriched in F and Cl (Müller et al., 2001), are light REE enriched, heavy REE depleted, and possess large ion lithophile element enrichments as indicated by unaltered alkaline igneous rocks spatially associated with the Porgera, Mount Kare, Ladolam, Emperor and Tuvatu deposits (Richards and Ledlie, 1993; Müller et al., 2001; Scherbarth and Spry, 2006). Some high field strength elements are depleted at Emperor and Tuvatu (Nb, Th, Ta, and U: Scherbarth and Spry, 2006) but are enriched at Porgera and Mount Kare (Nb, Th, and U: Richards and Ledlie, 1993), reflecting differences in the intraplate setting of the deposits from the highlands of Papua New Guinea versus the relatively greater contribution of ocean-floor basalts associated with the Fijian deposits. High field strength elements are also depleted in alkalic rocks associated with the Ladolam deposit (Müller et al., 2001), which reflect

Table 1. Characteristics of Major Alkaline Igneous Rock-Related Epithermal Gold

District, location, type	Gold endowment: Tonnage and grade; contained Au (t)	Age (Ma)	Alkalic rocks	Tectonic/geologic setting
Porgera (Papua New Guinea) Epithermal Au	51 Mt at 7 g/t Au; 387 t	5	Mafic alkaline volcanics; hawaiite-mugearite	Fold-thrust belt formed by continent-island arc collision; intrusions/mineralization controlled by crustal suture
Mount Kare (Papua New Guinea) Epithermal Au	51.5 Mt at 6.5 g/t Au; 335 t	5.5	Mafic alkaline volcanics; tephrite-basanite, alkali basalt, phonotephrite, mugearite	Fold-thrust belt formed by continent-island arc collision; intrusions/mineralization controlled by crustal suture
Ladolam (Lihir Island, Papua New Guinea) Epithermal Au(±Cu) transitional to porphyry Au(+Cu)	29.1 Mt at >1 g/t Au; 497 t	1.5–0.18	Trachybasalts intruded by monzonite, syenite, and latite porphyry dikes	Tholeiites, trachybasalt, and trachyandesites formed during oceanic subduction; shoshonites formed during incipient rifting that followed
Tuvatu (Fiji) Epithermal Au-Te transitional to porphyry Cu	Unknown tonnage/grade; 13 t	5.4–4.6	Shoshonites intruded by monzonite stocks	Island-arc magmatism preceded alkaline magmatism during waning stages of subduction; faults are N-NE, parallel to NE-trending Viti Levu lineament
Emperor (Fiji) Epithermal Au-Te(±Cu) transitional to porphyry Cu	14.7 Mt at 8.1 g/t Au; 280 t	4.8–3.8	Mafic alkaline volcanics intruded by monzonite stocks	Island-arc magmatism preceded alkaline magmatism during waning stages of subduction; faults are N-NE, parallel to NE-trending Viti Levu lineament
Tsav (eastern Mongolia) Epithermal Ag-Pb-Zn	Tonnage unkown; 7.21 wt % Pb, 3.42 wt % Zn, 0.23 wt % Cu; 141 g/t Ag		Hypabyssal shoshonites to high K calc-alkaline	Veins controlled by vertical NW faults in extensional environment
Dong'an (eastern Dragon) (NE China) Epithermal Au	14 Mt at 5.04 g/t; 63.8 t	108–107	Shoshonites to high K calcalkaline subvolcanics	Collisional belt; magmatic arcs formed by subduction; veins/intrusions controlled by postorogenic tensile shears and faults
Sandaowanzi (NE China) Low sulfide Au-Te(-Ag)	15 t Au at avg 8.03 g/t	135–124	Trachytes, trachytic andesites, basalts, andesites, rhyolites overlying a monzogranite; postore (116.6 ± 2.4 Ma) diabase, syenite, syenodiorite dikes	Mesozoic oceanic subduction followed by regional extension; igneous activity controlled by large-scale extensional structures
Pingyi area (Western Shangdong, E China) Guilaizuang, Lifanggou, and Mofanggou deposits	45 total t Au at grades avg 4.9–11.54 g/t (total of three deposits)	175.7	Diorite porphyry and pyroxene-hornblende monzosyenite porphyry	Mesozoic oceanic subduction followed by regional extension; igneous activity controlled by large-scale extensional structures
Dashuigou and Majiagou (southwest China) Epithermal Te (Au)	Unknown Au tonnage; Dashuigou contains estimated 30,200 t of ore (indicated and inferred) grading 1.09% Te; Majiagou contains 13,400 at 3.26% Te	Late Triassic to mid-Cretaceous	Permian-Triassic basalt and metabasalt/marble intruded by syenite and quartz diorite	Western margin of Yangtze craton that has been tectonically active since Late Paleozoic; continental rifting in Permian, followed by compression in Late Jurassic-Cretaceous
Sari Gunay (NW Iran) Epithermal Au	52 Mt at 1.77 g/t Au; 92 t	11.7–11.0	Alkaline latites and trachytes	Structural lineament-trending NNW controls volcanic centers
Fakos (Aegean Sea, Greece) Porphyry Cu-Au(Mo) to epithermal Au-Te	Tonnage unknown; bulk rock samples up to 13 ppm Au, 780 ppm Cu, 83 ppm Mo	21–18	Quartz monzonite, late-stage dikes w/shoshonitic affinities	Collision and oceanic subduction followed by extension; late-stage epithermal veins overprint porphyry veins related to arc volcanism/plutonism during extension
Mount Milligan (British Columbia, Canada) Porphyry Cu-Au; Late stage Au-Te-Bi-PGE	706 Mt at 0.33 g/t; 232 t	183	Monzonite, monzodiorite, syenite w/shoshonitic affinities	Magmatic arc complex with intrusives and volcanics; regional NW-SE and NNE-SSW faults and structures
Galore Creek (British Columbia, Canada) Porphyry Cu-Au	125 Mt at 0.4 g/t; 50 t	Jurassic	Alkaline volcanics, syenite, monzonite and late alkalic basalts and lamprophyres	Intrusions: intraoceanic island arcs prior to or during accretion; intrusions hosted by Upper Triassic volcanic and sedimentary rocks
Boundary area (Washington, United States; British Columbia, Canada) Republic, Dusty Mac, Shasket Creek, Sappho deposits Epithermal Au and porphyry Cu-Au	13.5 at avg 11 g/t; 192 t	Jura-Cretaceous (Sappho, Shasket Cr) and Tertiary (Dusty Mac, Republic)	Alkaline igneous intrusions (dikes, plugs, sills, porphyry), including quartz monzonite and syenite	Accreted magmatic-arc; N-NE-trending extensional faults and grabens served to localize alkaline intrusions and associated mineralization

Deposits of the World, Modified and Updated after Jensen and Barton (2000)

Mineralization style/structure	Ore and gangue minerals	Trace element association	References
Disseminated Au-pyrite with Au-Te epithermal veins controlled by normal faults	aspy, Au, bar, cpy, elec, gn, hm, mc, po, py, ro, sp, te, tt	Au, Ag, Ba, Te, V	Richards et al. (19910; Richards and Kerrich (1993); Jensen and Barton (2000); Ronacher et al. (2004)
Quartz-roscoelite veins and breccias controlled by steeply-dipping shear zone; secondary Au found in colluvial deposits	Au, Au-Ag alloy, gn, py, pyr, ro, sp, te, tt	Au, Ag, Te, V	Richards and Ledlie (1993)
Deep stockwork qtz veins overlain by breccias hosting high Au	ad, an, aspy, Au, bar, carb, cin, cpy, en, gn, mc, mo, mt, po, py, qtz, rt, sp, te, tn	Au, Ag, Ba, Te	Jensen and Barton (2000); Carman (2003); Müller et al. (2001, 2002); White et al. (2010)
Au-Te veins, stockworks, hydrothermal breccias; porphyry Cu-style mineralization adjacent to epithermal deposits	ad, Au, bis, elec, fl, gn, karelianite, nolanite, mt, py, qtz, ro, schreyerite, rt (V-rich), ser, sp, te, tn	Au, Ag, As, Bi, F, Sb, Se, Te, and V	Scherbarth and Spry (2006); Spry and Scherbarth (2006)
High-grade Au-Te epithermal veins overlying deep Cu porphyry mineralization	ad, ank, aspy, Au, cpy, do, native Te, mc, py, qtz, ro, ser, sp, te, tt	Au, As, Cu, Te, V	Ahmad et al. (1987); Begg (1996); Pals and Spry (2003)
3-4.5 km long, 0.3–3 m wide, banded qtz veins and veinlets	aspy, ar, Au, bis, carb, cpy, elec, fr, gn, native Ag, py, pyr, qtz, sp, tt	Au, Ag, Cu, Pb, Zn	Gantumur et al. (2005)
1–7 m wide qtz veins and disseminated ore minerals	ad, aspy, cc, cpy, elec, fl, gn, hm, mt, native Ag, py, ser, sp	Au, Ag, Cu, F	Zhang et al. (2010)
Au-Te (with lesser sulfides) in quartz veins; fine disseminations of ore minerals in adjacent host rocks	ad, Au, cc, cpy, gn, py, qtz, ser, sp, te	Au, Ag, Cu, Te; more than 95% of ore is in telluride minerals	Liu et al. (2011)
Guilaizuiang: Qtz veins and mineralized breccias hosted in limestone/dolostone Lifanggou and Mofanggou: stratiform ore in limestone/dolostone	Guilaizuang: Au, cov, cpy, do, elec, fl, gn, hm, mc, mt, py, qtz, ser, te, tt; Lifanggou and Mofanggou: Au, cal, dol, elec, fl, gn, py, qtz, ser, sp, te	Au, Ag, Cu, F, Te	Hu et al. (2006)
Series of 13 subparallel veins within metabasalt that end at contact with marble; intense wall-rock alteration is associated with veins	Au, bi, bis (Te-bearing), cal, cpy, do, fl, hm, native Bi, po, py, qtz, ser, sp, tet, tour	Au, Ag, Bi, Cu, F, Se, Te; noted for its extreme Te enrichment	Mao et al. (2002); http://www.prnewswire.com/news-releases/apollo-solar-announces-results-of-independent-technical-review-of-dashuigou-and-majiagou-tellurium-projects-61824367.html, accessed on 09/18/14
Qtz veins, massive sulfides, vuggy infillings and diseminations; epithermal veins overprinting early, barren, porphyry veins	aspy, cin, gn, mc, orp, py, rl, sp, stb	Au, As, Hg, Sb	Richards et al. (2006)
1–10 cm qtz veins crosscut earlier porphyry mineralization and alteration	Porphyry: bn, cpy, gn, ht, mo, mt, py, sp Epithermal: Au, elec, pr, bour, eng, Au, elec, te, tn-tt	Au, As, Pb, Sb, Te	Fornadel et al. (2012)
Late-stage epithermal veins overprint and crosscut porphyry veins	Porphyry: cpy, elec, hm, mt; Epithermal: aspy, elec, gn, pge, sp, te, tn-tt, spr	Au, As, Cu, Pb, PGE, Sb, Te	DeLong (1996); Jago (2008); LeFort et al. (2011)
Disseminated Cu(Au) porphyry with peripheral Fe skarns	Au, bn, cpy, tt, mt, py, te; Au closely related to bn in core of deposit	Au, Ag, Cu, PGE	Enns et al. (1995); Lang et al. (1995)
Epithermal: veins and disseminated in breccias with some replacements (Dusty Mac); porphyry: semimassive to massive veins and sulfide disseminations	Epithermal: bn, cpy, gn, py, sp, native Ag, selenide minerals (Republic), te rare; Porphyry: cpy, mt, py	Au, Ag, Cu, PGE (Sappho; Shasket Cr), Se (Republic), Te	Zhang et al. (1989); Mutschler et al. (1985); Nixon and Archibald (2001)

Table 1.

District, location, type	Gold endowment: Tonnage and grade; contained Au (t)	Age (Ma)	Alkalic rocks	Tectonic/geologic setting
Little Rocky Mountains (Montana, United States) Zortman-Landusky Epithermal Au	109 Mt at 0.55 g/t; 59.4 t	67–60	Stocks and laccoliths of syenite porphyry; breccia pipes and breccia dikes were emplaced in altered syenite porphyry	Igneous activity: Laramide subduction; orebodies: repeated fault movement along intrusive contact; passive hot spot beneath the Great Falls tectonic zone a result of oblique subduction
Judith Mountains (Montana, United States) Spotted Horse, Gies, New Year, Warm Springs deposits Epithermal Au-Te	Tonnage and grades unknown; 21.5 t	69–62 to 47	Stocks, laccoliths, sills, and dikes of qtz diorite, monzonite, syenite, alkali syenite, and tinguaite; some breccia pipes intrude alkaline igneous rocks	Orebodies located along faults at intrusive contact; passive hot spot beneath the Great Falls tectonic zone a result of oblique subduction
Moccasin Mountains (Montana, United States) Kendall, Muleshoe deposits Epithermal Au-Te	4 Mt at 1.7 g/t; 20.8 t	66–65	Laccolith complex (sills and dikes) of alkali syenite, qtz monzonite, and syenite porphyry; development of breccia pipes within syenite porphyry	Orebodies located along faults at intrusive contact; passive hot spot beneath the Great Falls tectonic zone a result of oblique subduction
Golden Sunlight (Montana, United States) Porphyry Mo, epithermal Au-Ag telluride	70.8 Mt at 0.054 g/t; 107.7 t	~79 Ma	Dikes, sills, and stocks of quartz monzodiorite, latite porphyry, and lamprophyres	Alkaline magmas and Mineral Hill porphyry/breccia pipe developed along pre-Laramide NE transtensional Great Falls tectonic zone zone
Northern Black Hills (South Dakota, United States) Gilt Edge, Annie Creek, Foley Ridge, Golden Reward, Richmond Hill Epithermal Au-Ag	88.5 Mt at 1.4 g/t; 208.3 t	60–40	Quartz monzonites, latites, rhyolites, trachytes, and phonolites	Black Hills uplift during Laramide deformation; east-west localization of alkaline sills and lacoliths during Paleocene to Eocene
Bear Lodge (Wyoming, United States) Epithermal Au; REE	Unknown	60–38	Trachyte and phonolite stocks, sills, and laccoliths and minor carbonatite	Black Hills uplift occurred during Laramide deformation; the alkalic complex intruded during Paleocene to Eocene
Cripple Creek (Colorado, United States) Epithermal Au-Te	Historic production: 731 t Au and ore reserves (vein and disseminated) of 119.1 Mt at 1.2 g/t Au; 871 t	32–27	Diatreme and hydrothermal breccias, phonolite, tephriphonolite, lamprophyre	Incipient phases of extension (Rio Grande rift) following compression (Laramide orogeny); diatreme emplaced 40 km off axis of Rio Grande rift
Boulder County (Colorado, United States) Jamestown, Ward, Gold Hill, Central City Epithermal Au-Te	Tonnage and grade unknown; ~67.3 t (~30 from Jamestown, Gold Hill, Ward; ~37.3 from alkaline-related Au deposits from Central City)	59–44	Stocks, sills, dikes of granodiorite and monzonite, and bostonite porphyry (Central City); monzonite and syenite stocks and dikes (Ward, Gold Hill, Jamestown)	Waning Laramide subduction with slab flattened to low angle; immediately preceded extension (Rio Grande rift)
La Plata (Colorado, United States) Porphyry Cu, epithermal Au-Te	32.1 Mt at 37 g/t (epith) and 0.069 g/t (porph); 13.7 t	70–65	Alkaline diorite, monzonites, syenites (+lamprophyres?)	Late Cretaceous/Paleocene Laramide alkaline magmatism contemporaneous with subduction; intrusions occupy a 25-km structural dome
Rosita (Colorado, United States) Epithermal Au-Ag-Te	Tonnage and grades unknown; 3 t	33–27	Syenogabbro-diorite-monzonite-tracyte plutons; lamprophyry dikes; coeval high Si rhyolites and other calc-alkaline intrusions	Incipient phases of crustal extension (Rio Grande rift) following compression related to Laramide orogeny
Ortiz Mountains (New Mexico, United States) Cunningham Hill, Dolores, Lukas Canyon, Carache Canyon Epithermal Au, skarn	15.3 Mt at 1.5 g/t; 29.5 t	36–28	Nepheline-bearing monzodiorite to monzonite stocks, phreatic breccia pipes, and trachyte dikes	Incipient phases of extension (Rio Grande rift) following compression (Laramide orogeny)
Lincoln County (New Mexico, United States) Jicarilla, White Oaks, Gallinas Mountains, Nogal deposits Epithermal Au, REE (Gallinas Mountains)	Nogal: 0.6 Mt at 4.5 g/t; 0.55 t (all deposits combined)	38–26	Syenite, monzonite intrusions	Incipient phases of extension (Rio Grande rift) following compression (Laramide orogeny)
Elizabethtown-Baldy and Red River districts (New Mexico, Unted States)	0.13 Mt at 29.5 g/t; 15 t	29–26	Quartz monzonite to monzonite stocks	Incipient phases of extension (Rio Grande rift) following compression (Laramide orogeny)

Grade/tonnage and contained Au for many USA deposits are from Mutschler (1992); critical, near-critical, or energy-critical elements that are important trace element associations in these deposits

Abbreviations: act = acanthite, ad = adularia, alt = altaite, an = anydrite, ank = ankerite, ar = argentite, aspy = arsenopyrite, Au = native gold, bar = barite, bi = biotite, bis = bismuthinite, bn = bornite, cal = calcite, carb = carbonates, cc = chalcocite, cin = cinnabar, cs = celestite, cov = covellite, cpy = chalcopyrite, do = dolomite, en = enargite, fl = fluorite, fer = ferberite, fr = friebergite, gn = galena, hm = hematite, kr = krennerite, mc = marcasite, mo =

(Cont.)

Mineralization style/structure	Ore and gangue minerals	Trace element association	References
Vein and disseminated mineralization in syenite; higher grade zones are localized in regional shears	Au, py (only in deeper parts of deposit; much of the deposit is oxidized)	Au, Ag	Lindsey and Fisher (1985); Wilson and Kyser (1988)
Mineralized breccia along contact of limestone and porphyry; fissure fillings, stockwork veins, breccia cement, and replacement styles common; Au-Te is latest stage	Mineralogy complex but primarily Au, gn, fl, py, ro, sp, te	Au, Ag, F, Te, V	Woodward and Giles (1993); Mutschler et al. (1991); Zhang and Spry (1994); Woodward (1995)
Disseminated and stockwork veins; replacement in carbonate sedimentary rocks along contact with intrusive syenite	gn, py, sp, te	Au, Ag, F, Te, V	Mutschler et al. (1995); Lindsey (1985); Lindsey and Naeser (1985)
Proterozoic stratabound sulfides; Cretaceous porphyry Mo/epithermal Au in Mineral Hill breccia pipe; Au occurs in disseminations and structurally controlled veins with four stages identified	Breccia pipe: aspy, Au, bn, cpy, gn, py, sp, te (incl Bi), sulfosalts	Au, Ag, Bi, Cu, Mo, Te	Lindquist (1966); Porter and Ripley (1985); Spry et al. (1996, 1997)
Disseminated and stockwork veins; replacement in carbonate sedimentary rocks	Intrusion/breccia-hosted: Au, bar, cpy, fl, gn, mo, mt, py, te; Sedimentary replacement deposits adjacent to intrusions: Au, gn, sch, sp, te, wol	Au, Ag, As, Ba, Cu, F, Te (Pb, W, Mo)	Lisenbee (1981); Paterson et al. (1989); Mutschler (1992)
Veins and mineralized intrusive and volcanic breccias; deep base metal Ag mineralization; carbonatite dikes and breccias have REE mineralization	Auriferous py, Au; bastnaesite	Te, As, Sb, Ba, Mo, REE	Staatz (1983)
Au-telluride veins; K-alteration halos contain disseminated native gold and tellurides; deep base metal-rich zones	Veins: Au, cin (rare), cpy, do, fl, gn, hm, mo, py, sp, te, tt, stb; Disseminated Au, auriferous py	Vein-style: Au, Ag, F, Mo, Te, V; Disseminated: Au, Te	Thompson et al. (1985); Kelley et al. (1998); Jensen (2003); Jensen and Barton (2000); Vardiman et al. (2006)
Sulfide and/or telluride-bearing quartz veins; spatially (and genetically?) associated porphyry Mo (Central City, Jamestown); spatially (and genetically?) associated W-rich veins	Au, fer, fr, gn, py, sp, native Te, te, wol	Ba, Au, F, Te, V	Kelly and Goddard (1969); Geller (1994); Saunders (1991); Kelley and Ludington (2002)
Cu (Au) ± PGE porphyry-style superimposed by epithermal Au-Te veins	Porphyry: Au, bn, cpy, py, te; Epithermal: Au, bn, cpy, gn, py, sp, te, tt	Au, Te, Ba, Cu, F, PGE, Te, V	Eckel (1949); Werle et al. (1984)
Veins and disseminations in breccia pipe, following lamprophyre emplacement	cpy, gn, mo (minor), py, Sb-Ag sulfosalts, tn-tt	Au, Ag, Ba, Te	McEwan et al. (1996)
Au-bearing breccias, Au-bearing skarns, Au-bearing Cu skarns, polymetallic veins	Au, gn (minor), py, sch, sp	Au, Ag, Te, W	McLemore (1996, 2013); Kelley and Ludington (2002); Schutz (1995)
Porphyry/veins (Nogal), fracture zones (White Oaks, Jicarilla) and disseminated in breccias (Gallinas)	Nogal: Au, cpy, do, elec, gn, hm, py, qtz, sp, Gallinas: bastnaesite, fl; White Oaks/Jicarilla: Au, fl, auriferous py, sch	Nogal: Au, Ag, Mo, Pb, Te, and Zn; Gallinas: Au, Ag, REE, Fl, Te; White Oaks/Jicarilla: Au, Ag, Cu, Te, W	Griswold (1959); Campbell et al. (1991); Douglass and Campbell (1994); McLemore and North (1987); McLemore (1996, 2013)
Veins and Au-Cu skarns with molybdenite mineralization at depth; 20 km east of Questa porphyry Mo deposit	Au, auriferous py; tet (at Aztec mine)	Au, Ag, Cu, Te, W	McLemore and North (1987); McLemore (1996, 2013)

molybdenite, mt = magnetite, nm = naumannite, orp = orpiment, pge = platinum- or palladium-bearing telluride mineral (merenskyite, temagamite), or sulfosalt (stibiopalladinite, naldretteite), po = pyrrhotite, py = pyrite, pyl = pyrolusite, pyr = pyrargyrite/proustite, pz = petzite, qtz = quartz, rl = realgar, ro = roscoelite, rt = rutile, sch = scheelite, ser = sericite, sp = sphalerite, spr = sperrylite, stb = stibnite, stn = stannite, te = tellurides, tn = tennantite, tt = tetrahedrite, tet = tetradymite, teb = tellurobismutite, tour = tourmaline, wol = wolframite

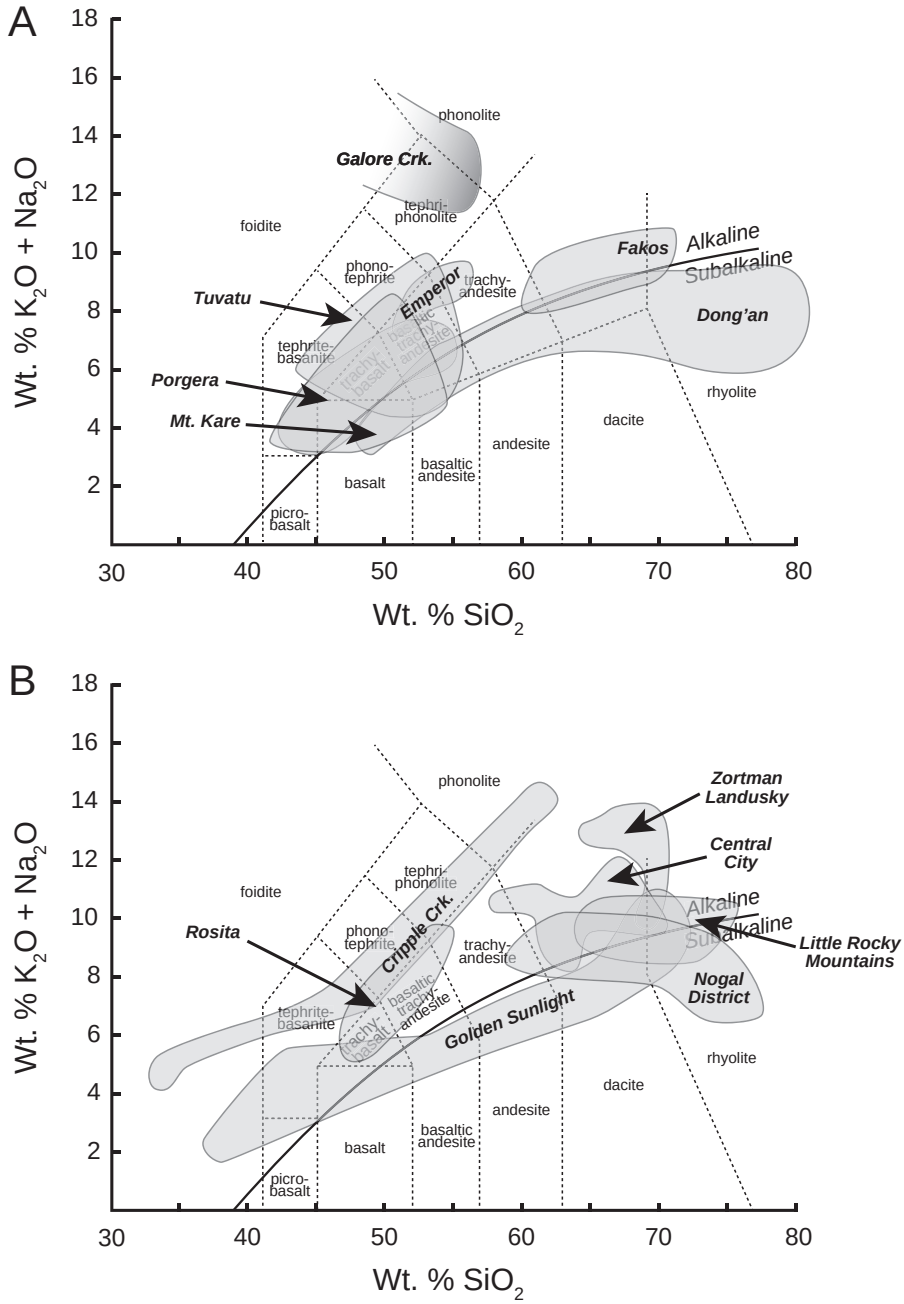

Fig. 2. Total alkali vs. silica diagrams (Le Bas et al., 1986) of igneous rock compositions spatially associated with alkaline igneous rock-related epithermal gold deposits: A. Non-United States occurrences. B. United States occurrences (see Table 1 for references). The alkalic-subalkalic boundary is derived from Irvine and Baragar (1971).

the oceanic arc setting of Lihir Island. For some deposits, compositions may be transitional to calc-alkaline rocks. Although not discussed here, it should be noted that epithermal gold-silver-telluride deposits also form in calc-alkaline rocks (see Cook et al., 2009; Goldfarb et al., 2016), and include the Baguio district, Philippines (Cooke and McPhail, 2001), the Golden Quadrilateral, Romania (e.g., Săcărâmb; Alderton and Fallick, 2000; Cook et al., 2004), the Kochbulak deposit in Uzbekistan (Kovalenker et al., 1997, 2003), and the Kassiteres, Pefka, Petrota, and Pagoni Rachi deposits, northern Greece (Voudouris, 2006).

Radiogenic isotopes are commonly used to better understand the origin of the alkaline magmas associated with epithermal gold deposits. The presence of xenoliths and the common occurrence of gold deposits in regions underlain by thin crust suggest that most gold deposits are associated with mantle-derived magmas (Jensen and Barton, 2000). At Ladolam, the presence of peridotite xenoliths and Os isotope evidence suggests the magmas were derived from a mantle source that underwent an extreme degree of noble metal enrichment (McInnes et al., 1998). Mantle sources for alkaline magmas associated with the Porgera deposit are indicated

by depleted Nd ($^{143}Nd/^{144}Nd$ ~0.512950; ε_{Nd} ~+6) and Sr ($^{87}Sr/^{86}Sr$ ~0.7035) isotope signatures (Richards et al., 1991). Major, trace, and radiogenic isotope data (Sr, Pb, and Nd) for alkaline lavas associated with mineralization at the Emperor deposit in Fiji suggest high degrees of mantle melting during subduction (Rogers and Setterfield, 1994; Pals and Spry, 2003).

In contrast to the many gold deposits associated with the more primitive magmatic systems, strontium and lead isotope compositions of Cretaceous and Tertiary alkaline rocks associated with gold deposits in the Rocky Mountain region, including Cripple Creek and deposits in Boulder County, Colorado, and those in New Mexico, reflect mantle sources that were influenced by crustal contamination. Generally low Sr isotope ratios (<0.706; Simmons and Hedge, 1978; Stein and Crock, 1990; Kelley et al., 1998) are consistent with a mantle source, but ε_{Nd} values ranging from –1.9 to –9.8 (Stein and Crock, 1990) require significant contributions from lower crust. Numerous other studies have similarly used radiogenic isotopes to determine a contribution from crustal rocks. Zhang et al. (2010) interpreted high $^{87}Sr/^{86}Sr$ ratios (>0.707253) and negative ε_{Nd} values of alkaline intrusions associated with the Dong'an deposit in northeastern China to indicate magma derivation from differentiates of parental andesitic magmas generated during partial melting of mafic lower crust, immediately preceding extension.

Geologic and tectonic setting

Assuming there is a direct genetic relationship between epithermal Au deposits and hydrous alkalic magmatism, the tectonic environment in which the magmas are generated is important. Alkalic rocks are commonly associated with rifting, convergent margins, and intraplate environments (Jensen and Barton, 2000). Alkaline rock provinces are typically characterized by low volumes of magma; therefore, these systems occur in isolation or as clusters of magmatic centers, but generally not as regionally extensive provinces (Richards, 1995).

Most gold-related alkaline igneous rocks occur in rift- and arc-related settings. Deposits in the western United States form a belt along the eastern side of the Rocky Mountains, stretching from near the border with Mexico to northern Montana and Canada (e.g., Mutschler et al., 1998; Kelley and Ludington, 2002). They are rift related, but in some areas the alkaline rock-related gold deposits are located above the easternmost part of the subducted Farallon plate. Slab subduction was responsible for the compressional Laramide orogeny (70–40 Ma) in and adjacent to the Colorado mineral belt and the transition to an extensional regime (~35–27 Ma) during slab rollback.

Some of the largest deposits (e.g., Cripple Creek, Colorado; Golden Sunlight, Montana) in the western United States are spatially associated with regional lineaments, such as deep-seated faults of the Colorado mineral belt and Great Falls tectonic zone (Montana). These reflect a first-order structural control on the localization of the alkaline rock-related epithermal gold deposits. Chaplin (2012) recently proposed that the Colorado mineral belt was defined by a NE-trending extensional zone within the underlying Farallon slab, although Richards (1995) noted evidence that the location of the belt was in part controlled by the reactivation of Precambrian basement structures associated with the Rio Grande rift, a conclusion similar to that proposed by Foster and Childs (1993) for the Great Falls tectonic zone.

Regardless of whether the alkaline igneous rock-related gold deposits formed in a continent-arc collision zone (e.g., Porgera and Mount Kare, Papua New Guinea: Richards, 1990; Richards and Ledlie, 1993), back-arc rift (e.g., Cripple Creek, Colorado: Jensen and Barton, 2000), or a postsubduction rift (e.g., Emperor, Fiji: Eaton and Setterfield, 1993; Begg and Gray, 2002; Begg et al., 2007; Fakos, Greece: Fornadel et al. 2012; and Ladolam, Papua New Guinea: Carman, 2003), the deposits are invariably associated with a transition from convergent tectonic processes to extensional or transpressive tectonics (Jensen and Barton, 2000) and are spatially related to deep-seated regional-scale faults (Richards, 1995; Carman, 2003). For example, other than the aforementioned faults associated with the Colorado mineral belt and the Great Falls tectonic zone, the two largest alkaline-rock related epithermal gold deposits in Fiji, Emperor, and Tuvatu, occur along the >250-km ENE-trending Viti-Levu lineament (e.g., Begg and Gray, 2002; Scherbarth and Spry, 2006). According to Begg and Gray (2002), this lineament was the result of northeast-southeast extension caused by a reversal of subduction direction during initial formation of the Vanuatu trench. The E-W-trending faults spatially associated with the alkaline igneous rock-related Fakos porphyry-epithermal system in Greece, are parallel to and at the western end of the major E-W-trending Intra-Pontide suture zone that extends from the northeastern part of the Aegean Sea eastward into Turkey. Similarly, the Porgera and Mount Kare deposits are located 25 and 40 km, respectively, south of a major suture zone, the Stolle-Lagaip fault. In places, these large-scale faults may facilitate the formation of cross-orogen faults that form oblique to the stress direction (e.g., Porgera, Golden Sunlight, and Cripple Creek: Richards, 1995). At the deposit scale, mineralization may occur at the intersection of major faults (e.g. Emperor: Begg, 1996), in vertical or steeply dipping structures (e.g., Mayflower mine near Golden Sunlight, Montana: Cocker, 1983; Gies, Montana: Zhang and Spry, 1994), or shallowly dipping structures (e.g., Tuvatu, Emperor). Zones of brecciation are commonly the locus of high-grade mineralization (e.g., Gies, Emperor).

Mineralization, alteration, and geochemistry

Epithermal gold deposits associated with alkaline magmatism are characterized by high-grade veins and disseminated Au, microfracture controlled in some cases, within alteration halos or hydrothermal or diatreme breccias (Table 1). Mineralization may be distributed over large vertical distances. For example, high-grade mineralization extends throughout ~1,000 m in some vein systems at Cripple Creek (Thompson et al., 1985; Vardiman et al., 2006), more than 700 m at Porgera (Richards, 1995), and more than 500 m at Emperor (Ahmad et al., 1987).

The mineralogy of epithermal deposits overlaps, in part, with that of porphyry-style mineralization formed at higher temperatures and greater depths, as discussed elsewhere in the paper. Epithermal veins typically contain native Au, gold-bearing telluride minerals, and/or auriferous pyrite. A wide variety of telluride minerals, in addition to Au-bearing

tellurides, have been reported, including Hg-, Pb-, Ag-, and Ni-bearing telluride minerals, along with selenides (naumannite) and sulfosalt minerals (Mutschler et al., 1985). Although specific PGE-rich phases are typically not evident, accompanying minerals in PGE-rich ore zones are hypogene chalcocite, bornite, and arsenide minerals (e.g., La Plata, Galore Creek, Mount Milligan), suggesting that the PGEs are hosted in these minerals. More detail about PGE enrichments in alkaline rock-related epithermal gold deposits are included in a later section.

High Au/Ag ratios are typical of vein mineralization (Mutschler and Mooney, 1995; Jensen and Barton, 2000), with some exceptions, including Zortman-Landusky in the Little Rocky Mountains, Montana; Ortiz Mountains, New Mexico; and the Republic deposit in Washington (Boundary area; Mutschler et al., 1985). Most deposits have low total sulfide, but where present, the most common sulfides are pyrite, sphalerite, and galena with subordinate tennantite-tetrahedrite, chalcopyrite, and molybdenite (Table 1; Jensen and Barton, 2000). In addition to vein gold, disseminated grains of native gold or auriferous pyrite are widespread in alteration halos or hydrothermal and diatreme breccias. Distributed gold in pyrite is most commonly reported as micron-sized native gold, but gold concentrations of as much as 100 ppm in solid solution in pyrite have been determined by secondary ion mass spectroscopy analyses from Cripple Creek and Emperor (Jensen and Barton, 2000; Pals et al., 2003). Where sizeable, the disseminated Au may constitute economic gold resources, such as at Zortman-Landusky in the Little Rocky Mountains (Hastings, 1988; Wilson and Kyser, 1988), Cripple Creek (Thompson et al., 1985; Kelley et al., 1998; Jensen and Barton, 2000), and Porgera (Richards, 1995).

Roscoelite (V-rich mica) is commonly present in veins and alteration halos, particularly in deposits with mafic wall rocks (Mutschler et al., 1985; Richards, 1995; Jensen and Barton, 2000; Pals and Spry, 2003). However, V may occur in other minerals including karelianite, vanadian muscovite, Ti-free nolanite, vanadian rutile, schreyerite, and an unnamed vanadium silicate as was described by Spry and Scherbarth (2006) for the Tuvatu deposit, Fiji.

Fluorite is common in systems hosted by felsic alkaline rocks (Cripple Creek, Colorado: Kelley et al., 1998; Boulder County, Colorado: Geller, 1994), and scheelite, ferberite, or wolframite is present in some breccia and alkalic gold epithermal vein deposits (e.g., Ortiz Mountains, New Mexico: Maynard, 1995; Boulder County, Colorado: Lovering and Tweto, 1953). Other common gangue or trace minerals in the veins include varying proportions of quartz, carbonates (ankerite, calcite, dolomite, and rare rhodochrosite), adularia, and sulfates (anhydrite, barite, celestite, and rare alunite). Many epithermal deposits also contain hematite or magnetite (Thompson et al., 1985; Ahmad et al., 1987; Zhang and Spry, 1994; Spry et al., 1996), consistent with relatively oxidized fluids (Jenson and Barton, 2000).

Potassium metasomatism has been described in nearly all epithermal gold deposits associated with alkaline rocks. In almost all examples, significant amounts of potassium were added during the process of alteration, whereas sodium and calcium were leached (Jensen and Barton, 2000). The style of alteration varies with magma type and host-rock composition. Potassium alteration is dominant in systems with felsic rocks, commonly occurring as broad zones of K feldspathized wall rocks (e.g., Cripple Creek, Zortman-Landusky), whereas zones of sericite + carbonate + K feldspar assemblages predominate in mafic-intermediate rocks (e.g., Porgera-Mount Kare: Richards et al., 1991; Emperor: Ahmad et al., 1987; Pals and Spry, 2003). During potassium metasomatism, K-silicate phases replace nepheline, plagioclase, or Na-rich alkali feldspar (Richards et al., 1991). Mafic mineral sites are typically replaced by sulfides (pyrite ± arsenopyrite, pyrrhotite, marcasite, and base metals), Fe-Mg carbonates, leucoxene, and clays (illite-montmorillonite), which give the rock a bleached appearance (Jensen and Barton, 2000).

In some alkalic-related epithermal gold deposits, pervasive alteration assemblages formed prior to ore deposition in epithermal deposits, including phyllic (argillization and sericitization) and carbonate alteration (Mutschler et al., 1985). Phyllic alteration associated with the Porgera deposit is extensive and is associated with large tonnages of low-grade refractory gold mineralization (Richards et al., 1991). Regional peripheral propylitic alteration is variably developed, most likely having formed prior to epithermal mineralization, sometimes in association with deeper porphyry-style deposits (Ladolam: Moyle et al., 1990; Emperor: Pals and Spry, 2003).

Epithermal gold deposits associated with alkaline rocks are sometimes characterized by low abundances of hydrothermal quartz and lack the acid alteration assemblages that characterize high-sulfidation epithermal deposits (Jensen and Barton, 2000), although there are many exceptions as noted below. For example, although of uncertain origin due to a sparsity of information, the Dong'anor Eastern Dragon deposit in northeastern China (Zhang et al., 2010), Lifanggou deposit in the Pingyi area near the Tan-Lu fault in eastern China (Hu et al., 2006), and the Sandaowanzi deposit in northeastern China (Liu et al., 2011) have silica-rich alteration zones, particularly adjacent to veins. Several deposits contain zones of advanced argillic alteration, including the Ladolam (Moyle et al., 1990; Richards, 1995), Fakos (Fornadel et al., 2012), Emperor (Eaton and Setterfield, 1993), and Rosita (Mutschler et al., 1998) deposits, which are characterized by kaolinite (±pyrophyllite or dickite), alunite, and quartz alteration superimposed upon earlier potassic alteration (Jensen and Barton, 2000). Restricted zones of acid alteration (quartz-dickite) are also noted in some deposits such as Cripple Creek (Jensen and Barton, 2000), Golden Sunlight (Spry et al., 1996), and the Bessie G deposit (La Plata Mountains, southwest Colorado; (Saunders and May, 1986) as narrow, late-stage veins that cut across all other assemblages (Jensen and Barton, 2000).

Source of metals and origin of fluid

Strontium and lead isotope compositions of ore and gangue minerals (apatite, carbonates, roscoelite, and galena) from veins in the Porgera deposit fall between the compositions of the Porgera intrusions and their host sedimentary rocks (Richards et al., 1991), suggesting a mixed magmatic-sedimentary source for both Pb and Sr, whereas the bulk of the precious-metal content was likely of magmatic origin (Richards, 1995). Vein galena samples from the Cripple Creek deposit almost entirely overlap those of K feldspar from alkaline igneous rocks, suggesting a genetic relationship between alkaline

magmatism and mineralization. However, higher $^{207}Pb/^{204}Pb$ and $^{208}Pb/^{204}Pb$ ratios of some galenas suggest a contribution to the ore fluid from surrounding early Proterozoic rocks, probably through leaching by mineralizing fluids (Kelley et al., 1998).

Stable isotope compositions ($\delta^{18}O$ and δD) are commonly used to constrain the origin of ore-forming fluids. Reported fluid compositions in equilibrium with gangue minerals show significant enrichment in ^{18}O and depletion in D, inconsistent with present-day meteoric water (Fig. 3). Ore fluids from some alkalic-related Au deposits at least partly overlap with the field for volcanic vapor produced by magmatic boiling (Hedenquist et al., 1998) and/or the arc magmatic water field (Taylor, 1997; Fig. 3). The range in values for the Porgera (Richards and Kerrich, 1993), Emperor (Ahmad et al., 1987), Dashuigou (Mao et al., 2002), Tuvatu (Scherbarth and Spry, 2006), Golden Sunlight (Spry et al., 1996), and Cripple Creek deposits (Kelley et al., 1998), and epithermal deposits (Annie Creek and Gilt Edge) from the northern Black Hills, South Dakota (Paterson et al., 1989), Central City area in the Boulder County district, Colorado (Rice et al., 1985), and deposits in the Pingyi area in eastern China (Hu et al., 2006) are similar to each other but are displaced to lower δD values compared to the magmatic water field (Fig. 3), although they overlap with respect to $\delta^{18}O$ values (Fig. 3). These deposits may have formed almost exclusively from magmatic fluids, although contributions from meteoric or other external fluids (seawater, evolved groundwater) were likely important to different degrees in the genesis of these deposits.

Excursions in $\delta^{18}O$ and δD suggest contributions from external fluids in late stages of deposit formation.The Mount Milligan and Dusty Mac deposits (British Columbia) are depleted in either δD or $\delta^{18}O$ or both compared to magmatic fluids, or most other epithermal Au deposits associated with alkaline rocks (Fig. 3). LeFort et al. (2011) stated that the stable isotope systematics for porphyry- and epithermal-style veins are similar at Mount Milligan, and that the δD depletion in fluids is typical of other porphyry systems in British Columbia. This shift in δD is attributed to mixing or contamination of magmas or magmatic fluids with evolved groundwater or assimilation of D-depleted country rocks.

Many epithermal Au deposits associated with alkaline rocks are characterized by light sulfur isotopes, attributed to the oxidation state of sulfur in alkaline systems or the progressive oxidation of hydrothermal fluids through boiling, or to leaching of sedimentary sulfur (Richards and Kerrich, 1993; Jensen and Barton, 2000). Sulfur isotope compositions of sulfides from the porphyry and epithermal deposits suggest a common sulfur source for the two styles of mineralization. Examples of such overlapping values include those from the Fakos porphyry-epithermal (Fornadel et al., 2012), Golden Sunlight (Spry et al., 1996), and Porgera deposits (Richards and Kerrich, 1993).

Link with Porphyry-Style Deposits

The genetic link between alkaline rock-related gold deposits and porphyry-style Cu or Mo deposits has long been known and is well documented (e.g., Richards, 1995; Jensen and Barton, 2000). The ore-forming processes for both porphyry and epithermal types of mineralization is part of a continuum of magmatic high-temperature conditions to later lower temperature hydrothermal epithermal-style mineralization. Such a spatial relationship has been recognized between porphyry Cu and gold telluride mineralization for example at Emperor (e.g., Eaton and Setterfield, 1993; Begg, 1996), LaPlata (Werle et al., 1984), Tuvatu (Scherbarth and Spry, 2006), Fakos (Fornadel et al., 2012), Ladolam (Müller et al., 2002; Carman, 2003), and Porgera (Ronacher et al., 2004; Cooke et al., 2006). Similarly, such a spatial relationship exists among low-grade porphyry Mo and gold tellurides at Golden Sunlight (Spry et al., 1996) and Central City (Rice et al., 1985).

Increased dissolved H_2O (and CO_2, F, Cl) of these magmas may have resulted in more productive gold deposits due to more efficient magmatic-hydrothermal systems. High volatile contents (e.g., H_2O, F, CO_2) may also have promoted F, Te, and V enrichment, explaining the presence of fluorite, roscoelite, and/or telluride minerals in these deposits. Nonetheless, there are several alkaline igneous rock epithermal gold deposits devoid of these minerals (Table 1). Although reasons for enrichment in some deposits and not others are still unclear, variations in the source regions of the magmas (e.g., composition of underlying crust) and composition of the magmas themselves have been proposed as possible mechanisms (Kelley and Luddington, 2002).

Critical Elements in Alkaline Rock-Related Epithermal Gold Deposits

Many epithermal gold deposits associated with alkaline igneous rocks show enrichments in critical, near-critical, or energy-critical elements (as defined above) such as F, PGEs, REEs, Te, V, and W (Mutschler et al., 1991, 1998). As discussed previously, a clear genetic relationship among epithermal alkalic-related gold deposits and porphyry Cu-style mineralization has been demonstrated at several localities. In other cases, porphyry-style mineralization and epithermal mineralization are associated with alkaline igneous rocks of similar age within a single district, but a direct genetic link between the deposit types has not been determined. The following sections describe the distribution of F, PGE, REE, Te, V, and W in alkalic igneous rock-related epithermal gold deposits and/or associated porphyry deposits that have a clear temporal and genetic link with the epithermal ores. More details on alkalic-related porphyry deposits are in John and Taylor (2016).

Fluorine (F)

Fluorine is one of five halogen elements along with chlorine, bromine, iodine, and astatine. The ionic radius of 1.36 angstroms (Å) allows it to substitute in mineral structures for the hydroxyl ion (ionic radius 1.40Å; Fleischer and Robinson, 1963). Fluorine is considered incompatible in igneous systems because it is not incorporated in common silicates that crystallize from the melt. As a result, it is concentrated in the residual magma during differentiation. Therefore, highly differentiated magmas tend to contain relatively higher fluorine contents (Shawe, 1976). The average fluorine concentrations in unmineralized alkaline intrusive igneous rocks are high, ranging from a mean of 1,100 ppm in alkalic ultramafic rocks to 2,640 ppm in some felsic alkaline intrusions (Shawe, 1976).

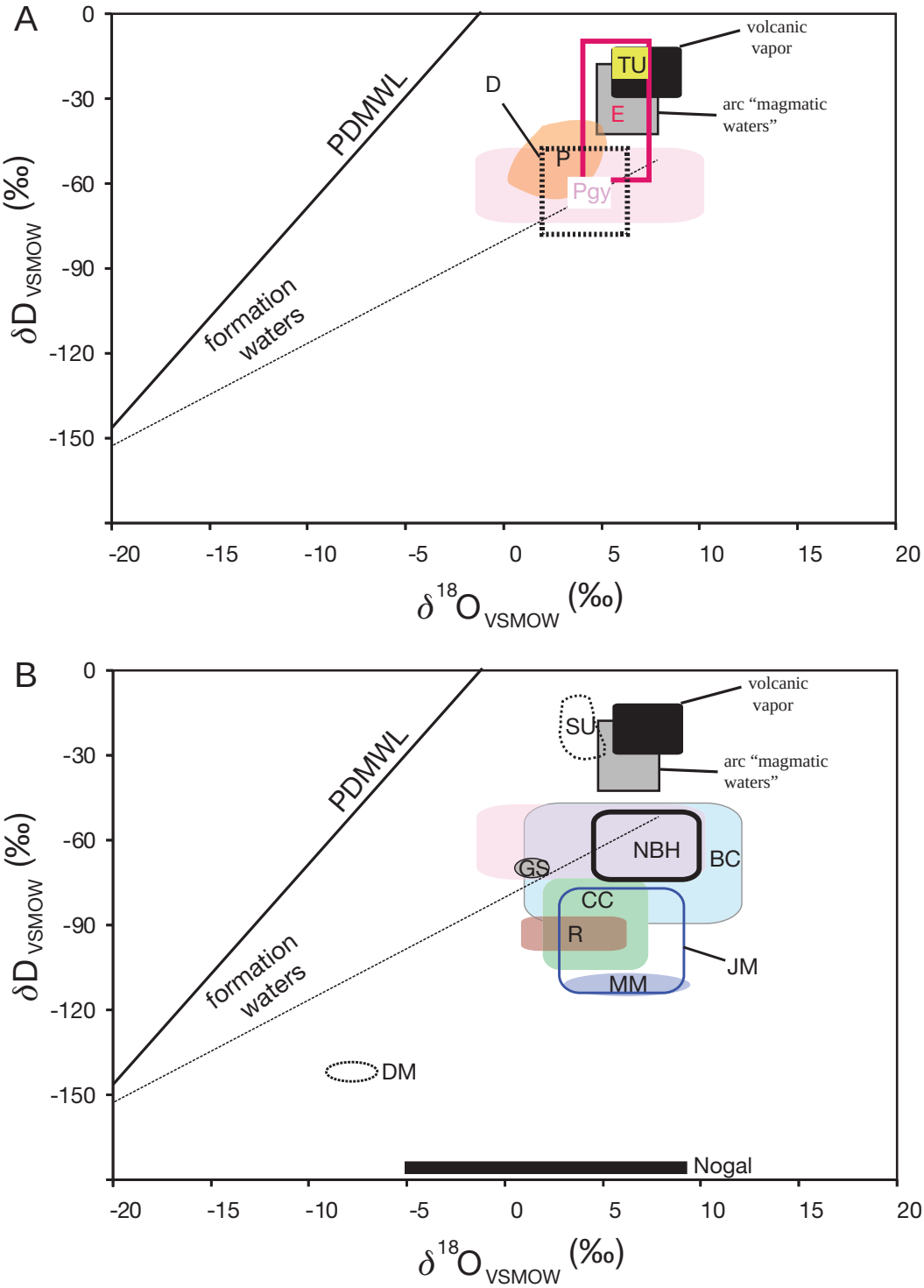

Fig. 3. Oxygen and hydrogen fluid compositions for select deposits in (A) non-North American, and (B) North American occurrences for which data are available. The present-day meteoric water line (PDMWL) and field of compositions for formation waters (Craig, 1961, 1963) are shown, along with the field for volcanic vapor (solid black; Hedenquist et al., 1998) and arc magma field (shaded gray; Taylor, 1997). Abbreviations: BC = Boulder County (Central City; Rice et al., 1985); CC = Cripple Creek (Kelley et al., 1998); D = Dashuigou deposit (Mao et al., 2002); DM = Dusty Mac (Zhang et al., 1989); E = Emperor (Ahmad et al., 1987); GS = Golden Sunlight (Spry et al., 1996); JM = Judith Mountains (Gies deposit; Zhang and Spry, 1994); MM = Mount Milligan—data for subepithermal veins only (LeFort et al., 2011); NBH = Northern Black Hills (Gilt Edge, Annie Creek; Paterson et al., 1989); P = Porgera Au-Te stage (Richards and Kerrich, 1993); Pgy = Pingyi area (Hu et al., 2006); R = Rosita (McEwan et al., 1996); SU = Sulphurets (Margolis, 1993); TU = Tuvatu (Scherbarth and Spry, 2006). Calculated $\delta^{18}O$ fluid compositions (in equilibrium with quartz) for Nogal gold deposits (without available hydrogen isotope compositions) are shown along x-axis of diagram (from Douglass and Campbell, 1994).

Fluorspar (commercial name for fluorite CaF_2) is the only fluorine mineral that is mined on a large scale. Fluorspar is used directly as a fluxing material and as an additive in different manufacturing processes, including aluminum- and steelmaking, glass manufacture, enamels, refrigerants, insulating foams, gasoline refining, and uranium fuel production. It is also used to produce hydrogen fluoride or hydrofluoric acid (HF). The importance of fluorine in numerous civilian and military uses and the dependence of the United States on a limited number of foreign suppliers (primarily Mexico, China, and South Africa) are reasons that F is a critical element and fluorspar is a critical mineral for the United States. A peak in consumption of fluorspar in the 1970s coincided with a peak in steel production. Currently, the United States imports most of its fluorine compounds (McRae, 2015).

The presence of fluorite in alkaline igneous rock-related epithermal gold deposits is common (Table 1), although with one exception discussed below, generally not high enough to be considered an economic resource. Where present in deposits, it typically forms early in the mineralizing process, prior to the gold (±telluride) event (Kelly and Goddard, 1969; Nash and Cunningham, 1973; Thompson et al., 1985; Spry and Scherbarth, 2006), and may be associated with base metal sulfide deposition (Kelly and Goddard, 1969).

The Jamestown district in Boulder County, Colorado, produced fluorspar from 1940 through 1973 from the Burlington and Emmett mines (Kelly and Goddard, 1969; Nash and Cunningham, 1973). Several hundred thousand metric tons of fluorspar was produced. Fluorite occurs in the alkalic Jamestown stock and in large lenticular breccia bodies in and adjacent to the stock. Breccias contain fluorite fragments cemented by a fine-grained mixture of fluorite and clay minerals. Most fluorite is associated with sulfides including galena, sphalerite, chalcopyrite, pyrite, tennantite, and enargite (Kelly and Goddard, 1969). Breccia fragments of massive galena are common in some fluorspar orebodies (Nash and Cunningham, 1973). Fluorite also occurs in veins that range from a few inches to 20 feet in width, and up to 1,000 feet long (Kelly and Goddard, 1969). Gold and telluride mineralization occurs with and without fluorite in veins peripheral to the stock (Nash and Cunningham, 1973). Fluids that formed the fluorite-bearing veins have temperatures ranging from 500° to 100°C, with a wide range in salinities (Nash and Cunningham, 1973). Together with oxygen isotope studies, results suggest that mineralizing fluids were mixtures of magmatic and meteoric waters.

Currently, fluorite is not mined as a by-product from alkaline epithermal gold deposits. However, if the future world market of fluorine is dominated by one or two foreign nations, it may be beneficial for the United States to develop high-grade, but relatively low-tonnage resources of fluorite, and therefore, many of the alkalic-related epithermal gold deposits that are enriched in fluorine have potential.

Platinum group elements (PGEs)

The PGEs include iridium, osmium, palladium, platinum, rhodium, and ruthenium, all of which have similar physical and chemical properties. PGEs have many industrial applications. They are used to reduce carbon monoxide, hydrocarbon, and nitrous oxide emissions in automobile exhaust. The chemical industry requires platinum or platinum-rhodium alloy to manufacture nitric oxide, which is the raw material for explosives, fertilizers, and nitric acid. In the petrochemical industry, platinum-supported catalysts are needed to refine crude oil and to produce aromatic compounds and high-octane gasoline. Alloys of PGEs are exceptionally hard and durable, making them the best known coating for industrial crucibles used in the manufacture of chemicals and synthetic materials. PGEs are used by the glass manufacturing industry in the production of fiberglass and flat-panel and liquid crystal displays. In the electronics industry, PGEs are used in computer hard disks, multilayer ceramic capacitors, and hybridized integrated circuits (Implats, 2012).

High concentrations of Pd or Pt are contained in a few alkaline-related epithermal gold vein deposits (Table 1). Many others may contain PGE enrichments, but analyses are not available. Furthermore, the genetic link between porphyry-stage events and the deposition of Au in late-stage veins implies that epithermal Au deposits may have been present in the shallower parts of some magmatic-hydrothermal complexes in weathered and eroded regions, and therefore, potential exists for the discovery of PGE-enriched epithermal veins in less deeply exhumed terranes.

Owing to the fact that much larger known PGE resources occur in deposits in which these elements are the primary commodities, it is unlikely that alkaline-related epithermal gold deposits will become a major source of PGEs. Nevertheless, it is worth noting the deposits that are enriched, in the event that PGEs may become economic as by-products of gold production in the future.

Epithermal veins associated with the Mount Milligan porphyry deposit typically contain>100 parts per billion (ppb) Pd, with some values exceeding 1,000 ppb (LeFort et al., 2011). Other epithermal and porphyry deposits in British Columbia and Washington (Finch et al., 1983; Nixon and Archibald, 2001), Colorado (Werle et al., 1984), and Greece (Eliopoulos and Economou-Eliopoulos, 1991) contain similar values (Fig. 4A, B). Only a few for which data are available contain high concentrations of both platinum and palladium, including the La Plata (Colorado) and Sappho deposits (British Columbia). Skouries (Greece) and Galore Creek (British Columbia) have high concentrations of palladium but lower platinum contents, and the Shasket Creek deposit (Washington) contains elevated platinum relative to palladium (Fig. 4A, B). Aside from platinum and palladium, other PGE concentrations are low (Mutschler et al., 1985).

The PGE enrichment typically occurs in semimassive to massive veins, stockworks, and disseminations in chalcopyrite-rich ore (Werle et al., 1984; Mutschler et al., 1985, 1998; Nixon and Archibald, 2001). In epithermal veins at the Mount Milligan deposit, the PGEs reside in Pd-Pt arsenide minerals that are associated with tellurides, electrum, Au-Ag-Bi-Te minerals, antimonides, arsenopyrite, tetrahedrite-tennantite, galena, chalcopyrite, and Fe-poor sphalerite (LeFort et al., 2011). However, most deposits have no recognized specific PGE-rich phases. Accompanying minerals in the PGE-rich chalcopyrite ore zones at the LaPlata (Allard stock) and Skouries deposits are hypogene chalcocite, bornite, and gangue hematite and magnetite (Werle et al., 1984; Eliopoulos and Economou-Eliopoulos, 1991); copper arsenide minerals and/

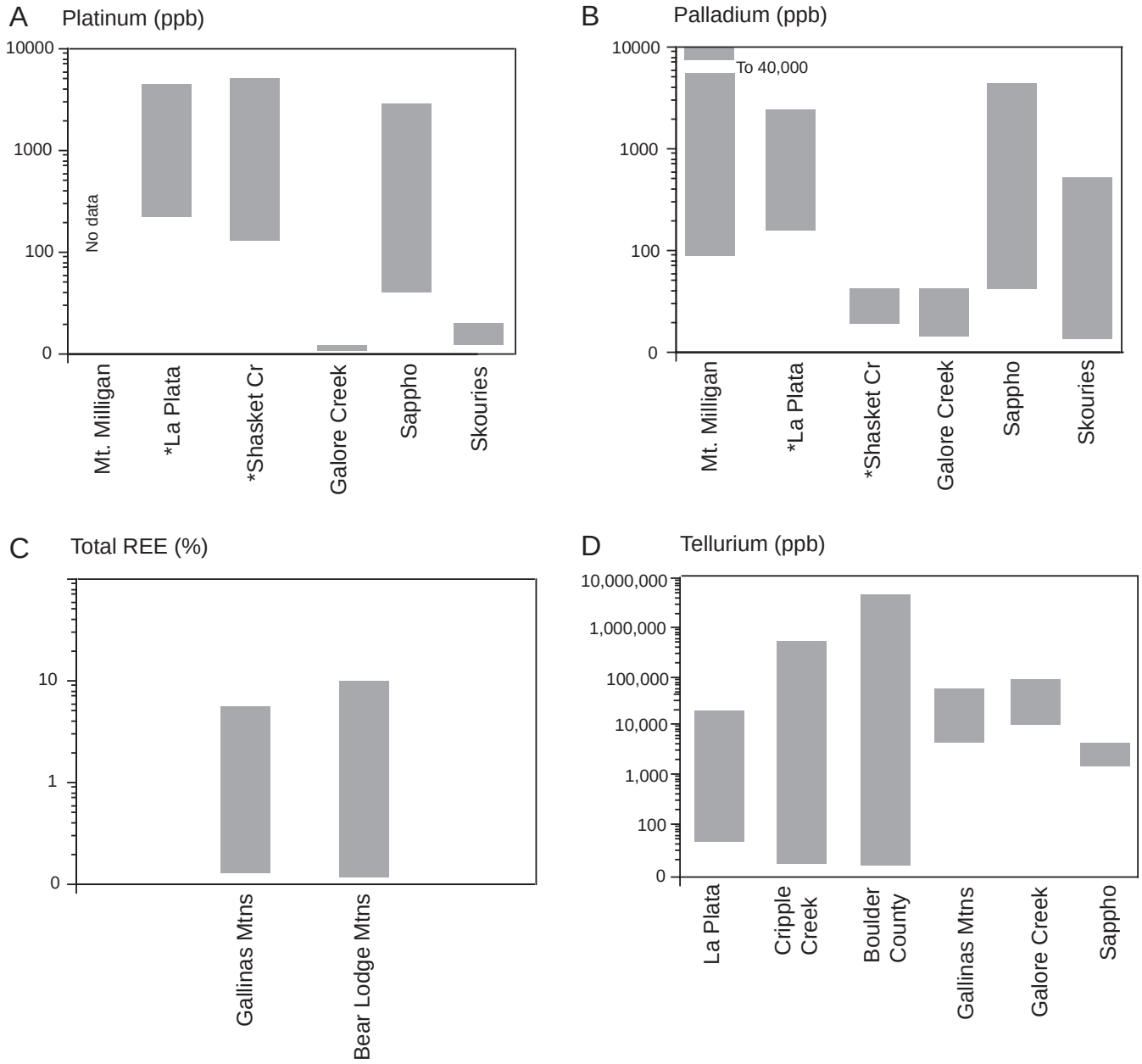

Fig. 4. A and B. Distribution of Pt and Pd (ppb) in whole-rock samples from select deposits for which data are available. Note that Ru data for Skouries range from 8 to 41 ppb. Sources of data: Galore Creek (Allen et al., 1976); La Plata (Eckel, 1949; Werle et al., 1984); Mount Milligan (LeFort et al., 2011); Sappho (Nixon and Archibald, 2001; Mutschler et al., 1998); Shasket Creek (Mutschler et al., 1985); Skouries (Eliopoulos and Economou-Eliopoulos, 1991). * = data are for samples of porphyry-style mineralized rocks, not epithermal veins, but epithermal gold mineralization of similar age is known in the district (but PGE data for epithermal style are unavailable). C. Total REE abundances (%). Sources of data: Bear Lodge Mountains (Staatz, 1983); Gallinas Mountains (McLemore, 2010). D. Te contents (ppb). Sources of data: Boulder County (K.D. Kelley, unpub. data, 2011); Cripple Creek (Cripple Creek and Victor Gold Mining Co., unpub. data, 2012); Gallinas Mountains (McLemore, 2013); Galore Creek, Sappho (Mutschler et al., 1985); La Plata (Werle et al., 1984).

or fluorite are common in some (La Plata: Eckel, 1949; Galore Creek: Enns et al., 1995) deposits.

At the Mount Milligan deposit, LeFort et al. (2011) suggested that PGEs were partitioned into and transported by a low-salinity, contracted vapor phase generated by porphyry-stage fluid boiling, and later deposited as As-Sb-Te-Bi-Hg phases in epithermal veins at relatively low temperature (<300°C). As such, the deposition of PGEs was not associated directly with porphyry-stage mineralizing events, suggesting that correlation between PGEs and Cu may only be spatially coincidental to overprinting of early porphyry-stage events by epithermal fluids (LeFort et al., 2011).

If the ore fluids in alkaline igneous rock-related epithermal gold systems are in large part magmatically derived, the composition of the alkaline magmas that produce these is likely a factor in PGE enrichment in these deposits (Tarkian and

Stribrny, 1999; Richards, 2009). Peach et al. (1990) and Richards (2009) demonstrated that chalcophile and siderophile elements preferentially partition into sulfide phases compared to silicate melts. The overall low abundance and high partition coefficients, particularly of PGEs, result in depletion in the magma but enrichment in residual sulfides (Richards, 2009). Therefore, early magmas tend to generate Cu-rich but precious metal-poor deposits, and Au- (and Pt, Pd)-rich residue remains in the lower crust and lithospheric mantle. A second stage of melting of the hydrous residue could then generate magmas with relatively high Au/Cu ratios and perhaps also PGE enrichments. Such magmas have the potential to form porphyry Cu-Au and epithermal Au deposits with high PGE concentrations (Richards, 2009).

Rare earth elements (REEs)

The rare earth elements are part of the lanthanide series. Although average crustal abundances are not low, concentrated deposits of REEs are limited. Due to their unusual physical and chemical properties, the REEs have diverse industrial, military defense, and energy technology applications (Long, 2011). The glass industry is the largest consumer of REE raw materials, which uses them for glass polishing and as additives that provide color and special optical properties. In petroleum refining, La-based catalysts are used whereas Ce-based catalysts are used for automotive catalytic converters. An increasingly important use of REEs is in the making of exceptionally strong neodymium-iron-boron (Nd-Fe-B) magnets that are used when space and weight are restrictions. Also, nickel-metal hydride batteries use a lanthanum-base alloy as anodes (Goonan, 2011; Long, 2011).

A few alkaline-carbonatite intrusive complexes that contain anomalous concentrations of gold or were prospected for gold in the past are also host to REE occurrences.The best examples of alkaline igneous rock-related epithermal gold deposits with abundant REEs are the Bear Lodge Mountains in northeast Wyoming (Staatz, 1983), and the Gallinas Mountains in Lincoln County, New Mexico (Griswold, 1959; McLemore, 2010). The Bear Lodge Mountains were initially prospected for gold during the late nineteenth century; rare earth and thorium mineralization was discovered in 1949. In 1972, Duval Corporation explored the area for porphyry-style copper and located high-grade copper, molybdenum, precious- and rare-earth metals within an altered carbonatite-alkaline intrusive complex (http://www.rareelementresources.com/). Tertiary igneous rocks associated with the REEs in the Bear Lodge Mountains are silica undersaturated phonolitic, syenitic, and trachytic intrusive and extrusive rocks, but minor lamprophyre and carbonatite occur (Staatz, 1983). Numerous breccias occur within the alkaline complex and at least one diatreme body has been identified (http://www.rareelementresources.com/). The REEs and Th occur as disseminated and vein deposits, primarily in monazite, brockite, and bastnaesite, with gangue K-feldspar, quartz, hematite and magnetite, and rare fluorite and barite (Staatz, 1983). The total rare earth content of mineralized disseminated and vein deposits (no. of samples = 376) is 0.23 to 9.8% (Fig. 4C). Very little is known about the gold prospects in the area, and particularly about how they relate spatially or genetically to the REE mineralization.

Igneous rocks associated with REE occurrences in the Gallinas Mountains are metaluminous to peraluminous alkaline volcanic rocks (Griswold, 1959) with chemical compositions similar to A-type granites (McLemore, 2010). REEs are associated with four types of deposits, including breccia pipes, iron skarn, Cu-REE-F (±Ag, Au) veins, and REE-F veins. In 1991 to 1992, the U.S. Bureau of Mines calculated an inferred resource of about 487,000 t with a grade of 2.95% total REEs. Gold is anomalous (up to 1,711 ppb) in some of the vein samples. The mineralogy of Cu-REE-F (Ag, Au) veins in the Gallinas Mountains is diverse and includes fluorite, quartz, barite, pyrite, calcite, chalcopyrite, and a variety of REE minerals such as bastnaesite, agardite, parasite, xenotime, and monazite (McLemore, 2010). Total REE contents (n = 278) range from <1 to 5.6% (Fig. 4C).

The Rosita Au-Ag telluride deposit in Colorado has reported REE minerals in apatite-magnetite veins and breccia-pipe deposits (Mutschler et al., 1998), and alkaline rocks within the Trans-Pecos magmatic province in southern New Mexico and northern Texas have been examined for potential deposits of Au, Ag, REEs, Nb, and U (McLemore and Guilinger, 1993), but no economic deposits have been discovered.

Tellurium (Te)

The most common critical element associated with alkaline igneous rock-related gold deposits is Te. Tellurium is an unusual element in that its cosmic abundance is greater than that of any other element with atomic number >40 (Anders and Ebihara, 1982); however, it is one of the rarest elements in the Earth's crust (0.4–10 ppb; Parker, 1967; McDonough and Sun, 1995; Reimann and de Caritat, 1998) and seawater (up to 9×10^{-4} ppb; Andreae, 1984; Lee and Edmond, 1985). For most unaltered terrestrial rocks, Te ranges in concentration from ~2 to 3 to ~10 to 20 ppb (e.g., volcanic rocks, ultramafic rocks, gabbro, syenite, basalt), but granitoids may contain average concentrations of ~100 ppb Te (e.g., Beaty and Manuel, 1973; Yi et al., 2000). Manganese nodules, Fe-Mn crusts, limestone, and shale contain up to 206 ppm, 52 ppm, 1.7 ppm, and 0.8 ppm Te, respectively (Beaty and Manuel, 1973; Haynes et al., 1985; Hein et al., 2003). Based on the elevated Te contents of these rocks, Jensen and Barton (2000) suggested that subduction of these highly enriched Te-bearing sediments could produce anomalous enrichment in the mantle and produce magmas that contain elevated Te contents.

Tellurium has a wide variety of uses (ceramics, glass fiber, vulcanized rubber, electronics industry), but it is used primarily in industry to form copper-, lead-, and iron-alloys, and stainless steel with more favorable machining characteristics, particularly thermoelectric cooling applications. Tellurium as cadmium telluride (CdTe) is also used in solar panels and research is underway to investigate whether (Cd,Zn)Te can be used in solid-state X-ray detectors. The photovoltaic solar and thermoelectric applications account for more than two-thirds of the world's Te usage (George, 2012). Its use in solar panels is particularly critical for development of alternative sources of energy in the United States and elsewhere. Current demand for Te is primarily met as a by-product of the processing of porphyry copper ores (George, 2012; Goldfarb et al., 2016; John and Taylor, 2016).

The price of tellurium has steadily increased since 2000: ~$6/kg - 2000, ~$45/kg - 2006, $110/kg - 2007, $175/kg - 2008, $130/kg - 2009, $221/kg - $300/kg in 2011 (Moss et al., 2011; George, 2012). However, the price dropped in January 2013 to about $180/kg owing to a softening in the metals market. Nonetheless, due to tellurium shortages worldwide, the price is expected to increase significantly over the coming decade and is a desirable commodity.

Tellurium commonly bonds with Au to produce more Au-bearing minerals than any other element. Minerals in the system Au-Ag-Te are calaverite ($AuTe_2$), krennerite ($AuTe_2$), petzite (Ag_3AuTe_2), muthmannite [(Ag,Au)Te], sylvanite [$(AgAu)_2Te_4$],hessite (Ag_2Te), empressite (AgTe), and stützite ($Ag_{5-x}Te_3$), but there are several other Au-bearing tellurides or sulphotellurides, including bilibinskite ($PbCuAu_3Te_2$), bezsmertnovite [$Au_4Cu(Te,Pb)$], bogdanovite [$(Au,Te,Pb)_3(Cu,Fe)$], buckhornite ($AuPb_2BiTe_2S_3$), kostovite ($CuAuTe_4$), montbrayite [$(Au,Sb)_2Te_3$], museumite [$Pb_2(Pb,Sb)_2S_8$][$(Te,Au)_2$], nagyágite [[$Pb(Pb,Sb)S_2$][Au,Te], and an unnamed Au-bearing telluride (Au_3TlTe_3). In addition, there are several Ag and nonprecious metal tellurides/sulfotellurides/tellurides/tellurates.

The predominant hosts for Te in alkalic-related epithermal gold deposits are precious metal telluride minerals that include many of those listed above. Most occur in veins, but they may also be disseminated in wall rocks adjacent to veins. It is difficult to assess the percentage of telluride minerals compared to other Au-bearing phases in most deposits due to a paucity of data. At the Sandaowanzi deposit in northeast China, 95% of the ores comprise telluride minerals (Liu et al., 2011). Generally, the telluride minerals are unevenly distributed within a given deposit, as shown by mapping their distribution, for example, in the Emperor (Pals and Spry, 2003) and Golden Sunlight deposits (Paredes, 1994). In addition to the occurrence of precious metal tellurides as disseminations and veins, bonanza-grade masses (with >1,000 oz/t Au) occur in some locations (e.g., Cripple Creek, Gies, Mayflower). Bonanza-grade gold (with tellurium) occurs in dilational zones (e.g., Gies), open vugs (e.g., Cresson Vug at Cripple Creek), and can form by a variety of processes including phase separation, hydrothermal flashing, and throttling.

Two districts contain native Te (Emperor, Fiji, and Boulder County, Colorado), and tetradymite (Bi_2Te_2S) has been reported at the Aztec mine in the Elizabethtown-Baldy district, New Mexico (McLemore, 2013). Although the classification of the Dashigou and adjacent Majiagou deposits in Sichuan province, China, as alkalic-related epithermal gold deposits is uncertain, both deposits contain abundant and dominant tetradymite (associated with gold, silver, and selenium), and assuming they are correctly assigned to this deposit class, they represent the only producers of Te as a primary product of mining (Mao et al., 1995, 2002; George, 2012).

Many alkalic-related epithermal gold deposits lack data for tellurium; those with reported concentrations show highly variable ranges depending on the distribution of telluride minerals (Fig. 4D). At Cripple Creek, among 72 samples of vein and disseminated ore collected throughout the district, average Te concentrations are 38 ppm, but many vein samples contain concentrations of 300 to 690 ppm (Cripple Creek and Victor Gold Mining Company, unpub. data, 2012). Similarly, 39 vein samples collected from multiple deposits within the Boulder County district have average Te contents of 53 ppm, with two samples containing >1,000 ppm (K.D. Kelley, unpub. data, 2011). Although tellurium is enriched in many deposits, it is currently not produced as a by-product. However, it could be considered a future commodity if global demand increases and as developments in the processing of Au-Te ores advance.

Some workers have suggested that the common occurrence of gold-bearing telluride minerals implies the transport of gold as a soluble tellurium complex (e.g., Jensen and Barton, 2000; Cooke and McPhail, 2001; Brugger et al., 2012; Grundler et al., 2013), in the vapor phase (Grundler et al., 2013), or as both chloride and sulfide complexes (Frank et al., 2011). Crustal fluids with anomalous tellurium concentrations, as is obvious from abundance of telluride minerals, include both CO_2-rich fluids that form alkalic-related epithermal gold deposits, and CO_2-poor fluids that typify most low- and high-sulfidation precious metal-bearing epithermal ores. Therefore, it is unlikely that CO_2 plays a significant role in the transport or concentration of tellurium. Studies of both liquid and vapor fluid inclusions from porphyry and epithermal deposits have indicated hundreds of parts per million Te in the fluids that have formed some occurrences (Wallier et al., 2006; Pudack et al., 2009). Studies have suggested that tellurium is transported as Te (IV) in oxidized magmatic fluids and/or in a fluid with basic pH, with reduction by wall-rock reactions or by fluid mixing causing precipitation of telluride minerals (Grundler et al., 2013). Change in fluid conditions, including decreases in temperature, wall-rock sulfidation, phase separation, pH shifts, and/or redox change, can destabilize tellurium-bearing complexes (e.g., Cooke and McPhail, 2001; Ciobanu et al., 2006). Most of the hypogene tellurides probably were deposited at temperatures between 300° and 100°C (e.g., Zhang and Spry, 1994), although in some magmatic Ni-Cu-PGE deposits, Pd- and/or Pb-bearing tellurides are stable at temperatures of 400°C (Vymazalova and Drabek, 2011).

Vanadium (V)

Vanadium (V) is a strategic metal with a principal use in the production of metal alloys such as high-strength steel and alloys for use in the aerospace industry. Lesser uses are in catalysts for the chemical industry, ceramics, glasses, and pigments. Vanadium consumption demand trends are heavily influenced by trends in steel production. The emerging need for large-scale electricity (vanadium-redox-flow batteries or VRBs) storage is a major potential future use of vanadium, making it an essential energy critical element. Development of VRBs will potentially increase the use of wind, solar, and other renewable, intermittent power sources. Lithium-vanadium-phosphate batteries produce higher voltages and higher energy to weight ratios, ideal for use in electric cars. Vanadium demand in lithium batteries is expected to increase from 200 t in 2012 to 1,700 t in 2017 (TTP Squared, Inc., 2013).

The close spatial relationship between vanadium minerals and gold, particularly gold-bearing tellurides in alkalic igneous-related epithermal gold deposits, has long been recognized (Lindgren, 1933). Some alkaline intrusive complexes contain historic or current economic resources of vanadium. For example, deposits in Arkansas (Magnet Cove, Wilson Springs) produced nearly 4.3 Mt of 1.2% V_2O_5 (Howard and Owens, 1995). However, none of the complexes with

economic vanadium are related to precious metal deposits. Epithermal gold deposits related to alkaline rocks have high vanadium contents but are presently uneconomic and are unlikely to be considered vanadium resources in the future.

The most common vanadium-bearing minerals in alkaline igneous rock-related epithermal gold deposits are roscoelite and vanadium mica, where they occur as fine-grained intergrowths with quartz and other gangue minerals (Richards, 1995). Roscoelite occurs in the Cripple Creek deposit in Colorado (Thompson et al., 1985; Jensen and Barton, 2000), Boulder County, Colorado deposits (Kelly and Goddard, 1969; Saunders, 1991), Emperor deposit, Fiji (Ahmad et al., 1987), many deposits in the Judith Mountains, Montana (Forrest, 1971; Zhang and Spry, 1994), and the Porgera deposit, Papua New Guinea (Richards et al., 1991; Richards and Kerrich, 1993). It has not been reported for epithermal deposits in New Mexico (North and McLemore, 1986; McLemore, 1996). Vanadium minerals other than roscoelite and/or vanadium muscovite are rare in most epithermal gold telluride deposits; however, the Tuvatu deposit in Fiji contains karelianite, Ti-free nolanite, vanadium rutile, schreyerite, and an unnamed vanadium silicatein addition to roscoelite and vanadium muscovite (Spry and Scherbarth, 2006). Rutile in the Tuvatu deposit contains up to 5.2 wt % V_2O_3; roscoelite contains 32.71 wt % V_2O_3, which is among the highest reported vanadium concentrations for roscoelite from an epithermal Au-Te deposit (Spry and Scherbarth, 2006).

Tungsten (W)

Tungsten is a lithophile element that occurs in nature as W^{+4} and W^{+6}. The ionic radius and electronegativity of tungsten is similar to that of Mo, Nb, and Ta (Hobbs and Elliott, 1973). Tungsten has the highest melting point of all metals, and because of this it is used for filaments in light bulbs, fluorescent lighting, electron tubes, and television tubes. Tungsten carbide is extremely hard and is therefore used in metal-working industries such as the mining and petroleum industries (drill bits) and space exploration. Its hardness and stability make it an important product for touch screen technology in smart phones and tablet devices. In 2013, more than 80% of tungsten was sourced from Chinese mines. Since 2008, Chinese domestic demand has exceeded its own supply, resulting in a near doubling of price for tungsten concentrate over the period of 2008 to 2013 (Shedd, 2014).

Some alkalic igneous rock-related epithermal gold deposits contain tungsten-bearing minerals such as scheelite, ferberite, or wolframite (Table 1). Deposits with well-known occurrences of tungsten include the Black Hills, South Dakota (Gilt Edge; Paterson et al., 1989), Boulder County, Colorado (Lovering and Tweto, 1953; Kelly and Goddard, 1969), and Ortiz Mountains in New Mexico (Maynard, 1995; Schutz, 1995; McLemore, 1996). Although the abundance of tungsten minerals in these deposits is generally not economic, small ferberite- and scheelite-bearing orebodies in Boulder County were mined historically (Kelly and Goddard, 1969), and in fact the Boulder County tungsten deposits were the chief source of tungsten in the United States from about 1900 to 1918 (Lovering and Tweto, 1953). As with fluorite and REEs, it is unclear in all cases how the tungsten mineralization is related temporally or genetically to the Au-Te stage. For example, in Boulder County, the tungsten ores largely occur in a belt that is separate and distinct from the telluride belt, but in the area of overlap, some tungsten mineralization occurs in telluride veins. Tungsten-rich deposits in the Ortiz Mountains occur in association with gold and sulfide minerals in breccias that are spatially distinct from Au-rich veins, but both are temporally related to alkaline magmatism and diatreme emplacement (Maynard, 1995).

Similar to F and Te, the abundance of W in mineralized samples is highly variable depending on the distribution of tungsten-bearing minerals. Vein and disseminated mineralized samples from across the Cripple Creek district (n = 72) contain an average of 20 ppm W (Cripple Creek and Victor Gold Mining Company, unpub. data, 2012), and Au-Te veins from mines in the Boulder County district (n = 39) have average contents of 528 ppm with some values >5,000 ppm (K.D. Kelley, unpub. data, 2011).

In the Boulder County veins, the predominant tungsten mineral is ferberite or wolframite. In most veins, it forms the matrix of a breccia consisting of quartz and country rock, but in some mines there are solid seams of high-grade ferberite and locally there are vuggy parts of veins containing ferberite crystals. The average width of the tungsten veins that were mined was 15 to 30 cm, but some shoots were as thick as 1.5 m. No vertical zoning is evident, other than changes in wall-rock alteration with depth (Kelly and Goddard, 1969). In the zone of overlap with the telluride belt, the small tungsten ore shoots were mostly separate from the telluride bodies, and Lovering and Tweto (1953) concluded that the tungsten ore was deposited later than tellurides.

In the Ortiz Mountains, scheelite is associated with micron-sized gold and other minerals such as pyrite, magnetite, calcite, siderite, quartz, and chalcopyrite in clast-supported breccias. Scheelite and gold occur as crystals in open spaces. About 250,000 oz of gold was recovered, but no record of production of tungsten exists (Maynard, 1995).

Exploration Implications

The permissive future by-products from alkaline igneous rock-related epithermal gold deposits include F, Te, and W, in addition to Au and Ag. Therefore, large deposits are primary exploration targets and identifying distinct geologic, geophysical, and geochemical signatures are of critical importance. These deposits occur in areas that underwent extensional or transtensional tectonics after subduction terminated (Richards, 1995, 1997; Jensen and Barton, 2000); therefore, such areas (e.g., back-arc regions) should be located and considered prospective (Richards, 1997). It is tempting to assume that the size of parental magma systems correlates directly with the size/grade of the resulting deposit. However, although alkaline igneous rock-related gold deposits can contain tens of millions of ounces of gold and are extremely attractive targets, they are generally spatially associated with smaller stocks and laccoliths rather than large-scale batholiths (Richards, 1997). Such igneous rocks commonly occur in clusters (e.g., Judith Mountains, Montana) and generally host more than one gold occurrence. For example, regional field exploration near the Porgera deposit revealed additional alkaline igneous rocks spatially associated with the Mount Kare deposit.

At a regional scale, the crustal architecture in which epithermal alkalic gold deposits occur can be imaged using aeromagnetic, gravity, radiometric, and seismic techniques. These methods may also be effective for mapping favorable lithologies at depth. In Fiji, there is a close relationship of deposits (e.g., Tuvatu) with the Viti Levu lineament and volcanic calderas (Begg, 1996; Scherbarth and Spry, 2006; Begg et al., 2007). The location of the shoshonitic volcanoes is clearly shown by medium wavelength gravity data (Colley and Flint, 1995, their fig. 12, p. 25), providing a good targeting method. Although the total magnetic intensity map of the Tuvatu region showed a complex magnetic pattern, the first vertical derivative was used to map the volcanic rocks (Gunn et al., 2009a, b). When these anomalies were aligned with gravity highs along the NE-trending Viti lineament, regional-scale targets for additional epithermal alkalic resources were identified. All of the newly identified epithermal targets (Vuda, Ba, Raki Raki) occur within the coincident magnetic and gravity highs along this trend, spatially related to shoshonitic volcanic rocks in or adjacent to the calderas (Colley and Flint, 1995; Scherbarth and Spry, 2006).

Large alkaline gold systems are spatially associated with rocks that are brecciated, fractured, and altered. Structures at the local scale commonly mimic the direction of regional structures (e.g., Emperor, Tuvatu). Moreover, there appears to be a spatial association with low-grade porphyry-style mineralization. The spatial association at Emperor (Eaton and Setterfield, 1993) and Tuvatu (Scherbarth and Spry, 2006) and the presence of the low-grade Kingston porphyry Cu deposit in the Navilawa caldera that hosts the Tuvatu and Banana Creek gold prospects have made the caldera a focus of exploration. Geophysical studies at the local scale have been instrumental in targeting prospects and deposits. For example, large inductively polarized chargeability and potassium radiometric anomalies obtained by Golden Rim Resources extend from the Tuvatu deposit through the center of the caldera through to the Banana Creek prospect that is related to hydrothermal alteration spatially associated with gold mineralization (http://www.sharescene.com/index.php?showtopic=269&st=80).

Similar aerial gamma ray surveys were used by Pitkin and Long (1977) to identify a potassic alteration zone in the Cripple Creek area. Aeromagnetic and gravity surveys as well as remote sensing may also be useful to identify alteration intensity, as was also done at Cripple Creek (Kleinkopf et al., 1970; Livo, 1994; Kelley et al., 1995). Satellite- (e.g., ASTER), airborne-(e.g., Hymap), and field-based infrared spectroscopy (e.g., Pima) have been used to aid alteration mapping around gold systems (Robert et al., 2007). Integrated Pima, Hylogger, Hychipper, and mineralogical studies may prove useful for identifying subtleties in alteration mineral associations (e.g., V-rich mica vs. others) as was done successfully for an orogenic Au deposit by Halley and Walshe (2006; see Robert et al., 2007, their fig. 13, p. 707).

Alkalic gold deposits are characterized by potassic and phyllic alteration, carbonates, fluorite, and also various sulfides, sulfosalts, tellurides, and, in some cases, selenides. They are generally low in S but also enriched in CO_2. Potassically altered rocks, along with the presence of colored fluorite and bright green vanadian mica/roscoelite, are relatively easy to recognize in the field and serve as initial indicators to precious metal mineralization. Geochemical surveys (whole rock, rock chip, soil) should include analyses of several pathfinder elements, including Ag, As, Au, Ba, Bi, Cu, F, Fe, Hg, Mo, Ni, Pb, REE, Sb, Se, Te, V, W, and Zn (Kelley et al., 1995).

Conclusions

Alkaline igneous rock-related epithermal gold deposits are a subset of low-sulfidation deposits that are temporally and genetically related to igneous rocks with high alkali-element contents. Ranging in age primarily from Mesozoic to Neogene, these deposits vary in size and grade, but some contain greater than 100 t Au, which are of major economic significance. Alkalic-related epithermal gold deposits are important primary producers of Au and Ag. Other metals, including many of the critical and near-critical elements like F, PGEs, REEs, Te, V, and W are enriched in these deposits, but with two exceptions have never been mined as primary products or as by-products.

Fluorine (from fluorspar) was mined from large breccia bodies and veins adjacent to alkalic igneous stocks in the Boulder County Au-Te district from 1940 through 1973. The latter part of this period coincided with a peak in consumption of fluorite in the United States, concurrent with a peak in steel production. The importance of fluorine in numerous civilian and military uses and the dependence of the United States on a limited number of foreign suppliers, namely Mexico, China, and South Africa, are reasons that it is a critical element. Although there are larger resources of fluorine in other deposit types, alkaline igneous rock-related epithermal gold deposits may be viable candidates for small tonnage fluorspar resources.

Tungsten is another critical element because its hardness and stability make it an important product for touch screen technology in smart phone and tablet devices. In 2013, more than 80% of produced tungsten was sourced from Chinese mines. Similar to fluorine, dependence of the United States on a limited number of foreign suppliers may lead to exploration for small tonnage, high-grade tungsten resources. Small tungsten orebodies in the Boulder County Au-Te district were mined historically. The tungsten ores are assumed to be at least temporally if not genetically associated with the gold deposits. Tungsten-rich deposits in the Ortiz Mountains are spatially distinct from Au-rich veins, but both are temporally related to alkaline magmatism and diatreme emplacement.

The most common critical element associated with alkaline igneous rock-related gold deposits is Te, which is one of the rarest elements in the Earth's crust. Tellurium is used primarily as steel alloys and photovoltaic solar and thermoelectric applications. The price of tellurium increased significantly in the first decade of the 21stcentury (~$6/kg in 2000 to $300/kg in 2011), but dropped by about half in 2013. Nonetheless, due to tellurium shortages worldwide, the price is expected to increase over the coming decade. The predominant hosts for Te in alkalic-related epithermal gold deposits are precious metal telluride minerals that occur dominantly in veins that are unevenly distributed within a given deposit. Native Te and tetradymite (Bi_2Te_2S) have been reported locally. Although the classification of the Dashigou and adjacent Majiagou deposits in Sichuan province, China, as alkalic-related epithermal gold deposits is uncertain, both deposits contain abundant and dominant

tetradymite, and these deposits represent the only producers of Te as a primary product of mining. Tellurium could be considered a future commodity if global demand increases and if advances are made in the processing of Au-Te ores.

Some alkaline igneous rock-related epithermal gold vein deposits (and spatially or genetically related porphyry deposits) contain high contents of Pt or Pd, or both, but due to the presence of other large known PGE resources in deposits in which PGEs are the primary commodities, it is unlikely that alkaline-related epithermal gold deposits will become a major source of PGEs. High V contents (dominantly in V-rich mica or roscoelite) are also characteristic of many deposits but are unlikely to be considered vanadium resources in the future. Rare earth element (REE) enrichments are associated with alkaline igneous complexes that are spatially and temporally associated with Au-rich zones, the best examples of which are the Bear Lodge Mountains in Wyoming and Cu-REE-F (± Ag, Au) vein deposits in the Gallinas Mountains in New Mexico. However, a genetic link between them is ambiguous.

Acknowledgments

Andrew Fornadel is thanked for reading an earlier draft of this contribution and for his suggestions and comments and his assistance in compiling tables and drafting figures. Stuart Giles (USGS) assisted with figures, and Cripple Creek and Victor Gold Mining Company provided recent tellurium data and resource estimates for Cripple Creek. We thank Jeremy Richards and Rich Goldfarb for their helpful and thorough reviews. Any use of trade, product, or firm names is for descriptive purposes only and does not imply endorsement by the U.S. Government.

REFERENCES

Ahmad, M., Solomon, M., and Walshe, J.L., 1987, Mineralogical and geochemical studies of the Emperor gold telluride deposit, Fiji: Economic Geology, v. 82, p. 345–370.

Alderton, D.H.M., and Fallick, A.E., 2000, The nature and genesis of gold-silver-tellurium mineralization in the Metaliferi Mountains of western Romania: Economic Geology, v. 95, p. 495–516.

Allen, D.G., Panteleyev, A., and Armstrong, A.T., 1976, Galore: Canadian Institute of Mining and Metallurgy Special Volume 15, p. 402–414.

Anders, E., and Ebihara, M., 1982, Solar system abundances of the elements: Geochimica et Cosmochimica Acta, v. 46, p. 2363–2380.

Andreae, M.O., 1984, Determination of inorganic tellurium species in natural waters: Analytical Chemistry, v. 56, p. 2064–2066.

Beaty, R.D., and Manuel, O.K., 1973, Tellurium in rocks: Chemical Geology, v. 12, p.155–159.

Begg, G., 1996, Genesis of the Emperor gold deposit, Fiji: Ph.D. thesis, Australia, Monash University, 466 p.

Begg, G., and Gray, D.R., 2002, Arc dynamics and tectonic history of Fiji based on stress and kinematic analysis of dikes and faults of the Tavua Volcano, Viti Levu Island, Fiji: Tectonics, v. 21, p. 5(1)-5(14).

Begg, G., Loucks, R., Gray, D., Foster, D., Kent, A., and Cooke, D.R., 2007, Gold and tectonics: A dynamic link [abs.]. Ores and Orogenesis: A Symposium Honoring the Career of William R. Dickinson, Tucson, Arizona, September 24–30, Program with Abstracts, p. 90–91.

Bonham, H.F., 1984, Three major types of epithermal precious-metal deposits [abs.] : Geological Society of America Abstracts with Programs, v. 16, p. 449.

——1986, Models for volcanic-hosted epithermal precious metal deposits: a review: Volcanism, Hydrothermal Systems and Related Mineralization Symposium, 5th, International Volcanology Congress, University of Auckland, Proceedings, p. 13–17.

Bonham, H.F., and Giles, D.L., 1983, Epithermal gold/silver deposits: the geothermal connection: Geothermal Resources Council Special Report, v. 13, p. 257–262.

Brugger, J., Etschmann, B.E., Grundler, P.V., Liu, W-H., Testemale, D., and Pring, A., 2012, XAS evidence for stability of polytellurides in hydrothermal fluids up to 599°C, 800 bar: American Mineralogist, v. 97, p. 1519–1522.

Campbell, A.R., Porter, J.A., and Douglass, S.E., 1991, Fluid inclusion investigation of the mid-Tertiary Helen Rae gold mine, Nogal district, New Mexico: New Mexico Geological Society Field Conference, 42nd, Sierra Blanca, Sacramento, Capitan Ranges, Guidebook, p. 317–321.

Carman, G.D., 2003, Geology, mineralization, and hydrothermal evolution of the Ladolam gold deposit, Lihir Island, Papua New Guinea: Society of Economic Geologists Special Publication 10, p. 247–283.

Chaplin, C.E., 2012, Origin of the Colorado mineral belt: Geosphere, v. 8, p. 28–43.

Ciobanu, C.L., Cook, N.J., and Spry, P.G., 2006, Preface—Special issue: Telluride and selenide minerals in gold deposits—How and why?: Mineralogy and Petrology, v. 87, p. 163–169.

Cocker, M.D., 1983, Primary element dispersion patterns in carbonate-hosted, epithermal, high-grade Au-Ag telluride system: Mayflower mine, Madison County, USA: Journal of Geochemical Exploration, v. 47, p. 377–390.

Colley, H., and Flint, D.J., 1995, Metallic mineral deposits of Fiji: Fiji Mineral Resources Department Memoir 4, 196 p.

Cook, N.J., Ciobanu, C.L., Damian, C.L. and Damian, F., 2004, Tellurides and sulphosalts from deposits in the Golden Quadrilateral: International Association on the Geology of Ore Deposits Guidebook Series, v. 12, p. 111–144.

Cook, N.J., Ciobanu, C.L., Spry, P.G., and Voudouris, P., 2009, Understanding gold-(silver)-telluride-(selenide) mineral deposits: Episodes, v. 32, p. 249–263.

Cooke, D.R., and McPhail, D.C., 2001, Epithermal Au-Ag-Te mineralization, Acupan, Baguio district, Philippines: Numerical simulations of mineral deposition: Economic Geology, v. 96, p. 109–131.

Cooke, D.R., and Simmons, S.F., 2000, Characteristics and genesis of epithermal gold deposits: Reviews in Economic Geology, v. 13, p. 221–244.

Cooke, D.R., Tosdale, D. Chamberlain, C., and Deyell, C., 2006, Alkalic porphyries and epithermal deposits [ext. abs.]: Sydney Minerals Exploration Discussion Group, Mines and Wines 2006, Mineral Exploration in New South Wales, Extended Abstracts, p. 7–10.

Craig, H., 1961, Isotopic variations in meteoric waters: Science, v. 133, p. 1702–1703.

——1963, The isotopic geochemistry of water and carbon in geothermal areas, *in* Toniorgi, E., ed., Nuclear geology in geothermal areas: Pisa, Consiglio Nazionale dell Richerche, p. 17–53.

Delong, R.C., 1996, Geology, alteration, mineralization and metal zonation of the Mount Milligan porphyry copper-gold deposits: M.Sc. thesis, Vancouver, BC, University of British Columbia, 121 p.

Douglass, S.E., and Campbell, A.R., 1994, Characterization of alkaline rock-related mineralization in the Nogal mining district, Lincoln County, New Mexico: Economic Geology, v. 89, p. 1306–1321.

Eaton, P.C., and Setterfield, T.N., 1993, The relationship between epithermal and porphyry hydrothermal systems within the Tavua caldera, Fiji: Economic Geology, v. 88, p. 1053–1083.

Eckel, E.B., 1949, Geology and ore deposits of the La Plata district, Colorado: U.S. Geological Survey Professional Paper 219, 179 p.

Eliopoulos, D.G., and Economou-Eliopoulos, M., 1991, Platinum-group element and gold contents in the Skouries porphyry copper deposit, Chalkidiki Penninsula, northern Greece: Economic Geology, v. 86, p. 740–749.

Enns, S.G., Thompson, J.F.H., Stanley, C.R., and Yarrow, E.W., 1995, The Galore Creek porphyry copper-gold deposits, northwest British Columbia: Canadian Institute of Mining, Metallurgy, and Petroleum Special Volume 46, p. 640–644.

Finch, R.J., Ikramuddin, M., Mutschler, F.E., and Shannon, S.S., Jr., 1983, Precious metals in alkaline suite porphyry copper systems in western North America [abs]: Geological Society of America Abstracts with Programs, v. 15, p. 572.

Fleischer, M., and Robinson, W.O., 1963, Some problems of the geochemistry of fluorine: Royal Society of Canada Special Publication 6, p. 58–75.

Fornadel, A.P., Voudouris, P. Ch., Spry, P.G., and Melfos, V., 2012, Mineralogical, stable isotope, and fluid inclusion studies of spatially related porphyry Cu-Mo and epithermal Au-Te mineralization, Fakos Peninsula, Limnos Island, Greece: Mineralogy and Petrology, v. 102, p. 85–111.

Forrest, R.A., 1971, geology and mineral deposits of the Warm Springs-Gilt Edge district, Fergus County, Montana: M.S. thesis, Butte, Montana College of Mineral Science and Technology, 191 p.

Foster, F., and Childs, J.F., 1993, An overview of significant lode gold systems in Montana, and their regional geologic setting: Exploration and Mining Geology, v. 2, p. 217–244.

Frank, M.R., Simon, A.C., Pettke, T., Candela, P.A., and Piccoli, P., 2011, Gold and copper partitioning in magmatic-hydrothermal systems at 800°C and 100 MPa: Geochimica et Cosmochimica Acta, v. 75, p. 2470–2482.

Gantumur, H., Batulzii, D., Wang, L., and Zhu, H., 2005, Tsav: A shoshonite-hosted intermediate sulfidation epithermal Ag-Pb-Zn deposit, eastern Mongolia: Mineral Deposits Research: Meeting the Global Challenge: Biennial Society of Geology Applied to Ore Deposits Meeting, 8th, Proceedings, p. 389–392.

Gast, P.W., 1968, Trace element fractionation and the origin of tholeiitic and alkaline magma types: Geochimica et Cosmochimica Acta, v. 32, p. 1057–1086.

Geller, B.A., 1994, Mineralogy and origin of telluride deposits in Boulder County, Colorado: Ph.D. dissertation, Boulder, University of Colorado, 731p.

George, M.W., 2012, Selenium and tellurium: U.S. Geological Survey 2011 Minerals Yearbook [Advance Release], p. 65.1–65.9.

Goldfarb, R.J., Hofstra, A.H., and Simmons, S.F., 2016, Critical elements in Carlin, epithermal, and orogenic gold deposits: Reviews in Economic Geology, v. 18, p. 217–244.

Goonan, T.G., 2011, Rare earth elements—end use and recyclability: U.S. Geological Survey Scientific Investigations Report 2011-5094, 15 p. Available only at http://pubs.usgs.gov/sir/2011/5094/.

Griswold, G.B., 1959, Mineral deposits of Lincoln County, New Mexico: New Mexico Bureau of Mines and Mineral Resources, Bulletin 67, 117 p.

Grundler, P.V., Brugger, J., Etschmann, B., Helm, L., Liu, W., Spry, P.G., Tian, Y., Testemale, D., and Pring, A., 2013, Speciation of aqueous tellurium (IV) in hydrothermal solutions and vapors and the role of oxidized tellurium species in gold metallogenesis: Geochimica et Cosmochimica Acta, v. 120, p. 298–325.

Gunn, P.J., Mackey, T., and Meixner, A.J., 2009a, The Fiji airborne geophysical survey project, *in* Petterson, M.G., ed., Pacific minerals in the new millennium: Science, exploration, mining, and community: Suva, Fiji Islands, Pacific Islands Applied Geoscience Commission (SOPAC), The Jackson Lum volume, p. 59–81.

——2009b, Magnetic, radiometric and gravity signatures of localities of epithermal gold deposits in Fiji, *in* Petterson, M.G., ed., Pacific minerals in the new millennium: Science, exploration, mining, and community: Suva, Fiji Islands, Pacific Islands Applied Geoscience Commission (SOPAC), The Jackson Lum volume, p. 83–90.

Halley, S., and Walshe, J.L., 2006, Alteration vectors to blind, high grade, Archean gold deposits: West Australian Geologist Newsletter 459, p. 4.

Hastings, J.S., 1988, Gold deposits of the Zortman-Landusky, Little Rocky Mountains, Montana, *in* Schafer, R.W., Cooper, J.J., and Vikre, P.G., eds., Bulk mineable precious metal deposits of the western United States: Geological Society of Nevada, p. 187–205.

Haynes, B.W., Law, S.L., Barron, D.C., Kramer, G.W., Maeda, R., and Magyar, M.J., 1985, Pacific manganese nodules: Characterization and processing: U.S. Geological Survey Bulletin 679, 48 p.

Hedenquist, J.W., 1987, Mineralization associated with volcanic-related hydrothermal systems in the Circum-Pacific basin: Circum Pacific Conference on Energy and Mineral Resources, American Association of Petroleum Geologists, 4th, Singapore, August 1986, Transactions, p. 513–524.

Hedenquist, J.W., Arribas, A., Jr., and Reynolds, T.J., 1998, Evolution of an intrusion-centered hydrothermal system: Far southeast-Lepanto porphyry and epithermal Cu-Au deposits, Philippines: Economic Geology, v. 93, p. 373–404.

Hedenquist, J.W., Arribas, A., Jr., and Gonzalez-Urien, E., 2000, Exploration for epithermal gold deposits: Reviews in Economic Geology, v. 13, p. 245–277.

Hein, J.R., Koschinsky, A., and Halliday, A.N., 2003, Global occurrence of tellurium-rich ferromanganese crusts and a model for the enrichment of tellurium: Geochimica et Cosmochimica Acta, v. 67, p. 1117–1127.

Hobbs, S.W., and Elliott, J.E., 1973, Tungsten: U.S. Geological Survey Professional Paper 820, p. 667–678.

Howard, J.M., and Owens, D.R., 1995, Minerals of the Wilson Springs vanadium mines, Potash Sulphur Springs, Arkansas: Rocks and Minerals, v. 70, p. 154–170.

Hu, H.B., Mao, J.W., Niu, S.Y., Li, Y.F., and Li, M.W., 2006, Geology and geochemistry of telluride-bearing Au deposits in the Pingyi area, western Shandong, China: Mineralogy and Petrology, v. 87, p. 209–240.

Implats, 2012, Metals usage: Implats Web page, accessed January 31, 2013, at http://www.implats.co.za/implats/Metals-usage.asp.

Irvine, T.N., and Baragar, W.R.A., 1971, A guide to the chemical classification of the common volcanic rocks: Canadian Journal of Earth Sciences, v. 8, p. 523–548.

Jaffe, R., Price, J., Ceder, G., Eggert, R., Graedel, T., Schneider, K., Hitzman, M., Houle, F., Hurd, A., Kelley, R., King, A., Milliron, D., Skinner, B., and Slakey, F., 2011, Energy critical elements—developing new technologies to foster U.S. energy independence: American Physical Society and Materials Research Society, Unpublished Report, 23 p. (http://www.mrs.org/advocacy/ece/).

Jago, C.P., 2008, Metal- and alteration-zoning, and hydrothermal flow paths at the moderately-tilted, silica-saturated Mount Milligan Cu-Au alkalic porphyry deposit: M.Sc. thesis, Vancouver, University of British Columbia, 210 p.

Jensen, E.P., 2003, Magmatic and hydrothermal evolution of the Cripple Creek gold deposit, Colorado, and comparisons with regional and global magmatic-hydrothermal systems associated with alkaline magmatism: Ph.D. dissertation, Tucson, University of Arizona, 846 p.

Jensen, E.P., and Barton, M.D., 2000, Gold deposits related to alkaline magmatism: Reviews in Economic Geology, v. 13, p. 279–314.

John, D.A., and Taylor, R.D., 2016, By-products of porphyry copper and molybdenum deposits: Reviews in Economic Geology, v. 18, p. 137–164.

Kelley, K.D., and Ludington, S., 2002, Cripple Creek and other alkaline-related gold deposits in the southern Rocky Mountains, USA: Influence of regional tectonics: Mineralium Deposita, v. 37, p. 38–60.

Kelley, K.D., Armbrustmacher, T.J., and Klein, D.P., 1995, Au-Ag-Te vein deposits, *in* du Bray, E.A., ed., Preliminary compilation of descriptive geoenvironmental mineral deposit models: U.S. Geological Survey, Open File Report 95-0831, p. 130–136.

Kelley, K.D., Romberger, S.B., Beaty, D.W., Pontius, J.A., Snee, L.W., Stein, H.J., and Thompson, T.B., 1998, Geochemical and geochronological constraints on the genesis of Au-Te deposits at Cripple Creek, Colorado: Economic Geology, v. 93, p. 981–1012.

Kelly, W.C., and Goddard, E.N., 1969, Telluride ores of Boulder County, Colorado: Geological Society of America Memoir 109, 237 p.

Kleinkopf, M.D., Peterson, D.L., and Gott, G., 1970, Geophysical studies of the Cripple Creek mining district, Colorado: Geophysics, v. 35, p. 490–500.

Kovalenker, V.A., Safonov, Y.G., Naumov, V.B. and Rusimov, V.L., 1997, Epithermal gold-telluride deposits of Kochbulak (Uzbekistan): Geology of Ore Deposits, v. 39, p. 127–152.

Kovalenker, V.A., Plotinskaya, O.Y., Prokof'ev, V.Y., Gertman, Y.L., Koneev, R.I. and Pomortsev, V.V., 2003, Mineralogy, geochemistry, and genesis of gold-selenide-telluride ores from the Kairagach deposit (Uzbekistan): Geology of Ore Deposits, v. 45, p. 171–200.

Lang, J.R., Lueck, B., Mortensen, J.K., Russel, J.K., Stanley, C.R., and Thompson, J.F.H., 1995, Triassic-Jurassic silica-undersaturated and silica-saturated alkali intrusions in the Cordillera of British Columbia: Implications for arc magmatism: Geology, v. 23, p. 451–454.

Le Bas, M.J., Le Maitre, R.W., Streckeisen, A., and Zenettin, B., 1986, A chemical classification of volcanic rocks based on the total alkali-silica diagram: Journal of Petrology, v. 27, p. 745–750.

Lee, D.S., and Edmond, J.M., 1985, Tellurium species in seawater: Nature, v. 313, p. 782–785.

LeFort, D., Hanley, J., and Guillong, M., 2011, Subepithermal Au-Pd mineralization associated with an alkali porphyry Cu-Au deposit, Mount Milligan, Quesnel terrane, British Columbia, Canada: Economic Geology, v. 106, p. 781–808.

Lindgren, W., 1933, Mineral deposits: New York, McGraw-Hill, 930 p.

Lindquist, A.E., 1966, Structure and mineralization of the Whitehall mining district, Jefferson County, Montana: M.S. thesis, Butte, Montana College of Mineral Science and Technology, 104 p.

Lindsey, D.A., 1985, A gold-mineralized breccia at Kendall, North Moccasin Mountains, Fergus County, Montana: U.S. Geological Survey Professional Paper 1301-C, p. 43–56.

Lindsey, D.A., and Fisher, F.S., 1985, Mineralized breccias in intrusive complexes of Late Cretaceous and Palaeocene age, north-central Montana: U.S. Geological Survey Professional Paper 1301-A, p. 1–34.

Lindsey, D.A., and Naeser, C.W., 1985, Relation between igneous intrusion and gold mineralization in the North Moccasin Mountains, Fergus County, Montana: U.S. Geological Survey Professional Paper 1301-B, p. 35–41.

Lisenbee, A.L., 1981, Studies of the Tertiary intrusions of the northern Black Hills uplift, South Dakota and Wyoming: A historical review: Geological

Society of America Rocky Mountain Section, 1981, Annual Meeting, Rapid City, Field Trip Guidebook, p. 106–125.
Liu, J., Bai, X., Zhao, S., Tran, M., Zhang, Z., Zhao, Z., Zhao, H., and Lu, J., 2011, Geology of the Sandaowanzi telluride gold deposit of the northern Great Xing'an Range, NE China: Geochronology and tectonic controls: Journal of Asian Earth Sciences, v. 41, p. 107–118.
Livo, K.E., 1994, Use of remote sensing to characterize hydrothermal alteration of the Cripple Creek area, Colorado: M.S. thesis, Golden, Colorado School of Mines, 135 p.
Long, K.R., 2011, The future of rare earth elements—will these high-tech industry elements continue in short supply?: U.S. Geological Survey Open-File Report 2011-1189, 41 p. Available at http://pubs.usgs.gov/of/2011/1189/.
Lovering, T.S., and Tweto, O.L., 1953, Geology and ore deposits of the Boulder County tungsten district, Colorado: U.S. Geological Survey Professional Paper 245, 199 p.
Mao, J., Chen, Y., and Wang, P., 1995, Geology and geochemistry of the Dashuigou tellurium deposit, western Sichuan, China: International Geology Review, v. 37, p. 526–546.
Mao, J., Wang, Y., Ding, T., Chen, Y., Wei, J., and Yin, J., 2002, Dashuigou tellurium deposit in Sichuan province, China: S, C, O, and H isotope data and their implications on hydrothermal mineralization: Resource Geology, v. 52, p. 15–23.
Margolis, J., 1993, Geology and intrusion related copper-gold mineralization, Sulphurets, British Columbia: Ph.D. dissertation, University of Oregon.
Maynard, S.R., 1995, Gold mineralization associated with mid-Tertiary magmatism and tectonism, Ortiz Mountains, Santa Fe County, New Mexico: Geology of the Santa Fe Region, New Mexico Geological Society Field Conference, 46th, Guidebook, p. 161–166.
McDonough, W.F., and Sun, S.-S., 1995, The composition of the Earth: Chemical Geology, v. 120, p. 223–254.
McEwan, C.J.A., Fallick, A.E., and Rice, C.M., 1996, The Rosita Hills epithermal Ag-base metal deposits, Colorado, USA: A stable isotope and fluid inclusion study: Mineralium Deposita, v. 31, p. 41–51.
McInnes, B.I.A., Evans, N.J., McBride, J.S., and Lambert, D.D., 1998, Osmium isotope and noble metal enrichment of the mantle source region of the Ladolam gold deposit Lihir Island, PDG [abs.]: Geological Society of America Abstracts with Programs, v. 30, p. 302.
McLemore, V.T., 1996, Great Plains Margin (alkaline-related) gold deposits in New Mexico, *in* Coyner, A.R., and Fahey, P.L., eds., Geology and ore deposits of the American Cordillera: Geological Society of Nevada Symposium Proceedings, v. 2, p. 935–950.
——2010, Geology and mineral deposits of the Gallinas Mountains, Lincoln and Torrance Counties, New Mexico: New Mexico Bureau of Geology and Mineral Resources Open-File Report OF-532, 92 p.
Mclemore, V. T., and North, R. M., 1987, Metallic mineral deposits in Colfax and Union Counties, northeastern New Mexico: New Mexico Geological Society, Guidebook to 38th Field Conference, p. 323–329.
McLemore, V.T., and Guilinger, J.R., 1993, Geology and mineral resources of the Cornudas Mountains, Otero County, New Mexico and Hudspeth County, Texas: Carlsbad Region, New Mexico and West Texas, New Mexico Geological Society Field Conference, 44th, Guidebook, p. 145–154.
McRae, M.E., 2015, Fluorspar: U.S. Geological Survey Mineral Commodity Yearbook 2015, p. 56–57.
Melfos, V., and Voudouris, P.C., 2012, Geological, mineralogical and geochemical aspects for critical and rare metals in Greece: Minerals, v. 2, p. 300–317.
Moss, R.L., Tzimas, E., Kara, H., Willis, P., and Kooroshy, J., 2011, Critical metals in strategic energy technologies: Unpublished JRC Scientific and Technical Reports, 164 p.
Moyle, A.L., Doyle, B.J., Hoogvliet, H., and Ware, A.R., 1990, Ladolam gold deposit, Lihir Island: Australian Institute of Mining and Metallurgy Monograph Series, v. 14, p. 1793–1805.
Müller, D., Franz, L., Herzig, P.M., and Hunt, S., 2001, Potassic igneous rocks from the vicinity of epithermal gold mineralization, Lihir Island, Papua New Guinea: Lithos, v. 57, p. 163–186.
Müller, D., Kaminski, K., Uhlig, S., Graupner, T., Herzig, P.M., and Hunt, S., 2002, The transition from porphyry- to epithermal-style gold mineralization at Ladolam, Lihir Island, Papua New Guinea: A reconnaissance study: Mineralium Deposita, v. 37, p. 61–74.
Mutschler, F.E., 1992, Alkaline igneous systems and related mineral deposits: 1992 Annual Pacific Northwest Mining and Metals Conference Short Course Notes, April 6–10.
Mutschler, F.E., and Mooney, T.C., 1995, Precious metal deposits related to alkaline igneous rocks—provisional classification, grade-tonnage data, and exploration frontiers: Geological Association of Canada Special Paper—IAGOD 1990 Symposium on Ore Deposit Models, 22 p.
Mutschler, F.E., Griffen, M.E., Stevens, D.S., and Shannon, S.S., Jr., 1984, Precious metal deposits related to alkaline rocks in the North American Cordillera [abs]: Geological Society of America Abstracts with Programs, v. 16, p. 606.
——1985, Precious metal deposit related to alkaline rocks in the North American Cordillera: An interpretive review: Transactions of the Geological Society of South Africa, v. 88, p. 355–377.
Mutschler, F.E., Mooney, T.C., and Johnson, D.C., 1991, Precious metal deposits related to alkaline igneous rocks, a space-time trip through the Cordillera: Mining Engineering, v. 43, p. 304–309.
Mutschler, F.E., Larson, E.E., and Ross, M.L., 1998, Potential for alkaline igneous rock-related gold deposits in the Colorado Plateau Laccolithic Centers: U.S. Geological Bulletin 2158, p. 233–252.
Nash, J.T., and Cunningham, C.G., 1973, Fluid-inclusion studies of the fluorspar and gold deposits, Jamestown district, Colorado: Economic Geology, v. 68, p. 1247–1262.
National Institute of Advanced Industrial Science and Technology, 2008, Rare metals: Tsukuba, Japan, Publication Office, AIST, 12 p.
National Research Council, 2008, Minerals, critical minerals, and the U.S. Economy: National Academy of Sciences, 263 p.
Niu, Y., 2008, The origin of alkaline lavas: Science, v. 320, p. 883–884.
Nixon, G.T., and Archibald, D.A., 2001, Age of platinum-group-element mineralization in the Sappho alkaline complex, south-central British Columbia: British Columbia Geological Survey Paper 2002-I, p. 171–176.
North, R.M., and McLemore, V.T., 1986, Silver and gold occurrences in New Mexico: New Mexico Bureau of Mines and Mineral Resources, Resource Map 15, 32 p., scale 1:1,000,000.
Pals, D.W., and Spry, P.G., 2003, Telluride mineralogy of the low-sulfidation epithermal Emperor gold deposit, Vatukoula, Fiji: Mineralogy and Petrology, v. 79, p. 285–307.
Pals, D.W., Spry, P.G., and Chryssoulis, S., 2003, Invisible gold and tellurium in arsenic-rich pyrite from the Emperor gold deposit, Fiji: Implications for gold distribution and deposition: Economic Geology, v. 98, p. 493–514.
Paredes, M.M., 1994, A fluid inclusion, stable isotope, and multi-element study of the Golden Sunlight deposit, Montana: M.S. thesis, Iowa State University, 174 p.
Parker, R.L., 1967, Composition of the Earth's crust: U.S. Geological Survey Professional Paper 440-D, 19 p.
Paterson, C.J., Groff, N.U. and Longstaffe, F.J., 1989, A view through an epithermal-mesothermal precious metal system in the northern Black Hills, South Dakota: A magmatic origin for the ore-forming fluids: Economic Geology Monograph 6, p. 564–570.
Peach, C.L., Mathez, E.A., and Keays, R.R., 1990, Sulfide melt-silicate melt distribution coefficients for noble metals and other chalcophile elements as deduced from MORB: Implications for partial melting: Geochimica et Cosmochimica Acta, v. 54, p. 3379–3389.
Peccerillo, A., and Taylor, R.P., 1976, Geochemistry of the Eocene calc-alkaline volcanic rocks in the Kastamonu area, northern Turkey: Mineralogy and Petrology, v. 56, p. 63–81.
Pilet, S., Baker, M.B., and Stolper, E.M., 2008, Metasomatized lithosphere and the origin of alkaline lavas: Science, v. 320, p. 916–919.
Pitkin, J.A., and Long, C.L., 1977, Interpretation of data from an aerial gamma-ray survey in the Cripple Creek district, Teller County, Colorado: U.S. Geological Survey Open-File Report 77-534, 12 p.
Porter, E.W., and Ripley, E.M., 1985, Petrologic and stable isotope study of the gold-bearing breccia pipe at the Golden Sunlight deposit, Montana: Economic Geology, v. 80, p. 1689–1706.
Pudack, C., Halter, W.E., Heinrich, C.A., and Pettke, T., 2009, Evolution of magmatic vapor to gold-rich epithermal liquid: the porphyry to epithermal transition at Nevados de Famatina, northwest Argentina: Economic Geology, v. 104, p. 449–477.
Reimann, C., and de Caritat, P., 1998, Chemical elements in the environment: Fact sheets for the geochemist and environmental scientist: Berlin, Springer-Verlag, 398 p.
Rice, C.M., Harmon, R.S., and Shepherd, T.J., 1985, Central City, Colorado: The upper part of an alkaline porphyry molybdenum system: Economic Geology, v. 80, p. 1769–1796.
Richards, J.P., 1990, Petrology and geochemistry of alkalic intrusives at the Porgera gold deposit, Papua New Guinea: Journal of Geochemical Exploration, v. 35, p. 141–199.

——1995, Alkalic-type epithermal gold deposits—a review: Mineralogical Association of Canada Short Course Series, v. 23, p. 367–400.
——1997, Controls on scale of Porgera-type porphyry/epithermal gold deposits associated with mafic, alkalic magmatism: Transactions Institution of Mining and Metallurgy, v. 106, p. B1–B8.
——2009, Postsubduction porphyry Cu-Au and epithermal Au deposits: Products of remelting of subduction-modified lithosphere: Geology, v. 37, p. 247–250.
Richards, J.P., and Kerrich, R., 1993, The Porgera gold mine, Papua New Guinea: Magmatic hydrothermal to epithermal evolution of an alkali-type precious metal deposit: Economic Geology, v. 88, p. 1017–1052.
Richards, J.P., and Ledlie, I., 1993, Alkalic intrusive rocks associated with the Mount Kare gold deposit, Papua New Guinea: Comparison with the Porgera intrusive complex: Economic Geology, v. 88, p. 755–781.
Richards, J.P., McCulloch, M.T., Chappel, B.W., and Kerrich, R., 1991, Sources of metals in the Porgera gold deposit, Papua New Guinea: Evidence from alteration, isotope, and noble metal geochemistry: Geochimica et Cosmochimica Acta, v. 55, p. 565–580.
Richards, J.P., Wilkinson, D., and Ulrich, T., 2006, Geology of the Sari Gunay epithermal gold deposit, northwest Iran: Economic Geology, v. 101, p. 1455–1496.
Robert, F., Brommecker, R., Bourne, B.T., Dobak, P.J., McEwan, C.J., Rowe, P.R., and Zhou, X., 2007, Models and exploration methods for major gold deposit types, *in* Milkereit, B., ed., Proceedings of Exploration 07: Fifth Decennial International Conference on Mineral Exploration, p. 691–711.
Ronacher, E., Richards, J.P., Reed, M.H., Bray, C.J., Spooner, E.T.C., and Adams, P.D., 2004, Characteristics and evolution of the hydrothermal fluid in the North zone high-grade area, Porgera gold deposit, Papua New Guinea: Economic Geology, v. 99, p. 843–867.
Rogers, N.W., and Setterfield, T.N., 1994, Potassium and incompatible-element enrichment in shoshonitic lavas from the Tavua volcano, Fiji: Chemical Geology, v. 118, p. 43–62.
Saunders, J.A., 1991, Gold deposits of the Boulder County gold district: U.S. Geological Survey Bulletin 1857-I, p. 137–148.
Saunders, J.A., and May, E.R., 1986, Bessie G, a high-grade epithermal gold telluride deposit, La Plata County, Colorado, U.S.A., *in* Macdonald, J.A., ed., Geology of gold deposits: Gold '86, Toronto, Proceedings, p. 436–444.
Scherbarth, N.L., and Spry, P.G., 2006, Mineralogical, petrological, stable isotope, and fluid inclusion characteristics of the Tuvatu gold-silver telluride deposit, Fiji: Comparisons with the Emperor deposit: Economic Geology, v. 101, p. 135–158.
Schutz, J.L., 1995, Gold mineralization associated with alkaline intrusives at the Carache Canyon breccia pipe prospect, Ortiz Mountains, New Mexico: New Mexico Geological Society Guidebook,46th Field Conference, p. 167–177.
Shawe, D.R., ed., 1976, Geology and resources of fluorine in the United States, with sections by D.R. Shawe, R.E. Van Alstine, R.G. Worl, A.V. Heyl, R.D. Trace, R.L. Parker, W.R. Griffitts, C.L. Sainsbury, and J.B. Cathcart: U.S. Geological Survey Professional Paper 933, 99 p.
Shedd, K.B., 2014, Tungsten: U.S. Geological Survey Mineral Commodity Yearbook 2013, p. 174–175.
Simmons, E.C., and Hedge, C.E., 1978, Minor element geochemistry and strontium isotopes of Tertiary stocks in Colorado mineral belt: U.S. Geological Survey Professional Paper 1100, p. 192–193.
Simmons, S.F., White, N.C., and John, D.A., 2005, Geological characteristics of epithermal precious and base metal deposits: Society of Economic Geologists 100th Anniversary Volume, p. 485–522.
Spry, P.G., and Scherbarth, N.L., 2006, The gold-vanadium-tellurium association at the Tuvatu gold-silver prospect, Fiji: Conditions of ore deposition: Mineralogy and Petrology, v. 87, p. 171–186.
Spry, P.G., and Thieben, S. E., 2000, The distribution and recovery of gold in the Golden Sunlight gold-silver telluride deposit, Montana, U.S.A.: Mineralogical Magazine, v. 64, p. 31–42.
Spry, P.G., Paredes, M.M., Foster, F., Truckle, J.S., and Chadwick, T.H., 1996, Evidence for a genetic link between gold-silver telluride and porphyry molybdenum mineralization at the Golden Sunlight deposit, Whitehall, Montana: Fluid inclusion and stable isotope studies: Economic Geology, v. 91, p. 507–526.
Spry, P.G., Foster, F., Truckle, J.S., and Chadwick, T.H., 1997, The mineralogy of the Golden Sunlight gold-silver telluride deposit, Whitehall, Montana, U.S.A.: Mineralogy and Petrology, v. 59, p. 143–164.
Staatz, M. H., 1983, Geology and description of thorium and rare-earth deposits in the southern Bear Lodge Mountains, northeast Wyoming: U.S. Geological Survey Professional Paper 1049-D, p. D1–D52.
Stein, H.J., and Crock, J.G., 1990, Late Cretaceous-Tertiary magmatism in the Colorado mineral belt: Rare earth element and samarium-neodymium isotopic studies: Geological Society of America Memoir, v. 174, p. 195–223.
Tarkian, M., and Stribrny, B., 1999, Platinum-group elements in porphyry copper deposits: A reconnaissance study: Mineralogy and Petrology, v. 65, p. 161–183.
Taylor, H.P., 1997, Oxygen and hydrogen isotope relationships in hydrothermal mineral deposits, *in* Barnes, H.L., ed., Geochemistry of hydrothermal ore deposits: New York, Wiley Interscience, p. 229–302.
Thompson, T.B., Trippel, A.D., and Dwelley, P.C., 1985, Mineralized veins and breccias of the Cripple Creek district, Colorado: Economic Geology, v. 80, p. 1669–1688.
TTP Squared, Inc., 2013. Atlantic Ltd.-Vanadium Market Outlook Presentation, TTP Squared, Inc., 25 p. Accessed March 22, 2013, at: http://atlanticltd.com.au/upload/documents/VanadiumInformation/Vanadium-MarketOutlook.pdf.
U.S. Department of Energy, 2010, Critical materials strategy: Washington, D.C., United States Department of Energy, 166 p.
Vardiman, D.M., Roy, E., Thornton, D., Nicholson, D., White, D., and Melker, M., 2006, Geology and exploration developments Cripple Creek mining district, Colorado U.S.A.: Unpublished Cripple Creek and Victor Field Trip Guidebook, 12 p. (http://www.ccvgoldmining.com/downloads/Geology%20Field%20Guide%202006.pdf)
Voudouris, P., 2006, A comparative mineralogical study of Te-rich magmatic-hydrothermal systems in northeastern Greece: Mineralogy and Petrology, v. 87, p. 241–275.
Vymazalová, A., and Drábek, M., 2011, The Pd-Pb-Te system: Pašavaite phase relations, experimental approach: Canadian Mineralogist, v. 49, p. 1679–1686.
Wallier, S., Rey, R., Kouzmanov, K., Pettke, T., Heinrich, C.A., Leary, S., O'Connor, G., Tamas, C.G., Vennemann, T., and Ullrich, T., 2006, Magmatic fluids in the breccia-hosted epithermal Au-Ag deposit of Rosia Montana, Romania: Economic Geology, v. 101, p. 923–954.
Werle, J.L., Ikramuddin, M., and Mutschler, F.E., 1984, Allard stock, La Plata Mountains, Colorado: An alkaline rock-hosted porphyry copper-precious metal deposit: Canadian Journal of Earth Science, v. 21, p. 630–641.
White, N.C., and Hedenquist, J.W., 1990, Epithermal environments and styles of mineralization: Variations and their causes, and guidelines for exploration: Journal of Geochemical Exploration, v. 36, p. 445–473.
——1995, Epithermal gold deposits: Styles, characteristics and exploration: Society of Economic Geologists Newsletter 23, p. 1–13.
White, P., Ussher, G., and Hermoso, D., 2010, Evolution of the Ladolam geothermal system on Lahir Island, Papua New Guinea: World Geothermal Congress 2010, Bali, Indonesia, 25–29 April, Proceedings, 7 p.
Wilson, M.R., and Kyser, T.K., 1988, Geochemistry of porphyry-hosted Au-Ag deposits in the Little Rocky Mountains, Montana: Economic Geology, v. 83, p. 1329–1346.
Woodward, L.A., 1995, Metallic mineral deposits of the Judith Mountains, central Montana: Montana Bureau of Mines and Geology Memoir 67, 78 p.
Woodward, L.A., and Giles, D.L., 1993, Lode mineralization in the Judith Mountains, Montana, *in* Hunter, L.D., ed., Energy and mineral resources of central Montana: Montana Geological Society Guidebook, p. 197–214.
Yi, W., Halliday, A.N., Alt, J.C., Lee, D.-C., Rehkämper, M., Garcia, M.O., Langmuir, C.H., and Su, Y., 2000, Cadmium, indium, tin, tellurium, and sulfur in oceanic basalts: Implications for chalcophile element fractionation in the Earth: Journal of Geophysical Research, v. 105, p. 18,927–18,948.
Zhang, X., and Spry, P.G., 1994, Petrological, mineralogical, fluid inclusion, and stable isotope studies of the Gies gold-silver telluride deposit, Judith Mountains, Montana: Economic Geology, v. 89, p. 602–627.
Zhang, X., Nesbitt, B.E., and Muehlenbachs, K., 1989, Gold mineralization in the Okanagan Valley, southern British Columbia: Fluid inclusion and stable isotope studies: Economic Geology, v. 84, p. 410–424.
Zhang, Z., Mao, J., Wang, Y., Pirajno, F., Liu, J., and Zhao, Z., 2010, Geochemistry and geochronology of the volcanic rocks associated with the Dong'an adularia-sericite epithermal gold deposit, Lesser Hinggan Range, Heilongjiang province, NE China: Constraints on the metallogenesis: Ore Geology Reviews, v. 37, p. 158–174.

©2016 Society of Economic Geologists, Inc.
Reviews in Economic Geology, v. 18, pp. 217–244

Chapter 10

Critical Elements in Carlin, Epithermal, and Orogenic Gold Deposits

Richard J. Goldfarb,[1,2,3,†] Albert H. Hofstra,[1] and Stuart F. Simmons[4,5]

[1] *State Key Laboratory of Geological Processes and Mineral Resources, School of Earth Sciences and Resources, China University of Geosciences, Beijing 100083, China*

[2] *U.S. Geological Survey, Box 25046, MS 973, Denver Federal Center, Denver, Colorado 80225-0046*

[3] *Centre for Exploration Targeting, School of Earth and Geographical Sciences, University of Western Australia, Crawley, Western Australia, Australia 6094*

[4] *Hot Solutions Ltd., PO Box 32-125, Devonport, Auckland, New Zealand 0744*

[5] *Energy and Geoscience Institute, University of Utah, 423 Wakara Way, Suite 300, Salt Lake City, Utah 84108*

Abstract

Carlin, epithermal, and orogenic gold deposits, today mined almost exclusively for their gold content, have similar suites of anomalous trace elements that reflect similar low-salinity ore fluids and thermal conditions of metal transport and deposition. Many of these trace elements are commonly referred to as critical or near-critical elements or metals and have been locally recovered, although typically in small amounts, by historic mining activities. These elements include As, Bi, Hg, In, Sb, Se, Te, Tl, and W. Most of these elements are now solely recovered as by-products from the milling of large-tonnage, base metal-rich ore deposits, such as porphyry and volcanogenic massive sulfide deposits.

A combination of dominance of the world market by a single country for a single commodity and a growing demand for many of the critical to near-critical elements could lead to future recovery of such elements from select epithermal, orogenic, or Carlin-type gold deposits. Antimony continues to be recovered from some orogenic gold deposits and tellurium could potentially be a primary commodity from some such deposits. Tellurium and indium in sphalerite-rich ores have been recovered in the past and could be future commodities recovered from epithermal ores. Carlin-type gold deposits in Nevada are enriched in and may be a future source for As, Hg, Sb, and/or Tl. Some of the Devonian carbonaceous host rocks in the Carlin districts are sufficiently enriched in many trace elements, including Hg, Se, and V, such that they also could become resources. Thallium may be locally enriched to economic levels in Carlin-type deposits and it has been produced from Carlin-like deposits elsewhere in the world (e.g., Alsar, southern Macedonia; Lanmuchang, Guizhou province, China). Mercury continues to be recovered from shallow-level epithermal deposits, as well as a by-product of many Carlin-type deposits where refractory ore is roasted to oxidize carbon and pyrite, and mercury is then captured in air pollution control devices.

Introduction

The gold-only (e.g., Phillips and Powell, 1993, 2014) or lode-gold deposits are generally classified as orogenic, epithermal, and Carlin types. They are universally mined for their gold content and, in the case of the epithermal deposits, commonly for their silver content. Base metal concentrations are typically low in orogenic, Carlin, and many epithermal ores where hydrothermal solutions have low to moderate salinity, generally no greater than about 5 to 8 wt % NaCl equiv. Some epithermal deposits, however, can be rich in base metals because higher salinity ore fluids can transport metals in this environment.

Many commodities that are commonly enriched in the gold-only deposits are defined as critical, energy critical, or near-critical in various reports on critical elements or rare metals that have been released over the past decade (e.g., National Institute of Advanced Industrial Science and Technology, 2008; National Research Council, 2008; European Commission, 2010; U.S. Department of Energy, 2010; Moss et al., 2011). These include Bi, Co, Hg, In, PGM, Ni, Sb, Se, Te, Tl, W, and graphite. Many of these are recovered as by-products from the refining of other commodities, such as tellurium and selenium from copper production (e.g., John and Taylor, 2016) and indium from zinc production. They are very rarely recovered as a primary commodity in any deposit, including the gold-only deposits. Some are defined as critical because their supply is dominated by a single or a few countries, such as In, Sb, and W by China, platinum group metals by Russia and South Africa, or cobalt by the Democratic Republic of the Congo (European Commission, 2010). With global industrialization and more complex energy needs, many of these commodities, which were of little to no economic interest in the past, are now of major importance in industries such as the automotive, computer, desalinization, electronic, solar, and space.

Below we describe the enrichments of critical elements in Carlin-type, epithermal, and orogenic gold deposits. We omit the alkaline intrusion-related epithermal gold ores, such as those at Cripple Creek, northern Black Hills, Zortman-Landusky, Mount Milligan, Lihir, Porgera, and Emperor, because this important subgroup of epithermal deposits is described by Kelley and Spry (2016) in a separate chapter. One purpose of this chapter is to indicate what critical elements have been historically produced (Table 1) or likely

† Corresponding author: e-mail, Goldfarb@usgs.gov

Table 1. Past Production of Various Critical Elements from Carlin-Type, Epithermal, and Orogenic Gold Deposits

Commodity	Deposit	Gold deposit type	Past production (tonnes of metal)	Reported enrichments
As	Getchell, Nevada	Carlin	~10 t/day in 1943	
	Yata, Guizhou, China	Carlin-like	Historic production	
	Giant, Yellowknife, Canada	Orogenic	237,000 t As tri-oxide	
	Ashanti (Obuasi), Ghana	Orogenic	Minor As in early 1990s	
	Salisgne, France	Orogenic	400,000 t As	
Bi	Potosi district, Bolivia	IS epithermal	Byproduct of Ag-Sn mining; at Tasna, sulfides with 10–15% Bi	
	Julcani, Peru	H-I epithermal	Significant production; 100 t Bi in 1990 from Pb concentrates	
	Cerro de Pasco, Peru	H-I epithermal	1920s from ores grading 1.5–2.0%Bi	
Hg	Alligator Ridge, Nevada	Shallow Carlin	0.086 t in 1999	
	Carlin trend (Barrick mines), Nevada	Carlin	Approx. 6 to 83 t/yr 1999–2002	
	Jerritt Canyon	Carlin	Approx. 2 t/yr 1999–2002	
	Pipeline	Carlin	Approx. 0.4 t/yr 1999–2003	
	Carlin trend (Newmont mines)	Carlin	Approx. 8 t/yr 2000–2003	
	Getchell trend (Newmont mines)	Carlin	Approx. 4 t/yr 2001–2003	
	Mercur, Utah	Carlin	1.23 t 1903–1907	
	Hycroft, Sulfur Dist., Nevada	Hot springs, L-I epithermal	50 t Hg (1941–1943, 1995,2000–2001)	
	McDermitt, Nevada	Hot springs Hg, L-I epithermal	5,900 t Hg (1974-1990)	7,000 t Hg
	Knoxville and Manhattan (McLaughlin), California	Hot springs, L-I epithermal Au-Hg	4,200 t Hg (1862–1948)	
	Moschellandsberg, SW Germany	Epithermal	Intermittent production (1440–1942)	
	Paradise Peak, Nevada	Shallow H-I epithermal	≥457 t Hg (1986–1994)	
In	Toyoha mine, Japan	L-I epithermal	>4,600 t In @138 g/t (1909–2006)	
	Pinguino district, Argentina	L-I epithermal		Sphalerite with 1 to >1,000 ppm In
	San Roque, Argentina	L-I epithermal		Intersections (1–12 m) with 30–1,500 ppm In
	Nagyborzsony, Hungary	IS epithermal		Sphalerite with 100–800 ppm In
Sb	Jerritt Canyon, Nevada	Carlin	<100 t	
	Bootstrap, Nevada	Carlin	<100 t	
	Cortez, Nevada	Carlin	Prospect	
	Getchell, Nevada	Carlin	Prospect	
	Xikuangshan	Carlin-like or orogenic?	World's largest, mined for 500 years	Almost exhausted
	Bolivia tin belt	IS epithermal	Intermittent unrecorded production	
	Murchinson belt, South Africa	Orogenic	550,000 t Sb @ 3.0–3.5% Sb	65,000 t Sb @ 1.87% Sb
	Otago, South Island, New Zealand	Orogenic	Minor from late 1800s–mid-1900s	
	Ollympiada, Russia	Orogenic		100,000 t Sb @ 1%Sb
	Reefton, South Island, New Zealand	Orogenic		Gold ores averaging 0.4% Sb
	Sarylakh, Yana-Kolyma, Russia	Orogenic		180,000 t Sb @ 20-30% Sb
	Sentachan, Yana-Kolyma, Russia	Orogenic		110,000 t Sb @ 20-30% Sb
	Yellow Pine, Idaho, USA	Orogenic	Production during WW III for Sb and W	47,000 t Sb @ 0.06% Sb
Se	Laerma, W. Qinling, China	Carlin-like		Locally >500 ppm Se
Te	Sacarimb, Romania	L-I epithermal	60 t Te @ 20 g/t Te (1700s–1941)	
	Bambolla, Somora, Mexico	L-I epithermal(?)	Minor production from ores average 2.5 g/t Te	
Tl	Alsar, Macedonia	L-I epithermal or Carlin-like?	20,000 t Sb (some remains)	500 t Tl (and 15,000 t As)
	Lanmuchang, Guizhou, China	Carlin-like	Historic Hg prod., Tl produced in the 1990s	500 t Tl
	Xiangquan, China	Epithermal or VMS?		250 t Tl @ 0.3% Tl
	North Island, New Zealand	Shallow (hot springs) L-I epithermal		As much as 1,000s ppm Tl
W	Hillgrove, NSW, Australia	Orogenic	Minor W, along with Sb and Au	
	Yellow Pine, Idaho, USA	Orogenic	Production during WW II for W and Sb	
	Otago, South Island, New Zealand	Orogenic	Minor from late 1800s to mid-1900s	
	Southern Cross, Western Australia	Orogenic	Minor W production at least through the 1970s	
	Hollinger mine, Timmins, Ontario, Canada	Orogenic	47,878 t W (1940–1953) from rock averaging 0.78% W	
	Julcani, Peru	H-I epithermal	Production during WW II	11,800 tons W ore reserves

Table 1. *(Cont.)*

Commodity	Host rocks	Deposit age	Ore style	Mineralogy hosting critical elements	References
As	Cambrian-Ordovician siltstone and limestone	Late Eocene	Disseminated	Orpiment, realgar	Berger and Tingley (1985)
	Triassic siliciclastics and limestone	J-K?	Disseminated	Realgar	Xia et al. (2012)
	Archean greenstone	Archean	Vein	Arsenopyrite	Aboriginal Affairs Canada (2010)
	Paleoproterozoic volcanosedimentary	Paleoproterozoic	Vein	Arsenopyrite	Edelstein (1995)
	Cambrian-Ordovician schists	Late Paleozoic	Vein	Arsenopyrite	Demange et al. (2006)
Bi	Late Paleogene dacite dome	14 Ma	Fractures	Ag minerals, cassiterite, wolframite	Pohl (2011)
	Late Miocene dacite/rhyodacite domes	10 Ma	Fractures in sulfides	Bismuthinite, wolframite	Petersen et al. (1977); Mobbs (1990)
	Middle Miocene quartz monzonite	15 Ma	Replacement and vein	Cuprobismutite, matildite, bismuthinite	Baumgartner et al. (2008)
Hg	Devonian-Mississippian limestone and shale	Late Eocene	Disseminated	Hg resides in pyrite, cinnabar	Ilchik (1990); Jones and Miller (2005)
	Devonian silty limestones, dolomite	Late Eocene	Disseminated	Hg resides in pyrite, cinnabar	Jones and Miller (2005)
	Ordovician-Devonian silty limestones	Late Eocene	Disseminated	Hg resides in pyrite, cinnabar	Jones and Miller (2005)
	Silurian-Devonian silty limestones	Late Eocene	Disseminated	Hg resides in pyrite, cinnabar	Jones and Miller (2005)
	Silurian-Devonian siltstones and limestone	Late Eocene	Disseminated	Hg resides in pyrite, cinnabar	Jones and Miller (2005)
	Cambrian-Ordovician siltstone and limestone	Late Eocene	Disseminated	Hg resides in pyrite, cinnabar	Jones and Miller (2005)
	Mississippian limestone	Late Eocene	Disseminated	Cinnabar	Stanger (1992)
	Tertiary volcanics/volcaniclastics	4 Ma	Disseminated, vein	Pyrite, maracaiste, electrum, cerargyrite, lodarggyrite, cinnabar	Jones and Miller (2005); Moore et al. (2013)
	Sedimentary rocks in Miocene caldera	16 Ma	Stratabound bodies	Cinnabar, radtkeite, corderoite	Rytuba (1976); Jones and Miller (2005)
	Siliceous sinter, altered serpentinite	Neogene-Quaternary	Fractures	Cinnabar, native mercury, metacinnabar	Rytuba et al. (1993)
	Sedimentary rocks in late Pz caldera	Late Paleozoic	Breccia, veinlets	Cinnabar, native mercury	Krupp (1989)
	Early Miocene ash flow tuff	19–18 Ma	Stratabound bodies	Cinnabar, native sulfur, corderoite	Rytuba and Heropoulos (1992); Sillitoe and Lorson (1994)
In	Volcanic and sedimentary rocks	Miocene	Veins	Splaerite, stannite, chalcopyrite	Ohta (1989); Shimizu and Aoki (2011)
	Jurassic vx and sed rocks	Jurassic	Veins	Sphalerite, chalcopyrite, cassiterite	Jovic et al. (2011a, b)
	Triassic-Jurassic volcanics and volcaniclastics	Jurassic(?)	Veins	Sphalerite, chalcopyrite, roquestite	Dill et al. (2013)
	Miocene dacite and andesite	Miocene	Stockworks	Sphalerite	Schwarz-Schampera and Herzig (2002)
Sb	Ordovician-Devonian silty limestones	Late Eocene	Disseminated	Stibnite	Lawrence (1963)
	Devonian limestone	Late Eocene	Disseminated	Stibnite	Lawrence (1963)
	Silurian-Devonian silty limestones	Late Eocene	Disseminated	Stibnite	Lawrence (1963
	Cambrian-Ordovician siltstone and limestone	Late Eocene	Disseminated	Stibnite	Lawrence (1963
	Devonian carbonate and argillite	Paleozoic(?), Mesozoic(?)	Massive	Stibnite	Fan et al. (2004); Goldfarb et al. (2014)
			Vein	Stibnite	Ahlfeld (1941); Dill et al. (1995)
	3.0 Ga volcanics and volcaniclastics	2.97 Ga	Vein, veinlet	Stibnite	Vearncombe et al. (1988); Schwarz-Schampera (2014)
	Early Mesozoic metasediments	Jurassic	Vein	Stibnite	Thompson et al. (1995)
	Late Neoproterozoic schist	Late Neoproterozoic(?)	Veinlet, disseminated	Stibnite	Yakubchuk et al. (2005)
	Early Paleozoic metasediments	Early Paleozoic	Vein	Stibnite	Thompson et al. (1995)
	Late Triassic argillite	Early Cretaceous	Breccia, lenses	Stibnite	Bortnikov et al. (2010)
	Late Triassic argillite	Early Cretaceous	Breccia, lenses	Stibnite	Bortnikov et al. (2010)
	Cretaceous-Tertiary intrusions and metasediments	Tertiary(?)	Veins, disseminated	Stibnite	Midas Gold Corp (2013)

Table 1. *(Cont.)*

Commodity	Host rocks	Deposit age	Ore style	Mineralogy hosting critical elements	References
Se	Cambrian carbonaceous cherts and slates	Triassic(?)	Veins to lenses	Se-bearing stibnite, various selenides	Liu et al. (2000)
Te	Neogene quartz andesite	Neogene	Vein	Nagyagite, sylvanite	Alderton and Fallick (2000); Popescu and Neacsu (2004)
	Tertiary rhyolite in Proterozoic metaseds	Tertiary	Vein	Hessite, benleonardite	Mexivada Mining Corp (2009); W. Atkinson (writ. commun., 2014)
Tl	Pliocene-Pleistocene subvolcanic intrusions	5–4 Ma	Steep shears and fractures	Fe-sulfide, As- and Tl-minerals, cinnabarite, Pb-Sb-sulfosalts, gold, sulfur	Boev and Jelenkovic (2012)
	Permian limestone, shale,coal	Jurassic-Cretaceous(?)	Disseminated	Lorandite, christite, cinnabar	Xiao et al. (2004)
	E. Ordovician limestone/mudstone	Paleozoic(?), Mesozoic(?)	Massive to vein	Pyrite, lafossaite, lorandite	Zhou et al. (2005); Fan et al. (2014)
	Hot spring precipitates	Modern			Weissberg (1969); Reyes et al. (2002)
W	Late Paleozoic metasediments and granitoids	255–245 Ma	Veins, disseminated	Scheelite	Ashley and Craw (2004)
	Cretaceous-Tertiary intrusions and metasediments	Tertiary(?)	Veins, disseminated	Scheelite	Midas Gold Corp (2013)
	Early Mesozoic metasediments	Jurassic	Vein	Scheelite	Thompson et al. (1995)
	Late Archean greenstone sequences	Late Archean	Vein	Scheelite, wolframite	Baxter (19780
	Late Archean tholeiitic basalt	Late Archean	Vein	Scheelite	Wood (1991)
	Late Miocene dacite/rhyodacite domes	10 Ma	Fractures in sulfides	Bismuthinite, wolframite	Petersen et al. (1977)

Abbreviations: H-I = high-intermediate sulfidation, IS = intermediate sulfidation, L-I = low-intermediate sulfidation, t = tonnes

are being produced from present-day gold mining activities; although rare, there are such present-day examples from each of the three gold deposit types. More significantly, we attempt to point out important element enrichments in these deposits that could become future primary resources at times of increased degree of criticality.

Carlin-Type and Carlin-Like Gold Deposits

The well-defined late Eocene Carlin-type gold deposits are located in north-central Nevada, USA (Fig. 1A) and their combined gold endowment (5,500 metric tons (t)) is enormous and is exceeded only by the Witwatersrand in South Africa. The bulk of this gold is in the northern Carlin trend (3,000 t). The Carlin-type deposits are epigenetic, disseminated, auriferous pyrite deposits that are generally hosted in calcareous sedimentary rocks. In these deposits, gold ore commonly occurs at intersections between faults and permeable reactive strata below an impermeable cap rock and generally exhibits a central high-grade zone of carbonate dissolution and argillic alteration with micron-sized disseminated pyrite. Pervasively silicified rock, called jasperoid, is often present within or near ore. In unsilicified rocks, open fractures and pores are often lined with macroscopic crystals of orpiment, realgar, and calcite. In jasperoid, most fractures and vugs are lined with drusy quartz and may contain kaolinite, stibnite, barite, or calcite (Hofstra and Cline, 2000; Cline et al., 2005). The deposits are typically enriched in As, Sb, Hg, and Tl, and minor amounts of Hg and Sb were recovered historically as a main product from some workings in what became large Carlin-type gold mines. In 1976, Carlin itself was the second largest mercury producer after the McDermitt epithermal mercury deposit in the United States (Tingley et al., 1993). Today, mercury is a significant by-product from processing of Carlin gold ores. In the period of 2004 to 2006, about 110 to 115 t Hg were produced annually in Nevada, mostly from Carlin gold orebodies, and about 75% of this was from the giant Goldstrike deposit (http://www.epa.gov/mercury/archive/stocks/Byproduct%20Mercury%20Production%20in%20Modern%20Precious%20Metals%20Mines%20in%20Nevada.pdf).

Carlin-type gold ore is mined by both open-pit and underground operations, with grades as low as less than 1 g/t mined from the former and as high as 34 g/t from the latter. Because most of the gold resides in pyrite, it must be first oxidized in a roaster or autoclave to allow recovery of gold with cyanide solutions. Natural weathering and oxidation of the pyritic ores eliminate this step and permit direct recovery of gold by cyanide heap leaching methods.

The geochemistry of Carlin-type deposit ores, described herein, is fairly well documented, but the origin of these deposits continues to be the subject of debate. Recent models for Nevada Carlin-type deposits call upon magmatic (Muntean et al., 2011) or sedimentary (Large et al., 2011a, b) sources for gold and transport to the site of ore deposition by H_2S-rich fluids of magmatic or metamorphic/meteoric derivation, respectively.

Two areas along the margins of the Yangtze craton in China are commonly stated to contain Carlin-type deposits (Fig. 1B;

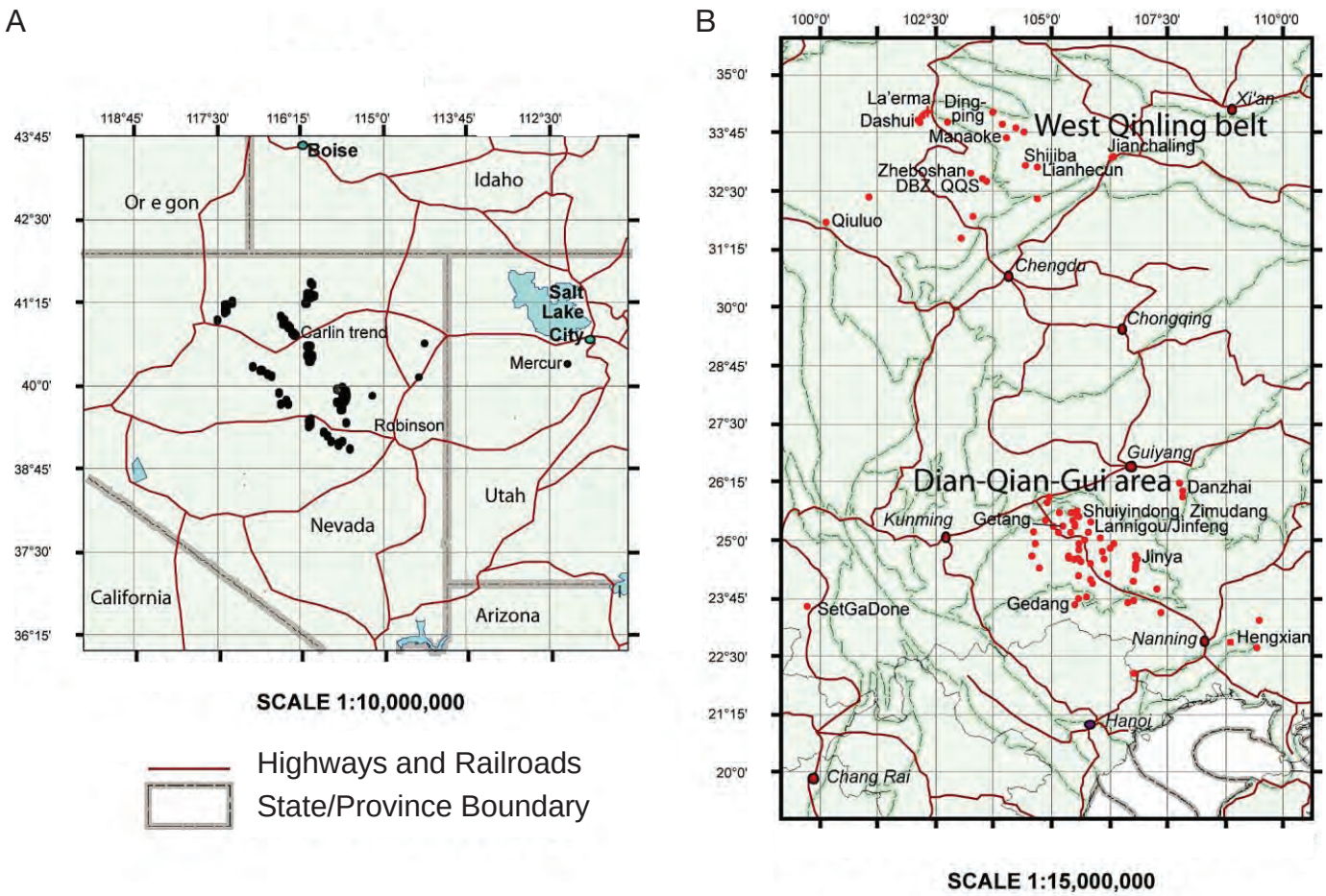

Fig. 1. Location of Carlin-type gold deposits in the western United States (A) and Carlin-like deposits in southwestern China (B).

Hofstra et al., 2005). These are in the Dian-Qian-Gui area and in the West Qinling belt and each contains about 800 t Au, but these areas are not as thoroughly explored as northern Nevada. These deposits show some features similar to many of the Nevada Carlin-type deposits, but other features resemble orogenic gold deposits (e.g., Cline et al., 2013). In this paper, we refer to deposits that have some features resembling Carlin-type gold deposits, but which classification remains uncertain, as Carlin-like gold deposits. Evidence from Carlin-like deposits in the West Qinling belt suggests they may be epizonal analogues of nearby mesozonal orogenic gold deposits (Mao et al., 2002; Hofstra et al., 2005). Likewise, evidence from Carlin-like deposits in the Dian-Qian-Gui area, mainly in Guizhou province, is in part consistent with a Carlin-type gold model and in part with an epizonal orogenic gold model (Hu et al., 2002; Hofstra et al., 2005).

Older mineralization in Eocene Carlin-type gold districts

Eocene-age Carlin-type gold deposits in Nevada occur in mining districts that have long and complex histories of sedimentation, deformation, magmatism, and hydrothermal activity, such that different types of mineralization are locally superimposed (Hofstra and Cline, 2000; Emsbo et al., 2003, 2006; Cline et al., 2005). Events that predate formation of the main Carlin gold resource are (1) deposition of Paleozoic metalliferous black shales or marls enriched in Zn, V, Ni, Cu, Pb, Se, Mo, As, Ag, Au ± bedded barite deposits (Poole et al., 1981; Papke, 1984; Emsbo et al., 1999, 2003, 2006; Large et al., 2011a, b); (2) replacement of Paleozoic carbonate rocks by banded (zebra) dolomite ± barite ± base metal sulfides (Diehl et al., 2010); (3) formation of Jurassic iron oxide ± Cu mineralization and polymetallic skarn, replacement, and vein deposits (Cortez: Barton et al., 2011), and reduced intrusion-related gold deposits (Bald Mountain: Nutt and Hofstra, 2007); (4) Cretaceous W skarn (Getchell: Silberman et al., 1974), polymetallic skarn (Gold Acres: Hays and Foo, 1991), and polymetallic vein and replacement deposit formation (Eureka: Vikre, 1998); and (5) formation of Paleogene intrusion-related Cu and W skarn and polymetallic replacement deposits (Railroad: Rayias, 1999). Some of the Carlin-type gold deposits also are locally overprinted by Neogene epithermal Au-Ag ± Hg deposits, notably where the northern Carlin trend and the northern Nevada rift intersect (Wallace, 2003; Cluer, 2012).

Consequently, the gold ore in Carlin-type deposits in Nevada may contain critical elements in adjacent older deposits or in material remobilized from such deposits into the Carlin ores during Eocene hydrothermal activity. These elements potentially could be exploited along with gold. Although the geochemical signatures of pre-Carlin-type gold ore mineralization must be considered on a case by case basis for the

above deposit types, carbonaceous strata deposited under dysoxic to anoxic conditions enriched in Zn, V, Ni, Cu, Pb, Se, Mo, As, Ag, Au, ± (Ba or P) are the most common elemental anomalies. Within these strata, most anomalous trace elements are concentrated in Paleozoic syngenetic pyrite and related sulfide minerals or in organic matter (Emsbo et al., 1999; Emsbo and Koenig, 2005; Large et al., 2009). The exception is vanadium, which is concentrated in mica and organic matter (Emsbo et al., 1999; Poul Emsbo, oral commun., 2014). Such strata may locally contain barite enriched in strontium and/or phosphate nodules that may be enriched in rare earth elements (REE). Thus, where Carlin-type gold mineralization is hosted in carbonaceous strata, it may some day be possible, if there is need, to recover the aforementioned trace elements from concentrates of organic matter (Ni, V, Se, Mo, Au), sulfides (Zn, Ni, Cu, Se, Mo, As, Ag, Au), micas (V), bedded barite (Sr), or phosphate (REE).

Carlin-type deposit mineralization and paragenesis

Most of the trace elements introduced with gold in Carlin-type deposits reside either in main ore-stage pyrite or in late ore-stage sulfide and sulfosalt minerals. Ore-stage arsenian pyrite, and locally marcasite or arsenopyrite, occur as isolated micron-sized grains and commonly form 1- to 30-μm-thick rims on preexisting pyrite in the host rocks (e.g., Fig. 2). Arsenic facilitates the incorporation of gold into the pyrite lattice up to a solubility limit (Fig. 3A) above which pyrite contains nanoparticles of native gold (Bakken et al., 1989; Fleet and Mumin, 1997; Palenik et al., 2004; Reich et al., 2005; Deditius et al., 2011a; Large et al., 2009). Arsenic also facilitates the incorporation of other trace elements into the pyrite lattice, and, although the solubility limits are poorly known, nanoparticles of Ag, Ag-Pb-S, Pb-S, and Hg-S have been documented in such pyrite (Deditius et al., 2011b). Microanalysis of ore-stage pyrite by LA-ICP-MS (Fig. 3B) or SIMS show that it generally contains elevated As, Sb, Hg, Tl, and Au, as well as less consistently Cu, Te, Se, Pb, Zn, Ag, and W (e.g., Emsbo et al., 2003; Cline et al., 2005; Barker et al., 2009; Large et al., 2009; Muntean et al., 2011).

The high trace element content of ore-stage pyrite has been attributed to the H_2S-rich composition of ore-forming fluids, the relatively low temperature of ore formation, and the fast rate of pyrite precipitation (Hofstra and Cline, 2000; Deditius et al., 2011a). Such ore-stage pyrite is routinely oxidized in the mill prior to gold recovery with cyanide solutions. During the process, the contained trace elements also may potentially be liberated and recovered with additional processing and, thus, they might constitute a future economic resource.

During the late ore stage of Carlin-type deposits, a variety of sulfide minerals precipitate locally in open fractures and

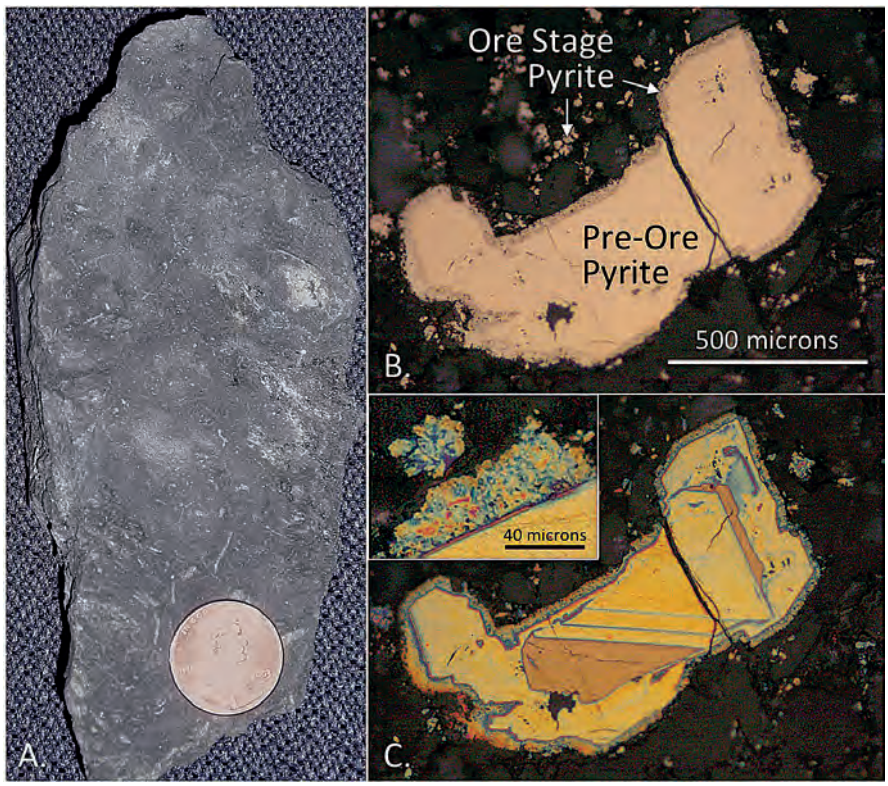

Fig. 2. (A). Cut slab of pervasively argillized and sulfidized high-grade gold ore from the Deep Star deposit, northern Carlin trend (23-mm U.S. penny for scale) with an abundance of fine-grained "sooty" ore pyrite. Ore is hosted in calc-silicate hornfels produced by the emplacement of Jurassic intrusions into calcareous siltstones of the Devonian Popovich Formation. (B). Reflected light image of Jurassic preore pyrite rimmed by Eocene ore pyrite in a matrix comprised of quartz and kaolinite containing disseminated ore pyrite. (C). Reflected light image of tarnished pyrite (shown in B) highlights both trace element-rich growth zones in the Jurassic pyrite and rims comprised of Eocene ore pyrite. Inset shows that ore pyrite is comprised of a polycrystalline aggregate of zoned crystals.

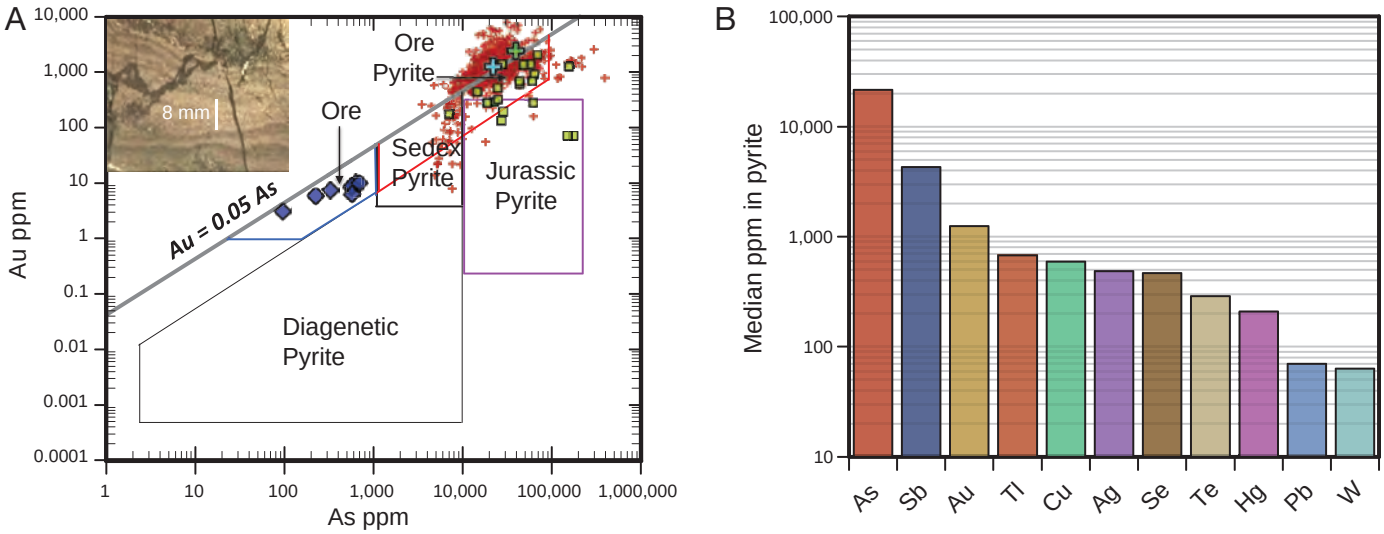

Fig. 3. (A). Au vs. As data (n = 1,150; red crosses) relative to reference fields for Silurian and Devonian diagenetic pyrite (black hair line), Devonian sedex pyrite (black line), Jurassic intrusion-related pyrite (magenta line), Eocene gold ore (blue line), Eocene ore-stage pyrite (red line), and the solubility limit of gold in arsenian-pyrite (gray line) from Large et al. (2011a). For comparison, the median compositions of gold ore (blue diamonds) and pyrite (yellow squares) in different ore types and host rocks from the northern Carlin trend are plotted (data from Almeida et al., 2010). About one-half of the LA-ICP-MS data points, as well as their median composition (cyan cross) and electron microprobe data on ore pyrite (green cross; from Emsbo et al., 2003) plot above the solubility limit of Au in arsenian-pyrite. Thus, gold nanoparticles may be present in some of the ore pyrite at Meikle. The other one-half of the LA-ICP-MS data points plot below the solubility limit within the field of typical ore-stage pyrite. The minority of data that plot in the sedex field are reasonable given that most of the preore pyrite at Meikle was deposited with hydrothermal dolomite in the footwall alteration zone of a sedex hydrothermal system (Emsbo et al., 2003). (B). Bar chart showing the median abundance of trace elements in ore pyrite (n = 1,150). (Inset) Polished slab of high-grade gold ore hosted in Devonian hydrothermal dolomite from the Meikle mine, northern Carlin trend. It is comprised of silicified internal sediment in a dissolution collapse cavity that consists mainly of ore pyrite, quartz, and preore pyrite (Emsbo et al., 2003). The LA-ICP-MS data plotted in (A) and (B) were collected along the 8-mm white line.

pores. Arsenic minerals such as orpiment (As_2S_3) and realgar (AsS) are relatively common, arsenopyrite (FeAsS) is uncommon, and microscopic native arsenic is rarely present. Stibnite (Sb_2S_3) is a common antimony mineral, which in some deposits contains significant concentrations of selenium (Lu, 1994). Although cinnabar (HgS) is the main mercury mineral, it is uncommon and generally microscopic in size. The most common thallium mineral, lorandite ($TlAsS_2$), is a minor constituent in some deposits and typically occurs with orpiment and realgar (Radtke et al., 1974). Other rare minerals include carlinite (Tl_2S) (Radtke and Dickson, 1975), christite ($TlHgAsS_3$) (Radtke, et al., 1977), weissbergite ($TlSbS_2$) (Dickson and Radtke, 1978), ellisite (Tl_3AsS_3) (Dickson, et al., 1979), gillulyite ($Tl_2(As, Sb)_8 S_{13}$) (Wilson et al., 1991), coloradoite (HgTe) and calaverite ($AuTe_2$) (Simon et al., 1999), and galkhaite $(Cs,Tl)(Hg,Cu,Zn)_6(As,Sb)_4S_{12}$ (Tretbar et al., 2000).

In Nevada, there are several Carlin-type deposits that have exploited orpiment and realgar veins for arsenic (Getchell) and stibnite veins for antimony (Jerritt Canyon) (Table 1; Cline et al., 2005). During World War II, when government wartime restrictions forced the shutdown of many gold producers, the Getchell mine in Nevada was permitted to continue operations as a producer of "strategic" arsenic (Berger and Tingley, 1985). Historic As, Sb, Tl, or Hg mines also are present in China in areas subsequently defined as hosting Carlin-like gold deposits (Hu et al., 2002). At the Yata Carlin-type deposit in southwestern Guizhou, realgar has been recovered for many years as a source of arsenic (Xia et al., 2012). The stibnite-bearing jasperoids in Carlin-type gold deposits closely resemble those at the Xikuangshan deposit in Hunan province, China (A. Hofstra, field observation, 2012), which is the world's largest antimony deposit, but lacks gold (Fan et al., 2004). It is, therefore, possible that significant antimony resources may be present in Carlin-type districts in Nevada and Carlin-like districts in China. Thallium was the principal commodity produced from lorandite and christite in the Lanmuchang deposit in China's Guizhou province, which is associated with arsenic and mercury occurrences and Carlin-like gold deposits along the Hujiabao anticline (Xiao et al, 2004). Jasperoid in the Laerma deposit, West Qinling belt, is unique in that it contains selenium-bearing stibnite and the Sb_2Se_3 analogue antimonselite (Liu et al., 1999); the selenium was derived from Lower Cambrian metalliferous black shales (Wen and Carignan, 2011).Thus, the vugs and veins of late ore-stage minerals in Carlin-type and Carlin-like deposits are high-grade, low-tonnage sources for As, Sb, Tl, and Hg, as well as locally selenium, which potentially could meet some future economic needs.

Characteristics of Carlin-type ore-forming solutions

The common geochemistry of Carlin-type gold deposits suggests that they all formed from ore fluids with similar chemical compositions. Gold typically was deposited at 180° to 240°C and at depths of 1 to 3 km from a low to moderate salinity (3–6 wt % NaCl equiv) fluid, with 1 to 4 mol % CO_2;

fluid source is highly debated (Hofstra and Cline, 2000; Cline et al., 2005; Saunders et al., 2014). Fluid inclusion studies and equilibrium chemical models show that the hydrothermal fluids contained significant concentrations of reduced sulfur ($\Sigma H_2S + HS^- > 10^{-2}$ m) and that Au was transported predominantly as sulfide complexes ($AuHS^\circ$, $Au[HS]_2^-$) (e.g., Hofstra et al., 1991; Hofstra and Cline 2000). Although other complexes may be present, most of the trace elements present in ore pyrite (As, Sb, Hg, Tl, Te) can form sulfide complexes at the temperatures of ore formation. Chemical models show that as pyrite precipitates by sulfidation of host-rock iron, the concentration of H_2S and gold in the fluid steadily decrease. During the sulfidation process, it is likely that other sulfide-complexed elements also are incorporated into ore pyrite. Consequently, the chemical composition of ore pyrite may reflect the abundance of sulfide complexed elements in ore fluids. The common trace element assemblage (As, Sb, Hg, Tl, Au, ±W, ±Te) in ore-stage pyrite may be derived from the ultimate source of reduced sulfur, whereas the idiosyncratic elements (e.g., base metals, Se, Mo) may reflect local scavenging of elements from preore mineralization encountered along fluid pathways.

Geochemistry of Carlin-type deposits

Unlike epithermal and orogenic gold deposits that are described below, there is little production or resource data for critical elements in Carlin-type deposits. Evaluation of the geochemistry of these ores, however, emphasizes some anomalies that potentially could be of future economic interest.

There have been several multielement geochemical studies of the northern Carlin trend (Bakken, 1990; Kuehn and Rose, 1992; Kesler et al., 2003; de Almeida et al., 2010; Hofstra et al., 2011). Element abundances shown in Figure 4 are representative of mill-grade Carlin ore. The plots provide an indication of the typical abundance of some critical elements in Carlin-type gold deposits. Below we show how various statistical approaches have been used to identify the suite of elements in these Carlin-type deposits. The results show that the most consistently anomalous elements in decreasing order of abundance are S, As, Sb, Hg, ±W, Tl, Au, ±Te.

Factor analysis has been employed to identify ore-related element associations in multielement lithogeochemical data sets from Nevada Carlin-type gold districts (e.g., Hofstra and Cline, 2000; Jerritt Canyon: Hofstra, 1994; Patterson and Muntean, 2011; Carlin trend: Emsbo et al., 1999, 2003;

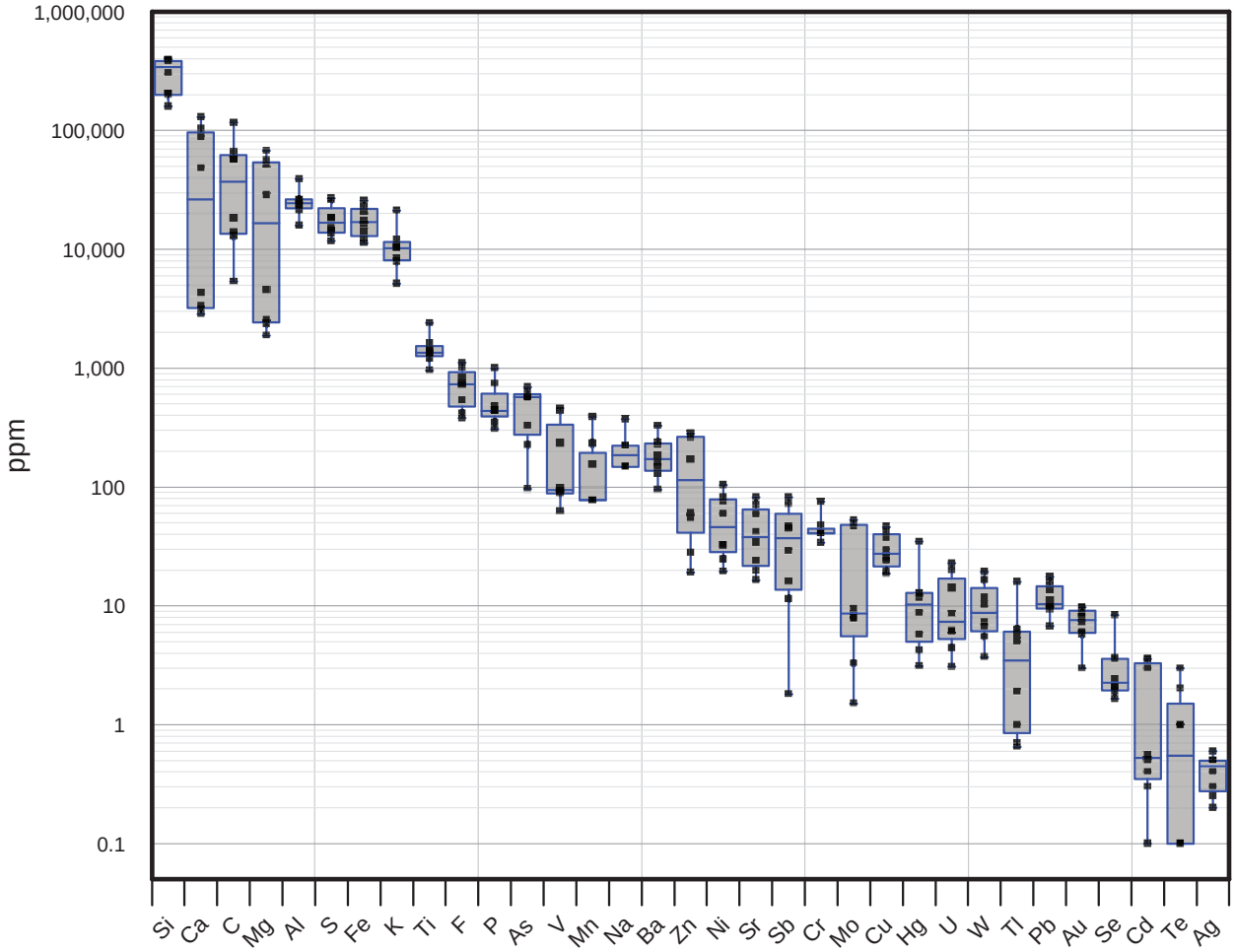

Fig. 4. Box plots (extremes, 25th, 50th, and 75th percentile values) of the median abundance of 33 elements detected in two ore types hosted in six different sedimentary rock units in three formations (Roberts Mountains, Popovich, Rodeo Creek) on the Goldstrike property in the northern Carlin trend (from de Almeida et al., 2011). Elements sorted in decreasing order of the highest median value. Black squares show the median abundance of elements in each ore type and unit.

de'Almeida et al., 2010; Hofstra et al., 2011; Gold Bar: Yigit and Hofstra, 2003). These studies show that Au, As, Sb, Hg, and Tl are consistently anomalous in Carlin-type gold ores. In some data sets, other trace elements (e.g., W, Te, Cu, Pb, Se, Ag, Sn, In, Mn, Li, or Cs) may be associated with the Carlin ore signature.

Isocon diagrams (Grant, 1986) have been used to document mass transfer between unaltered host rocks and mineralized equivalents in several Carlin-type gold deposits (Table 2, Fig. 5A, B; e.g., Hofstra and Cline, 2000). These diagrams show that in most gold ores, the elements of the Carlin suite (As, Sb, Hg, Tl, Au, ± W, ±Te) are enriched by one to four orders of magnitude relative to local background (e.g., Fig. 5A, B). These diagrams also show that a large amount of sulfur is introduced with the Carlin suite of elements and that iron is generally immobile (e.g., Fig. 5A, B). The general immobility of iron, as well as introduction of sulfur, gold, and trace elements, indicates that ore-stage pyrite precipitated from H_2S-bearing fluids by sulfidation of reactive iron in the host rocks (Hofstra et al., 1991). The introduction of iron in some ore zones suggests that ore-stage pyrite may also precipitate by sulfidation of an iron-bearing fluid (Table 2; Kesler et al., 2003). In support of the results from factor analysis, the isochon diagrams indicate that other trace elements, such as Ag, Pb, Zn, Cu, Se, Mo, and Cs, are introduced in some samples and ore zones (Table 2).

Another approach to defining element additions is to divide the average trace element concentrations in the ores by the average trace element concentrations in the crust to obtain enrichment factors. These factors can provide an indication of the most strongly anomalous elements in a deposit area. Lithogeochemical data on ore samples with >1 ppm Au from several deposits were used to calculate enrichment factors for Tl, Hg, Sb, As, Au, Ag, Pb, Zn, Cu, Mo, and W (Fig. 6A-C; Hofstra and Christensen, 2002). Elements are arranged from the classic Carlin suite (Tl, Hg, Sb, As, Au) on the left, through Ag and base metals (Pb, Zn, Cu) to Mo and W on the right in Figure 6A. The common ligands for these elements also progress from sulfide to chloride to oxyanions. In the few deposits with tellurium analyses, concentrations are notably high (e.g., Kesler et al., 2005). Element enrichments in Carlin trend deposits (Fig. 6A, colored symbols) are essentially the same as those of Carlin-type deposits in other Nevada gold districts (Fig. 6A, black squares). Likewise, Figure 6B and C show that element enrichments in the Dian-Qian-Gui area and West Qinling belt Carlin-like gold deposits (colored symbols) are essentially the same as those Carlin-type deposits in Nevada (black squares).

Conclusions

Historically, small amounts of mercury, antimony, and arsenic were recovered at some of the sites of today's giant Carlin-type gold deposits in Nevada. Today, mercury is a significant by-product of much of the gold ore processing. Thallium is a highly enriched element within the Carlin-type ores, but it has never been recovered from Nevada deposits. The Alsar deposit in Macedonia (see epithermal section below), classified by some workers as a Carlin-type deposit, and the

Table 2. Introduced Elements in Carlin-Type Deposits Based on Isocon Diagrams

Deposit/district	Age-Formation[1]	Strongly introduced elements[2]	Reference (comment)[1]
Carlin/Carlin trend	D-Roberts Mountains	S, As, Hg, Au, Tl, Sb	Bakken et al. (1989)
Screamer/Carlin trend	D-Popovich	Fe, S, Mn, As, Sb, Au, W	Kesler et al. (2003)
Meikle/Carlin trend	D-Bootstrap dolomite	S, As, Sb, Tl, Hg, Au, Ag, Te	Emsbo et al. (2003)
Meikle/Carlin trend	J-lamprophyre	S, As, Sb, W,Tl, Hg, Au, Ag, Te	Emsbo et al. (2003)
Meikle/Carlin trend	J-diorite	S, As, W, Hg, Au, Sb, Tl, Te, Ag	Emsbo et al. (2003)
Meikle/Carlin trend	J-monzonite	S, As, Sb, Tl, Hg, Au, W, Te, Ag	Emsbo et al. (2003)
Deep Star/Carlin trend	J-endoskarn	S, As, W, Hg, Sb, Au, Pb, Tl, Cd, Ag	Hofstra (unpub. data)
Meikle/Carlin trend	Eo-dacite	S, As, Sb, Hg, W, Tl, Te, Au	Emsbo et al. (2003)
Griffin/Carlin trend	Eo-dacite	S, As, Sb, Mo, W, Au, Ag, Se	Henry and Ressel (2000)
Beast/Carlin trend	Eo-rhyolite	As, Sb, Ni, Co, Cu, Tl, W, Hg, Mo, Au, Ag	Ressel et al. (2000) *(S na)*
N Generator Hill/ Jerritt Canyon	OS-Hanson Creek	S, As, Sb, Hg, Au, Tl, Se, Ag	Hofstra et al. (1999)
N Generator Hill/ Jerritt Canyon	SD-Roberts Mountains	S, As, Au	Hofstra et al. (1999)
DASH/Jerritt Canyon	M-andesite	S, As, W, Hg, Sb, Au	Hofstra et al. (1999)
W Generator Hill/Jerritt Canyon	Eo-basalt	S, As, Sb, W, Tl, Au, Hg, Se, Ag, Te	Hofstra et al. (1999)
Getchell/Getchell trend	CO-Comus A	Sb,Tl, Hg, Te, W, Au, Se	Cail and Cline (2001) *(in S As halo)*
Getchell/Getchell trend	CO-Comus C	As, Hg, Sb, Tl, Te, Cs, Au	Cail and Cline (2001) *(in S As halo)*
Getchell/Getchell trend	CO-Comus G	Sb, Hg, Tl, Mo, Te, Cu, Au, Se	Cail and Cline (2001) *(in S As halo)*
Getchell/Getchell trend	K-rhyodacite	S, As, Sb, Hg, Tl, Au, Te	Cail and Cline (2001) *(in S As halo)*
Gold Bar/BMET	D-Denay	As, Zn, Sb, Hg, Au, Ag	Yigit and Hofstra (2003)
Alligator Ridge	MD-Pilot	As, Sb, Hg, Tl, Au	Nutt and Hofstra (2003) *(S na)*
	D-Guilmette	As, Sb, Hg, Tl, Au	Nutt and Hofstra (2003) *(S na)*
Generalized order of abundance		S>As>Sb>Hg>(±W)>Tl>Au≈(±Te)>(±Ag)	

[1] Abbreviations: C = Cambrian, D = Devonian, Eo = Eocene, J = Jurassic, K-Cretaceoous, M = Mississippian, O = Ordovician, S = Silurian; S na = Sulfur not analyzed, *in S As halo* = inside the sulfur and arsenic halo

[2] In decreasing order of abundance

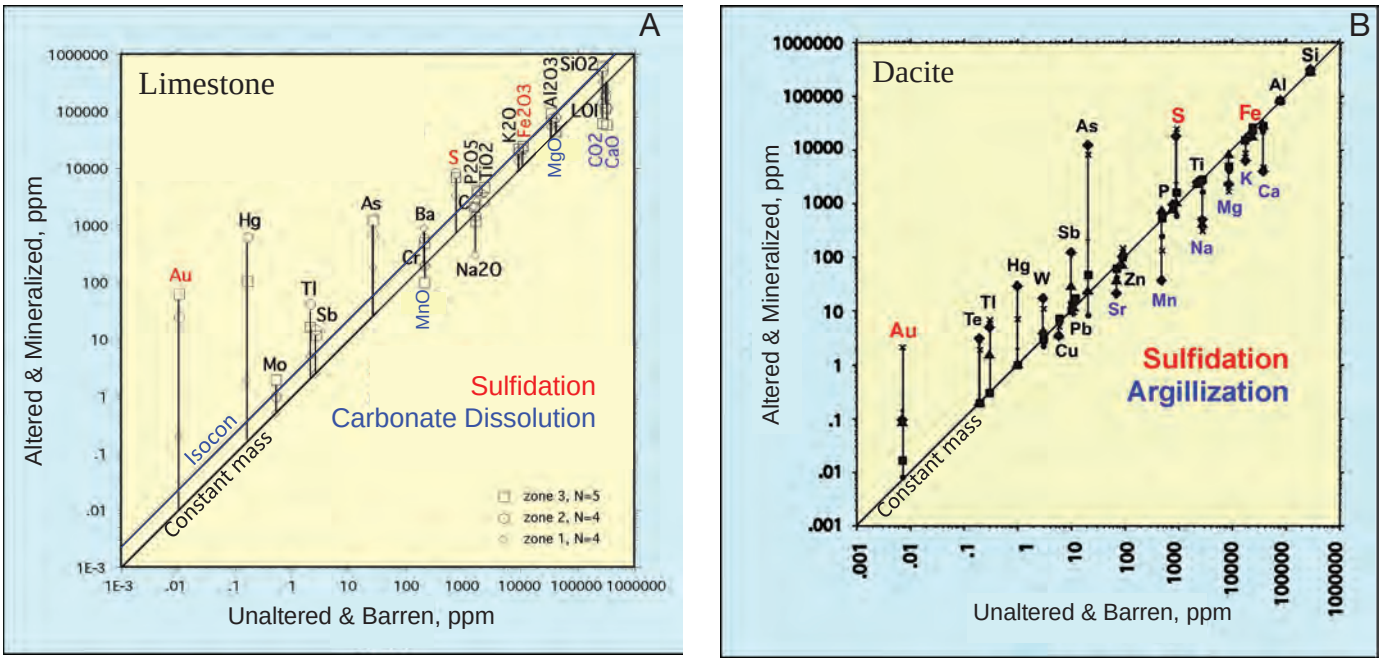

Fig. 5. (A). Isocon diagram showing mass transfer associated with alteration and mineralization in silty laminated limestones of the Silurian and Devonian Roberts Mountains Formation at the Carlin mine in the Carlin trend (based on data for alteration zones 1, 2, and 3 in Bakken et al., 1989). The introduction of Au and S, together with the immobility of Fe_2O_3 (labeled in red), indicate that ore pyrite precipitated from H_2S-rich fluids by sulfidation of host rock iron. The introduction of S and Au is accompanied by other elements that form sulfide complexes, such as As, Hg, Tl and Sb. The depletion of CO_2, CaO, MgO, and MnO (labeled in blue) by carbonate dissolution explains the increased concentration of immobile components (SiO_2, Al_2O_3, Fe_2O_3, K_2O, TiO_2, P_2O_5) that define the isocon. The depletion of Na_2O may reflect clay alteration of detrital or diagenetic albite. (B). Isocon diagram showing mass transfer associated with alteration and mineralization in an Eocene dacite porphyry dike at the Betze mine in the northern Carlin trend (based on data in Emsbo et al., 2003). As in (A), the introduction of Au and S together with the immobility of Fe (labeled in red) indicates that ore-stage pyrite precipitated from H_2S-rich fluids by sulfidation of host-rock iron. The introduction of S and Au is accompanied by other elements that form sulfide complexes, such as As, Sb, Hg, Tl, and Te, as well as W, which (3b) shows that it also can reside in pyrite. The depletion of Ca, K, Mg, Na, Mn, and Sr (blue labels) by argillization of silicate minerals is balanced by the introduction of S and trace elements such that immobile components (Si, Al, Fe, Ti, P) lie along the line of constant mass. Note that Zn, Pb, and Cu are relatively immobile.

Lanmuchang deposit in Guizhou province China, are examples of Carlin-like systems from which thallium was recovered as a primary commodity. The common occurrence of stibnite in jasperoids associated with Carlin-type and Carlin-like deposits in Nevada and China, respectively, allows that significant resources might be defined, if antimony were targeted. Future recovery of other critical elements in the Nevada Carlin districts might come from some of the more massive proto-ores, such as the Paleozoic metalliferous black shales or carbonate replacements, rather than from the Eocene gold orebodies. Carlin-type and Carlin-like deposits are unlikely to be an important global producer of critical elements other than mercury, unless the value of these elements increase or their recovery is mandated by environmental regulations.

Epithermal Deposits

Epithermal deposits form in shallow parts of subaerial hydrothermal systems induced by magmatism along convergent plate margins. Most occur around the circum-Pacific and in the Mediterranean region in Mesozoic-Cenozoic volcanic rock sequences. Epithermal deposits display a diversity of characteristics in terms of orebody geometry, mineralogy, and contained metals, and they have been mined for Cu, Hg, Mn, Pb, Sn, W, and Zn, in addition to gold and silver (Simmons et al. 2005). They form at ≤1.5-km paleodepth and at temperatures <300°C. Orebodies are typically confined to narrow vertical intervals <500 m, but in a few examples can reach a 1,000-m vertical extent. This setting is highly conducive to metal precipitation and accumulation due to sharp physical and chemical gradients that form in and around fluid upflow zones.

Variably anomalous concentrations of As, Bi, Hg, In, Sb, Se, Te, Tl, and W are found in and surrounding epithermal precious metal deposits, and some of these metals are routinely used as pathfinders for exploration (e.g.,White and Hedenquist, 1995; Hedenquist et al., 2000; Simmons et al., 2005). These metals are found with silica sinters, hydrothermally altered rocks, hydrothermal breccias, and mineralized veins at concentrations of a few tens of ppb to a few thousands of ppm, and rarely attain percent levels. The occurrences of metals show crude zonation, which in part reflects temperature gradients, but also reflects changes in fluid chemistry in and surrounding boiling zones (e.g., White and Hedenquist, 1995). The maximum concentrations of elements, such as As, Hg, Sb, and Tl, may be offset and isolated from the ore-grade concentrations of gold and silver (Fig. 7). In the case of

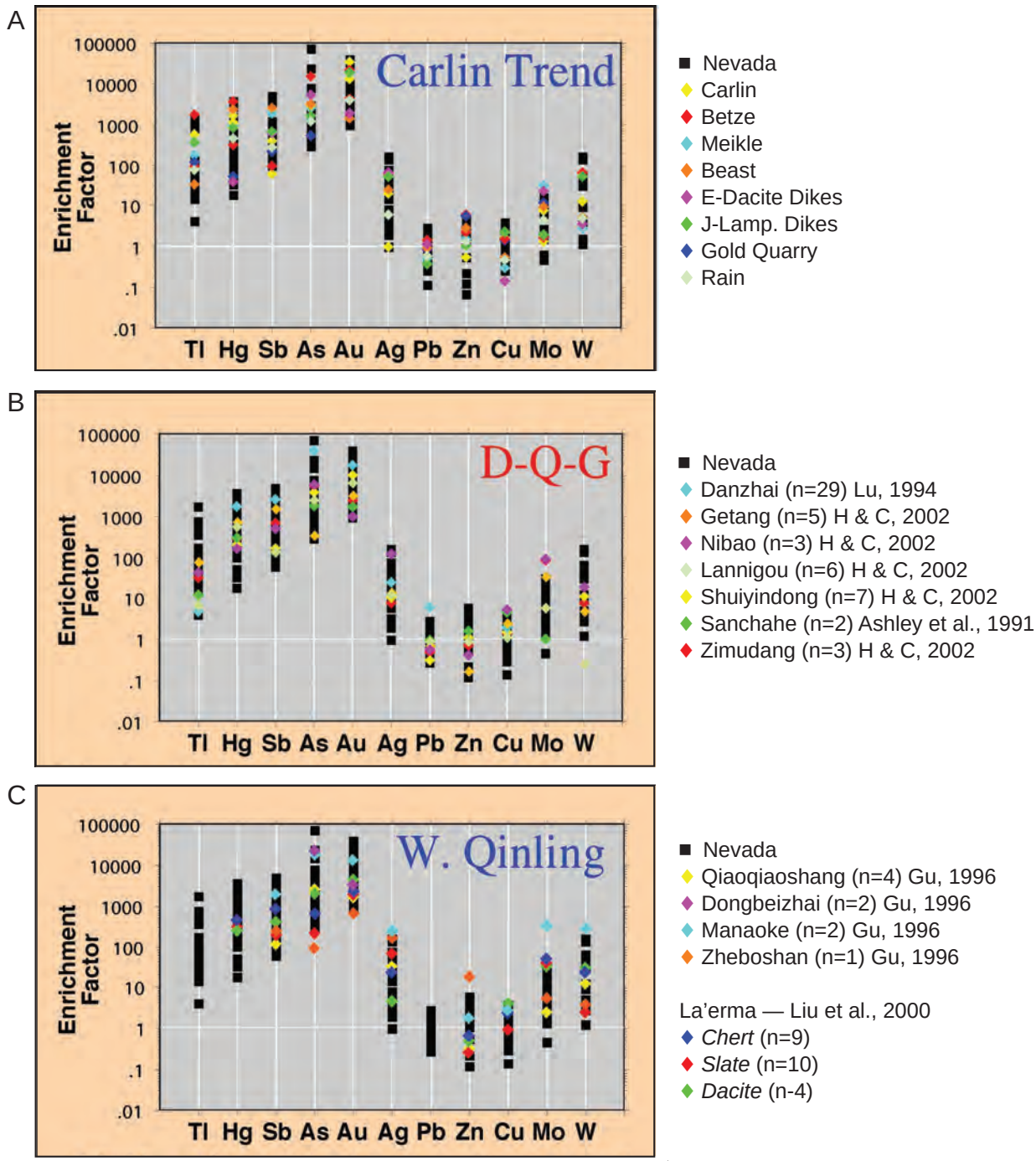

Fig. 6. (A). Trace element enrichments relative to average crust composition in gold ores (Au ≥1 ppm) from several Carlin trend deposits (colored symbols) relative to data from other Carlin-type deposits in Nevada (black symbols). (B). Trace element enrichments relative to average crust in gold ores (Au ≥1 ppm) from several Dian-Qian-Gui area deposits compared to data from 25 Carlin-type deposits in Nevada (black symbols). (C). Trace element enrichments relative to average crust in gold ores (Au ≥1 ppm) from several West Qinling belt deposits compared to data from 25 Carlin-type deposits in Nevada (black symbols). Adapted from Hofstra and Christensen (2002).

mercury deposits, this is a consequence of vapor-phase transport (Christensen and Mroczek, 2003).

The following review of the geochemistry of epithermal deposits discusses Bi, Hg, In, Sb, Te, and Tl, but not As, Se,or W. Arsenic, although very consistently enriched in epithermal ores, particularly in sulfosalt minerals, is almost never considered as a potential economic commodity in the deposits. Selenide minerals are documented at Hishikari (Japan), Sleeper and numerous other deposits in the western United States, Guanajuato (Mexico), and some Coromandel (New Zealand) epithermal deposits, although not in economic amounts (Simon et al., 1997; Christie et al., 2007). However,

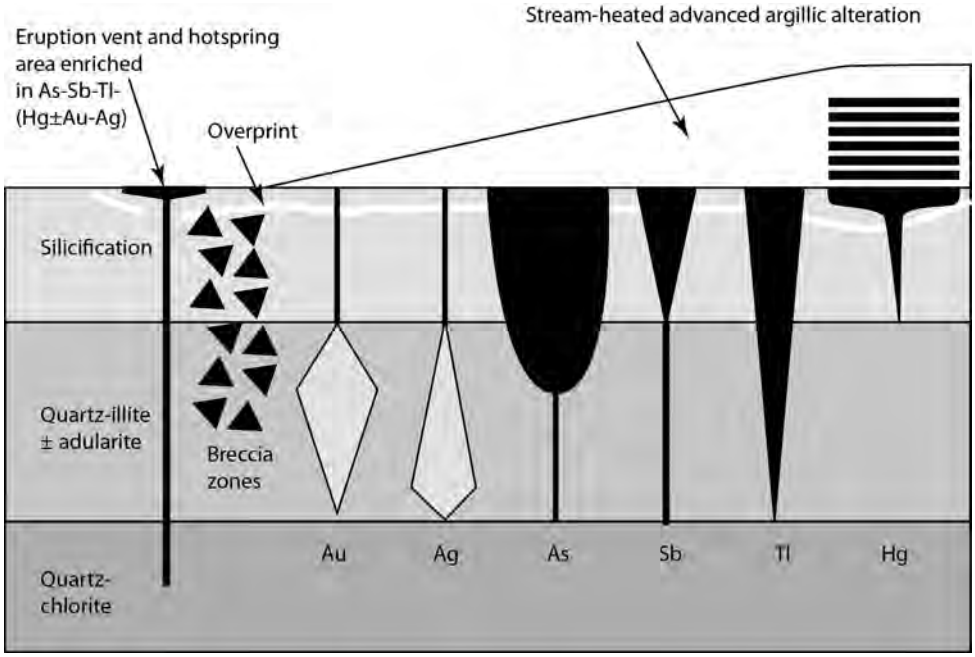

Fig. 7. Low-intermediate sulfidation epithermal deposits showing separation of trace elements As, Hg, Sb, and Tl from the main zone of precious metal mineralization. After Hedenquist et al. (1996). The overprint region refers to changes in the shallow environment due to rise and fall of the water table during hydrothermal activity. Because the zone of steam-heated acid alteration can only form above or at the water table, any rise and fall creates an overprint on earlier formed alteration-mineralization (e.g. Simmons, 1991).

selenium concentrations in these deposits are much greater, probably by at least one order of magnitude, than in porphyry copper deposits, the principal source of selenium (John and Taylor, 2016). Dill (2010) noted that selenium was likely historically produced from epithermal veins in the Harz Mountains (Germany) and in Potosi (Bolivia). Some epithermal deposits contain elevated concentrations of tungsten in the form of wolframite, such as Baia Mare (Romania), Cirotan (Indonesia), Cerro de Pasco (Peru), and Julcani (Peru), and in huebnerite at Tonapah and Sunnyside (United States), Victoria (Philippines), and El Indio (Chile). However, the tungsten is not present in economic quantities in these deposits.

Epithermal deposit subtypes

Epithermal gold deposits can be divided into two main subtypes based on gangue mineralogy, comprising alunite-dickite-pyrophyllite, which form from acidic, oxidized fluids of mainly magmatic origin, and adularia-illite-calcite deposits, which form from near-neutral pH reduced solutions dominated by meteoric water (e.g., White and Hedenquist, 1990, 1995; Simmons et al., 2005). The deposits can also be subdivided into three main subtypes based on sulfide mineralogy (Hedenquist et al., 2000; Sillitoe and Hedenquist, 2003), in which key indicator minerals are distinguished on the basis of their stability relative to sulfur fugacity (f_{S_2}). Enargite, famatinite, and orpiment are high-sulfidation state minerals that are stable at high f_{S_2}; tennantite and tetrahedrite are intermediate-sulfidation state minerals, and arsenopyrite and pyrrhotite are low-sulfidation state minerals (Einaudi et al., 2003). High- and intermediate-sulfidation state minerals occur in mineralized bodies associated with alunite-dickite-pyrophyllite gangue minerals, whereas low- and intermediate-sulfidation state minerals form in mineralized bodies associated with adularia-illite-calcite gangue minerals. Below, we will refer to the two groups as high- and low-intermediate sulfidation deposits. Generally, epithermal ores form from dilute to moderate salinity solutions (<6 wt % NaCl) with <1 mol % CO_2, but clear evidence for higher salinity solutions (>10 wt % NaCl) exists in some deposits (e.g., Simmons, 1991; Davies et al., 2008). Metals are deposited via physical processes that include boiling, fluid mixing, and cooling, which sharply reduce metal solubility in and surrounding the upflow zone of the ore-forming environment.

The epithermal deposits within different subdivisions have a modest influence on the occurrences of critical metals as discussed below. Indium appears restricted to polymetallic veins containing sphalerite, in association with low-intermediate sulfidation state minerals. Cook et al. (2009) noted that gallium may also be significantly enriched in some sphalerites from epithermal ores, and Rytuba et al. (2003) indicated that gallium may be significantly enriched in alunite in some zones of quartz-alunite alteration to the point that it is near economic. Tellurium and bismuth are most consistently associated with high-intermediate sulfidation state ores. For comparison, many critical metals are elevated in fluids and precipitates from high-temperature volcanic fumaroles, including As, Bi, Hg, I, Re, Sb, Se, Te, Tl, and W (e.g., Greenland and Aruscavage, 1986; Symonds et al., 1987; Hedenquist et al., 1994; Korzhinsky et al., 1994; Taran et al., 1995; Fulignati and Sbrana, 1998; Wardell et al., 2008; Moune et al., 2010; Calabrese et al., 2011; Mather et al., 2011; Henley and Berger, 2013). Many of these elements (i.e., As, Hg, Sb,

Se, Te, Tl, and W) occur in geothermal fluids and precipitates sampled from hot springs and production wells (e.g., Weissberg, 1969; Ewers and Keays, 1977; Hedenquist and Henley, 1985; Krupp and Seward, 1987; Reyes et al., 2002; Christenson and Mroczek, 2003; Pope et al., 2005; Simmons and Brown, 2006, 2007).

Historic and present critical and near-critical element resources

Antimony: Antimony occurs in stibnite, tetrahedrite, famatinite, and Ag sulfosalt minerals. Stibnite is an accessory mineral in some low- and high-intermediate sulfidation deposits, such as Cerro de Pasco (Baumgartner et al., 2008), Creede (Plumlee and Whitehouse-Veaux, 1994), Hishikari (Izawa et al., 1990), Kelian (Davies et al., 2008), McLaughlin (Sherlock et al., 1995), Paradise Peak (Sillitoe and Lorson, 1994), and Sari Gunay (Richards et al., 2006); it is fairly common in low-intermediate sulfidation deposits of the Great Basin that are related to bimodal volcanism, such as Sleeper, Hog Ranch, Rosebud, and those of the National district (Vikre, 1985; Dave John, writ. commun., 2014). The epithermal stibnite veins of the Bolivian tin belt are a rare example of deposits in which antimony is the main commodity (Ahlfeld, 1941; Dill et al., 1995). Tetrahedrite, by contrast, is widespread and commonly found in many high- and low-intermediate sulfidation deposits (e.g., Sillitoe and Hedenquist, 2003). At Cerro de Pasco, Baumgartner et al. (2008) reported carbonate replacement ores containing as much as 5.6% Sb. The ores are comprised of an inner zone of famatinite-pyrite and an outer zone of tetrahedrite, and bismuthinite-stibnite solid solution, and enargite-pyrite vein ores containing as much as 2% Sb. Low-intermediate sulfidation ores in Mexican epithermal silver-base metal deposits contain antimony in tetrahedrite and Ag sulfosalts (e.g., Gemmell et al., 1988; Camprubi and Albinson, 2007). These minerals are also found in ginguro bands in Japanese epithermal deposits (Shikazono, 1985). Trace metal dispersion halos, which enclose epithermal orebodies, extend up to the surface where hot-springs deposit sinters contain one to hundreds of ppm Sb (e.g., Silberman and Berger, 1985; Simmons and Browne, 2000; Warren et al., 2004). Presumably, the antimony substitutes into mainly pyrite and possibly other coexisting sulfide minerals (Ewers and Keays, 1977; Baker et al., 2006) or precipitates as amorphous sulfur compounds, such as those found in the Champagne Pool in New Zealand (Weissberg, 1969; Hedenquist and Henley, 1985).

Bismuth: Bismuth occurs as bismuthinite in a few high-intermediate sulfidation deposits, including Beregovo (Biruk and Skakun, 2000), Cerro de Pasco (Baumgartner et al., 2008), Goldfield (Vikre, 1989), Julcani (Benavides, 1983), Paradise Peak (Sillitoe and Lorson, 1994), and Rodalquilar (Arribas et al., 1995). The high-grade Au-Ag ores at Paradise Peak commonly contain 500 to 3,500 ppm Bi (John et al., 1991). Bismuth is also present in high concentrations in the Bi-Ag-Sn ± base metal intermediate-sulfidation veins of Bolivia, such as at Rosario and Candelaria. Anomalous bismuth concentrations are rare in low-intermediate sulfidation deposits, although a few bismuth-bearing minerals are known (e.g., Sillitoe et al., 2002).

Most bismuth is recovered as a by-product of lead and copper refining of ores from large tonnage deposits, although bismuth conceivably could be recovered from sulfide-rich epithermal deposits. In the Potosi district, Bolivia, bismuth is recovered as a by-product of silver and tin mining (Pohl, 2011). However, available present-day production data regarding specific deposits are not readily available. Bismuth was produced at some of the Andean epithermal deposits during the 20th century. Petersen et al. (1977) noted that significant bismuth was being recovered at Julcani, at least through the 1970s, primarily from bismuthinite that occurs along fractures with Ag-, Cu-, and Pb-rich minerals. At Cerro de Pasco, bismuth was recovered in the 1920s from ore containing 1.5 to 2.0% Bi (Ward, 1921).

Indium: Indium occurs in sphalerite and, less commonly, in chalcopyrite, stannite, and rare indium minerals (Wood and Samson, 2006; Dill et al., 2013). Significant indium concentrations are reported for a few low-intermediate sulfiation epithermal deposits (Schwarz-Schampera and Herzig, 2002; Ishihara et al., 2006, 2011; Cook et al., 2009; Jovic et al. 2011a, b; Dill et al., 2013). The best-known deposit is Toyoha in southwest Hokkaido, Japan (Fig. 8). Indium-rich epithermal occurrences are also now recognized in southern Argentina (Jovic et al., 2011a, b). These examples, summarized below, are mainly associated with low-intermediate sulfidation state

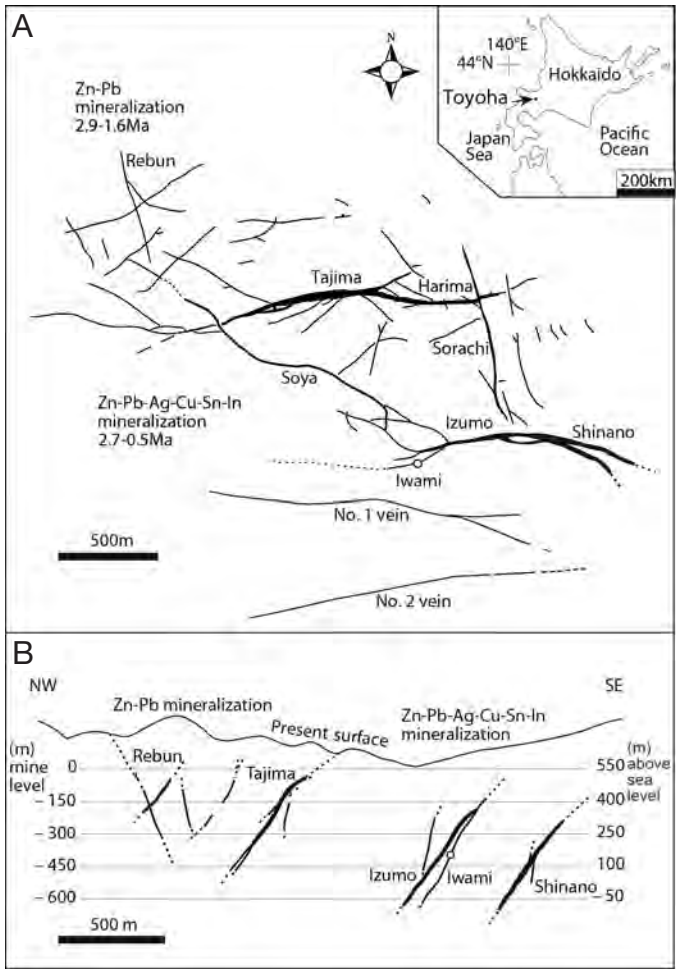

Fig. 8. Distribution (A) and vertical extent (B) of vein systems at the Toyoha epithermal deposit, Japan. The zinc-rich ore contains bands of indium-rich sphalerite. Modified from Shimzu and Morishita (2012).

mineralization. To date, indium has only been produced from deposits in Japan, because indium is recovered more easily as a by-product from the refining of ores mined from large tonnage zinc-rich deposit types.

The Toyoha deposit in Japan, which was mined between 1909 and 2006, is the largest of many epithermal vein deposits in the Sapporo-Iwamai district and was one of the world's largest indium producers (Fig. 8). Total production at Toyoha exceeded 4,600 t In at an average grade of 138 g/t. Base metal-rich mineralization is present as steeply dipping veins, each extending for 500 to 1,500 m along strike within a district covering 8 km², and hosted by hydrothermally altered Miocene volcanic and sedimentary rocks (Fig. 8; Shimizu and Aoki, 2011). The early-formed northern veins are zinc- and lead-rich with sphalerite, galena, pyrite, hematite, magnetite, chalcopyrite, whereas the late-formed southern veins contain pyrrhotite, pyrite, galena, chalcopyrite, arsenopyrite, tetrahedrite, tennantite, and wolframite characterized by a Zn-Pb-Ag-Cu-Sn-In geochemical association (Yajima and Ohta, 1979; Ohta, 1991). Within the latter group, the Izumo and Sorachi veins contained bonanza shoots grading 400 to >1,000 g/t In (Ishihara et al., 2006). Indium-bearing minerals comprise sphalerite, an unnamed zinc-indium mineral ($CuZn_2InS_4$), stannite, kesterite ($Cu_2[Zn,Fe]SnS_4$), roquesite ($CuInS_2$), sakuraiite (Cu,Zn,Fe,In,SnS), chalcopyrite, and laforêtite ($AgInS_2$; Ohta, 1989), which were deposited below about 300°C (Shimizu and Morishita, 2012).

Pinguino is an epithermal vein district covering 20 km², located in the Deseado Massif, Patagonia, Argentina, that is currently being explored for gold-silver mineralization. Quartz veins extend for 2 to >4 km along strike. The veins are hosted in hydrothermally altered, Early to Middle Jurassic volcanic and sedimentary rocks. An indicated resource containing 18,385,000 oz Ag and 106,000 oz Au is reported (Argentex news release, January 31, 2013, http://www.argentexmining.com/s/Home.asp). Two vein types, each attaining widths >10 m, are identified; one is an early sulfide-rich type, with associated enrichments in Au, Ag, Bi, Cu, In, Pb, Sn, Sb, W, and Zn, and a second later type contains silver- and gold-rich quartz (Jovic et al., 2011a, b). Indium occurs in the early-formed veins, which are comprised of three stages of mineralization that include (1) arsenopyrite, pyrite, and quartz; (2) iron-rich sphalerite and galena; and (3) greenockite (CdS) and iron-poor sphalerite. Indium concentrations range from 1 to >1,000 ppm, with iron-rich sphalerite from stage 2 being the volumetrically important host phase (Jovic et al., 2011a). Other indium-bearing minerals found in stage 1 include chalcopyrite, cassiterite, and ferrokësterite ($Cu_2[Fe,Zn]SnS_4$]; Jovic et al. 2011b). Sphalerite-hosted fluid inclusions contain moderate salinity (4–9 wt % NaCl equiv) solutions that homogenize to liquid between 250° and 315°C (Jovic et al., 2011a).

The San Roque Au-Ag prospect in the Rio Negro Province, Argentina, hosts two epithermal quartz veins exposed at the surface over short strike lengths of ~200 m within Triassic-Jurassic lavas and volcaniclastic rocks. Indium concentrations ranging from 30 to 1,500 ppm within intervals of 1 to 12 m have been reported (Dill et al., 2013). Indium occurs in sphalerite, chalcopyrite, roquestite, and skuraiite; associated sulfides comprise galena and pyrite. Sphalerite-hosted fluid inclusions contain moderate-salinity solutions (4.5–6.5 wt % NaCl equiv) that homogenize to liquid between 210° and 250°C (Dill et al., 2013).

Characteristics of a few other indium-rich epithermal deposits are summarized in Schwarz-Schampera and Herzig (2002). The Nagyborzsony deposit in northern Hungary is associated with Miocene dacites and andesites of the Borzsony volcanic complex. High-temperature polymetallic stockworks in the intermediate-sulfidation ores include sphalerite with 0.01 to 0.08 wt % In. The Kirki (or St. Phillipe) Zn-Pb-Ag high-sulfidation epithermal deposit in western Thrace, Greece, is hosted by late Eocene to early Oligocene rhyodacite, andesite, and volcaniclastic rocks. The Zn-Pb ores contain as much as 1,000 ppm In in sphalerite and wurtzite. At the Pleistocene andesite-related McLaughlin hot springs low-sulfidation gold deposit in central California, anhedral grains of gallium-indium-tin oxide are disseminated throughout petroleum-bearing opal in veins. Indium-rich sphalerites are also recognized in low-sulfidation epithermal gold-silver deposits of the Kuril Island arc and Kamchatka of eastern Russia. Sphalerites in these deposits contain as much as 4.67 and 9.3 wt % In, respectively.

Mercury: Mercury, which occurs in its native form or as cinnabar, is concentrated in the shallowest levels of the epithermal environments, such as in hot-spring silica sinters, due to its high solubility and volatility (e.g., Christenson and Mroczek, 2003). Mercury concentrations in epithermal gold-silver deposits generally range between 100 ppb and 50 ppm (Bagby and Berger, 1985). In the early 1990s, the Paradise Peak deposit was producing 12 t Hg annually (Rytuba and Heropoulos, 1992) from silver-gold ores deposited in a hot-springs environment. McLaughlin is an example where gold-silver mineralization was discovered at the site of the Manhattan mercury mine. Bonanza epithermal Au-Ag vein mineralization there contained tens to hundreds of ppm Hg, and hundreds to tens of thousands of ppm Sb (Sherlock et al., 1995; Sherlock, 2005). At McDermitt, Nevada, epithermal hot-springs deposits lack significant gold, but they originally contained 13,000 t Hg (Rytuba, 1976). Several modern hot-spring areas in New Zealand and in the United States are known to be active sites of mercury mineralization that contain 0.2 to 5% Hg (Weissberg, 1969; White, 1981; Christenson and Mroczek, 2003).

Although some epithermal deposits are mercury rich, the classification of mercury deposits remains problematic. The largest historic mercury deposits are not typical epithermal deposits, and although they may have formed in shallow hydrothermal environments, they are generally not classified as epithermal. The Almaden deposit in Spain, the largest known mercury deposit in the world, is unique and difficult to classify (Saupe, 1990). The New Almaden and New Idria mercury deposits in California, many mercury deposits in the Kuskokwim basin in southwestern Alaska, and mercury deposits in the Tien Shan of southwestern Kyrgyzstan may be the shallowest parts of metamorphic hydrothermal systems that would form orogenic gold deposits (see below) at greater depth (Goldfarb et al., 2005) and thus are not truly examples of epithermal deposits.

Tellurium: Tellurium typically occurs in relatively greater abundance and mineralogical variety in epithermal deposits than in other magmatic-related mineral deposit types.

Tellurium occurs in the form of telluride minerals, native tellurium, and tellurium-bearing sulfosalts in unoxidized ores, and as tellurites in secondary ores. It can be found in both high- and low-intermediate sulfidation ores. Gold- and silver-bearing tellurides deposit as scales in two-phase pipelines in the Rotokawa geothermal system, New Zealand (Reyes et al., 2002).

Low-intermediate sulfidation state epithermal ores in some calc-alkaline volcanic rocks contain tellurium minerals (Cook and Ciobanu, 2005). For example, a diversity of economically important telluride ores occur across a region of 600 km^2 in the Metaliferi Mountains, western Romania, one of Earth's richest epithermal ore regions (Alderton and Fallick, 2000). Many of the telluride minerals are uncommon elsewhere and tend to occur in the shallowest parts of deposits; they include rucklidgeite ($[Bi,Pb]_3Te_4$), tsumoite (BiTe), and hedleyite (Bi_7Te_3; Cook and Ciobanu, 2004). The Sacarimb deposit in the Metaliferi Mountains is estimated to have cumulatively produced 30 t Au, 85 t Ag, and 60 t Te from ores containing nagyagite and sylvanite that averaged 20 g/t Te and 10 g/t Au. The ores were mainly present as nagyagite ($Pb_5Au[Te,Sb]_4S_{5-8}$) and sylvanite (($[Ag,Au]Te_2$) within the Neogene calc-alkaline volcanic rocks (Popescu and Neacsu, 2004). This deposit is the type locality for nagyagite, krennerite ($AuTe_2$), petzite (Ag_3AuTe_2), stutzite (Ag_7Te_4), muthmannite ($AuAgTe_2$), and museumite($Pb_5AuSbTe_2S_{12}$). The tellurides were deposited at temperatures between 200° and 300°C from very dilute hydrothermal solutions (Cook et al., 2005). Telluride minerals also occur in the Baguio district, Philippines (Cooke and Bloom, 1990; Cooke et al., 1996), in the Thames district, New Zealand (Christie et al., 2007), and at Bereznyakovskoe in the Urals (Lehmann et al., 1999). Saunders and Brueske (2012) suggested a zonation of low-sulfidation deposits may characterize the western United States, from selenium- to tellurium-rich from west to east (Fig. 9), argued as reflecting subduction-related changes in mantle fertilization. The Jefferson Au-Ag-Te-In project, a few kilometers east of the giant Round Mountain epithermal deposit in Nevada, is being evaluated as a potential tellurium resource (http://www.mexivada.com/s/Home.asp).

A small, underground operation along the eastern side of the Mojave-Sonora Mega shear zone in northern Sonora, Mexico, the Bambolla deposit, produced small amounts of gold and silver from quartz-hematite-pyrite veins in volcanic rocks (E.O. Monteagudo, unpub. report, Mexivada Mining Corp., 2009). The mineralogy at Bambolla includes a variety of telluride minerals and native tellurium, and the deposit is being reevaluated for its tellurium potential by First Solar of Denver. It appears to be a shallow, perhaps hot-springs level, low-intermediate sulfidation deposit with microcrystalline quartz textures and zoning to base metals with depth (William Atkinson, writ. commun., 2014).

Notable high-intermediate sulfidation deposits containing high concentrations of tellurium include El Indio, Chile (Jannas et al., 1999), Pueblo Viejo, Dominican Republic (Kesler et al., 1981, 2003; Muntean et al., 1990), Mulatos, Mexico

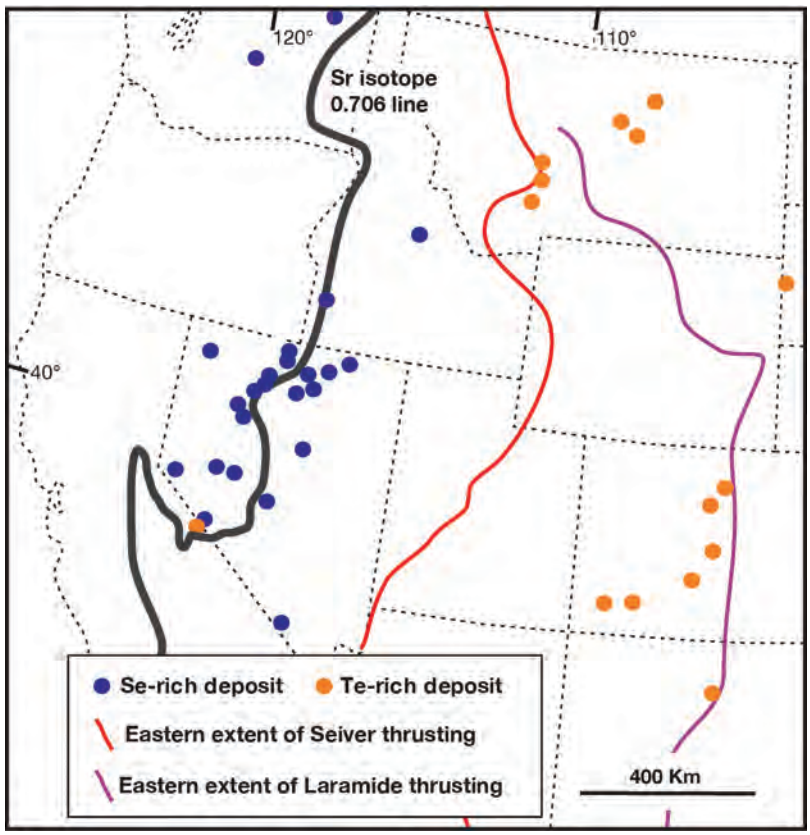

Fig. 9. Map showing distribution of Laramide and younger tellurium vs. selenium-rich epithermal ore deposits in the western United States. Modified from Saunders and Brueseke (2012).

(Staude, 2001), Enasen, Sweden (Hallberg, 1994) and Goldfield, United States (Vikre, 1989, although some workers do not recognize such—see Fig. 9). Calaverite, krennerite, petzite, sylvanite, and hessite are the most common telluride minerals, and tellurium can substitute for arsenic and antimony in tennantite in sufficient abundance to form goldfieldite, the tellurian tennantite. In all well-studied deposits, precious metal tellurides have been documented, although they are generally less economically important than native gold and electrum. The tellurium content of ores averages 101.6 ppm at Kochbulak, Uzbekistan (Plotinskaya et al., 2006), and enargite grains from Lepanto, Philippines, contain many hundreds of ppm Te(Deyell and Hedenquist, 2011). Secondary tellurite minerals, including emmonsite ($Fe_2[TeO_3]_3\ 2[H_2O]$), blakeite ($Fe_2[TeO_3]_3$), and rodalquilarite ($Fe_2[TeO_2OH]_3TeO_3Cl$), occur at Rodalquilar, Spain (Arribas et al., 1995).

Thallium: There are rare examples of epithermal deposits containing highly anomalous thallium. At the Alsar (or Allchar) epithermal deposit in the Kozuf mining district in southern Macedonia, ores are characterized by an Au-As-Sb-Tl signature (Percival and Radtke, 1994; Boev and Jelenkovic, 2012). Significant thallium was recovered during production from 1881 to 1913, and the deposit still contains an estimated 500 t Tl. In addition to pyrite, stibnite, orpiment, and realgar, thallium-bearing sulfosalts in the deposit include lorandite ($TiAsS_2$), jankovicite ($Tl_5Sb9[As,Sb]_4S_{22}$), fangite (Tl_3AsS_4), and bernardire ($(Ti[Sb,As]_5S_5]$ (Cvetkovic et al., 1995).The deposit is associated with a large Pliocene volcanic complex ranging in composition from alkali basalt through rhyolite, with disseminated ores hosted by Triassic carbonates, Tertiary tuffs and dolomite, and Pliocene tuff. The classification of the Alsar deposit remains problematic. Although its clear association with the Pliocene volcanism is consistent with typical epithermal deposits, the disseminated nature of the ore has led to some workers defining this as a Carlin-like deposit (e.g., Radtke and Dickinson, 1984).

Xiangquan is a unique Tl-only deposit, located along the northeastern margin of the South China block, and described by Zhou et al. (2005) and Fan et al. (2014). The present resource (Fan et al., 2014) is 250 t Tl at an average grade of 0.3% Tl. The faulted and folded strata-bound ores are hosted in Early Ordovician limestones, mudstones, and marls. The thallium is mainly in massive to disseminated pyrite, but also occurs as fine grains of lafossaite (Tl[Cl,Br]) and lorandite, all associated with quartz, fluorite, barite, and calcite. Zhou et al. (2005) first suggested that Mesozoic igneous activity reworked the thallium concentrated in early Paleozoic seafloor pyrite into much younger Tl-rich epithermal veins. However, Fan et al. (2014) argue that the epithermal overprint was the cause of the deposition of the calcite, fluorite, and barite, but the thallium resource was entirely Paleozoic in age and not concentrated in the Mesozoic epithermal event.

In other deposits that are unequivocally epithermal, thallium may be enriched in ores, although it has never been recovered from these ores. At Cisimuet, one of the low-intermediate sulfidation deposits of West Java, Indonesia, Marcoux and Milesi (1994) reported 620 to 1,730 ppm Tl in auriferous pyrite, although overall thallium concentrations are probably no more than a few parts per million. Gemmel (2007) indicated that the thallium in altered rocks surrounding low-sulfidation ores at the Gosowong deposit in eastern Indonesia can be preferentially concentrated in adularia, rather than in sulfide minerals. Gray and Coolbaugh (1994) noted high thallium concentrations in argillically altered rocks of the Summitville high-sulfidation epithermal deposit. Precious metal-rich precipitates in New Zealand hot springs contain tens to thousands of ppm Tl (Weissberg, 1969; Hedenquist and Henley, 1985; Krupp and Seward, 1987; Reyes et al., 2002), indicating that thallium mobilization in the epithermal environment occurs in places.

Conclusions

In the modern context, indium and tellurium are the only critical elements known to occur in economic concentrations large enough to make them commercially valuable. The diverse range of elements found in epithermal deposits, however, suggests that epithermal deposits potentially could be discovered with possibly recoverable amounts of other critical elements.

Orogenic Gold Deposits

Orogenic gold deposits are most readily defined as gold deposits in deformed metamorphic rocks (e.g., Groves et al., 1998; Goldfarb et al., 2005). As their name implies, this type of hydrothermal gold deposit represents regional fluid flow that is inherent to orogeny. These gold-bearing orebodies typically form in host rocks 20 to 200 m.y. after their deposition and relatively late in their deformational history. These gold deposits are hosted by a variety of mafic to felsic igneous and sedimentary rocks in Precambrian cratons and late Neoproterozoic-Phanerozoic fold belts. A diversity of structures, from shear zones to fold hinges, control the ores, which possess highly variable gold grades. Syngold mineralization intrusions generally occur within a few kilometers of the deposits, but there are notable exceptions Lower greenschist to lower amphibolite metamorphic conditions represent peak P-T conditions in the country rocks for almost all deposits. Geochemical signatures of many ores are Ag-Au-As-Bi-Sb-Te-W-B ± Hg (Figs. 10–12).

The genetic model most widely accepted for the orogenic gold deposits is that they are a product of metamorphic devolatilization (see summary in Phillips and Powell, 2010). During greenschist to amphibolite facies metamorphism of most sedimentary and volcanic rock sequences, approximately 3 to

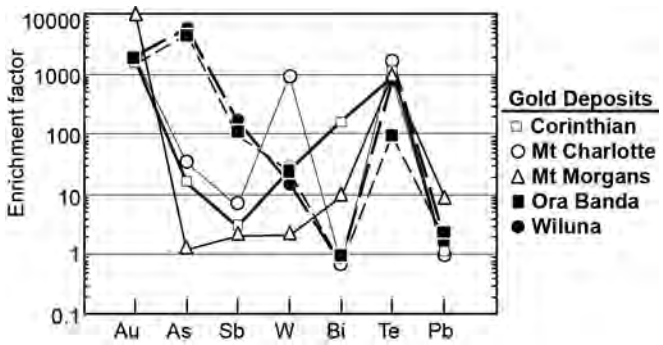

Fig. 10. Trace element enrichment factors for orogenic gold deposits, Yilgarn craton, Western Australia. Note that As, Sb, W, and Te concentrations are significantly enriched over crustal abundance levels for most deposits; Bi and W are locally enriched in some ores. After Eilu and Groves (2001).

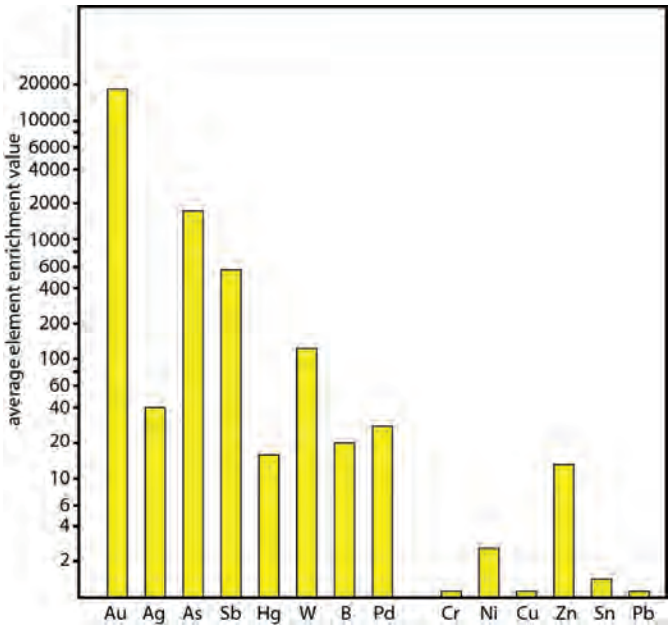

Fig. 11. Element enrichments relative to background concentrations for altered basalt at the orogenic gold deposit at the Dickenson mine, Red Lake, Ontario, Canada. Elements enrichments of Au, As, Sb, and W are notably greater than those of the base metals. After Kerrich and Fryer (1981).

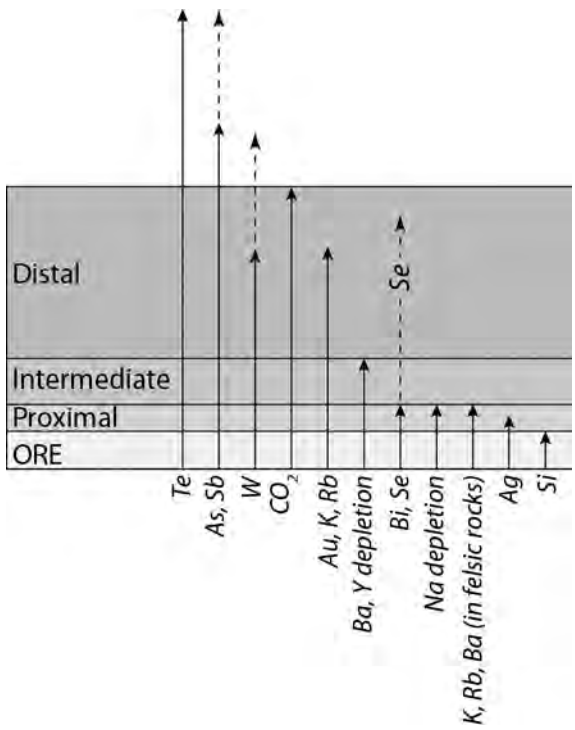

Fig. 12. Typical alteration halos, showing relative distributions of added and depleted elements surrounding greenschist facies-hosted orogenic gold deposits, Yilgarn craton, Western Australia. Note the broad extent of enrichment zones of As, Sb, Te, and W. Solid lines are for typical relative relationships, whereas dashed extensions are for some less common examples. In most examples, proximal assemblages are shown within about 10 m of the ore, intermediate at about 10 to 50 m, and distal beyond 50 and locally as far as 200 m from ore. After Eilu and Groves (2001).

5 vol % of the rock is converted to a fluid phase. The prograde metamorphic fluid moves upward along these major structural channelways during episodic seismic events (e.g., Sibson et al., 1988). Gold and associated metals are transported in the fluid phase to shallower deposition sites in rocks already on a retrograde metamorphic path (e.g., Stuwe, 1998), often located in greenschist facies brittle-ductile transition zone. The gold is sourced and released from elevated concentrations in preexisting pyrite, which is syngenetic to diagenetic in origin in sedimentary rocks (Goldfarb et al., 1997), during the prograde desulfidation to form pyrrhotite. In greenstone belts, the pyrite might be present in altered areas of metabasic rocks or within minor, but widely distributed chert beds. Goldfarb et al. (2005) summarized supporting evidence for such a metamorphic model. which includes (1) common H_2O-CO_2-CH_4-N_2-H_2S, low-salinity ore fluids formed during metamorphic devolatilization, (2) isotopically heavy $\delta^{18}O$ and δD values for hydrothermal minerals, (3) highly variable $\delta^{34}S$ values of pyrite and other ore-related sulfide minerals, which reflect variable host terranes undergoing a regional metamorphism, (4) a general lack of ores in high-grade (upper amphibolite and granulite) metamorphic rocks, and (5) a gradual decrease in ore-related elements at increasing metamorphic grades (e.g., Pitcairn et al., 2006) in a Barrovian metamorphic sequence (Fig. 13).

Mineralogy and paragenesis

The quartz-carbonate veins and altered wall rocks that define orogenic gold ores typically contain 2 to 5% ore and related minerals (Goldfarb et al., 2005). Pyrite and arsenopyrite typically are the dominant phases that were deposited with the gold. In most deposits, much of the gold appears paragenetically late in fractures cutting pyrite and arsenopyrite grains, but this reflects the ductile behavior of gold relative to the sulfides during tens of millions of years of deformation and uplift. The abundance of arsenopyrite is greater than pyrite in deposits hosted by relatively reduced metasedimentary rocks, although at relatively high temperatures (approx >350°C) pyrrhotite is generally dominant in clastic metasedimentary rocks.

Most orogenic gold deposits form at depths of between 3 and 20 km (Groves et al., 1998). However, the ore-forming fluids must be able to reach shallower crustal levels in some circumstances. In such scenarios, extending upward at shallower crustal levels, stibnite-gold, stibnite, stibnite-cinnabar, and cinnabar are deposited as metals in cooler and more brittle environments; also realgar and orpiment may become more abundant than arsenopyrite as the main arsenic-bearing mineral phases. This is consistent with the continuum model of Groves (1993), which indicates differences in structural styles and ore/alteration assemblages with variations in P-T. The telescoping of cinnabar, stibnite, and gold, common in many magmatic hydrothermal systems, is generally absent in these orogenic gold and related stibnite and cinnabar deposits because of the lower (approx 25°–30°C/km) geothermal gradient associated with the regional metamorphism relative to that surrounding a locally emplaced intrusion.

Orogenic gold deposits may contain high abundances of tellurium-bearing minerals. Similar to the epithermal deposits, these high concentrations of tellurium have thus far not been recovered, although gold-bearing tellurides can make

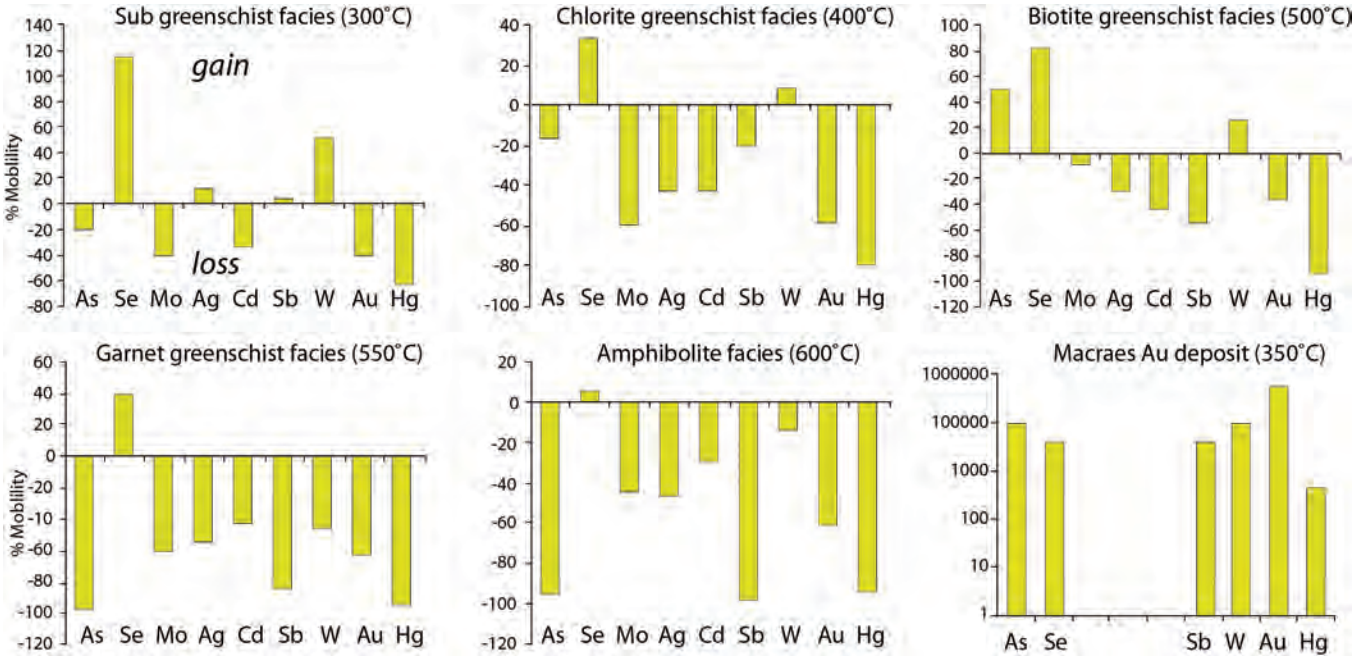

Fig. 13. Relative mass loss or gain of various elements from different metamorphic grades of schist in the Otago orogenic gold region of South Island, New Zealand. Note that during prograde metamorphism between 300° and 600°C, Ag, As, Au, Cd, Hg, Mo, Sb, Se, and W are lost from schist to the hydrothermal fluid system, and added to the Macraes and other gold deposits. From Pitcairn et al. (2006).

up much of the recovered gold ore. In many districts, specific deposits hosted by local intrusions, rather than by the widespread metavolcanic or metasedimentary country rocks, tend to contain an abundance of telluride minerals (e.g., Kirkland Lake, Kensington), suggesting the relatively oxidizing environment provided by the felsic to intermediate igneous host rocks provides a major control on precipitating telluride minerals. Abundant tellurides and the presence of hydrothermal hematite in other deposits, such as the Gold Mile, Western Australia, and Commoner deposit, Zimbabwe, also suggests some degree of oxidation of the ore fluids. A variety of telluride minerals are common in orogenic gold deposits, including mainly Au-, Ag-, Bi-, Pb- and Pd-bearing phases (e.g., Goldfarb et al., in press). The gold-bearing tellurides have been shown to reflect the main ore stages (e.g., Yellowknife: Boyle, 1979; Kensington: Casey, 2000) or a hydrothermal pulse subsequent to the main gold-depositing event (e.g., Ashanti: Bowell et al., 1990; Golden Mile: Mueller and Muhling, 2013).

Scheelite is a common mineral in many orogenic gold deposits, both in Precambrian greenstone belts and in Phanerozoic metasedimentary rock belts. In most paragenetic descriptions, the scheelite is defined as an early-stage hydrothermal mineral. Similar to gold, tungsten is soluble over a wide range of hydrothermal conditions (Foster, 1977) and in low- to moderate-salinity fluids typical of orogenic gold ores, polytungstate ions may be important for tungsten transport (e.g., Wood and Samson, 2000).

Hydrothermal fluid geochemistry

Most orogenic gold deposits form between about 220° to 375°C and over a variety of depths ranging between about 3 to 5 and 15 to 20 km. Ore-forming fluids are rich in CO_2, typically containing at least 5 mol % CO_2; they contain significant amounts of CH_4, N_2, and H_2S; and they have salinities of about 4 to 9 wt % NaCl equiv. Gold in orogenic gold deposits is widely recognized as being carried in metamorphic ore-forming fluids as bisulfide complexes. In addition, As, Hg, and Sb are also strongly complexed with sulfur and thus are commonly anomalous in orogenic deposits. Although also commonly present at anomalous levels, the transport mechanisms for Bi, Te, and W anomalies in these deposits are still highly debated. Extreme drops in pressure and wall-rock sulfidation are the two main causes of metal deposition in orogenic gold deposits. As stated previously, there is a general zoning upward from the gold-rich ores at deep levels to more antimony-rich ores at shallower levels and mercury-rich ores in the near-surface environment (Fig. 14).

Historic and present-day critical and near-critical element resources

Arsenic: Arsenic is the most abundant trace metal in many orogenic gold deposits, particularly those in the mesozonal and hypozonal environments that contain abundant arsenopyrite. Historically, minor amounts of arsenic were recovered from some orogenic gold deposits. During mining of the Archean Giant deposit in Yellowknife, Slave province, Canada, 237,000 t of arsenic trioxide dust was recovered, but rather than being used for industrial purposes, it was removed during the roasting of ores and stored to prevent environmental contamination (Aboriginal Affairs and Northern Development Canada, 2010). In the early 1990s, minor amounts of arsenic were recovered as a by-product from mining of the Precambrian Ashanti and Bogosu orogenic gold deposits in

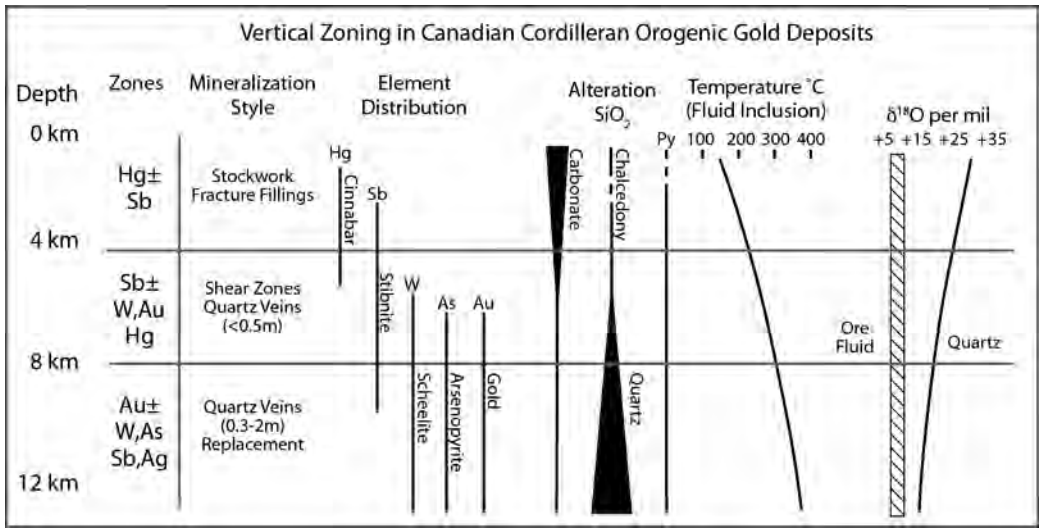

Fig.14. Summary of vertical zoning in orogenic gold and related deposits in the Canadian Cordillera, showing changes in mineralization style, mineralogy/geochemistry, and oxygen isotope composition of metalliferous quartz with changing depth and fluid temperature. Significant concentrations of As and W characterize many mesozonal and hypozonal orogenic gold deposits, whereas along many deep crustal faults in Cordilleran orogens, the vein systems are Sb rich at shallower levels and Hg rich at shallowest levels. From Nesbitt et al. (1989).

Ghana (Edelstein, 1995). The world's largest producer of arsenic in the early 1990s was the late Paleozoic Salisgne orogenic gold deposit in the French Massif Central (Le Guen et al., 1992), which has yielded a total of almost 400,000 t As (Demange et al., 2006).

Because of the environmental concerns related to arsenic and the limited demand for it, it is currently rare for present-day orogenic gold deposits to be considered as potential resources of by-product arsenic in most countries; in fact, Canada and the United States produce no arsenic. Much of the world's arsenic demand, exclusive of what is produced from China, is met as the by-product arsenic trioxide that is recovered during production from large-tonnage copper, lead, and zinc ores, particularly those porphyry ores mined in the Andes and Philippines. However, more than 50% of the world's arsenic in 2012 was recovered from the roasting of gold-bearing sulfide minerals in China (http://mcgroup.co.uk/researches/arsenic). Specific source deposits are not known, but it is likely many of these are the Phanerozoic orogenic gold deposits that are widespread in China. Much of China's arsenic production is suggested to come from realgar and orpiment in gold deposits in Sichuan province (Edelstein, 2013), which are most likely either Carlin-like ores (e.g., Hofstra and Christensen, 2002) and/or epizonal orogenic ores (e.g., Goldfarb et al., 2014).

Antimony: Antimony has historically been recovered from relatively shallow-level orogenic gold deposits. In many cases, small historic antimony mines are now the sites of much larger orogenic gold mining activities. For example, on the eastern side of the South Island of New Zealand, antimony mining from Mesozoic massive stibnite-bearing veins occurred in the Otago and Marlborough provinces from the late 1800s until the middle 1900s (Thompson et al., 1995). A small antimony mining operation at Macres, East Otago, is now the site of a major open-pit gold mine with approx 150 t Au of past production and reserves. On the western side of the South Island, the Paleozoic gold-bearing veins at Reefton were mined historically underground and are now being mined in a small open pit. Thompson et al. (1995) indicated that these 40 t Au ores also average 0.4% Sb, which is a potential by-product.

Similar to Macraes, the 1,200 t Au resource at the Late Cretaceous Donlin Creek deposit, southwestern Alaska (Goldfarb et al., 2004), surrounds a small historic antimony prospect at Snow Gulch. The Late Cretaceous Bralorne-Bridge River district in southwestern British Columbia hosts both western Canada's largest historic orogenic lode gold deposit and widespread auriferous stibnite prospects (Hart and Goldfarb, 2007). In the Fairbanks district of east-central Alaska, mid-Cretaceous orogenic gold deposits and the historic Scrafford antimony mine are associated with similar local NE-trending faults. In southwestern Kyrgyzstan, widespread antimony deposits previously mined prior to the 1990s are located along the southern side of the Fergana Valley (United Nations, 1998), between the giant, late Paleozoic orogenic gold deposits at Kumtor to the east and Zarmitan to the west. Russia's largest gold resource (700 t Au), the late Neoproterozoic Olympiada orogenic gold deposits in the Yenisei ridge province along the southwestern margin of the Siberia craton, was originally evaluated as an antimony resource (Yakubchuk et al., 2005). The Early Cretaceous Sarylakh and Sentachan orogenic gold deposits of the Yana-Kolyma fold belt in the Russian Far East contain 20 to 30% antimony grades and are estimated to contain 5% of the global antimony reserve. The deposits contain 180,000 and 110,000 t Sb, respectively (Bortnikov et al., 2010).

Most of the antimony in the United States, as well as tungsten, used during World War II, and shortly thereafter, was recovered from the Stibnite-Yellow Pine gold district in Idaho, where stibnite forms massive replacement zones in

carbonate strata (Cookro et al., 1988) and some features of the ores resemble structurally controlled orogenic gold deposits. The Golden Meadows project at the site of the historic Yellow Pine deposit has indicated resources of 78.2 Mt of 1.68 g/t Au and 0.06% Sb (Midas Gold Corp., 2013), stated in a U.S. Geological Survey report as defining the present world's largest antimony resource (Sutphin et al., in press). Beaver Brook, in the Paleozoic orogenic gold belt of central Newfoundland, is presently the only antimony producer in North America. It has resources estimated at 100,000 t Sb (Schwarz-Schampera, 2014).

China is responsible for about 90% of the global annual production of about 15,000 t Sb (Schwarz-Schampera, 2014). Much of this continues to come from the world's largest historic antimony producer, now nearing the end of its more than 500-year mine life, the Xikuangshan deposit in the poorly understood group of Au, W, and Sb ores in the Jiangnan fold belt in southeastern China (Goldfarb et al., 2014). Many of the middle Paleozoic and/or late Mesozoic gold ores have characteristics typical of orogenic gold deposits, but the Xikuangshan deposit type is uncertain. It has many features resembling the Carlin-like ores described above, in particular abundant jasperoid formation and a replacement texture for the stibnite in a local carbonate unit in a Devonian argillite sequence; however, the massive stibnite ore lacks anomalous gold (A. Hofstra, unpub. data). Therefore it is uncertain as to whether this should be classified as a Carlin-like replacement deposit or as an epizonal Sb deposit formed at a slightly shallower level than the orogenic gold lodes in the Jiangnan belt.

These epizonal orogenic antimony-gold deposits may also occur in Precambrian cratons. The best example is defined by the 50-km-long Antimony Line in the Murchinson greenstone belt within the Kaapvaal craton, South Africa (Vearncombe et al., 1988). Production from veins and veinlets since 1932 includes more than 550,000 t Sb in concentrate, with remaining resources and reserves of about 65,000 t Sb in material averaging 1.87% Sb (Schwarz-Schampera, 2014).

In summary, many epizonal orogenic gold districts also contain widespread antimony prospects and deposits; some of the deposits, where the two metals occur within the same vein systems, may be defined as Au-Sb deposits. Many of these deposits were generally small to moderate producers during war times in the 20th century. They now reflect potential easily minable, high-grade, low-tonnage antimony resources, as well as some low-grade, high-tonnage deposits (i.e., Yellow Pine), which could be developed given increased future demand. The relatively most abundant antimony resources appear to be associated with districts containing carbonate units, where large stibnite replacement bodies develop.

Tungsten: Historically, tungsten has also been recovered during the mining of orogenic gold deposits, typically from scheelite. Many Phanerozoic orogenic gold provinces are characterized by an Au-Sb-W signature, such as Yellow Pine, Hillgrove (NSW, Australia), Otago, and the Jiangnan fold belt. In addition, Archean gold lodes contain abundant scheelite in world-class provinces such as the Yilgarn craton (e.g., Southern Cross, Coolgardie, Norseman) and Superior province (e.g., Timmins). All these deposits produced small amounts of tungsten in the early 1890s (Maitland, 1919; Rastall and Wilcockson, 1920). The world's largest orogenic gold deposit, Muruntau, shows a strong correlation between gold and tungsten enrichments (Uspenskiy and Aleshin, 1993). Felsic quartz-bearing rocks typically have greatest scheelite concentrations in Precambrian greenstone belts (e.g., Hodgson and MacGeehan, 1982), but this relationship does not apply to younger sedimentary rock terranes. Throughout the latter half of the 20th century to the present, large tonnage tungsten resources in deposit types such as skarns and magmatic veins have met the world demand, and therefore, orogenic gold deposits rarely are considered as potential sources of tungsten.

Tellurium: The world's largest Archean orogenic gold deposit, the Golden Mile, hosted in predominantly mafic metavolcanic rocks of the Yilgarn craton of Western Australia, contains 1,500 t Au. Although the majority of the ore is hosted in arsenic-rich pyrite, about 20% of the resource is hosted in late-stage telluride minerals (Lindgren, 1906; Mueller and Muhling, 2013). Many of the higher grade gold zones contain hundreds of ppm Te. Recognized minerals that concentrate mercury, silver, and /or gold, as well as the tellurium, include coloradoite (HgTe), calverite, petzite, and hessite, with a total of 19 distinct telluride phases identified. Mueller and Muhling (2013) described zoning of tellurides from and inner zone of calaverite, to hessite, and then to an outer, very late coloradoite zone. Shackleton et al. (2003) noted the tellurides at the Golden Mile occur as fine-grained composite aggregates, massive segregations, composite grains with native gold, inclusions in and intergrowths with pyrite and tetrahedrite-group minerals, and inclusions in carbonates, quartz, and tourmaline. Eilu et al. (1998) indicated that tellurium anomalies greater than 10 ppm in mafic volcanic rocks extend for more than 100 m beyond ore zones in various orogenic gold deposits in Western Australia and suggested tellurium as an important geochemical pathfinder for orogenic gold deposits in the Yilgarn craton.

Similarly, many of the world-class Archean gold deposits of the Abitibi and Yellowknife greenstone belts in Canada may have anomalous concentrations of tellurium, typically in gold-bearing tellurides. Telluride minerals are common in deposits in the Kirkland Lake and Red Lake districts of Ontario. As in other deposits, the tellurides, as well as much of the gold, are typically interpreted to have formed paragentically late (e.g., Thomson, 1928). Native gold in the syenite-hosted gold-bearing veins at the Kirkland Lake deposit occurs with altaite (PbTe), calaverite, petzite, and coloradoite, as well as sericite. Highest grade ore samples of about 200 to 400 ppm Au also contain about 200 to 500 ppm Mo and 300 to 700 ppm Te, with the atypical Au-Te-Mo signature interpreted as suggesting an alkali magmatic ore fluid source that is rather unique in the district (Ispolatov et al., 2008). In contrast, in the Yellowknife mining district, Boyle (1979) reported the tellurium in the ore was contained in the main sulfide stage, with as much as 1,000 ppm Te in galena, 100 ppm Te in stibnite, and 100 ppm Te in lead-bearing sulfosalts.

A strong gold-tellurium association is also recognized at Ashanti in Ghana, the world's largest Paleoproterozoic orogenic gold deposit. Eleven telluride minerals are known at Ashanti within a telluride-quartz-hematite assemblage deposited with minor amounts of gold, after an earlier event that deposited the bulk of the gold (Bowell et al., 1990). The

tellurides are zoned from an inner coloradoite-rich assemblage in the veins to an assemblage dominated by altaite along the vein walls and in the country rocks. The telluride event was shown to reflect a cooling of ore fluids and associated oxidation, and hypogene hematite and goethite were deposited with the telluride minerals.

The Phanerozoic deposits in accreted metasedimentary rock belts are also commonly characterized by an abundance of gold- and silver-rich telluride minerals. Calaverite, petzite, sylvanite, altaite, and melonite ($NiTe_2$) are associated with the main gold vein, stockwork, and breccias events in the early Paleozoic clastic rocks at the Kumtor deposit, Kyrgyzstan (Ivanov et al., 2000). The Cretaceous California Mother Lode deposits have been long recognized for their common silver-, gold-, nickel-, and lead-bearing tellurides that are associated with native gold (Turner, 1894). As noted above, intrusions emplaced into these terranes, which are often structurally favorable hosts for the vein deposits, tend to have greater abundances of tellurides. The Eocene Kensington gold deposit, Juneau gold belt, southeastern Alaska, is dominated by veins within an intermediate stock with native gold, petzite, and calaverite, with lesser volynskite ($AgBiTe_2$), sylvanite, tellurobismuthite (Bi_2Te_3), alatite, and hessite (Casey, 2000). Much of the gold endowment is hosted in the two main telluride minerals. Similarly, the tonalite-hosted Willow Creek district, south-central Alaska, contains abundant tellurides in the main ore assemblage, with coloradoite dominant, and lesser nagyagite and altaite (Burleigh, 1987). Interestingly, the main gold ores of the Grass Valley district, California, are hosted by N-striking veins cutting granodiorite, but these lack telluride mineralization; only auriferous east-west veins in adjacent mafic and ultramafic country rocks contain silver- and lead-bearing telluride minerals (Johnston, 1940).

Many Russian and central Asian Phanerozoic gold deposits report significant platinum and palladium grades. Whereas some of this may reflect high natural backgrounds of PGM in black shale host rocks, some PGM are clearly associated with numerous tellurium-bearing minerals. At Sukhoi Log, Baikal region, eastern Russia, palladium-bearing tellurides are present, as well as many silver-, gold-, bismuth-, and lead-rich tellurides (Distler and Yudovskaya, 2005).

Conclusions

Historically, many orogenic gold deposits of all ages were mined for tungsten, antimony, and, rarely arsenic contents. A very few deposits in the future could continue to provide economic amounts of antimony and tungsten when the need is present. An abundance of telluride-bearing minerals in many orogenic gold deposits could be a potentially important future source for tellurium.

Discussion

Elements that are most consistently recognized as anomalous in one or more of the gold-only deposit types are mainly Ag, As, Au, Bi, Hg, In, Sb, Se, Te, Tl, and W. This reflects the geochemistry of the hydrothermal systems that form the auriferous ores. As a result, the fluid geochemistry is the ultimate control on which critical to near-critical elements might be recovered, if future demands require new sources for these elements.

Hydrothermal geochemistry of gold systems and associated critical elements

Above 400°C and under acidic conditions gold is mostly transported as $AuCl_2^-$, but at the relatively lower temperatures that characterize the orogenic, Carlin-type, and epithermal gold deposits, $Au(HS)_2^-$ is the dominant gold species in acidic, sulfur-bearing fluids (e.g., Gammons and Williams-Jones, 1997). Other metals, such as As, Hg, and Sb, which are consistently present in elevated concentrations within these gold deposits, also form sulfur complexes in aqueous and aqueous-carbonic solutions, and are deposited along with gold during desulfidation reactions. Thermodynamic studies, however, indicate that uncharged hydroxide species, such as $As(OH)_3$ and $Sb(OH)_3$, as well as uncharged Hg^o, are dominant species in hydrothermal fluids (e.g., Varekamp and Buseck, 1984; Ballantyne and Moore, 1988; Krupp, 1988). Nevertheless, in deposits in which ore fluids have relatively high H_2S concentrations, such as recognized from fluid inclusion studies of many gold deposits, these metals are likely to be transported as sulfur species (e.g., Krupp, 1988; Zotov et al., 2003).

The arsenic-bearing mineral phase that precipitates with gold varies with temperature. As a consequence, loellingite precipitates at high temperatures above about 350°C in orogenic gold deposits, arsenian pyrite and arsenopyrite are deposited during the gold event in many gold deposits, and realgar, orpiment, and native arsenic are commonly precipitated as hydrothermal systems cool below about 200°C during post-gold ore events.

Antimony and mercury are typically undersaturated in hydrothermal fluids to temperatures lower than most of the gold (Saunders et al., 2014). In many epithermal and Carlin-type deposits, these elements may be concentrated in gold ores as temperatures decrease. In contrast, the relatively low geothermal gradient deposits along fault zones that host orogenic gold deposits results in less telescoping of these metals. Thus, epizonal Hg, Sb, and Au lode deposits are commonly separated into areas that expose differing crustal levels; shallowest mercury deposits may spatially overlap with deeper antimony deposits, and deeper antimony deposits may continue downward into epizonal orogenic gold deposits. Therefore, these orogenic gold deposits may be enriched in antimony, but they are unlikely to contain significant amounts of mercury.

Silver is typically recovered from many epithermal deposits in which Ag/Au ratios range from <10 to >1,000 (Simmons et al., 2005), in contrast to the Carlin and orogenic gold deposit types where silver may be anomalous, but is seldom recovered. The anomalous silver in all these deposits also reflects the fact that the highly stable Ag bisulfide complex is an important species in ore fluids (e.g., Seward and Barnes, 1997; Stefansson and Seward, 2003) likely controlled by contributions from deep magmatic sources. Important selenium concentrations in some epithermal silver-gold deposits reflect selenide mineral deposition along with minor silver sulfosalt precipitation under such oxidizing conditions (e.g., Simon et al., 1997).

The solubility and transport of many of the other elements in hydrothermal fluids is much less understood. Tungsten, an important by-product in many orogenic gold deposits, is commonly inferred to be transported as a simple tungstate species (Pokrovski et al., 2013), such as H_2WO_4. Although the

CO_2-rich character of the ore fluids that form orogenic gold deposits makes the possibility of some type of carbonate complexing appealing. Wood and Samson (2000) indicated that such complexing is highly unlikely. They suggest that tungsten solubility is mostly controlled by fluid chloride concentration and pH of the fluid, the latter which could explain the common gold-tungsten association in orogenic gold deposits. Large increases in pH values could be related to wall-rock reactions, but the lack of significant scheelite in the Carlin-type ores and the fact that the orogenic gold fluids are initially near-neutral pH make such increases unlikely. More likely, the increase in pH that accompanies fluid immiscibility during large pressure fluctuations would cause precipitation of scheelite along with the gold.

Tellurium and bismuth are notably elevated in some epithermal and orogenic gold deposits. The relative low solubility of tellurium in hydrothermal fluids has suggested to many workers that it may be transported preferentially in the vapor phase (e.g., Cooke and McPhail, 2001). However, such a vapor phase is not necessary in many gold deposits that show a lack of evidence of fluid unmixing and the presence of a vapor phase. Perhaps gold-tellurium complexes, as suggested by Jensen and Barton (2000) and Brugger et al. (2012), are common in many hydrothermal systems. Available data suggest any drastic change in fluid conditions, including decrease in temperature, wall-rock sulfidation, phase separation, pH shifts, and/or redox change, can destabilize tellurium-bearing complexes (e.g., Cooke and McPhail, 2001; Ciobanu et al., 2006; Maslennikov et al., 2013). The hydrothermal speciation of bismuth is very poorly known (Wood et al., 1987), but its enrichment in high-intermediate sulfidation relative to low-intermediate sulfidation epithermal ores suggests that in the few cases where bismuth is recovered, it may be exceptionally concentrated during magmatic-hydrothermal processes. In orogenic gold deposits, the common existence of gold-bearing bismuth telluride minerals suggests a common precipitation mechanism for the Bi, Te, and some Au.

Thallium typically occurs as Tl^+ and $TlHS^o$ in hydrothermal solutions (Xiong, 2007). As noted above, it can behave both as a lithophile element, substituting for K^+ in feldspars and illite, and as a chalcophile element deposited in sulfide minerals. Oxidation, increase in fluid pH, or decrease in temperature are suggested processes of destabilization of dissolved Tl species (Xiong, 2007). Its relative abundance in epithermal deposits, as well as its association with antimony and arsenic in geothermal systems (Fig. 7), suggests that steep temperature gradients and oxidation processes in the epithermal environment precipitate thallium. This commonly will be associated with boiling events. Hydrothermal fluids in Carlin-type ores tend to be neutralized due to interaction with carbonate-rich host rocks, which destabilizes thallium complexes because of increasing fluid pH. Because these processes are not common in orogenic gold hydrothermal systems, thallium is rarely anomalous in these orebodies.

Where are these critical elements enriched in lode gold systems produced today and which elements are most likely to be future resources in these deposits?

The deposits discussed in this paper (epithermal, Carlin-type, and orogenic gold) are presently being mined generally only for their gold content, although many epithermal deposits are also important silver producers. The various gold deposit types are typically not primary sources for other metals, including many of the critical and near-critical elements that nevertheless may be enriched in some epithermal, Carlin-type, and/or orogenic gold deposits. Much of the global demand for elements that are commonly enriched in the gold deposits, such as As, Bi, In, Se, Te, and Tl, is met adequately from by-product recovery of the refining of ores from large tonnage, base metal-rich deposits such as porphyry Cu and Mo and volcanogenic massive sulfide deposits. One concern for many nations remains the domination of the world market for many commodities by China, which would include elements such as As, Bi, Hg, In, Sb, and W (e.g., Gunn, 2014). Such control of world supply of a commodity by a single country could lead to future need for some countries to develop high-grade, but relatively low-tonnage resources of some of these elements that are enriched in gold ores.

Orogenic gold deposits potentially could be a source of antimony. Arsenic and tungsten, although also enriched in orogenic gold ores, are available from other sources and are unlikely to approach critical status in future years. Epithermal deposits are potential future sources of tellurium and indium. The Neogene Tethyan arc region of southern Europe includes large amounts of past production of tellurium from low-intermediate sulfidation ores in Romania and anomalous indium in other low-intermediate sulfidation deposits. High-intermediate sulfidation ores in young arcs in the Andes and Philippines are also sites of tellurium enrichment. With the growing global importance of solar energy, the abundant tellurium in the epithermal ores, as well as in many orogenic gold deposits, could have future economic importance. Thallium potentially could also be produced in the future from some Carlin-like gold deposits, such as the Alsar deposit in southern Macedonia, although the classification of this deposit is uncertain.

Acknowledgments

Reviews by Karen Kelley and David John are greatly appreciated, as they have improved the content of this paper. The authors also thank the editors, Philip Verplanck and Murray Hitzman for the invitation to contribute.

REFERENCES

Aboriginal Affairs and Northern Development Canada, 2010, How much is 237,000 tonnes of arsenic trioxide dust?: Available from: http://www.aadnc-aandc.gc.ca/eng/1100100027425/1100100027429.

Ahlfeld, F., 1941, Zoning in the Bolivian tin belt: Economic Geology, v. 36, p. 569–588.

Alderton, D.H.M., and Fallick, A.E., 2000, The nature and genesis of gold-silver-tellurium mineralization in the Metaliferi Mountains of western Romania: Economic Geology, v. 95, p. 495–516.

Arribas, A., Jr., Cunningham, C.G., Rytuba, J.J., Rye, R.O., Kelly, W.C., Podwysocki, M.H., McKee, E.H., and Tosdal, R.M., 1995, Geology, geochronology, fluid inclusions, and isotope geochemistry of the Rodalquilar Au alunite deposit, Spain: Economic Geology, v. 90, p. 795–822.

Ashley, P.M., and Craw, D., 2004, Structural controls on hydrothermal alteration and gold-antimony mineralization in the Hillgrove area, NSW, Australia: Mineralium Deposita, v. 39, p. 223–239.

Bagby, W.C., and Berger, B.R., 1985, Geologic characteristics of sediment-hosted, disseminated precious-metal deposits in the western United States: Reviews in Econimic Geology, v. 2, p. 169–202.

Baker, T., Mustard, R., Brown, V., Pearson, N., Stanley, C.R., Radford, N.W., and Butler, I., 2006, Textural and chemical zonation of pyrite at Pajingo: A

potential vector to epithermal gold veins: Geochemistry: Exploration, Environment, Analysis, v. 6, p. 283–293
Bakken, B.M., 1990, Gold mineralization, wall-rock alteration, and the geochemical evolution of the hydrothermal system in the main orebody, Carlin mine, Nevada: Ph.D. dissertation, Palo Alto, CA, Stanford University, 256 p.
Bakken, B.M., Hochella, M.F., Jr., Marshall, A.F., and Turner, A.M., 1989, High-resolution microscopy of gold in unoxidized ore from the Carlin mine, Nevada: Economic Geology, v. 84, p. 171–179.
Ballantyne, J.M., and Moore, J.N., 1988, Arsenic geochemistry in geothermal systems: Geochimica et Cosmochimica Acta, v. 52, p. 475–483.
Barker, S.L.L., Hickey, K.A., Cline, J.S., Dipple, G.M., Kilburn, M.R., Vaughan, J.R., and Longo, A.A., 2009, Uncloaking invisible gold: Use of nanoSIMS to evaluate gold, trace elements, and sulfur isotopes in pyrite from Carlin-type gold deposits: Economic Geology, v. 104, p. 897–904.
Barton, M.D., Girardi, J.D., Kreiner, D.C., Seedorff, E., Zurcher, L., Dilles, J.H., Haxel, G.B., and Johnson, D.A, 2011, Jurassic igneous-related metallogeny of southwestern North America: Great Basin Evolution and Metallogeny, Geological Society of Nevada 2010 Symposium, Proceedings, p. 373–398.
Baumgartner, R., Fontboté, L., and Vennemann, T., 2008, Mineral zoning and geochemistry of epithermal polymetallic Zn-Pb-Ag-Cu-Bi mineralization at Cerro de Pasco, Peru: Economic Geology, v. 103, p. 493–537.
Baxter, J.L., 1978, Molybdenum, tungsten, vanadium, and chromium in Western Australia: Geological Survey of Western Australia Mineral Resources Bulletin, v. 11, 140 p.
Benavides, J.D., 1983, Wall-rock alteration and mineralogic zoning in a section of the Julcani mining district, Peru: M.S. thesis, Palo Alto, CA, Stanford University, 199 p.
Berger, B.R., and Tingley, J.V., 1985, History of discovery, mining, exploration of the Getchell mine, Humboldt County, Nevada, *in* Hollister, V. F., ed., Discoveries of epithermal precious metal deposits, case histories of mineral discoveries: Society of Mining Engineers, New York, v. 1, p. 49–51.
Biruk, S.V., and Skakun, L.Z., 2000, Bismuth minerals of the Beregovo ore field: Mineral assemblages and spatial zonation (Transcarpathian, Ukraine): Geological Quarterly, v. 44, p. 39–46.
Boev, B., and Jelenkovic, R., 2012, Allchar deposit in the Republic of Macedonia—petrology and age determination, *in* Al-Juboury, A., ed., Petrology—new perspectives and applications: Rijeka, Croatia, InTech, Chapter 6, 39 p.
Bortnikov, N.S., Gamynin, G.N., Vikent'eva, O.V., Prokof'ev, V.Yu., and Prokop'ev, A.V., 2010, The Sarylakh and Sentachan gold-antimony deposits, Sakha-Yakutia: A case of combined mesothermal gold-quartz and epithermal stibnite ores: Geology of Ore Deposits, v. 52, p. 339–372.
Bowell, R.J., Foster, R.P., and Stanley, C.J., 1990, Telluride mineralization at Ashanti gold mine, Ghana: Mineralogical Magazine, v. 54, p. 617–627.
Boyle, R.W., 1979, The geochemistry of gold and its deposits: Geological Survey of Canada Bulletin 280, 584 p.
Brugger, J., Etschmann, B.E., Grundler, P.V., Liu, W-H., Testemale, D., and Pring, A., 2012, XAS evidence for stability of polytellurides in hydrothermal fluids up to 599°C, 800 bar: American Mineralogist, v. 97, p. 1519–1522.
Burleigh, R.E., 1987, A stable isotope, fluid inclusion, and ore petrographic study of gold-quartz veins in the Willow Creek mining district, Alaska: M.S. thesis, Fairbanks, University of Alaska, 246 p.
Cail, T.L., and Cline, J.S., 2001, Alteration associated with gold deposition at the Getchell Carlin-type gold deposit, north-central Nevada: Economic Geology, v. 96, p. 1343–1359.
Calabrese, S., Aiuppa, A., Allard, P., Bagnato, E., Bellomo, S., Brusca, L., D'Alessandro, W., and Parello, F., 2011, Atmospheric sources and sinks of volcanogenic elements in a basaltic volcano (Etna, Italy): Geochimica et Cosmochimica Acta, v. 75, p. 7401–7425.
Camprubi, A., and Albinson, T., 2007, Epithermal deposits in Mexico—update of current knowledge, and an empirical reclassification: Geological Society of America Special Paper 422, p. 377–415.
Casey, S.D., 2000, Mineralogy and stable isotope geochemistry of gold-silver telluride mineralization in the Berner Bay district, Alaska: M.Sc. thesis, Ames, Iowa State University, 117 p.
Christenson, B.W., and Mroczek, E.K., 2003, Potential reaction pathways of Hg in some New Zealand hydrothermal environments: Society of Economic Geologists, Special Publication 10, p. 111–132.
Christie, A.B., Simpson, M.P., Brathwaite, R.L., Mauk, J.L., and Simmons, S.F., 2007, Epithermal Au-Ag and related deposits of the Hauraki goldfield, Coromandel volcanic zone, New Zealand: Economic Geology, v. 102, p. 785–816.
Ciobanu, C.L., Cook, N.J., and Spry, P.G., 2006, Preface—Special issue: Telluride and selenide minerals in gold deposits—how and why?: Mineralogy and Petrology, v. 87, p. 163–169.
Cline, J.S., Hofstra, A.H., Muntean, J.L., Tosdal, R.M., and Hickey, K.A., 2005, Carlin-type gold deposits in Nevada: Critical geologic characteristics and viable models: Economic Geology 100th Anniversary Volume, p. 451–484.
Cline, J.S., Muntean, J.L., Gu, X-X., and Xia, Y., 2013, A comparison of Carlin-type gold deposits: Guizhou province, Golden Triangle, southwest China, and northern Nevada, USA: Earth Science Frontiers, v. 20, p. 1–18.
Cluer, J.K., 2012, Remobilized geochemical anomalies related to deep gold zones, Carlin trend, Nevada: Economic Geology, v. 107, p. 1343–1349.
Cook, N.J., and Ciobanu, C.L., 2004, Bismuth tellurides and sulphosalts from the Larga hydrothermal system, Metaliferi Mts., Romania-Paragenesis and genetic significance: Mineralogical Magazine, v. 68, p. 301–321.
——2005, Tellurides in Au deposits—implications for modeling, *in* Mao, J.W., and Bierlein, F.P., eds. Mineral deposit research—meeting the global challenge: Berlin-Heidelberg-New York, Springer, p. 1387–1390.
Cook, N., Ciobanu, C.L., Capraru, N., Damian, G., and Crist, P., 2005, Mineral assemblages from the vein salband at Sacarimb, Golden Quadrilateral, Romania—II. Tellurides: Geochemistry, Mineralogy and Petrology, v. 43, p. 56–63.
Cook, N.J., Ciobanu, C.L., Pring, A., Skinner, W., Shimizu, M., Danyushevsky, L., Saini-Eidukat, B., and Melcher, F., 2009, Trace and minor elements in sphalerite: A LA-ICPMS study: Geochimica et Cosmochimica Acta, v. 73, p. 4761–4791.
Cooke, D.R., and Bloom, M.S., 1990, Epithermal and subjacent porphyry mineralization, Acupan, Baguio district, Philippines: A fluid-inclusion and paragenetic study: Journal of Geochemical Exploration, v. 35, p. 297–340.
Cooke, D.R., and McPhail, D.C., 2001, Epithermal Au-Ag-Te mineralization, Acupan, Baguio district, Philippines: Numerical simulations of mineral deposition: Economic Geology, v. 96, p. 109–131.
Cooke, D.R., McPhail, D.C., and Bloom, M.S., 1996, Epithermal gold mineralization, Acupan, Baguio district, Philippines: Geology, mineralization, alteration, and thermochemical environment of ore deposition: Economic Geology, v. 91, p. 243–272.
Cookro, T.M., Silberman, M.L., and Berger, B.R., 1988, Gold-tungsten bearing hydrothermal deposits in the Yellow Pine mining district, Idaho, *in* Schafer, R.W., Cooper, J.J., and Vikre, P.G., eds., Bulk Minable Precious Metal Deposits of the Western United States: Reno, Geological Society of Nevada, Symposium Proceedings, p. 577–624.
Cvetkovic, L., Boronikhin, V.A., Pavicevic, M.K., Krajnovic, D.,Grzetic, I., Libowitzky, E., Giester, G., and Tillmanns, E., 1995, Jankovicite, $Tl_5Sb_9(As,Sb)_4S_{22}$, A new Tl-sulfosalt from Allchar, Macedonia: Mineralogy and Petrology, v. 53, p. 125–131.
Davies, A.G.S., Cooke, D.R., Gemmell, J.B., van Leeuwen, T., Cesare, P., and Hartshorn, G., 2008, Hydrothermal breccias and veins at the Kelian gold mine, Kalimantan, Indonesia: Genesis of a large epithermal gold deposit: Economic Geology, v. 103, p. 717–757.
de Almeida, C.M., Olivo, G.R., Chouinard, A., Weakly, C., and Poirier, G., 2010, Mineral paragenesis, alteration, and geochemistry of the two types of gold ore and the host rocks from the Carlin-type deposits in the southern part of the Goldstrike property, northern Nevada: Implications for sources of ore-forming elements, ore genesis, and mineral exploration: Economic Geology, v. 105, p. 971–1004.
Deditius, A.P., Kesler, S.E., Reich, M.. Utsunomiya, S., and Ewing, R.C., 2011a, Chemical limits of trace elements in pyrite: Mineralogical Magazine, v. 75, p. 733.
Deditius, A.P., Utsunomiya, S., Reich, M., Kesler, S.E, and Ewing, R.C., 2011b, Trace metal nanoparticles in pyrite: Ore Geology Reviews, v. 42, p. 32–46.
Demange, M., Pascal, M.L., Raimbault, L., Armand, J., Forette, M.C., Serment, R., and Touil, A., 2006, The Salsigne Au-As-Bi-Ag-Cu deposit, France: Economic Geology, v. 101, p. 199–234.
Deyell, C.L., and Hedenquist, J.W., 2011, Trace element geochemistry of enargite in the Mankayan district, Philippines: Economic Geology, v. 106, p. 1465–1478.
Dickson, F.W., and Radtke, A.S., 1978, Wesissbergite, $TlSbS_2$, a new mineral from the Carlin gold deposit, Nevada: American Mineralogist, v. 63, p. 720–724.
Dickson, F.W., Radtke, A.S., and Peterson, J. A., 1979, Ellisite, Tl_3AsS_3 , a new mineral from the Carlin gold deposit, Nevada, and associated sulfide and sulfosalt minerals: American Mineralogist, v. 64, p. 701–707.

Diehl, S.F., Hofstra, A.H., Koenig, A.E., Emsbo, P., Christiansen, W., and Johnson, C., 2010, Hydrothermal zebra dolomite in the Great Basin, Nevada—attributes and relation to Paleozoic stratigraphy, tectonics, and ore deposits: Geosphere, v. 6, p. 663–690.

Dill, H.G., 2010, The "chessboard" classification scheme of mineral deposits—mineralogy and geology from aluminum to zirconium: Earth Science Reviews, v. 100, p. 1–420.

Dill, H.G., Weiser, T., Berhardt, I. R., and Kilibarda, C.R., 1995, The composite gold-antimony vein deposit at Kharma (Bolivia): Economic Geology, v. 90, p. 51–66.

Dill, H.G., Garrido, M.M., Melcher, F., Gomez, M.C., Weber, B., Luna, L.I., and Bahr, A., 2013, Sulfidic and non-sulfidic indium mineralization of the epithermal Au-Cu-Zn-Pb-Ag deposit San Roque (Provincia Rio Negro, SE Argentina)—with special reference to the "indium window" in zinc sulfide: Ore Geology Reviews, v. 51, p. 103–128.

Distler, V.V., and Yudovskaya, M.A., 2005, Polymetallic PGE-Au mineralization of the Sukhoi Log deposit, Russia: Mineralogical Association of Canada Short Course Series, v. 35, p. 457–485.

Edelstein, D., 1995, Arsenic: U.S. Geological Survey Minerals Yearbook 1995, p. 71–74.

——2013, Arsenic: U.S. Geological Survey Minerals Yearbook 1995, p. 2–21.

Eilu, P., and Groves, D.I., 2001, Primary alteration and geochemical dispersion haloes of Archean orogenic gold deposits in the Yilgarn craton: the preweathering scenatio: Geochemistry: Exploration, Environment, Analysis, v. 1, p. 183–200.

Eilu, P., Mikucki, E.J., and Groves, D.I., 1998, Wallrock alteration and primary geochemical dispersion in lode-gold exploration: SGA Short Course Series Volume 1, 65 p.

Einaudi, M.T., Hedenquist, J.W., and Inan, E., 2003, Sulfidation state of fluids in active and extinct hydrothermal systems: Transitions from porphyry to epithermal environments: Society of Economic Geologists Special Publication 10, p. 285–314.

Emsbo, P., and Koenig, A. E.,2005, Discovery and significance of gold-rich bitumen in the Rodeo deposit, northern Carlin trend, Nevada: Geochimica et Cosmochimica Acta, v. 69, no. 10 supplement, p. 123.

Emsbo, P., Hutchinson, R.W., Hofstra, A.H., Volk, J.A., Bettles, K.H., Baschuk, G.J., and Johnson, C.A., 1999, Syngenetic Au on the Carlin trend: Implications for Carlin-type deposits: Geology, v. 27, p. 59–62.

Emsbo, P., Hofstra, A.H., Lauha, E.A., Griffin, G.L., and Hutchinson, R.W., 2003, Origin of high-grade gold ore, source of ore fluid components, and genesis of Meikle and neighboring Carlin-type deposits, northern Carlin trend, Nevada: Economic Geology, v. 98, p. 1069–1106.

Emsbo, P., Groves, D.I., Hofstra, A.H., and Bierlein, F.P., 2006, The giant Carlin gold province: A protracted interplay of orogenic, basinal, and hydrothermal processes above a lithospheric boundary: Mineralium Deposita, v. 41, p. 517–525.

European Commission, 2010, Critical raw materials for the EU: Report of the Ad-hoc working group on defining critical raw materials, 84 p.

Ewers, G.R., and Keays, R.R., 1977, Volatile and precious metal zoning in the Broadlands geothermal field, New Zealand: Economic Geology, v. 72, p. 1337–1354.

Fan, D., Zhang, T., and Ye, J., 2004, The Xikuangshan Sb deposit hosted by the Upper Devonian black shale series, Hunan, China: Ore Geology Reviews, v. 24, p. 121–133.

Fan, Y., Zhou, T-F., Yuan, F., and Wu, M-G., 2014, Geological and geochemical constraints on the genesis of the Xiangquan Tl-only deposit, eastern China: Ore Geology Reviews, v. 59, p. 97–108.

Fleet, M.E., and Mumin, A. H., 1997, Gold-bearing arsenian pyrite and marcasite and arsenopyrite from Carlin trend gold deposits and laboratory synthesis: American Mineralogist, v. 82, p. 182–193.

Foster, R.P., 1977, Solubility of scheelite in hydrothermal chloride solutions: Chemical Geology, v. 20, p. 27–43.

Fulignati, P., and Sbrana, A., 1998, Presence of native gold and tellurium in active high-sulfidation hydrothermal system of La Fossa volcano (Vulcano, Italy): Journal of Volcanology and Geothermal Research, v. 86, p. 187–198.

Gammons, C.H., and Williams-Jones, A.E., 1997, Chemical mobility of gold in the porphyry-epithermal environment: Economic Geology, v. 92, p. 45–59.

Gemmell, J.B., 2007, Hydrothermal alteration associated with the Gosowong epithermal Au-Ag deposit, Halmahera, Indonesia: Mineralogy, geochemistry, and exploration implications: Economic Geology, v. 102, p. 893–922.

Gemmell, J.B., Simmons, S.F., and Zantop, H., 1988, The St. Niño silver-lead-zinc vein, Fresnillo district, Zacatecas, Mexico: Part I. Structure, vein stratigraphy and mineralogy: Economic Geology, v. 83, p. 1597–1618.

Goldfarb, R.J., Miller, L.D., Leach, D.L., and Snee, L.W., 1997, Gold deposits in metamorphic rocks of Alaska: Economic Geology Monograph 9, p. 151–190.

Goldfarb, R.J., Ayuso, R., Miller, M.L., Ebert, S.W., Marsh, E.E., Petsel, S.A., Miller, L.D., Bradley, D., Johnson, C., and McClelland, W., 2004, The Late Cretaceous Donlin Creek gold deposit, southwestern Alaska: Controls on epizonal ore formation: Economic Geology, v. 99, p. 643–671.

Goldfarb, R.J., Baker, T., Dube, B., Groves, D.I., Hart, C.J.R., and Gosselin, P., 2005, Distribution, character, and genesis of gold deposits in metamorphic terranes: Economic Geology 100th Anniversary Volume, p. 407–450.

Goldfarb, R.J., Taylor, R.D., Collins, G.S., Goryachev, N.A., and Orlandini, O.F., 2014, Phanerozoic continental growth and gold metallogeny of Asia: Gondwana Research, v. 25, p, 48–102.

Goldfarb, R.J., Berger, B.R., George, M.W., and Seal, R.R. III, in press, Tellurium—economic and environmental geology, and prospects for future supply: U.S. Geological Survey Professional Paper.

Grant, J.A., 1986, The isocon diagram: A simple solution to Gresens' equation for metasomatic alteration: Economic Geology, v. 81, p. 1976–1982.

Gray, J.E., and Coolbaugh, M.F., 1994, Geology and geochemistry of Summitville, Colorado: An epithermal acid sulfate deposit in a volcanic dome: Economic Geology, v. 89, p. 1906–1923.

Greenland, L.P., and Aruscavage, P., 1986, Volcanic emission of Se, Te, and As from Kilauea volcano, Hawaii: Journal of Volcanology and Geothermal Research, v. 27, p. 195–201.

Groves D.I., 1993, The crustal continuum model for late-Archaean lode-gold deposits of the Yilgarn Block, Western Australia: Mineralium Deposita, v. 28, p. 366–374.

Groves, D.I., Goldfarb, R.J., Gebre-Mariam, M., Hagemann, S.G., and Robert F., 1998, Orogenic gold deposits: A proposed classification in the context of their crustal distribution and relationship to other gold deposit types: Ore Geology Reviews, v. 13, p. 7–27.

Gunn, G., ed., 2014, Critical metals handbook: Oxford, UK, John Wiley and Sons, 439 p.

Hallberg, A., 1994, The Enåsen gold deposit, central Sweden: Mineralium Deposita, v. 29, p. 150–162.

Hart, C.J.R., and Goldfarb, R.J., 2007, Geochronological and regional metallogenic investigations in the Bralorne-Bridge River mining district (Parts of NTS 092D, J, I, O), southwestern British Columbia: Project Rationale: British Columbia Ministry of Energy, Mines and Petroleum Resources Paper 2007-1, p. 291–296.

Hays, R.C., Jr., and Foo, S.T., 1991, Geology and mineralization of the Gold Acres deposit, Lander County, Nevada, *in* Raines, G.L., Lisle, R.E., Schafer, R.W., Wilkinson, WH., eds., Geology and Ore Deposits of the Great Basin, Symposium Proceedings: Reno, NV, Geological Society of Nevada, p. 677–685.

Hedenquist, J.W., and Henley, R.W., 1985, Hydrothermal eruptions in the Waiotapu geothermal system, New Zealand: Their origin, associated breccias, and relation to precious metal mineralization: Economic Geology, v. 80, p. 1640–1668.

Hedenquist, J.W., Aoki, M., and Shinohara, H., 1994, Flux of volatiles and ore-forming metals from the magmatic-hydrothermal system of Satsuma Iwojima volcano: Geology, v. 22, p. 585–588.

Hedenquist, J.W., Izawa, E., Arribas, A., and White, N.C., 1996, Epithermal-gold deposits: Styles, characteristics, exploration: Society of Resource Geology, Resource Geology Special Publication 1, 18 p.

Hedenquist, J.W., Arribas, A., Jr., and Gonzales-Urien, E., 2000, Exploration for epithermal gold deposits: Reviews in Economic Geology, v. 13, p. 245–277.

Henley, R.W., and Berger, B.R., 2013, Nature's refineries—metals and metalloids in arc volcanoes: Earth-Science Reviews, v. 125, p. 146–170.

Henry, C.D., and Ressel, M.W., 2000, Eocene magmatism of northeastern Nevada: The smoking gun for Carlin-type gold deposits, *in* Cluer, J.K., Price, J.G., Struhsacker, E.M., Hardyman, R.F., and Morris, C.L., eds., Geology and Ore Deposits 2000: The Great Basin and Beyond: Reno, Geological Society of Nevada, p. 365–388.

Hodgson, C.J., and MacGeehan, P.J., 1982, Geological characteristics of gold deposits in the Superior province of the Canadian Shield: Canadian Institute of Mining and Metallurgy Special Volume 24, p. 211–229.

Hofstra, A.H., 1994, Geology and genesis of the Carlin-type gold deposits in the Jerritt Canyon district, Nevada: Ph.D. Dissertation, Boulder, CO, University of Colorado, 719 p.

Hofstra, A.H., and Christensen, O.D., 2002, Comparison of Carlin-type Au deposits in the United States, China, and Indonesia: Implications for

genetic models and exploration: U.S. Geological Survey Open-File Report 02-131, p. 61–94.
Hofstra, A.H., and Cline, J.S., 2000, Characteristics and models for Carlin-type gold deposits: Reviews in Economic Geology, v. 13, p. 163–220.
Hofstra, A.H., Leventhal, J.S., Northrop, H.R., Landis, G.P., Rye, R.O., Birak, D.J., and Dahl, A.R., 1991, Genesis of sediment-hosted diseminated gold deposits by fluid mixing and sulfidization: Chemical-reaction-path modeling of ore-depositional processes documented in the Jerritt Canyon district, Nevada: Geology, v. 19, p. 36–40.
Hofstra, A.H., Snee, L.W., Rye, R.O., Folger, H.W., Phinisey, J.D., Loranger, R.J., Dahl, A.R., Naeser, C.W., Stein, H.J., and Lewchuk, M., 1999, Age constraints on Jerritt Canyon and other gold deposits in the western United States—Relationship to Mid-Tertiary extension and magmatism: Economic Geology, v. 94, no. 6, p. 769–802.
Hofstra, A.H., Zhang, X-C., Emsbo, P., Hu, R-H., Su,W-C., Christiansen, W.D., Fu, S-H., and Theodorakos, P., 2005, Source of ore fluids in Carlin-type gold deposits in the Dian-Qian-Gui area and West Qinling belt, P.R. China: Implications for genetic models: Mineral Deposit Research: Meeting the Global Challenge, SGA Meeting, 8th Biennial, Beijing, China, 18–21 August 2005, Proceedings, p. 533–536.
Hofstra, A.H., Christiansen, W.D., Zohar, P.B., and Tousignant, G., 2011, Lithogeochemistry of the Devonian Popovich Formation in the northern Carlin trend, Nevada: Great Basin Evolution and Metallogeny, Geological Society of Nevada, Symposium 2010, Proceedings, p. 63–96.
Hu, R-Z., Su, W-C., Bi, X-W., Tu, G-Z., and Hofstra, A. H., 2002, Geology and geochemistry of Carlin-type gold deposits in China: Mineralium Deposita, v. 37, p. 378–392.
Ilchik, R.P., 1990, Geology and geochemistry of the Vantage gold deposits, Alligator Ridge-Bald Mountain mining district, Nevada: Economic Geology, v. 85, p. 50–75.
Ishihara, S., Hoshino, K, Murakami, H., and Endo, Y., 2006, Resource evaluation and some genetic aspects of indium in the Japanese ore deposits: Resource Geology, v. 56, p. 347–364.
Ishihara, S., Murakami, H., and Marquez-Zavalia, M. F., 2011, Inferred indium resources of the Bolivian tin-polymetallic deposits: Resource Geology, v. 61, p. 174–191.
Ispolatov, V., Lafrance, B., Dubé, B., Creaser, R., and Hamilton, M., 2008, Geologic and structural setting of gold mineralization in the Kirkland Lake-Larder Lake gold belt, Ontario: Economic Geology, v. 103, p. 1309–1340.
Ivanov, S.M., Ansdell, K.M., and Melsore, D.L., 2000, Ore texture and stable isotope constraints on ore deposition mechanisms at the Kumtor lode gold deposit [ext. abs.]: Society of Economic Geologists, Short Course Poster Session, Extended Abstract Volume, p. 47–52.
Izawa, E., Urashima, Y., Ibaraki, K., Suzuki, R., Yokoyama, T., Kawasaki, K., Koga, A., and Taguchi, S., 1990, The Hishikari gold deposit: High-grade epithermal veins in Quaternary volcanics of southern Kyushu, Japan: Journal of Geochemical Exploration, v. 36, p. 1–56.
Jannas, R.R., Bowers, T.S., Petersen, U., and Beane, R.E., 1999, High sulfidation deposit types in the El Indio district, Chile: Society of Economic Geologists Special Publication 7, p. 219–266.
Jensen, E.P., and Barton, M.D., 2000, Gold deposits related to alkaline magmatism: Reviews in Economic Geology, v. 13, p. 279–313.
John, D.A., and Taylor, R.D., 2016, By-products of porphyry copper and molybdenum deposits: Reviews in Economic Geology, v. 18, p. 137–164.
John, D.A., Nash, J.T., Clark, C.W., and Wulftange, W., 1991, Geology, hydrothermal alteration, and mineralization at the Paradise Peak gold-silver-mercury deposit, Nye County, Nevada, *in* Raines, G.L., Lisle, R.E.,Schafer, R.W., and Wilkinson, W.H., eds., Geology and ore deposits of the Great Basin. Symposium proceedings: Reno, Geological Society of Nevada and U.S. Geological Survey, p. 1020–1050.
Johnston, W.D., Jr., 1940, The gold quartz veins of Grass Valley. California: U.S. Geological Survey Professional Paper 194, 101 p.
Jones, G., and Miller, G., 2005, Mercury and modern gold mining in Nevada: Final report to U.S. Environmental Protection Agency Region IX, 41 p.
Jovic, S.M., Guido, D.M., Schalamuk, I.B., Rios, F.J., Tassinari, C.C.G., and Recio, C., 2011a, Pingüino In-bearing polymetallic vein deposit, Deseado Massif, Patagonia, Argentina: Characteristics of mineralization and ore-forming fluids: Mineralium Deposita, v. 46, p. 257–271.
Jovic, S.M., Guido, D.M., Melgarejo, J.C., Páez, G.N., Ruiz, R., and Schalamuk, I.B., 2011b, The indium-bearing minerals of the Pingüino polymetallic vein system, Deseado Massif, Patagonia, Argentina: Canadian Mineralogist, v. 49, p. 931–946.
Kelley, K.D., and Spry, P.G., 2016, Critical elements in alkaline igneous rock-related epithermal gold deposits: Reviews in Economic Geology, v. 18, p. 195–216.
Kerrich, R., and Fryer, B.J., 1981,The separation of rare elements from abundant base metals in Archean lode gold deposits: Implications of low water/rock source regions: Economic Geology, v. 76, p. 160–166.
Kesler, S.E., Russell, N., Seaward, M., Rivera, J., McCurdy, K., Cumming, G.L., and Sutter, J.F., 1981, Geology and geochemistry of sulfide mineralization underlying the Pueblo Viejo gold-silver oxide deposit, Dominican Republic: Economic Geology, v. 76, p. 1096–1117.
Kesler, S.E., Fortuna, J., Ye, Z., Alt, J.C., Core, D.P., Zohar, P., Borhauer, J., and Chryssoulis, S.L., 2003, Evaluation of the role of sulfidation in deposition of gold, Screamer section of the Betze-Post Carlin-type deposit, Nevada: Economic Geology, v. 98, p. 1137–1157.
Kesler, S.E., Campbell, I.H., Smith, C.N., Hall, C.M., and Allen, C.M., 2003, Ages of the Pueblo Viejo gold-silver deposit and its significance to models for high-sulfidation epithermal mineralization: Economic Geology, v. 100, p. 253–272.
Kesler, S.E., Riciputi, L.C., and Ye, Z., 2005, Evidence for a magmatic origin for Carlin-type gold deposits: Isotopic composition of sulfur in the Betze-Post-Screamer deposit, Nevada, USA: Mineralium Deposita, v. 41, p. 127–136.
Korzhinsky, M.A., Tkachenko, S.I., Shmulovich, K.I., Taran, Y.A., and Steinberg, G.S., 1994, Discovery of pure rhenium mineral at Kudriavy volcano: Nature, v. 369, p. 51–52.
Krupp, R., 1988, Physiochemical aspects of mercury metallogenesis: Chemical Geology, v. 69, p. 345–356.
——1989, Paragenesis and conditions of formation of the Moschellandsberg mercury deposit, SW Germany: Mineralium Deposita, v. 24, p. 69–76.
Krupp, R.E., and Seward, T.M., 1987, The Rotokawa geothermal system, New Zealand: An active epithermal gold-depositing environment: Economic Geology, v. 82, p. 1109–1129.
Kuehn, C.A., and Rose, A.W., 1992, Geology and geochemistry of wall-rock alteration at the Carlin gold deposit, Nevada: Economic Geology, v. 87, p. 1697–1721.
Large, R.R, Danyushevsky, L., Hollit, C., Maslennikov, V., Meffre, S., Gilbert, S., Bull, S., Scott, R., Emsbo, P., Thomas, H., Singh, B., and Foster, J., 2009, Gold and trace element zonation in pyrite using a laser imaging technique: Implications for the timing of gold in orogenic and Carlin-style sediment-hosted deposits: Economic Geology, v. 104, p. 635–668.
Large, R.R., Bull, S.W., and Maslennikov, V.V., 2011a, A carbonaceous sedimentary source-rock model for Carlin-type and orogenic gold deposits: Economic Geology v. 106, p. 331–358.
Large, R.R., Bull, S.W., and Gilbert, S., 2011b, Multiple syngentic metalliferous horizons enriched in V, As, Mo, Se, Ni, Ag, Zn, and Au in the northern Carlin trend: Implications for the genesis of world class gold-arsenic deposit, *in* Steiniger, R., and Pennell, B., eds., Great basin evolution and metallogeny: Reno, Geological Society of Nevada, p. 1–16.
Lawrence, E.F., 1963, Antimony deposits of Nevada: Nevada Bureau of Mines and Geology, Bulletin 61, 248 p.
Le Guen, M., Lescuyer, J.L., and Marcoux, E., 1992, Lead-isotope evidence for a Hercynian origin of the Salsigne gold deposit (southern Massif Central France): Mineralium Deposita, v. 27, p. 129–136.
Lehmann, B., Heinhorst, J., Hein, M., and others, 1999, The Bereznjakovskoje gold trend, Southern Urals, Russia: Mineralium Deposita, v. 34, p. 241–249.
Lindgren, Waldemar, 1906, Metasomatic processes in the gold deposits of Western Australia: Economic Geology, v. 1, p. 530–544.
Liu, J-J., Liu, J-M., Liu, C-Q., Lu, W-Q., Liu, S-R., and Su, W-C., 1999, Mineralogy of the stibnite-antimonselite series: International Geology Review, v. 41, p. 1042–1050.
Liu, J-J., Zheng, M-H., Liu, J-M., and Su, W-C., 2000, Geochemistry of the La'erma and Qiongmo Au-Se deposits in the western Qinling Mountains, China: Ore Geology Reviews, v. 17, p. 91–111.
Lu, G-Q., 1994, A genetic link between the gold-mercury mineralization and petroleum evolution—a case of the Danzhai gold-mercury deposit: Ph.D. dissertation, Chicoutimi, Quebec, Universite du Quebec, 209 p.
Maitland, A.G., 1919, A summary of the geology of Western Australia: The gold deposits of Western Australia: Geological Survey of Western Australia, 380 p.
Mao, J-W., Qiu, Y-M., Goldfarb, R.J., Zhang, Z-C., Garwin, S., and Ren, F-S., 2002, Geology, distribution, and classification of gold deposits in the western Qinling belt, central China: Mineralium Deposita, v. 37, p. 352–377.

Marcoux, E., and Milesi, J.P., 1994, The epithermal gold deposits in West Java, Indonesia: Geology, age and crustal source: Journal of Geochemical Exploration, v. 50, p. 393–408.
Maslennikov, V.V., Maslennikova, S.P., Large, R.R., Danyushevsky, L.V., Herrington, R.J., and Stanley, C.J., 2013, Tellurium-bearing minerals in zoned sulfide chimneys from Cu-Zn massive sulfide deposits of the Urals, Russia: Mineralogy and Petrology, v. 107, p. 67–99.
Mather, T.A., Witt, M.L.I., Pyle, D.M., Quayle, B.M., Aiuppa, A., Bagnato, E., Martin, R.S., Sims, K.W., Edmond, M., Sutton, A.J., and Ilyinskaya, E., 2011, Halogens and trace metalemissions from the ongoing 2008 summit eruption of Kilauea volcano, Hawaii: Geochimica et Cosmochimica Acta, v. 83, p. 292–323.
Midas Gold Corporation, 2103, Mineral resources: http://www.midasgoldinc.com/s/goldenmeadows.asp?ReportID=542245.
Mobbs, P.M., 1990, Latin America and Canada 1990: U.S. Bureau of Mines Minerals Yearbook, v. 3, p. 276–290.
Moore, D.B., Gorman, M., Harris, D., Peterson, A. T., Reeeves, M., and Wilson, S.E., 2013, Technical report—Hycroft mine, Winnemucca, Nevada, USA: Allied Nevada Gold Corp., Unpub. report, 145 p.
Moss, R.L., Tzimas, E., Kara, H., Willis, P., and Kooroshy, J., 2011, Critical metals in strategic energy technologies—assessing rare metals as supply-chain bottlenecks in low-carbon energy technologies: European Commission Joint Research Centre Scientific and Technical Report, 164 p.
Moune, S., Gauthier, P.J., and Delmelle, P., 2010, Trace elements in the particulate phase of the plume of Masaya volcano, Nicaragua: Journal of Volcanology and Geothermal Research, v. 193, p. 232–244.
Mueller, A.G., and Muhling, J.R., 2013, Silver-rich telluride mineralization at the Mount Charlotte and Au-Ag zonation in the giant Golden Mile deposit, Kalgoorlie, Western Australia: Mineralium Deposita, v. 48, p. 295–311.
Muntean, J.L., Kesler, S.E., Russell, N., and Polanco, J., 1990, Evolution of the Monte Negro acid-sulfate Au-Ag deposit, Pueblo Viejo, Dominican Republic: Important factors in grade control: Economic Geology, v. 85, p. 1738–1758.
Muntean, J.L., Cline, J.S., Simon, A.C., and Longo, A.A., 2011, Magmatic-hydrothermal origin of Nevada's Carlin-type gold deposits: Nature Geoscience, v. 4, p. 122–127.
National Institute of Advanced Industrial Science and Technology, 2008, Rare metals: Tsukuba, Japan, Publication Office, AIST, 12 p.
National Research Council, 2008, Minerals, critical minerals, and the U.S. economy: National Academy of Sciences, 263 p.
Nesbitt, B.E., Muehlenbachs, K., and Murowchick, J.B., 1989, Genetic implications of stable isotope characteristics of mesothermal Au deposits and related Sb and Hg deposits in the Canadian Cordillera: Economic Geology, v. 84, p. 1489–1506.
Nutt, C.J., and Hofstra, A.H., 2007, Bald Mountain gold mining district, Nevada: A Jurassic reduced intrusion-related gold system: Economic Geology, v. 102, p. 1129–1155.
Nutt, C.J., and Hofstra, A.H., 2003, Alligator Ridge: A shallow Carlin-type gold district: Economic Geology, v. 98, p. 1225–1241.
Ohta, E., 1989, Occurrence and chemistry of indium-containing minerals from the Toyoha mine, Hokkaido, Japan: Mining Geology, v. 39, p. 355–372.
——1991, Polymetallic mineralization at the Toyoha mine, Hokkaido, Japan: Mining Geology, v. 41, p. 279–295.
Palenik, C.S., Utsunomiya, S., Reich, M., Kesler, S.E., Wang, L., and Ewing, R.C., 2004, "Invisible" gold revealed: Direct imaging of gold nanoparticles in a Carlin-type deposit: American Mineralogist, v. 89, p. 1359–1366.
Papke, K.G., 1984, Barite in Nevada: Nevada Bureau of Mines and Geology Bulletin 98, 125 p.
Patterson, L.M., and Muntean, J.L., 2011, Multi-element geochemistry across a Carlin-type gold district: Jerritt Canyon, Nevada: Great Basin Evolution and Metallogeny, Geological Society of Nevada, Symposium 2010, Proceedings, p. 1119–1151.
Percival, J.C., and Radtke, A.S., 1994, Sedimentary-rock-hosted disseminated gold mineralization in the Alsar district, Macedonia: Canadian Mineralogist, v. 32, p. 649–665.
Petersen, U., Noble, D.C., Arenas, M.J., and Goodell, P.C., 1977, Geology of the Julcani mining district, Peru: Economic Geology, v. 72, p. 931–949.
Phillips, G.N., and Powell, R., 1993, Link between gold provinces: Economic Geology, v. 88, p. 1084–1098.
——2010, Formation of gold deposits: A metamorphic devolatilization model: Journal of Metamorphic Geology, v. 28, p. 689–718.
——2014, A practical classification of gold deposits, with a theoretical basis: Ore Geology Reviews, v. 85, pt. 3, p. 568–573.
Pitcairn, I.K., Teagle, D.A.H., Craw, D., Olivo, G.R., Kerrich, R., and Brewer T.S., 2006, Sources of metals and fluids in orogenic gold deposits: Insights from the Otago and Alpine schists, New Zealand: Economic Geology, v. 101, p. 1525–1546.
Plotinskaya, O.Yu., Kovalenker, V.A., Seltmann, R., and Stanley, C.J., 2006, Te and Se mineralogy of the high-sulfidation Kochbulak and Kairagach epithermal gold telluride deposits (Kurama Ridge, Middle Tien Shan, Uzbekistan): Mineralogy and Petrology, v. 87, p. 187–207.
Plumlee, G.S., and Whitehouse-Veaux, P.H., 1994, Mineralogy, paragenesis and mineral zoning of the Bulldog Mountain vein system, Creede district, Colorado: Economic Geology, v. 89, p. 1883–1905.
Pohl, W.L., 2011, Economic geology: Principles and practice: Wiley-Blackwell, 680 p.
Pokrovski, G.S., Borisova, A.Y., and Bychkov, A.Y., 2013, Speciation and transport of metalloids in geological vapors: Reviews in Mineralogy and Geochemistry, v. 76, p. 165–218.
Poole, F.G., Ketner, K.B., Smith, J.F., Jr., Harris, A.G., and Oversby, B., 1981, Bedded barite in Mississippian rocks of northeastern Nevada: U.S. Geological Survey Professional Paper 1275, 74 p.
Pope, J.G., Brown, K.L., and McConchie, D.M., 2005, Gold concentrations in springs at Waiotapu, New Zealand: Implications for precious metal deposition in geothermal systems: Economic Geology, v. 100, p. 677–687.
Popescu, G.C., and Neacsu, A., 2004, Tellurium—mineralogy, resources, energetic implications, *in* Gold-silver-telluride deposits of the golden quadrilateral, South Apuseni Mountains, Romania: IAGOD Guidebook Series 12, p. 19–25.
Radtke, A.S.,and Dickson, F.W., 1975, Carlinite, Tl_2S, a new mineral from Nevada: American Mineralogist, v. 60, p. 559–565.
——1984, Genesis and vertical position of fine-grained disseminated replacement type gold deposits in Nevada and Utah, USA: Problems of Ore Deposition, IAGOD Symposium, 4th, Varna, Proceedings, v. 1, p. 71–78.
Radtke, A.S., Taylor, C.M., Erd, R.C., and Dickson, F.W., 1974, Occurrence of lorandite $TlAsS_2$, at the Carlin gold deposit, Nevada: Economic Geology, v. 69, p. 121–123.
Radtke, A.S., Dickson, F.W., Slack, J.F., and Brown, K.L., 1977, Christite, a new thallium mineral from the Carlin gold deposit, Nevada: American Mineralogist, v. 62, p. 421–425.
Rastall, R.H., and Wilcockson, W.H., 1920, Tungsten ores: London, Imperial Institute, Imperial Institute Monographs on Mineral Resources, 81 p.
Rayias, A.C., 1999, Stratigraphy, structural geology, alteration and geochemistry of the northeastern Railroad district, Elko County, Nevada: M.S. thesis, Reno, NV, University of Nevada, Reno, 180 p.
Reich, M., Kesler, S.E., Utsonumiya, S., Palenik, C.S., Chryssoulis, S.L., and Ewing R.C., 2005, Solubility of gold in arsenian pyrite: Geochimica et Cosmochimica Acta, v. 69, p. 2781–2796.
Ressel, M.W., Noble, D.C., Heizler, M.T., Volk, J.A., Lamb, J.B., Park, D.E., Conrad, J.E., and Mortensen, J.K., 2000, Gold-mineralized Eocene dikes at Griffin and Meikle—bearing on the age and origin of deposits of the Carlin Trend, Nevada, *in* Cluer, J.K., Price, J.G., Struhsacker, E.M., Hardyman, R.F., and Morris, C.L., eds., Geology and ore deposits 2000—The Great Basin and beyond: Reno, Geological Society of Nevada, v. 1, p. 79–101.
Reyes, A., Trompetter, W., Britten, K., and Searle, J., 2002, Mineral deposits in the Rotokawa geothermal pipelines, New Zealand: Journal of Volcanology and Geothermal Research, v. 119, p. 215–239.
Richards, J.P., Wilkinson, D., and Ullrich, T., 2006, Geology of the Sari Gunay epithermal gold deposit, northwest Iran: Economic Geology, v. 101, p. 1455–1496.
Rytuba, J.J., 1976, Geology and ore deposits of the McDermitt caldera, Nevada-Oregon: U.S. Geological Survey Open-File Report 76-535, p. 1–9.
Rytuba, J.J., and Heroopoulos, C., 1992, Mercury: An important byproduct in epithermal gold systems: U.S. Geological Survey Bulletin 1877, p. D1–D8.
Rytuba, J.J., Enderlin, D.A., Donnelly-Nolan, J.M., and McLaughlin, R., 1993, Mclaughlin gold and Knoxville mercury: Road log: Society of Economic Geologists Guidebook Series 16, p. 350–361.
Rytuba, J.J., John, D.A., Foster, A., Ludington, S.D., and Kotlyar, B., 2003, Hydrothermal enrichment of gallium in zones of advanced argillic alteration—examples from the Paradise Peak and McDermitt ore deposits, Nevada: U.S. Geological Survey Bulletin 2209-C, 16 p.
Saunders, J.A., and Brueseke, M.E., 2012, Volatility of Se and Te during subduction-related distillation and the geochemistry of epithermal ores of the western United States: Economic Geology, v. 107, p. 165–172.
Saunders, J.A., Hofstra, A.H., Goldfarb, R.J., and Reed, M.H., 2014, Geochemistry of hydrothermal gold deposits: Treatise on Geochemistry, 2nd ed., v. 13, p. 383–424.

Saupe, F., 1990, Geology of the Almaden mercury deposit, Province of Ciudad Real, Spain: Economic Geology, v. 85, p. 482–510.
Schwarz-Schampera, U., 2014, Antimony, *in* Gunn, G., ed., Critical metals handbook: Oxford, UK, John Wiley and Sons, p. 70–121.
Schwarz-Schampera, U., and Herzig, P., 2002, Indium: Geology, mineralogy, and economics: Berlin, Springer Verlag, 263 p.
Seward, T.M., and Barnes, H.L., 1997, Metal transport by hydrothermal ore fluids, *in* Barnes, H.L., ed., Geochemistry of hydrothermal ore deposits: New York, John Wiley and Sons, p. 435–486.
Shackleton, J.M., Spry, P.G., and Bateman, R., 2003, Telluride mineralogy of the Golden Mile deposit, Kalgoorlie, Western Australia: Canadian Mineralogist, v. 41, p. 1503–1524.
Sherlock R.L., 2005, The relationship between the McLaughlin gold-mercury deposit and active hydrothermal systems in the Geysers-Clear Lake area, northern Coast Ranges, California: Ore Geology Reviews, v. 26, p. 349–382.
Sherlock, R.L., Tosdal, R.M., Lehrman, N.J., Graney, J.R., Losh, S., Jowett, E.C., and Kesler, S.E., 1995, Origin of the McLaughlin mine sheeted vein complex: Metal zoning, fluid inclusion, and isotopic evidence: Economic Geology, v. 90, p. 2156–2181.
Shikazono, N., 1985, A comparison of temperatures estimated from the electrum-sphalerite-pyrite-argentite assemblage and filling temperatures of fluid inclusions from epithermal Au-Ag vein-type deposits in Japan: Economic Geology, v. 80, p. 1415–1424.
Shimizu, T., and Aoki, M., 2011, Hydrothermal alteration and K-Ar ages of Neogene-Quaternary magmatic-hydrothermal systems at Toyoha-Muine area in southwest Hokkaido, Japan: Resource Geology, v. 61, p. 192–209.
Shimizu, T., and Morishita, Y., 2012, Petrography, chemistry, and near-infrared microthermometry of indium-bearing sphalerite from the Toyoha polymetallic deposit, Japan: Economic Geology, v. 107, p. 723–735.
Sibson, R.H., Robert, F., and Poulsen, H.K., 1988, High-angle reverse faults, fluid-pressure cycling, and mesothermal gold-quartz deposits: Geology, v. 16, p. 551–555.
Silberman, M.L., and Berger, B.R., 1985, Relationship of trace element patterns to alteration and morphology in epithermal precious-metal deposits: Reviews in Economic Geology, v. 2, p. 203–232.
Silberman, M.L., Berger, B.R., and Koski, R.A., 1974, K-Ar age relations of granodiorite emplacement and tungsten and gold mineralization near the Getchell mine, Humboldt County, Nevada: Economic Geology, v. 69, p. 646–656.
Sillitoe, R. H., and Hedenquist, J.W., 2003, Linkages between volcanotectonic settings, ore fluid compositions, and epithermal precious metal deposits: Society of Economic Geologists Special Publication 10, p. 315–343.
Sillitoe, R.H., and Lorson, R.C., 1994, Epithermal gold-silver-mercury deposits at Paradise Peak, Nevada: Ore controls, porphyry gold association, detachment faulting, and supergene oxidation: Economic Geology, v. 89, p. 1228–1248.
Sillitoe, R.H., Cooper, C., Sale, M.J., Soechiting, W., Echavarria, D., and Gallardo, J.L., 2002, Discovery and geology of the Esquel low-sulfidation epithermal gold deposit, Patagonia, Argentina: Society of Economic Geologists Special Publication 9, p. 227–240.
Simmons, S.F., 1991, Hydrologic implications of alteration and fluid inclusion studies in the Fresnillo district: Evidence for a brine reservoir and a descending water table and during the formation of hydrothermal Ag-Pb-Zn orebodies: Economic Geology, v. 86, p. 1579–1602.
Simmons, S.F., and Brown, K.L., 2007, The flux of gold and related metals through a volcanic arc, Taupo volcanic zone: Geology, v. 35, p. 1099–1102.
Simmons, S.F., and Browne, P.R.L., 2000, Hydrothermal minerals and precious metals in the Broadlands-Ohaaki geothermal system: Implications for understanding low-sulfidation epithermal environments: Economic Geology, v. 95, p. 971–999.
Simmons, S. F. and Brown, K. L., 2006, Gold in magmatic hydrothermal solutions and the rapid formation of a giant ore deposit: Science, v. 314, p. 288–291.
Simmons, S.F., White, N.C., and John, D., 2005, Geological characteristics of epithermal precious and base metal deposits: Economic Geology 100th Anniversary Volume, p. 485–522.
Simon, G., Kesler, S.E., and Essene, E.J., 1997, Phase relationships among selenides, tellurides, and oxides: II. Applications to selenide-bearing ore deposits: Economic Geology, v. 92, p. 468–484.
Simon, G., Kesler, S.E., and Chryssoulis, S., 1999, Geochemistry and textures of gold-bearing arsenian pyrite, Twin Creeks, Nevada: Implications for deposition of gold in Carlin-type deposits: Economic Geology, v. 94, p. 405–421.
Stanger, L.W., 1992, Barrick mercury gold mine, Mercur, Utah, *in* Wilson, J.R., ed., Field guide to geologic excursions in Utah and adjacent areas of Nevada, Idaho, and Wyoming: Geological Society of America Rocky Mountains Section, Ogden, Utah, May 13–15, University of Utah, p. 319–323.
Staude, J-M., 2001, Geology, geochemistry and formation of Au-(Cu) mineralization and advanced argillic alteration in the Mulatos district, Sonora, Mexico: Society of Economic Geologists Special Publication 8, p. 199–216.
Stefansson, A., and Seward, T.M., 2003, Stability of chloridogold(I) complexes in aqueous solutions from 300° to 600°C and from 500 to 1800 bar: Geochimica et Cosmochimica Acta, v. 67, p. 4559–4576.
Stuwe, K., 1998, Tectonic constraints on the timing relationships of metamorphism, fluid production and gold-bearing quartz vein emplacement: Ore Geology Reviews, v. 13, p. 219–228.
Sutphin, D.M., Drew, L.J., Carlin, J.F., Jr., and Seal, R.R., III, in press: Antimony: U.S. Geological Survey Professional Paper.
Symonds, R.B., Rose, W.I., Reed, M.H., Lichte, F.E., and Finnegan, D.L., 1987, Volatilization, transport and sublimation of metallic and non-metallic elements in high temperature gases at Merapi volcano, Indonesia: Geochimica et Cosmochimica Acta, v. 51, p. 2083–2101.
Taran, Y.A., Hedenquist, J.W., Korzhinksky, M.A., Tkachenko, S.I., and Shmulovich, K.I., 1995, Geochemistry of magmatic gases from Kudryavy volcano, Iturup, Kuril Islands: Geochimica et Cosmochimica Acta, v. 59, p. 1749–1761.
Thompson, B., Brathwaite, B., and Chrisite, T., 1995, Mineral wealth of New Zealand: Institute of Geological and Nuclear Sciences Information Series 33, 170 p.
Thomson, E., 1928, A new telluride occurrence in Quebec: University of Toronto Studies, Geologic Series, v. 36, p. 33–36.
Tingley, J.V., Horton, R.C., and Lincoln, F.C., 1993, Outline of Nevada mining history: Nevada Bureau of Mines and Geology Special Publication 15, 48 p.
Tretbar, D.R., Arehart, G.B., and Christensen, J.N., 2000, Dating gold deposition in a Carlin-type gold deposit using Rb/Sr methods on the mineral galkhaite: Geology, v. 28, p. 947–950.
Turner, H.W., 1894, Jackson folio, California: U.S. Geological Survey, Geological Atlas of the United States, folio 11, 6 p.
United Nations, 1998, Geology and mineral resources of Kyrgyzstan: Atlas of Mineral Resources of the ESCAP Region, 163 p.
United States Department of Energy, 2010, Critical materials strategy: Washington, D.C, United States Department of Energy, 166 p.
Uspenskiy, Y.I., and Aleshin, A.P., 1993, Patterns of scheelite mineralization in the Muruntau gold deposit, Uzbekistan: International Geology Review, v. 35, p. 1037–1051.
Varekamp, J.C., and Buseck, P.R., 1984, The speciation of mercury in hydrothermal systems, with applications to ore deposition: Geochimica et Cosmochimica Acta, v. 48, p. 77–185.
Vearncombe, J.R., Cheshire, P.E., De Beer, J.H., Mallinson, W.S., McCourt, S., and Stettler, E.H., 1988, Strucutres related to the antimony line, Murchinson schist belt, Kaapvaal craton, South Africa: Tectonophysics, v. 154, p. 285–308.
Vikre, P.G., 1985, Precious metal vein systems in the National district, Humboldt County, Nevada: Economic Geology, v. 80, p. 360–393.
——1989, Ledge formation at the Sandstorm and Kendell gold mines, Goldfield, Nevada: Economic Geology, v. 84, p. 2115–2138.
——1998, Intrusion-related, polymetallic carbonate replacement deposits in the Eureka district, Eureka County, Nevada: Nevada Bureau of Mines and Geology Bulletin 110, 52 p.
Wallace, A.R., 2003, Geology of the Ivanhoe Hg-Au district, northern Nevada: Influence of Miocene volcanism, lakes, and active faulting on epithermal mineralization: Economic Geology, v. 98, p. 409–424.
Ward, A.T., 1921, Bismuth, *in* Roush, G.A., and Butts, A., eds., The Mineral Industry: Its Statistics, Technology and Trade during 1920, Volume XXIX: New York, McGraw-Hill Book Company, 895 p.
Wardell, L.J., Kyle, P.R., and Counce, D., 2008, Volcanic emissions of metals and halogens from White Island (New Zealand) and Erebus volcano (Antarctica) determined with chemical traps: Journal of Volcanology and Geothermal Research, v. 177, p. 734–742.
Warren, I., Zuluaga, J.I., Robbins, C.H., Wulftange, W., and Simmons, S.F., 2004, Characterization of epithermal alteration and mineralization at El Peñon, northern Chile: Society of Economic Geologists Special Publication 11, p. 113–139.
Weissberg, B.G., 1969, Gold-silver ore-grade precipitates from New Zealand thermal waters: Economic Geology, v. 64, p. 95–108.

Wen, H., and Carignan, J., 2011, Selenium isotopes trace the source and redox processes in the black shale-hosted Se-rich deposits in China: Geochimica et Cosmochimica Acta, v. 75, p. 1411–1427.

White, D.E., 1981, Active geothermal systems and hydrothermal ore deposits: Economic Geology 75th Anniversary Volume, p. 392–424.

White, N.C., and Hedenquist, J.W., 1990, Epithermal environments and styles of mineralization: Variations and their causes, and guidelines for exploration: Journal of Geochemical Exploration, v. 36, p. 445–474.

——1995, Epithermal gold deposits: Styles, characteristics, and exploration: Society of Economic Geologists Newsletter 23, p. 1–13.

Wilson, J.R., Robinson, P.D., Wilson, P.N., Stanger, L.W., and Salmon, G.L., 1991, Gillulyite, $Tl_2(As,Sb)_8S_{13}$, a new thallium arsenic sulfosalt from the Mercur gold deposit, Utah: American Mineralogist, v. 76, p. 653–656.

Wood, P.C., 1991, The Hollinger-McIntyre gold-quartz vein system, Timmins, Ontoria: Geologic characteristics, fluid properties and light stable isotope geochemistry: Ontario Geological Survey, Open-File Report 5756, 289 p.

Wood, S.A., and Samson, I.M., 2000, The hydrothermal geochemistry of tungsten in granitoid environments: I. Relative solubilities of ferberite and scheelite as a function of T, P, pH, and m_{NaCl}: Economic Geology, v. 95, p. 143–182.

——2006, The aqueous geochemistry of gallium, germanium, indium and scandium: Ore Geology Reviews, v. 28, p. 57–102.

Wood, S.A., Crerar, D.A., and Borcsik, M.P., 1987, Solubility of the assemblage pyrite-pyrrhotite-magnetite-sphalerite-galena-gold-stibnite-bismuthinite-argentite-molybdenite in H_2O-NaCl-CO_2 solutions from 200° to 350°C: Economic Geology, v. 82, p. 1864–1887.

Xia, Y., Su, W.C., Zhang, X.C., and Liu, J.Z., 2012, Geochemistry and metallogenic model of Carlin-type gold deposits in southwest Guizhou province, China, *in* Panagiotarus, D., Geochemistry-earth's system processes, Chapter 7: Croatia, InTech, Rijeka, 31 p., http://www.intechopen.com/books/geochemistry-earth-s-system-processes

Xiao, T., Guha, J., Boyle, D., Liu, C-Q., and Chen, J., 2004, Environmental concerns related to high thallium levels in soils and thallium uptake by plants in southwest Guizhou, China: The Science of the Total Environment, v. 318, p. 223–244.

Xiong, Y-L., 2007, Hydrothermal thallium mineralization up to 300°C: A thermodynamic approach: Ore Geology Reviews, v. 32, p. 291–313.

Yajima, J., and Ohta, E., 1979, Two-stage mineralization and formation process of the Toyoha deposits, Hokkaido, Japan: Mining Geology, v. 29, p. 291–306.

Yakubchuk, A.S., Shatov, V.V., Kirwin, D., Edwards, A., Tommurtogoo, O., Badarch, G., and Buryak, V.A., 2005, Gold and base metal metallogeny of the central Asian orogenic supercollage: Economic Geology 100th Anniversary Volume, p. 1035–1068.

Yigit, O., and Hofstra, A.H., 2003, Lithogeochemistry of Carlin-type gold mineralization in the Gold Bar district, Battle Mountain-Eureka trend, Nevada: Ore Geology Reviews, v. 22, p. 201–224.

Zhou, T.-F., Fan, Y., Yuan, F., Wu, M.-A., Hou, M.-J., Voicu, G., Hu,Q.-H., Zhang, Q.-M., and Yue, S.C., 2005, A preliminary geological and geochemical study of the Xiangquan thallium deposit, eastern China: the world's first thallium-only mine: Mineralogy and Petrology, v. 85, p. 243–251.

Zotov, A.V., Shikina, N.D., and Akinfiev, N.N., 2003, Thermodynamic properties of the Sb(III) hydroxide complex $Sb(OH)_{3(aq)}$ at hydrothermal conditions: Geochimica et Cosmochimica Acta, v. 67, p. 1821–1836.

©2016 Society of Economic Geologists, Inc.
Reviews in Economic Geology, v. 18, pp. 245–306

Chapter 11

The Minor Element Endowment of Modern Sea-Floor Massive Sulfides and Comparison with Deposits Hosted in Ancient Volcanic Successions

Thomas Monecke,[1,†] Sven Petersen,[2] Mark D. Hannington,[2,3] Hannah Grant,[2] and Iain M. Samson[4]

[1] *Department of Geology and Geological Engineering, Colorado School of Mines, 1516 Illinois Street, Golden, Colorado 80401*

[2] *GEOMAR, Helmholtz Center for Ocean Research Kiel, Wischofstrasse 1-3, 24148 Kiel, Germany*

[3] *Department of Earth and Environmental Sciences, University of Ottawa, 140 Louis Pasteur, Ottawa, Ontario K1N 6N5, Canada*

[4] *Department of Earth and Environmental Sciences, University of Windsor, Windsor, Ontario N9B 3P4, Canada*

Abstract

Sea-floor massive sulfide deposits represent a new type of base and precious metal resources that may be exploited by future deep-sea mining operations. These deposits occur in diverse tectonic environments and are mostly located along the global mid-ocean ridge system within international waters and arc-related settings within the exclusive economic zones of the world's oceans. Much controversy is currently centered on the question whether sea-floor massive sulfide deposits represent a significant resource of metals that could be exploited to meet the metal demand of modern technology-based society.

Chemical analysis of sulfide samples from sea-floor hydrothermal vent sites worldwide shows that sea-floor massive sulfides can be enriched in the minor elements Bi, Cd, Ga, Ge, Hg, In, Mo, Sb, Se, Te, and Tl, with concentrations ranging up to several tens or hundreds of parts per million. The minor element content of sea-floor sulfides broadly varies with volcanic and tectonic setting. Massive sulfides on mid-ocean ridges commonly show high concentrations of Se, Mo, and Te, whereas arc-related sulfide deposits can be enriched in Cd, Hg, Sb, and Tl. Superposed on the volcanic and tectonic controls, the minor element content of sea-floor sulfides is strongly influenced by the temperature-dependent solubility of these elements. The high- to intermediate-temperature suite of minor elements, Bi, In, Mo, Se, and Te, is typically enriched in massive sulfides composed of chalcopyrite, while the low-temperature suite of minor elements, Cd, Ga, Ge, Hg, Sb, and Tl, is more typically associated with sphalerite-rich massive sulfides. Temperature-related minor element enrichment trends observed in modern sea-floor hydrothermal systems are broadly comparable to those encountered in fossil massive sulfide deposits.

Although knowledge on the mineralogical sequestration of the minor elements in sea-floor massive sulfide deposits is limited, a significant proportion of the total amount of minor elements contained in massive sulfides appears to be incorporated into the crystal structure of the main sulfide minerals, including pyrite, pyrrhotite, chalcopyrite, sphalerite, wurtzite, and galena. In addition, the over 80 trace minerals recognized represent important hosts of minor elements in massive sulfides. As modern sea-floor sulfides have not been affected by metamorphic recrystallization and remobilization, the minor element distribution and geometallurgical properties of the massive sulfides may differ from those of ancient massive sulfide deposits.

The compilation of geochemical data from samples collected from hydrothermal vent sites worldwide now permits a first-order evaluation of the global minor element endowment of sea-floor sulfide deposits. Based on an estimated 600 million metric tons (Mt) of massive sulfides in the neovolcanic zones of the world's oceans, the amount of minor elements contained in sea-floor deposits is fairly small when compared to land-based mineral resources. Although some of the minor elements are potentially valuable commodities and could be recovered as co- or by-products from sulfide concentrates, sea-floor massive sulfide deposits clearly do not represent a significant or strategic future resource for these elements.

Introduction

The discovery of hydrothermal venting on the modern sea floor over 35 years ago represented one of the most significant scientific discoveries ever made. It resulted in the identification of chemosynthetic vent communities (Lonsdale, 1977; Corliss et al., 1979; Jannasch and Wirsen, 1979; Jannasch, 1985) and the possible link between sea-floor high-temperature processes and the origin of life (Corliss et al., 1981; Baross and Hoffman, 1985; Maher and Stevenson, 1988; Huber and Wächtershäuser, 1998; Martin et al., 2008). In addition, early workers already recognized that sea-floor hydrothermal vent sites can be associated with significant accumulations of polymetallic sulfides (Francheteau et al., 1979, 1981; Hekinian et al., 1980; Koski et al., 1984), resembling ancient massive sulfide deposits hosted by volcanic rocks emplaced in submarine settings (Franklin et al., 2005; Hannington, 2014).

Today, sea floor research and exploration has resulted in the discovery of over 600 active and inactive hydrothermal sites in the world's oceans (Beaulieu et al., 2013; S. Petersen, unpub. data). They occur primarily at mid-ocean ridges, but also in submarine volcanic arcs and related back-arc basins. Over 330 active and inactive hydrothermal vent sites in these settings are known to be associated with sulfide and sulfide precipitates. However, sea-floor massive sulfide deposits have

† Corresponding author: e-mail, tmonecke@mines.edu

only been described from 237 sites (Baker and German, 2004; Hannington et al., 2005; Beaulieu et al., 2013; Monecke et al., 2014; this study).

Chemical analysis of recovered sample material has shown that sea-floor massive sulfide deposits formed in association with high-temperature venting may contain significant contents of base and precious metals (Herzig and Hannington, 1995; Hannington et al., 2005, 2010; Monecke et al., 2014), with grades that are not unlike those encountered in ancient massive sulfide deposits (Barrie and Hannington, 1999; Galley and Koski, 1999; Franklin et al., 2005). Recent developments suggest that the high base and precious metal grades of some sea-floor massive sulfide deposits make them potentially viable targets for deep-sea mining (Hannington et al., 2010, 2011; Hoagland et al., 2010; Van Dover, 2011). For legal reasons, commercial exploration for sea-floor massive sulfide deposits has so far been largely restricted to active volcanic arcs and related back-arc basins located in the exclusive economic zones of the world's oceans. However, recently implemented new regulations by the United Nations, through the International Seabed Authority, now also allow prospecting and exploration of sea-floor massive sulfide deposits in international water (Decision of the Assembly of the International Seabed Authority, ISBA/16/A/12/Rev.1, 49 p., 11/15/10), where some of the largest known sea-floor massive sulfide deposits are located. So far, this has resulted in six contracts between national agencies (China, France, Germany, India, Russia, and South Korea) and the International Seabed Authority, focusing on exploration in the Indian Ocean and the Atlantic. The onset of commercial mineral exploration of the world's oceans has raised the question how significant sea-floor massive sulfide deposits really are as a potential future source of base metals and other elements (Glasby, 2000; Scott, 2001; Rona, 2003; Cathles, 2011a, b; Hannington, 2011; Hannington et al., 2011; Singer, 2014).

The present contribution provides a comprehensive review of the different tectonic settings of sea-floor massive sulfide deposits and discusses the links between geodynamic setting and the size and composition of the deposits. Information on the minor element content of sea-floor massive sulfide deposits and the mineralogical sequestration of these elements in the massive sulfides has been compiled to constrain the geochemical behavior of these elements in sea-floor hydrothermal systems. Based on the available size and compositional data of sea-floor massive sulfide deposits, an initial assessment of the global minor element endowment of this deposit type is conducted. This assessment provides a first-order answer to the question whether sea-floor massive sulfide deposits represent a possible future source of minor elements for modern technology-based society.

Tectonic Settings and Global Distribution

Following the discovery of low-temperature venting at the Galapagos rift in 1977 (Corliss et al., 1979; Williams et al., 1979) and sea-floor sulfides and high-temperature venting at the East Pacific Rise in 1978 and 1979 (Francheteau et al., 1979, 1981; Hekinian et al., 1980; Macdonald et al., 1980; Spiess et al., 1980; Haymon and Kastner, 1981), marine research largely focused on the exploration of the global mid-ocean ridges, even in remote locations such as the high Arctic (Edmonds et al., 2003; Pedersen et al., 2010a, b). As a result, discoveries have been made in almost all parts of the oceans (Fig. 1).

Mid-ocean ridges

A total of 129 basalt-hosted sea-floor massive sulfide deposits are located along the ca. 54,700 km (cf. Bird, 2003) of mid-ocean ridges (Table 1; Fig. 1). These are largely situated along fast-spreading ridges (full spreading rates of >60 mm/yr) such as the East Pacific Rise (Francheteau et al., 1979, 1981; Hekinian et al., 1980; McConachy et al., 1986; Auzende et al., 1996b; Haymon and White, 2004; Hey et al., 2006) and the Pacific-Antarctic Ridge (Stoffers et al., 2002). Fast-spreading ocean ridges develop in relatively thin oceanic crust and are typified by abundant eruptions of mid-ocean ridge basalt (Hannington et al., 2005). Eruption rates are high and occur at intervals of tens of years in cycles lasting hundreds to thousands of years (Haymon et al., 1991, 1993). During the frequent volcanic eruptions, sulfide deposits accumulating at the sea floor can be buried by the lavas (Auzende et al., 1994). Due to the frequent eruptions and the rapid displacement of the deposit from the heat source, hydrothermal vent complexes are short-lived, producing comparably small sea-floor massive sulfide deposits (Fouquet, 1997).

Mid-ocean ridges that have an intermediate-spreading rate (40–60 mm/yr) are characterized by lower rates of magma supply, deeper axial valleys and a higher proportion of off-axis volcanism (Hannington et al., 2005). Sea-floor massive sulfide deposits on intermediate-rate spreading ridges include those on the Central Indian Ridge (Herzig and Plüger, 1988; Halbach et al., 1998; Münch et al., 1999; Van Dover et al., 2001; Kumagai et al., 2008; Nakamura et al., 2012), the Juan de Fuca Ridge (Normark et al., 1983; Delaney et al., 1992; Koski et al., 1994a; Glickson et al., 2007; Kelley et al., 2012; Jamieson et al., 2014a), the Galapagos rift (Corliss et al., 1979; Embley et al., 1988; Haymon et al., 2008), and the Gorda Ridge (Koski et al., 1988; Zierenberg et al., 1993). The axial magma chambers of these spreading centers typically occur 2.5 to 3.5 km below the sea floor (Perfit et al., 1999) and volcanic eruptions take place in intervals of hundreds of years (Embley et al., 2000). Although intermediate-rate spreading centers are dominated by mid-ocean ridge basalt, more evolved lavas may occur locally (Perfit et al., 1999).

Slow-spreading mid-ocean ridges (20–40 mm/yr) occur in relatively thick oceanic crust and show intermittent volcanism between periods of volcanic quiescence that are tens of thousands of years in length (Hannington et al., 2005). Slow-spreading takes place along the Mid-Atlantic Ridge, which is host to a number of large hydrothermal vent systems (Rona et al., 1993, 1996; Humphris et al., 1995; Haase et al., 2007; Ondréas et al., 2009; Fouquet et al., 2010; Cherkashev et al., 2013; Wheeler et al., 2013), and the Carlsberg Ridge, where sea-floor massive sulfide occurrences were first documented in 2012 (Tao et al., 2013). Lava compositions at slow-spreading ridges range from normal incompatible element-depleted basalt to enriched basalt, but serpentinized mantle rocks are also present. Subaxial magma chambers are deep or may be even absent. Penetration of seawater into the oceanic crust occurs mostly along deeply penetrating faults to as much as 10 km below the sea floor (deMartin et al., 2007; McCaig et al., 2007; Andersen et al., 2015).

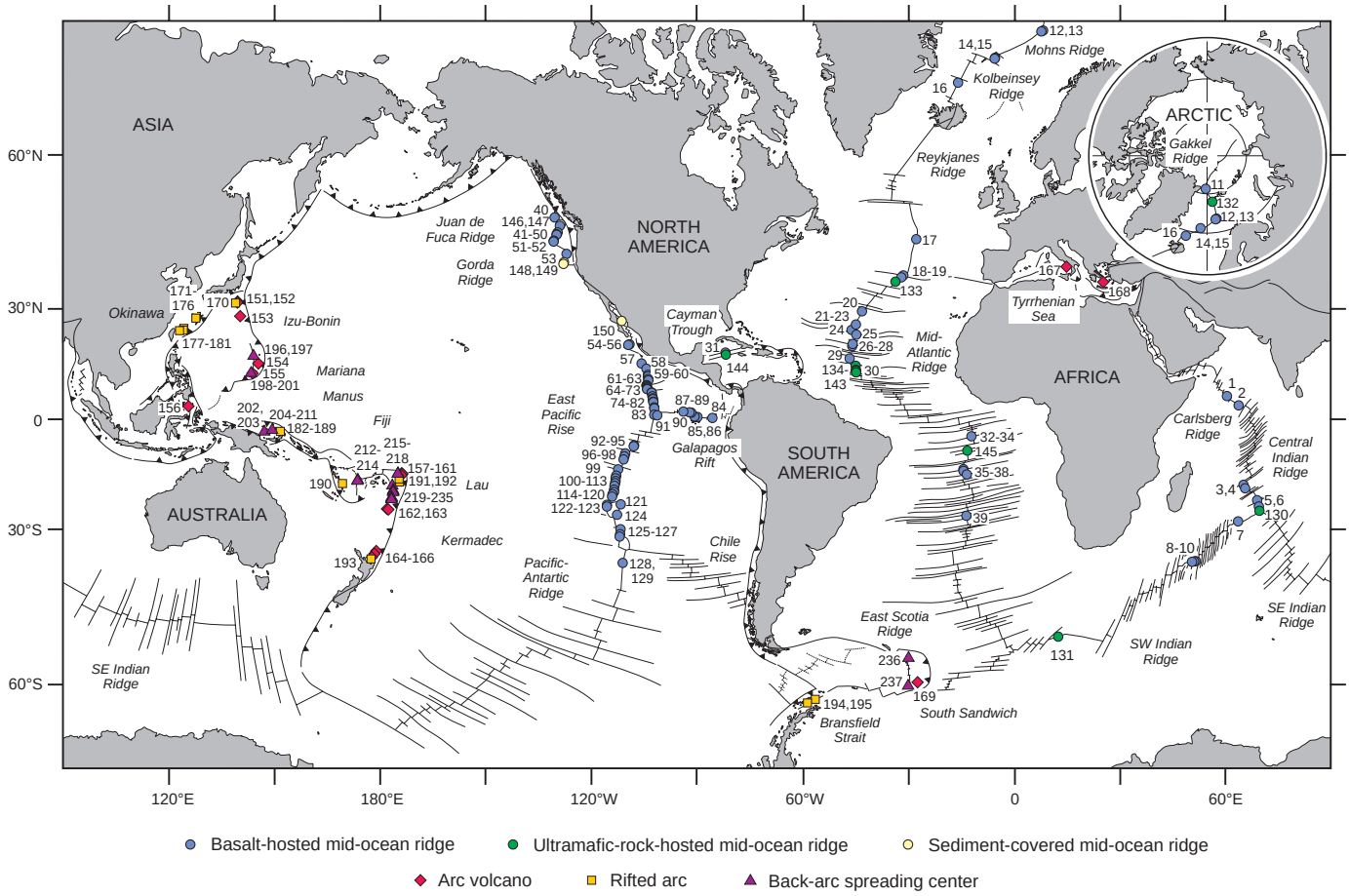

Fig. 1. Locations of sea-floor massive sulfide deposits in the world's oceans. The distribution partly reflects the amount of sea-floor exploration done in any region. The deposits are keyed to Tables 1 and 2. Major mid-ocean ridges and subduction zones are indicated.

Sea-floor massive sulfide deposits associated with ultraslow-spreading centers (<20 mm/yr) account for only a small percentage of all deposits located along the global mid-ocean ridges (Table 1). Examples include those on the Southwest Indian Ridge in the Indian Ocean (Münch et al., 2001; Bach et al., 2002; Tao et al., 2012), the Arctic mid-ocean ridge segments (Edmonds et al., 2003; Pedersen et al., 2010a, b), and the Cayman trough (Kinsey and German, 2013; Webber et al., 2015). Sea-floor massive sulfide deposits at these spreading centers are hosted by mid-ocean ridge basalt or serpentinized abyssal peridotite.

Sea-floor massive sulfide deposits have also been identified on mid-ocean ridges that are covered by sediments derived from nearby continental margins. This includes sites at Middle Valley (Davis et al., 1992; Fouquet et al., 1998; Zierenberg et al., 1998; Zierenberg and Miller, 2000), the Escanaba trough (Koski et al., 1988; Zierenberg et al., 1993, 1994), and the Guaymas basin (Koski et al., 1985; Peter and Scott, 1988). The sedimentation rates at these locations are very high, ranging from 0.1 to 1 mm/yr, when compared to the open ocean pelagic sedimentation rate of approximately 0.01 mm/yr (Hannington et al., 2005). Due to the thick turbidite cover (200 to >1,000 m), volcanic activity in this setting is largely restricted to shallow subseafloor intrusions (Einsele, 1985; Davis and Villinger, 1992). As a consequence, sea-floor massive sulfide deposits on sediment-covered ridges are mostly associated with sill complexes, with the largest part of the massive sulfide accumulation formed through subseafloor replacement within the sediments (Fouquet et al., 1998; Zierenberg et al., 1998).

Arc-related settings

Although early research already suggested the existence of hydrothermal vent sites in arc-related settings (Bertine and Keene, 1975; Craig et al., 1987), marine exploration in this environment only commenced with the discovery of hydrothermal vent fields in the Manus basin in 1986 (Both et al., 1986; Binns and Scott, 1993), the Okinawa trough in 1988 (Halbach et al., 1989, 1993), the Lau basin in 1989 (Fouquet et al., 1993a), and the North Fiji basin in 1989 (Auzende et al., 1989; Bendel et al., 1993). However, the majority of the marine exploration of submarine volcanic arc volcanoes has only been carried out in recent years (Iizasa et al., 1999; de Ronde et al., 2001, 2007; Embley et al., 2004; Stoffers et al., 2006; Monecke et al., 2009; Petersen et al., 2014).

Over the past decades, a total of 140 sea-floor hydrothermal vent sites with associated sulfide and sulfate precipitates have been discovered in arc-related settings worldwide (Monecke et al., 2014; this study), which includes 87 sea-floor massive sulfide deposits (Table 2; Fig. 1).

Table 1. Sea-floor Massive Sulfide Deposits at Mid-Ocean Ridges (modified from Hannington et al., 2005)

No.	Deposit	Location	Setting	Depth (m)	Spreading rate (mm/yr)[1]	Temp. (°C)
Basalt-hosted mid-ocean ridge						
1	60°31'E	Carlsberg Ridge	Slow-spreading ridge	2,900–3,100	25	-
2	63°50'E	Carlsberg Ridge	Slow-spreading ridge	3,500	28	-
3	Dodo	Central Indian Ridge	Intermediate-rate spreading ridge	2,750	41	356
4	Solitaire	Central Indian Ridge	Intermediate-rate spreading ridge	2,610	42	296
5	MESO zone	Central Indian Ridge	Intermediate-rate spreading ridge	2,850–2,900	45	-
6	Edmond	Central Indian Ridge	Intermediate-rate spreading ridge	3,290–3,320	46	382
7	Mount Jourdanne	Southwest Indian Ridge	Ultra-slow spreading ridge	2,940–2,960	13	-
8	SWIR 51°44'E	Southwest Indian Ridge	Ultra-slow spreading ridge	1,600	15	-
9	SWIR 50°28'E	Southwest Indian Ridge	Ultra-slow spreading ridge	1,740–1,770	15	-
10	Longqi	Southwest Indian Ridge	Ultra-slow spreading ridge	2,760	15	379
11	Aurora	Gakkel Ridge	Ultra-slow spreading ridge	4,100	13	-
12	Loki's Castle	Mohns Ridge	Ultra-slow spreading ridge	2,350	15	317
13	Mohn's Treasure	Mohns Ridge	Ultra-slow spreading ridge	2,600	15	-
14	Trollvegen	Mohns Ridge	Ultra-slow spreading ridge	520–590	17	260
15	Soria Moria	Mohns Ridge	Ultra-slow spreading ridge	710	17	270
16	Squid Forest	Kolbeinsey Ridge	Ultra-slow spreading ridge	900	17	-
17	Moytirra	Mid-Atlantic Ridge	Slow-spreading ridge	2,100	22	-
18	Menez Gwen	Mid-Atlantic Ridge	Slow-spreading ridge	810–870	20	284
19	Lucky Strike	Mid-Atlantic Ridge	Slow-spreading ridge	1,620–1,740	20	333
20	Broken Spur	Mid-Atlantic Ridge	Slow-spreading ridge	3,050–3,110	23	364
21	Alvin zone	Mid-Atlantic Ridge	Slow-spreading ridge	3,400–3,600	23	-
22	Mir zone	Mid-Atlantic Ridge	Slow-spreading ridge	3,430–3,580	23	-
23	TAG	Mid-Atlantic Ridge	Slow-spreading ridge	3,630–3,670	23	369
24	MAR 24°30'N	Mid-Atlantic Ridge	Slow-spreading ridge	3,900	24	-
25	Snake Pit	Mid-Atlantic Ridge	Slow spreading ridge	3,430–3,530	24	366
26	Puy des Folles	Mid-Atlantic Ridge	Slow spreading ridge	1,940–2,000	24	-
27	Zenith-Victory	Mid-Atlantic Ridge	Slow spreading ridge	2,370–2,600	24	-
28	Peterburgskoe	Mid-Atlantic Ridge	Slow spreading ridge	2,850–3,050	25	-
29	Krasnov	Mid-Atlantic Ridge	Slow spreading ridge	3,700–3,750	25	-
30	Semyenov-4	Mid-Atlantic Ridge	Slow spreading ridge	2,560–2,950	24	-
31	Beebe	Cayman trough	Ultra-slow spreading ridge	4,940–5,010	19	401
32	Red Lion	Mid-Atlantic Ridge	Slow-spreading ridge	3,050	31	348
33	Comfortless Cove	Mid-Atlantic Ridge	Slow-spreading ridge	3,000	31	400
34	Turtle Pits	Mid-Atlantic Ridge	Slow-spreading ridge	2,990	31	407
35	Baily's Beads	Mid-Atlantic Ridge	Slow-spreading ridge	2,290	32	-
36	Rainbow Bay North	Mid-Atlantic Ridge	Slow-spreading ridge	1,900	32	-
37	Rainbow Bay South	Mid-Atlantic Ridge	Slow-spreading ridge	2,900	32	-
38	MAR 15°10'S	Mid-Atlantic Ridge	Slow-spreading ridge	2,790	32	-
39	Merian	Mid-Atlantic Ridge	Slow-spreading ridge	2,550	33	-
40	Southern Explorer	Juan de Fuca Ridge	Intermediate-rate spreading ridge	1,850	53	306
41	Sasquatch	Juan de Fuca Ridge	Intermediate-rate spreading ridge	2,200	52	287
42	Salty Dawg	Juan de Fuca Ridge	Intermediate-rate spreading ridge	2,130	52	305
43	High-Rise, Endeavour	Juan de Fuca Ridge	Intermediate-rate spreading ridge	2,160–2,170	52	352
44	Main vent field, Endeavour	Juan de Fuca Ridge	Intermediate-rate spreading ridge	2,200–2,220	52	402
45	Mothra, Endeavour	Juan de Fuca Ridge	Intermediate-rate spreading ridge	2,270	52	319
46	JdFR 46°41'N	Juan de Fuca Ridge	Intermediate-rate spreading ridge	2,400–2,410	51	223
47	Co-Axial	Juan de Fuca Ridge	Intermediate-rate spreading ridge	2,055	51	294
48	CASM, Axial Smt.	Juan de Fuca Ridge	Intermediate-rate spreading ridge	1,570–1,580	51	-
49	ASHES, Axial Smt.	Juan de Fuca Ridge	Intermediate-rate spreading ridge	1,540–1,550	51	345
50	International District, Axial Smt.	Juan de Fuca Ridge	Intermediate-rate spreading ridge	1,520–1,530	51	347
51	North Cleft	Juan de Fuca Ridge	Intermediate-rate spreading ridge	2,245–2,270	50	327
52	South Cleft	Juan de Fuca Ridge	Intermediate-rate spreading ridge	2,200–2,220	49	342
53	Sea Cliff	Gorda Ridge	Intermediate-rate spreading ridge	2,730	49	308
54	EPR 20°54'N	East Pacific Rise	Fast-spreading ridge	2,620	59	-
55	EPR 20°50'N	East Pacific Rise	Fast-spreading ridge	2,600	60	355
56	Green Smt.	East Pacific Rise	Fast-spreading ridge	1,830–1,950	61	-
57	Teotihuacan	East Pacific Rise	Fast-spreading ridge	2,300	85	-
58	EPR 14°09'N	East Pacific Rise	Fast-spreading ridge	2,600	90	-
59	EPR 12°49'N	East Pacific Rise	Fast-spreading ridge	2,600–2,700	94	350
60	EPR 12°42'N Seamount	East Pacific Rise	Fast-spreading ridge	2,500–2,600	94	-
61	87D-C Smt.	East Pacific Rise	Fast-spreading ridge	2,240	98	-
62	87D-D1 Smt.	East Pacific Rise	Fast-spreading ridge	2,190	98	-
63	EPR 10°56'N	East Pacific Rise	Fast-spreading ridge	2,520–2,530	99	347
64	EPR 9°50'N	East Pacific Rise	Fast-spreading ridge	2,520	102	386
65	EPR 9°47'N	East Pacific Rise	Fast-spreading ridge	2,530	102	403
66	EPR 9°41'N	East Pacific Rise	Fast-spreading ridge	2,560	103	313
67	EPR 9°39'N	East Pacific Rise	Fast-spreading ridge	2,570	103	345

Table 1. *(Cont.)*

No.	Deposit	Location	Setting	Depth (m)	Spreading rate (mm/yr)[1]	Temp. (°C)
Basalt-hosted mid-ocean ridge *(Cont.)*						
68	EPR 9°33'N	East Pacific Rise	Fast-spreading ridge	2,570	103	308
69	EPR 9°30'N	East Pacific Rise	Fast-spreading ridge	2,580	103	263
70	EPR 9°17'N	East Pacific Rise	Fast-spreading ridge	2,590	104	388
71	Medusa	East Pacific Rise	Fast-spreading ridge	2,580	104	330
72	EPR 8°53'N	East Pacific Rise	Fast-spreading ridge	2,500–2,600	105	-
73	EPR 8°38'N	East Pacific Rise	Fast-spreading ridge	2,550	105	-
74	EPR 7°54'N	East Pacific Rise	Fast-spreading ridge	2,700–2,800	108	-
75	EPR 7°43'N	East Pacific Rise	Fast-spreading ridge	2,740–2,860	109	-
76	EPR 6°50'N	East Pacific Rise	Fast-spreading ridge	2,700–2,800	111	-
77	EPR 6°14'N	East Pacific Rise	Fast-spreading ridge	2,700–2,800	112	-
78	EPR 6°00'N	East Pacific Rise	Fast-spreading ridge	2,700–2,800	113	-
79	EPR 5°15'N	East Pacific Rise	Fast-spreading ridge	2,700–2,800	115	-
80	EPR 5°00'N	East Pacific Rise	Fast-spreading ridge	2,700–2,800	115	-
81	EPR 3°35'N	East Pacific Rise	Fast-spreading ridge	2,700–2,800	119	-
82	EPR 2°40'N	East Pacific Rise	Fast-spreading ridge	3,020–3,090	122	-
83	EPR 1°44'N	East Pacific Rise	Fast-spreading ridge	2,850	111	-
84	85°51'W	Galapagos rift	Intermediate-rate spreading ridge	2,540–2,600	60	-
85	89°14'W	Galapagos rift	Intermediate-rate spreading ridge	1,720	57	-
86	90°33'W	Galapagos rift	Intermediate-rate spreading ridge	1,530	56	-
87	91°14'W	Galapagos rift	Intermediate-rate spreading ridge	1,750	56	-
88	91°23'W	Galapagos rift	Intermediate-rate spreading ridge	1,620	56	-
89	Iguanos-Pinguinos	Galapagos rift	Intermediate-rate spreading ridge	1,620–1,650	55	-
90	Navidad	Galapagos rift	Intermediate-rate spreading ridge	2,390–2,400	53	-
91	Precious Stone Mountain	Galapagos Microplate	Slow-spreading ridge	1,450–1,700	32	-
92	EPR 7°22'S	East Pacific Rise	Fast-spreading ridge	2,735	133	-
93	EPR 7°24'S	East Pacific Rise	Fast-spreading ridge	2,740–2,750	133	-
94	EPR 7°25'S	East Pacific Rise	Fast-spreading ridge	2,740–2,750	133	-
95	EPR 7°45'S	East Pacific Rise	Fast-spreading ridge	2,720	133	-
96	EPR 9°41'S	East Pacific Rise	Fast-spreading ridge	2,630	135	-
97	EPR 10°34'S	East Pacific Rise	Fast-spreading ridge	2,660–2,670	136	-
98	EPR 11°18'S	East Pacific Rise	Fast-spreading ridge	2,650	137	-
99	EPR 13°59'S	East Pacific Rise	Fast-spreading ridge	2,620–2,640	139	374
100	EPR 15°45'S	East Pacific Rise	Fast-spreading ridge	2,620–2,630	141	-
101	EPR 16°43'S	East Pacific Rise	Fast-spreading ridge	2,650–2,660	141	-
102	EPR 17°12'S	East Pacific Rise	Fast-spreading ridge	2,600–2,620	142	-
103	EPR 17°22'S	East Pacific Rise	Fast-spreading ridge	2,630–2,740	142	-
104	EPR 17°25'S	East Pacific Rise	Fast-spreading ridge	2,570–2,740	142	376
105	EPR 17°35'S	East Pacific Rise	Fast-spreading ridge	2,590–2,620	142	349
106	EPR 17°37'S	East Pacific Rise	Fast-spreading ridge	2,590–2,620	142	350
107	EPR 17°44'S	East Pacific Rise	Fast-spreading ridge	2,620–2,640	142	350
108	EPR 18°11'S	East Pacific Rise	Fast-spreading ridge	2,670	142	305
109	EPR 18°15'S	East Pacific Rise	Fast-spreading ridge	2,650–2,680	142	310
110	EPR 18°25'S	East Pacific Rise	Fast-spreading ridge	2,630–2,660	142	382
111	EPR 18°26'S	East Pacific Rise	Fast-spreading ridge	2,620–2,630	142	345
112	EPR 18°32'S	East Pacific Rise	Fast-spreading ridge	2,640	142	-
113	EPR 18°37'S	East Pacific Rise	Fast-spreading ridge	2,640–2,660	142	-
114	EPR 20°06'S	East Pacific Rise	Fast-spreading ridge	2,900	143	-
115	EPR 20°40'S	East Pacific Rise	Fast-spreading ridge	3,050	143	-
116	EPR 20°50'S	East Pacific Rise	Fast-spreading ridge	3,000	144	-
117	EPR 21°25'S	East Pacific Rise	Fast-spreading ridge	2,800–2,830	144	354
118	EPR 21°29'S	East Pacific Rise	Fast-spreading ridge	2,800–2,830	144	-
119	Rapa Nui (EPR 21°33'S)	East Pacific Rise	Fast-spreading ridge	2,800–2,860	144	405
120	EPR 21°40'S	East Pacific Rise	Fast-spreading ridge	2,700	144	-
121	Pito Smt.	East Pacific Rise	Slow-spreading ridge	2,240–2,270	36	-
122	EPR 23°32'S	East Pacific Rise	Fast-spreading ridge	2,600	107	-
123	EPR 23°50'S	East Pacific Rise	Fast-spreading ridge	2,650–2,660	100	-
124	EPR 26°12'S	East Pacific Rise	Fast-spreading ridge	2,600	101	-
125	EPR 29°45'S	East Pacific Rise	Fast-spreading ridge	2,500–2,520	146	-
126	EPR 31°09'S	East Pacific Rise	Fast-spreading ridge	2,330	146	378
127	EPR 31°52'S	East Pacific Rise	Fast-spreading ridge	2,330	187	370
128	PAR 37°40'S	Pacific-Antarctic Ridge	Fast-spreading ridge	2,180–2,210	95	-
129	PAR 37°48'S	Pacific-Antarctic Ridge	Fast-spreading ridge	2,210–2,230	95	-
Ultramafic rock-hosted mid-ocean ridge						
130	Kairei	Central Indian Ridge	Intermediate-rate spreading ridge	2,420–2,460	47	365
131	SWIR 12°30'E	Southwest Indian Ridge	Ultra-slow spreading ridge	3,730	15	-
132	Lucky B	Lena trough	Ultra-slow spreading ridge	3,010–3,700	14	-

Table 1. *(Cont.)*

No.	Deposit	Location	Setting	Depth (m)	Spreading rate (mm/yr)[1]	Temp. (°C)
Ultramafic rock-hosted mid-ocean ridge *(Cont.)*						
133	Rainbow	Mid-Atlantic Ridge	Slow-spreading ridge	2,260–2,400	20	370
134	Logatchev-1	Mid-Atlantic Ridge	Slow spreading ridge	2,910–3,060	24	359
135	Logatchev-2	Mid-Atlantic Ridge	Slow spreading ridge	2,700	24	320
136	Semyenov-1	Mid-Atlantic Ridge	Slow spreading ridge	2,570–2,620	24	-
137	Semyenov-2	Mid-Atlantic Ridge	Slow spreading ridge	2,420–2,480	24	317
138	Semyenov-3	Mid-Atlantic Ridge	Slow spreading ridge	2,400–2,600	24	-
139	Semyenov-5	Mid-Atlantic Ridge	Slow spreading ridge	2,160–2,340	24	-
140	Irinovskoe	Mid-Atlantic Ridge	Slow spreading ridge	2,700–2,770	24	364
141	Ashadze-2	Mid-Atlantic Ridge	Slow spreading ridge	3,260	24	296
142	Ashadze-3	Mid-Atlantic Ridge	Slow spreading ridge	4,100–4,200	24	-
143	Ashadze-1	Mid-Atlantic Ridge	Slow spreading ridge	4,065–4,120	24	372
144	Von Damm	Mid-Cayman trough	Ultra-slow spreading ridge	2,300	19	226
145	Nibelungen	Mid-Atlantic Ridge	Slow-spreading ridge	2,890–2,900	32	372
Sediment-covered mid-ocean ridge						
146	Dead Dog, Middle Valley	Juan de Fuca Ridge	Intermediate-rate spreading ridge	2,420–2,430	53	276
147	Bent Hill and ODP Mound, Middle Valley	Juan de Fuca Ridge	Intermediate-rate spreading ridge	2,440–2,460	53	265
148	Northern Escanaba trough	Gorda Ridge	Intermediate-rate spreading ridge	3,250–3,330	47	218
149	Southern Escanaba trough	Gorda Ridge	Intermediate-rate spreading ridge	3,180–3,260	47	-
150	Southern trough, Guaymas basin	Gulf of California	Sediment-filled pull-apart basin	2,000–2,020	51	359

[1] Spreading rates were calculated using the MORVEL56 model (DeMets et al., 2010)

Site descriptions: [1] Chen and Li (2013), X. Han (unpub. data); [2] Tao et al. (2013); [3, 4] Nakamura et al. (2012); [5] Herzig and Plüger (1988), Halbach et al. (1998), Münch et al. (1999); [6] Van Dover et al. (2001), Kumagai et al. (2008); [7] Fujimoto et al. (1999), Münch et al. (2000, 2001); [8-10] Tao et al. (2009, 2012, unpub. data); [11] Edmonds et al. (2003), Baker et al. (2004); [12] Pedersen et al. (2010a, b), Eickmann et al. (2014); [13] Pedersen et al. (2010b); [14, 15] Pedersen et al. (2010b), Schander et al. (2010), Sweetman et al. (2013); [16] Pedersen et al. (1999, 2010b); [17] Wheeler et al. (2013); [18] Charlou et al. (2000), Marcon et al. (2013), Dubilier et al. (2015); [19] Charlou et al. (2000), Ondréas et al. (2009); [20] Butler et al. (1998); [21, 22] Rona et al. (1993, 1996); [23] Rona et al. (1993, 1996), Humphris et al. (1995), Petersen et al. (2000); [24] Sudarikov et al. (1990); [25] Detrick et al. (1986), Karson and Brown (1988), Fouquet et al. (1993b); [26, 27] Cherkashov et al. (2010a); [28] Shilov et al. (2011), Gablina et al. (2015); [29] Beltenev et al. (2004), Cherkashov et al. (2010a); [30] Beltenev et al. (2007, 2009), Cherkashov et al. (2010a); [31] Connelly et al. (2012), Kinsey and German (2013), Webber et al. (2015); [32, 33] Haase et al. (2007); [34] Haase et al. (2007), Koschinsky et al. (2008); [35] Tao et al. (2011a); [36, 37] Tao et al. (2011b), Li et al. (2014); [38, 39] Ye et al. (2014); [40] Tunnicliffe et al. (1986); [41, 42] Kelley et al. (2012); [43] Kelley et al. (2012), Jamieson et al. (2014a); [44] Delaney et al. (1992); Kelley et al. (2012), Jamieson et al. (2014a); [45] Kelley et al. (2001, 2012), Glickson et al. (2007), Jamieson et al. (2014a); [46] Bobbitt (2007); [47] Butterfield et al. (1997); [48] Hannington and Scott (1988); [49] Butterfield et al. (1990); [50] Kelley et al. (2014); [51] Koski et al. (1994a); [52] Normark et al. (1983, 1987); [53] Von Damm et al. (2006); [54] Francheteau et al. (1979, 1981), Hekinian et al. (1980); [55] Spiess et al. (1980), Macdonald et al. (1980), Haymon and Kastner (1981); [56] Alt et al. (1987), Alt (1988); [57] Gente et al. (2010); [58] Vanko et al. (1991); [59] Hekinian et al. (1983), Fouquet et al. (1988), Desbruyères (1995); [60] Hekinian et al. (1983), Fouquet et al. (1988); [61, 62] Kuriyama et al. (1994); [63] McConachy et al. (1986), Ballard et al. (1988); [64-70] Haymon et al. (1991), Von Damm (2000); [71] National Science Foundation 04/18/07; [72] Krasnov et al. (1995a); [73] Bohnenstiehl et al. (2003); [74] Krasnov et al. (1995a); [75] Boulegue et al. (1984); [76-81] Krasnov et al. (1995a); [82] Klein et al. (2003); [83] Shank et al. (2000); [84] Corliss et al. (1979), Embley et al. (1988); [85] Werner et al. (2010); [86-90] Haymon et al. (2008); [91] Tao et al. (2011c); [92] Jollivet et al. (2004); [93] Marchig (1989), Marchig et al. (1997); [94] Jollivet et al. (2004); [95-97] Marchig (1989); [98] Marchig (1989), Lupton et al. (1999); [99] Fujioka et al. (1995), Jollivet et al. (2004); [100] Marchig (1989); [101] Marchig (1989), Marchig et al. (1997); [102] Marchig (1989), Auzende et al. (1996b); [103] Auzende et al. (1996b), Halanych et al. (1999); [104] Auzende et al. (1996b), Charlou et al. (1996), Halanych et al. (1999), Jollivet et al. (2004); [105] Jollivet et al. (2004); [106] Haymon and White (2004); [107] R.M. Haymon (unpub. data); [108] Auzende et al. (1996b), Charlou et al. (1996); [109] Auzende et al. (1996b); [110] Gundlach and Marchig (1986); [111] Auzende et al. (1996b), Charlou et al. (1996); [112] Tufar et al. (1984), Bäcker et al. (1985), Gundlach and Marchig (1986); [113] Auzende et al. (1996b), Jollivet et al. (2004); [114] Francheteau and Ballard (1983); [115, 116] Macdonald et al. (1988); [117] Marchig et al. (1987), Jollivet et al. (2004); [118] Tufar et al. (1984), Bäcker et al. (1985), Gundlach and Marchig (1986), Marchig et al. (1987); [119] Von Damm et al. (2003), Jollivet et al. (2004); [120] Krasnov et al. (1995a); [121] Verati et al. (1999); [122] Marchig et al. (1987); [123] Marchig (1989); [124] Marchig et al. (1987); [125] Marchig (1989); [126, 127] Hey et al. (2006); [128, 129] Stoffers et al. (2001, 2002); [130] Hashimoto et al. (2001), Van Dover et al. (2001); [131] Bach et al. (2002); [132] Jokat (2000), Snow et al. (2001); [133] Marques et al. (2006), Dyment et al. (2009); [134] Petersen et al. (2009); [135] Fouquet et al. (2008); [136-138] Beltenev et al. (2007); [139] Beltenev et al. (2009); [140] Jamieson et al. (2014b), Melekestseva et al. (2014a); [141] Beltenev et al. (2005), Ondréas et al. (2012); [142] Beltenev et al. (2005); [143] Ondréas et al. (2012); [144] Connelly et al. (2012); [145] Melchert et al. (2008); [146] Ames et al. (1993), Fouquet et al. (1998), Zierenberg and Miller (2000); [147] Davis et al. (1987, 1992), Ames et al. (1993), Fouquet et al. (1998), Zierenberg et al. (1998), Zierenberg and Miller (2000); [148] Koski et al. (1988, 1994b), Fouquet et al. (1998), Zierenberg et al. (1993, 1994), Zierenberg and Miller (2000); [149] Koski et al. (1988, 1994b), Zierenberg et al. (1993, 1994); and [150] Koski et al. (1985), Peter and Scott (1988)

Vent temperatures: [3, 4] Nakamura et al. (2012); [6] Van Dover et al. (2001); [10] Tao et al. (unpub. data); [12, 14] Pedersen et al. (2010b); [15] Sweetman et al. (2013); [18, 19] Charlou et al. (2000); [20] James et al. (1995); [23] Edmonds et al. (1996); [25] Butterfield et al. (2003); [31] Webber et al. (2015); [32, 33] Haase et al. (2007); [34] Koschinsky et al. (2008); [40] Hannington et al. (1991); [41, 42] Kelley et al. (2012); [43] Merle (2011); [44] Kelley et al. (2012); [45] Glickson et al. (2007); [46] Bobbitt (2007); [47] Butterfield et al. (1997); [49] Merle (2011); [50] Kelley et al. (2014); [51] Butterfield and Massoth (1994); [52] Butterfield et al. (2003); [53] Von Damm et al. (2006); [55] Butterfield et al. (2003); [59] Pester et al. (2011); [63] McConachy et al. (1986); [64-70] Von Damm (2000); [71] National Science Foundation 04/18/07; [99] Fujioka et al. (1995); [104-107] Shanks (2001); [108] Charlou et al. (1996); [109] Auzende et al. (1996b); [110, 111, 117] Shanks (2001); [119] Von Damm et al. (2003); [126] Hey et al. (2006); [127] Butterfield et al. (2003); [130] Van Dover et al. (2001); [133] Seyfried et al. (2011); [134] Charlou et al. (2010); [135] Fouquet et al. (2008); [137, 140] Destrigneville et al. (2015); [141, 143] Charlou et al. (2010); [144] Seewald et al. (2012); [145] Schmidt et al. (2011); [146, 147] Butterfield et al. (1994); [148] Von Damm et al. (2005); and [150] Peter and Scott (1988)

Table 2. Sea-floor Massive Sulfide Deposits in Volcanic Arcs and Related Extensional Settings (modified from Monecke et al., 2014)

No.	Deposit	Location	Setting	Depth (m)	Rate of extension/ spreading (mm/yr)[1]	Temp. (°C)
Arc volcano						
151	Sunrise	Izu-Ogasawara arc	Intraoceanic arc	1,210–1,360	-	278
152	Myojinsho	Izu-Ogasawara arc	Intraoceanic arc	1,100	-	-
153	Suiyo	Izu-Ogasawara arc	Intraoceanic arc	1,320–1,370	-	317
154	Black Forrest	Mariana arc	Intraoceanic arc	340–380	-	239
155	Forecast	Mariana arc	Intraoceanic arc	1,450–1,470	-	210
156	Kawio Barat	Sangihe arc	Transitional rear-arc	1,850	-	-
157	Mata Fitu	Tonga arc	Intraoceanic rear-arc	2,580–2,650	-	331
158	Mata Tolu	Tonga arc	Intraoceanic rear-arc	1,810–1,850	-	271
159	Mata Ua	Tonga arc	Intraoceanic rear-arc	2,350–2,370	-	>360[2]
160	Niua South	Tonga arc	Intraoceanic arc	900, 1,150–1,180	-	315
161	Volcano O	Tonga arc	Intraoceanic rear-arc	1,470, 1,635	-	-
162	Volcano 18	Tonga arc	Intraoceanic arc	930–1,030	-	260
163	Volcano 19	Tonga arc	Intraoceanic arc	385–540	-	265
164	Brothers	Kermadec arc	Intraoceanic arc	1,450, 1,540–1,690	-	302
165	Rumble II West	Kermadec arc	Intraoceanic arc	1,250–1,300, 1,300–1,350	-	-
166	Clark	Kermadec arc	Intraoceanic arc	870–895	-	221
167	Palinuro	Aeolian arc	Transitional arc	600–630	-	-
168	Kolumbo	Hellenic arc	Continental margin arc	500	-	220
169	Macintosh	South Sandwich arc	Intraoceanic arc	1,420–1,440	-	212
Rifted arc						
170	Bayonnaise knoll	Izu-Ogasawara arc	Back-arc rift in intraoceanic arc	680–820	no data	-
171	Minami-Ensei knoll	Okinawa trough	Intracontinental back-arc rift	690–710	27	278
172	Iheya North knoll	Okinawa trough	Intracontinental back-arc rift	970–1,000	30	311
173	Clam	Okinawa trough	Intracontinental back-arc rift	1,370–1,400	30	220
174	Yoron Hole	Okinawa trough	Intracontinental back-arc rift	580–600	28	247
175	JADE	Okinawa trough	Intracontinental back-arc rift	1,335–1,550	31	320
176	Hakurei	Okinawa trough	Intracontinental back-arc rift	1,600–1,650	31	326
177	Irabu NE Volcano	Okinawa trough	Intracontinental back-arc rift	1,850	43	-
178	Irabu SW Volcano	Okinawa trough	Intracontinental back-arc rift	1,640–1,660	43	-
179	Knoll E	Okinawa trough	Intracontinental back-arc rift	1,470	47	-
180	Hatoma knoll	Okinawa trough	Intracontinental back-arc rift	1,450–1,520	48	310
181	Dai-Yon	Okinawa trough	Intracontinental back-arc rift	1,320–1,390	52	328
182	Pacmanus	Manus basin	Back-arc rift in old arc crust	1,650–1,800	140	358
183	NE Pual	Manus basin	Back-arc rift in old arc crust	1,880	141	-
184	Solwara 13	Manus basin	Back-arc rift in old arc crust	1,995–2,010	141	-
185	Solwara 12	Manus basin	Back-arc rift in old arc crust	1,865–1,925	143	-
186	Solwara 5	Manus basin	Back-arc rift in old arc crust	1,650–1,680	144	-
187	Solwara 1	Manus basin	Back-arc rift in old arc crust	1,490–1,660	144	303
188	SuSu	Manus basin	Back-arc rift in old arc crust	1,150–1,260, 1,300–1,370	144	332
189	Solwara 9	Manus basin	Back-arc rift in old arc crust	1,680	144	-
190	Nifonea Ridge	Vate trough	Back-arc rift in intraoceanic arc	1,860–1,880	no data	370
191	FRSC-2	Lau basin	Back-arc rift in intraoceanic arc	1,640–1,820	76	-
192	Fonualei South	Lau basin	Back-arc rift in intraoceanic arc	940–970, 1,540–1,580	55	254
193	Calypso Vents	Taupo Volcanic zone	Fore-arc extensional zone in continental crust	160–185, 150–180, 190–200	no data	201
194	Hook Ridge	Bransfield Strait	Post-subduction marginal basin in continental crust	1,070–1,130	10	-
195	Three Sisters	Bransfield Strait	Post-subduction marginal basin in continental crust	975	10	-
Back-arc spreading center						
196	Alice Springs	Mariana trough	Spreading center distal to arc	3,595–3,640	32	287
197	18°03'N	Mariana trough	Spreading center distal to arc	3,675	33	-
198	Yamanaka	Mariana trough	Spreading center distal to arc	2,830	51	-
199	Fryer	Mariana trough	Spreading center distal to arc	2,860–2,880	51	248
200	Archean	Mariana trough	Spreading center distal to arc	2,990	51	343
201	Pika knoll	Mariana trough	Spreading center distal to arc	2,830, 2,920	51	330
202	Solwara 11	Manus basin	Spreading center intersecting hot-spot trail	1,300–1,500	123	-
203	Solwara 18	Manus basin	Spreading center intersecting hot-spot trail	1,310	124	-
204	Solwara 16	Manus basin	Spreading center distal to arc	2,145–2,165	68	-
205	Solwara 15	Manus basin	Spreading center distal to arc	2,210–2,220	54	-
206	Solwara 14	Manus basin	Spreading center distal to arc	2,240–2,250	52	-
207	Solwara 10	Manus basin	Spreading center distal to arc	2,230–2,255	50	-
208	Vienna Woods	Manus basin	Spreading center distal to arc	2,470–2,500	29	302

Table 2. *(Cont.)*

No.	Deposit	Location	Setting	Depth (m)	Rate of extension/ spreading (mm/yr)[1]	Temp. (°C)
Back-arc spreading center *(Cont.)*						
209	Solwara 3	Manus basin	Spreading center distal to arc	2,470–2,490	28	-
210	Bronze-Age Fort	Manus basin	Spreading center distal to arc	2,430–2,440	25	-
211	150°22'E	Manus basin	Spreading center distal to arc	2,560–2,630	18	194
212	SO99	North Fiji basin	Spreading center distal to arc	1,960–2,000	58	-
213	Père Lachaise	North Fiji basin	Spreading center distal to arc	1,950–1,980	58	-
214	White Lady-Starmer	North Fiji basin	Spreading center distal to arc	1,980–2,020	58	285
215	Tahi Moana 7	Lau basin	Spreading center proximal to arc	1,880–1,940	108	-
216	Maka	Lau basin	Spreading center proximal to arc	1,520–1,530, 1,660	105	315
217	Papatua	Lau basin	Spreading center distal to arc	2,100	107	-
218	Kings Triple Junction A2	Lau basin	Spreading center distal to arc	2,080	105	-
219	Central Lau Spreading Center A3	Lau basin	Spreading center distal to arc	2,250	88	-
220	Kilo Moana	Lau basin	Spreading center distal to arc	2,610–2,640	84	336
221	Tow Cam	Lau basin	Spreading center distal to arc	2,690–2,730	80	325
222	Tahi Moana 1	Lau basin	Spreading center distal to arc	2,200–2,250	74	311
223	ABE	Lau basin	Spreading center distal to arc	2,100–2,160	73	317
224	White Church	Lau basin	Spreading center proximal to arc	1,890–1,970	54	-
225	Northern Valu Fa Ridge 2	Lau basin	Spreading center proximal to arc	1,780–1,840	54	-
226	Tahi Moana 2	Lau basin	Spreading center proximal to arc	1,830–1,870	53	-
227	Northern Valu Fa Ridge 3	Lau basin	Spreading center proximal to arc	1,805–1,850	53	-
228	Tu'i Malila	Lau basin	Spreading center proximal to arc	1,820–1,930	52	315
229	Tahi Moana 4	Lau basin	Spreading center proximal to arc	1,640–1,690	49	-
230	Mariner	Lau basin	Spreading center proximal to arc	1,880–1,950	49	365
231	Vai Lili	Lau basin	Spreading center proximal to arc	1,680–1,770	48	342
232	Tahi Moana 6	Lau basin	Spreading center proximal to arc	1,880–1,940	47	-
233	Tahi Moana 3	Lau basin	Spreading center proximal to arc	2,010–2,030	44	-
234	Tahi Moana 5	Lau basin	Spreading center proximal to arc	2,000–2,050	44	-
235	Hine Hina	Lau basin	Spreading center proximal to arc	1,790–1,920	43	-
236	Mermaids Purse	East Scotia Ridge	Spreading center distal to arc	2,600–2,620	59	353
237	Devils Punchbowl	East Scotia Ridge	Spreading center distal to arc	2,395	69	383

[1] Rates of extension/spreading were calculated using the MORVEL56 model (DeMets et al., 2010)

[2] Measured maximum temperature is slightly below boiling point at the water depth; as two-phase venting has been observed, it is possible that the sensor of the remotely operated vehicle slightly underestimated temperature (Merle, 2012)

Site descriptions: [151] Iizasa et al. (1999), Glasby et al. (2000, 2008); [152] Iizasa et al. (1992), Iizasa (1993); [153] Kasuga and Kato (1992), Watanabe and Kajimura (1994), Watanabe et al. (1994), Glasby et al. (2000, 2008), Marumo et al. (2008); [154] Merle et al. (2004); Hein et al. (2014); [155] Gamo et al. (1993), Iwaida and Ueno (2005), Merle et al. (2006); [156] Butterfield et al. (2010); [157] Merle (2012); [158] Nautilus Minerals 11/01/12, Merle (2012); [159] Nautilus Minerals 11/01/12, Merle (2012); [160] Nautilus Minerals 09/17/08, P. Jankowski (Nautilus Minerals NI43-101 Technical Report, 03/03/10); [161] Nautilus Minerals 09/17/08, Kim et al. (2009), P. Jankowski (Nautilus Minerals NI43-101 Technical Report, 03/03/10); [162] Se-Jong Ju (unpub. data), Lee et al. (2015); [163] Stoffers et al. (2006), Schwarz-Schampera et al. (2007); [164] de Ronde et al. (2003b, 2005, 2011); [165] Wright et al. (1998), de Ronde et al. (2003b), Leybourne et al. (2012); [166] Merle et al. (2005), de Ronde et al. (2014); [167] Tufar (1991), Monecke et al. (2009), Petersen et al. (2014); [168] Sigurdsson et al. (2006), Kilias et al. (2013); [169] Rogers (2010); [170] Iizasa et al. (2004), Tanahashi et al. (2008), Watanabe and Hayashi (2014); [171] Chiba et al. (1992; 1993), Nedachi et al. (1992), Glasby and Notsu (2003); [172] Chiba et al. (1996), Kataoka et al. (2000), Glasby and Notsu (2003), Ueno et al. (2003); [173] Kimura et al. (1989), Tanaka et al. (1989), Sakai et al. (1990a), Glasby and Notsu (2003); [174] Fukuba et al. (2015); [175] Halbach et al. (1989, 1993), Kimura et al. (1989), Nakamura et al. (1990), Sakai et al. (1990a, b), Tanaka et al. (1990), Noguchi et al. (2011), Ishibashi et al. (2014); [176] Glasby and Notsu (2003), Noguchi et al. (2011), Ishibashi et al. (2014); [177, 178] Matsumoto et al. (2001), Watanabe et al. (2006); [179] Watanabe et al. (1995); [180] Fujikura et al. (2001), Watanabe (2001); [181] Fujikura et al. (2001), Matsumoto et al. (2001), Konno et al. (2006), Suzuki et al. (2008); [182] Binns and Scott (1993), Moss and Scott (2001), Binns et al. (2002), Petersen et al. (2005), Tivey et al. (2006), Monecke et al. (2007), P. Jankowski (Nautilus Minerals NI43-101 Technical Report, 03/03/10), Craddock et al. (2010), Reeves et al. (2011), Thal et al. (2014); [183] Tivey et al. (2006); [184] Nautilus Minerals 11/04/09, P. Jankowski (Nautilus Minerals NI43-101 Technical Report, 03/03/10); [185] Nautilus Minerals 11/04/09, 02/11/11, P. Jankowski (Nautilus Minerals NI43-101 Technical Report, 03/03/10); [186] Nautilus Minerals 06/20/07, P. Jankowski (Nautilus Minerals NI43-101 Technical Report, 03/03/10); [187] Moss and Scott (2001), Binns (2004), Tivey et al. (2006), I. Lipton (Nautilus Minerals NI 43-101 Compliant Resource Report, 02/01/08), P. Jankowski (Nautilus Minerals NI43-101 Technical Report, 03/03/10), Craddock et al. (2010), Nautilus Minerals 01/25/11; [188] Moss and Scott (2001), Binns (2004), Tivey et al. (2006), P. Jankowski (Nautilus Minerals NI43-101 Technical Report, 03/03/10), Craddock et al. (2010), Yeats et al. (2014); [189] P. Jankowski (Nautilus Minerals 2008 Exploration Program, 12/31/08), Nautilus Minerals 09/11/08, P. Jankowski (Nautilus Minerals NI43-101 Technical Report, 03/03/10); [190] Haase et al. (2013); [191] Kim et al. (2009), Nautilus Minerals 05/27/09, 06/11/09; [192] Nautilus Minerals 11/01/12, Merle (2012); [193] Pantin and Wright (1994), Stoffers et al. (1999), Hocking et al. (2010) [194] Bohrmann et al. (1999), Klinkhammer et al. (2001), Petersen et al. (2004); [195] Klinkhammer et al. (2001), Petersen et al. (2004); [196] Craig et al. (1987), Hawkins et al. (1990), Kusakabe et al. (1990), Iwaida and Ueno (2005); [197] Hawkins et al. (1990); [198, 199] Kakegawa et al. (2008), Ikehata et al. (2015); [200] Ishibashi et al. (2006), Ikehata et al. (2015); [201] Kakegawa et al. (2008), Nakamura et al. (2013), Ikehata et al. (2015); [202] Nautilus Minerals 12/12/08, 02/25/10, P. Jankowski (Nautilus Minerals, NI43-101 Technical Report, 03/03/10); [203] Nautilus Minerals 01/14/08, 02/25/10, P. Jankowski (Nautilus Minerals, NI43-101 Technical Report, 03/03/10); [204] Nautilus Minerals 01/14/08, 02/25/10, P. Jankowski (Nautilus Minerals, NI43-101 Technical Report, 03/03/10); [205] Nautilus Minerals 01/14/08, P. Jankowski (Nautilus Minerals, NI43-101 Technical Report, 03/03/10); [206] P. Jankowski (Nautilus Minerals 2008 Exploration Program, 12/31/08), Nautilus Minerals 01/14/08, P. Jankowski (Nautilus Minerals NI43-101 Technical Report, 03/03/10); [207] P. Jankowski (Nautilus Minerals 2008 Exploration Program, 12/31/08), Nautilus Minerals 09/08/08, P. Jankowski (Nautilus Minerals NI43-101 Technical Report, 03/03/10); [208] Both et al. (1986), Tufar (1990), Auzende et al. (1996a), Tivey et al. (2006); [209] Tufar (1990), Tivey et al. (2006); [210] Tivey et al. (2006); [211] Tufar (1990), Lisitsyn et al. (1993), Tivey

Table 2. *(Cont.)*

et al. (2006); [212] Halbach et al. (1995), Kim et al. (2006); [213] Auzende et al. (1989), Bendel et al. (1993), Halbach et al. (1995); [214] Auzende et al. (1989), Grimaud et al. (1991), Bendel et al. (1993), [215] Nautilus Minerals 05/27/09, 06/11/09, P. Jankowski (Nautilus Minerals NI43-101 Technical Report, 03/03/10); [216] Merle (2008, 2009), Nautilus Minerals 09/17/08, Kim et al. (2009), P. Jankowski (Nautilus Minerals NI43-101 Technical Report, 03/03/10); [217] Hawkins (1986); [218] Malahoff and Falloon (1991), Lisitsyn et al. (1992), Paropkari et al. (2010); [219] Malahoff and Falloon (1991), Lisitsyn et al. (1992); [220, 221] Ferrini et al. (2008), Mottl et al. (2011); [222] Nautilus Minerals 02/18/09, P. Jankowski (Nautilus Minerals NI43-101 Technical Report, 03/03/10); [223] Ferrini et al. (2008), Nautilus Minerals 02/18/09, Mottl et al. (2011); [224] Fouquet et al. (1993a), Herzig et al. (1993, 1998), Nautilus Minerals 02/18/09, P. Jankowski (Nautilus Minerals NI43-101 Technical Report, 03/03/10); [225] Fouquet et al. (1993a), Nautilus Minerals 02/18/09, P. Jankowski (Nautilus Minerals NI43-101 Technical Report, 03/03/10); [226] Nautilus Minerals 02/18/09, P. Jankowski (Nautilus Minerals NI43-101 Technical Report, 03/03/10); [227] Fouquet et al. (1993a), Nautilus Minerals 02/18/09, P. Jankowski (Nautilus Minerals NI43-101 Technical Report, 03/03/10); [228] Ferrini et al. (2008), Nautilus Minerals 02/18/09, P. Jankowski (Nautilus Minerals NI43-101 Technical Report, 03/03/10), Mottl et al. (2011); [229] Nautilus Minerals 02/18/09, P. Jankowski (Nautilus Minerals NI43-101 Technical Report, 03/03/10); [230] Ferrini et al. (2008), Nautilus Minerals 02/18/09, P. Jankowski (Nautilus Minerals NI43-101 Technical Report, 03/03/10), Mottl et al. (2011); [231] Fouquet et al. (1993a), Herzig et al. (1993, 1998), Ferrini et al. (2008), Mottl et al. (2011); [232-234] Nautilus Minerals 02/18/09, P. Jankowski (Nautilus Minerals NI43-101 Technical Report, 03/03/10); [235] Fouquet et al. (1993a), Herzig et al. (1993, 1998), Nautilus Minerals 02/18/09, P. Jankowski (Nautilus Minerals NI43-101 Technical Report, 03/03/10), Schwarz-Schampera et al. (2007); and [236, 237] Rogers et al. (2012)

Vent temperatures: [151] Iizasa et al. (1999); [153] Watanabe et al. (1994); [154] Merle et al. (2004); [155] Iwaida and Ueno (2005); [157-160] Merle (2012); [162] Se-Jong Ju (unpub. data); [163] Stoffers et al. (2006); [164] de Ronde et al. (2011, 2014); [166] de Ronde et al. (2014); [168] Sigurdsson et al. (2006); [169] Rogers (2010); [171] Chiba et al. (1993); [172] Glasby and Notsu (2003); [173] Sakai et al. (1990a); [174] Fukuba et al. (2015); [175] Sakai et al. (1990a); [176] Ishibashi et al. (2014); [180] Fujikura et al. (2001); [181] Suzuki et al. (2008); [182] Reeves et al. (2011); [187] Tivey et al. (2006); [188] Bach et al. (2011); [190] Haase et al. (2013); [192] Merle (2012); [193] Botz et al. (2002); [196] Kusakabe et al. (1990); [199] Wheat et al. (2003); [200, 201] Ishibashi et al. (2006); [208] Gamo et al. (1996); [211] Tivey et al. (2006); [214] Auzende et al. (1989); [216] Merle (2009); [220, 221] Tivey et al. (2005); [222, 223, 228, 230] Flores et al. (2012); [231] Fouquet et al. (1993a); and [236, 237] Rogers et al. (2012)

Many of the sea-floor massive sulfide deposits recognized are located on arc volcanoes along the ~16,000 km of global submarine arcs (cf. de Ronde et al., 2003a; Monecke et al., 2014). Well-endowed intraoceanic arcs include the Izu-Ogasawara arc (Iizasa et al., 1992, 1999; Watanabe and Kajimura, 1994), the Mariana arc (Iwaida and Ueno, 2005; Hein et al., 2014), the Tonga arc (Stoffers et al., 2006), and the Kermadec arc (de Ronde et al., 2003b, 2005, 2011, 2014). Examples of sea-floor massive sulfide deposits located in transitional arcs include those in the Sanghie arc (Butterfield et al., 2010) and the Aeolian arc (Tufar, 1991; Monecke et al., 2009; Petersen et al., 2014). The only known sea-floor massive sulfide deposits associated with continental margin volcanism are located in the Hellenic arc (Sigurdsson et al., 2006; Kilias et al., 2013). Most of the arc volcanoes hosting sea-floor massive sulfide deposits are simple cones, with basal diameters of 30 km and heights of 1 to 2 km above the surrounding sea floor. However, sea-floor massive sulfide deposits also occur on arc volcanoes that are characterized by summit calderas, which can range up to 5 or 6 km in diameter (de Ronde et al., 2003a).

In many submarine volcanic arcs, sea-floor massive sulfide formation is associated with arc-related rifts (Table 2). Back-arc rifts in intraoceanic arcs hosting sea-floor massive sulfide deposits include those in the Izu-Ogasawa arc (Iizasa et al., 2004; Tanahashi et al., 2008), the Tonga arc (Kim et al., 2009), and the rifts developing in continental crust in the Okinawa trough behind the Ryukyu arc (Halbach et al., 1989, 1993; Matsumoto et al., 2001; Glasby and Notsu, 2003; Watanabe et al., 2006; Suzuki et al., 2008; Ishibashi et al., 2014). Some of the most important sites in arc-related rifts on the modern sea floor are located in the eastern Manus basin (Binns and Scott, 1993; Moss and Scott, 2001; Binns et al., 2002; Petersen et al., 2005; Monecke et al., 2007; Thal et al., 2014; Yeats et al., 2014) where back-arc rifting takes place in a basement of Eocene to Oligocene arc crust (Martinez and Taylor, 1996). Hydrothermal activity in the Bransfield Strait of Antarctica occurs in a postsubduction marginal basin within continental crust (Klinkhammer et al., 2001; Petersen et al., 2004).

Sea-floor massive sulfide deposits are also located along the 9,600-km-long (cf. Bird, 2003) back-arc spreading centers (Table 2). They occur in young back-arc basins proximal to the arc front such as those in the southern portion of the Lau basin (Fouquet et al., 1991a, b, 1993a; Herzig et al., 1993, 1998; Ferrini et al., 2008) or in more mature back-arc basins distal to the arc front. Examples include those in the Mariana trough (Craig et al., 1987; Hawkins et al., 1990; Kakegawa et al., 2008; Nakamura et al., 2013) and the Manus basin (Tufar, 1990; Auzende et al., 1996a; Tivey et al., 2006), the northern part of the Lau basin (Lisitsyn et al., 1992; Ferrini et al., 2008; Mottl et al., 2011), the North Fiji basin (Auzende et al., 1989; Bendel et al., 1993; Halbach et al., 1995), and the East Scotia Ridge (Rogers et al., 2012). Most back-arc spreading centers resemble intermediate-rate mid-ocean ridge spreading centers, implying similar rates of magma supply. However, spreading rates are highly variable and can range from less than 20 to over 120 mm/yr (Table 2). The depth to the subaxial magma chamber ranges from as little as 1.1 to over 3.5 km (Collier and Sinha, 1990, 1992).

Size and Tonnage Characteristics

The dimensions of sea-floor massive sulfide deposits are generally not well constrained. Most known deposits have been investigated only through sea-floor video surveys employing tools towed by research vessels or, more recently, the use of remotely operated vehicles and autonomous underwater vehicles. High-resolution bathymetric and geophysical surveys have so far only been conducted across a limited number of vent sites and associated sea-floor massive sulfide deposits (Tivey et al., 2006; Glickson et al., 2007; Ferrini et al., 2008; Soule et al., 2008; Yoshikawa et al., 2012; Jamieson et al., 2014a; Thal et al., 2014).

The available data shows that the surface expression of sea-floor massive sulfide deposits can vary significantly in size, ranging from tens to several hundreds of meters in diameter. Hannington et al. (2010, 2011) compiled the sizes of the 62 best studied sea-floor massive sulfide deposits worldwide and showed that these have surface areas ranging from less than 100

to about 300,000 m². Out of the group of 62 deposits, approximately half have explored dimensions of 5,000 m² or more.

Although the surface areas of sea-floor massive sulfide deposits can be fairly readily determined from sea floor surveys, the amount of sulfide contained in these deposits cannot be inferred simply from the surface area. The sulfides accumulations may be of variable thickness or even discontinuous with large areas of barren substrate between adjacent chimneys and sulfide mounds. Extensive dusting of the sea floor by metalliferous sediments and debris derived from collapsed chimneys essentially precludes visual assessment of the continuity of sulfide outcrops (Hannington et al., 2010). Even in high-resolution bathymetric surveys, it is often difficult to distinguish between sulfide accumulations on the sea floor and irregularly shaped volcanic substrate (Jamieson et al., 2014a).

Estimates of the tonnage of sea-floor massive sulfide deposits are possible only in few cases where drilling information is available. During deep drilling at Bent Hill at Middle Valley, 95 m of massive sulfide was intersected below the sea floor (ODP Leg 139, Davis et al., 1992). The ODP Mound, located only 300 m to the south, was also shown to mostly consist of massive sulfide (ODP Leg 169, Zierenberg and Miller, 2000). Both mounds were estimated to contain a combined tonnage of between 10 and 15 Mt, excluding the Cu stringer zones located below the massive sulfide lenses (Zierenberg et al., 1998; Hannington et al., 2010). ODP drilling to a maximum depth of 125 m at the TAG hydrothermal mound on the Mid-Atlantic Ridge indicated 2.7 Mt of massive sulfides and 1.2 Mt of stockwork sulfides (ODP Leg 158, Hannington et al., 1998).

However, deep drilling at Central Hill in the northern Escanaba trough demonstrated that massive sulfides at this location only form a thin (5–15 m) veneer over sediments. No major intersection of massive sulfides was recovered (ODP Leg 169, Zierenberg and Miller, 2000). Similarly, deep drilling at the Pacmanus vent field in the eastern Manus basin did not reveal the presence of a thick massive sulfide lens (ODP Leg 193, Binns et al., 2002) although subsequent shallow drilling to a maximum depth of 5 m using a lander-type system recovered up to 2-m-long intervals of massive sulfides and sulfates (Petersen et al., 2005). Drilling at the Snake Pit site at the Mid-Atlantic Ridge established a maximum thickness of massive sulfides of over 10 m at the base of an active vent, with the sulfide lens thinning to a few meters within 20 m from the vent (ODP Leg 106, Detrick et al., 1986). Shallow drilling to a maximum depth of 15 m using a lander-type system at the Logatchev hydrothermal vent field showed that the massive sulfides at this location only form a thin blanket on top of an intensely clay-altered substrate (Petersen et al., 2009).

Shallow drilling to a maximum depth of 5 m at the Palinuro volcanic complex in the Aeolian arc revealed the presence of an extensive subseafloor massive sulfide deposit located tens of centimeters to several meters below a cover of unconsolidated sediments. This blind sulfide lens is potentially of significant thickness as all holes drilled in a 3,500-m² area ended in massive sulfides (Monecke et al., 2009; Petersen et al., 2014).

To date, the most comprehensive delineation of a sea-floor massive sulfide deposit through shallow drilling to a maximum depth of 20 m has been conducted at the Solwara 1 site in the eastern Manus basin (Binns, 2004). Based on a total of 146 holes drilled within the 90,000-m² large vent field and the use of a deep-towed electromagnetic survey, a NI43-101 compliant resource of 2.1 Mt of massive sulfide ore was established. An indicated resource of 870,000 t grading 6.8 wt % Cu, 0.4 wt % Zn, 4.8 g/t Au, and 23 g/t Ag, as well an inferred resource of 1,300,000 t of 7.5 wt % Cu, 0.8 wt % Zn, 7.2 g/t Au, and 37 g/t Ag at a 4.0 wt % Cu cut-off were defined (I. Lipton, Nautilus Minerals Inc., NI 43-101 Compliant Resource Report, 02/01/08).

Using the tonnage versus area relationship for the Solwara 1 sea-floor massive sulfide deposit, which is ~28 t/m², as well as available drilling information as a guide, Hannington et al. (2010, 2011) estimated that the 62 best studied sea-floor massive sulfide deposits in the world's oceans have a combined tonnage of approximately 50 Mt. Over 60% of the total tonnage is contained in the seven largest deposits, which are Middle Valley (~10–15 Mt), Semyenov (~9 Mt), Krasnov (3 Mt), Sunrise (~3 Mt), the TAG hydrothermal mound (2.7 Mt), Solwara 1 (2.1 Mt), and the Alvin zone (2 Mt). Assuming that the size distribution of the 62 best studied sea-floor massive sulfide deposits is representative of sea-floor sulfides that remain to be discovered on the modern sea floor, only one in ten future discoveries would be expected to contain more than 2 Mt of massive sulfides (Hannington et al., 2010, 2011).

Based on a study of the spatial distribution for known hydrothermal vent sites on the mid-ocean ridges and in subduction-related environments, Hannington and Monecke (2009) as well as Hannington et al. (2010, 2011) determined that the total number of sea-floor massive sulfide deposits along the neovolcanic zones of the world's oceans is on the order of ~1,000. Applying the size distribution of the test group of well-studied deposits, the total sulfide tonnage contained in 1,000 deposits ranging from 100 t to 10 Mt in size is expected to be ~600 Mt. This estimated global tonnage of massive sulfides clearly only represents a first-order approximation, as a true resource estimation cannot be conducted at the present time due to the lack of drilling (Hannington et al., 2010, 2011). Moreover, the area included in the study represents only the currently active volcanic zones of the mid-ocean ridges, arcs, and back-arcs. Depending on preservation, massive sulfides may also be present in the vast areas of crust outside the neovolcanic zones.

Base and Precious Metal Grades

Over the past decades, a large number of samples have been collected from sea-floor massive sulfide deposits worldwide and analyzed for their base and precious metal contents. The most comprehensive database of geochemical analyses of massive sulfide samples has been compiled by Hannington et al. (1994, 2005, 2010) and Monecke et al. (2014).

It is important to note that the base and precious metal values compiled from the literature cannot be directly compared to grade data of ancient massive sulfide deposits on land (Hannington et al., 2010; Monecke et al., 2014). Sampling of sea-floor sulfides is inherently difficult and commonly yields only chimney fragments or samples from the surface of sulfide accumulations that may not be representative of the deposit as a whole. In many cases, small samples collected from the surface of massive sulfide accumulations have anomalously high base and precious metal grades. As such outlier values

strongly influence the arithmetic mean, median values are used in the present contribution as a more accurate measure of statistical trends.

The presently available data (Hannington et al., 1994, 2005, 2010; Monecke et al., 2014) indicate that the metal content of sea-floor massive sulfide deposits broadly varies by volcanic and tectonic setting. Sea-floor massive sulfide deposits located on basalt-hosted mid-ocean ridges contain 3.2 wt % combined Cu + Zn + Pb. The median Au and Ag values are 0.3 and 27.3 ppm, respectively (Hannington et al., 1994, 2005, 2010). By comparison, ultramafic-rock-hosted sea-floor massive sulfide deposits have significantly higher combined Cu + Zn + Pb content of 13.2 wt %, but the summary statistics may be less reliable due to the smaller number of samples analyzed. The median Au and Ag concentrations of ultramafic-rock-hosted sea-floor massive sulfide deposits are 2.8 and 26 ppm, respectively (Hannington et al., 1994, 2005, 2010). Sea-floor massive sulfide deposits hosted by sediment-covered ridges have a deviating metal signature. These deposits contain only 1.5 wt % combined Cu + Zn + Pb. The precious metal contents of the massive sulfides are low when compared to sea-floor massive sulfide deposits located on basalt-hosted mid-ocean ridges, with median Au and Ag concentrations of 0.05 and 3.0 ppm, respectively (Hannington et al., 1994, 2005, 2010).

Sea-floor massive sulfide deposits associated with more evolved volcanic rocks at convergent plate margins show a large compositional variability (Hannington et al., 1994, 2005, 2010; Monecke et al., 2014). Sea-floor massive sulfide deposits located on arc volcanoes contain 3.6 wt % combined Cu + Zn + Pb. The massive sulfide samples have median Au and Ag values of 1.9 and 100 ppm, respectively (Monecke et al., 2014). By comparison, massive sulfides formed by hydrothermal systems associated with rifted arc crust are characterized by generally higher base metal contents, with a median base metal content of 11.1 wt % combined Cu + Zn + Pb. The precious metal grades in sea-floor massive sulfide deposits associated with arc rifting are also higher, with median Au and Ag values of 7.5 and 166 ppm, respectively (Monecke et al., 2014). Sea-floor massive sulfide deposits located in back-arc spreading centers yielded samples that have a median base metal content of 16.1 wt % combined Cu + Zn + Pb. The precious metal grades are lower than those encountered in sea-floor massive sulfide deposits located in rifted arcs. The median Au content is 2.5 ppm, while the median Ag value is 94.7 ppm (Monecke et al., 2014).

Assuming that sea-floor massive sulfide deposits contain on average 5 wt % combined Cu + Zn + Pb, the average concentration of these elements in ancient deposits occurring on land, the ~600 Mt of massive sulfides in the neovolcanic zones of the world's oceans contain ~30 Mt of base metals (Hannington et al., 2010, 2011). Singer (2014) arrived at a similar estimate based on metal grades extrapolated from land-based deposits.

Temperature Controls on Base Metal Enrichment

Metal solubility in black smoker liquids is strongly temperature dependent. As a consequence, the grades of sea-floor massive sulfide deposits depend on the temperature evolution of the hydrothermal liquids during their ascent to the sea floor. The occurrence of subseafloor boiling represents a key control on temperature as boiling liquids cool rapidly due to the heat loss required for vaporization. Venting of high-temperature liquids is, therefore, restricted to deep-water environments where hydrostatic pressures are high, inhibiting subseafloor boiling (Butterfield et al., 1990; Hannington et al., 2005; Monecke et al., 2014). As Cu can only be transported in high-temperature black smoker liquids (chalcopyrite precipitation mostly occurs at temperatures between 280° and 350°C; Large, 1992), significant Cu enrichment (>2 wt %) is only encountered in sea-floor massive sulfide deposits forming in deep water (Monecke et al., 2014). In contrast, Zn and Pb can be transported by hydrothermal liquids of lower temperatures (sphalerite and galena precipitation mostly occurs at temperatures between 175° and 250°C; Large, 1992). This allows sea-floor massive sulfide deposits enriched in these base metals to be formed over a wider range of water depths, including shallow marine systems where subseafloor boiling causes significant cooling of the liquids during their ascent to the sea floor (Hannington et al., 2005; Monecke et al., 2014).

The strong temperature control on metal solubility also causes pronounced compositional zoning within sea-floor massive sulfide deposits. In the shallow subseafloor environment and within sulfide mounds, the hydrothermal liquids cool due to conductive heat transfer and mixing with cold seawater (Hannington et al., 1995, 1998; Hannington, 2014). As a consequence, the interior of the deposits and the underlying stockwork zones, where hydrothermal liquids cool from >350° to 280°C (Large, 1992), are typically enriched in Cu. Chalcopyrite and isocubanite are the dominant Cu-rich sulfide minerals, which are commonly associated with pyrrhotite and sometimes magnetite. A distinct enrichment of Zn and Pb occurs within the outer margins of the sea-floor massive sulfide deposits where the sulfide-forming liquids become saturated in sphalerite and galena upon cooling and mixing with seawater (Janecky and Seyfried, 1984; Large, 1992). In these peripheral lower temperature zones, pyrite or marcasite is the dominant Fe sulfide mineral (Herzig and Hannington, 1995; Hannington et al., 1995, 1998).

The same temperature-dependent compositional zonation can be observed at various scales within sea-floor massive sulfide deposits. In black smoker chimneys, conduits of the high-temperature liquids are usually lined by chalcopyrite, with the outer parts of the chimneys being composed of minerals deposited at lower temperatures, including sphalerite, galena, wurtzite, pyrite, marcasite, amorphous silica, and barite (Haymon and Kastner, 1981; Goldfarb et al., 1983; Haymon, 1983; Fouquet et al., 1993b; Herzig et al., 1993; Berkenbosch et al., 2012). In addition, anhydrite represents an important component in the outer parts of chimneys where hydrothermal liquids percolating through the chimney walls encounter cold seawater. The anhydrite is precipitated from the Ca^{2+} contained in the vent liquids and the SO_4^{2-} in ambient seawater, although the anhydrite may also form simply by conductive heating of seawater to temperatures above 150°C (Janecky and Seyfried, 1984; Mills and Elderfield, 1995; Mills et al., 1998; Humphris and Bach, 2005).

Despite the simple temperature control on mineral formation, paragenetic relationships are typically complex. The highly variable thermal history of the deposits, commonly

involving multiple periods of high-temperature upflow over the life of the deposit (Lalou et al., 1995, 1996, 1998; Hannington et al., 1998; Kuznetsov et al., 2006; Wang et al., 2012), results in complex overprinting and replacement relationships. During periods of high-temperature fluid flow, mineral precipitation within the growing deposit occurs through infilling and replacement of previously formed minerals. In a thermally intensifying system, continuous dissolution of earlier formed sulfide minerals and replacement by minerals stable at higher temperatures results in pronounced metal zoning, a process referred to as zone refining (Knuckey et al., 1982; Eldridge et al., 1983; Ohmoto, 1996). Over time, most Zn and Pb is stripped from the high-temperature interior of the deposit and reprecipitated in the cooler outer zones, leaving a high-grade Cu-rich core behind. Continued refining and stripping of Cu from the lower and interior part of the deposits will eventually leave behind a barren pyrite body (Eldridge et al., 1983; Ohmoto, 1996; Hannington et al., 1998).

Base metal zoning within sea-floor massive sulfide deposits caused by zone refining have been well documented for sea-floor massive sulfide deposits that have been drilled, including the Bent Hill and ODP Mound at Middle Valley (Zierenberg et al., 1998), the TAG hydrothermal mound (Hannington et al., 1998), Palinuro (Petersen et al., 2014), and Pacmanus (Petersen et al., 2005).

Minor Element Content

Table 3 contains a summary of minor element analyses performed on almost 5,000 samples from sea-floor massive sulfide deposits worldwide. The compilation comprises analytical results from the literature as well as from samples collected by the authors during numerous research cruises over the past decades. Compilation of the data shows that the minor element content of sea-floor sulfides varies over several orders of magnitude between samples and hydrothermal vent sites. Median minor element concentrations of sea-floor massive sulfide deposits in different tectonic settings are 1.0 ppm Bi, 70.0 ppm Cd, 16.0 ppm Ga, 8.8 ppm Ge, 3.1 ppm Hg, 3.1 ppm In, 41.0 ppm Mo, 21.2 ppm Sb, 17.0 ppm Se, 1.0 ppm Te, and 8.6 ppm Tl (Table 3).

Basalt-hosted mid-ocean ridges

The concentrations of the minor elements Bi, Hg, In, and Te in samples collected from basalt-hosted mid-ocean ridge sea-floor massive sulfide deposits are typically below 10 ppm (Figs. 2–4). Only 25% of massive sulfide samples have Bi concentrations exceeding 2.5 ppm. High Bi concentrations ranging from 20 to 95 ppm have been reported in some samples from 12°49'N on the East Pacific Rise (Schwarz-Schampera, 2000) and from the TAG hydrothermal mound (Miller, 1998). The concentration of Hg is mostly below 7 ppm, with elevated concentrations being reported from the TAG hydrothermal mound (Hannington et al., 1991) as well as several sites along the Juan de Fuca Ridge (Hannington et al., 1991; Kristall et al., 2011) and the East Pacific Rise (Moss and Scott, 1996; Marchig et al., 1997). Indium concentrations exceeding about 5 ppm, with maximum concentrations reaching 20 to 134 ppm, have been reported for samples from Snake Pit on the Mid-Atlantic Ridge (Fouquet et al., 1993b), the Main vent field at Endeavour (U. Schwarz-Schampera, unpub. data), as well as several deposits along the East Pacific Rise (Marchig et al., 1997) and the Galapagos rift (S. Petersen, unpub. data). High Te concentrations above 50 ppm have only been reported from North Cleft on the Juan de Fuca Ridge (Smith and Koski, 1994).

The concentrations of Ga, Ge, Sb, and Tl in basalt-hosted massive sulfides commonly do not exceed concentrations of 50 ppm. Only 25% of all sulfide samples collected from basalt-hosted mid-ocean ridge sea-floor massive sulfide have Ga concentrations above 40 ppm. High Ga concentrations have been reported from white smoker chimneys at the TAG hydrothermal mound (Hannington et al., 1991), sulfide samples from the Southern Explorer (Hannington et al., 1991), Mothra at Endeavour (Kristall et al., 2011), Axial Seamount (Hannington et al., 1991), and several sites at the East Pacific Rise (Marchig et al., 1997). Sea-floor sulfides from basalt-hosted mid-ocean ridge sea-floor massive sulfide deposits having Ge concentrations above 35 ppm are considered anomalous. Some of the highest Ge concentrations on the modern sea floor have been reported from the MESO zone on the Central Indian Ridge, where pyrite-marcasite samples exhibit concentrations of Ge up to 393 ppm (Münch et al., 1999). In addition to this site, only few samples with Ge contents above 100 ppm have been reported, which includes some samples from the Mir zone (Mozgova et al., 1998) and South Cleft (Bischoff et al., 1983). Antimony concentrations exceeding 25 ppm have been reported for Mount Jourdanne on the Southwest Indian Ridge (Münch et al., 2001), the Southern Explorer site (Hannington et al., 1991), the hydrothermal fields along the Endeavour Segment of the Juan de Fuca Ridge (Kristall et al., 2011), Axial Seamount (Hannington and Scott, 1988; Hannington et al., 1991), and North Cleft (Koski et al., 1994a). Only 25% of all samples collected from basalt-hosted sea-floor massive sulfide deposits have Tl concentrations above 20 ppm. Elevated Tl concentration have been documented from Mothra at the Endeavour Segment of the Juan de Fuca Ridge (Kristall et al., 2011) as well as Axial Seamount (Hannington et al., 1991).

In contrast to the elements discussed above, Cd, Mo, and Se commonly occur at concentrations above 100 ppm in sulfide samples from basalt-hosted sea-floor massive sulfide deposits. The highest Cd concentrations of over 2,000 ppm have been reported from North Cleft (Smith and Koski, 1994). High concentrations of this element have also been encountered in samples from Mount Jourdanne (Münch et al., 2001), TAG (Hannington et al., 1991), and Mothra (Kristall et al., 2011). Samples having Mo and Se concentrations above 110 ppm are considered to be anomalous. Sites with anomalous Mo concentrations include the MESO zone (Münch et al., 1999) and 16°43'S on the East Pacific Rise (Marchig et al., 1997). High Se concentrations of over 1,000 ppm have been encountered at several sea-floor massive sulfide deposits, including Axial Seamount (S. Petersen, unpub. data), 9°50'N on the East Pacific Rise (Rouxel et al., 2008), and 16°43'S on the East Pacific Rise (Marchig et al., 1997).

Ultramafic rock-hosted mid-ocean ridges

Minor element analyses are available only for a limited number of mid-ocean ridge sea-floor massive sulfide deposits hosted by ultramafic rocks. The element concentrations of Bi, Ga, Hg, In, Te, and Tl are typically below 10 ppm in samples

Table 3. Minor Element Content of Sulfide Samples Collected from Vent Sites Located in Different Plate Tectonic Settings (all data in ppm)

	Basalt-hosted mid-ocean ridge	Ultramafic rock-hosted mid-ocean ridge	Sediment-covered mid-ocean ridge	Arc volcano	Rifted arc	Back-arc spreading center	All settings
Bi							
Median	1.0	2.5	2.2	1.0	1.0	1.0	1.0
Average	3.8	8.6	25.7	60.4	12.0	3.2	13.3
Min	0.01	0.10	0.05	0.10	0.01	0.25	0.01
Max	95.0	316	820	2,000	524	45	2,000
N	672	184	90	160	436	89	1,631
Cd							
Median	40.0	10.8	19.0	117	308	310	70.0
Average	242	156	85.6	402	576	572	364
Min	0.10	0.10	0.50	0.10	0.10	0.10	0.10
Max	2,800	1,880	1,975	4,140	4,440	6,302	6,302
N	1,388	262	157	251	656	579	3,293
Ga							
Median	16.0	4.0	-	10.0	70.0	7.1	16.0
Average	34.1	10.3	-	51.1	146	29.5	62.6
Min	0.05	0.10	-	0.05	0.65	0.50	0.05
Max	653	75	-	1,870	3,700	210	3,700
N	576	117	-	204	318	50	1,265
Ge							
Median	9.3	12.0	3.0	5.2	12.0	52.0	8.8
Average	26.0	29.3	8.5	13.3	40.7	183	29.6
Min	0.10	0.25	0.50	0.50	0.05	0.30	0.05
Max	393	400	150	194	352	918	918
N	512	112	71	65	139	19	918
Hg							
Median	2.0	0.5	8.5	36.0	11.2	2.0	3.1
Average	6.1	2.2	23.8	249	301	4.7	104
Min	0.0025	0.001	0.50	0.10	0.01	0.03	0.001
Max	152	19	270	6,400	95,000	470	95,000
N	1,026	207	46	241	545	172	2,237
In							
Median	2.5	0.3	-	0.2	12.5	10.0	3.1
Average	4.8	2.0	-	6.6	42.4	43.9	20.5
Min	0.025	0.025	-	0.025	0.003	0.01	0.003
Max	134	29	-	144	502	592	592
N	537	117	-	154	303	260	1,371
Mo							
Median	62.0	16.5	24.0	47.0	23.0	25.0	41.0
Average	84.6	29.1	31.2	78.8	81.5	44.3	72.6
Min	0.05	0.50	0.50	0.30	0.50	0.10	0.05
Max	1,500	469	275	910	2,350	549	2,350
N	1,618	226	158	234	598	346	3,180
Sb							
Median	9.0	6.1	5.8	222	535	47.0	21.2
Average	38.1	40.8	217	1,304	1,760	73.1	513
Min	0.01	0.05	0.05	0.05	0.20	0.10	0.01
Max	1,025	1,110	16,000	22,400	43,500	523	43,500
N	1,636	250	174	276	699	323	3,358
Se							
Median	40.0	110	32.0	1.5	1.5	2.5	17.0
Average	105	259	85.5	50.6	177	23.4	116
Min	0.10	0.40	0.16	0.50	0.05	0.10	0.05
Max	1,632	1,505	1,400	1,690	9,700	1,080	9,700
N	1,503	209	174	179	432	265	2,762
Te							
Median	1.0	3.0	4.7	0.3	0.2	2.8	1.0
Average	2.5	11.1	0.71	4.9	7.1	3.3	5.6
Min	0.01	0.005	0.10	0.025	0.0025	0.10	0.0025
Max	164	96	57	83.7	431	7.9	431
N	441	143	20	142	418	10	1,174
Tl							
Median	6.5	2.5	2.9	13.0	37.0	7.5	8.6
Average	14.4	6.7	4.6	81.8	78.9	22.2	38.8
Min	0.01	0.025	0.50	0.05	0.10	0.01	0.01
Max	160	82.0	43.0	1,000	1,600	120	1,600
N	550	163	56	201	314	41	1,325

Notes: N = number of samples analyzed; there are no analyses for Ga and In available for sulfide occurrences located at sediment-covered ridges; some of the earliest geochemical analyses of In have been excluded from the calculation of the median and average In concentrations due to the high detection limit of 10 ppm; element concentrations given in the table are not weighted using sample sizes

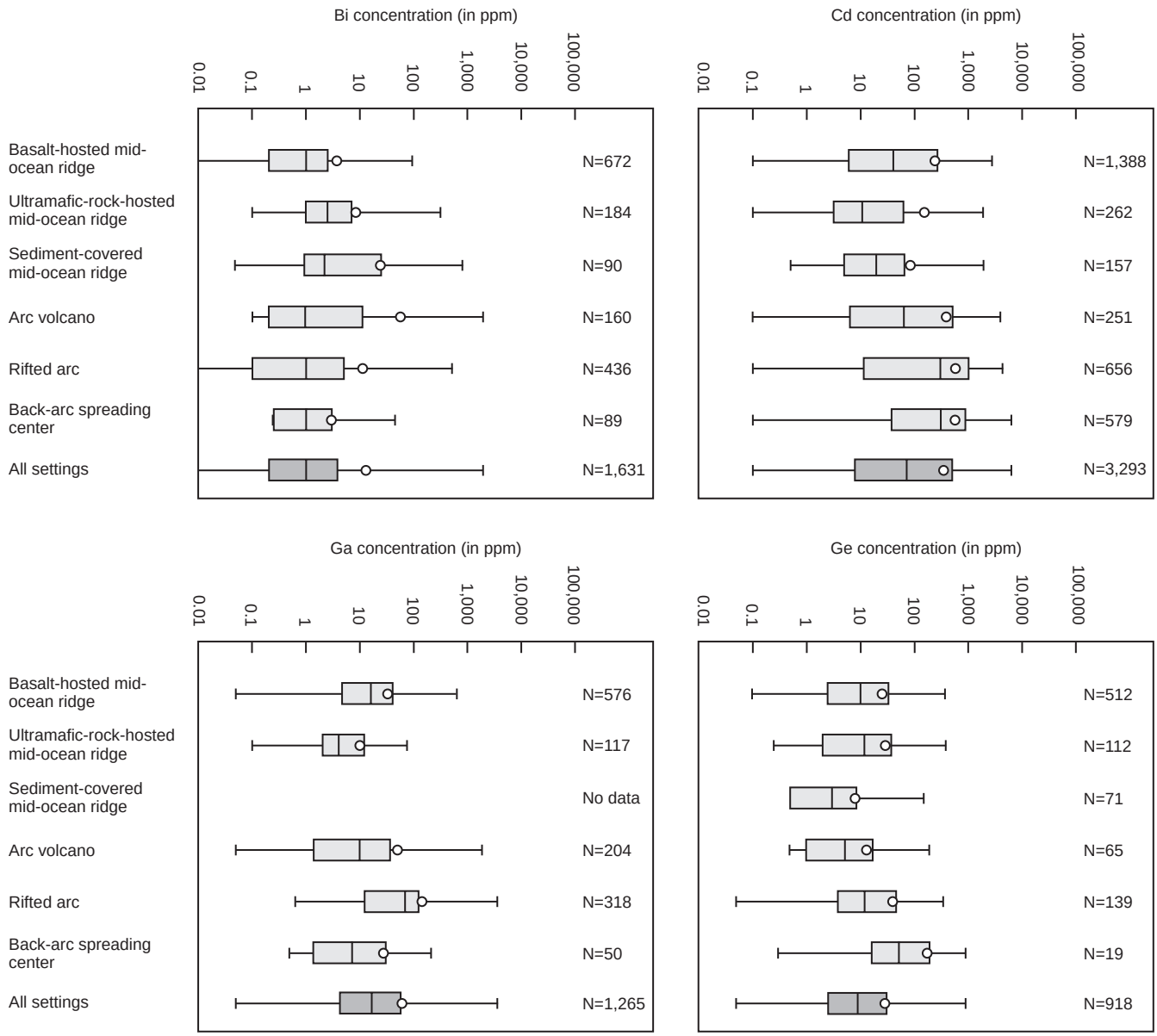

Fig. 2. Whisker-and-box-plot representation of the Bi, Cd, Ga, and Ge concentrations in sulfide samples collected from sea-floor massive sulfide deposits in different volcanic and tectonic settings worldwide. The box encloses the interquartile range with the median displayed as a line. The average value is represented by the open circle. The horizontal lines extending outside of the box mark the minimum and maximum element concentrations encountered. N = number of samples analyzed.

recovered from these sea-floor massive sulfide deposits. About 25% of all samples have Bi concentrations exceeding 7 ppm. The highest concentrations of this element, reaching up to 316 ppm, have been documented at the Logatchev and Nibelungen sites on the Mid-Atlantic Ridge (S. Petersen, unpub. data). Anomalous Ga concentrations, ranging from 30 to 75 ppm have been documented at the Kairei vent field and Logatchev (S. Petersen, unpub. data). The Hg content of sulfide samples from sea-floor massive sulfide deposits hosted by ultramafic rocks is typically below 2 ppm. Elevated concentrations of up to 19 ppm have been noted at Kairei and Logatchev (Wang et al., 2014; S. Petersen, unpub. data). The concentrations of In are similarly low. Only some samples from the Rainbow and Logatchev sites have In concentrations of 5 to 29 ppm (Marques et al., 2007; S. Petersen, unpub. data). About 25% of the samples have Te and Tl concentrations exceeding 15 and 10 ppm, respectively. Anomalous concentrations of these elements, ranging up to 96 ppm Te and 82 ppm Tl, occur at Logatchev and Semyenov (A. Firstova, unpub. data; S. Petersen, unpub. data).

The minor elements Cd, Ge, Mo, and Sb typically occur at concentrations below 50 ppm in samples from ultramafic rock-hosted sea-floor massive sulfide deposits, while Se concentrations up to about 400 ppm are common. The highest Cd concentrations, ranging up to 1,880 ppm, have been documented at the Rainbow hydrothermal field (Bogdanov et al.,

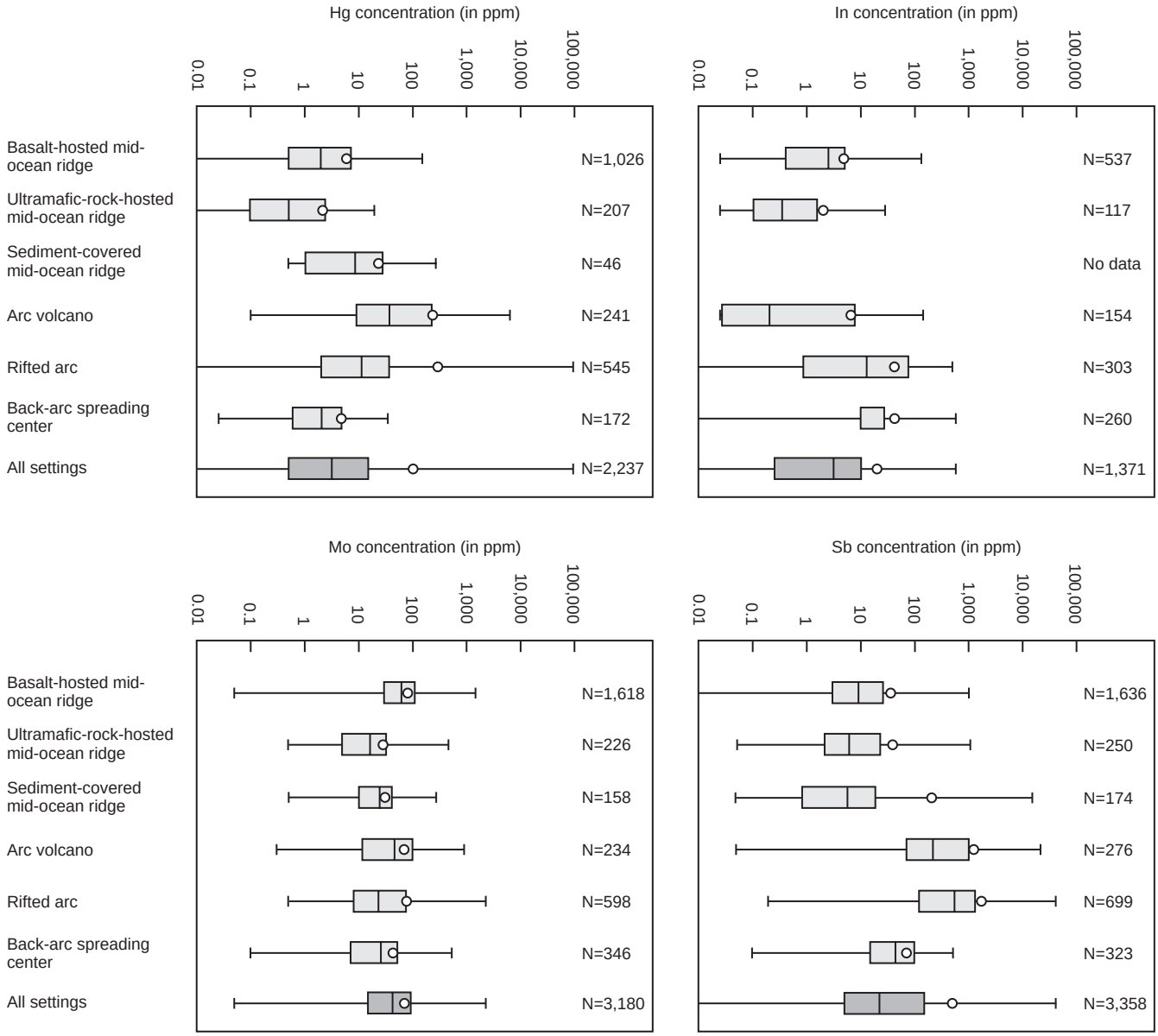

Fig. 3. Whisker-and-box-plot representation of the Hg, In, Mo, and Sb concentrations in sulfide samples collected from sea-floor massive sulfide deposits in different volcanic and tectonic settings worldwide. The box encloses the interquartile range with the median displayed as a line. The average value is represented by the open circle. The horizontal lines extending outside of the box mark the minimum and maximum element concentrations encountered. N = number of samples analyzed.

2002). Anomalous Ge concentrations of 100 to 400 ppm have so far only been documented from Kairei and Nibelungen (S. Petersen, unpub. data). About 25% of all samples have Mo concentrations above 30 ppm. Massive sulfides with Mo concentrations between 100 and 469 ppm have been recovered from Logatchev and Semyenov (S. Petersen, unpub. data). Anomalous Sb concentrations of 150 to 1,110 ppm occur at Logatchev and Nibelungen (Murphy and Meyer, 1998; S. Petersen, unpub. data). The highest concentrations of Se, ranging from 800 to 1,505 ppm, in sulfide samples from ultramafic rock-hosted sea-floor massive sulfide deposits have been documented at Logatchev and Semyenov (Murphy and Meyer, 1998; A. Firstova, unpub. data; S. Petersen, unpub. data).

Sediment-covered mid-ocean ridges

Many of the minor elements, including Bi, Cd, Ge, Hg, Mo, Sb, Te, and Tl occur at concentrations below 50 ppm in sulfide samples from sea-floor massive sulfide deposits located on sediment-covered ridges. Samples from the Escanaba trough have anomalous Bi concentrations exceeding 25 ppm (Benninger and Koski, 1987; Koski et al., 1988, 1994b). Samples having concentrations above 65 ppm are considered to be anomalously enriched in Cd. Concentrations ranging from 200 to 1,975 ppm have been encountered at Middle Valley (Krasnov et al., 1994; M.D. Hannington, unpub. data) and in the Escanaba trough (Benninger and Koski, 1987; Koski et al., 1988, 1994b). Similarly, some sulfide samples from the

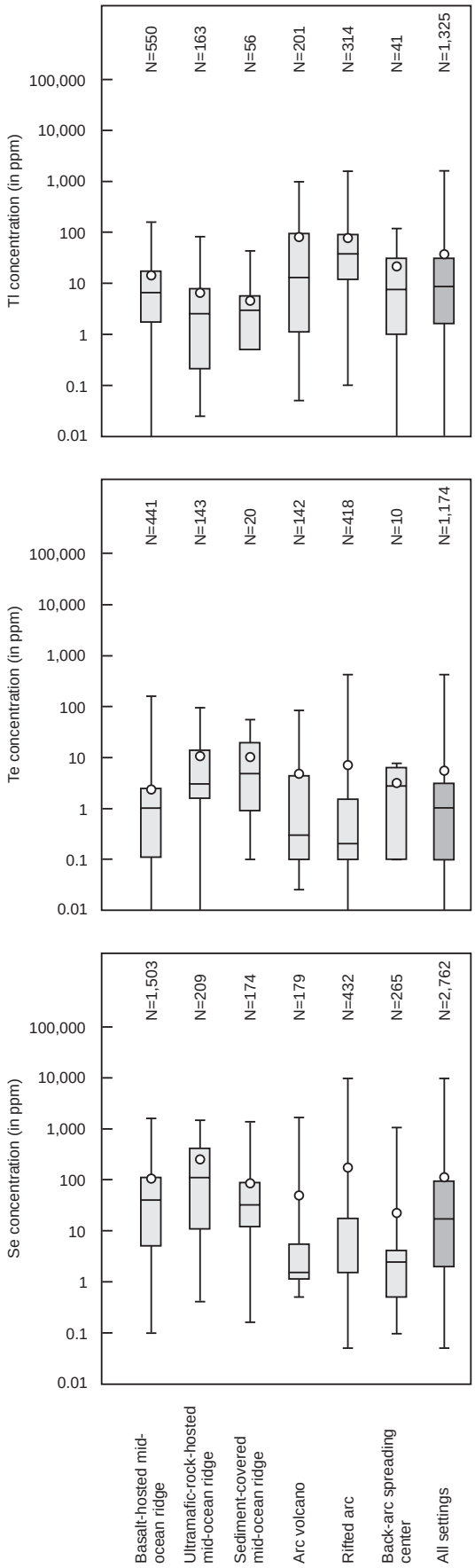

Fig. 4. Whisker-and-box-plot representation of the Se, Te, and Tl concentrations in sulfide samples collected from sea-floor massive sulfide deposits in different volcanic and tectonic settings worldwide. The box encloses the interquartile range with the median displayed as a line. The average value is represented by the open circle. The horizontal lines extending outside of the box mark the minimum and maximum element concentrations encountered. N = number of samples analyzed.

Escanaba trough exhibit anomalous Ge concentrations of 25 to 150 ppm (Benninger and Koski, 1987; Koski et al., 1994b). About 25% of all samples from sediment-covered ridges have Hg concentrations above 30 ppm. Enrichment of this element to concentration levels of 50 to 270 ppm have been documented for some samples from Middle Valley (Krasnov et al., 1994) and the Escanaba trough (Benninger and Koski, 1987; Koski et al., 1988, 1994b). Molybdenum typically occurs at concentrations below 40 ppm, with the highest values being reported from Middle Valley (Krasnov et al., 1994; M.D. Hannington, unpub. data) and the Escanaba trough (Koski et al., 1994b). The concentrations of Sb in sulfide samples from sediment-covered ridges do not typically exceed 20 ppm. However, anomalous enrichment at concentration levels of up to 16,000 ppm have been noted for some samples from the Escanaba trough (Benninger and Koski, 1987; Koski et al., 1988, 1994b). The concentration of Te has only been determined in a few samples from sediment-covered ridges, with the highest concentrations occurring at Middle Valley (M.D. Hannington, unpub. data). Sulfide samples having concentrations above 6 ppm Tl are considered anomalous. High values of up to 43 ppm Tl occur at the Escanaba trough (Benninger and Koski, 1987; Koski et al., 1994b).

Samples from sea-floor massive sulfide deposits located on sediment-covered ridges can have elevated Se concentrations. Approximately 25% of the samples have Se values exceeding 90 ppm. The highest Se concentrations, ranging up to 1,400 ppm have been reported from the Escanaba trough (Benninger and Koski, 1987; Koski et al., 1988, 1994b) and the Guaymas basin (Peter and Scott, 1988).

Arc volcanoes

Sea-floor massive sulfide deposits located on arc volcanoes have been the focus of several detailed studies. Massive sulfide samples from these deposits typically have Bi, In, Se, and Te concentrations below 10 ppm. Bismuth concentrations exceeding 50 ppm have been reported from Palinuro (Petersen et al., 2014), Suiyo (Watanabe and Kajimura, 1994), and Brothers (de Ronde et al., 2011). About 25% of all samples from sea-floor massive sulfide deposits of this tectonic setting have In concentrations exceeding 10 ppm. Anomalously high In concentrations, ranging up to 144 ppm, have been reported from Sunrise (Glasby et al., 2008), Black Forrest (Hein et al., 2014), and Brothers (de Ronde et al., 2011). Anomalous Se concentrations, ranging from 30 to 1,690 ppm, occur in sulfide samples from Brothers (de Ronde et al., 2011). Sulfide samples with Te concentrations exceeding 30 ppm have been reported from Palinuro (Petersen et al., 2014).

The minor elements Ga and Ge typically occur in concentrations below 50 ppm in sulfide samples from sea-floor massive sulfide deposits on arc volcanoes. Sulfide samples with anomalous Ga concentrations ranging from 150 ppm to a maximum of 1,870 ppm have been recovered from Suiyo (Noguchi et al., 2007) and Brothers (de Ronde et al., 2011). Concentrations exceeding 17 ppm Ge are considered to be anomalous. Germanium concentrations above 30 ppm have been reported from Brothers (de Ronde et al., 2011).

In contrast to the elements mentioned above, Cd, Hg, Mo, Sb, and Tl commonly occur in concentrations exceeding 100 ppm. About 25% of all samples recovered from

sea-floor massive sulfide deposits on arc volcanoes have Cd values above 500 ppm. Sulfide samples with concentrations above 1,500 ppm Cd have been reported from Sunrise (Glasby et al., 2008), Myojinsho caldera (Iizasa et al., 1992), Suiyo (Watanabe and Kajimura, 1994; Noguchi et al., 2007), Brothers (de Ronde et al., 2011), and Palinuro (H. Puchelt, unpub. data). Concentrations above 220 ppm Hg are considered anomalous for sulfide samples from sea-floor massive sulfide deposits located on arc volcanoes. So far, only samples from Palinuro have yielded Hg concentrations exceeding 1,000 ppm Hg (Petersen et al., 2014; H. Puchelt, unpub. data). Sulfide samples from arc volcanoes generally have Mo concentrations below 100 ppm. Samples with exceptionally high Mo concentrations, ranging from 200 to 910 ppm have been recovered from Suiyo (Watanabe and Kajimura, 1994; Glasby et al., 2008), Brothers (de Ronde et al., 2011), and Palinuro (Petersen et al., 2014; S. Petersen, unpub. data). The concentrations of Sb are generally high in sea-floor massive sulfide deposits located on arc volcanoes, with enrichments above 5,000 ppm Sb reported from Sunrise (Glasby et al., 2008), Palinuro (Petersen et al., 2014), and Kolumbo (Kilias et al., 2013). Thallium concentrations above 100 ppm are not common in sea-floor massive sulfide deposits located on arc volcanoes. Some of the highest Tl concentrations, ranging from 300 to over 1,000 ppm, have been reported from Palinuro (Petersen et al., 2014) and Kolumbo (Kilias et al., 2013).

Rifted arcs

Samples from sea-floor massive sulfide deposits in rifted arcs generally have minor element concentration ranges comparable to those from sea-floor massive sulfide deposits on arc volcanoes (Figs. 2–4). The concentrations of Bi and Te are low, with only 25% of the samples exceeding concentrations of 5 and 2 ppm, respectively. Sulfide samples with high Bi concentrations, ranging from 200 to 524 ppm, have been recovered from Pacmanus and Solwara 1 (Moss, 2000; S. Petersen, unpub. data), while elevated Te concentrations, with values above 100 ppm, have been recorded for sulfide samples from JADE (Urabe, 1989) as well as Pacmanus and SuSu (Moss, 2000; S. Petersen, unpub. data).

Minor elements occurring at concentrations of up to 100 ppm in sulfide samples recovered from sea-floor massive sulfide deposits in rifted arcs include Ga, Ge, Hg, In, Mo, Se, and Tl. Enrichments of Ga above 125 ppm are considered anomalous. High Ga concentrations, ranging from 1,000 to 3,700 ppm have been observed at JADE, Hakurei, Iheya North knoll (Noguchi et al., 2007), and Pacmanus (S. Petersen, unpub. data). About 25% of all samples collected from rifted arcs have Ge concentrations above 50 ppm, with the highest Ge values, ranging from 100 to 352 ppm, occurring in samples from Pacmanus (Moss, 2000; S. Petersen, unpub. data). The concentration of Hg in samples from rifted arcs does not typically exceed 40 ppm. Anomalous Hg enrichments above 1,000 ppm have been reported from Iheya North knoll (Noguchi et al., 2007), JADE (Nakamura et al., 1990), and the Calypso vents (Hocking, 2007) where native Hg occurs in massive cinnabar samples (Stoffers et al., 1999). The concentrations of In and Mo exceeds 70 ppm only in about 25% of the samples collected from sea-floor massive sulfide deposits in rifted arcs. Samples with elevated In contents, ranging from 100 to 502 ppm, have been collected from Pacmanus (Binns, 2014; S. Petersen, unpub. data) while anomalous Mo concentrations, ranging from 500 to 2,350 ppm have been reported from Pacmanus, Solwara 1, and SuSu (Moss, 2000; Craddock, 2009; Yeats et al., 2014; S. Petersen, unpub. data). Concentrations of Se are typically below 20 ppm, although concentrations as high as 3,000 to 9,700 ppm have been reported from JADE (Aoki and Nakamura, 1989; Urabe, 1989). Thallium concentrations above 90 ppm are considered to be anomalous and enrichments have been reported for samples from JADE (Aoki and Nakamura, 1989; Nakamura et al., 1990), Pacmanus (S. Petersen, unpub. data), the Calypso vents (Hocking, 2007), and Three Sisters in the Bransfield Strait (Petersen et al., 2004).

Cadmium and Sb are the minor elements with the highest concentrations in sulfide samples from rifted arcs. About 25% of the samples analyzed have Cd concentrations above 1,000 ppm and Sb contents above 1,300 ppm. High Cd concentrations have been reported from JADE (Zeng et al., 2009), Pacmanus, and Solwara 1 (Moss, 2000; Craddock, 2009; S. Petersen, unpub. data). Concentrations of Sb exceeding 15,000 ppm have been reported for several sites from the Okinawa trough, including JADE (Urabe, 1989; Aoki and Nakamura, 1989) and Hakurei (Noguchi et al., 2007, 2011).

Back-arc spreading centers

Minor element analyses are available for a number of sea-floor massive sulfide deposits located along back-arc spreading centers. Trace elements typically occurring in concentrations below 10 ppm include Bi, Hg, and Se. Only about 25% of all samples collected from this setting have Bi concentrations exceeding 3 ppm. Concentrations exceeding 10 ppm have been recorded from White Church, Vai Lili, and Hine Hina in the Lau basin (U. Schwarz-Schampera, unpub. data). Concentrations of Hg exceeding 5 ppm are not common. However, anomalous Hg concentrations of up to 35 ppm have been recorded for some samples from the Mariana trough (Noguchi et al., 2011) and the Lau basin (P. M. Herzig, unpub. data). Selenium concentrations exceeding 5 ppm are considered to be anomalous. High Se concentrations above 500 ppm have been recorded for several sites in the Lau basin (Tivey et al., 2005; P.M. Herzig, unpub. data). Only a limited number of Te analyses are available for sulfide samples from sea-floor massive sulfide deposits located along back-arc spreading centers.

The Ga and In concentrations of sea-floor massive sulfides collected from back-arc spreading centers are largely below 50 ppm. Elevated Ga concentrations, ranging from 50 to 210 ppm, have been reported from Maka, White Church, and Vai Lili in the Lau basin (Kim et al., 2011; U. Schwarz-Schampera, unpub. data). About 25% of the samples contain more than 25 ppm In. Maximum concentrations of this element reach 592 ppm in samples from Vai Lili (Schwarz-Schampera and Herzig, 2002). Most samples have Mo concentrations below 50 ppm. Elevated Mo concentrations of 250 to 549 ppm have been reported from White Lady-Starmer in the North Fiji basin (Bendel et al., 1993) as well as Tow Cam, ABE, and White Church in the Lau basin (Fouquet et al., 1993a; Tivey et al., 2005; U. Schwarz-Schampera, unpub. data).

The minor elements Cd, Ge, and Sb have the highest concentrations in samples from sea-floor massive sulfide deposits

located at back-arc spreading centers. Concentrations exceeding 870 ppm Cd are considered to be anomalous. High Cd concentrations of up to 6,300 ppm have been reported from the SO99 site in the North Fiji basin (P. Halbach, unpub. data) as well as Vienna Woods in the Manus basin (Lisitsyn et al., 1993) and Kings Triple Junction A2 in the Lau basin (Lisitsyn et al., 1992). Concentrations above 200 ppm Ge have so far only been noted at Vai Lili (U. Schwarz-Schampera, unpub. data). About 25% of all samples contain more than 100 ppm Sb. Anomalously high Sb concentrations ranging from 250 to 523 ppm occur in individual samples from the Mariana trough and the Lau basin (Herzig et al., 1993; Tivey et al., 2005; Ikehata et al., 2015; M.D. Hannington, unpub. data).

Mineralogical Sequestration of Minor Elements

Polymetallic sea-floor massive sulfide deposits contain sulfide minerals formed over a wide range of temperatures (Haymon and Kastner, 1981; Goldfarb et al., 1983; Haymon, 1983; Fouquet et al., 1993b; Herzig et al., 1993; Hannington et al., 1995; Berkenbosch et al., 2012). High-temperature sulfide minerals typically occur in sulfide-bearing stockworks, in the interior of sulfide mounds, and as linings within the black smoker chimneys. These minerals include chalcopyrite and isocubanite together with pyrrhotite and pyrite, and occasionally wurtzite and bornite (Fig. 5; Haymon and Kastner, 1981; Goldfarb et al., 1983; Haymon, 1983; Fouquet et al., 1993b; Herzig et al., 1993; Berkenbosch et al., 2012). Disseminated sulfides, the outer portions of sulfide mounds, the rims of black smoker chimneys, and white smoker chimneys are made up of lower-temperature sulfide minerals, including sphalerite, marcasite, and pyrite in addition to gangue minerals such as anhydrite, barite, and amorphous silica (Fig. 6; Haymon and Kastner, 1981; Goldfarb et al., 1983; Haymon, 1983; Fouquet et al., 1993b; Herzig et al., 1993; Berkenbosch et al., 2012). Sea-floor massive sulfide deposits formed in suprasubduction settings may also contain tennantite-tetrahedrite and galena as major components (Table 4). Covellite, digenite, and other Cu sulfides are common secondary minerals forming as a result of supergene processes occurring on the sea floor (Hannington et al., 1995).

The major minerals forming the polymetallic massive sulfides of sea-floor massive sulfide deposits can contain small amounts of the elements reviewed in the present contribution, either through substitution into the crystal structure or incorporation into submicroscopic mineral inclusions. So far, most trace element studies on ore minerals from sea-floor massive sulfide deposits have been conducted by electron microprobe (EMP) analysis, which limits detection of these elements to concentrations in the parts per million ranges. In addition to the main sulfide minerals, over 80 trace minerals have been recognized, including a wide range of base metal sulfide, sulfate, and oxide minerals. This includes about 30 trace minerals containing the minor elements discussed in the present review (Table 4).

Bismuth

Bismuth in sea-floor massive sulfide deposits primarily occurs in the accessory phases bismuthinite, tellurobismuthite, and tetradymite. In pyrrhotite-rich massive sulfides from the Escanaba trough, trace amounts of native Bi occur as intergrowths with chalcopyrite and as small (<2 μm) inclusions in löllingite (Zierenberg et al., 1993) that contain up to 10 wt % Sb (Koski et al., 1988; Törmänen and Koski, 2005) and 1.2 wt % Te (Törmänen and Koski, 2005). In polymetallic sulfides, native Bi forms inclusions in arsenopyrite (Koski et al., 1988). Törmänen and Koski (2005) showed that a range of additional Bi-bearing phases are also present, including Bi tellurides, Bi-Te sulfides, and bismuthinite. These Bi minerals represent the most frequent host for gold in the massive sulfide samples from the Escanaba trough. Approximately 75% of native gold, maldonite, and an unnamed Au-bearing phase with the composition of $AuBi_5S_4$ are in contact with the Bi phases as inclusions or intergrowths. EMP analyses showed that the Bi content of the Bi tellurides range from about 40 to 70 wt %, which encompasses compositions of the minerals tsumoite, pilsenite, and hedleyite. The analyses of the Bi-Te sulfides correspond to Bi-enriched joseite-B and S-enriched joseite. In addition, a phase with the approximate composition Bi_3S_2 was identified, which could be Bi-rich ikunolite. Secondary Bi oxide minerals formed as a result of sulfide oxidation at the sea floor include bismite and bismoclite (Törmänen and Koski, 2005).

Dekov and Savelli (2004) described the occurrence of bismuthinite from Palinuro. At the Myojinsho caldera, tellurobismuthite forms small lath-shaped crystals or granular (<10 μm) inclusions in pyrite (Iizasa et al., 1992). Bismuth tellurides with compositions between tellurobismuthite, tetradymite, and kawazulite occur in chalcopyrite-bornite chimneys from Brothers volcano. In addition, native Bi forms wispy, radiating aggregates within the pore space of Cu-rich sulfide samples (Berkenbosch et al., 2012). Bismuthinite is a rare accessory phase in massive sulfides from the Dai-Yon deposit in the southern Okinawa trough. Bismuthinite in chimneys from this field contain Pt concentrations of 1.30 to 1.69 wt % (Gena et al., 2005). In some sea-floor massive sulfide deposits, tellurobismuthite is texturally associated with minerals of the tennantite-tetrahedrite solid solution (Fig. 7).

Cadmium

Sphalerite and wurtzite are the main hosts of Cd in sea-floor massive sulfide deposits (Table 5). Cadmium concentrations in these minerals can reach up to about 1.0 wt %. Enrichment of Cd in sphalerite above this threshold has so far only been recorded from Menez Gwen (Lein et al., 2010), Green Seamount (Alt et al., 1987), Palinuro (Petersen et al., 2014), and Bayonnaise knoll (Watanabe and Hayashi, 2014). In contrast to sphalerite and wurtzite, other sulfide minerals in sea-floor massive sulfide deposits commonly show only low Cd concentrations. Chalcopyrite from Menez Gwen contains <0.01 to 0.09 wt % Cd, while concentrations of <1 to 79 ppm Cd were encountered in pyrite (Lein et al., 2010). Cubanite from Broken Spur grades <0.01 to 0.05 wt % Cd and pyrrhotite contains <0.01 to 0.08 wt % Cd (Bogdanov et al., 2008). Pyrite concentrates from the Southern Explorer site at the Juan de Fuca Ridge yielded concentrations ranging from <10 to 60 ppm Cd (Hannington et al., 1991). Chalcopyrite and isocubanite from the South Cleft site of the Juan de Fuca Ridge contain 0.01 to 0.07 wt % Cd. Maximum concentrations of 0.04 wt % Cd were encountered in pyrrhotite (Paradis et al., 1988). Wang et al. (2014) reported concentrations of <0.02 to 0.03 wt % Cd for chalcopyrite and pyrite from Kairei. At Rainbow, chalcopyrite contains 0.01 to 0.06 wt % Cd, pyrite has Cd

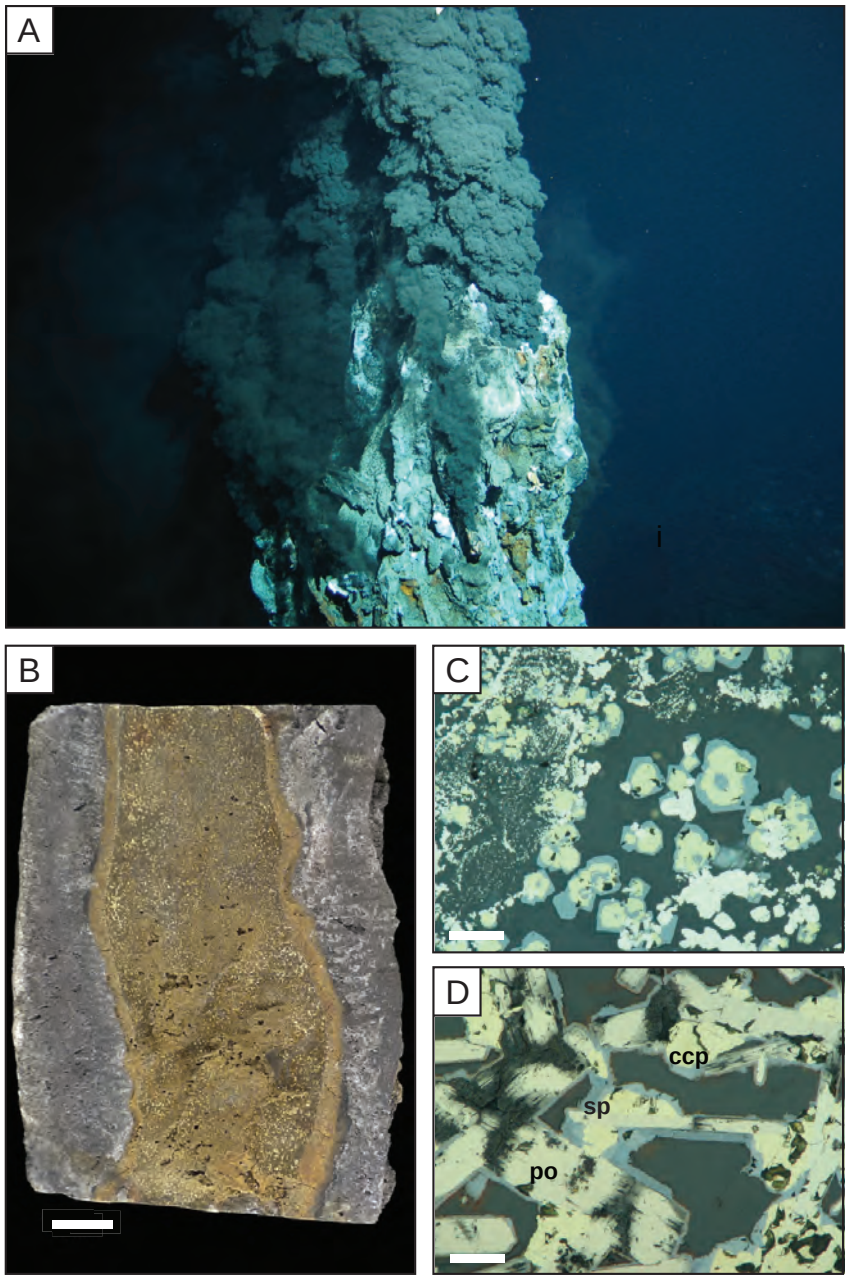

Fig. 5. Characteristics of black smoker chimneys. A. Black smoker chimney at the Turtle Pits hydrothermal field, Mid-Atlantic Ridge (photo: ROV Kiel 6000, GEOMAR). The field of view is approximately 1 m. B. Cross section through a high-temperature chimney showing a central lining of chalcopyrite. The rim of the smoker consists of a mixture of anhydrite and sphalerite. The chimney originates from the Vai Lili hydrothermal field, Lau basin (R/V Nadir cruise Nautilau, sample NL-20-04). C. Reflected light microphotograph of a black smoker sample from the Turtle Pits hydrothermal field, Mid-Atlantic Ridge. The image shows an assemblage of pyrite and chalcopyrite/isocubanite that is overgrown by sphalerite (medium gray). Open space is dark gray. Chalcopyrite and isocubanite cannot be distinguished at this magnification (R/V Meteor cruise M68/1, sample 07ROV-01). Scale bar is 100 μm. D. Reflected light microphotograph of a black smoker sample from the ultramafic rock-hosted Logatchev-1 hydrothermal field, Mid-Atlantic Ridge. The image shows an assemblage of pyrrhotite (po), chalcopyrite (ccp), and sphalerite (sp), which are all rimmed by late Fe oxyhydroxides. Pyrrhotite is showing dissolution textures due to its interaction with cold seawater (R/V Meteor cruise M60/3, sample 73ROV-02). Scale bar is 100 μm.

concentrations of 0.01 wt %, and pyrrhotite contains 0.02 to 0.03 wt % Cd (Marques et al., 2006). Chalcopyrite and pyrite at Palinuro are characterized by <0.02 to 0.04 wt % Cd, while galena contains between 0.04 and 0.11 wt % Cd (Petersen et al., 2014). Petersen et al. (2004) recorded Cd concentrations of 0.03 to 0.11 wt % in galena from Hook Ridge.

Distinct Cd minerals are rare in sea-floor massive sulfide deposits. At Rainbow, Lein et al. (2003) identified a Cd-rich mineral, presumably native Cd. So far, greenockite has only been described from the Myojinsho caldera where small grains of this mineral are in contact with chalcopyrite and sphalerite (Iizasa et al., 1992).

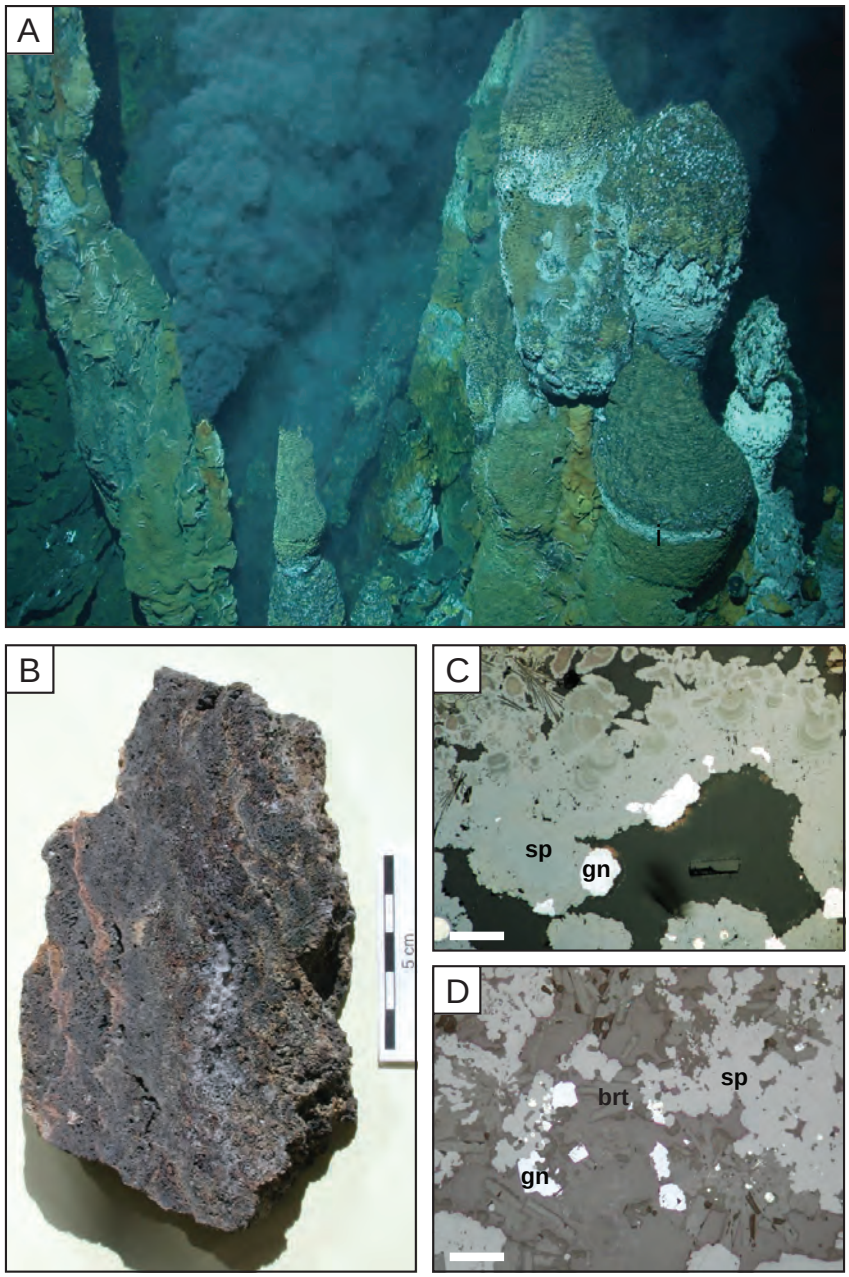

Fig. 6. Characteristics of white smoker chimneys. A. White to gray smoker chimneys at the Roman Ruins site of the Pacmanus hydrothermal field, Manus basin (photo: ROV Quest 4000, MARUM, University of Bremen). The field of view is approximately 2.5 m. B. Cross section through a sphalerite-rich chimney from the Roman Ruins site of the Pacmanus hydrothermal field, Manus basin. The image shows the common association between brown sphalerite and white barite (R/V Sonne cruise SO166, sample 70GTV-1C2). C. Reflected light microphotograph of a sphalerite-rich sample from the Pacmanus hydrothermal field, Manus basin. The image shows an assemblage of medium gray sphalerite (sp) and galena (gn)/jordanite. Note the colloform texture of early sphalerite, which is intimately intergrown with opal-A. Open space is dark gray (R/V Sonne cruise SO216, sample 34GTV-01). Scale bar is 100 μm. D. Reflected light microphotograph of a sphalerite-rich sample from the Roman Ruins site at the Pacmanus hydrothermal field, Manus basin. The image shows an assemblage of sphalerite (sp) and barite (brt), which is overgrown by opal-A (globular, dark gray) and late galena (gn) grains (R/V Sonne cruise SO166, sample 70GTV-1A2). Scale bar is 200 μm.

Gallium and germanium

At present, little is known about the mineralogical sequestration of Ga and Ge in sea-floor massive sulfide deposits. An exception is a study by Petersen et al. (2004) showing that sphalerite from Hook Ridge contains <0.02 to 0.15 wt % Ga.

Mercury

In many sea-floor massive sulfide deposits, Hg is present in solid solution in tennantite and tetrahedrite. For instance, tetrahedrite from Palinuro contains between <0.02 and 7.24 wt % Hg. In addition, a distinct Hg-rich sulfosalt (Fig. 8A)

Table 4. Mineralogical Composition of Sea-Floor Massive Sulfide Deposits (minerals in italic are mainly, although not always exclusively, of secondary origin; gangue minerals are not listed)

Mineral	Formula	Basalt-hosted mid-ocean ridge	Ultramafic rock-hosted mid-ocean ridge	Sediment-covered mid-ocean ridge	Arc volcano	Rifted arc	Back-arc spreading center
Main minerals							
Bornite	Cu_5FeS_4	++	++	-	+	++	++
Chalcopyrite/ISS	$CuFeS_2$	+++	+++	+++	+++	+++	+++
Covellite	CuS	++	++	+	++	++	++
Galena	PbS	++	++	++	+++	+++	++
Isocubanite/cubanite	$CuFe_2S_3$	+++	+++	+++	-	++	-
Marcasite	FeS_2	+++	+++	+++	+++	+++	+++
Pyrite	FeS_2	+++	+++	++	+++	+++	+++
Pyrrhotite	$Fe_{1-x}S$	+++	+++	+++	+	+	+
Sphalerite	ZnS	+++	+++	+++	+++	+++	+++
Wurtzite	ZnS	++	+	++	+++	+++	++
Minor and trace minerals							
Acanthite/argentite	Ag_2S	+	+	+	-	-	-
Alabandite	MnS	-	-	+	-	+	-
Anglesite	$PbSO_4$	+	-	-	+	++	+
Anilite	Cu_7S_4	-	+	-	-	-	-
Argentopyrite	$AgFe_2S_3$	-	+	-	-	-	-
Arsenopyrite	FeAsS	-	-	++	+	+	-
Atacamite/paratacamite/ botallackite	$Cu_2Cl(OH)_3$	+	+	-	-	+	-
Bismite	Bi_2O_3	-	-	+	-	-	-
Bismoclite	BiOCl	-	-	+	-	-	-
Bismuthinite	Bi_2S_3	-	-	+	+	+	-
Boulangerite	$Pb_5Sb_4S_{11}$	+	-	+	-	-	-
Bravoite	$(Ni,Fe)S_2$	-	-	-	+	-	-
Calaverite	$AuTe_2$	-	-	-	+	-	-
Cerussite	$PbCO_3$	-	-	-	+	+	-
Cassiterite	SnO_2	-	+	-	-	-	-
Chalcanthite	$CuSO_4{\cdot}5H_2O$	+	+	-	-	-	-
Chalcocite	Cu_2S	+	++	-	+	+	-
Chlorargyrite	AgCl	-	-	-	-	+	-
Cinnabar	HgS	-	-	-	+	+	-
Cobaltite	CoAsS	-	+	-	-	-	-
Coloradoite	HgTe	-	+	-	-	-	-
Cuprite	Cu_2O	-	+	-	-	+	-
Digenite	Cu_9S_5	++	++	+	+	+	+
Djurleite	$Cu_{31}S_{16}$	-	+	-	-	-	-
Dufrenoysite	$Pb_2As_2S_5$	-	-	-	-	++	-
Enargite	Cu_3AsS_4	-	-	-	++	++	-
Eskebornite	$CuFeSe_2$	-	-	-	+	-	-
Famatinite	Cu_3SbS_4	-	-	-	+	-	-
Franckeite	$(Pb,Sn)_6FeSn_2Sb_2S_{14}$	-	-	+	-	-	-
Freieslebenite	$AgPbSbS_3$	-	-	-	-	+	-
Fukuchilite	$(Cu,Fe)S_2$	-	-	-	-	+	-
Geerite	Cu_8S_5	-	+	-	-	-	-
Glaucodot/alloclasite	(Co,Fe)AsS	-	-	+	-	-	-
Gordaite	$NaZn_4(SO_4)(OH)_6Cl{\cdot}6H_2O$	+	-	-	-	-	-
Goslarite	$ZnSO_4{\cdot}7H_2O$	+	-	-	-	-	-
Gratonite	$Pb_9As_4S_{15}$	-	-	-	-	-	+
Greenockite	CdS	-	-	-	+	-	-
Greigite	$FeFe_2S_4$	-	+	-	-	-	-
Hessite	Ag_2Te	-	(?)	-	-	-	-
Idaite	Cu_3FeS_4	+	+	-	+	-	+
Jalpaite	Ag_3CuS_2	-	-	-	-	+	-
Jordanite-geocronite	$Pb_{14}(As,Sb)_6S_{23}$	+	-	+	+	++	+
Kawazulite	$Bi_2(Te,Se,S)_3$	-	-	-	+	-	-
Kermesite	Sb_2S_2O	-	-	-	-	+	-
Linnaeite	$CoCo_2S_4$						
Löllingite-safflorite	$(Fe,Co)As_2$	+	+	+	-	-	-

Table 4. *(Cont.)*

Mineral	Formula	Basalt-hosted mid-ocean ridge	Ultramafic rock-hosted mid-ocean ridge	Sediment-covered mid-ocean ridge	Arc volcano	Rifted arc	Back-arc spreading center
Minor and trace minerals *(Cont.)*							
Luzonite	Cu_3AsS_4	-	+	-	-	+	-
Maldonite	Au_2Bi	-	-	+	-	-	-
Melonite	$NiTe_2$	-	+	-	-	-	-
Mimetite	$Pb_5(AsO_4)_3Cl$	-	-	-	+	-	-
Millerite	NiS	-	+	-	-	-	-
Molybdenite	MoS_2	-	+	-	-	-	-
Nantokite	CuCl	+	-	-	-	-	-
Native Ag	Ag	-	+	-	-	+	-
Native As	As	-	+	-	+	+	-
Native Au-electrum	Au	+	+	+	+	+	++
Native Bi	Bi	-	-	+	+	-	-
Native Cd	Cd	-	+	-	-	-	-
Native Cu	Cu	+	+	-	-	-	-
Native Hg	Hg	-	-	-	-	+	-
Native Pb	Pb	-	+	-	-	-	-
Native Pt	Pt	-	+	-	-	-	-
Native Te	Te	-	-	-	+	-	-
Nukundamite	$(Cu,Fe)_4S_4$	-	-	-	-	+	-
Orpiment	As_2S_3	-	-	-	+	+	-
Pearceite	$(Ag,Cu)_{16}As_2S_{11}$	-	-	-	+	-	-
Pentlandite	$(Fe,Ni)_9S_8$	-	+	-	-	-	-
Proustite-pyrargyrite	$Ag_3(As,Sb)S_3$	-	-	-	+	+	+
Realgar	AsS	+	-	-	++	++	-
Robinsonite	$Pb_4Sb_6S_{13}$	-	-	-	-	+	-
Roxbyite	Cu_9S_5	+	+	-	-	-	-
Samsonite	$Ag_4MnSb_2S_6$	-	-	-	-	+	-
Seligmannite-bournonite	$PbCu(As,Sb)S_3$	-	-	-	+	-	-
Semseyite	$Pb_9Sb_8S_{21}$	-	-	-	+	-	-
Spionkopite	$Cu_{39}S_{28}$	-	+	-	-	-	-
Stannite	Cu_2FeSnS_4	-	-	+	-	-	-
Stephanite	Ag_5SbS_4	-	-	-	-	-	+
Stibnite	Sb_2S_3	-	-	+	++	++	-
Tellurobismuthite	Bi_2Te_3	-	-	-	++	-	-
Tennantite-tetrahedrite	$(Cu,Ag,Zn,Fe)_{12}(As,Sb)_4S_{13}$	+	+	+	++	++	++
Tenorite	CuO	-	+	-	-	-	-
Tetradymite	Bi_2Te_2S	-	-	-	+	-	-
Troilite	FeS	-	+	-	-	-	-
Umangite	Cu_3Se_2	-	-	-	+	-	-
Uraninite	UO_2	-	+	-	-	-	-
Yarrowite	Cu_9S_8	-	+	-	-	-	-

Notes: +++ = abundant, ++ = common, + = rare, - = not reported, (?) = uncertain occurrence

Basalt-hosted mid-ocean ridge: Alt et al. (1987), Bischoff et al. (1983), Bogdanov et al. (2008), Butler et al. (1998), Detrick et al. (1986), Dill et al. (1992), Duckworth et al. (1995), Embley et al. (1988), Fouquet et al. (1988, 1993b), Goldfarb et al. (1983), Graham et al. (1988), Haase et al. (2007), Halbach et al. (1998), Hannington (1993), Hannington and Scott (1988), Hannington et al. (1986, 1988, 1991), Haymon and Kastner (1981), Hekinian et al. (1980), Herzig et al. (1991), Humphris et al. (1995), Koski et al. (1994a), Krasnov et al. (1995b), Kristall et al. (2006), Lalou et al. (1998), Langmuir et al. (1997), Lein et al. (2010), Marchig et al. (1997), Moss and Scott (1988), Mozgova et al. (1998), Münch et al. (1999, 2000, 2001), Normark et al. (1986), Nygård et al. (2003), Paradis et al. (1988), Petersen et al. (2000), Rona et al. (1993), Sudarikov et al. (1990), Thompson et al. (1988), Tivey and Delaney (1986), Tufar et al. (1984), Verati et al. (1999), Zierenberg et al. (1984); Ultramafic-rock-hosted mid-ocean ridge: Bach et al. (2002), Cherkashov et al. (2010b), Dekov et al. (2011), Fouquet et al. (2010), Gablina et al. (2000, 2006), Lein et al. (2003), Marques et al. (2006), Melekestseva (2010), Melekestseva et al. (2010, 2014a, b), Mozgova et al. (1996, 1999, 2005, 2008), S. Petersen (unpub. data), Torokhov et al. (2002), Wang et al. (2012, 2014); Sediment-covered mid-ocean ridge: Ames et al. (1993), Davis et al. (1987), Koski et al. (1985; 1988; 1994b), Lawrie and Miller (2000), Peter and Scott (1988), Törmänen and Koski (2005), Zierenberg and Miller (2000), Zierenberg et al. (1993); Arc volcano: Berkenbosch et al. (2012), Dekov and Savelli (2004), de Ronde et al. (2003b, 2005, 2014), Glasby et al. (2008), Hein et al. (2014), Iizasa (1993), Iizasa et al. (1992, 1999), Iwaida and Ueno (2005), Kasuga and Kato (1992), Kilias et al. (2013), Leybourne et al. (2012), Marumo et al. (2008), Petersen et al. (2014), Sigurdsson et al. (2006), Stoffers et al. (2006), Tufar (1991); Rifted arc: Binns (2014), Binns and Scott (1993), Binns et al. (1997), Chiba et al. (1996), Fukuba et al. (2015), Gena et al. (2005), Halbach et al. (1993), Iizasa et al. (2004), Kim et al. (2009), Lüders et al. (2001), Moss and Scott (2001), Nakashima et al. (1993, 1995), Nedachi et al. (1992), Okamoto et al. (2002), Petersen et al. (2004), Stoffers et al. (1999), Suzuki et al. (2008), Ueno et al. (2003), Watanabe and Hayashi (2014), Watanabe et al. (2006), Yeats et al. (2014); Back-arc spreading center: Bendel et al. (1993), Fouquet et al. (1993a), Herzig et al. (1993), Ikehata et al. (2015), Iwaida and Ueno (2005), Kakegawa et al. (2008), Kim et al. (2006), Lisitsyn et al. (1992, 1993), Paropkari et al. (2010), Shadlun et al. (1993), and Tufar (1990)

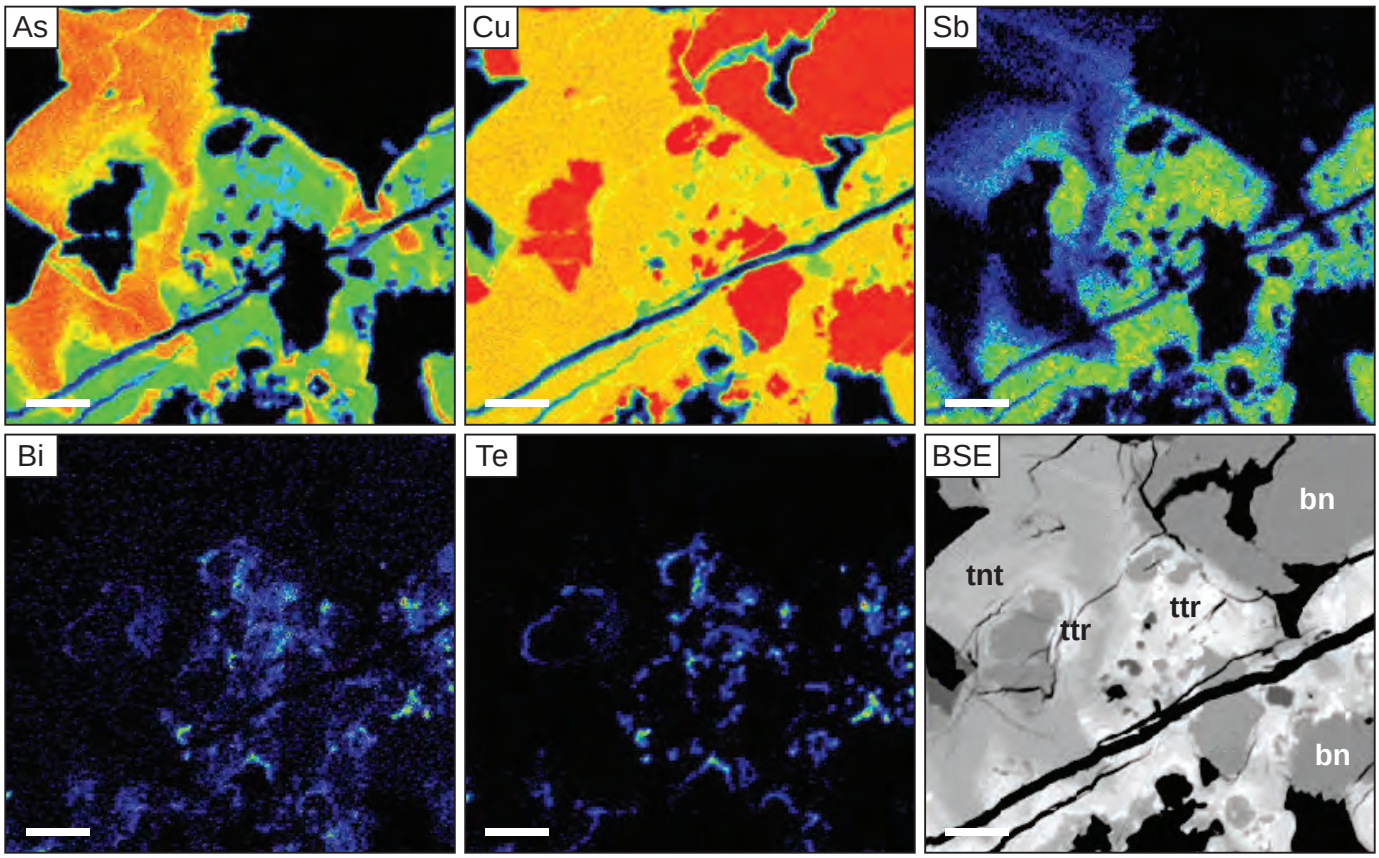

Fig. 7. Electron microprobe element distribution maps across tennantite-tetrahedrite grains from the Satanic Mills site at the Pacmanus hydrothermal vent field, Manus basin (R/V Sonne cruise SO-216, station 43ROV). The maps show the distribution of As, Cu, Sb, Bi, and Te. Hot colors are indicative for high element concentrations, while cold colors indicate low concentrations. The backscattered electron (BSE) image is given for comparison. The tennantite-tetrahedrite shows pronounced compositional zoning, characterized by tetrahedrite cores (ttr) and tennantite rims (tnt). The tennantite-tetrahedrite is in contact with bornite (bn), which is essentially devoid of As. Abundant small tellurobismuthite grains occur within the Sb-rich zones of the tennantite-tetrahedrite grains, in close contact with the bornite. Scale bar is 20 μm.

was recognized that contains 19.6 to 21.5 wt % Hg (Petersen et al., 2014). Minerals belonging to the tennantite-tetrahedrite solid solution from Hook Ridge contain between <0.02 and 0.54 wt % Hg (Petersen et al., 2004). Mercury may also be present in sphalerite, pyrite, and galena. Petersen et al. (2014) analyzed sphalerite and pyrite from Palinuro and recorded Hg concentrations of <0.02 to 7.41 and <0.02 to 0.69 wt %, respectively. Chalcopyrite and galena are characterized by <0.02 to 0.09 wt % Hg. At Hook Ridge, Petersen et al. (2004) noted Hg concentrations of <0.02 to 1.00 wt % Hg in sphalerite.

The rare Hg-bearing mineral coloradoite has been observed at the Rainbow and Logatchev deposits (Torokhov et al., 2002; Lein et al., 2003; Mozgova et al., 2005). Massive sulfides at Palinuro (Petersen et al., 2014) and in sea-floor massive sulfide deposits of the Okinawa trough (Halbach et al., 1993; Nakashima et al., 1995; Lüders et al., 2001; Okamoto et al., 2002) contain trace amounts of cinnabar (Fig. 8B). Massive amounts of cinnabar occur in shallow marine hot spring deposits in the Bay of Plenty of the Taupo volcanic zone (Stoffers et al., 1999). This is, so far, also the only site where native Hg is present, forming small droplets within porous cinnabar.

Indium

As discrete In-bearing phases have so far not been reported from sea-floor massive sulfide deposits, much of the In contained in bulk massive sulfide samples probably occurs as impurities or microinclusions in the main sulfide phases. Lein et al. (2010) showed that chalcopyrite from Menez Gwen contains up to 0.12 wt % In, while sphalerite contains up to 0.09 wt % In. At Broken Spur, cubanite and pyrrhotite contain up to 0.11 and 0.06 wt % In, respectively (Bogdanov et al., 2008). Schwarz-Schampera and Herzig (2002) suggested that In enrichment of chalcopyrite-rich massive sulfide samples from the Lau basin can be related to the presence of chalcopyrite-roquesite solid solution, microinclusions of roquesite in chalcopyrite, or the substitution of In into the crystal structure of high Fe sphalerite.

Molybdenum

Molybdenum is largely contained as an impurity in the main iron and copper sulfides. Instrumental neutron activation analysis (INAA) by Hannington et al. (1991) showed that pyrite concentrates from Snake Pit have Mo contents of 47 to

Table 5. Cadmium Content of Sphalerite (Sp) and Wurtzite (Wur) in Sea-floor Massive Sulfide Deposits (concentrations in wt %)

No.	Deposit and location	Mineral	Cd
18	Menez Gwen, Mid-Atlantic Ridge	Sp	<0.02–1.73
20	Broken Spur, Mid-Atlantic Ridge	Sp	0.01–0.53
48	CASM, Axial Smt., Juan de Fuca Ridge	Sp	0.18–0.32
51	North Cleft, Juan de Fuca Ridge	Sp	0.03–0.42
		Wur	0.04–0.70
52	South Cleft, Juan de Fuca Ridge	Sp	<0.01–0.56
		Wur	0.04–0.71
55	EPR 20°50'N, East Pacific Rise	Wur	<0.01–0.42
56	Green Smt., East Pacific Rise	Sp	0.57–1.19
130	Kairei, Central Indian Ridge	Sp	<0.02–0.14
133	Rainbow, Mid-Atlantic Ridge	Sp	0.06–0.33
134	Logatchev-1, Mid-Atlantic Ridge	Sp/wur	0.03–0.40
148	Northern Escanaba trough, Gorda Ridge	Sp	0.05–0.53
150	Southern trough, Guaymas basin, Gulf of California	Sp	0.03–0.17
155	Forecast, Mariana arc	Sp	0.02–0.04
167	Palinuro, Aeolian arc	Sp	<0.02–1.44
170	Bayonnaise knoll, Izu-Ogasawara arc	Sp	<0.01–1.84
171	Minami-Ensei knoll, Okinawa trough	Sp	0.18–0.73
		Wur	0.30–0.39
172	Iheya North knoll, Okinawa trough	Sp	0.12–0.33
		Wur	0.17–0.42
173	Clam, Okinawa trough	Wur	<0.01–0.04
180	Hatoma knoll, Okinawa trough	Sp	0.10–0.20
181	Dai-Yon, Okinawa trough	Sp	0.14
194	Hook Ridge, Bransfield Strait	Sp	<0.02–0.47
196	Alice Springs, Mariana trough	Sp	0.17–0.50
208	Vienna Woods, Manus basin	Sp	<0.01–0.56

References: [18] Lein et al. (2010); [20] Bogdanov et al. (2008); [48] Hannington et al. (1991); [51] Koski et al. (1984, 1994a); [52] Normark et al. (1983), Paradis et al. (1988); [55] Zierenberg et al. (1984); [56] Alt et al. (1987); [130] Wang et al. (2014); [133] Marques et al. (2006); [134] Mozgova et al. (1999); [148] Zierenberg et al. (1993); [150] Koski et al. (1985); [155] Iwaida and Ueno (2005); [167] Petersen et al. (2014); [170] Watanabe and Hayashi (2014); [171] Nedachi et al. (1992), Nakashima et al. (1993); [172] Ueno et al. (2003); [173] Nakashima et al. (1993); [180, 181] Okamoto et al. (2002); [194] Petersen et al. (2004); [196] Iwaida and Ueno (2005); and [208] Shadlun et al. (1993)

71 ppm. The Mo content of chalcopyrite concentrates from the TAG hydrothermal mound range from 98 to 498 ppm. Pyrite concentrates from the Southern Explorer site yielded concentrations ranging from 66 to 104 ppm Mo, while chalcopyrite concentrates have 77 to 443 ppm Mo (Hannington et al., 1991). Pyrite and marcasite from Vienna Woods contain up to 30 ppm Mo (Shadlun et al., 1993). Molybdenite as a discrete phase is extremely rare and has so far only been recognized at Rainbow (Lein et al., 2003). However, anomalously high Mo concentrations of up to 6,790 ppm in pyrite were recorded by laser ablation-inductively coupled plasma-mass spectrometry (LA-ICP-MS) in samples from Menez Gwen and can probably be accounted for by the presence of microinclusions of molybdenite in the analyzed pyrite (Lein et al., 2010).

Antimony

In many sea-floor massive sulfide deposits, significant amounts of Sb are contained in the main sulfide minerals, especially sphalerite. LA-ICP-MS investigation by Lein et al. (2010) demonstrated that pyrite from Menez Gwen is typified by 0.48 to 255 ppm Sb. Chalcopyrite from the same location contains up to 0.07 wt % Sb, while sphalerite contains up to 0.13 wt % Sb (Lein et al., 2010). At Turtle Pits, LA-ICP-MS analyses yielded average Sb concentrations of 0.5 ppm for chalcopyrite, 4.9 ppm for pyrite, and 47.9 ppm for sphalerite (Wohlgemuth-Ueberwasser et al., 2015). Trace element analyses of pyrite and chalcopyrite concentrates from the Southern Explorer site yielded Sb concentrations of 2 to 26 and 0.6 to 0.7 ppm, respectively (Hannington et al., 1991). Hannington et al. (1991) showed that sphalerite concentrates from the CASM and ASHES vent sites at Axial Seamount contain 355 to 1,580 ppm Sb. Up to 400 ppm Sb is contained in sphalerite from the ODP Mound at Middle Valley (Lawrie and Miller, 2000), while galena contains on average 0.05 wt % Sb (Ames et al., 1993). Trace element analyses on pyrrhotite, pyrite, and sphalerite from Middle Valley performed by Houghton et al. (2004) confirmed that sphalerite represents a major sink for Sb at this deposit. LA-ICP-MS analyses of chalcopyrite and pyrite from Logatchev yielded average concentrations of 22.5 and 11.6 ppm, respectively (Wohlgemuth-Ueberwasser et al., 2015).

Petersen et al. (2014) analyzed pyrite from Palinuro and noted concentrations of <0.02 to 2.71 wt % Sb. Chalcopyrite in the same samples contains <0.02 to 1.14 wt % Sb, while sphalerite hosts <0.02 to 3.49 wt % Sb. Concentrations of <0.02 to 2.27 wt % Sb were encountered in galena. Enargite at the Bayonnaise knoll in the Izu-Ogasawara arc contains <0.01 to 0.07 wt % Sb (Watanabe and Hayashi, 2014). At the Iheya North knoll in the Okinawa trough, Ueno et al. (2003) measured concentrations of 0.02 to 1.00 wt % Sb in galena. Galena from Pacmanus contains 0.5 to 3.0 wt % Sb (Binns, 2014). Based on LA-ICP-MS analyses, Wohlgemuth-Ueberwasser et al. (2015) reported average Sb concentrations of 164 ppm for chalcopyrite, 175 ppm for pyrite, and 1,480 ppm for sphalerite. Petersen et al. (2004) noted Sb concentrations of <0.02 to 0.17 wt % in sphalerite, <0.02 to 0.10 wt % in galena, and <0.02 to 0.04 wt % in covellite from Hook Ridge. Iwaida and Ueno (2005) reported concentrations of up to 0.25 wt % Sb in galena from Alice Springs. Sphalerite from Vienna Woods has Sb concentrations ranging from 0.15 to 1.38 wt %, while galena has 0.36 to 2.50 wt % Sb (Shadlun et al., 1993).

In addition to the main sulfide phases, elevated Sb concentrations in massive sulfide samples may be related to the presence of minerals of the tennantite-tetrahedrite solid solution. A wide range of compositions, spanning from tennantite to tetrahedrite, can be encountered. This is particularly true for deposits located in volcanic arcs and associated rifts where the most comprehensive data is available (Table 6). In many cases, tennantite and tetrahedrite grains show pronounced compositional zoning (Figs. 7, 9).

Besides tennantite-tetrahedrite minerals, Sb-bearing trace minerals are rare in sea-floor massive sulfide deposits located on mid-ocean ridges. Münch et al. (2001) documented boulangerite at Mount Jourdanne on the Southwest Indian Ridge. Boulangerite and franckeite are present in trace amounts in massive sulfides from the Escanaba trough (Koski et al., 1988; Zierenberg et al., 1993; Törmänen and Koski, 2005). A possible occurrence of stibnite has been recorded from ODP Mound at Middle Valley (Lawrie and Miller, 2000).

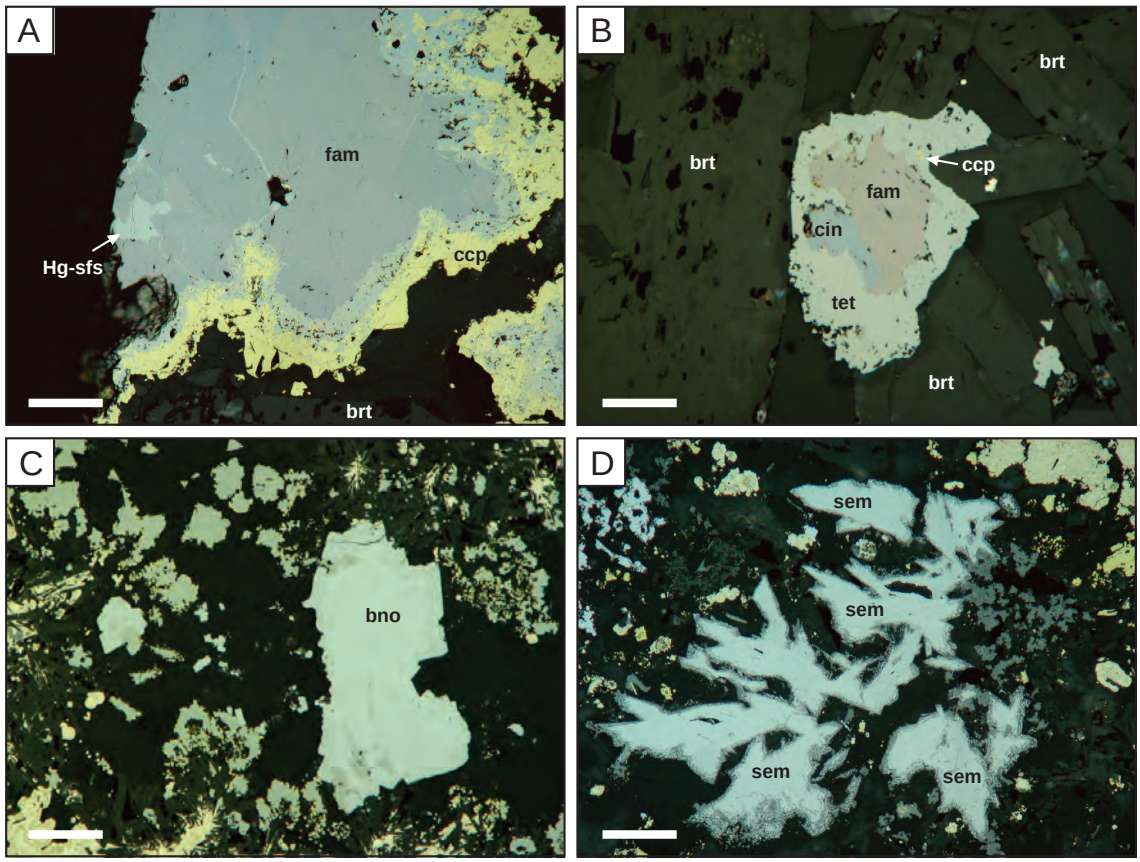

Fig. 8. Reflected light microphotographs of trace minerals contained in sulfide samples recovered by shallow drilling from the sea-floor massive sulfide deposit at the Palinuro volcanic complex in the Aeolian arc, Tyrrhenian Sea. A. Intergrowth of famatinite Cu_3SbS_4 (fam) and chalcopyrite (ccp). The grain hosts an Hg-rich sulfosalt (Hg-sfs) that contains 19 to 21.5 wt % Hg. A euhedral barite (brt) grain is located in the lower part of the image (R/V Meteor cruise M72/3, station 857RD, sample 41-45 cm). B. Intergrown mineral aggregate consisting of a core of famatinite Cu_3SbS_4 (fam) and cinnabar HgS (cin) surrounded by tetrahedrite (tet). The tetrahedrite is host to small grains of chalcopyrite (ccp). The matrix is composed mainly of barite (brt) and small pyrite grains (R/V Meteor cruise M72/3, station 851RD, sample 72-76 cm). C. Large bournonite $PbCuSbS_3$ crystal (bno) that is surrounded by a barely visible rim of seligmannite $PbCuAsS_3$. The matrix consists of amorphous silica with abundant small grains of tetrahedrite and barite. Also present are trace amounts of chalcopyrite and pyrite (R/V Meteor cruise M72/3, station 932RD, sample 156-159 cm). D. Sb-bearing Pb sulfosalt grain that is compositionally close to semseyite $Pb_9Sb_8S_{21}$ (sem). The grain has diffuse grain boundaries and is set in a matrix of amorphous silica and fine-grained pyrite, chalcopyrite, tetrahedrite, galena, and sphalerite (R/V Meteor cruise M72/3, station 857RD, sample 41-45 cm). Scale bar is 100 μm in all images.

In contrast to mid-ocean ridge systems, Sb-bearing trace minerals are common in deposits located on arc volcanoes. Palinuro represents a well-documented example for the occurrence of stibnite and proustite-pyrargyrite (Dekov and Savelli, 2004). In addition to those minerals, bournonite and members of the seligmanite-bournonite solid solution occur in association with galena and sphalerite at this site (Fig. 8C; Petersen et al., 2014). Petersen et al. (2014) also documented a rare Sb-bearing Pb sulfosalt, which contains between 25.4 and 28.9 wt % Sb and is compositionally close to semseyite (Fig. 8D). Famatinite is a minor mineral at Palinuro (Fig. 8B), containing between 12.2 and 25.3 wt % Sb. Enargite in the massive sulfides has Sb concentrations of 0.11 to 2.99 wt % (Petersen et al., 2014). Besides Palinuro, members of the proustite-pyrargyrite solid solution have been reported from the Sunrise deposit in the Izu-Ogasawara arc (Iizasa et al., 1999).

A range of Sb-bearing minerals have been identified in the deposits of the Okinawa trough. Stibnite is present in the outer zones of black smoker chimneys at the JADE deposit (Halbach et al., 1993; Lüders et al., 2001), but is also present at the Minami-Ensei knoll (Nedachi et al., 1992; Nakashima et al., 1995), and in the sulfate-rich portions of black smoker chimneys at the Hatoma knoll (Okamoto et al., 2002) and Dai-Yon (Okamoto et al., 2002; Gena et al., 2005; Suzuki et al., 2008). Freieslebenite at the Iheya North knoll contains between 14.2 and 23.3 wt % Sb, while luzonite hosts 1.91 to 3.09 wt % Sb (Ueno et al., 2003). Fine, hair-like, and sometimes radial aggregates of kermesite have been described from the JADE site (Halbach et al., 1993; Lüders et al., 2001) as well as from the Hatoma knoll and Dai-Yon (Okamoto et al., 2002). Enargite contained in an Mn-rich chimney from Dai-Yon has average Sb concentrations of 0.24 wt % (Suzuki et al., 2008). Members of the proustite-pyrargyrite solid solution are also present at the JADE vent field (Halbach et al., 1993). Suzuki et al. (2008) described the occurrence of samsonite from Dai-Yon. The Minami-Ensei knoll vent site currently

Table 6. Antimony Content of Tennantite-Tetrahedrite in Sea-Floor Massive Sulfide Deposits (concentrations in wt %)

No.	Deposit and location	Sb
167	Palinuro, Aeolian arc	6.01–30.0
170	Bayonnaise knoll, Izu-Ogasawara arc	<0.01–3.83
171	Minami-Ensei knoll, Okinawa trough	<0.10–23.9
172	Iheya North knoll, Okinawa trough	2.17–26.1
175	JADE, Okinawa trough	0.3–26.1
181	Dai-Yon, Okinawa trough	0.02–3.38
182	Pacmanus, Manus basin	0.03–1.10
194	Hook Ridge, Bransfield Strait	<0.02–15.7

References: [167] Petersen et al. (2014); [170] Watanabe and Hayashi (2014); [171] Nedachi et al. (1992); [172] Ueno et al. (2003); [175] Halbach et al. (1993); [181] Suzuki et al. (2008); [182] Binns and Scott (1993), Wohlgemuth-Ueberwasser et al. (2015); and [194] Petersen et al. (2004)

represents the only known occurrence of robinsonite on the modern sea floor (Nedachi et al., 1992).

Minerals of the jordanite-geocronite solid solution have been recorded from a number of sea-floor massive sulfide deposits, including Broken Spur (Duckworth et al., 1995), Snake Pit (Detrick et al., 1986), Axial Seamount (Hannington and Scott, 1988; Hannington et al., 1991), the massive sulfides of the Escanaba trough (Törmänen and Koski, 2005), the Sunrise deposit at the Myojin knoll (Iizasa et al., 1999; Glasby et al., 2008), Brothers volcano (Berkenbosch et al., 2012), Palinuro (Tufar, 1991), and the Bayonnaise knoll in the Izu-Ogasawara arc (Iizasa et al., 2004). A sphalerite-rich siliceous chimney recovered from Pacmanus was found to contain both Sb-free jordanite and phases compositionally intermediate between jordanite and geocronite, indicating that significant variations in the composition of this sulfosalt can occur at

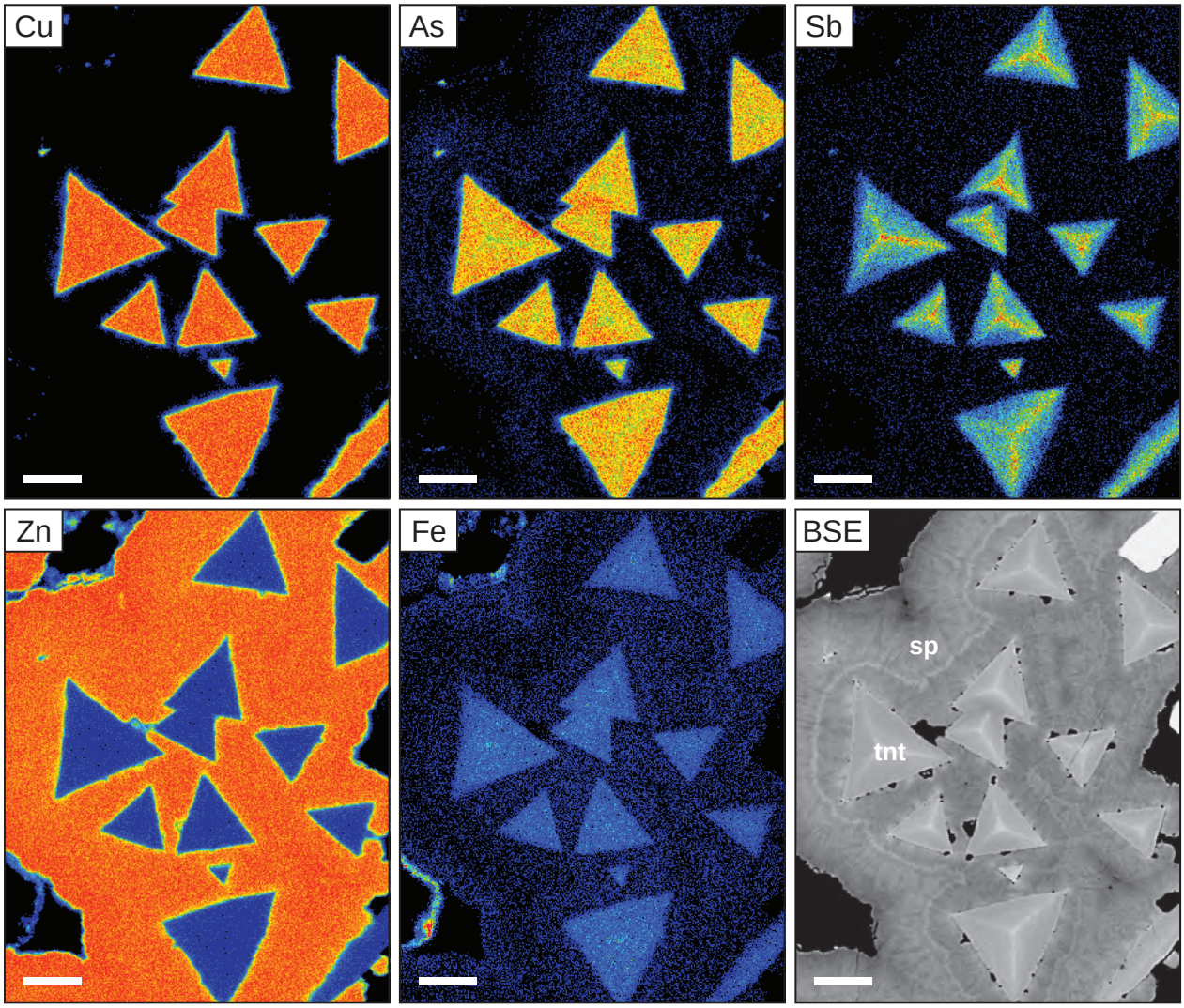

Fig. 9. Electron microprobe element distribution maps across tennantite (tnt) from the Satanic Mills site at the Pacmanus hydrothermal vent field, Manus basin (R/V Sonne cruise SO-166, station 58GTV). The maps show the distribution of Cu, As, Sb, Zn, and Fe. Hot colors are indicative for high element concentrations, while cold colors indicate low concentrations. The backscattered electron (BSE) image is given for comparison. The euhedral tennantite (tnt) crystals are enclosed by collomorph sphalerite (sp). Note the crystallographic control on the distribution of Sb within the tennantite crystals. Early sphalerite surrounding the tennantite is slightly enriched in Fe when compared to sphalerite in the outer growth bands. Scale bar is 20 μm.

small scales, even within individual chimneys (Binns, 2014). Sea-floor massive sulfide deposits located at back-arc spreading centers contain few Sb-bearing trace minerals. Proustite-pyrarygyrite and stephanite have so far only been documented from Vienna Woods (Shadlun et al., 1993).

Selenium

Selenium is an impurity in the main sulfide phases pyrite, chalcopyrite, sphalerite, and galena. Halbach et al. (1998) demonstrated that pyrite from the MESO zone on the Central Indian Ridge is enriched in Se, with maximum concentrations ranging up to 180 ppm. Pyrite concentrates from Snake Pit showed that this mineral has Se contents of <2 to 98 ppm (Hannington et al., 1991). Chalcopyrite separates from the TAG hydrothermal mound have Se contents of 205 to 640 ppm (Hannington et al., 1991). Halbach et al. (2003) even reported maximum concentrations of up to 2,800 ppm Se in chalcopyrite from this deposit. At Turtle Pits, average Se concentrations of 204 ppm in chalcopyrite, 25.5 ppm in pyrite, and 28.2 ppm in sphalerite were recorded by Wohlgemuth-Ueberwasser et al. (2015). Pyrite concentrates from the Southern Explorer site yielded concentrations ranging from 20 to 200 ppm Se, while chalcopyrite concentrates have Se concentrations of 190 to 310 ppm (Hannington et al., 1991). Wang et al. (2014) reported concentrations of <0.02 to 0.05 wt % Se for pyrite and <0.02 to 0.20 wt % Se for chalcopyrite from Kairei. Covellite from the same location hosts <0.02 to 0.05 wt % Se, digenite <0.02 to 0.03 wt % Se, isocubanite 0.14 to 0.20 wt % Se, and sphalerite <0.02 to 0.04 wt % Se. Chalcopyrite from Logatchev contains on average 530 ppm, while pyrite has average concentrations of only 15.5 ppm Se (Wohlgemuth-Ueberwasser et al., 2015). Galena from Logatchev was found to contain as much as 4 wt % Se, possibly due to the presence of clausthalite microinclusions (Torokhov et al., 2002). LA-ICP-MS analyses of chalcopyrite from Pacmanus yielded average Se concentrations of 17.7 ppm, while pyrite and sphalerite contained on average 7.3 and 4.3 ppm Se, respectively (Wohlgemuth-Ueberwasser et al., 2015). Petersen et al. (2004) demonstrated that galena from Hook Ridge has Se concentrations of <0.02 to 0.08 wt %.

Selenium-bearing trace minerals have so far only been described from a few sea-floor massive sulfide deposits. Unidentified silver and gold selenides have been recorded at Semyenov at the Mid-Atlantic Ridge (Cherkashov et al., 2010b). Selenium-bearing Bi tellurides occur in black smoker chimneys at Brothers volcano (Berkenbosch et al., 2012). Eskebornite and umangite form inclusions in pyrite at Palinuro (Dekov and Savelli, 2004).

Tellurium

The Te content of the main sulfide phases contained in sea-floor massive sulfide deposits is typically low. LA-ICP-MS analyses of chalcopyrite, pyrite, and sphalerite from Turtle Pits yielded average Te concentrations of 4.7, 1.2, and 0.6 ppm, respectively. At Logatchev, chalcopyrite contains on average 39.6 ppm Te, while pyrite has average Te concentrations of only 0.6 ppm (Wohlgemuth-Ueberwasser et al., (2015). Average Te concentrations of below 1 ppm were reported for chalcopyrite, pyrite, and sphalerite from Pacmanus (Wohlgemuth-Ueberwasser et al., 2015).

The occurrence of discrete Te minerals has been described for a number of sea-floor massive sulfide deposits. Melonite is a trace mineral at the Rainbow deposit where it is present in textural association with native gold in the interior of Cu-rich black smoker chimneys (Fouquet et al., 2010). Coloradoite forms an accessory phase at Rainbow and Logatchev (Torokhov et al., 2002; Lein et al., 2003; Mozgova et al., 2005). The possible occurrence of hessite (Melekestseva et al., 2010) and an unidentified silver telluride phase (Cherkashov et al., 2010b; Melekestseva, 2010; Melekestseva et al., 2010) have been reported from Semyenov. Bismuth tellurides and Bi-Te sulfide phases also occur in massive sulfides of the Escanaba trough (Zierenberg et al., 1993; Törmänen and Koski, 2005). At Brothers volcano, Bi tellurides have been recognized. In addition to these phases, calaverite and native Te are present in chalcopyrite-sulfate chimneys (Berkenbosch et al., 2012). Tellurobismuthite also forms a rare trace mineral at the Myojinsho caldera (Iizasa et al., 1992).

Thallium

In some sea-floor massive sulfide deposits, pyrite, marcasite, and sphalerite contain trace amounts of Tl. LA-ICP-MS investigations revealed that colloform pyrite in the outer parts of a black smoker chimney from Menez Gwen has Tl contents ranging from 23 to 668 ppm (Lein et al., 2010). Pyrite in a barite-rich sample contained lower Tl concentrations of <0.01 to 308 ppm. At Vienna Woods, pyrite and marcasite contain 0.01 to 0.05 wt % Tl (Shadlun et al., 1993). Sphalerite from Hook Ridge contains <0.02 to 0.11 wt % Tl (Petersen et al., 2004).

Source Controls on Minor Element Enrichment

The geodynamic setting of sea-floor hydrothermal systems represents a first-order control on the geochemical composition of sea-floor massive sulfide deposits (Table 3). The minor element geochemistry of sea-floor hydrothermal systems is influenced by the composition of the igneous rocks undergoing high-temperature reactions with the hydrothermal fluids in the reaction zone of the convection system. Basalt and ultramafic rocks predominate in the reaction zone of mid-ocean ridge hydrothermal systems, with more evolved lavas occurring in volcanic arcs and related extensional settings, and sedimentary rocks in both oceanic and continental crust (Hannington et al., 2010). In addition to source-rock controls, the direct input of volatiles from subvolcanic magmas may result in the addition of metals to sea-floor hydrothermal convection systems (Hannington et al., 1999d).

Source-rock controls on the composition of sea-floor massive sulfide deposits can probably be best evaluated in diagrams normalizing the median composition of massive sulfides to mid-ocean ridge basalt, with the elements being plotted in the order of decreasing enrichment (Fig. 10). The normalized plot highlights that the minor elements considered in the present review are enriched in sea-floor massive sulfide deposits in comparison to mid-ocean ridge basalt, with enrichment factors varying from about 1 to over 10,000 (Fig. 10).

Basalt-hosted mid-ocean ridge sea-floor massive sulfide deposits show a fairly flat pattern. With the exception of Ga and Ge, enrichment factors vary from about 30 to 1,000. In comparison to sea-floor massive sulfide deposits in other

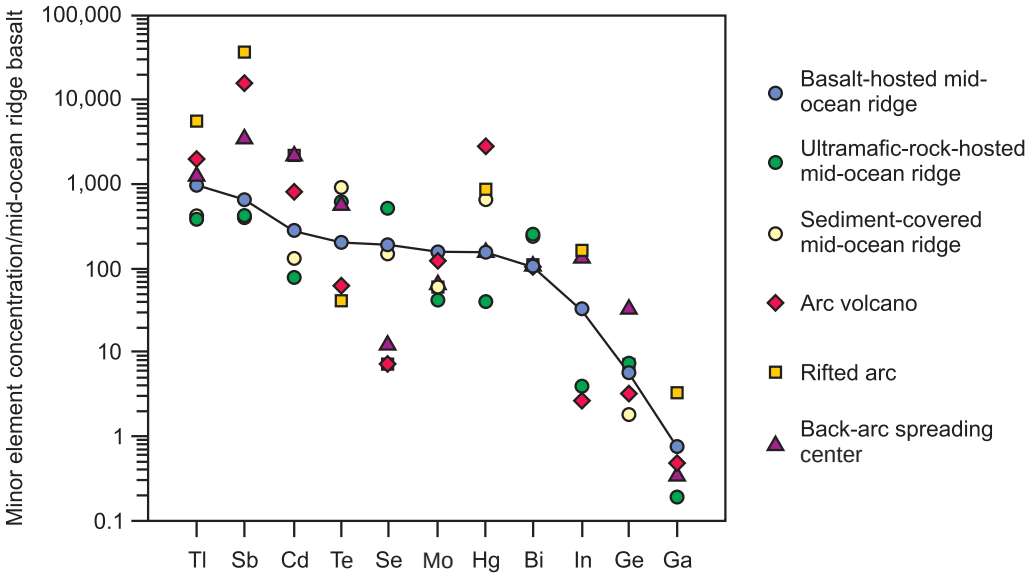

Fig. 10. Diagram showing the median element abundances in sea-floor massive sulfide deposits normalized to mid-ocean ridge basalt, with the elements plotted in the order of decreasing enrichment. The plot highlights source rock controls on minor element content in deposits located in different geodynamic settings. Element abundances are given in Table 3. Values of mid-ocean ridge basalt from Arevalo and McDonough (2010).

settings, mid-ocean ridge sea-floor massive sulfide deposits are characterized by only moderate enrichments of Cd, Sb, Hg, and Tl. This is in contrast to relatively high Se, Mo, and Te enrichment factors (Fig. 10). Of all elements analyzed, Ga and Ge show the lowest enrichment factors, suggesting that uptake of these elements in the high-temperature reaction zone of mid-ocean ridge sea-floor hydrothermal systems is inefficient. In comparison to sea-floor massive sulfide deposits hosted by basalt, ultramafic rock-hosted sea-floor massive sulfide deposits have low enrichment factors of Ga, Cd, In, Hg, and Tl, while sediment-covered mid-ocean ridge sea-floor massive sulfide deposits show significant Hg and Te enrichments (Fig. 10).

Sea-floor massive sulfide deposits in volcanic arcs and related rifts show remarkable enrichments in Cd, Sb, Hg, and Tl. Enrichment of these elements in the hydrothermal systems may perhaps be related to direct magmatic contributions to the sea-floor hydrothermal systems in these settings (Hannington et al., 1999d). In contrast to this suite of elements, the Se, Mo, and Te enrichment of sea-floor massive sulfide deposits in suprasubduction settings is similar or lower than those encountered in mid-ocean ridge sea-floor massive sulfide deposits (Fig. 10).

Fluid Controls on Minor Element Enrichment and Mineralogical Sequestration

The total concentrations of metals in hydrothermal liquids forming sea-floor massive sulfide deposits is low. Iron occurs in concentrations ranging from about <1 to 2,500 mmol/kg. The Cu contents of vent liquids ranges from <1 to 162 μmol/kg, while Zn concentrations between <1 and 3,000 μmol/kg are common. The Pb contents of end-member black smoker liquids are comparably low and reach up to 3.9 μmol/kg (German and Von Damm, 2003).

Minor element concentrations in end-member liquids have been measured at several hydrothermal vent sites on the modern sea floor (Table 7). The most comprehensive data are currently available for Cd, which occurs in concentrations ranging from 1 to 4,000 nmol/kg. The highest Cd concentrations documented so far occur in the hydrothermal systems of the Manus basin (Craddock, 2009). The concentrations of Ga and Ge range from 25 to 243 and 126 to 170 nmol/kg, respectively. The limited data available suggests that Hg concentrations in end-member hydrothermal liquids are <0.01 nmol/kg. The concentration of In is also low in vent liquids, with values ranging from <1 to 3.5 nmol/kg. With values between 1 and 148 nmol/kg, the Mo content of end-member hydrothermal liquids is commonly below the seawater value of 105 nmol/kg (Sohrin et al., 1989). The contents of Sb and Se range from <3 to 13,000 and <0.6 to 103 nmol/kg, respectively. The highest Sb concentrations in end-member fluids have been reported for hydrothermal systems in arc-related rifts (Craddock, 2009). Data compilation shows that end-member liquids have Tl concentrations between 6.8 and 92 nmol/kg (Table 7).

Observed variations in the minor element content of end-member hydrothermal liquids can be related to variations in source rock, processes of subseafloor phase separation, the complexation behavior of these elements during transport at high temperatures and variable redox conditions, and the temperature-dependent partitioning of these elements into the different sulfide phases forming at the hydrothermal vent sites (Trefry et al., 1994; Douville et al., 1997, 2002; Metz and Trefry, 2000; Seyfried et al., 2003).

However, irrespective of the potentially complex processes controlling the minor element concentrations in end-member hydrothermal liquids, the different elements almost always display consistent temperature-dependent enrichment and depletion trends within any given sea-floor massive

Table 7. Minor Element Composition of End-Member Hydrothermal Fluids (all data in nmol/kg)

No.	Deposit and location	Cd	Ga	Ge	Hg	In	Mo	Sb	Se	Tl
6	Edmond, Central Indian Ridge	218–277								
18	Menez Gwen, Mid-Atlantic Ridge	<9–12				<1	10–11	3.0–4.7		11–12
19	Lucky Strike, Mid-Atlantic Ridge	18–79				<1	2.7–84	<3–6.3		7.1–16
20	Broken Spur, Mid-Atlantic Ridge	75–145								
23	TAG, Mid-Atlantic Ridge	66–570	60–243			2.2	5–148	3.9		7–13
25	Snake Pit, Mid-Atlantic Ridge	440				<1	3	11		25
44	Main vent field, Endeavour, Juan de Fuca Ridge	25–225					37–101			
49	ASHES, Axial Smt. Juan de Fuca Ridge			126–148						
51	North Cleft, Juan de Fuca Ridge	216–700	25–40				5–30	7–15		40–74
52	South Cleft, Juan de Fuca Ridge	370–910	34–67				31–33	8–18		42–92
53	Sea Cliff, Gorda Ridge	13.5–14.7			0.004–0.01					
55	EPR 20°50'N, East Pacific Rise	17–180		130–170					<0.6–72	
59	EPR 12°49'N, East Pacific Rise	55–70								
63	EPR 10°56'N, East Pacific Rise	1–43								
130	Kairei, Central Indian Ridge	69.9–114					2			
133	Rainbow, Mid-Atlantic Ridge	105–178				2.8–3.5	1.3–3.2	3.0–3.2		6.8–11.0
134	Logatchev-1, Mid-Atlantic Ridge	63				<1	1	<3		7
150	Southern trough, Guaymas basin, Gulf of California	<10–46							38–103	
153	Suiyo, Izu-Ogasawara arc						5			
180	Hatoma knoll, Okinawa trough						7			
182	Pacmanus, Manus basin	23–4,000						98–5,717		
187	Solwara 1, Manus basin	85–800						178–750		
188	SuSu, Manus basin	13–160						105–13,000		
208	Vienna Woods, Manus basin	36–57						<30		
231	Vai Lili, Lau basin	700–1,500								

References: [6] Gallant and Von Damm (2006); [18, 19] Douville et al. (2002); [20] James et al. (1995); [23] Metz and Trefry (2000), Douville et al. (2002); [25] Douville et al. (2002); [44] Seyfried et al. (2003); [49] Mortlock et al. (1993); [51, 52] Trefry et al. (1994), Metz and Trefry (2000); [53] Lamborg et al. (2006), Von Damm et al. (2006); [55] Von Damm (1990), Mortlock et al. (1993); [59, 63] Von Damm (1990); [130] Kishida et al. (2004), Gallant and Von Damm (2006); [133, 134] Douville et al. (2002); [150] Von Damm (1990); [153, 180] Kishida et al. (2004); [182, 187, 188, 208] Craddock (2009); and [231] Fouquet et al. (1993a)

sulfide deposit (Auclair et al., 1987; Hannington et al., 1991). Observed coenrichments of the minor elements together with Cu or Zn as well as experimental studies establishing temperature-dependent solubility controls (Wood et al., 1987; Seward and Barnes, 1997; Wood and Samson, 1998, 2006; Seward et al., 2014) provide first-order indications of the behavior of the minor elements during the formation of sea-floor massive sulfide deposits.

Enrichments of Bi are common in chalcopyrite-rich massive sulfides, implying that this element shows a high- to intermediate-temperature affinity. Bismuth is most likely transported mainly as hydroxide complexes (Tooth et al., 2013), although Bi chloride complexes are also known. Bismuthinite, one of the most common Bi-bearing minerals in sea-floor massive sulfide deposits, has a low solubility except at temperatures greater than 350°C and salinities of at least 5 mol/kg NaCl (cf. Wood et al., 1987), which is consistent with the predominance of Bi in Cu-rich massive sulfides. In the geochemical data set compiled for the present study, Bi correlates with Te, suggesting that Bi and Te frequently occur together in Cu-rich sulfides (Fig. 11). A high-temperature affinity of Te has also been proposed by Butler and Nesbitt (1999) based on systematic LA-ICP-MS analyses across a black smoker chimney sample from Broken Spur.

In black smoker liquids, Cd is transported as chloride complexes (cf. Bazarkina et al., 2010). The molar Zn/Cd ratio in the liquids does not show a strong temperature dependence between about 200° and 350°C, suggesting that both elements exhibit a similar geochemical behavior over this temperature range (Metz and Trefry, 2000). In the case of basalt-hosted vent sites, the Zn/Cd ratio of the end-member hydrothermal liquids is similar to this ratio in mid-ocean ridge basalt, suggesting a similar extraction efficiency for these elements in the recharge zone of the sea-floor hydrothermal systems (Metz and Trefry, 2000). However, at some vent sites, the overall Zn and Cd concentrations of the end-member liquids appear to slightly increase with decreasing temperature, presumably because dissolution of previously formed sulfides provides additional dissolved Zn and Cd to the liquids during their ascent through vent mounds and chimneys (Trefry et al., 1994).

During sea-floor sulfide formation, Cd is incorporated into sphalerite and wurtzite due to the similarity in ionic radius of Cd^{2+} and Zn^{2+}. Thermodynamic modeling has shown that sphalerite precipitated at higher temperature is expected to be richer in Cd than sphalerite forming at low temperature (Schwartz, 2000). As expected, bulk geochemical data from sea-floor massive sulfide deposits worldwide show a correlation between Cd and Zn (Fig. 12), highlighting the general intermediate- to low-temperature affinity of Cd.

Relatively little information is available on the mobilization, transport, and speciation of Ga and Ge in sea-floor hydrothermal systems. The presently available data suggests that Zn/Ga ratios in black smoker liquids sampled from basalt-hosted vent sites are significantly higher than this ratio in mid-ocean ridge basalt, implying that Ga uptake in

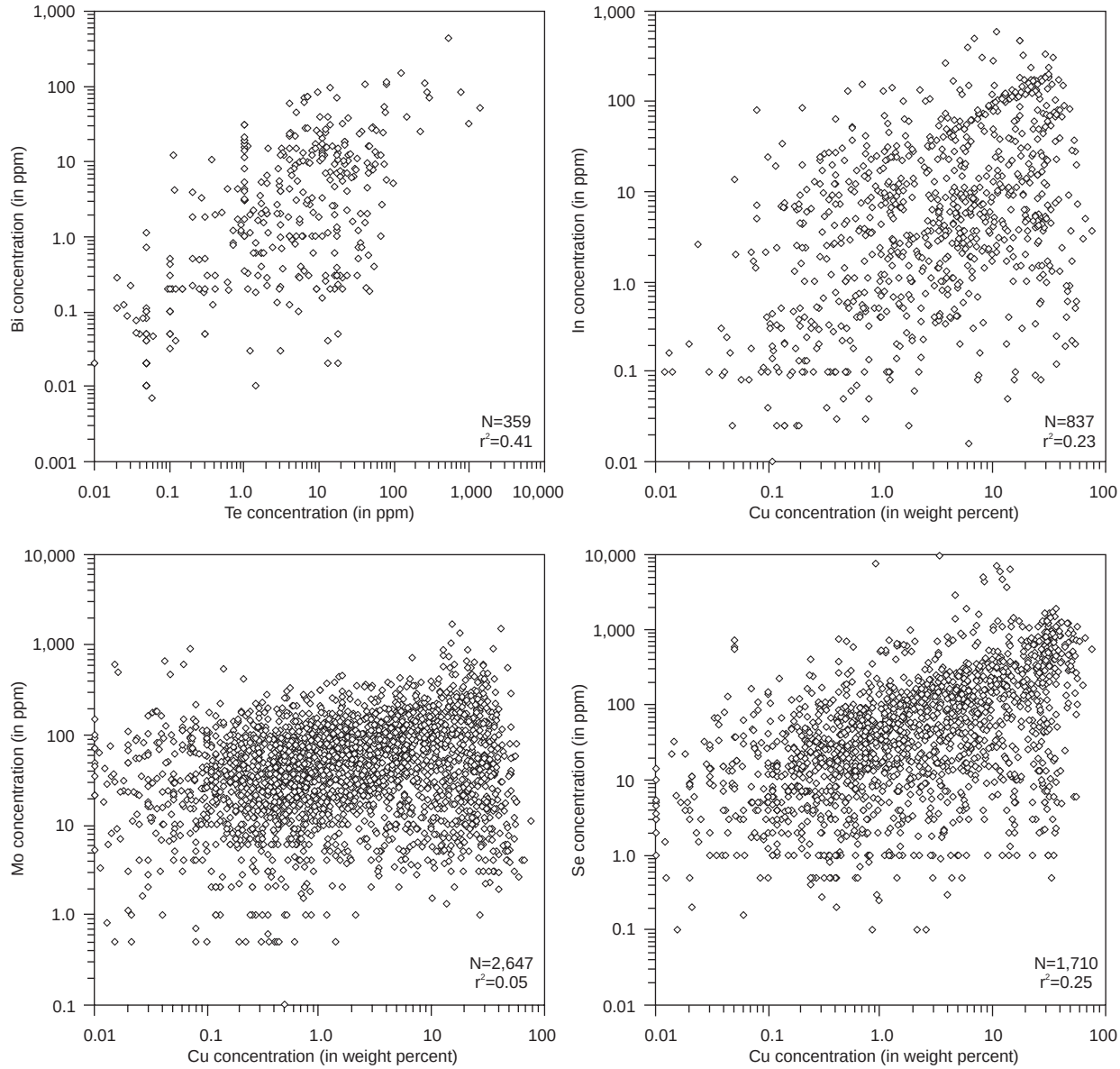

Fig. 11. Scatter diagram showing the relationships between elements with a high- to intermediate-temperature affinity in sulfide samples collected from sea-floor massive sulfide deposits worldwide. The concentrations of Bi and Te show a positive correlation. The concentrations of In and Se exhibit a broad relationship with Cu.

the recharge zone of sea-floor hydrothermal systems is not as efficient as for Zn (Metz and Trefry, 2000). Wood and Samson (2006) predicted that Ga is transported as hydroxide complexes in hydrothermal liquids with low fluorine activity, such as black smoker liquids. Gallium appears to have an intermediate- to low-temperature affinity. However, there is no strong correlation between Ga and Zn (Fig. 12), presumably due to the variability of Zn/Ga ratios in the hydrothermal liquids. In contrast to Ga, which forms hydroxide complexes at elevated temperatures, germanic acid and its dissociation products may represent the most important Ge species in hydrothermal liquids with low fluorine activity (Wood and Samson, 2006). Although Ge also has an intermediate- to low-temperatures affinity, correlation between Ge and Zn in bulk samples is not strong (Fig. 12).

Mercury may be transported in hydrothermal liquids as elemental Hg species. However, in aqueous solutions with high hydrogen sulfide content, Hg transport is likely to occur as sulfide complexes (Barnes and Seward, 1997). Mercury transport in the vapor phase is possible if Hg is present as an elemental species before vapor separation (Varekamp and Buseck, 1984). In sea-floor hydrothermal systems, Hg appears to have an intermediate- to low-temperature affinity as Hg enrichment is common in Zn-rich massive sulfides. There is a broad correlation between Hg and Sb in the compiled geochemical dataset, which may indicate that Hg is primarily incorporated into sulfosalts (Fig. 13). In fluids with high sulfide concentrations, Sb is probably transported as $Sb(HS)_4^-$ and $Sb(HS)_{4-n}(OH)_n^-$ complexes (cf. Sherman et al., 2000), while mixed hydroxide-chloride complexes may predominate

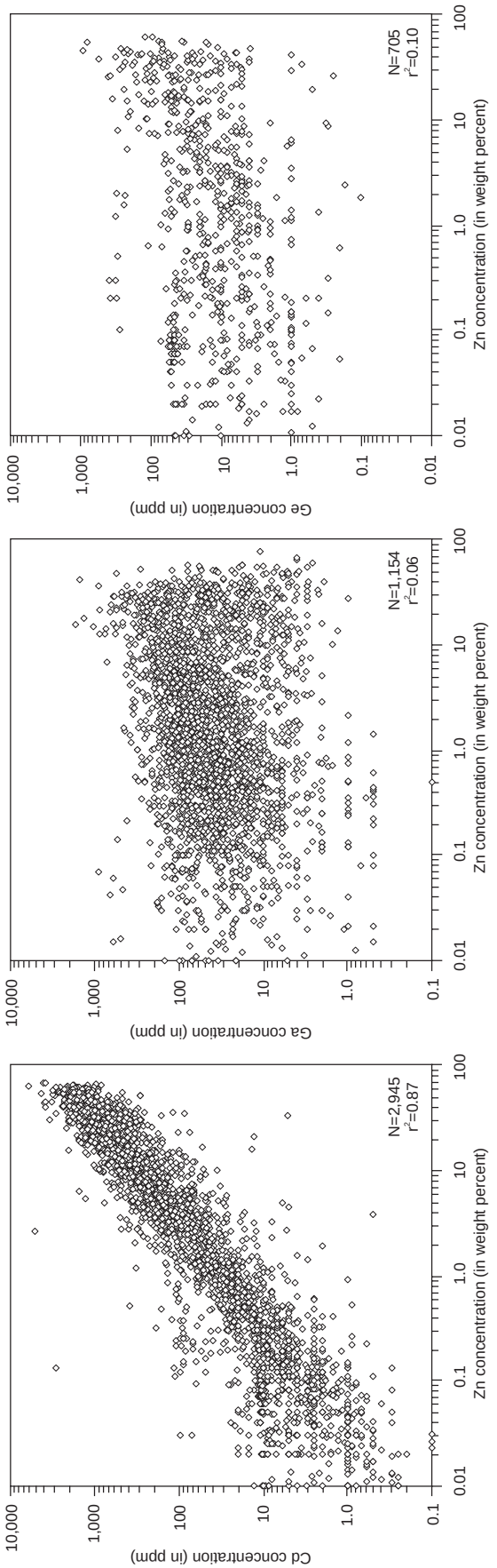

Fig.12. Scatter diagram showing the relationships between elements with an intermediate- to low-temperature affinity in sulfide samples collected from sea-floor massive sulfide deposits worldwide. The Cd and Zn concentrations of the sulfide samples show a strong positive correlation.

in acidic saline solutions (Pokrovski et al., 2006). In sea-floor massive sulfide deposits, Sb appears to be preferentially incorporated in sulfosalts precipitating at lower temperatures. Bulk samples from sea-floor massive sulfide deposits show a broad relationship between Sb and Zn (Fig. 13).

Sulfide samples from sea-floor massive sulfide deposits exhibit a broad relationship between In and Cu (Fig. 11). Coenrichment of In and Cu in sea-floor massive sulfide deposits may be best explained by the fact that In forms stable chloride and bisulfide complexes at high temperatures (Seward et al., 2000) and can be incorporated into chalcopyrite through a coupled substitution of Fe by Cu and In (Yamanaka and Kato, 1976). Fouquet et al. (1993a) as well as Schwarz-Schampera and Herzig (2002) demonstrated that In is deposited with chalcopyrite and high-temperature sphalerite in the cores of black smoker chimneys from Vai Lili in the Lau basin, indicating that this element in sea-floor massive sulfide deposits is most likely introduced together with Cu at high temperatures. The high-temperature affinity of In has also been demonstrated for the Broken Spur site by Butler and Nesbitt (1999).

At the high temperatures of the recharge zone of sea-floor hydrothermal systems, Mo is probably transported as MoO_4^{2-} (Seyfried et al., 2003). Molybdenum coprecipitates with chalcopyrite at high temperatures (Hannington et al., 1991; Halbach et al., 2003), presumably due to the formation of Mo^{2+} under the acidic conditions caused by mineralization reactions near the sea floor (Seyfried et al., 2003). High-temperature precipitation of Mo is also suggested by the observation that Mo solubility in vent liquids sharply decreases at temperatures below 350°C (Metz and Trefry, 2000). Despite its high-temperature affinity, Mo displays only a weak relationship with Cu in bulk geochemical data (Fig. 11).

Selenium also shows a broad correlation with Cu in sea-floor massive sulfide deposits (Fig. 11). Unlike other minor elements, Se is carried in the liquid phase as a volatile species similar to H_2S. As a consequence, Se partitioning will be strongly influenced by the Se/S ratio of the hydrothermal liquids (Huston et al., 1995). Auclair et al. (1987) demonstrated that the highest Se contents in chimney fragments from the East Pacific Rise are found in chalcopyrite. Sphalerite and wurtzite show distinctly lower Se abundances. Studies by Hannington et al. (1991) and Halbach et al. (2003) confirm that Se has a high-temperature affinity.

Thallium transport in aqueous solutions likely occurs as the free thallium ion at low temperatures and acidic conditions, while bisulfide complexes may be important in less acidic solutions (Xiong, 2007). With increasing temperature, the formation of thallium chloride complexes becomes important (Xiong, 2007). In end-member hydrothermal liquids, Tl shows a strong linear correlation with K and Rb, suggesting effective extraction from the host rocks in the recharge zone of sea-floor hydrothermal systems (Metz and Trefry, 2000). Thallium shows an intermediate- to low-temperature affinity. Ewers and Keays (1977) established that appreciable quantities of Tl only precipitate from subaerial geothermal liquids at temperatures below 160°C. As these temperatures are lower than the typical temperature range of sphalerite precipitation, the Tl concentrations of bulk sulfide samples only show a weak correlation with Zn (Fig. 13).

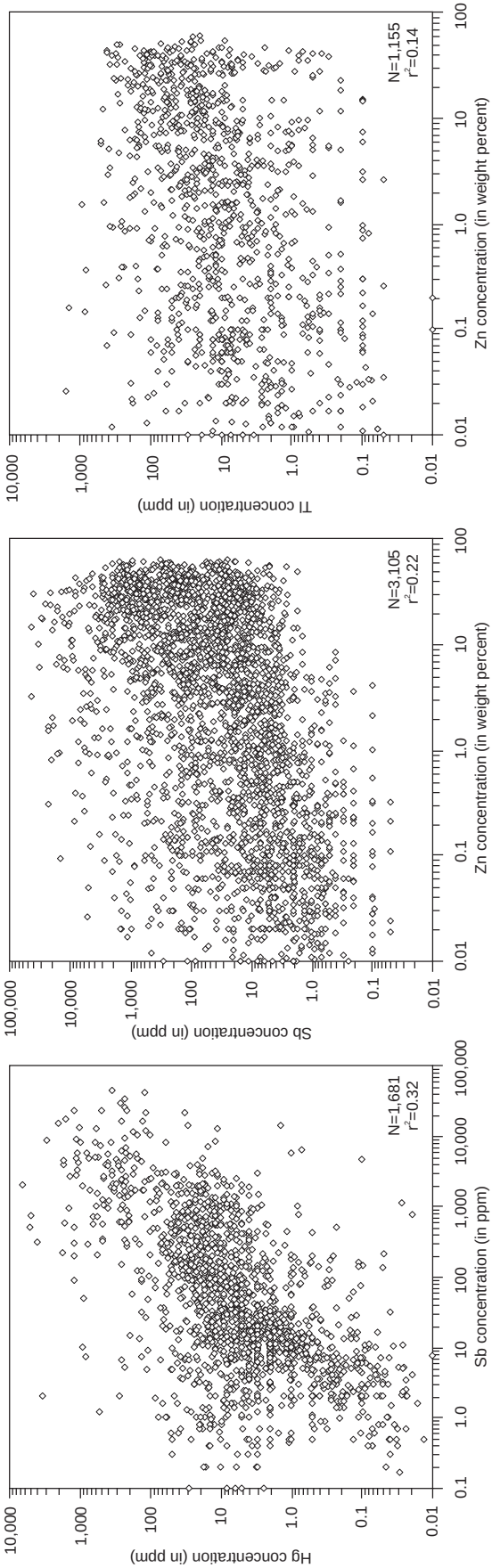

Fig. 13. Scatter diagram showing the relationships between elements with an intermediate- to low-temperature affinity in sulfide samples collected from sea-floor massive sulfide deposits worldwide. The concentrations of Hg and Sb show a broad positive correlation. The Sb and Tl concentrations exhibit a broad relationship with Zn.

Estimate of the Global Minor Element Endowment

The data available today allow a first-order estimate of the minor element endowment of sea-floor massive sulfide deposits to provide an answer to the question whether the world's oceans represent a significant future source of metals for mankind (Glasby, 2000; Scott, 2001; Rona, 2003; Cathles, 2011a, b; Hannington, 2011; Hannington et al., 2011; Singer, 2014).

Using the median minor element concentrations determined for almost 5,000 sulfide samples collected on the modern sea floor as described above, the minor element endowment of the ~50 Mt of known sea-floor massive sulfide deposits can be estimated (Table 8). In addition, the global minor element endowment of the estimated ~600 Mt of sea-floor massive sulfide deposits inferred to be present in the neovolcanic zones of the world's oceans can be calculated (Table 8). As discussed above, these calculations clearly only yield broad estimates as grade and tonnage information comparable to ancient deposits located on land are not available for modern sea-floor hydrothermal systems.

For comparison, Table 8 also lists the world's refinery production of the minor elements enriched in sea-floor massive sulfide deposits. Comparison of the data reveals that sea-floor massive sulfide deposits only represent a significant repository for selected elements. The global Ga and Ge endowments of sea-floor massive sulfide deposits are estimated to be about 20 to 30 times higher than the current annual production of these elements. Sea-floor sulfides may also represent a significant repository for Tl. Elements such as Cd, Hg, In, Se, and Te are enriched in sea-floor massive sulfide deposits. In contrast, Bi, Mo, and Sb clearly are not concentrated sufficiently in sea-floor massive sulfide deposits to be significant from a resource perspective.

Table 8 also lists the world reserves for minor elements where known. Data comparison shows that the global Bi endowment of sea-floor massive sulfide deposits equals only 0.2% of the Bi reserves contained in land-based ore deposits. The global Mo endowment of sea-floor massive sulfide deposits is also equivalent to only 0.2% of the world reserves of this element, which can be largely accounted for by low-grade porphyry Mo deposits. Clearly, sea-floor massive sulfide deposits are not major repositories of Bi and Mo when compared to deposits located on land. By comparison, the global Se and Te endowments in sea-floor massive sulfide deposits are perhaps more significant (Table 8).

The available data clearly demonstrate that the minor element endowment of sea-floor massive sulfide deposits is small by comparison to mineral resources located on land. Despite significant uncertainties in estimating the global endowment, it does not appear likely that sea-floor massive sulfide deposits will ever play a major role as a future source of minor elements for modern society.

Furthermore, it is important to note that the generally low concentrations of minor elements in sea-floor massive sulfide deposits will not allow these elements to become the economic driver of future deep-sea mining. Assuming minor element grades of 16 ppm Ga, 8.9 ppm Ge, and 3.1 ppm In (Table 3) and the average base and precious metal grades from the Solwara 1 deposit in the Manus basin as guidelines, these minor elements account for less than 5% of the metal

Table 8. Comparison Between the Estimated Minor Element Endowment in Sea-Floor Massive Sulfide Deposits, the World's Refinery Production, and Reserves of These Elements in 2014 (data from the U.S. Geological Survey Mineral Commodity Summaries 2015; all data in metric tons)

	Estimated endowment in known sea-floor massive sulfide deposits (~50 Mt of sulfides)[1]	Estimated global endowment in sea-floor massive sulfide deposits (~600 Mt of sulfides)[1]	World refinery production in 2014	World reserves in land-based deposits 2014
Bi	50	600	8,500	320,000
Cd	3,350	40,200	22,200	-
Ga	800	9,600	440	-
Ge	445	5,340	165	-
Hg	155	1,860	1,870	-
In	155	1,860	820	-
Mo	2,050	24,600	266,000	11,000,000
Sb	1,065	12,780	160,000	1,800,000
Se	830	9,960	>2,275	120,000
Te	50	600	>95	24,000
Tl	430	5,160	>10	-

[1] Estimate based on median minor element concentrations of sulfide samples collected from sea-floor massive sulfide deposits worldwide (see Table 3)
Note: - = no data available

value of a ton of massive sulfides in sea-floor massive sulfide deposits, depending on metal prices (see U.S. Geological Survey Mineral Commodity Summaries 2015 for metal prices of minor elements). Clearly, economically feasibility of deep-sea mining will depend on the base and precious metal grades of the sea-floor massive sulfide deposits to be exploited, not their minor element contents. However, assuming that technical, legal, and environmental challenges of sea-floor mining can be overcome, recovery of minor elements as co- or by-products during smelting and refining may be feasible and potentially economically beneficial.

Comparison to Ancient Massive Sulfide Deposits

Volcanogenic massive sulfide (VMS) deposits are the fossil analogs of sea-floor massive sulfides. These deposits located in Archean to Cenozoic volcanic belts are predominately comprised of stratiform sulfide lenses although related crosscutting stringer zones and massive replacement pipes also occur. The ore lenses consist of >60% sulfide minerals, mainly pyrite and/or pyrrhotite, with variable amounts of chalcopyrite, sphalerite, and galena (Franklin et al., 2005). The ores formed at or immediately below an ancient sea floor and are hosted by coherent and volcaniclastic rocks that were emplaced essentially coeval to the mineralization. Sedimentary rocks such as pelagic or hemipelagic mudstone are present in the host stratigraphy of many VMS deposits (McPhie and Allen, 1992; Gibson et al., 1999; Doyle and Allen, 2003; Tornos et al., 2015).

VMS deposits formed throughout Earth history. Some of the oldest examples of this deposit type are located in pre-3.7 Ga old volcanic rocks at Isua in Greenland (Appel, 1979), the 3.5 Ga Warrawoona greenstone belt of East Pilbara in Australia (Sangster and Brook, 1977; Barley, 1992), and the 3.3 Ga Strelley greenstone belt of East Pilbara (Vearncombe et al., 1995; Brauhart et al., 2001). The fossil record of sea-floor hydrothermal activity is impressive as approximately 800 VMS deposits have been recognized in ancient volcanic belts worldwide (cf. data compilation in Franklin et al., 2005).

Lithostratigraphic classification

Most VMS deposits are thought to have formed near plate margins in arc-related extensional settings that were inverted and strongly deformed during subsequent orogenesis (Allen et al., 2002). Based on the composition of the volcanic host-rock successions, five different lithostratigraphic types of massive sulfide deposits are distinguished (Barrie and Hannington, 1999; Franklin et al., 2005).

Massive sulfide deposits hosted in mafic-dominated volcanic successions, including ophiolite and ophiolite-like assemblages, are thought to have formed in intraoceanic back arcs (Barrie and Hannington, 1999; Galley and Koski, 1999; Franklin et al., 2005). The immediate host rocks are predominately pillowed and massive basaltic flows. Felsic volcanic rocks, ultramafic flows, and intrusions form only a minor component of the host-rock successions. Prominent examples include the deposits in the Cretaceous Troodos Complex of Cyprus (Constantinou and Govett, 1973; Adamides, 1987; Hannington et al., 1998) and the Cretaceous Semail Ophiolite in Oman (Lescuyer et al., 1988; Haymon et al., 1989; Gilgen et al., 2014). Pelitic-mafic volcanic successions hosting VMS deposits likely originated in back-arc settings located close to an eroding continental hinterland (Barrie and Hannington, 1999; Franklin et al., 2005). Mafic volcanic rocks and pelite are subequal in abundance, or pelite may dominate. The late Paleozoic to Mesozoic Besshi deposits of Japan represent examples for this VMS type (Kamiyama et al., 1964; Nozaki et al., 2010; Ikehata et al., 2011).

Volcanic successions containing a significant proportion of felsic volcanic rocks are among the most important hosts to VMS deposits. Bimodal-mafic successions probably largely represent incipient rifts formed in intraoceanic volcanic arcs (Barrie and Hannington, 1999; Franklin et al., 2005). Deposits located in these successions, dominated by basalt with up to 25% of felsic volcanic strata, include those of the Archean Noranda camp in Quebec, Canada (Gibson and Watkinson, 1990; Kerr and Gibson, 1993; Gibson and Galley, 2007) and the Paleoproterozoic Flin Flon district of Manitoba, Canada (Syme and Bailes, 1993; DeWolfe et al., 2009). Bimodal-felsic volcanic assemblages hosting VMS deposits largely formed in rifted transitional or continental margin arcs and related back-arc settings (Barrie and Hannington, 1999; Franklin et al., 2005). Felsic volcanic rocks predominate in these successions, with basalt accounting for 20 to 50% of the volcanic strata.

Examples of these deposits include those of the Paleoproterozoic Skellefte and Bergslagen districts in Sweden (Allen et al., 1996a, b), the Cambrian Mount Read district in Tasmania (Corbett, 1992; Large, 1992; Large et al., 2001a; Mortensen et al., 2015), the Cretaceous Pontides of Turkey (Çağatay, 1993), and the Miocene Hokuroku district in Japan (Ohmoto, 1983; Ohmoto and Takahashi, 1983; Tanimura et al., 1983).

VMS deposits hosted in siliciclastic-felsic volcanic successions presumably formed in intracontinental back-arc rifts and spreading centers (Barrie and Hannington, 1999; Franklin et al., 2005). In deposits of this type, such as those of the Late Devonian to Middle Carboniferous Iberian Pyrite Belt of Spain and Portugal (Schermerhorn, 1975; Boulter, 1993; Leistel et al., 1998a; Carvalho et al., 1999) and the Ordovician Bathurst district in Canada (McCutcheon, 1992; Goodfellow and McCutcheon, 2003; van Staal et al., 2003), siliciclastic strata account for about 80% of the volcanic successions, while felsic volcaniclastic rocks with minor flows, domes, and sills form the remainder of the host-rock successions.

Tonnage and grade

In terms of total geologic resource, sea-floor massive sulfide deposits are dwarfed in comparison with their ancient analogues. The total tonnage contained in known VMS deposits worldwide is nearly 13.5 Bt (cf. data compilation in Franklin et al., 2005), which is over twenty times the estimated global tonnage of all sea-floor massive sulfide deposits. The metal contained in the giant Kidd Creek deposit in the Archean Abitibi greenstone belt in Ontario, Canada (Hannington et al., 1999a-c), alone is equal to approximately 50% of the estimated metal endowment of the neovolcanic zones in the world's oceans. With a total past production, reserve, and resource of over 170 Mt of ore grading 2.25 wt % Cu, 5.88 wt % Zn, 0.22 wt % Pb, and 77 g/t Ag (M.D. Hannington, unpub. data), Kidd Creek is the deepest base metal mine in the world and exploited from surface to a depth of over 3 km.

Individual VMS deposits vary in size from a few hundred thousand to several million tons in size (Fig. 14). The size characteristics of the five different lithostratigraphic types of VMS deposits vary significantly (cf. data compilation in Franklin et al., 2005). Deposits in mafic-dominated volcanic successions, including ophiolite and ophiolite-like assemblages, have a median size of 2.3 Mt. Volcanogenic massive sulfide deposits located in bimodal-mafic and bimodal-felsic volcanic successions have a median size of approximately 3.0 Mt. Massive sulfide deposits hosted in pelitic-mafic and siliciclastic-felsic successions can be significantly larger, with median sizes of 4.1 and 7.0 Mt, respectively. This contrasts strongly with the median size of currently known sea-floor massive sulfide deposits of less than 100,000 t (Fig. 14), as constrained by Hannington et al. (2010) for the test group of the 62 best studied sea-floor massive sulfide deposits.

The apparent differences in size between sea-floor massive sulfide and VMS deposits can, at least in part, be accounted for by the processes of sulfide formation. Careful volcanological studies on VMS deposits have shown that large deposits are almost universally hosted by volcaniclastic strata or siliciclastic rocks (Franklin et al., 2005). Sulfide formation in these deposits occurs at least in part through processes of subsea-floor infilling and replacement of the host rocks. The sulfides precipitate within wet, porous, and poorly consolidated rocks at depth of 10 to 200 m below the sea floor (Doyle and Allen,

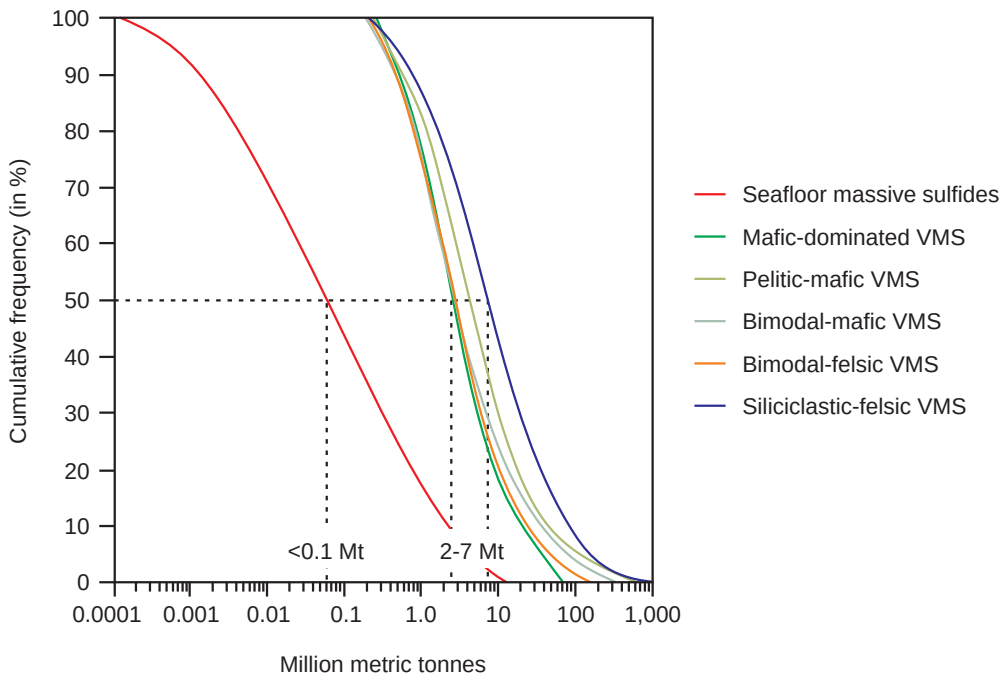

Fig. 14. Comparison of the cumulative size distributions of sea-floor massive sulfide deposits and volcanogenic massive sulfide deposits. The size distribution of sea-floor massive sulfide deposits is taken from Hannington et al. (2010). The distributions of the five lithostratigraphic types of volcanogenic massive sulfide deposits were constructed using the data given by Franklin et al. (2005). The plot illustrates that the median size of sea-floor massive sulfide deposits is <0.1 Mt whereas the different types of ancient deposits have median sizes ranging from 2 to 7 Mt.

2003). Subseafloor infiltration and replacement are efficient mechanisms of metal precipitation. In contrast, most sea-floor massive sulfide deposits discovered today represent mound-style deposits formed through successive growth at the sea floor, which is not an efficient process of metal accumulation as much of the metals carried by the black smoker liquids is lost into the oceans. At present, only one example of a blind subseafloor massive sulfide deposit has been discovered and drilled (Petersen et al., 2014). The development of geophysical tools allowing the discovery of ore lenses located below significant overburden in volcaniclastic and siliciclastic successions represents a frontier in sea-floor exploration, perhaps leading to future discovery of more deposits comparable in size to their ancient analogues.

Irrespective of size considerations, both VMS and sea-floor massive sulfide deposits are typically polymetallic in nature. Volcanogenic massive sulfide deposits contain an average of 5 wt % of combined Cu, Zn, and Pb (Large, 1992; Barrie and Hannington, 1999; Galley and Koski, 1999; Franklin et al., 2005). In general, Cu enrichment is more common in VMS deposits hosted by mafic-dominated or pelitic-mafic volcanic successions, although high Cu grades are also frequently encountered in compositionally bimodal-mafic volcanic successions, with the felsic volcanic rocks commonly occurring in close association with the deposits. Deposits enriched in Zn and Pb are most frequently located in bimodal-felsic or siliciclastic-felsic volcanic successions (Barrie and Hannington, 1999; Franklin et al., 2005). In addition to the base metals, some VMS deposits contain economic grades of Au and Ag (Hannington et al., 1999d; Huston, 2000; Franklin et al., 2005; Monecke and Mercier-Langevin, 2014; Grant et al., 2015). A small number of VMS deposits are exploited primarily for their precious metal content (Bergman Weihed et al., 1996; Roth et al., 1999; Gibson et al., 2000; Mercier-Langevin et al., 2007a, b, 2011; Monecke et al., 2008; Dubé et al., 2014).

Pyrite or pyrrhotite are the dominant sulfide minerals in VMS deposits. They are accompanied by sphalerite, chalcopyrite, and/or galena as the principal economic minerals. Just like their modern sea-floor analogues, most VMS deposits are compositionally zoned according to the solubilities of the different ore minerals in cooling hydrothermal liquids, with Cu- and Fe-rich sulfides being most abundant in the interiors and in the underlying stockwork zones, and Zn- and Pb-rich sulfides deposited at the cooler outer margins (Roscoe, 1965; Large, 1977, 1992; Knuckey et al., 1982; Eldridge et al., 1983; Ohmoto, 1996). Because of the consistency in zonation, metal distribution has long been used in mineral exploration as an indicator of stratigraphic-facing direction in deformed deposits.

Minor element content

In VMS deposits, the minor elements Bi, Cd, Ga, Ge, Hg, In, Mo, Sb, Se, Te, and Tl occur in abundance ranging from several parts per million to thousands parts per million, which is comparable with concentration ranges observed in sea-floor massive sulfide deposits (Table 9). At smelters and refineries processing ores from VMS deposits, many of these elements are routinely recovered as by-products. Examples include the recovery of Bi, Cd, In, and Se from the ores at Kidd Creek (Walker et al., 1975; Hannington et al., 1999a) and the production of Hg from deposits in the Skellefte district in Sweden (Rytuba, 2003). Cadmium, Se, and Te are recovered as by-products from smelting and refining of Zn and Cu concentrates produced from Australian VMS deposits (Skirrow et al., 2013). However, some of the minor elements are considered to be deleterious, attracting smelter penalties, in particular Sb and Hg (Skirrow et al., 2013).

Table 9. Concentration Ranges of Minor Elements in Volcanogenic Massive Sulfide Deposits (modified from Hannington, 2014)

Concentrations	Trace elements
To 10,000 ppm	Cd and Sb
To 1,000 ppm	Se
To 500 ppm	Bi, In, and Mo
To 100 ppm	Ga, Ge, Hg, Te, and Tl

Despite obvious implications to processing and waste management, comparably little quantitative data constraining the mineralogical sequestration of minor elements in ancient massive sulfides is available. In general, elements such as Bi, In, Mo, and Se are enriched in chalcopyrite-rich ores, whereas other minor elements such as Cd, Hg, Sb, and Tl have higher abundances in sphalerite-rich ores (Hannington, 2014), which is in agreement with the observations from sea-floor massive sulfide deposits. Minor element enrichment in the massive sulfide ores can be related to element substitution into the crystal structure of the main ore minerals pyrite, pyrrhotite, chalcopyrite, sphalerite, and galena or the occurrence of trace minerals. A large number of trace ore minerals have been documented (Shimazaki, 1974; Mosier et al., 1983; Eremin et al., 2007), including over 110 minerals containing the minor elements discussed in this contribution (Table 10).

Bismuth

Bismuth is common in the ores of VMS deposits in concentrations of up to 500 ppm (Table 9). The ore at Kidd Creek averages approximately 20 ppm Bi (Hannington et al., 1999c). Much of the Bi in VMS ores appears to be contained in accessory phases (Table 10). Approximately 15% of all well-documented VMS deposits contain at least one Bi-bearing accessory mineral (Mosier et al., 1983). Marcoux et al. (1996) demonstrated that the VMS deposits of the Iberian Pyrite Belt contain close to 30 different Bi-bearing minerals. Eremin et al. (2007) identified 25 different Bi-bearing accessory minerals in the Devonian VMS deposits of the Rudny Altai of Russia and Kazakhstan. Bismuthinite and native Bi are among the most common Bi-bearing trace minerals in VMS deposits (Table 10). In many deposits, including Kidd Creek (Hannington et al., 1999c), Bi-rich trace ore minerals are particularly abundant in Cu-rich ores.

Cadmium

In VMS deposits, Cd mainly occurs in solid solution in sphalerite, although some VMS deposits contain the rare Cd-bearing accessory minerals cadmoselite and greenockite (Table 10). The Kidd Creek deposit, which is estimated to have an overall grade of about 700 ppm Cd (Hannington et al., 1999c), represents a well-studied example of a Cd-rich VMS deposit.

Table 10. Minor Element Minerals and Examples of Their Occurrence in Volcanogenic Massive Sulfide Deposits[1,2]

Mineral	Formula	Age	Location
Bi-bearing ore minerals			
Aikinite	$PbCuBiS_3$	Miocene	Kurosawa, Hokuroku, Japan
		Cretaceous	Elshitsa, Sredna Gora, Bulgaria
			Murgul, Pontides, Turkey
		Devonian-Carboniferous	Neves-Corvo, Iberian Pyrite Belt, Portugal
			Nuestra Senora del Carmen, Iberian Pyrite Belt, Spain
			Rio Tinto, Iberian Pyrite Belt, Spain
			Tharsis, Iberian Pyrite Belt, Spain
		Devonian	Artemievskoe, Rudney Altai, Kazakhstan
			Kamyshinskoe, Rudney Altai, Kazakhstan
			Maleevskoe, Rudney Altai, Kazakhstan
			Safyanovskoe, Urals, Russia
Aleksite	$PbBi_2Te_2S_2$	Devonian	Ridder-Sokolnoe, Rudney Altai, Kazakhstan
Bismuthinite	Bi_2S_3	Cretaceous	Lahanos, Pontides, Turkey
		Devonian-Carboniferous	Algares, Iberian Pyrite Belt, Portugal
			Aznalcóllar, Iberian Pyrite Belt, Spain
			Concepción, Iberian Pyrite Belt, Spain
			Neves-Corvo, Iberian Pyrite Belt, Portugal
			Nuestra Senora del Carmen, Iberian Pyrite Belt, Spain
			Rio Tinto, Iberian Pyrite Belt, Spain
			San Miguel, Iberian Pyrite Belt, Spain
			Tharsis, Iberian Pyrite Belt, Spain
		Devonian	Artemievskoe, Rudney Altai, Kazakhstan
			Kamyshinskoe, Rudney Altai, Kazakhstan
			Mount Morgan, Queensland, Australia
			Novo-Berezovskoe, Rudney Altai, Kazakhstan
			Podolskoe, Urals, Russia
		Silurian	Currawong, Benambra, Australia
			Woodlawn, New South Wales, Australia
		Cambrian	Rosebery, Mount Read Volcanics, Tasmania, Australia
			Thalanga, Queensland, Australia
		Mesoproterozoic	Ambaji, Gujarat, India
			Deri, Rajasthan, India
		Paleoproterozoic	Hällefors, Bergslagen, Sweden
		Neoarchean	Hackett River, Nunavut, Canada
			Kidd Creek, Abitibi, Ontario, Canada
		Mesoarchean	Gossan Hill, Western Australia, Australia
Bohdanowiczite	$AgBiSe_2$	Devonian-Carboniferous	Neves-Corvo, Iberian Pyrite Belt, Portugal
		Neoarchean	Kidd Creek, Abitibi, Ontario, Canada
Bursaite	$Pb_5Bi_4S_{11}$	Cambrian	Cofer, Virginia, USA
Cosalite	$Pb_2Bi_2S_5$	Devonian-Carboniferous	Algares, Iberian Pyrite Belt, Portugal
			Aljustrel, Iberian Pyrite Belt, Portugal
			Lomero-Poyatos, Iberian Pyrite Belt, Spain
			Neves-Corvo, Iberian Pyrite Belt, Portugal
			Rio Tinto, Iberian Pyrite Belt, Portugal
			Sotiel-Migollas, Iberian Pyrite Belt, Spain
		Devonian	Kamyshinskoe, Rudney Altai, Kazakhstan
			Maleevskoe, Rudney Altai, Kazakhstan
		Cambrian	Cofer, Virginia, USA
			Rosebery, Mount Read Volcanics, Tasmania, Australia
		Paleoproterozoic	Hällefors, Bergslagen, Sweden
Emplectite	$CuBiS_2$	Devonian-Carboniferous	Concepción, Iberian Pyrite Belt, Spain
			Rio Tinto, Iberian Pyrite Belt, Portugal
			Tharsis, Iberian Pyrite Belt, Spain
		Devonian	Kamyshinskoe, Rudney Altai, Kazakhstan
			Novo-Berezovskoe, Rudney Altai, Kazakhstan
Friedrichite	$Pb_5Cu_5Bi_7S_{18}$	Devonian-Carboniferous	Rio Tinto, Iberian Pyrite Belt, Portugal
Galenobismutite	$PbBi_2S_4$	Devonian-Carboniferous	Neves-Corvo, Iberian Pyrite Belt, Portugal
			Nuestra Senora del Carmen, Iberian Pyrite Belt, Spain
		Devonian	Artemievskoe, Rudney Altai, Kazakhstan
			Kamyshinskoe, Rudney Altai, Kazakhstan
			Maleevskoe, Rudney Altai, Kazakhstan
		Silurian	Currawong, Benambra, Australia
			Wilga, Benambra, Australia
		Paleoproterozoic	Hällefors, Bergslagen, Sweden
Giessenite	$Pb_{28}Cu_2(Bi,Sb)_{19}S_{57}$	Devonian-Carboniferous	Rio Tinto, Iberian Pyrite Belt, Portugal
		Devonian	Novo-Berezovskoe, Rudney Altai, Kazakhstan
Gladite	$PbCuBi_5S_9$	Devonian-Carboniferous	Algares, Iberian Pyrite Belt, Portugal
Guanajuatite/paraguanajuatite	$Bi_2(Se,S)_3$	Devonian-Carboniferous	Neves-Corvo, Iberian Pyrite Belt, Portugal

Table 10. *(Cont.)*

Mineral	Formula	Age	Location
Bi-bearing ore minerals *(Cont.)*			
Gustavite	$PbAgBi_3S_6$	Devonian-Carboniferous	Algares, Iberian Pyrite Belt, Portugal
			Concepción, Iberian Pyrite Belt, Spain
			Rio Tinto, Iberian Pyrite Belt, Portugal
Hammarite	$Pb_2Cu_2Bi_4S_9$	Devonian-Carboniferous	Rio Tinto, Iberian Pyrite Belt, Portugal
		Devonian	Maleevskoe, Rudney Altai, Kazakhstan
Heyrovskyite	$Pb_4AgBi_3S_9$	Neoarchean	Hackett River, Nunavut, Canada
Joseite	Bi_4TeS_2	Devonian-Carboniferous	Tharsis, Iberian Pyrite Belt, Spain
Joseite-B	Bi_4Te_2S	Devonian-Carboniferous	Neves-Corvo, Iberian Pyrite Belt, Portugal
			Sotiel-Migollas, Iberian Pyrite Belt, Spain
			Tharsis, Iberian Pyrite Belt, Spain
		Devonian	Ridder-Sokolnoe, Rudney Altai, Kazakhstan
Junoite	$Pb_3Cu_2Bi_8(S,Se)_{16}$	Neoarchean	Kidd Creek, Abitibi, Ontario, Canada
Kobellite	$Cu_2Pb_{10}(Bi,Sb)_{16}S_{35}$	Devonian-Carboniferous	Neves-Corvo, Iberian Pyrite Belt, Portugal
			Sotiel-Migollas, Iberian Pyrite Belt, Spain
			Tharsis, Iberian Pyrite Belt, Spain
		Devonian	Maleevskoe, Rudney Altai, Kazakhstan
			Novo-Berezovskoe, Rudney Altai, Kazakhstan
		Cambrian	Cofer, Virginia, USA
			Rosebery, Mount Read Volcanics, Tasmania, Australia
		Paleoproterozoic	Boliden, Skellefte, Sweden
Krupkaite	$PbCuBi_3S_6$	Devonian-Carboniferous	Neves-Corvo, Iberian Pyrite Belt, Portugal
			Rio Tinto, Iberian Pyrite Belt, Portugal
Laitakarite	$Bi_4(Se,S)_3$	Devonian-Carboniferous	Neves-Corvo, Iberian Pyrite Belt, Portugal
			San Miguel, Iberian Pyrite Belt, Spain
		Mesoproterozoic	Ambaji, Gujarat, India
			Deri, Rajasthan, India
		Paleoproterozoic	Boliden, Skellefte, Sweden
		Neoarchean	Kidd Creek, Abitibi, Ontario, Canada
Lillianite	$Pb_3Bi_2S_6$	Devonian-Carboniferous	Rio Tinto, Iberian Pyrite Belt, Portugal
		Neoarchean	Hackett River, Nunavut, Canada
Lindströmite	$Pb_3Cu_3Bi_7S_{15}$	Devonian-Carboniferous	Rio Tinto, Iberian Pyrite Belt, Portugal
		Devonian	Artemievskoe, Rudney Altai, Kazakhstan
			Kamyshinskoe, Rudney Altai, Kazakhstan
			Maleevskoe, Rudney Altai, Kazakhstan
			Novo-Berezovskoe, Rudney Altai, Kazakhstan
Maldonite	Au_2Bi	Cambrian	Rosebery, Mount Read Volcanics, Tasmania, Australia
Matildite	$AgBiS_2$	Cretaceous	San Fernando, Cuba
		Devonian	Kamyshinskoe, Rudney Altai, Kazakhstan
		Neoarchean	Hackett River, Nunavut, Canada
Miharaite	$PbCu_4FeBiS_6$	Devonian-Carboniferous	Neves-Corvo, Iberian Pyrite Belt, Portugal
Native Bi	Bi	Devonian-Carboniferous	Algares, Iberian Pyrite Belt, Portugal
			Aljustrel, Iberian Pyrite Belt, Portugal
			Aznalcóllar, Iberian Pyrite Belt, Spain
			Neves-Corvo, Iberian Pyrite Belt, Portugal
			Nuestra Senora del Carmen, Iberian Pyrite Belt, Spain
			Rio Tinto, Iberian Pyrite Belt, Spain
			San Miguel, Iberian Pyrite Belt, Spain
			Sotiel-Migollas, Iberian Pyrite Belt, Spain
			Tharsis, Iberian Pyrite Belt, Spain
		Devonian	Artemievskoe, Rudney Altai, Kazakhstan
			Kamyshinskoe, Rudney Altai, Kazakhstan
			Novo-Berezovskoe, Rudney Altai, Kazakhstan
		Cambrian	Cofer, Virginia, USA
			Henty, Mound Read Volcanics, Tasmania, Australia
			Rosebery, Mount Read Volcanics, Tasmania, Australia
			Thalanga, Queensland, Australia
		Mesoproterozoic	Ambaji, Gujarat, India
			Deri, Rajasthan, India
		Paleoproterozoic	Boliden, Skellefte, Sweden
			Hällefors, Bergslagen, Sweden
			Ruttan, Rusty Lake, Manitoba
		Neoarchean	Hackett River, Nunavut, Canada
			Kidd Creek, Abitibi, Ontario, Canada
			Taivaljärvi, Finland
Nuffieldite	$Pb_2Cu(Bi,Sb,Pb)Bi_2S_7$	Devonian-Carboniferous	Aznalcóllar, Iberian Pyrite Belt, Spain
			Concepción, Iberian Pyrite Belt, Spain
			Rio Tinto, Iberian Pyrite Belt, Portugal
		Devonian	Maleevskoe, Rudney Altai, Kazakhstan

Table 10. *(Cont.)*

Mineral	Formula	Age	Location
Bi-bearing ore minerals *(Cont.)*			
Pekoite	$PbCuBi_{11}(S,Se)_{18}$	Devonian-Carboniferous	Neves-Corvo, Iberian Pyrite Belt, Portugal
			Rio Tinto, Iberian Pyrite Belt, Spain
Pilsenite	Bi_4Te_3	Devonian	Ridder-Sokolnoe, Rudney Altai, Kazakhstan
		Paleoproterozoic	Trout Lake, Flin Flon, Manitoba
Tellurobismuthite	Bi_2Te_3	Devonian	Gaiskoe, Urals, Russia
			Molodezhnoe, Urals, Russia
			Mount Morgan, Queensland, Australia
			Safyanovskoe, Urals, Russia
			Uchalinskoe, Urals, Russia
			Uzelginskoe, Urals, Russia
		Silurian	Tarnyerskoe, Urals, Russia
			Valentorskoe, Urals, Russia
			Yaman-Kasy, Urals, Russia
		Neoarchean	Bousquet 2-Dumagami, Abitibi, Quebec, Canada
Tetradymite	Bi_2Te_2S	Cretaceous	Elshitsa, Sredna Gora, Bulgaria
			Lahanos, Pontides, Turkey
			Murgul, Pontides, Turkey
		Devonian-Carboniferous	Neves-Corvo, Iberian Pyrite Belt, Portugal
			Tharsis, Iberian Pyrite Belt, Spain
		Devonian	Maleevskoe, Rudney Altai, Kazakhstan
			Mount Morgan, Queensland, Australia
			Novo-Berezovskoe, Rudney Altai, Kazakhstan
			Ridder-Sokolnoe, Rudney Altai, Kazakhstan
			Safyanovskoe, Urals, Russia
		Silurian	Tarnyerskoe, Urals, Russia
		Paleoproterozoic	Hällefors, Bergslagen, Sweden
Wittichenite	Cu_3BiS_3	Miocene	Kurosawa, Hokuroku, Japan
		Devonian-Carboniferous	Concepción, Iberian Pyrite Belt, Spain
			Neves-Corvo, Iberian Pyrite Belt, Portugal
			Rio Tinto, Iberian Pyrite Belt, Spain
		Devonian	Kamyshinskoe, Rudney Altai, Kazakhstan
			Safyanovskoe, Urals, Russia
		Silurian	Currawong, Benambra, Australia
			Valentorskoe, Urals, Russia
			Wilga, Benambra, Australia
Cd-bearing ore minerals			
Cadmoselite	CdSe	Neoarchean	Kidd Creek, Abitibi, Ontario, Canada
Greenockite	CdS	Devonian	Kamyshinskoe, Rudney Altai, Kazakhstan
		Silurian	Yaman-Kasy, Urals, Russia
Ge-bearing ore minerals			
Argyrodite	Ag_8GeS_6	Devonian	Babaryk, Urals, Russia
Ge-bearing colusite	$Cu_{26}V_2(As,Sn,Sb,Ge)_6S_{32}$	Miocene	Ezuri, Hokuroku, Japan
		Cretaceous	San Fernando, Cuba
		Permian	Yanahara, Okayama, Japan
		Devonian	Gaiskoe, Urals, Russia
		Ordovician	Waterloo, Queensland, Australia
		Neoarchean	Bousquet 2-Dumagami, Abitibi, Quebec, Canada
Germanite	$Cu_{13}Fe_2Ge_2S_{16}$	Miocene	Kamikita, Japan
			Shakanai, Hokuroku, Japan
		Devonian	Aleksandrinskoe, Urals, Russia
			Babaryk, Urals, Russia
			Bakr-Tau, Urals, Russia
			Gaiskoe, Urals, Russia
			Tash-Tau, Urals, Russia
Germanocolusite	$Cu_{26}V_2(Ge,As)_6S_{32}$	Devonian	Maykain, Rudney Altai, Kazakhstan
			Urup, North Caucasus, Russia
Renierite	$(Cu,Zn)_{11}Fe_4(Ge,As)_2S_{16}$	Devonian	Aleksandrinskoe, Urals, Russia
			Artemievskoe, Rudney Altai, Kazakhstan
			Kamyshinskoe, Rudney Altai, Kazakhstan
		Silurian	Valentorskoe, Urals, Russia
		Neoarchean	Bousquet 2-Dumagami, Abitibi, Quebec, Canada
Hg-bearing ore minerals			
Au-Ag-Hg alloy	(Au,Ag,Hg)	Jurassic	Eskay Creek, British Columbia, Canada
		Devonian-Carboniferous	Rio Tinto, Iberian Pyrite Belt, Spain
		Ordovician	Ming, Baie Verte, Newfoundland, Canada
		Cambrian	Mount Lyell, Mound Read Volcanics, Tasmania, Australia
			South Hercules, Mound Read Volcanics, Tasmania, Australia

Table 10. *(Cont.)*

Mineral	Formula	Age	Location
Hg-bearing ore minerals *(Cont.)*			
		Paleoproterozoic	Boliden, Skellefte, Sweden
			Långsele, Skellefte, Sweden
			Rakkejaur, Skellefte, Sweden
			Trout Lake, Flin Flon, Manitoba
Cinnabar/metacinnabar	HgS	Miocene	Kali Kuning, Wetar, Indonesia
		Jurassic	Eskay Creek, British Columbia, Canada
		Devonian	Gaiskoe, Urals, Russia
			Zapadno-Ozernoe, Urals, Russia
		Ordovician	Murray Brook, Bathurst, New Brunswick, Canada
		Paleoproterozoic	Långsele, Skellefte, Sweden
Coloradoite	HgTe	Devonian-Carboniferous	Neves-Corvo, Iberian Pyrite Belt, Portugal
		Devonian	Gaiskoe, Urals, Russia
			Molodezhnoe, Urals, Russia
			Mount Morgan, Queensland, Australia
			Uchalinskoe, Urals, Russia
			Uzelginskoe, Urals, Russia
		Silurian	Yaman-Kasy, Urals, Russia
		Ordovician	Ming, Baie Verte, Newfoundland, Canada
Moschellandsbergite	Ag_2Hg_3	Miocene	Kali Kuning, Wetar, Indonesia
Perroudite	$Hg_5Ag_4S_5(Cl,I,Br)_4$	Miocene	Kali Kuning, Wetar, Indonesia
Tiemannite	HgSe	Devonian-Carboniferous	Neves-Corvo, Iberian Pyrite Belt, Portugal
		Devonian	Zapadno-Ozernoe, Urals, Russia
In-bearing ore minerals			
Roquesite	$CuInS_2$	Devonian-Carboniferous	Neves-Corvo, Iberian Pyrite Belt, Portugal
		Neoarchean	Kidd Creek, Abitibi, Ontario, Canada
Sakuraiite	(Cu,Zn,In,Fe,Sn)S	Devonian-Carboniferous	Neves-Corvo, Iberian Pyrite Belt, Portugal
Mo-bearing ore minerals			
Molybdenite	MoS_2	Devonian	Bakr-Tau, Urals, Russia
			Chessy, Massif Central, France
			Mount Morgan, Queensland, Australia
			Uzelginskoe, Urals, Russia
		Silurian	Letnee, Urals, Russia
		Ordovician	Ming, Baie Verte, Newfoundland, Canada
		Cambrian	Cofer, Virginia, USA
			Thalanga, Queensland, Australia
			Western Tharsis, Mount Read Volcanics, Tasmania, Australia
		Neoproterozoic	Um Samiuki, Eastern Desert, Egypt
		Paleoproterozoic	Hällefors, Bergslagen, Sweden
			Ruttan, Rusty Lake, Manitoba
Sb-bearing ore minerals[3]			
Andorite	$PbAgSb_3S_6$	Cretaceous	Barika, Iran
Arsenquatrandorite	$Ag_{17.6}Pb_{12.8}Sb_{38.1}As_{11.5}S_{96}$	Cretaceous	Barika, Iran
Aurostibnite	$AuSb_2$	Ordovician	Sulitjelma, Norway
		Paleoproterozoic	Boliden, Skellefte, Sweden
			Långsele, Skellefte, Sweden
Barikaite	$Pb_{10}Ag_3Sb_8As_{11}S_{40}$	Cretaceous	Barika, Iran
Berthierite	$FeSb_2S_4$	Cretaceous	La Esmeralda, Mexico
		Devonian	Maleevskoe, Rudney Altai, Kazakhstan
		Paleoproterozoic	Rakkejaur, Skellefte, Sweden
Bindheimite	$Pb_2Sb_2O_6(O,OH)$	Ordovician	Murray Brook, Bathurst, New Brunswick, Canada
Boulangerite	$Pb_5Sb_4S_{11}$	Miocene	Kali Kuning, Wetar, Indonesia
			Uwamuki, Hokuroku, Japan
		Cretaceous	La Esmeralda, Mexico
		Jurassic	Eskay Creek, British Columbia, Canada
		Carboniferous	Kudz Ze Kayah, Finlayson Lake, Canada
			Wolferine, Finlayson Lake, Canada
		Devonian-Carboniferous	Aznalcóllar, Iberian Pyrite Belt, Spain
		Ordovician	Ming, Baie Verte, Newfoundland, Canada
		Cambrian	Cofer, Virginia, USA
			Rosebery, Mount Read Volcanics, Tasmania, Australia
		Paleoproterozoic	Boliden, Skellefte, Sweden
			Hällefors, Bergslagen, Sweden
			Näsliden, Skellefte, Sweden
			Rakkejaur, Skellefte, Sweden
			Trout Lake, Flin Flon, Manitoba
		Neoarchean	Mattabi, Sturgeon Lake, Ontario, Canada

Table 10. *(Cont.)*

Mineral	Formula	Age	Location
Sb-bearing ore minerals[3] *(Cont.)*			
Bournonite	$PbCuSbS_3$	Miocene	Kali Kuning, Wetar, Indonesia
			Uwamuki, Hokuroku, Japan
		Cretaceous	La Esmeralda, Mexico
		Jurassic	Eskay Creek, British Columbia, Canada
		Devonian-Carboniferous	Aznalcóllar, Iberian Pyrite Belt, Spain
			Neves-Corvo, Iberian Pyrite Belt, Portugal
			Tharsis, Iberian Pyrite Belt, Spain
		Silurian	Currawong, Benambra, Australia
		Cambrian	Rosebery, Mount Read Volcanics, Tasmania, Australia
		Mesoproterozoic	Montauban, Quebec
		Paleoproterozoic	Boliden, Skellefte, Sweden
			Hällefors, Bergslagen, Sweden
			Långsele, Skellefte, Sweden
			Näsliden, Skellefte, Sweden
			Rakkejaur, Skellefte, Sweden
			Trout Lake, Flin Flon, Manitoba
		Neoarchean	Mattabi, Sturgeon Lake, Ontario, Canada
			Taivaljärvi, Finland
Breithauptite	NiSb	Devonian	Chessy, Massif Central, France
		Ordovician	Sulitjelma, Norway
		Paleoproterozoic	Hällefors, Bergslagen, Sweden
			Långsele, Skellefte, Sweden
Chalcostibite	$CuSbS_2$	Devonian-Carboniferous	Neves-Corvo, Iberian Pyrite Belt, Portugal
Costibite/paracostibite	CoSbS	Paleoproterozoic	Hällefors, Bergslagen, Sweden
			Trout Lake, Flin Flon, Manitoba
Diaphorite	$Pb_2Ag_3Sb_3S_8$	Devonian	Zyryanovskoe, Rudney Altai, Kazakhstan
Dyscrasite	Ag_3Sb	Devonian	Zyryanovskoe, Rudney Altai, Kazakhstan
		Mesoproterozoic	Montauban, Quebec
		Paleoproterozoic	Trout Lake, Flin Flon, Manitoba
		Neoarchean	Kidd Creek, Abitibi, Ontario, Canada
			Taivaljärvi, Finland
Famatinite	Cu_3SbS_4	Miocene	Kali Kuning, Wetar, Indonesia
		Devonian-Carboniferous	Tharsis, Iberian Pyrite Belt, Spain
Ferdowsiite	$Ag_8Sb_5As_3S_{16}$	Cretaceous	Barika, Iran
Fizelyite	$Pb_{14}Ag_5Sb_{21}S_{48}$	Mesoproterozoic	Montauban, Quebec
Freibergite	$(Ag,Cu,Fe,Zn)_{12}(Sb,As)_4S_{13}$	Cretaceous	La Esmeralda, Mexico
		Jurassic	Eskay Creek, British Columbia, Canada
		Devonian	Artemievskoe, Rudney Altai, Kazakhstan
			Ashele, Rudney Altai, Xinjiang, China
			Kamyshinskoe, Rudney Altai, Kazakhstan
			Novo-Leninogorskoe, Rudney Altai, Kazakhstan
			Ridder-Sokolnoe, Rudney Altai, Kazakhstan
			Shemonaikhinskoe, Rudney Altai, Kazakhstan
			Strezhanskoe, Rudney Altai, Kazakhstan
		Silurian	Woodlawn, New South Wales, Australia
		Ordovician	Sulitjelma, Norway
		Cambrian	Cofer, Virginia, USA
		Neoproterozoic	Um Samiuki, Eastern Desert, Egypt
		Paleoproterozoic	Lynne, Penokean, Wisconsin, USA
			Trout Lake, Flin Flon, Manitoba
		Neoarchean	Hackett River, Nunavut, Canada
			Kidd Creek, Abitibi, Ontario, Canada
			Taivaljärvi, Finland
Freieslebenite	$AgPbSbS_3$	Paleoproterozoic	Trout Lake, Flin Flon, Manitoba
		Neoarchean	Taivaljärvi, Finland
Geocronite	$Pb_{14}(Sb,As)_6S_{23}$	Miocene	Kali Kuning, Wetar, Indonesia
		Cretaceous	Barika, Iran
		Mesoproterozoic	Montauban, Quebec
Gudmundite	FeSbS	Devonian-Carboniferous	Neves-Corvo, Iberian Pyrite Belt, Portugal
		Devonian	Maleevskoe, Rudney Altai, Kazakhstan
		Ordovician	Sulitjelma, Norway
		Cambrian	Cofer, Virginia, USA
		Mesoproterozoic	Montauban, Quebec
		Paleoproterozoic	Boliden, Skellefte, Sweden
			Hällefors, Bergslagen, Sweden
			Rakkejaur, Skellefte, Sweden
			Trout Lake, Flin Flon, Manitoba

Table 10. *(Cont.)*

Mineral	Formula	Age	Location
Sb-bearing ore minerals[3] *(Cont.)*			
		Neoarchean	Bousquet 1, Abitibi, Quebec, Canada
			Hackett River, Nunavut, Canada
			Taivaljärvi, Finland
Guettardite/twinnite	$Pb(Sb,As)_2S_4$	Cretaceous	Barika, Iran
		Mesoproterozoic	Montauban, Quebec
Jamesonite/parajamesonite	$Pb_4FeSb_6S_{14}$	Cretaceous	La Esmeralda, Mexico
		Jurassic	Eskay Creek, British Columbia, Canada
		Paleoproterozoic	Boliden, Skellefte, Sweden
			Rakkejaur, Skellefte, Sweden
Jaskolskiite	$Pb_{2+x}Cu_x(Sb,Bi)_{2-x}S_5$	Devonian-Carboniferous	Aznalcóllar, Iberian Pyrite Belt, Spain
Meneghinite	$Pb_{13}CuSb_7S_{24}$	Miocene	Uwamuki, Hokuroku, Japan
		Carboniferous	Wolferine, Finlayson Lake, Canada
		Devonian-Carboniferous	Aznalcóllar, Iberian Pyrite Belt, Spain
			Neves-Corvo, Iberian Pyrite Belt, Portugal
			Tharsis, Iberian Pyrite Belt, Spain
		Cambrian	Cofer, Virginia, USA
			Rosebery, Mount Read Volcanics, Tasmania, Australia
		Mesoproterozoic	Ambaji, Gujarat, India
			Deri, Rajasthan, India
		Paleoproterozoic	Hällefors, Bergslagen, Sweden
			Näsliden, Skellefte, Sweden
Miargyrite	$AgSbS_2$	Cretaceous	Barika, Iran
		Carboniferous	Wolferine, Finlayson Lake, Canada
		Devonian	Berezovskoe, Rudney Altai, Kazakhstan
			Strezhanskoe, Rudney Altai, Kazakhstan
		Ordovician	Ming, Baie Verte, Newfoundland, Canada
		Mesoproterozoic	Montauban, Quebec
		Neoarchean	Taivaljärvi, Finland
Native Sb	Sb	Paleoproterozoic	Hällefors, Bergslagen, Sweden
		Neoarchean	Taivaljärvi, Finland
Nisbite	$NiSb_2$	Devonian	Maleevskoe, Rudney Altai, Kazakhstan
		Paleoproterozoic	Hällefors, Bergslagen, Sweden
			Långsele, Skellefte, Sweden
Owyheeite	$Ag_3Pb_{10}Sb_{11}S_{28}$	Cretaceous	La Esmeralda, Mexico
Polybasite	$(Ag,Cu)_{16}Sb_2S_{11}$	Miocene	Uchinotai-Higashi, Hokuroku, Japan
		Devonian	Zarechenskoe, Rudney Altai, Russia
			Zyryanovskoe, Rudney Altai, Kazakhstan
		Paleoproterozoic	Lynne, Penokean, Wisconsin, USA
Pyrargyrite/pyrostilpnite	Ag_3SbS_3	Cretaceous	Barika, Iran
			San Fernando, Cuba
		Devonian	Berezovskoe, Rudney Altai, Kazakhstan
			Kamyshinskoe, Rudney Altai, Kazakhstan
			Ridder-Sokolnoe, Rudney Altai, Kazakhstan
			Shemonaikhinskoe, Rudney Altai, Kazakhstan
		Silurian	Lewis Pond, New South Wales, Australia
		Ordovician	Ming, Baie Verte, Newfoundland, Canada
		Cambrian	Rosebery, Mount Read Volcanics, Tasmania, Australia
		Mesoproterozoic	Montauban, Quebec
		Paleoproterozoic	Hällefors, Bergslagen, Sweden
			Lynne, Penokean, Wisconsin, USA
			Trout Lake, Flin Flon, Manitoba
		Neoarchean	Selbaie, Abitibi, Quebec, Canada
Semseyite	$Pb_9Sb_8S_{21}$	Cretaceous	La Esmeralda, Mexico
Stephanite	Ag_5SbS_4	Cretaceous	Barika, Iran
		Devonian	Strezhanskoe, Rudney Altai, Kazakhstan
			Zyryanovskoe, Rudney Altai, Kazakhstan
		Ordovician	Ming, Baie Verte, Newfoundland, Canada
		Neoproterozoic	Um Samiuki, Eastern Desert, Egypt
		Mesoproterozoic	Montauban, Quebec
		Paleoproterozoic	Crandon, Penokean, Wisconsin, USA
		Neoarchean	Hackett River, Nunavut, Canada
			Selbaie, Abitibi, Quebec, Canada
Sterryite	$Ag_2Pb_{10}(Sb,As)_{12}S_{29}$	Cretaceous	Barika, Iran
Stibnite/metastibnite	Sb_2S_3	Cretaceous	Barika, Iran
		Jurassic	Eskay Creek, British Columbia, Canada
		Paleoproterozoic	Långsele, Skellefte, Sweden
Tintinaite	$Cu_2Pb_{10}(Sb,Bi)_{16}S_{35}$	Devonian-Carboniferous	Sotiel-Migollas, Iberian Pyrite Belt, Spain
Ullmannite	NiSbS	Paleoproterozoic	Hällefors, Bergslagen, Sweden
			Långsele, Skellefte, Sweden

Table 10. *(Cont.)*

Mineral	Formula	Age	Location
Se-bearing ore minerals			
Clausthalite	PbSe	Cretaceous	Murgul, Pontides, Turkey
		Carboniferous	Kudz Ze Kayah, Finlayson Lake, Canada
			Wolferine, Finlayson Lake, Canada
		Devonian	Zapadno-Ozernoe, Urals, Russia
		Mesoproterozoic	Ambaji, Gujarat, India
			Deri, Rajasthan, India
		Paleoproterozoic	Trout Lake, Flin Flon, Manitoba
		Neoarchean	Bousquet 2-Dumagami, Abitibi, Quebec, Canada
			Kidd Creek, Abitibi, Ontario, Canada
Dzharkenite	$FeSe_2$	Devonian	Zapadno-Ozernoe, Urals, Russia
Eucairite	CuAgSe	Neoarchean	Kidd Creek, Abitibi, Ontario, Canada
Klockmannite	CuSe	Neoarchean	Kidd Creek, Abitibi, Ontario, Canada
Native Se	Se	Devonian	Zapadno-Ozernoe, Urals, Russia
Naumannite	Ag_2Se	Devonian-Carboniferous	Neves-Corvo, Iberian Pyrite Belt, Portugal
		Devonian	Yubileynoe, Urals, Russia
			Zapadno-Ozernoe, Urals, Russia
		Paleoproterozoic	Trout Lake, Flin Flon, Manitoba
		Neoarchean	Kidd Creek, Abitibi, Ontario, Canada
			Selbaie, Abitibi, Quebec, Canada
Petrovskaite	AgAu(S,Se)	Devonian	Uchalinskoe, Urals, Russia
Te-bearing ore minerals			
Altaite	PbTe	Cretaceous	Antonio, Cuba
			Elshitsa, Sredna Gora, Bulgaria
		Devonian	Bakr-Tau, Urals, Russia
			Gaiskoe, Urals, Russia
			Molodezhnoe, Urals, Russia
			Oktyabrskoe, Urals, Russia
			Uchalinskoe, Urals, Russia
			Uzelginskoe, Urals, Russia
		Silurian	Komsomolskoe, Urals, Russia
			Tarnyerskoe, Urals, Russia
			Yaman-Kasy, Urals, Russia
		Ordovician	Waterloo, Queensland, Australia
		Neoarchean	Bousquet 1, Abitibi, Quebec, Canada
			Bousquet 2-Dumagami, Abitibi, Quebec, Canada
			Mattagami Lake, Matagami, Quebec, Canada
Benleonardite	$Ag_8(Sb,As)Te_2S_3$	Silurian	Yaman-Kasy, Urals, Russia
		Neoproterozoic	Um Samiuki, Eastern Desert, Egypt
Calaverite/krennerite	$AuTe_2$	Devonian	Gaiskoe, Urals, Russia
			Mount Morgan, Queensland, Australia
			Uchalinskoe, Urals, Russia
		Silurian	Komsomolskoe, Urals, Russia
			Tarnyerskoe, Urals, Russia
		Ordovician	Waterloo, Queensland, Australia
		Cambrian	Mount Lyell, Mound Read Volcanics, Tasmania, Australia
		Neoarchean	Bousquet 1, Abitibi, Quebec, Canada
Cervelleite	Ag_4TeS	Devonian	Babaryk, Urals, Russia
			Tash-Tau, Urals, Russia
		Silurian	Valentorskoe, Urals, Russia
			Yaman-Kasy, Urals, Russia
		Neoproterozoic	Um Samiuki, Eastern Desert, Egypt
Empressite	AgTe	Devonian	Molodezhnoe, Urals, Russia
			Uchalinskoe, Urals, Russia
		Silurian	Valentorskoe, Urals, Russia
			Yaman-Kasy, Urals, Russia
Frohbergite	$FeTe_2$	Silurian	Yaman-Kasy, Urals, Russia
Goldfieldite	$Cu_{12}(Te,Sb,As)_4S_{13}$	Cretaceous	Elshitsa, Sredna Gora, Bulgaria
		Silurian	Yaman-Kasy, Urals, Russia
Hessite	Ag_2Te	Cretaceous	Murgul, Pontides, Turkey
			San Fernando, Cuba
		Devonian	Aleksandrinskoe, Urals, Russia
			Ashele, Rudney Altai, Xinjiang, China
			Bakr-Tau, Urals, Russia
			Gaiskoe, Urals, Russia
			Maleevskoe, Rudney Altai, Kazakhstan
			Molodezhnoe, Urals, Russia
			Mount Morgan, Queensland, Australia

Table 10. *(Cont.)*

Mineral	Formula	Age	Location
Te-bearing ore minerals *(Cont.)*			
			Oktyabrskoe, Urals, Russia
			Ridder-Sokolnoe, Rudney Altai, Kazakhstan
			Safyanovskoe, Urals, Russia
			Strezhanskoe, Rudney Altai, Kazakhstan
			Tash-Tau, Urals, Russia
			Uchalinskoe, Urals, Russia
			Uzelginskoe, Urals, Russia
			Yubileinoe, Urals, Russia
			Zarechenskoe, Rudney Altai, Russia
			Zyryanovskoe, Rudney Altai, Kazakhstan
		Silurian	Komsomolskoe, Urals, Russia
			Tarnyerskoe, Urals, Russia
			Valentorskoe, Urals, Russia
			Yaman-Kasy, Urals, Russia
		Ordovician	Waterloo, Queensland, Australia
		Cambrian	Henty, Mound Read Volcanics, Tasmania, Australia
		Neoproterozoic	Um Samiuki, Eastern Desert, Egypt
		Paleoproterozoic	Hällefors, Bergslagen, Sweden
			Långsele, Skellefte, Sweden
			Trout Lake, Flin Flon, Manitoba
		Neoarchean	Bousquet 2-Dumagami, Abitibi, Quebec, Canada
			Mattagami Lake, Matagami, Quebec, Canada
Kochkarite	$PbBi_4Te_7$	Cretaceous	Antonio, Cuba
Mattagamite	$CoTe_2$	Neoarchean	Mattagami Lake, Matagami, Quebec, Canada
Montbrayite	Au_2Te_3	Devonian	Gaiskoe, Urals, Russia
Muthmannite	(Ag,Au)Te	Devonian	Gaiskoe, Urals, Russia
Native Te	Te	Cretaceous	Elshitsa, Sredna Gora, Bulgaria
		Devonian	Uzelginskoe, Urals, Russia
		Silurian	Valentorskoe, Urals, Russia
			Yaman-Kasy, Urals, Russia
Petzite	Ag_3AuTe_2	Devonian	Mount Morgan, Queensland, Australia
			Uzelginskoe, Urals, Russia
		Silurian	Tarnyerskoe, Urals, Russia
			Yaman-Kasy, Urals, Russia
		Ordovician	Waterloo, Queensland, Australia
		Cambrian	Mount Lyell, Mound Read Volcanics, Tasmania, Australia
		Neoarchean	Bousquet 2-Dumagami, Abitibi, Quebec, Canada
Rucklidgeite	$(Bi,Pb)_3Te_4$	Cretaceous	Antonio, Cuba
		Paleoproterozoic	Trout Lake, Flin Flon, Manitoba
Stützite	$Ag_{5-x}Te_3$	Devonian	Uzelginskoe, Urals, Russia
		Silurian	Valentorskoe, Urals, Russia
			Yaman-Kasy, Urals, Russia
Sylvanite	$(Au,Ag)_2Te_4$	Cretaceous	Elshitsa, Sredna Gora, Bulgaria
		Devonian	Ridder-Sokolnoe, Rudney Altai, Kazakhstan
			Uzelginskoe, Urals, Russia
			Zarechenskoe, Rudney Altai, Russia
		Silurian	Valentorskoe, Urals, Russia
			Yaman-Kasy, Urals, Russia
Tellurantimony	Sb_2Te_3	Neoarchean	Mattagami Lake, Matagami, Quebec, Canada
Volynskite	$AgBiTe_2$	Silurian	Yaman-Kasy, Urals, Russia
		Paleoproterozoic	Trout Lake, Flin Flon, Manitoba

[1] Minor element minerals in some volcanogenic massive sulfide deposits may be of secondary origin

[2] Minerals containing more than one minor element are listed under the element having the highest concentration

[3] Occurrences of tetrahedrite are not listed as this Sb-bearing mineral is present in about 50% of VMS deposits with well-documented trace mineralogy (Mosier et al., 1983)

References: Agnew et al. (2005), Almodóvar et al. (1998), Barrie and Krogh (1996), Barrie et al. (2005), Belogub et al. (2003, 2008), Benzaazoua et al. (2003), Bergman Weihed et al. (1996), Berry et al. (1992), Bodon and Valenta (1995), Bogdanov et al. (1997), Boyle (1995), Brueckner et al. (2014), Callaghan (2001), Cook et al. (1990), DeMatties (1994), Eremin et al. (2007), Fedorov (1993), Franklin et al. (1975), Frets and Balde (1975), Gaspar (2002), Grant et al. (2015), Hannington et al. (1999b, c), Healy and Petruk (1990, 1992), Herrmann et al. (2001), Huston and Large (1988), Huston et al. (1992b), Kachalovskaya et al. (1975), Kase et al. (1990, 1994), Komuro and Kajiwara (2004), Krapiva et al. (1986), Lambe and Rowe (1987), Lawrence (1967), Layton-Matthews et al. (2008), Leitch (1981), Leistel et al. (1998b), Lescuyer et al. (1998), Makovicky et al. (2013), Marcoux et al. (1996), Maslennikov et al. (2013), McKay and Hazeldene (1987), Miller and Craig (1997), Mozgova et al. (1994), Novoselov et al. (2006), Nysten (1986), Özgür (1993), Papunen et al. (1989), Pringle and Thorpe (1980), Prokin and Buslaev (1999), Pshenichnyy et al. (1975), Roth et al. (1999), Rubinovich-Kogan (1988), Scotney et al. (2005), Shalaby et al. (2004), Sharpe and Gemmell (2002), Sherlock et al. (1999), Shimazaki (1974), Spiridonov et al. (1992), Thorpe and Harris (1973), Thorpe et al. (1976), Tiwary and Cook (1999), Tomkins (2007), Tornos et al. (1998), Torró et al. (2016), Tourigny et al. (1989, 1993), Trepka-Bloch (1985, 1989), Vikentyev (2006, 2015), Vikentyev et al. (2004, 2006), Wagner and Jonsson (2001), Wagner and Monecke (2005), Wagner et al. (2005), Wang (1999), Zakrzewski et al. (1980), and Zaw and Large (1992)

Sphalerite from this deposit has Cd concentrations ranging from 0.2 to 0.6 wt % (Hannington et al., 1999b). Similar concentration ranges occur in the deposits in the Hokuroku district, such as Uchinotai-Nishi where sphalerite is typified by Cd concentrations of 0.24 to 0.59 wt % (Urabe and Sato, 1978). Sphalerite at the Crandon deposit in the Penokean volcanic belt of Wisconsin contains an average of 0.09 wt % Cd (Lambe and Rowe, 1987), while sphalerite at the Ruttan deposit in northern Manitoba averages 0.17 wt % Cd, with a range of up to 0.29 wt % (Barrie et al., 2005). At the Rosebery deposit in Tasmania, the Cd and Zn concentrations of the ore correlate strongly, suggesting that Cd is also primarily contained in sphalerite. At an average concentration of 273 ppm Cd, the 23.5 Mt Rosebery deposit contains an estimated 6,400 t Cd (Skirrow et al., 2013).

Gallium

Gallium is present in trace amounts in VMS deposits (Table 9). Barrie et al. (2007) reported average concentrations of 0.12 wt % Ga in sphalerite from the Neoproterozoic Bisha deposit in Eritrea. A study on the deposits of the Iberian Pyrite Belt revealed the presence of up to 150 ppm Ga in ores with elevated concentrations of Ag, Pb, and Zn. LA-ICP-MS analyses showed that Ga in these deposits is primarily contained in sphalerite (Marcoux et al., 1996). An association between Ga and Zn was also noted at the Cambro-Ordovician Balcooma and Dry River South deposits in northern Queensland (Huston et al., 1992a). The Dry River South deposit has an approximate Ga grade of 60 ppm. At a total tonnage of 0.73 Mt of ore, this deposit contains an estimated 44 t Ga (Skirrow et al., 2013). In addition to sphalerite, tourmaline contained in some VMS deposits can have detectable amounts of Ga (Griffin et al., 1996). However, Ga is currently not recoverable from silicate minerals contained in sulfide ores.

Germanium

In comparison, little is known on the mineralogical sequestration of Ge in VMS ores. Early studies by Takeuchi et al. (1956) indicated that Ge can be enriched in sphalerite at levels ranging from 50 to 250 ppm. Similar Ge concentrations have been reported in sphalerite from Bisha in Eritrea (Barrie et al., 2007). In some deposits, Ge is also present in Ge-bearing colusite and germanocolusite (Table 10). Wagner and Monecke (2005) showed that Ge-bearing colusite at the Ordovician Waterloo deposit in Queensland contains 4 to 5 wt % Ge. At the Bousquet 2-Dumagami deposit in the Archean Abitibi greenstone belt of Quebec, Canada, Ge is enriched in Cu-rich ores and occurs primarily in trace minerals such as Ge-bearing colusite and renierite (Tourigny et al., 1993). Argyrodite and germanite are rare trace minerals in some VMS deposits (Table 10).

Mercury

The Hg content of VMS deposits is highly variable, but typically below 100 ppm (Table 9). The Rosebery deposit has an estimated average Hg content of 44 ppm. The Nimbus deposit in Western Australia contains on average 66 ppm Hg (Skirrow et al., 2013). At Kidd Creek, the ore averages 1.1 ppm Hg (Hannington et al., 1999c). Much of the Hg in VMS ores is likely contained in solid solution in sphalerite (Jonasson and Sangster, 1975; Grammatikopoulos and Roth, 2002; Barrie et al., 2005). However, low concentrations of this element have been detected in other sulfide minerals such as chalcopyrite, galena, pyrite, and pyrrhotite (Jonasson and Sangster, 1975; Ryall, 1979; Barrie et al., 2005). Elevated concentrations of Hg can be present in tetrahedrite (Ryall, 1979). In some deposits, such as the Neogene Kali Kuning deposits on Wetar Island in Indonesia (Scotney et al., 2005) or the Jurassic Eskay Creek deposit in British Columbia, Canada (Roth et al., 1999), Hg forms cinnabar. Some deposits also contain an alloy of Au, Ag, and Hg (Table 10). Coloradoite, moschellandsbergite, perroudite, and tiemannite are additional rare Hg hosts (Table 10).

Indium

Roquesite is a major host of In, typically forming inclusions in massive chalcopyrite and chalcopyrite stringers. At Kidd Creek, chalcopyrite ores containing roquesite inclusions are typified by In concentrations between 250 and 400 ppm (Hannington et al., 1999c). Indium is also present in solid solution in the crystal structures of chalcopyrite through a coupled substitution of Fe by Cu and In, causing an excess of Cu atoms (Yamanaka and Kato, 1976). Smaller amounts of In occur in solid solution in sphalerite through the coupled substitution of Zn by Cu and In (Bente and Doering, 1995). Roquesite can occur as inclusions in sphalerite as "roquesite disease," similar to "chalcopyrite disease" (Kieft and Damman, 1990). In some VMS deposits, In is present in tennantite-tetrahedrite (Ishihara and Endo, 2007), Cu-Sn sulfosalts such as stannite and stannoidite (Schwarz-Schampera and Herzig, 2002; Benzaazoua et al., 2003), and the trace ore mineral sakuraiite (Table 10).

Molybdenum

Molybdenum is commonly found in trace amounts in massive sulfides (Table 9), but molybdenite is not an important ore constituent (Table 10). Elevated Mo concentrations are commonly noted in Cu-rich massive sulfides (Ashley et al., 1988). Copper concentrate from the Mount Lyell deposits in Tasmania contained on average 0.1 wt % Mo (Skirrow et al., 2013). In addition to molybdenite, Mo can be contained in solid solution in pyrite (Huston et al., 1995). For example, pyrite present in the altered mudstone hosting the Eskay Creek deposit contains up to several hundred ppm Mo (Ritts, 2012). In some cases, Mo enrichments occur in ores with high Te contents, presumably related to the presence of telluride phases (Maslennikov et al., 2009).

Antimony

Many VMS deposits contain elevated Sb concentrations (Table 9). Skirrow et al. (2013) estimated that the Rosebery deposit in Tasmania contains an average grade of 271 ppm Sb for a total of 6,400 t. Zinc-rich ores from Dry River South contained 20 to 100 ppm Sb, while <50 ppm Sb are present in ores from the Mount Chalmers deposit in Queensland (Skirrow et al., 2013). Ore samples from Kidd Creek have an average Sb content of about 30 ppm (Hannington et al., 1999c). About 50% of VMS deposits with well-documented trace mineralogy contain at least one Sb-bearing mineral. In nearly all of these deposits, members of the tennantite-tetrahedrite

solid solution were recognized as the main Sb-bearing sulfide phases (Mosier et al., 1983). In addition, a wide range of minor phases, including boulangerite, bournonite, freibergite, pyrargyrite, and stephanite, as well as accessory minerals such as dyscrasite, gudmundite, jamesonite, meneghinite, miargyrite, polybasite, and stibnite have been reported from VMS deposits (Table 10).

Selenium

Selenium occurs in concentrations of up to 1,000 ppm in VMS deposits (Table 9). The Cu concentrate produced from the Mount Lyell deposits in Tasmania contained on average 80 ppm Se (Skirrow et al., 2013). The ore at Kidd Creek contains on average 170 ppm Se (Hannington et al., 1999c). Selenium mainly substitutes for sulfur in Cu and Fe sulfides, including pyrite, pyrrhotite, chalcopyrite, bornite, and digenite (Huston et al., 1995; Hannington et al., 1999c; Layton-Matthews et al., 2008). Huston et al. (1995) showed that the Se content of pyrite in Zn-rich deposits is typically low (<5 ppm), while high Se contents of 10 to 200 ppm can be observed in pyrite in the stringer zones or lower parts of Cu-rich deposits. Selenium levels in chalcopyrite in Besshi deposits are typically higher than in coexisting pyrite (Yamamoto et al., 1984). At the Kidd Creek deposit, bornite and digenite are important Se hosts. Bornite contains on average 0.2 wt % Se, up to a maximum of 2.1 wt % (Hannington et al., 1999c). In some deposits, a significant proportion of the total Se content of the ores can be accounted for by the presence of selenide trace minerals (Table 10).

Tellurium

Tellurium is typically present in VMS deposits at concentration levels below 100 ppm (Table 9). Copper concentrates from the Mount Lyell deposits in Tasmania had an average Te content of 40 ppm (Skirrow et al., 2013). Tellurium is complexed with elements such as Pb and Bi and the precious metals and at least 10% of all VMS deposits contain Te-bearing accessory phases (Mosier et al., 1983). In deposits containing elevated Au and Ag grades, a large proportion of the precious metals is present as the tellurides calaverite, cervelleite, hessite, petzite, and sylvanite. Tellurobismuthite and tetradymite have been identified in some deposits (Table 10).

Thallium

Thallium occurs in low concentrations in ores from VMS deposits (Table 9). Most of the Tl is hosted by pyrite. Analysis of pyrite mill concentrates showed that pyrite at Rosebery contained about 80 ppm Tl, while galena contained 30 ppm Tl (Smith and Huston, 1992). LA-ICP-MS analysis of pyrite present in the hydrothermally altered mudstone host of the Eskay Creek deposit revealed the presence of tens to hundreds of ppm of Tl (Ritts, 2012). Thallium incorporation into pyrite has also been suggested as the primary reason for the enrichment of this element in ores from the Hokuroku district (Murao and Itoh, 1992) and the Mount Chalmers deposit in Queensland (Huston et al., 1995). At Kidd Creek, the highest Tl concentrations are recorded in massive pyrite and pyrite stringers (Hannington et al., 1999b). Ore samples from this deposit have an average Tl content of 10 ppm (Hannington et al., 1999c). In fossil black smoker chimneys from the Silurian Yaman-Kasy deposit in the Urals, high Tl values occur in the outer portions of the chimneys that are enriched in colloform pyrite (Maslennikov et al., 2009).

In many VMS deposits, the ore lenses are surrounded by pronounced low-temperature alteration halos, showing a distinct Tl enrichment (Möller et al., 1983; Smith and Huston, 1992; Large et al., 2001b). Based on the analysis of mineral separates, Smith and Huston (1992) suggested that approximately 95% of the Tl enrichment in the alteration halo surrounding the Rosebery deposit in Tasmania is related to the incorporation of this element into secondary white mica, while about 5% of the whole-rock Tl content can be accounted for by the presence of sulfide minerals such as pyrite.

Effects of metamorphic recrystallization and remobilization

Despite of the general mineralogical similarities between VMS and sea-floor massive sulfide deposits, there are a number of notable differences in the mineralogical sequestration of the minor elements, including the number and abundance of minor element minerals recognized in both deposit types. Differences in the mineralogical sequestration may, at least in part, be related to the fact that most ancient massive sulfide deposits have been affected by extensive deformation associated with basin inversion and orogenesis as well as metamorphic recrystallization and remobilization at greenschist facies and higher metamorphic grades. These processes have a major impact on the mineralogical distribution of the minor elements as impurities originally contained in the major ore minerals are expelled from the crystal structure during recrystallization to form new accessory minerals. Strain-induced textural changes and metamorphic recrystallization and remobilization are reflected in the nearly stoichiometric compositions of the major ore minerals (pyrite, pyrrhotite, chalcopyrite, sphalerite, and galena), which are nearly devoid of trace elements in the majority of metamorphosed VMS deposits, as well as the abundance of minor and trace sulfosalts and other minerals that occur at the margins of the recrystallized grains, at triple junction contacts, or in late remobilization veins (Marshall and Gilligan, 1987, 1993; Vokes and Craig, 1993; Huston et al., 1995; Wagner and Jonsson, 2001, Wagner et al., 2005; Tomkins, 2007).

Concluding Remarks

Since the first discovery of black smokers on the mid-ocean ridges over 35 years ago, remarkable advances have been made in the understanding of sea-floor hydrothermal systems and associated sea-floor massive sulfide deposits. The data available today indicate that modern sea-floor hydrothermal systems exhibit significant diversity. The geodynamic setting represents a first-order control on the physical and chemical properties of sea-floor massive sulfide deposits. The data discussed in the present review suggest that the minor element content and mineralogical sequestration of these elements in sea-floor massive sulfide deposits differs systematically for sulfide accumulations formed in different tectonic environments, while the temperature of sulfide formation dictates the enrichment and distribution of the minor elements at the deposit scale.

Although sea-floor massive sulfide deposits are widely regarded to be close analogues of VMS deposits located in

ancient volcanic successions, important differences exist between modern and ancient sea-floor hydrothermal systems. Sea-floor massive sulfide deposits on the modern sea floor represent massive sulfide accumulations that have formed in recent times and most deposits are typified by ongoing hydrothermal activity. Massive sulfide lenses forming through subseafloor replacement or deposits that have been covered by younger volcanic or sedimentary rocks are inherently difficult to find on the modern sea floor with current sea-floor exploration methodologies. The size and tonnage characteristics of the presently known sea-floor sulfide accumulations deviate significantly from their fossil analogues. A large percentage of the total tonnage of VMS deposits is contained in a small number of high tonnage deposits. These deposits are thought to largely represent the product of subseafloor replacement processes of the volcanic host rocks. This contrasts with the known distribution of sea-floor massive sulfide deposits on the modern sea floor, which are mostly low tonnage. Many of the sea-floor massive sulfide deposits, in particular those at mid-ocean ridges or on arc volcanoes, are formed in environments that have a low geologic preservation potential and are for this reason not, or not likely, represented in the ancient rock record.

Modern sea-floor sulfide accumulations possess fundamentally different geometallurgical properties compared to most of their fossil analogues. Although massive sulfides are formed in response to rapid quenching of hydrothermal solutions at, or immediately below the sea floor, sea-floor massive sulfide deposits are pristine and have not been affected by deformation occurring during basin inversion and orogenesis as well as metamorphic recrystallization and remobilization. Deformation and metamorphism of the ores in ancient deposits are important processes causing grain coarsening and the redistribution of trace elements on a local to deposit scale. Trace elements originally contained in the main sulfide minerals are expelled during recrystallization to form new accessory phases or late remobilization veins. As a consequence, the mineralogical sequestration of trace elements, including the minor elements discussed in the present contribution, varies as a function of the degree of postdepositional recrystallization of the massive sulfide ores.

Based on the currently available data, a first assessment of the global minor element inventory of sea-floor massive sulfide deposits is attempted in the present contribution. Although grade and tonnage information for sea-floor massive sulfide deposits are far from being reliable, the compiled data set provides an answer to the question whether sea-floor sulfides in the world's oceans represent a significant or strategic future source of minor elements for modern technology-based society. The first-order approximation of the present study suggests that the endowment of these elements in sea-floor massive sulfide deposits is limited when compared to land-based mineral resources. Although some of the elements represent valuable commodities, the minor elements will not likely become economic drivers for deep-sea mining of sea-floor massive sulfide deposits in the foreseeable future. The feasibility of deep-sea mining operations exploiting sea-floor massive sulfide deposits in an economically competitive climate will depend on the base and precious metal content of the sea-floor resources, not their minor element content. However, once deep-sea mining operations exploit sea-floor massive sulfide deposits, some of the minor elements could be recovered as co- or by-products from sulfide concentrates using technology already in use at smelter and refinery plants.

The review of the present study demonstrates that many questions remain. Of these, the probably most important to the understanding of sea-floor hydrothermal processes is whether direct magmatic degassing of deep intrusions contributes metals to hydrothermal systems forming sea-floor massive sulfide deposits, potentially accounting for the enrichment of certain minor elements in massive sulfides. Developing predictive guidelines for these processes has significant implications for exploration, both in modern and ancient volcanic terranes. Future geometallurgical research should focus on a quantitative evaluation of how the minor elements are distributed among the main ore minerals and accessory phases contained in massive sulfides and how this distribution is changed by deformation and metamorphic recrystallization in ancient deposits. Quantitative understanding of the mineralogical sequestration of the minor elements in modern and ancient deposits is key to economic recovery of these commodities from massive sulfide ores.

Acknowledgments

This contribution is based on the available literature and data gathered by the authors on samples recovered during numerous research cruises, many of which have been led by P.M. Herzig and P. Stoffers. We are indebted to I. Jonasson who helped us collect and analyze hundreds of modern sea-floor sulfides samples over the past decades. This manuscript benefited from initial discussions with R. Goldfarb, M. Hitzman, D. Sinclair, and P. Verplanck. We acknowledge reviews by J. Franklin and D. Huston that helped to improve an earlier version of the manuscript.

REFERENCES

Adamides, N.G., 1987, Diverse modes of occurrence of Cyprus sulphide deposits and comparison with recent analogues: Geological Survey of Canada Paper 85-29, p. 153–168.

Agnew, M.W., Large, R.R., and Bull, S.W., 2005, Lewis Ponds, a hybrid carbonate and volcanic-hosted polymetallic massive sulphide deposit, New South Wales, Australia: Mineralium Deposita, v. 39, p. 822–844.

Allen, R.L., Lundström, I., Ripa, M., Simeonov, A., and Christofferson, H., 1996a, Facies analysis of a 1.9 Ga, continental margin, back-arc, felsic caldera province with diverse Zn-Pb-Ag-(Cu-Au) sulfide and Fe oxide deposits, Bergslagen region, Sweden: Economic Geology, v. 91, p. 979–1,008.

Allen, R.L., Weihed, P., and Svenson, S.Å., 1996b, Setting of Zn-Cu-Au-Ag massive sulfide deposits in the evolution and facies architecture of a 1.9 Ga marine volcanic arc, Skellefte district, Sweden: Economic Geology, v. 91, p. 1,022–1,053.

Allen, R.L., Weihed, P., Blundell, D., Crawford, T., Davidson, G., Galley, A., Gibson, H., Hannington, M., Herrington, R., Herzig, P., Large, R., Lentz, D., Maslennikov, V., McCutcheon, S., Peter, J., and Tornos, F., 2002, Global comparisons of volcanic-associated massive sulphide districts: Geological Society, London, Special Publication, v. 204, p. 13–37.

Almodóvar, G.R., Sáez, R., Pons, J.M., Maestre, A., Toscano, M., and Pascual, E., 1998, Geology and genesis of the Aznalcóllar massive sulphide deposits, Iberian Pyrite Belt, Spain: Mineralium Deposita, v. 33, p. 111–136.

Alt, J.C., 1988, The chemistry and sulfur isotope composition of massive sulfide and associated deposits on Green Seamount, eastern Pacific: Economic Geology, v. 83, p. 1,026–1,033.

Alt, J.C., Lonsdale, P., Haymon, R., and Muehlenbachs, K., 1987, Hydrothermal sulfide and oxide deposits on seamounts near 21°N, East Pacific Rise: Geological Society of America Bulletin, v. 98, p. 157–168.

Ames, D.E., Franklin, J.M., and Hannington, M.D., 1993, Mineralogy and geochemistry of active and inactive chimneys and massive sulfide, Middle

Valley, northern Juan de Fuca Ridge: An evolving hydrothermal system: Canadian Mineralogist, v. 31, p. 997–1,024.
Andersen, C., Rüpke, L., Hasenclever, J., Grevemeyer, I., and Petersen, S., 2015, Fault geometry and permeability contrast control vent temperatures at the Logatchev 1 hydrothermal field, Mid-Atlantic Ridge: Geology, v. 43, p. 51–54.
Aoki, M., and Nakamura, K., 1989, The occurrence of chimneys in Izena Hole No. 2 ore body and texture and mineral composition of the sulfide chimneys: Proceedings of JAMSTEC Symposium on Deep Sea Research, v. 5, p. 197–210.
Appel, P.W.U., 1979, Stratabound copper sulfides in a banded iron-formation and in basaltic tuffs in the Early Precambrian Isua supracrustal belt, West Greenland: Economic Geology, v. 74, p. 45–52.
Arevalo, R., Jr., and McDonough, W.F., 2010, Chemical variations and regional diversity observed in MORB: Chemical Geology, v. 271, p. 70–85.
Ashley, P.M., Dudley, R.J., Lesh, R.H., Marr, J.M., and Ryall, A.W., 1988, The Scuddles Cu-Zn prospect, and Archean volcanogenic massive sulfide deposit, Golden Grove district, Western Australia: Economic Geology, v. 83, p. 918–951.
Auclair, G., Fouquet, Y., and Bohn, M., 1987, Distribution of selenium in high-temperature hydrothermal sulfide deposits at 13°North, East Pacific Rise: Canadian Mineralogist, v. 25, p. 577–587.
Auzende, J.M., Urabe, T., Deplus, C., Eissen, J.P., Grimaud, D., Huchon, P., Ishibashi, J., Joshima, M., Lagabrielle, Y., Mével, C., Naka, J., Ruellan, E., Tanaka, T., and Tanahashi, M., 1989, Le cadre géologique d'un site hydrothermal actif: La campagne STARMER 1 du submersible Nautile dans le Bassin Nord-Fidjien: Comptes Rendues de l'Académie des Sciences, Série II, Mécanique, Physique, Chimie, Sciences de l'Univers, Sciences de la Terre, v. 309, p. 1,787–1,795.
Auzende, J.M., Ballu, V., Batiza, R., Bideau, D., Cormier, M.H., Fouquet, Y., Geistdoerfer, P., Lagabrielle, Y., Sinton, J., and Spadea, P., 1994, Activité magmatique, tectonique et hydrothermale actuelle sur la Dorsale Est Pacifique entre 17° et 19°S (campagne NAUDUR): Comptes Rendues de l'Académie des Sciences, Série II, Mécanique, Physique, Chimie, Sciences de l'Univers, Sciences de la Terre, v. 319, p. 811–818.
Auzende, J.M., Urabe, T., Binns, R., Charlou, J.L., Gena, K., Gamo, T., Henry, K., Matsubayashi, O., Matsumoto, T., Moss, R., Naka, J., Nagaya, Y., Okamura, K., and Ruellan, E., 1996a, Activité tectonique, magmatique et hydrothermale dans le bassin de Manus (SW Pacifique, Papouasie-Nouvelle Guinée): Campagne MANUSFLUX du Shinkai-6500: Comptes Rendues de l'Académie des Sciences, Série II, Mécanique, Physique, Chimie, Sciences de l'Univers, Sciences de la Terre, v. 323, p. 501–508.
Auzende, J.M., Ballu, V., Batiza, R., Bideau, D., Charlou, J.L., Cormier, M.H., Fouquet, Y., Geistdoerfer, P., Lagabrielle, Y., Sinton, J., and Spadea, P., 1996b, Recent tectonic, magmatic, and hydrothermal activity on the East Pacific Rise between 17°S and 19°S: Submersible observations: Journal of Geophysical Research, v. 101, p. 17,995–18,010.
Bach, W., Banerjee, N.R., Dick, H.J.B., and Baker, E.T., 2002, Discovery of ancient and active hydrothermal systems along the ultra-slow spreading Southwest Indian Ridge 10°–16°E: Geochemistry Geophysics Geosystems, v. 3, doi: 10.1029/2001GC000279.
Bach, W., Dubilier, N., Borowski, C., Breuer, C., Brunner, B., Franke, P., Herschelmann, O., Hourdez, S., Jonda, L., Jöns, N., Klar, S., Koloa, K., Mai, A., Meyerdierks, A., Müller, I., Petersen, S., Pjevac, P., Ratmeyer, V., Reeves, E., Rehage, R., Reuter, C., Schaen, A., Shu, L., Thal, J., and Zarrouk, M., 2011, Cruise report R/V Sonne cruise SO 216: Back-arc Manus basin underwater Solfataras (BAMBUS), Townsville, Australia, June 14, 2011 – Makassar, Indonesia, July 23, 2011: Berichte aus dem Fachbereich Geowissenschaften der Universität Bremen, v. 280, 86 p.
Bäcker, H., Lange, J., and Marchig, V., 1985, Hydrothermal activity and sulphide formation in axial valleys of the East Pacific Rise crest between 18 and 22°S: Earth and Planetary Science Letters, v. 72, p. 9–22.
Baker, E.T., and German, C.R., 2004, On the global distribution of hydrothermal vent fields: Geophysical Monograph Series, v. 148, p. 245–266.
Baker, E.T., Edmonds, H.N., Michael, P.J., Bach, W., Dick, H.J.B., Snow, J.E., Walker, S.L., Banerjee, N.R., and Langmuir, C.H., 2004, Hydrothermal venting in magma deserts: The ultraslow-spreading Gakkel and Southwest Indian Ridges: Geochemistry Geophysics Geosystems, v. 5, doi: 10.1029/2004GC000712.
Ballard, R.D., Uchupi, E., Blackman, D.K., Cheminee, J.L., Francheteau, J., Hékinian, R., Schwab, W.C., and Sigurdsson, H., 1988, Geological mapping of the East Pacific Rise axis (10°19'-11°53'N) using the Argo and Angus imaging systems: Canadian Mineralogist, v. 26, p. 467–486.
Barley, M.E., 1992, A review of Archean volcanic-hosted massive sulfide and sulfate mineralization in western Australia: Economic Geology, v. 87, p. 855–872.
Barnes, H.L., and Seward, T.M., 1997, Geothermal systems and mercury deposits, *in* Barnes, H.L., ed., Geochemistry of hydrothermal ore deposits, 3rd ed.: New York, Wiley, p. 699–736.
Baross, J.A., and Hoffman, S.E., 1985, Submarine hydrothermal vents and associated gradient environments as sites for the origin and evolution of life: Origins of Life and Evolution of Biospheres, v. 15, p. 327–345.
Barrie, C.T., and Hannington, M.D., 1999, Classification of volcanic-associated massive sulfide deposits based on host-rock composition: Reviews in Economic Geology, v. 8, p. 1–11.
Barrie, C.T., and Krogh, T.E., 1996, U-Pb zircon geochronology of the Selbaie Cu-Zn-Ag-Au mine, Abitibi subprovince, Canada: Economic Geology, v. 91, p. 563–575.
Barrie, C.T., Taylor, C., and Ames, D.E., 2005, Geology and metal contents of the Ruttan volcanogenic massive sulfide deposit, northern Manitoba, Canada: Mineralium Deposita, v. 39, p. 795–812.
Barrie, C.T., Nielsen, F.W., and Aussant, C.H., 2007, The Bisha volcanic-associated massive sulfide deposit, western Nakfa terrane, Eritrea: Economic Geology, v. 102, p. 717–738.
Bazarkina, E.F., Pokrovski, G.S., Zotov, A.V., and Hazemann, J.L., 2010, Structure and stability of cadmium chloride complexes in hydrothermal fluids: Chemical Geology, v. 276, p. 1–17.
Beaulieu, S.E., Baker, E.T., German, C.R., and Maffei, A., 2013, An authoritative global database for active submarine hydrothermal vent fields: Geochemistry Geophysics Geosystems, v. 14, p. 4,892–4,905, doi: 10.1002/2013GC004998.
Belogub, E.V., Novoselov, C.A., Spiro, B., and Yakovleva, B.A., 2003, Mineralogical and S isotopic features of the supergene profile of the Zapadno-Ozernoe massive sulphide and Au-bearing gossan deposit, South Urals: Mineralogical Magazine, v. 67, p. 339–354.
Belogub, E.V., Novoselov, K.A., Yakovleva, V.A., and Spiro, B., 2008, Supergene sulphides and related minerals in the supergene profiles of VHMS deposits from the South Urals: Ore Geology Reviews, v. 33, p. 239–254.
Beltenev, V., Shagin, A., Markov, V., Rozhdestvenskaya, I., Stepanova, T., Cherkashev, G., Fedorov, I., Rumyantsev, A., and Poroshina, I., 2004, A new hydrothermal field at 16°38.4'N, 46°28.5'W on the Mid-Atlantic Ridge: InterRidge News, v. 13, p. 5–6.
Beltenev, V., Ivanov, V., Shagin, A., Sergeyev, M., Rozhdestvenskaya, I., Shilov, V., Dobretzova, I., Cherkashev, G., Samovarov, M., and Poroshina, I., 2005, New hydrothermal sites at 13°N, Mid Atlantic Ridge: InterRidge News, v. 14, p. 14–16.
Beltenev, V., Ivanov, V., Rozhdestvenskaya, I., Cherkashov, G., Stepanova, T., Shilov, V., Pertsev, A., Davydov, M., Egorov, I., Melekestseva, I., Narkevsky, E., and Ignatov, V., 2007, A new hydrothermal field at 13°30'N on the Mid-Atlantic Ridge: InterRidge News, v. 16, p. 9–10.
Beltenev, V., Ivanov, V., Rozhdestvenskaya, I., Cherkashov, G., Stepanova, T., Shilov, V., Davydov, M., Laiba, A., Kaylio, V., Narkevsky, E., Pertsev, A., Dobretzova, I., Gustaytis, A., Popova, Y., Amplieva, Y., Evrard, C., Moskalev, L., and Gebruk, A., 2009, New data about hydrothermal fields on the Mid-Atlantic Ridge between 11°-14°N: 32nd cruise of R/V Professor Logatchev: InterRidge News, v. 18, p. 13–17.
Bendel, V., Fouquet, Y., Auzende, J.M., Lagabrielle, Y., Grimaud, D., and Urabe, T., 1993, The White Lady hydrothermal field, North Fiji back-arc basin, southwest Pacific: Economic Geology, v. 88, p. 2,237–2,249.
Benninger, L.M., and Koski, R.A., 1987, Descriptions and chemical analyses of sulfide samples dredged in 1986 from Escanaba trough, southern Gorda Ridge: U.S. Geological Survey Open-File Report 87-375-B, 26 p.
Bente, K., and Doering, T., 1995, Experimental studies on the solid state diffusion of Cu + In in ZnS and on "disease," DIS (diffusion induced segregations), in sphalerite and their geological applications: Mineralogy and Petrology, v. 53, p. 285–305.
Benzaazoua, M., Marion, P., Pinto, A., Migeon, H., and Wagner, F.E., 2003, Tin and indium mineralogy within selected samples from the Neves Corvo ore deposit (Portugal): A multidisciplinary study: Minerals Engineering, v. 16, p. 1,291–1,302.
Bergman Weihed, J., Bergström, U., Billström, K., and Weihed, P., 1996, Geology, tectonic setting, and origin of the Paleoproterozoic Boliden Au-Cu-As deposit, Skellefte district, northern Sweden: Economic Geology, v. 91, p. 1,073–1,097.
Berkenbosch, H.A., de Ronde, C.E.J., Gemmell, J.B., McNeill, A.W., and Goemann, K., 2012, Mineralogy and formation of black smoker chimneys

from Brothers submarine volcano, Kermadec arc: Economic Geology, v. 107, p. 1,613–1,633.
Berry, R.F., Huston, D.L., Stolz, A.J., Hill, A.P., Beams, S.D., Kuronen, U., and Taube, A., 1992, Stratigraphy, structure, and volcanic-hosted mineralization of the Mount Windsor subprovince, North Queensland, Australia: Economic Geology, v. 87, p. 739–763.
Bertine, K.K., and Keene, J.B., 1975, Submarine barite-opal rocks of hydrothermal origin: Science, v. 188, p. 150–152.
Binns, R.A., 2004, Eastern Manus basin, Papua New Guinea: Guides for volcanogenic massive sulphide exploration from a modern seafloor analogue, *in* McConachy, T.F., and McInnes, B.I.A., eds., Copper-zinc massive sulphide deposits in Western Australia: Clayton South, Victoria, Commonwealth Scientific and Industrial Research Organisation, p. 59–80.
——2014, Bikpela: A large siliceous chimney from the Pacmanus hydrothermal field, Manus basin, Papua New Guinea: Economic Geology, v. 109, p. 2,243–2,259.
Binns, R.A., and Scott, S.D., 1993, Actively forming polymetallic sulfide deposits associated with felsic volcanic rocks in the eastern Manus back-arc basin, Papua New Guinea: Economic Geology, v. 88, p. 2,226–2,236.
Binns, R.A., Scott, S.D., Gemmell, J.B., Crook, K.A.W., and Shipboard Scientific Party, 1997, The SuSu knolls hydrothermal field, eastern Manus basin, Papua New Guinea [abs.]: American Geophysical Union Fall Meeting, San Francisco, California, 1997, Supplement to EOS Transaction American Geophysical Union, v. 78, p. V22E-2.
Binns, R.A., Barriga, F.J.A.S., Miller, D.J., Asada, R., Bach, W., Bartetzko, A.C.M., Benning, L.G., Bjerkgård, T., Christiansen, L.B., Elswick, E.R., Findlay, R., Iturrino, G.J., Kimura, H., Kulange, J.B., Lackschewitz, K.S., Lee, S.M., Masta, A., Paulick, H., Pinto, Á.M., Roberts, S., Scott, S.D., Vanko, D.A., Warden, I., and Yeats, C.J., 2002, Leg 193 summary: Proceedings of the Ocean Drilling Program, Initial Reports, v. 193, p. 1–84.
Bird, P., 2003, An updated digital model of plate boundaries: Geochemistry Geophysics Geosystems, v. 4, doi: 10.1029/2001GC000252.
Bischoff, J.L., Rosenbauer, R.J., Aruscavage, P.J., Baedecker, P.A., and Crock, J.G., 1983, Sea-floor massive sulfide deposits from 21°N, East Pacific Rise; Juan de Fuca Ridge; and Galapagos rift: Bulk chemical composition and economic implications: Economic Geology, v. 78, p. 1,711–1,720.
Bobbitt, A., 2007, Cruise report R/V Atlantis cruise AT15-21: Axial Volcano, Endeavour Segment, and Cobb Segment, Juan de Fuca Ridge (NeMO 2007), Astoria, Oregon, August 3, 2007, Astoria, Oregon, August 20, 2007: Newport, Pacific Marine Environmental Laboratory, National Oceanic and Atmospheric Administration, 166 p.
Bodon, S.B., and Valenta, R.K., 1995, Primary and tectonic features of the Currawong Zn-Cu-Pb(-Au) massive sulfide deposit, Benambra, Victoria: Implications for ore genesis: Economic Geology, v. 90, p. 1,694–1,721.
Bogdanov, K., Tsonev, D., and Kuzmanov, K., 1997, Mineralogy of gold in the Elshitsa massive sulphide deposit, Sredna Gora zone, Bulgaria: Mineralium Deposita, v. 32, p. 219–229.
Bogdanov, Y.A., Bortnikov, N.S., Vikent'ev, I.V., Lein, A.Y., Gurvich, E.G., Sagalevich, A.M., Simonov, V.A., Ikorskii, S.V., Stavrova, O.O., and Apollonov, V.N., 2002, Mineralogical-geochemical peculiarities of hydrothermal sulfide ores and fluids in the Rainbow field associated with serpentinites, Mid-Atlantic Ridge (36°14'N): Geology of Ore Deposits, v. 44, p. 444–473.
Bogdanov, Y.A., Lein, A.Y., Maslennikov, V.V., Li, S., and Ul'yanov, A.A., 2008, Mineralogical-geochemical features of sulfide ores from the Broken Spur hydrothermal vent field: Oceanology, v. 48, p. 679–700.
Bohnenstiehl, D.R., Tolstoy, M., Fox, C.G., Dziak, R.P., Chapp, E., Fowler, M., Haxel, J., Fisher, C., Van Hilst, C., Laird, R., Collier, R., Cowen, J., Lilley, M., Simons, K., Carbotte, S.M., Reynolds, J.R., and Langmuir, C.H., 2003, Anomalous seismic activity at 8°37-42'N on the East Pacific Rise: Newsletter of Ridge 2000 Program, v. 1, p. 18–20.
Bohrmann, G., Chin, C., Petersen, S., Sahling, H., Schwarz-Schampera, U., Greinert, J., Lammers, S., Rehder, G., Daehlmann, A., Wallmann, K., Dijkstra, S., and Schenke, H.W., 1999, Hydrothermal activity at Hook Ridge in the central Bransfield basin, Antarctica: Geo-Marine Letters, v. 18, p. 277–284.
Both, R., Crook, K., Taylor, B., Brogan, S., Chappell, B., Frankel, E., Liu, L., Sinton, J., and Tiffin, D., 1986, Hydrothermal chimneys and associated fauna in the Manus back-arc basin, Papua New Guinea: EOS Transaction American Geophysical Union, v. 67, p. 489–490.
Botz, R., Wehner, H., Schmitt, M., Worthington, T.J., Schmidt, M., and Stoffers, P., 2002, Thermogenic hydrocarbons from the offshore Calypso hydrothermal field, Bay of Plenty, New Zealand: Chemical Geology, v. 186, p. 235–248.
Boulegue, J., Perseil, E.A., Bernat, M., Dupré, B., Stouff, P., and Francheteau, J., 1984, A high-temperature hydrothermal deposit on the East Pacific Rise near 7°N: Earth and Planetary Science Letters, v. 70, p. 249–259.
Boulter, C.A., 1993, Comparison of Rio Tinto, Spain, and Guaymas basin, Gulf of California: An explanation of a supergiant massive sulfide deposit in an ancient sill-sediment complex: Geology, v. 21, p. 801–804.
Boyle, D.R., 1995, Geochemistry and genesis of the Murray Brook precious metal gossan deposit, Bathurst mining camp, New Brunswick: Exploration and Mining Geology, v. 4, p. 341–363.
Brauhart, C.W., Huston, D.L., Groves, D.I., Mikucki, E.J., and Gardoll, S.J., 2001, Geochemical mass-transfer patterns as indicators of the architecture of a complete volcanic-hosted massive sulfide hydrothermal alteration system, Panorama district, Pilbara, Western Australia: Economic Geology, v. 96, p. 1,263–1,278.
Brueckner, S.M., Piercey, S.J., Sylvester, P.J., Maloney, S., and Pilgrim, L., 2014, Evidence for syngenetic precious metal enrichment in an Appalachian volcanogenic massive sulfide system: The 1806 zone, Ming mine, Newfoundland, Canada: Economic Geology, v. 109, p. 1,611–1,642.
Butler, I.B., and Nesbitt, R.W., 1999, Trace element distributions in the chalcopyrite wall of a black smoker chimney: Insights from laser ablation inductively coupled plasma mass spectrometry (LA-ICP-MS): Earth and Planetary Science Letters, v. 167, p. 335–345.
Butler, I.B., Fallick, A.E., and Nesbitt, R.W., 1998, Mineralogy, sulphur isotope geochemistry and the development of sulphide structures at the Broken Spur hydrothermal vent site, 29°10'N, Mid-Atlantic Ridge: Journal of the Geological Society London, v. 155, p. 773–785.
Butterfield, D.A., and Massoth, G.J., 1994, Geochemistry of north Cleft segment vent fluids: Temporal changes in chlorinity and their possible relation to recent volcanism: Journal of Geophysical Research, v. 99, p. 4,951–4,968.
Butterfield, D.A., Massoth, G.J., McDuff, R.E., Lupton, J.E., and Lilley, M.D., 1990, Geochemistry of hydrothermal fluids from Axial Seamount hydrothermal emissions study vent field, Juan de Fuca Ridge: Subseafloor boiling and subsequent fluid-rock interaction: Journal of Geophysical Research, v. 95, p. 12,895–12,921.
Butterfield, D.A., McDuff, R.E., Franklin, J., and Wheat, C.G., 1994, Geochemistry of hydrothermal vent fluids from Middle Valley, Juan de Fuca Ridge: Proceedings of the Ocean Drilling Program, Scientific Results, v. 139, p. 395–410.
Butterfield, D.A., Jonasson, I.R., Massoth, G.J., Feely, R.A., Roe, K.K., Embley, R.E., Holden, J.F., McDuff, R.E., Lilley, M.D., and Delaney, J.R., 1997, Seafloor eruptions and evolution of hydrothermal fluid chemistry: Philosophical Transactions of the Royal Society of London, v. A355, p. 369–386.
Butterfield, D.A., Seyfried, W.E., Jr., and Lilley, M.D., 2003, Composition and evolution of hydrothermal fluids, *in* Halbach, P.E., Tunnicliffe, V., and Hein, J.R., eds., Energy and mass transfer in marine hydrothermal systems: Berlin, Dahlem University Press, p. 123–161.
Butterfield, D.A., Holden, J.F., Shank, T.M., Tunnicliffe, V., Sherrin, J., Herrera, S., Baker, E.T., Lovalvo, D., Makarim, S., Malik, M.A., Wirasantosa, S., and Hammond, S.R., 2010, Video observations by telepresence reveal two types of hydrothermal venting on Kawio Barat seamount [abs.]: American Geophysical Union Fall Meeting, San Francisco, California, 2010, OS13C–1236.
Çağatay, M.N., 1993, Hydrothermal alteration associated with volcanogenic massive sulfide deposits: Examples from Turkey: Economic Geology, v. 88, p. 606–621.
Callaghan, T., 2001, Geology and host-rock alteration of the Henty and Mount Julia gold deposits, western Tasmania: Economic Geology, v. 96, p. 1,073–1,088.
Carvalho, D., Barriga, F.J.A.S., and Munhá, J., 1999, Bimodal siliciclastic systems—the case of the Iberian Pyrite Belt: Reviews in Economic Geology, v. 8, p. 375–408.
Cathles, L.M., 2011a, What processes at mid-ocean ridges tell us about volcanogenic massive sulfide deposits: Mineralium Deposita, v. 46, p. 639–657.
——2011b, Reply to comment by Hannington "Are black smokers copper plating the ocean floor?": Mineralium Deposita, v. 46, p. 665–669.
Charlou, J.L., Fouquet, Y., Donval, J.P., Auzende, J.M., Jean-Baptiste, P., Stievenard, M., and Michel, S., 1996, Mineral and gas chemistry of hydrothermal fluids on an ultrafast spreading ridge: East Pacific Rise, 17° to 19°S (Naudir cruise, 1993) phase separation processes controlled by volcanic and tectonic activity: Journal of Geophysical Research, v. 101, p. 15,899–15,919.
Charlou, J.L., Donval, J.P., Douville, E., Jean-Baptiste, P., Radford-Knoery, J., Fouquet, Y., Dapoigny, A., and Stievenard, M., 2000, Compared geochemical signatures and the evolution of Menez Gwen (37°50'N) and Lucky

Strike (37°17'N) hydrothermal fluids, south of the Azores Triple Junction on the Mid-Atlantic Ridge: Chemical Geology, v. 171, p. 49–75.
Charlou, J.L., Donval, J.P., Konn, C., Ondréas, H., Fouquet, Y., Jean-Baptist, P., and Fourré, E., 2010, High production and fluxes of H_2 and CH_4 and evidence of abiotic hydrocarbon synthesis by serpentinization in ultramafic-hosted hydrothermal systems on the Mid-Atlantic Ridge: Geophysical Monograph Series, v. 188, p. 265–296.
Chen, Y.J., and Li, J., 2013, China national update 2013: InterRidge News, v. 22, p. 4–5.
Cherkashov, G., Poroshina, I., Stepanova, T., Ivanov, V., Beltenev, V., Lazareva, L., Rozhdestvenskaya, I., Samovarov, M., Shilov, V., Glasby, G.P., Fouquet, Y., and Kuznetsov, V., 2010a, Seafloor massive sulfides from the northern equatorial Mid-Atlantic Ridge: New discoveries and perspectives: Marine Georesources and Geotechnology, v. 28, p. 222–239.
Cherkashov, G., Lazareva, L., and Stepanova, T., 2010b, Massive sulfide deposits at Semyenov cluster: Mineralogy, age and evolution [abs.]: Minerals of the Ocean-5 and Deep-Sea Minerals and Mining-2 Joint International Conference, St. Petersburg, Russia, 2010, Abstract Volume, p. 52–57.
Cherkashev, G.A., Ivanov, V.N., Bel'tenev, V.I., Lazareva, L.I., Rozhdestvenskaya, I.I., Samovarov, M.L., Poroshina, I.M., Sergeev, M.B., Stepanova, T.V., Dobretsova, I.G., and Kuznetsov, V.Y., 2013, Massive sulfide ores of the northern equatorial Mid-Atlantic Ridge: Oceanology, v. 53, p. 607–619.
Chiba, H., Sakai, H., Gamo, T., Ishibashi, J., Nakashima, K., Minami, H., and Dobashi, F., 1992, Chemistry and isotopic composition of bubbles emerging from the seafloor at the Minami-Ensei knoll, Okinawa trough: Proceedings of JAMSTEC Symposium on Deep Sea Research, v. 8, p. 81–87.
Chiba, H., Nakashima, K., Gamo, T., Ishibashi, J., Tsunogai, U., and Sakai, H., 1993, Hydrothermal activity at the Minami-Ensei knoll, Okinawa trough: Chemical characteristics of hydrothermal solutions: Proceedings of JAMSTEC Symposium on Deep Sea Research, v. 9, p. 271–282.
Chiba, H., Ishibashi, J., Ueno, H., Oomori, T., Uchiyama, N., Takeda, T., Takamine, C., Ri, J., and Itomitsu, A., 1996, Seafloor hydrothermal systems at the North knoll, Iheya Ridge, Okinawa trough: JAMSTEC Journal of Deep Sea Research, v. 12, p. 211–219.
Collier, J., and Sinha, M., 1990, Seismic images of a magma chamber beneath the Lau basin back-arc spreading center: Nature, v. 346, p. 646–648.
——1992, Seismic mapping of a magma chamber beneath the Valu Fa Ridge, Lau basin: Journal of Geophysical Research, v. 97, p. 14,031–14,053.
Connelly, D.P., Copley, J.T., Murton, B.J., Stansfield, K., Tyler, P.A., German, C.R., Van Dover, C.L., Amon, D., Furlong, M., Grindlay, N., Hayman, N., Hühnerbach, V., Judge, M., Le Bas, T., McPhail, S., Meier, A., Nakamura, K., Nye, V., Pebody, M., Pedersen, R.B., Plouviez, S., Sands, C., Searle, R.C., Stevenson, P., Taws, S., and Wilcox, S., 2012, Hydrothermal vent fields and chemosynthetic biota on the world's deepest seafloor spreading centre: Nature Communications, v. 3, doi: 10.1038/ncomms1636.
Constantinou, G., and Govett, G.J.S., 1973, Geology, geochemistry, and genesis of Cyprus sulfide deposits: Economic Geology, v. 68, p. 843–858.
Cook, N.J., Halls, C., and Kaspersen, P.O., 1990, The geology of the Sultjelma ore field, northern Norway—some new interpretations: Economic Geology, v. 85, p. 1,720–1,737.
Corbett, K.D., 1992, Stratigraphic-volcanic setting of massive sulfide deposits in the Cambrian Mount Read Volcanics, Tasmania: Economic Geology, v. 87, p. 564–586.
Corliss, J.B., Dymond, J., Gordon, L.I., Edmond, J.M., von Herzen, R.P., Ballard, R.D., Green, K., Williams, D., Bainbridge, A., Crane, K., and van Andel, T.H., 1979, Submarine thermal springs on the Galápagos rift: Science, v. 203, p. 1,073–1,083.
Corliss, J.B., Baross, J.A., and Hoffman, S.E., 1981, An hypothesis concerning the relationship between submarine hot springs and the origin of life on Earth: Oceanologica Acta, 1981, p. 59–69.
Craddock, P.R., 2009, Geochemical traces of processes affecting the formation of seafloor hydrothermal fluids and deposits in the Manus back-arc basin: Ph.D. thesis, Cambridge, Massachusetts Institute of Technology, 370 p.
Craddock, P.R., Bach, W., Seewald, J.S., Rouxel, O.J., Reeves, E., and Tivey, M.K., 2010, Rare earth element abundances in hydrothermal fluids from the Manus basin, Papua New Guinea: Indicators of sub-seafloor hydrothermal processes in back-arc basins: Geochimica et Cosmochimica Acta, v. 74, p. 5,494–5,513.
Craig, H., Horibe, Y., Farley, K.A., Welhan, J.A., Kim, K.R., and Hey, R.N., 1987, Hydrothermal vents in the Marina trough: Results of the first Alvin dives [abs.]: American Geophysical Union Fall Meeting, San Francisco, California, 1987, Supplement to EOS Transaction American Geophysical Union, v. 68, p. 1,531.
Davis, E.E., and Villinger, H., 1992, Tectonic and thermal structure of the Middle Valley sedimented rift, northern Juan de Fuca Ridge: Proceedings of the Ocean Drilling Program, Initial Reports, v. 139, p. 9–41.
Davis, E.E., Goodfellow, W.D., Bornhold, B.D., Adshead, J., Blaise, B., Villinger, H., and Le Cheminant, G.M., 1987, Massive sulfides in a sedimented rift valley, northern Juan de Fuca Ridge: Earth and Planetary Science Letters, v. 82, p. 49–61.
Davis, E.E., Mottl, M.J., Fisher, A.T., Baker, P.A., Becker, K., Boni, M., Boulègue, J.J., Brunner, C.A., Duckworth, R.C., Franklin, J.M., Goodfellow, W.D., Gröschel-Becker, H.M., Kinoshita, M., Konyukhov, B.A., Körner, U., Krasnov, S.G., Langseth, M.G., Mao, S., Marchig, V., Marumo, K., Oda, H., Rigsby, C.A., Simoneit, B.R.T., Stakes, D.S., Villinger, H.W., Wheat, C.G., Whelan, J.K., and Zierenberg, R.A., 1992, Site 856: Proceedings of the Ocean Drilling Program, Initial Reports, v. 139, p. 161–281.
Dekov, V.M., and Savelli, C., 2004, Hydrothermal activity in the SE Tyrrhenian Sea: An overview of 30 years of research: Marine Geology, v. 204, p. 161–185.
Dekov, V., Boycheva, T., Hålenius, U., Petersen, S., Billström, K., Stummeyer, J., Kamenov, G., and Shanks, W., 2011, Atacamite and paratacamite from the ultramafic-hosted Logatchev seafloor vent field (14°45'N, Mid-Atlantic Ridge): Chemical Geology, v. 286, p. 169–184.
Delaney, J.R., Robigou, V., McDuff, R.E., and Tivey, M.K., 1992, Geology of a vigorous hydrothermal system on the Endeavour Segment, Juan de Fuca Ridge: Journal of Geophysical Research, v. 97, p. 19,663–19,682.
deMartin, B.J., Sohn, R.A., Pablo Canales, J., and Humphris, S.E., 2007, Kinematics and geometry of active detachment faulting beneath the Trans-Atlantic Geotraverse (TAG) hydrothermal field on the Mid-Atlantic Ridge: Geology, v. 35, p. 711–714.
DeMatties, T.A., 1994, Early Proterozoic volcanogenic massive sulfide deposits in Wisconsin: An overview: Economic Geology, v. 89, p. 1,122–1,151.
DeMets, C., Gordon, R.G., and Argus, D.F., 2010, Geologically current plate motions: Geophysical Journal International, v. 181, p. 1–80.
de Ronde, C.E.J., Baker, E.T., Massoth, G.J., Lupton, J.E., Wright, I.C., Feely, R.A., and Greene, R.R., 2001, Intra-oceanic subduction-related hydrothermal venting, Kermadec volcanic arc, New Zealand: Earth and Planetary Science Letters, v. 193, p. 359–369.
de Ronde, C.E.J., Massoth, G.J., Baker, E.T., and Lupton, J.E., 2003a, Submarine hydrothermal venting related to volcanic arcs: Society of Economic Geologists Special Publication 10, p. 91–110.
de Ronde, C.E.J., Faure, K., Bray, C.J., Chappell, D.A., and Wright, I.C., 2003b, Hydrothermal fluids associated with seafloor mineralization at two southern Kermadec arc volcanoes, offshore New Zealand: Mineralium Deposita, v. 38, p. 217–233.
de Ronde, C.E.J., Hannington, M.D., Stoffers, P., Wright, I.C., Ditchburn, R.G., Reyes, A.G., Baker, E.T., Massoth, G.J., Lupton, J.E., Walker, S.L., Greene, R.R., Soong, C.W.R., Ishibashi, J., Lebon, G.T., Bray, C.J., and Resing, J.A., 2005, Evolution of a submarine magmatic-hydrothermal system: Brothers volcano, southern Kermadec arc, New Zealand: Economic Geology, v. 100, p. 1,097–1,133.
de Ronde, C.E.J., Baker, E.T., Massoth, G.J., Lupton, J.E., Wright, I.C., Sparks, R.J., Bannister, S.C., Reyners, M.E., Walker, S.L., Greene, R.R., Ishibasi, J., Faure, K., Resing, J.A., and Lebon G.T., 2007, Submarine hydrothermal activity along the mid-Kermadec arc, New Zealand: Large-scale effects on venting: Geochemistry Geophysics Geosystems, v. 8, doi: 10.1029/2006GC001495.
de Ronde, C.E.J., Massoth, G.J., Butterfield, D.A., Christenson, B.W., Ishibasi, J., Ditchburn, R.G., Hannington, M.D., Brathwaite, R.L., Lupton, J.E., Kamenetsky, V.S., Graham, I.J., Zellmer, G.F., Dziak, R.P., Embley, R.W., Dekov, V.M., Munnik, F., Lahr, J., Evans, L.J., and Takai, K., 2011, Submarine hydrothermal activity and gold-rich mineralization at Brothers volcano, Kermadec arc, New Zealand: Mineralium Deposita, v. 46, p. 541–584.
de Ronde, C.E.J., Walker, S.L., Ditchburn, R.G., Caratori Tontini, F., Hannington, M.D., Merle, S.G., Timm, C., Handler, M.R., Wysoczanski, R.J., Dekov, V.M., Kamenov, G.D., Baker, E.T., Embley, R.W., Lupton, J.E., and Stoffers, P., 2014, The anatomy of a buried submarine hydrothermal system, Clark volcano, Kermadec arc, New Zealand: Economic Geology, v. 109, p. 2,261–2,292.
Desbruyères, D., 1995, Temporal variations of deep-sea hydrothermal communities at 13°N/EPR: InterRidge News, v. 4, p. 6–10.
Destrigneville, C., Chavagnac, V., Olive, J.A., Leleu, T., Rommevaux, C., Escartin, J., Jamieson, J.W., and Petersen, S., 2015, Thermo-chemical fluxes, reactions and mixing in hydrothermal plumes at oceanic core complexes (Mid-Atlantic Ridge, 13°30'N and 13°20'N) [abs.]: American Geophysical Union Fall Meeting, San Francisco, California, 2015, OS43A-2024.

Detrick, R.S., Honnorez, J., Adamson, A.C., Brass, G., Gillis, K.M., Humphris, S.E., Mevel, C., Meyer, P., Petersen, N., Rautenschlein, M., Shibata, T., Staudigel, H., Yamamoto, K., and Wooldridge, A.L., 1986, Drilling the Snake Pit hydrothermal sulfide deposit on the Mid-Atlantic Ridge, lat 23°22'N: Geology, v. 14, p. 1,004–1,007.

DeWolfe, Y.M., Gibson, H.L., Lafrance, B., and Bailes, A.H., 2009, Volcanic reconstruction of Paleoproterozoic arc volcanoes: The Hidden and Louis formations, Flin Flon, Manitoba, Canada: Canadian Journal of Earth Sciences, v. 46, p. 481–508.

Dill, H.G., Gauert, C., Holler, G., and Marchig, V., 1992, Hydrothermal alteration and mineralisation of basalts from the spreading zone of the East Pacific Rise (7°S-23°S): Geologische Rundschau, v. 81, p. 717–728.

Douville, E., Charlou, J.L., Donval, J.P., Knoery, J., Fouquet, Y., Bienvenu, P., and Appriou, P., 1997, Trace elements in fluids from the new Rainbow hydrothermal field (36°14 N, MAR): A comparison with other Mid-Atlantic Ridge fluids [abs.]: American Geophysical Union Fall Meeting, San Francisco, California, 1997, V51E-7.

Douville, E., Charlou, J.L., Oelkers, E.H., Bienvenu, P., Jove Colon, C.F., Donval, J.P., Fouquet, Y., Prieur, D., and Appriou, P., 2002, The Rainbow vent fluids (36°14'N, MAR): The influence of ultramafic rocks and phase separation on trace metal content in Mid-Atlantic Ridge hydrothermal fluids: Chemical Geology, v. 184, p. 37–48.

Doyle, M.G., and Allen, R.L., 2003, Subsea-floor replacement in volcanic-hosted massive sulfide deposits: Ore Geology Reviews, v. 23, p. 183–222.

Dubé, B., Mercier-Langevin, P., Kjarsgaard, I., Hannington, M., Bécu, V., Côte, J., Moorhead, J., Legault, M., and Bédard, N., 2014, The Bousquet 2-Dumagami world-class Archean Au-rich volcanogenic massive sulfide deposit, Abitibi, Quebec: Metamorphosed submarine advanced argillic alteration footprint and genesis: Economic Geology, v. 109, p. 121–166.

Dubilier, N., Borowski, C., Büttner, H., Colaço, Contreira, L., dos Santos Ferreira, C., Fink, D., Franke, P., Hach, P., Hentscher, M., Hourdez, S., Köhler, J., Lartaud, F., LeBris, N., Lino, S., Lott, C., Mai, A.H., Marcon, Y., Meyerdierks, A., Petersen, S., Prieto Mollar, X., Ratmeyer, V., Reevers, E., Rehage, R., Reuter, M., Reuter, C., Schulz, H., Truscheit, T., Vidoudez, C., Wilkop, T., Winkel, M., Zabel, M., and Zarrouk, M., 2015, Cruise report R/V Meteor cruise M82/3: Interdisciplinary geological, chemical and biological studies at the Menez Gwen hydrothermal vent field, Mid-Atlantic Ridge at 37°50'N, Ponta Delgada, Portugal, September 6, 2010, Las Palmas, Spain, October 11, 2010: Bremen, Germany, DFG-Senatskommision für Ozeanographie am Zentrum für Marine Umweltwissenschaften, Universität Bremen, 342 p.

Duckworth, R.C., Knott, R., Fallick, A.E., Rickard, D., Murton, B.J., and Van Dover, C., 1995, Mineralogy and sulphur isotope geochemistry of the Broken Spur sulphides, 29°N, Mid-Atlantic Ridge: Geological Society, London, Special Publication 87, p. 175–189.

Dyment, J., Bissessur, D., Bucas, K., Cueff-Gauchard, V., Durand, L., Fouquet, Y., Gaill, F., Gente, P., Hoisé, E., Ildefonse, B., Konn, C., Lartaud, F., LeBris, N., Musset, G., Nunes, A., Renard, J., Riou, V., Tasiemski, A., Thibaud, R., Torres, P., Yatheesh, V., Vodjdani, I., and Zbinden, M., 2009, Detailed investigation of hydrothermal site Rainbow, Mid-Atlantic Ridge, 36°13'N: Cruise MoMARDream: InterRidge News, v. 18, p. 22–24.

Edmonds, H.N., German, C.R., Green, D.R.H., Huh, Y., Gamo, T., and Edmond, J.M., 1996, Continuation of the hydrothermal fluid chemistry time series at TAG, and the effects of ODP drilling: Geophysical Research Letters, v. 23, p. 3,487–3,489.

Edmonds, H.N., Michael, P.J., Baker, E.T., Connelly, D.P., Snow, J.E., Langmuir, C.H., Dick, H.J.B., Mühe, R., German, C.R., and Graham, D.W., 2003, Discovery of abundant hydrothermal venting on the ultraslow-spreading Gakkel Ridge in the Arctic Ocean: Nature, v. 421, p. 252–256.

Eickmann, B., Thorseth, I.H., Peters, M., Strauss, H., Bröcker, M., and Pedersen, R.B., 2014, Barite in hydrothermal environments as a recorder of subseafloor processes: A multiple-isotope study from the Loki's Castle vent field: Geobiology, v. 12, p. 308–321.

Einsele, G., 1985, Basaltic sill-sediment complexes in young spreading centers: Genesis and significance: Geology, v. 13, p. 249–252.

Eldridge, C.S., Barton, P.B., Jr., and Ohmoto, H., 1983, Mineral textures and their bearing on formation of the Kuroko orebodies: Economic Geology Monograph 5, p. 241–281.

Embley, R.W., Jonasson, I.R., Perfit, M.R., Franklin, J.M., Tivey, M.A., Malahoff, A., Smith, M.F., and Francis, T.J.G., 1988, Submersible investigation of an extinct hydrothermal system on the Galapagos Ridge: Sulfide mounds, stockwork zone, and differentiated lavas: Canadian Mineralogist, v. 26, p. 517–539.

Embley, R.W., Chadwick, W.W., Perfit, M.R., Smith, M.C., and Delaney, J.R., 2000, Recent eruptions on the CoAxial segment of the Juan de Fuca Ridge: Implications for mid-ocean ridge accretion processes: Journal of Geophysical Research, v. 105, p. 16,501–16,525.

Embley, R.W., Baker, E.T., Chadwick, W.W., Jr., Lupton, J.E., Resing, J.A., Massoth, G.L., and Nakamura, K., 2004, Explorations of Mariana arc volcanoes reveal new hydrothermal systems: EOS Transaction American Geophysical Union, v. 85, p. 37 and 44.

Eremin, N.I., Sergeeva, N.E., and Dergachev, A.L., 2007, Rare minerals from massive sulfide ores: Typomorphic features and geochemical trend: Moscow University Geology Bulletin, v. 62, p. 98–106.

Ewers, G.R., and Keays, R.R., 1977, Volatile and precious metal zoning in the Broadlands geothermal field, New Zealand: Economic Geology, v. 72, p. 1,337–1,354.

Fedorov, D.T., 1993, Massive sulfide-polymetallic deposits of the Kamyshin ore field, eastern Kazakhstan: International Geology Review, v. 35, p. 758–774.

Ferrini, V.L., Tivey, M.K., Carbotte, S.M., Martinez, F., and Roman, C., 2008, Variable morphologic expression of volcanic, tectonic, and hydrothermal processes at six hydrothermal vent fields in the Lau back-arc basin: Geochemistry Geophysics Geosystems, v. 9, doi: 10.1029/2008GC002047.

Flores, G.E., Shakya, M., Meneghin, J., Yang, Z.K., Seewald, J.S., Wheat, C.G., Podar, M., and Reysenbach, A.L., 2012, Inter-field variability in the microbial communities of hydrothermal vent deposits from a back-arc basin: Geobiology, v. 10, p. 333–346.

Fouquet, Y., 1997, Where are the large hydrothermal sulphide deposits in the oceans?: Philosophical Transactions of the Royal Society of London, v. A355, p. 427–441.

Fouquet, Y., Auclair, G., Cambon, P., and Etoubleau, J., 1988, Geological setting and mineralogical and geochemical investigations on sulfide deposits near 13°N on the East Pacific Rise: Marine Geology, v. 84, p. 145–178.

Fouquet, Y., von Stackelberg, U., Charlou, J.L., Donval, J.P., Erzinger, J., Foucher, J.P., Herzig, P., Mühe, R., Soakai, S., Wiedicke, M., and Whitechurch, H., 1991a, Hydrothermal activity and metallogenesis in the Lau back-arc basin: Nature, v. 349, p. 778–781.

Fouquet, Y., von Stackelberg, U., Charlou, J.L., Donval, J.P., Foucher, J.P., Erzinger, J., Herzig, P., Mühe, R., Wiedicke, M., Soakai, S., and Whitechurch, H., 1991b, Hydrothermal activity in the Lau back-arc basin: Sulfides and water chemistry: Geology, v. 19, p. 302–306.

Fouquet, Y., von Stackelberg, U., Charlou, J.L., Erzinger, J., Herzig, P.M., Mühe, R., and Wiedicke, M., 1993a, Metallogenesis in back-arc environments: The Lau basin example: Economic Geology, v. 88, p. 2,154–2,181.

Fouquet, Y., Wafik, A., Cambon, P., Mevel., C., Meyer, G., and Gente, P., 1993b, Tectonic setting and mineralogical and geochemical zonation in the Snake Pit sulfide deposit (Mid-Atlantic Ridge at 23°N): Economic Geology, v. 88, p. 2,018–2,036.

Fouquet, Y., Zierenberg, R.A., Miller, D.J., Bahr, J.M., Baker, P.A., Bjerkgården, T., Brunner, C.A., Duckworth, R.C., Gable, R., Gieskes, J., Goodfellow, W.D., Gröschel-Becker, H.M., Guèrin, G., Ishibashi, J., Iturrino, G., James, R.H., Lackschewitz, K.S., Marquez, L.L., Nehlig, P., Peter, J.M., Rigsby, C.A., Schultheiss, P., Shanks, W.C., III, Simoneit, B.R.T., Summit, M., Teagle, D.A.H., Urbat, M., and Zuffa, G.G., 1998, Investigation of hydrothermal circulation and genesis of massive sulfide deposits at sediment-covered spreading centers at Middle Valley and Escanaba trough: Proceedings of the Ocean Drilling Program, Initial Reports, v. 169, p. 7–16.

Fouquet, Y., Cherkashov, G., Charlou, J.L., Ondréas, H., Birot, D., Cannat, M., Bortnikov, N., Silantyev, S., Sudarikov, S., Cambon-Bonavita, M.A., Desbruyères, D., Fabri, M.C., Querellou, J., Hourdez, S., Gebruk, A., Sokolova, T., Hoisé, E., Mercier, E., Kohn, C., Donval, J.P., Etoubleau, J., Normand, A., Stephan, M., Briand, P., Crozon, J., Fernagu, P., and Buffier, E., 2008, Serpentine cruise—ultramafic hosted hydrothermal deposits on the Mid-Atlantic Ridge: First submersible studies on Ashadze 1 and 2, Logatchev 2 and Krasnov vent fields: InterRidge News, v. 17, p. 15–19.

Fouquet, Y., Cambon, P., Etoubleau, J., Charlou, J.L., Ondréas, H., Barriga, F.J.A.S., Cherkashov, G., Semkova, T., Poroshina, I., Bohn, M., Donval, J.P., Henry, K., Murphy, P., and Rouxel, O., 2010, Geodiversity of hydrothermal processes along the Mid-Atlantic Ridge and ultramafic-hosted mineralization: A new type of oceanic Cu-Zn-Co-Au volcanogenic massive sulfide deposit: Geophysical Monograph Series, v. 188, p. 321–367.

Francheteau, J., and Ballard, R.D., 1983, The East Pacific Rise near 21°N, 13°N and 20°S: Inferences for along-strike variability of axial processes of the mid-ocean ridge: Earth and Planetary Science Letters, v. 64, p. 93–116.

Francheteau, J., Needham, H.D., Choukroune, P., Juteau, T., Séguret, M., Ballard, R.D., Fox, P.J., Normark, W., Carranza, A., Cordoba, D., Guerrero, J., Rangin, C., Bougault, H., Cambon, P., and Hekinian, R., 1979, Massive deep-sea sulphide ore deposits discovered on the East Pacific Rise: Nature, v. 277, p. 523–528.

Francheteau, J., Needham, H.D., Choukroune, P., Juteau, T., Séguret, M., Ballard, R.D., Fox, P.J., Normark, W.R., Carranza, A., Cordoba, D., Guerrero, J., and Rangin, C., 1981, First manned submersible dives on the East Pacific Rise at 21°N (Project Rita): General results: Marine Geophysical Researches, v. 4, p. 345–379.

Franklin, J.M., Kasarda, J., and Poulsen, K.H., 1975, Petrology and chemistry of the alteration zone of the Mattabi massive sulfide deposit: Economic Geology, v. 70, p. 63–79.

Franklin, J.M., Gibson, H.L., Jonasson, I.R., and Galley, A.G., 2005, Volcanogenic massive sulfide deposits: Economic Geology 100th Anniversary Volume, p. 523–560.

Frets, D.C., and Balde, R., 1975, Mount Morgan copper-gold deposit: Australasian Institute of Mining and Metallurgy Monograph Series, v. 5, p. 779–785.

Fujikura, K., Fujiwara, Y., Ishibashi, J., Katayama, S., Komatsu, T., Maezawa, Y., Maki, Y., Miyazaki, J., Miyake, H., Okamoto, K., Okoshi, K., Toth, L.G., Tsuchida, S., Yamaguchi, T., Yamanaka, T., Watabe, H., Watanabe, H., Zielinski, S., and Kato, K., 2001, Report on investigation of hydrothermal vent ecosystems by the crewed submersible "Shinkai 2000" on the Dai-Yon (No. 4) Yonaguni knoll and the Hatoma knoll, the Okinawa trough: JAMSTEC Journal of Deep Sea Research, v. 19, p. 141–154.

Fujimoto, H., Cannat, M., Fujioka, K., Gamo, T., German, C., Mével, C., Münch, U., Ohta, S., Oyaizu, M., Parson, L., Searle, R., Sohrin, Y., and Yama-ashi, T., 1999, First submersible investigations of mid-ocean ridges in the Indian Ocean: InterRidge News, v. 8, p. 22–24.

Fujioka, K., Massoth, G., de Ronde, C., Tanaka-Nakano, A., Gendron, J., Kinoshita, M., Nishizawa, A., Okano, O., Paradis, G., Roe, K., Shinohara, M., Shitashima, K., Tsunogai, U., and Ytow, N., 1995, Active hydrothermal systems of a super-fast spreading ridge, southern East Pacific Rise (13°58'S to 18°26'S): InterRidge News, v. 4, p. 7–10.

Fukuba, T., Noguchi, T., and Fujii, T., 2015, The Yoron Hole: The shallowest hydrothermal system in the Okinawa trough, *in* Ishibashi, J., Okino, K., and Sunamura, M., eds., Subseafloor biosphere linked to hydrothermal systems: TAIGA concept: Tokyo, Springer, p. 489–492.

Gablina, I.F., Mozgova, N.N., Borodaev, Y.S., Stepanova, T.V., Cherkashev, G.A., and Il'in, M.I., 2000, Copper sulfide associations in recent oceanic ores of the Logachev hydrothermal field (Mid-Atlantic Ridge, 14°45'N): Geology of Ore Deposits, v. 42, p. 296–316.

Gablina, I.F., Semkova, T.A., Stepanova, T.V., and Gor'kova, N.V., 2006, Diagenetic alterations of copper sulfides in modern ore-bearing sediments of the Logatchev-1 hydrothermal field (Mid-Atlantic Ridge 14°45'N): Lithology and Mineral Resources, v. 41, p. 27–44.

Gablina, I.F., Dmitrenko, O.B., Os'kina, N.S., Khusid, T.A., and Popova, E.A., 2015, Impact of hydrothermal activity on carbonate fossils in bottom sediments of the tropical Atlantic: Oceanology, v. 55, p. 100–111.

Gallant, R.M., and Von Damm, K.L., 2006, Geochemical controls on hydrothermal fluids from the Kairei and Edmond vent fields, 23°-25°S, Central Indian Ridge: Geochemistry Geophysics Geosystems, v. 7, doi: 10.1029/2005GC001067.

Galley, A.G., and Koski, R.A., 1999, Setting and characteristics of ophiolite-hosted volcanogenic massive sulfide deposits: Reviews in Economic Geology, v. 8, p. 221–246.

Gamo, T., Chiba, H., Fryer, P., Ishibashi, J., Ishii, T., Johnson, L.E., Kelly, K., Masuda, H., Ohta, S., Reysenbach, A.L., Rona, P.A., Shibata, T., Tamaoka, J., Tanaka, H., Tsunogai, U., and Yamaguchi, T., 1993, Revisits to the mid-Mariana trough hydrothermal site and discovery of new venting in the southern Mariana region by the Japanese submersible Shinkai 6500: InterRidge News, v. 2, p. 11–14.

Gamo, T., Okamura, K., Kodama, Y., Charlou, J.L., Urabe, T., Auzende, J.M., Shipboard Scientific Party, and Ishibashi, J., 1996, Chemical characteristics of hydrothermal fluids from the Manus back-arc basin, Papua New Guinea, I. Major chemical components [abs.]: Western Pacific Geophysics Meeting, Brisbane, Australia, 1996, Supplement to EOS Transactions of the American Geophysical Union, v. 77, T32A-5.

Gaspar, O.C., 2002, Mineralogy and sulfide mineral chemistry of the Neves-Corvo ores, Portugal: Insight into their genesis: Canadian Mineralogist, v. 40, p. 611–636.

Gena, K., Kase, K., Chiba, H., and Nakashima, K., 2005, Tin-bearing chalcopyrite and platinum-bearing bismuthinite in the active Tiger sulfide chimney, Yonaguni knoll IV seafloor hydrothermal system, Okinawa trough, Japan [abs.]: American Geophysical Union Fall Meeting, San Francisco, California, 2005, V51C-1492.

Gente, P., Agranier, A., Aguillòn-Robles, A., Benoit, M., Deschamps, A., Dyment, J., Hémond, C., Janin, M., Maia, M., Rodrigues-Leon, L., Szitkar, F., Thibaud, R., and Tilot, V., 2010, Cruise PARISUB on EPR 16°N: Magmatism and hydrothermalism over a ridge-hotspot interaction: InterRidge News, v. 19, p. 17–20.

German, C.R., and Von Damm, K.L., 2003, Hydrothermal processes: Treatise on Geochemistry, 1st ed., v. 6, p. 181–222.

Gibson, H.L., and Galley, A.G., 2007, Volcanogenic massive sulphide deposits of the Archean, Noranda district, Quebec: Mineral Deposits Division, Geological Association of Canada, Special Publication 5, p. 533–552.

Gibson, H.L., and Watkinson, D.H., 1990, Volcanogenic massive sulphide deposits of the Noranda cauldron and shield volcano, Quebec: Canadian Institute of Mining and Metallurgy, Special Volume 43, p. 119–132.

Gibson, H.L., Morton, R.L., and Hudak, G.J., 1999, Submarine volcanic processes, deposits, and environments favorable for the location of volcanic-associated massive sulfide deposits: Reviews in Economic Geology, v. 8, p. 13–51.

Gibson, H.L., Kerr, D.J., and Cattalani, S., 2000, The Horne mine: Geology, history, influence on genetic models, and a comparison to the Kidd Creek mine: Exploration and Mining Geology, v. 9, p. 91–111.

Gilgen, S.A., Diamond, L.W., Mercolli, I., Al-Tobi, K., Maidment, D.W., Close, R., and Al-Towaya, A., 2014, Volcanostratigraphic controls on the occurrence of massive sulfide deposits in the Semail Ophiolite, Oman: Economic Geology, v. 109, p. 1,585–1,610.

Glasby, G.P., 2000, Lessons learned from deep-sea mining: Science, v. 289, p. 551–553.

Glasby, G.P., and Notsu, K., 2003, Submarine hydrothermal mineralization in the Okinawa trough, SW of Japan: An overview: Ore Geology Reviews, v. 23, p. 299–339.

Glasby, G.P., Iizasa, K., Yuasa, M., and Usui, A., 2000, Submarine hydrothermal mineralization on the Izu-Bonin arc, south of Japan: An overview: Marine Georesources and Geotechnology, v. 18, p. 141–176.

Glasby, G.P., Iizasa, K., Hannington, M., Kubota, H., and Notsu, K., 2008, Mineralogy and composition of Kuroko deposits from northeastern Honshu and their possible modern analogues from the Izu-Ogasawara (Bonin) arc south of Japan: Implications for mode of formation: Ore Geology Reviews, v. 34, p. 547–560.

Glickson, D.A., Kelley, D.S., and Delaney, J.R., 2007, Geology and hydrothermal evolution of the Mothra hydrothermal field, Endeavour Segment, Juan de Fuca Ridge: Geochemistry Geophysics Geosystems, v. 8, doi: 10.1029/2007GC001588.

Goldfarb, M.S., Converse, D.R., Holland, H.D., and Edmond, J.M., 1983, The genesis of hot spring deposits on the East Pacific Rise, 21°N: Economic Geology Monograph 5, p. 184–197.

Goodfellow, W.D., and McCutcheon, S.R., 2003, Geologic and genetic attributes of volcanic sediment-hosted massive sulfide deposits of the Bathurst mining camp, northern New Brunswick—a synthesis: Economic Geology Monograph 11, p. 245–301.

Graham, U.M., Bluth, G.J., and Ohmoto, H., 1988, Sulfide-sulfate chimneys on the East Pacific Rise, 11° and 13°N latitudes. Part I: Mineralogy and paragenesis: Canadian Mineralogist, v. 26, p. 487–504.

Grammatikopoulos, T.A., and Roth, T., 2002, Mineralogical characterization and Hg deportment in field samples from the polymetallic Eskay Creek deposit, British Columbia, Canada: International Journal of Surface Mining, Reclamation and Environment, v. 16, p. 180–195.

Grant, H.L.J., Layton-Matthews, D., and Peter, J.M., 2015, Distribution and controls on silver mineralization in the Hackett River Main zone, Nunavut, Canada: An Ag- and Pb-enriched Archean volcanogenic massive sulfide deposit: Economic Geology, v. 110, p. 943–982.

Griffin, W.L., Slack, J.F., Ramsden, A.R., Win, T.T., and Ryan, C.G., 1996, Trace elements in tourmalines from massive sulfide deposits and tourmalinites: Geochemical controls and exploration applications: Economic Geology, v. 91, p. 657–675.

Grimaud, D., Ishibashi, J., Lagabrielle, Y., Auzende, J.M., and Urabe, T., 1991, Chemistry of hydrothermal fluids from the 17°S active site on the North Fiji basin Ridge (SW Pacific): Chemical Geology, v. 93, p. 209–218.

Gundlach, H., and Marchig, V., 1986, Cruise report R/V Sonne cruise SO-40: GEOMETEP 4, Callao, Peru, October 20, 1985, Callao, Peru, January 17,

1986: Hannover, Germany, Federal Institute for Geosciences and Natural Resources, 292 p.

Haase, K.M., Petersen, S., Koschinsky, A., Seifert, R., Devey, C.W., Keir, R., Lackschewitz, K.S., Melchert, B., Perner, M., Schmale, O., Süling, J., Dubilier, N., Zielinski, F., Fretzdorff, S., Garbe-Schönberg, D., Westernströer, U., German, C.R., Shank, T.M., Yoerger, D., Giere, O., Kuever, J., Marbler, H., Mawick, J., Mertens, C., Stöber, U., Walter, M., Ostertag-Henning, C., Paulick, H., Peters, M., Strauss, H., Sander, S., Stecher, J., Warmuth, M., and Weber, S., 2007, Young volcanism and related hydrothermal activity at 5°S on the slow-spreading southern Mid-Atlantic Ridge: Geochemistry Geophysics Geosystems, v. 8, doi: 10.1029/2006GC001509.

Haase, K.M., Abegg, F., Abegg, J., Allen, K.M., Anderson, M., Beier, C., Bodendorfer, M., Bühring, B., Brandl, P.A., Cuno, P., Franke, H., Garbe-Schönberg, D., Greß, M., Hannington, M., Haruel, C., Hennke, J., Huusmann, H., Kemner, F., Kleint, C., Kuckuck, J., Nasemann, P., Pieper, M., Rose, J., Schwarz-Schampera, U., and Suck, I., 2013, Cruise report R/V Sonne cruise SO-229: Volcanism, hydrothermal activity and vent biology in the Coriolis troughs, New Hebrides island arc, Townsville, Australia, July 1, 2013, Nouméa, New Caledonia, July 26, 2013: Erlangen, Germany, GeoZentrum Nordbayern, 244 p.

Halanych, K.M., Tieger, M., O'Mullan, G.D., Lutz, R.A., and Vrijenhoek, R.C., 1999, Brief description of biological communities at 7°S on the East Pacific Rise: InterRidge News, v. 8, p. 23–27.

Halbach, P., Nakamura, K., Wahsner, M., Lange, J., Sakai, H., Käselitz, L., Hansen, R.D., Yamano, M., Post, J., Prause, B., Seifert, R., Michaelis, W., Teichmann, F., Kinoshita, M., Märten, A., Ishibashi, J., Czerwinski, S., and Blum, N., 1989, Probable modern analogue of Kuroko-type massive sulphide deposits in the Okinawa trough back-arc basin: Nature, v. 338, p. 496–499.

Halbach, P., Pracejus, B., and Märten, A., 1993, Geology and mineralogy of massive sulfide ores from the central Okinawa trough, Japan: Economic Geology, v. 88, p. 2,210–2,225.

Halbach, P., Blum, N., and Auzende, J.M., 1995, The SO 99 field—a new chimney field of massive sulfides in the North Fiji basin, *in* Pašava, J., Kříbek, B., and Žák, K., eds., Mineral deposits: From their origin to their environmental impacts: Rotterdam, Balkema, p. 225–228.

Halbach, P., Blum, N., Münch, U., Plüger, W., Garbe-Schönberg, D., and Zimmer, M., 1998, Formation and decay of a modern massive sulfide deposit in the Indian Ocean: Mineralium Deposita, v. 33, p. 302–309.

Halbach, P.E., Fouquet, Y., and Herzig, P., 2003, Mineralization and compositional patterns in deep-sea hydrothermal systems, *in* Halbach, P.E., Tunnicliffe, V., and Hein, J.R., eds., Energy and mass transfer in marine hydrothermal systems, Berlin, Dahlem University Press, p. 85–122.

Hannington, M.D., 1993, The formation of atacamite during weathering of sulfides on the modern seafloor: Canadian Mineralogist, v. 31, p. 945–956.

——2011, Comments on "What processes at mid-ocean ridges tell us about volcanogenic massive sulfide deposits" by L.M. Cathles: Mineralium Deposita, v. 46, p. 659–663.

——2014, Volcanogenic massive sulfide deposits: Treatise on Geochemistry, 2nd ed., v. 13, p. 463–488.

Hannington, M., and Monecke, T., 2009, Global exploration models for polymetallic sulphides in the Area: An assessment of lease block selection under the draft regulations on prospecting and exploration for polymetallic sulphides: Marine Georesources and Geotechnology, v. 27, p. 132–159.

Hannington, M.D., and Scott, S.D., 1988, Mineralogy and geochemistry of a hydrothermal silica-sulfide-sulfate spire in the caldera of Axial Seamount, Juan de Fuca Ridge: Canadian Mineralogist, v. 26, p. 603–625.

Hannington, M.D., Peter, J.M., and Scott, S.D., 1986, Gold in sea-floor polymetallic sulfide deposits: Economic Geology, v. 81, p. 1,867–1,883.

Hannington, M.D., Thompson, G., Rona, P.A., and Scott, S.D., 1988, Gold and native copper in supergene sulphides from the Mid-Atlantic Ridge: Nature, v. 333, p. 64–66.

Hannington, M., Herzig, P., Scott, S., Thompson, G., and Rona, P., 1991, Comparative mineralogy and geochemistry of gold-bearing sulfide deposits on the mid-ocean ridges: Marine Geology, v. 101, p. 217–248.

Hannington, M.D., Petersen, S., Jonasson, I.R., and Franklin, J.M., 1994, Hydrothermal activity and associated mineral deposits on the seafloor: Geological Survey of Canada Open File Report 2915C, map 1:35,000,000 and CD-ROM.

Hannington, M.D., Jonasson, I.R., Herzig, P.M., and Petersen, S., 1995, Physical and chemical processes of seafloor mineralization at mid-ocean ridges: Geophysical Monograph Series, v. 91, p. 115–157.

Hannington, M.D., Galley, A.G., Herzig, P.M., and Petersen, S., 1998, Comparison of the TAG mound and stockwork complex with Cyprus-type massive sulfide deposits: Proceedings of the Ocean Drilling Program, Scientific Results, v. 158, p. 389–415.

Hannington, M.D., Barrie, C.T., and Bleeker, W., 1999a, The giant Kidd Creek volcanogenic massive sulfide deposit, western Abitibi Subprovince, Canada: Preface and introduction: Economic Geology Monograph 10, p. 1–30.

Hannington, M.D., Bleeker, W., and Kjarsgaard, I., 1999b, Sulfide mineralogy, geochemistry, and ore genesis of the Kidd Creek deposit: Part I. North, Central, and South orebodies: Economic Geology Monograph 10, p. 163–224.

——1999c, Sulfide mineralogy, geochemistry, and ore genesis of the Kidd Creek deposit: Part II. The Bornite zone: Economic Geology Monograph 10, p. 225–266.

Hannington, M.D., Poulsen, K.H., Thompson, J.F.H., and Sillitoe, R.H., 1999d, Volcanogenic gold in the massive sulfide environment: Reviews in Economic Geology, v. 8, p. 325–356.

Hannington, M.D., de Ronde, C.E.J., and Petersen, S., 2005, Sea-floor tectonics and submarine hydrothermal systems: Economic Geology 100th Anniversary Volume, p. 111–141.

Hannington, M., Jamieson, J., Monecke, T., and Petersen, S., 2010, Modern sea-floor massive sulfides and base metal resources: Toward an estimate of global sea-floor massive sulfide potential: Society of Economic Geology Special Publication 15, p. 317–338.

Hannington, M., Jamieson, J., Monecke, T., Petersen, S., and Beaulieu, S., 2011, The abundance of seafloor massive sulfide deposits: Geology, v. 39, p. 1,155–1,158.

Hashimoto, J., Ohta, S., Gamo, T., Chiba, H., Yamaguchi, T., Tsuchida, S., Okudaira, T., Watabe, H., Yamanaka, T., and Kitazawa, M., 2001, Hydrothermal vents and associated biological communities in the Indian Ocean: InterRidge News, v. 10, p. 21–22.

Hawkins, J., 1986, "Black Smoker" vent chimneys: EOS Transactions of the American Geophysical Union, v. 67, p. 430.

Hawkins, J.W., Lonsdale, P.F., Macdougall, J.D., and Volpe, A.M., 1990, Petrology of the axial ridge of the Mariana trough backarc spreading center: Earth and Planetary Science Letters, v. 100, p. 226–250.

Haymon, R.M., 1983, Growth history of hydrothermal black smoker chimneys: Nature, v. 301, p. 695–698.

Haymon, R.M., and Kastner, M., 1981, Hot spring deposits on the East Pacific Rise at 21°N: Preliminary description of mineralogy and genesis: Earth and Planetary Science Letters, v. 53, p. 363–381.

Haymon, R.M., and White, S.M., 2004, Fine-scale segmentation of volcanic/hydrothermal systems along fast-spreading ridge crests: Earth and Planetary Science Letters, v. 226, p. 367–382.

Haymon, R.M., Koski, R.A., and Abrams, M.J., 1989, Hydrothermal discharge zones beneath massive sulfide deposits mapped in the Oman Ophiolite: Geology, v. 17, p. 531–535.

Haymon, R.M., Fornari, D.J., Edwards, M.H., Carbotte, S., Wright, D., and Macdonald, K.C., 1991, Hydrothermal vent distribution along the East Pacific Rise crest (9°09'-54'N) and its relationship to magmatic and tectonic processes on fast-spreading mid-ocean ridges: Earth and Planetary Science Letters, v. 104, p. 513–534.

Haymon, R.M., Fornari, D.J., Von Damm, K.L., Lilley, M.D., Perfit, M.R., Edmond, J.M., Shanks, W.C., III, Lutz, R.A., Grebmeier, J.M., Carbotte, S., Wright, D., McLaughlin, E., Smith, M., Beedle, N., and Olson, E., 1993, Volcanic eruption of the mid-ocean ridge along the East Pacific Rise crest at 9°45-52'N: Direct submersible observations of seafloor phenomena associated with an eruption event in April, 1991: Earth and Planetary Science Letters, v. 119, p. 85–101.

Haymon, R.M., White, S.M., Baker, E.T., Anderson, P.G., Macdonald, K.C., and Resing, J.A., 2008, High-resolution surveys along the hot spot-affected Galápagos Spreading Center: 3. Black smoker discoveries and the implications for geological controls on hydrothermal activity: Geochemistry Geophysics Geosystems, v. 9, doi: 10.1029/2008GC002114.

Healy, R.E., and Petruk, W., 1990, Petrology of Au-Ag-Hg alloy and "invisible" gold in the Trout Lake massive sulfide deposit, Flin Flon, Manitoba: Canadian Mineralogist, v. 28, p. 189–206.

——1992, Graphic galena-clausthalite solid solution in low Fe sphalerite from the Trout Lake massive sulfide ores, Flin Flon, Manitoba: Economic Geology, v. 87, p. 1,906–1,910.

Hein, J.R., de Ronde, C.E.J., Koski, R.A., Ditchburn, R.G., Mizell, K., Tamura, Y., Stern, R.J., Conrad, T.A., Ishizuka, O., and Leybourne, M.I.,

2014, Layered hydrothermal barite-sulfide mound field, East Diamante caldera, Mariana volcanic arc: Economic Geology, v. 109, p. 2,179–2,206.
Hekinian, R., Fevrier, M., Bischoff, J.L., Picot, P., and Shanks, W.C., 1980, Sulfide deposits from the East Pacific Rise near 21°N: Science, v. 207, p. 1,433–1,444.
Hekinian, R., Fevrier, M., Avedik, F., Cambon, P., Charlou, J.L., Needham, H.D., Raillard, J., Boulegue, J., Merlivat, L., Moinet, A., Manganini, S., and Lange, J., 1983, East Pacific Rise near 13°N: Geology of new hydrothermal fields: Science, v. 219, p. 1,321–1,324.
Herrmann, W., Blake, M., Doyle, M., Huston, D., Kamprad, J., Merry, N., and Pontual, S., 2001, Short wavelength infrared (SWIR) spectral analysis of hydrothermal alteration zones associated with base metal sulfide deposits at Rosebery and Western Tharsis, Tasmania, and Highway-Reward, Queensland: Economic Geology, v. 96, p. 939–955.
Herzig, P.M., and Hannington, M.D., 1995, Polymetallic massive sulfides at the modern seafloor: A review: Ore Geology Reviews, v. 10, p. 95–115.
Herzig, P.M., and Plüger, W.L., 1988, Exploration for hydrothermal activity near the Rodriguez Triple Junction, Indian Ocean: Canadian Mineralogist, v. 26, p. 721–736.
Herzig, P.M., Hannington, M.D., Scott, S.D., Maliotis, G., Rona, P.A., and Thompson, G., 1991, Gold-rich sea-floor gossans in the Troodos Ophiolite and on the mid-Atlantic Ridge: Economic Geology, v. 86, p. 1,747–1,755.
Herzig, P.M., Hannington, M.D., Fouquet, Y., von Stackelberg, U., and Petersen, S., 1993, Gold-rich polymetallic sulfides from the Lau back arc and implications for the geochemistry of gold in sea-floor hydrothermal systems of the southwest Pacific: Economic Geology, v. 88, p. 2,182–2,209.
Herzig, P.M., Hannington, M.D., and Arribas, A., Jr., 1998, Sulfur isotopic composition of hydrothermal precipitates from the Lau back-arc: Implications for magmatic contributions to seafloor hydrothermal systems: Mineralium Deposita, v. 33, p. 226–237.
Hey, R.N., Massoth, G.J., Vrijenhoek, R.C., Rona, P.A., Lupton, J., and Butterfield, D.A., 2006, Hydrothermal vent geology and biology at Earth's fastest spreading rates: Marine Geophysical Researches, v. 27, p. 137–153.
Hoagland, P., Beaulieu, S., Tivey, M.A., Eggert, R.G., German, C., Glowka, L., and Lin, J., 2010, Deep-sea mining of seafloor massive sulfides: Marine Policy, v. 34, p. 728–732.
Hocking, M.W.A., 2007, The Calypso hydrothermal vent field: The seafloor expression of an active submarine low-sulphidation epithermal system, Bay of Plenty, New Zealand: M.Sc. thesis, Ottawa, University of Ottawa, 177 p.
Hocking, M.W.A., Hannington, M.D., Percival, J.B., Stoffers, P., Schwarz-Schampera, U., and de Ronde, C.E.J., 2010, Clay alteration of volcaniclastic material in a submarine geothermal system, Bay of Plenty, New Zealand: Journal of Volcanology and Geothermal Research, v. 191, p. 180–192.
Houghton, J.L., Shanks, W.C., III, and Seyfried, W.E., Jr., 2004, Massive sulfide deposition and trace element remobilization in the Middle Valley sediment-hosted hydrothermal system, northern Juan de Fuca Ridge: Geochimica et Cosmochimica Acta, v. 68, p. 2,863–2,873.
Huber, C., and Wächtershäuser, G., 1998, Peptides by activation of amino acids with CO on (Ni,Fe)S surfaces: Implications for the origin of life: Science, v. 281, p. 670–672.
Humphris, S.E., and Bach, W., 2005, On the Sr isotope and REE compositions of anhydrites from the TAG seafloor hydrothermal system: Geochimica et Cosmochimica Acta, v. 69, p. 1,511–1,525.
Humphris, S.E., Herzig, P.M., Miller, D.J., Alt, J.C., Becker, K., Brown, D., Brügmann, G., Chiba, H., Fouquet, Y., Gemmell, J.B., Guerin, G., Hannington, M.D., Holm, N.G., Honnorez, J.J., Iturrino, G.J., Knott, R., Ludwig, R., Nakamura, K., Petersen, S., Reysenbach, A.L., Rona, P.A., Smith, S., Sturz, A.A., Tivey, M.K., and Zhao, X., 1995, The internal structure of an active sea-floor massive sulphide deposit: Nature, v. 377, p. 713–716.
Huston, D.L., 2000, Gold in volcanic-hosted massive sulfide deposits: Distribution, genesis, and exploration: Reviews in Economic Geology, v. 13, p. 401–426.
Huston, D.L., and Large, R.R., 1988, Distribution, mineralogy, and geochemistry of gold and silver in the North End orebody, Rosebery, Tasmania: Economic Geology, v. 83, p. 1,181–1,192.
Huston, D.L., Taylor, T., Fabray, J., and Patterson, D.J., 1992a, A comparison of the geology and mineralization of the Balcooma and Dry River South volcanic-hosted massive sulfide deposits, northern Queensland: Economic Geology, v. 87, p. 785–811.
Huston, D.L., Bottrill, R.S., Creelman, R.A., Zaw, K., Ramsden, T.R., Rand, S.W., Gemmell, J.B., Jablonski, W., Sie, S.H., and Large, R.R., 1992b, Geologic and geochemical controls on the mineralogy and grain size of gold-bearing phases, eastern Australian volcanic-hosted massive sulfide deposits: Economic Geology, v. 87, p. 542–563.
Huston, D.L., Sie, S.H., Suter, G.F., Cooke, D.R., and Both, R.A., 1995, Trace elements in sulfide minerals from eastern Australian volcanic-hosted massive sulfide deposits: Part I. Proton microprobe analyses of pyrite, chalcopyrite, and sphalerite, and Part II. Selenium levels in pyrite: Comparison with $\delta^{34}S$ values and implications for the source of sulfur in volcanogenic hydrothermal systems: Economic Geology, v. 90, p. 1,167–1,196.
Iizasa, K., 1993, Assessment of the hydrothermal contribution to seafloor sediments in the Myojinsho submarine caldera, Shichito-Iwojima Ridge, Izu-Ogasawara arc, Japan: Marine Geology, v. 114, p. 119–132.
Iizasa, K., Yuasa, M., and Yokoto, S., 1992, Mineralogy and geochemistry of volcanogenic sulfides from the Myojinsho submarine caldera, the Shichito-Iwojima Ridge, Izu Ogasawara arc, northwestern Pacific: Marine Geology, v. 108, p. 39–58.
Iizasa, K., Fiske, R.S., Ishizuka, O., Yuasa, M., Hashimoto, J., Ishibashi, J., Naka, J., Horii, Y., Fujiwara, Y., Imai, A., and Koyama, S., 1999, A Kuroko-type polymetallic sulfide deposit in a submarine silicic caldera: Science, v. 283, p. 975–977.
Iizasa, K., Sasaki, M., Matsumoto, K., Shiokawa, S., Tanahashi, M., and Shipboard Scientific Party, 2004, A first extensive hydrothermal field associated with Kuroko-type deposit in a silicic submarine caldera in a nascent rift zone, Izu-Ogasawara (Bonin) arc, Japan [abs.]: Oceans 2004 MTTS/IEEE Conference: Kobe, Marine Technology Society, Proceedings, p. 991–996.
Ikehata, K., Notsu, K., and Hirata, T., 2011, Copper isotope characteristics of copper-rich minerals from Besshi-type volcanogenic massive sulfide deposits, Japan, determined using a femtosecond LA-MC-ICP-MS: Economic Geology, v. 106, p. 307–316.
Ikehata, K., Suzuki, R., Shimada, K., Ishibashi, J., and Urabe, T., 2015, Mineralogical and geochemical characteristics of hydrothermal minerals collected from hydrothermal vent fields in the southern Mariana spreading center, *in* Ishibashi, J., Okino, K., and Sunamura, M., eds., Subseafloor biosphere linked to hydrothermal systems: TAIGA concept: Tokyo, Springer, p. 275–287.
Ishibashi, J., Suzuki, R., Yamanaka, T., Toki, T., Kimura, H., Noguchi, T., and Urabe, T., 2006, Seafloor hydrothermal activity at off-axial seamounts of backarc spreading in southern Mariana trough [abs.]: Goldschmidt Conference, 16th, Melbourne, Australia, 2006, Geochimica et Cosmochimica Acta, v. 70, A279.
Ishibashi, J., Noguchi, T., Toki, T., Miyabe, S., Yamagami, S., Onishi, Y., Yamanaka, T., Yokoyama, Y., Omori, E., Takahashi, Y., Hatada, K., Nakaguchi, Y., Yoshizaki, M., Konno, U., Shibuya, T., Takai, K., Inagaki, F., and Kawagucci, S., 2014, Diversity of fluid geochemistry affected by processes during fluid upwelling in active hydrothermal fields in the Izena Hole, the middle Okinawa trough back-arc basin: Geochemical Journal, v. 48, p. 357–369.
Ishihara, S., and Endo, Y., 2007, Indium and other trace elements in volcanogenic massive sulfide ores from the Kuroko, Besshi and other types in Japan: Bulletin of the Geological Survey of Japan, v. 58, p. 7–22.
Iwaida, C., and Ueno, H., 2005, Ore and gangue minerals of seafloor hydrothermal deposits in the Mariana trough: JAMSTEC Report of Research and Development, v. 1, p. 1–12.
James, R.H., Elderfield, H., and Palmer, M.R., 1995, The chemistry of hydrothermal fluids from the Broken Spur site, 29°N Mid-Atlantic Ridge: Geochimica et Cosmochimica Acta, v. 59, p. 651–659.
Jamieson, J.W., Clague, D.A., and Hannington, M.D., 2014a, Hydrothermal sulfide accumulation along the Endeavour Segment, Juan de Fuca Ridge: Earth and Planetary Science Letters, v. 395, p. 136–148.
Jamieson, J.W., Petersen, S., Augustin, N., Steinführer, A., Escartin, J., and ODEMAR Scientific Party, 2014b, Seafloor massive sulfide formation on oceanic core complexes: Recent exploration of the Semyenov and Irinovskoe hydrothermal fields, Mid-Atlantic Ridge [abs.]: Minerals of the Ocean-7 and Deep-Sea Minerals and Mining-4, St. Petersburg, Russia, 2014, Abstract Volume, p. 42–45.
Janecky, D.R., and Seyfried, W.E., Jr., 1984, Formation of massive sulfide deposits on oceanic ridge crests: Incremental reaction models for mixing between hydrothermal solutions and seawater: Geochimica et Cosmochimica Acta, v. 48, p. 2,723–2,738.
Jannasch, H.W., 1985, The chemosynthetic support of life and the microbial diversity at deep-sea hydrothermal vents: Proceedings of the Royal Society of London, v. B255, p. 277–297.
Jannasch, H.W., and Wirsen, C.O., 1979, Chemosynthetic primary production at East Pacific sea floor spreading centers: BioScience, v. 29, p. 592–598.

Jokat, W., 2000, The expedition ARKTIS-XV/2 of "Polarstern" in 1999: Berichte zur Polarforschung, v. 368, p. 1–142.

Jollivet, D., Lallier, F.H., Barnay, A.S., Bienvenue, N., Bonnivard, E., Briand, P., Cambon-Bonavita, M.A., Comtet, T., Cosson, R., Daguin, C., Donval, J.P., Faure, B., Gaillard, M., Glippa, V., Guillou, L., Hourdez, S., Le Bris, N., Morand, S., Pradillon, F., Rees, J.F., Segonzac, M., Shillito, B., Thiébaut, E., and Viard, F., 2004, The BIOSPEEDO cruise: A new survey of hydrothermal vents along the South East Pacific Rise from 7°24'S to 21°33'S: InterRidge News, v. 13, p. 20–26.

Jonasson, I.R., and Sangster, D.F., 1975, Variations in the mercury content of sphalerite from some Canadian sulphide deposits [ext. abs.]: International Geochemical Exploration Symposium, 5th, Vancouver, Canada, 1974, Proceedings, p. 313–332.

Kachalovskaya, V.M., Osipov, B.S., Kukoev, V.A., and Koslova, E.V., 1975, Germanium bearing minerals from the bornite ore of the Urup deposit: Zapiski Vsesoiuznogo Mineralogicheskogo Obshchestvat, v. 104, p. 94–97.

Kakegawa, T., Utsumi, M., and Marumo, K., 2008, Geochemistry of sulfide chimneys and basement pillow lavas at the southern Mariana trough (12.55°N–12.58°N): Resource Geology, v. 58, p. 249–266.

Kamiyama, T., Kojima, G., Iwahashi, T., Hide, K., Yoshida, H., Nakamura, T., Fukumoto, H., Yonebayashi, S., Hamajima, I., Kamura, Y., Okubo, Y., Yui, S., Kanehira, K., Nureki, T., Kanda, S., Miura, F., Nakagawa, M., and Oyagi, N., 1964, Geology and situation of ore deposits in the region of the Iimori mine: Collaborative studies on geology and ore deposits of the region of the Iimori mine, No. 1: Mining Geology, v. 14, p. 336–349.

Karson, J.A., and Brown, J.R., 1988, Geologic setting of the Snake Pit hydrothermal site: An active vent field on the Mid-Atlantic Ridge: Marine Geophysical Researches, v. 10, p. 91–107.

Kase, K., Yamamoto, M., Nakamura, T., and Mitsuno, C., 1990, Ore mineralogy and sulfur isotope study of the massive sulfide deposit of Filon Norte, Tharsis mine, Spain: Mineralium Deposita, v. 25, p. 289–296.

Kase, K., Yamamoto, M., and Mitsuno, C., 1994, Germanium-bearing colusite from the Yanahara mine, Japan, and its significance to ore genesis: Resource Geology, v. 44, p. 33–38.

Kasuga, S., and Kato, Y., 1992, Discovery of hydrothermal ore deposits in the crater of the Suiyo Smt. on the Izu-Ogasawara arc: Proceedings of JAMSTEC Symposium on Deep Sea Research, v. 8, p. 249–256.

Kataoka, S., Ishibashi, J., Yamanaka, T., and Chiba, H., 2000, Topography and fluid geochemistry of the Iheya North knoll seafloor hydrothermal system in the Okinawa trough: JAMSTEC Journal of Deep Sea Research, v. 16, p. 1–7.

Kelley, D.S., Delaney, J.R., and Yoerger, D.R., 2001, Geology and venting characteristics of the Mothra hydrothermal field, Endeavour segment, Juan de Fuca Ridge: Geology, v. 29, p. 959–962.

Kelley, D.S., Carbotte, S.M., Caress, D.W., Clague, D.A., Delaney, J.R., Gill, J.B., Hadaway, H., Holden, J.F., Hooft, E.E.E., Kellogg, J.P., Lilley, M.D., Stoermer, M., Toomey, D., Weekly, R., and Wilcock, W.S.D., 2012, Endeavour Segment of the Juan de Fuca Ridge: One of the most remarkable places on Earth: Oceanography, v. 25, p. 44–61.

Kelley, D.S., Delaney, J.R., and Juniper, S.K., 2014, Establishing a new era of submarine volcanic observatories: Cabling Axial Seamount and the Endeavour Segment of the Juan de Fuca Ridge: Marine Geology, v. 352, p. 426–450.

Kerr, D.J., and Gibson, H.L., 1993, A comparison of the Horne volcanogenic massive sulfide deposit and intracauldron deposits of the Mine sequence, Noranda, Quebec: Economic Geology, v. 88, p. 1,419–1,442.

Kieft, K., and Damman, A.H., 1990, Indium-bearing chalcopyrite and sphalerite from the Gåsborn area, West Bergslagen, central Sweden: Mineralogical Magazine, v. 54, p. 109–112.

Kilias, S.P., Nomikou, P., Papanikolaou, D., Polymenakou, P.N., Godelitsas, A., Argyraki, A., Carey, S., Gamaletsos, P., Mertzimekis, T.J., Stathopoulou, E., Goettlicher, J., Steininger, R., Betzelou, K., Livanos, I., Christakis, C., Bell, K.C., and Scoullos, M., 2013, New insights into hydrothermal vent processes in the unique shallow-submarine arc-volcano, Kolumbo (Santorini), Greece: Nature Scientific Reports, v. 3, doi: 10.1038/srep02421.

Kim, J., Lee, I., Halbach, P., Lee, K.Y., Ko, Y.T., and Kim, K.H., 2006, Formation of hydrothermal vents in the North Fiji basin: Sulfur and lead isotope constraints: Chemical Geology, v. 233, p. 257–275.

Kim, J., Son, S.K., Son, J.W., Kim, K.H., Shim, W.J., Kim, C.H., and Lee, K.Y., 2009, Venting sites along the Fonualei and Northeast Lau Spreading Centers and evidence of hydrothermal activity at an off-axis caldera in the northeastern Lau basin: Geochemical Journal, v. 43, p. 1–13.

Kim, J., Lee, K.Y., and Kim, J.H., 2011, Metal-bearing molten sulfur collected from a submarine volcano: Implications for vapor transport of metals in seafloor hydrothermal systems: Geology, v. 39, p. 351–354.

Kimura, M., Tanaka, T., Kyo, M., Ando, M., Oomori, T., Izawa, E., and Yoshikawa, I., 1989, Study of topography, hydrothermal deposits and animal colonies in the middle Okinawa trough hydrothermal areas using the submersible "SHINKAI 2000" system: Proceedings of JAMSTEC Symposium on Deep Sea Research, v. 5, p. 223–244.

Kinsey, J.C., and German, C.R., 2013, Sustained volcanically-hosted venting at ultraslow ridges: Piccard hydrothermal field, Mid-Cayman Rise: Earth and Planetary Science Letters, v. 380, p. 162–168.

Kishida, K., Sohrin, Y., Okamura, K., and Ishibashi, J., 2004, Tungsten enriched in submarine hydrothermal fluids: Earth and Planetary Science Letters, v. 222, p. 819–827.

Klein, E.M., Smith, D.K., Williams, C.M., Hanna, H., Zhu, W., Rudnicki, M., Cheney, R., and Vancouver Leg01 Scientific Party, 2003, Tectonic and geologic characterization of the incipient rift, east of the East Pacific Rise at 2°40'N [abs.]: American Geophysical Union Fall Meeting, San Francisco, California, 2003, V12C-0602.

Klinkhammer, G.P., Chin, C.S., Keller, R.A., Dählmann, A., Sahling, H., Sarthou, G., Petersen, S., Smith, F., and Wilson, C., 2001, Discovery of new hydrothermal vent sites in Bransfield Strait, Antarctica: Earth and Planetary Science Letters, v. 193, p. 395–407.

Knuckey, M.J., Comba, C.D.A., and Riverin, G., 1982, Structure, metal zoning and alteration at the Millenbach deposit, Noranda, Quebec: Geological Association of Canada Special Paper 25, p. 255–295.

Komuro, K., and Kajiwara, Y., 2004, Germanium-bearing colusite in siliceous black ore from the Ezuri Kuroko deposit, Hokuroku district, Japan: Resource Geology, v. 54, p. 447–452.

Konno, U., Tsunogai, U., Nakagawa, F., Nakaseama, M., Ishibashi, J., Nunoura, T., and Nakamura, K., 2006, Liquid CO_2 venting on the seafloor: Yonaguni knoll IV hydrothermal system, Okinawa trough: Geophysical Research Letters, v. 33, L16607.

Koschinsky, A., Garbe-Schönberg, D., Sander, S., Schmidt, K., Gennerich, H.H., and Strauss, H., 2008, Hydrothermal venting at pressure-temperature conditions above the critical point of seawater, 5°S on the Mid-Atlantic Ridge: Geology, v. 36, p. 615–618.

Koski, R.A., Clague, D.A., and Oudin, E., 1984, Mineralogy and chemistry of massive sulfide deposits from the Juan de Fuca Ridge: Geological Society of America Bulletin, v. 95, p. 930–945.

Koski, R.A., Lonsdale, P.F., Shanks, W.C., Berndt, M.E., and Howe, S.S., 1985, Mineralogy and geochemistry of a sediment-hosted hydrothermal sulfide deposit from the Southern trough of Guaymas basin, Gulf of California: Journal of Geophysical Research, v. 90, p. 6,695–6,707.

Koski, R.A., Shanks, W.C., III, Bohrson, W.A., and Oscarson, R.L., 1988, The composition of massive sulfide deposits from the sediment-covered floor of Escanaba trough, Gorda Ridge: Implications for depositional processes: Canadian Mineralogist, v. 26, p. 655–673.

Koski, R.A., Jonasson, I.R., Kadko, D.C., Smith, V.K., and Wong, F.L., 1994a, Compositions, growth mechanisms, and temporal relations of hydrothermal sulfide-sulfate-silica chimneys at the northern Cleft segment, Juan de Fuca Ridge: Journal of Geophysical Research, v. 99, p. 4,813–4,832.

Koski, R.A., Benninger, L.M., Zierenberg, R.A., and Jonasson, I.R., 1994b, Composition and growth history of hydrothermal deposits in Escanaba trough, southern Gorda Ridge: U.S. Geological Survey Bulletin v. 2022, p. 293–324.

Krapiva, L.Y., Dobrovol'skaya, M.G., Malov, V.S., Chvileva, T.N., and Estrugo, M., 1986, Colusite from the San Fernando deposits, Cuba: Transactions (Doklady) of the U.S.S.R. Academy of Sciences, Earth Science Sections, v. 287, p. 118–122.

Krasnov, S., Stepanova, T., and Stepanov, M., 1994, Chemical composition and formation of a massive sulfide deposit, Middle Valley, northern Juan de Fuca Ridge (Site 856): Proceedings of the Ocean Drilling Program, Scientific Results, v. 139, p. 353–372.

Krasnov, S.G., Poroshina, I.M., and Cherkashev, G.A., 1995a, Geological setting of high-temperature hydrothermal activity and massive sulphide formation on fast- and slow-spreading ridges: Geological Society, London, Special Publication 87, p. 17–32.

Krasnov, S.G., Cherkashev, G.A., Stepanova, T.V., Batuyev, B.N., Krotov, A.G., Malin, B.V., Maslov, M.N., Markov, V.F., Poroshina, I.M., Samovarov, M.S., Ashadze, A.M., Lazareva, L.I., and Ermolayev, I.K., 1995b, Detailed geological studies of hydrothermal fields in the North Atlantic: Geological Society, London, Special Publication 87, p. 43–64.

Kristall, B., Kelley, D.S., Hannington, M.D., and Delaney, J.R., 2006, Growth history of a diffusely venting sulfide structure from the Juan de Fuca Ridge: A petrological and geochemical study: Geochemistry Geophysics Geosystems, v. 7, doi: 10.1029/2005GC001166.

Kristall, B., Nielsen, D., Hannington, M.D., Kelley, D.S., and Delaney, J.R., 2011, Chemical microenvironments within sulfide structures from the Mothra hydrothermal field: Evidence from high-resolution zoning of trace elements: Chemical Geology, v. 290, p. 12–30.

Kumagai, H., Nakamura, K., Toki, T., Morishita, T., Okino, K., Ishibashi, J., Tsunogai, U., Kawagucci, S., Gamo, T., Shibuya, T., Sawaguchi, T., Neo, N., Joshima, M., Sato, T., and Takai, K., 2008, Geological background of the Kairei and Edmond hydrothermal fields along the Central Indian Ridge: Implications of their vent fluids' distinct chemistry: Geofluids, v. 8, p. 239–251.

Kuriyama, T., Matsumoto, K., and Fujioka, H., 1994, Polymetallic sulfides on the off-axis volcanoes around the East Pacific Rise; 11°30' North latitude: Resource Geology, v. 44, p. 187–199.

Kusakabe, M., Mayeda, S., and Nakamura, E., 1990, S, O and Sr isotope systematics of active vent materials from the Mariana backarc basin spreading axis at 18°N: Earth and Planetary Science Letters, v. 100, p. 275–282.

Kuznetsov, V., Cherkashev, G., Lein, A., Shilov, V., Maksimov, F., Arslanov, K., Stepanova, T., Baranova, N., Chernov, S., and Tarasenko, D., 2006, ^{230}Th/U dating of massive sulfides from the Logatchev and Rainbow hydrothermal fields (Mid-Atlantic Ridge): Geochronometria, v. 25, p. 51–55.

Lalou, C., Reyss, J.L., Brichet, E., Rona, P.A., and Thompson, G., 1995, Hydrothermal activity on a 10^5-year scale at a slow-spreading ridge, TAG hydrothermal field, Mid-Atlantic Ridge 26°N: Journal of Geophysical Research, v. 100, p. 17,855–17,862.

Lalou, C., Reyss, J.L., Brichet, E., Krasnov, S., Stepanova, T., Cherkashev, G., and Markov, V., 1996, Initial chronology of a recently discovered hydrothermal field at 14°45'N, Mid-Atlantic Ridge: Earth and Planetary Science Letters, v. 144, p. 483–490.

Lalou, C., Münch, U., Halbach, P., and Reyss, J.L., 1998, Radiochronological investigation of hydrothermal deposits from the MESO zone, Central Indian Ridge: Marine Geology, v. 149, p. 243–254.

Lambe, R.N., and Rowe, R.G., 1987, Volcanic history, mineralization, and alteration of the Crandon massive sulfide deposit, Wisconsin: Economic Geology, v. 82, p. 1,204–1,238.

Lamborg, C.H., Von Damm, K.L., Fitzgerald, W.F., Hammerschmidt, C.R., and Zierenberg, R., 2006, Mercury and monomethylmercury in fluids from Sea Cliff submarine hydrothermal field, Gorda Ridge: Geophysical Research Letters, v. 33, doi: 10.1029/2006GL026321.

Langmuir, C., Humphris, S., Fornari, D., Van Dover, C., Von Damm, K., Tivey, M.K., Colodner, D., Charlou, J.F., Desonie, D., Wilson, C., Fouquet, Y., Klinkhammer, G., and Bougault, H., 1997, Hydrothermal vents near a mantle hot spot: The Lucky Strike vent field at 37°N on the Mid-Atlantic Ridge: Earth and Planetary Science Letters, v. 148, p. 69–91.

Large, R.R., 1977, Chemical evolution and zonation of massive sulfide deposits in volcanic terrains: Economic Geology, v. 72, p. 549–572.

——1992, Australian volcanic-hosted massive sulfide deposits: Features, styles, and genetic models: Economic Geology, v. 87, p. 471–510.

Large, R.R., McPhie, J., Gemmell, J.B., Herrmann, W., and Davidson, G.J., 2001a, The spectrum of ore deposit types, volcanic environments, alteration halos, and related exploration vectors in submarine volcanic successions: Some examples from Australia: Economic Geology, v. 96, p. 913–938.

Large, R.R., Allen, R.L., Blake, M.D., and Herrmann, W., 2001b, Hydrothermal alteration and volatile element halos for the Rosebery K lens volcanic-hosted massive sulfide deposit, western Tasmania: Economic Geology, v. 96, p. 1,055–1,072.

Lawrence, L.J., 1967, A mineragraphic study of Mount Morgan copper-gold ore: The Australasian Institute of Mining and Metallurgy Proceedings, v. 223, p. 29–47.

Lawrie, D., and Miller, D.J., 2000, Sulfide mineral chemistry and petrography from Bent Hill, ODP Mound, and TAG massive sulfide deposits: Proceedings of the Ocean Drilling Program, Scientific Results, v. 169, p. 1–34.

Layton-Matthews, D., Peter, J.M., Scott, S.D., and Leybourne, M.I., 2008, Distribution, mineralogy, and geochemistry of selenium in felsic volcanic-hosted massive sulfide deposits of the Finlayson Lake district, Yukon Territory, Canada: Economic Geology, v. 103, p. 61–88.

Lee, S., Kim, S.J., Ju, S.J., Pak, S.J., Son, S.K., Yang, J., and Han, S., 2015, Mercury accumulation in hydrothermal vent mollusks from the southern Tonga arc, southwestern Pacific Ocean: Chemosphere, v. 127, p. 246–253.

Lein, A.Y., Cherkashev, G.A., Ul'yanov, A.A., Ul'yanova, N.V., Stepanova, T.V., Sagalevich, A.M., Bogdanov, Y.A., Gurvich, E.G., and Torokhov, M.P., 2003, Mineralogy and geochemistry of sulfide ores from the Logatchev-2 and Rainbow fields: Similar and distinctive features: Geochemistry International, v. 41, p. 271–294.

Lein, A.Y., Bogdanov, Y.A., Maslennikov, V.V., Li, S., Ulyanova, N.V., Maslennikova, S.P., and Ulyanov, A.A., 2010, Sulfide minerals in the Menez Gwen nonmetallic hydrothermal field (Mid-Atlantic Ridge): Lithology and Mineral Resources, v. 45, p. 305–323.

Leistel, J.M., Marcoux, E., Thiéblemont, D., Quesada, C., Sánchez, A., Almodóvar, G.R., Pascual, E., and Sáez, R., 1998a, The volcanic-hosted massive sulphide deposits of the Iberian Pyrite Belt: Mineralium Deposita, v. 33, p. 2–30.

Leistel, J.M., Marcoux, E., Deschamps, Y., and Joubert, M., 1998b, Antithetic behaviour of gold in the volcanogenic massive sulphide deposits of the Iberian Pyrite Belt: Mineralium Deposita, v. 33, p. 82–97.

Leitch, C.H.B., 1981, Mineralogy and textures of the Lahanos and Kizilkaya massive sulfide deposits, northeastern Turkey, and their similarity to Kuroko ores: Mineralium Deposita, v. 16, p. 241–257.

Lescuyer, J.L., Oudin, E., and Beurrier, M., 1988, Review of the different types of mineralization related to the Oman ophiolitic volcanism [ext. abs.]: Quadrenniel International Association on the Genesis of Ore Deposits Symposium, 7th, Luleå, Sweden, Proceedings, p. 489–500.

Lescuyer, J.L., Leistel, J.M., Marcoux, E., Milési, J.P., and Thiéblemont, D., 1998, Late Devonian-Early Carboniferous peak sulphide mineralization in the western Hercynides: Mineralium Deposita, v. 33, p. 208–220.

Leybourne, M.I., de Ronde, C.E.J., Wysoczanski, R.J., Walker, S.L., Timm, C., Gibson, H.L., Layton-Matthews, D., Baker, E.T., Clark, M.R., Caratori Tontini, F., Faure, K., Lupton, J.E., Fornari, D.J., Soule, S.A., and Massoth, G.J., 2012, Geology, hydrothermal activity, and sea-floor massive sulfide mineralization at the Rumble II West mafic caldera: Economic Geology, v. 107, p. 1,649–1,668.

Li, B., Yang, Y., Shi, X., Ye, J., Gao, J., Zhu, A., and Shao, M., 2014, Characteristics of a ridge-transform inside corner intersection and associated mafic-hosted seafloor hydrothermal field (14.0°S, Mid-Atlantic Ridge): Marine Geophysical Research, v. 35, p. 55–68.

Lisitsyn, A.P., Malahoff, A.R., Bogdanov, Y.A., Soakai, S., Zonenshayn, L.P., Gurvich, Y.G., Murav'yev, K.G., and Ivanov, G.V., 1992, Hydrothermal formations in the northern part of the Lau basin, Pacific Ocean: International Geology Review, v. 34, p. 828–847.

Lisitsyn, A.P., Crook, K.A.W., Bogdanov, Y.A., Zonenshayn, L.P., Murav'yev, K.G., Tufar, W., Gurvich, Y.G., Gordeyev, V.V., and Ivanov, G.V., 1993, A hydrothermal field in the rift zone of the Manus basin, Bismarck Sea: International Geology Review, v. 35, p. 105–126.

Lonsdale, P., 1977, Clustering of suspension-feeding macrobenthos near abyssal hydrothermal vents at oceanic spreading centers: Deep-Sea Research, v. 24, p. 857–863.

Lüders, V., Pracejus, B., and Halbach, P., 2001, Fluid inclusion and sulfur isotope studies in probable modern analogue Kuroko-type ores from the JADE hydrothermal field (central Okinawa trough, Japan): Chemical Geology, v. 173, p. 45–58.

Lupton, J., Butterfield, D., Lilley, M., Ishibashi, J., Hey, D., and Evans, L., 1999, Gas chemistry of hydrothermal fluids along the East Pacific Rise, 5°S to 32°S [abs.]: American Geophysical Union Fall Meeting, San Francisco, California, 1999, V12D-13.

Macdonald, K.C., Becker, K., Spiess, F.N., and Ballard, R.D., 1980, Hydrothermal heat flux of the "black smoker" vents on the East Pacific Rise: Earth and Planetary Science Letters, v. 48, p. 1–7.

Macdonald, K.C., Haymon, R.M., Miller, S.P., Sempere, J.C., and Fox, P.J., 1988, Deep-tow and sea beam studies of dueling propagating ridges on the East Pacific Rise near 20°40'S: Journal of Geophysical Research, v. 93, p. 2,875–2,898.

Maher, K.A., and Stevenson, D.J., 1988, Impact frustration of the origin of life: Nature, v. 331, p. 612–614.

Makovicky, E., Topa, D., Tajeddin, H., Putz, H., and Zagler, G., 2013, Ferdowsiite: A new mineral from the Barika ore deposit, Iran: Canadian Mineralogist, v. 51, p. 727–737.

Malahoff, A., and Falloon, T., 1991, Cruise report R/V Akademik Mstislav Keldysh/MIR cruise 21 Leg 2: Preliminary report of the Lau basin leg, Honiara, Solomon Islands, April 29, 1990, Nuku'alofa, Tonga, May 21, 1990, SOPAC Cruise Report 137: Suva: South Pacific Applied Geoscience Commission, 27 p.

Marchig, V., 1989, Cruise report R/V Sonne cruise SO-62: GEOMETEP 5, Callao, Peru, April 4, 1989, Valparaiso, Chile, July 2, 1989: Hannover, Germany, Federal Institute for Geosciences and Natural Resources, 390 p.
Marchig, V., Gundlach, H., and the Shipboard Scientific Part, 1987, Ore formation at rapidly diverging plate margins: Results of cruise GEOMETEP 4: Bundesanstalt für Geowissenschaften und Rohstoffe Circular, v. 4, p. 3–22.
Marchig, V., Blum, N., and Roonwal, G., 1997, Massive sulfide chimneys from the East Pacific Rise at 7°24'S and 16°43'S: Marine Georesources and Geotechnology, v. 15, p. 49–66.
Marcon, Y., Sahling, H., Borowski, C., dos Santos Ferreira, C., Thal, J., and Bohrmann, G., 2013, Megafaunal distribution and assessment of total methane and sulfide consumption by mussel beds at Menez Gwen hydrothermal vent, based on geo-referenced photomosaics: Deep-Sea Research I, v. 75, p. 93–109.
Marcoux, E., Moëlo, Y., and Leistel, J.M., 1996, Bismuth and cobalt minerals as indicators of stringer zones to massive sulphide deposits, Iberian Pyrite Belt: Mineralium Deposita, v. 31, p. 1–26.
Marques, A.F.A., Barriga, F., Chavagnac, V., and Fouquet, Y., 2006, Mineralogy, geochemistry, and Nd isotope composition of the Rainbow hydrothermal field, Mid-Atlantic Ridge: Mineralium Deposita, v. 41, p. 52–67.
Marques, A.F.A., Barriga, F.J.A.S., and Scott, S.D., 2007, Sulfide mineralization in an ultramafic-rock hosted seafloor hydrothermal system: From serpentinization to the formation of Cu-Zn-(Co)-rich massive sulfides: Marine Geology, v. 245, p. 20–39.
Marshall, B., and Gilligan, L.B., 1987, An introduction to remobilization: Information from ore-body geometry and experimental considerations: Ore Geology Reviews, v. 2, p. 87–131.
——1993, Remobilization, syn-tectonic processes and massive sulphide deposits: Ore Geology Reviews, v. 8, p. 39–64.
Martin, W., Baross, J., Kelley, D., and Russell, M.J., 2008, Hydrothermal vents and the origin of life: Nature Reviews, v. 6, p. 805–814.
Martinez, F., and Taylor, B., 1996, Backarc spreading, rifting, and microplate rotation, between transform faults in the Manus basin: Marine Geophysical Researches, v. 18, p. 203–224.
Marumo, K., Urabe, T., Goto, A., Takano, Y., and Nakaseama, M., 2008, Mineralogy and isotope geochemistry of active submarine hydrothermal field at Suiyo Seamount, Izu-Bonin arc, West Pacific Ocean: Resource Geology, v. 58, p. 220–248.
Maslennikov, V.V., Maslennikova, S.P., Large, R.R., and Danyushevsky, L.V., 2009, Study of trace element zonation in vent chimneys from the Silurian Yaman-Kasy volcanic-hosted massive sulfide deposit (southern Urals, Russia) using laser ablation-inductively coupled plasma mass spectrometry (LA-ICPMS): Economic Geology, v. 104, p. 1,111–1,141.
Maslennikov, V.V., Maslennikova, S.P., Large, R.R., Danyushevsky, L.V., Herrington, R.J., and Stanley, C.J., 2013, Tellurium-bearing minerals in zoned sulfide chimneys from Cu-Zn massive sulfide deposits of the Urals, Russia: Mineralogy and Petrology, v. 107, p. 67–99.
Matsumoto, T., Kinoshita, M., Nakamura, M., Sibuet, J.C., Lee, C.S., Hsu, S.K., Oomori, T., Shinjo, R., Hashimoto, Y., Hosoya, S., Imamura, M., Ito, M., Tukuda, K., Yagi, H., Tatekawa, K., Kagaya, I., Hokakubo, S., Okada, T., and Kimura, M., 2001, Volcanic and hydrothermal activities and possible "segmentation" of the axial rifting in the westernmost part of the Okinawa trough—preliminary results from the YOKOSUKA/SHINKAI 6500 Lequios Cruise: JAMSTEC Journal of Deep Sea Research, v. 19, p. 95–107.
McCaig, A.M., Cliff, R.A., Escartin, J., Fallick, A.E., and MacLeod, C.J., 2007, Oceanic detachment faults focus very large volumes of black smoker fluids: Geology, v. 35, p. 935–938.
McConachy, T.F., Ballard, R.D., Mottl, M.J., and Von Herzen, R.P., 1986, Geologic form and setting of a hydrothermal vent field at lat 10°56'N, East Pacific Rise: A detailed study using Angus and Alvin: Geology, v. 14, p. 295–298.
McCutcheon, S.R., 1992, Base-metal deposits of the Bathurst-Newcastle district: Characteristics and depositional models: Exploration and Mining Geology, v. 1, p. 105–119.
McKay, W.J., and Hazeldene, R.K., 1987, Woodlawn Zn-Pb-Cu sulfide deposit, New South Wales, Australia: An interpretation of ore formation from field observations and metal zoning: Economic Geology, v. 82, p. 141–164.
McPhie, J., and Allen, R.L., 1992, Facies architecture of mineralized submarine volcanic sequences: Cambrian Mount Read Volcanics, western Tasmania: Economic Geology, v. 87, p. 587–596.
Melchert, B., Devey, C.W., German, C.R., Lackschewitz, K.S., Seifert, R., Walter, M., Mertens, C., Yoerger, D.R., Baker, E.T., Paulick, H., and Nakamura, K., 2008, First evidence for high-temperature off-axis venting of deep crustal/mantle heat: The Nibelungen hydrothermal field, southern Mid-Atlantic Ridge: Earth and Planetary Science Letters, v. 275, p. 61–69.
Melekestseva, I.Y., 2010, Sulfur isotopic composition of massive sulfides from the Semenov hydrothermal cluster, 13°31'N, MAR [abs.]: Minerals of the Ocean-5 and Deep-Sea Minerals and Mining-2 Joint International Conference, St. Petersburg, Russia, 2010, Abstract Volume, p. 70–73.
Melekestseva, I.Y., Kotlyarov, V.A., Khvorov, P.V., Ivanov, V.N., Beltenev, V.E., and Dobretsova, I.G., 2010, Noble-metal mineralization in the Semenov-2 hydrothermal field (13°31'N), Mid-Atlantic Ridge: Geology of Ore Deposits, v. 52, p. 800–810.
Melekestseva, I.Y., Beltenev, V.E., and Ivanov, V.N., 2014a, Peterburgskoe and Irinovskoe hydrothermal fields, MAR: A diversity of massive sulfides and mineralized rocks [abs.]: Minerals of the Ocean-7 and Deep-Sea Minerals and Mining-4, St. Petersburg, Russia, 2014, Abstract Volume, p. 65–67.
Melekestseva, I.Y., Tret'yakov, G.A., Nimis, P., Yuminov, A.M., Maslennikov, V.V., Maslennikova, S.P., Kotlyarov, V.A., Beltenev, V.E., Danyushevsky, L.V., and Large, R., 2014b, Barite-rich massive sulfides from the Semenov-1 hydrothermal field (Mid-Atlantic Ridge, 13°30.87'N): Evidence for phase separation and magmatic input: Marine Geology, v. 349, p. 37–54.
Mercier-Langevin, P., Dubé, B., Hannington, M.D., Davis, D.W., Lafrance, B., and Gosselin, G., 2007a, The LaRonde Penna Au-rich volcanogenic massive sulfide deposit, Abitibi greenstone belt, Quebec: Part I. Geology and geochronology: Economic Geology, v. 102, p. 585–609.
Mercier-Langevin, P., Dubé, B., Hannington, M.D., Richer-Laflèche, M., and Gosselin, G., 2007b, The LaRonde Penna Au-rich volcanogenic massive sulfide deposit, Abitibi greenstone belt, Quebec: Part II. Lithogeochemistry and paleotectonic setting: Economic Geology, v. 102, p. 611–631.
Mercier-Langevin, P., Hannington, M.D., Dubé, B., and Bécu, V., 2011, The gold content of volcanogenic massive sulfide deposits: Mineralium Deposita, v. 46, p. 509–539.
Merle, S., 2008, Cruise report R/V Thompson cruise TN227: Northeast Lau basin, Apia, Western Samoa, November 13, 2008, Apia, Western Samoa, November 28, 2008: Newport, Pacific Marine Environmental Laboratory, National Oceanic and Atmospheric Administration, 34 p.
——2009, Cruise report R/V Thompson cruise TN234: Northeast Lau basin response cruise, Apia, Western Samoa, May 5, 2009, Apia, Western Samoa, May 13, 2009: Newport, Pacific Marine Environmental Laboratory, National Oceanic and Atmospheric Administration, 242 p.
——2011, Cruise report R/V Atlantis cruise AT18-08: Endeavour Segment and Axial Seamount, Juan de Fuca Ridge (NeMO 2011), Astoria, Oregon, July 19, 2011, Astoria, Oregon, August 1, 2011: Newport, Pacific Marine Environmental Laboratory, National Oceanic and Atmospheric Administration, 247 p.
——2012, Cruise report R/V Roger Revellle cruise RR1211: Submarine Ring of Fire - Northeast Lau basin (SroF-12), Suva, Fiji, September 9, Apia, Samoa, September 25, 2012: Newport, Pacific Marine Environmental Laboratory, National Oceanic and Atmospheric Administration, 260 p.
Merle, S., Ristau, S., Embley, R.W., and Chadwick, W., 2004, Cruise report R/V Thomas G. Thompson cruise TN167: Submarine Ring of Fire-Mariana arc submarine volcanoes, Apra, Guam, March 27, 2004, Yokahama, Japan, April 17, 2004: Newport, Pacific Marine Environmental Laboratory, National Oceanic and Atmospheric Administration, 274 p.
Merle, S., Embley, R.W., and Chadwick, W., 2005, Cruise report R/V Ka'imikai-o-Kanaloa cruises KoK05-05 and KoK05-06: New Zealand American Submarine Ring of Fire-Kermadec arc submarine volcanoes, Pago Pago, American Samoa, April 3, 2005, Tauranga, New Zealand, May 10, 2005: Newport, Pacific Marine Environmental Laboratory, National Oceanic and Atmospheric Administration, 125 p.
——2006, Cruise report R/V Melville cruise MGLN02MV: Submarine Ring of Fire-Mariana arc submarine volcanoes, Apra, Guam, April 18, 2006, Yokahama, Japan, May 13, 2006: Newport, Pacific Marine Environmental Laboratory, National Oceanic and Atmospheric Administration, 234 p.
Metz, S., and Trefry, J.H., 2000, Chemical and mineralogical influences on concentrations of trace metals in hydrothermal fluids: Geochimica et Cosmochimica Acta, v. 64, p. 2,267–2,279.
Miller, D.J., 1998, Geochemical analyses of massive sulfide and sediment samples from the TAG hydrothermal mound: Proceedings of the Ocean Drilling Program, Scientific Results, v. 158, p. 41–46.
Miller, J.W., and Craig, J.R., 1997, Ore minerals of the Cofer volcanogenic massive sulfide deposit, Louisa County, Virginia: Canadian Mineralogist, v. 35, p. 1,465–1,483.

Mills, R.A., and Elderfield, H., 1995, Rare earth elements geochemistry of hydrothermal deposits from the active TAG Mound, 26°N Mid-Atlantic Ridge: Geochimica et Cosmochimica Acta, v. 59, p. 3,511–3,524.

Mills, R.A., Teagle, D.A.H., and Tivey, M.K., 1998, Fluid mixing and anhydrite precipitation within the TAG mound: Proceedings of the Ocean Drilling Program, Scientific Results, v. 158, p. 119–127.

Möller, P., Dieterle, M.A., Dulski, P., Germann, K., Schneider, H.J., and Schütz, W., 1983, Geochemical proximity indicators of massive sulphide mineralization in the Iberian Pyrite Belt and the East Pontic Metallotect: Mineralium Deposita, v. 18, p. 387–398.

Monecke, T., and Mercier-Langevin, P., 2014, Gold in the massive sulfide environment: A comparison of ancient and modern seafloor hydrothermal systems [ext. abs.]: Quadrennial International Association on the Genesis of Ore Deposits Symposium, 14th, Kunming, China, 2014, Acta Geologica Sinica, v. 88, suppl. 2, p. 190–191.

Monecke, T., Giorgetti, G., Scholtysek, O., Kleeberg, R., Götze, J., Hannington, M.D., and Petersen, S., 2007, Textural and mineralogical changes associated with the incipient hydrothermal alteration of glassy dacite at the submarine Pacmanus hydrothermal system, eastern Manus basin: Journal of Volcanology and Geothermal Research, v. 160, p. 23–41.

Monecke, T., Gibson, H., Dubé, B., Laurin, J., Hannington, M.D., and Martin, L., 2008, Geology and volcanic setting of the Horne deposit, Rouyn-Noranda, Quebec: Initial results of a new research project: Geological Survey of Canada Current Research 2008-9, 16 p.

Monecke, T., Petersen, S., Lackschewitz, K., Hügler, M., Hannington, M.D., and Gemmell, J.B., 2009, Shallow submarine hydrothermal systems in the Aeolian volcanic arc: EOS Transaction American Geophysical Union, v. 90, p. 110–111.

Monecke, T., Petersen, S., and Hannington, M.D., 2014, Constraints on water depth of massive sulfide formation: Evidence from modern seafloor hydrothermal systems in arc-related settings: Economic Geology, v. 109, p. 2,079–2,101.

Mortensen, J.K., Gemmell, J.B., McNeill, A.W., and Friedman, R.M., 2015, High-precision U-Pb zircon chronostratigraphy of the Mount Read Volcanic belt in western Tasmania, Australia: Implications for VHMS deposit formation: Economic Geology, v. 110, p. 445–468.

Mortlock, R.A., Froelich, P.N., Feely, R.A., Massoth, G.J., Butterfield, D.A., and Lupton, J.E., 1993, Silica and germanium in Pacific Ocean hydrothermal vents and plumes: Earth and Planetary Science Letters, v. 119, p. 365–378.

Mosier, D.L., Singer, D.A., and Salem, B.B., 1983, Geologic and grade-tonnage information on volcanic-hosted copper-zinc-lead massive sulfide deposits: U.S. Geological Survey Open-File Report 83-89, 78 p.

Moss, R., 2000, Geochemistry and mineralogy of gold in the Pacmanus and SuSu knolls hydrothermal systems, eastern Manus basin, Papua New Guinea: Ph.D. thesis, Toronto, University of Toronto, 219 p.

Moss, R., and Scott, S.D., 1996, Silver in sulfide chimneys and mounds from 13°N and 21°N, East Pacific Rise: Canadian Mineralogist, v. 34, p. 697–716.

——2001, Geochemistry and mineralogy of gold-rich hydrothermal precipitates from the eastern Manus basin, Papua New Guinea: Canadian Mineralogist, v. 39, p. 957–978.

Mottl, M.J., Seewald, J.S., Wheat, C.G., Tivey, M.K., Michael, P.J., Proskurowski, G., McCollom, T.M., Reeves, E., Sharkey, J., You, C.F., Chan, L.H., and Pichler, T., 2011, Chemistry of hot springs along the Eastern Lau spreading center: Geochimica et Cosmochimica Acta, v. 75, p. 1,013–1,038.

Mozgova, N.N., Nenasheva, S.N., Borodaev, Y.S., and Yudovskaya, M.A., 1994, Nuffieldite from the Maleevskoe massive sulfide deposit, Russia: Canadian Mineralogist, v. 32, p. 359–364.

Mozgova, N.N, Krasnov, S.G., Batuyev, B.N., Borodaev, Y.S., Efimov, A.V., Markov, V.F., and Stepanova, T.V., 1996, The first report of cobalt pentlandite from a Mid-Atlantic Ridge hydrothermal deposit: Canadian Mineralogist, v. 34, p. 23–28.

Mozgova, N.N., Krasnov, S.G., Borodaev, Y.S., Stepanova, T.V., Cherkashev, G.A., Lalou, C., and Samovarov, M.S., 1998, The structure, mineral associations, and noble metals of the Mir oceanic ore mound, the TAG hydrothermal field (Mid-Atlantic Ridge, 26°N latitude): Geology of Ore Deposits, v. 40, p. 228–249.

Mozgova, N.N., Efimov, A.V., Borodaev, Y.S., Krasnov, S.G., Cherkashov, G.A., Stepanova, T.V., and Ashadze, A.M., 1999, Mineralogy and chemistry of massive sulfides from the Logatchev hydrothermal field (14°45'N Mid-Atlantic Ridge): Exploration and Mining Geology, v. 8, p. 379–395.

Mozgova, N.N., Borodaev, Y.S., Gablina, I.F., Cherkashev, G.A., and Stepanova, T.V., 2005, Mineral assemblages as indicators of the maturity of oceanic hydrothermal sulfide mounds: Lithology and Mineral Resources, v. 40, p. 293–319.

Mozgova, N.N., Trubkin, N.V., Borodaev, Y.S., Cherkashev, G.A., Stepanova, T.V., Semkova, T.A., and Uspenskaya, T.Y., 2008, Mineralogy of massive sulfides from the Ashadze hydrothermal field, 13°N, Mid-Atlantic Ridge: Canadian Mineralogist, v. 46, p. 545–567.

Münch, U., Blum, N., and Halbach, P., 1999, Mineralogical and geochemical features of sulfide chimneys from the MESO zone, Central Indian Ridge: Chemical Geology, v. 155, p. 29–44.

Münch, U., Halbach, P., Fujimoto, H., and Shipboard Scientific Party INDOYO Diving Cruise (MODE198 Leg 3), 2000, Sea-floor hydrothermal mineralization from the Mt. Jourdanne, Southwest Indian Ridge: JAMSTEC Journal of Deep Sea Research, v. 16, p. 125–132.

Münch, U., Lalou, C., Halbach, P., and Fujimoto, H., 2001, Relict hydrothermal events along the super-slow Southwest Indian spreading ridge near 63°56'E—mineralogy, chemistry and chronology of sulfide samples: Chemical Geology, v. 177, p. 341–349.

Murao, S., and Itoh, S., 1992, High thallium content in Kuroko-type ore: Journal of Geochemical Exploration, v. 43, p. 223–231.

Murphy, P.J., and Meyer, G., 1998, A gold-copper association in ultramafic-hosted hydrothermal sulfides from the mid-Atlantic Ridge: Economic Geology, v. 93, p. 1,076–1,083.

Nakamura, K., Marumo, K., and Aoki, M., 1990, Discovery of a black smoker vent and a pockmark emitting CO_2-rich fluid on the seafloor hydrothermal mineralization field at the Izena Cauldron in the Okinawa trough: Proceedings of JAMSTEC Symposium on Deep Sea Research, v. 6, p. 33–50.

Nakamura, K., Watanabe, H., Miyazaki, J., Takai, K., Kawagucci, S., Noguchi, T., Nemoto, S., Watsuji, T., Matsuzaki, T., Shibuya, T., Okamura, K., Mochizuki, M., Orihashi, Y., Ura, T., Asada, A., Marie, D., Koonjul, M., Singh, M., Beedessee, G., Bhikajee, M., and Tamaki, K., 2012, Discovery of new hydrothermal activity and chemosynthetic fauna on the Central Indian Ridge at 18°–20°S: PloS ONE, v. 7, doi: 10.1371/journal.pone.0032965.

Nakamura, K., Toki, T., Mochizuki, N., Asada, M., Ishibashi, J., Nogi, Y., Yoshikawa S., Miyazaki, J., and Okino, K., 2013, Discovery of a new hydrothermal vent based on an underwater, high-resolution geophysical survey: Deep-Sea Research I, v. 74, p. 1–10.

Nakashima, K., Sakai, H., Yoshida, H., Chiba, H., Tanaka, Y., Gamo, T., Ishibashi, J., and Tsunogai, U., 1993, Mineralogical and fluid inclusion studies on some hydrothermal deposits at the Iheya Ridge and Minami-Ensei knoll, Okinawa trough: Report of research dive 621 and hydrothermal precipitates collected by dives 487 and 622 of "Shinkai 2000": Proceedings of JAMSTEC Symposium on Deep Sea Research, v. 9, p. 253–269.

——1995, Hydrothermal mineralization in the Mid-Okinawa trough, *in* Sakai, H., and Nozaki, Y., eds., Biogeochemical processes and ocean flux in the Western Pacific: Tokyo, Terra Scientific Publishing, p. 487–508.

Nedachi, M., Ueno, H., Ossaka, J., Nogami, K., Hashimoto, J., Fujikura, K., and Miura, T., 1992, Hydrothermal ore deposits on the Minami-Ensei knoll of the Okinawa trough—mineral assemblages: Proceedings of JAMSTEC Symposium on Deep Sea Research, v. 8, p. 95–106.

Noguchi, T., Oomori, T., Tanahara, A., Taira, N., Takada, J., and Taira, H., 2007, Chemical composition of hydrothermal ores from Mid-Okinawa trough and Suiyo Seamount determined by neutron activation analysis: Geochemical Journal, v. 41, p. 141–148.

Noguchi, T., Shinjo, R., Ito, M., Takada, J., and Oomori, T., 2011, Barite geochemistry from hydrothermal chimneys of the Okinawa trough: Insight into chimney formation and fluid/sediment interaction: Journal of Mineralogical and Petrological Sciences, v. 106, p. 26–35.

Normark, W.R., Morton, J.L., Koski, R.A., Clague, D.A., and Delaney, J.R., 1983, Active hydrothermal vents and sulfide deposits on the southern Juan de Fuca Ridge: Geology, v. 11, p. 158–163.

Normark, W.R., Morton, J.L., Bischoff, J.L., Brett, R., Holcomb, R.T., Kappel, E.S., Koski, R.A., Ross, S.L., Shanks, W.C., III, Slack, J.F., Von Damm, K.L., and Zierenberg, R.A., 1986, Submarine fissure eruptions and hydrothermal vents on the southern Juan de Fuca Ridge: Preliminary observations from the submersible Alvin: Geology, v. 14, p. 823–827.

Normark, W.R., Morton, J.L., and Ross, S.L., 1987, Submersible observations along the southern Juan de Fuca Ridge: 1984 Alvin program: Journal of Geophysical Research, v. 92, p. 11,283–11,290.

Novoselov, K.A., Belogub, E.V., Zaykov, V.V., and Yakovleva, V.A., 2006, Silver sulfotellurides from volcanic-hosted massive sulfide deposits in the southern Urals: Mineralogy and Petrology, v. 87, p. 327–349.

Nozaki, T., Kato, Y., and Suzuki, K., 2010, Re-Os geochronology of the Iimori Besshi-type massive sulfide deposit in the Sanbagawa metamorphic belt, Japan: Geochimica et Cosmochimica Acta, v. 74, p. 4,322–4,331.

Nygård, T.E., Bjerkgård, T., Kelly, D., Thorseth, I., and Pedersen, R.B., 2003, Hydrothermal chimneys and sulphide mineralised breccias from the Kolbeinsey and the Mohns Ridge [abs.]: EGS-AGU-EUG Joint Assembly, Nice, France, 2003, 11,863.

Nysten, P., 1986, Gold in the volcanogenic mercury-rich sulfide deposit Långsele, Skellefte ore district, northern Sweden: Mineralium Deposita, v. 21, p. 116–120.

Ohmoto, H., 1983, Geologic setting of the Kuroko deposits, Japan: Part I. Geologic history of the Green tuff region: Economic Geology Monograph 5, p. 9–24.

——1996, Formation of volcanogenic massive sulfide deposits: The Kuroko perspective: Ore Geology Reviews, v. 10, p. 135–177.

Ohmoto, H., and Takahashi, T., 1983, Geologic setting of the Kuroko deposits, Japan: Part III. Submarine calderas and Kuroko genesis: Economic Geology Monograph 5, p. 39–54.

Okamoto, K., Ishibashi, J., Motomura, Y., Yamanaka, T., and Fujikura, K., 2002, Mineralogical studies of hydrothermal deposits collected from the Dai-Yon Yonaguni knoll and the Hatoma knoll in the Okinawa trough: JAMSTEC Journal of Deep Sea Research, v. 21, p. 75–82.

Ondréas, H., Cannat, M., Fouquet, Y., Normand, A., Sarradin, P.M., and Sarrazin, J., 2009, Recent volcanic events and the distribution of hydrothermal venting at the Lucky Strike hydrothermal field, Mid-Atlantic Ridge: Geochemistry Geophysics Geosystems, v. 10, doi: 10.1029/2008GC002171.

Ondréas, H., Cannat, M., Fouquet, Y., and Normand, A., 2012, Geological context and vents morphology of the ultramafic-hosted Ashadze hydrothermal areas (Mid-Atlantic Ridge 13°N): Geochemistry Geophysics Geosystems, v. 13, doi: 10.1029/2012GC004433.

Özgür, N., 1993, Volcanogenic massive sulfide deposits in the East Pontic Metallotect, NE Turkey: Resource Geology Special Issue, v. 17, p. 180–185.

Pantin, H.M., and Wright, I.C., 1994, Submarine hydrothermal activity within the offshore Taupo volcanic zone, Bay of Plenty continental shelf, New Zealand: Continental Shelf Research, v. 14, p. 1,411–1,438.

Papunen, H., Kopperoinen, T., and Tuokko, I., 1989, The Taivaljärvi Ag-Zn deposit in the Archean greenstone belt, eastern Finland: Economic Geology, v. 84, p. 1,262–1,276.

Paradis, S., Jonasson, I.R., Le Cheminant, G.M., and Watkinson, D.H., 1988, Two zinc-rich chimneys from the Plume site, southern Juan de Fuca Ridge: Canadian Mineralogist, v. 26, p. 637–654.

Paropkari, A.L., Ray, D., Balaram, V., Prakash, L.S., Mirza, I.H., Satyanarayana, M., Rao, T.G., and Kaisary, S., 2010, Formation of hydrothermal deposits at Kings Triple Junction, northern Lau back-arc basin, SW Pacific: The geochemical perspectives: Journal of Asian Earth Sciences, v. 38, p. 121–130.

Pedersen, R., Kelley, D., Thorseth, I., Torsvik, T., Hamnes, G., Stensby, B., and Pedersen, L., 1999, ROV exploration of the Kolbeinsey Ridge: Preliminary results of the SUBMAR-99 cruise: InterRidge News, v. 8, p. 32–34.

Pedersen, R.B., Rapp, H.T., Thorseth, I.H., Lilley, M.D., Barriga, F.J.A.S., Baumberger, T., Flesland, K., Fonseca, R., Früh-Green, G.L., and Jorgensen, S.L., 2010a, Discovery of a black smoker vent field and vent fauna at the Arctic mid-ocean ridge: Nature Communications, v. 1, doi: 10.1038/ncomms1124.

Pedersen, R.B., Thorseth, I.H., Nygård, T.E., Lilley, M.D., and Kelley, D.S., 2010b, Hydrothermal activity at the Arctic mid-ocean ridges: Geophysical Monograph Series, v. 188, p. 67–89.

Perfit, M.R., Ridley, W.I., and Jonasson, I.R., 1999, Geologic, petrologic, and geochemical relationships between magmatism and massive sulfide mineralization along the Eastern Galapagos Spreading Center: Reviews in Economic Geology, v. 8, p. 75–100.

Pester, N.J., Rough, M., Ding, K., and Seyfried, W.E., Jr., 2011, A new Fe/Mn geothermometer for hydrothermal systems: Implications for high-salinity fluids at 13°N on the East Pacific Rise: Geochimica et Cosmochimica Acta, v. 75, p. 7,881–7,892.

Peter, J.M., and Scott, S.D., 1988, Mineralogy, composition, and fluid-inclusion microthermometry of seafloor hydrothermal deposits in the Southern trough of Guaymas basin, Gulf of California: Canadian Mineralogist, v. 26, p. 567–587.

Petersen, S., Herzig, P.M., and Hannington, M.D., 2000, Third dimension of a presently forming VMS deposit: TAG hydrothermal mound, Mid-Atlantic Ridge, 26°N: Mineralium Deposita, v. 35, p. 233–259.

Petersen, S., Herzig, P.M., Schwarz-Schampera, U., Hannington, M.D., and Jonasson, I.R., 2004, Hydrothermal precipitates associated with bimodal volcanism in the Central Bransfield Strait, Antarctica: Mineralium Deposita, v. 39, p. 358–379.

Petersen, S., Herzig, P.M., Kuhn, T., Franz, L., Hannington, M.D., Monecke, T., and Gemmell, J.B., 2005, Shallow drilling of seafloor hydrothermal systems using the BGS Rockdrill: Conical Seamount (New Ireland fore-arc) and Pacmanus (eastern Manus basin), Papua New Guinea: Marine Georesources and Geotechnology, v. 23, p. 175–193.

Petersen, S., Kuhn, K., Kuhn, T., Augustin, N., Hékinian, R., Franz, L., and Borowski, C., 2009, The geological setting of the ultramafic-hosted Logatchev hydrothermal field (14°45'N, Mid-Atlantic Ridge) and its influence on massive sulfide formation: Lithos, v. 112, p. 40–56.

Petersen, S., Monecke, T., Westhues, A., Hannington, M.D., Gemmell, J.B., Sharpe, R., Peters, M., Strauss, H., Lackschewitz, K., Augustin, N., Gibson, H., and Kleeberg, R., 2014, Drilling shallow-water massive sulfides at the Palinuro volcanic complex, Aeolian island arc, Italy: Economic Geology, v. 109, p. 2,129–2,158.

Pokrovski, G.S., Borisova, A.Y., Roux, J., Hazemann, J.L., Petdang, A., Tella, M., and Testemale, D., 2006, Antimony speciation in saline hydrothermal fluids: A combined X-ray absorption fine structure spectroscopy and solubility study: Geochimica et Cosmochimica Acta, v. 70, p. 4,196–4,214.

Pringle, G.J., and Thorpe, R.I., 1980, Bohdanowiczite, junoite and laitakarite from the Kidd Creek mine, Timmins, Ontario: Canadian Mineralogist, v. 18, p. 353–360.

Prokin, V.A., and Buslaev, F.P., 1999, Massive copper-zinc sulphide deposits in the Urals: Ore Geology Reviews, v. 14, p. 1–69.

Pshenichnyy, G.N., Shaldun, T.N., Vyal'sov, L.N., and Tsepin, A.I., 1975, First find of germanium-bearing colusite: Transactions (Doklady) of the U.S.S.R. Academy of Sciences, Earth Science Sections, v. 221, p. 140–143.

Reeves, E.P., Seewald, J.S., Saccocia, P., Bach, W., Craddock, P.R., Shanks, W.C., Sylva, S.P., Walsh, E., Pichler, T., and Rosner, M., 2011, Geochemistry of hydrothermal fluids from the Pacmanus, Northeast Pual and Vienna Woods hydrothermal fields, Manus basin, Papua New Guinea: Geochimica et Cosmochimica Acta, v. 75, p. 1,088–1,123.

Ritts, A., 2012, Texture and composition of pyrite contained in the mudstone host of the Eskay Creek sulfide and sulfosalt deposit, British Columbia: M.Sc. thesis, Golden, Colorado, Colorado School of Mines, 185 p.

Rogers, A.D., 2010, Cruise report RRS James Cook cruise 42: Chemosynthetic ecosystems of the southern ocean (CHESSO), Punta Arenas, Chile, January 7, 2010, Montevideo, Uruguay, February 21, 2010: Southampton, England, School of Ocean and Earth Science, University of Southampton, 240 p.

Rogers, A.D., Tyler, P.A., Connelly, D.P., Copley, J.T., James, R., Larter, R.D., Linse, K., Mills, R.A., Naveira Garabato, A., Pancost, R.D., Pearce, D.A., Polunin, N.V.C., German, C.R., Shank, T., Boersch-Supan, P.H., Alker, B.J., Aquilina, A., Bennett, S.A., Clarke, A., Dinley, R.J.J., Graham, A.G.C., Green, D.R.H., Hawkes, J.A., Hepburn, L., Hilario, A., Huvenne, V.A.I., Marsh, L., Ramirez-Llodra, E., Reid, W.D.K., Roterman, C.N., Sweeting, C.J., Thatje, S., and Zwirglmaier, K., 2012, The discovery of new deep-sea hydrothermal vent communities in the Southern Ocean and implications for biogeography: PLoS Biology, v. 10, doi: 10.1371/journal.pbio.1001234.

Rona, P.A., 2003, Resources of the sea floor: Science, v. 299, p. 673–674.

Rona, P.A., Hannington, M.D., Raman, C.V., Thompson, G., Tivey, M.K., Humphris, S.E., Lalou, C., and Petersen, S., 1993, Active and relict seafloor hydrothermal mineralization at the TAG hydrothermal field, Mid-Atlantic Ridge: Economic Geology, v. 88, p. 1,989–2,017.

Rona, P.A., Petersen, S., Becker, K., Von Herzen, R.P., Hannington, M.D., Herzig, P.M., Naka, J., Lalou, C., and Thompson, G., 1996, Heat flow and mineralogy of TAG relict high-temperature hydrothermal zones: Mid-Atlantic Ridge 26°N, 45°W: Geophysical Research Letters, v. 23, p. 3,507–3,510.

Roscoe, S.M., 1965, Geochemical and isotopic studies, Noranda and Matagami areas: Canadian Institute of Mining and Metallurgy Transactions, v. 68, p. 279–285.

Roth, T., Thompson, J.F.H., and Barrett, T.J., 1999, The precious metal-rich Eskay Creek deposit, northwestern British Columbia: Reviews in Economic Geology, v. 8, p. 357–373.

Rouxel, O., Shanks, W.C., III, Bach, W., and Edwards, K.J., 2008, Integrated Fe- and S-isotope study of seafloor hydrothermal vents at East Pacific Rise 9-10°N: Chemical Geology, v. 252, p. 214–227.

Rubinovich-Kogan, R., 1988, Mineralogía y paragénesis del depósito de sulfuros masivos sinsedimentarios La Esmeralda, Estado de México: M.Sc. thesis, Mexico City, Mexico, Universidad Nacional Autónoma de México, 147 p.

Ryall, W.R., 1979, Mercury distribution in the Woodlawn massive sulfide deposit, New South Wales: Economic Geology, v. 74, p. 1,471–1,484.
Rytuba, J.J., 2003, Mercury from mineral deposits and potential environmental impact: Environmental Geology, v. 43, p. 326–338.
Sakai, H., Gamo, T., Kim, E.S., Shitashima, K., Yanagisawa, F., Tsutsumi, M., Ishibashi, J., Sano, Y., Wakita, H., Tanaka, T., Matsumoto, T., Naganuma, T., and Mitsuzawa, K., 1990a, Unique chemistry of the hydrothermal solution in the mid-Okinawa trough backarc basin: Geophysical Research Letters, v. 17, p. 2,133–2,136.
Sakai, H., Gamo, T., Kim, E.S., Tsutsumi, M., Tanaka, T., Ishibashi, J., Wakita, H., Yamano, M., and Oomori, T., 1990b, Venting of carbon dioxide-rich fluid and hydrate formation in mid-Okinawa trough backarc basin: Science, v. 248, p. 1,093–1,096.
Sangster, D.F., and Brook, W.A., 1977, Primitive lead in an Australian Zn-Pb-Ba deposit: Nature, v. 270, p. 423.
Schander, C., Rapp, H.T., Kongsrud, J.A., Bakken, T., Berge, J., Cochrane, S., Oug, E., Byrkjedal, I., Todt, C., Cedhagen, T., Fosshagen, A., Gebruk, A., Larsen, K., Levin, L., Obst, M., Pleijel, F., Stöhr, S., Warén, A., Mikkelsen, N.T., Hadler-Jacobsen, S., Keuning, R., Petersen, K.H., Thorseth, I.H., and Pedersen, R.B., 2010, The fauna of hydrothermal vents on the Mohn Ridge (North Atlantic): Marine Biology Research, v. 6, p. 155–171.
Schermerhorn, L.J.G., 1975, Spilites, regional metamorphism and subduction in the Iberian Pyrite Belt: Some comments: Geologie en Mijnbouw, v. 54, p. 23–35.
Schmidt, K., Garbe-Schönberg, D., Koschinsky, A., Strauss, H., Jost, C.L., Klevenz, V., and Königer, P., 2011, Fluid elemental and stable isotope composition of the Nibelungen hydrothermal field (8°18'S, Mid-Atlantic Ridge): Constraints on fluid–rock interaction in heterogeneous lithosphere: Chemical Geology, v. 280, p. 1–18.
Schwartz, M.O., 2000, Cadmium in zinc deposits: Economic geology of a polluting element: International Geology Review, v. 42, p. 445–469.
Schwarz-Schampera, U, 2000, Indium-tin association in volcanogenic massive sulfide deposits: Evidences from active seafloor hydrothermal systems and ancient massive sulfide deposits on land: Ph.D. thesis, Freiberg, Germany, TU Bergakademie Freiberg, 481 p.
Schwarz-Schampera, U., and Herzig, P.M., 2002, Indium—geology, mineralogy, and economics: Berlin, Springer, 257 p.
Schwarz-Schampera, U., Botz, R., Hannington, M., Adamson, R., Anger, V., Cormany, D., Evans, L., Gibson, H., Haase, K., Hirdes, W., Hocking, M., Juniper, K., Langley, S., Leybourne, M., Metaxas, A., Mills, R., Ostertag-Henning, C., Rauch, M., Rutkowski, J., Schmidt, M., Shepherd, K., Stevens, C., Tamburri, K., Tracey, D., and Westernstroer, U., 2007, Cruise report R/V Sonne cruise SO-192/2: Marine geoscientific research on input and output in the Tonga-Kermadec subduction zone, Auckland, New Zealand, April 26, 2006, Suva, Fiji, May 17 2007: Hannover, Germany, Federal Institute for Geosciences and Natural Resources, 92 p.
Scotney, P.M., Roberts, S., Herrington, R.J., Boyce, A.J., and Burgess, R., 2005, The development of volcanic hosted massive sulfide and barite-gold orebodies on Wetar Island, Indonesia: Mineralium Deposita, v. 40, p. 76–99.
Scott, S.D., 2001, Deep ocean mining: Geoscience Canada, v. 28, p. 87–96.
Seewald, J., McDermott, J.M., German, C.R., Sylva, S.P., Reeves, E.P., and Klein, F., 2012, Geochemistry of hydrothermal fluids from the ultra-slow spreading Mid-Cayman Rise [abs.]: American Geophysical Union Fall Meeting, San Francisco, California, 2012, OS22B-06.
Seward, T.M., and Barnes, H.L., 1997, Metal transport by hydrothermal ore fluids, *in* Barnes, H.L., ed., Geochemistry of hydrothermal ore deposits, 3rd ed.: New York, Wiley, p. 435–486.
Seward, T.M., Henderson, C.M.B., and Charnock, J.M., 2000, Indium(III) chloride complexing and solvation in hydrothermal solutions to 350°C: An EXAFS study: Chemical Geology, v. 167, p. 117–127.
Seward, T.M., Willams-Jones, A.E., and Migdisov, A.A., 2014, The chemistry of metal transport and deposition by ore-forming hydrothermal fluids: Treatise on Geochemistry, 2nd ed., v. 13, p. 29–57.
Seyfried, W.E., Jr., Seewald, J.S., Berndt, M.E., Ding, K., and Foustoukos, D.I., 2003, Chemistry of hydrothermal vent fluids from the Main Endeavour Field, northern Juan de Fuca Ridge: Geochemical controls in the aftermath of June 1999 seismic events: Journal of Geophysical Research, v. 108, doi: 10.1029/2002JB001957.
Seyfried, W.E., Jr., Pester, N.J., Ding, K., and Rough, M., 2011, Vent fluid chemistry of the Rainbow hydrothermal system (36°N, MAR): Phase equilibria and in situ pH controls on subseafloor alteration processes: Geochimica et Cosmochimica Acta, v. 75, p. 1,574–1,593.
Shadlun, T.N., Bortnikov, N.S., Bogdanov, Y.A., Tufar, W., Murav'yev, K.G., Gurvich, Y.G., Muravitskaya, G.N., Korina, Y.A., and Topa, T., 1993, Mineralogy, textures, and formation conditions of modern sulfide ores, Manus basin rift zone: International Geology Reviews, v. 35, p. 127–145.
Shalaby, I.M., Stumpfl, E., Helmy, H.M., El Mahallawi, M.M., and Kamel, O.A., 2004, Silver and silver-bearing minerals at the Um Samiuki volcanogenic massive sulphide deposit, Eastern Desert, Egypt: Mineralium Deposita, v. 39, p. 608–621.
Shank, T.M., Fornari, D.J., Wigham, B., Scheirer, D., Getsiv, J., Perfit, M., and Tolstoy, M., 2000, Biology of newly-discovered "AHA" hydrothermal vent fields near 1°44'N on the East Pacific Rise axis [abs.]: American Geophysical Union Fall Meeting, San Francisco, California, 2000, T51D-15.
Shanks, W.C., III, 2001, Stable isotopes in seafloor hydrothermal systems: Vent fluids, hydrothermal deposits, hydrothermal alteration, and microbial processes: Reviews in Mineralogy and Geochemistry, v. 43, p. 469–525.
Sharpe, R., and Gemmell, J.B., 2002, The Archean Cu-Zn magnetite-rich Gossan Hill volcanic-hosted massive sulfide deposit, Western Australia: Genesis of a multistage hydrothermal system: Economic Geology, v. 97, p. 517–539.
Sherlock, R.L., Roth, T., Spooner, E.T.C., and Bray, C.J., 1999, Origin of the Eskay Creek precious metal-rich volcanogenic massive sulfide deposit: Fluid inclusion and stable isotope evidence: Economic Geology, v. 94, p. 803–824.
Sherman, D.M., Ragnarsdottir, K.V., and Oelkers, E.H., 2000, Antimony transport in hydrothermal solutions: An EXAFS study of antimony(V) complexation in alkaline sulfide and sulfide-chloride brines at temperatures from 25°C to 300°C at P_{sat}: Chemical Geology, v. 167, p. 161–167.
Shilov, V., Cherkashev, G., Beltenev, V., Ivanov, V., Rozhdestvenskaya, I., Gablina, I., Dobretsova, I., Melekestseva, I., Narkevskiy, E., Gustaitis, A., and Kuznetsov, V., 2011, New hydrothermal field on the Mid-Atlantic Ridge: Interridge News, v. 20, p. 40–41.
Shimazaki, Y., 1974, Ore minerals of the Kuroko-type deposits: Mining Geology Special Issue, v. 6, p. 311–322.
Sigurdsson, H., Carey, S., Alexandri, M., Vougioukalakis, G., Croff, K., Roman, C., Sakellariou, D., Anagnostou, C., Rousakis, G., Ioakim, C., Gogou, A., Ballas, D., Misaridis, T., and Nomikou, P., 2006, Marine investigations of Greece's Santorini volcanic field: EOS Transactions of the American Geophysical Union, v. 87, p. 337, 342.
Singer, D.A., 2014, Base and precious metal resources in seafloor massive sulfide deposits: Ore Geology Reviews, v. 59, p. 66–72.
Skirrow, R.G., Huston, D.L., Mernagh, T.P., Thorne, J.P., Dulfer, H., and Senior, A.B., 2013, Critical commodities for a high-tech world: Australia's potential to supply global demand: Canberra, Geoscience Australia, 126 p.
Smith, R.N., and Huston, D.L., 1992, Distribution and association of selected trace elements at the Rosebery deposit, Tasmania: Economic Geology, v. 87, p. 706–719.
Smith, V.K., and Koski, R.A., 1994, Descriptive and chemical data for hydrothermal sulfide-sulfate-silica chimneys from the northern Cleft segment, Juan de Fuca Ridge: U.S. Geological Survey Open-File Report 94-15, 20 p.
Snow, J., Hellebrand, E., Jokat, W., and Mühe, R., 2001, Magmatic and hydrothermal activity in Lena trough, Arctic Ocean: EOS Transactions American Geophysical Union, v. 82, p. 193, 197–198.
Sohrin, Y., Isshiki, K., Nakayama, E., Kihara, S., and Matsui, M., 1989, Simultaneous determination of tungsten and molybdenum in sea water by catalytic current polarography after preconcentration on a resin column: Analytica Chimica Acta, v. 218, p. 25–35.
Soule, S.A., Ferrini, V.L., Kinsey, J.C., Fornari, D.J., Sellers, C., White, S.M., Von Damm, K., and Carbotte, S.M., 2008, Navigational infrastructure at the East Pacific Rise 9°50'N area following the 2005-2006 eruption: Seafloor benchmarks and near-bottom multibeam surveys: Geochemistry Geophysics Geosystems, v. 9, doi: 10.1029/2008GC002070.
Spiess, F.N., Macdonald, K.C., Atwater, T., Ballard, R., Carranza, A., Cordoba, D., Cox, C., Diaz Garcia, V.M., Francheteau, J., Guerrero, J., Hawkins, J., Haymon, R., Hessler, R., Juteau, T., Kastner, M., Larson, R., Luyendyk, B., Macdougall, J.D., Miller, S., Normark, W., Orcutt, J., and Rangin, C., 1980, East Pacific Rise: Hot springs and geophysical experiments: Science, v. 207, p. 1,421–1,433.
Spiridonov, E.M., Kachalovskaya, V.M., Kovachev, V.V., and Krapiva, L.Y., 1992, Germanocolusite $Cu_{26}V_2(Ge,As)_6S_{32}$—a new mineral: Moscow University Geology Bulletin, v. 47, p. 42–45.
Stoffers, P., Hannington, M., Wright, I., Herzig, P., de Ronde, C., Arpe, T., Battershill, C., Botz, R., Britten, K., Browne, P., Cheminée, J.L., Fricke, H.W., Garbe-Schönberg, D., Hekinian, R., Hissman, K., Huber, R.,

Robertson, J., Schauer, J., Schmitt, M., Scholten, J., Schwarz-Schampera, U., and Smith, I., 1999, Elemental mercury at submarine hydrothermal vents in the Bay of Plenty, Taupo volcanic zone, New Zealand: Geology, v. 27, p. 931–934.

Stoffers, P., Worthington, T., Petersen, S., Hannington, M., Türkay, M., Ackermand, D., Borowski, C., Dankert, S., Fretzdorff, S., Haase, K., Hekinian, R., Hoppe, A., Jonasson, I., Kuhn, T., Lancaster, R., Monecke, T., Renno, A., Stecher, J., and Weiershäuser, L., 2001, Cruise report R/V Sonne cruise SO-157: Magmatic and hydrothermal processes at a spreading axis influenced by a hotspot: The Pacific-Antarctic Ridge and off-axis seamounts near 37°S (Foundation 3), Valparaiso, Chile, June 15, 2001, Easter Island, Chile, July 14, 2001: Berichte des Institutes für Geowissenschaften an der Universität Kiel, Germany, v. 17, 132 p.

Stoffers, P., Worthington, T., Hekinian, R., Petersen, S., Hannington, M., Türkay, M., Ackermand, D., Borowski, C., Dankert, S., Fretzdorff, S., Haase, K., Hoppe, A., Jonasson, I., Kuhn, T., Lancaster, R., Monecke, T., Renno, A., Stecher, J., and Weiershäuser, L., 2002, Widespread silicic volcanism and hydrothermal activity on the northern Pacific-Antarctic Ridge: InterRidge News, v. 11, p. 30–32.

Stoffers, P., Worthington, T.J., Schwarz-Schampera, U., Hannington, M.D., Massoth, G.J., Hekinian, R., Schmidt, M., Lundsten, L.J., Evans, L.J., Vaiomo'unga, R., and Kerby, T., 2006, Submarine volcanoes and high-temperature hydrothermal venting on the Tonga arc, southwest Pacific: Geology, v. 34, p. 453–456.

Sudarikov, S.M., Ashadze, A.M., Stepanova, T.V., Neshcheretov, A.V., Vorob'yev, P.V., Kasabov, R.V., and Gutnikov, A.S., 1990, Hydrothermal activity and ore deposition in the rift valley of the Mid-Atlantic Ridge (new data): Transactions (Doklady) of the U.S.S.R. Academy of Sciences, Earth Science Sections, v. 311, p. 89–93.

Suzuki, R., Ishibashi, J., Nakaseama, M., Konno, U., Tsunogai, U., Gena, K., and Chiba, H., 2008, Diverse range of mineralization induced by phase separation of hydrothermal fluid: Case study of the Yonaguni knoll IV hydrothermal field in the Okinawa trough back-arc basin: Resource Geology, v. 58, p. 267–288.

Sweetman, A.K., Levin, L.A., Rapp, H.T., and Schander, C., 2013, Faunal trophic structure at hydrothermal vents on the southern Mohn's Ridge, Arctic Ocean: Marine Ecology Progress Series, v. 473, p. 115–131.

Syme, E.C., and Bailes, A.H., 1993, Stratigraphic and tectonic setting of Early Proterozoic volcanogenic massive sulfide deposits, Flin Flon, Manitoba: Economic Geology, v. 88, p. 566–589.

Takeuchi, T., Nambu, M., Suzuki, M., and Okada, K., 1956, Germanium bearing black ores from the Kamikita mine, Aomori Prefecture: Mining Geology, v. 6, p. 231–243.

Tanahashi, M., Fujioka, K., and Machida, S., 2008, Myojin rift, Izu-Bonin arc as the modern analog of Hokuroku basin, northeast Japan: Geotectonic significance of the new hydrothermal deposit in the back-arc rift: Resource Geology, v. 58, p. 301–312.

Tanaka, T., Mitsuzawa, K., and Hotta, H., 1989, "SHINKAI2000" diving surveys in the east of Iheya small ridge in the central Okinawa trough: Proceedings of JAMSTEC Symposium on Deep Sea Research, v. 5, p. 267–281.

Tanaka, T., Hotta, H., Sakai, H., Ishibashi, J., Oomori, T., Izawa, E., and Oda, N., 1990, Occurrence and distribution of the hydrothermal deposits in the Izena Hole, central Okinawa trough: Proceedings of JAMSTEC Symposium on Deep Sea Research, v. 6, p. 11–26.

Tanimura, S., Date, J., Takahashi, T., and Ohmoto, H., 1983, Geologic setting of the Kuroko deposits, Japan: Part II. Stratigraphy and structure of the Hokuroku district: Economic Geology Monograph 5, p. 24–38.

Tao, C., Wu, G., Ni, J., Zhao, H., Su, X., Zhou, N., Li, J., Chen, Y.J., Cui, R., Deng, X., Egorov, I., Dobretsova, I.G., Sun, G., Qiu, Z., Deng, X., Zhou, J., Gu, C., Li, J., Yang, J., Zhang, K., Wu, X., Chen, Z., Lei, J., Huang, W., Zhou, P., Ding, T., Jin, W., Li, H., and Lin, J., 2009, New hydrothermal fields found along the SWIR during the Legs 5-7 of the Chinese DY115-20 expedition [abs.]: American Geophysical Union Fall Meeting, San Francisco, California, 2009, OS21A-1150.

Tao, C.H., Li, H.M., Yang, Y.M., Yu, Ni, J.Y., Cui, R.Y., Chen, Y.S., Li, J.B., He, Y.H., Huang, W., Lei, J.J., Wang, Y.J., and DY115-21 Leg 4 Science Party, 2011a, Two hydrothermal fields found on the southern Mid-Atlantic Ridge: Science China Earth Sciences, v. 54, p. 1,302–1,303.

Tao, C., Li, H., Shao, Z., Bao, G., Su, X., Chen, J.Y., Deng, X., Qiu, Z., Zhang, K., Li, J., and COMRA' 22 Cruise Science Party, 2011b, Three new hydrothermal fields found at 13-14°S Mid-Atlantic Ridge: Interridge News, v. 20, p. 48.

Tao, C., Li, H., Wu, G., Su, X., Zhang, G., and Chinese DY115-21 Leg 3 Scientific Party, 2011c, First hydrothermal active vent discovered on the Galapagos microplate [abs.]: American Geophysical Union Fall Meeting, San Francisco, California, 2011, OS11B-1488.

Tao, C., Lin, J., Guo, S., Chen, Y.J., Wu, G., Han, X., German, C.R., Yoerger, D.R., Zhou, N., Li, H., Su, X., Zhu, J., and the DY115-19 (Legs 1-2) and DY115-20 (Leg 4-7) Science Parties, 2012, First active hydrothermal vents on an ultraslow-spreading center: Southwest Indian Ridge: Geology, v. 40, p. 47–50.

Tao, C., Wu, G., Deng, X., Qiu, Z., Han, C., and Long, Y., 2013, New discovery of seafloor hydrothermal activity on the Indian Ocean Carlsberg Ridge and southern North Atlantic Ridge—progress during the 26th Chinese COMRA cruise: Acta Oceanologica Sinica, v. 32, p. 85–88.

Thal, J., Tivey, M., Yoerger, D., Jöns, N., and Bach, W., 2014, Geologic setting of Pacmanus hydrothermal area—high resolution mapping and in situ observations: Marine Geology, v. 355, p. 98–114.

Thompson, G., Humphris, S.E., Schroeder, B., Sulanowska, M., and Rona, P.A., 1988, Active vents and massive sulfides at 26°N (TAG) and 23°N (Snakepit) on the Mid-Atlantic Ridge: Canadian Mineralogist, v. 26, p. 697–711.

Thorpe, R.I., and Harris, D.C., 1973, Mattagamite and tellurantimony, two new telluride minerals from Mattagami Lake mine, Matagami area, Quebec: Canadian Mineralogist, v. 12, p. 55–60.

Thorpe, R.I., Pringle, G.J., and Plant, A.G., 1976, Occurrence of selenide and sulphide minerals in bornite ore of the Kidd Creek massive sulphide deposit, Timmins, Ontario: Geological Survey of Canada Paper 76-1A, p. 311–317.

Tivey, M.K., and Delaney, J.R., 1986, Growth of large sulfide structures on the Endeavour Segment of the Juan de Fuca Ridge: Earth and Planetary Science Letters, v. 77, p. 303–317.

Tivey, M.K., Seewald, J., Wheat, C.G., Mottl, M., Reysenbach, A.L., and Kim, S., 2005, Cruise report R/V Melville/DSV cruise TUIM05MV: Lau basin vent characterization cruise, Nuku'alofa, Tonga, April 5, 2005, Nuku'alofa, Tonga, May 7, 2005: Woods Hole, MA, Woods Hole Oceanographic Institution, 115 p.

Tivey, M., Bach, W., Seewald, J., Tivey, M., and Vanko, D., 2006, Cruise report R/V Melville cruise MGLN06: Hydrothermal systems in the eastern Manus basin: Fluid chemistry and magnetic structure as guides to subseafloor processes, Rabaul, Papua New Guinea, July 21, 2006, Suva, Fiji, September 1, 2006: Woods Hole, MA, Woods Hole Oceanographic Institution, 132 p.

Tiwary, A., and Cook, N.J., 1999, Trace mineralogy of metamorphosed VMS deposits at Deri and Ambaji, South Delhi fold belt, India [ext. abs.]: Fifth biennial SGA meeting and tenth quadrennial IAGOD symposium, London, United Kingdom, 1999, Proceedings, p. 987–990.

Törmänen, T.O., and Koski, R.A., 2005, Gold enrichment and the Bi-Au association in pyrrhotite-rich massive sulfide deposits, Escanaba trough, southern Gorda Ridge: Economic Geology, v. 100, p. 1,135–1,150.

Tomkins, A.G., 2007, Three mechanisms of ore re-mobilisation during amphibolite facies metamorphism at the Montauban Zn-Pb-Au-Ag deposit: Mineralium Deposita, v. 42, p. 627–637.

Tooth, B., Etschmann, B., Pokrovski, G.S., Testemale, D., Hazemann, J.L., Grundler, P.V., and Brugger J., 2013, Bismuth speciation in hydrothermal fluids: An X-ray absorption spectroscopy and solubility study: Geochimica et Cosmochimica Acta, v. 101, p. 156–172.

Tornos, F., González Clavijo, E., and Spiro, B., 1998, The Filon Norte orebody (Tharsis, Iberian Pyrite Belt): A proximal low-temperature shale-hosted massive sulphide in a thin-skinned belt: Mineralium Deposita, v. 33, p. 150–169.

Tornos, F., Peter, J.M., Allen, R., and Conde, C., 2015, Controls on the siting and style of volcanogenic massive sulphide deposits: Ore Geology Reviews, v. 68, p. 142–163.

Torokhov, M.P., Cherkashev, G.A., Stepanova, T.V., and Zhirnov, E.A., 2002, Uranium, its minerals and paragenesis in massive sulphides of the Logatchev-2, MAR ore field: InterRidge News, v. 11, p. 32–33.

Torró, L., Proenza, J.A., Melgarejo, J.C., Alfonso, P., Farré de Pablo, J., Colomer, J.M., García-Casco, A., Gubern, A., Gallardo, E., Cazanas, X., Chávez, C., Del Carpio, R., León, P., Nelson, C.E., and Lewis, J.F., 2016, Mineralogy, geochemistry and sulfur isotope characterization of Cerro de Maimón (Dominican Republic), San Fernando and Antonio (Cuba) lower Cretaceous VMS deposits: Formation during subduction initiation of the proto-Caribbean lithosphere within a fore-arc: Ore Geology Reviews, v. 72, p. 794–817.

Tourigny, G., Brown, A.C., Hubert, C., and Crépeau, R., 1989, Synvolcanic and syntectonic gold mineralization at the Bousquet mine, Abitibi greenstone belt, Quebec: Economic Geology, v. 84, p. 1,875–1,890.
Tourigny, G., Doucet, D., and Bourget, A., 1993, Geology of the Bousquet 2 mine: An example of a deformed, gold-bearing, polymetallic sulfide deposit: Economic Geology, v. 88, p. 1,578–1,597.
Trefry, J.H., Butterfield, D.B., Metz, S., Massoth, G.J., Trocine, R.P., and Feely, R.A., 1994, Trace metals in hydrothermal solutions from Cleft segment on the southern Juan de Fuca Ridge: Journal of Geophysical Research, v. 99, p. 4,925–4,935.
Trepka-Bloch, C., 1985, Cyclic ore formation of some volcanogenic massive sulfide deposits in the Skellefte district, Sweden: Mineralium Deposita, v. 20, p. 23–29.
——1989, Volcanogenic and tectonic features of the Rakkejaur sulfide deposit, Skellefte district, Sweden: Mineralium Deposita, v. 24, p. 279–288.
Tufar, W., 1990, Modern hydrothermal activity, formation of complex massive sulfide deposits and associated vent communities in the Manus back-arc basin (Bismarck Sea, Papua New Guinea): Mitteilungen der Österreichischen Geologischen Gesellschaft, v. 82, p. 183–210.
——1991, Paragenesis of complex massive sulfide ores from the Tyrrhenian Sea: Mitteilungen der Österreichischen Geologischen Gesellschaft, v. 84, p. 265–300.
Tufar, W., Gundlach, H., and Marchig, V., 1984, Zur Erzparagenese rezenter Sulfid-Vorkommen aus dem südlichen Pazifik: Mitteilungen der Österreichischen Geologischen Gesellschaft, v. 77, p. 185–245.
Tunnicliffe, V., Botros, M., de Burgh, M.E., Dinet, A., Johnson, H.P., Juniper, S.K., and McDuff, R.E., 1986, Hydrothermal vents of Explorer Ridge, northeast Pacific: Deep-Sea Research, v. 33, p. 401–412.
Ueno, H., Hamasaki, H., Murakawa, Y., Kitazono, S., and Takeda, T., 2003, Ore and gangue minerals of sulfide chimneys from the North knoll, Iheya Ridge, Okinawa trough, Japan: JAMSTEC Journal of Deep Sea Research, v. 22, p. 49–62.
Urabe, T., 1989, Mineralogical characteristics of the hydrothermal ore body at Izena Hole No. 1 in comparison with Kuroko deposits: Proceedings of JAMSTEC Symposium on Deep Sea Research, v. 5, p. 191–196.
Urabe, T., and Sato, T., 1978, Kuroko deposits of the Kosaka mine, northeast Honshu, Japan–Products of submarine hot springs on Miocene sea floor: Economic Geology, v. 73, p. 161–179.
Van Dover, C.L., 2011, Tighten regulations on deep-sea mining: Nature, v. 470, p. 31–33.
Van Dover, C.L., Humphris, S.E., Fornari, D., Cavanaugh, C.M., Collier, R., Goffredi, S.K., Hashimoto, J., Lilley, M.D., Reysenbach, A.L., Shank, T.M., Von Damm, K.L., Banta, A., Gallant, R.M., Götz, D., Green, D., Hall, J., Harmer, T.L., Hurtado, L.A., Johnson, P., McKiness, Z.P., Meredith, C., Olson, E., Pan, I.L., Turnipseed, M., Won, Y., Young, C.R., III, and Vrijenhoek, R.C., 2001, Biogeography and ecological setting of Indian Ocean hydrothermal vents: Science, v. 294, p. 818–823.
van Staal, C.R., Wilson, R.A., Rogers, N., Fyffe, L.R., Langton, J.P., McCutcheon, S.R., McNicoll, V., and Ravenhurst, C.E., 2003, Geology and tectonic history of the Bathurst Supergroup, Bathurst mining camp, and its relationships to coeval rocks in southwestern New Brunswick and adjacent Maine—a synthesis: Economic Geology Monograph 11, p. 37–60.
Vanko, D.A., Milby, B.J., and Heinzquith, S.W., 1991, Massive sulfides with fluid-inclusion-bearing quartz from a young seamount on the East Pacific Rise: Canadian Mineralogist, v. 29, p. 453–460.
Varekamp, J.C., and Buseck, P.R., 1984, The speciation of mercury in hydrothermal systems, with applications to ore deposition: Geochimica et Cosmochimica Acta, v. 48, p. 177–185.
Verati, C., Lancelot, J., and Hékinian, R., 1999, Pb isotope study of black-smokers and basalts from Pito Seamount site (Easter microplate): Chemical Geology, v. 155, p. 45–63.
Vearncombe, S., Barley, M.E., Groves, D.I., McNaughton, N.J., Mikucki, E.J., and Vearncombe, J.R., 1995, 3.26 Ga black smoker-type mineralization in the Strelley belt, Pilbara craton, Western Australia: Journal of the Geological Society of London, v. 152, p. 587–590.
Vikentyev, I.V., 2006, Precious metal and telluride mineralogy of large volcanic-hosted massive sulfide deposits in the Urals: Mineralogy and Petrology, v. 87, p. 305–326.
——2015, Invisible and microscopic gold in pyrite: Methods and new data for massive sulfide ores of the Urals: Geology of Ore Deposits, v. 57, p. 237–265.
Vikentyev, I.V., Yudovskaya, M.A., Mokhov, A.V., Kerzin, A.L., and Tsepin, A.I., 2004, Gold and PGE in massive sulfide ore of the Uzelginsk deposit, southern Urals, Russia: Canadian Mineralogist, v. 42, p. 651–665.
Vikentyev, I.V., Moloshag, V.P., and Yudovskaya, M.A., 2006, Speciation of noble metals and conditions of their concentration in massive sulfide ores of the Urals: Geology of Ore Deposits, v. 48, p. 77–107.
Vokes, F.M., and Craig, J.R., 1993, Post-recrystallisation mobilisation phenomena in metamorphosed stratabound sulphide ores: Mineralogical Magazine, v. 57, p. 19–28.
Von Damm, K.L., 1990, Seafloor hydrothermal activity: Black smoker chemistry and chimneys: Annual Reviews in Earth and Planetary Science, v. 18, p. 173–204.
——2000, Chemistry of hydrothermal vent fluids from 9°-10°N, East Pacific Rise: "Time zero," the immediate posteruptive period: Journal of Geophysical Research, v. 105, p. 11,203–11,222.
Von Damm, K.L., Lilley, M.D., Shanks, W.C., III, Brockington, M., Bray, A.M., O'Grady, K.M., Olson, E., Graham, A., Proskurowski, G., and SouEPR Science Party, 2003, Extraordinary phase separation and segregation in vent fluids from the southern East Pacific Rise: Earth and Planetary Science Letters, v. 206, p. 365–378.
Von Damm, K.L., Parker, C.M., Zierenberg, R.A., Lilley, M.D., Olson, E.J., Clague, D.A., and McClain, J.S., 2005, The Escanaba trough, Gorda Ridge hydrothermal system: Temporal stability and subseafloor complexity: Geochimica et Cosmochimica Acta, v. 69, p. 4,971–4,984.
Von Damm, K.L., Parker, C.M., Lilley, M.D., Olson, E.J., Clague, D.A., Zierenberg, R.A., and McClain, J.S., 2006, Chemistry of vent fluid and its implications for subsurface conditions at Sea Cliff hydrothermal field, Gorda Ridge: Geochemistry Geophysics Geosystems, v. 7, doi: 10.1029/2005GC001034.
Wagner, T., and Jonsson, E., 2001, Mineralogy of sulfosalt-rich vein-type ores, Boliden massive sulfide deposit, Skellefte district, northern Sweden: Canadian Mineralogist, v. 39, p. 855–872.
Wagner, T., and Monecke, T., 2005, Germanium-bearing colusite from the Waterloo volcanic-rock-hosted massive sulfide deposit, Australia: Crystal chemistry and formation of colusite-group minerals: Canadian Mineralogist, v. 43, p. 655–669.
Wagner, T., Jonsson, E., and Boyce, A.J., 2005, Metamorphic ore remobilization in the Hällefors district, Bergslagen, Sweden: Constraints from mineralogical and small-scale sulphur isotope studies: Mineralium Deposita, v. 40, p. 100–114.
Walker, R.R., Matulich, A., Amos, A.C., Watkins, J.J., and Mannard, G.W., 1975, The geology of the Kidd Creek mine: Economic Geology, v. 70, p. 80–89.
Wang, D., 1999, Geological setting and features of the Ashele Cu-Zn deposit, Xinjiang, China: Exploration and Mining Geology, v. 8, p. 197–210.
Wang, Y., Han, X., Jin, X., Qiu, Z., Ma, Z., and Yang, H., 2012, Hydrothermal activity events at Kairei field, Central Indian Ridge 25°S: Resource Geology, v. 62, p. 208–214.
Wang, Y., Han, X., Petersen, S., Jin, X., Qiu, Z., and Zhu, J., 2014, Mineralogy and geochemistry of hydrothermal precipitates from Kairei hydrothermal field, Central Indian Ridge: Marine Geology, v. 354, p. 69–80.
Watanabe, K., 2001, Mapping the hydrothermal activity area on the Hatoma knoll in the southern Okinawa trough: JAMSTEC Journal of Deep Sea Research, v. 19, p. 87–94.
Watanabe, S., and Hayashi, K., 2014, Mineralogy, sulfur isotope and fluid inclusion studies of hydrothermal ore at the Hakurei deposit, Bayonnaise knoll, Izu-Bonin arc: Resource Geology, v. 64, p. 77–90.
Watanabe, K., and Kajimura, T., 1994, The hydrothermal mineralization at Suiyo Seamount, in the central part of the Izu-Ogasawara arc: Resource Geology, v. 44, p. 133–140.
Watanabe, K., Shibata, A., and Kajimura, T., 1994, Mapping the hydrothermal area in the caldera on Suiyo Seamount: JAMSTEC Journal of Deep Sea Research, v. 10, p. 55–62.
Watanabe, K., Shibata, A., Furukawa, H., and Kajimura, T., 1995, Topography of submarine volcanoes off the north-northeast coast of Iriomote island, the Ryukyu Islands: Bulletin of the Volcanological Society of Japan, v. 40, p. 91–97.
Watanabe, M., Hoshino, K., Shiokawa, R., Takaoka, Y., Fukumoto, H., Shibata, Y., Shinjo, R., and Oomori, T., 2006, Metallic mineralization associated with pillow basalts in the Yaeyama Central Graben, southern Okinawa trough, Japan: JAMSTEC Report of Research and Development, v. 3, p. 1–8.
Webber, A.P., Roberts, S., Murton, B.J., and Hodgkinson, M.R.S., 2015, Geology, sulfide geochemistry and supercritical venting at the Beebe hydrothermal vent field, Cayman trough: Geochemistry Geophysics Geosystems, v. 16, p. 2,661–2,678, doi: 10.1002/2015GC005879.

Werner, R., Hauff, F., and Hoernle, K., 2010, Cruise report R/V Sonne cruise SO-208 Leg 1&2: Propagation of Galápagos plume material in the equatorial East Pacific (PLUMEFLUX), Caldera, Costa Rica, July 15, 2010, Guayaquil, Ecuador, August 29, 2010: Berichte aus dem Leibniz-Institut für Meereswissenschaften an der Universität Kiel, v. 39, 230 p.

Wheat, C.G., Fryer, P., Hulme, S., Becker, N., Curtis, A., and Moyer, C., 2003, Hydrothermal venting in the southern most portion of the Mariana backarc spreading center at 12.57°N [abs.]: American Geophysical Union Fall Meeting, San Francisco, California, 2003, T32A-0920.

Wheeler, A.J., Murton, B., Copley, J., Lim, A., Carlsson, J., Collins, P., Dorschel, B., Green, D., Judge, M., Nye, V., Benzie, J., Antoniacomi, A., Coughlan, M., and Morris, K., 2013, Moytirra: Discovery of the first known deep-sea hydrothermal vent field on the slow-spreading Mid-Atlantic Ridge north of the Azores: Geochemistry Geophysics Geosystems, v. 14, p. 4,170–4,184, doi: 10.1002/gggge.20243.

Williams, D.L., Green, K., van Andel, T.H., Von Herzen, R.P., Dymond, J.R., and Crane, K., 1979, The hydrothermal mounds of the Galapagos rift: Observations with DSRV Alvin and detailed heat flow studies: Journal of Geophysical Research, v. 84, p. 7,467–7,484.

Wohlgemuth-Ueberwasser, C.C., Viljoen, F., Petersen, S., and Vorster, C., 2015, Distribution and solubility limits of trace elements in hydrothermal black smoker sulfides: An in-situ LA-ICP-MS study: Geochimica et Cosmochimica Acta, v. 159, p. 16–41.

Wood, S.A., and Samson, I.M., 1998, Solubility of ore minerals and complexation of ore metals in hydrothermal solutions: Reviews in Economic Geology, v. 10, p. 33–80.

——2006, The aqueous geochemistry of gallium, germanium, indium and scandium: Ore Geology Reviews, v. 28, p. 57–102.

Wood, S.A., Crerar, D.A., and Borcsik, M.P., 1987, Solubility of the assemblage pyrite-pyrrhotite-magnetite-sphalerite-galena-gold-stibnite-bismuthinite-argentite-molybdenite in H_2O-NaCl-CO_2 solutions from 200° to 350°C: Economic Geology, v. 82, p. 1,864–1,887.

Wright, I.C., de Ronde, C.E.J., Faure, K., and Gamble, J.A., 1998, Discovery of hydrothermal sulfide mineralization from southern Kermadec arc volcanoes (SW Pacific): Earth and Planetary Science Letters, v. 164, p. 335–343.

Xiong, Y., 2007, Hydrothermal thallium mineralization up to 300°C: A thermodynamic approach: Ore Geology Reviews, v. 32, p. 291–313.

Yamamoto, M., Kase, K., and Tsutsumi, M., 1984, Fractionation of sulfur isotopes and selenium between coexisting sulfide minerals from the Besshi deposit, Central Shikoku, Japan: Mineralium Deposita, v. 19, p. 237–242.

Yamanaka, T., and Kato, A., 1976, Mössbauer effect study of ^{57}Fe and ^{119}Sn in stannite, stannoidite, and mawsonite: American Mineralogist, v. 61, p. 260–265.

Ye, J., Shi, X., Yang, Y., Li, B., and Ren, X., 2014, Hydrothermal mineralization at 15°S and 26°S on South Atlantic Ridge [abs.]: Minerals of the Ocean-7 and Deep-Sea Minerals and Mining-4, St. Petersburg, Russia, 2014, Abstract Volume, p. 47.

Yeats, C.J., Parr, J.M., Binns, R.A., Gemmell, J.B., and Scott, S.D., 2014, The SuSu knolls hydrothermal field, eastern Manus basin, Papua New Guinea: An active submarine high-sulfidation copper-gold system: Economic Geology, v. 109, p. 2,207–2,226.

Yoshikawa, S., Okino, K., and Asada, M., 2012, Geomorphological variations at hydrothermal sites in the southern Mariana trough: Relationship between hydrothermal activity and topographic characteristics: Marine Geology, v. 303-306, p. 172–182.

Zakrzewski, M.A., Burke, E.A.J., and Nugteren, H.W., 1980, Cobalt minerals in the Hällefors area, Bergslagen, Sweden: New occurrences of costibite, paracostibite, nisbite and cobaltian ullmannite: Canadian Mineralogist, v. 18, p. 165–171.

Zaw, K., and Large, R.R., 1992, The precious metal-rich South Hercules mineralization, western Tasmania: A possible subsea-floor replacement volcanic-hosted massive sulfide deposit: Economic Geology, v. 87, p. 931–952.

Zeng, Z.G., Yu, S.X., Yin, X.B., Wang, X.Y., Zhang, G.L., Wang, X.M., and Chen, D.G., 2009, Element enrichment and U-series isotopic characteristics of the hydrothermal sulfides at Jade site in the Okinawa trough: Science in China Series D: Earth Sciences, v. 52, p. 913–924.

Zierenberg, R.A., and Miller, D.J., 2000, Overview of Ocean Drilling Program Leg 169: Sedimented ridges II: Proceedings of the Ocean Drilling Program, Scientific Results, v. 169, p. 1–39.

Zierenberg, R.A., Shanks, W.C., III, and Bischoff, J.L., 1984, Massive sulfide deposits at 21°N, East Pacific Rise: Chemical composition, stable isotopes, and phase equilibria: Geological Society of America Bulletin, v. 95, p. 922–929.

Zierenberg, R.A., Koski, R.A., Morton, J.L., Bouse, R.M., and Shanks, W.C., III, 1993, Genesis of massive sulfide deposits on a sediment-covered spreading center, Escanaba trough, southern Gorda Ridge: Economic Geology, v. 88, p. 2,069–2,098.

Zierenberg, R.A., Morton, J.L., Koski, R.A., and Ross, S.L., 1994, Geologic setting of massive sulfide mineralization in Escanaba trough: U.S. Geological Survey Bulletin, v. 2022, p. 171–197.

Zierenberg, R.A., Fouquet, Y., Miller, D.J., Bahr, J.M., Baker, P.A., Bjerkgård, T., Brunner, C.A., Duckworth, R.C., Gable, R., Gieskes, J., Goodfellow, W.D., Gröschel-Becker, H.M., Guèrin, G., Ishibashi, J., Iturrino, G., James, R.H., Lackschewitz, K.S., Marquez, L.L., Nehlig, P., Peter, J.M., Rigsby, C.A., Schultheiss, P., Shanks, W.C., III, Simoneit, B.R.T., Summit, M., Teagle, D.A.H., Urbat, M., and Zuffa, G.G., 1998, The deep structure of a sea-floor hydrothermal deposit: Nature, v. 392, p. 485–488.

©2016 Society of Economic Geologists, Inc.
Reviews in Economic Geology, v. 18, pp. 307–321

Chapter 12

Critical Elements in Sediment-Hosted Deposits (Clastic-Dominated Zn-Pb-Ag, Mississippi Valley-Type Zn-Pb, Sedimentary Rock-Hosted Stratiform Cu, and Carbonate-Hosted Polymetallic Deposits): A Review

Erin E. Marsh,[1,†] Murray W. Hitzman,[2] and David L. Leach[2]

[1] *U.S. Geological Survey, Box 25046 MS 973, Denver, Colorado 80305*

[2] *Department of Geology and Geological Engineering, Colorado School of Mines, Golden, Colorado 80401*

Abstract

Some sediment-hosted base metal deposits, specifically, the clastic-dominated Zn-Pb deposits, carbonate-hosted Mississippi Valley-type (MVT) deposits, sedimentary rock-hosted stratiform copper deposits, and carbonate-hosted polymetallic ("Kipushi-type") deposits, are or have been important sources of critical elements including Co, Ga, Ge, PGEs, and Re. Cobalt is noted in only a few clastic-dominated and MVT deposits, whereas sedimentary rock-hosted stratiform copper deposits are major producers. Gallium occurs in sphalerite from clastic-dominated and MVT deposits. Little is reported of germanium in clastic-dominated deposits; it is more commonly noted in MVT deposits (up to 4,900 ppm within sphalerite) and has been produced from carbonate-hosted polymetallic deposits (Kipushi, Tsumeb). Indium is known to be elevated in sphalerite and zinc concentrates from some MVT and clastic-dominated deposits, produced from Rammelsberg and reported from Sullivan, Red Dog, Tri-State, Viburnum Trend, Lisheen, San Vincente, and Shalipayco. Platinum and palladium have been produced from sedimentary rock-hosted stratiform copper deposits in the Polish Kupferschiefer. Sedimentary rock-hosted stratiform copper deposits in the Chu-Sarysu basin are known to have produced rhenium. Although trace element concentrations in these types of sediment-hosted ores are poorly characterized in general, available data suggest that there may be economically important concentrations of critical elements yet to be recognized.

Introduction

Critical elements are defined as elements that are important to modern society and have the potential for supply restriction (National Research Council, 2008; American Physical Society, 2011; British Geological Survey, 2012). Sediment-hosted base metal deposits, including clastic-dominated Zn-Pb deposits, carbonate-hosted Mississippi Valley-type (MVT) deposits, sedimentary rock-hosted stratiform copper deposits, and carbonate-hosted polymetallic ("Kipushi type") deposits are major producers of Pb, Zn, and Cu, all of which are important for modern society, but none of which are in danger of becoming scarce. Some sediment-hosted base metal deposits contain critical elements that are, or potentially could be, exploited. The distinction of an element as critical is subject to change with new discoveries or production developments, as well as with shifts in market and political climates. For this review we are considering the top 20 critical elements listed by the British Geological Survey (2012).The most common critical elements associated with the sediment-hosted deposits we review are Co, Ga, Ge, In, Pt, Pd, and Re (Tables 1, 2).

Critical elements associated with sediment-hosted deposits may occur within specific ore minerals (e.g., Ga, Ge, and In within sphalerite; Cook et al., 2009) or as trace elements in nonore minerals. Regrettably, the information on critical element abundance in sediment-hosted deposits is relatively sparse. Data for this contribution were gathered from both publicly available references and smelting company data. Smelter data commonly report elemental concentrations from mixed ore concentrates, making it impossible to determine the exact proportion of elements from specific minerals or even deposits. The available analytical results were derived from a variety of techniques, including solution chemistry, electron microscope analysis (EMPA), and laser ablation inductively coupled plasma mass spectrometry (LA-ICP-MS). As an example of the problems inherent in this review, indium is a common midweight standard for many ICP-MS methods and is therefore excluded from many solution chemistry analyses. To follow is a summary of critical elements found in sediment-hosted deposits reported in the literature and a discussion of what allows for these poorly congregated elements to potentially concentrate in select sediment-hosted deposits.

† Corresponding author: e-mail, emarsh@usgs.gov

Sediment-Hosted Base Metal Deposits

Sediment-hosted base metal (Cu, Pb, Zn) deposits are hosted by a variety of carbonate and siliciclastic rocks. They formed from a range of processes in several tectonic environments over at least the last two billion years of Earth history (Hitzman et al., 2005; Leach et al., 2010a, b). Historically, these deposits have been the world's most important sources of lead and zinc and they continue to dominate world production of these metals. These deposits also account for approximately 23% of world copper production.

The two main groups of sediment-hosted Zn-Pb ores are clastic-dominated deposits hosted in primarily siliciclastic rock sequences and Mississippi Valley-type (MVT) deposits hosted in carbonate-dominated rock sequences. The

Table 1. Concentrations of Ga, Ge, and In Reported in Sediment-Hosted Ores for Clastic-

District	Deposit	Country	Ge (ppm)	Ga (ppm)	In (ppm)	Co (ppm)	Co (%)
Clastic-dominated (CD) sediment-hosted deposits							
	Rammelsberg	Germany			50		
	Red Dog	United States	79	26			
	Red Dog	United States	17	10			
	Sullivan	Canada					0.08–0.17
	Sullivan	Canada			14.6		
	Sullivan	Canada			19.21–93		
	Sullivan	Canada	0.8–22				
	Howards Pass	Canada					0.004–0.01
	Black Butte	United States					1,200.00
Mississippi Valley-type (MVT) deposits							
Viburnum Trend		United States	60–400				
Central Tennessee	Elmwood-Gordonsville	United States	400				
Upper Silesia		Poland		15			
Huize		China	354				
Alpine	Bleiberg	Austria	8.6–1,400	0.5–127			
Alpine	Bleiberg	Austria	5–2,250	<1–5			
Alpine	Bleiberg	Austria	1–700	<1–50			
Alpine	Bleiberg	Austria	200–1,350	<1–5			
Alpine	Bleiberg	Austria	193				
Alpine	Bleiberg	Austria	22–1,500				
Alpine	Lafatsch	Austria	10–250	5–40			
Alpine	Gorno - Val Vedra	Italy	20–1,200	10–200			
Alpine	Hochobir	Austria	1–4,000	1–200			
Alpine	Jauken	Austria	100–1,200	<1–5			
Alpine	Jauken	Austria	200–7,250	<1–5			
Alpine	Rubland	Austria	40–3,000				
Alpine	Forolach	Austria	5–210	5–80	<0.1–2		
Alpine	Raibl	Italy	50–2,100	<1–8			
Alpine	Cave di Predil (Raibl)	Italy	2–3,000				
Alpine	Mezica	Slovenia	20–1,100				
Apline	Mezica	Slovenia	190				
	Reocin	Spain	53				
	Reocin	Spain			37		
Cevennes	Tréves	France	160				
Cevennes	Tréves	France	74				
	Pomerzany	Poland	30–800				
	Bushy Park	South Africa	98.5	46			
	Elimhof	South Africa	32	35			
	Pering	South Africa	43.5	36.55			
	Pering SP-2	South Africa	57.5	0.295			
	Balloch	South Africa	1.8	0.04			
	Kalkfontein	South Africa	17.125	11.9			
Irish Midlands	Tynagh	Ireland	1–27				
Irish Midlands	Navan	Ireland	1–72				
Irish Midlands	Lisheen	Ireland	400–900	300–1,600	400–900		
Irish Midlands	Lisheen	Ireland	0.4–1.3	1–73			
	Nanisivik	Canada			20		
	Greenex (Black Angel)	Greenland			14		
	Balmat	United States			40		
Bafq		Iran			5		
	San Vicente	Peru	11–62				
	San Vicente	Peru	34–116				
	San Vicente	Peru	8–30		5		
	Cercapuquio	Peru	10		10		
	Shalipayco	Peru	100–130		10		
	Cave di Predil (Raibl)	Italy	544				
Carbonate-hosted polymetallic deposits							
	Apex	United States	5,000–7,000				
	Apex	United States		7,000–20,000			
	Tsumeb	Namibia	50				

[1] Data are from individual mineral analyses, whole-rock samples, and concentrates; a variety of analytical techniques are reported in these sources, including atomic adsorption spectrophotometry, X-ray fluorescence analysis (XRF), secondary ion mass spectrometry (SIMS), electron microscope analysis (EMPA), and inductively coupled plasma mass spectrometry (ICP-MS); given the differences in precision and accuracy between these techniques only qualitative comparison can be made between the data

Dominated, MVT, and Carbonate-Hosted Polymetallic Deposit Types (with data sources given)[1]

Sample type	Notes	Source
Average grade for the deposit		Large and Walcher (1999); Schwarz-Shamera and Herzig (2002)
Zinc concentrate		Alaska Department of Environmental Conservation (2002)
Lead concentrate		Alaska Department of Environmental Conservation (2002)
Arsenopyrite	Electron microprobe analysis	Ethier et al. (1976)
	Average	Hamilton et al. (1983)
Sphalerite	TIMS	Yi et al. (1995)
	ICP-AES	Slack et al. (2000)
Pyrite	Atomic absorption spectrophotometry	Goodfellow et al. (1983)
		Tetra Tech, 2013
Zinc concentrate		Bernstein (1985); Holl (2006)
Zinc concentrate		Misra et al. (1996)
Sphalerite		Hagni (1983)
Sphalerite		Melcher and Buchholz (2014)
Sphalerite	Mainly Rudolf Shaft; emmisions spectroscopy	Pimminger et al. (1985)
Sphalerite	Bleiberg, pit Maxer Banke; SIMS	Pimminger et al. (1985)
Sphalerite	Bleiberg, pit Maxer Banke, light fissure sphalerite; SIMS	Pimminger et al. (1985)
Sphalerite	Bleiberg, pit Max, colloform sphalerite; SIMS	Pimminger et al. (1985)
Zinc concentrate		Cerny and Schroll (1985); Höll et al. (2007)
Sphalerite		Cerny and Schroll (1985); Höll et al. (2007)
Sphalerite	SIMS	Pimminger et al. (1985)
Sphalerite	SIMS	Pimminger et al. (1985)
Sphalerite	SIMS	Pimminger et al. (1985)
Sphalerite	Fine-grained sphalerite	Pimminger et al. (1985)
Sphalerite	SIMS	Pimminger et al. (1985)
Sphalerite	SIMS	Pimminger et al. (1985)
Sphalerite	Mineralization in breccia; SIMS	Pimminger et al. (1985)
Sphalerite	Colloform sphalerite; SIMS	Pimminger et al. (1985)
Sphalerite		Schroll (unpub.); Höll et al. (2007)
Sphalerite		Schroll (unpub.); Höll et al. (2007)
Zinc concentrate		Schroll (unpub.); Höll et al. (2007)
Sphalerite		Seebold et al. (1992)
Whole ore samples		Seebold et al. (1992)
Sphalerite		Geldron (1983)
Sphalerite		Geldron (1983)
Sphalerite		Sass-Gustkiewicz (2001); Höll et al. (2007)
Sphalerite	ICP-MS	Schaefer et al. (2004)
Sphalerite	ICP-MS	Schaefer et al. (2004)
Sphalerite	ICP-MS	Schaefer et al. (2004)
Sphalerite	ICP-MS	Schaefer et al. (2004)
Sphalerite	ICP-MS	Schaefer et al. (2004)
Sphalerite	ICP-MS	Schaefer et al. (2004)
Sphalerite		Schroll (unpub.); Höll et al. (2007)
Sphalerite		Schroll (unpub.); Höll et al. (2007)
Sphalerite	EMPA	Wilkinson et al. (2005)
Whole ore samples	ICP-MS	Hitzman et al. (2002)
Zinc concentrate		Rodier (1990) (appendix)
Zinc concentrate		Rodier (1990) (appendix)
Zinc concentrate		Rodier (1990) (appendix)
Zinc concentrate		Rodier (1990) (appendix)
Sphalerite	Atomic absorption spectrophotometry	Fontboté and Gorzawski (1990)
Ore samples	XRF	Fontboté and Gorzawski (1990)
Zinc concentrate		Soler and Lara (1990)
Zinc concentrate		Soler and Lara (1990)
Zinc concentrate		Soler and Lara (1990)
Zinc concentrate		Schroll (unpub.); Holl et al. (2007)
Iron oxides	Semiquantitative emission spectroscopy	Bernstein (1986)
Iron oxides	Semiquantitative emission spectroscopy	Bernstein (1986)
Average grade for the deposit		Lombaard et al. (1986)

Table 2. Cobalt and Copper in Sedimentary Rock-Hosted Stratiform Copper Deposits

Deposit	Country	Co (%)	Cu (%)	Mt	Source
Nchanga-Chingola group	Zambia	0.48	2.16	1,082.5	Hitzman et al. (2012)
Nkana-Mindola group	Zambia	0.13	2.5	612.7	Hitzman et al. (2012)
Frontier (Lufua)	DRC	0.017	1.17	160.80	Selley et al. (2005); Hitzman et al. (2012)
Baluba	Zambia	0.16	2.38	71.20	Selley et al. (2005); Hitzman et al. (2005)
Chibuluma (East and West)	Zambia	0.19	4.26	36.40	Hitzman et al. (2012)
Mwambashi B	Zambia	0.08	2.63	8.4	Selley et al. (2005)
Chambishi (Main and West)	Zambia	0.12	2.55	123.90	Hitzman et al. (2012)
Luanshya-Baluba	Zambia	0.15	2.66	406.5	Hitzman et al. (2012)
Kakanda group	DRC	0.14	3.13	41.3	Hitzman et al. (2012)
Kambove-Kamoya group	DRC	0.2	5.7	44.5	Hitzman et al. (2012)
Kinsevere group	DRC	1.8	3	52	Booth et al. (2010); MMG Ltd. (2012)
Kisanfu	DRC	1.08	2.32	55	Hitzman et al. (2012)
Kolwezi district	DRC	0.33	4.48	726	Hitzman et al. (2012)
Luishia-Kasnogwe group	DRC	0.09	2.82	62.9	Hitzman et al. (2012)
Luiswishi	DRC	0.95	4.32	12.4	Hitzman et al. (2012)
Tenke-Fungurume district	DRC	0.27	3.5	547	Hitzman et al. (2012)
Tilwezembe	DRC	0.6	1.8	23	Broughton (2013); Glencore (2012)
Desiwa	DRC	0.12	1.44	319	Broughton (2013)
Mutanda	DRC	0.59	1.48	299.5	Broughton (2013)
Kalumbwe	DRC	2.87 Cu + Co		2.5	Broughton (2013)
Kisanfu	DRC	1.08	2.62	108	Broughton (2013)
Lumwana project	Zambia	0.02	0.74	342.5	43-101 2009
Boleo	Mexico	0.06	0.76	264.7	43-101 Baja Mining Corp. (2010)
Kilembe	Uganda	0.17	1.98	16.2	www.vangold.ca/s/Kilembe.asp

[1]Nchanga upper orebody

clastic-dominated deposits include the so-called sedimentary exhalative (SEDEX) deposits. The defining factor between clastic-dominated and MVT deposits is their tectonic setting (Leach et al., 2005, 2010a, b). Copper-rich sediment-hosted ores are dominated by the sedimentary rock-hosted stratiform copper deposits (Hitzman et al., 2005). Copper, together with zinc, and commonly a diverse suite of other metals, are produced from the carbonate-hosted polymetallic deposits, also termed Kipushi-type deposits (Hitzman et al., 2005).

Clastic-dominated sediment-hosted Zn-Pb-Ag deposits

Most clastic-dominated sediment-hosted Zn-Pb-Ag deposits have traditionally been termed SEDEX (Carne and Cathro, 1982; Lydon, 1986; Lavery et al., 1994; Large et al., 2005; Leach et al., 2005, 2010a; Goodfellow and Lydon, 2007). Within this group are some deposits with well-documented exhalative ores (e.g., Sullivan in British Columbia; Lydon, 2007, Fig. 1) and deposits that clearly formed as subsea-floor replacement (e.g., Red Dog deposits, Alaska; Kelley and Jennings, 2004; Kelley et al., 2004) or in a more deeply buried diagenetic environment (e.g., Century in North Australia; Broadbent et al., 1998).

Clastic-dominated Zn-Pb-Ag deposits mainly formed in siliciclastic-dominated sediments along passive margins. Fewer examples are known from marine-filled continental back-arc basins and continental rifts. The formation of clastic-dominated sediment-hosted deposits is confined to evaporative latitudes(~5°–40° N and S),where evaporites formed on cratonic margins and dense concentrated seawater was able to infiltrate downward along structures into reduced sediments in the flanking marine basins (Leach et al., 2010a). Clastic-dominated ores are hosted in shale, sandstone, siltstone, or mixed clastic rocks and commonly occur as replacements of carbonate, barite, pyrite, and organic material in a clastic-dominated sedimentary rock sequence. Economically, the most important clastic-dominated sediment-hosted deposits occur within Proterozoic rocks of the northern Australia zinc belt (Gulson, 1985; Cooke et al., 2000, 2003; Large et al., 2005), Proterozoic metasedimentary rocks of Rajasthan in eastern India (Deb and Pal, 2004), Devonian sedimentary rocks in Germany (Krebs, 1981; Large and Walcher, 1999), Carboniferous sedimentary rock of the Brookian passive margin in Alaska (Kelley et al., 2004), and in Cambrian, Lower Silurian and Upper Devonian rocks of the Selwyn basin, Canada (Goodfellow et al., 1983). Previously published research has shown that clastic-dominated Zn-Pb-Ag deposits generally do not contain significant amounts of critical elements; only a few are noted to have recovered by-product indium (i.e., Rammelsberg and Sullivan; Table 1).

Mississippi Valley-type Zn-Pb-Ag deposits

Mississippi Valley-type deposits are epigenetic deposits hosted in dolostone, limestone, and occasionally sandstone in platform carbonate sequences inboard of major orogenic belts (Leach and Sangster, 1993; Leach et al., 2001, 2005, 2010b). Mississippi Valley-type deposits formed a few million to hundreds of millions years following deposition of their host rocks. Mississippi Valley-type ores first appeared in the rock record during the Late Archean. They became abundant in the late Neoproterozoic and continued to form through the Phanerozoic.

Mississippi Valley-type districts are typically spatially adjacent to orogenic zones and are related to closure of a facing ocean basin (Bradley and Leach, 2003). Within these overall contractional settings, the single most important tectonic controls at the deposit or district scale are extensional (normal, transtensional, and wrench) faults along with associated fractures and dilatancy zones. Ore deposition is generally related

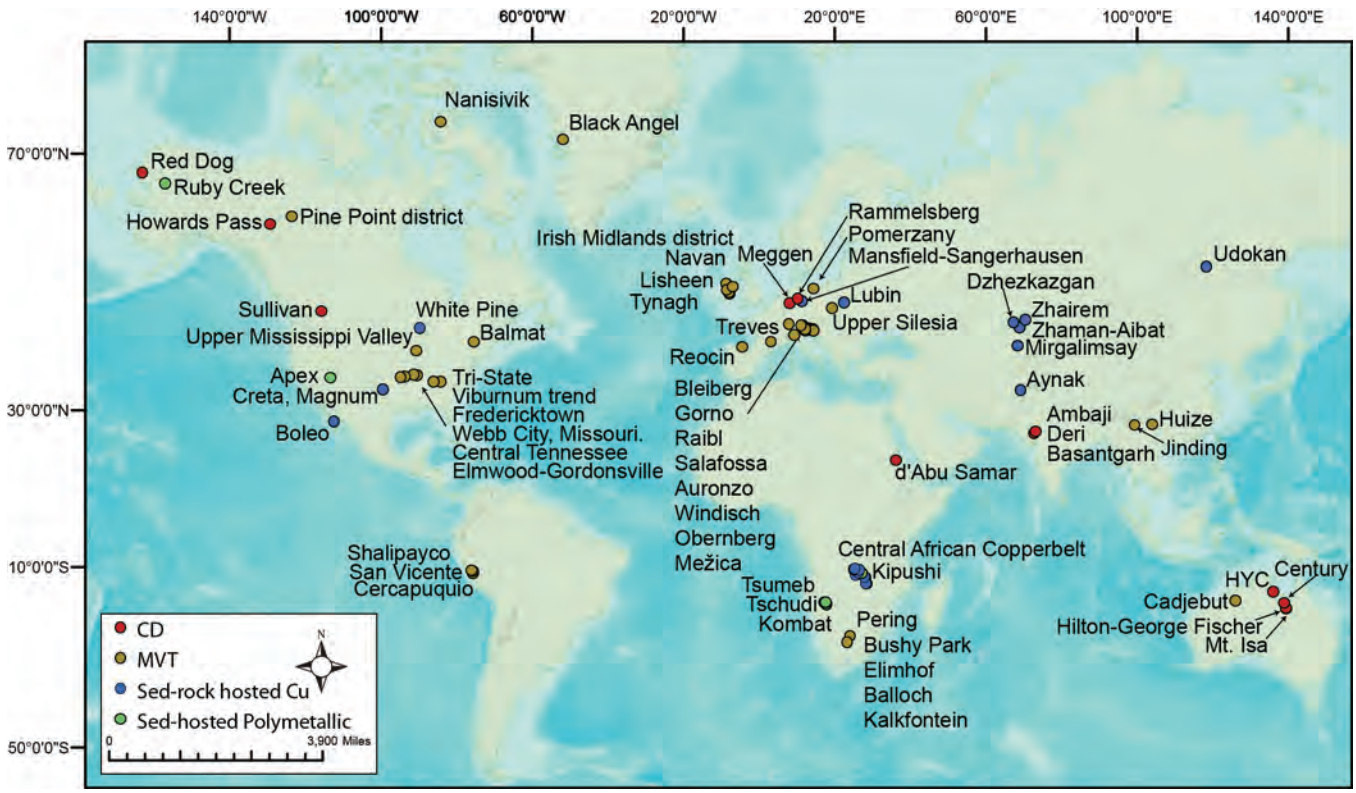

Fig. 1. World map with deposit and district locations. CD = clastic-dominated, MVT = Mississippi Valley-type, Sed = sedimentary.

to zones where an oxidized metal-bearing fluid, which originated from evaporated seawater, mixed with a fluid containing reduced sulfur.

The largest concentrations of MVT deposits occur inboard of two orogenic belts, the late Paleozoic Hercynian-Appalachian-Ouachita orogenic belt and the Mesozoic-Cenozoic Tethyian belt. The late Paleozoic Hercynian-Appalachian-Ouachita orogenic belt contains the Appalachian, East Tennessee, Central Tennessee, and Ozark districts of the United States (Leach et al., 2001, 2005), deposits in Nova Scotia, Canada (Leach et al., 2001), and the Irish Midlands districts (Hitzman and Large, 1986). The Tethyian orogenic belt contains deposits in northern Spain (Velasco et al., 1994, 2003), North Africa (Rouvier et al., 1985), the Upper Silesia district of Poland (Symons et al., 1995; Leach et al., 1996), the Alpine district of Europe (Leach et al., 2003; Schroll, 2005), and Iran (Bazargani-Gullani et al., 2011). Mississippi Valley-type deposits have been responsible for production of significant gallium and germanium, and one district (southeast Missouri) locally contains potentially economic concentrations of cobalt (Table 1).

Sedimentary rock-hosted stratiform copper deposits

Sedimentary rock-hosted stratiform copper deposits comprise disseminated to veinlet Cu and Cu-Fe sulfides in siliciclastic or dolomitic sedimentary rocks (Hitzman et al., 2005). These deposits account for approximately 23% of the world's Cu production and known reserves (Singer, 1995). They are important sources of Ag and Co; some deposits contain significant Pb, Ni, Re, U, and Zn, and a few contain very minor Au and platinum group elements (PGEs).

Sediment-hosted stratiform copper deposits consist of relatively thin (generally <30 m and commonly less than 3 m in thickness) ore-stage sulfide-bearing zones that are peneconcordant with bedding. These deposits commonly occur in basins that contain marine or lacustrine rocks immediately overlying continental red beds and in isolated nonred units within continental red-bed sequences (Kirkham, 1989; Hitzman et al., 2005). They commonly display a sequence of mineral zonation from the contact with the red beds into the reduced, ore-bearing sediments of hematite-chalcocite-bornite-chalcopyrite- pyrite. In many deposits, ore-stage galena and sphalerite may occur with chalcopyrite or between the chalcopyrite and widespread pyrite zones. The Fe^{3+}-Cu-Pb-Zn-Fe^{2+} zoning, together with the oxide and sulfide mineral zoning and paragenetic mineral sequence, indicate that reduction of an initially hematite-stable, Cu-(Pb-Zn)-transporting fluid is the primary cause of base metal sulfide precipitation. The reductants responsible for sulfide precipitation may include both in situ organic matter and mobile hydrocarbons (Hitzman et al., 2005).

Sulfides and associated nonsulfide minerals in the deposits display textures and fabrics, indicating that they were precipitated after host-rock deposition. However, the timing of mineralization in these systems in relationship to the timing of host-rock deposition is variable (Hitzman et al., 2005). Mineralization may take place relatively early in the diagenetic history of the host sediments (e.g., White Pine, Michigan: Wiese, 1960, 1973; White and Wright, 1966; Brown, 1971; Kamoto, Democratic Republic of Congo (DRC): Bartholomé, 1962, 1974; Creta, Magnum deposits: Hagni and Gann, 1976;

Johnson, 1976; Smith, 1976; Redstone deposit: Chartrand and Brown, 1985; Chartrand et al., 1989; Lustwerk and Wasserman, 1989) or very late in the diagenetic or postdiagenetic history of the sedimentary rocks (e.g., Central African Copperbelt: Selley et al., 2005; Hitzman et al., 2012).

Sediment-hosted stratiform copper deposits are abundant worldwide, indicating that this style of mineralization results from ore-forming processes that are relatively common. However, only three basins are known to contain supergiant deposits—the Neoproterozoic Katangan basin (Central African Copperbelt; Hitzman et al., 2012), the Permian basin of Europe (Kupferschiefer; Borg et al., 2012), and the Paleoproterozoic Kodaro-Udokan basin of Siberia (Udokan; Volodin et al., 1994). Three other basins, the Devonian to Carboniferous Chu-Sarysu basin of Kazakhstan (Box et al., 2012), the Middle Proterozoic Midcontinent rift of United State of America (Brown, 1971; White, 1971; Mauk et al., 1992), and a Neoproterozoic-Cambrian basin in Afghanistan (Abdullah et al., 1977) contain giant sedimentary rock-hosted deposits.

The Central African Copperbelt is a major producer of cobalt and contains deposits that have been mined for U and Ni (Hitzman et al., 2012; Table 1). The Central African Copperbelt deposits are unusual relative to other deposits of this type as they lack significant silver. Many sedimentary rock-hosted deposits contain minor Zn and Pb, though these metals are not commercially produced. Prior to the end of the Cold War, the sedimentary rock-hosted Kupferschiefer deposits of Poland produced a number of metals including Au, Cd, Co, Ni, Mo, Pd, Pt, Se, Re, Tl, V, and Tl (Borg et al., 2012). The deposits in the Chu-Sarysu basin of Kazakhstan produce significant rhenium (Box et al., 2012). Though many sedimentary rock-hosted stratiform copper deposits contain minor amounts of hydrothermal apatite and other phosphate minerals, none are known to contain significantly anomalous amounts of rare earth elements.

Carbonate-hosted polymetallic deposits

This group of Cu-Zn-Pb-(Ag)-bearing replacement deposits, also termed "Kipushi-type" (Bernstein and Cox, 1986), contains anomalous germanium, and most deposits have significant contents of other minor metals. Deposits thought to be part of this group include copper-rich deposits: Kipushi in the DRC (Intiomale and Oosterbosch, 1974; De Magnée and François, 1988; Heijlen et al., 2008; Kampunzu et al., 2009), Tsumeb (Lombaard et al., 1986; Hughes, 1987; Maiden and Hughes, 2000), Khusib Springs, Tschudi, and Kombat deposits (Innes and Chaplin, 1986; Osterman, 1999) in the Damaran region of northern Namibia, the Ruby Creek deposit in Alaska (Bernstein and Cox, 1986; Hitzman, 1986), and the Apex deposit in Utah, United States (Berstein, 1986). Copper-poor examples of this deposit type include the Lombe and Kengere deposits in the Congolese Copperbelt and the Kabwe (Broken Hill) deposit in Zambia (Kamona, 1993; Hitzman et al., 2003).

A number of these deposits, including Kipushi, Tsumeb and Apex, form in elongate, vertically oriented pipes. The pipes appear to have formed by either karst processes (Tsumeb: Maiden and Hughes, 2000; Apex: Bernstein, 1986) or through salt diapirism (Kipushi: De Magnée and François, 1988). Other deposits such as Kombat and Ruby Creek are strata bound. The Namibian strata-bound deposits appear to be related to a major unconformity and karst surface (Innes and Chaplin, 1986).

The genesis of most of these deposits is contentious. While some (e.g., Kombat) probably formed from oxidized hydrothermal basinal fluids (Osterman, 1999), others (e.g., Ruby Creek) probably formed from reduced basinal fluids (Hitzman, 1986).

Critical Elements in Sediment-Hosted Deposits

Some sediment-hosted deposits are important sources of critical elements. The following discussion examines specific critical element (Co, Ga, Ge, In, PGE, and Re) abundance in the different types of sediment-hosted base metal deposits.

Cobalt

The average crustal abundance of Co is 20 to 29 ppm (Taylor, 1964; Smith and Huyck, 1999; Dill, 2010), whereas mafic and ultramafic rocks contain approximately 150 ppm (Goldschmidt, 1958). Cobalt sits in the periodic table between iron and nickel and shares many geochemical characteristics with these elements. In aqueous solutions, cobalt can be transported by both hydrosulfide and chloride complexes (Migdisov et al., 2011). Increasing fluid temperature and salinity increases cobalt solubility (Liu et al., 2011).

The clastic-dominated sediment-hosted deposits generally contain little cobalt. An exception is the Black Butte Cu-Co-Ag deposit in Montana, United States (Graham et al., 2012; White et al., 2014), which contains 9.1 Mt of ore at 2.83% Cu and 0.12% Co (Tetra Tech, 2013). Cobaltiferous pyrite and minor siegenite ($(Ni,Co)_3S_4$) compose a paragenetically early stage of mineralization at the Black Butte deposit (White et al., 2014). The clastic-dominated sediment-hosted deposits of northern Australia contain anomalous cobalt, although not as a major constituent of the ores. Copper mill feed from the Mount Isa deposit contains 0.05 wt % Co, whereas framboidal pyrite-pyrrhotite-bearing zinc and lead concentrates at Mount Isa contain ~0.1 wt % Co (Croxford, 1974). The Walford Creek clastic-dominated deposit in northern Australia contains up to 0.5 wt % Co in pyrite (Rohrlach et al., 1998; Copper Strike Limited, 2005). Arsenopyrite in the Sullivan clastic-dominated orebody contained up to 0.17% Co (Ethier et al., 1976), though cobalt was not produced. The Howards Pass clastic-dominated deposit in the Selwyn Basin, Canada, locally contains cobaltiferous pyrite with some drill intersections having up to 0.01% Co (Goodfellow et al., 1983).

Some MVT deposits have produced a minor amount of cobalt. The most prominent example of cobalt in MVT ores is in the Southeast Missouri lead district that was reported to contain 120 Mlbs Co (Hagni, 1983). Cobalt is most prominent in copper-rich portions of orebodies. Cobalt in Southeast Missouri occurs in siegenite, fletcherite, and nickelean carrolite, as well as in small amounts within sphalerite. There are little data on cobalt concentrations in other MVT districts.

Although most sedimentary rock-hosted stratiform copper deposits appear to contain only minor amounts of cobalt, the deposits of the Central African Copperbelt are one of the world's major sources of cobalt (Roberts and Gunn, 2013). Economic (>0.1 wt % Co) concentrations of cobalt are only present in deposits of the western portion of the Zambian

Copperbelt (Annels, 1974; Fleischer et al., 1976; Selley et al., 2005; Fig. 2), whereas virtually all the deposits in the Congolese portion of the Copperbelt contain some cobalt (Hitzman et al., 2012), with the prominent exception of the newly discovered giant Kamoa copper deposit situated to the west of the Kolwezi deposits, DRC (Schmandt et al., 2013). Most of the Congolese deposits display higher Co:Cu than those of the Co-bearing deposits in the Zambian Copperbelt (Cailteux et al., 2005). Extremely high Co values (~1%) are present in deposits located along the Tilwezembe anticline to the south of the Kolwezi district in the Congolese Copperbelt (Broughton, 2013).

Cobalt in the Copperbelt deposits is hosted primarily in carrollite ($CuCo_2S_4$), though minor cobalt is also present in linnaeite($Co^{+2}Co^{+3}{}_2S_4$), cobaltiferous pyrite, cattierite, cobaltite (CoS_2), siegenite ($(Ni,Co)_3S_4$), violarite ($Fe^{2+}Ni^{3+}{}_2S_4$), cobaltiferous vaesite ($(Ni,Co)S_2$) and cobaltiferous pentlandite ($(Fe, Ni, Co)_9S_8$) (Cailteaux et al., 2005). Carrollite is intergrown with copper sulfides and appears to have been precipitated throughout the period of copper mineralization (Annels and Simmonds, 1984; Schuh et al., 2012). Especially in the Congolese Copperbelt, cobalt has also been produced from supergene cobalt oxide minerals, primarily heterogenite.

Significant cobalt is also present in the Boleo sedimentary rock-hosted stratiform copper deposit in Baja California Sur, Mexico (Wilson and Rocha, 1955; Ochoa-Landin, 1998). This previously mined deposit has measured and indicated reserves of 172.4 Mt with 0.073% Co (Baja Mining Corp., 2010). The Boleo deposit occurs within Miocene sedimentary rocks that overlie a thick sequence of mafic volcanic rocks. Cobalt is also present in the sedimentary rock-hosted stratiform deposits of the Permian Kupferschiefer in Poland and Germany, though information on grades and tonnages is not available (Borg et al., 2012). Higher concentrations of cobalt are present in the Kupferschiefer district within late veins that also contain nickel and silver. These vein systems may not be directly genetically linked to the disseminated sulfides of the dominant stratiform copper mineralization (Friedrich et al., 1984). Trace cobalt is also present in the Dzhezkazgan sedimentary rock-hosted stratiform copper deposit in Kazakhstan (Yefimenko, 2008), though average concentrations from Dzhezkazgan ore are not publicly available.

The source of cobalt in the sedimentary rock-hosted stratiform deposits is generally unknown. In the Zambian Copperbelt, there is a spatial association of Co-rich deposits with gabbroic bodies (Annels and Simmonds, 1984). However, a mafic igneous source of cobalt is not supported by lead isotope data (Selley et al., 2005). Furthermore, mafic rocks are virtually unknown in the Congolese Copperbelt where cobalt is most pervasive (Cailteux, 1994), although little is known of basement rocks in most of the district. At Boleo, the source of cobalt is presumably footwall mafic volcanic rocks due to their elevated cobalt content.

Several of the carbonate-hosted polymetallic deposits contain significant cobalt. The Kipushi deposit in the Central African Copperbelt contains cobalt in carrollite and in

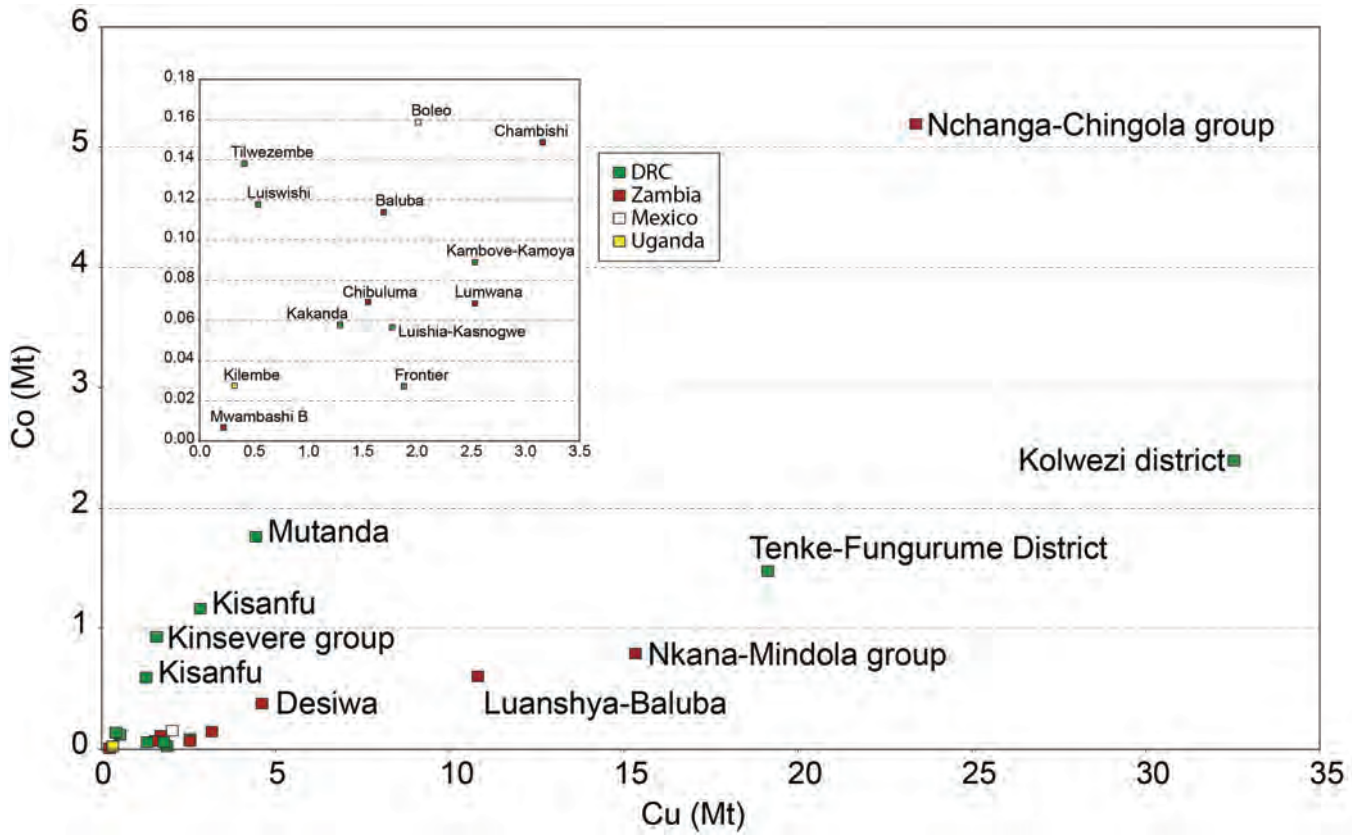

Fig. 2. Cobalt vs. copper tonnage values for sediment-hosted copper deposits with reported cobalt production (data listed in Table 2).

cobaltiferous sphalerite (Intiomale and Oosterbosch, 1974). Average Co values of produced and remaining ore are not publicly available. The Ruby Creek deposit contains significant intervals with over 0.1% Co (Nova Copper Inc., 2013) distributed between cobaltiferous pyrite, which may contain up to 4.3 wt % Co (Bernstein and Cox, 1986), and carrollite.

Gallium

The crustal abundance of gallium is similar to that of lead (5–19 ppm) and gallium is chemically similar to Zn, with chalcophile tendencies and the same electron structure (Vershkoksaya, 1966). Gallium is a post-transition metal between zinc and germanium and below aluminum in the periodic table and can exhibit similar geochemical associations with each. Both hydroxide and fluoride complexes are thought to be important for gallium transport in hydrothermal fluids (Wood and Samson, 2006). Gallium occurs as a minor or trace element in clays and sphalerite, as well as in Ga-bearing sulfides and oxides (Borisenko, 1993; Downs, 1993). Gallium is extracted from zinc ores and from residues from germanium production from zinc ores (Burton and Culkin, 1969; Bautista, 1989; Gray et al., 2007). Gallium abundance in sphalerite is thought to be temperature dependent, with higher gallium concentrations (100–1,000 ppm) in sphalerite precipitated at low temperature (Gray et al., 2007).

Data on the gallium contents of clastic-dominated sediment-hosted deposits are sparse. Zinc concentrates from the Red Dog district have 26 ppm Ga (Alaska Department of Environmental Conservation, 2002). There are relatively abundant data on the gallium content of MVT ores. Sphalerite in MVT ores in the United States contains 7 to 50 ppm Ga (Wellmer et al., 1994; Ullman's Encyclopaedia of Industrial Chemistry, 2002). Samples from MVT deposits in the Alps display gallium contents ranging up to 200 ppm (Schroll, 1984; Pimminger et al., 1985; Fig. 3). Mineralized samples from the Lisheen deposit in Ireland contain up to 73 ppm Ga (Hitzman et al.,

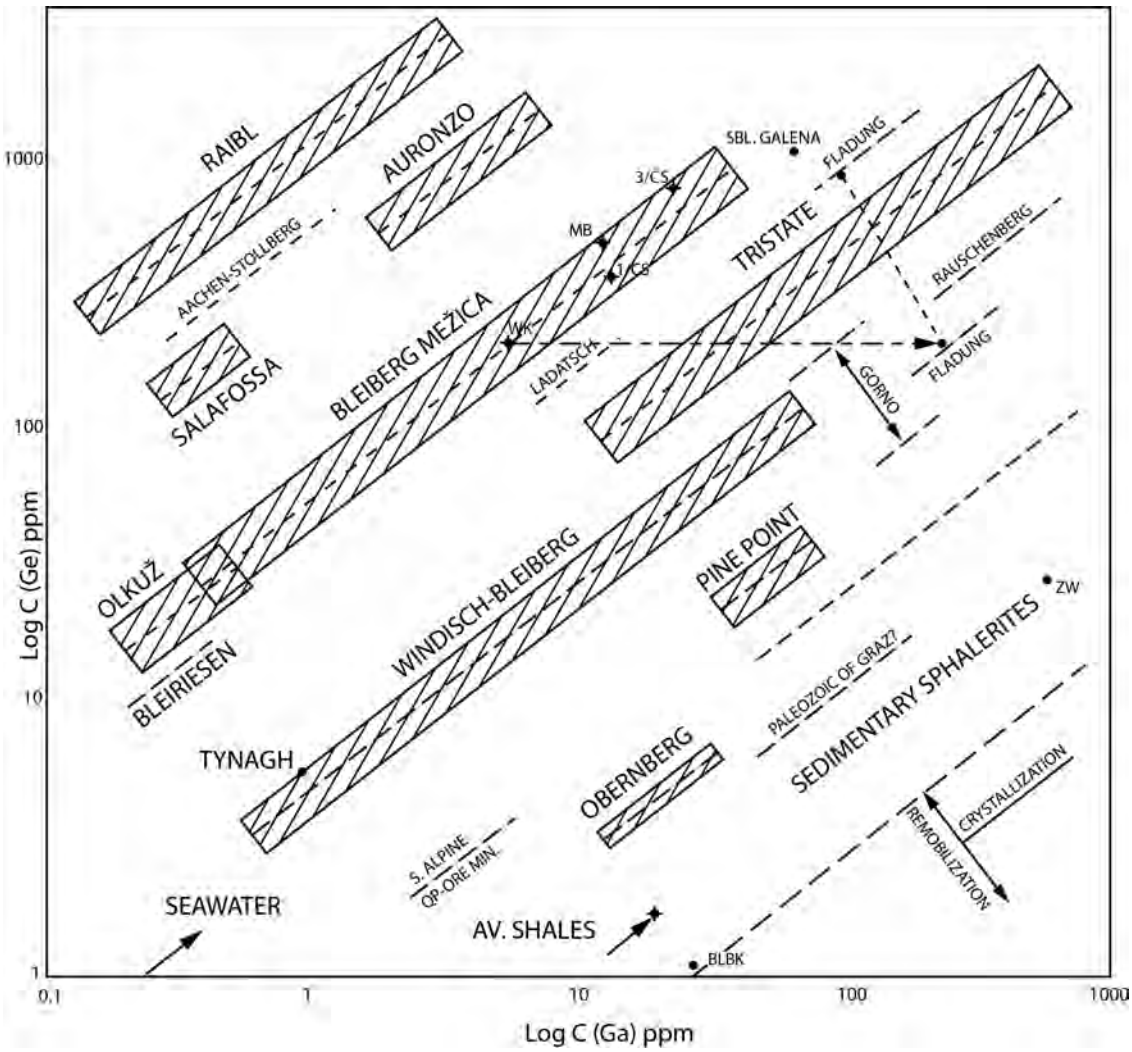

Fig. 3. Gallium vs. germanium content in sphalerite from various MVT ores, shales, and igneous related mineralization reported in Schroll (1984). Ratios illustrate an increase of Ga with increased temperature, similarities between Upper Silesia (Olkuz), Bleiberg, and Bleiriesen, as well as a relationship between higher Ga in deposits hosted in clay-rich sediment (BLBK = Bleiglanzbank; MB = Maxer Bank; QP-ORE MIN = Permian quartz porphyry extrusions of the South Alps; WK = Wetterstein; ZW = Zwickau; 1/CS - first Cardita; 3/CS = third Cardita; modified from Schroll, 1984).

2002) and individual sphalerite grains have gallium values up to 600 ppm (Wilkinson et al., 2005). In United States MVT deposits, paragenetically late iron-rich sphalerite appears to contain higher amounts of gallium than paragenetically early iron-poor sphalerite (Hagni, 1983; Schaeffer et al., 2004). Worldwide, gallium extraction from MVT sphalerite ores was reported to be 6,500 t in 2002 (Ullman's Encyclopaedia of Industrial Chemistry, 2002; Moskalyk, 2003).

There are virtually no data on the gallium concentrations in the sedimentary rock-hosted copper deposits. Gallium is known to be present in several carbonate-hosted polymetallic deposits, though the data are poor. At Kipushi, gallium occurs in gallite ($CuGaS_2$) as small inclusions in renierite, germanite, and Cd-rich sphalerite (DeVos et al., 1974).

Germanium

Germanium abundance in the Earth's crust is 1.6 ppm. It is a metalloid between gallium and arsenic in the periodic table and similar to these elements forms sulfides and oxides such as germanite ($Cu_{26}Ge_4Fe_4S_{32}$), renierite ($(Cu,Zn)_{11}(Ge,As)_2Fe_4S_{16}$), argyrodite ($Ag_8GeS_6$), briarite ($Cu_2(Zn,Fe)GeS_4$),and kriesselite ($Al_2GeO_4(OH)_2$) (all of which appear to form at high sulfur fugacities (Bernstein, 1985; Höll et al., 2007). At moderate temperatures, germanium can be incorporated into copper and arsenic minerals and, at low temperatures and low to moderate sulfur fugacities, it substitutes for zinc in sphalerite and can be present at concentrations up to 3,000 ppm (Vlassov, 1964; Hörmann, 1969; Geldron, 1983; Bernstein, 1985; Höll et al., 2007). Germanium-rich sphalerite may be either iron rich (Lougnon, 1963) or iron poor (Brewers et al., 1955; Vlasov, 1964).

Germanium is transported in hydrothermal fluids as germanic acid, and with fluoride complexes (Wood and Samson, 2006). Based on the presence of germanium in sulfur-rich hot springs (White and Roberson, 1962), Bernstein (1986) speculated that sulfide complexes could also be important for germanium transport.

There are very little data on the germanium contents of clastic-dominated sediment-hosted deposits or sedimentary rock-hosted stratiform copper deposits. Zinc concentrates from the Red Dog clastic-dominated district contain 79 ppm Ge (Alaska Department of Environmental Conservation, 2002). Whole-rock massive and bedded sulfide samples from Sullivan, B.C., contain between 0.8 to 22 ppm Ge (Slack et al., 2000).

There are relatively abundant data on the germanium content of MVT ores. The MVT ores in the United States contain between 20 and 450 ppm Ge (Wellmer et al., 1994) and germanium is a common by-product of zinc smelters utilizing United States MVT zinc concentrates (Nyrstar, 2013). The MVT deposits of the Alps contain sphalerite with germanium values up to 4,900 ppm (Pimminger et al., 1985; Schroll, 1984, 2005; Fig. 3). In contrast, the Irish MVT deposits appear to have low germanium contents. The ICP-MS analysis of whole-rock ore samples from the Lisheen deposits have maximum germanium values of 1.3 ppm (Hitzman et al., 2002), whereas microprobe analyses of sphalerite from Lisheen yield values up to 500 ppm Ge (Wilkinson et al., 2005). Analyses of sphalerite from the Tynagh and Navan deposits in Ireland show germanium concentrations up to 27 and 72 ppm, respectively (Höll et al., 2007). Trace element analyses of sphalerite from various MVT deposits in southern China reveal enriched germanium (Ye et al., 2011). One deposit, Huize, contains sphalerite with up to 354 ppm Ge; this deposit has a production of 10 t/yr of by-product germanium (Melcher and Buchholz, 2014). Germanium content in zinc concentrates from MVT in South America ranges from ~10 to 130 ppm (Soler and Lara, 1990; Fig. 4).

The carbonate-hosted polymetallic deposits have historically been major sources of germanium. The Kipushi and Tsumeb deposits were major producers, with average grades of 0.3 and 0.005% Ge, respectively. The Kipushi mine produced 278 t Ge from 1956 to 1978 (Ivanplats Limited, 2012). Mineralized samples from the Khusib Springs deposit contain up to 0.011% Ge (Melcher et al., 2006). The Apex deposit in Utah is cited as containing 220,235 t of 0.064% Ge (Bernstein and Cox, 1986). The Ruby Creek deposit contains germanium (Bernstein and Cox, 1986), but average grades are not available.

Germanium in sediment-hosted polymetallic deposits generally occurs in the minerals renierite [$(Cu,Zn)_{11}(Ge,As)_2Fe_4S_{16}$] and germanite [$Cu_{11}Ge(Cu,Ge,Fe,Zn,W,Mo,As,V)_{4\text{-}6}S_{16}$] and more rarely in briartite [$Cu_2(Fe,Zn)GeS_4$]. At Kipushi (Intiomale and Oosterbosch, 1974; Intiomale, 1983), Tsumeb (Lombaard et al., 1986; Maiden and Hughes, 2000), and Ruby Creek (Bernstein and Cox, 1986), germanium sulfides are concentrated in high-grade copper zones and occur as inclusions in, or are intergrown with bornite and, in some cases, chalcocite-digenite. At Kipushi germanium also occurs in cadmium-rich sphalerite assemblages, with some of the germanium apparently present within sphalerite itself (Intiomale, 1983).

Indium

Average indium concentrations in continental and oceanic crust rocks are 0.05 ppm and 0.072 ppm, respectively (Shaw, 1952; Taylor and McLennon, 1985; Phipps et al., 2008; Schwarz-Schampera, 2013). Indium is a post-transition metal and sits between cadmium and tin in the periodic table. In sediment-hosted Zn-Pb deposits, indium occurs most commonly in sphalerite and chalcopyrite (Yi et al., 1995; Schwarz-Schampera and Herzig, 2002; Schwarz-Schampera, 2013), but it may also occur in indium-bearing minerals such as roquesite ($CuInS_2$), laforetite ($AgInS_2$), indite ($Fe^{2+}In_2S_4$), and tolovkite (InSbS). Cook et al. (2009) show that indium and copper concentrations co-vary, and presumably represent coupled substitution for Zn^{+2}; they also suggest that indium occurs preferentially in higher temperature mineral assemblages.

The Rammelsburg clastic-dominated sediment-hosted deposit contained up to 300 ppm indium in copper-rich material from within a feeder zone beneath the stratiform deposit (Large and Walcher, 1999; Schwarz-Schampera and Herzig, 2002). Samples of concentrate from the Sullivan clastic-dominated sediment-hosted deposit contained an average of 14.6 ppm indium (Hamilton et al., 1983), with sphalerite having values up to 93 ppm In (Yi et al., 1995). Though no indium analyses are publicly available for the Red Dog deposits, the Trail Metallurgical Operation produced by-product indium from ore that was primarily from Red Dog and Sullivan (Roskill, 1992). There is no indication from available

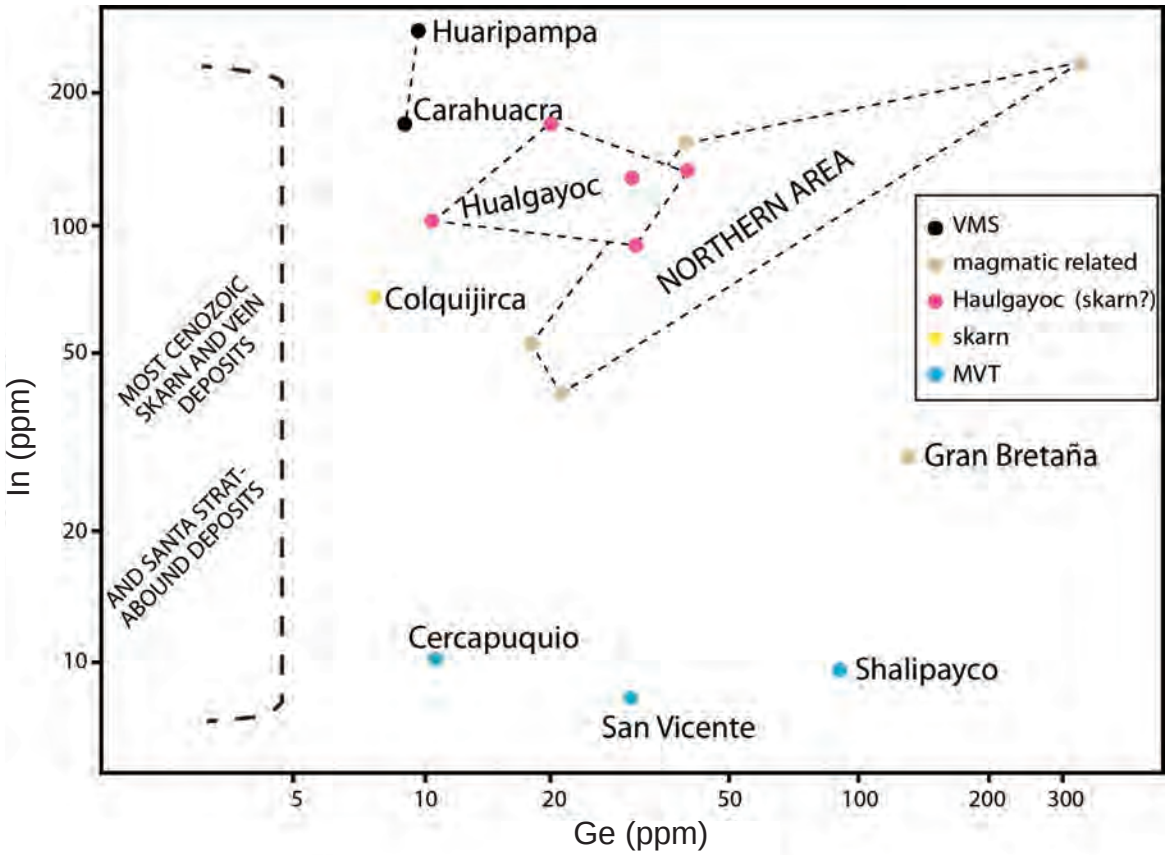

Fig. 4. Germanium vs. indium concentrations from various deposits in South America (modified from Soler and Lara, 1990). MVT = Mississippi Valley-type, VMS = volcanogenic massive sulfide.

metallurgical data that the northern Australian clastic-dominated sediment-hosted deposits contain significant indium.

The enhanced indium contents of higher-temperature "feeder zone" type mineralized rockexemplified by the copper-rich ore at Rammelsburg suggests that the hydrothermal fluid temperature may have been a control on the presence of indium. The higher temperature copper-rich sulfide zones within volcanogenic massive sulfide deposits commonly contain up to 300 ppm indium (Schwarz-Schampera and Herzig, 2002). Future work could investigate whether copper-rich clastic-dominated sediment-hosted deposits such as Ambaji, Basantgarh, and Deri in India (SRK Consulting and Gustavson Associates, 2004), d'Abu Samar in Sudan (El Samani, 1986), and small copper-rich portions of the HYC deposit in Australia contain significant indium.

Little data are available for the indium contents of MVT ores. The San Vincente and Shalipayco deposits in Peru produced concentrates with low indium values (~10 ppm; Rodier, 1990; Soler and Lara, 1990; Fig. 4). Hagni (1983) noted that paragenetically late, iron-rich sphalerite in the Tri-State and Viburnum Trend deposits contains elevated indium relative to earlier, lessiron-rich sphalerite. Sphalerite from the Lisheen MVT deposit contains indium values up to 500 ppm In (Wilkinson et al., 2005). Additional work is required to determine if iron-rich sphalerites or sphalerites rich in other trace elements such as Cu, Ag, or Cd in MVT deposits are also enriched in indium.

Sedimentary rock-hosted copper deposits and carbonate-hosted polymetallic deposits do not appear to contain significant indium. Whether this is due to the lack of analysis or occurrence is uncertain as data are scarce.

Platinum group elements (PGEs)

Platinum and palladium are enriched in ultramafic rocks (10–20 ppb) and black shales (50 ppb) (Goldschmidt, 1958; Wedepohl, 1969; Coveney et al., 1992, Dill, 2010; Gunn, 2013). Palladium and platinum are transition metals and occur near Au, Ag, and Ni in the periodic table. Chloride complexes transport the platinum group metals at moderate temperatures, low pH, and high oxidation states (Jaireth, 1992; Gammons et al., 1992; Pašava, 1993). Transport of these metals at low temperatures (<150°C) has not been thoroughly investigated.

No significant occurrences of PGEs have been recognized in clastic-dominated sediment-hosted deposits, MVT deposits, or in carbonate-hosted polymetallic deposits. However, several sedimentary rock-hosted stratiform copper districts have produced small amounts of palladium and platinum. Platinum group elements (PGEs) production has occurred in the sedimentary rock-hosted stratiform copper deposits of the Polish Kupferschiefer (Hitzman et al., 2005). Several tens of kilograms of Pt+Pd slime have been produced from the Lubin area mines in Poland where platinum and palladium values range up to 370 and 120 ppm, respectively (Kucha,

1982, 1994; Borg et al., 2012). In the Polish Kupferschiefer deposits, PGEs (principally platinumand palladium) are concentrated in narrow zones that straddlethe redox front between underlying hematitic redbeds and the overlying, organic-rich Kupferschiefer shale (Pašava, 1993; Betchel et al., 2001; Oszczepolski et al., 2002; Piestrzynski et al., 2002; Borg et al., 2005, 2012; Walther et al., 2009). Platinum occurs as a native metal and palladium occurs as native palladium and in haycockite ($Cu_4Fe_5S_8$), sobolevskite (PdBi), palladium arsenides, and nickel-cobalt arsenides (Kucha, 1982; Peterson, 1994). Detailed mineralogical studies by Piestrzynski et al. (2002), Pieczonka and Piestrzynski (2008), and Pieczonka et al. (2008) indicate that mineralized zones in the Polish sedimentary rock-hosted deposits also contain trace amounts of gold, noble metal alloys, tellurides, selenides, arsenides, and arsenates. In some instances the PGEs and other trace metals are associated spatially with organic matter and enhanced vanadium values indicative of organic matter (Kucha, 1982, 1994; Borg et al., 2012). There are no reports of PGE production from the German Kupferschiefer deposits, though Borg et al. (2005) describe PGE mineralization within the Mansfeld/Sangerhausen district of Germany that appears to be similar to that in the Polish Kupferschiefer.

Very minor amounts of palladium, platinum, and gold have also been produced from several of the sedimentary rock-hosted deposits in the Kolwezi district of the Congolese Copperbelt, and PGEs have been noted in assays from several other deposits in the Congolese Copperbelt, including the Kambove, Shinkolobwe, Mutoshi, Swambo, and Musonoi deposits (François, 1974).

Rhenium

In crustal rocks, rhenium typically ranges between 0.2 and 2 ppb, with the greatest concentrations in black shales and sapropels that may contain up to 2556 ppb Re (Lipinski et al., 2003). Rhenium is a transition metal and has physical properties similar to Mo and W (Millensifer et al., 2014) At low temperatures rhenium is apparently precipitated by redox reactions (Xiong and Wood, 2001; Xiong et al., 2006). Rhenium can substitute for molybdenum within molybdenite and castaingite ($CuMo_2S_5$) (McCandless et al., 1993) and also occurs in rhenium sulfides such as rheniite (ReS_2), tarkianite ($(Cu,Fe)(Re,Mo)_4S_8$), and dzhezkazganite ($(Pb,Cu,Rh)S_2$) (Millensifer et al., 2014). Rhenium sulfides are commonly associated with bornite (Samonov and Pozharisky, 1977).

The majority of the world's rhenium comes from molybdenite in porphyry-style deposits. There are no reports of rhenium in clastic-dominated sediment-hosted or MVT deposits. Sedimentary rock-hosted stratiform copper deposits contain approximately 10 to 15% of the global rhenium resources (Millensifer et al., 2014). The sedimentary rock-hosted Dzhezkazgan and Zhaman-Aibat copper deposits in the Chu-Sarysu basin of Kazakhstan produce by-product rhenium. Dzhezkazgan ores average 1 to 2 g/t Re, whereas the Zhaman-Aibat deposit has an average grade of 1.45 g/t Re (Seyfullin et al., 1974; Yefimenko, 2008). It is unclear if the rhenium in these deposits occurs as lattice substitutions in copper sulfides or as small inclusions of Re sulfides (Poplavko et al., 1962; Fleischer, 1963). The Mansfeld-Sangerhausen deposit of the German Kupferschiefer is reported to contain 21 g/t Re (Kirkham, 1989; Xiong and Wood, 2001). It is likely that other sedimentary rock-hosted stratiform copper deposits contain minor amounts of rhenium, as reported from Lubin (5.3 ppm in the Cu-rich samples; 1.5 ppm in the Rote Faule; Piestrzynski and Sawlowicz, 1999). It has probably not been recognized due to the general absence of geochemical analysis for rhenium.

Conclusions and Recommendations for Future Research

There are relatively sparse data on the concentrations of critical elements in most sediment-hosted deposits and in concentrates produced from these deposits. However, several sediment-hosted deposits and districts are significant repositories of critical elements. Generally, clastic-dominated deposits appear to lack critical elements, with significant concentrations of cobalt and indium only in the higher temperature, commonly copper-rich portions of orebodies. Mississippi Valley-type deposits have been significant producers of both gallium and, more importantly, germanium. Unusually copper-rich, and probably higher temperature, portions of several MVT deposits may contain cobalt. The sedimentary rock-hosted stratiform copper deposits are one of the world's most important sources of cobalt, though major production has come from only one district, the Central African Copperbelt. Sedimentary rock-hosted stratiform copper deposits may also contain significant rhenium; the deposits of the Chu-Sarysu basin of Kazakhstan are an important source of this element. Portions of several sedimentary rock-hosted stratiform copper deposits contain anomalous concentrations of PGEs. Historically, the polymetallic sediment-hosted deposits have been an important source of germanium, and they may contain other critical elements such as gallium and rhenium.

More work is needed to understand the distribution of critical elements in sediment-hosted deposits. Critical element contents vary both by deposit type and between mine districts belonging to the same deposit type. It is likely that spatially limited portions of a number of sediment-hosted deposits contain unrecognized elevated concentrations of critical elements. Better understanding of the spatial and temporal distribution of these critical elements in individual deposits should lead to a better understanding of critical element geochemistry and favorable environments for their enrichment, and thereby allow for better prediction of their presence. Given the relatively low cost of high-precision geochemical analyses, more multielement geochemical data on the ores and concentrates from these deposits are possible.

Acknowledgments

We would like to thank Alan Koenig, Philip Verplanck, and Rich Goldfarb for discussions and encouragement. Alex Brown, Jeff Mauk, and Janet Slate are thanked for thorough reviews that significantly improved the manuscript.

REFERENCES

Abdullah, S., Chmyriov, V.M., Stazhilo-Alekseev, K.F., Dronov, V.I., Gannon, P.J., Lubemov, B.K., Kafarskiy, A.K., and Malyarov, E.P., 1977, Mineral resources of Afghanistan: Ministry of Mines and Industries, Afghan Geological and Mines Survey, Republic of Afghanistan, v. 2, 419 p.

Alaska Department of Environmental Conservation, 2002, Table 2–1: Composition of Red Dog lead and zinc concentrates: Accessed March 6, 2013 (dec.alaska.gov/spar/csp/docs/reddog/03dmts_ra_tables-april2005.pdf)

American Physical Society, 2011, The energy critical elements: Securing materials for emerging technologies: 28 p. (http://www.aps.org/policy/reports/popa-reports/upload/elementsreport.pdf)

Annels, A.E., 1974, Some aspects of the stratiform ore deposits of the Zambian Copperbelt and their genetic significance, *in* Bartholomé, P., ed., Gisements stratiformes et provinces cuprifères: Liège, Société Géologique de Belgique, p. 235–254.

Annels, A.E., and Simmonds, J.R., 1984, Cobalt in the Zambian Copperbelt: Precambrian Research, v. 25, p. 75–98.

Baja Mining Corp, 2010, Technical report update, Baja south, Mexico: NI 43-101, 206 p.

Bartholomé, P., 1962, Les minerais cupro-cobaltifères de Kamoto (Katanga-Ouest), I. Pétrographie—II. Paragenèses. Studia Universitatis "Lovanium", Faculté des Sciences, University of Kinshasa, v. 14, 40 p. and v. 16, 24 p.

——1974, On the diagenetic formation of ores in sedimentarybeds, with special reference to Kamoto, Shaba, Zaïre, *in* Bartholomé, P., ed., Gisements stratiformes et provinces cuprifères: Liège, Société Géologique de Belgique, p. 203–213.

Bautista, R.G., 1989, Gallium metal recovery: JOM, Journal of the Minerals, Metals and Materials Society, v. 41, p. 30–31.

Bazargani-Guilani, K., Nekouvaght Tak, M.A., and Faramarzi, M., 2011, Pb-Zn deposits in Cretaceous carbonate host rocks, northeast Shahmirzad, central Alborz, Iran: Australian Journal of Earth Sciences, v. 58, p. 297–307.

Bernstein, L.R., 1985, Germanium geochemistry and mineralogy: Geochimica et Cosmochimica Acta, v. 49, p. 2409–2422.

——1986, Geology and mineralogy of the Apex germanium-gallium mine, Washington County, Utah: Utah Geological Association Publication 15, p. 119–127.

Bernstein, L.R., and Cox, D.P., 1986, Geology and sulfide mineralogy of the Number One orebody, Ruby Creek copper deposit, Alaska: Economic Geology, v. 81, p. 1675–1689.

Betchel, A., Bechtel, A., Ghazi, A.M., Elliott, W.C., and Oszczepalski, S., 2001, The occurrences of the rare earth elements and the platinum group elements in relation to base metal zoning in the vicinity of Rote Fäule in the Kupferschiefer of Poland: Applied Geochemistry, v. 16, p. 375–386.

Borg, G., Frotzscher, M., and Ehling, B., 2005, Metal content and spatial distribution of Au and PGE in the Kupferschiefer of the Mansfeld/Sangerhausen mining district, Germany, *in* Mao, J., and Bierlein, J.P. , eds., Mineral deposit research: Meeting the global challenge: Berlin-Heidelberg, Springer, p. 885–888.

Borg, G., Piestrzynski, A., Bachmann, G.H., Püttmann, W., Walther, S., and Fiedler, M., 2012, An overview of the European Kupferschiefer deposits: Society of Economic Geologists Special Publication 16, p. 444–486.

Borisenko, L.F., 1993, Promising types of gallium bearing deposits: Lithology and Mineral Resources, v. 28, p. 25–37.

Box, S.E., Syusyura, B., Sletmann, R., Creaser, R.A., Dolgopolova, A., and Zientek, M.L., 2012, Dzhezkazgan and associated sandstone copper deposits of the Chu-Sarysu basin, central Kazakhstan: Society of Economic Geologists Special Publication 16, p. 303–328.

Bradley, D.C., and Leach, D.L., 2003, Tectonic controls of Mississippi Valley-type lead-zinc mineralization in orogenic forelands: Mineralium Deposita, v. 38, p. 652–667.

Brewers, F.M., Cox, J.D., and Morris, D.F.C., 1955, The occurrence of germanium in blende: Geochimica et Cosmochimica Acta, v. 8, p. 131–136.

British Geological Survey, 2012, Risk list—current supply risk index for chemical elements or element groups which are of economic value: 12 p. (http://www.bgs.ac.uk/downloads/start.cfm?id=2643)

Broadbent, G.C., Myers, R.E., and Wright, J.V., 1998, Geology and origin of shale-hosted Zn-Pb-Ag mineralization at the Century deposit, northwest Queensland, Australia: Economic Geology, v. 93, p. 1264–1294.

Broughton, D.W., 2013, Geology and ore deposits of the Central African Copperbelt: Ph.D. dissertation, Golden, Colorado, Colorado School of Mines, 140 p.

Brown, A.C., 1971, Zoning in the White Pine copper deposit, Ontonagon County, Michigan: Economic Geology, v. 66, p. 543–573.

Burton, J.D., and Culkin, F., 1969, Gallium, *in* Wedepohl, K.H., ed., Handbook of geochemistry, Vol. 2: Berlin, Springer, p. 31-1–31-O-11.

Cailteux, J., 1994, Lithostratigraphy of the Neoproterozoic Shaba-type (Zaire) Roan Supergroup and metallogenesis of associated stratiform mineralization: Journal of African Earth Sciences, v. 19, p. 279–301.

Cailteux, J.L.H., Kampunzu, A.B., Lerouge, C., Kaputo, A.K., and Milesi, J.P., 2005, Genesis of sediment-hosted stratiform copper-cobalt deposits, Central African Copperbelt: Journal of African Earth Sciences, v. 42, p. 134–158.

Carne, R., and Cathro, R., 1982, Sedimentary exhalative (Sedex) zinc-lead-silver deposits, northern Canadian Cordillera: Canadian Institute of Mining and Metallurgy Bulletin, v. 1, p. 66–78.

Cerny, I., and Schroll, E., 1985.Heimische Vorräte an Spezialmetallen (Ga, In, Tl, Ge, Se, Te und Cd) in Blei-Zink und anderen Erzen: Archivfür Lagerstättenforschung der Geologischen Bundesanstalt, Wien 18, p. 5–33.

Chartrand, F.M., and Brown, A.C., 1985, The diagenetic origin of stratiform copper mineralization, Coates Lake, Redstone copper belt, N.W.T., Canada: Economic Geology, v. 80, p. 325–343.

Chartrand, F.M., Brown, A.C., and Kirkham, R.V., 1989, Diagenesis, sulphides, and metal zoning in the Redstone copper deposit, Northwest Territories: Geological Association of Canada Special Paper 36, p. 189–206.

Cook, N.J., Ciobanu, C.L., Pring, A., Skinner, W., Shimizu, M., Danyushevsky, L., Saini-Eidukat, B., and Melcher, F., 2009, Trace and minor elements in sphalerite: A LA-ICPMS study: Geochimica et Cosmochimica Acta, v. 73, p. 4761–4791.

Cooke, D.R., Bull, S.W., Large, R.R., and McGoldrick, P.J., 2000, The importance of oxidized brines for the formation of Australian Proterozoic stratiform sediment-hosted Pb-Zn (Sedex) deposits: Economic Geology, v. 95, p. 1–18.

Cooke, D.R., Bull, S., and Large, R.R., 2003, Processes of ore formation in the stratiform sediment-hosted Zn-Pb deposits of northern Australia: Testing the Century model: Journal of Geochemical Exploration, v. 78, p. 519–524.

Copper Strike Limited, 2005, Final drill results from Walford Creek, 9 November 2005: (http://www.infomine.com/index/prPA313299.pdf)

Coveney, R.M., Jr., Murowchick, J.B., Grauch, R.I., Glascock, M.D., and Denison, J.R., 1992, Gold and platinum in shales with evidence against extraterrestrial sources of metals: Chemical Geology, v. 99, p. 101–114.

Croxford, N.J.W., 1974, Cobalt mineralization at Mount Isa, Queensland, Australia, with references to Mount Cobalt: Mineralium Deposita, v. 9, p. 105–115.

Deb, M., and Pal, T., 2004, Geology and genesis of the base metal sulphide deposits in the Dariba-Rajpura-Bethumni belt, Rajasthan, India, in the light of basin evolution, *in* Deb, M., and Goodfellow, W.D., eds., Sediment hosted lead-zinc sulphide deposits: Attributes and models of some major deposits in India, Australia and Canada: New Delhi, India, Narosa Publishing House, p. 304–327.

De Magnée, I., and François, A., 1988, The origin of the Kipushi (Cu, Zn, Pb) deposit in direct relation with a Proterozoic salt diapir, Copperbelt of central Africa, Shaba, Republic of Zaïre, *in* Friedrich, G.H., and Herzig, P.M., eds., Base metal sulfide deposits: Berlin-Heidelberg, Springer-Verlag, p. 74–93.

DeVos, W., Viaene, W., Moreau, J., and Wautier, J., 1974, Minéralogie du gisement de Kipushi, Shaba, Zaire, *in* Bartholomé, P., ed., Gisements stratiformes et provinces cuprifères: Liège, Société Géologique de Belgique, p. 165–183.

Dill, H.G., 2010, The "chessboard" classification scheme of mineral deposits: Mineralogy and geology from aluminum to zirconium: Earth Science Reviews, v. 100, p. 1–420.

Downs, A.J., 1993, Chemistry of aluminum, gallium, indium, and thallium: Glasgow, Blackie Academic and Professional, 533 p.

El Samani Y., Touray, J.C., Pouit, G., and Guyot, G., 1986, La Mineralisation en Zn-Cu-Mn-Ba d'Abu Samar et les Indices de la Plaine d'Allaikaleib (Soudan): Des Accumulation Metalliferes Metamophisees d'Origin Exhalative-Sedimentaire: Chronique de la Récherche Miniére, v. 483, p. 3–18.

Ethier, V.G., Campbell, F.A., Both, R.A., and Krouse, H.R., 1976, Geological setting of the Sullivan orebody and estimates of temperatures and pressure of metamorphism: Economic Geology, v. 71, p. 1570–1588.

Fleischer, M., 1963, New mineral names—Dzhezkazganite: American Mineralogist, v. 48, p. 209.

Fleischer, V.D., Garlick, W.G., and Haldane, R., 1976, Geology of the Zambian Copperbelt, *in* Wolf, K.H., ed., Handbook of strata-bound and stratiform ore deposits: Elsevier Science v. 6, p. 223–352.

Fontbote, L., and Gorzawski, H., 1990, Genesis of the Mississippi Valley-type Zn-Pb deposit of San Vicente, central Peru; geologic and isotopic (Sr, O, C, S, Pb) evidence: Economic Geology, v. 85, p. 1402–1437.

François, A., 1974, Stratigraphie, tectonique et minéralisations dans l'arc cuprifère du Shaba (République du Zaïre), *in* Bartholomé, P., ed., Gisement

stratiformes et provinces cuprifères: Liège, Société Géologique de Belgique, p. 79–101.
Friedrich, G., Diedel, R., Schmitdt, F.P., and Schumacher, C., 1984, Untersuchungen an Cu-As-Sulfiden und Arseniden des basalen Zechsteins der Gebiete Spessart/Rhön und Richelsdorf: Fortschritte der Mineralogie, v. 62, p. 63–65.
Gammons, C.H., Bloom, M.S., and Yu, Y., 1992, Experimental investigation of the hydrothermal geochemistry of platinum and palladium: I. Solubility of platinum and palladium sulfide minerals in $NaCl/H_2O/SO_4$ solutions at 300°C: Geochimica et Cosmochimica Acta, v. 56, p. 3881–3894.
Geldron, A., 1983, Le germanium: un élément valorisant des gisements hydrothermaux a Zn-Cu-(Pb): Chron. Rech. Min., no. 470, p. 25–32.
Glencore, 2012, Annual Report 2012: http://www.glencore.com/assets/investors/doc/reports_and_results/2012/GLEN-Annual-Report-2012.pdf, 170 p.
Goldschmidt, V.M., 1958, Geochemistry: London, Oxford University Press, 730 p.
Goodfellow, W.D., and Lydon, J.W., 2007, Sedimentary-exhalative (SEDEX) deposits: Geological Association of Canada, Mineral Deposits Division, Special Publication 5, p. 163–183.
Goodfellow, W.D., Lydon, J.W., and Turner, R.W., 1983, Geology and genesis of stratiform sediment-hosted (SEDEX) Zn-Pb-Ag sulphide deposits: Geological Association of Canada Special Paper 40, p. 201–251.
Graham, G.E., Hitzman, M.W., and Zieg, J., 2012, Geologic setting, sedimentary architecture, and paragenesis of the sediment-hosted Sheep Creek Cu-Co-Ag deposit, Helena embayment, Montana: Economic Geology, v. 107, p. 1115–1141.
Gray, F., Kramer, D.H., and Bliss, J.D., 2007, Gallium and gallium compounds, *in* Kirk-Othmer concise encyclopedia of chemical technology 5th ed: Hoboken, N.J.,Wiley-Interscience, p. 337–364.
Gulson, B.L., 1985, Shale-hosted lead-zinc deposits in northern Australia: Lead isotope variations: Economic Geology, v. 80, p. 2001–2012.
Gunn, G., 2013 Platinum-group metals, *in* Gunn, G., ed., Critical metals handbook, 1st ed.: Oxford, John Wiley and Sons, p. 284–311.
Hagni, R., 1983, Minor elements in Mississippi Valley-type ore deposits, *in* Shanks, W.C., ed., Cameron volume on unconventional mineral deposits: New York, Society of Mining Engineers AIME, p. 71–88.
Hagni, R.D., and Gann, D.E., 1976, Microscopy of copper ore at the Creta mine, southwestern Oklahoma: Oklahoma Geological Survey Circular, v. 77, p. 40–50.
Hamilton, J.M., Delaney, G.D., Hauser, R.L., and Ransom, P.W., 1983, Geology of the Sullivan deposit, Kimberley, BC, Canada: Mineralogical Association of Canada, Short Course Handbook, v. 8, p. 31–83.
Heijlen, W., Banks, D.A., Muchez, P., Stensgard, B.M., and Yardley, B.W.D., 2008, The nature of mineralizing fluids of the Kipushi Zn-Cu deposit, Katanga, Democratic Republic of Congo: Quantitative fluid inclusion analysis using laser ablation ICP-MS and bulk crush-leach methods: Economic Geology, v. 103, p. 1459–1482.
Hitzman, M.W., 1986, Geology of the Ruby Creek copper deposit, southwestern Brooks Range, Alaska: Economic Geology, v. 81, p. 1644–1674.
Hitzman, M.W., and Large, D., 1986, A review and classification of the Irish carbonate-hosted base metal deposits, *in* Andrew, C.J., Crowe, R.W.A., Finlay, S., Pennell, W.M., and Pyne, J.F., eds., Geology and genesis of mineral deposits in Ireland: Dublin, Irish Association for Economic Geology, p. 217–238.
Hitzman, M.W., Redmond, P.B., and Beaty, D.W., 2002, The carbonate-hosted Lisheen Zn-Pb-Ag deposit, County Tipperary, Ireland: Economic Geology, v. 97, p. 1627–1655.
Hitzman, M.W., Reynolds, N.A., Sangster, D.F., Allen, C.R., and Carman, C.E., 2003, Classification, genesis, and exploration guides for nonsulfide zinc deposits: Economic Geology, v. 98, p. 685–714.
Hitzman, M.W., Kirkham, R., Broughton, D., Thorson, J., and Selley, D., 2005, The sediment-hosted stratiform copper ore system: Economic Geology 100th Anniversary Volume, p. 609–642.
Hitzman, M.W., Broughton, D., Selley, D., Woodhead, J., Wood, D., and Bull, S., 2012, The Central African Copperbelt: Diverse stratigraphic, structural, and temporal settings in the world's largest sedimentary copper district: Society of Economic Geologists Special Publication 16, p. 487–514.
Höll, R., Kiling, M., and Schroll, R., 2007, Metallogenesis of germanium: Ore Geology Reviews, v. 30, p. 145–180.
Hörmann, P.K., 1969, Germanium, *in* Wedepohl, K.H., Handbook of geochemistry II: Berlin-Heidelberg, Springer, p. 32–A-1–32–O-9.
Hughes, M.J., 1987, The Tsumeb ore body, Namibia, and related dolostone-hosted base metal ore deposits of central Africa: Ph.D. dissertation, Johannesburg, South Africa, University of the Witwatersrand, 448 p.
Innes, J., and Chaplin, R.C., 1986, Ore bodies of the Kombat mine, south west Africa (Namibia), *in* Anhaeusser, C.R., and Maske, S., eds., Mineral deposits of southern Africa: Geological Society of South Africa, v. 2, p. 1789–1805.
Intiomale, M.M., 1983, Le Gisement Zn-Pb-Cu de Kipushi (Shaba-Zaïre). Etude Géologique et Metallogénique: Ph.D. thesis, Louvainla-Neuve, Belgium, Université Catholique de Louvain, 170 p.
Intiomale, M.M., and Oosterbosch, R., 1974, Géologie et géochimie du gisement de Kipushi, Zaïre, *in* Bartholomé, P. , ed., Gisements stratiformes et provinces cuprifères: Liège, Belgium, Sociéte Géologique de Belgique, p. 123–164.
Ivanplats Limited, 2012, Kipushi Project Dominican Republic of Congo: Technical Report NI 43-101 (Revision 2), 53 p.
Jaireth, S., 1992, The calculated solubility of platinum and gold in oxygen-saturated fluids and the genesis of platinum-palladium and gold mineralization in the unconformity-related uranium deposits: Mineralium Deposita, v. 27, p. 42–54.
Johnson, K.S., 1976, Permian copper shales of southwestern Oklahoma: Oklahoma Geological Survey Circular 77, p. 3–14.
Kamona, F., 1993, The carbonate hosted Kabwe Pb-Zn deposit, central Zambia: Ph.D. dissertation, Aachen, Germany, Rheinisch-Westfalischen Technischen Hoschschule, 207 p.
Kampunzu, A.B., Cailteux, J.L.H., Kamoa, A.F., Intiomale, M.M., and Melcher, F., 2009, Sediment-hosted Zn-Pb-Cu deposits in the Central African Copperbelt: Ore Geology Reviews, v. 35, p. 263–297.
Kelley, K.D., and Jennings, S., 2004, A special issue devoted to barite and Zn-Pb-Ag deposits in the Red Dog district, Western Brooks Range, northern Alaska: Economic Geology, v. 99, p. 1–14.
Kelley, K.D., Dumoulin, J.A., and Jennings, S., 2004, The Anarraaq Zn-Pb-Ag and barite deposit, northern Alaska: Evidence for replacement of carbonate by barite and sulfides: Economic Geology, v. 99, p. 1577–1591.
Kirkham, R.V., 1989, Distribution, settings, and genesis of sediment-hosted stratiform copper deposits: Geological Association of Canada Special Paper 36, p. 3–38.
Krebs, W., 1981, The geology of the Meggen ore deposit, *in* Wolf.K.H., ed., Handbook of stratabound and stratiform ore deposits: Amsterdam, Elsevier, p. 509–549.
Kucha, H., 1982, Platinum-group metals in the Zechstein copper deposits, Poland: Economic Geology, v. 77, p. 1578–1591.
——1994, PIXE analysis of Kupferschiefer samples: Geological Quarterly, v. 38, no. 4, p. 687–700.
Large, D., and Walcher, E., 1999, The Rammelsberg massive sulphide Cu-Zn-Pb-Ba-deposit, Germany: An example of sediment-hosted, massive sulphide mineralization: Mineralium Deposita, v. 34, p. 522–538.
Large, R.R., Bull, S.W., McGoldrick, P.J., Derrick, G., Carr, G., and Walters, S., 2005, Stratiform and stratabound Zn-Pb-Ag deposits of the Proterozoic sedimentary basins of northern Australia: Economic Geology 100th Anniversary Volume, p. 931–963.
Lavery, N.G., Leach, D.L., and Saunders, J.A., 1994, Lithogeochemical investigations applied to exploration for sediment-hosted lead-zinc deposits, *in* Fontbote, L., and Boni M., eds., Sediment-hosted Zn-Pb ores: Berlin-Heidelberg, Springer, p. 393–428.
Leach, D.L., and Sangster, D.F., 1993, Mississippi Valley-type lead-zinc deposits: Geological Association of Canada Special Paper 40, p. 289–314.
Leach, D.L., Viets, J.G., Kozlowski, A., and Kibletski, S., 1996, Geology, geochemistry, and genesis of the Krakow-Silesia zinc-lead district, southern Poland: Society of Economic Geology Special Publication 4, p. 144–170.
Leach, D.L., Bradley, D., Lewchuk, M.T., Symons, D.T., de Marsily, G., and Brannon, J., 2001, Mississippi Valley-type lead-zinc deposits through geological time: Implications from recent age-dating research: Mineralium Deposita, v. 36, p. 11–740.
Leach, D.L., Bechstadt, T., Boni, M., and Zeeh, S., 2003, Triassic-hosted MVT Zn-Pb ores of Poland, Austria, Slovenia and Italy, *in* Kelley, J.G., Andrew, C.J., Ashton, J.H., Boland, M.B., Earls, G., Fusciardi, L., and Stanley, G., eds., Europe's major base metal deposits: Dublin, Irish Association for Economic Geology, p. 169–214.
Leach, D.L., Sangster, D.F., Kelley, K.D., Large, R.R., Garven, G., Allen, C.R., Gutzmer, J., and Walters, S., 2005, Sediment-hosted lead-zinc deposits: A global perspective: Economic Geology 100th Anniversary Volume, p. 561–608.
Leach, D.L., Bradley, D.C., Huston, D., Pisarevsky, S.A., Taylor, R.D., and Gardoll, S.J., 2010a, Sediment-hosted lead-zinc deposits in Earth history: Economic Geology, v. 105, p. 593–625.

Leach, D.L., Taylor, R.D., Fey, D.L., Diehl, S.F., and Saltus, R.W., 2010b, A deposit model for Mississippi Valley-type lead-zinc ores: U.S. Geological Survey Scientific Investigations Report 2010-5070-A, 52 p.

Lipinski, M., Warning, B., and Brumsack, H.J., 2003, Trace metal signatures of Jurassic/Cretaceous black shales from the Norwegian Shelf and the Barents Sea: Paleogeography, Paleoclimatology, Paleoecology, v. 190, p. 459–475.

Liu, W., Borg, S.J., Testemale, D., Etschmann, B., Hazemann, J.L., and Brugger, J., 2011, Speciation and thermodynamic properties for cobalt chloride complexes in hydrothermal fluids at 35–440°C and 600 bar: An in-situ XAS study: Geochimica et Cosmochimica Acta, v. 75, p. 1227–1248.

Lombaard, A.F., Günzel, A., Innes, J., and Kruger, T.L., 1986, The Tsumeb lead-copper-zinc-silver deposit, south west Africa/Namibia, *in* Anhaeusser, C.R., Maske, S., eds., Mineral deposits of Southern Africa: Geological Society of South Africa, v. 2, p. 1761–1787.

Lougnon, J., 1963, Geology of the lead-zinc deposits of Valauria mine, Tende, Maritime Alps: France: Rep., Bur. Rech. Geol. Minieves, Mem. 4, p. 1–61.

Lustwerk, R.L., and Wasserman, M.D., 1989, Water escape structures in the Coates Lake Group, Northwest Territories, Canada: Geological Association of Canada Special Paper 36, p. 207–224.

Lydon, J.W., 1986, Models for the generation of metalliferous hydrothermal systems within sedimentary rocks, and their applicability to the Irish Carboniferous Zn-Pb deposits, *in* Andrew, C.J., Crowe, R.W.A., Finlay, S., Pennell, W.M., and Pyne, J.F., eds., Geology and genesis of mineral deposits in Ireland: Dublin, Irish Association for Economic Geology, p. 555–577.

——2007, Geology and metallogeny of the Belt-Purcell basin: Geological Association of Canada, Mineral Deposits Division, p. 581–607.

Maiden, K., and Hughes, M., 2000, Mount Isa and Tsumeb: A comparative metallogenic study: Communication of the Geological Survey Namibia, v. 12, p. 167–177.

Mauk, J.L., Brown, A.C., Seasor, R.W., and Eldridge, C.S., 1992, Geology and stable isotope and organic geochemistry of the White Pine sediment-hosted stratiform copper deposit: Society of Economic Geologists Guidebook Series 13, p. 63–98.

McCandless, T.E., Ruiz, J., and Campbell, A.R., 1993, Rhenium behavior in molybdenite in hypogene and near-surface environments: Implications for Re-Os geochronometry: Geochimica et Cosmochimica Acta, v. 57, p. 889–905.

Melcher, F., and Buchholz, P., 2014, Germanium, *in* Gunn, G., Critical metals handbook, 1st ed.: Oxford, John Wiley and Sons, p. 177–203.

Melcher, F., Oberthür, T., and Rammlmair, D., 2006, Geochemical and mineralogical distribution of germanium in the Khusib Springs Cu-Zn-Pb-Ag sulfide deposit, Otavi Mountain Land, Namibia: Ore Geology Reviews, v. 28, p. 32–56.

Migdisov, A.A., Zezin, D., and Williams-Jones, A.E., 2011, An experimental study of cobalt (II) complexation in Cl- and H_2S-bearing hydrothermal solutions: Geochimica et Cosmochimica Acta, v. 75, p. 4065–4079.

Millensifer, T., Sinclair, D., Jonasson, I., and Lipmann, A., 2014, Rhenium, *in* Gunn, G., ed., Critical metals handbook: Oxford, John Wiley and Sons, p. 340–360.

Misra, K. C., Gratz, J. F., and Lu, C., 1996, Carbonate-hosted Mississippi Valley-type mineralization in the Elmwood-Gordonsville deposits, Central Tennessee zinc district: A synthesis: Society of Economic Geologists Special Publication 4, p. 58–73.

MMG Ltd., 2012, Minerals Resources and Ore Reserve Statement: http://www.mmg.com/services/downloadmedia.aspx?mediaid=%7B5ACB6833-9083-46E1-AB9A-6157666608ED%7D, 17 p.

Moskalyk, R.R., 2003, Gallium: the backbone of the electronics industry: Minerals Engineering, v. 16, p. 921–929.

National Research Council, 2008, Minerals, critical minerals, and the U.S. economy: Washington, DC, National Academy Press, 264 p.

Nyrstar, 2013, Clarksville Fact Sheet, 2 p. (http://www.nyrstar.com/operations/Documents/Fact%20Sheet%20CLARKSVILLE%20EN.pdf)

Nova Copper Inc., 2013, Technical report for the Bornite deposit: South Reef and Ruby Creek zones, northwest Alaska, USA, 129 p. (http://www.novacopper.com/i/pdf/reports/Technical_Report_for_the_Bornite_Deposit_31January2013_.pdf).

Ochoa-Landin, L., 1998, Geological sedimentalogical, and geochemical studies of the Boleo Cu-Co-Zn deposit, Santa Rosalia, Baja California, Mexico: Ph.D. thesis, University of Arizona, 145 p.

Osterman, C., 1999, The geology and genesis of the orebodies of the Kombat mine, Namibia: Ph.D. dissertation, Golden, Colorado, Colorado School of Mines, 215 p.

Oszczepalski, S., Nowak, G.J., Bechtel, A., and Zak K., 2002, Evidence of oxidation of the Kupferschiefer in the Lubin-Sieroszowice deposit, Poland: Implications for Cu-Ag and Au-Pt-Pd mineralization: Geological Quarterly, v. 46, p. 1–23.

Pašava, J., 1993, Anoxic sediments—an important environment for PGE: An overview: Ore Geology Reviews, v. 8, p. 425–445.

Peterson, J.A., 1994, Platinum-group elements in sedimentary environments in the conterminous United States: U.S. Geological Survey Bulletin 2049-A, 37 p.

Phipps, G., Mikolajczak, C., and Guckes, T., 2008, Indium and gallium: Long-term supply: Renewable Energy Focus, v. 9, p. 56–59.

Pieczonka, J., and Piestrzynski, A., 2008, Mineralogy and geochemistry of ore minerals from secondary oxidized zones: Annales Societatis Geologorum Poloniae, v. 78, no. 3, p. 195–241.

Piestrzynski, A., and Sawlowicz, Z., 1999, Exploration for Au and PGE in the Polish Zechstein copper deposits (Kupferschiefer): Journal of Geochemical Exploration, v. 66, p. 17–25.

Piestrzynski, A., Pieczonka, J., and Gluszek, A., 2002, Redbed-type gold mineralization, Kupferschiefer, south-west Poland: Mineralium Deposita, v. 37, p. 512–528.

Pieczonka, J., Piestrzynski, A., Mucha, J., Gluszek, A., Kotarba, M., and Wieclaw, D., 2008, The red-bed-type precious metal deposit in the Sieroszowice-Polkowice copper mining district, SW Poland: Annales Societatis Geologorum Poloniae, v. 78, p. 151–280.

Pimminger, M., Grasserbauer, M., Schroll, E., and Cerny, I., 1985, Trace element distribution in sphalerites from Pb-Zn-ore occurrences of the Eastern Alps: Tschermaks Mineralogische und Petrographische Mitteilungen, v. 34, p. 131–141.

Poplavko, E.M., Zak, S., and Marchukova, I., 1962, Rhenium mineral from ores of Djezkazgan deposit: Dolkay Akaemii Nauk SSR, v. 146, p. 433.

Roberts, S., and Gunn, G., 2013, Cobalt, *in* Guss, G., ed., Critical metals handbook, 1st ed.: Oxford, John Wiley and Sons, p. 122–149.

Rodier, D.D., 1990, An overview of silver and trace metal recovery strategies in the zinc industry: Lead-Zinc '90, *in* Mackey, T.S., and Prengaman, R.D. eds., Proceedings of a World Symposium on Metallurgy and Environmental Control, held during the 119th TMS Annual Meeting, Anaheim, California: Minerals, Metals and Materials Society (TMS), p. 57–85.

Rohrlach, B.D., Fu, M., and Clarke, J.D.A., 1998, Geological setting, paragenesis and fluid history of the Walford Creek Zn-Pb-Cu-Ag prospect, Mt. Isa basin, Australia: Australian Journal of Earth Sciences, v. 45, p. 63–81.

Roskill, 1992, The economics of idium 1992: London, Roskill Information Services Ltd., 101 p.

Rouvier, H., Perthuisot, V., and Mansouri, A., 1985, Pb-Zn deposits and salt-bearing diapirs in Southern Europe and North Africa: Economic Geology, v. 80, p. 666–687.

Samonov, I.Z., and Pozharisky, I.F., 1977, Deposits of copper, *in* Smirnov, V.E., ed., Ore deposits of the USSR, v. 2: London, Pitman Publishing, p. 164–170.

Sass-Gustkiewicz, M., 2001,The Pomerzany mine—characteristics of the ore deposit: Joint Biennial SGA-SEG Meeting, 6th, Krakow, Poland, Geological Excursion Guide, p. 64–78.

Schaefer, M.O., Gutzmer, J., Beukes, N.J., and Greyling, L.N., 2004, Mineral chemistry of sphalerite and galena from Pb-Zn mineralization hosted by the Transvaal Supergroup in Griqualand West, South Africa: South African Journal of Geology, v. 107, p. 341–354.

Schmandt, D., Broughton, D., Hitzman, M.W., Plink-Bjorklund, P., Edwards, D., and Humphrey, J., 2013, The Kamoa copper deposit, Democratic Republic of Congo: Stratigraphy, diagenetic and hydrothermal alteration, and mineralization: Economic Geology, v. 108, p. 1301–1324.

Schroll, E., 1984, Geochemical indicator parameters of lead-zinc ore deposits in carbonate rocks, *in* Wauschkuhn, A., Kluth, C., and Zimmermann, R.A., eds., Syngenesis and epigenesis in the formation of deposits: Berlin Heidelberg, Springer, p. 294–305.

——2005, Alpine type Pb-Zn-deposits (APT) hosted by Triassic carbonates, *in* Mao, Jingwen, and Frank P. Bierlein, eds, Mineral deposit research: Meeting the Global Challenge: Proceedings of the Eighth Biennial SGA Meeting, v. 18, p. 175–178.

Schuh, W., Leveille, R.A., Fay, I., and North, R., 2012, Geology of the Tenke-Fungurume sediment-hosted strata-bound copper-cobalt district, Katanga, Democratic Republic of Congo: Society of Economic Geologists Special Publication 16, p. 269–301.

Schwarz-Schampera, U., 2013, Indium, *in* Gunn, G., ed., Critical metals handbook, 1st ed.: Oxford, John Wiley and Sons, p. 204–229.

Schwarz-Schampera, U., and Herzig, P.M, 2002, Indium: Geology, mineralogy, and economics: New York, Springer, 257 p.

Seebold, I., Fernández, G., Reinoso, J., Alonso, A., Escayo,M.A., and Gómez F., 1992, Yacimientos estratioligados de blenda, galena y marcasita en dolomías. Mina de Reocín (Cantabria), *in* García-Guinea, J., and Martínez-Frías, J., eds., Recursos minerals de España: Madrid, Spain, Consejo Superior de Investigaciones Científicas, p. 947–967.

Selley, D., Broughton, D., Scott, R., Hitzman, M., Bull, S., Large, R., McGoldrick, P., Croaker, M., Pollington, N., and Barra, F., 2005, A new look at the glogy of the Zambian Copperbelt: Economic Geology 100th Anniversary Volume, p. 965–1000.

Seyfullin, S.S., Kalinin, S.K., Strutynskiy, A.V., and Fayn, E.Y., 1974, Rhenium in stratified copper deposits and showings in west central Kazakhstan: Geochemistry International, v. 11, p. 414–418.

Shaw, D.M., 1952, The geochemistry of indium: Geochimica et Cosmochimica Acta, v. 2, p. 185–206.

Singer, D.A., 1995, World-class base and precious metal deposits: A quantitative analysis: Economic Geology, v. 90, p. 88–104.

Slack, J.F., Meier, A.L., Malcom, M.J., Fey, D.L., Doughten, M.W., and Wandless, G.A., 2000, Trace element and rare-earth element geochemistry of bedded and massive sulphides from the Sullivan Pb-Zn-Ag deposit, British Columbia—a reconnaissance study: Geological Association of Canada, Mineral Deposits Division, Special Publication 1, p. 720–735.

Smith, G.E., 1976, Sabkha and tidal-flat facies control of stratiform copper deposits in north Texas: Oklahoma Geological Survey Circular 77, p. 25–39.

Smith, K.S., and Huyck, H.L., 1999, An overview of the abundance, relative mobility, bioavailability, and human toxicity of metals: Reviews in Economic Geology, v. 6A, p. 29–70.

Soler, P., and Lara, M.A., 1990, Minor and trace elements in polymetallic stratabound ore deposits of the central Peruvian Andes: Society Applied to Mineral Deposits Special Publication 8, p. 735–748

SRK Consulting (US), Inc., and Gustavson Associates, LLC, 2004, Independent technical report summarizing the Ambaji group of mines feasibility study, Gurjarat and Rajasthan States, India, 109 p.

Symons, D.T.A., Sangster, D.F., and Leach, D.L., 1995, A Tertiary age from paleomagnetism for Mississippi Valley-type zinc-lead mineralization in Upper Silesia, Poland: Economic Geology, v. 90, p. 782–794.

Taylor, S.R., 1964, Abundance of chemical elements in the continental crust: A new table: Geochimica et Cosmochimica Acta, v. 28, p. 1273–1285.

Taylor, S.R., and McLennan, S.M., 1985, The continental crust: Its composition and evolution, an examination of the geochemical record preserved in sedimentary rocks: Oxford and Palo Alto, CA, Blackwell Scientific Publications, 312 p.

Tetra Tech, 2013, Updated technical report and preliminary economic assessment for the Black Butte copper project, Montana: National Instrument 43-101, 342 p.

Ullmann's Encyclopaedia of Industrial Chemistry, 2002, Gallium and gallium compounds, 6th ed.: Rexdale, Ontario, John Wiley and Sons, p. 337–364.

Velasco, F., Herrero, J.M., Gil, P.P., Alvarez, L., and Yusta, I., 1994, Mississippi Valley-type, sedex, and iron deposits in Lower Cretaceous Rocks of the Basque-Cantabrian basin, northern Spain: Society Applied to Mineral Deposits Special Publication 10, p. 246–270.

Velasco, F., Herrero, J.M., Yusta, I., Alonso, J.A., Seebold, I., and Leach, D., 2003, Geology and geochemistry of the Reocín zinc-lead deposit, Basque-Cantabrian basin, northern Spain: Economic Geology, v. 98, p. 1371–1396.

Vershkovskaya, O.V., 1966, Gallium, *in* Vlasov, K.A., ed., Geochemistry and mineralogy of rare elements and genetic types of their deposits, Vol. 1: Jerusalem, Israel Program for Scientific Translations, p. 437–458.

Vlassov, K.A., 1964, Geochemistry and mineralogy of rare elements and genetic types of their deposits, v. 1 and 3: Academy of Sciences, U.S.S.R., Institute for Mineralogy, Geochemistry and Crystal Chemistry of Rare Elements, Moscow. Israel Program for Scientific Translation, 1966, p. 525–551.

Volodin, R.N., Chechetkin, V.S., Bogdanov, Y.V., Narkelyun, L.F., and Trubachev, A.I., 1994, The Udokan cupriferous sandstones deposit (eastern Siberia): Geology of Ore Deposits, v. 36, p. 1–25.

Walthers, S., Borg, G., and Ehling, B.C., 2009, The German Kupferschiefer deposits—what about the precious metals, smart science for exploration and mining: Townsville, Australia, Economic Geologist Research Unit, James Cook University, v. 2, p. 229–504.

Wedepohl, K.H., 1969, Handbook of geochemistry: Berlin, Springer Verlag, 245 p.

Wellmer, F.-W., Atmaca, T., Gunther, M., Kastner, H., and Thorman, A., 1994, The economics of sediment-hosted zinc and lead deposits: Society Applied to Mineral Deposits Special Publication 10, p. 429–462.

White, W.S., 1971, A paleohydrological model for mineralization of the White Pine copper deposit, northern Michigan: Economic Geology, v. 66, p. 1–13.

White, D.E., and Roberson, C.E.,1962, Sulphur Bank, California, a major hot-spring quicksilver deposit, *in* Holland, H.D., Engel, A.E.J., James, H.L., and Leonard, B.F., Petrologic studies—a volume to honor A.F. Buddington: Geological Society of America, p. 397–428.

White, W.S., and Wright, J.C., 1966, Sulfide-mineral zoning in the basal Nonesuch Shale, northern Michigan: Economic Geology, v. 61, p. 1171–1190.

White, J., Gammons, C.H., and Zieg, G.A., 2014, Paragenesis of cobalt and nickel in the Black Butte shale-hosted copper deposit, Belt basin, Montana, USA: Mineralium Deposita, v. 49, p. 335–351.

Wiese, R.G., Jr., 1960, Petrology and geochemistry of a copper-bearing Precambrian shale, White Pine, Michigan: Ph.D. thesis, Cambridge, MA, Harvard University.

——1973, Mineralogy and geochemistry of the parting shale, White Pine, Michigan: Economic Geology, v. 68, p. 317–331.

Wilkinson, J.J., Eyre, S.L., and Boyce, A.J., 2005, Ore-forming processes in Irish-type carbonate-hosted Zn-Pb deposits: Evidence from mineralogy, chemistry, and isotopic composition of sulfides at the Lisheen mine: Economic Geology, v. 100, p. 63–86.

Wilson, I.F., and Rocha, V.S., 1955, Geology and mineral deposits of the Boléo copper district, Baja California, Mexico: U.S. Geological Survey Professional Paper 273, 134 p.

Wood, S.A., and Samson, I.M., 2006, The aqueous geochemistry of gallium, germanium, indium and scandium: Ore Geology Reviews, v. 28, p. 57–102.

Xiong, Y., and Wood, S.A., 2001, Hydrothermal transport and deposition of rhenium under subcritical conditions (up to 200°C) in light of experimental studies: Economic Geology, v. 96, p. 1429–1444.

Xiong, Y., Wood, S., and Kruszewski, J., 2006, Hydrothermal transport and deposition of rhenium under subcritical conditions revisited: Economic Geology, v. 101, p. 471–478.

Ye, L., Cook, N.J., Ciobanu, C.L., Yuping, L., Qian, Z., Tiegeng, L., and Danyushevskiy, L., 2011, Trace and minor elements in sphalerite from base metal deposits in South China: A LA-ICPMS study: Ore Geology Reviews, v. 39, p. 188–217.

Yefimenko, S.A., 2008, Nuclear-geophysical methods of investigation of the Dzhezkazgan's ores: Informational Bulletin of the Annual Seminar of Experimental Mineralogy, Petrology and Geochemistry, v. 1, p. 26.

Yi, W., Halliday, A.N., Der-Chuen, L., and Christensen, J.N., 1995, Indium and tin in basalts, sulfides, and the mantle: Geochimica et Cosmochimica Acta, v. 59, p. 5081–5090.

©2016 Society of Economic Geologists, Inc.
Reviews in Economic Geology, v. 18, pp. 323–337

Chapter 13

Resource Potential for Commodities in Addition to Uranium in Sandstone-Hosted Deposits

George N. Breit[†,*]

U.S. Geological Survey, Box 25046 MS 964D, Denver Federal Center, Denver, Colorado 80225

Abstract

Sandstone-hosted deposits mined primarily for their uranium content also have been a source of vanadium and modest amounts of copper. Processing of these ores has also recovered small amounts of molybdenum, rhenium, rare earth elements, scandium, and selenium. These deposits share a generally common origin, but variations in the source of metals, composition of ore-forming solutions, and geologic history result in complex variability in deposit composition. This heterogeneity is evident regionally within the same host rock, as well as within districts. Future recovery of elements associated with uranium in these deposits will be strongly dependent on mining and ore-processing methods.

Introduction

Epigenetic sandstone-hosted deposits currently supply 30 to 40% of the uranium produced annually (Burrows, 2010). Although recent mining of these deposits has been primarily for their uranium content, some of these deposits contain enrichments of other elements of potential economic interest. Elements variably enriched in the deposits include arsenic, chromium, cobalt, copper, lead, molybdenum, nickel, rare earth elements (REE), rhenium, scandium, selenium, and vanadium. Of these, copper, molybdenum, REE, rhenium, scandium, selenium, and vanadium have been recovered. Significant amounts of vanadium have been produced from deposits in the United States, along with some copper, molybdenum, and scandium. Deposits in the former Soviet Union (Kazakhstan, Uzbekistan, and Russian Federation) produced molybdenum, rhenium, rare earth elements, scandium, and selenium (Dahlkamp, 2009). In addition, copper was recovered from sandstone deposits in Argentina. With the exception of vanadium recovered from sandstone-hosted uranium deposits on the Colorado Plateau, United States, the value of commodities other than uranium has been small. Nonetheless, advances in processing technology suggest that additional coproduction of commodities from these deposits is possible. This report presents an overview of information on the abundance and distribution of elements sufficiently enriched in sandstone-hosted uranium deposits to be considered of potential economic interest. Unfortunately, available compositional data and production records are incomplete for many deposits. Accordingly, this review should be considered an introduction rather than a thorough review of the potential of sandstone-hosted uranium deposits. Compositional attributes of selected deposits, emphasizing those with known enrichments of elements in addition to uranium, are listed in Table 1 and their locations are shown in Figure 1.

Sandstone-hosted U deposits are estimated to contain ~27% of known global uranium reasonably assured resources when low-grade resources in phosphorites and black shales are excluded (<$130/kg U; OECD/NEA-IAEA, 2010). The uranium deposit database (UDEPO) compiled by the International Atomic Energy Agency (IAEA) lists 526 sandstone-hosted uranium deposits in 44 countries (IAEA, 2009). Deposits listed in the database produced or have resources exceeding 300 t (t) uranium. Particularly large uranium resources of this deposit type are recognized in Australia, Kazakhstan, Niger, the United States, and Uzbekistan.

Sandstone-hosted uranium deposits vary in the assemblage and concentration of associated elements among regions as well as among and within districts in a region. The conditions responsible for the variations are incompletely understood, partly because of uncertainties in the origin of individual deposits beyond generally described processes and conditions. An understanding of the observed element enrichments is expected to include an evaluation of the sources of enriched elements, the ore-forming solutions, chemical reductants responsible for primary ore formation, diagenetic transformations, and for some deposits, alteration by later mineralizing fluids.

Deposit Description

General characteristics of sandstone-hosted uranium deposits are summarized in numerous publications including Nash et al. (1981), Adams (1991), Cuney and Kyser (2009), IAEA (2009), and Burrows (2010). Sandstone-hosted uranium deposits are epigenetic accumulations formed, at least initially, at low temperatures (<100°C) by precipitation or adsorption of uranium that was supplied in meteoric water. Uranium grades in these deposits typically range from 0.02 to 0.5 wt % as U. Total uranium contents of deposits are typically <50,000 t, though a few larger deposits are known (IAEA, 2009). Host rocks are typically younger than Silurian, with the greatest number of known deposits in late Paleozoic, Mesozoic, and Tertiary units. The host sandstones are commonly quartzose to arkosic fluvial units that were deposited on cratonic platforms or within intermontane basins, although some host rocks were deposited in marginal marine settings (Everhart, 1985).

Uranium accumulation in the sandstone-hosted deposits is the result of an abrupt change in redox conditions as

[†] E-mail, gbreit@usgs.gov
[*]Emeritus scientist

Table 1. Characteristics of Selected Sandstone-Hosted Uranium Deposits Including the Concentration of Associated Elements

Identifier	Deposit/district	Ore (Mt)	Deposit type	Geologic area	Country	Host rock age	Reductant
1	Cerro Solo deposit	1.5	Tabular	San Jorge gulf basin	Argentina	Cretaceous	Detrital plant matter
2	Sierra Pintada district	1.7	Tabular	Sierra Pintada	Argentina	Permian	Detrital plant matter
3	Tonco-Amblaya district	1.7	Tabular	Norte Subandino	Argentina	Cretaceous	Detrital plant matter
4	Marlagüe district	0.5	Basal channel	Neuquen basin	Argentina	Cretaceous	Bitumen; sulfide
5	Mulga Rocks area	44	Tabular	Narnoo basin	Australia	Tertiary	Detrital plant matter
6	Bigryli deposit	7.5	Tabular	Ngalia basin	Australia	Carboniferous	V mica/plant matter?
7	Figueira deposit	2.3	Tabular	Parana basin	Brazil	Permian	Detrital plant matter
8	Blizzard deposit	2	Basal channel	Omineca crystalline belt	Canada	Tertiary	Detrital plant matter
9	Hailaer basin	nr	Tabular	Hailier basin	China	Cretaceous	Detrital plant matter
10	Mecsek district	25 to 50	Tabular	Tisza terrane	Hungary	Permian	Detrital plant matter
11	Mynkuduk deposit	317	Roll front	Chu-sarysu basin	Kazakhstan	Cretaceous	Petroleum; H_2S?
12	Inkay deposit	550	Roll front	Chu-sarysu basin	Kazakhstan	Cretaceous	Petroleum,; H_2S?
13	Semizbai deposit	63	Basal channel	Shokay zone	Kazakhstan	Cretaceous	Detrital plant matter; sulfide minerals
14	Burgos basin	2		Burgos basin	Mexico	Tertiary	Petroleum; H_2S
15	Southwestern Karoo Basin	38	Tabular	Karoo basin	South Africa	Permian	Detrital plant matter
16	White Canyon district	2*	Tabular	Colorado Plateau	United States	Triassic	Detrital plant matter
17	Monument Valley district	1.4*	Tabular	Colorado Plateau	United States	Triassic	Detrital plant matter
18	Uravan Mineral Belt	15*	Tabular	Colorado Plateau	United States	Jurassic	Detrital plant matter
19	Primary ore - Grants Uranium Region	20	Tabular	Colorado Plateau	United States	Jurassic	Humate
20	Shirley basin	14	Roll front	Wyoming basins	United States	Tertiary	Detrital plant matter
21	South Texas	42	Roll front	Texas Gulf Coast	United States	Tertiary	Petroleum; H_2S
22	Uchkuduk deposit	125	Roll front	Beshbulak basin	Uzbekistan	Cretaceous	Detrital plant matter; petroleum
23	Sugraly deposit	30	Roll front	Beshbulak basin	Uzbekistan	Cretaceous	Petroleum; H_2S

Table 1. *(Cont.)*

Identifier	U (wt %)	V (wt %)	Mo (wt %)	Cu (wt%)	Re (ppm)	Se (ppm)	Other (ppm)	Comment	References
1	0.3	nr	0.2	nr	+	nr	nr	Summary values in report	CNEA (2000)
2	0.09	0.01	<0.001	nr	nr	nr	nr	Average values	Castillo (2004); Dahlkamp (2010)
3	0.1	0.1 to 0.29	nr	nr	nr	nr	nr	Production value and measured range	Antonietti et al. (1984)
4	0.15	+	nr	2	nr	nr	nr	Averages from production; includes the Huemul deposit	Antonietti et al. (1984)
5	0.055	nr	nr	0.05	nr	500	As - 12 Co - 200 Cr - 131 Pb - 88 ΣREE ->500 Sc - 54	Limited data; average values?; ore hosted in sandstone and lignite	Douglas et al. (2003); Macfarlane and Inwood (2010)
6	0.1	0.12	nr	nr	nr	nr	nr	Vanadium in detrital micas average values	Schmid et al. (2012)
7	0.2 to 0.4	nr	0.08 to 0.28	+	nr	nr	nr	Ranges of mineralized samples	Barretto (1985)
8	0.2	0.003	<0.001	<0.001	nr	<0.1	As - 2.5 Co - 36 Ni - 72 Pb – 8.0	Associated metal values are geometric means for U >100 ppm	Boyle (1982); Christopher (2005)
9	0.01 to 0.38	<0.06	<0.08	nr	<1.4	<18	Sc - <13	Max values listed	Ziying et al. (2004)
10	0.12	0.08	nr	+	nr	nr	Cr - 10,000 to 30,000	Average values	Kiss (1958); IAEA (2009)
11	0.04	nr	nr	nr	nr	100 to 600	Sc - > 2 ΣREE - <100	7 stacked ore zones; representative values	As summarized in Dahlkamp (2009)
12	0.06	nr	nr	nr	<0.1	nr	ΣREE - 100 Sc - 4	Representative values	As summarized in Dahlkamp (2009)
13	0.027	nr	nr	nr	nr	nr	nr	Representative values	As summarized in Dahlkamp (2009)
14	0.12	+	+	nr	nr	nr	nr	Representative values; extension of Texas Gulf coast province	As summarized in Dahlkamp (2010)
15	0.1	<0.01	0.02	<0.001	nr	nr	As - 97 Co - 46 Ni - 12 Pb - 95	Geometric means for samples with >100 ppm U	le Roux (1993); Cole and Wipplinger (2001)
16	0.26	0.1	nr	0.7	nr	nr	nr	Size and contents based on past production;	Nash et al. (1981); Chenoweth (1993); Malan (1968)
17	0.4	0.6	nr	0.7	nr	nr	nr	Size and contents based on past production	Malan (1968), Nash et al. (1981)
18	0.2	0.7	0.001	0.009	nr	12	As - 70 Co - 10 Cr - 17 Ni - 8.4 Pb - 88 Sc - <10	Geometric means	Shoemaker et al. (1959); Nash et al. (1981)
19	0.14	0.07	0.002	<0.001	nr	31	As - 22 Co <5 Ni - <5 Pb – 35	Geometric means for samples with >100 ppm U	Spirakis and Pierson (1983)
20	0.2	0.014	<0.001	0.005	nr	<0.1	As - <0.5 Co - <1 Cr - 53 Ni - 11 Pb - 30	Geometric means for samples with >100 ppm U	Spirakis et al. (1984a, b)
21	0.12	0.003	0.001	<0.001	nr	9	As - 30 Co - 7 Cr - 9 Ni - 4 Pb - 14	Geometric means for Oakville and Whitsett Fm. deposits	Spirakis et al. (1984a, b)
22	0.04	nr	0.01	nr	nr	100	nr	None	As summarized in Dahlkamp (2009)
23	0.2	nr	0.004 to 0.26	nr	10	0.06 to 0.12	nr	None	As summarized in Dahlkamp (2009)

Notes: + = described as enriched but values not given, ΣREE = sum of rare earth elements, Fm. = Formation, max = maximum, Mt = million metric tons, nr = not reported, ppm = parts per million, wt % = weight percent

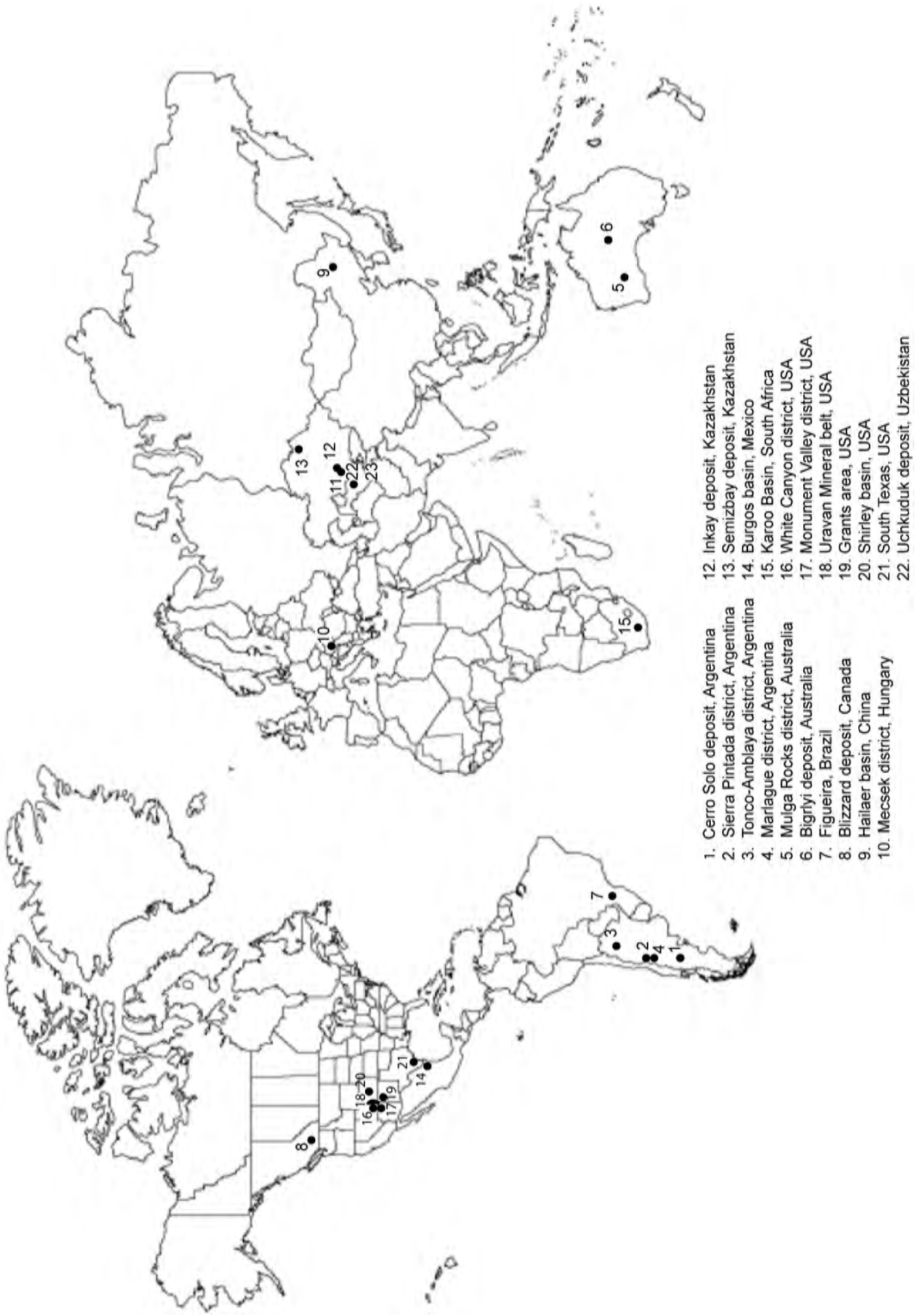

Fig. 1. World map showing the location of sandstone-hosted uranium deposits listed in Table 1.

uraniferous groundwater moves through the host rock. Oxidizing conditions dominate the environment where uranium enters solution and likewise the characteristics of the transporting groundwater (Cuney and Kyser, 2009). Sulfate, phosphate, and carbonate complexes facilitate uranium transport depending on pH and solution composition (Langmuir, 1978; Bastrakov et al., 2010). The assemblage of carbonate, clay, and feldspar minerals common in most host rocks is consistent with circum-neutral to alkaline solutions. If the uraniferous groundwater encounters chemical reductants or adsorbants, uranium will accumulate. Reducing conditions convert the uranyl ion to low-solubility U(IV) species. Potential reductants include detrital carbonaceous matter (Hostetler and Garrels, 1962), H_2S (Goldhaber et al., 1983), pyrite, humate, petroleum, metastable sulfur species (Granger and Warren, 1969), and reactive ferrous iron accessible at the surface of mineral grains (Liger et al., 1999; Latta et al., 2012). Reduction of uranyl is likely facilitated by bacteria either through formation of reductants (H_2S, Fe(II)) or direct reduction of U(VI) (Lovely et al., 1993; Wall and Krumholz, 2006). Common U(IV) phases include coffinite ($USiO_4$), uraninite (UO_2), brannerite (UTi_2O_6), and pitchblende ($UO_2 \cdot UO_3$). Adsorption to plant fragments, extrinsic organic matter such as humate or bitumen, and poorly crystalline TiO_2 phases may be important in the accumulation of the uranyl ion prior to reduction. Supergene oxidation of primary sandstone-hosted deposits can result in a range of uranium minerals including autinite ($Ca(UO_2)_2(PO4)_2 \cdot 10–12H_2O$), boltwoodite ($(H,K)(UO_2)(SiO_4) \cdot 1.5H_2O$, carnotite ($K_2(UO_2)_2(VO_4)_2 \cdot 3H_2O$),), schoepite ($((UO_2)_8O_2(OH)_{12} \cdot 12H_2O$), and tyuymanite ($Ca(UO_2)_2(VO_4)_2 \cdot 8H_2O$).

Four classes of sandstone-hosted deposits have been defined (IAEA, 2009). The classification is largely based on the relationship of the deposit position and shape within the host sandstone. These classes include: roll-front, tabular, basal channel, and tectonic/lithologic deposits. Although tabular orebodies tend to contain the greatest amount of elements in addition to uranium, the content of associated commodities varies only broadly among the deposit classes. Sandstone-hosted deposits considered herein have attributes in common with uranium deposits in lacustrine sediment, caldera-fill and volcaniclastic sediments (Nash, 2010), and lignites, but this summary will limit its scope to the sandstone-hosted deposits.

Roll-front uranium deposits are presently the most prolific uranium producers of the sandstone type. These deposits are distinguished by the approximately crescent shape of the orebodies in vertical cross section. The bulge of the "C" commonly occupies an approximate midpoint of the host sandstone bed (greatest permeability) while the upper and lower limbs lag because they are usually adjacent to low permeability layers or diastems that bound the host sandstone. Evidence of a steep redox gradient that resulted in uranium accumulation in these deposits is typically provided by the varied color of the sandstone. Red to yellow sands, indicative of an oxidized condition, exist up hydrologic gradient from the orebody, whereas gray sandstone, indicative of reducing conditions, is dominant down gradient from ore. In some areas, mobile reductants (H_2S, petroleum) introduced after ore formation can obscure the color contrast. Mineralization along this interface can extend laterally on sinuous trends for tens of kilometers and multiple interfaces can be established vertically in discrete sand units that are bounded by intervening low permeability layers. Distribution of orebodies along the sinuous mineralized trend is discontinuous and irregular, likely as a result of local variations in permeability, metal concentrations, and reducing potential. The resulting distribution of orebodies has been likened to "beads on a string." Individual orebodies are typically a few to tens of meters thick and extend laterally for tens to hundreds of meters. Associated elements enriched in roll-front deposits are typically arranged spatially from oxidized to reduced rock in the sequence of selenium, uranium-vanadium, rhenium, arsenic, and molybdenum. This sequence is consistent with the expected reduction potential of each element as it moves through the defining redox gradient at the site of ore formation (Harshman, 1974). The position of these elements can be centimeters to tens of meters from the core of the uranium orebody. Significant roll-type sandstone-hosted uranium deposits are recognized in Australia, Kazakhstan, the United States, Uzbekistan, and in several other countries.

Tabular sandstone-hosted uranium deposits are broadly peneconcordant with the host sandstones. They generally have a lensoid shape that is elongate parallel to the depositional trend of the host rock. Recognizable mineralization can extend for tens of kilometers on trend with ore-grade material extending irregularly for tens to hundreds of meters. Ore is typically a few to several meters thick. In detail, the position of uranium and associated elements varies from tight conformity to small-scale sedimentary structures such as cross beds, to sweeping irregular shapes that cross depositional structures at steep angles, locally forming "rolls" (Shawe, 2011). Associated elements typically enriched in these orebodies include copper, molybdenum, rhenium, and vanadium. The distribution of these elements is irregular relative to the uranium distribution. Enrichments have been reported to be within, or centimeters to meters above or below the core of the uranium ore. Although commonly hosted in red-bed continental sediments, tabular ores lack the proximal systematic position of oxidized and reduced rock common to roll-front deposits.

The IAEA (2009) defined three subtypes of tabular sandstone uranium deposits. They include: (1) those attributed to detrital carbonaceous debris and lack vanadium (Niger, South Africa, and France), (2) deposits found with extrinsic organic matter (humate deposits, New Mexico, United States), and (3) those deposits associated with high contents of vanadium (Colorado Plateau, United States). Various explanations are offered to account for the compositional differences and tabular geometry of these deposits. In explaining the tabular uraniferous humate ore zones in the Jurassic Morrison Formation, San Juan basin, New Mexico, United States, Turner-Peterson (1985) proposed that neutralization of an alkaline solution that transported the humate, or cation loading of the humate, resulted in its precipitation. The complexing ability of the functional groups in the humate molecules accumulated uranium from flowing groundwater eventually resulting in ore-grade accumulations. To explain the vanadium-rich orebodies that lack humate elsewhere in the Morrison Formation, Northrop et al. (1990) examined deposits in the Henry basin, Utah, and provided comprehensive isotopic and chemical data to support a genesis tied to a solution interface. The

interface was between underlying saline water and overlying circulating dilute meteoric water that supplied metals to the ore zone. Ore formed where the interface intersected detrital carbonaceous matter that supported the reducing conditions necessary to form the ore phases. Hansley and Spirakis (1992) attempted to link the ores in the San Juan basin and the Henry basin by proposing that diagenetic changes at higher temperatures removed humate and favored accumulation of vanadium in the Henry basin ores.

Basal channel deposits are hosted by sands that fill channels incised into underlying crystalline basement rock, the basement rock is characteristically uraniferous. The general conceptual model proposes that uranium leached from the underlying rock is reduced by reaction with carbonaceous matter accumulated in the overlying sands. Attributes of these orebodies resemble the more significant tabular-type deposits, but they remain unique in the supply of ore metals directly from adjacent crystalline rocks and the sediment derived from them. Example deposits include the Blizzard deposit, Canada (Boyle, 1982), and Dolmatovskoye, Russian Federation (Dahlkamp, 2009).

Tectonic-lithologic deposits are those in which the interaction of reducing and oxidized solutions was directly linked to fault conduits such that faults control the shape and position of orebodies. This deposit type is least common of the sandstone-hosted category. Such deposits are concentrated in clastic sediments adjacent to faults and may be a product of redistribution of existing orebodies by a superimposed hydrologic regime facilitated by the structural disruption. Example tectonic-lithologic deposits include Lodeve, France (IAEA, 2009), the stacked ores within the San Juan basin, New Mexico, United States (Granger et al., 1961), and possibly the Mulga Rocks deposits, Western Australia (Macfarlane and Inwood, 2010). A number of sandstone-hosted orebodies in other classes are genetically linked to faults, but lack the close spatial control on deposit geometry. These deposits are known in Texas (Goldhaber et al., 1983), Wyoming (Hancock, 2012), Kazakhstan (Dahlkamp, 2009), and elsewhere (Dahlkamp, 2009, 2010).

Associated Commodities

Redox changes responsible for accumulation of uranium also resulted directly in reduction of dissolved arsenic, chromium, molybdenum, rhenium, selenium, and vanadium (Table 2). The lower valence states of these elements are less soluble and therefore accumulate in or near the orebodies. The valence states of the cobalt, lead, nickel, REE, and scandium are not directly altered by the reducing environment. Solubility limitations result in accumulation of these elements in sulfides, clays, oxides, and other phases formed in the orebody. Although a fraction of the Cu(II) is reduced to Cu(I) (chalcocite; Cu_2S) in the orebodies, the bulk of the copper is accumulated by formation of Cu(II) sulfides.

Vanadium

Many sandstone-hosted uranium deposits in the western United States have vanadium contents equal to or substantially greater than their content of uranium. Few deposits elsewhere contain similar vanadium enrichments (Table 1). The average resource and ore grades for deposits that are potential vanadium producers range from 0.1 to 1 wt % vanadium. The relative abundances of vanadium and uranium in some sandstone-hosted uranium districts of the United States are illustrated in Figure 2. Elsewhere, deposits with vanadium enrichments include those at the Bigrlyi prospect, Australia (0.13 wt % V; McKay and Miezitis, 2001); Tonco-Amblyo district, Argentina (0.1–0.3 wt % V; Dahlkamp, 2010); and the Karamurun district, Kazakhstan (Dahlkamp, 2009). Minor production of vanadium is reported for deposits in the former Soviet Union and in Argentina (Dahlkamp, 2009, 2010).

Vanadium is a prominent coproduct of sandstone deposits hosted by the Salt Wash Member of the Jurassic Morrison Formation in Colorado and Utah. Vanadium in these deposits typically ranges to 1 wt %, which is as much as five times the uranium content. On an atomic basis, the amount of vanadium is 10 to 30 times the uranium content in these deposits, which emphasizes that the supply and processes of accumulation favored vanadium. For several decades in the 20th century, production from sandstone uranium-vanadium deposits dominated the global supply of vanadium (Colorado School of Mines, 1961; Schmidt et al., 1981). During World War II, the deposits were mined principally for their vanadium content and uranium was a by-product. In total, these deposits produced approximately 150,000 t of vanadium (U.S. Department of Energy, U.S. Energy Information Administration, 2009, proprietary uranium producing mines database). In

Table 2. Species of Elements Transported and Chemically Reduced during Formation of Sandstone-Hosted Uranium Deposits

Element	Oxic valence state	Oxic aqueous species	Complexing ions	Primary ore valence state	Primary ore phases
Arsenic	As(V)	$H_xAsO_4^{(x-3)}$ $H_xAsO_3^{(x-2)}$	na	As(0), As(III)	Sulfide minerals; arsenopyrite
Chromium	Cr(VI))	CrO_4^{2-}	na	Cr(III)	Clay minerals
Copper	Cu(II)	Cu^{2+}	Cl^-	Cu(II) some Cu(I)	Sulfide minerals, selenides
Molybdenum	Mo(VI)	MoO_4^{2-}	na	Mo(IV)	Jordisite; molybdenite
Rhenium	Re(VII)	ReO_4^-	na	Re(IV)	Sulfide minerals; ReO_2
Selenium	Se(VI)	$H_xSeO_4^{(x-2)}$ $H_xSeO_3^{(x-2)}$	na	Se(0), Se(-II)	Selenides; sulfide minerals; native Se
Uranium	U(VI)	UO_2^{2+}	SO_4^{2-} HPO_4^-		
			F^-, CO_3^{2-}	U(IV) possibly some U(VI)	Uraninite; coffinite; Brannerite; pitchblende
Vanadium	V(V)	$H_xVO_4^{(x-3)}$ VO^{2+}	VO^{2+} with OH^-, C_{org}	V(III)	Oxides; clay minerals

Notes: na = not applicable

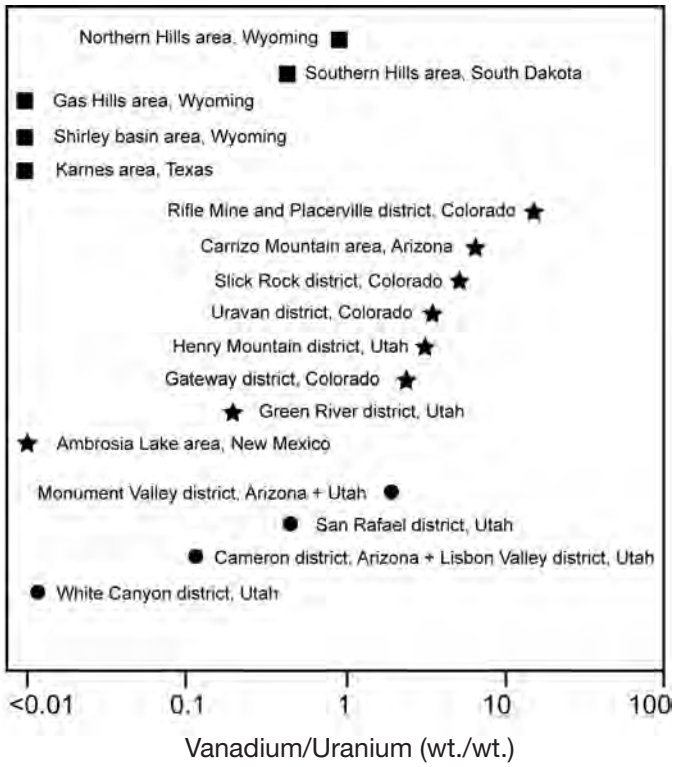

Fig. 2. Cumulative vanadium to uranium ratio of material recovered from processing sandstone-hosted uranium ores from selected areas within the United States. Note the amount of vanadium recovered for some areas is less than the content in the ore. Data from the U.S. Department of Energy, U.S. Energy Information Administration, 2009, proprietary uranium producing mines database. Symbols indicate the host rocks of the deposits. ■ = various Cretaceous and Tertiary formations; ★ = Jurassic Morrison Formation; ● = Triassic Chinle Formation.

recent years, only the White Mesa Mill near Blanding, Utah, has recovered vanadium from sandstone ores. In 2010, production from this facility was sufficient to meet 20% of the vanadium demand for the United States, which amounted to nearly 2% of global V production (Polyak, 2010). In addition to the Salt Wash deposits, V was produced within the United States from deposits in the Shinarump and Moss Back Members of the Triassic Chinle Formation in Arizona and Utah (11,000 t V) and a substantially lesser amount from Cretaceous sandstones in southwestern South Dakota and northeastern Wyoming (U.S. Department of Energy, U.S. Energy Information Administration, 2009, proprietary uranium producing mines database).

Vanadium abundance varies regionally across the Colorado Plateau both in the Jurassic Morrison and Triassic Chinle Formation ores. Ores hosted by the Salt Wash Member of the Morrison Formation (northern Colorado Plateau) have much greater vanadium contents than those in the Westwater Canyon Member (San Juan basin; Hansley and Spirakis, 1992). Vanadium content of the Salt Wash-hosted ores varies spatially. Deposits in southeastern Utah and southwestern Colorado have greater vanadium to uranium weight ratios (>3.4) than those in east-central Utah and west-central Colorado (V:U <3.4; U.S. Department of Energy, U.S. Energy Information Administration, 2009, proprietary uranium producing mines database). Vanadium contents of the Chinle Formation are less than those in most Salt Wash-hosted ores and are not spatially systematic. Vanadium was recovered from deposits in the Monument Valley area of northern Arizona and southern Utah (V:U ~2). Malan (1968) noted that vanadium decreased from 0.8 to 0.1 wt % moving east to west across the Monument Valley district. Ratios in other producing areas where the Chinle Formation was mined, including the Cameron, Lisbon Valley, San Rafael, and White Canyon districts, are less than 0.6.

Vanadium-enriched ores in southwestern South Dakota and northeastern Wyoming are considered part of the Wyoming basins uranium province (Boberg, 2010). These deposits are distinguished from other deposits in the province by their substantially higher vanadium contents. Ore from the Northern Hills, Wyoming, contained a weight V:U of approximately 0.8, whereas those in the Southern Hills, South Dakota area had a value of 0.3. Ratios in typical sandstone ores elsewhere in the Wyoming province are <0.01 (Fig. 2).

Vanadium is generally coextensive with uranium in most deposits, although slight offsets in maximum concentrations of each commodity are common (Harshman, 1974; Northrop et al., 1990). Vanadium is present within the orebodies in diverse minerals, partly reflecting the three oxidation states of vanadium possible under natural conditions and its behavior as a siderophile element. In chemically reduced environments, V(III) is dominant and forms karelianite (V_2O_3), montroseite (VOOH), V chlorite, and V illite (roscoelite). Under weakly reducing conditions, V(IV) is stable and forms phases such as paramontroseite (VO_2), duttonite ($VO(OH)_2$), and doloresite ($H_8V_6O_{16}$), typically as oxidation products of the primary (V(III)) minerals. Vanadium forms many phases in supergene environments of which corvusite ((Na, Ca, K)$V_8O_{20}\cdot 4H_2O$), carnotite ($K_2(UO_2)_2(VO_4)_2\cdot 3H_2O$), and tyuyamunite ($Ca(UO_2)_2(VO_4)_2\cdot 5\text{-}8H_2O$) are the most common.

Molybdenum

Molybdenum is second to vanadium in abundance of potentially recoverable commodities in sandstone-hosted uranium deposits. Reported deposit-scale concentrations of molybdenum range from <0.001 to 0.2 wt % (Table 1). Molybdenum was reportedly a by-product of processing sandstone uranium deposits within countries of the former Soviet Union (Dahlkamp, 2009). Some production of molybdenum also occurred from deposits in South Dakota, which were processed with molybdenum-rich uraniferous lignite ash (King et al., 1973) and from ores on the Texas Gulf Coast (McCulloh, 1982). The amount of total production is unknown. Select deposits in Africa and South America are noted for their high molybdenum contents. Cole and Wipplinger (2001) presented a detailed description of the molybdenum content of uranium deposits in the southwestern portion of the Karoo basin, South Africa. Molybdenum contents in samples from those deposits have a geometric mean of 0.02 wt %. A major challenge in considering molybdenum as a potential coproduct is that most of the molybdenum is spatially offset from uranium. For example, typical roll-front deposits have maximum molybdenum enrichments a few centimeters to tens of meters down gradient from the redox interface (Harshman,

1974; Dahlkamp, 2009). In Salt Wash-hosted sandstone ores molybdenum enrichments were detected both above and below tabular ores; in one deposit, a zone containing 1 wt % molybdenum was present 2 m above an ore layer containing 1 wt % uranium (H.C. Granger, 1988, USGS, writ. commun.). In contrast to these reported offsets, a particularly rich sample of ore from the Karoo basin contained 0.87 wt % U and 1.4% Mo.

The mineraloids jordisite (MoS_2), femolite ($(Mo,Fe)S_2$) (Dymkov et al., 2009) and ilsemannite ($Mo_3O_8 \cdot nH_2O$) are the principal forms of molybdenum recognized in sandstone U deposits. Le Roux (1993) identified molybdenite, as well as jordisite, in deposits in the Karoo basin. Ilsemannite is formed by oxidation of jordisite and is commonly observed as a bright blue "bloom" on freshly exposed surfaces of the orebody.

Copper

Copper enrichment of sandstone-hosted uranium deposits varies from a few parts per million to values as great as 2 wt %. Few deposits have sufficient copper to be of economic interest. Deposits with large contents of copper (>0.5 wt %) include the mined out Huemul deposit, Argentina (produced 4,000 t Cu; Antonietti et al.,1984), the Monument Valley and White Canyon districts, Arizona and New Mexico, United States (produced 8,500 t, Chenoweth, 1993). Copper is also inferred to be a significant component of the Imouraren deposit, Niger (Pagel et al., 2005). The unusual Falea deposit, Mali, is reported to contain a measured and indicated resource of 14.2 Mt of ore containing 0.08 wt % U and 0.22 wt % Cu (Muller and Umpire, 2012). Shawe (2011) reported the copper enrichment of uranium deposits in the Morrison Formation in the Slick Rock district, Colorado, was as high as 0.7 wt %. Copper enrichment within this district is greatest near faults. Elsewhere on the Colorado Plateau, Malan (1968) noted that the abundance of copper varied systematically among deposits within the Monument Valley, Arizona and White Canyon, Utah districts. Harshman (1974) reported that copper enrichment is absent in roll-front deposits in the Wyoming basin province and the Texas Gulf Coast. Chalcopyrite, covellite, chalcocite, and bornite are common in sandstone uranium deposits that are enriched in copper. Oxidation of these phases typically forms azurite, malachite, tenorite, and volborthite ($Cu_3V_2O_7(OH)_2 \cdot 2H_2O$).

Rhenium

The enrichment of sandstone uranium deposits with rhenium has been known since the 1950s. The recognition that molybdenum was enriched in these deposits and the known association of rhenium with molybdenum in other orebodies prompted the evaluation of rhenium abundance. Petersen et al. (1959) reported rhenium contents as great as 1,000 ppm in a small uranium deposit hosted by the Chinle Formation at the Sun Valley mine, Arizona. The authors noted that the deposit was unusually rich in rhenium compared to other deposits on the Colorado Plateau. Shortly after, Myers et al. (1960) reported as much as 70 ppm rhenium in a molybdenum-rich sandstone uranium deposit in the Cretaceous Fall River Formation in southwestern South Dakota. Concentrations reported for deposits in the Russian Federation and Kazahkstan typically approach a few ppm (Troshkina, 2011), which is sufficient for recovery. Some production of rhenium is also reported from sandstone ores in Texas (McCulloh, 1982). Based on its high molybdenum content, the Cerro Solo deposit in Argentina is also expected to be enriched in rhenium. Procedures have been developed for recovery of rhenium from in situ recovery (ISR) operations (Abisheva et al., 2011); although it is unclear if the processes have been implemented. Sampling across ore layers revealed that rhenium is typically coextensive with uranium (Dahlkamp, 2009). The mineral form of rhenium in the sandstone-hosted uranium deposits is poorly known. It has been speculated to be bound primarily within molybdenum sulfides, but this contrasts with the spatial offset of rhenium and molybdenum concentrations in roll-type deposits as illustrated in Dahlkamp (2009). Kislyakov and Shchetochkin (2000) reported that ReS_2 and ReO_2 occur in deposits within the Kyzylkum region of Uzbekistan. Mingkuan and Ruiquan (1997) reported that rhenium in a deposit in China is present as ReO_2 that is bound to organic matter.

Selenium

Selenium enrichment near and within uranium deposits is common in roll-front (Harshman, 1974) and tabular deposits (Granger et al., 1961; Shawe, 2011). Generally, the enrichment is spatially offset to the oxidized side of roll-front deposits (Harshman, 1974; Dahlkamp, 2009) and may be offset from the main uranium orebody by centimeters to meters. Selenium concentrations are typically a few to hundreds of ppm (Table 1). Despite being considered as a possible by-product of uranium ores in the United States during the 1950s (Shoemaker et al., 1959), no production from U.S. deposits is known. Selenium was reportedly produced from sandstone ore in the former Soviet Union, but amounts of production are not available (Dahlkamp, 2009).

Native Se, selenides, and selenium within iron sulfide minerals have been detected near and within sandstone-hosted uranium deposits (Howard, 1977). Among the selenides reported are clausthalite (PbSe), ferroselite (FeSe), berzelianite (Cu_2Se), eucairite (CuAgSe), greenockite (CdSe), and naumannite (Ag_2Se).

Scandium

Consideration of scandium as a by-product of sandstone-hosted uranium deposits is unusual, considering that the enrichment relative to barren host rocks is slight (<2 times) and the measured concentration in ore is typically less than the 22 ppm considered representative of continental crust (Rudnick and Gao, 2003). Consideration as a coproduct is the result of milling processes. During processing some types of uranium ore, an iron-rich slag was generated that reportedly contained 0.1 to 0.2 wt % scandium. The slag was then subjected to further processing to recover the scandium (Ross and Rosenbaum, 1962; Adams, 1973). Although processing of uranium ores for scandium ceased in the United States in 1964 (Adams, 1973), it continues to be extracted from uranium ores in Kazakhstan (Gambogi, 2013).

Scandium is a siderophile element and is not redox sensitive. The stable valence state is Sc(III), which favors inclusion of scandium in ferric ion phases including pyroxenes, micas, and clays, and also is consistent with its enrichment in REE

minerals. The controls on scandium contained in sandstone-hosted uranium deposits are not known. High scandium content is reported for brannerite ($UTiO_3$), which is known to occur in some sandstone-hosted deposits. Troshkina (2011) illustrated a zone of scandium enrichment in the roll front of the Kanimeh uranium deposit Uzbekistan. In the Akdala deposit in the Chu Sarysu basin, Kazakhstan scandium contents of 2.8 ppm are reported (Dahlkamp, 2009). Within this deposit, coffinite is reported to be the dominant uranium mineral such that the increase in scandium and REE reported for this deposit may be related to REE in coffinite as observed elsewhere by Hansley and Fitzpatrick (1989). Kislyakov and Shchetochkin (2000) proposed that scandium phases in Uzbekistan sandstone uranium ore include oxides and phosphates.

Other element enrichments

Other elements variably enriched in the sandstone-hosted uranium deposits include arsenic, cobalt, chromium, lead, nickel, and REE. Published analyses for the full list of these elements are limited. The concentrations for these elements typically are limited to a few tens to hundreds of ppm, though some deposits locally contain greater amounts. With the exception of REE, these other ore constituents have not been produced from sandstone ores.

Arsenic contents of deposits in the southwestern portion of the Karoo basin (le Roux, 1993; Cole and Wipplinger, 2001) are greater than other sandstone uranium deposits with reported concentrations (Table 1). Karoo samples with >100 ppm U have a geometric mean of 97 ppm As and many exceed 1,000 ppm (Cole and Wipplinger, 2001). Harshman (1974) investigated the distribution of arsenic across roll-front deposits in Wyoming and Texas and found that only deposits in the Gas Hills district, Wyoming, contained concentrations consistently exceeding 100 ppm. Recognized minerals containing arsenic in the Karoo basin include arsenopyrite, löllingite ($FeAs_2$), as well as nickel and cobalt sulfides (le Roux, 1993). Arsenic in other deposits is thought to be contained in pyrite and marcasite.

Chromium is notably enriched in the Mecsek deposits in Hungary (1 wt %; Kiss, 1958), and several deposits on the Colorado Plateau. Enriched deposits on the Colorado Plateau include the Rifle deposit (0.1 wt %; Fischer, 1960), the Placerville district, Colorado (Breit, 1995), small accumulation marginal to deposits in the Salt Wash deposits in the Uravan mineral belt (Breit and Goldhaber, 1989), and in the Temple Mountain area, Utah (Hawley et al., 1965). On the Colorado Plateau, the chromium-rich clays are associated with uranium deposits that contain significant vanadium enrichments. Illite-smectite is the only chromium-rich phase recognized in these deposits (Kiss, 1958; Fisher, 1960; Hawley et al., 1965). Zones of chromium enrichment are typically positioned marginal to the uranium orebodies in the direction of red or brown sandstones. The position of chromium enrichment is consistent with the conversion of soluble Cr(VI) to Cr(III), the form in the clay minerals, under weakly reducing conditions.

Cobalt contents of the sandstone uranium orebodies, where reported, are low and variable. Harshman (1974) noted the enrichment of cobalt to a maximum of 20 ppm in roll-front deposits in Wyoming and Texas. This enrichment coincided with zones of maximum pyrite content, the presumed host for the cobalt. Ore with >0.01wt % U had a geometric mean of 31 ppm cobalt relative to the 7 ppm reported for barren sandstone in the Chinle Formation on the Colorado Plateau (Pierson and Spirakis, 1986); whereas ores in the Salt Wash Member of the Morrison had a geometric mean of only 11 ppm (Shoemaker et al., 1959). In the tabular sandstone deposits of the Karoo basin, samples with >0.01 wt % U have a geometric mean of 46 ppm cobalt with a maximum sample value of 936 ppm (Cole and Wipplinger, 2001). Le Roux (1993) found that cobalt was hosted by cobaltite (CoAsS) and nickel-bearing sulfides.

Lead contents of samples from sandstone-hosted uranium deposits range from a few tens of ppm to 5,000 ppm (Fischer, 1960). Ores with >0.01 wt % U contained 102 ppm of lead in Chinle Formation ores (Pierson and Spirakis, 1986). Near Grants, New Mexico, lead contents of ore have a geometric mean of 35 ppm and a range of 5 to 1,500 ppm (Spirakis and Pierson, 1983). Deposits in the Morrison Formation proximal to faults in the Slick Rock district, Colorado, contain as much as 3,200 ppm lead. Samples from the Karoo basin (>0.01 wt % U) have a geometric mean of 95 ppm, with a maximum of 1,900 ppm (Cole and Wipplineger, 2001). Small grains of galena and clausthalite (PbSe) have been detected in primary sandstone uranium ores with some anglesite detected in supergene deposits. Lead is expected to accumulate in uranium deposits as a result of radioactive decay, but isotopic analyses indicate that deposits with substantial lead contents are the result of addition of common lead.

Information on the nickel content of sandstone uranium ores is relatively limited. Nickel is enriched 20 times in uranium ore deposits of the Salt Wash Member of the Morrison Formation, relative to the composition of barren sandstone (Shoemaker et al., 1959). Those results are consistent with the findings of Northrop et al. (1990) who noted an enrichment of nickel in Salt Wash deposits within the Henry basin, Utah. Shawe (2011) noted an enrichment of nickel in uranium deposits marginal to faults in the Slick Rock district to values as great as 460 ppm relative to the 3 ppm detected in deposits distal from faults. The Karoo basin uranium deposits are also enriched in nickel. Data of Cole and Wipplinger (2001) yielded a geometric mean of 12 ppm nickel (>0.01 wt % U) with the maximum sample value being 616 ppm. Nickel phases recognized by le Roux (1993) in the Karoo basin include thin late-stage veinlets of gersdorffite (NiAsS) and bravoite ($(Fe,Ni)S_2$).

Rare earth elements

REE are reported to be enriched in some uranium deposits to as much as a few hundred ppm of total REE. Unfortunately data for the deposits are typically limited, such that the relative enrichments of light and heavy rare earth elements cannot be described. In the ores hosted by the Chinle Formation on the Colorado Plateau contents of lanthanum increase to about twice the content in barren sandstone to achieve geometric mean concentrations of 37 ppm. Lower concentrations are reported for ores in the Grants uranium region (Spirakis et al., 1981), which is consistent with the findings of Della Valle and Brookins (1983) who resolved that a detectable enrichment in REE was limited to the clay-sized fraction in the vicinity of deposits in the Grants area. A table of Maksimova et al.

(1995) presented in Dahlkamp (2009) compares the content of selected REE in roll-type deposits in the Chu Sarysu basin, Kazahkstan. In the Budenovskoye and Inkay districts, mean contents in high-grade uranium ores were respectively: lanthanum 71 and 17 ppm; cerium 39 and 49 ppm; neodymium 38 and 10 ppm; ytterbium 2.3 and 4 ppm; and yttrium 91 and 67 ppm. The form of REE in these orebodies is uncertain though Hansley and Fitzpatrick (1989) recognized a significant enrichment in REE in coffinite in the humate ores of the San Juan basin area, New Mexico. If other deposits have a similar distribution of REE, extraction would be related to dissolution of coffinite and retaining REE in the leach solution. Recovery of REE is reported for deposits in Uzbekistan (Dahlkamp, 2009).

Origin of the Varying Composition

The diverse mineral and chemical assemblages observed among sandstone-hosted uranium deposits are the product of varied conditions of primary ore formation, diagenetic alteration, and superimposed mineralization processes. Accumulation of elements during formation of these deposits requires a source of metals that are soluble during weathering or shallow diagenesis, groundwater of an appropriate composition to transport the elements, hydrologic conditions conducive to transport of the metals to the site of ore formation (permeability and gradient), and sufficient reductant to precipitate the ore constituents. A full review of these variables is beyond the scope of this paper; nonetheless, some comment on known contrasts and proposed explanations is presented to provide a context to consider deposit composition.

The accumulation of elements in sandstone-hosted uranium deposits is thought to require inputs beyond the element abundances available in typical continental sandstones (Table 3). Considering the concentrations characteristic of common geologic materials (Table 3), weathering of no single igneous rock type can readily account for all of the elements enriched in sandstone-hosted uranium deposits. Commonly proposed sources of uranium include granitic rock (Stuckless and Nkomo, 1978; Penny, 2012) and silicic volcanic ash (Zielinski, 1978). These materials characteristically have greater contents of uranium than other major lithologies and are significant contributors of detritus in the sediments hosting the deposits or in adjacent units. Silicic igneous rocks also tend to have greater contents of lead and REE (Table 3). In contrast to uranium, the elements cobalt, chromium, copper, nickel, scandium, and vanadium have higher concentrations in mafic igneous rocks (Table 3). Weathering of mafic minerals may be a particularly good source of vanadium. For example, mafic rocks or their metamorphosed equivalents are thought to be included in the sediment source area for sandstones hosting the V-rich sandstone uranium deposits in the Tonco Amblaya district, Argentina (Puncoviscana belt; Omarini et al., 1999). As a further example, mafic rocks (greenstones) are proposed to explain the supply of vanadium to form the uranyl vanadate minerals in Australian calcrete uranium deposits (Mann and Deutscher, 1978). Although molybdenum does not vary among the igneous rock types (Table 3), silicic igneous rocks are also a likely source. Molybdenum is known to be concentrated in volcanogenic uranium deposits (Breit and Hall, 2011), which are hosted by silicic volcanics. Cole and Wipplinger (2001) also noted that molybdenum enrichment in deposits within the Karoo basin corresponds to detritus derived from an area of granitic rocks known to host molybdenum mineralization. The volatility of selenium during igneous processes suggests that the primary means of supply and dispersion into the environment, including systems forming sandstone-hosted U

Table 3. Representative Concentrations of Trace Elements in Selected Rock Types to Compare with the Assemblage Enriched in Sandstone-Hosted Uranium Deposits (values in ppm)

Source material	As	Co	Cr	Cu	Mo	Ni	Pb	Re	ΣREE	Sc	Se	U	V	References
Flood basalt	2.3	47	200	144	nr	70	4	nr	110	34	nr	0.9	320	Smedley and Kinniburgh (2002); Farmer (2007)
N-MORB	0.05	43	250	68	0.9	119	2.6	0.001	50	44	0.24	0.03	280	Sun et al. (2003); Klein (2004); Jenner et al. (2010)
Granite	0.77	12	31	13	1.1	9	23	nr	285	8	0.04	2.9	39	Gao et al. (1998); Kemp and Hawkesworth (2003)
Rhyolite	3.2	1	1.7	5	1	5	17	nr	nr	3	<0.2	5	10	Compiled from USGS data in National Geochemical Database: Rock. http://mrdata.usgs.gov/ngdb/rock/
Upper continental crust	4.8	17.3	92	28	1.1	47	17	0.0002	148	14	0.09	2.7	97	Rudnick and Gao (2003)
Continental sandstone	4.1	2.5	12	5	<3	8	19	nr	45	2.0	<1	1.1	15	Spirakis et al. (1981); Spirakis et al. (1984a, b); Pierson and Spirakis (1986); Condie (1993); Smedley and Kinniburgh (2002)
Average shale	13	19	90	45	2.6	58	20	nr	136	15	0.6	2.7	130	Li (1991); Condie (1993)
Black shale	29	17	110	70	65	50	20	0.15	200	16	6	15	500	Vine and Tourtelot (1970); Quinby-Hunt et al. (1989); Rhenium value averaged from: Jaffe et al. (2002); Lipinski et al. (2003); Pašava et al. (2010); Georgiev et al. (2012); Harris et al. (2013); Xu et al. (2014)

Notes: nr = not reported, ΣREE = sum of rare earth elements, N-MORB = normal type mid-ocean ridge basalt

deposits, may be the weathering of volcanic ash (Floor and Roman-Ross, 2012).

Although mafic rocks may be a plausible source of several elements in the sandstone deposits, they are generally not considered a significant source of detritus that formed most host rocks. A common, albeit minor, component of the clastic host rocks that may have supplied the mafic associated metals is detrital magnetites. Dissolution of detrital magnetite and spinel has been offered to account for the high vanadium content of ores in the Salt Wash Member of the Morrison Formation (Shawe, 1976; Wanty et al., 1990; Adams, 1991). Paramagnetic grains (magnetite, ilmenite, and martite grains with magnetite remnants) extracted from red sandstone in the Salt Wash Member contain 0.07 to 0.15 wt % V, as well as significant amounts of chromium, copper, and nickel (Shawe, 1976). Although spinels are generally considered refractory during weathering and diagenesis, magnetite dissolution is noted to occur in gray, chemically reduced sandstones that host uranium deposits (Adams et al., 1974; Shawe, 1976; Harris, 1984). Details of the dissolution and potential redistribution of trace elements are not known. In addition, detrital magnetite dissolution is also recognized near sandstone uranium deposits that lack significant vanadium enrichment (Adams et al., 1974; Harris, 1984).

Among the lithologies listed in Table 3, black shales have enrichments in the entire suite of elements enriched in the sandstone uranium deposits. Thamm et al. (1981) considered black shales as a source of vanadium in the deposits hosted by the Salt Wash Member of the Morrison Formation in Colorado and Utah. Metals and sediment mobilized during shale weathering could have provided a dispersed source of metal entrained in the host sediment that could have been redistributed into the orebodies during diagenesis.

The provenance of detritus for many rocks that host sandstone uranium deposits suggests a significant component of silicic crystalline rocks, with a contribution of volcanic ash. Characteristically, deposits in these units have an assemblage of substantially enriched elements limited to uranium, molybdenum, selenium, and possibly arsenic. Host rocks in which sedimentary rocks were recognized as a significant component of the detritus typically have a more diverse assemblage of enriched elements. Such a contrast in sediment sources may partly account for the differences in ore composition between the Westwater Canyon (low vanadium ore) and Salt Wash Members (vandiferous ore) of the Morrison Formation. Black shales were a likely constituent of the Paleozoic section that provided sediment that formed the Salt Wash Member, in contrast to the crystalline rocks that provided much of the sediment for the Westwater Canyon Member (Craig et al., 1977). In further support of black shales as a metal source, the supply of rhenium to surface waters during weathering of typical silicic volcanic or crystalline rocks is small, whereas substantial amounts are released from black shales (Hodge et al., 1996; Dalai et al., 2002; Jaffe et al., 2002). A similar contribution of rhenium is expected to groundwater capable of forming sandstone uranium deposits.

The composition of groundwater responsible for the uranium mineralization likely had considerable influence on the transport of elements accumulated in the sandstone-hosted ore deposits. Generally, an alkaline solution is favored because uranyl carbonate complexes enable high dissolved uranium concentrations by inhibiting adsorption to mineral surfaces and precipitation of uranyl (UO_2^{2+}) phases (Langmuir, 1978; Bastrakov et al., 2010). An alkaline solution (pH >8.5) would also favor the transport of elements such as arsenic, chromium, molybdenum, rhenium, selenium, and vanadium. These elements are stable as oxyanions under oxidizing conditions (Table 2), and high pH would limit their adsorption to ferric oxyhydroxides that are expected to be present in the zone of oxidation (Howard, 1977; Brinza et al., 2008; Leybourne and Cameron, 2008; Wright and Belitz, 2010). This is a particularly important consideration for arsenic, molybdenum, and vanadium. Cotransport of uranyl and vanadate (V(V)) species also may be limited by the solubility of uranyl vanadate minerals (carnotite and tyuyamunite), but the solubility is greatly enhanced by high contents of dissolved carbonate species (Langmuir, 1978). Bastrakov et al. (2010) noted that sulfate complexes of the uranyl and vanadyl ion promote solubility at low solution pH (pH <5). Low pH solutions would similarly enhance the mobility of oxyanions by limiting adsorption. Nonetheless, the significant abundance of carbonate minerals and preservation of feldspars common in sandstones hosting uranium deposits is inconsistent with low pH ore-forming solutions.

Two examples of the effectiveness of metal transport by oxidizing, alkaline solutions are found in the groundwaters of the Central Oklahoma aquifer, Oklahoma, and beneath the Franklin Lake playa, southeastern California. These are offered as examples of potential ore-forming solutions. Circulation of meteoric water in the Permian red beds in the Central Oklahoma aquifer results in pH values >8.5 as a result of exchange of Ca^{2+} for Na^{+} on clay minerals in the presence of carbonate minerals and in isolation from the atmosphere (Schlottmann et al., 1998). The high pH favors desorption of arsenic (max 140 μg/L), chromium (max 180 μg/L), molybdenum (max 94 μg/L) selenium (max 380 μg/L), uranium (max 360 μg/L), and vanadium (max 910 μg/L) from iron oxide surfaces that are abundant in the aquifer (Schlottmann et al., 1998). Groundwater discharging from springs in the area of the Franklin Lake playa contains equivalents of bicarbonate greater than calcium plus magnesium. Evaporation results in precipitation of calcite and dolomite until dissolved calcium and magnesium are depleted and the residual water evolves to a pH >9. The solution also has high contents of arsenic (max 16 mg/L), chromium (max 0.2 mg/L), molybdenum (max 14 mg/L), selenium (max 0.6 mg/L), uranium (max 4 mg/L), and vanadium (max 0.6 mg/L; Goldstein et al., 2011). Note the contrasting relative amounts of vanadium and uranium in the groundwater from the two areas. Sediment in the Central Oklahoma aquifer was derived from a marine Paleozoic sedimentary sequence that included black shales, whereas sediment in the Franklin Lake playa was derived principally from silicic volcanic deposits and Paleozoic carbonate rocks. An additional consideration of the alkaline pH, carbonate-rich solutions is that the solubility of divalent base metals will be low.

Hydrologic conditions responsible for transport of ore constituents to the site of accumulation can be generalized as flow of meteoric water down the gravimetric gradient through the host sandstone. Upon encountering reductants

and adsorbants, the relative accumulation of each element in solution was a product of the favorability of possible reactions that could result in deposition. The spatial distribution and varied ability of detrital plant fragments, petroleum, H_2S, metastable sulfur species, sulfide minerals, and ferrous iron to reduce the suite of metals delivered by meteoric water is expected to influence which elements accumulate and their relative position in the ore deposit.

Modification of sandstone uranium deposits by mineralizing processes subsequent to the initial accumulation of uranium is indicated in several deposits. The geometry and position of orebodies has been modified in response to hydrologic changes and diagenesis. Actively forming roll-front deposits is thought to advance down gradient as long as the hydrologic and geochemical regimes are sustained. Uplift of the western San Juan basin, New Mexico, during the Tertiary created roll-front deposits from the primary Jurassic-age tabular ores as a result of an increased gradient driving oxygenated meteoric water through reduced sandstones (Nash et al., 1981). Meunier et al. (1990) argued that radiation damage to quartz grains beyond the extent of current tabular sandstone uranium ores in the Salt Wash sandstones, Colorado and Utah, indicated that the ore had been redistributed. Breit (1995) interpreted the similar age of illite in sandstone ore and in barren rock near Placerville, Colorado, was the product of a pervasive recrystallization of clays subsequent to ore formation. The role of redistribution and recrystallization on associated elements in most deposits typically has not been described.

Significant copper accumulations in sandstone-hosted uranium deposits likely are the product of processes that were variable and separate in time from conditions and processes responsible for uranium accumulation. This is consistent with the contrast in the alkaline solutions likely to transport uranium (Langmuir, 1978) and the lower pH, saline solutions favorable for copper transport in sedimentary basins (Rose, 1989). Precipitation of uranium on preexisting sulfide minerals has been proposed for the uranium enrichment of the Cu-Ag orebody at Falea, Mali (Muller and Umpire, 2012), and small accumulations of uranium in the sandstone-hosted silver deposits in the Silver Reef district, Utah (James and Newman, 1986). In contrast, the copper (and small silver) content of Salt Wash-hosted uranium deposits Slick Rock district, Colorado was added to preexisting uranium deposits (Shawe, 2011). Breit and Meunier (1990) determined that the added copper was the result of saline solutions that entered the Morrison Formation along faults. Copper sulfide formed by replacement of preexisting iron sulfide minerals within the uranium deposits. The copper content of the White Canyon and Monument Valley deposits has not been genetically evaluated, but considering that the copper content varies spatially within each district (Malan, 1968), the copper mineralization likely postdates the accumulation of uranium.

All sandstone-hosted deposits of significance are volumes of rock in variably permeable sandstone that contained accumulation of reactive reduced species. The deposits could function as effective sinks for metals transported in subsequent mineralizing fluids. Shawe (2011) noted that Salt Wash-hosted uranium deposits near faults in the Slick Rock district, Colorado, were enriched in copper, nickel, lead, and other elements relative to deposits more distant from faults. The complex Mulga Rock deposits, although in the tectonic/lithologic class, may represent a new type of sandstone-hosted uranium deposits because of the high contents of a range of associated elements including gold (Douglas et al., 2003). The Akouta deposit in Niger was also subjected to superimposed hydrothermal alteration (Pagel et al., 2005).

Processing

Recovery of uranium and associated elements from the sandstone-hosted deposits is highly dependent on the methods of ore processing. For example, historic production of copper from cupriferous ores on the Colorado Plateau was dependent not only on the composition of the ore, but also the availability of appropriate mill circuits, which varied during the mining of those deposits. Similarly, in the 1950s and 1960s mills throughout the United States recovered vanadium from uranium ores with low vanadium grades (<0.1 wt % V) because mill designs were based on high vanadium Colorado Plateau ores. Scandium was recovered in the United States and Australia only if uranium mills produced a scandium-enriched iron slag, perhaps an unintended consequence.

Processing methods for sandstone uranium ores are variable, but generally are designed to oxidize the low valence state of the ore phases and thereby promote dissolution of those phases. Both alkaline- and acid-processing circuits have been used in traditional uranium mill operations, depending on the properties of the ore. Roasting of some ores was applied to enhance recovery of elements, such as vanadium, that are bound in refractory silicates. Such processing is expected to dissolve a wide range of elements enriched in the deposits. Recovery of those elements was dependent on processing of the pregnant extract solutions.

Beginning in the early 1960s, tests of in situ recovery (ISR; also known as in situ leach (ISL)) were conducted in the United States and the former Soviet Union. In situ recovery operations effectively dissolve uranium phases by passing reactive solutions through the permeable orebodies. Both alkaline (carbonate and bicarbonate) and acid (sulfuric or nitric acid) solutions are used in in situ recovery mining. Oxidants such as hydrogen peroxide, oxygen gas, and chlorates are added to the alkaline solutions. The ability of in situ recovery solutions to leach commodities other than uranium is dependent on the reactivity of the phases hosting those elements to the lixiviant composition. As shown by leach solution composition at the Honeymoon deposit, Australia, in situ recovery lixiviants are effective in extracting commodities in addition to uranium (Ackland and Hunter, 2002). Recovery of vanadium oxides and supergene phases may be amenable to in situ recovery. Such a recovery system would require the formation of the relatively soluble V(V) species (vanadate), but inhibit formation of low-solubility uranyl vanadates. Vanadiferous silicates, which are abundant in the Salt Wash deposits, are expected to be refractory to both alkaline and acid in situ recovery lixiviants and would likely require conventional milling to assure vanadium recovery.

The value of other elements in sandstone-hosted uranium deposits requires consideration of the processing metallurgy. In some uranium ore-processing circuits, the associated elements are difficult to recover (Churchward and Rosenbaum,

1963) or are considered a problem as they degrade the quality of resulting uranium oxides or foul exchange resins used in purification (Gupta, 1992; Sole et al., 2011). For example, a U.S. patent issued for an in situ recovery extraction solution of bicarbonate and sodium chlorate emphasized the ability of the lixiviant to preferentially extract uranium relative to other metals within the ore such as molybdenum, selenium, and vanadium (Hunkin et al., 1979). Nonetheless, improvements in processing technologies and greater value for some commodities have increased the potential to gain credits for molybdenum, rhenium, scandium, and vanadium (Mikhaylenko and van Deventer, 2009).

Summary

Sandstone-hosted uranium deposits variably accumulate a diverse assemblage of elements. Historic mining and milling practices enabled the recovery of large amounts of vanadium, minor copper, and small amounts of several other commodities. The form and abundance of these metals and metalloids vary greatly among deposits. Conditions and processes responsible for the variation are the product of source materials for the elements, composition of the transport solutions, abundance and reactivity of reductants and adsorbants in the ore zone, and transformations during diagenesis and subsequent episodes of mineralization. Although these orebodies are sought primarily for their uranium content, choice of mining and milling approaches may provide substantial credits for other constituents that are mobilized during extraction.

REFERENCES

Abisheva, Z.S., Zagorodnyaya, A.N., and Bekturganov, N.S., 2011, Review of technologies for rhenium recovery from mineral raw materials in Kazakhstan: Hydrometallurgy, v. 109, p. 1–8.

Ackland, M.C., and Hunter, T.C., 2002, Australia's Honeymoon project—from acquisition to approval—1997–2002: International Atomic Energy Agency TECDOC-1396, p. 115–137.

Adams, J.W., 1973, Scandium: U.S. Geological Survey Professional Paper 820, p. 425–435.

Adams, S.S., 1991, Evolution of genetic concepts for the principal types of sandstone uranium deposits in the United States: Economic Geology Monograph 8, p. 225–248.

Adams, S.S., Curtis, H.S., and Hafen, P.L., 1974, Alteration of detrital magnetite-ilmenite in continental sandstones of the Morrison Formation, New Mexico: International Atomic Energy Agency Proceedings Series STI/PUB/374, p. 219–253.

Antonietti, C., Gorustovich, S., Valdiviezo, A., Benitez, A., and Saucedo, P., 1984, Geologia y metalogenesis de los depositos uraniferos de Argentina Parte 1: Acumulaciones con control sedimentario: in Geology and metallogenesis of uranium deposits of South America: International Atomic Energy Agency, Vienna, Austria, p. 6–34.

Barretto, P.M.C., 1985, Sedimentary and tectonic environments for uranium mineralization on the Parana basin Brazil: Geological environments of sandstone-type uranium deposits: International Atomic Energy Agency TEDOC-328, p. 173–195.

Bastrakov, E.N., Jaireth, S., and Mernagh, T.P., 2010, Solubility of uranium in hydrothermal fluids at 25° to 300°C: Implications for the formation of uranium deposits: Geoscience Australia Record 2010/29, 91p.

Boberg, W.W., 2010, The nature and development of the Wyoming uranium province: Society of Economic Geologists Special Publication 15, p. 653–674.

Boyle, D.R., 1982, The formation of basal-type uranium deposits in south central British Columbia: Economic Geology, v. 77, p. 1176–1209.

Breit, G.N., 1995, Origin of clay minerals associated with V-U deposits in the Entrada Sandstone, Placerville mining district, southwestern Colorado: Economic Geology, v. 90, p. 407–419.

Breit, G.N., and Goldhaber, M.B., 1989, Hematite-enriched sandstones and chromium-rich clays—clues to the origin of vanadium-uranium deposits in the Morrison Formation, southwestern Colorado and southeastern Utah: International Atomic Energy Agency TEDOC-500, p. 201–225.

——1995, Diagenesis of sandstone in the Morrison Formation within the Paradox basin: Utah Geological Association Guidebook 25, p.197–210.

Breit, G.N., and Hall, S.M., 2011, Deposit model for volcanogenic uranium deposits: U.S. Geological Survey Open-File Report 2011-1255, 8 p.

Breit, G.N., and Meunier, J-D., 1990, Fluid inclusion, $\delta^{18}O$, $^{87}Sr/^{86}Sr$ evidence for the origin of fault-controlled copper mineralization, Lisbon Valley, Utah and Slick Rock district, Colorado: Economic Geology, v. 85, p. 884–891.

Brinza, L., Benning, L.G., and Statham, P.J., 2008, Adsorption studies of Mo and V onto ferrihydrite: Mineralogical Magazine, v. 72, p. 385–388.

Burrows, D.R., 2010, Uranium exploration in the past 15 years and recent advances in uranium metallogenic models: Society of Economic Geologists Special Publication 15, p. 599–652.

Castillo, A., 2004, Leaching method: Changes in Sierra Pintada mine in recent developments: Uranium resources and production with emphasis on in-situ leach mining: International Atomic Energy Agency TECDOC 1396, p. 223–229.

Chenoweth, W.L., 1993, The geology and production history of the uranium deposits in the White Canyon mining district, San Juan County: Utah Geological Survey Miscellaneous Publication 93-3, 26 p.

Christopher, P.A., 2005, Technical report on Blizzard uranium deposit Beaverdell area, British Columbia, Canada: for Santoy Resources Ltd., (http://www.santoy.ca/i/pdf/BlizzardAug05.pdf; accessed Feb 26, 2013).

Churchward, P.E., and Rosenbaum, J.B., 1963, Sources and recovery methods for rhenium: U.S. Bureau of Mines Report of Investigations 6246, 16 p.

CNEA, 2000, Cerro Solo uranium ore deposit: Chubut Province—a promising enterprise (http://caebis.cnea.gov.ar/geologia/cerrsolo/FOLLETO.htm; accessed May, 2014).

Cole, D.I., and Wipplinger, P.E., 2001, Sedimentology and molybdenum potential of the Beaufort Group in the main Karoo basin, South Africa: Council for Geoscience Memoir, South Africa, v. 80, 225 p.

Colorado School of Mines Research Foundation, 1961, Colorado vanadium: A composite study: State of Colorado Mining Board, 155 p.

Condie, K.C., 1993, Chemical composition and evolution of the upper continental crust: Contrasting results from surface samples and shales: Chemical Geology, v. 104, p. 1–37.

Craig, L.C., Holmes, C.N., Freeman, V.L., Mullens, R.E., and Weira, G.W., 1977, Maps showing thickness of the Morrison Formation and thickness and generalized facies of the members of the Morrison Formation in the Colorado Plateau region: U.S. Geological Survey Open-File Report 77-516.

Cuney, M., and Kyser, K., 2009, Recent and not-so-recent developments in uranium deposits and implications for exploration: Mineralogical Association of Canada, Short Course Series 39, 257 p.

Dahlkamp, F.J., 2009, Uranium deposits of the world, v. 1, Asia: Berlin, Springer-Verlag, 945 p.

——2010, Uranium deposits of the world, v. 2, USA and Latin America: Berlin, Springer-Verlag, 423 p.

Dalai, T.K., Singh, S.K., Trivedi, J.R., and Krishnaswami, S., 2002, Dissolved rhenium in the Yamuna river system and the Ganga in the Himalaya: Role of black shale weathering on the budgets of Re, Os, and U in rivers and CO_2 in the atmosphere: Geochimica et Cosmochimica Acta, v. 66, p. 29–43.

Della Valle, R.S., and Brookins, D.G., 1983, Geochemical studies of the Grants mineral belt, New Mexico, *in* Augustithis, A.A., ed., The significance of trace elements in solving petrogenetic problems and controversies: Athens, Theophrastus, p. 793–818.

Douglas, G.B., Butt, C.R.M., and Gray, D.J., 2003, Mulga Rock uranium and multielement deposits, Officer basin, Western Australia: CSIRO Exploration and Mining, CRC LEME, p. 1–3.

Dymkov, Y.M., Doinikova, O.A., and Volkov, N.I., 2009, Femolite from the exogenic-epigenetic Khokhlovskoe uranium deposit (Transural region) and hetero organic products of its thermochemical transformation: Geochemistry International, v. 47, p. 803–814.

Everhart, D.L., 1985, Tectonic settings of the world's sandstone-type uranium deposits: International Atomic Energy Agency TECDOC-328, p. 21–46.

Farmer, G.L., 2007, 3.03 Continental basaltic rocks, *in* Holland, H.D., and Turekian, K.K., eds., Treatise on Geochemistry: Elsevier, v. 3, 39 p.

Fischer, R.P., 1960, Deposits of the Rifle Creek area, Garfield County, Colorado: U.S. Geological Survey Bulletin 1101, 52 p.

Floor, G.H., and Roman-Ross, G., 2012, Selenium in volcanic environments: A review: Applied Geochemistry, v. 27, p. 517–531.

Gambogi, J., 2013, Scandium: U.S. Geological Survey Mineral Commodity Summaries, 2013, p. 140–141.

Gao, S., Luo, T-C., Zhang, B-R., Zhang, H-F., Hanm Y-W., Zhao, Z-D., and Hu, Y-K., 1998, Chemical composition of the continental crust as revealed by studies in East China: Geochimica et Cosmochimica Acta, v. 62, p. 1959–1975.

Georgiev, S., Stein, H.J., Hannah, J.L., Weiss, H.M., Bingen, B., Guangping X., Rein, E., Hatlø, V., Løseth, H., Nali, M., and Piasecki, S., 2012, Chemical signals for oxidative weathering predict Re-Os isochroneity in black shales, East Greenland: Chemical Geology, v. 324–325, p. 108–121.

Goldhaber, M.B., Reynolds, R.L., and Rye, R.O., 1983, Role of fluid mixing and fault-related sulfide in the origin of the Ray Point uranium district, South Texas: Economic Geology, v. 78, p. 1043–1063.

Goldstein, H.L., Breit, G.N., Yount, J.C., Reynolds, R.L., Reheis, M.C., Skipp, G.L., Fisher, E.M., and Lamothe, P.J., 2011, Physical, chemical, and mineralogical data from surficial deposits, groundwater levels, and water composition in the area of Franklin Lake playa and Ash Meadows, California and Nevada: U.S. Geological Survey Data Series 607.

Granger, H.C., and Warren, C.G., 1969, Unstable sulfur compounds and the origin of roll-type uranium deposits: Economic Geology, v. 64, p. 160–171.

Granger, H.C., Santos, E.S., Dean, B.G., and Moore, F.B., 1961, Sandstone-type uranium deposits at Ambrosia Lake, New Mexico: An interim report: Economic Geology, v. 56, p. 1179–1210.

Gupta, C.K., 1992, Extractive metallurgy of molybdenum: Boca Raton, CRC Press, 404 p.

Hancock, S., 2012, The geology and hydrogeology of the Lost Creek roll-front uranium deposit, Wyoming, USA: Ph.D. dissertation, Golden, Colorado, Colorado School of Mines.

Hansley, P.L., and Fitzpatrick, J.J., 1989, Compositional and crystallographic data on REE-bearing coffinite from the Grants uranium region, northwestern New Mexico: American Mineralogist, v. 74, p. 263–370.

Hansley, P.L., and Spirakis, C.S., 1992, Organic matter diagenesis as the key to a unifying theory for the genesis of tabular uranium-vanadium deposits in the Morrison Formation, Colorado Plateau: Economic Geology, v. 87, p. 352–365.

Harris, N.B., Mnich, C.A., Selby, D., and Korn, D., 2013, Minor and trace element and Re-Os chemistry of the upper Devonian Woodford Shale, Permian basin, west Texas: Insights into metal abundance and basin processes: Chemical Geology, v. 356, p. 76–93.

Harris, R.E., 1984, Alteration and mineralization associated with sandstone uranium occurrences, Morton Ranch Area, Wyoming: Geological Survey of Wyoming Report of Investigations 25, 44 p.

Harshman, E.N., 1974, Distribution of elements in some roll-type uranium deposits in formation of uranium deposits: International Atomic Energy Agency Panel Proceedings STI/PUB374, p. 169–183.

Hawley, C.C., Wyant, D.G., and Brooks, D.B., 1965, Geology and uranium deposits of the Temple Mountain district, Emery Count, Utah: U.S. Geological Survey Bulletin 1192, 154 p.

Hodge, V.F., Johannesson, K.H., and Stetzenbach, K.J., 1996, Rhenium, molybdenum, and uranium in groundwater from the southern Great Basin, USA: Evidence for conservative behavior: Geochimica et Cosmochimica Acta, v. 60, p. 3192–3212.

Hostetler, P.B., and Garrels, R.M., 1962, Transportation and precipitation of uranium and vanadium at low temperatures, with special reference to sandstone-type uranium deposits: Economic Geology, v. 57, p. 137–167.

Howard, J.H., III, 1977, Geochemistry of selenium: Formation of ferroselite and selenium behavior in the vicinity of oxidizing sulfide and uranium deposits: Geochimica et Cosmochimica Acta, v. 41, p.1665–1678.

Hunkin, G.G., Fife, T.P., and Stano, J.R., 1979, In situ carbonate leaching and recovery of uranium from ore deposits: U.S. Patent Office, Patent 4,155,982.

IAEA, 2009, World distribution of uranium deposits (UDEPO) with uranium deposit classification: International Atomic Energy Agency TEC-DOC-1629, 117 p.

Jaffe, L.A., Peucker-Ehrenbrink, B., and Petsch, S.T., 2002, Mobility of rhenium, platinum group elements and organic carbon during black shale weathering: Earth and Planetary Science Letters, v. 198, p. 339–353.

James, L.P., and Newman, E.W., 1986, Subsurface character of mineralization at Silver Reef, Utah, and a possible model for ore genesis: Utah Geological Association Report UGA-15, p. 149–158.

Jenner, F.E., O'Neill, H.S.C., Arculus, R.J., and Mavrogenes, J.A., 2010, The magnetite crisis in the evolution of arc-related magmas and the initial concentration of Au, Ag and Cu: Journal of Petrology, v. 51, p. 2445–2464.

Kemp, A.I.S., and Hawkesworth, C.J., 2003, 3.11 Granitic perspectives on the generation and secular evolution of the continental crust: Treatise on Geochemistry, v. 3, p. 349–410.

King, R.U., Shawe, D.R., and MacKevett, E.M. Jr., 1973, Molybdenum: U.S. Geological Survey Professional Paper 820, p. 425–435.

Kislyakov Y.M., and Shchetochkin, V.N., 2000, Hydrogenic ore-forming systems: Geology of Ore Deposits, v. 42, p. 369–396.

Kiss, Jean, 1958, Uraniferous chromium ore and its paragenetic role in the Mecsek Permian aggregate: Geneva, United Nations International Conference Peaceful uses of Atomic Energy, 2nd, Proceedings, Sept. 1–13, v. 2, p. 396–401.

Klein, E.M., 2004, 3.13 Geochemistry of the igneous oceanic crust: Treatise on Geochemistry, v. 3, p. 433–463.

Langmuir, D., 1978, Uranium solution-mineral equilibria at low temperatures with application to sedimentary ore deposits: Geochimica et Cosmochimica Acta, v. 42, p. 547–569.

Latta, D.E., Boyanov, M.I., Kemner, K.M., O'Loughlin, E.J., and Scherer, M.M., 2012, Abiotic reduction of uranium by Fe(II) in soil: Applied Geochemistry, v. 27, p. 1515–1524.

Le Roux, J.P., 1993, Genesis of stratiform U-Mo deposits in the Karoo basin of South Africa: Ore Geology Reviews, v. 7, p. 485–509.

Leybourne, M.I., and Cameron, E.M., 2008, Source, transport, and fate of rhenium, selenium, molybdenum, arsenic and copper in groundwater associated with porphyry-Cu deposits, Atacama Desert, Chile: Chemical Geology, v. 247, p. 208–228.

Li, Y.H., 1991, Distribution patterns of the elements in the ocean: A synthesis: Geochimica et Cosmochimica Acta, v. 55, p. 3223–3240.

Liger, E., Charlet, L., and Van Cappellen, P., 1999, Surface catalysis of uranium (VI) reduction by Fe(II): Geochimica et Cosmoshimica Acta, v. 63, p. 2939–2955.

Lipinski, M., Warning, B., and Brumsack, H-J., 2003, Trace metal signatures of Jurassic/Cretaceous black shales from the Norwegian Shelf and the Barents Sea: Palaeogeography, Palaeoclimatology, Palaeoecology, v. 190, p. 459–475.

Lovely, D.R., Roden, E.E., Phillips, E.J.P., and Woodward, J.C., 1993, Enzymatic iron and uranium reduction by sulfate-reducing bacteria: Marine Geology, v. 113, p. 41–53.

Macfarlane, I., and Inwood, N., 2010, Mulga Rock project—Ambassador uranium deposit, June 2010 resource estimate: Coffey Mining Pty Ltd., JORC compliant report (http://www.eama.com.au/projects/reports/ accessed April 1, 2013).

Maksimova, M.F., Brovin, K.G., Goldstein, R.I., and Natalchenko, B.I., 1995, Rare earth elements concentration in the areas of gray rocks and thinning out oxidation zone, *in*, Rare metal-uranium ore formation within sedimentary rocks: Moscow, Nauka, p. 90–106.

Malan, R.C., 1968, The uranium industry and geology of the Monument Valley and White Canyon districts, Arizona and Utah, *in* Ridge, J.D., ed., Ore deposits of the United States 1933–1967: American Institute of Mining and Metallurgical, and Petroleum Engineers, v. 1, p. 790–804.

Mann, A.W., and Deutscher, R.L., 1978, Genesis principles for the precipitation of carnotite in calcrete drainages in Western Australia: Economic Geology, v. 73, p. 1724–1737.

McKay, A.D., and Mieztis, Y., 2001, Australia's uranium resources, geology, and development of deposits: AGSO—Geoscience Australia Mineral Resource Report 1, 184 p.

McCulloh, R.P., 1982, A preliminary assessment of Lousiana's uranium potential: Gulf Coast Association of Geological Societies Transactions, v. 32, p. 221–231.

Meunier, J-D., Sellier, E., and Pagel, M., 1990, Radiation-damage rims in quartz from uranium-bearing sandstones: Journal of Sedimentary Petrology, v. 60, p. 53–58.

Mikhaylenko, M., and van Deventer, J., 2009, Notes of practical application of ion exchange resins in uranium extractive metallurgy: Alta Uranium 2009, Melbourne, 2009. (http://www.purolite.com/customized/uploads/u_purolite_alta09.pdf).

Mingkuan, Q., and Ruiquan, Z., 1997, The geochemistry and significance of rhenium in uranium deposit no. 512: Uranium Geology, v.15 p. 273–278.

Muller, C.J., and Umpire, A., 2012, An independent technical report on the Falea uranium, copper and silver deposit Mali, West Africa: Roodeport, South Africa, Minxcon (Pty) Ltd., 109 p.

Myers, A.T., Hamilton, J.C., and Wilmarth, V.R., 1960, A study of rhenium and molybdenum in uranium ore from the Runge mine, Fall River County, South Dakota, by means of a spectrographic and concentration method: U.S. Geological Survey Professional Paper 400, p. B39–B41.

Nash, J.T., 2010, Volcanogenic uranium deposits: Geology, geochemical processes, and criteria for resource assessment: U.S. Geological Survey Open-File Report 2010-1001, 99 p.

Nash, J.T., Granger, H.C., and Adams, S.S., 1981, Geology and concepts of genesis of important types of uranium deposits: Economic Geology 75th Anniversary Volume, p. 63–116.

Northrop, H.R., Goldhaber, M.B. et al., 1990, Genesis of the tabular-type vanadium-uranium deposits of the Henry basin, Utah: Economic Geology, v. 85, p.215–269.

OECD/NEA-IAEA, 2010, Uranium 2009: Resources, production and demand (the Red Book): Paris, Organization for Economic Co-operation and Development, 452 p.

Omarini, R.H., Sureda, R.J., Gotze, H-J., Seilacher, A., and Pfluger, F., 1999, Puncoviscana folded belt in northwestern Argentina: Testimony of Late Proterozoic Rodinia fragmentation and pre-Gondwana collisional episodes: International Journal of Earth Sciences, v. 88, p. 76–97.

Pagel, M., Cavellec, S., Forbes, P., Ferbaud, O., Vergely, P., and Wagani, I., 2005, Uranium deposits in the Arlit area (Niger), *in* Jingwen M., and Bierlien, F.P., eds., Mineral deposit research: Meeting the global challenge: Berlin, Springer-Verlag, p. 303–305.

Pašava, J., Oszczepalski, S., and Du, A., 2010, Re-Os age of non-mineralized black shale from the Kupferschiefer, Poland, and implications for metal enrichment: Mineralium Deposita, v. 45, p. 189–199.

Penny, R., 2012, Australian sandstone-hosted uranium deposits: Transactions of the Institution of Mining and Metallurgy, pt. B, v. 121, no. 11, p. 65–75.

Petersen, R.J., Hamilton, J.C., and Myers, A.T., 1959, An occurrence of rhenium associated with uraninite in Coconino County, Arizona: Economic Geology, v. 54, p. 254–267.

Pierson, C.T., and Spirakis, C.S., 1986, Comparison of the chemical composition of mineralized and umineralized sandstone and conglomerate samples from the uranium-bearing Chinle Formation of the Colorado Plateau: U.S. Geological Survey Open-File Report 86-281, 15 p.

Polyak, D.E., 2010, Vanadium: U.S. Geological Survey Mineral Commodity Summaries 2010, p. 80.1–80.10.

Quinby-Hunt, M.S., Wilde, P., Orth, C.J., and Berry, W.B.N., 1989, Elemental geochemistry of black shales—statistical comparison of low calcic shales with other shales: U.S. Geological Circular 1037, p. 8–15.

Rose, A.W., 1989, Mobility of copper and other heavy metals in sedimentary environments: Geological Association of Canada Special Paper, v. 36, p. 97–110.

Ross, J.R., and Rosenbaum, J.B., 1962, Reconnaissance of scandium sources and recovery of scandium from uranium mill solutions: U.S. Bureau of Mines Report of Investigations 6064, 16 p.

Rudnick, R.L., and Gao, S., 2003, 3.01 Composition of the continental crust: Treatise on Geochemistry, v. 3, p. 1–64.

Schlottmann, J.L., Mosier, E.L., and Breit, G.N., 1998, Arsenic, chromium, selenium, and uranium in the Central Oklahoma aquifer: U.S. Geological Survey Water-Supply Paper 2357-A, p. 119–177.

Schmid, S., Foss, C., Hill, J., Quigley, M., Schaubs, P., Cleverley, J., and Robinson, J., 2012, JSU Ngalia basin uranium mineral system project: Ngalia basin uranium mineral system project: Northern Territory Geological Survey Record 2012-003, 96 p.

Schmidt, H., Kruszona, M., Kippenberger, C., and Thormann, A., 1981, XIV Vanadium: Hanover, Bundesanstalt fur Geowissenschaften und Rohstoffe, 200 p.

Shawe, D.R., 1976, Sedimentary rock alteration in the Slick Rock district, San Miguel and Dolores Counties, Colorado: U.S. Geological Survey Professional Paper 576-E, 19 p.

——2011, Uranium-vanadium deposits of the Slick Rock district, Colorado: U.S. Geological Survey Professional Paper 576-F, 80 p.

Shoemaker, E.M., Miesch, A.T., Newman, W.L., and Riley, L.B., 1959, Element composition of the sandstone-type deposits: U.S. Geological Survey Professional Paper 320, pt. 3, p. 25–54.

Smedley, P.L., and Kinniburgh, D.G., 2002, A review of the source, behavior and distribution of arsenic in natural waters: Applied Geochemistry, v. 17, p. 517–568.

Sole, K.C., Cole, P.M., Feather, A.M., and Marthie, H.K., 2011, Solvent extraction and ion exchange applications in Africa's resurging uranium industry: A review: Solvent Extraction and Ion Exchange, v. 29, p. 868–899.

Spirakis, C.S., and Pierson, C.T., 1983, Comparison of the chemical characteristics of the uranium deposits of the Morrison Formation in the Grants uranium region, New Mexico: U.S. Geological Survey Open-File Report 83-380, 20 p.

Spirakis, C.S., Pierson, C.T., and Granger, H.C., 1981, Comparison of the chemical composition of mineralized and unmineralized (barren) samples of the Morrison Formation in the Ambrosia Lake uranium area, New Mexico: U.S. Geological Survey Open-File Report 81-508, 43 p.

Spirakis, C.S., Pierson, C.T., and Peterson, F., 1984a, Chemical characteristics of uranium-vanadium deposits of the Henry Mountains mineral belt, Utah: U.S. Geological Survey Open-File Report 84-367, 11 p.

Spirakis, C.S., Pierson, C.T., and Santos, E.S., 1984b, Chemical characteristics of roll-type uranium deposits in Wyoming and Texas: U.S. Geological Survey Open-File Report 84-366, 18 p.

Stuckless, J.S., and Nkomo, I.T., 1978, Uranium-lead isotope systematics in uraniferous alkali-rich granites from the Granite Mountains, Wyoming: Implications for uranium source rocks: Economic Geology, v. 73, p. 427–441.

Sun, W., Bennett, M.C., Eggins, S.M., Arculus, R.J., and Perfit, M.R., 2003, Rhenium systematics in submarine MORB and back-arc basin glasses: Laser ablation ICP-MS results: Chemical Geology, v. 196, p. 259–281.

Thamm, J.K., Kovschak, A.A. Jr., and Adams, S.S., 1981, Geology and recognition criteria for sandstone uranium deposits of the Salt Wash type, Colorado Plateau province: U.S. Department of Energy, GJBX-6(81), 136 p.

Troshkina, I.D., 2011, Rhenium in nuclear fuel cycle: International Symposium on Technetium and Rhenium Science and Utilization, 7th, July 4–8, Moscow, (http://www.technetium-99.ru/Presentations/Troshkina.pdf, accessed May 15, 2014)

Turner-Peterson, C.E., 1985, Lacustrine-humate model for primary uranium ore deposits, Grants uranium region, New Mexico: American Association of Petroleum Geologists Bulletin, v. 69, p. 1999–2020.

Vine, J.D., and Tourtelot, E.B., 1970, Geochemistry of black shale deposits—a summary report: Economic Geology, v. 65, p. 253–272.

Wall, J.D., and Krumholz, L.R., 2006, Uranium reduction: Annual Reviews in Microbiology, v. 60, p. 149–166.

Wanty, R.B., Goldhaber, M.G., and Northrop, H.R., 1990, Geochemistry of vanadium in an epigenetic, sandstone-hosted vanadium-uranium deposit, Henry basin, Utah: Economic Geology, v. 85, p. 270–284.

Wright, M.T., and Belitz, K., 2010, Factors controlling the regional distribution of vanadium in groundwater: Ground Water, v. 48, p. 515–525.

Xu, G., Hannah, J.L., Stein, H.J., Mørk, A., Os Vigran, J., Bingen, B., Schutt, D.L., and Lundschien, B.A., 2014, Cause of Upper Triassic climate crisis revealed by Re-Os geochemistry of Boreal black shales: Palaeogeography, Palaeoclimatology, Palaeoecology, v. 395, p. 222–232.

Zielinski, R.A., 1978, Uranium abundances and distribution in associated glassy and crystalline rhyolites of the western United States: Geological Society of America Bulletin, v. 89, p. 409–414.

Ziying, L., Wenming, D., and Qingyin, G., 2004, Metallogenic features and perspective evaluation of sandstone-type uranium mineralization in Hailaer basin, NE, China: Recent developments in uranium resources and production with emphasis on in situ leach method: International Atomic Energy Agency TECDOC-1396, p. 91–102.

©2016 Society of Economic Geologists, Inc.
Reviews in Economic Geology, v. 18, pp. 339–365

Chapter 14

Lithium Brines: A Global Perspective

Lee Ann Munk,[1,†] Scott A. Hynek,[2] Dwight C. Bradley,[3,*] David Boutt,[4] Keith Labay,[3] and Hillary Jochens[1]

[1] *Department of Geological Sciences, University of Alaska Anchorage, 3101 Science Cir., Anchorage, Alaska 99508*

[2] *Earth and Environmental Systems Institute and Department of Geosciences, Pennsylvania State University, 302 Hosler, University Park, Pennsylvania 16802*

[3] *U.S. Geological Survey, 4210 University Drive, Anchorage, Alaska 99508*

[4] *Department of Geosciences, University of Massachusetts Amherst, 611 N. Pleasant St., 248 Morrill IV South, Amherst, Massachusetts 01002*

Abstract

Lithium is a critical and technologically important element that has widespread use, particularly in batteries for hybrid cars and portable electronic devices. Global demand for lithium has been on the rise since the mid-1900s and is projected to continue to increase. Lithium is found in three main deposit types: (1) pegmatites, (2) continental brines, and (3) hydrothermally altered clays. Continental brines provide approximately three-fourths of the world's Li production due to their relatively low production cost. The Li-rich brine systems addressed here share six common characteristics that provide clues to deposit genesis while also serving as exploration guidelines. These are as follows: (1) arid climate; (2) closed basin containing a salar (salt crust), a salt lake, or both; (3) associated igneous and/or geothermal activity; (4) tectonically driven subsidence; (5) suitable lithium sources; and (6) sufficient time to concentrate brine. Two detailed case studies of Li-rich brines are presented; one on the longest produced lithium brine at Clayton Valley, Nevada, and the other on the world's largest producing lithium brine at the Salar de Atacama, Chile.

Introduction

Lithium is a critical and technologically important element used in ceramics, glass, lubricants, light-weight alloys, medicine, and batteries. The use of Li ion batteries in electric cars and electronic devices has increased the global demand for lithium, a trend that is likely to continue. Lithium-rich brines are the most economically recoverable Li source on the planet. Therefore, it is important to understand the genesis of these deposits in order to develop exploration models for continued discovery of new deposits.

Lithium is found in three main types of deposits: (1) pegmatites, (2) continental brines, and (3) hydrothermally altered clays. Lithium is a lithophile element because it has a low density of 0.53 g/cm^3, an ionic charge of +1, and an ionic radius of 0.79. For comparison Na^+ has an ionic charge of +1 but a larger ionic radius of 0.99, and Mg^{2+} has an ionic charge of +2 and an ionic radius of 0.72. The lithophilic characteristics of Li and the fact that it is a trace element explain why it concentrates in the late phases of both hydrothermal and low-temperature fluids. This generally explains its association and geochemical behavior in the three deposit types. In particular, for continental brines there is evidence that both evaporative concentration and hydrothermal inputs have a significant impact on concentrating Li in brines. These concentrating processes are effective for Li because it is relatively incompatible and geochemically conservative, both in magmatic systems and low-temperature solutions. From a Li brine production standpoint the Mg/Li ratio of the starting and final processed brines is important because Mg causes chemical interferences in the brine purification process. Ultimately, the initial brine composition determines the production process.

Lithium-rich brine deposits account for about three-fourths of the world's lithium production (U.S. Geological Survey, 2011). These Li-rich continental (nonmarine) brines are the focus of this paper. Economically viable Li-rich brines contain varying amounts of the major cations and anions (Na, K, Mg, Ca, Cl, SO_4, and CO_3), which can form a range of ionic salts (Warren, 2010). The composition of the source rocks, inflow waters, and the resulting brine composition dictate how the brine will evolve once it undergoes evaporation and mineral precipitation (Eugster, 1980). These brines can also contain appreciable Li, B, Ba, Sr, Br, I, and F, and in the case where Li is concentrated on the order of 100s of mg/L these deposits can be classified as having potential economic viability with respect to Li extraction.

It is known that Li can also accumulate in deep oilfield brines, such as those associated with the Smackover Formation in the Gulf Coast of the United States (Collins, 1976) or the Devonian strata of the Appalachian Plateau of Pennsylvania (Dresel and Rose, 2010). Some brines are reported to contain 100s of mg/L but typically they have low concentrations of Li and are usually greater than 1 km deep, preventing development (Gruber et al., 2011). There are also occurrences of closed basins with abundant saline ground and surface waters which are not enriched in Li. One example is the ephemeral lakes of southwestern Australia, many of which may have occupied closed basins since the Eocene and are hosted by diverse and highly weathered igneous and metamorphic rocks of the Archean Yilgarn craton (Benison and Bowen, 2006). These unusual waters have salinities that in all but a few cases are 5 to 10 times greater than seawater (Bowen and Benison,

† Corresponding author: e-mail, lamunk@uaa.alaska.edu
*Present address: 11 Cold Brook Rd., Randolph, NH 03593, USA.

2009). These studies further demonstrate that the fluids are Na-Cl and Na-Mg-Cl-SO_4 brines, the majority of which have a pH <4. Although extreme weathering and evaporation have played critical roles in the development of these brines, their Li content is quite low. Only a single brine sample exceeds 1 mg/L Li, and the vast majority of brines contain less than 0.5 mg/L (B. Bowen, pers. commun.) The climate and hydrology of these systems is favorable for enrichment of Li, but clearly a sufficient Li source and/or concentrating mechanism is absent.

Studies of continental Li-rich brines are most extensive for those in the Central Andes of Bolivia and northern Chile as reported in Risacher and Fritz (2009) and references therein. Hundreds of geochemical analyses for brines from this region are published by Moraga et al. (1974), Rettig et al. (1980), Risacher and Fritz (1991), and Risacher et al. (1999, 2003). The focus of most of this work was to examine the origin of the salts in the salars. Risacher and Fritz (2009) also provided a general classification for these brines (alkaline, sulfate-rich, and calcium-rich), and noted that alkaline salars are absent in Chile due to the presence of high-sulfur volcanic rocks that release hydrogen ions during weathering. The origin of solutes to salars in the Central Andes has been addressed by the major and trace element and isotopic investigations of Alpers and Whitmore (1990), Spiro and Chong (1996), Carmona et al. (2000), and Boschetti et al. (2007). However, none of these studies specifically addressed the origin and accumulation of Li. At Clayton Valley, Nevada, Kunasz (1974), Davis et al. (1986), Price et al. (2000), and Zampirro (2004) have explored the sources and concentrating processes of Li in the Clayton Valley brines. More recent work by Jochens and Munk (2011) and Munk et al. (2011) and current work by the authors of this paper on the Li-rich brines in Clayton Valley and the Salar de Atacama, Chile, is focused primarily on understanding the sources, transport, and accumulation of Li, and the age of the brines.

Bradley et al. (2013) identified common characteristics of Li-rich continental brines as the basis for an ore deposit model. In this paper, we elaborate on these common characteristics and focus on how they can be used as general exploration guidelines for locating future Li brine deposits on a global scale. We also include a discussion of the general geology, hydrogeochemistry, and climate of Li-rich brine systems followed by detailed discussion in the form of two case studies from the Salar de Atacama, Chile, and Clayton Valley, Nevada, which are currently two of the most well-studied Li-rich brine systems.

Six Characteristics Common to Continental Lithium Brines

The Li-rich brine systems in our compilation (Table 1) share six common (global) characteristics that provide clues to deposit genesis while also serving as exploration guidelines. These include: (1) arid climate; (2) closed basin containing a salar (salt crust), a salt lake, or both; (3) associated igneous and/or hydrothermal activity; (4) tectonically driven subsidence; (5) suitable Li sources; and (6) sufficient time to concentrate Li in the brine. Table 1 summarizes information related to the six common characteristics of continental Li-rich brines.

Climate is the first characteristic and is perhaps the most important, as it is linked to all the others because it (1) contributes to the formation of the salars in a closed-basin setting, (2) is a factor in the concentration of Li in brines over time, and (3) is essential for the concentration of Li in evaporation ponds for economic purposes. Table 1 indicates the classification of the climate for each Li-rich brine location in terms of hyperarid, arid, or semiarid.

The second characteristic, shared by all continental Li-rich brines, is a closed basin with a salar(s) or salt lake(s). This characteristic is controlled primarily by climate and tectonic setting. Salars or salt crusts are common where brines exist in shallow subsurface aquifers. The aquifers may be composed of halite and other interbedded salts—commonly gypsum, as well as volcanic ash or ignimbrites, alluvial gravels and sands, and tufa (commonly evidence of modern or past hydrothermal activity). Most of the locations in Table 1 are classified as salars. Salt lakes may also contain enrichments of Li, although these are typically in the lower range of the concentration spectrum and there are only a few (Table 1) considered here. Most salt lakes do not produce Li because of low concentrations.

The third characteristic is evidence of hydrothermal activity. This likely plays a significant role in the formation of Li-rich brines for several reasons: (1) it provides a hot water source for enhanced leaching of Li from source rocks; (2) it is also likely a direct source of Li from shallow magmatic brines and/or magmatic activity; (3) it may play a role in the concentration of Li through distillation or "steaming" of thermal waters in the shallow subsurface; (4) thermally driven circulation may be an effective means for advecting Li from source areas to regions of brine accumulation; and (5) it can result in the formation of the Li-rich clay mineral hectorite, which can in turn be a potential source of Li to brines if leaching and transport occur from the clay source.

A fourth characteristic of all Li-rich brine deposits is that they occur in basins that are undergoing tectonically driven subsidence. The basins listed in Table 1 have a number of different tectonic drivers, including extension, transtension, and orogenic loading. In contrast, significant Li brine accumulations have not been reported from intracratonic basins in arid regions, such as the shallow sabhkas that rest on Precambrian basement of Australia or North Africa.

The fifth characteristic or requirement for the formation of Li-rich brines is a viable source(s) of Li. Lithium sources in various basins appear to include magmatic fluids, high-silica vitric volcanic rocks, hectorite, and ancient salt deposits. These along with the "time factor," discussed below, are probably the least well understood of the six characteristics. Despite the observation that multiple potential sources of Li exist they are yet to be definitively identified and quantified.

The sixth characteristic or requirement for the formation of Li-rich brines is time. The time it takes to leach, transport, and concentrate Li in continental brines is not well understood. However, it appears that most Li brines of economic interest are geologically young (Neogene). Currently we are working on dating the brines at Clayton Valley, Nevada, United States, and the Salar de Atacama, Chile, as well as developing hydrogeologic models for these environments to understand the transport and accumulation of Li in the closed basins. These studies will be the first to address the time factor for Li brines using a quantitative approach.

General geology of Li brines (basins, tectonics, and stratigraphy)

Figure 1 shows the global distribution of the locations of Li brines or salt lakes detailed in Table 1. We include the best known brines from North America, South America (Argentina, Bolivia, and Chile), and Asia (China) that are enriched in Li, irrespective of whether the brines are in production or not. Other well-known brines that contain Li include those with relatively lower Li concentration in lakes such as Great Salt Lake, Searles Lake, and the Dead Sea (Table 1), as well as oil field brines such as that from the Smackover Formation (Gulf Coast, United States) or the Devonian strata of the northeastern United States.

The majority of important Li-rich brines are located in the Altiplano-Puna region of the Central Andes of South America. Houston et al. (2011) classified the salars in the Altiplano-Puna region of the Central Andes in terms of two end members, "immature clastic" or "mature halite," primarily using (1) the relative amount of clastic versus evaporite sediment; (2) climatic and tectonic influences, as related to altitude and latitude; and (3) basin hydrology, which controls the influx of fresh water. The immature classification refers to basins that generally occur at higher (wetter) elevations, contain alternating clastic and evaporite sedimentary sequences dominated by gypsum, have recycled salts, and a general low abundance of halite. Mature refers to salars in arid to hyperarid climates, which occur in the lower elevations of the region, reach halite saturation, and have intercalated clay and silt and/or volcanic deposits. An important point made by Houston et al. (2011) is the relative significance of aquifer permeability which is controlled by the geological and geochemical composition of the aquifers. For example, immature salars may contain large volumes of easily extractable Li-rich brines simply because they are comprised of a mixture of clastic and evaporite aquifer materials that have higher porosity and permeability.

Our conceptual model for Li brines is shown in Figure 2. The model seeks to account for the sources, sinks, and processes that mobilize, sequester, and concentrate Li. This model is developed primarily from the information we have gathered over the past few years on the brines at Clayton Valley, Nevada, United States, and Salar de Atacama, Chile, which are further described in the following sections. The concepts of Houston et al. (2011) are specific to the range of salars observed in the Altiplano-Puna region of the Central Andes and are not necessarily transferable, in a global sense, to other Li-rich brines. Our conceptual model captures the framework of Houston et al. (2011), albeit with less specificity. We also recognize the earlier summaries by Asher-Bolander (1982, 1991), which describe a model for the formation of Li-rich clays and provide a brief description of factors contributing to the formation of Li-rich brines, in particular emphasizing the importance of hydrothermal activity in concentrating Li.

Effects of geochemistry, climate, and hydrogeology on evolution of the Li brine resource

Geochemical characteristics: The minimum, maximum and average Li concentrations for the brines and lakes in this study are listed in Table 1. These values are compiled from various sources detailed in Appendix 1. Because some of the basins do not have minimum and maximum Li concentration data reported in the literature we use the average Li concentrations to compare basins. The lowest average Li concentration is 10 mg/L in Searles Lake, California, and the highest average Li concentration is 1,400 mg/L for the brine in Salar de Atacama, Chile. Average seawater contains 0.2 mg/L Li.

The potentially important sources of Li to brines include high-silica volcanic rocks, preexisting evaporites and brines, hydrotherm clays, and hydrothermal fluids. The relative role of Li leaching from source rocks by low- and high-temperature fluids versus Li sourced in magmatic fluids themselves is not known and studies addressing this topic are scant. A study by Price et al. (2000) suggests that Li in the Clayton Valley, Nevada, brine is leached by groundwater from volcanic tuffs and that process alone can account for all the Li in the brines. However, experimental weathering studies by Jochens and Munk (2011) have shown that less than 10 μg/L Li are released from these volcanic rocks when exposed to water at ambient conditions. Godfrey et al. (2013) reported similar findings from low-temperature leaching of Li from volcanic rocks near Salar del Hombre Muerto, Argentina. Risacher and Fritz (2009) concluded that Li and B in Andean salars are derived from the weathering of ignimbrites. Yu et al. (2013) demonstrated that playas in the Qaidam basin receive Li transported by streams that is ultimately sourced from upstream hydrothermal inputs. They also hypothesized that source(s) of Li are from alteration of volcanic rocks by hydrothermal fluids and/or from direct connection to differentiated magmatic sources. Hofstra et al. (2013) reported that fluid inclusions in quartz phenocrysts from high-silica volcanic rocks in the Great Basin region of the United States contain elevated Li concentrations relative to their host vitric matrices, suggesting that volcanic glass is a significant and readily available source of Li released to the environment via weathering processes and that fluid inclusions in erupted volcanic rocks may ultimately be an important Li source.

The predictive sequence of evaporite formation in closed-basin salt lakes was established by Hardie and Eugster (1970) and Eugster and Hardie (1978). Their model indicates that there are three major fluid pathways or "chemical divides" that result during evaporation, which are dictated by the initial ionic composition of the fluid. Here we summarize the essence of their models in order to set a context for Li-enriched brines, but the reader is referred to Eugster (1980), Eugster and Hardie (1978), and Hardie and Eugster (1970) for more details. Path 1 occurs when there is an excess of bicarbonate compared to the alkaline earth elements (referred to as "soft water"), which produces the typical precipitation path from calcite to trona with no gypsum because the parent water is low in Ca and Mg. Examples from Eugster (1980) include Alkali Valley, Oregon, and Lake Magadi, Kenya. The Wilkins Peak member of the Eocene Green River Formation in southwestern Wyoming contains 25 major trona beds and is an example of a large volume geologic trona deposit. Path 2 occurs when there is an excess of alkaline earth elements compared to bicarbonate (referred to as "hard water") and in this case gypsum is precipitated after calcite and the path divides into a sulfate-rich system such as Saline Valley, California, or sulfate-poor system such as Bristol Dry Lake,

Table 1. Summary of Lithium

Basin	Region	Lat.	Long.	Min Li (mg/L)	Max Li (mg/L)	Avg Li (mg/ L)	Li nearby hot springs (mg/L)	Total Li resource (Mt)	Mean annual temp (°C)	Precip. (mm/yr)
Clayton Valley	Nevada	37.76724	–117.58481	100	300	160	40	0.3	13	122
Searles Lake	California	35.73175	–117.32930	10	80	65	NA	NA	19.5	85
Salton Sea	California and Mexico	33.25239	–115.71031	100	400	200	5–100	0.316	22.7	65
Great Salt Lake	Utah	41.25311	–112.70506	18 (north) 40 (south)	43 (north) 64 (south)	52	1.8-6.5	0.53	10.5	186
Dead Sea	Israel	31.15663	35.43786	NA	NA	10	very low	NA	16.7	58
Salar de Atacama	Chile	–23.50069	–68.24984	900	7,000	1,400	40 (El Tatio)	6.3	13.9	39
Salar de Maricunga	Chile	–26.93605	–69.06936	NA	NA	920	NA	0.22	6.6	52
Salar de Surire	Chile	–18.83700	–69.005	NA	NA	340	8.3	NA	3.8	247
Salar del Hombre Muerto	Argentina	–25.38555	–67.13364	190	900	521	3.2-5.5	0.8	6.7	91
Salar del Rincon	Argentina	–24.07478	–67.08165	NA	NA	400	1,500	0.223	8	61
Salar de Olaroz and Salar de Cauchari	Argentina	–23.45187	–66.68484	282 (Olaroz) 200 (Cauchari)	1,207 (Olaroz) 2,150 (Cauchari)	650 (Olaroz) 510 (Cauchari)	NA	0.9–1.0	7.2	90
Salar de Llullaillaco (Mariana)	Argentina	–24.80602	–68.29033	250	650	450	NA	NA	7.8	30
Salar de Uyuni	Bolivia	–20.15888	–67.56912	80	1,150	321	NA	10.2	9.3	62
Salar de Copaisa	Bolivia	–19.36163	–68.16860	NA	NA	243	NA	NA	8.1	320
Salar de Pastos Grandes	Bolivia	–21.64429	–67.79809	353	1,787	1,062	5.2 (edge) 67 (playa)	NA	4.1	57
Taijanier (Taijner) Lake	Qaidam, China	37.49260	93.95323	NA	NA	290	NA	2.02	4.2	167
Zhabuye Lake	Tibet, China	31.34586	84.04752	500	1,000	680	NA	1.53	0.2	287
Dangxiongcuo (DXC)	Tibet, China	31.57053	86.73580	NA	NA	430 (5)	NA	0.181	0.5	184

Notes: APVC = Altiplano-Puna volcanic complex, NA = not available
[1] All references for data in this table are detailed in the Appendix
[2] See Appendix for additional details on tectonics and geologic setting

California (Eugster, 1980). Path 3 is considered intermediate and describes waters with neither a dominance of bicarbonate nor the alkaline earth elements, which result in the formation of alkaline earth carbonates. In this case Mg is concentrated over Ca in the water and high Mg calcite or dolomite can form. At some point either the alkaline earth elements or bicarbonate are exhausted and the brine composition moves toward the alkaline earth path or forms gypsum, respectively. The gypsum path may follow either a sulfate-rich or -poor pathway (Eugster, 1980). These pathways control major element brine evolution through mineral precipitation, depending on the starting composition of the fluids. These three pathways can account for the majority of brine compositions indicating that closed basin brine composition is, on a first order, controlled by the composition of input waters. After precipitation of the alkaline earth elements, the brines are enriched in the alkali metals with a mixture of anions. Eugster (1980) noted that if the alkalis (Na and K) are treated separately, minor constituents and Si are included and the sulfide-sulfate equilibriums are considered, then other mechanisms in addition to mineral precipitation are required to account for the observed differences between inflow and brine waters. This led Eugster and

Brine Basins and Characteristics[1]

Evap (mm/yr)	Aridity index	Aridity class	Min elevation (m)	Max elevation (m)	Relief (m)	Basin floor area (km²)	Basin area (km²)	Tectonic setting[2]
1,425	0.0856	Arid	1,297	2,841	1,544	97	1,437	Basin and Range extensional province; between Neogene core complex and its breakway zone
1,659	0.05	Arid	482	1,984	1,502	187	1,891	Basin and Range extensional province
1,842	0.0336	Arid	–71	3,497	3,568	972	20,051	Pull-apart basin along intracontinental portion of San Andreas transform fault
1,156	0.1428	Arid	1,281	3,959	2,678	18,075	86,896	Basin and Range extensional province
1,467	0.0343	Arid	–415	2,805	3,220	1,111	43,272	Pull-apart basin along intracontinental portion of Dead Sea transform fault
1,440	0.0326	Arid	2,302	6,208	3,906	2,115	15,659	Volcanic arc, plateau margin basin, active subsidence, ~6 km of Cenozoic strata
950	0.0554	Arid	3,748	6,695	2,947	136	2,421	Volcanic arc, high-elevation plateau margin basin
1,100	0.2276	Semiarid	4,260	5,783	1,523	106	586	Volcanic arc, high-elevation plateau margin basin
1,106	0.0696	Arid	3,963	5,835	1,872	581	3,888	Tectonic basin bound by crustal fault blocks, adjacent large silicic volcanic caldera, and resurgent dome dominate hydrographic basin
1,233	0.0568	Arid	3,718	5,590	1,872	421	2,811	Typical Puna, contractional basin and range, bound by crustal fault blocks and also by alluvium and volcanic edifices
1,246	0.0707	Arid	3,886	6,136	2,250	480	5,699	Typical Puna, contractional basin and range, bound by crustal fault blocks and also by alluvium and volcanic edifices
1,148	0.0261	Hyperarid	5,755	6,648	893	128	1,234	Volcanic arc, intra-arc basin
1,318	0.0541	Arid	3,653	6,136	2,483	13,768	47,351	Altiplano, low relief, minor volcanism, APVC to the south and thin skinned fold-thrust belt to the east
1,316	0.2402	Semiarid	3,661	6,549	2,888	3,055	145,279	Altiplano, low relief, minor volcanism, APVC to the south and thin skinned fold-thrust belt to the east
1,094	0.0521	Arid	4,430	5,817	1,387	142	634	Altiplano plateau, occupies an ~5.2 Ma caldera in the northern APVC
989	0.0313	Arid	2,686	6,824	4,138	210	34,148	Growth syncline within intracontintal foreland basin in the far field of the Himalayan-Tibet collisional orogen
750	0.3333	Semiarid	4,424	6,580	2,156	3,055	16,768	Neogene rift oriented at a high angle to the orogenic grain in the upper plate of the Himalayan Tibet collisional orogen
783	0.2868	Semiarid	4,464	6,308	1,844	54	906	Neogene rift oriented at a high angle to the orogenic grain in the upper plate of the Himalayan Tibet collisional orogen

Jones (1978) to propose five major fractionation mechanisms that could account for brine evolution, including mineral precipitation, dissolution of efflorescent crusts and sediment coatings, sorption, degassing, and redox.

The world's most enriched Li brines appear to correspond to the late-stage fluids in the model of Eugster and Hardie (1978). For example, the Li-rich brine at Salar de Atacama, Chile, contains on average 1,400 mg/L Li with a minimum of 900 mg/L and a maximum of nearly 7,000 mg/L, and it is produced from a halite aquifer with carbonate and sulfate flanking the basin. This indicates that carbonate and sulfate mineral precipitation may have played a role in producing the existing Na-Cl brine that is enriched in Li.

In addition to evaporative concentration processes as described above, the distillation of Li from geothermal heating of fluids may play a significant role in concentrating Li in these brines, and perhaps causes prolonged replenishment of brines that are in production. Since many of the Li-rich brines exist over, or in close proximity, to relatively shallow magma chambers it may be that through faults and fractures, the late-stage magmatic fluids and vapors have pathways to migrate into the closed basins.

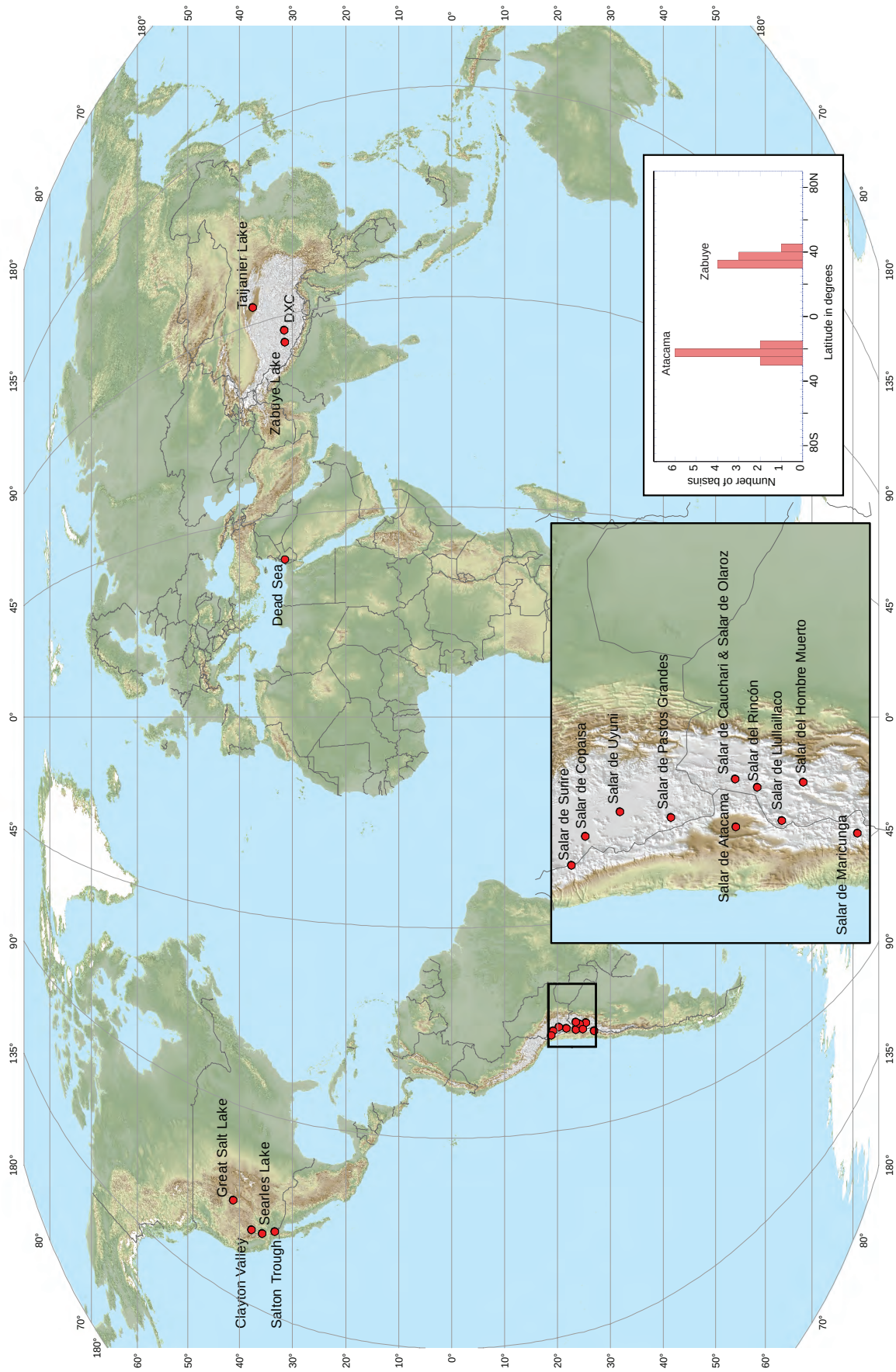

Fig. 1. World map of lithium brine deposits with inset showing detail in South America. Histogram showing the bimodal latitudinal distribution of Li brine deposits in northern and southern arid belts (adapted from Bradley et al., 2013).

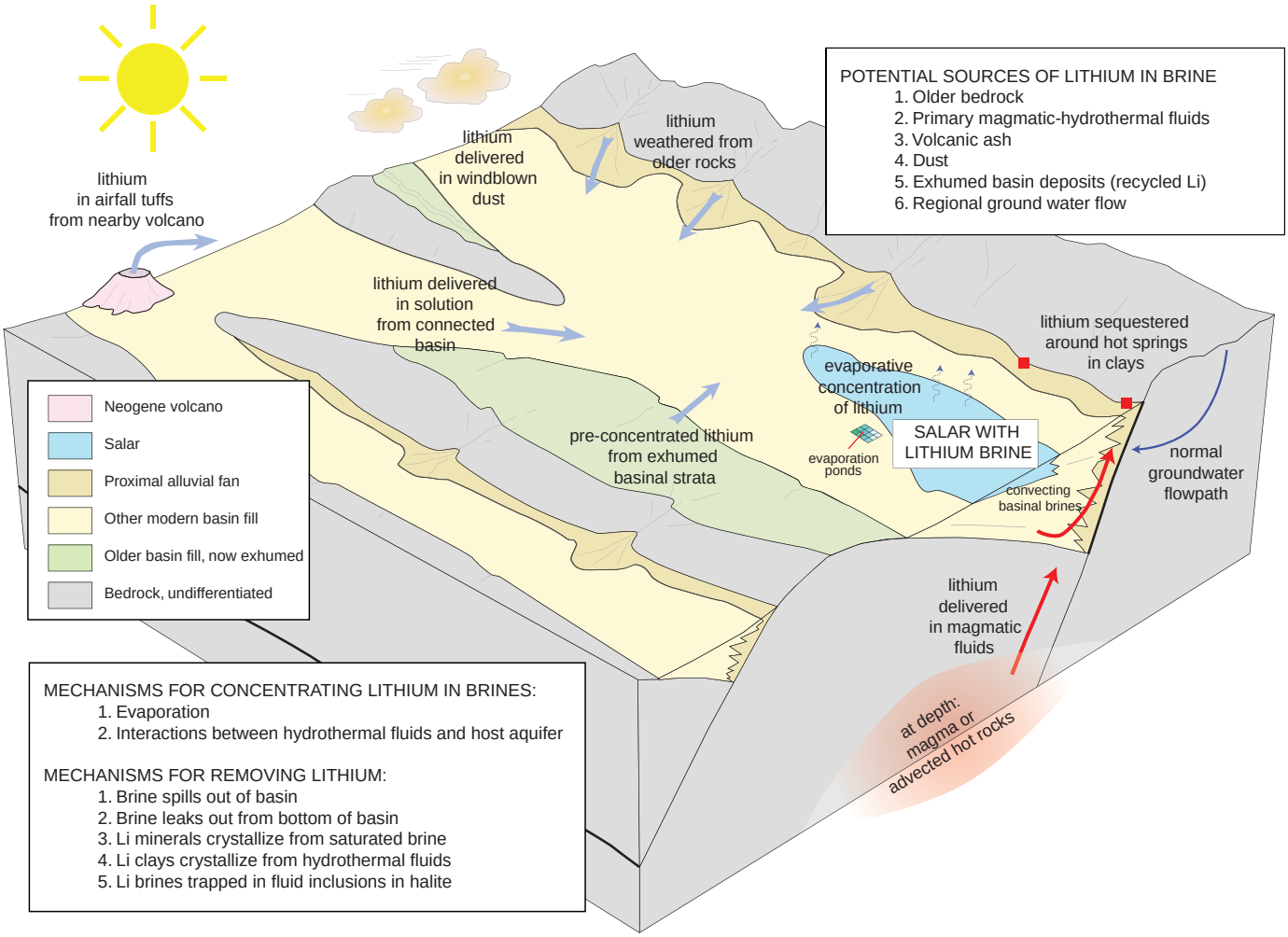

Fig. 2. Summary diagram of the geologic, geochemical, and hydrogeologic features of lithium brines emphasizing the sources, transport, and fate of lithium (adapted from Bradley et al., 2013).

Climatic factors in the generation of Li brines: Certain climatic characteristics are shared by all basins hosting Li-rich brines. Typically these basins are in subtropical and midlatitudes where arid climates are expected (Fig. 1). An arid climate is imperative for evaporative concentration of surface and shallow subsurface brines. Indeed, all of the basins investigated herein have evaporation far exceeding precipitation (Table 1; aridity index). As a first assessment, arid climate and a low precipitation/evaporation ratio are very favorable for the development of Li-rich brines. However, what is critical for generating economical brines is a large flux of water to the basin—seemingly at odds with the importance of arid climates in generating Li-rich brines. For example, on the Salar de Atacama evaporation greatly exceeds precipitation , irrespective of whether precipitation estimates are 10 mm/a (Jordan et al., 2002a), 25 mm/a (Houston et al., 2011), 39 mm/a (Table 1), or anything <50 cm/a (e.g., Bookhagen and Strecker, 2008). Under any scenario there is a net water deficit on the Salar de Atacama and evaporative concentration of inflow waters is possible, but without significant inflow water it would be impossible to generate the enormous volume of highly concentrated brine present there.

The magnitude of water flux through an Li-rich brine-generating basin that is necessary for economical brines is dependent, in turn, on the Li content of the average inflow waters. Economical Li brines contain a minimum of 100 mg/L Li, and more commonly 500 to 5,000 mg/L Li, whereas the inflow waters may only contain Li in the range of 1–10 mg/L or less. Therefore, at an absolute minimum, inflow waters must be concentrated by one full order of magnitude. Given that most Li brine-generating basins have many inflows that are not enriched in Li, it is assumed that the average Li content of inflow waters is less than 1 mg/L Li. Thus, the combined effects of evaporation and precipitation of evaporite minerals must concentrate inflow waters by many orders of magnitude and the time-integrated flux of water through the basin must be sufficient to create a Li brine deposit that contains enough total Li to be economical, irrespective of Li concentration.

There are a number of ways in which large influxes of water can be combined with high evaporation rates to create favorable conditions for generation of Li-rich brines. One example is that of a seasonal climate where wet seasons alternate with hot and dry conditions. To generate both sufficient inflow and evaporation with seasonal climatic variation, each year

must be split between one of these two functions. Essentially the recharge area (precipitation) and the concentration area (evaporation) are identical, but they must each serve these functions for only a part of the year; thereby increasing the amount of time required to generate a brine of given Li concentration. Similarly, alternating between wet and dry climates on longer (climatic) timescales is a possible mechanism for evaporative concentration of large volumes of water in a closed basin. Again, time is the limiting factor in this scenario as the same land surface must serve both functions. Climatic cycles likely played an important role in the generation of the Li-rich brine in Salars de Copaisa and Uyuni, where at least 130 ka of climatically driven lake-level cycles have been documented on the Bolivian Altiplano (Placzek et al., 2011). Alternatively, recharge and evaporative concentration can operate simultaneously in different areas of the hydrographic basin. As for the Salar de Atacama, precipitation elsewhere in the drainage basin can serve as the Li influx while the low-elevation salar surface can serve to concentrate the inflow waters. Likewise, the nearly 5,900-m-high resurgent dome of the Cerro Galán caldera may be an important recharge area for the Salar del Hombre Muerto at ~4,000-m elevation.

In addition to elevation differences, the size of a drainage basin relative to the salar/playa surface is an important consideration (Table 1). Importantly, the size of the drainage basin is not limited to surface drainage. Regional groundwater flow below topographic divides is one additional factor that can contribute significant amounts of water to a closed basin. For example, at Clayton Valley, Nevada, a large regional groundwater flow system contributes the majority of the water flux to the basin (Rush, 1968; Belcher, 2004). Subsurface flow paths provide ample water to aid in mobilization and evaporative enrichment of Li within a closed basin and may also provide significant additional sources of Li.

The climatic condition requisite for generation of Li brines is a net water deficit at the basin floor. A wide range of localities satisfy this condition; however, water cannot be evaporated and Li cannot be concentrated unless there is a sufficient influx of both. For this reason, localities favorable to generation of Li-rich brines juxtapose wetter conditions with the hot, dry conditions characteristic of basin floors. This can be accomplished many ways, including seasonality, climatic cycles, and climatic variation within the surface and/or subsurface drainage basins. Therefore, the role of climate can be complicated by other factors and these must be assessed for each basin.

Hydrogeology. As discussed above most known Li brine deposits occur in the shallow subsurface of tectonically active, closed basins in arid regions (Fig. 1). In these settings, basin hydrology and hydrogeology are inextricably linked through depositional and tectonic processes and have important impacts on the geometry and nature of subsurface flow paths. Host aquifers in these systems range from clastic sedimentary units associated with alluvial fans and playa sediments (including volcanic deposits) to halite and other salts. Fresh water enters the system either on the flanks through permeable alluvial sediments and is confined to the more permeable facies (fan gravels, sands), or through subsurface paths from upgradient basins. Fresh water mixes and floats on the denser basin brines and is ultimately driven upward by a moisture gradient which is maintained by sufficiently arid conditions. This results in significant loss of water through evaporation and concentration of dissolved constituents.

Lithium can enter a basin from leaching of rocks and alluvial fans and hydrothermal fluids associated with magma at shallow depths. Many closed basins are actually connected via subsurface flow paths and can act as sinks for regional transport of ground water. Large fault systems can often act as preferential flow paths allowing Li to be delivered via magmatic-derived fluids from depth. Because brines have extremely high total dissolved solids, they are denser than fresh water, which affects the movement of these fluids in the subsurface. Often there are strong feedbacks between the dissolution of halite, moving ground water, and density changes resulting in complex flow paths that act to mix subsurface fluids. Through a combination of evaporation and hydrothermal distillation brines can reach Li concentrations on the order of 1,000s of mg/L.

The permeability of the host aquifer for the brine plays an important role in the development of and exploitation of the resource. Immature salars, those with significant clastic sediments (Houston et al., 2011) have porosity and permeability dominated by primary depositional processes. Coarse-grained sediments tend to accumulate at the margins of the basin and commonly fine upward and basinward. These sediments have high permeability and well-connected porosity. Clastic sediments at the center of the basin, such as lacustrine facies, commonly have high porosity but low permeability. These sediments often have intercalated evaporite deposits that act as confining units to brines deeper in the basin. Mature salars are dominated by evaporite deposits that have little connected primary porosity. Brines in these environments tend to be transported and hosted in fractures and dissolution features that vary in occurrence in both time and space. The spacing of these features is small (<1 m) such that the shallow evaporite aquifers can be treated as a well-connected porous medium at the km scale. These aquifers often exhibit strong depth dependence in hydrologic characteristics, where the higher porosity and permeability are located closer to the land surface.

Lithium Brine Case Studies

Case study 1: Clayton Valley, Nevada

Clayton Valley is located in Esmeralda County, Nevada, United States, approximately 160 km north of Death Valley, California (Fig. 3) and is the location of the only Li-rich brine deposit in production in North America. Clayton Valley is a closed basin with an area of 1,342 km^2 and a playa surface of 72 km^2. The basin lies in the eastern rain shadow of the Sierra Nevada Mountains and is arid with an annual average precipitation of about 12 cm, average evaporation rates of 142 cm/yr, and an average temperature of 13°C. The elevation of the valley floor is 1,298 m, lower than any of the adjacent basins.

The basement consists of late Neoproterozoic to Ordovician carbonate and clastic rocks that were deposited along the ancient western passive margin of North America. During late Paleozoic and Mesozoic orogenies, the region was shortened and subjected to low-grade metamorphism (Oldow et

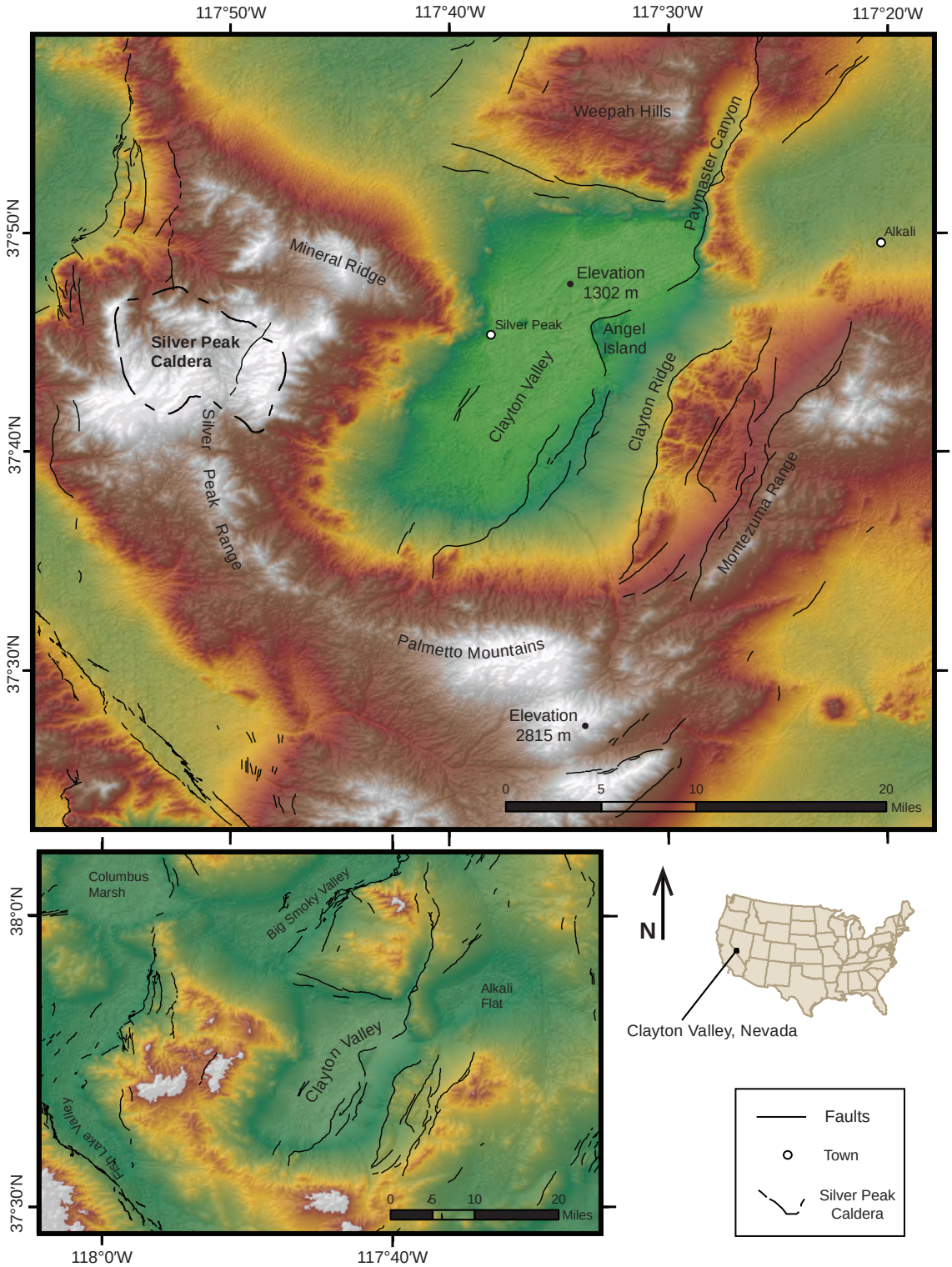

Fig. 3. Shaded relief map of Clayton Valley, showing major features noted in text and Appendix. Fault locations from U.S. Geological Survey (ftp://hazards.cr.usgs.gov/maps/qfaults) and the location of the Silver Peak caldera is from Robinson (1972).

al., 1989). Granitoids were emplaced at ca. 155 and 85 Ma. Extension commenced at ca. 16 Ma and has continued to the present, with changes in structural style. A metamorphic core complex just west of Clayton Valley was exhumed from midcrustal depths during Neogene extension. The basin is bounded to the east by a steep normal fault system toward which basin strata thicken. Late Miocene to Pliocene tuffaceous lacustrine facies (Esmeralda Formation of older usage from Albers and Stewart, 1972) contains up to 1,300 ppm Li and an average of 100 ppm Li (Kunasz, 1974; Davis and Vine,

1979). Miocene silicic tuffs and rhyolites along the basin's eastern flank have Li concentrations as high as 228 ppm (Price et al., 2000). Multiple wetting and drying periods during the Pleistocene resulted in the formation of lacustrine deposits, salt beds, and Li-rich brines. Hectorite in the surface playa sediments contains from 350 to 1,171 ppm Li (Kunasz, 1974). Prior to development of the brine resource, a salt flat and brine pool existed in the northern part of the basin, but groundwater pumping has eliminated the surface brine pool.

At Clayton Valley, brines are pumped from six aquifer units (Zampirro, 2004). Volcanic glass in the main ash aquifer shares strong compositional affinities with the ~760-ka Bishop Tuff. However, this ash bed could also be correlated with some of the 0.8 to 1.2 Ma tuffs of Glass Mountain (Sarna-Wojcicki et al., 2005). In Clayton Valley, this aquifer system ranges between 5 to 20 m thick. Other aquifers (and their thicknesses) include the salt aquifer system comprised of thick-bedded halite deposits interbedded with silt (30–100 m); the tufa aquifer system, an aquifer of consolidated travertine in the uppermost strata localized in the northeastern part of the basin (6–20 m); the lower ash system, an extensive zone of thin volcanic ash deposits, interbedded with silt and sand (10–90 m), also exposed in outcrop in the basin; the marginal gravel aquifer, a localized aquifer of mixed gravel, sand, and silt along the eastern margin of the basin (10–70 m); and the lower gravel aquifer, a poorly sorted deposit of coarse to fine gravel, sand, and silt at ~1-km depth (50–100 m).

The Li content of the waters in Clayton Valley ranges from less than 1 μg/L in snow up to 407 mg/L in groundwater from one of the aquifers composed of volcanic ash. The cold springs surrounding Clayton Valley have Li concentrations of less than 1 mg/L. One hot spring in the area located east of Clayton Valley near Alkali, Nevada, contains 1.6 mg/L Li. Lithium content of the groundwater from a freshwater well in an alluvial fan located near Silver Peak, Nevada, is less than 1 mg/L. Two groundwaters, one located just north of the town of Silver Peak and the other on the far northeast part of the basin, contain about 40 mg/L Li.

Davis et al. (1986) proposed that the Li at Clayton Valley, Nevada was concentrated by the same processes as Cl and therefore must have been trapped as an Li-rich fluid when the halite formed. They also hypothesized that in the last 10,000 years meteoric water entered the basin and dissolved the halite to form brines with evaporative signatures. Munk et al. (2011) indicated that other sources and processes were likely involved in the formation of the brines in the system because nonhalite aquifers produce brine with higher Li concentrations than the halite aquifer. It may be that a combination of hydrothermal activity and leaching from volcanic ash and clays are major sources of Li in the aquifers in Clayton Valley, Nevada. We have found that one of the aquifers composed predominantly of pumice ash has nearly identical major and trace element glass composition to the Bishop tuff; however, the Li content in glass from this aquifer is approximately 12 ppm higher (72 ppm) than the Bishop tuff from a number of other localities. This may be an indication that the volcanic glass in this aquifer exchanges Li over time.

Figure 4 indicates that snow, hot and cold springs, and cold groundwater in Clayton Valley are more dilute (have lower Na concentrations) than the hot groundwater and brines. Additionally, the cold springs have enriched δD values compared to the hot groundwater, most likely caused by evaporation at the surface. It appears that there are two mixing pathways that can account for the composition of waters in the basin (Fig. 4). We interpret these mixing lines as dilute inflow waters interacting and leaching chemical constituents from the rocks

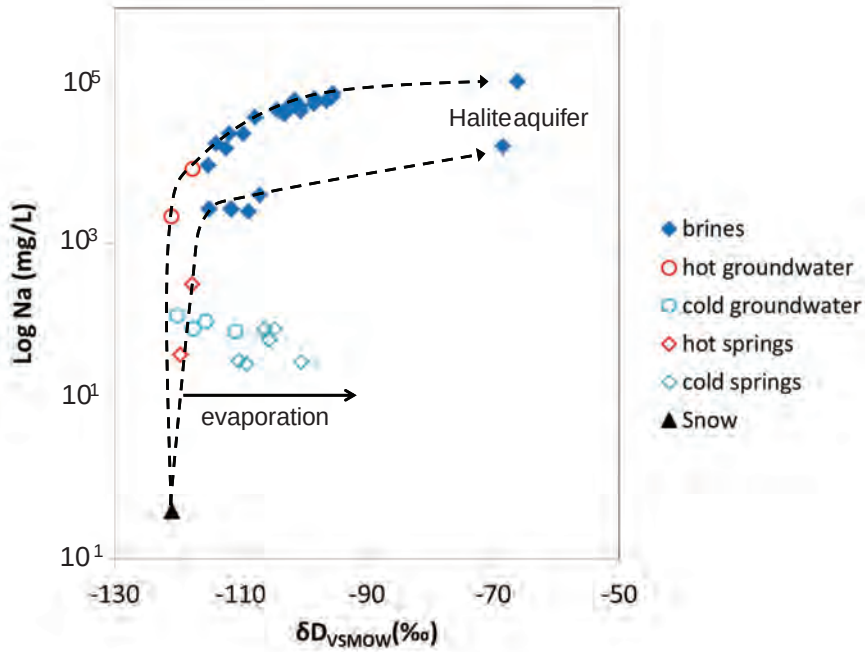

Fig. 4. Log Na vs. δD_{VSMOW} for waters in the Clayton Valley, Nevada, basin. Cold shallow groundwaters and springs exhibit dilute concentrations and an evaporation trend as a function of increasing δD_{VSMOW}. Hypothetical mixing/evaporation curves are represented by dashed arrows from the meteoric water (snow) to brine in the halite aquifer.

in the basin with the possibility of hydrothermal inputs contributing water with higher total dissolved solids (TDS) to the brines. These processes could then be followed by mixing with other brines, concentration through evaporation, and/or halite precipitation to form the various brine compositions in the basin.

Case study 2: Salar de Atacama, Chile

The Salar de Atacama is a large closed basin which lies on the Tropic of Capricorn in the Atacama Desert approximately 200 km east of the Pacific Ocean and immediately to the west of the Altiplano-Puna plateau (Fig. 5). The basin coincides with a sharp bend in the modern Andean volcanic arc which retreats 60 km east from its regional north-south trend. The salar has a surface area of 3,000 km^2 and a drainage basin flanked on all sides by substantial topography; the Andean volcanic arc dominates recharge to the salar. The salar surface is 2,300 m above sea level and is ~2,000 m lower than the volcanic arc on the western plateau margin. As in the rest of the Atacama Desert, precipitation on the salar surface is rare. The adjacent Andean highlands receive precipitation more often but are still arid to hyperarid (Strecker et al., 2007). Evaporation at the elevation of the salar varies between 0 to 2.8 mm/d, depending on the surface characteristics (Kampf et al., 2005); relative to an estimated mean annual precipitation of 39 mm, the P/E ratio (aridity index) is ~0.033. Interestingly, no evaporation was measured by Kampf et al. (2005) from the rough halite nucleus of Salar de Atacama that comprises approximately half of the surface area and hosts the Li-rich brine at 30-m depth.

Water in the Salar de Atacama basin and the adjacent Andean arc varies in Li concentration from approximately 0.05 to 5 mg/L in the Andean inflow waters, 5 to 100 mg/L in shallow groundwaters in the southern and eastern flanks of the basin, and up to 5,000 mg/L in brines. This indicates that the brines in the basin can be significantly more concentrated, by up to five orders of magnitude, compared to water entering the basin.

The geologic history of the Salar de Atacama basin can be summarized as follows. Sedimentary, volcanic, and plutonic rocks indicate its position during the Paleozoic along the western margin of Gondwana. During the Jurassic and Early Cretaceous this region was an extensional backarc basin, with inversion and basin-scale tectonic subsidence initiating in the Late Cretaceous. This continental backarc setting persisted through the Paleogene, transitioning to a forearc basin in the Neogene. Uplift and predominantly clastic deposition have been ongoing since the Cretaceous, and during the Plio-Pleistocene thick halite deposits have accumulated in the center of the basin.

Details of the Cenozoic geologic history highlight several relevant observations in the Salar de Atacama (additional details on the older geologic history can be found in the Appendix). There was first a foreland basin originating in mid-Cretaceous, with thrusting and coeval sedimentation occurring during the Cretaceous and Paleogene (Arriagada et al., 2006). During the Oligocene-early Miocene normal faulting, perhaps in a transtensional environment, controlled the western margin of the basin and accommodated thousands of meters of strata (Jordan et al., 2007). Much of this sedimentation was accommodated by a normal fault along the western basin margin with as much as 6 km of vertical displacement (Pananont et al., 2004). From ~12 Ma onward the volcanic arc was established east of the Salar de Atacama and shortening resumed, uplifting the intrabasinal Cordillera de la Sal and later resulting in development of blind thrust faults within the basin (Jordan et al., 2007). Interpretation of seismic data by Pananont et al. (2004) suggest that the Cordillera de la Sal, a prominent N-S-trending anticlinal feature that separates the Salar de Atacama from the Cordillera Domeyko, results from diapiric flow of Oligocene to middle Miocene strata initiated in the Miocene and is associated with a deep reverse fault. Following initiation of diapiric flow in the western Salar de Atacama basin, uplift of the Altiplano-Puna plateau is accommodated by monoclinal folding which is expressed in the geomorphology and westward tilted strata at the plateau margin (Jordan et al., 2010). A number of late Miocene and Pliocene ignimbrites derived from calderas on the plateau can be traced westward into the subsurface of the Atacama basin. These ingimbrites interfinger with halite deposits that are typically 1 km thick, and establish the age of these strata as Plio-Pleistocene with a lower age limit likely to be sometime in the late Miocene. In the southern portion of the salar these deposits are offset by the Salar fault system, which exhibits close to a kilometer of down-to-the-east offset on a reverse fault during this interval (Jordan et al., 2002b). The Salar fault system can be followed to the south-southwest into the Tilomonte (Tilocalar) Valley as moderate- to high-angle reverse faults which offset a Pliocene ignimbrite and Paleozoic rocks of the eastern Cordón de Lila. Some of the features of this fault system as exposed in the Tilocalar (Tilomonte) Valley suggest the influence of major pre-Andean basement structures (Kuhn, 2002).

Several aspects of this geologic history are relevant to the generation of Li-rich brine in Salar de Atacama. There are a number of fault systems with kilometers of offset, which may be crustal scale features and preferential flow paths for fluids. During the Miocene and Pliocene several voluminous ignimbrite pulses related to development of the large Altiplano-Puna volcanic complex indicate major magmatic activity to the east on the plateau (Salisbury et al., 2011). It is possible that this volcanism is intimately related to late Miocene uplift of the plateau via lower crustal delamination (cf. Hoke and Garzione, 2008). If large-scale tectonic factors play a role in the generation of Li brines these processes might be relevant to generation of the Li-enriched brine in Salar de Atacama, particularly if the mantle is considered to be the ultimate source of Li to brines. Crustal scale faults within the Atacama basin itself are not necessarily good candidates for communication between the mantle and brine aquifers in light of the fact that the lithosphere below the Atacama basin is widely believed to be a cold, rigid block on the basis of seismological data (Schurr and Rietbrock, 2004).

However, numerous faults exist between the salar and the magmatic arc in the southern half of the Atacama basin and these are more attractive fluid conduits. As their coincidence with young lavas and recent volcanic edifices document, magmatic fluids have exploited these faults as conduits. Further, these faults do not express themselves in the northern half of the basin and instead are confined to the portion of the basin that is known to exhibit the highest concentration Li brines

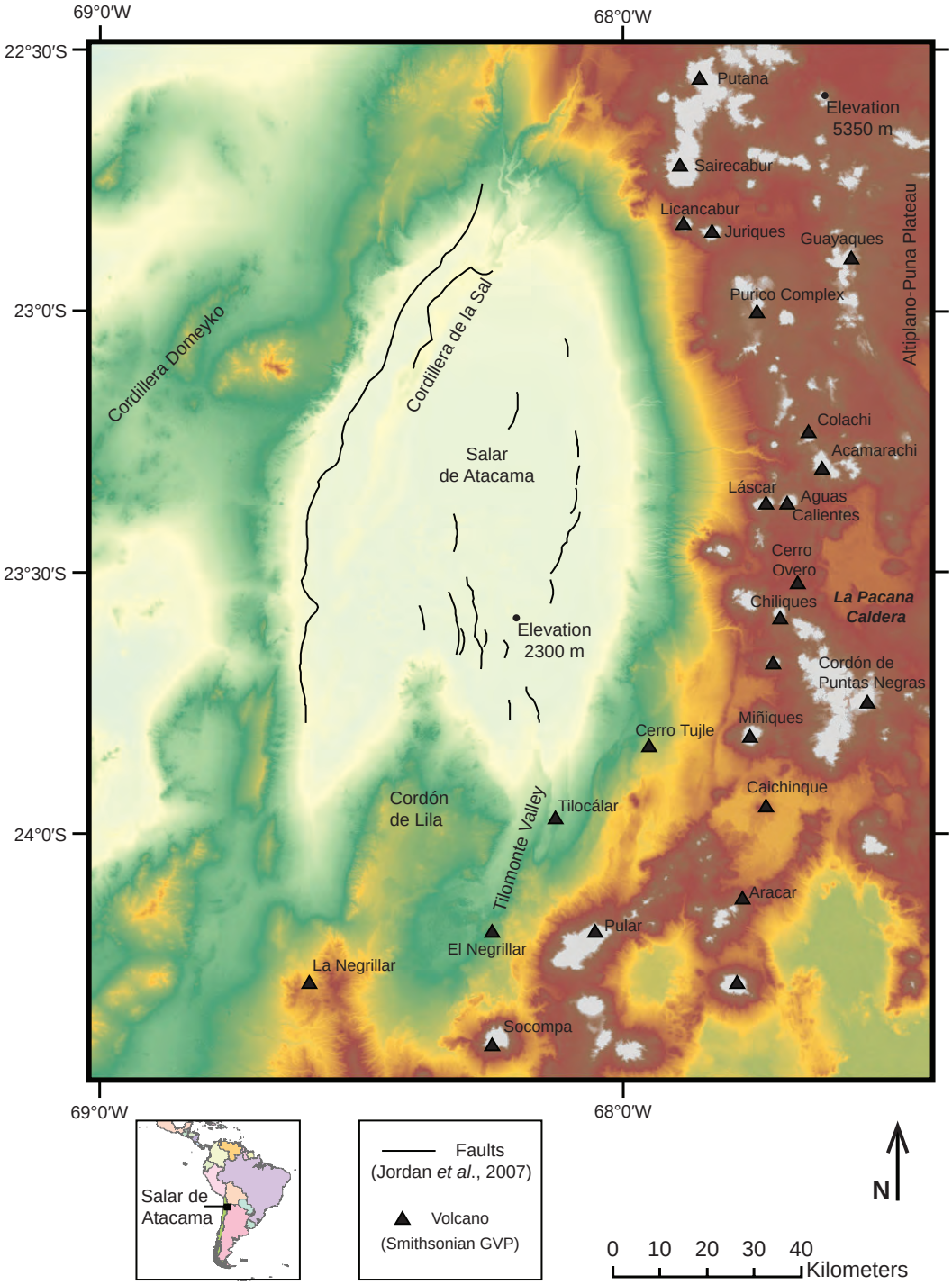

Fig. 5. Shaded relief map of Salar de Atacama, Chile, showing major features noted in text and Appendix. Fault locations from Jordan et al. (2007) and the Andean volcano locations are from the Smithsonian Global Volcanism Program (GVP; http://www.volcano.si.edu).

(Ide and Kunasz, 1989). We have observed high dissolved ^{3}He concentrations in shallow groundwater and brine in the southeastern part of the Atacama basin. These high ^{3}He concentrations have not been observed in water and brine sampled from the western half of the Atacama basin, and we interpret the ^{3}He as an indicator of the influence of mantle-derived gases in the southeastern sector of the basin.

The interaction of groundwater and magmatic systems in the Andean arc and on the Altiplano-Puna plateau is another potential mechanism for transporting Li, ultimately mantle derived, from volcanic systems to the Salar de Atacama. The huge volcanic centers of the Altiplano-Puna volcanic complex contain large volumes of highly evolved and low-temperature magma at shallow crustal levels; melt inclusion data demonstrate that

magmatic Li contents of 100 to 1,000 ppm are common in this region (Lindsay et al., 2001; Schmitt, 2001). Whether and how these magmatic systems are connected to the Salar de Atacama by thermal waters and the regional groundwater system remains a major question. Crustal-scale and smaller faults may serve either as conduits for or barriers to fluid flow (cf. Caine et al., 1996). Multiple ignimbrites exist at depth within the northern half of the basin. These interfinger with halite and are likely to be permeable enough to transport fluids, especially under the large topographic gradient along the western plateau margin. It seems conceivable to connect the giant magmatic systems of the Altiplano-Puna volcanic complex as a Li source to Salar de Atacama brines, but understanding of the regional groundwater systems at the plateau margin is limited. Jordan et al. (2002a, b) have proposed that the accumulation of halite in the Atacama basin is coincident with monoclinal folding, and uplift of the Altiplano-Puna plateau immediately to the east. Indeed, deep groundwater flow driven by the elevation contrast across the western plateau margin may be a consequence of plateau uplift and result in initiation of the thick halite sequence in the Atacama basin, but in order to evaluate this possibility much work characterizing the modern deep groundwater system is needed.

Certainly, Andean magmatic systems have a large role to play as Li sources either directly or indirectly via surface and subsurface weathering of silicic volcanic rocks. It is important to note that the rock units which comprise the Atacama basin and its strata control to a large degree the evolution and ultimate composition of brines. Bedrock and basinal strata of Salar de Atacama are essentially devoid of limestone, with the exception of Jurassic strata exposed in the Cordillera Domyeko (Flint et al., 1993) and minor Maastrictian(?) marine carbonates (Mpodozis et al., 2005). As described in previous sections, catchment lithologies control the chemical composition of inflow waters, volcanic sulfide results in sulfate-rich brines, and the dearth of limestone results in brines that are Ca-poor relative to sulfate. For this reason, the evaporite mineral sequence in the Atacama brines is prone to precipitate Mg and Li sulfate salts in the absence of Ca (Boschetti et al., 2007). This chemical divide (cf. Eugster and Hardie, 1978) has implications, not only for the evolution of brine chemistry but also for the logistics and economics of processing brines for Li.

Finally, the hydrographic history of the Salar de Atacama basin has implications for the origin and evolution of the Li-rich brine. It is possible that the basin has been closed continuously since the uplift of the Cordillera Domeyko in the Cretaceous, and almost certain that the basin has been hydrographically closed with respect to surface waters since the late Miocene. Jordan et al. (2007) suggested that the western margin of the modern basin was established by a major down-to-the-east normal fault during an Oligocene period of extension or transtension. Irrespective of the exact timing, any of these scenarios for hydrographic closure of the basin permit accumulation and concentration of brines on the timescale of 1 to 10 m.y. at a minimum.

Lithium Uses, Demand, and Global Li Brine Resources

Lithium was not discovered until the early 1800s and was little more than a scientific curiosity at first. After many decades at low levels, Li production has increased exponentially since the 1950s (Mohr et al., 2010; Fig. 6), with more growth expected. Lithium is alloyed with other elements such as aluminum, cadmium, manganese, and copper to produce high strength-to-weight metals. It is used as a coolant in nuclear breeder reactors. Compounds of Li are used as heat-resistant glass, ceramics, and lubricants. It is the key ingredient of drugs used to treat bipolar disease. But the most important modern use of Li is in rechargeable Li ion batteries for cell phones, laptops, and hybrid and electric cars (Garrett, 2004). Lithium ion batteries are superior because they are lightweight and can be efficiently recharged. Lithium's use in cars is what gives it a key role in global efforts to reduce greenhouse gas emissions and minimize global warming.

Projections by Gruber et al. (2011) and Kesler et al. (2012) indicate that demand for Li will increase through the year 2100, with nonbattery, portable electronic batteries, and vehicle batteries each contributing to this demand. Depending on the global economic growth scenario adopted, and accounting for 90% recycling, they concluded that between 12 and 20 million metric tons (Mt) of Li will be needed. Global Li resources have recently been estimated by several authors. Gruber et al. (2011) estimated 39 Mt of Li metal; Tahil (2008) estimated 19.2 Mt; U.S. Geological Survey (2011) estimated 33 Mt; Evans (2010) estimated 34.5 Mt; and Yaksic and Tilton (2009) estimated 64 Mt. Barring major new uses for Li, global demand is unlikely to exceed supply in the next century.

Exploration for lithium-rich brine deposits

Identification of prospective basins: All of the Li-rich brine basins in Table 1 are closed basins, and they are all marked by a saline lake or a salar (i.e., a salt flat or salt-encrusted depression). Closed basins form because of tectonics but they are maintained only where, over longer time-spans, evaporation exceeds precipitation. If the long-term rate of precipitation in a basin increases sufficiently, eventually lake water will overtop some point along the drainage divide and drain, carrying the dissolved Li away. Evidently, the aridity classification must be semiarid or drier, but the numerical aridity index for the basins in Table 1 ranges through an order of magnitude,

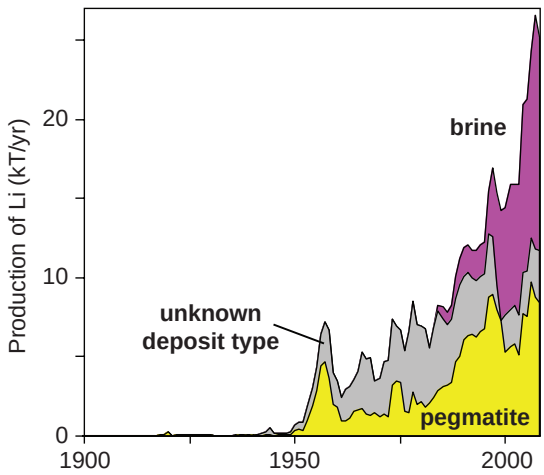

Fig. 6. Lithium production since 1900 (modified from Mohr, 2010).

from 0.03 to 0.33. Judging from the present-day distribution of basins, the favorable zones lie between about 19° and 37° north or south (Fig. 1). Rain-shadow effects probably stretch the north-south span of favorable latitudes. Mean annual temperature does not appear to be a critical factor, with values ranging through two orders of magnitude from 0.2° to 22.7°C.

All of the world's Li-rich brine basins cataloged in Table 1 are tectonically active, subsiding basins as evidenced by thick accumulations of Quaternary to recent sediment, and in most cases, also evidenced by faults with Quaternary to recent displacements. In contrast, shallow, internally drained depressions on the stable cratons (e.g., Australia: Benison and Bowen, 2006; Algeria: Hacini et al., 2008) do not appear to be prospective. Lithium-brine resources are found in a range of tectonic settings from extensional to strike-slip to contractional (Table 1, Appendix). The overall tectonic setting where Li-rich brines occur appears to vary and may not be the primary factor in determining favorability for Li-rich brines, although at the local scale, tectonics control basin geometry. Most of the Li-rich brine basins in Table 1 show evidence for elevated heat flow. The most obvious evidence includes young volcanoes, hot springs, and geothermal resources. Only one basin in our compilation, Lake Zabuye, appears to have none of these.

Evidence of older hydrothermal activity is seen in several instances and should be regarded as a favorable characteristic. For example, at Clayton Valley, Nevada, some Miocene to Pliocene basinal deposits were hydrothermally enriched in the Li-rich clay hectorite; this took place a few million years ago, before these altered strata were uplifted and exposed. Hectorite concentration halos have been reported from several basins that lack Li-rich brines in the U.S. Basin and Range province (Vine, 1980). In such cases, a hectorite halo may be all that remains of a former brine system that has since leaked away. Borate deposits appear to be hybrids involving both hydrothermal and evaporative processes; their presence is also a favorable indicator for Li brines. At Salar del Rincón, hot-spring deposits which appear inactive contain residual water with up to 1,500 mg/L Li (Toledo et al., 2009).

Source rocks such as felsic, vitric tuffs that have abundant and readily leached Li are favorable (Price et al., 2000) but perhaps not the sole source of Li as it is present in most crustal rocks at tens of parts per million. There are extensive ignimbrite deposits flanking the east side of the Salar de Atacama basin that can contain up to nearly 700 ppm Li in quartz melt inclusions (Lindsay et al., 2001). Similarly, in the western United States quartz inclusions from large silicic eruptions contain appreciable Li. Hofstra et al. (2013) have suggested that Li in melt inclusions is the best estimate of preeruptive magmatic concentrations and that subsequent loss of Li during eruption, lithification, and weathering of a moderate volume eruption is sufficient to generate an economical brine deposit if it can be efficiently mobilized and concentrated. If there are hydrothermal inputs of Li to the brines that are associated with silicic magmatic systems we would argue that this type of source has the potential to bring high concentrations of Li to the brine. It then becomes a question of how to get the Li-rich fluids from the hydrothermal source to the brine; this may occur along faults and fractures in the case of the Salar de Atacama system.

Physiographic aspects of Li-rich brine basins do not appear to be that important to the existence or size of the resource. Of the basins in Table 1, basin-floor areas range from 54 to 18,075 km^2, catchment areas range from 634 to 145,279 km^2, and basin-floor elevations range from –415 to +4,464 m. A special situation exists at Clayton Valley, Nevada, which may be partly responsible for the size of the resource. Clayton Valley is one of five adjacent closed basins. Although they are hydrologically unconnected at the surface, groundwater ultimately flows into Clayton Valley, the lowest elevation of the five (Zampirro, 2004). In fact Clayton Valley may be the end of very long regional groundwater flow paths in the western Basin and Range (Belcher, 2004, plate l).

Basin-scale exploration: Within a closed basin that is prospective for Li-rich brines based on the above criteria, the most convenient exploration tool is surface sampling of waters and/or sediments. Because many Li brines are located within 1 m of the surface salt crust, water sampling is relatively easy to use as a general exploration tool. However, for deeper brines it may be useful to perform geophysical surveys to identify high conductivity anomalies that could then be drilled for sampling.

Another exploration strategy is surface sampling of sediment. This approach, however, has produced mixed results. During reconnaissance exploration for Li resources by the U.S. Geological Survey in the 1970s, surface samples were analyzed from 41 closed basins in the U.S. Basin and Range Province. Whereas four basins were identified as having anomalous Li concentrations (defined as >300 ppm; Vine, 1980), neither Great Salt Lake Desert nor Searles Valley were found to be prospective by this measure, despite the known occurrence of Li brines at depth.

Geologic reconnaissance: Several important observations related to the youthfulness of a prospective basin and it's tectonic, sedimentary, and heat-flow characteristics can be assessed with a boots-on-the-ground approach. Basins likely to host Li-rich brines should include young high-silica volcanic rocks, evidence for Quaternary faulting, thick accumulations of clastic and/or evaporite strata, and hot-springs or hot-spring deposits. Given the observations of Hofstra et al. (2013) on the Li content of quartz melt inclusions versus host rocks, it is clear that whole-rock geochemistry of vitric rocks may be of limited value for exploration purposes. Rather, if much of this Li has already been mobilized an analysis of quartz-hosted melt inclusions in potential source rocks may be a better measure of whether the rocks are (were) a potential Li source. In addition heat flow can be assessed by estimating the temperatures of formation for hot-spring carbonates or by application of chemical thermometers to hot-spring water. A critical determination to be made is whether the water temperature can be explained by deep circulation of meteoric water with reasonable geothermal gradients or whether a temperature anomaly (e.g., a magma body) might be present at shallow depths. An assessment of tectonics and heat flow over longer periods can be provided by low-temperature thermochronology of bedrock in fault bounded mountain blocks. Granitic lithologies are ideal for this approach, though any rocks containing apatite and zircon are potential targets. Bedrock which has cooled very rapidly and/or recently would be indicative of tectonically active basins and by analysis of

apatite-zircon pairs it may be possible to understand the timing of changes in exhumation rate or the geothermal gradient. These approaches would be most fruitfully targeted to bedrock at the lowest elevations possible. A similar approach can be applied to basinal strata that are exhumed. Cooling ages which are significantly younger than depositional ages can constrain depth of burial and/or geothermal gradients within sedimentary basins.

Mining and production of lithium-rich brines

As noted above, the arid climate that is necessary for the genesis of Li-rich brines in closed basins is also a key to production, because the first step in the extraction of Li is solar evaporation. Brines that are pumped to the surface typically carry 200 to 1,400 ppm Li and ideally have a low Mg/Li ratio (<10) as the geochemical behavior of Mg ions can be similar to Li ions in low-temperature aqueous solution and interfere with the Li purification process. Brines are evaporated in a succession of artificial ponds; in the case of Clayton Valley, Nevada, there are nine ponds with a total area of 16 km^2 (Garrett, 2004). In each pond in the chain, brine enters at one end, loses some of its water during the ensuing weeks or months, and is transmitted from the other end into the next pond. Multiple ponds are used in order to separate the various evaporite minerals that crystallize out in sequence, and to compensate for the fact that evaporation rate decreases as TDS increases. The evaporite species depend on the initial brine chemistry: at Clayton Valley, calcite, gypsum, halite, sylvite, and glaserite precipitate out, and at one stage, calcium hydroxide is added to induce precipitation of magnesium, as hydroxide (Garrett, 2004). Depending on climate, it takes a few months to two years to achieve a concentrate that is both enriched in Li (to 5,000 ppm at Clayton Valley) and depleted in other cations. This concentrate is pumped from the last pond to a chemical plant where various end products such as Li carbonate, Li hydroxide, and Li metal are produced. Garrett (2004) described the processes at Clayton Valley and Salar de Atacama in considerable detail.

In most instances, Li-enriched oilfield and geothermal brines do not owe their very existence to present-day climate. Extraction of Li from these brines by solar evaporation is therefore not always an option. In the Salton trough geothermal field, fluids that are pumped to the surface to exploit their heat content also contain elevated Li, Mn, and Zn, which are recovered in a proprietary process not involving solar evaporation (Simbol Materials, 2013). This is also a newly prospective approach for pressurized brines beneath the Rock Springs anticline, Greater Green River basin, Wyoming (University of Wyoming, 2013).

Summary

Because of the extensive use of Li in industrial and technological applications the demand for this critical element will continue to increase. Continental brines enriched in Li are the most economically recoverable form of Li deposits and account for the source of 75% of current Li production. Therefore, it is imperative to develop an understanding of the genesis of these deposits. We have identified and outlined the six common characteristics of the environments for 18 different basins and their respective brines or salt lakes ranging in Li concentration from 10 to 7000 mg/L. These characteristics are (1) arid climate, (2) closed basin containing a salar (salt crust) or saline lake, (3) associated igneous or geothermal activity (4) tectonically driven subsidence, (5) suitable Li source(s), and (6) ample time to concentrate brine. The relative importance of each of these characteristics has not yet been quantified but these characteristics lay the framework for future studies and exploration for continental Li-rich brines.

Acknowledgments

The authors would like to thank Rockwood Lithium, Ltd. for their continued support of our research at Clayton Valley, Nevada, and at Salar de Atacama, Chile. Their interest and commitment to helping develop a better understanding of the formation of continental Li brines has greatly enhanced our ability to address this important resource. We also thank the USGS for earlier support of the work at Clayton Valley, Nevada through USGS MRERP award G10AP00056 to L. Munk and C.P. Chamberlain. Melissa Jennings is thanked for her review of the paper as well as Terry Jordan for discussions on the geology of Salar de Atacama, Chile. Constructive reviews from Lisa Stillings and Stephen Kesler improved the quality of this manuscript.

REFERENCES

Albers, J.P., and Stewart, J.H., 1972, Geology and mineral deposits of Esmeralda County, Nevada: Nevada Bureau of Mines and Geology Bulletin, v. 78, 88 p.

Alpers, C.N., and Whittemore, D.O., 1990, Hydrogeochemistry and stable isotopes of ground and surface waters from 2 adjacent closed basins, Atacama Desert, northern Chile: Applied Geochemistry, v. 5, p. 719–734.

Arriagada, C., Cobbold, P.R., and Roperch, P., 2006, Salar de Atacama basin: A record of compressional tectonics in the central Andes since the mid-Cretaceous: Tectonics, v. 25, p. 41–44.

Asher-Bolander, S., 1982, Lithium-rich clays, *in* Erickson, R.L. ed., Characteristics of mineral deposit occurrences, U.S. Geological Survey Open-File Report 82-795, p. 225–229.

——1991, Descriptive model of lithium-rich playa brine: U.S. Geological Survey Open-File Report 91-11A, p. 53–54.

Belcher, W.A., ed., 2004, Death Valley regional ground-water flow system, Nevada and California—hydrogeologic framework and transient groundwater flow model: U.S. Geological Survey Scientific Investigations Report 2004-5205.

Benison, K.C., and Bowen, B.B., 2006, Acid saline lake systems give clues about past environments and the search for life on Mars: Icarus, v. 183, p. 225–229.

Bookhagen, B., and Strecker, M.R., 2008, Orographic barriers, high-resolution TRMM rainfall, and relief variations along the eastern Andes: Geophysical Research Letters, v. 35, p. 1–6.

Boschetti, T., Cortecci, G., Barbieri, M., and Mussi, M., 2007, New and past geochemical data on fresh to brine waters of the Salar de Atacama and Andean altiplano, northern Chile: Geofluids, v. 7, p. 33–50.

Bowen, B.B., and Benison, K.C., 2009, Geochemical characteristics of naturally acid and alkaline saline lakes in southern Western Australia: Journal of Applied Geochemistry, v. 24, p. 268–284.

Bradley, D., Munk, L., Jochens, H., Hynek, S., and Labay, K., 2013, A preliminary deposit model for lithium brines: U.S. Geological Survey Open-File Report: 2013-1006, 6 p.

Caine, J.S., Evans, J.P., and Forster, C.B., 1996, Fault zone architecture and permeability structure: Geology, v. 24, p. 1025–1028.

Carmona, V., Pueyo, J.J., Taberner, C., Chong, G., and Thirlwall, M., 2000, Solute inputs in the Salar de Atacama (N. Chile): Journal of Geochemical Exploration, v. 69, p. 449–452.

Collins, A.G., 1976, Lithium abundances in oil field waters, *in* Vine, J.D., ed., Lithium resources and requirements by the year 2000: Geological Society of America, p. 116–122.

Davis, J.R., and Vine, J.D., 1979, Stratigraphic and tectonic setting of the lithium brine field, Clayton Valley, Nevada: Basin and Range Symposium and Great Basin Field Conference, p. 421–430.
Davis, J.R., Friedman, I., and Gleason, J.D., 1986, Origin of the lithium-rich brine, Clayton Valley, Nevada, US: U.S. Geological Survey Bulletin 1622, p. 131–138.
Dresel, P.E., and Rose, A.W., 2010, Chemistry and Origin of Oil And Gas Well Brines in Western Pennsylvania: Pennsylvania Geological Survey Open-File Oil and Gas Report 10-01.0, 48 p.
Eugster, H.P., 1980, Geochemistry of evaporitic lacustrine deposits: Annual Reviews in Earth and Planetary Science, v. 8, p. 35–63.
Eugster, H.P., and Hardie, L.A., 1978, Saline lakes: Springer, New York.
Eugster, H.P., and Jones, B.F., 1979, Behavior of major solutes during closed-basin brine evolution: American Journal of Science, v. 279, p. 609–631.
Evans, K., 2010, The lithium-brine reserve conundrum: Northern Miner, v. 96, p. 2–6.
Flint, S., Turner, P., Jolley, E.J., and Hartley, A.J., 1993, Extensional tectonics in convergent margin basins: An example from the Salar de Atacama, Chilean Andes: Geological Society of America Bulletin 105, p. 603–617.
Garrett, D.E., 2004, Handbook of lithium and natural calcium chloride: Their deposits, processing, uses and properties: Elsevier, 476 p.
Godfrey, L.V., Chan, L.H., Alonso, R.N., Lowenstein, T.K., McDonough, W.F., Houston, J., Li, J., Bobst, A., and Jordan, T.E., 2013, The role of climate in the accumulation of lithium-rich brine in the Central Andes: Journal of Applied Geochemistry, v. 38, p. 92–102.
Gruber, P.W., Medina, P.A., Keoleian, G.A., Kesler, S.E., Everson, M.P., and Wallington, T.J., 2011, Global lithium availability a constraint for electric vehicles?: Journal of Industrial Ecology, v. 15, p. 760–775.
Hacini, M., Kherici, N., and Oelkers, E.H., 2008, Mineral precipitation rates during the complete evaporation of the Merouane Chott ephemeral lake: Geochimica et Cosmochimica Acta, v. 72, p. 1583–1597.
Hardie, L.A., and Eugster, H.P., 1970, The evolution of closed-basin brines: Mineralogical Society of America Special Paper, v. 3, p. 273–290.
Hofstra, A.H., Todorov, T.I., Mercer, C.N., Adams, D.T., and Marsh, E.E., 2013, Silicate melt inclusion evidence for extreme pre-eruptive enrichment and post-eruptive depletion of lithium in silicic volcanic rocks of the Western United States: Implications for the origin of lithium-rich brines: Economic Geology, v. 108, p. 1691–1701.
Hoke, G.D., and Garzione, C.N., 2008, Paleosurfaces, paleoelevation, and the mechanisms for the late Miocene topographic development of the Altiplano plateau: Earth and Planetary Science Letters, v. 271, p. 192–201.
Houston, J., Butcher, A., Ehren, P., Evans, K., and Godfrey, L., 2011, The evaluation of brine prospects and the requirement for modifications to filing standards: Economic Geology, v. 106, p. 1225–1239.
Ide, F., and Kunasz, I.A., 1989, Origin of lithium in Salar de Atacama, northern Chile: Geology of the Andes and its relation to hydrocarbon and mineral resources: Circum-Pacific Council for Energy and Mineral Resources Earth Science Series, Houston, Texas, Proceedings, p. 165–172.
Jochens, H., and Munk, L.A., 2011, Experimental weathering of lithium-bearing source rocks, Clayton Valley, Nevada, USA: Biennial Meeting SGA 2011, 11th, Antofagasta, Chile, Proceedings, p. 238–240.
Jordan, T.E., Godfrey, L.V., Muñoz, N., Alonso, R.N., Lowenstein, T.L., Hoke, G., Peranginangin, N., Isacks, B.L., and Cathles, L., 2002a, Orogenic-scale ground water circulation in the Central Andes: Evidence and consequences: International Symposium on Andean Geodynamics (ISAG), 5th, Toulouse, France, Institut de Recherche Pour le Développement, and Université Paul Sabatier, Proceedings, p. 331–334.
Jordan, T.E., Munoz, N., Hein, M., Lowenstein, T., Godfrey, L., and Yu, J., 2002b, Active faulting and folding without topographic expression in an evaporite basin, Chile: Geological Society of America Bulletin v. 114, p. 1406–1421.
Jordan, T.E., Mpodozis, C., Munoz, N., Blanco, N., Pananont, P., and Gardeweg, M., 2007, Cenozoic subsurface stratigraphy and structure of the Salar de Atacama basin, northern Chile: Journal of South American Earth Sciences, v. 23, p. 122–146.
Jordan, T.E., Nester, P.L., Blanco, N., Hoke, G.D., Davila, F., and Tomlinson, A.J., 2010, Uplift of the Altiplano-Puna plateau: A view from the west: Tectonics v. 29, TC5007, doi:10.1029/2010TC002661.
Kampf, S.K., Tyler, S.W., Ortiz, C.A., Muñoz, J.F., and Adkins, P.L., 2005, Evaporation and land surface energy budget at the Salar de Atacama, northern Chile: Journal of Hydrology, v. 310, p. 236–252.
Kesler, S.E., Gruber, P.W., Medina, P.A., Keoleian, G.A., Everson, M.P., and Wallington, T.J., 2012, Global lithium resources: Relative importance of pegmatite, brine and other deposits: Ore Geology Reviews, v. 48, p. 55–69.
Kuhn, D., 2002, Fold and thrust belt structures and strike-slip faulting at the SE margin of the Salar de Atacama basin, Chilean Andes: Tectonics, v. 21, 1026, doi:10.1029/2001TC901042.
Kunasz, I.A., 1974, Lithium occurrence in the brines of Clayton Valley, Esmeralda County, Nevada: Symposium on Salt, 4th, Northern Ohio Geological Survey, Proceedings, p. 57–66.
Lindsay, J.M., Schmitt, A.K., Trumbull, R.B., De Silva, S.L., Siebel, W., and Emmermann, R., 2001, Magmatic evolution of the La Pacana caldera system, Central Andes, Chile: Compositional variation of two cogenetic, large-volume felsic ignimbrites: Journal of Petrology v. 42, p. 459–486.
Mohr, S., Mudd, G., and Giurco, D., 2010, Lithium resources and production: A critical global assessment: Prepared for CSIRO Minerals Down Under Flagship, by the Institute for Sustainable Futures (University of Technology, Sydney) and Department of Civil Engineering (Monash University), 99 p.
Moraga, A., Chong, G., Fortt, M.A., and Henriquez, H., 1974, Estudio geolo´gico del salar de Atacama, Provincia de Antofagasta: Santiago, Chile, Boletin Instituto de Investigaciones Geológicas, v. 29, p. 1–56.
Mpodozis, C., Arriagada, C., Basso, M., Roperch, P., Cobbold, P., and Reich, M., 2005, Late Mesozoic to Paleogene stratigraphy of the Salar de Atacama Basin, Antofagasta, Northern Chile: Implications for the tectonic evolution of the Central Andes: Tectonophysics, v. 399, p. 125–154.
Munk, L., Jennings, M., Bradley, D., Hynek, S., Godfrey, L., and Jochens, H., 2011, Geochemistry of lithium-rich brines in Clayton Valley, Nevada, USA: Biennial Meeting SGA 2011, 11th, Antofagasta, Chile, Proceedings, p. 211–213.
Oldow, J.S., Bally, A.W., Avé Lallemant, H.G., and Leeman, W.P., 1989, Phanerozoic evolution of the North American cordillera, United States and Canada, Bally, A.W., and Palmer, A.R., eds., The Geology of North America-Vol. A. An Overview: Geological Society of America, p. 139–232.
Pananont, P., Mpodozis, C., Blanco, N., Jordan, T.E., and Brown, L.D., 2004, Cenozoic evolution of the northwestern Salar de Atacama basin, northern Chile: Tectonics, v. 23, TC6007, doi:10.1029/2003TC001595.
Placzek, C.J., Quade, J., and Patchett, P.J., 2011, Isotopic tracers of paleohydrologic change in large lakes of the Bolivian Altiplano: Quaternary Research, v. 75, p. 231–244.
Price, J.G., Lechler, P.J., Lear, M.B., and Giles, T.F., 2000, Possible volcanic sources of lithium in brines in Clayton Valley, Nevada: Geology and Ore Deposits 2000: The Great Basin and Beyond, Geological Society of Nevada, Proceedings, p. 241–248.
Rettig, S.L., Jones, B.F., and Risacher, F., 1980, Geochemical evolution of brines in the Salar of Uyuni, Bolivia: Chemical Geology, v. 30, p. 57–79.
Risacher, F., and Fritz, B. G., 1991, Geochemistry of Bolivian Salars, Lipez, southern Altiplano—origin of solutes and brine evolution: Geochimica et Cosmochimica Acta, v. 55, p. 687–705.
——2009, Origin of salts and brine evolution of Bolivian and Chilean salars: Aquatic Geochemistry, v. 15, p. 123–157.
Risacher, F., Alonso, H., and, Salazar, C., 1999, Geoquímica de aguas en cuencas cerradas, I, II, III Regiones, Chile: Santiago, Chile, Series de Informes Tecnicos Ministerio de Obras Públicas, Dirección General de Aguas, Technical Report.
——2003, The origin of brines and salts in Chilean salars: A hydrochemical review: Earth-Science Reviews, v. 63, p. 249–293.
Robinson, P.T., 1972, Petrology of the potassic Silver Peak volcanic center, western Nevada: Geological Society of America Bulletin, v. 83, p. 1693–1708.
Rush, F.E., 1968, Index of hydrographic areas in Nevada: Nevada Division of Water Resources Information Report 6, 38 p.
Salisbury, M.J., Jicha, B.R., de Silva, S.L., Singer, B.S., Jimenez, N.C., and Ort, M.H., 2011, Ar^{40}/Ar^{39} chronostratigraphy of Altiplano-Puna volcanic complex ignimbrites reveals the development of a major magmatic province: Geological Society of America Bulletin, v. 123, p. 821–840.
Sarna-Wojcicki, A.M., Reheis, M.C., Pringle, M.S., Fleck, R.J., Burbank, D., Meyer, C.E., Slate, J.L., Wan, E., Budahn, J.R., Troxel, B., and Walker, J.P., 2005, Tephra layers of blind Spring Valley and related upper Pliocene and Pleistocene tephra layers, California, Nevada, and Utah: Isotopic ages, correlation, and magnetostratigraphy: U.S. Geological Survey Professional Paper 1701, 63 p.
Schmitt, A.K., 2001, Gas-saturated crystallization and degassing in large-volume, crystal-rich dacitic magmas from the Altiplano-Puna, northern Chile: Journal of Geophysical Research-Solid Earth, v. 106, p. 30,561–30,578.

Schurr, B., and Rietbrock, A., 2004, Deep seismic structure of the Atacama basin, northern Chile: Geophysical Research Letters v. 31, L12601, doi:10.1029/2004GL019796.

Simbol Materials, 2013, http://www.simbolmaterials.com/breakthrough_technology.htm

Spiro, B., and Chong, G., 1996, Origin of sulfate in the Salar de Atacama and the Cordillera de la Sal, initial results of an isotopic study: International Symposium on Andean Geodynamics, 3rd, Paris, Saint Malo, France, Orstom Editions, Collection Colloques et Seminaires, p. 703–705.

Strecker, M.R., Alonso, R.N., Bookhagen, B., Carrapa, B., Hilley, G.E., Sobel, E.R., and, Trauth, M.H., 2007, Tectonics and climate of the southern central Andes: Annual Review of Earth and Planetary Sciences, v. 35, p. 747–787.

Tahil, W., 2008, The trouble with lithium 2: Under the microscope: Martainville, France, Meridian International Research.

Toledo, A.O., Alonso, R.N., V. Ruiz, T., and Quiroga, A.G., 2009, Evapofacies Halítica en el Salar del Rincón, Departamento Los Andes, Salta: Revista de la Asociación Geológica Argentina, v. 64, p. 493–500.

University of Wyoming, 2013, UW researchers' lithium discovery could boost CO_2 storage prospects: (http://www.uwyo.edu/uw/news/2013/04/uw-researchers-lithium-discovery-could-boost-co2-storageprospects.html).

U.S. Geological Survey, 2011, Mineral commodity summaries 2011: Lithium.

Vine, J.D., 1980, Where in the world is all the lithium? U.S. Geological Survey Open-File Report 80-1234, 107 p.

Warren, J.K., 2010, Evaporites through time: Tectonic, climatic and eustatic controls in marine and nonmarine deposits: Earth-Science Reviews v. 98, p. 217–268.

Yaksic, A., and, Tilton, J.E., 2009. Using the cumulative availability curve to assess the threat of mineral depletion: The case of lithium: Resources Policy v. 34, p. 185–194.

Yu, J., Gao, C., Cheng, A., Liu, Y., Zhang, L., and, He, X., 2013, Geomorphic, hydroclimatic and hydrothermal controls on the formation of lithium brine deposits in the Qaidam basin, northern Tibetan plateau, China: Ore Geology Reviews, v. 50, p. 171–183.

Zampirro, D., 2004, Hydrogeology of Clayton Valley brine deposits, Esmeralda County, Nevada: Forum on the Geology of Industrial Minerals, 39th, Reno, Nevada, Proceedings.

APPENDIX

Summary

This Appendix provides detailed information on the geology and tectonics of each basin listed in Table 1 of the main paper. References for other information included in Table 1 are also detailed here. Table S1 at the end of this Appendix contains various geochemical data for hot springs, thermal water, and nonthermal water in some Li-rich brine-bearing basins. This data, collected by the authors, augment Table 1 and the Appendix text.

Middle East

The Dead Sea is the only saline water considered from the Middle East. Importantly, this saline water has developed in extremely arid conditions. It is surrounded by the eastern Mediterranean, the Horn of Africa, and the Arabian Peninsula—three of the most arid regions on the planet.

Dead Sea

The Dead Sea is not part of the world ocean but rather is a terminal salt lake. The lake is the most saline in the world (>30% dissolved solids; Garfunkel and Ben-Avraham, 1996), and the basin contains the topographically lowest dry land. The Dead Sea occupies an intracontinental pull-apart basin along the sinistral transform boundary between the Arabian and African plates (Garfunkel and Ben-Avraham, 1996). Recent drawdown of the Dead Sea, which is due to agricultural overuse of surface water from the River Jordan, has resulted in the separation of lake water into northern and southern lakes. The southern lake is largely divided into evaporating ponds where potash and bromide are produced (Garrett, 2004). The end liquor reportedly has subeconomic Li concentrations of 30 mg/L (Garrett, 2004). The shores of the southern lake are dotted with hot springs. In a synthesis of evidence for active faulting in along this plate boundary zone, Garfunkel et al. (1981) noted that a late Pliocene to early Pleistocene basaltic unit (cover basalt) is widely distributed.

Notes for Table 1: Average Li concentration from Garrett (2004). Garrett (2004) also estimated 2 Mt of Li resource in the Dead Sea, although it is not identified as a major source of Li to date because the concentration of Li is quite low.

North American Basins Containing Li Brines

Salton trough, California

The Salton trough is a strike-slip basin located at a releasing bend along an intracontinental segment of the San Andreas transform fault (Axen and Fletcher, 1998). Looking to the south, the San Andreas fault is seen to be the northernmost of a series of transforms that connect short ridge segments across which the Gulf of California has opened by seafloor spreading in the past few million years. The Salton trough, then, is akin to one of the ridge segments, a key difference being that extension has not yet reached the stage of seafloor spreading. The lithium-enriched brines in the Salton trough are geothermal fluids at 100° to 300°C (Garrett, 2004, p. 37) that are produced from young basin-fill strata in the transtensional basin. The Colorado River was probably a major sediment source (Winker and Kidwell, 1986). Robinson et al. (1976) reported that sediments of the Colorado River delta are intruded by Quaternary rhyolite domes. The lithium resource has been known for decades but only recently did production start, by Simbol, Inc., as a byproduct of geothermal energy production(http://www.simbolmaterials.com/breakthrough_technology.htm).

Notes for Table 1: All reported Li values from Garrett (2004). Total Li resource from Gruber et al. (2011).

Searles Lake, California

Searles Valley is a Neogene basin within the broad intersection between the E-striking, sinistral Garlock fault system and the eastern California shear zone of Dokka and Travis (1990), a N-striking zone of diffuse dextral shear. Extension appears to be the main driver of subsidence. A normal fault system marked by a pronounced surface graben follows the basin's eastern edge at the foot of the Slate Range (Smith, 2009). The Garlock fault, near the southern limit of the basin, is active, as revealed by a Quaternary sinistral offset of about 90 m (McGill and Sieh, 1993). During relatively wet intervals in the past few million years, Searles Lake was the third in a chain of five lakes on the east side of the Sierra Nevada Mountains, the lowest and final one being Death Valley (Smith, 2009). The spillways, through which each of the first four paleolakes drained to the next one, are now far above the present lake or playa surfaces. Searles Valley does not appear to be prospective for geothermal resources; however, the Coso geothermal field lies within the next basin upstream (China Lake; Smith, 1976). Quaternary tufa pinnacles of lacustrine origin are inferred to line up along buried faults (Smith, 2009). Mafic lavas as young as 1.75 Ma crop out nearby. The Lava Creek ash (0.64 Ma) has been identified in the basin fill (Izett and Wilcox, 1982). Curiously, some brines and muds in Searles Valley are enriched in tungsten (Ririe, 1989).

Notes for Table 1: Minimum, maximum, and average Li concentrations from Garrett (2004), the average is from the middle part of the lake.

Great Salt Lake, Utah

The geology of Great Salt Lake is dominated by Paleozoic marine strata exposed in horsts of the Basin and Range extensional province. Great Salt Lake is bordered on the east by the Wasatch Mountains, the largest and most continuous fault-bounded mountain block in the eastern Basin and Range. The Wasatch Mountains define the edge of Basin and Range extension in northern Utah, and by virtue of their abundant snowpack they provide a major source of water to Great Salt Lake. However, the three major freshwater sources for Great Salt Lake, the Provo/Jordan River system, the Weber River, and the Bear River, all drain the quartzite-dominated Neoproterozoic Uinta Mountain Group in the western Uinta Mountains before traversing the Wasatch Mountains. The Wasatch and adjacent Oquirrh Mountains are intruded by granodiorite and quartz monzonite intrusions, which precede and coincide with an Oligocene and early Miocene ignimbrite flareup in the Basin and Range (Best et al., 2013). This ignimbrite flareup has drawn comparison with the Mio-Pliocene Central Andean flareup, and it is likely that crustal thickness in the

Basin and Range at this time was similar to the present-day Andean Plateau (Best et al., 2009). The 36 to 18 Ma flareup is related to a variety of metal deposits of economic importance, including Marysvale volcanic field in central Utah. In the Oquirrh Mountains, immediately south of Great Salt Lake the Bingham Canyon mine exploits a large porphyry copper deposit related to this event. During paleoclimatic intervals where lake levels were higher, the Great Salt Lake subbasin has also been connected to the Sevier subbasin, which contains younger volcanic rocks. These young volcanic rocks are much more interesting from a Li source perspective. They contain basaltic flows and tuff cones (Pushkar and Condie, 1973)—some of which were subaqueous eruptions in Lake Bonneville (White, 1996), and topaz rhyolites that contain extraordinary enrichments in Rb, Cs, Li, and Be (Congdon and Nash, 1988) and host the important volcanogenic beryllium deposit at Spor Mountain, Utah (Foley et al., 2010).

Great Salt Lake is the remnant of the glacial Lake Bonneville, whose climatically driven lake-level record is well known for the last 30 ka (Oviatt, 1997). The late Quaternary Bonneville highstand (pre 17.5 ka) was contemporaneous with maximum glaciation in the Wasatch Mountains, which began its retreat at ~16 ka (Laabs et al., 2011). A longer term history of lake-level fluctuations in the Bonneville basin is known to extend back at least 750 ka and is broadly correlated with extensive Northern Hemisphere glactiation (Oviatt et al., 1999). It is believed that rapid desiccation of deep freshwater lakes led to deposition of thick evaporite units (Balch et al., 2005).

Two important aspects of the late Quaternary and modern hydrology of the Bonneville basin and Great Salt Lake are salient to sources of Li and concentration of Li in Great Salt Lake and Sevier Lake (in the Sevier subbasin). The first (paleo)hydrologic point of interest is the geomorphic threshold that separates the two subbasins at the Old River Bed, near Table Mountain, Utah. At ~14,500 ka Lake Bonneville fell below the threshold that separates the Sevier subbasin from the Great Salt Lake subbasin; from this point until ~11,500 ka Lake Gunnison occupied the Sevier subbasin and overflowed into the Great Salt Lake subbasin (Oviatt et al., 2003). Lake Gunnison was fed by the Beaver and Sevier Rivers originating in the Tushar Mountains (Marysvale volcanic field); this drainage is assumed to be the same as modern and freshwater inputs dominated by the Sevier River. Since ~11,500 ka the Sevier River has been the major source of freshwater to Sevier Lake, though in recent times irrigation has effectively reduced this input to zero. A subsurface brine exists within a meter of the land surface underneath Sevier Lake playa. This Na-Cl brine contains ~30 mg/L lithium and appears to be perched in the upper 10 m of Sevier Lake above fresher water (Whelan, 1969). Almost nothing is known about groundwater flux to the basin, but presumably the Sevier Lake brine is perched on lacustrine clays related to Lake Bonneville and Lake Gunnison. Consequently, it can be assumed that the lithium in this brine has been concentrated over the Holocene. A number of interesting thermal springs exist in the region, including Baker Hot Springs ~60 km north of Sevier Lake, but within the drainage basin, and the Roosevelt Known Geothermal Resource Area (KGRA) at the southeastern margin of the drainage basin. However, the Sevier River likely provided the vast majority of the influx over this period and may be the major source of Li to the Sevier Lake basin.

The second (paleo)hydrologic point of interest is the potential Quaternary diversions of the Bear River into and out of the Great Salt Lake subbasin. At present the Bear River is one of the three major sources of freshwater to Great Salt Lake, though at different points in the late Quaternary it may have been diverted into and out of the Bonneville (Great Salt Lake) basin repeatedly (Bouchard et al., 1998). The input of the Bear River is important from the perspective of the Sr isotope hydrology and paleohydrology of Great Salt Lake (Jones and Faure, 1972; Hart et al., 2004). In fact, the Bear River dominates the Sr isotope hydrology not only because of its high discharge, but also because of its high Sr concentrations owing to contributions from Crystal Hot Springs. Influx from Crystal Hot Springs changes the composition of the Bear River, and adds substantial Li. Our samples from hot and cold springs in this region contain 1.8 to 6.5 mg/L Li (cf. Table S1) and presumably this is the major Li source for Great Salt Lake. Analyses from the 1960s (Handy, 1967; Whelan, 1969) converge on Li concentrations in the range of 40 to 70 mg/L, though more recent analyses report Li concentrations <30 mg/L (Jones et al., 2009).

Although Li is not economical to extract from Great Salt Lake, the minerals industry is very active in Great Salt Lake—as of 2005, six mining companies extracted dissolved and solid components from the lake, including common salts, potassium sulfate, magnesium chloride, magnesium (metal), chloride (gas), sodium sulfate, and calcium sulfate (http://www.deq.utah.gov/workgroups/gsl_wqsc/docs/2005/Mar/GSLChemistry.pdf).

Notes for Table 1: Minimum, maximum, average Li concentration and total Li resource from Garrett (2004). Li concentration of nearby hot springs and associated surface water from S. Hynek (this paper).

Clayton Valley, Nevada

A good overview of the geology and physiography of Clayton Valley can be found in Kunasz (1974). Clayton Valley is an extensional basin with a valley floor occupied by a 20-km^2 playa (Kunasz, 1974). It is located in the Basin and Range province, the world's widest hyperextended terrain. Extension in the Basin and Range province, in turn, has taken place above an asthenospheric slab window along a former convergent margin, the extension being the consequence of complex ridge-trench-transform interactions (Dickinson and Snyder, 1979). Deformation in this part of the Basin and Range province is relatively young (mid-Miocene to Pliocene) and related to transtension within the broad structure known as Walker Lane (Oldow et al., 2009). In detail, Clayton Valley is hosted in an extensional half-graben system between a young metamorphic core complex to the west (Mineral Ridge Core Complex: Oldow et al., 2009) and its breakaway zone to the east (Montezuma Range). Low-angle extension has pulled the rocks of the core complex up from their original position at depth; this process has juxtaposed the basin fill against hot rocks. Before the groundwater system was disrupted by lithium brine production, hot springs were located at the eastern and western basin margins (Davis and Vine, 1979). The basin is being evaluated for geothermal resources (Anonymous, 2012). A well-formed

basaltic cinder cone is located within a few kilometers of the brine field; this volcano is undated but probably Quaternary in age. The basin fill sequence includes many horizons of glassy, felsic tuff from a variety of local and distant Neogene eruptive centers, including the Bishop tuff (Sarna-Wojcicki et al., 2000) that blanketed much of the Basin and Range and which constitutes an important Li-rich brine aquifer in the Clayton Valley brine field (Zampirro, 2004). Price et al. (2000) reported Li concentrations as high as 228 ppm in silicic tuffs within the Clayton Valley drainage area.

Notes for Table 1: Average Li concentration is from Harben and Edwards (1998) and the minimum and maximum Li concentrations are from Garrett (2004). Lithium in nearby hotsprings from Davis et al. (1986). Lithium resource estimate from Gruber et al. (2011).

Evaporite Basins (Salars) of the Central Andes

The Central Andes of South America host the largest and most numerous Li brine deposits in the world. Two important physiographic features if the Central Andes figure prominently in the generation of Li brines; the Central Andean plateau and the Atacama Desert. In these environments, the combination of volcanism, hydrothermal activity, closed basins, and hyperarid climate has led to extensive deposition of evaporite deposits since ~15 Ma (Alonso et al., 1991). The extreme size and longevity of these closed basins is very favorable for generation of Li brines, particularly where thick evaporite deposits (halite, gypsum, and less commonly borates) have removed ions from solution, further concentrating Li. A general overview of the geology and mineral resources of Central Andean salars can be found in Ericksen et al. (1990).

The Central Andean plateau is the world's second largest and highest orogenic plateau; only the Tibetan plateau is higher or more extensive (Allmendinger et al., 1997; Strecker et al., 2007). This high-altitude plateau is a hydrographically closed topographic feature in the back arc of the Neogene Andes. A series of closed basins at tropical and subtropical southern latitudes comprise the Central Andean plateau. Although the full extent of the plateau includes Bolivia, northwestern Argentina, and portions of Chile and Peru, the salars of interest belong to three main groups; those of the Bolivian Altiplano, those of the Argentine Puna, and those of the Chilean Atacama Desert at the western margin of the plateau. The Altiplano of Bolivia has more subdued reflief and is dominated by the extremely large Salar de Uyuni and its satellite salar, Copaisa. Additionally, Salar de Pastos Grandes is a smaller closed basin within the Uyuni hydrographic basin, which sits at a higher elevation (~4,450 m) than Uyuni and Copaisa (~3,650 m). The salars in the Argentine portion of the plateau share more characteristics with the Bolivian Salar de Pastos Grandes (not to be confused with the Argentine Salar de Pastos Grandes) than they do with the giant Uyuni/Copaisa system. These salars on the Argentine Puna plateau have much smaller surface areas and typically their hydrographic boundaries are defined by some combination of volcanic edifices, crystalline mountain blocks, and alluvial deposits. The Chilean salars discussed span the latitudinal range of the Atacama Desert (18°–27° S); at the northern and southern ends, the Salars de Surire and Maricunga, respectively, lie at the western margin of the Puna-Altiplano plateau with elevations exceeding 4,000 m. In the central Atacama, the giant Salar de Atacama lies on the Tropic of Capricorn at 2,300-m elevation.

Salars of the Altiplano plateau

Salars on the Altiplano plateau discussed herein are (from north to south) Copaisa, Uyuni, and Pastos Grandes. These salars occupy the same hydrographic basin and contain a rich record of climatically driven lake-level history. The Andean volcanic arc defines the western margin of the Altiplano. The topography on the Altiplano is generally subdued relative to the southern portion of the Central Andean plateau and recent volcanic activity is also less abundant. The Li resources in the Bolivian Altiplano are substantial, but the Mg/Li ratio of these brines is not favorable for Li production using current technology.

Salar de Copaisa: This is a satellite lake to Uyuni; they were connected during periods of higher lake level. This connection occurred as recently as the latest Quaternary or early Holocene. A thorough discussion of lake-level histories and the connections between basins can be found in Plazcek et al. (2006, 2011). Modern Salar de Copaisa is fed by drainages from the north.

Notes for Table 1: Average Li concentration from Garrett (2004).

Salar de Uyuni: Salar de Uyuni is the remnant of a large glacial lake, and the world's largest salt flat. The climatic history of the region from ~120 ka to present is documented by paleolake shores in the Uyuni, and adjacent Poopo and Coipasa basins (Plazcek et al., 2006). Modern Salar de Uyuni is fed by the Río Grande de Lipez from the south; this drainage area includes young rhyolites.

Notes for Table 1: Lithium concentrations from Garrett (2004) and total Li resource from Gruber et al. (2011).

Salar de Pastos Grandes: Altiplano plateau, southeastern Bolivia. The Salar de Pastos Grandes occupies a small portion of the ~60- × 35-km oval collapse caldera first identified by Baker (1981), using satellite imagery. This caldera presumably formed during eruption of the 5.45 Ma Chuhuilla Ignimbrite and was last active during eruption of the 2.89 Ma Pastos Grandes Ignimbrite which erupted ~1,500 km^3 of Dense Rock Equivalent (DRE) material (Salisbury et al., 2011). The Pastos Grandes caldera is the northernmost caldera in the Altiplano-Puna volcanic complex, and the Pastos Grandes Ignimbrite formed during the youngest documented supereruption in the complex. Currently, the Salar de Pastos Grandes is bordered to the south and the west by resurgent lava domes; whereas the northern and eastern boundaries of the salar are the caldera scarp. With respect to generation of the lithium brine at Pastos Grandes, de Silva and Francis (1991) made two relevant observations: (1) in addition to Pastos Grandes, several other lakes "may be remnants of a much more extensive lake which once occupied much of the moat of Pastos Grandes caldera," and (2) "Of several hot springs associated with the caldera, the largest is in the Laguna Pastos Grandes. These provide evidence for continuing geothermal activity within the underlying plutonic system."

Notes for Table 1: Lithium concentrations from Lando (2010).

Salars of the Puna plateau

The Puna plateau is the southern portion of the high elevation internally drained Central Andean plateau. The Puna is distinct from the northern portion (Altiplano) of the Central Andean plateau in that it has more youthful topography characterized by basins and ranges; these are often composed of Ordovician bedrock and also exposed Tertiary sediments. Volcanism on the Puna consists of the Andean arc at its western margin and bimodal volcanism in the back arc. Young back-arc mafic rocks are widely distributed throughout the plateau (Kay et al., 1994). Both large and small silicic calderas are also present (de Silva and Francis, 1991; Siebel et al., 2001). Trumbull et al. (2006) conducted a thorough review of the spatiotemporal dynamics of volcanism in both the frontal magmatic arc and the back-arc plateau. More recent work has improved understanding of geochronology and geochemistry of both mafic (Risse et al., 2008) and silicic (Kay et al., 2010) volcanic centers. There are several large, potentially crustal-scale, lineaments or faults that play an important role in the magmatism and fluid flow of the region. These NW-SE-trending lineaments are closely associated with many of the Li-rich salars in the region and have had dynamic interactions with volcanism and individual volcanic centers (Ramelow et al., 2006; Petrinovic et al., 2010). In fact, these lineaments can be considered an important first-order feature in ore deposit models and exploration geology (Chernicoff et al., 2002). The surficial geology of the Puna is dominated by the crustal blocks that constitute the ranges, late Cenozoic sediments and volcanoes, Quaternary alluvium and salar surfaces. The basins commonly contain volcanic, clastic, and evaporite deposits 3 to 5 km thick (Alonso et al., 1991). Internally drained, evaporite depositional centers have existed in the region since ~15 Ma (Vandervoort et al., 1995). Presently, salars are estimated to occupy ~5% of the surface of the Puna plateau, a ~5,000 km^2 area (Toledo et al., 2009).

Salar de Olaroz/Cauchari, Puna plateau, northwestern Argentina: The Salars de Olaroz and Cauchari are in the same tectonic basin but are separated by alluvial deposits related to the Ola River, which flows into the northern Salar de Cauchari. The southern portion of Salar de Cauchari is fed by the Río Tocomar, originating at the Tocomar volcanic center (see the Salar del Rincón section for further information). Salar de Olaroz is fed from the north by Río El Rosario (also Río El Toro). Little information can be found about springs or thermal waters in the basin, but a study of opaline silica nodules in alluvial fans on the margin of Salar Olaroz concluded that these nodules were indicative of high-silica thermal waters (Bustillo and Alonso, 1989).

There is a history of borate mining in the basin by several companies, and currently two lithium exploration/production companies are active in the basin. It is from their publically available information that most of the data regarding Li concentrations and reserves are derived. A resource evaluation presented for Lithium Americas Corporation in 2010 provides significant data on both Olaroz and Cauchari (http://www.lithiumamericas.com/downloads/Inferred-Resource-Estimate-May_6_2010.pdf; last accessed August 27, 2013). This report details the Li concentrations in surface and subsurface brines, in addition to developing an initial hydrostratigraphic model.

A total of 55 surface brines sampled from hand-dug pits mostly yielded brines containing between 200 and 1,000 mg/L Li. Lithium concentrations in surface brines reached a minimum (<200 mg/L) at the south end of Cauchari and in the boundary zone between Olaroz and Cauchari, and they reached a maximum (>1,000 mg/L) in the central zone of Cauchari. Subsurface brines were evaluated by sampling nine boreholes at 1-m-depth increments; a total of 760 brine samples yielded Li concentrations similar to the mean surface brine value. Three holes in Olaroz yielded average Li concentrations of 347, 456, and 552 mg/L. The weighted mean of all brines sampled from six boreholes in Cauchari is 681 mg/L Li and one of these boreholes yielded an average of 869 mg/L Li (n = 114). These Li concentration data, combined with lithological and hydrological characterization of the basins, were used to arrive at an estimated Li reserve of 0.93 Mt. A subsequent report provides information on additional drilling, geophysical surveys, and hydrologic modeling, but the details of brine volume and lithium concentration changed very little (http://www.lithiumamericas.com/downloads/LAC_NI_43-101_Updated_12062010.pdf; last accessed August 27, 2013). Li reserve estimates of Lithium Americas Corporation combined with estimates (~0.27 Mt Li) put forth by Orocobre Limited for its property on Olaroz (http://www.orocobre.com.au/Projects_Olaroz.htm; last accessed August 27, 2013) put the estimated lithium in this system well over 1 Mt. As of November 2012, Orocobre was developing this property with the aim of producing battery-grade lithium carbonate late in the spring of 2014.

Notes for Table 1: Lithium concentrations in Table 1 from Mohr et al. (2010) and references within and are similar to the values reported by Lithium Americas above. Total Li resource taken from the above estimates.

Salar del Rincón, Puna plateau, northwestern Argentina: The Salar del Rincón is a typical Puna basin, delimited by a combination of fault-bounded mountain blocks, stratovolcanoes, and coarse alluvial deposits. To the north, the basin is bound by alluvium and to the east by Sierra de Guayaos, which are composed of Ordovician sedimentary rocks and exposed Tertiary strata. Along its western and southern margins, Salar del Rincón is bound by volcanoes. Less than 50 km west of Salar de Rincón is the Tocomar volcanic center, which is known to have volcanic eruptions within the last 1 Ma and has associated springs and geothermal features associated with the NW-SE-trending,regional-scale Calama-Olacapato-El Toro fault (Petrinovic and Piñol, 2006). The older three volcanic edifices separate this basin from Salar de Pocitos to the south (Cerro Tul-Tul, Cerro del Medio, and Cerro Pocitos) and are also associated with the Calama-Olacapato-El Toro fault zone (Petrinovic et al., 2006). Within the basin, paleohot-spring deposits are identified, and residual water within these deposits was observed to contain as much as 1,500 mg/L of Li (Toledo et al., 2009). Toledo et al. (2009) also presented an assessment of the Li resources in the salar, based upon a drilling program that targeted both solids and brines. They observe an average Li content of 400 mg/L in the brines and present information on the hydrologic characteristics and stratigraphic architecture of the basin. A zone of effective porosity in excess of 30% is identified as well as a zone of lower effective porosity (<10%), together these zones host Li reserves estimated at ~0.2 Mt.

Notes for Table 1: Lithium concentrations in Table 1 from Toledo et al. (2009), as described above.

Salar de Llullaillaco, Puna plateau, northwestern Argentina: The Salar de Llullaillaco is located adjacent to a volcano of the same name, which is the world's highest historically active volcano. This lies just outside of the Salar de Atacama surface drainage and due west of the Salar de Arizaro. The Salar de Arizaro, the largest basin preserved within the Puna, contains ~5 km of strata, more than 3 km of them being Miocene lacustrine and eolian deposits (Boyd, 2010). It has been speculated that this basin records delamination of lower crustal material (DeCelles et al., 2011). The potential of lithospheric removal has implications for the generation of lithium-rich brines, as reduced crustal thickness and an influx of hot asthenospheric mantle may play important roles in lithium transport. The potential for lithospheric delamination in an overthickened orogen is supported by geophysical observations, which indicate that the crust is on the order of 42 km thick in this region (Yuan et al., 2002), substantially less thick than predicted based upon the elevation of this region.

Notes for Table 1: Maximum and minimum Li concentrations from Mohr et al. (2010) and references within. Average Li concentration reported in Table 1 is the midpoint of the maximum and minimum.

Salar del Hombre Muerto, Puna plateau, northwestern Argentina: Geology in the region of Salar del Muerto is typical of the Puna: Ordovician rocks compose most ranges, basins are filled with late Cenozoic clastic sediments and volcanic rocks, and magmatism is associated with faults in the region (Aceñolaza et al., 1976). The basin containing the Salar del Hombre Muerto is delimited and dissected by faults. Accommodation space within the sedimentary basin was created by Plio-Pleistocene strike-slip deformation (Jordan et al., 1999). Hombre Muerto can be divided into two subbasins and several important differences exist between the two subbasins. Bedrock along the eastern sector of Salar del Hombre Muerto contains metamorphic rocks, which may be some of the oldest rocks in the region (Quenardelle, 1990). The eastern basin also contains borates and has low chloride content, whereas the western basin contains nearly 1 km of halite and almost no borates (Vinante and Alonso, 2006). This is probably related to the surface hydrology of the basin, which is dominated by inflow to the eastern subbasin. These waters drain predominantly young silicic volcanic rocks (Quenardelle, 1987).

In fact, the surface waters that enter the eastern subbasin also drain the interior of one of the world's largest silicic calderas, Cerro Galán. This caldera is an important feature of the southern Puna plateau that was first recognized with spacecraft imagery (Francis et al., 1978, 1983, 1989). An accurate geochronology of the most recent explosive silicic volcanism at Cerro Galan is just emerging (Kay et al., 2011). Based on this data, it is clear that caldera-forming eruptions clustered in a <100-ka interval, the youngest of which is very precisely dated at 2.060 ± 0.004 Ma (Hynek et al., 2011), in close agreement with early Rb-Sr ages (2.03 ± 0.07 Ma; Sparks et al., 1985). These silicic ignimbrites and intracaldera rocks have $^{87}Sr/^{86}Sr$ ratios >0.710 (Sparks et al., 1985; Kay et al., 2011). Thermal water in the region has been observed to have more radiogenic Sr isotope ratios than these ignimbrites (Jordan et al., 1999). This has been interpreted to indicate interaction between thermal waters and radiogenic basement rocks. These data and interpretations are in accord with data we have collected from hot-spring and surface water in the Río Aguas Calientes drainage, which drains the Cerro Galan caldera and feeds the eastern subbasin of the Salar del Hombre Muerto (Table S1). These samples indicate this drainage may be a significant Li source to the salar. A hill slope hot spring discharging into Río Aguas Calientes has an Li content of 5.5 mg/L, and the river into which it flows (Río Aguas Calientes) has an Li content of 3.2 mg/L. Both this hot spring and the river have radiogenic $^{87}Sr/^{86}Sr$ ratios (0.71584 and 0.71763, respectively), considering that these are draining a large silicic volcanic caldera filled with a young rhyodacite ignimbrite.

If the Río Aguas Calientes drainage is the dominant source of Li over the last 2 Ma, its predicted that Li influx must agree with other constraints. Typically it is assumed that halite has been accumulating in the Salar del Hombre Muerto at a rate of ~500 m/Ma for the last 2 Ma (Jordan et al., 1999). This gives a minimum time for generation of the Li brine, which prior to production had between 234 and 1,100 mg/L of Li, with the majority of brines samples containing between 700 to 800 mg/L Li (Nicolli et al., 1982). The climatic history over this interval is less certain, but some constraints do exist. Sediment cores from the Salar del Hombre Muerto indicate that shallow saline lakes have existed in the past, but the region has become progressively drier since ~45 ka (Godfrey et al., 2003).

Notes for Table 1: Maximum, minimum, and average Li concentrations from Garrett (2004). Lithium concentrations of nearby hotsprings from S. Hynek (this paper) and total Li resource from Gruber et al. (2011).

Salars of the Atacama Desert

The Atacama Desert lies in the rain shadow of the hyper-arid Central Andean Plateau. Although the salars of the Atacama are at lower elevations than those of the adjacent plateau, they share many characteristics. Most importantly, salars of the Atacama Desert are intimately associated with volcanism and hydrothermal activity of the Andean magmatic arc. The lacustrine basins of interest all fall between the Cordillera Domeyko and the Altiplano-Puna plateau, a late Quaternary history for many of these basins is provided by Valero-Garcés et al. (2000).

Salar de Surire, northern Atacama Desert, Chile: The Salar de Surire is an interesting feature at a high elevation, close to the Altiplano, Volcan Parinacota, and Arica, Chile. Salar de Surire is close to the Uyuni and Coipasa hydrologic basins in Bolivia but is well isolated topographically from them. Geologic studies in a hydrographically closed basin immediately to the north of Salar de Surire provide a relevant tectonic and sedimentary context. The Lauca basin appears to have initiated in the late Miocene and since then has accumulated lacustrine sediments. Plio-Plesitocene evaporite deposits exist and little deformation has occurred since ~6 Ma (Kött et al., 1995).

Notes for Table 1: Average Li concentration and Li concentration of nearby hot springs from Garrett (2004).

Salar de Atacama, central Atacama Desert, Chile: The geology of the Salar de Atacama is discussed at length in the text. Here we provide additional information about the older

geologic history. The Cordón de Lila, an anticlinal feature plunging northward into the southern Salar de Atacama, is composed of Paleozoic rocks including marine strata, volcanic successions, and plutonic rocks of predominantly Ordovician age. This block has recently been interpreted to represent a continental magmatic arc at the western margin of Gondwana (Zimmerman et al., 2010). Magmatism along the Gondwanan margin continued into the Late Permian as recorded by volcanic and volcaniclastic strata along the eastern margin of the salar (Breitkreuz, 1995). Thick Permo-Triassic volcanic and continental strata were deposited in the Domeyko basin and are overlain by a Jurassic mixed carbonate/clastic sequence (Flint et al., 1993). These units crop out in the Cordillera Domeyko on the western margin of the salar and are unconformably overlain by Cretaceous and Cenozoic sedimentary rocks associated with the initial uplift of the Cordillera Domeyko and inception of the Salar de Atacama basin (Mpodozis et al., 2005). There was first a foreland basin here, starting in the mid-Cretaceous, with thrusting and coeval sedimentation occurring during the Cretaceous and Paleogene (Arriagada et al., 2006).

Notes for Table 1. Maximum, minimum, and average Li concentrations from Garrett (2004). Lithium concentration of El Tatio hot spring from L.Munk (this paper). Total Li resource estimate from Gruber et al. (2011).

Salar de Maricunga, southern Atacama Desert, Chile: The Salar de Maricunga occupies a high elevation intermontane basin between the Cordillera Domeyko and the Andean Cordillera. Salar de Maricunga is situated near the southernmost portion of the Central Andean plateau and also near the southernmost limit of the Atacama Desert. Latorre et al. (2005) remarked that, "With very little rainfall either from tropical or extratropical sources, this sector is undisputedly the driest portion of the Atacama Desert."

Notes for Table 1. The average Li concentration is actually the average Li grade reported by Yaksic and Tilton (2009) and the total Li resource is from Gruber et al. (2011).

Asian Basins Containing Li Brines

These basins all occur within or on the margins of the Tibetan plateau, therefore, thick orogenic crust is a commonality.

Lake Zabuye

Lake Zabuye is one of a series of high-altitude, terminal lakes in the Shigatse Prefecture of the Tibet Autonomous Region. The Tibetan plateau is the upper plate of the Himalayan-Tibetan collisional orogen, with Tibet comprising the widest and topographically highest orogenic hinterland in the world. Lake Zabuye lies within a Neogene graben that is oriented at high angles to the structural grain of the orogen. The geometry of extension in the basin of Lake Zabuye has not been documented, but 50 km to the west in the Lunggar extensional basin, Woodruff et al. (2013) have shown that extension was asymmetric with the basin having formed above a low-angle, E-dipping detachment. The thrust belt appears to be extending parallel to its strike. The Lake Zabuye area does not appear to have any young volcanic activity or hot springs, although the English-language literature is sparse. A map of Tibetan geothermal resources (Ji, 2008) shows abundant hot springs in many parts of Tibet but none in the Lake Zabuye area. Fourteen elevated strand lines show that Zabuye Lake was once many times larger than today (Yu, 2001). Lake Zabuye has northern and southern arms; the southern one has the brine resource. A notable aspect of this lithium resource is that Lake Zabuye is the only known evaporite system where lithium carbonate precipitates naturally; this is the type locality of the mineral zabuyelite. Wikipedia lists a number of alternate renditions for the name of the lake: Drangyer, Zabayu, Zabuye Caka, Zhabuye, Chabyêr, and Chabyer (http://en.wikipedia.org/wiki/Lake_Zabuye).

Notes for Table 1: Minimum and maximum Li concentrations from Garrett (2004).Average Li concentration and total Li resource from Gruber et al. (2011).

Dangxiongcuo (DXC) Lake, Tibet

English-language information on this Tibetan basin is limited. The most thorough treatment, though far from comprehensive, is from a 2005 vintage industry webpage (essentially, a Powerpoint presentation for investors) by Sterling Group Ventures http://www.sterlinggroupventures.com/Sterling_-_Li_Only_presentation_Sep2005.pdf. The geographic setting and presumably the tectonic origin are similar to those of Lake Zabuye. That is, the lake appears to be in a Neogene graben that is oriented at high angles to the structural grain of the Himalayan-Tibetan collisional orogen. The Sterling Group presentation mentioned hot springs. The name is transliterated as Lake Dangqiongcuo in Google Earth. Transliterated as Damzung Co by Zheng (1997).

Notes for Table 1: Average Li concentration and total Li resource from Gruber et al. (2011).

Taijanier Lake, Qaidam, China

The Qaidam basin is a huge, terminal depocenter in northern Tibet that has subsided since the Paleogene (Yin et al., 2008). On the broadest scale, it can be viewed as an intracontinental foreland basin in the distal, upper-plate hinterland of the Himalayan-Tibetan collisional orogen. The Qaidam basin is bound on the northeast, and loaded by, the Qilian Shan Mountains (Yin et al., 2008). The Qaidam basin is bound by the Kunlun transpressional orogen on the southwest and by the Altyn Tagh strike-slip orogen to the northwest (Yin et al., 2008). Taijanier Lake is one of a number of lakes and salt pans within the greater Qiadam basin. In a series of basin-scale isopach maps, Quaternary sediments are shown as anomalously thick in the area of Taijanier Lake (Yin et al., 2008, fig. 12). Indeed, Taijanier Lake appears to be localized in a growth syncline above a fault-bend fold like those documented and interpreted by Yin et al. (2008) on a nearby basin-scale cross section. An intriguing, newly recognized possibility is that the growth of live folds in the Qaidam basin has been enhanced by wind erosion (Kapp et al., 2011). Boron- and lithium-enriched hydrothermal waters are reported from the Qaidam basin (Zheng M., 1997). A review of the chemistry of lakes in this region is presented by Zheng and Liu (2009).

Notes for Table 1: Average Li concentration from Gruber et al. (2011) and total Li resource from Yaksic and Tilton (2009).

Table 1: General Information Summary

Topographical and environmental characteristics of the lithium basins were determined through the use of the

Environmental Systems Research Institute (ESRI®) Geographic Information System (GIS) software ArcGIS® Version 10. Several datasets with global coverage were acquired from public sources to provide elevation, drainage, and climatic information. The data included 90-m Shuttle Radar Topograpy Mission (SRTM) Digital Elevation Models (DEMs) from Jarvis et al. (2008), drainage basins from Lehner et al. (2008), temperature and precipitation from Hijmans et al. (2005), and aridity and evapotranspiration from Trabucco and Zomer (2009). The resolutions of the climate datasets were about 1 km.

The outer boundaries and total areas of each closed lithium basin were defined by polygons extracted from the drainage basins dataset. Each of these polygons defined a zone that could be used to extract information from the elevation and climate datasets using statistical tools. The latitude and longitude for a basin were identified by the location of the lowest elevation point within each basin. The area of the basin floor where water could collect was also determined from the elevation data. By isolating a range of elevations, from the minimum elevation up to a threshold value, a section of the topography that matched the maximum extent of the shoreline as shown in satellite imagery could be extracted and its area found. Values for temperature, precipitation, evapotranspiration, and aridity were obtained using zonal statistics to identify the majority value for each parameter in the basins delineated by the drainage polygons.

NOTES

SRTM 90m Digital Elevation Data: http://srtm.csi.cgiar.org/index.asp

Jarvis, A., H.I. Reuter, A. Nelson, E. Guevara, 2008, Hole-filled SRTM for the globe Version 4, available from the CGIAR-CSI SRTM 90m Database http://srtm.csi.cgiar.org).

Drainage divides: http://hydrosheds.cr.usgs.gov/

Lehner, B., Verdin, K., Jarvis, A. (2008): New global hydrography derived from spaceborne elevation data. Eos, Transactions, AGU, 89(10): 93-94.

Aridity and evapotranspiration: http://csi.cgiar.org/Aridity/

Trabucco, A., and Zomer, R.J. 2009. Global Aridity Index (Global-Aridity) and Global Potential Evapo-Transpiration (Global-PET) Geospatial Database.CGIAR Consortium for Spatial Information. Published online, available from the CGIAR-CSI GeoPortal at: http://www.csi.cgiar.org/

Temperature and precipitation: http://www.worldclim.org/bioclim

Hijmans, R.J., S.E. Cameron, J.L. Parra, P.G. Jones and A. Jarvis, 2005. Very high resolution interpolated climate surfaces for global land areas. International Journal of Climatology 25: 1965–1978.

REFERENCES

Aceñolaza, F.G., Toselli, A.J., and Gonalez, O., 1976, Geologia de la region comprendida entre el Salar del Hombre Muerto y Antofagasta de la Sierra, Provincia de Catamarca: Revista de la Asociación Geológica Argentina, v. 31, p. 127–136.

Allmendinger, R.W., Jordan, T.E., Kay, S.M., and Isacks, B.L., 1997, The evolution of the Altiplano-Puna plateau of the Central Andes: Annual Review of Earth and Planetary Sciences, v. 25, p. 139–174.

Alonso, R.N., Jordan, T.E., Tabbutt, K.T., and Vandervoort, D.S., 1991, Giant evaporite belts of the Neogene central Andes: Geology, v. 19, p. 401–404.

Anonymous, 2012, Silver Peak area geothermal exploration project environmental assessment DOI-BLM-NV-B020-2012-0214-EA DOE/EA-1921: U.S. Bureau of Land Management, 47 p. [accessed Dec. 26, 2012 at http://www.blm.gov/pgdata/etc/medialib/blm/nv/field_offices/battle_mountain_field/blm_information/nepa/rockwood_silver_peak.Par.86685.File.dat/Rockwood (CFC) Silver Peak Area EA (508 Compliant).pdf].

Arriagada, C., Cobbold, P.R., and Roperch, P., 2006, Salar de Atacama basin: A record of compressional tectonics in the central Andes since the mid-Cretaceous: Tectonics, v. 25, p. TC1008.

Axen, G.J., and Fletcher, J.M., 1998, Late Miocene-Pleistocene extensional faulting, northern Gulf of California, Mexico and Salton trough, California: International Geology Review, v. 40, p. 217–244.

Baker, M.C.W., 1981, The nature and distribution of Upper Cenozoic ignimbrite centers in the central Andes: Journal of Volcanology and Geothermal Research, v. 11, p. 293–315.

Balch, D.P., Cohen, A.S., Schnurrenberger, D.W., Haskell, B.J., Garces, B.L.V., Beck, J.W., Cheng, H., and Edwards, R.L., 2005, Ecosystem and paleohydrological response to Quaternary climate change in the Bonneville basin, Utah: Palaeogeography, Palaeoclimatology, Palaeoecology, v. 221, p. 99–122.

Best, M.G., Barr, D.L., Christiansen, E.H., Gromme, S., Deino, A.L., and Tingey, D.G., 2009, The Great Basin altiplano during the middle Cenozoic ignimbrite flareup: Insights from volcanic rocks: International Geology Review, v. 51, p. 589–633.

Best, M.G., Christiansen, E.H., and Gromme, S., 2013, Introduction: The 36-18 Ma southern Great Basin, USA, ignimbrite province and flareup: Swarms of subduction-related supervolcanoes: Geosphere, v. 9, p. 260–274.

Bouchard, D.P., Kaufman, D.S., Hochberg, A., and Quade, J., 1998, Quaternary history of the Thatcher basin, Idaho, reconstructed from the $^{87}Sr/^{86}Sr$ and amino acid composition of lacustrine fossils: Implications for the diversion of the Bear River into the Bonneville basin: Palaeogeography, Palaeoclimatology, Palaeoecology, v. 141, p. 95–114.

Boyd, J.D., 2010, Tectonic evolution of the Arizaro basin of the Puna plateau, NW Argentina: Implications for plateau-scale processes: M.S. thesis, University of Wyoming, 83 p.

Breitkreuz, C., 1995, The Late Permian Peine and Cas Formations at the eastern margin of the Salar de Atacama, northern Chile: Stratigraphy, volcanic facies, and tectonics: Revista Geológica de Chile, v. 22, 323 p.

Bustillo, M.A., and Alonso, R., 1989, Nodulos Opalinos en Facies Marginales del Salar Olaroz (Puna Argentina): Estudios Geologicos, v. 45, p. 55–59.

Chernicoff, C.J., Richards, J.P., and Zappettini, E.O., 2002, Crustal lineament control on magmatism and mineralization in northwestern Argentina: Geological, geophysical, and remote sensing evidence: Ore Geology Reviews, v. 21, p. 127–155.

Congdon, R.D., and Nash, W.P., 1988, High-fluorine rhyolite: An eruptive pegmatite magma at the Honeycomb Hills, Utah: Geology, v. 16, p. 1018–1021.

Davis, J.R., and Vine, J.D., 1979, Stratigraphic and tectonic setting of the lithium brine field, Clayton Valley, Nevada: RMAG-UGA 1979 Basin and Range Symposium, Proceedings, p. 421–430.

Davis, J.R., Friedman, I., and Gleason, J.D., 1986, Origin of the lithium-rich brine, Clayton Valley, Nevada: U.S. Geological Survey Bulletin 1622, p. 131–138.

DeCelles, P.G., Carrapa, B., Horton, B.K., McNabb, J., and Boyd, J., 2011, Cordilleran hinterland basins as recorders of lithospheric removal in the central Andes [abs.]: American Geophysical Union, Fall Meeting 2011, Abstract T131-06.

de Silva, S.L., and Francis, P.W., 1991, Volcanoes of the central Andes: New York, Springer-Verlag, 216 p.

Dickinson, W.R., and Snyder, W.S., 1979, Geometry of subducted slabs related to San Andreas transform: Journal of Geology, v. 87, p. 609–627.

Dokka, R.K., and Travis, D.J., 1990, Role of the eastern California shear zone in accommodating Pacific-North American plate motion: Geophysical Research Letters, v. 17, p. 323–326.

Ericksen, G.E., Salas O., and Raul, 1990, Geology and resources of salars in the central Andes: Geology of the Andes and its relation to hydrocarbon and mineral resources 11, 151 p.

Flint, S., Turner, P., Jolley, E.J., and Hartley, A.J., 1993, Extensional tectonics in convergent margin basins: An example from the Salar de Atacama, Chilean Andes: Geological Society of America Bulletin, v. 105, p. 603–617.

Foley, N.K., Seal, R.R., Piatak, N.M., and Hetland, B., 2010, An occurrence model for the national assessment of volcanogenic beryllium deposits: U.S. Geological Survey Open-File Report 2010-1195.

Francis, P.W., Hammill, M., Kretzschmar, G.A., and Thorpe, R.S., 1978, The Cerro Galan caldera, north-west Argentina and its tectonic setting: Nature, v. 274, p. 749–751.

Francis, P.W., O'Callaghan, L., Kretzschmar, G.A., Thorpe, R.S., Sparks, R.S.J., Page, R.N., de Barrio, R.E., Gillou, G., and Gonzalez, O.E., 1983, The Cerro Galan ignimbrite: Nature, v. 301, p. 51–53.

Francis, P.W., Sparks, R.S.J., Hawkesworth, C.J., Thorpe, R.S., Pyle, D.M., Tait, S.R., Mantovani, M.S., and McDermott, F., 1989, Petrology and geochemistry of volcanic rocks of the Cerro Galan caldera, northwest Argentina: Geological Magazine, v. 126, p. 515–547.

Garfunkel, Z., and Ben-Avraham, Z., 1996, The structure of the Dead Sea basin: Tectonophysics, v. 266, p. 155–176.
Garfunkel, Z., Zak, I., and Freund, R., 1981, Active faulting in the Dead Sea rift: Tectonophysics, v. 80, p. 1–26.
Garrett, D.E., 2004, Handbook of lithium and natural calcium chloride. Their deposits, processing, uses and properties: Elsevier, 476 p.
Godfrey, L.V., Jordan, T.E., Lowenstein, T.K., and Alonso, R.L., 2003, Stable isotope constraints on the transport of water to the Andes between 22° and 26°S during the last glacial cycle: Palaeogeography, Palaeoclimatology, Palaeoecology, v. 194, p. 299–317.
Gruber, P.W., Medina, P.A., Keoleian, G.A., Kesler, S.E., Everson, M.P., and Wallington, T.J., 2011, Global lithium availability a constraint for electric vehicles?: Journal of Industrial Ecology, v. 15, p. 760–775.
Handy, A.H., 1967, Distinctive brines in Great Salt Lake, Utah: U.S. Geological Survey Professional Paper 575-B, p. B225–B227.
Harben, P., and Edwards, G., 1998, "Lithium: Times are Changing:" Canadian Institue of Mining and Metallurgy Special Volume 50, p. 171–182.
Hart, W.S., Quade, J., Madsen, D.B., Kaufman, D.S., and Oviatt, C.G., 2004, The $^{87}Sr/^{86}Sr$ ratios of lacustrine carbonates and lake-level history of the Bonneville paleolake system: Geological Society of America Bulletin, v. 116, p. 1107–1119.
Hynek, S.A., Brown, F.H., and Fernandez, D.P., 2011, A rapid method for handpicking potassium rich feldspar from silicic tephra: Quaternary Geochronology, v. 6, p. 285–288.
Izett, G.A., and Wilcox, R.E., 1982, Map showing localities and inferred distributions of the Huckleberry Ridge, Mesa Falls, and Lava Creek ash beds (Pearlette family ash beds) of Pliocene and Pleistocene age in the Western United States and Southern Canada: U.S. Geological Survey Miscellaneous Investigation Series Map I-1325, scale 1:4,000,000.
Ji, D., 2008, Geothermal resources and utilization in Tibet and the Himalayas, *in* Fridleifsson, E.B., Workshop for decision makers on direct heating use of geothermal resources in Asia: Iceland: Orkustofnun, 9 p.
Jones, B.F., Naftz, D.L., Spencer, R.J., and Oviatt, C.G., 2009, Geochemical evolution of Great Salt Lake, Utah, USA: Aquatic Geochemistry, v. 15, p. 95–121.
Jones, L.M., and Faure, G., 1972, Strontium isotope geochemistry of Great Salt Lake, Utah: Geological Society of America Bulletin 83, p. 1875–1880.
Jordan, T.E., Alonso, R.N., and Godfrey, L.V., 1999, Tectónica, subsidencia y aguas en el salar del Hombre Muerto, Puna Argentina: Congreso Geológico Argentino, 14th, Actas I, p. 254–256.
Kapp, P., Pelletier, J.D., Rohrmann, A., Heermance, R., and Russell, J., 2011, Wind erosion in the Qaidam basin, central Asia: Implications for tectonics, paleoclimate, and the source of the Loess plateau: GSA Today, v. 21, no. 4/5, doi: 10.1130/GSATG99A.1
Kay, S.M., Coira, B., and Viramonte, J., 1994, Young mafic back arc volcanic rocks as indicators of continental lithospheric delamination beneath the Argentine Puna plateau, central Andes: Journal of Geophysical Research, v. 99, p. 24,323–24,339.
Kay, S.M., Coira, B.L., Caffe, P.J., and Chen, C-H, 2010, Regional chemical diversity, crustal and mantle sources and evolution of central Andean Puna plateau ignimbrites: Journal of Volcanology and Geothermal Research, v. 198, p. 81–111.
Kay, S.M., Coira, B., Worner, G., Kay, R.W., and Singer, B.S., 2011, Geochemical, isotopic and single crystal $^{40}Ar/^{39}Ar$ age constraints on the evolution of the Cerro Galan ignimbrites: Bulletin of Volcanology, v. 73 p. 1487–1511.
Kött, A., Gaupp, R., and Wörner, G., 1995, Miocene to Recent history of the western atiplano in northern Chile revealed by lacustrine sediments of the Lauca basin (18°15'–18°40'S/69°30'–69°05'W): Geologische Rundschau, v. 84, p. 770–780.
Kunasz, I.A., 1974, Lithium occurrence in the brines of Clayton Valley Esmeralda County, Nevada, *in* Coogan, A.H., ed., Fourth International Symposium on Salt, Houston, Tex., April 8–12. 1973, Proceedings: Cleveland, Northern Ohio Geological Society, p. 57–65. (Also available at http://www.saltinstitute.org/content/download/1270/7052).
Laabs, B.J.C., Marchetti, D.W., Munroe, J.S., Refsnider, K.A., Gosse, J.C., Lips, E.W., Becker, R.A., Mickelson, D.M., and Singer, B.S., 2011, Chronology of latest Pleistocene mountain glaciation in the western Wasatch Mountains, Utah, U.S.A.: Quaternary Research, v. 76, p. 272–284.
Lando, J., 2010, Pastos Grandes, lithium brine project, Bolivia: New World Resource Corp. website, http://www.newworldresource.com/s/PastosGrandes.asp (23/07/10).
Latorre, C., Betancourt, J.L., Rech, J.A., Quade, J., Homgren, C., Placzek, C., Maldonado, A., Vuille, M., and Rylander, K.A., 2005, Late Quaternary history of the Atacama Desert *in* Smith, M., and Hesse, P., eds., The archaeology and environmental history of the southern deserts: Canberra, Australia, National Museum of Australia Press, p. 73–90.
McGill, S., and Sieh, K., 1993, Holocene slip rate of the Central Garlock fault in southeastern Searles Valley, California: Journal of Geophysical Research, v. 98, p. 14,217–14,231.
Mohr, S., Mudd, G., and Giurco, D., 2010, Lithium resources and production: A critical global assessment: Prepared for CSIRO Minerals Down Under Flagship, by the Institute for SustainableFutures (University of Technology, Sydney) and Department of Civil Engineering (Monash University), October, 2010, 99 p.
Mpodozis, C., Arriagada, C., Basso, M., Roperch, P., Cobbold, P., and Reich, M., 2005, Late Mesozoic to Paleogenestratigraphy of the Salar de Atacama basin, Antofagasta, northern Chile: Implications for the tectonic evolution of the central Andes: Tectonophysics, v. 399, p. 125–154.
Nicolli, H.B., Surlano, J.M., Méndez, V., and Gómez Peral, M.A., 1982, Salmueras ricas en metales alcalinos del Salar del Hombre Muerto, Provincia de Catamarca, Republica Argentina: Quinto Congreso Lationamericano de Geologia, Argentina, Actas 3, p. 187–204.
Oldow, J.S., Elias, E.A., Ferranti, L., McClelland, W.C., and McIntosh, W.C., 2009, Late Miocene to Pliocene synextensional deposition in fault-bounded basins within the upper plate of the western Silver Peak-Lone Mountain extensional complex, west-central Nevada: Geological Society of America, Special Papers 2009, v. 447, p. 275–312, doi: 10.1130/2009.2447(14). (Also available at http://specialpapers.gsapubs.org/content/447/v.full.pdf+html).
Oviatt, C.G., 1997, Lake Bonneville fluctuations and global climate change: Geology, v. 25, p. 155–158.
Oviatt, C.G., Thompson, R.S., Kaufman, D.S., Bright, J., and Forester, R.M., 1999, Reinterpretation of the Burmester core, Bonneville basin, Utah: Quaternary Research, v. 52, p. 180–184.
Oviatt, C.G., Madsen, D.B., and Schmitt, D.N., 2003, Late Pleistocene and early Holocene rivers and wetlands in western Utah: Quaternary Research, v. 60, p. 200–210.
Petrinovic, I.A., and Piñol, F.C., 2006. Phreatomagmatic and phreatic eruptions in locally extensive settings of southern central Andes: The Tocomar volcanic centre (24°10'S–66°34'W), Argentina: Journal of Volcanology and Geothermal Research, v. 158, p. 37–50.
Petrinovic, I.A., Riller, U., Brrod, J.A., Alvarado, G., and Arnosio, M., 2006, Bimodal volcanism in a tectonic transfer zone: Evidence for tectonically controlled magmatism in the southern central Andes, NW Argentina: Journal of Volcanology and Geothermal Research, v. 152, p. 240–252.
Petrinovic, I.A., Martí, J., Aguirre-Díaz, G.J., Guzmáan, S., Geyer, A., and Salado Paz, N., 2010, The Cerro Aguas Calientes caldera, NW Argentina: An example of a tectonically controlled, polygenetic collapse caldera, and its regional significance: Journal of Volcanology and Geothermal Research, v. 194, p. 15–26.
Placzek, C., Quade, J., and Patchett, P.J., 2006, Geochronology and stratigraphy of late Pleistocene lake cycles on the southern Bolivian altiplano: Implications for causes of tropical climate change: Geological Society of America Bulletin, v. 118, p. 515–532.
——2011, Isotopic tracers of paleohydrologic change in large lakes of the Bolivian altiplano: Quaternary Research, v. 75, p. 231–244.
Price, J.G., Lechler, P.J. et al., 2000, Possible volcanic sources of lithium in brines in Clayton Valley, Nevada: Geology and Ore Deposits 2000: The Great Basin and Beyond Proceedings, v. 1, p. 241–248.
Pushkar, P., and Condie, K.C., 1973, Origin of the Quaternary basalts from the Black Rock Desert region, Utah: Strontium isotopic evidence: Geological Society of America Bulletin, v. 84, p. 1053–1058.
Quenardelle, S.M., 1987, Unidades geomorfologicas en el area del Salar del Hombre Muerto, Puna Argentina, determinadas mediante analisis digital interactivo de imagenes LANDSAT: Decimo Congreso Geologico Argentino, Actas I, p. 365–368.
——1990, Geologia y petrologia del basamento metamorphico del sector oriental del Salar del Hombre Muerto, Puna Argentia: Decimo Primer Congreso Geologico Argentino, Actas I, p. 166–169.
Ramelow, J., Riller, U., Romer, R.L., and Oncken, O., 2006, Kinematic link between episodic trapdoor collapse of the Negra Muerta caldera and motion on the Olacapato-El Toro fault zone, southern central Andes: International Journal of Earth Sciences (Geologische Rundschau), v. 95, p. 529–541.
Ririe, G.T., 1989, Evaporites and strata-bound tungsten mineralization: Geology, v. 17, p. 139–143.
Risse, A., Trumbull, R.B., Coira, B., Kay, S.M., and van den Bogaard, P., 2008, $^{40}Ar/^{39}Ar$ geochronology of mafic volcanism in the back-arc region of the

southern Puna plateau, Argentina: Journal of South American Earth Sciences, v. 26, p. 1–15.
Robinson, P.T., Elders, W.A., and Muffler, L.J.P., 1976, Quaternary volcanism in the Salton Sea geothermal field, Imperial Valley: Geological Society of America Bulletin, v. 87, p. 347–360. doi: 10.1130/0016-7606(1976)87<347:QVITSS>2.0.CO;2
Salisbury, M.J., Jicha, B.R., de Silva, S.L., Singer, B.S., Jiméez, N.C., and Ort, M.H., 2011, $^{40}Ar/^{39}Ar$ chronostratigraphy of Altiplano-Puna volcanic complex ignimbrites reveals the development of a major magmatic province: Geological Society of America Bulletin, v. 123, p. 821–840.
Sarna-Wojcicki, A.M., Pringle, M.S., and Wijbrans, J., 2000, New $^{40}Ar/^{39}Ar$ age of the Bishop tuff from multiple sites and sediment rate calibration for the Matuyama-Brunhes boundary: Journal of Geophysical Research, v. 105, p. 21,431–21,443.
Siebel, W., Schnurr, W.B.W., Hahne, K., Kraemer, B., Trumbull, R.B., van den Bogaard, P., and Emmermann, R., 2001, Geochemistry and isotope systematics of small- to medium-volume Neogene-Quaternary ignimbrites in the southern central Andes: Evidence for derivation from andesitic magma sources: Chemical Geology, v. 171, p. 213–237.
Smith, G.I., 1976, Origin of lithium and other components in the Searles Lake evaporites: U.S. Geological Survey Professional Paper 1005, p. 92–103.
——2009, Late Cenozoic geology and lacustrine history of Searles Valley, Inyo and San Bernardino Counties, California: U.S. Geological Survey Professional Paper 1727, 115 p.
Sparks, R.S.J., Fracnis, P.W., Hamer, R.D., Pankhurst, R.J., O'Callaghan, L.O., Thorpe, R.S., and Page, R., 1985, Ignimbrites of the Cerro Galan caldera, NW Argentina: Journal of Volcanology and Geothermal Research, v. 24, p. 205–248.
Strecker, M.R., Alonso, R.N., Bookhagen, B., Carrapa, B., Hilley, G.E., Sobel, E.R., and Trauth, M.H., 2007, Tectonics and climate of the southern central Andes: Annual Review of Earth and Planetary Sciences, v. 35, p. 747–787.
Toledo, A.O., Alonso, R.N., V. Ruiz, T., and Quiroga, A.G., 2009, Evapofacies Halítica en el Salar del Rincón, Departamento Los Andes, Salta: Revista de la Asociación Geológica Argentina, v. 64, p. 493–500.
Trumbull, R.B., Riller, U., Oncken, O., Scheuber, E., Munier, K., and Hongn, F., 2006, The time-space distribution of Cenozoic volcanism in the south-central Andes: A new data compilation and some tectonic implications, *in* Oncken, O., Chong, G., Franz, G., Giese, P., Götze, H-J., Ramos, V.A., Strecker, M.R., Wigger, P., eds., The Andes—active subduction orogeny: Springer, Berlin, Frontiers in Earth Sciences, v. 1, p. 29–43.
Valero-Garcés, B.L., Grosjean, M., Messerli, B., Schwalb, A., and Kelts, K., 2000, Later Quaternary lacustrine deposition in the Chilean altiplano (18°–28°S): AAPG Studies in Geology, v. 46, p. 625–636.
Vandervoort, D.S., Jordan, T.E., Zeitler, P.K., and Alonso, R.N., 1995, Chronology of internal drainage development and uplift, southern Puna plateau, Argentine central Andes: Geology, v. 23, p. 145–148.
Vinante, D., and Alonso, R.N., 2006, Evapofacies del Salar Hombre Muerto, Puna Argentina: Distribucion y Genesis: Revista de la Asociación Geológica Argentina, v. 61, p. 286–297.
Whelan, J.A., 1969, Subsurface brines and soluble salts of subsurface sediments, Sevier Lake, Millard County, Utah: Utah Geological and Mineral Survey Special Studies 30, 13 p.
White, J.D.L., 1996, Pre-emergent construction of a lacustrine basaltic volcano, Pahvant Butte, Utah (USA): Bulletin of Volcanology, v. 58, p. 249–262.
Winker, C.D., and Kidwell, S.M., 1986, Paleocurrents of the Pliocene Colorado delta plain, Fish bCreek-Vallecito Basin, southern California: Implications for paleogeography of the early northern Gulf of California: Geology, v. 14, p. 788–791.
Woodruff, W.H., Jr., Horton, B.K., Kapp, P., and Stockli, D.F., 2013, Late Cenozoic evolution of the Lunggar extensional basin, Tibet: Implications for basin growth and exhumation in hinterland plateaus: Geological Society of America Bulletin, v. 125, p. 343–358. doi: 10.1130/B30664.1.
Yaksic, A., and Tilton, J., 2009, Using the cumulative availability curve to assess the threat of mineral depletion: The case of lithium: Resources Policy, v. 34, p. 185–194.
Yin, A., Dang, Y.Q., Zhang, M., Chen, X.H., and McRivette, M.W., 2008, Cenozoic tectonic evolution of the Qaidam basin and its surrounding regions (Part 3): Structural geology, sedimentation, and regional tectonic reconstruction: Geological Society of America Bulletin, v. 120, p. 847–876.
Yu, G., Harrison, S.P., and Xue, B., 2001, Lake status records from China: Data Base Documentation: Max Planck Institute for Biogeochemistry (MPI-BGC), MPI-BGC Technical Report 4, 243 p.
Yuan, X., Sobolev, S., and Kind, R., 2002, Moho topography in the central Andes and its geodynamic implications: Earth and Planetary Science Letters, v. 199, p. 389–402.
Zampirro, D., 2004, Hydrogeology of Clayton Valley brine deposits, Esmeralda County, Nevada: Nevada Bureau of Mines and Geology Special Publication 33, p. 271–280.
Zheng, M., 1997, An introduction to saline lakes on the Qinghai-Tibet plateau: Kluwer Academic Publisher, v. 76.
Zheng, M., and Liu, X., 2009.Hydrochemistry of Salt Lakes of the Qinghai-Tibet plateau, China: Aquatic Geochemistry, v. 15, p. 293–320.
Zimmerman, U., Niemeyer, H., and Meffre, S., 2010, Revealing the continental margin of Gondwana: The Ordovician arc of the Cordón de Lila (northern Chile): International Journal of Earth Science (Geologische Rundschau), v. 99, Supplement 1, p. S39–S56.

Table S1. Geochemical Data for Hot Springs, Thermal Water, and Associated Surface Water in Some Li-Rich Brine-Bearing Basins[1]

Sample no.	Sample date	Sample notes	Sample type	Lat (N)	Long (E)	Elev (m)	δ^2H	$\delta^{18}O$	$^{87}Sr/^{86}Sr$	se	Li mg/L	Na mg/L	K mg/L	Rb µg/L	Cs µg/L	Mg mg/L	Ca mg/L	Sr µg/L	Ba µg/L	As µg/L	U µg/L
Puna Plateau and plateau margin, northwestern Argentina																					
TUC-870	27-Mar-07	Draining metamorphic	River	–27.0915	–65.5540	412	–28	–5.9	0.72031	0.00004	0.003	3	1.8	1.2	<0.03	1.1	9	19	18	0.25	0.03
TUC-872	27-Mar-07	Draining metamoprhic	River	–27.0834	–65.6655	747	–28	–5.8	0.71802	0.00003	0.003	6	2.8	1.1	<0.03	2.1	11	39	13	0.74	0.13
SAL-962	3-Apr-07	Angastaco basin	River	–25.7011	–66.0295	1,772	–36	–6.0	0.71705	0.00001	0.497	132	7.9	14	1.2	9.5	37	488	110	21	5.3
PUN-1053	16-Apr-07	Rio Aguas Calientes	River	–25.8258	–66.9247	4,461	–50	–7.0	0.71763	0.00002	3.25	246	11	164	1207	6.0	32	349	8	799	2.7
PUN-1054	16-Apr-07	Hillslope hotspring	Hotspring	–25.8258	–66.9247	4,468	–50	–6.5	0.71584	0.00002	5.53	389	10	174	1842	3.1	22	315	25	1806	1.5
CAT-1004	7-Apr-07	Termas de Fiambala	Spring (warm)	–27.7430	–67.5514	1,906	–40	–6.7	0.73561	0.00002	0.205	130	3.1	38	4.6	0.63	15	157	53	0.19	0.05
PUN-1010	9-Apr-07	Salar Carachi Pampa	Lake/ playa	–26.5127	–67.4092	3,014	22	10.0	0.71791	0.00001	6.48	>2000	201	705	168	86	708	8018	115	33	8.0
CAT-1014	10-Apr-07	Termas Villavil	Spring (warm)	–27.1123	–66.8227	2,113	–30	–4.7	0.70959	0.00018	0.020	87	1.2	1.5	0.18	0.08	7	6	3	4.9	0.25
PUN-1051	15-Apr-07	Laguna Grande	Lake/ playa	–26.2379	–67.0503	4,250	–52	–6.8	0.71897	0.00002	0.927	185	13	89	121	6.8	45	393	98	140	14
Bear River Drainage and Crystal Hot Spring, Great Salt Lake Basin, Utah, USA																					
BR-2	Nov-12	Bear River-upstream	River	41.6384	–112.1180	1,292			0.71400	0.00001	0.049	57	8.2	15	0.29	35	59	383	77	2.3	1.5
BR-5	Nov-12	Bear River-upstream	River	41.6384	–112.1185	1,292			0.71408	0.00001	0.049	55	8.3	16	0.33	34	59	383	76	2.5	1.3
BR-3	Nov-12	Salt Creek	Creek	41.6345	–112.0884	1,298			0.72330	0.00002	2.37	5,249	365	675	63	87	337	13,016	233	13	1.6
BR-4A	Nov-12	Crystal Hot Spring	Hotspring	41.6593	–112.0874	1,306			0.72349	0.00002	6.65	14,863	1,012	1,899	176	186	806	35,499	386	16	0.37
BR-4B	Nov-12	Crystal Hot Spring	Cold spring	41.6593	–112.0874	1,306			0.72297	0.00002	1.75	3,896	268	501	45	79	279	10,063	202	15	3.0
BR-1	Nov-12	Bear River-downstream	River	41.5446	–112.1080	1,289			0.71623	0.00001	0.077	127	11	23	0.92	35	62	493	79	2.6	1.4
Hot Springs and cold groundwater from the region near Clayton Valley, NV																					
Silver Peak tap	26-May-11	454 Rocky Way	Tap	37.7568	–117.6371	1,334	–113	–14.8	0.71019	0.00001	0.05	90	3.9	4.7	0.02	24	101	1,464	130	1.1	12
NHW	22-May-11	North Hot Well	Well	37.7739	–117.6322	1,300	–117	–13.1	0.71003	0.00002	39.7	10,418	899	4,060	289	69	641	34,643	597	6.6	1.0
CV-24W	25-May-11	Groundwater	Well	37.7146	–117.5903	1,304			0.70980	0.00001	6.7	1,544	288	219	1.247	6	37	4,789	279	41	0.45
CV-29W	26-May-11	Paymaster Hot Well	Well	37.8314	–117.4811	1,321	–120	–14.0	0.71175	0.00002	31.9	8,974	787	3,743	293	41	180	8,872	177	1.1	0.05
CV-30W	26-May-11	Paymaster Well	Well	37.8573	–117.4762	1,420	–124	–15.6	0.71568	0.00002	0.08	87	5.9	11	<0.007	25	52	759	75	0.05	0.43
CV-2W	14-May-12	Alkali Hot Springs	Hotspring	37.8246	–117.3376	1,532			0.71173	0.00001	1.7	314	22	124	83	3.7	42	1,381	33	5.8	0.02
CV-5aW	13-May-12	"The Hot Box"	Hotspring	37.8601	–117.9840	1,448			0.71250	0.00003	0.7	288	28	93	6	0.12	4	24	11	54	2.9
CV-15W	13-May-12	Old Borax Works	Hotspring	37.9095	–117.9552	1,436			0.71147	0.00001	5.3	1,382	151	962	320	7.4	120	3,127	144	711	0.08
CV-29W	15-May-12	Paymaster Hot Well	Well	37.8314	–117.4811	1,321			0.71169	0.00001	28.2	8,974	755	3,470	236	35	113	8,451	382	0.41	0.03
NHW	16-May-12	North Hot Well	Well	37.7739	–117.6322	1,300			0.71004	0.00001	34.4	10,418	852	4,075	313	60	656	31,719	523	4.4	1.4

[1] Elemental data measured by ICP-MS, Sr isotope ratios by MC-ICP-MS, and H and O isotope ratios cavity ring-down spectroscopy